NOVEMBER 1979

analytical chemistry

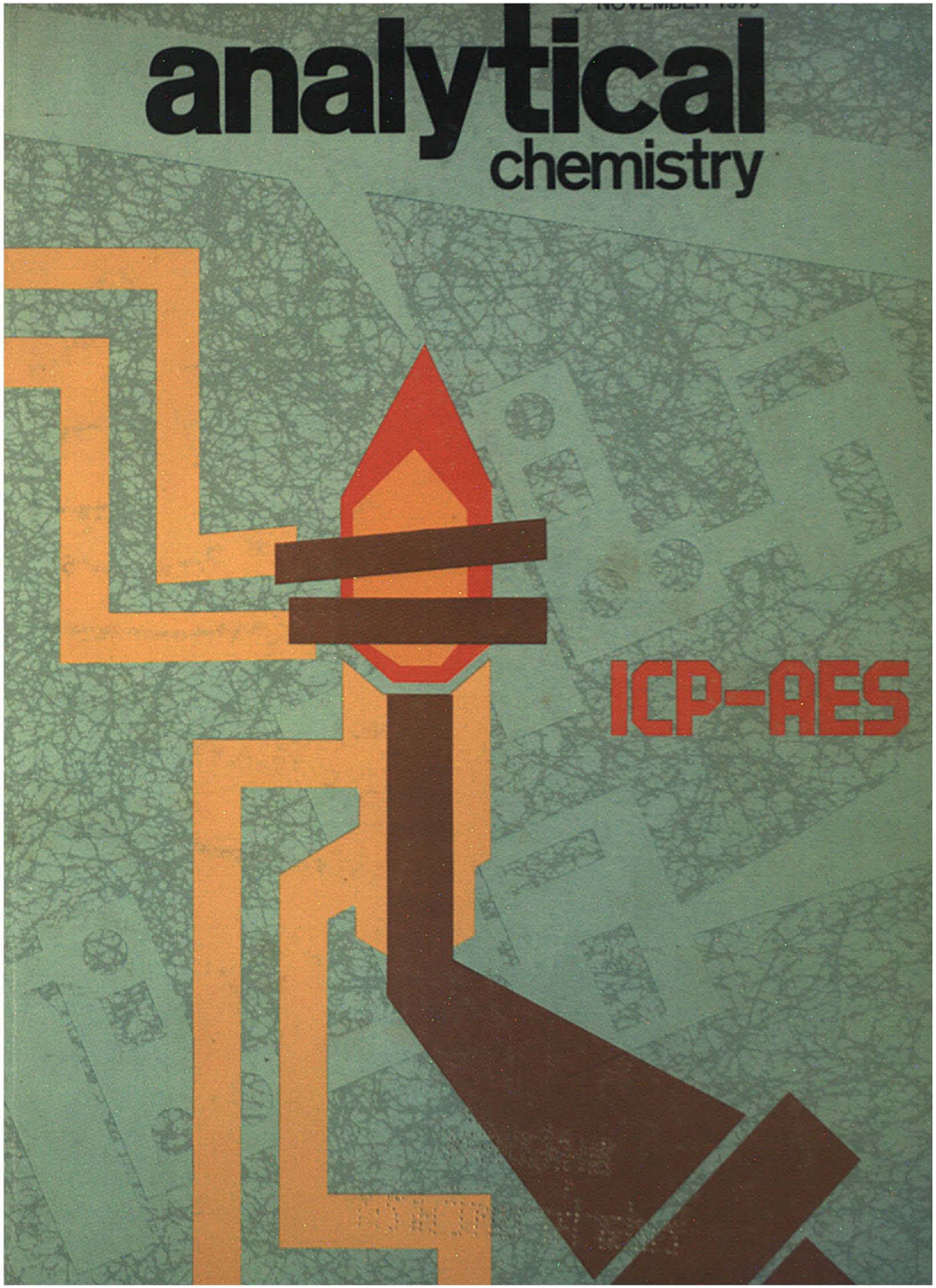

Kevex has the best multi-element analyzer you can buy today.

But the big payoff comes tomorrow.

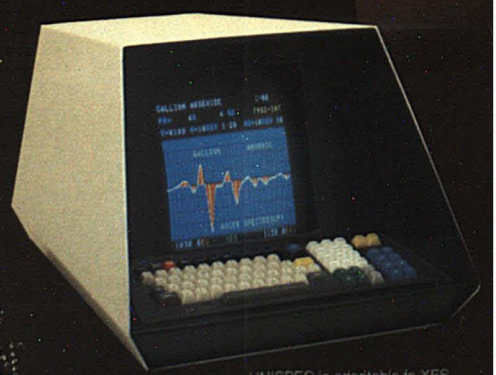

Introducing UNISPEC™

UNISPEC—Universal Spectroscopy—is a bold concept that solves an age-old problem for the materials analyst: how to select analytical instruments that serve both today's and tomorrow's needs.

UNISPEC unites many disparate spectroscopy methods by applying a common and powerful capability to 12 different spectrometry and signal analysis modes.

Specifically, UNISPEC combines (1) microprocessor-based data gathering and processing, (2) interchangeable instrument modules, (3) color-coded video display and (4) bulk information storage on mini-disks.

UNISPEC gives every materials analyst an open-ended option if he has a requirement for X-ray spectrometry. For example, you may wish to perform surface analyses (Auger/ESCA) next year. It's simple and economical with UNISPEC and Kevex. You just add the proper module.

No longer does the demand for immediate results force the allocation of substantial funds to satisfy today's needs without due consideration of tomorrow's.

Because now there is UNISPEC from Kevex. Find out more about it.

UNISPEC is adaptable to XES (XRF, Ultra-Trace,™ microanalysis), Alpha-X,™ WDX, Auger, ESCA, SIMS, ISS, APS, EELS and now, color-coded transient and general purpose signal averaging.

kevex

KEVEX CORPORATION

1101 Chess Drive • Foster City, CA 94404 • Phone (415) 573-5866

CIRCLE 86 ON READER SERVICE CARD

Discover the big drop...

in time, effort and expense.

Now moisture analysis is faster, easier and more economical than ever before.

Aquatest IV gets to the heart of moisture determination because microprocessor control is the heart of Aquatest IV.

Savings start immediately. You never waste time determining a titer because Aquatest IV needs no standardization. It's always in calibration.

Frequent handling of noxious reagents is eliminated. The Karl Fischer reagent is self-generating, allowing you to test hundreds of samples without adding reagent. Burettes are unnecessary.

Your savings continue through the testing process. Once you depress the start key, Aquatest IV automatically performs all functions and calculations, then the result is displayed in percent, ppm or micrograms.

The Aquatest IV automatically compensates for interfering reactions. The instrument also features programmable extraction time and solvent blank correction.

Discover the big drop in time, effort and expense.

Discover the Aquatest IV moisture analyzer.

Aquatest IV
automated moisture analyzer

If moisture affects your products or your profits...

PHOTOVOLT CORPORATION
1115 BROADWAY, NEW YORK, N.Y. 10010

Call our toll-free number: 800-221-5182. From New York State, call collect (212) 989-0484.

CIRCLE 170 ON READER SERVICE CARD

Part of the solution, not the problem.

It isn't simply that Whatman AIEC's outperform other ion exchange celluloses (they do, of course) or that they are unique (they are). A key thing is that they're Whatman AIEC's.

If you are separating and/or purifying enzymes, proteins, nucleotides and the like*, and the separations are at all critical, we suggest that you can profitably ignore the lesser breeds.

With Whatman AIEC's you can confidently expect better resolution, higher capacity, particularly for macromolecules, good to excellent flow rates, among other virtues. And, far from least, Whatman product quality: uniformity, reliability, consistency of performance.

Whatman AIEC's are available in both fibrous and microgranular form (either anion or cation). They pack easily and exceptionally well. They aren't the least expensive—the best rarely is.

Interesting new technical data supporting these contentions are available on request. We appreciate your requests.

*e.g., peptides, nucleosides, hormones, viruses, polysaccharides, lipids, among others.

Whatman Inc. ■ 9 Bridewell Place, Clifton, New Jersey 07014 ■ Tel. (201) 777-4825 ■ Telex 133426.

Whatman

CIRCLE 240 ON READER SERVICE CARD

Volume 51, No. 13, November 1979
ANCHAM
51(13) 1269A-1392A/2065-2304(1979)
ISSN 0003-2700

analytical chemistry

CONTENTS

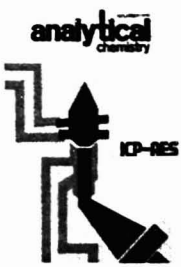

Our cover design depicts an ICP source. See REPORT, page 1290 A

Published monthly with review issue added in April and Laboratory Guide in August by the American Chemical Society, from 20th and Northampton Sts., Easton, Pa. 18042. Executive and Editorial headquarters, American Chemical Society, 1155 16th St., N.W., Washington, D.C. 20036 (202) 872-4600. Second class postage paid at Washington, D.C., and at additional mailing offices.

1979 Subscription prices—including surface postage

	1 yr	2 yr	3 yr
MEMBERS:			
Domestic	$12	$22	$30
Canada, Foreign	21	40	57
NONMEMBERS:			
Domestic	16	29	42
Canada	25	47	69
Other Foreign	33	61	89

Airmail and air freight rates are available from Membership & Subscription Services, ACS, P.O. Box 3337, Columbus, Ohio 43210 (614) 421-7230.

New and renewal subscriptions should be sent with payment to the Office of the Controller at the ACS Washington address.

Subscription service inquiries and changes of address (include both old and new addresses with ZIP code and *recent mailing label*) should be directed to the ACS Columbus address noted above. Please allow six weeks for change of address to become effective.

Claims for missing numbers will not be allowed if loss was due to failure of notice of change of address to be received in the time specified; if claim is dated (a) North America: more than 90 days beyond issue date, (b) all other foreign: more than one year beyond issue date; or if the reason given is "missing from files."

Microfilm and microfiche editions are available by single volume or back issue collection. Inquiries and payments to Microforms Program, ACS Washington address.

Single issues, current year, $3.00 except review issue and Labguide, $4.00; **back issues and volumes:** *write or call* Special Issues Sales, ACS Washington address (202) 872-4365.

Advertising Management: Centcom, Ltd., 25 Sylvan Road South, Westport, Conn. 06880 (203) 226-7131

Briefs

Time and Spatially Resolved Atomic Absorption Measurements with a Dye Laser Plume Atomizer and Pulsed Hollow Cathode Lamps 2066

Pulsed hollow cathode lamps with pulses as short as 1-μs are used as primary sources for atomic absorption measurements. Influences of sample chamber pressure are studied.

R. M. Manabe and Edward H. Piepmeier,* Department of Chemistry, Oregon State University, Corvallis, Ore. 97331
Anal. Chem., 51 (1979)

Inductively-Coupled Argon Plasma as an Excitation Source for Flame Atomic Fluorescence Spectrometry 2071

Sensitivity and noise sources of the technique are evaluated. Detection limits for 14 elements are compared to detection limits obtained by other radiation sources and to those obtained by other atomic spectrometric techniques.

M. S. Epstein, S. Nikdel, N. Omenetto, R. Reeves, J. Bradshaw, and J. D. Winefordner,* Department of Chemistry, University of Florida, Gainesville, Fla. 32611 *Anal. Chem., 51 (1979)*

Lophine Chemiluminescence for Metal Ion Determinations 2077

Emission intensity is a function of analyte reduction potential. Detection limits are OCl^-, 1×10^{-6} M; Co(II), 8×10^{-7} M; Cr(III), 5×10^{-6} M; Cu(II), 5×10^{-6} M. RSDs are in the range of 2–5%.

Allan MacDonald, Kenneth W. Chan, and Timothy A. Nieman,* School of Chemical Sciences, University of Illinois, Urbana, Ill. 61801 *Anal. Chem., 51 (1979)*

Enzyme Amplification Laser Fluorimetry 2082

Detection limits for glucose-6-phosphate, α-ketoglutaric acid, and NADP are 2 nM, 4×10^{-12} mol, and 1×10^{-14} mol, respectively. Sensitivity for NADP is 0.1 nM.

T. Imasaka and R. N. Zare,* Department of Chemistry, Stanford University, Stanford, Calif. 94305 *Anal. Chem., 51 (1979)*

Microdetermination of Manganese in Animal Tissues by Flameless Atomic Absorption Spectrometry 2086

Treatment with HCl liberates Mn from animal tissues. RSD for a 10-μL sample of plasma extract, containing 2.07 ng Mn/mL, is 3.5%. Matrix and other interferences are not detected.

David I. Paynter, Department of Animal Science and Production, University of Western Australia, Nedlands, Western Australia 6009 *Anal. Chem., 51, (1979)*

Determination of Aluminum in Blood, Urine, and Water by Inductively Coupled Plasma Emission Spectrometry 2089

Optimum working conditions and interferences by metals and metalloids common in biological samples are studied using a concentric pneumatic nebulizer. Detection limits are 0.4 μg/L in water, 1 μg/L in urine, and 4 μg/L in blood.

Pierre Allain* and Yves Mauras, Laboratoire de Pharmacologie, C.H.U., 49036 Angers Cedex, France *Anal. Chem., 51 (1979)*

* Corresponding author.

Chemiluminescent Determination of Clinically Important Organic Reductants 2092

Detection limits (in mg/L) are: ascorbic acid, 0.17; creatinine, 4.7; uric acid, 0.64; glutathione, 1.0; glucuronic acid, 9.1; lactose, 5.2; glucose, 21. The RSD of the chemiluminescent signal is 0.5–5%.

Robert L. Veazey and Timothy A. Nieman,* School of Chemical Sciences, University of Illinois, Urbana, Ill. 61801 *Anal. Chem., 51 (1979)*

Laser Fluorometry of Fluorescein and Riboflavin 2096

The detection limits of fluorescein and riboflavin are determined to be 0.02 and 0.6 parts-per-trillion, obtained by a nitrogen-laser-pumped dye laser and pulse-gated photon counter.

Nobuhiko Ishibashi,* Teiichiro Ogawa, Totaro Imasaka, and Mikio Kunitake, Faculty of Engineering, Kyushu University, Fukuoka 812, Japan *Anal. Chem., 51 (1979)*

Flame Photometric Determination of Carbon Disulfide in Air after Specific Preconcentration 2100

Atmospheric CS_2 samples are analyzed by headspace technique and flame photometry after concentration on sodium azide and hexamethylphosphorotriamide treated chromatographic support. Temperature-dependent CS_2 hydrolysis is studied for its effect on quantitative determinations.

Jean Godin,* Jean-Louis Cluet, and Claude Boudène, INSERM U 122, Laboratoire de Toxicologie, UER des Sciences Pharmaceutiques, 92290 Chatenay-Malabry, France *Anal. Chem., 51 (1979)*

Quantitative Electron Spectroscopy for Chemical Analyses of Bitumen Processing Catalysts 2102

ESCA is used to analyze Mo/Al_2O_3 hydrodesulfurization catalysts containing nickel and cobalt as promoters.

G. M. Bancroft and R. P. Gupta, Department of Chemistry, University of Western Ontario, London, Ontario, Canada, and **A. H. Hardin* and M. Ternan,** Energy Research Laboratories, Department of Energy, Mines and Resources, Ottawa, Ontario, Canada *Anal. Chem., 51 (1979)*

Determination of Elemental Concentration Maps from Digital Secondary Ion Images 2107

A numerical correction routine applied in each pixel of digitized ion images can be performed at a rate of approximately 0.2 s/pixel on a PDP 11 minicomputer.

Wolfgang Steiger and Friedrich G. Rudenauer,* SGAE, Lenaugasse 10, A-1082 Vienna, Austria *Anal. Chem., 51 (1979)*

Processing Elemental Microanalytical Data 2112

CNHS ratios are calculated from data on unweighed analyzed samples using three linear equations correlating binary atomic ratios of organic compounds with binary signal ratios of their four combustion gases.

Bruno Colombo and Guido Giazzi, Carlo Erba Strumentazione, Rodano, Milan, Italy, and **Ermes Pella,*** Farmitalia Carlo Erba, Ricerca e Sviluppo Chimico, Milan, Italy *Anal. Chem., 51 (1979)*

ORION just wrote the book on specific ion methods. Again.

And it's yours for the asking.

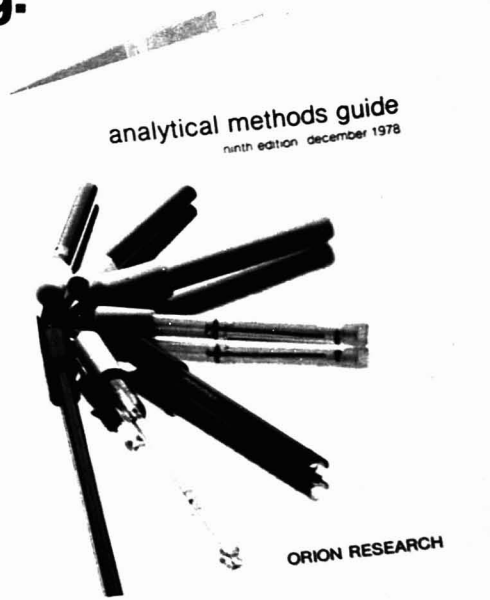

The newly-revised ninth edition of the Analytical Methods Guide is now available from ORION Research. The result of 15 years of leadership in specific ion technology, this unique, comprehensive guide is an indispensible tool for the analyst seeking the simplicity, time-savings, and precision inherent in analysis by electrode.

More than 80 species readily measurable by electrode and hundreds of applications in research, industry, and biomedicine are listed. You'll also find detailed information on sample preparation and the several direct and incremental analytical techniques utilized in electrode measurements. Complete references are included for each method.

In addition, the Analytical Methods Guide is a storehouse of facts on specific ion and pH electrodes, instrumentation, accessories and solutions, and more.

To obtain your free copy of the ORION Analytical Methods Guide mail the coupon today.

ORION RESEARCH
380 Putnam Avenue, Cambridge, MA 02139, U.S.A.

Gentlemen: Please send my free copy of the new Analytical Methods Guide.

☐ Add my name to your mailing list.

Name _____
Department _____
Organization _____
_____
Street and No. _____
City _____
Country _____ Postal Code _____

CIRCLE 156 ON READER SERVICE CARD

Briefs

Sensitivities and Interferences in Activation Analysis of Thin Samples by means of 25-MeV to 30-MeV Protons 2116

Activation properties of Na, Mg, Cl, Ca, Ti, Cr, Mn, Fe, Ni, Cu, Zn, As, Br, Sr, Cd, Sn, Sb, and Pb through bombardment of thin samples by 25-MeV to 30-MeV protons for routine analysis are considered. Detection limits are in the nanogram to microgram levels.

P. Priest, Laboratoire de Chimie Inorganique et Nucléaire, Université Catholique de Louvain 2, Chemin du Cyclotron, B-1348 Louvain-la-Neuve, Belgium, and **G. Desaedeleer,*** Service de Radioprotection, Université Catholique de Louvain, 2, Chemin du Cyclotron, B-1348 Louvain-la-Neuve, Belgium

Anal. Chem., 51 (1979)

Thermometric Titrations of Polyprotic Acids 2122

The formulation of n equivalent equations for the thermometric titration curve of a polyprotic acid H_nA are given, the pK values of which are comparable.

Maurice A. Bernard and Jean-Louis Burgot,* Laboratoire de Chimie Minérale B, Groupe de Cristallographie et Chimie Solide, L.A. 251, Universite de Caen, 14032 Caen Cedex, France

Anal. Chem., 51 (1979)

Cathodic Stripping Voltammetric Determination of Organic Halides in Drug Dissolution Studies 2127

Determination of organic hydrochlorides and hydrobromides at concentration orders of 10^{-6} M gives accurate and precise (3.1% and 2.9% coefficients of variation) results by stripping voltammetry following mercurous halide electrolyte saturation.

Ian E. Davidson,* Wyeth Laboratories, Huntercombe Lane South, Taplow, Maidenhead, Berkshire, SL6 OPH, England, and **W. Franklin Smyth,** Department of Chemistry, Chelsea College, University of London, Manresa Road, London SW3, England

Anal. Chem., 51 (1979)

Pseudopolarographic Determination of Metal Complex Stability Constants in Dilute Solution by Rapid Scan Anodic Stripping Voltammetry 2133

No complexation of lead and cadmium occurs with glycine at pH 4.68. Lead speciation in geothermal water is a $PbCl^+$ complex. Arsenic(III) structure at 1.0 ng/mL in acid solutions in $As(OH)_3$.

Steven D. Brown and Bruce R. Kowalski,* Department of Chemistry, University of Washington, Seattle, Wash. 98195

Anal. Chem., 51 (1979)

Potassium Titanium(IV) Oxalate as a Reagent for Automated Pulse Polarographic Determination of Seromucoids 2139

The system operates at 60 samples/h with approximately ±0.5% precision and less than 2% carry-over for determinations in the range 1–30 mg L^{-1}.

P. W. Alexander* and M. H. Shah, Department of Analytical Chemistry, University of New South Wales, P.O. Box 1, Kensington, N.S.W., Australia 2033 *Anal. Chem., 51 (1979)*

Amperometric Membrane Electrode for Measurement of Ozone in Water 2144

A current sensitivity of 0.484 μA $(mg/L)^{-1}$ $(cm)^{-2}$ is observed at an applied voltage of +0.6 V (vs. SCE) at 22 °C. A detection limit of 62 μg/L is predicted at twice the observed residual current.

John H. Stanley and J. Donald Johnson,* Department of Environmental Sciences and Engineering, School of Public Health, University of North Carolina at Chapel Hill, Chapel Hill, N.C. 27514

Anal. Chem., 51 (1979)

Copper Ion-Selective Electrode for Determination of Inorganic Copper Species in Fresh Water 2148

Distributions of $CuOH^+$, $Cu_2(OH_2)^{2+}$, $CuCO_3(aq)$, $Cu(CO_3)_2^{2-}$ are deduced measuring Cu^{2+}, OH^-, and CO_3^{2-} concentrations as functions of pH in controlled media. $CuCO_3(aq)$ predominates at natural pH and alkalinity levels.

Renato Stella* and M. T. Ganzerli-Valentini, Laboratorio di Radiochimica e Centro di Radiochimica ed Analisi per Attivazione del C.N.R., Istituto di Chimica Generale ed Inorganica, Università di Pavia, Viale Taramelli 12, 27100 Pavia, Italy

Anal. Chem., 51 (1979)

Quantitative Examination of Thin-Layer Chromatography Plates by Photoacoustic Spectroscopy 2152

Twenty ng of fluorescein in 4.5 mg of silica gel is detectable with an RSD of 0.08–0.1.

S. L. Castleden,* C. M. Elliott, G. F. Kirkbright, and D. E. M. Spillane, Department of Chemistry, Imperial College, London SW7 2AY, U.K. *Anal. Chem., 51 (1979)*

Mass Spectrometric Tracer Pulse Chromatography 2154

Mass spectrometric tracer pulse (MSTP) chromatography measures vapor–liquid or vapor–solid equilibrium data. The technique is based on normal tracer pulse chromatography, but utilizes stable isotopes and a mass specific detection system.

J. F. Parcher* and M. I. Selim, Chemistry Department, The University of Mississippi, University, Miss. 38677

Anal. Chem., 51 (1979)

Effect of Temperature on the Separation of Conformational Isomers of Cyclic Nitrosamines by Thin-Layer Chromatography 2157

Resolution of conformational isomers not separable at room temperature is achieved at −77 °C. Better separation occurs at low temperatures with improved resolution occurring with continued development.

Haleem J. Issaq,* Mario M. Mangino, George M. Singer, David J. Wilbur, and Nelson H. Risser, Chemical Carcinogenesis Program, Frederick Cancer Research Center, Frederick, Md. 21701 *Anal. Chem., 51 (1979)*

Thin Layer Chromatographic Separation of Pesticides, Decachlorobiphenyl, and Nucleosides with Micellar Solutions 2160

Aqueous solutions of sodium dodecyl sulfate with polyamide separates p,p'-DDT, p,p'-DDD, p,p'-DDE, and decachlorobiphenyl on alumina thin-layer sheets. Reversed micellar solution separates adenosine, cytidine, guanosine, and uridine.

Daniel W. Armstrong* and Robert Q. Terrill, Department of Chemistry, Bowdoin College, Brunswick, Me. 04011

Anal. Chem., 51 (1979)

BREAK THE GLASS HABIT

Nalgene®
FEP Sep Funnels are as chemical resistant as glass.

Like glass, Nalgene® Sep Funnels of Teflon* FEP resist *any* chemical used in an extraction. But unlike glass, they won't break or crack, even when dropped, so you can reduce replacement costs. And both the screw cap on top and the stopcock at the bottom make these Nalgene Sep Funnels leakproof when they're shaken.

Teflon* FEP construction lets you see clearly the interface of even colorless liquids all the way down to the stopcock housing.

Nalgene Sep Funnels are non-wetting, so they drain completely. They're non-stick, so they're easy to clean. The stopcock housing can be removed for easier cleaning, too.

Get extraordinary chemical resistance and convenience with these economical alternatives to fragile glass sep funnels.

Put Nalgene Labware to the test, and see why so many laboratories are breaking the glass habit. Send for our free Nalgene Labware catalog, featuring over 250 products for professional use. Write: Nalge Company, Division of Sybron Corporation, Nalgene Labware Department, Box 365, Rochester, New York 14602.

And unbreakable Nalgene Labware lasts longer.

SYBRON | Nalge

CIRCLE 150 ON READER SERVICE CARD

Briefs

N,N'-Bis(*p*-phenylbenzylidene)-α,α'-bi-*p*-toluidine as Stationary Phase in a Packed and in a Micropacked Column 2163

Combined thermal and chromatographic studies of *N,N'*-bis(*p*-phenylbenzylidene)-α,α'-bi-*p*-toluidine as a packing material reveal the highest separation of polycyclic aromatic hydrocarbons occurs at 275–280 °C.

F. Janssen, Chemistry Department, KEMA Laboratories, Utrechtseweg 310, Arnhem, The Netherlands *Anal. Chem., 51 (1979)*

Interactive Effects of Temperature, Salt Concentration, and pH on Head Space Analysis for Isolating Volatile Trace Organics in Aqueous Environmental Samples 2167

Sixty-six-fold enrichment factors are obtained by increasing temperature from 30 to 50 °C and by increasing Na_2SO_4 solution concentrations from zero to saturation.

Stephen L. Friant, Academy of Natural Science, Philadelphia, Pa. 19104, and **Irwin H. Suffet,*** Department of Chemistry, Environmental Studies Institute, Drexel University, Philadelphia, Pa. 19104 *Anal. Chem., 51 (1979)*

Determination of Alkoxyl Substitution in Cellulose Ethers by Zeisel-Gas Chromatography 2172

Adipic acid catalyzes the hydriodic acid cleavage of substituted alkoxyl groups quantitatively to their corresponding alkyliodides. In-situ xylene extraction of alkyliodides allows for determination of alkoxy substitution in cellulosic ethers.

K. L. Hodges,* W. E. Kester, D. L. Wiederrich, and J. A. Grover, The Dow Chemical Company, Midland, Mich. 48640 *Anal. Chem., 51 (1979)*

Reduction in Sample Foaming in Purge and Trap Gas Chromatography/Mass Spectrometry Analyses 2176

Silicone surfactants and heat dispersion are used to reduce foaming in purge and trap GC/MS analyses of volatile priority pollutants. Qualitative and quantitative aspects of reduction are considered.

M. E. Rose and B. N. Colby,* Chemistry and Chemical Engineering Systems, Science and Software, P.O. Box 1620, La Jolla, Calif. 92038 *Anal. Chem., 51 (1979)*

Trace Enrichment with Hand-Packed CO:PELL ODS Guard Columns and Sep-Pak C_{18} Cartridges 2180

The efficiency of removing an organic compound from seawater using RP-18 packing depends on the water solubility of the compound and on the volume of water sampled.

William A. Saner,* J. Richard Jadamec, and Richard W. Sager, U.S. Coast Guard Research and Development Center, Avery Point, Groton, Conn. 06340, and **Timothy J. Killeen,** Statistics Department, University of Connecticut, Storrs, Conn. 06368 *Anal. Chem., 51 (1979)*

Survey of Carbon-13 Chemical Shifts in Aromatic Hydrocarbons and Its Application to Coal-Derived Materials 2189

A ^{13}C chemical shift assignment scheme yields structural information on the oxygen and aliphatic carbon groups in coal extracts.

C. W. Snape and W. R. Ladner,* National Coal Board, Coal Research Establishment, Stoke Orchard, Cheltenham, Glos. GL52 4RZ, England, and **K. D. Bartle,** Department of Physical Chemistry, University of Leeds, Leeds LS2 9JT, England *Anal. Chem., 51 (1979)*

Error Estimates for Finite Zero-Filling in Fourier Transform Spectrometry 2198

Four zero-fillings for the absorption mode and three zero-fillings for the magnitude mode will usually suffice to reduce the peak height error to less than 2%.

Melvin B. Comisarow* and Joe D. Melka, Chemistry Department, University of British Columbia, Vancouver, British Columbia, Canada V6T 1W5 *Anal. Chem., 51 (1979)*

Simulation of Nuclear Magnetic Resonance Spin Lattice Relaxation Time Measurements for Examination of Systematic and Random Error Effects 2203

Systematic and random errors in NMR spin lattice relaxation time (T_1) measurements are investigated by simulating relaxation data using various experimental parameters: pulse width, recovery delay, waiting times, and signal-to-noise.

T. Phil Pitner* and Jerry F. Whidby,* Philip Morris USA Research Center, P.O. Box 26583, Richmond, Va. 23261 *Anal. Chem., 51 (1979)*

Detection of Small Quantities of Photochemically Produced Oxygen by Reaction with Alkaline Pyrogallol 2206

A continuous flow system detects oxygen quantities of 3.5×10^{-7} mol by spectrophotometric monitoring of trap reagent alkaline pyrogallol.

I. A. Duncan,* A. Harriman, and G. Porter, Davy Faraday Research Laboratory of The Royal Institution, 21 Albemarle Street, London W1X 4BS England *Anal. Chem., 51 (1979)*

Neutron-Capture Prompt γ-Ray Activation Analysis for Multielement Determination in Complex Samples 2209

Up to 17 elements from among the set H, B, C, N, Na, Mg, Al, Si, P, S, Cl, K, Ca, Ti, V, Mn, Fe, Cd, Nd, Sm, and Gd are measurable in samples of coal, fly ash, orchard leaves, and bovine liver.

M. P. Failey, D. L. Anderson, W. H. Zoller, and G. E. Gordon,* Department of Chemistry, University of Maryland, College Park, Md. 20742, and **R. M. Lindstrom,** Center for Analytical Chemistry, National Bureau of Standards, Washington, D.C. 20234 *Anal. Chem., 51 (1979)*

The Antlia™ hand pump puts pressure on the liquid, not on you.

You've seen this little drama in your lab: you homogenize some tissue into liquid, put it into a standard syringe, then try to separate the plasma from the debris by running it through a membrane. Only it takes more muscle than you have to drive down the plunger to push the solution through the debris-clogged membrane . . . and then, to add to your problems, the syringe starts to leak.

S&S puts an end to all this with the S&S Antlia system — because its unique hand pump can build and sustain pressures as high as 75 psi — far more than can be developed by a standard syringe. It's designed to separate out the soluble fractions from homogenized cells without impossible effort, without leaking, without clogging. And that's why, in the fields of immunochemistry and immunology, it's the most-used device of its kind.

For greatest efficiency in using the Antlia system for this application, we recommend S&S BA85 membrane filters (0.45μm). The Antlia is used for any number of other applications as well, e.g., cold-sterilization of tissue culture media where we recommend low-extractable BA83 1 (0.2μm).

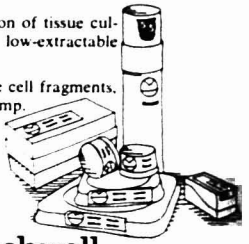

To remove the effort, as well as the cell fragments, use the Antlia pneumatic hand pump. For complete information on the Antlia system and S&S membranes, ask Schleicher & Schuell, Inc., Keene, New Hampshire 03431; (603) 352-3810.

Schleicher & Schuell

Schleicher & Schuell, Inc.
Keene, New Hampshire 03431

Schleicher & Schull GmbH, D-3354, Dassel, West Germany
Schleicher & Schull AG, 8714, Feldbach ZH, Switzerland

CIRCLE 187 ON READER SERVICE CARD

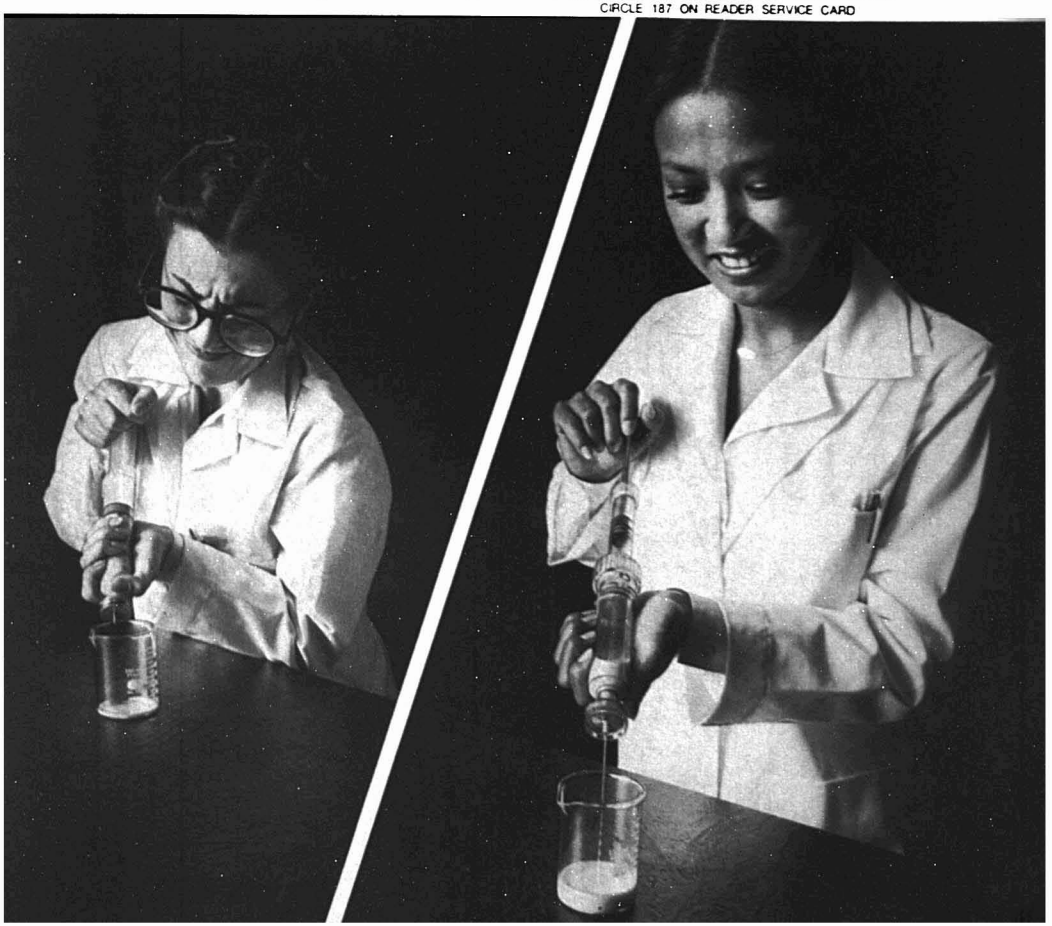

Briefs

Frequency Modulated Correlation Chromatography 2222

By frequency modulating a signal, signal processing techniques previously useful only in linear areas of an isotherm are made useful in nonlinear areas.

Dan C. Villalanti and M. F. Burke,* Analytical Division, Department of Chemistry, University of Arizona, Tucson, Ariz. 85721, and **J. B. Phillips,** Department of Chemistry and Biochemistry, Southern Illinois University, Carbondale, Ill. 62901
Anal. Chem., 51 (1979)

Inductively Coupled Plasma Emission Spectrometric Detection of Simulated High Performance Liquid Chromatographic Peaks 2225

Separation and detection of Al, As, B, Ba, Ca, Cd, Co, Cr, Cu, Fe, K, Li, Mg, Mn, Mo, Na, Ni, P, Pb, Sb, Se, Sr, Ti, V, and Zn are evaluated. Comparisons are made between ICP and AAS for HPLC peak detection of EDTA and NTA copper chelates, and to UV solution absorption for Cu chelate detection.

David M. Fraley, Dennis Yates, and Stanley E. Manahan,* Department of Chemistry, University of Missouri, Columbia, Mo. 65211
Anal. Chem., 51 (1979)

Selective Electrocatalytic Method for the Determination of Nitrite 2230

A Mo-catalyst permits nitrite determination in the presence of nitrate. With 0.01–1 mM NO_2^-, the working curve slope is 8.18 ± 0.04 nA/M and linear correlation coefficient, 0.9997.

James A. Cox* and Anna F. Brajter, Department of Chemistry and Biochemistry, Southern Illinois University at Carbondale, Carbondale, Ill. 62901
Anal. Chem., 51 (1979)

Hydroxyl Anion Chemical Ionization Screening of Liquid Fuels 2232

Mass spectra of screened aromatic components in liquid fuels using hexane as the solvent are characterized by the absence of measurable signals from aliphatic components.

L. Wayne Sieck,* National Bureau of Standards, National Measurement Laboratory, Washington, D.C. 20234, and **K. R. Jennings and P. D. Burke,** Department of Chemistry and Molecular Sciences, University of Warwick, Coventry CV4 7AL, England
Anal. Chem., 51 (1979)

Interlaboratory Study of the Determination of Polychlorinated Biphenyls in a Paper Mill Effluent 2235

A method for determining PCBs in paper mill effluent is satisfactory for effluents having greater than 2 μg/L PCB content and easily removed interferences.

Joseph J. Delfino,* Laboratory of Hygiene, 465 Henry Mall, University of Wisconsin—Madison, Madison, Wis. 53706 and **Dwight B. Easty,** The Institute of Paper Chemistry, P.O. Box 1039, Appleton, Wis. 54912
Anal. Chem., 51 (1979)

Quaternized Porous Beads for Exclusion Chromatography of Water-Soluble Polymers 2239

Molecular weight calibration graphs, theoretical plate height plots, and concentration effects are obtained for cationic polyelectrolytes chromatographed on quaternized porous glass.

C. P. Talley and L. M. Bowman,* Research and Development, Calgon Corporation, Post Office Box 1346, Pittsburgh, Pa. 15230
Anal. Chem., 51 (1979)

Electrochemical Studies of the Oxidation Pathways of Apomorphine 2243

In the absence of strong nucleophiles, an irreversible chemical reaction follows the initial $2e^-/2H^+$ oxidation of apomorphine and eventually produces a new redox couple.

H.-Y. Cheng, E. Strope, and R. N. Adams,* Department of Chemistry, University of Kansas, Lawrence, Kan. 66045
Anal. Chem., 51 (1979)

Determination of Urinary Ammonia by Osmometry 2247

Urinary ammonia trapped in acid is measured osmometrically with precision of ±1.2 SE and accuracy of 1.5%.

Man S. Oh,* Kenneth R. Phelps, Ruth L. Lieberman, and Hugh J. Carroll, Department of Medicine, State University of New York, Downstate Medical Center, Brooklyn, N.Y. 11203
Anal. Chem., 51 (1979)

Ligand Exchange Chromatography of Alkyl Phenyl Sulfides 2248

The contribution of polar, molecular weight, and steric effects E_S to R_M values on chromatographic behavior is examined using Hg^{2+}, Ag^+, Cd^{2+}, and Pb^{2+} impregnated silica gel plates.

Vaclav Horak,* Mercedes De Valle Guzman, and George Weeks, Department of Chemistry, Georgetown University, Washington, D.C. 20057
Anal. Chem., 51 (1979)

Observation of Electrochemical Concentration Profiles by Absorption Spectroelectrochemistry 2253

Optical path length of 0.5 cm or greater increases spectroelectrochemical sensitivity. Spatial resolution of the diffusion layer gives information about mass transfer and additional insight into reactions accompanying charge transfer.

Richard Pruiksma and Richard L. McCreery,* Department of Chemistry, Ohio State University, Columbus, Ohio 43210
Anal. Chem., 51 (1979)

Rotating-Ring-Disc Analysis of Iron Tetra(*N*-methylpyridyl)porphyrin in Electrocatalysis of Oxygen 2257

The rate of reaction of ferrous porphyrin with O_2 is about 4×10^7 $M^{-1}s^{-1}$. The main product of the catalytic reduction is hydrogen peroxide.

Armand Bettelheim and Theodore Kuwana,* Department of Chemistry, The Ohio State University, 140 West 18th Avenue, Columbus, Ohio 43210
Anal. Chem., 51 (1979)

Chromatography Products From

SGE

Syringes for gas and liquid chromatography

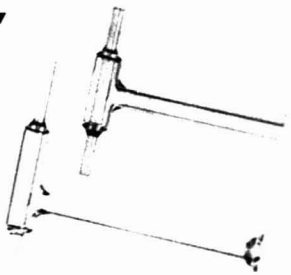

Graphite ferrules, glass lined tubing in standard lengths or cut to specifications

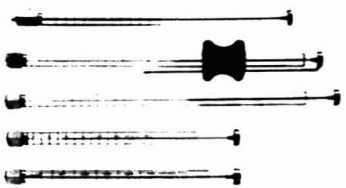

Molecular jet separators.

WCOT-SCOT capillary columns in quartz, borosilicate and stainless steel.

High temperature micro needle valve.

Scientific Glass Engineering

SGE

Head Office — 111 Arden St., North Melbourne, Victoria AUSTRALIA
U.S. Office — Kramer Ln. & Metric Blvd., Austin, Texas 78759
European Office — 567 North Circular Rd., London NW 27AY GREAT BRITAIN

CIRCLE 194 ON READER SERVICE CARD

Briefs

Radiation-Induced Surface Redox and Shake-Up Structure in X-Ray Photoelectron Spectra of Copper(II) Chelates 2260

X-ray photoelectron spectroscopy of copper(II) complex, 1,8-bis(2′-pyridyl)-3,6-dithiaoctane, in the S 2p and Cu $2p_{3/2}$ regions confirms X-ray-induced surface redox reaction of the chelate. Shake-up satellite peaks are discussed in terms of known optical absorption data.

Michael Thompson,* Bruce R. Lennox, and Deborah J. Zemon, Department of Chemistry, University of Toronto, 80 St. George Street, Toronto, Ontario, Canada, M5S 1A1

Anal. Chem., 51 (1979)

Analysis of Metal Alloys by Inductively Coupled Argon Plasma Optical Emission Spectrometry 2264

Samples are acid-diluted and analyzed by a direct-reading inductively coupled argon plasma (ICAP) spectrometer for elemental concentrations. The spectrometer is programmed with a concentration ratio method.

Arthur F. Ward* and Louis F. Marciello, Jarrell-Ash Division, Fisher Scientific Company, 590 Lincoln Street, Waltham, Mass. 02154

Anal. Chem., 51 (1979)

Synthesis and Identification of the 22 Tetrachlorodibenzo-*p*-dioxin Isomers by High Performance Liquid Chromatography and Gas Chromatography 2273

Applications to determination of tetrachlorodibenzo-*p*-dioxins in a variety of samples are discussed.

T. J. Nestrick,* L. L. Lamparski, and R. H. Stehl, Analytical Laboratory, Dow Chemical U.S.A., Midland, Mich. 48640

Anal. Chem., 51 (1979)

Correspondence

Diffusion Control in Linear Sweep Voltammetry 2282

Brian R. Eggins,* School of Physical Science, Ulster Polytechnic, Shore Road, Newtownabbey, Co. Antrim, BT37 0QB, N. Ireland, and **Norman H. Smith,** School of Mathematics, Ulster Polytechnic, Shore Road, Newtownabbey, Co. Antrim, BT37 0QB, N. Ireland

Anal. Chem., 51 (1979)

Direct Sample Insertion Device for Inductively Coupled Plasma Emission Spectrometry 2284

Eric D. Salin and Gary Horlick,* Department of Chemistry, University of Alberta, Edmonton, Alberta, Canada T6G 2G2

Anal. Chem., 51 (1979)

Effects of Switching Potential and Finite Drop Size on Cyclic Voltammograms at Spherical Electrodes 2287

J. Everett Spell and Robert H. Philp, Jr.,* Department of Chemistry, University of South Carolinia, Columbia, S.C. 29208

Anal. Chem., 51 (1979)

No. 450 Gas Stream Purifier

The model 450 purifier with model 454 replaceable cartridge is specially designed for controlling the acetone vapor in acetylene. The cartridge contains activated charcoal. It belongs in an AA system. Circle 144

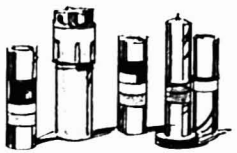

Automatic Regulators 1PA-510 and 1L 326

If you are using AA, choose the correct regulators. In the laboratory, use regulators designed for the specific gas. Information on these regulators can be obtained. Circle 147

Cylinder Scale, Model 8510

To judge accurately when a liquefied gas is nearing empty, Matheson has designed and sells a cylinder scale. We recommend this for nitrous oxide because it will let you know ... and it's the only way ... when the cylinder is empty. Invaluable! Circle 145

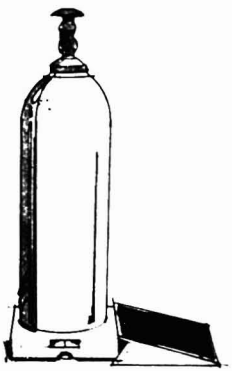

Series 6103 Flash Arrestor

A flash arrestor is installed as a part of the AA system downstream, after the regulator and cylinder. Some instruments have a built-in flash arrestor. If yours does not, two should be installed. Acetylene is highly flammable. Should flashback occur, with the accompanying shock wave, this device will instantly seal off the path to both regulator and cylinder ... preventing an explosion of much greater magnitude in either regulator or cylinder, both of which contain more gas. Flash arrestors are recommended for both fuel gas and oxidizer gas lines. For more information, circle 148

Nitrous Oxide Heater

Because nitrous oxide, frequently used as an oxidizer gas in AA, is liquefied gas, or a gas over liquid in a cylinder, it often cools or ices on expansion, causing problems in automatic control. The heater we offer is installed between cylinder and regulator and eliminates icing and allows for higher flows. Thermostatically controlled, the N_2O is not overheated and the operator can concentrate on his instrument. Works simply with 115 VAC. Circle 146

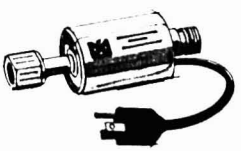

Acetylene 99.6% and Nitrous Oxide 99.0%

These are pure gases containing less impurities than commercial grades. We recommend them and specially purify them for AA instrument use. The purer the gas, the less interference in final results. Circle 149

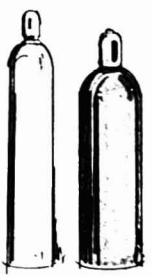

Improved Operation Of An Atomic Absorption Spectrophotometer

Chemical analysis by atomic absorption spectroscopy is achieved by converting the sample into an atomic vapor and measuring its absorbance at a selected wavelength. The measured absorbance is proportional to concentration. The analysis is made by comparing this absorbance with a reference sample of known composition under similar conditions.

Atomic absorption lines are so narrow that the use of a conventional monochromator is impractical to measure them. Commercial instruments overcome this by the use of hollow cathode lamps which emit atomic spectral lines of the element to be determined.

Elements are measured after they have been put into solution either aqueous or organic. The solution is then sprayed into a flame, generally, air-acetylene. Some compounds, like the rare earths, require a highly reducing flame. This is done most safely by burning the acetylene in nitrous oxide which gives more available oxygen than air.

For years Matheson has been servicing scientists using AA spectroscopy, not only with gases but with other equipment which makes operation easier, and more important, safer. These items are at left. If you're not familiar with them we will be delighted to rush literature to you.

Matheson

Lyndhurst, N.J. 07071

East Rutherford, N.J. 07073
Morrow, Georgia 30260
Bridgeport, N.J. 08014
Gloucester, Massachusetts 01930
Joliet, Illinois 60434
Dayton, Ohio 45424
La Porte, Texas 77571
Cucamonga, California 91730

Newark, California 94560
Dorsey, Maryland 21227
Gonzales, Louisiana 70737
Whitby, Ontario, Canada L1N 5R9
Edmonton, Alberta, Canada T5B 4N8
B-2411 Oevel, Belgium
8046 Heusenstamm, West Germany

Briefs

Aids for Analytical Chemists

Gas Chromatography News

Double your GC speed!

Analysis time reduced 50 %

SERIES 3000-3 HI-EFF gas chromatography columns are only 3 ft. long, yet they fully resolve mixtures normally requiring a 6 ft. column for separation. Best of all, SERIES 3000-3 HI-EFF columns cut the time required for analysis by one-half.

Twice the efficiency

SERIES 3000-3 HI-EFF (3 ft.) columns provide 3000-4000 theoretical plates with a HETP of 0.23-0.30 mm. A minimum of 1000 plates/foot is obtained over a carrier gas flow range of 6 to 20 ml/min, producing twice the efficiency of ordinary packed columns.

No modifications required

SERIES 3000-3 HI-EFF (3 ft.) columns can be used in conventional gas chromatographs without any modifications — no make-up gas, special pressure regulators, etc., are required. A carrier gas flow of 30 ml/min is readily obtained with a 60 psig pressure regulator or with standard flow controllers.

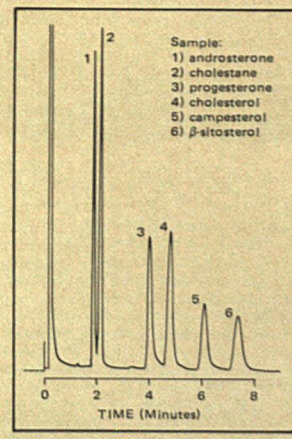

Separation of a mixture of free steroids on a 3 ft. OV-17 SERIES 3000-3 HI-EFF column.

Immediate availability

SERIES 3000-3 HI-EFF (3 ft.) columns are made of 3 ft. x 2 mm ID x ¼" OD glass and are presently available with the following four packings:

3% OV-101 on GAS CHROM Q
1.5% OV-17 on GAS CHROM Q
3% OV-210 on GAS CHROM Q
15% SILAR-10C on GAS CHROM R

Column configurations designed to fit a number of standard commercial gas chromatographs are available from stock.

Configurations to fit other commercial gas chromatographs are available on a custom-made basis with 2-week delivery.

Please write for more information to:

Applied Science Division
(formerly Applied Science Laboratories, Inc.)
Milton Roy Company Laboratory Group
P.O. Box 440, State College, Pennsylvania 16801 Phone 814-238-2406

CIRCLE 2 ON READER SERVICE CARD

Letters

Typographical Error

Sir: A reader has called my attention to an unfortunate typographical error in my April 1979 ANALYTICAL APPROACH article on the JFK Assassination (pages 484 A–493 A). The error occurs in the second column of page 492 A, in lines 8–10. In my typed manuscript, the wording is correct, but a portion of the parenthetical expression was lost in the typesetting, leading to an erroneous statement.

Whereas the published article states ". . .(Q4,5 being fragments recovered from two different areas in the Dallas limousine). . . ," *it should read:* ". . .(Q4,5 being fragments recovered from President Kennedy's brain, and Q2 and Q14 being fragments recovered from two different areas in the Dallas limousine). . . ."

Vincent P. Guinn
Department of Chemistry
University of California
Irvine, Calif. 92717

Any Volunteers for Niobium Analysis?

Sir: The Canadian Certified Reference Materials Project (CCRMP) is currently certifying a pyrochlore ore from Oka, Quebec, encoded OKA-1, at ~0.5% Nb. The usual practice of the CCRMP is to request a minimum of 20 laboratories to participate on a voluntary basis in a round-robin certification program for the chosen element(s) in the candidate material. The lack of laboratories experienced in niobium analysis, however, requires a significant departure from this practice, and it is planned to certify OKA-1 for niobium with the participation of considerably fewer but experienced laboratories.

Anyone interested in participating in this round-robin certification should contact the writer for further information.

Henry F. Steger
Coordinator, CCRMP
555 Booth St.
Ottawa, Ont. K1A 0G1
Canada

The Varian Cary 210/219 UV-Vis Spectrophotometers let you go from basic to ultrasophisticated...

...without ever leaving the medium price range!

Both Models 210 and 219 have been bred for the modestly funded laboratory that's unwilling to compromise on high performance and simplicity in operation.

But here's the best part: for only a little more than the single-purpose "budget" UV-Vis spectrophotometers, you get the 210/219's building-block-like expandability. You can start out with just enough UV-Vis spectrophotometer to handle immediate needs, then later "build on" inexpensively to venture into additional techniques as your analytical requirements grow.

For example, you can add a Routine Sampling System, and the touch of a button cools or heats 500 microliters of sample to achieve one of five temperatures within 0.1°C in less than fifteen seconds. Or, as a significant operating convenience, you can add the Wavelength Programmer, which automatically provides repetitive scanning at any of a number of chosen wavelengths. The Temperature Readout expands the 210/219 into thermodynamic or kinetic studies, when photometric measurements are temperature-dependent. Add the Gel Scanner Accessory for automatic scanning of gel matrices from electrophoretic separations or sheet film. For quantitating kinetic data or for qualitative analysis of spectral detail, let the Derivative/Log A Accessory give you first- and second-derivative spectra. You can add the microprocessor-based Smart Printer for a reliable source of neatly organized hard-copy data—complete with sample or cell number, absorbance versus wavelength, or absorbance versus time.

The list goes on. You can make either Varian Cary Model 210 or 219 as sophisticated as you wish, as versatile as you wish—whenever you are ready. And the 210/219 will still be in the medium price range.

Get all the facts by circling Reader Service No. 218. Better yet, circle 219 to have a Varian Cary representative tell you in person.

varian

For immediate assistance contact: 611 Hansen Way, Palo Alto, CA 94303 • Florham Park, NJ (201) 822-3700 • Park Ridge, IL (312) 825-7772 Houston, TX (713) 783-1800 • Los Altos, CA (415) 968-8141. In Europe: Steinhauserstrasse, CH-6300 Zug, Switzerland.

For gas chromatography you

For price/performance, versatility and reliability you can't beat the Varian 3700 series. In addition, every 3700 comes with full service and applications support to assure your success.

can't beat the Varian 3700 series

The Varian 3700 series is a family of powerful gas chromatographs that puts the emphasis on performance. On chromatography. On giving you the greatest capability to handle your specific application plus unmatched flexibility to meet changing needs.

You can choose the right gas chromatograph.

The 3700 is modular so you can easily choose a chromatograph that is exactly right for your laboratory. All components —injectors, detectors, temperature programmers, flow controllers and automation systems—are upgradeable and interchangeable. You can begin with a basic dual column unit and add capability as you need it. Or, you can start right now with the world's most powerful, versatile and fully automatic GC system. And the 3700 continues to grow so you can always have the newest and best gas chromatograph.

You have better control of the analysis.

The 3700 controls, with ESP monitor and self-diagnostic display, give you more clear information about operating parameters and better control of injectors, column oven, detectors and flows. You don't have to interrogate the system and wait for a printout. You always know what is going on so you can take timely action.

Large dual-column oven makes it easier to do more.

It gives you more room to install columns side by side. Greater freedom to use any columns your application demands: packed or capillary, single or multiple, with column switching and valving inside the oven.

You can use the best detector for your application.

TCD, FID, ECD, FPD, TSD and multi-detector models are offered. Each of these new detectors is designed to provide excellent performance for its range of applications. See Figures 1, 2, and 3. Universal ionization detector bases let you interchange FID, ECD, FPD, and TSD detectors yourself in minutes.

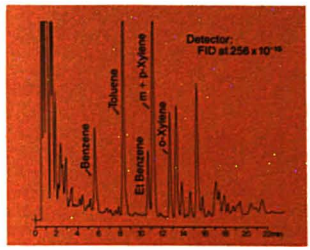

Figure 1. Benzene in Working Environment. The 3700 is widely used in industrial hygiene for detection and quantitation of solvents in the working environment.

Figure 2. Haloforms in Drinking Water. Analysis of drinking water injected directly onto a porous polymer column. Trihaloforms at ppb levels can be detected with this technique.

Figure 3. Volatile Nitrosamines. The 3700 equipped with a TSD, which is very selective for nitrogen, is excellent for screening food and cosmetics products for nitrosamines.

You can choose the best injection technique for your sample.

The versatile 3700 injector system permits you to choose: (1) heated or unheated true on-column injection right into the column packing, (2) heated, flash-vaporization with replaceable glass inserts, (3) two all glass capillary injectors with a choice of modes, or (4) valve injection using gas and liquid sampling valves.

You can use all the speed and power of capillary GC.

There are two high resolution, easy-to-use capillary systems to choose from. The new low cost system makes the power of capillary available to everyone. In both systems columns can be installed in minutes without tedious end straightening. A new capillary effluent splitter lets you detect your capillary separation with any two different ionization detectors. See Figure 4.

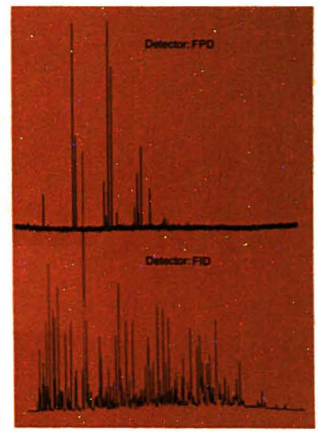

Figure 4. Coal Hydrogenation Product. In the analysis of very complex samples such as this coal hydrogenation product the 3700's capillary system gives high resolution of sample components. The capillary effluent splitter permits detection of the sulfur compounds with the FPD and the organics with FID.

Proven, powerful automation..

For total automation Model 3700 Gas Chromatograph combines with the proven Model 8000 AutoSampler™ and the powerful CDS-111 Chromatography Data System. These components can be purchased and used separately, or they can be combined in many different configurations to meet individual requirements. Result, you can choose the automation you want and you don't have to buy anything that you don't need.

Let us give you detailed information about an unbeatable 3700 system that will do great gas chromatography for you. **Circle Reader Service Numbers: 244** 3700 Series Gas Chromatographs, **245** CDS-111 Chromatography Data System, **246** Model 8000 AutoSampler, **247** Model 3711 Automatic Gas Chromatographs, **248** Have a representative call.

varian

611 Hansen Way, Palo Alto, CA 94303 • Florham Park NJ (201) 822-3700 • Park Ridge, IL (312) 825-7772 • Houston, TX (713) 783-1800 • Los Altos, CA (415) 968-8141

Here's why analytical chemists choose the

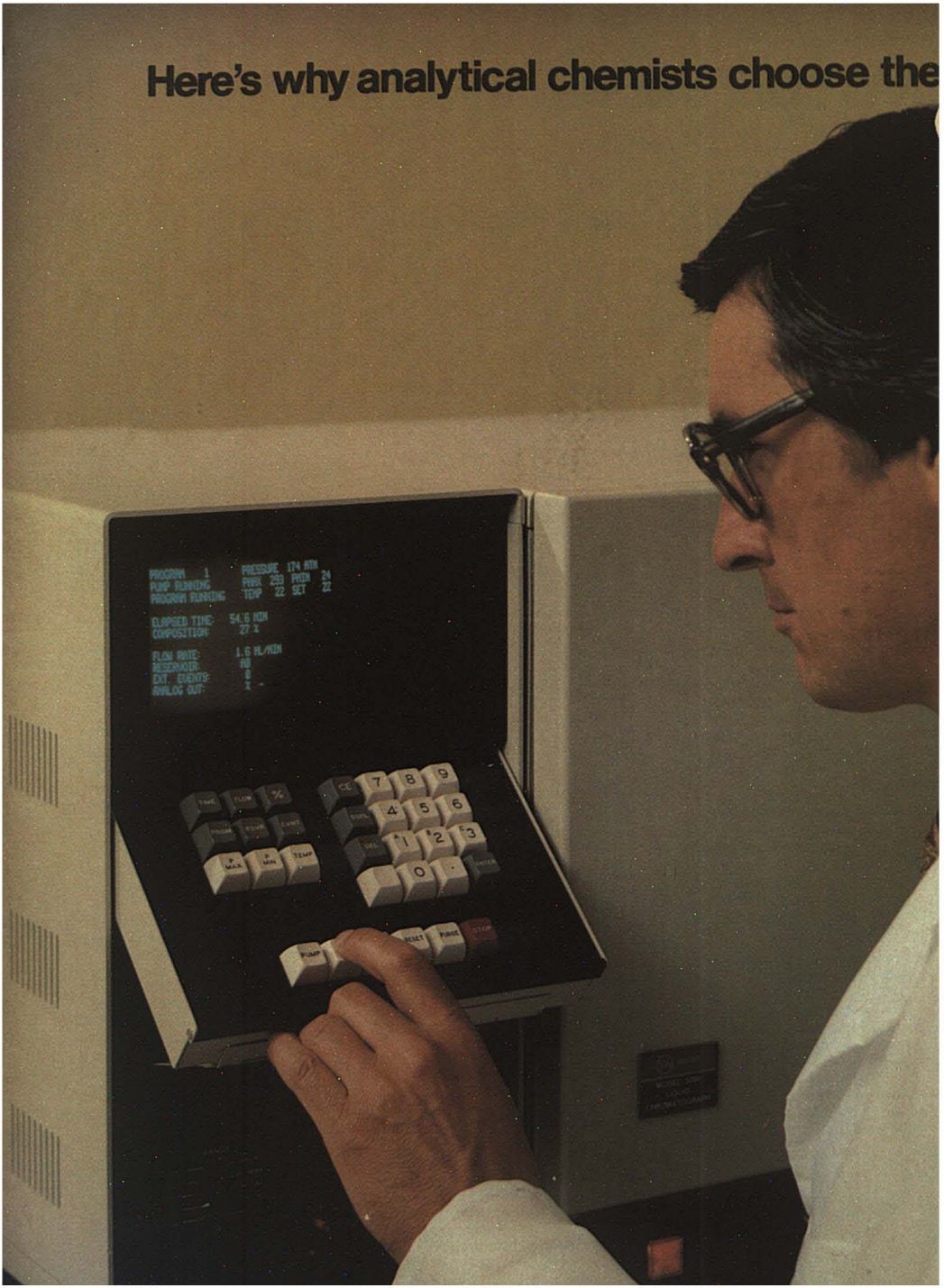

ıew Varian Model 5000 Liquid Chromatograph

Analytical chemists choose the new Varian Model 5000 liquid chromatograph for all manner of applications ranging from pesticides to petrochemicals to pills to PTH amino acids. Here are some of the reasons why.

The 5000 is easy to use. Separations such as those shown at right are easier to do on the 5000 than on any other liquid chromatograph.

The interactive CRT and simple keyboard make program building so easy anyone can do it. The CRT guides you and prompts you and it continuously displays *all* instrument conditions so you always know what is happening in your analysis.

You get outstanding performance. Flow rates and gradient profiles are microcomputer controlled for accuracy and reproducibility.

You can depend on it. The 5000's proprietary single-piston pump is designed to provide a new high level of LC reliability. Inlet check valve problems are eliminated by a new inlet valve design that opens and closes by positive mechanical action.

It's modular so you can choose a 5000 configuration that is right for your application. For example, the 5000 combines with Varian UV, fluorescence, refractive index, and variable wavelength detectors. You can use any LC column and you can select whatever injection system you need from manual to fully automatic sampling. For total automation you can add the CDS-111L Chromatography Data System.

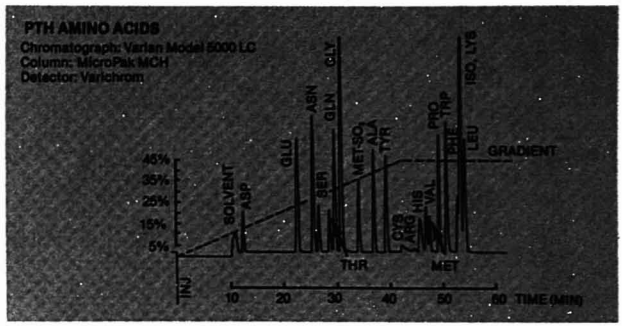

Twenty PTH amino acids can be separated in a single gradient run on the Varian Model 5000 Liquid Chromatograph. For more information circle ***Reader Service Number 235.***

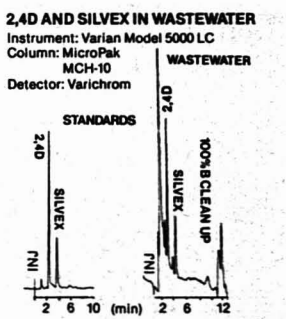

The method used in this separation provides a fast and reproducible analysis for monitoring 2,4D and Silvex in wastewaters. For more information circle ***Reader Service Number 236.***

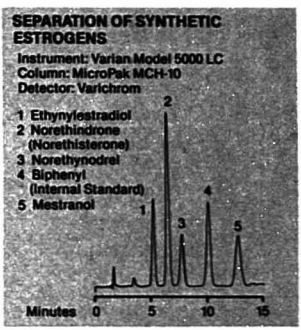

This separation of oral contraceptives demonstrates the use of Model 5000 for tablet assay and content uniformity. For more information circle ***Reader Service Number 237.***

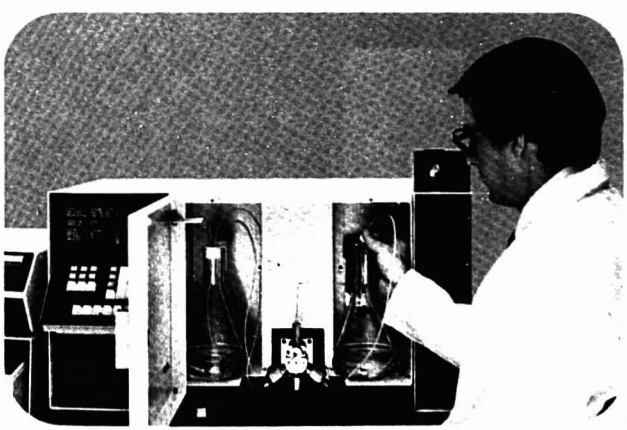

More and more chemists are choosing the new Varian Model 5000 liquid chromatograph because it provides the excellent performance they require. Also, the 5000 is so easy to use it makes difficult separations seem simple.

The price is right. There are five basic models in the 5000 Series: from simple isocratic to completely automatic gradient systems. Each is designed to offer unbeatable price/performance, to provide a new level of LC capability at affordable system prices lower than most LC components.

For full details on a 5000 that may be exactly right for you, circle **Reader Service Number 238.**

To have a Varian representative contact you, circle **Reader Service Number 239.**

varian

For immediate assistance contact:
611 Hansen Way, Palo Alto, CA 94303 • Florham Park, NJ (201) 822-3700 • Park Ridge, IL (312) 825-7772 • Houston, TX (713) 783-1800 • Los Altos, CA (415) 968-8141
In Europe: Steinhauserstrasse, CH-6300 Zug, Switzerland.

Simultaneous or Sequential Determination of the Elements at All Concentration Levels– the Renaissance of an Old Approach

Velmer A. Fassel

Ames Laboratory—U.S. Department of Energy and
Department of Chemistry
Iowa State University
Ames, Iowa 50011

An award acceptance address provides the award recipient with a timely opportunity to contemplate, to predict, and to offer personal commentary on the nature and direction of the science in which he has been involved. In the remarks that follow I shall avail myself of this opportunity. I shall mostly proceed in a serious manner but will occasionally punctuate my remarks with lighthearted commentary and historical reminiscences that are responsive to several provocative questions posed later in this address.

On the occasion of this award symposium, I can boast enthusiastically about the fields of analytical chemistry and spectroscopy. As noted in recent editorial commentary in this JOURNAL (*1, 2*), the strength and stature of these disiplines, both in academia and in industry, have climbed steadily during the past decade. Those of us who are now active analytical chemists or spectroscopists should therefore take pride in the contributions of chemical analysts in years past, but with the full recognition that leaders in these fields have often expressed concern, or chided their colleagues, or were critical of developing trends. In this context, it is appropriate to take a backward journey to 1933 when G. E. F. Lundell published a perceptive article that should be required reading for anyone striving to be identified as an analytical chemist.

Velmer Fassel (right) receives the ACS Award in Analytical Chemistry (Fisher Award) from Gardner Stacy, President of the Society, at the ACS/CSJ Chemical Congress which was held in Honolulu, Hawaii, April 1–6, 1979.

This REPORT is based on Dr. Fassel's Award Address

0003-2700/79/A351-1290$01.00/0

This paper entitled "The Chemical Analysis of Things as They Are" (*3*), contained a number of classic sentences, including the following: "The determinator's salvation lies in the development of selective methods of analysis, and his final resting place will be a heaven in which he has a shelf containing 92 reagents, one for each element, where No. 13 is the infallible specific for Al, No. 26 the sure shot for Fe, No. 39 the unfailing relief for Y, and so on to U."

The heavenly hopes expressed by Lundell have never been realized. Even today, the most optimistic analytical chemist sees little hope of ever reaching the utopian state of specific reagents for each element, especially for those elements that have nearly identical (the lanthanides) or very similar chemical properties, e.g., Hf and Zr. The thrust of Lundell's statement was to chide some of his analytical chemistry contemporaries for not giving adequate consideration to an important requirement of an acceptable analytical method, namely, sufficient selectivity so that it would be useful for the "chemical analysis of things as they are." During Lundell's professional career—and occasionally even today—new analytical methodologies are proposed when it is quite obvious that they suffer from interferences to such a degree that they are not useful for the analysis of "things as they are." Lundell aptly commented:

> *There is no dearth of methods that are entirely satisfactory for the determination of elements when they occur alone. The rub comes in because elements never occur alone, for nature and man frown on celibacy. Methods of determination must therefore be judged by their 'selectivity.' It is in this respect that most methods are weak and improvements must come . . . .*

During the 46 years that have elapsed since Lundell's paper was published, these improvements have indeed materialized, and they have followed many different pathways. The remainder of my address will be devoted to a historical walk along one of these pathways.

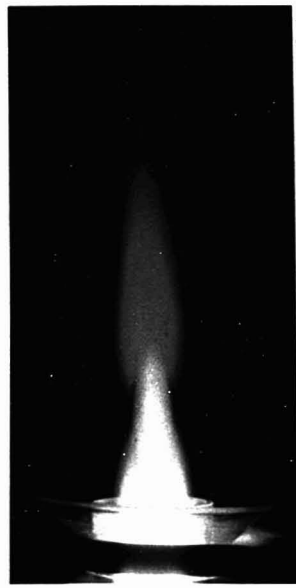

Iowa State University Photo Service

Inductively Coupled Plasma—Atomic Emission Spectroscopy

The Early Years. For the past 17 years my associates and I have devoted a fraction of our efforts to the development of the basic science, the investigative methods and the hardware for an analytical approach that would eventually provide the capability of determining the chemical elements selectively, at all concentration levels, i.e., major, minor, and trace constituents, simultaneously if so desired, or in a rapid sequential manner, with a single analytical technique, and with accuracy and precision. A new analytical approach, usually identified as inductively coupled plasma—atomic emission spectroscopy (ICP-AES) has emerged from these studies. I use the term "new analytical approach" advisedly, because the AES portion of this technique is certainly not new; quantitative determinations have been made via AES for at least 40 years. The use of ICP's as vaporization-atomization-excitation cells is not new either. The first analytical studies of ICP's were launched independently 17 years ago, by Stanley Greenfield and associates at Albright and Wilson, Ltd., Oldbury, England, and by our research group at the Ames Laboratory, Iowa State University. The exciting possibilities offered by ICP's as vaporization-atomization-excitation-ionization (VAEI) cells for analytical atomic spectroscopy were first communicated ~15 years ago (*4, 5*), and a decade has passed since a landmark paper, as described by Barnes (*6*), was published (*7*). The analytical community, however, including academia, almost completely ignored these and subsequent papers until approximately five years ago. The surprising lack of interest in the ICP-AES approach to elemental determinations is reminiscent of Sir Allen Walsh's experience (*8*) following the publication of the pioneering papers in flame atomic absorption spectroscopy (AAS). His experience and ours are, I believe, excellent examples of how tacit acceptance of methodologies as they are, and perhaps a liberal sprinkling of mental paralysis, can influence the timely acceptance of new ideas. Because ICP-AES was originally conceived as an alternative approach for the determination of minor and trace constituents, it had to vie for attention at a time when AAS was experiencing its phenomenal growth and wide acceptance. The fact that AAS provided a relatively simple, highly specific way for elemental determination at the minor or trace concentration level contributed so much to its popularity that the use of alternative techniques for performing the same tasks suffered precipitous declines. The technique that experienced the greatest decline in usage was atomic emission spectroscopy, which during the period from the mid-1930's to the early 1960's was often, if not usually, the method of choice for multielement determinations at the minor or trace concentration level. Although spark-arc excitation AES retained its important role for compositional control in the metals industries, there is no doubt that its use as a gen-

If you can't observe solids as readily as liquids on your superconducting FT NMR...

...you just don't have an XL-200!

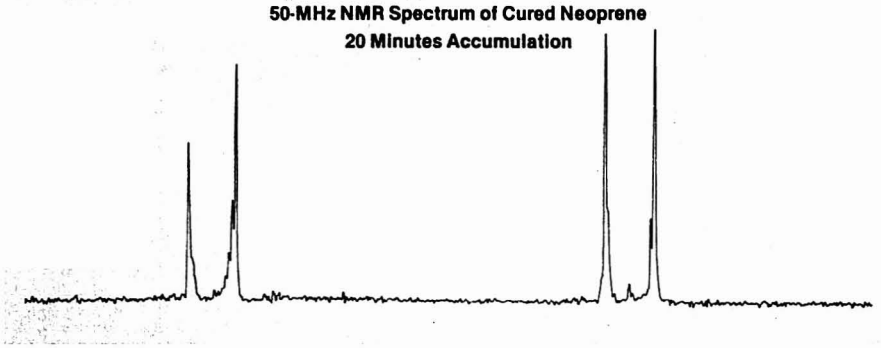

^{13}C spectrum of cured neoprene with carbon black in a Kel F rotor using high power gated decoupling (400 transients at 3 second intervals). The resolution has been enhanced by a Lorentzian to Gaussian transformation to bring out the fine structure. The width of the plot is 10 kHz. *Sample courtesy of E. I. Du Pont de Nemours and Company.*

With the new ^{13}C solid-state accessory for the XL-200, you can spin solid or powdered samples at the magic angle, increase sensitivity using cross-polarization, and achieve efficient line narrowing with strong dipolar decoupling. Yet operation is surprisingly simple! You can introduce and eject the rotor pneumatically without disturbing the probe or the spinning axis adjustment. You monitor the spin rate on the spectrometer's built-in tachometer, just as in liquid-sample experiments. Front panel controls let you adjust optimal cross-polarization and decoupling conditions independently and conveniently.

There are other unique aspects to the XL-200 superconducting FT NMR Spectrometer, such as the data handling and spectrometer control system: a 13-bit ADC, which accommodates stronger signals on each transient; a standard 32K CPU, independent of the acquisition processor and programmed in PASCAL, a high-level, structured language; a built-in interactive 5M-word disk with dual platters; a large, flicker-free raster scan display.

The software, too, is exceptionally sophisticated. It permits multitasking (simultaneous acquisition, processing, printing, etc.) and queuing (automatic sequential execution of requested tasks) on the same or on different NMR experiments. You can also array parameters (up to three variables, including temperature) within a given experiment; generate your own convenient macro-commands; create your own special or general-purpose pulse sequences in a simple, English-like code; even do your own computer programming in PASCAL.

Then there's the matter of the XL-200's broadband accessory which, with only a single probe for liquid samples, enables you to observe a host of nuclei (including ^{13}C) between 20 and 81 MHz. And there's the remarkable low-loss dewar system, which operates over three months on only 25 liters of liquid helium.

The XL-200 is in a class by itself—with a price tag and an operating economy that belie its advanced design.

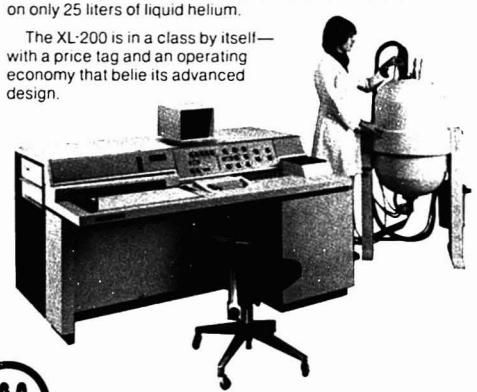

varian

For immediate assistance contact: 611 Hansen Way, Palo Alto, CA 94303 • Florham Park, NJ (201) 822-3700 • Park Ridge, IL (312) 825-7772
Houston, TX (713) 783-1800 • Los Altos, CA (415) 968-8141. In Europe: Steinhauserstrasse, CH-6300 Zug, Switzerland.

CIRCLE 222 ON READER SERVICE CARD

eral analytical tool experienced a sharp decline from the mid-1960's to the early 1970's, whereas AAS was ascending its steep popularity curve. The interest of analytical chemists or spectroscopists in AES was further undermined when some AAS enthusiasts directed intellectual darts at the principle of observing free atoms in emission rather than in absorption. These darts consisted of undocumented, and usually theoretically unsound, claims regarding the alleged superiority of observing free atoms in absorption rather than in emission. Thus, the claim that AAS should exhibit far superior powers of detection because the bulk of the free atoms in atomization cells were in the ground state in contrast to the far smaller number density in excited states, did not rest on sound theoretical bases. Neither did the claim that because the fraction of atoms in excited states was very small, the observation of free atoms in emission was subject to serious "excitation interferences" arising from collisional deactivation, preferential excitation, or energy transfer processes in general. Other assertions suggested that, in spite of recorded successes in the past, spectral line interferences were so inseparable, and temperature changes in the excitation cells so uncontrollable, that the observation of free atoms in emission for analytical purposes was surely destined for failure. These assertions were often read in amused astonishment by myself and others. Unfortunately, they were repeated often enough in the literature and advertising circulars to lead to their acceptance as fact by many analysts. The period from 1965 to 1970 saw the publication of a sufficient number of these unwise claims to fill part of an issue of the fictional journal *Acta Retracta*. Regrettably—but also fortunately—that journal has never become a reality. I use the term "fortunately" because emanations from my pen in other contexts would have been acceptable candidates for publication in the journal!

The publication of the scientific misdemeanors referred to above subsided rather abruptly after C. Th. J. Alkemade's perceptive paper entitled "Science vs. Fiction in Atomic Absorption Spectroscopy" appeared in 1968 (*9*). By that time the reputation of AES as a useful general analytical tool was sufficiently tarnished that its attractiveness as a research field in academia and as a commercial venture by instrument makers continued to decline. But decline in usage does not imply total stagnation in scientific development. Although basic research in analytical AES was confined to a limited number of academic, government, and industrial laboratories, significant advances emerged. In 1974 the revival of AES as a general analytical tool was presaged in a number of ways, for example, by provocative titles in several scientific communications. Thus, Boumans (*10*) used the title "Multielement Analysis by Optical Emission Spectroscopy—Rise and Fall of an Empire?" and I used the title "Optical Emission Spectroscopy: Stagnant or Pregnant?" (*11*). (I am indebted to Sir Allen Walsh who first used the descriptive "Stagnant or Pregnant" phraseology in his paper entitled "Atomic Absorption Spectroscopy—Stagnant or Pregnant?" (*8*).) The questions posed in these titles focused on the future role that AES would play in the elemental compositional analysis of materials. Both Boumans and I projected that AES would soon regain its appeal and again become a mainstay analytical technique. And now, five years later, AES is attracting the anticipated attention.

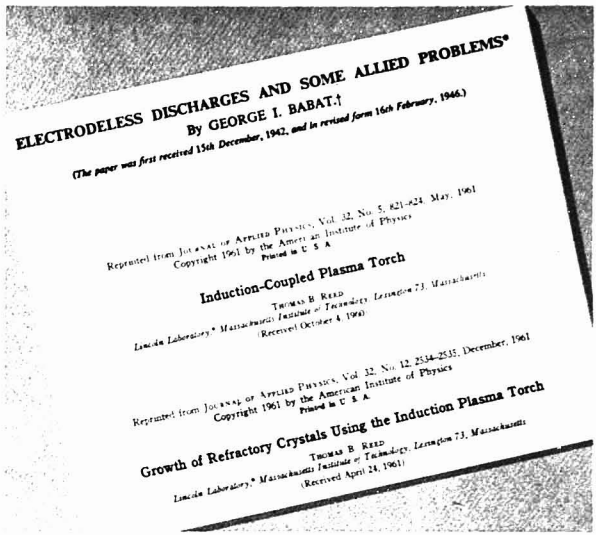
ELECTRODELESS DISCHARGES AND SOME ALLIED PROBLEMS*

By GEORGE I. BABAT.†

(The paper was first received 15th December, 1942, and in revised form 16th February, 1946.)

Reprinted from Journal of Applied Physics, Vol. 32, No. 5, 821–824, May, 1961
Copyright 1961 by the American Institute of Physics
Printed in U. S. A.

Induction-Coupled Plasma Torch

THOMAS B. REED
Lincoln Laboratory,* Massachusetts Institute of Technology, Lexington 73, Massachusetts
(Received October 4, 1960)

Reprinted from Journal of Applied Physics, Vol. 32, No. 12, 2534–2535, December, 1961
Copyright 1961 by the American Institute of Physics
Printed in U. S. A.

Growth of Refractory Crystals Using the Induction Plasma Torch

THOMAS B. REED
Lincoln Laboratory,* Massachusetts Institute of Technology, Lexington 73, Massachusetts
(Received April 24, 1961)

Figure 1. Photograph of title and author by-lines of several pioneer papers on inductively-coupled plasmas

What has brought this change? Three factors have been primarily responsible. First, analysts are increasingly faced with the necessity of determining many elements, in more and more samples, at all concentration levels, and sometimes on a real-time basis. The one-element-at-a-time limitation of classical chemical or AAS procedures, their limited powers of detection for some elements, their limited dynamic range, and their susceptibility to interelement interferences, are causing these techniques to lose some of their attractiveness for many analytical tasks. I chose to use the words "some of their attractiveness" because AAS in particular is still, and probably always will be, a very attractive way for performing elemental determinations.

The second factor is the increasing recognition among analysts that AES possesses some natural advantages for the simultaneous or rapid sequential determination of the elements. This adaptability rests on the comparatively simply way the characteristic line emission can be excited and observed.

The third factor, perhaps the most important, can be attributed to the emergence of a new "excitation" source, i.e., the component that is expected to vaporize the sample, dissociate the vapor, and excite and/or ionize the free atoms that are formed. For many years, perceptive analytical spectroscopists recognized that classical flames, arc, and spark discharges were not performing these tasks as well as they should, especially for the determination of elemental constituents in liquid samples. Many of the negative attitudes that analysts had generated vis-a-vis AES could in fact be traced to these deficiencies in classical atomization-excitation cells. The new excitation source referred to above is an electrodeless, argon-supported plasma, operated at atmospheric pressure and sustained by inductive coupling to high frequency electromagnetic fields. This plasma

possesses some unique physical properties that make it a remarkable VAEI cell for elemental analysis.

Before detailing the properties of these plasmas, it is appropriate to recognize the contributions of some of the pioneering investigators of ICP's. A recital of the historical development of ICP's requires a journey backwards in the corridors of time to 1942 when G. Babat published his first papers on the properties of ICP's (*12*). Babat continued his investigations at the "Svetlana" plant in Leningrad even while that city was experiencing the severe blockade during the early years of World War II. Babat's studies eventually ceased when the entire power system of the city failed and some of his colleagues perished during the hostilities (*13*). In spite of these adversities, Babat submitted an English manuscript to the *J. Inst. Electr. Eng.* in 1942 (*14*). As shown by the photograph of the title and byline of the published paper in Figure 1, four years elapsed before the revision was received. The importance of Babat's paper was that he apparently was the first individual to sustain electrodeless ICP's at atmospheric pressure. Approximately 20 years later, T. B. Reed described (see photo of bylines in Figure 1) some exceptionally effective ways of forming and stabilizing Ar supported inductively coupled plasmas (*15, 16*). Normally neither the *J. Appl. Physics* nor these papers would attract the attention of an analytical chemist. Because I majored in physics in undergraduate college, I did then—and still do—scan the physics journals. When I read Reed's papers, I recognized that these plasmas offered several unusually attractive possibilities as VAEI cells for analytical atomic spectroscopy. These attractive possibilities were, first, their high temperatures, which should make them effective VAEI cells; second, because the plasmas are sustained by pure Ar, the free atom lifetimes should be longer than in other atomization cells used for that purpose; and finally, because the discharges are electrodeless, there should be no contamination from electrode materials. The same thought processes must have gone through the mind of Stanley Greenfield at Albright and Wilson, Ltd., Oldbury, England. As best as we can ascertain, we independently initiated analytical studies on these plasmas in early 1962 within a few weeks of each other. It was not until late 1964 and early 1965 that we became aware of each others' activities.

Our initial goals were to establish whether these plasmas could be sustained under the low power conditions that would be comfortable for analytical chemists, while sample material

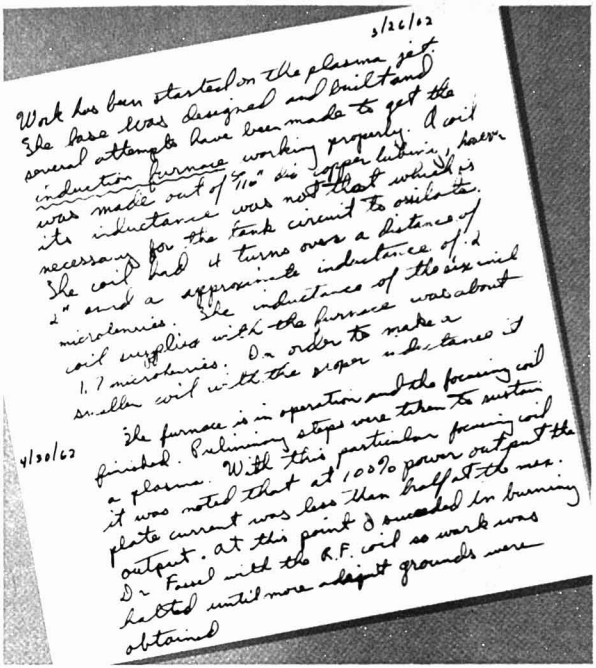

Figure 2. Photograph of research notebook entries

in the form of liquid aerosols was injected. Eventually both goals were achieved, but not without painful incidents. To place that statement in proper perspective, Figure 2 shows a photograph of two entries from the research notebook of the first graduate student assigned to this project. These two entries convey the information that our ICP investigations started on March 26, 1962, and that on April 30, 1962, this student acknowledged that he "succeeded in burning Dr. Fassel with the RF coil so work was halted until more adequate grounds were obtained." This incident provided us with an excellent example of the vagaries of high frequency fields, if not properly contained or grounded. At that time we were employing a relatively high-powered generator (15 KW) to evaluate the performance of various torch configurations. During these experiments an optical bench carriage was located on a laminated, maple-wood table, near the induction coil, but totally isolated electrically. When I reached toward the carriage, I was "zapped" by a miniature lightning bolt, resulting in considerable reflex action on my part and a small crater in my thumb. As I contemplated my position on the floor, I was heard to mutter that perhaps I should consider abandoning laboratory research! Subsequently, when this graduate student decided to abandon analytical chemistry (to become a physical chemist instead!), I assigned this project to R. Wendt.

Our initial evaluations of the analytical performance of these plasmas were not encouraging, especially in the context of the powers of detection that we measured. Because our measured detection limits were not competitive with the values published for AAS, which was then entering its period of phenomenal growth and acceptance, we were not inspired to publish our results. The inspiration to do so came just before the end of 1964 when we became aware of the publication of S. Greenfield's first paper in the November 1964 issue of the *Analyst* (*4*). Greenfield et al did not report detection limits as such but simply concentration levels at which they performed useful analyses. When we observed that our measured detection limits were lower, by as much as an order of magnitude or two, than those concentrations reported by Greenfield, et al, we cast our results into a brief communication which was submitted to ANALYTICAL CHEMISTRY in Febru-

ary of 1965. In due time we received a most unusual review of our paper; it was written in verse! Excerpts from this review follow:

A Review in Verse

Microwave sources are hardly new
Mavrodineanu and Boiteux cite quite a few
The important question: Is this one new?
Yes there are differences but they are relatively small
And I wonder if they justify publication at all . . . .
I hope that Editor Fassel will agree*
This manuscript has only a little novelty
But the sad and bitter fact is
We know very little in practice
Of what these discharges actually do
Solid data are exceedingly few
And far between; a detailed study could
Reveal a lot, and it would
Be a finer addition to the literature
Than this small note, I feel sure

(* I was co-editor of *Spectrochimica Acta* at the time.)

In a lighthearted manner, the reviewer implied that we were describing a microwave powered plasma, which we weren't, and that the plasma was capacitively coupled to the coil, which it wasn't. We noted these facts in our response to the Editor and further commented on the large difference in the physical properties of the ICP and the other plasmas mentioned by the reviewer. As shown by Figure 3, the paper was published in June 1965 (*5*). At the conclusion of our brief communication, we stated as follows: "Our observations indicate this combination of plasma and aerosol generator is a practical and versatile source for analytical spectroscopy." Three years later this rather conservative conclusion was questioned by two investigators, who concluded that "except for a few refractory elements, the plasma torch does not appear to be a suitable replacement for a chemical flame." Another candidate for *Acta Retracta?*

Progressive advancements at our and Greenfield's laboratory in reducing the radio frequency interference with the recording electronics; improving impedance matching between the high-frequency generator and the plasma; improving forward power regulation; refining techniques for generating aerosols of solutions; and improving the efficiency of injection of aerosols into properly shaped plasmas resulted in vast improvements in the analytical performance of these plasmas. Many of these improvements were discussed in the paper (*7*) whose publication by-line is shown in Figure 3. At the end of this paper we again closed with a rather conservative conclusion, as follows: ". . . the superior powers of detection and promising freedom from chemical interferences exhibited by the plasma . . . suggest that they offer distinct advantages over combustion flames for the emission spectrometric determination of trace elements in solution." It is perhaps not surprising that this conclusion was disputed by the coauthors of a review published three years later, who concluded "that the inductive plasmas are no better than atomic absorption and flame emission spectrometry of most elements with a C_2H_2/N_2O flame." Surely another entry for *Acta Retracta!*

Physical and Spectroscopic Properties of ICP's. Because the theoretical and practical aspects of the formation, thermal isolation, and stabilization of these plasmas have been adequately discussed in recent reviews (*17*), I shall not cover them in this presentation. Rather I will focus attention on those physical and spectroscopic properties that contribute to the remarkable performance of these plasmas as VAEI cells for analytical emission spectroscopy. I shall examine these properties in terms of the fate of sample aerosols or gases upon their injection into the plasma. The various physical and chemical forms of the aerosols and gases that have been successfully injected and analyzed are summarized in the diagram in Figure 4. The liquid aqueous, organic or metal aerosols are generated by pneumatic, ultrasonic, or electrical nebulizers, the various forms of which have been discussed in recent reviews (*18–20*). As an aside, the diagram in Figure 4 communicates how simply and directly virtually all sample types can be analyzed by ICP-AES.

The highly schematic representation of the ICP sketched in Figure 5 shows the now familiar annular, "doughnut hole" shape at the base of the plasma. This shape is readily developed through the proper choices of frequency of the current provided by the generator and of the aerosol-carrier flow rate that injects the sample material into the plasma (*7, 21*). The effective puncturing of this toroidal base of the plasma by the aerosol carrier flow assures injection and transport of the sample material into the heart of the plasma. It is the efficiency of this sample introduction process that distinguishes the ICP from other plasmas that have been used as VAEI cells. Upon injection into the plasma the aerosols or gases are heated indirectly by radiation, convection and conduction as they pass through the eddy current "tunnel." Because there is very little interaction of the sample with the eddy current flow that sustains the plasma, changes in sample composition have an unusually small or negligible effect on the properties of the plasma (*18, 22, 23*), a situation that does not prevail in most other VAEI cells.

Temperatures measured above the coil and estimated by extrapolation down into the induction region are

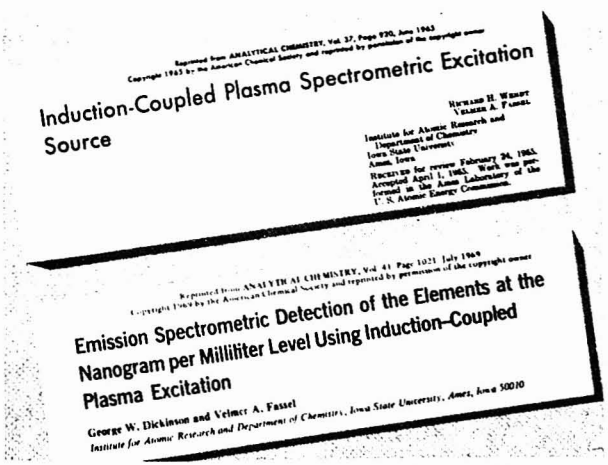
Induction-Coupled Plasma Spectrometric Excitation Source

Emission Spectrometric Detection of the Elements at the Nanogram per Milliliter Level Using Induction-Coupled Plasma Excitation

Figure 3. Photograph of title and author by-lines of several papers published by the author and associates

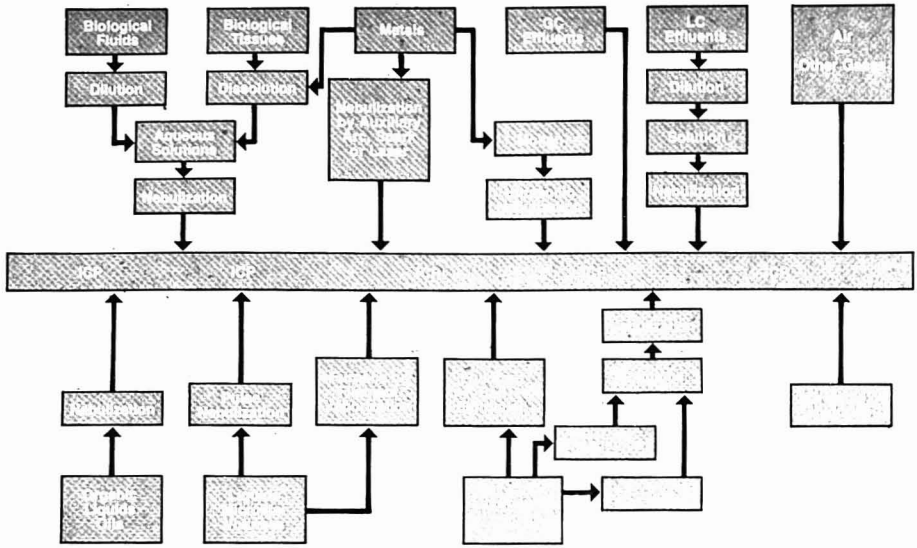

Figure 4. Modes of sample injection into ICP's

shown in Figure 5 (*24, 25*). By the time the sample species reach the observation height of 15 to 20 millimeters above the coil, they have had a residence time of ~2 milliseconds at temperatures ranging from ~8000 to ~5500 K. The residence times and temperatures experienced by the sample are approximately twice those found in nitrous oxide—acetylene flames, the hottest combustion flames commonly used in AAS. The combination of high temperature and relatively long interaction time leads to an unusually high, if not total, degree of atomization of the analyte species, especially for the small aerosol particles resulting from the processes shown in Figure 4. When atomization is essentially complete, dissociation equilibria play a less significant role.

Ionization equilibria, however, may play an important role, especially if the analyte is ionized to a considerable degree in the absence of other easily ionizable elements. Fortunately, under the plasma conditions now generally employed, ionization interference effects are surprisingly small. The search for a satisfying explanation for these unexpected observations has catalyzed extensive experimentation and discussion (*25–30*). The consensus view now is that the suprathermal electron number density in a "pure" Ar plasma is so high that the total is not significantly affected by the addition of easily ionizable elements to the plasma.

The considerations discussed above suggest that interelement effects in the vaporization-atomization-excitation and ionization process should be low or even negligible. There is voluminous documentation that a single analytical calibration curve often suffices for the determination of an analyte in a variety of samples of widely ranging composition. When interelement "effects" are observed they may usually be traced to the fact that the aerosol formation process is affected by large changes in the composition of the sample, or to residual ionization interferences, or to spectral line interferences or background shifts that have occurred and for which proper corrections have not been applied.

The plasma possesses other unique advantages. First, after the free atoms are formed, they flow downstream in a narrow cylindrical radiating channel. The optical aperture or viewing field of conventional spectrometers can be readily filled by this narrow radiating channel. In this way, the radiation emitted by the free atoms or ions is used effectively. Second, at the normal height of observation, the central axial channel containing the relatively high number density of analyte free atoms or ions has a rather uniform temperature profile (*24, 25*). The number density of free atoms in the hot argon sheath surrounding the axial channel is far lower. Under these conditions, the analyte free atoms or ions tend to behave as an optically thin emitting source. If a large range of emission intensities can be accommodated linearly by the measurement system, linear analytical calibration curves covering five orders of magnitude change in concentration can be readily achieved.

Simultaneous or Rapid Sequential Determination of the Elements at Major, Minor, and Trace Concentration Levels Without Changing Experimental Parameters. The analytical performance of these plas-

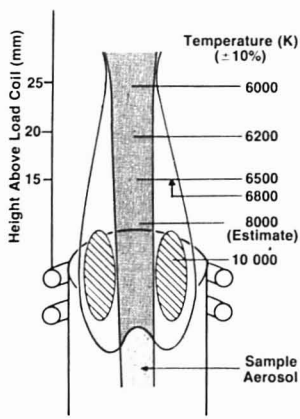

Figure 5. Schematic representation of a typical ICP used in analytical spectroscopy

ULTRASPHERE™ HPLC Columns. NEW! High Efficiency. Super Reproducibility. Extended Column Lifetime.

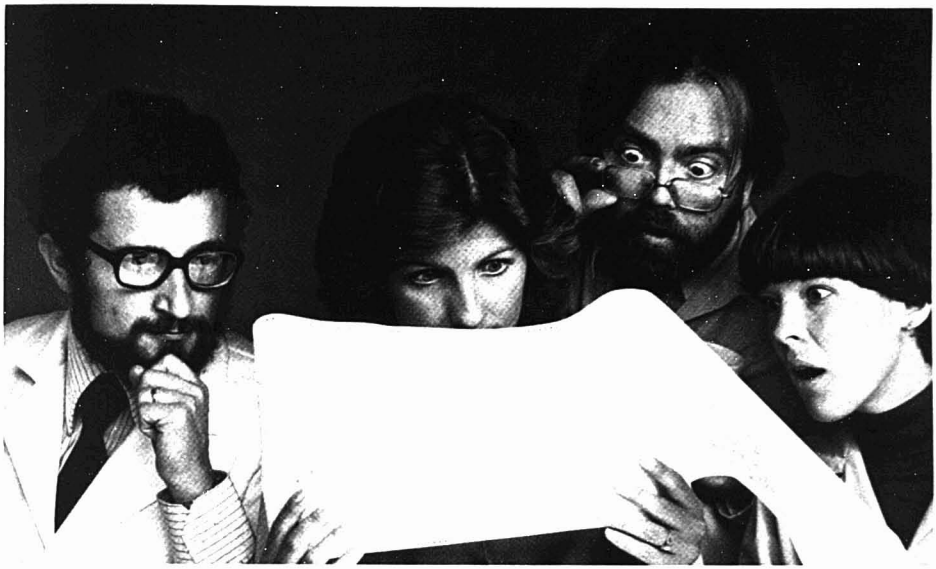

"That's what I call High Performance."

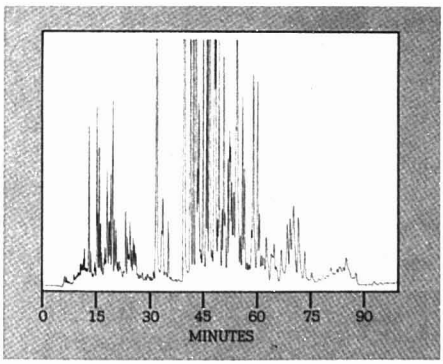

Gasoline Separation with ULTRASPHERE-ODS

New Altex Prepacked HPLC Columns Dramatically Improve Your Liquid Chromatography.

Altex introduces Maximum Coverage packings in ODS and Octyl columns for Reverse Phase LC. And a totally NEW column especially for Ion Pairing.

Densely packed 5μm spherical particles are endcapped for an unprecedented level of column stability. Minimum efficiency of 65,000 plates/meter and peak asymmetry between $0.9 \leq A_s \leq 1.4$.

Call your nearest Altex Dealer, or write to: Altex Scientific, Inc., a subsidiary of Beckman Instruments, Inc., 1780 Fourth Street, Berkeley, CA 94710 (415) 527-5900 Telex: 33-5403

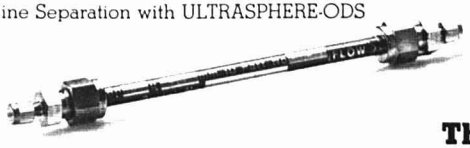

ALTEX

The Smart Components for HPLC

CIRCLE 1 ON READER SERVICE CARD

mas may be greatly affected by the choice of experimental parameters. If the assumption is made that the choice of frequency of the current flowing in the coil, the torch configuration, and the pattern of gas flows assure effective injection of the sample into the axial channel of the plasma, the remaining dominant experimental parameters are: power input into the plasma; Ar carrier-gas flow-rate; and observation height. Although the nominal power of the generators employed for analytical purposes has ranged from 1–15 KW, most investigators have worked in the 1–5 KW range and this trend has been reflected in the commercial units. There has been repeated documentation (*31–33*) that a compromise set of values for the parameters identified above can usually be identified that leads to the high powers of detection, extended linear dynamic range, and freedom of interelement effects characteristic of these plasmas. Thus, given the availability of spectrometers with adequate capabilities, major, minor, and trace constituents can be determined simultaneously or in a rapid sequential manner, without changing any experimental parameters other than the wavelength of observation (*34*). When the plasma is mated to a classical polychromator of the type shown in Figure 6, the chemical elements may be determined simultaneously in a single step. In these instruments, precisely located exit slits isolate the spectral lines of interest from the dispersed spectrum formed by the diffraction grating. Each exit channel has its own photomultiplier detector and electronic integrator. As many as 50 or more channels are provided in commercial instruments, allowing the simultaneous integration and determination of up to that many analyte signals. The technology represented by these polychromators is mature; thousands of these instruments are employed in the metals industries for composition control. In one corporation alone, over 13 million quantitative determinations based on direct spark or arc excitation of metal specimens were completed in 1977, with precision and accuracy comparable or superior to those obtained by classical chemical procedures. Yet, as late as the 1970's, repeated accounts in the published literature have referred to the complexity of these instruments and to problems associated with misalignment and drifting of the individual exit slits. I believe that the authors of these assertions would find a visit to a modern steel or aluminum control laboratory a revealing experience. It is not uncommon for these instruments to be employed for the simultaneous determination of up to 10 or more major and minor constituents, performing analyses at prodigious rates (up to 600/hour on 40 to 50 samples), often under alarming environmental conditions, with relative standard deviations of 0.5 to 1.0 for 24 hours per day. The above remarks are not meant to imply that the exit slits must not be aligned with care. They must, but misalignment and drift, if they do occur, are monitored, and appropriate alignment adjustments are conveniently applied.

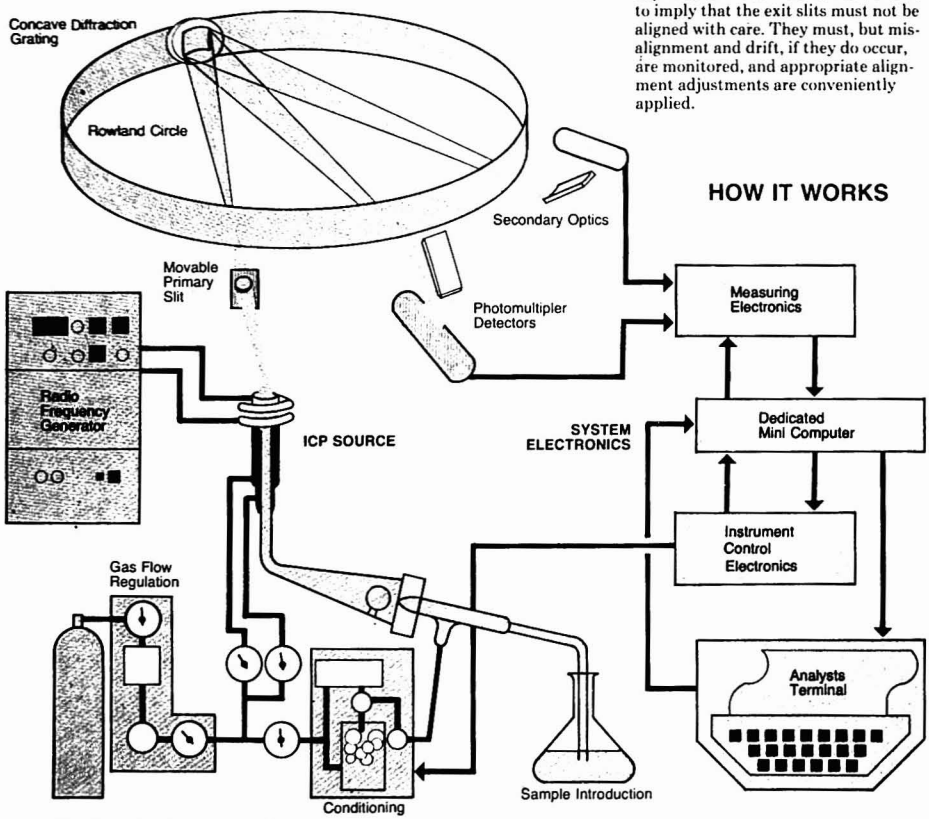

Figure 6. Schematic diagram of an ICP polychromator

Applied Research Laboratories

Presently, polychromators are employed in most ICP-AES systems that are extensively used for the routine, simultaneous determination of the same set of elements in matrices of similar composition. However, their application for the determination of a broader range of elements in samples of widely varying composition is restricted by the fixed array of exit slits employed for isolation of the spectral lines. In principle, scanning monochromators can be used for the sequential determination of most of the elements in the periodic table, and a number of lines may be measured for each element to enhance the reliability of the determinations. However, for multielement determinations, the operations involved in a sequential scan to the spectral lines of interest and in measuring the intensities of the lines relative to the spectral background usually require constant operator attention and lengthen the analysis time considerably as compared to the time required for simultaneous multielement determinations with a polychromator. As a solution to this problem we have recently described (*35*) a programmable scanning monochromator system that eliminates the inefficiencies mentioned above. This instrument, shown in schematic form in Figure 7, possesses the following characteristics and capabilities:

- A computer-controlled scanning monochromator with the ability to slew rapidly and accurately, under program control, from one successive analysis wavelength to another in a selected sequence of analytical wavelengths;
- Automated line search and peak-seeking routine for determination of the peak intensity of selected lines;
- Storage in memory of a selected, ordered list of the most prominent spectral lines for each of the 70 or so elements usually determined by ICP-AES, with prioritization of the selected lines in accordance with powers of detection and freedom from spectral line interferences;
- Preselection of one or more of the stored analyte lines for each element to be determined;
- Preselection of precise wavelengths at which the spectral background intensity measurement is to be made for each analysis line;
- Computer software rearrangement of the selected analysis lines and corresponding background wavelengths in ascending wavelength to facilitate orderly measurements and to minimize the analysis time;
- Video terminal for the visualization of difficult background situations and for the display of analytical calibration curve data. The video terminal also aids the judicious selection of the most useful lines for a particular analytical problem;
- Detection limit routine for monitoring instrument performance. Detection limit measurements that are based on signal to noise considerations provide a convenient and sensitive performance test of the entire system;
- A signal measurement range of 10^6 for exploitation of the wide dynamic range that is characteristic of the ICP.

Computer-controlled monochromator systems that possess some of the features and characteristics discussed above have been described (*36–38*), suggested (*39*), or are commercially available, but none of the versions previously described or marketed have possessed all of the capabilities specified above. For ICP-AES, these instruments present attractive possibilities. Because it is usually neither necessary nor desirable to change experimental parameters in the plasma for the determination of a broad range of elements at concentrations ranging from major constituents to trace levels, it is convenient to program the instrument to start at the low wavelengths and proceed up the scale unattended until the end of the analytical cycle. These simple operations should be contrasted, for example, with the sequence of steps required for sequential multielement determinations by conventional AAS. If a broad range of elements at various concentration levels is to be determined via flame atomization, the analyst is faced with the prior selection of the proper primary source, the nature of the flame and its operating stoichiometry, the height of observation, and the sample dilution appropriate to the concentration range for each element to be determined. If furnace atomization is employed, it is usually necessary to carefully select the best combination of drying, charring, ashing, and atomization temperatures for each element to be determined and for each sample type. Other analytical techniques are similarly burdened with the selection of optimum conditions for multielement determinations. To cite just one more example, the sequential determi-

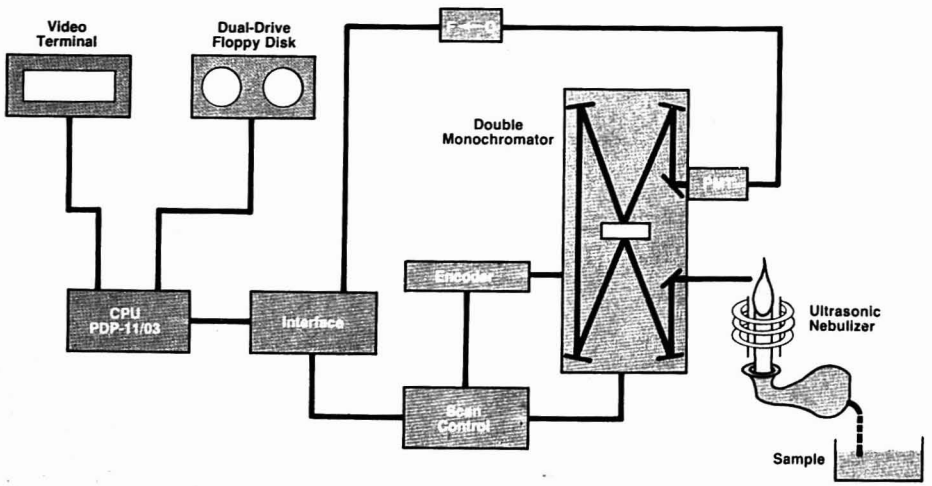

Figure 7. Schematic diagram of a programmable ICP scanning spectrometer

Can a gas chromatograph make your dream come true?

Carlo Erba Strumentazione, leader in capillary column instrumentation, has the right answer.

The Fractovap 4160 Series - the first high resolution dedicated gas chromatograph ensuring discrimination-free quantitative results and absolutely innovative performance breakthroughs in capillary gas chromatography.

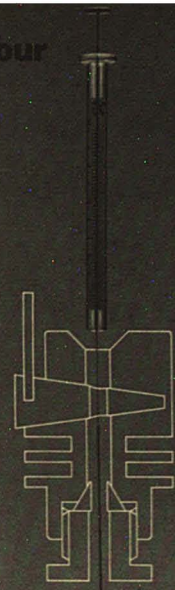

New revolutionary injection system
The Fractovap 4160 Series is the first gas chromatograph introducing a dual capillary dedicated injection system.
It in fact provides the new revolutionary on-column injector, besides the well established split-splitless injector, which definitely avoids any discrimination between low and high boiling point components contained in the same mixture.

Unique variable length temperature adjustable on-colum trapping system
This system allows the concentration effects of the sample components to be controlled. Very useful for volatile compounds and especially for automatic glass capillary head space analysis.

Zero dead volume true all glass system
Nothing but glass capillary column between the injection and detection point. No glass lined tubing configurations which cause dead volumes and active centres responsible for sample decomposition of thermolabile compounds.

New accurate all metal pneumatic system
Accurate and precise gas regulations are ensured by all metal diffusion-proof bleeding-free pressure controllers for the dual circuit of the carrier gas, auxiliary gases and standard make-up gas line. All lines are provided with metal shut-off valves for easier leak-check and flow-rate measurements. Interchangeable pneumatic plumbing allowing constant pressure or flow operations are also available.

Ultra rapid amplifier
Specially capillary column designed ultra rapid (50 msec constant time) high sensitivity and linear dynamic range electrometric amplifier to ensure reliable results even with very fast peaks.

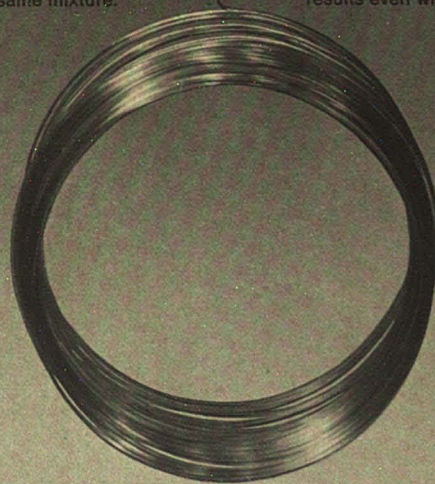

Can any other GC be greater than this?
The reply card enclosed to this journal will bring you the answer together with full details of what new technology has created and how surprisingly priced it is.

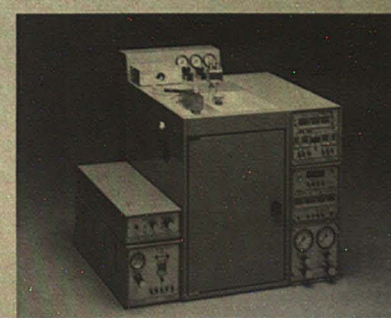

MONTEDISON GROUP
RMITALIA CARLO ERBA

CARLO ERBA STRUMENTAZIONE
P.O. BOX 4342 I-20100 MILANO
TELEX 333216 CEST

CIRCLE 33 ON READER SERVICE CARD

Table I. Simultaneous Determination of the Elements Requirements of an Ideal System

1. Applicable to all elements
2. Simultaneous or rapid sequential multielement determination capability at the major, minor, trace and ultratrace concentration level without change of operating conditions
3. No interelement interference effects
4. Applicable to the analysis of microliter or microgram sized samples
5. Applicable to the analysis of solids, liquids, and gases with minimal preliminary sample preparation or manipulation
6. Capable of providing rapid analyses; amenable to process control
7. Acceptable precision and accuracy
8. Nondestructive
9. Portable
10. Commercially available facilities at acceptable cost
11. Acceptance by the scientific community

nation of low and high atomic number elements of X-ray fluorescence spectroscopy involves major changes in the energy distribution of the exciting radiation and in the choice of diffracting crystals. For ICP-AES, a single set of operating conditions usually suffices for determination of all applicable elements at major constituent or trace levels. The value of this capability is often underestimated by analysts.

A facility that incorporates both a polychromator and a programmable scanning spectrometer provides the analyst with an unusually flexible instrument. The polychromator may then be used for the determination of those elements for which routine analyses are required, while the scanning instrument provides the flexibility of line choice for the rapid sequential determination of virtually all elements in the periodic system, at all concentration levels.

During the past five years there have been repeated demonstrations (*34*) by many analysts that the analytical approaches represented in Figures 6 and 7 or a combination thereof fulfill, to an unusually high degree, the requirements of an ideal system for the simultaneous or rapid sequential determination of the elements at all concentration levels in a single analytical operation. Such an analytical system must meet many requirements, most of which are shown in Table I. In a recent review I assessed the degree to which ICP-AES simultaneous or rapid sequential systems complied with these requirements (*18*). I shall not repeat this assessment here, other than to update the first requirement listed. If an Ar path is provided between the plasma and spectrometer and to the detector, Br, Cl, and I are also determinable (*40*).

The high degree of compliance of the ICP-AES technique with the requirements shown in Table I (*18*) is leading to a rapidly increasing acceptance of this approach by the scientific community. This acceptance has been manifested in a number of ways. First, the number of active ICP-AES laboratories has increased from less than 10 in 1969 to an estimated total exceeding 400 installations in 1979. Second, a privately published newsletter now appears monthly (*41*) and cover stories, with colorful cover photographs, have appeared in ANALYTICAL CHEMISTRY, *Science*, and *American Laboratory*. Third, as a result of a poll conducted by *American Laboratory* at the 1978 Pittsburgh Conference, the editorial staff of that periodical concluded that the percentage projected growth of "plasma spectrometers" exceeded all other analytical instruments (*42*). Finally, ICP-AES symposia at recent Pittsburgh Conferences and meetings of the Federation of Analytical Chemistry and Spectroscopy Societies have consistently been among the best attended.

Problem Areas. Lest the impression be conveyed that ICP-AES is a panacea for all elemental determinations at all concentration levels, I hasten to identify several problem areas. Spectral line interferences are common in AES, but there are well-known approaches for eliminating or drastically reducing their effects on analytical results. These line interferences can frequently be eliminated altogether by the judicious selection of the analysis lines. Although this selection process may lead to some compromise between optimum detecting power and least interference from spectral lines of the concomitants, such compromises are generally acceptable. The most definitive assessment of possible spectral line interferences is based on observations of spectra of pure reference samples free of the analyte species. The general unavailability of such reference samples remains a problem of ultratrace analysis by atomic spectroscopy. Weak spectral line interferences may not always be avoidable, and under these circumstances, correction schemes based on measurements of the concentrations of the interfering elements can be used. The latter approach is particularly appropriate when the concentrations of several elements are determined simultaneously with a polychromator. When determinations are made at trace concentration levels, the underlying spectral background will normally be a large fraction of the total measured signal, and precise background corrections are required for accurate analyses. Changes in the concentrations of concomitants may produce subtle changes in the background level. These background shifts may be caused by true spectral interference, as discussed above, by stray light (*43*), or by true spectral background shifts arising from radiative recombination continuum emission or from line-broadening processes (*44*). The stray light contributions, other than the portion arising from far scatter, can usually be reduced by use of high quality gratings, such as holographic gratings, and by proper design of the spectrometer. Residual far scatter, which may be considered a form of stray light, may often be rejected by mounting band-pass absorption or rejection filters immediately in front of the detector or the entrance slit of the spectrometer (*43, 45*).

True background shifts, if not measured accurately and subtracted from the total, may introduce an analytical bias that may masquerade as an interelement or matrix effect. The various approaches for accurately measuring background shifts have been reviewed recently (*46–48*), and automated minicomputer controlled, multielement background correction approaches to ensure precise correction data are now commercially available.

Another problem area resides in the aerosol generation processes; there is general agreement that the various aerosol generation techniques summarized in Figure 4 constitute the weakest link in ICP-AES system. Although these techniques have provided simple, direct, and adequately precise means for presenting sample material to the plasma for analysis, fragmentary experimental evidence and intuitive deduction indicate that these processes may limit the ultimate precision and accuracy attainable by the technique.

The Future. What does the future hold? Unfortunately, it is not revealed to us until it becomes the present. Polychromator-ICP systems should continue to exert a major impact in the routine simultaneous multiele-

Spectroscopists!

Look at the software we've added to the OMA® 2 System...

We've taken the industry standard in rapid-scan spectroscopy and made it even better! EG&G PARC's state-of-the-art Optical Multichannel Analyzer system, the OMA 2, now includes the following software at no extra cost:

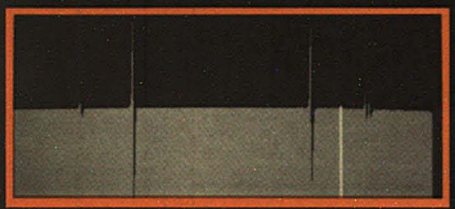

DIFFERENTIATION: Permits automatic calculation and display of 1st through 5th derivative of spectral curves. Also has smoothing function.

TIME HISTOGRAM: In conjunction with vidicon detectors and our Rotating Optical Slit accessory, permits display of the time evolution of a selected group of channels.

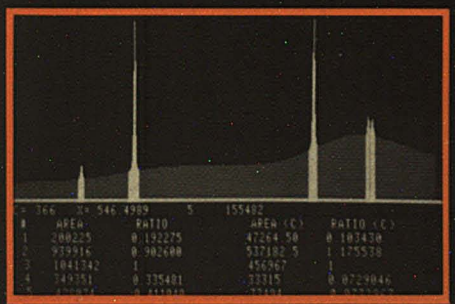

AREA AND RATIO CALCULATIONS: Calculates the area under the curve for up to six regions of interest and the ratios of the areas to the area of one selected region.

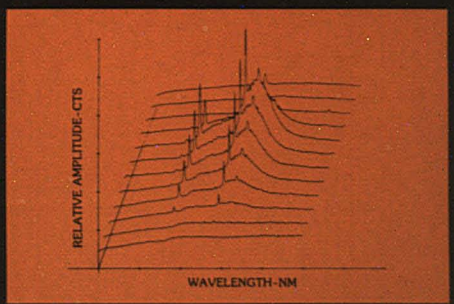

TIME RESOLVED PLOTTING: Provides hard-copy output on X-Y recorders of time resolved data. Allows plot rotation for view of peaks hidden behind foreground features.

In addition to the above new features, we've added such things as two-way "talk-listen" capability for communication with and operation by your computer, fast data acquisition modes for kinetic studies, data shifting along the X-axis for precise averaging of time resolved data containing baseline jitter (e.g., from streak cameras), and a whole lot of other functions. Want to know more about our SMART OMA 2? Call or write today. Electro-Optical Instrument Division.

NEW! An applications package has been developed for PHOTOMETRIC and RADIOMETRIC measurements. It allows keyboard entry of standard sources, and gives outputs of your experiment in radiometric or photometric units. It also calculates COLOR TEMPERATURE, COLORIMETRIC COORDINATES, and more. For details and prices, call or write today.

EG&G PRINCETON APPLIED RESEARCH
P. O. BOX 2565 • PRINCETON, NJ 08540 • 609/452-2111 • TELEX: 843409
Circle 178 for additional information only.

529

LC ANALYSES HAVE FINALLY BEEN REDUCED.

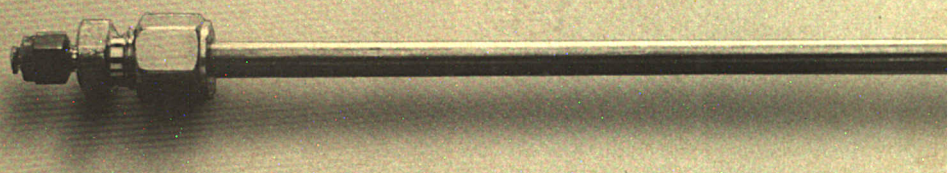

TO THIS.

Waters' new Radial-PAK™ cartridge is a sizable advance in LC separation technology. The cartridge is part of a whole new innovative concept. The Waters Radial Compression Separation System (RCSS).

RCSS improves LC analyses because separations occur while the Radial-PAK cartridge is under radial compression in the RCM-100 Module. This ensures consistent chromatographic results, greater performance, and eliminates column voiding.

For example, an analgesic assay was reduced from 8 minutes on a high efficiency steel column to only 3 minutes with RCSS, saving over 60% of the analysis time. The time for an aromatic hydrocarbon separation was reduced by more than two thirds, from 6.5 minutes to only 2 minutes, by transferring the work to RCSS.

Plus, it's more economical. In fact, the cartridges are inexpensive enough to dedicate a separate cartridge to each application. Radial-PAK cartridges are available for reverse phase and normal phase chromatography.

Now it takes very little to reduce the time and cost of LC analyses. RCSS. Another example of technological innovation from Waters. The people who provide total solutions for solving chemical analysis and purification problems. Write or call for further information. Waters Associates, Inc., 34 Maple Street, Milford, MA 01757. (617) 478-2000, Ext. 2612.

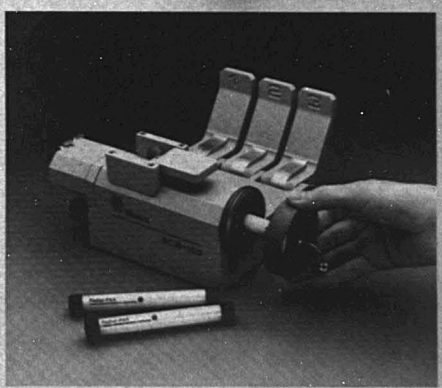

Waters

The Liquid Chromatography People

CIRCLE 232 ON READER SERVICE CARD

ment determination field. Although programmable scanning spectrometer-ICP systems are still in their infancy, they are likely to have an even greater impact in the general analytical laboratory. Thus, the way many elemental determinations are made is likely to undergo a considerable change in the future. The assumption should not be made, however, that state-of-the-art ICP-AES systems represent the ultimate solution to simultaneous or rapid multielement determinations at all concentration levels. Better ways may emerge—if the challenge of developing a better way is met.

Acknowledgment

The Fisher Award was established 32 years ago to recognize and encourage outstanding contributions to the science of analytical chemistry. I am keenly aware that the achievements attributed to me have resulted to a large extent from the dedicated effort and imagination of a large number of able associates and former students. So that I may express my gratitude to these individuals and to recognize their contributions, a list of the 84 coauthors of our 165 publications is given below. The coauthors are listed in order by decreasing number of publications, which are given in parentheses. The important contributions of R. N. Kniseley are particularly evident as are the sustaining influence and contributions of A. D'Silva, E. DeKalb, and R. Winge:

Kniseley, R. (61); D'Silva, A. (16); DeKalb, E. (13); Winge, R. (9); Reif, I. (8); Butler, C. C. (7); Gordon, W. A. (6); Heidel, R. H. (6); Kross, R. D. (6); Dallmann, W. E. (5); Evens, F. Monte (4); Haas, W. (4); Jasinski, R. J. (4); Margoshes, M. (4); Rasmuson, J. O. (4); Cowley, T. G. (3); Gray, L. S. (3); Hirschmann, R. P. (3); Kalnicky, D. J. (3); Kehres, P. W. (3); Larson, G. F. (3); Mossotti, V. G. (3); Quinney, B. B. (3); Tabeling, R. W. (3); Wendt, R. H. (3); West, A. C. (3); Barnett, W. B. (2); Brehm, R. K. (2); Cook, H. D. (2); Curry, R. H. (2); Dickinson, G. W. (2); Fiorino, J. A. (2); Goetzinger, J. W. (2); Golightly, D. G. (2); Hettel, H. J. (2); Hill, C. C. (2); Horrigan, V. M. (2); Krotz, L. C. (2); Lentz, C. F. (2); Myers, R. B. (2); Nixon, D. E. (2); Oestreich, G. J. (2); Saranathan, T. R. (2); Scott, R. H. (2); Smith, A. Lee (2); Willis, J. B. (2); Abercrombie, F. N. (1); Altpeter, L. L. (1); Amenson, C. C. (1); Anderson, C. H. (1); Anderson, D. (1); Banks, C. V. (1); Becker, D. A. (1); Conrad, E. E. (1); Farquhar, E. L. (1); Fillwalk, F. (1); Goldstein, S. A. (1); Grabau, F. (1); Grossmann, W. E. L. (1); Hayles, W. J. (1); Howard, A. M. (1); Huke, F. B. (1); Hurd, B. G. (1); Kamada, H. (1); Katzenberger, J. M. (1); Laabs, F. C. (1); Layton, E. M., Jr. (1); Lucas, W. V. (1); Matsumoto, C. (1); Mossholder, N. V. (1); Nakamoto, K. (1); Olson, K. W. (1); Peterson, C. A. (1); Peterson, V. J. (1); Rundle, R. E. (1); Skogerboe, R. (1); Slack, R. W. (1); Sutherland, W. L. (1); Taniguchi, T. (1); Tremmel, C. (1); Voter, R. C. (1); Weber, J. (1); Wilhelm, H. A. (1); Woo, C. S. (1).

References

(1) H. A. Laitinen, *Anal. Chem.*, **50**, 852A, 1233A (1978).
(2) J. Osteryoung, *ibid.*, **50**, 849A (1978).
(3) G. E. F. Lundell, *Ind. Eng. Chem., Anal. Ed.*, **5**, 221 (1933).
(4) S. Greenfield, I. L. Jones, and C. T. Berry, *Analyst*, **89**, 713 (1964).
(5) R. H. Wendt and V. A. Fassel, *Anal. Chem.*, **37**, 920 (1965).
(6) R. Barnes, Ed., "Emission Spectroscopy," pp 422–26; Dowden, Hutchison, and Ross, Stroudsburgh, Pa., 1978.
(7) G. W. Dickinson and V. A. Fassel, *Anal. Chem.*, **41**, 1021 (1969).
(8) A. Walsh, *Anal. Chem.*, **46**, 698 (1974).
(9) C. Th. J. Alkemade, *Appl. Opt.*, **7**, 1261 (1968).
(10) P. W. J. M. Boumans, *Philips Tech. Rev.*, **34**, 305 (1974).
(11) V. A. Fassel, Paper presented at the Federation of Analytical Chemistry and Spectroscopy Societies, 1st National Meeting, Atlantic City, N.J., Nov. 18–22, 1974.
(12) G. I. Babat, *Vestn. Elektroprom*, February 1942, No. 2, pp 1–12; No. 3, pp 2–8.
(13) S. V. Dresvin, A. V. Donskoi, V. M. Goldfarb, and V. S. Klubnikin, "Physics and Technology of Low Temperature Plasmas," p 10, translation by T. Cheron and H. V. Echert, Iowa State University Press, Ames, 1977.
(14) G. I. Babat, *J. Inst. Elect. Eng.*, **94**, 27 (1947).
(15) T. B. Reed, *Intern. Sci. Technol.*, **6**, 42 (1962).
(16) T. B. Reed, *Appl. Phys.*, **32**, 821, 2534 (1961); **34**, 2266 (1963).
(17) For a detailed discussion of the theory, formation, and properties of inductively coupled plasmas, the reader is referred to reference (13) and to H. V. Eckert, *High Temp. Sci.*, **6**, 99 (1974).
(18) V. A. Fassel, *Science*, **202**, 183 (1978).
(19) V. A. Fassel, *Pure Appl. Chem.*, **49**, 1533 (1977).
(20) R. M. Barnes, *CRC Critical Reviews in Analytical Chemistry*, **7**, 203 (1978).
(21) S. Greenfield, I. L. Jones, H. M. McGeachin, and P. B. Smith, *Anal. Chim. Acta*, **74**, 225 (1975).
(22) G. F. Larson, V. A. Fassel, R. H. Scott, and R. N. Kniseley, *Anal. Chem.*, **47**, 238 (1975).
(23) P. W. J. M. Boumans, and F. J. de-Boer, *Spectrochim. Acta Part B*, **31**, 355 (1976).
(24) D. J. Kalnicky, R. N. Kniseley, V. A. Fassel, *Spectrochim. Acta Part B*, **30**, 511 (1975).
(25) D. J. Kalnicky, V. A. Fassel, R. N. Kniseley, *Appl. Spectrosc.*, **31**, 137 (1977).
(26) J. Mermet, *Spectrochim. Acta Part B*, **30**, 383 (1975).
(27) G. R. Kornblum and L. de Galan, *ibid.*, **32**, 71 (1977).
(28) J. M. Mermet and C. Traisy, *Rev. Phys. Appl.*, **12**, 1219 (1977).
(29) J. Jarosz, J. M. Mermet, J. R. Robin, *Spectrochim. Acta Part B*, **33**, 55 (1978).
(30) P. W. J. M. Boumans and F. J. de Boer, *ibid.*, **32**, 365 (1977).
(31) V. A. Fassel and R. N. Kniseley, *Anal. Chem.*, **46**, 1110A, 1155A (1974).
(32) R. H. Scott, V. A. Fassel, R. N. Kniseley, D. E. Nixon, *ibid.*, **46**, 75 (1974).
(33) P. W. J. M. Boumans and F. J. de-Boer, *Spectrochim. Acta Part B*, **30**, 309 (1975).
(34) For the most recent reviews on the analytical applications of ICP-AES, the reader is referred to reference 20 and to R. B. Barnes, Ed., "Applications of Inductively Coupled Plasmas to Emission Spectroscopy," Franklin Institute Press, Philadelphia, Pa., 1978.
(35) M. A. Floyd, V. A. Fassel, R. K. Winge, J. M. Katzenberger, and A. P. D'Silva, Paper No. 351 presented at the 1979 Pittsburgh Conference on Analytical Chemistry and Applied Spectroscopy, Cleveland, Ohio, March 5–9, 1979.
(36) R. W. Spillman and H. V. Malmstadt, *Anal. Chem.*, **48**, 303 (1976).
(37) D. J. Johnson, F. W. Plankey, and J. D. Winefordner, *ibid.*, **47**, 1739 (1975).
(38) H. Kawaguchi, M. Okada, T. Ito, and A. Muzuike, *Anal. Chim. Acta*, **95**, 145 (1977).
(39) P. W. J. M. Boumans, G. H. van Gool, and J. A. J. Jansen, *Analyst*, **101**, 585 (1976).
(40) C. C. Wohlers and V. A. Fassel, unpublished data.
(41) "ICP Information Newsletter," R. Barnes, Ed., Dept. of Chemistry, Univ. of Massachusetts, Amherst, Mass.
(42) F. I. Scott, Jr., *Am. Lab.*, Jan. 1979, pp 105–109.
(43) G. F. Larson, V. A. Fassel, R. K. Winge, and R. N. Kniseley, *Appl. Spectrosc.*, **30**, 384 (1976).
(44) G. F. Larson and V. A. Fassel, accepted for publication in *Appl. Spectrosc.*
(45) V. A. Fassel, J. M. Katzenberger, R. K. Winge, *Appl. Spectrosc.*, **33**, 1 (1979).
(46) R. K. Skogerboe, P. J. Lamothe, G. J. Bastiaans, S. J. Freeland, G. N. Coleman, *ibid.*, **30**, 495 (1976).
(47) S. R. Koirtyohann, E. D. Glass, D. A. Yates, E. J. Hinterberger, F. E. Lichte, *Anal. Chem.*, **49**, 1121 (1977).
(48) W. J. Haas, R. K. Winge, V. A. Fassel, R. N. Kniseley, paper presented at the 29th Pittsburgh Conference on Analytical Chemistry and Applied Spectroscopy, Feb. 27–March 3, 1978.

This research was supported by the U.S. Department of Energy, Contract No. W-7405-Eng-82, Division of Chemical Sciences, Budget Code AK-01-03-02-3.

Velmer A. Fassel is Deputy Director of the Ames Laboratory DOE and the Energy and Mineral Resources Research Inst. at Iowa State University. He holds these positions while retaining his academic rank of professor of chemistry. The title of Distinguished Professor of Science and Humanities was bestowed in 1976. Dr. Fassel received his Ph.D in physical chemistry from Iowa State University in 1947. Previously he had received his B.A. at Southeast Missouri State University. He is the author of 166 publications on various aspects of atomic emission, absorption, and fluorescence spectroscopy, molecular spectra and structure, and high temperature analytical chemistry. He has received six major awards. His current research interests are atomic emission, absorption, and fluorescence spectroscopy, especially their analytical applications, X-ray excited optical luminescence, and other ultratrace analytical techniques.

If you know pH you should know Philips.

It's not always what you know but who you know that counts, and getting to know Philips will help solve your electrochemistry problems. Our comprehensive range of equipment and our wealth of knowledge and expertise can provide all your requirements in both laboratory and industrial pH, pX and conductivity.

Now established in our Cambridge laboratories, Philips electrochemists work side by side with their Pye Unicam colleagues in other disciplines in analytical chemistry.

This broad based pool of expertise is worth getting to know, so why not find out now what we have to offer by completing the Reader Reply Card or contacting your local Philips Science & Industry office or the address below.

pH, pX and conductivity meters: A range of analogue and digital instruments from simple low cost general purpose to sophisticated high accuracy with push button function control.
Reader Reply No 116.

Ion selective electrodes: Solid state and plastic membranes covering a wide range of ions, including the new ammonia probe.
Reader Reply No 117.

pH electrodes: pH, redox, reference and combined electrodes for an extensive range of applications.
Reader Reply No 118.

Conductivity cells: A complete range from the traditional glass and platinum to rugged wire wound cells in p.v.d.f.
Reader Reply No 119.

Industrial pH and conductivity: An extensive range of transmitters, electrodes, cells and housings.
Reader Reply No 120.

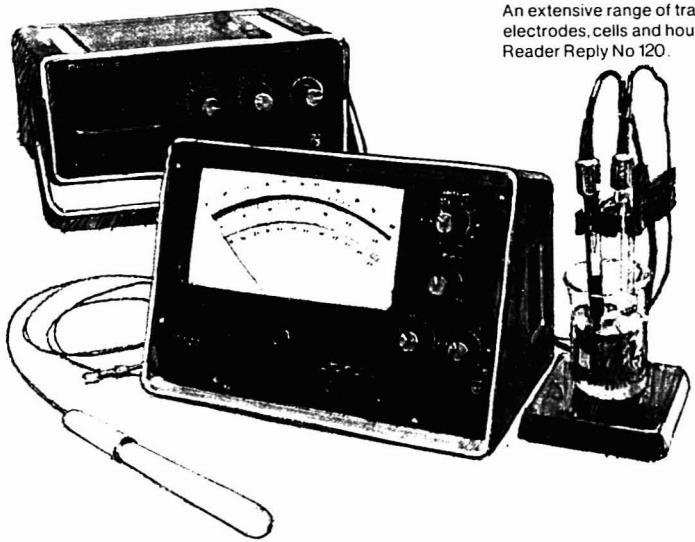

PHILIPS

Pye Unicam Ltd

York Street Cambridge CB1 2PX England
Telephone (0223) 58866 Telex 817331

Printed in England 7050.05.3143.11

Enzyme Immunoassay? The future is in the cards!

A great future is predicted for EMIT, Elisa and other new spectrophotometric immunoassays, but how can you be prepared for tomorrow's techniques?

Using Pye Unicam Software Cards as a basis, low-cost systems can be built around either the SP6 or SP8 Series Spectrophotometers and the HP97S Programmable Calculator.

All you have to do is slide the magnetic software card through the reader and the system is instantly programmed for immunoassays or conventional colorimetric or rate measurements.

And, the programs can easily be changed to keep you in touch with the rapidly developing world of immunoassay techniques, without the aid of a fortune teller – or a fortune!

For further information write, 'phone or use the reader reply service today.

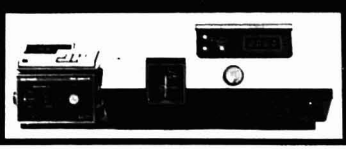

PHILIPS

Pye Unicam

A SCIENTIFIC INSTRUMENT COMPANY OF PHILIPS

York Street Cambridge CB1 2PX England
Telephone (0223) 358866 Telex 817331

CIRCLE 167 ON READER SERVICE CARD

1308 D

The LC Systems that

Pye Unicam's new LC-XP Series of liquid chromatographs allows the chromatographer to choose the system that will exactly suit his own specific requirements – requirements that may vary from quality control to complex research studies.
The Series consists of both isocratic and gradient elution liquid chromatographs which, while modular in design are essentially conceived as fully integrated systems. Not only can a liquid chromatograph be configured to suit any budget or application, but, when requirements change, the system can be readily updated with minimum expense.

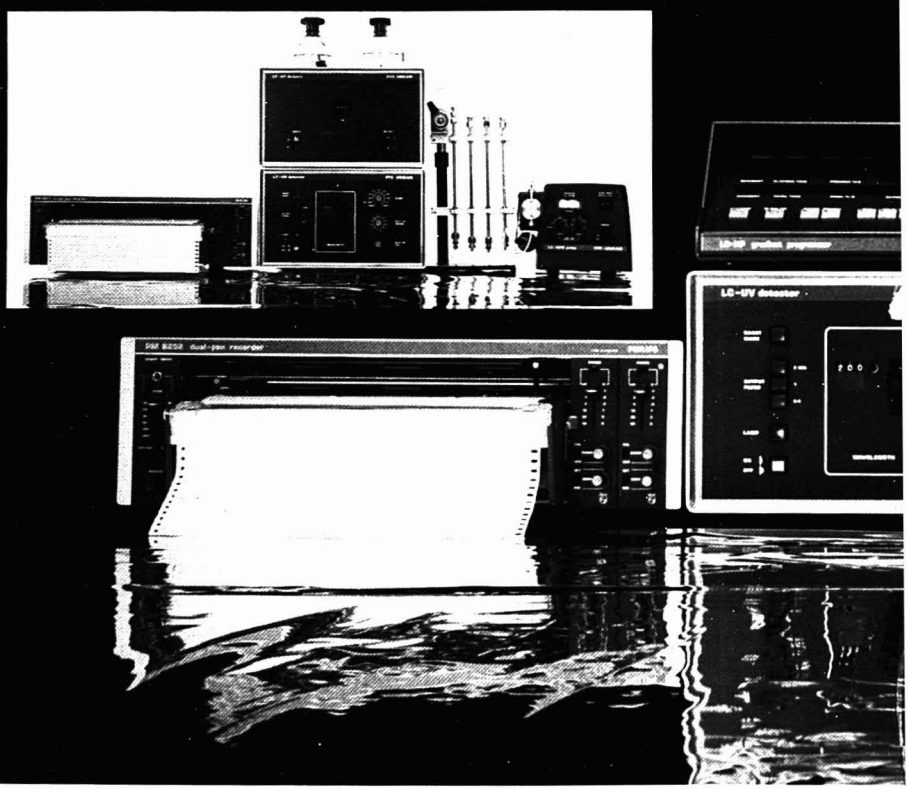

PHILIPS

You can vary the system but the reliability never changes.

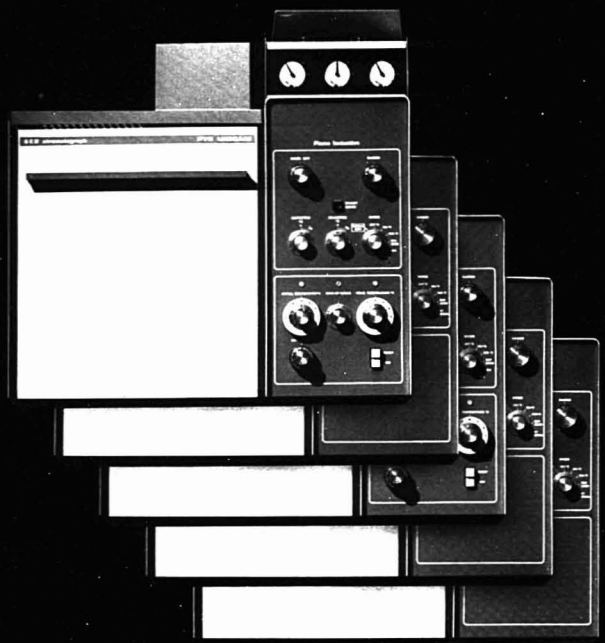

The great work-horses of gas chromatography: the five versions of the GCD system. Ideal for routine, repetitive applications. Economical, reliable. Simple to use, yet capable of high performance chromatography.

Each of these five popular versions is compact and self-contained; each is dedicated to a particular detection system: Temperature Programmed FID, Isothermal FID, Temperature Programmed and AutoDoor FID, Isothermal TCD and Isothermal ECD.

It's not only for these reasons of economy, ease and dependability that this simple system has enjoyed the continued approval of gas chromatographers everywhere; GCD instruments are supported by the excellent world wide facilities of Philips and Pye Unicam.

You can obtain details of GCD capability by writing to the address below, ringing, or using the reader reply service. If you're not already depending on the GCD system, contact us today.

PHILIPS

Pye Unicam

A SCIENTIFIC INSTRUMENT COMPANY OF PHILIPS

York Street Cambridge CB1 2PX England
Telephone (0223) 358866 Telex 817331

CIRCLE 163 ON READER SERVICE CARD

1308 G

Masters in UV/visible, the new SP8 Series.

The new SP8 Series share the world's most advanced optical design, incorporating master holographic gratings for ultra-low stray light levels, silica-coated optics for durability and angled mirrors and windows which improve photometric accuracy. Whatever your UV/visible scanning requirements, one of the four SP8 models can be tailored to your needs.

The SP8-100 and the new, extended range SP8-150 are designed on a modular basis so that high performance systems can meet, within a tight budget, the demands of almost any application.

The SP8-200 and the new, double monochromator SP8-250 offer the highest standards of precision currently available. Research performance is combined with the flexibility of keyboard operation and *full* microprocessor control and data handling – not just abscissa and ordinate control.

Write, 'phone or use the reader reply service to discover which of the new SP8 Series will benefit your analytical problems.

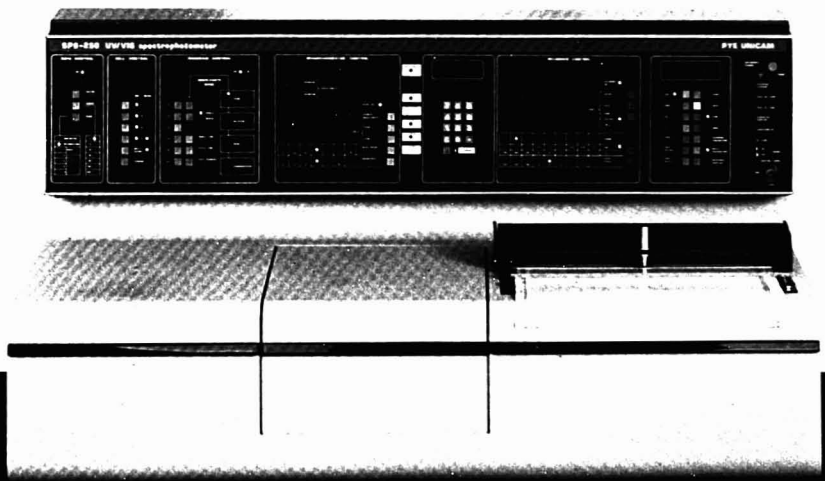

PHILIPS

Pye Unicam

A SCIENTIFIC INSTRUMENT COMPANY OF PHILIPS

York Street Cambridge CB1 2PX England
Telephone (0223) 58866 Telex 817331

CIRCLE 168 ON READER SERVICE CARD

1308 H

To those who think Beckman means only Gamma – here's the other side of the story: Beckman is also LS. More than half of all researchers purchasing LS instruments select Beckman. A decade of technical innovation improving simplicity of operation and data quality is the main reason. Beckman LS instruments offer:

1. **Automatic Quench Compensation.** Developed by Beckman, AQC is designed to ensure accurate quench correction of dual-labeled samples by automatic adjustment of each sample. Each isotope is, therefore, measured in its properly corrected window, thus ensuring a much more precise and meaningful final answer.

2. **H Number.** This technique of quench monitoring is based on instrumental determination of the Compton edge of an external gamma source. The H Number technique uses a microprocessor-directed scan to determine the inflection point, resulting in increased accuracy and the widest range of quench monitoring.

3. **Random Coincidence Monitor.** RCM eliminates errors in final results by automatically calculating the % of chance chemiluminescent events contributing to the observed count rate.

Features like these are why researchers feel so confident in Beckman LS instruments.

Beckman is LS.

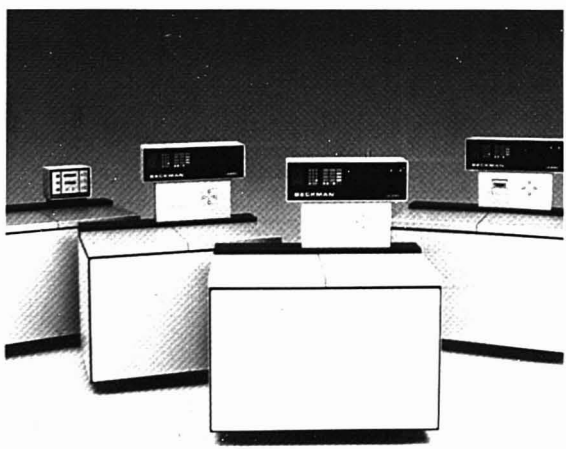

To those who think Beckman means only LS – here's the other side of the story: Beckman is also Gamma. Only Beckman offers a choice of four gamma-counters for the research and clinical laboratory:

1. Gamma 4000. This high-performance, bench-top unit has 200- or 400-sample capacity, and preset and variable windows. The optional DP-5000 computer/printer provides on-line data reduction capability – for radioimmunoassay final-answer calculations.

2. Gamma 7000. Microprocessor-controlled, this unit offers high performance with push-button simplicity. Permanently stored counting programs eliminate knobs, manual controls and switches to make operation fast, easy and reliable.

3. Gamma 8000. Takes microprocessor-control one step further, allowing the user to design special counting programs while maintaining simplicity of operation.

4. Gamma 9000. Built into the 9000 is a complete computer that both controls the operation of the instrument and takes your data through to final answer – the ultimate in data-handling capability.

These instruments make Beckman the state-of-the-art choice in Gamma.

Beckman is Gamma.

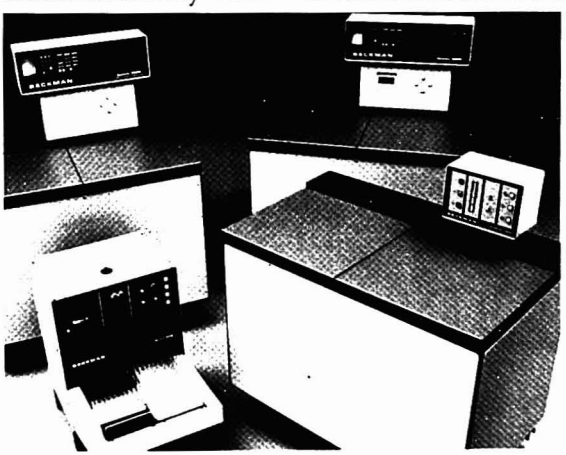

Facts from Beckman

For more information, send us the coupon, or use the reader-inquiry numbers indicated:

☐ Gamma Inquiry No. 27

☐ LS Inquiry No. 28

Name _____

Laboratory _____

Address _____

_____

Beckman Instruments International S.A.
17 rue des
Pierres-du-Niton
CH-1211 Geneva 6

BECKMAN

1308 J

a reliable and cost-effective line

flame photometers - spectrophotometers, fluorimeters
specific analysers (Cl, CO_2, bilirubin ...)

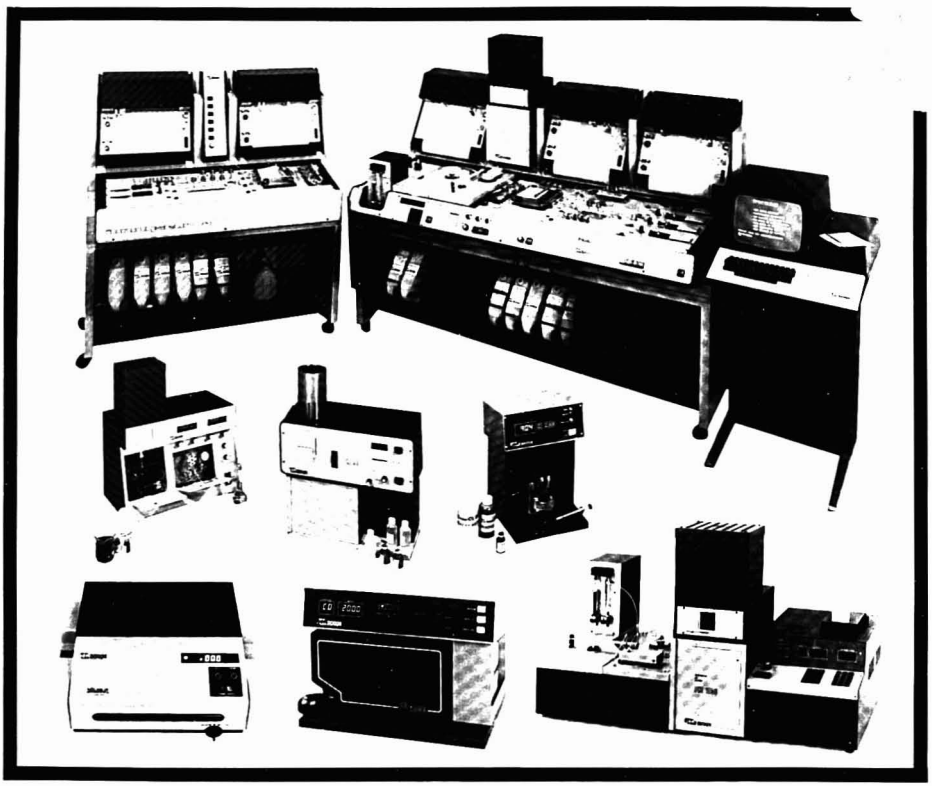

multiparametric analysers

ionolysers 4, 6, 8, 10

reagents and disposable items

biologie
DIVISION D'INSTRUMENTS S.A.
19, rue de la Gare
94230 CACHAN-(France).

Agencies:

West Germany, Brazil, U.S.A.,
Africa, Far East, Japan, Middle East.

CIRCLE 99 ON READER SERVICE CARD

1308 K

KONTRON®

UV/VIS SPECTROPHOTOMETERS

Uvikon Series

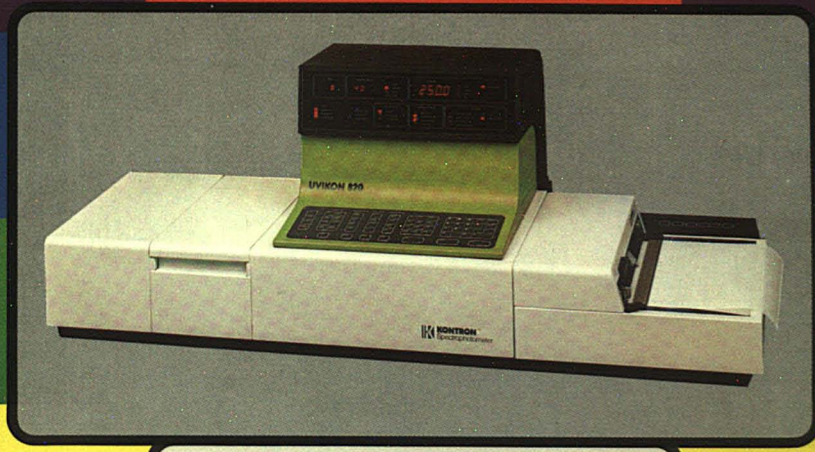

- The "Multi-User" instruments with the individually selectable program memories
- Every memorized program can be called for by touching of only 4 keys
- Simple programming – can be performed by everybody
- Erroneous operation no longer possible

The KONTRON UVIKON SERIES comprises 5 customers' oriented instruments.

CIRCLE 124 ON READER SERVICE CARD

KONTRON®
UV/VIS SPECTROPHOTOMETERS

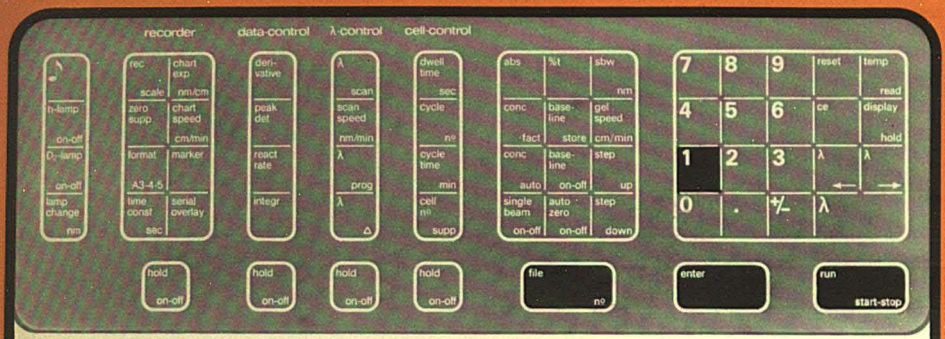

All instrument and accessory functions are controlled by the keyboard.

The large sample compartment is accessible from 3 sides and is designed for the accomodation of a wide variety of accessories (i. e. holder for 10 cm cells).

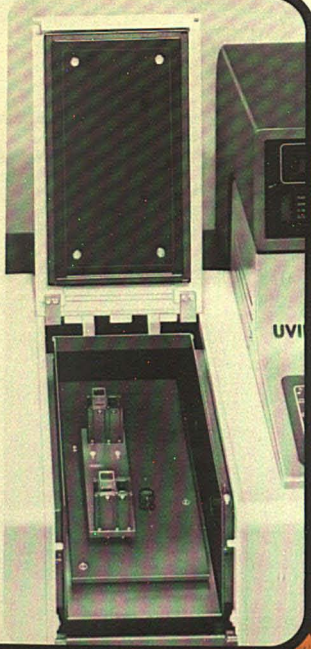

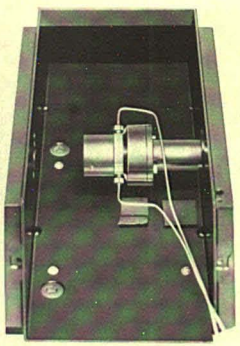

Refraction index free 8 µl flow through cell for applications in the liquid chromatography field.
Due to the high optical and mechanical precision the realignment of the cell is no longer necessary.
(UVIKON 720 LC)

KONTRON LTD
Head Office
Bernerstrasse-Sud 169
CH-8048 Zurich (Switzerland)
tel. (01) 62 92 62, twx 52115

The new approach to heavy metal analysis...

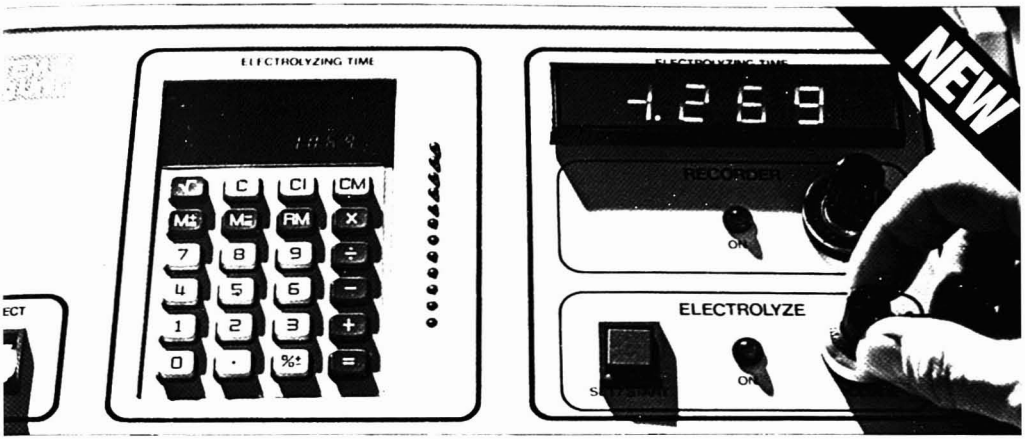

... Striptec!

The new, easy and economic way to make precise heavy metal determinations even at super-low concentrations

Striptec – the latest development from Tecator – uses new technology (potentiometric stripping analysis) that gives a very wide measuring range, with no special preparatory steps. The instrument is capable of simultaneous measurement of several metals including cadmium, lead, copper with high precision also at ppb-levels.

In combination with Tecator's programmable Digestion Systems for multisample preparation Striptec allows convenient and reproducible conditions for the measurment of trace metals not only in liquids and inorganic materials, but also in all kinds of organic materials.

Compared to existing analyzers, Striptec is more compact and less expensive. It offers great advantages in being simple to install and operate. The robust design and unique technology offer troublefree maintenance and minimize the service demand.

Step forward with the latest development from Tecator!

Send for more facts about Striptec.
Mail to Tecator
Box 70, S-263 01 Höganäs, Sweden.

Name .....

Inst./Company .....

Dept .....

Address .....

.....

Telephone .....

tecator

Box 70, S-263 01 Höganäs, Sweden.

CIRCLE 210 ON READER SERVICE CARD

KONTRON®
UV/VIS SPECTROPHOTOMETERS

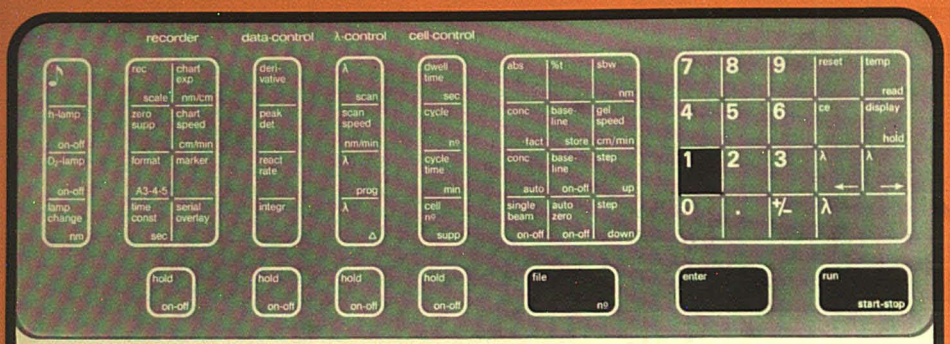

All instrument and accessory functions are controlled by the keyboard.

The large sample compartment is accessible from 3 sides and is designed for the accomodation of a wide variety of accessories (i. e. holder for 10 cm cells).

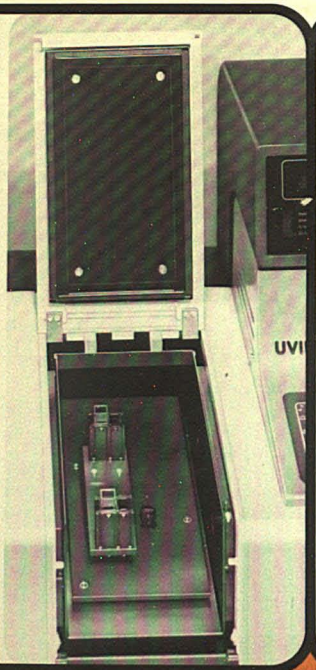

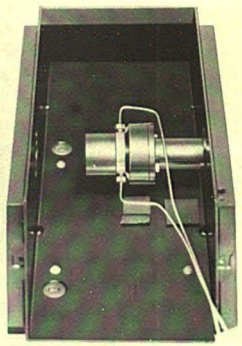

Refraction index free 8 µl flow through cell for applications in the liquid chromatography field.
Due to the high optical and mechanical precision the realignment of the cell is no longer necessary.
(UVIKON 720 LC)

KONTRON LTD
Head Office
Bernerstrasse-Sud 169
CH-8048 Zurich (Switzerland)
tel. (01) 62 92 62, twx 52115

The new approach to heavy metal analysis...

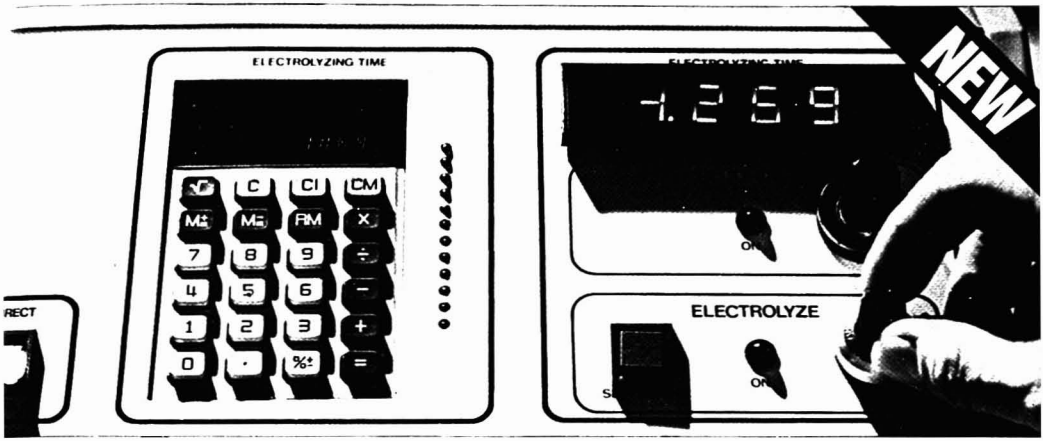

... Striptec!

The new, easy and economic way to make precise heavy metal determinations even at super-low concentrations

Striptec – the latest development from Tecator – uses new technology (potentiometric stripping analysis) that gives a very wide measuring range, with no special preparatory steps. The instrument is capable of simultaneous measurement of several metals including cadmium, lead, copper with high precision also at ppb-levels.

In combination with Tecator's programmable Digestion Systems for multisample preparation Striptec allows convenient and reproducible conditions for the measurment of trace metals not only in liquids and inorganic materials, but also in all kinds of organic materials.

Compared to existing analyzers, Striptec is more compact and less expensive. It offers great advantages in being simple to install and operate. The robust design and unique technology offer troublefree maintenance and minimize the service demand.

Step forward with the latest development from Tecator!

Send for more facts about Striptec.
Mail to Tecator
Box 70, S-263 01 Höganäs, Sweden.

Name .....

Inst./Company .....

Dept .....

Address .....

.....

Telephone .....

tecator

Box 70, S-263 01 Höganäs, Sweden.

CIRCLE 210 ON READER SERVICE CARD

Solve Your Materials Problems 6 Ways

More R&D and QC labs use Micromeritics proven, precision instruments to measure physical properties of material than those of any other manufacturer in the world. These measurements include:

1 **Automatic particle size distribution** gives rapid analysis from 100 to 0.1 μm diameter and 500 to 38 μm diameter.

2 **Manual and automatic physical adsorption** for B.E.T. surface area from 0.001m^2g up; adsorption and desorption isotherms; pore structure (volume, size and shape) from 600 to 20Å diameter.

3 **Manual and automatic chemisorption** measures active material availability; percent metal dispersion.

4 **Mercury porosimetry** measures pore structure (volume, size and shape) from 354 to 0.0035μm diameter; density, surface area and average particle size.

5 **Manual and automatic density** determines absolute volume to ± 0.02cc.

6 **Electorophoretic mass-transport analysis** to study flocculation and dispersion; particle-liquid systems behavior; zeta potential.

We also invite you to use our complete Materials Analysis Laboratory Services. Let us show you how to solve your material problems. Call or write the distributor in your area or contact Micromeritics Instrument Corporation, 5680 Goshen Springs Road, Norcross, Georgia 30093. U.S.A. (404) 448-8282. Telex: 70-7450.

micromeritics

CIRCLE 135 ON READER SERVICE CARD

EUROPEAN SALES OFFICE
2 Orchard Way
Eaton Bray
Bedfordshire
England
Telex 851-826249

AFRICA
North
Coultronics France S.A.
Margency 95580 Andilly
France
Telephone 989-9030

South
Coulter Electronics PTY. Ltd
Transvaal
South Africa
Telephone 805-2046 55 56

ARGENTINA
Instrumentalva S.R.L.
Buenos Aires
Telephone 85-3121 86-1436

AUSTRALIA
Townson & Mercer Ltd
Lane Cove, N.S.W.
Telephone 428-1199

BELGIUM
Anasis S.A.
Namur
Belgium
Telephone 081 22 50 85

BRAZIL
Danon Sociedade Importadora
Equipmentos Cientificos LTDA
Rio de Janeiro
Telephone 221-4480

DENMARK
Bie & Bernitsen Ltd
Roedovre
Telephone 45-294-8822

EASTERN EUROPE
Medata AB
Stockholm
Sweden
Telephone 08 303370

ENGLAND
Coulter Electronics Ltd
Harpenden, Herts
Telephone Harp 63151

FINLAND
Oy Tamro AB
Helsinki
Telephone 90-544011

FRANCE
Coultronics France S.A.
Margency 95580 Andilly
Telephone 989-9030

GERMANY
Coulter Scientific GmbH
Gathingspfad
West Germany
Telephone 02156-755011

GREECE
The GG Forum
Thessaloniki
Greece
Telephone 542 371

GUADELOUPE
Coultronics France S.A.
Margency 95580 Andilly
France
Telephone 989-9030

INDIA
Blue Star Limited
Bombay
Telephone 45-7887 or
45-6799

ITALY
Coulter Scientific S.p.A.
Milano
Telephone 98-80-108

JAPAN
Shimadzu Seisakusho Ltd
Kyoto
Telephone (075) 8111111

KUWAIT
Bader Sultan & Bros. Co.
Kuwait
Telephone 421291 92 93

MALAYSIA
Delta Electronics SDN. BHD
Bangsar Baru
Kuala Lumpur
Telephone 943629

MARTINIQUE
Coultronics France S.A.
Margency 95580 Andilly
France
Telephone 989-9030

NETHERLANDS
Chemical Laboratory Instrumen
Schijndel
Netherlands
Telephone 04104-4035

NEW ZEALAND
Selby Wilton Scientific Ltd
Lower Hutt
Telephone 697-099

REUNION
Coultronics France S.A.
Margency 95580 Andilly
France
Telephone 989-9030

SPAIN
Izasa S.L.
Barcelona 15
Telephone 2548100

SWITZERLAND
IG Instrumenten-Gesellschaft
Zurich
Telephone 0166331

TAIWAN
Vertex Corporation
Taipei, Taiwan
Telephone 752-6452(3)

U.S.S.R.
Coultronics France S.A.
Margency 95580 Andilly
France
Telephone 989-9030

...the new honestly priced Liquid Scintillation and Automatic Gamma Counters from Philips...

...the end to price confusion.

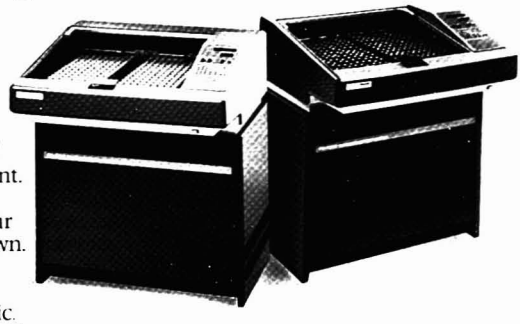

Just how important is price?

Of course price is important. But not price at any price.

Price not as a result of your ability to beat the salesman down. With Philips you won't have to argue about price.

The Philips price is realistic. Our price is based on the value of our products.

No more – no less.

The new Philips Liquid Scintillation and Automatic Gamma Counters.

The new generation for the eighties.

In styling and performance.

In our price the availability of service is included.
For at least 10 years.

In our price the availability of spare parts is guaranteed.
For at least 10 years.

Compare Philips with others in this field.
For price and performance.

We invite your comparison.
To find out the facts fill in the coupon, or write, telephone or telex, but whatever you do, contact us.

Please send me
detailed information on:

◯ Philips Liquid Scintillation Counter.
◯ Philips Automatic Gamma Counter.

Name:

Position:

Business Address:

Application:

Send to: Hein Diebels, Nuclear Analysis Manager,
N.V. Philips' Gloeilampenfabrieken,
Division of Science and Industry, A.C.
Lelyweg 1, 7602 EA Almelo,
the Netherlands.

Telephone:
05490-18291
Telex: 44191

PHILIPS

PHILIPS

CIRCLE 165 ON READER SERVICE CARD

NOW–THE FIRST FULL FLUORESCENCE LINE WITH MICROPROCESSOR CONVENIENCE.

You won't find a more complete line of fluorescence spectrophotometers anywhere. These Perkin-Elmer "multiple choice" instruments range from research to routine in performance – with microprocessor control and a variety of accessories to stretch their capabilities.

MODEL MPF-44B
NOTHING BETTER
FOR RESEARCH

No other research-grade instrument matches it in sophistication, resolution, and sensitivity. It incorporates every advance gained through Perkin-Elmer's long experience. It's shown here with our DCSU-2 Differential Corrected

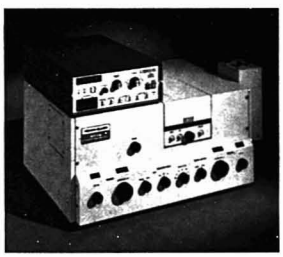

Spectra Unit, an ordinate microprocessor. This remarkable accessory enables you to perform spectra correction, subtraction, and polarization, and obtain first and second derivative curves of either corrected or uncorrected spectra.

MODEL 650-40
CONVENIENCE AND
CAPABILITY COMBINED

This is the abscissa-microprocessor-controlled member of the highly sensitive Perkin-Elmer 650

series – a medium priced line that offers many features found only in high priced units. The 650-40 operates with function keys and a numeric keyboard, includes automatic gain setting and auto zero, and gives you a digital display of fluorescence, wavelength, and other parameters. The Model 650-40/60 version has an ordinate microprocessor for such additional functions as spectra correction, CATing, rep scan, subtraction, and polarization.

MODEL 650-10
MORE SENSITIVITY
FOR THE DOLLAR

High-efficiency ruled concave grating monochromators and horizontal slit arrangements are combined in a proprietary optical design that gives this instrument extremely high sensitivity for a moderate price. Slit width is continuously adjustable down to 1.5 nm, another Perkin-Elmer exclusive that attains precision control of intensity and resolution you

won't find elsewhere except in high priced units. As little as 0.6 ml of sample is needed in the standard cell

MODEL 3000
THE UNCOMMON UNIT
FOR ROUTINE WORK

Features like pushbutton operation and abscissa microcomputer control of scanning monochromators make the Model 3000 an exclusive Perkin-Elmer breakthrough in its class. You get excitation spectra quantum corrected automatically, and digital display of fluorescence values. The Model 3000 also has three pairs of wavelength memories (three for excitation and three for emission). A pulsed xenon source, together with ratio-recording electronics, provides excellent stability for long-term measurement.

Get all the facts on this remarkable selection of fluorescence instruments and accessories. For literature or a demonstration, phone (203) 762-6095. Or write Perkin-Elmer Corporation, MS-12, Main Avenue, Norwalk, CT 06856.

PERKIN-ELMER
Expanding the world of analytical chemistry.

CIRCLE 174 ON READER SERVICE CARD

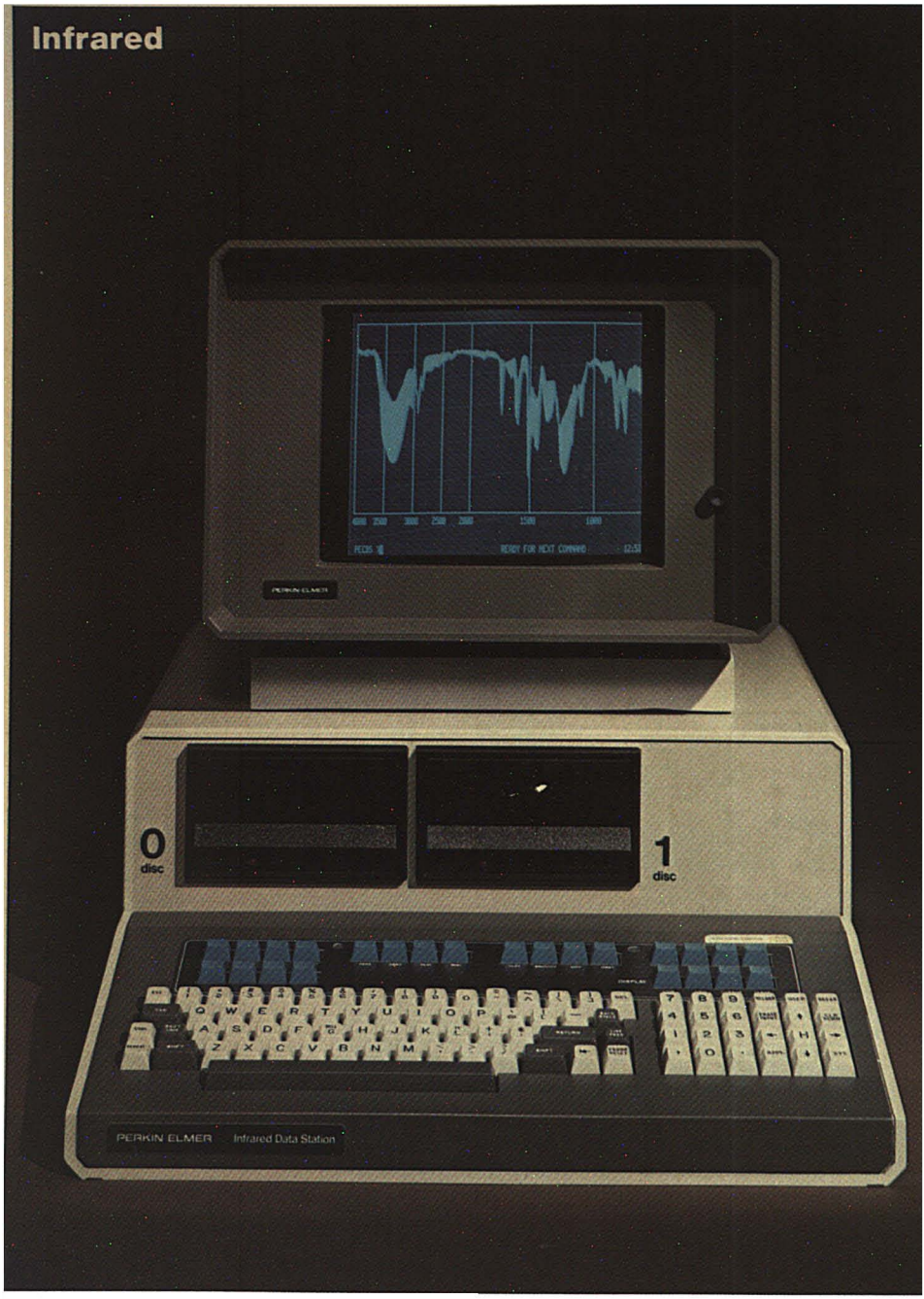
Infrared
0
disc
1
disc
PERKIN ELMER
Infrared Data Station

The spectral sleuth.

SEARCH software in our IR Data Station makes interpreting spectra fast, easy, and accurate.

The Perkin-Elmer IR Data Station is a desktop computer consisting of a processing module, keyboard, and CRT display. Connect it to a high-performance Perkin-Elmer infrared spectrophotometer and you can do dozens of unusual, important things. Store, retrieve, and manipulate data. Visually compare as many as three spectra at once on the CRT. Smooth, average, or accumulate spectra. Take spectral differences.

And when you add the SEARCH applications program, you get instant guidance on interpreting an IR spectrum, and a library search as well – quickly, easily, accurately. Pushing a button delivers years of experience.

Problem: identify this compound

Ordinarily, you use only a library of reference spectra to perform band-for-band matching with a spectrum from an unknown material.

In fact, you need a very large library, which hopefully contains the identical spectrum, as well as consistent calibration of your instrument. Otherwise, the best matches on band position alone may be very misleading.

First stage: possible structural units

The Perkin-Elmer SEARCH program takes an entirely new approach. When you place the SEARCH diskette into the Perkin-Elmer IR Data Station, the computer almost immediately delivers the kind of information you'd get only from an experienced spectroscopist. The computer does the cross-referencing that takes years to learn.

From its store of over 800 structural units, the screen shows you a list of the most likely possibilities.

```
POSSIBLE STRUCTURAL UNITS :     OCT20
 202  ALKYL GROUP - POSSIBLY METHYL SUBSTITUENT
 206  ALKYL GROUP - POSSIBLY WITH 4 CARBONS OR LONGER (CONSULT MANUAL)
 211  ALKYL GROUP - POSSIBLY CARBONYL COMPOUND
1001  ALIPHATIC KETONE - GENERAL
1002  ALIPHATIC METHYL KETONE
1003  ALIPHATIC KETONE - PROBABLY STRAIGHT CHAIN
4302  ALIPHATIC CARBONYL COMPOUND - KETONE OR ESTER CARBONYL
4913  ALIPHATIC CARBONYL COMPOUND - CLASS 3

 PSUs above may be subject to interference. Consult Manual
```

Turn to the comprehensive SEARCH manual, and you get a full explanation of each. It may be all you need to identify your compound.

Second stage: a library search in seconds

But you can go beyond this interpretation and have a library search. Perkin-Elmer's SEARCH library holds some 2300 representative spectra on a single microfloppy disk. You can get additional disks from Perkin-Elmer and, if desired, create your own specific library.

The SEARCH program compares about 80 spectra per second with the unknown spectrum. It matches them band-for-band, including the possible structural units. The screen then shows you a list of the 15 best matches:

```
NEAREST FIFTEEN SPECTRA FROM LIBRARY :     OCT20  SEARCH  05
9-7 CD336X 2-OCTANONE (SOLN) P217
9-5 PS407X METHYL HEPTYL KETONE
9-3 PS408X METHYL NONYL KETONE
9-3 PS409X DIISOBUTYL KETONE
9-2 CD599X HEXANENITRILE, 5-OXO P364
9-1 PS404X METHYL N-PROPYL KETONE
9-1 PS405X METHYL ISOAMYL KETONE
9-1 PS402X ACETONE
9-0 CD339X 5-DECANONE (SOLN) P219
9-0 CD333X METHYL ETHYL KETONE (SOLN) P215
9-0 PS403X METHYL ETHYL KETONE
9-0 PS405X METHYL ISOBUTYL KETONE
9-0 PS411X CYCLOHEXANONE
9-0 PS335X DIACETONE ALCOHOL
9-0 PS413X MESITYL OXIDE

 Always compare hard copy spectra before accepting identification
```

Pinpointing the solution

In matching your unknown spectrum with those in the library, the SEARCH program looks first for samples with the same structural units. Then it looks within these for matching band frequencies.

So even if your compound isn't in the library, the best matches turn up being chemically similar materials. Using this list of possible matches, you can compare your unknown spectrum with the known spectra illustrated in one of the books of corresponding spectra that's included with the SEARCH program.

More capability for less cost

You can enter data into the SEARCH routine directly from your Perkin-Elmer spectrophotometer, manually via the Data Station keyboard, from an optional digitizer accessory, or from a microfloppy disk containing a peak table generated earlier. No other comparable system does so much for so little. Besides its lower cost, the SEARCH applications program is a far-ranging asset to the less experienced operator. It's described fully in our literature. For your copy, write Perkin-Elmer Corp., Instrument Division, MS-12, Main Avenue, Norwalk, CT 06856.

PERKIN-ELMER

Responsive Technology

CIRCLE 175 ON READER SERVICE CARD

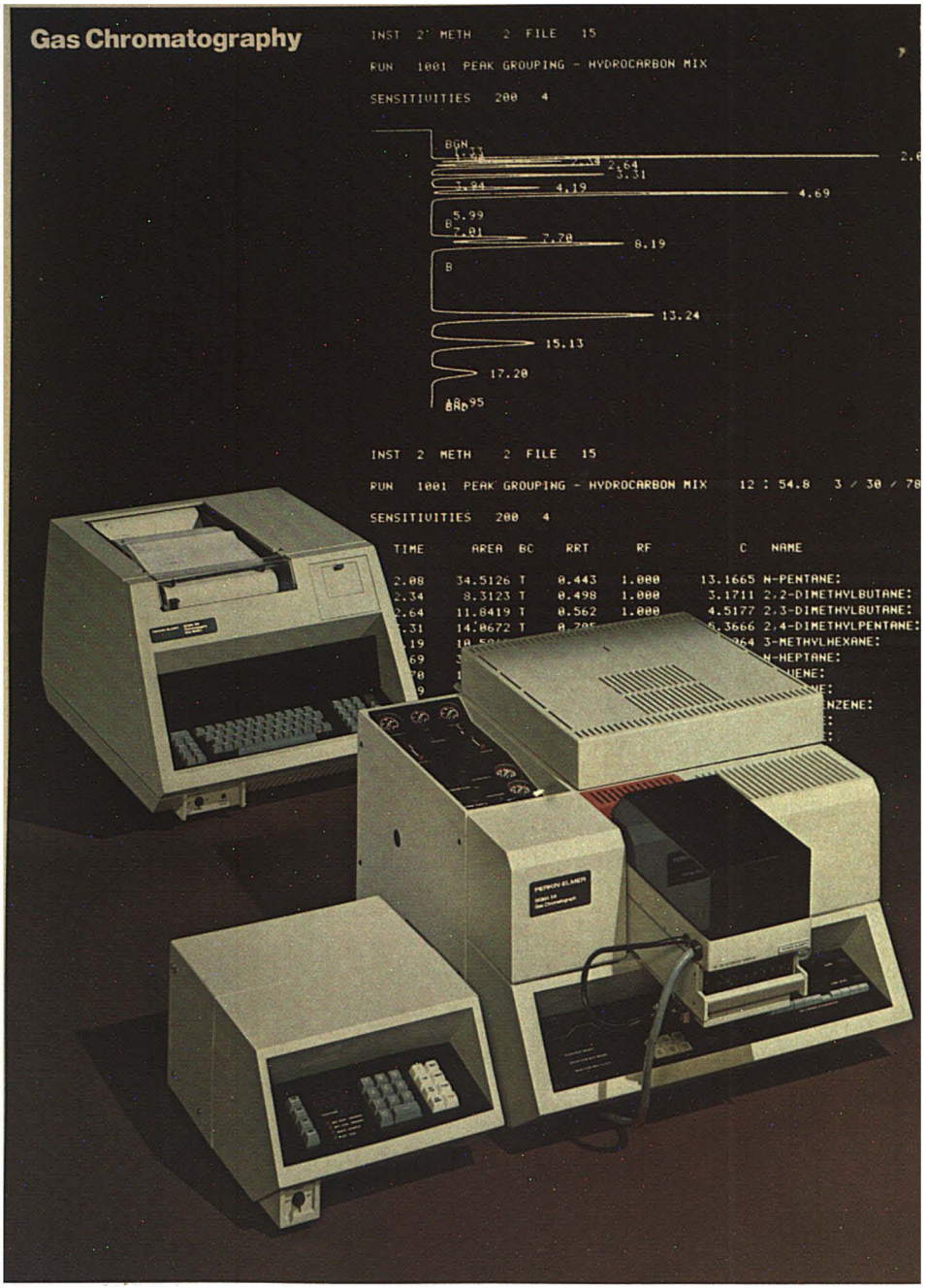
Gas Chromatography
INST 2' METH 2 FILE 15
RUN 1001 PEAK GROUPING - HYDROCARBON MIX
SENSITIVITIES 200 4
BGN
2.64
3.31
4.19
4.69
5.99
7.01
7.78
8.19
13.24
15.13
17.20
INST 2 METH 2 FILE 15
RUN 1001 PEAK GROUPING - HYDROCARBON MIX 12 : 54.8 3 / 30 / 78
SENSITIVITIES 200 4
TIME AREA BC RRT RF C NAME
2.08 34.5126 T 0.443 1.000 13.1665 N-PENTANE:
2.34 8.3123 T 0.498 1.000 3.1711 2,2-DIMETHYLBUTANE:
2.64 11.8419 T 0.562 1.000 4.5177 2,3-DIMETHYLBUTANE:
PERKIN ELMER

Perkin-Elmer's SIGMA 3B. If you're raising a GC family, start with all the advantages.

Our SIGMA 3B Gas Chromatograph is a series of instruments combining many advantages of more expensive units. Its cost is modest. Its size is compact. It has features that already place it at the head of its class. And it can be expanded to suit any application. So when you need more GC capability, you don't have to move up to a more expensive model. Simply add an accessory or change a component.

Unattended automatic sampling

Our AS-100 Automatic Sampler, for example, helps the SIGMA 3B to run round the clock unattended. Up to 100 samples can be analyzed three times each. A built-in microprocessor handles everything with simple keyboard instructions, and leads the operator through set-up and storage of up to four sampling programs. Add a SIGMA 10B Data Station with BASIC II, and you can program the AS-100 to make sampling decisions based on data obtained during the analysis period.

Microprocessor-controlled analyses

Single or dual column, the SIGMA 3B is ideal for routine temperature-programmed analyses. Independent temperature setting and control for injectors and detector are standard in 1°C increments to 449°C. Enter instructions on a keyboard as simple as a pocket calculator's, not cumbersome digital switches. Self-checking, the microprocessor rejects "impossible" entries. During operation, it continuously monitors and adjusts the control systems. Self-diagnostics provide pinpoint serviceability, and you can generate a chromatogram without an injection in order to verify operation of detector amplifiers and integrators or data reduction systems.

Multi-dimensional chromatography

The SIGMA 3B is ideally suited for use in multi-dimensional chromatography. It provides a wide array of customized component configurations. With our new valveless backflush and cut system, you can simultaneously use different columns with different stationary phases to perform separations of complex mixtures on a single injection. Simultaneous detection with any combination of five available detector types (FID, FPD, NPD, ECD, and HWD) expands the SIGMA 3B's multi-dimensional capabilities. The large column oven permits any combination of columns—metal or glass, packed or open tubular. With a parallel column adapter, it can house two packed columns without disturbing a capillary column already installed.

Data handling flexibility

Using the SIGMA 10B Data Station, you get hard copy reports and annotated chromatograms on a printer/plotter. You can link the SIGMA 10B to a central computer. Or, as a further option, write your own program using standard BASIC to achieve outstanding flexibility in calculations and report formatting.

Proven head space analysis

The exclusive Perkin-Elmer Head Space Sampler, installed in minutes, converts your SIGMA 3B into a powerful new type of analyzer. In head space analysis, only the volatile components present in the gas phase above the sample (the head space) are analyzed. The non-volatile residue never reaches the GC injection system to complicate the analysis. The sample can be solid, liquid, highly viscous or a complex matrix. The technique is ideal for many environmental analysis problems.

HS-6 Head Space Sampler

The SIGMA series

The SIGMA 3B gives you all this with a price tag lower than any other in its class. It's also part of a complete line of Perkin-Elmer gas chromatographs and accessories. In addition to the 3B, the SIGMA series includes: the low-cost isothermal model SIGMA 4B; the multi-detector, microprocessor-controlled SIGMA 2B; and the most sophisticated system, the SIGMA 1B, which combines one or more gas chromatographs with integral microprocessor control and multi-channel data handling.

Start raising your GC family now. Send for literature on the SIGMA 3B and the accessories that stretch its analytical output. Write Perkin-Elmer Corp., Instrument Division, MS-12, Main Ave., Norwalk, CT 06856.

SIGMA 3B with an AS-100 Automatic Sampler lower left and a SIGMA 10B Data Station at rear. Background is data station printout with annotated chromatogram and calculations.

PERKIN-ELMER

Responsive Technology

CIRCLE 176 ON READER SERVICE CARD


ULTRAVIOLET/VISIBLE
ORD
MAX
A complete line of up-to-date UV-VIS double-beam spectrophotometers with Keyboard Control is available only from Perkin-Elmer. Go no further in your decision making. From the low-cost, high performance Model 552, through the super high performance Model 559, to the ultra high performance Model 320/330, we have an instrument for your application and your budget. Perkin-Elmer's Responsive Technology provides the speed, accuracy, and precision of Keyboard Control.
For immediate information call (312) 887-0770
CLEAR

Keyboard Control with UV Performance you can Count On!

Model 552

Perkin-Elmer UV-VIS Recording Spectrophotometers begin with the low in price, high on features, Model 552.
Keyboard Control. Makes operating the instrument fast, accurate, and precise.
Automatic Baseline Compensator. Provides a flat baseline, even when using our scanning Super Sipper.

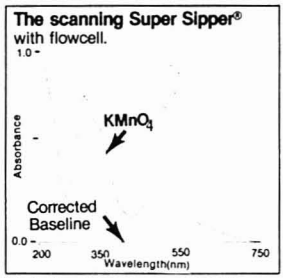

With the Super Sipper you can even scan. Shown above is a scan of $KMnO_4$ in our specially designed flowcell. A corrected baseline of the flowcell containing solvent water is shown beneath the scan.

Expandable Keyboard Operation. For a few dollars more, you can add Rep Scan, 1st and 2nd Derivative, and Automatic Concentration Factor. A high performance version is available which uses a fore-monochromator and incorporates a holographic grating to provide stray light of less than 0.002%T at 220 nm.

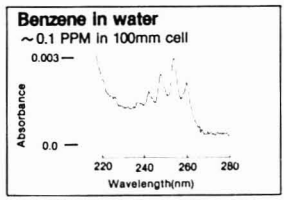

Trace determinations of aromatic hydrocarbons become routine with the baseline compensation power and low noise level of the M552. Benzene in water can easily be detected and quantified at the 100ppb level using 100 mm pathlength cells.

Model 559

The next member of the Perkin-Elmer family of UV-VIS Double-Beam Spectrophotometers is the Model 559. The Model 559's include keyboard control and all the features of the M552, PLUS
Holographic Grating for low stray light and enhanced photometric linearity. High performance version reduces stray light still further.

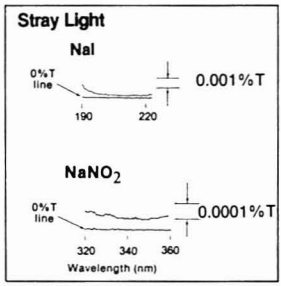

Measured stray light on a typical High Performance 559 (shown above) is well within the specification of 0.002%T at 220 nm and 0.001%T at 340 nm.

Patented Flowchart ® Recorder! The "intelligent recorder" from Perkin-Elmer automatically aligns chart to monochromator at all times.
Accessories Standard! Other instrument manufacturers make them expensive options; Perkin-Elmer provides them as standard.
1) Repetitive Scanning
2) Wavelength Programming
3) 1st and 2nd Derivative
4) Integration

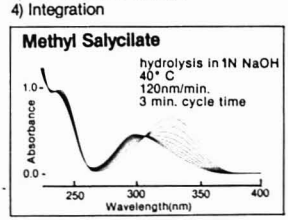

The patented Flowchart recorder makes repetitive scanning fast, accurate and precise.

Model 320/330

State of the art performance and features highlight the Model 320, for those demanding a research level, completely automatic spectrophotometer.
Double Monochromator provides better than 0.0001%T stray light at 220nm.
Keyboard Control of ALL operating parameters (even slit-width). You asked for, and you expect, unsurpassed versatility in an ultra-high performance instrument.
Smart Recorder. Just position to a grid line once and the 320 remembers. Again, accessories are standard.
1) Wavelength Programming
2) Repetitive Scanning
3) 1st, 2nd, 3rd and 4th Derivative.

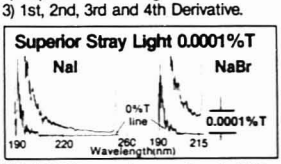

Stray light measurements were made on the M320 according to the ASTM method. Measured stray light at 220 nm with sodium iodide was well within the spec of 0.0001%T at 220 nm. Also shown is stray light using NaBr.

The Model 330 is the UV-VIS-NIR version, extending the wavelength range to 2600 nm.

Information or Demonstration
(use the reader service card)

Circle 100-for a Demonstration.
Circle 101-for information on M552/559
Circle 102-for information on M320/330
Circle 103-for an Application Data Bulletin describing derivative scanning with the Models 552 and 559.

or write directly to Perkin-Elmer Corporation, M/S-12, Main Ave., Norwalk Connecticut 06856, or Bodenseewerk Perkin-Elmer & Co.,GmbH, Postfach 1120, 7770 Uberlingen, Federal Republic of Germany.

PERKIN-ELMER
Responsive Technology

CIRCLE 171 ON READER SERVICE CARD

Varian's veteran MCP's are now available for commercial applications.

Four sizes available with quick delivery.

Varian has a distinguished history of supplying volume quantities of high performance microchannel plates to the military. This means industrial and scientific users have a new, high quality source for a complete line of high resolution electron multipliers.

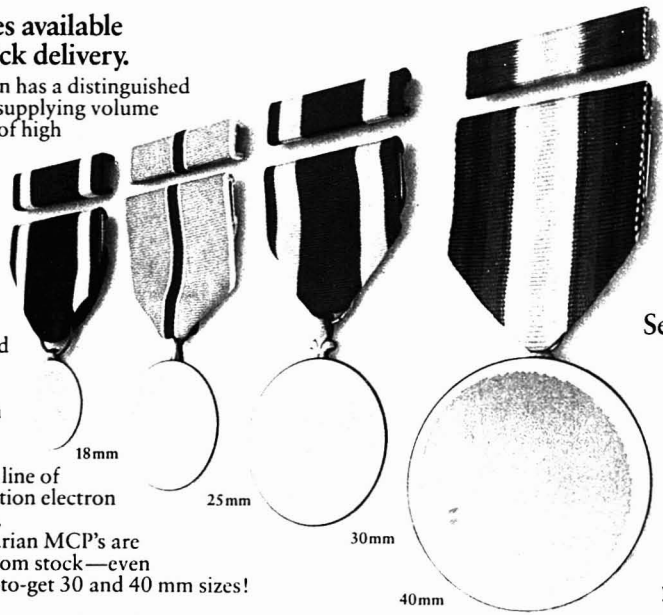

All Varian MCP's are available from stock—even those hard-to-get 30 and 40 mm sizes!

High gain and low dark noise

Whether your instrument is measuring electrons, positive ions, soft X-rays or ultra-violet, Varian MCP's provide a source of high gain, high speed and self saturating detection. They feature low dark noise, and excellent resolution is obtained with 12μm diameter channels spaced 15μm apart. Rugged construction and solid borders result in easier handling and mounting.

Send for a free applications brochure.

For a free brochure describing these microchannel plates, holder assemblies, and their uses, or to place your order now, contact Varian, LSE Division, 611 Hansen Way, Palo Alto, CA 94303. Or, call (415) 493-4000, EXT. 4100/3308, or any of the Varian EDG sales offices throughout the world.

varian

CIRCLE 228 ON READER SERVICE CARD

Report

Demand-Pull and Science-Push in Multielement Analysis

Marvin Margoshes
Technicon Instruments Corporation
Tarrytown, N.Y. 10591

Marvin Margoshes is technical director, Scientific Liaison, Technicon Instrument Corp., Tarrytown, N.Y. Prior to joining Technicon in 1971, he worked for the Digilab Division of Block Engineering; the Analytical Chemistry Division of the NBS; and the Biophysics Research Laboratory, Peter Bent Brigham Hospital and Harvard Medical School. Dr. Margoshes has authored over 50 scientific publications on various analytical methods including IR, flame and emission spectroscopy, computer applications, and chromatography. A member of the American Chemical Society since his undergraduate days, he was a member of the Instrumentation Advisory Panel of ANALYTICAL CHEMISTRY from 1970 through 1975. He is also a current member of the Advisory Board of the JOURNAL.

Material in this paper was presented at the Symposium on Multielement Analysis at the ACS National Meeting, March 4, 1979, on the occasion of the presentation of the ACS Award in Analytical Chemistry to Velmer A. Fassel.

I did not want to pass up the chance to take part in honoring Velmer Fassel on the occasion of the presentation to him of the 1979 ACS Award in Analytical Chemistry. I had a problem though, in that the topic of the symposium is multielement analysis, and I haven't done any work on this subject for several years. On reflection, I realized that combining my past experience on this subject with the work I have been doing for the past several years would allow me to bring to the topic an unusual point of view. In terms of the general tone of the symposium, I am taking the part of the devil's advocate.

Since I joined Technicon in 1971, I have entered into one of the fastest-growing industries in America—technology transfer. I look for technology emerging from research at universities and government laboratories that matches Technicon's needs and especially the needs of our customers. Many other companies have scientists doing similar work.

Most scientists operate as specialists, and they have been said to learn more and more about less and less until they know everything about nothing. In technology transfer, I need to be a generalist, and I may be headed toward knowing nothing about everything. It is demanding work, with many frustrations and many rewards.

To give you some idea of the size of the technology transfer industry, the U.S. Government published in 1975 a 200-page Directory of Federal Technology Transfer (*1*). It lists the addresses and telephone numbers of 62 offices in 18 departments, administrations, and agencies of the federal government whose sole or part-time responsibility is to assist in the transfer to industry of technological developments that have come from government-funded research. Most universities have some arrangement to patent and license inventions from their research. Often, the university has an office of its own to handle these matters. Others rely on nonprofit agencies such as the Research Corporation, or on for-profit organizations such as University Patents, Inc.

Those who have studied the processes of innovation have learned that most new technology can be classified as falling into one of two categories, called "demand-pull" and "science-push" (*2, 3*). Most industrial R&D is of the demand-pull type. A need is identified that can become a market for the company, and a project team is formed to develop a product to fit the need. In a well-run company, the R&D staff doesn't just wait for assignments. They will alert the company to new technical developments that could find a market. However, little or no research may be done unless it can be foreseen that the company will be able to apply the results of the research.

0003-2700/79/A351-1317$01.00/0

In science-push, the tendency is to do the research first and later look for the application. An unflattering description of the process is to call it "a cure looking for a disease." Spin-off is an intermediate case, where the aim is to find new uses for technology developed for one application. In either science-push or spin-off, the process of finding useful applications tends to be slow and to have a low yield. Efforts have been made to justify the expense of the moon flights by the spin-offs to earthly needs. The obvious rejoinder is that, if the spin-off process works so well, we might as well target the effort to the earthly needs and wait for the moon flight to come by spin-off.

Many studies have shown that the majority of successful innovations come from demand-pull rather than from technology-push or spin-off. James M. Utterback (*4*) summarized the results of eight studies which showed that three out of four innovations began with a recognition of a need and then sought a technology to meet the need. Other studies have found that the time lag for adoption of an innovation is significantly longer for technology-push than for demand-pull, usually about 15 to 20 years. (*5*) A long lapse for introduction of an innovation does not mean that the need is not there. Quite often, the technological base for application is incomplete and there needs to be more "gap-filling science" (*5*) to supply missing parts.

I don't intend to imply that all research should be directed toward recognized practical needs. It is certainly of great importance that there be excellent and well-supported basic research that is intended to explore areas where we lack knowledge or understanding, without regard to predictable uses. However, analytical chemistry is an applied science. Analyses are almost always done for very practical reasons, such as quality control in industrial production or to protect individuals from toxic materials. Even if an analytical chemist is engaged in analyzing moon rocks, he is not usually doing pure research. He may be supporting a team that is doing pure research, however. The best research in analytical chemistry is also devoted to practical ends. It sometimes happens that the research analytical chemist loses contact with the practical needs. I believe that when this happens the research tends to become sterile.

All of this does not downgrade analytical chemistry. If anything, analytical chemistry is a more demanding study than most pure sciences. A good analytical chemist must understand broad areas of science and technology that apply to chemical characterization; he must understand the science or the technology involved in the reason for doing the analysis; and he must be skilled at matching the analytical methods to the task at hand. A good analytical chemist never has the luxury of being a narrow specialist, learning more and more about less and less.

With this lengthy introduction, I return to the theme of these sessions—multielement analysis. There are needs for multielement analysis, and many of them are of scientific or technological importance. Emission spectroscopy has the inherent capacity to do multielement analyses. It is hard to say just when emission spectroscopy was first applied to measure two or more elements at once in the same sample. Perhaps it was when spectra were first recorded on a photographic plate. Before that, when all measurements were made visually and had to be one at a time, it was not usual to speak of multielement analyses. At any rate, books and articles of that early period did not dwell on this subject. For a long time, until about 1920, it was believed that quantitative analysis by emission spectroscopy was impossible, so the field languished. The rediscovery of the internal standard principle by Gerlach in 1925 changed all of that, and multielement analysis by emission spectroscopy became an accepted method. One can date the emergence of *simultaneous* multielement analysis to the development of the photoelectric emission spectrometer in the 1940's. This instrument made it possible for the first time to measure intensities of many lines at once and to have the results available within seconds after the end of the exposure. If we date research on multielement analysis from 1925, we have been doing research on this subject more than half a century. If we accept the later date, our period of research is about 35 years.

I can date my own involvement in this subject to 1954, when I worked on a five-channel flame emission spectrometer designed to measure sodium, potassium, calcium, magnesium, and strontium in biological fluids (*6*). The instrument was a technical success—it worked extremely well. I take special pride in having incorporated into it an automatic correction for background (*7*), which is now quite common but was entirely novel then. However, the instrument was a commercial failure. The reason for the lack of commercial success was quite simple: Flame photometers are used quite often to measure sodium and potassium in serum. Physicians are interested in measuring chloride at the same time as sodium and potassium,

We have the Ion Selective Electrode capability and performance you've always wanted.

Graphic Controls makes Ion Selective electrodes for fast, precise analysis of a wide range of ions, including electrodes for halides, heavy metals, cyanide and sulfide. Not only have we broadened the practical measuring range of analysis-by-electrode applications, but we've also managed major breakthroughs in performance.

For example, our new Ultra Sensitive Chloride Electrode responds to chloride in the 10 ppb range, without compromising selectivity. That's a range 25 times lower than can be measured with conventional electrodes.

This kind of performance is made possible by an important advance in electrode technology...the solid state sensing element found in all of our Ultra Sensitive Electrodes.

All our Ion Selective electrodes provide selectivity equal to or better than conventional electrodes...up to 25 times better. They assure fast, drift-free response. Bodies are of solvent resistant epoxy construction. Contacts are solid and located within the electrode body, so there's no need for filling solutions.

In addition to features like these, we're making electrode replacement easier than ever. Should any of our electrodes fail to operate properly upon receipt, just put it back in its own shipping carton, use our special "return" label and mail. We'll ship a replacement within 24 hours. It's just one more way for us to show that we care about your needs. We're on your side!

For more information, see your local GC representative. Or contact Graphic Controls, Recording Chart Division, Box 1271, Buffalo, NY 14240. 716/853-7500.

We're on Your Side

GRAPHIC CONTROLS
Recording Chart Division

CIRCLE 80 ON READER SERVICE CARD

but chloride determination is not convenient by flame photometry. There is little medical justification for measuring as a group all of the elements that can be measured in serum by flame emission. We had not bothered to ask if the technology matched the need. Even in our own laboratory, the instrument was used mainly for single-element analyses or for research on new flames. This instrument is an excellent example of technology-push.

The second instrument that I worked on (8) represents a good case of demand-pull. The measurement of enzyme activities in serum for medical diagnosis was then a new technique, but it was tying up our spectrophotometer that we needed for research. Rather than buying a new spectrophotometer, we put together a simple instrument for $20 in parts and a few hours of work. The Macalaster Scientific Corp. picked it up, and it was a reasonably successful product.

I won't dwell on my later efforts at multielement analysis. Most of them never reached a high level of technical success, and often the work was never published. My concept of the television spectrometer (9) was turned into a technical success by a group at Bell Telephone Laboratories (10), but it is still unproven that it will be a commercial success.

Most of us who have worked on multielement methods in emission spectroscopy, atomic absorption, and atomic fluorescence have had similar records. In fact, there isn't much about our current commercial emission spectrometers that is different from the designs of 30 years ago. One major design change was incorporating the computer, which is a clear case of demand-pull. The initial efforts to use on-line computers around 1960 were plagued by the limitations of computer technology of that period. In this case, the technology wasn't fully ready until several years later. I have already mentioned background correction. The only other major change that comes to mind is the introduction of vacuum spectrometry, which is also not recent.

One reason that we are honoring Velmer Fassel today is for his perseverance in introducing the induction-coupled plasma source for multielement emission spectrometry. In fact, we would not be using the plasma to any extent today if he had not persevered. His first publication on this subject was in 1965 (11), and there have been at least 16 more from his laboratory on this subject. The ICP may turn out to be one of the rare important innovations in multielement spectroscopy.

Despite the dismal record that most of us have established in achieving practical results from research on multielement analysis, we point to the few successes and use them to justify continuing to do what we know best. I think we should look for needs that are unmet or are poorly met, where we can apply our skills. I direct your attention particularly to the needs for simultaneous determination of several compounds, which can be met in many cases by molecular spectroscopy. If you want to find useful applications, you need only to read the literature on chromatography. Gas chromatography was a rapidly growing area of analytical chemistry a few years ago, and now liquid chromatography is growing in importance each year. Both methods enable the analytical chemist to determine several compounds in a sample. However, chromatography is slow by our standards. A typical chromatographic run takes about a quarter of an hour. There are some as short as one minute, but that is a rare exception. Many require an hour or more. Emission spectroscopists are accustomed to determining up to two dozen elements in a sample in less than a minute. Could we not apply that measuring skill to the determination of compounds?

In fact, there is ample historical backing for this idea. Starting in the 1940's and continuing for several years, there was important use of infrared and Raman spectrometry for multicomponent analyses, especially of hydrocarbon mixtures. Mixtures with up to 10 components were analyzed (12–15).

Why did the use of molecular spectrometry for multicomponent analyses die out? I think there are two reasons. First of all, chromatography evolved as a better way to analyze complex mixtures of hydrocarbons, which was the main application for the infrared and Raman methods. Secondly, the instrumentation of that time for the spectrometric methods wasn't adequate. Raman spectrometry was very slow and required fairly large samples. Infrared spectrometers had poor signal-to-noise ratios. The computations had to be done on analog computers since digital computers were scarce and expensive. All of these technical limitations have since been overcome. However, I am not aware of recent studies on analysis of complex molecular mixtures by infrared and Raman, except for work in the near infrared.

Karl Norris at the Department of Agriculture in Beltsville, Md., worked for several years on the near-infrared analysis of food materials (16). Analytical chemists have still not become much aware of this work, but the technique is already having a major impact in some important parts of agriculture. In what is so far the most impor-

All you've ever desired in a spectrophotometer

Introducing Hitachi's Computerized Double-Beam, Ratio Recording, UV-Visible Spectrophotometer

The Model 100-80 is not just a UV-Visible spectrophotometer but a spectrophotometric system. Many operating features which are standard equipment on the Model 80 have been previously available only as expensive hardware accessories. The highly advanced and unique software design provides methods and techniques of acquiring, processing and presenting photometric data never before available in a spectrophotometer.

Check These Standard Features

Wavelength Scanning • Repetitive Scanning • First & Second Derivatives • Auto/Manual Printing • Wavelength Programming • Time Scan Recording • Auto Zero • Automatic Baseline Correction • 5 Point Curve Correction • Temperature Readout Self Testing • Integration plus a wide variety of useful hardware accessories and extended software programs.

All this at an affordable price!

Let us prove what a truly outstanding instrument the Model 80 is. Send for more information or request a demo. HITACHI NSA Scientific Instruments, 450 E. Middlefield Road, Mountain View, CA 94043, (415) 969-1100.

HITACHI NSA
SCIENTIFIC INSTRUMENTS

CIRCLE 151 ON READER SERVICE CARD

tant application, a sample of grain, such as wheat, corn, or soybeans, is ground to a powder and packed into a cup. The sample cup is placed in a filter reflectance spectrophotometer, and the instrument measures reflectance at six wavelengths in the near infrared. The instrument then solves three simultaneous equations to compute percentages of protein, oil, and moisture in the grain. The whole procedure takes about one minute.

When I heard of Norris' work in 1973 and saw what it could do, I predicted that in a few years the instruments would be used to analyze grain when the farmer brings it for sale to the grain elevator. That procedure has now been proven, and is becoming commonplace. On a routine basis, these near-infrared instruments are measuring one compound (water) and two groups of compounds (protein and oil) in complex matrices. Furthermore, the precision of analysis is proving to be at least as good as the precision of the reference methods, even when the near-infrared instruments are operated by persons who have no previous experience in chemical analysis.

My initial doubt about Norris' method has proved to be the common reaction of analytical chemists. Fortunately, Karl Norris didn't believe that it was impossible to do analyses this way. Also, nobody told him that it is impossible to determine individual amino acids by near infrared reflectance. Norris and a Canadian colleague, Phil Williams, have tackled that problem. They have not yet published their results, but they claim to have made reasonably accurate determinations of the total amino acid content of grains from the near-infrared reflectance analysis of powders (17).

These recent successes should encourage us to look again at the needs and opportunities for the analysis of complex mixtures of organic compounds by spectrometry. There have been dramatic improvements in molecular spectrometer design and in computers, the essential hardware components. What is lacking is applications research and perhaps an adequate understanding of parts of the theory. I think that spectroscopists with experience in multielement analysis can bring a great deal of their knowledge to this important field.

References

(1) "Federal Technology Transfer. Directory of Programs, Resources, Contact Points," Federal Council for Science and Technology, Committee on Domestic Technology Transfer, June 1975. Superintendent of Documents, U.S. Government Printing Office, Washington, D.C. 20402.
(2) J. R. Bright, "Technological Forecasting for Industry and Government," pp 272–75, Prentice-Hall, Englewood Cliffs, N.J., 1968.
(3) J. P. Martino, "Technological Forecasting for Decisionmaking," pp 382–95, American Elsevier Publ. Co., New York, N.Y., 1972.
(4) J. M. Utterback, *Science*, **183**, 620 (1974).
(5) T. J. Allen, "Managing the Flow of Technology," pp 46–57, MIT Press, Cambridge, Mass., 1977.
(6) B. L. Vallee and M. Margoshes, *Anal. Chem.*, **28**, 175 (1956).
(7) M. Margoshes and B. L. Vallee, *ibid.*, p 1066.
(8) R. E. Thiers, M. Margoshes, and B. L. Vallee, *ibid.*, **31**, 1258 (1959).
(9) M. Margoshes, *Spectrochim. Acta*, **25B**, 113 (1970); *Opt. Spectra*, **4**, 26 (1970).
(10) D. L. Wood, A. B. Dargis, and D. L. Nash, *Appl. Spectrosc.*, **29**, 310 (1975).
(11) R. H. Wendt and V. A. Fassel, *Anal. Chem.*, **37**, 920 (1965).
(12) A. L. Smith, in "Treatise on Analytical Chemistry," I. M. Kolthoff and P. J. Elving, Eds., p 3695ff, Pt. I, Vol. 6, Interscience Publ., New York, N.Y., 1965.
(13) E. J. Rosenbaum, *ibid.*, p 3761.
(14) R. B. Barnes and R. C. Gore, *Anal. Chem.*, **21**, 7 (1949).
(15) R. P. Bauman, "Absorption Spectroscopy," pp 403ff, 545ff, J. Wiley & Sons, New York, N.Y., 1962.
(16) C. A. Watson, *Anal. Chem.*, **49**, 835A (1977).
(17) P. Williams, private communication.

MCB: THE SOURCE

for thousands of high purity reagents

MCB Reagents is the source for the finest in high purity, technologically advanced chemicals for use in analytical research, and industrial and clinical science.

To locate the reagents you need, consult the new 1979 MCB Buying Guide. It contains 600 pages of easy-to-find and easy-to-read product listings.

Included are special sections on EM Chromatography products, featuring the world famous LiChrosorb® sorbent line and Hibar®-II HPLC Columns; MCB Schuchardt Organics for Synthesis; specialized products, including Suprapur® Density Gradient Chemicals; and a full line of dyes and stains, acids, organics, and inorganics from reagent to high purity grade. Also in this edition, MCB is proud to introduce OmniSolv™, our brand new high purity, glass-distilled, multipurpose solvent line.

Reserve your free copy of the 1979 MCB Buying Guide by writing to us on your letterhead, or by circling the inquiry number below.

It's your link to the source of the highest quality chemicals available, from MCB Reagents.

MCB REAGENTS

MCB Reagents, Associate of E. Merck, Darmstadt, Germany, 2909 Highland Avenue, Cincinnati, Ohio 45212

CIRCLE 143 ON READER SERVICE CARD

Lanier introduces the No Problem™ typewriter for your technical typing.

Want to get your typing back faster than ever before? **NO PROBLEM**

Want to type Greek and math symbols right on the screen? **NO PROBLEM**

Want to type and edit multi-level equations with typewriter simplicity? **NO PROBLEM**

Want to add line drawings and charts to the page? **NO PROBLEM**

Most typewriters – even many of the latest electronic models – are limited to basic typing.

But the Lanier No Problem Electronic Typewriter is multi-use, with extraordinary powers for technical and scientific typing.

No Problem typing – a better way to type.

The No Problem concept

To begin with, the No Problem typewriter speeds up the typing of your proposals, manuals, and reports like no ordinary typewriter can.

It eliminates typing rough drafts on paper. Pages are prepared on a TV-like screen instead.

Changes and corrections are made right on the screen. So no whiteouts. No retyping. No false starts. Whole paragraphs can be moved with the touch of a few keys.

Letter quality printing is done at up to 540 words per minute.

Want to type Greek and math symbols right on the screen? **No Problem**

Want to type and edit multi-level equations with typewriter simplicity? **No Problem**

See the Lanier No Problem™ Electronic Typewriter in action.

YES, I want to see Lanier's unique demonstration of the *No Problem's* capabilities. Please arrange to have someone call for an appointment.

NAME_____ TITLE_____

PHONE_____ BEST TIME TO CALL_____

FIRM NAME_____ ADDRESS_____

COUNTY_____ CITY_____ STATE_____ ZIP_____

What kind of typing or word processing system are you using now?_____ 4 E 15 K9

Or call toll free: **(800) 241-1706** (except in Alaska or Hawaii). Georgia residents call collect: **(404) 321-1244.**

NO POSTAGE
NECESSARY
IF MAILED
IN THE
UNITED STATES

BUSINESS REPLY MAIL
FIRST CLASS PERMIT NO 2021 ATLANTA, GA

POSTAGE WILL BE PAID BY ADDRESSEE

Lanier Business Products
1700 Chantilly Drive NE
Atlanta, Georgia 30324

With the No Problem typewriter, one typist can now do work as fast as 3 or 4 people using ordinary electric typewriters.

Plus, the basic intelligence for the No Problem typewriter is contained on No Problem Smart Discs.™ So future functions and improvements can be added with new Smart Discs as they are developed.

One typewriter or a shared system

The No Problem Shared System™ offers you even greater typing capabilities.

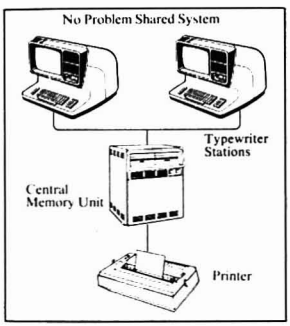

The No Problem Shared System™ adds new capabilities to the already versatile No Problem concept.

The heart of the system is the Central Memory Unit. It can store up to 30,000 pages, giving you lower storage costs per page, and eliminating the need for typists to handle numerous discs.

You can start with one or two typewriter stations connected to the Central Memory Unit, and add typewriter stations or printers as your needs increase.

There is also an attractive economic factor in sharing printers and other equipment.

Advanced features

Consider the old method of incorporating complex mathematical equations into your copy: leave the space blank, then hand letter them in after the page was typed. Or, you could run to the photocopier, then "cut and paste."

With the No Problem Shared System, you can incorporate *and edit* virtually any equation you may encounter—*right on the screen.* It will display *256 different characters,* including Greek and math symbols.

Line drawings can be constructed on the No Problem screen, too.

The No Problem Shared System automatically selects left, right or center page position for numbers, and chapter names on even and odd pages. Repagination automatically updates section numbers to accommodate your additions and deletions.

Advanced editing automatically positions footnotes on the proper page.

And the printing of the No Problem Shared System approaches typeset quality and flexibility. Proportional and bold printing, to fit any format or width, is easily done. Even in two typestyles and two colors on the same page at the same time.

Most of all, the No Problem Shared System can improve your cost/performance ratio dramatically with its increased workpower.

Modular design protects your investment

You can add Shared System typewriter stations, standalone No Problem typewriters, printers and Smart Discs to your office at will.

So your investment will *continue* to be a money-making problem solver as long as you own the equipment.

The No Problem demonstration

Your Lanier representative won't waste your time with a memorized sales pitch.

We would rather show you how No Problem typing can solve *your* problems.

Send us this coupon and we'll call immediately to set up an appointment. Or call toll free **(800) 241-1706.**

Except in Alaska or Hawaii. In Georgia, call collect (404) 321-1244.

The No Problem Electronic Typewriter from LANIER®

LANIER BUSINESS PRODUCTS, INC.

It does more than just type.

CIRCLE 126 ON READER SERVICE CARD

Want to see Lanier No Problem typing in action? NO PROBLEM.

Send us the information below and a Lanier representative will call for an appointment.

Name _____ Title _____

Phone _____

Best Time To Call _____

Firm Name _____

Address _____ County _____

City _____ State _____ Zip _____

What kind of typing or word processing system are you using now? _____

Lanier Business Products, Inc.
1700 Chantilly Dr. NE, Atlanta, GA 30324

 4 E 15 K9

CARBON
IN
ORGANICS AND INORGANICS

LECO® CR-12 Carbon Determinator

Range: 0.05 to 100% Sample size: 0.15 to 1.0 gram

Graphite Coal Hydrocarbons
Carbonates and organic compounds

- **Infrared detection**
- **Two minute analysis**
- **Integral balance & printer**

CONTACT LECO® TODAY!

LECO CORPORATION 3000 Lakeview Ave. St. Joseph, MI 49085, U.S.A. Phone: (616) 983-5531
Offices: California (714) 957-8227 • Texas (713) 931-0000 • Pittsburgh (412) 776-4891 • Canada (416) 270-6610 • Mexico City (905) 658-1877

LECO®

CIRCLE 129 ON READER SERVICE CARD

Hg Mercury Toxicity

Polarographers and other analytical chemists in contact with elemental mercury will be interested in the results of research on mercury toxicity reported on at the American Chemical Society Great Lakes Regional Meeting in Rockford, Ill., June 4, 1979, by a group of researchers from the American Dental Association Health Foundation Research Institute in Chicago, Ill. Two of the researchers have also prepared an extensive review chapter on Hg toxicity for a book to be published next year.

The American Dental Association Health Foundation group consists of D. J. Merdian, R. C. A. Chen, C. Siew, G. S. Rao and J. J. Hefferren. The first four researchers presented the Great Lakes paper, while Rao and Hefferren wrote the review chapter. The group's interest in Hg toxicity stems from the wide use of Hg based alloys in the restoration of teeth in current dental practice. Recent surveys suggest that one of 10 dental offices in the U.S. may be in technical violation of the Hg exposure limit as recommended by the National Institute for Occupational Safety and Health (NIOSH) at 0.05 mg Hg/cubic meter of air determined as a time-weighted average for an 8-hour work day.

At the Great Lakes Meeting, Merdian, Chen, Siew, and Rao reported that the most common signs of chronic exposure to high concentration Hg vapor are tremor, kidney and gastrointestinal disturbances, metallic taste, insomnia, and erethism, among others. Erethism is a peculiar form of emotional instability specific for Hg intoxication. The researchers exposed mice to Hg vapor (0.2 mg/m^3, 24 hours/day, continuously for seven days), and sacrificed them over a period of almost two months to determine time-dependent Hg concentration in blood, brain, heart, kidney, liver, lung, and testis.

On day zero after the seven day exposure period, the highest amount of Hg was found in kidney (92.15 μg/g), followed by brain (41.85 μg/g). Hg levels in the remaining tissues and blood were relatively low. Hg levels in all tissues except brain rapidly disappeared, and by day 56 after exposure no Hg could be detected. In contrast, brain Hg levels remained relatively steady up to 28 days after exposure and nearly 26% of the original Hg taken up by brain was retained on day 56 after the exposure. The researchers concluded: "These results clearly indicate that the central nervous system (CNS) is most susceptible to the toxic effects of trace Hg vapor exposure."

The review chapter, "Toxicity of Mercury," by Rao and Hefferren, will appear in the book, "Biocompatibility of Dental Materials," Volume IV of the Uniscience Series on "Biocompatibility," CRC Press, Inc., West Palm Beach, Fla. (in press, 1980). Rao and Hefferren report that Hg's vapor pressure is 2×10^{-3} mm at 25 °C., and that the equilibrium vapor concentration of Hg in a room at 25 °C. is calculated to be 20 mg/m^3. Its vapor pressure increases rapidly as temperature rises: There is about an eight-fold increase when the temperature rises from 20 to 50 °C.

Rao and Hefferren point out that Hg spilled on the floor is the major cause of Hg contamination in the dental office environment. The spilled Hg disperses into small droplets which increases its surface area and thus its vaporization. Hg droplets can collect in carpets and floor cracks making them inaccessible during routine office cleaning. Prompt cleanup after a spill and covering up any inaccessible spillage with powdered sulfur, calcium polysulfide, or activated alumina is recommended. Scrap Hg should be

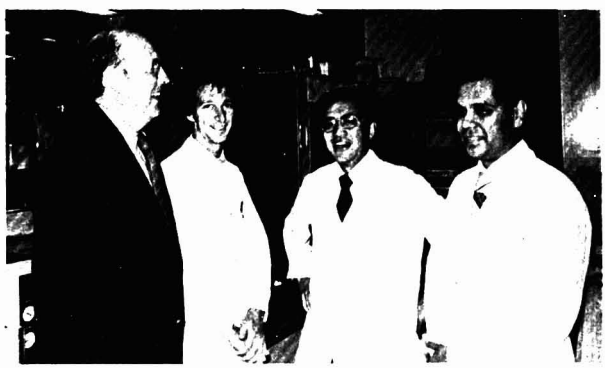

John J. Hefferren, Dennis J. Merdian, Chakwan Siew, and G. Subba Rao (left to right) in the Pharmacology-Toxicology Laboratory of the Division of Biochemistry at the American Dental Association Health Foundation Research Institute in Chicago. Hefferren is Director of the Institute, Merdian is a Research Assistant, Siew is Head of the Toxicology Laboratory, and Rao is Director of the Division of Biochemistry and Head of the Pharmacology Laboratory. The Hg toxicity studies are supported by research grants to Rao from the American Fund for Dental Health

stored under water or bacteriostatic solution. The fact that Hg vapor has been detected within 30 minutes after covering amalgam scrap with water emphasizes the need for tightly sealed containers for storage.

Employers are legally responsible under the Occupational Safety and Health Act of 1970 for maintaining Hg vapor concentration at a safe level. The Occupational Safety and Health Administration (OSHA) enforces a standard of 0.1 mg Hg/cubic meter of air in the workplace. Booklets on Hg health hazards and workers' rights may be obtained by writing to OSHA Publications, Room N3423, Occupational Safety & Health Administration, Washington, D.C. 20210. Single copies of "Mercury" (OSHA 2234) and "Worker's Rights Under OSHA" (OSHA 2253) are free.

Rao and Hefferren point out that there currently exists no simple clinical diagnostic test which can be correlated with Hg exposure hazards. Since the major concern is chronic exposure to elemental Hg vapor, any resulting adverse effects may not be manifested in readily measurable clinical signs and symptoms until a threshold limit is reached after many years. These threshold limits may vary among individuals depending on their body capacity to handle the Hg. While the CNS is considered the most likely target organ to be affected by chronic trace Hg inhalation exposures, these effects are the least quantifiable using current objective clinical measurements. Rao and Hefferren conclude that more research is needed in this important area to develop sensitive, reliable and practical methods of measuring any such effects of Hg exposure.

Monitoring for Hg, on the other hand, is now rather straightforward, thanks to the commercial availability of personal monitoring badges and dosimeters, as well as portable detectors. The badges and dosimeters contain gold, to which Hg adsorbs quantitatively. Quantitation is based on a change in conductivity that can be measured as the Hg-Au amalgam forms. The badges and dosimeters are worn by individual workers, and subsequent analysis provides information on time-weighted average (TWA) concentrations, usually on a daily basis.

Jerome Environmental Monitoring Service (P.O. Box 455, Concord, N.H. 03301) manufactures a gold coil dosimeter to be utilized with a low-flow pump. Gold film monitoring badges are available from 3M Company's Occupational Health & Safety Products Division (3M Center, Saint Paul, Minn. 55101). Badges and dosimeters may be returned to the companies after exposure, whereupon individual Hg vapor exposures and TWA concentrations will be determined. This service is quite cost-effective for short-term or one-shot Hg vapor concentration studies. Jerome also markets a complete analytical system for monitoring workplace environments and personnel exposure, which includes personal dosimeters and a portable detector for quantitation.

A. J. Sipin Company, Inc., 425 Park Avenue South, NY, N.Y. 10016, also provides personal Hg dosimeter service. The Sipin badges contain a specially treated sorbent capable of absorbing Hg vapor, which is subsequently analyzed by flameless atomic absorption spectrometry.

A variety of portable Hg vapor detectors and analyzers are currently marketed by the major instrument companies and companies specializing in the analysis of environmental pollutants. A copy of the list of companies that market Hg vapor analyzers and provide personal Hg monitor (badge) service may be obtained from Dr. G. S. Rao, ADAHF Research Institute, 211 E. Chicago Avenue, Chicago, Ill. 60611. A combination of personal Hg monitoring badge and Hg vapor analyzer is appropriate for extended studies on potential Hg vapor exposure in the laboratory or workplace.

NIOSH recommends a warning sign be posted in any work area where there is potential exposure to Hg: "WARNING! MERCURY. High Concentrations are Hazardous to Health. Maintain Adequate Ventilation."

Self-Testing of Blood Glucose Helps Diabetics

In recent tests at a major New York research center, diabetic patients were encouraged to do a little analytical biochemistry—on themselves. The research, conducted at the Rockefeller University by Charles M. Peterson and his colleagues [*Diabetes Care*, **2**, 329–35, 1979], has demonstrated the feasibility of improved blood glucose control with self-analysis.

Traditionally, patients have monitored their blood sugar levels with laboratory blood tests and urinalyses. The former are slow and expensive, and urinalysis will only indicate a hyperglycemic condition when blood sugar is so high it has exceeded the kidneys' ability to filter it out. Dr. Peterson points out that trying to maintain a proper blood sugar level with urinalysis is a little like trying to drive a car at a speed of 30 mph when the speedometer only works at 70 mph or greater.

The self-administered test for blood glucose is a product of enzyme research, and has led to an improvement in the ability of patients to routinely correct for abnormalities in their blood glucose levels with an accuracy that was not formerly possible. Doctors hope that such self-analysis will greatly facilitate regulation of diabetes and increase the likelihood of the attainment of a degree of control approximating euglycemia, a normal

The Rockefeller University on Manhattan's East Side as seen from the air

blood sugar level. Many physicians believe an improved ability to prevent swings in blood sugar may prevent the usual complications of diabetes, including heart disease, blindness, cataracts, blood vessel damage, nerve disorders, and kidney damage.

Such improvement in control is afforded by the use of reagent strips produced by a number of manufacturers. In one type of reagent strip, a drop of blood is placed on a semi-permeable membrane. Blood cells do not pass through the membrane, but blood filtrate is exposed to the reagent system underneath. Glucose oxidase in the reactive area dissolves in the filtrate, converting any glucose present to gluconic acid. Hydrogen, removed from the glucose in the glucose oxidase reaction, combines with atmospheric oxygen to form hydrogen peroxide. In the presence of peroxidase, the hydrogen peroxide oxidizes chromogen indicator, producing gray to blue-purple colors. The color may be visually compared to a color chart or analyzed in a reflectance colorimeter.

In the Rockefeller University study, patients were taught to monitor their own blood glucose with the reagent strips and were encouraged to maintain their blood glucose level between 70 and 140 mg/dL. They were also taught to calibrate exercise, food, and insulin in terms of their effects on blood glucose levels. For example, a given type of candy would be found to increase a patient's blood sugar by about 20 mg/dL. The patient could then use three of these candies to correct a hypoglycemic episode. Patients were encouraged to perform similar experiments with various types of foods. And blood glucose response to exercise and to particular doses of insulin was tested in a similar fashion by each patient. They were encouraged to perform blood tests before and one hour after each meal and to adjust their glucose levels when necessary with the variables at their command.

At the end of the study, Peterson concluded that improved control of blood glucose through the program of patient-monitored blood sugar had been demonstrated and that systolic blood pressure, alkaline phosphatase concentration, and nerve conduction abnormalities had been ameliorated. Peterson also suggested that the program was cost effective through the avoidance of diabetes-related hospitalizations that would occur in the absence of the close control made possible by the patient self-monitoring.

As Peterson puts it, "It gives people a chance to do something about their condition. That's what makes people with chronic diseases depressed—the sense of helplessness and hopelessness that comes with any chronic disease."

Now when you think powerful IR analysis, think compact.

Presenting the Beckman Microlab™ 620 MX Computing Infrared Spectrophotometer. An incredibly powerful and versatile analytical instrument designed in a uniquely compact and easy-to-operate configuration.

There is nothing else like it. Packed into its three-foot frame is the analytical horsepower of a mainframe external computer, floppy disk data storage center, and totally preprogrammed and interfaced software systems.

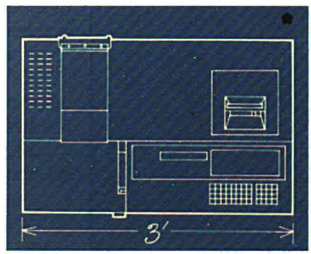

Besides drastically reducing space requirements, the Microlab 620 also slashes cost, lab work time and training requirements.

The more you use the Microlab, the more powerful it becomes. It can analyze, code and store a virtually unlimited number of spectra for qualitative comparison. It does sample identification without the need for separation. Plus, the Microlab memorizes and recalls at the push of a button a virtually unlimited number of quantitative protocols.

No matter what your area of analysis or range of applications, the Microlab's spectral library can be personalized to meet your lab's needs.

The Microlab also features multiple data output, fully automatic operation, repetitive scan and a whole lot more.

So if you think unlimited analytical capability requires unlimited space, money and time, think again. Then call your local Beckman representative for the full story on the Microlab 620 MX. Or write: Scientific Instruments Division, Beckman Instruments, Inc., P.O. Box C-19600, Irvine, CA 92713.

Innovation in IR since 1940

BECKMAN

CIRCLE 19 ON READER SERVICE CARD

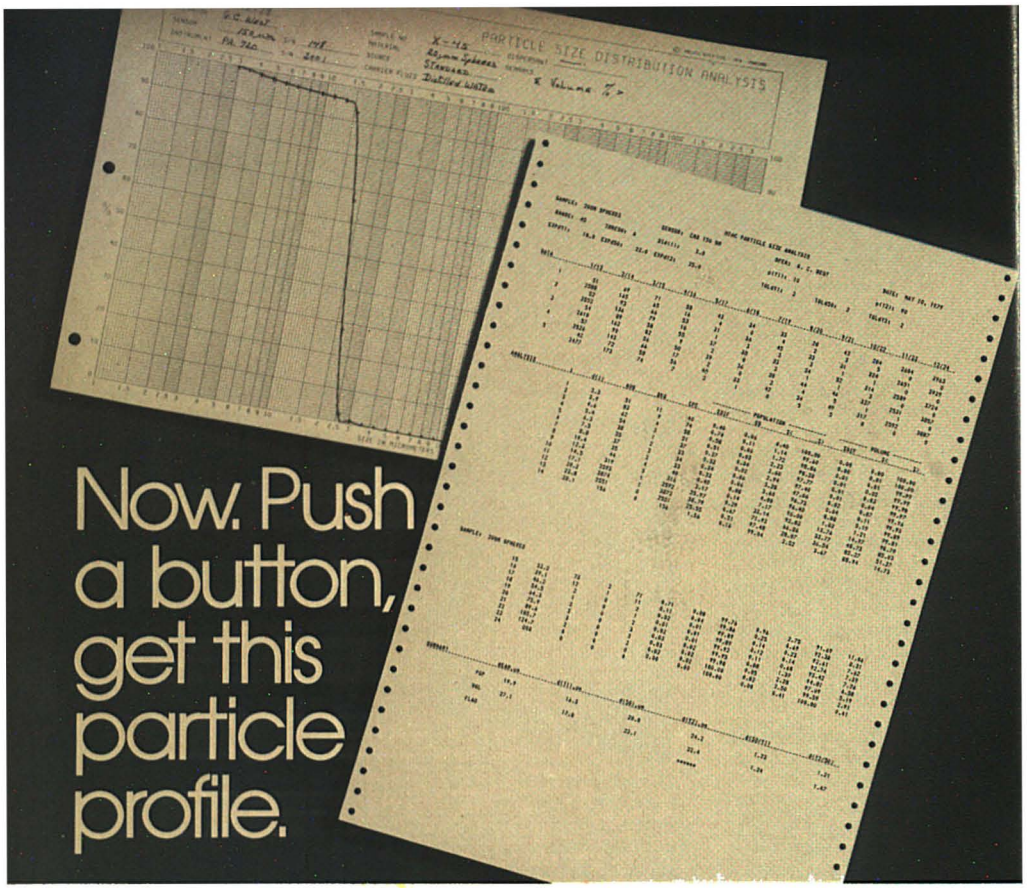

Now. Push a button, get this particle profile.

With any carrier, liquid or dry, the new HIAC PA-720 delivers the most comprehensive particle size analysis a single system can give you.

HIAC's new PA-720 Particle Size Analysis System counts, sizes, analyzes, summarizes. It computes, prints and plots. It gives you expanded-scale close-ups. Its powerful microprocessor provides insight into particle population and volume (weight) distribution *in any carrier.* Immediately.

In applications across the board—research, materials control, production control—the HIAC PA-720 overcomes long-standing restrictions. Your powder sample can be analyzed in water, alcohol, air, inert gases, solvents—even viscous oils. No electrolyte is needed. State-of-the-art light-blockage sensors size and count particles one at a time from 1μm to 2500μm with 24-channel characterization. And calibration is assured by traceability to NBS and ISO.

Multiple Data Outputs. Both printed and plotted size distribution data is provided. Replicate runs are automatically averaged and key information summarized. Included are particle diameters, background-corrected counts, standard deviation, and statistical profile by number and volume (weight). X-Y plots are presented in any of six modes. And you can pre-set values for production control, and be alerted when tolerances are exceeded.

No other system tells you so much about so broad a range of samples in so wide a choice of carriers. And no other system works so precisely, so quickly, so easily.

Ask us to show you. Write or call for literature and a free demonstration on your material, in your lab. See how simple particle size analysis has just become.

HIAC PA-720 Particle Size Analysis System: from right, vacuum sampler, analyzer-data processor, data printer, plotter. Pressure sampler and dry sample feeder also available.

Pacific Scientific® HIAC™ INSTRUMENTS DIVISION

P.O. Box 3007, 4719 West Brooks Street, Montclair, CA 91763; Phone: (714) 621-3965
Pacific Scientific Inc., Hauptstrasse 132, P.O. Box 69, CH-4450 Sissach, Switzerland; Phone: 061-984405

CIRCLE 169 ON READER SERVICE CARD

Pittsburgh Conference

Atlantic City, N.J.
March 10–14, 1980

"New Look in Analytical Chemistry and Applied Spectroscopy" is the theme of the 31st Pittsburgh Conference on Analytical Chemistry and Applied Spectroscopy, which will be held in the Atlantic City Convention Center, Atlantic City, N.J., on March 10–14, 1980. The 90 technical sessions scheduled include 16 planned symposia and a total of 800 papers. The Exposition of Modern Laboratory Equipment will feature more than 400 exhibitors in over 1000 booths showing the newest analytical instrumentation and related chemicals. This year the exhibits and technical sessions will continue simultaneously from Monday morning until Friday noon.

The following symposia have been arranged and will be presented as part of the technical program:

Advances and Applications of High Resolution Chromatography, arranged by Curt White, U.S. Department of Energy, and William Suits, Varian Instrument Division

Therapeutic Drug Monitoring, arranged by Rita Windisch, Mercy Hospital

Practical Solutions to Quantitative Capillary Gas Chromatography, arranged by John Q. Walker, McDonnell Douglas Research Laboratories, and William Suits, Varian Instrument Division

Analytical Support for Bioassay Involving Mutagenicity and Carcinogenicity, arranged by Robert W. Freedman, U.S. Bureau of Mines

Safe Drinking Water, Legislation, and Related Chemical Analysis, arranged by Robert W. Freedman, U.S. Bureau of Mines

Preparative Liquid Chromatography—New Support for the Analyst, Synthesist, and Spectroscopist, arranged by Peter C. Talarico, Waters Scientific Limited

ASTM E-42 Advances in Quantitative Surface Analysis of Materials, arranged by Yale E. Strausser, Hewlett-Packard

Ion Beams and Synchrotron Radiation for Surface Analysis, arranged by David M. Hercules, University of Pittsburgh

Analytical Instrumentation—Evolution in the Last 40 Years, arranged by Joseph Feldman, Duquesne University and L. Ettre, Perkin-Elmer Corporation

Innovations in Mass Spectrometry, arranged by Frank W. Plankey, University of Pittsburgh, and Ben Freiser, Purdue University

The Current State of Analytical Voltammetry, arranged by Howard Siegerman, EG&G Princeton Applied Research

Licensing, Accreditation, & Regulation: The Impact of Government on Analytical Chemistry, arranged by Gerst Gibbon, U.S. Department of Energy, and Harold Sweeney, Koppers Company, Inc.

Quality Assurance in Trace Organic Environmental Measurements, arranged by David H. Freeman, University of Maryland, and William Suits, Varian Instrument Division

Herbert A. Laitinen will receive SACP special award for his significant contributions to the field of analytical chemistry

Computer Software for Scientists, arranged by Frank W. Plankey, University of Pittsburgh

Dal Nogare Award Symposium, arranged by Mary E. Kaiser, E. I. Du Pont

Coblentz Award Symposium, arranged by Ira Levin, National Institutes of Health

The Society for Analytical Chemists of Pittsburgh (SACP) will present a special award to Herbert A. Laitinen, Editor of ANALYTICAL CHEMISTRY and Graduate Research Professor at the University of Florida in Gainesville, for his outstanding contributions to the field of analytical chemistry, his excellence in teaching, his editorial contributions to ANALYTICAL CHEMISTRY, and for the example he has set for the younger generation of analytical chemists. Dr. Laitinen's research interests include electroanalytical chemistry, with emphasis on surface chemistry, molten salt chemistry, and environmental chemistry.

The Spectroscopy Society of Pittsburgh will present its 1980 Spectroscopy Award to Harold J. Bernstein, who recently retired from the National Research Council of Canada. Dr. Bernstein had a distinguished 32-year career in infrared and Raman spectroscopy and nuclear magnetic resonance. He will be cited for his contributions in these fields and on a variety of other subjects, including vibrational spectra and assignments, Raman techniques and spectra, the resonance Raman effect, internal rotation and the energy of differences between rotamers, NMR spectroscopy, and bond properties and physical properties of molecules.

Other awards to be presented during the Conference will be listed in the Conference preliminary program in December. The social program and technical tours will also be listed in the preliminary program.

Advanced registration is urged. Registration forms mailed before February, 1980, will be processed so that a badge, vouchers for the final program, abstracts, and souvenir are mailed to the conferees. Registration fees are $10 for advanced registration, $20 for registration at the Conference, and $3.00 for students. A pocket admission tab for the exposition only will be available free of charge. Registration forms may be obtained from the preliminary program or by writing to Dr. Frank W. Plankey, Department of Chemistry, University of Pittsburgh, Pittsburgh, Pa. 15260. Return the completed registration form and the $10 fee to Dr. Plankey.

Housing forms may be obtained from the preliminary program or by writing to Mr. Ralph Raybeck, 4376 Frank St., Pittsburgh, Pa. 15227.

An employment bureau will be available to all registrants without charge. Job candidate and employer forms are available from Mrs. Marilyn V. Senneway, 405 Carmel Drive, Aliquippa, Pa. 15001.

The Spouses Program will be listed in the preliminary program. Additional information can be obtained from Mrs. Louise A. Manka, 1109 Lancaster Ave., Pittsburgh, Pa. 15218.

Conference preliminary programs will be mailed to the conferees who attended the Pittsburgh Conference during the past three years. Prospective conferees should write to Mrs. Linda Briggs, Program Secretary, 437 Donald Rd., Pittsburgh, Pa. 15235, for a copy of the program.

Further information on the meeting can be obtained from Dan P. Manka, Publicity Chairman, 1109 Lancaster Ave., Pittsburgh, Pa. 15218.

Helen Free Wins Garvan Medal

Helen Free, called "a pioneer in the field of diagnostic chemistry" and "an outstanding scientist, author, and teacher" by her colleagues, is the winner of the 1980 Garvan Medal sponsored by W. R. Grace & Company. The Medal is given to recognize distinguished service to chemistry by women chemists, and consists of $2000, an inscribed gold medal, and a bronze replica of the medal.

Free has been employed at Miles Laboratories and at their Ames Company division continuously for the last 25 years. During that time her work in research and development of convenient test systems involving chemical reagents and accompanying instrumentation has led to a great number of publications and patents.

Helen Free

Her work led to the expansion of the convenient tablet tests for urinalysis begun in the early 1940's by Dr. Walter Compton, and to the introduction and expansion of dip-and-read tests for various urinary constituents, now used as standard test procedures in clinical laboratories throughout the world.

After a successful two-decade career in the laboratory, Free has more recently chaired New Product Management Committees at Ames which, under her supervision, have introduced over 40 new products and product improvements. These have included chemical reagents, microbiology reagents, and instrumentation for blood chemistry, histology, and cytology, as well as urine study.

Free has taught biochemistry and a course on body fluids for medical technologists at Goshen College, and a continuing education course on management at Indiana University in South Bend. Most importantly, she has defined new teaching techniques for teachers of clinical chemistry, medical, and medical technology students, and has conducted creative workshops in clinical studies in the U.S., India, Pakistan, and Malaysia. Helen and Alfred Free are coauthors of "Urinalysis in Clinical Laboratory Practice" (1975), considered a classic in its field.

"By her own example," states a colleague, "she has championed the cause for women in science and serves as an excellent role model for others to follow."

Once you pick up the new Thomas catalog, you won't want to put it down.

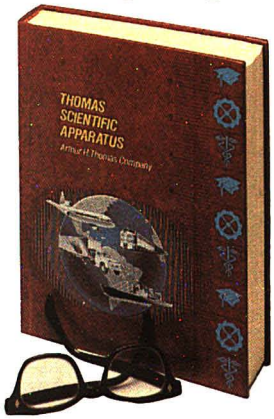

The plot of this book is very interesting but it's no mystery. It's clearly to make lab apparatus shopping easier for you.

This 1980 edition lists 19,192 apparatus items—3,344 new since the last catalog printing—and 2,868 reagents. There's a total of 1,512 pages of valuable purchasing information about products from many manufacturers, including our own brands.

The Thomas catalog format is similar to an encyclopedia's. Items are listed alphabetically and assigned numbers. The lowest number is the first item listed and the highest is the last item. Number, product name and price are on a single line.

In addition, the catalog has clear, detailed product descriptions with photographs or sketches and, occasionally, a diagram to give you a better understanding of the item.

When you need laboratory apparatus, our catalog will provide the information you require to shop more intelligently. For your free copy, write us on your company letterhead. Arthur H. Thomas Company, Vine Street at Third, Philadelphia, PA 19106.

ARTHUR H.
THOMAS
COMPANY
Serving labs the world over since 1900

CIRCLE 208 ON READER SERVICE CARD

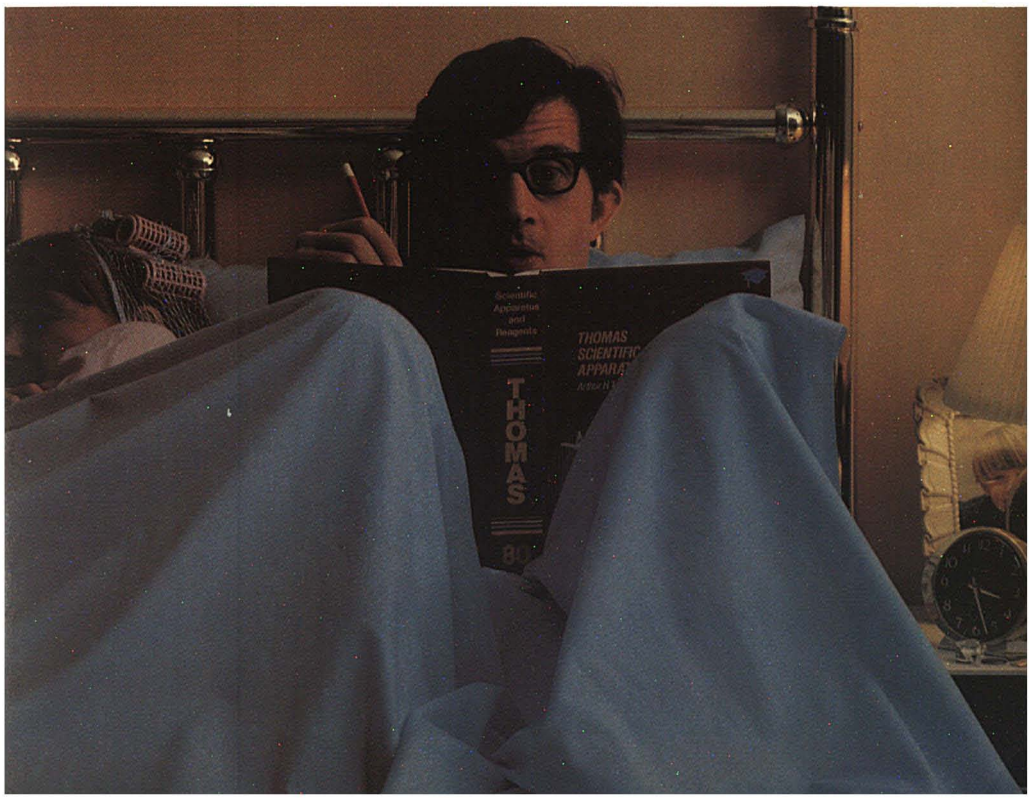

Delta Range Delta Range Delta Range

The movable fine range that simplifies precision weighing.

This photo of the new PC4400 balance demonstrates one of the great benefits of DeltaRange. Here's a big-capacity balance—4000 g—weighing a drop of fluid with .01 g readability, although the balance already has nearly 1000 g tared into it.

It is weighing the drop on the 400 g DeltaRange. If you press the control bar, the full 400 g fine range will be available again. And again. And again. Items that weigh more than 400 g will get a result with .1 g readability.

You can really appreciate DeltaRange if you've ever run out of range when weighing formulas. And you'll appreciate it if you're tired of going from one balance to another to weigh heavy and light items. This one balance can do all your weighing.

Because PC Series balances are available with a plug-in microprocessor-based Application Input Device, they can save time when you need to count small parts, measure moisture loss in percent, do reference comparison weighing, or to highlight intermediate and final results during compounding or formula weighings. The device accepts keys that program the balance for each function.

Mettler PC balances are available in several capacities/readabilities. Contact your Mettler dealer—or write for a brochure to Mettler Instrument Corporation, Box 71, Hightstown, NJ 08520.

Mettler

CIRCLE 153 ON READER SERVICE CARD

Correction: In the IR spectrum shown in Figure 6 in THE ANALYTICAL APPROACH, September, page 1129 A, the curve itself was inadvertently rotated by 180 degrees in the plane of the paper.

Call for Papers

12th Annual Symposium on Advanced Analytical Concepts for the Clinical Laboratory
Oak Ridge, Tenn. April 24–25, 1980. Papers on new ideas or new technology relating to the clinical laboratory are invited, and those describing components or systems that can be used in advanced technology may be considered. A 150–200 word abstract should be submitted by Jan. 15, 1980 to: Charles D. Scott, Oak Ridge National Laboratory, P.O. Box X, Oak Ridge, Tenn. 37830. Accepted papers must be available in a form suitable for publication at the time of presentation. The papers will be subjected to normal editorial review before being published in *Clinical Chemistry*.

Symposium on the Legal Implications of Environmental ASTM Standards for Forensic Purposes
Milwaukee, Wis. June 13–14, 1980. Papers are solicited to describe previously unpublished material on topics including claims and litigations, permit problems, and legal questioning of analytical results. A special technical publication on the symposium proceedings is anticipated by ASTM. Prospective authors are asked to submit an abstract and ASTM offer form by Dec. 1, 1979 to Dr. Alan P. Bentz, U.W. Coast Guard Research and Development Ctr., Avery Point, Groton, Conn. 07340. Manuscripts for the program are due May 1, 1980.

7th International Symposium on Mass Spectrometry in Biochemistry, Medicine and Environmental Research
Milan, Italy. June 16–18, 1980. All the latest aspects of mass spectrometry and their areas of application are within the scope of the symposium. Those authors wishing to present a communication are requested to submit the title and an abstract of up to 200 words before Jan. 25, 1980 to: Dr. Alberto Frigerio, Istituto di Ricerche Farmacologiche Mario Negri, Via Eritrea, 62-20157 Milan, Italy. The Proceedings will be published by Elsevier.

Meetings

- **Recent Advances in Mass Spectrometry in Analytical Chemistry.** Feb. 6, 1980. London. *Contact: The Secretary, Analytical Division, Chemical Society, Burlington House, London W1V OBN, England*
- **Research and Development Topics in Analytical Chemistry.** April 1–2, 1980. Kent University, Canterbury, England. *Contact: The Secretary, Analytical Division, Chemical Society, Burlington House, London W1V OBN, England*
- **Modern Techniques for Surface Characterization.** April 9–11, 1980. University of Durham, Durham, England. *Contact: The Secretary, Analytical Division, Chemical Society, Burlington House, London W1V OBN, England*

Get meaningful signal analysis through complete annotation of accurate data. Introducing the Gould ES 1000.

The new Gould ES 1000 electrostatic analog recorder automatically makes the exact chart notations you require for determining the nature of your signals. Chart speeds, amplifier sensitivity settings, units of measurement, real time, and test identification are all printed exactly according to your preprogrammed instructions. Even when you make additional, immediate notations through the auxiliary keyboard, there's no need to touch the chart or stop the recorder.

You'll also find the rugged, dependable Gould ES 1000 is a versatile performer whatever your application. Plug-in signal conditioners provide accurate monitoring of a wide range of input functions. There's even an optional plug-in digital converter. You get a peak capture capability of 40 microseconds and flat frequency response from DC to at least 10 kHz across all 16 channels.

For accuracy, the fixed electrostatic linear array of the ES 1000 generates its own grid pattern at the same time it is producing the high resolution 100 dots per inch trace. Traces overlap allowing all channels to record full scale across the 10" wide writing area. The unique 1000 electrode head eliminates pens, ink, and other moving parts that might have the potential for trouble.

Find out more about how meaningful your signal analysis can be with the new Gould ES 1000. Write Gould Inc. Instruments Divison, 3631 Perkins Ave., Cleveland, Ohio 44114.

GOULD

An Electrical/Electronics Company

- **1st International Workshop on Trace Element Analytical Chemistry in Medicine and Biology.** April 27–29, 1980. Neuherberg, Fed. Rep. of Germany. *Contact: P. Schramel, Gesellschaft fuer Strahlen- und Umweltforschung Physikalisch-Technische Abteilung, Ingolstadter Landstrasse 1, D-8042 Neuherberg, F.R. Germany. Page 1198 A, Oct.*
- **4th Symposium on Ion Exchange.** May 27–30, 1980. Balaton Lake, Hungary. *Contact: J. Inczedy, Organizing Committee, 4th Symposium on Ion Exchange, P.O.B. 28, Veszprem, Hungary H-8201*
- **10th Northeast Regional ACS Meeting.** June 30–July 3, 1980. Clarkson College, Potsdam, N.Y. *Contact: Tom McKinley, Clarkson College, Potsdam, N.Y. 13676*
- **6th International Conference on Thermal Analysis (ICTA '80).** July 6–12, 1980. Bayreuth, Fed. Rep. of Germany. *Contact: 6th ICTA '80, Postfach 1120, D-8672 Selb, Fed. Rep. of Germany*
- **38th Annual Electron Microscope Society of America Meeting and 15th Annual Microbeam Analysis Society Meeting.** Aug. 4–8, 1980. San Francisco. *Contact: David C. Joy, Bell Telephone Laboratories, Murray Hill, N.J. 07974*
- **7th Annual Meeting of the Federation of Analytical Chemistry and Spectroscopy Societies (FACSS).** Sept. 7–12, 1980. Philadelphia. *Contact: J. A. Williamson, Du Pont Co., Instrument Products Div., Wilmington, Del. 19801*
- **Trace and Ultratrace Analysis.** Sept. 23–25, 1980. Cardiff, England. *Contact: The Secretary, Analytical Division, Chemical Society, Burlington House, London W1V OBN, England*

Short Courses

University of Houston Courses. Contact: S. Deming, Department of Chemistry, University of Houston, Houston, Tex. 77004. 713-749-4809

Fundamentals of Experimental Design
U. of Houston. Dec. 3–4. S. Deming and S. Morgan. $300

Sequential Simplex Optimization
U. of Houston. Dec. 5–6. S. Deming and S. Morgan. $300

An Experimentalist's Approach to Liquid Chromatography
U. of Houston. Dec. 10–11. R. Henry and B. Bidlingmeyer. $300

Liquid Chromatography: Separation plus Spectroscopy
Cincinnati. Dec. 10–14. W. Shumaker. $625. *Contact:* Ann Woolley, Finnigan Institute, 11750 Chesterdale Rd., Bldg. 5, Cincinnati, Ohio 45246. 513-772-5500

The Center for Professional Advancement Courses. Contact: Mary Sobin, Dept. NR, The Center for Professional Advancement, P.O. Box H, East Brunswick, N.J. 08816. 201-249-1400

Fine Particle Measurement
E. Brunswick, N.J. Jan. 7–11. T. Allen. $770 (5 days), $650 (4 days)

Thermoanalytical Methods
E. Brunswick, N.J. Jan. 14–16. Miller. $490

Electroanalytical Chemistry
E. Brunswick, N.J. Jan. 14–17. G. Ewing and M. Miller. $620

Microprocessors and Microcomputers
Atlanta. Jan. 15–18. E. R. Garen and S. Smith, $695. *Contact:* ICS Enrollment Office, Integrated Computer Systems, Inc., 300 N. Washington St., Suite 103, Alexandria, Va. 22314. 703-548-1333

For Your Information

Highlights of a report containing an analysis of the 1980 budget for **Federal research and development funding** have been released by the National Science Foundation (NSF). Copies of *Science Resources Studies Highlights*, "Total Federal R&D Growth Slight in 1980 but Varies by Budget Function," can be obtained from the Division of Science Resources Studies, National Science Foundation, Washington, D.C. 20550. Copies of the special report on which *Highlights* was based, *Federal R&D Funding by Budget Function: Fiscal Years 1979–80*, can also be obtained from the Division of Science Resources Studies, NSF.

A paper entitled "**Priority Pollutant Analysis: Comparing Cost Effectiveness of GC/MS and GC**" is available upon request on your company letterhead from Finnigan Instruments, 845 W. Maude Avenue, Sunnyvale, Calif. 94086.

A report from the International Union of Pure and Applied Chemistry (IUPAC) Commission on Microchemical Techniques and Trace Analysis, written by Ewald Jackwerth, on **multi-element preconcentration from pure lead,** has been published in the May 1979 issue of *Pure and Applied Chemistry* (Vol. 51, No. 5, pp 1149–59). The report discusses preconcentration of trace elements from pure lead by precipitating the matrix as $PbCl_2$, $Pb(NO_3)_2$ or $PbSO_4$. A less technical article based on the report has been published in the IUPAC *Information Bulletin* (1979), No. 2, p 8.

Core Laboratories, Inc., Dallas-based international petroleum engineering company, has agreed in principle to acquire all the outstanding stock in **Chromaspec Labs, Inc.** of Houston, Tex., for an undisclosed number of shares of Core Lab common stock. Chromaspec, which provides analytical laboratory and pilot plant services to the petrochemical, refining and chemical industries, is expected to operate a wholly-owned subsidiary of Core Labs.

The National Commitee for Clinical Laboratory Standards (NCCLS) has published standard PSC-12, "**Definition of Quantities and Conventions Related to Blood pH & Gas Analysis.**" PSC-12 aids in answering the need for uniformity and for a handy laboratory reference. Copies of PSC-12 are available at $9.00 each, plus $1.00 additional per copy for out-of-U.S. orders. Check or money order is requested in advance. NCCLS, 771 E. Lancaster Ave., Villanova, Pa. 19085, 215-525-2435.

"**Safety in Academic Chemistry Laboratories,**" Third Edition (August 1979) is now available. The manual was prepared by the ACS Committee on Chemical Safety, and provides a benchmark as to what constitutes safety in laboratories and elsewhere. The first pages of text relate to philosophy, facilities, practices, and policies. The remainder of the manual is directed to the student. Send $1.00/copy to Committee on Chemical Safety, American Chemical Society, 1155 Sixteenth Street, N.W., Washington, D.C. 20036.

The Jarrell-Ash shopping guide to plasma spectrometers.

[Where else do you get such a selection!]

Only Jarrell-Ash makes it this easy for you to bring your laboratory into the **Plasma Age.** With five basic plasma emission spectrometers to choose from — plus an almost endless variety of options. Virtually a custom model for every budget, every need. **Plasma AtomComp™** from Jarrell-Ash. It's the comprehensive line. Send for data today.

Model 955

Extremely cost-effective tool for smaller facilities. PDP-8A computer. Maximum 30 analytical channels. Options: variable-wavelength channel; automatic background correction.

$

Model 965

Ideal for industrial and commercial lab applications. PDP-8A computer. Maximum 48 analytical channels. Dual floppy disks. Options: mercury profile monitor; basic storage-&-retrieval; statistics.

$$

Model 970

Versatile performer for a remarkable variety of needs. PDP-8E computer. Maximum 48 analytical channels. Options: sample-intro accessories; multiple sources; data-management functions.

$$$

Model 1140

A comprehensive plasma system that's easy-to-use, upwardly expandable, thanks to today's finest mini computer, the PDP-11/04 with RSX11M-based operating system. Maximum 61 analytical channels. Options: high-level languages for software development; spectrum-scanning.

$$$$

Model 1160

A veritable plasma powerhouse for sophisticated research. Multi-user, multi-tasking, real-time system produces, manages data efficiently, fast. PDP-11/34 computer with RSX11M-based operating system. Maximum 61 analytical channels. Options: additional memory; multiple-point automatic background correction.

$$$$$

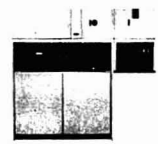

Leaders in Plasma Spectrometery

Jarrell-Ash Division
Fisher Scientific Company

590 Lincoln Street
Waltham, Massachusetts 02154
Phone (617) 890-4300

$ *is our way of telling you there's a remarkable range in prices . . . a model for every size and kind of facility.*

CIRCLE 121 ON READER SERVICE CARD

Robert G. Smerko
Department of Public Affairs
American Chemical Society
1155 16th Street, N.W.
Washington, D.C. 20036

The American Chemical Society and Regulatory Affairs

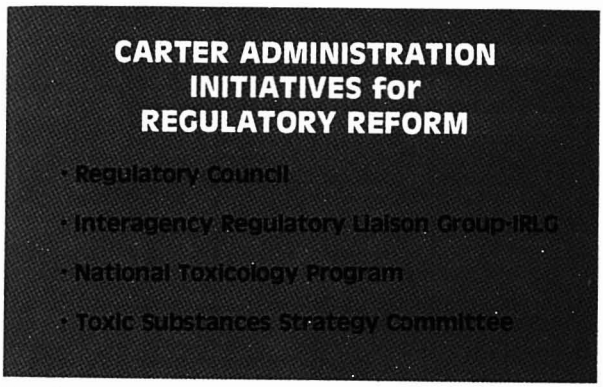

Figure 1.

My remarks will cover four related points:

- the current Administration's efforts at regulatory reform aimed at social regulations;
- the need to take into consideration the analytical chemistry component of regulations in this reform effort;
- the role of the Division of Analytical Chemistry in regulatory matters;
- ACS participation in regulatory matters over the past three years.

My first point is regulatory reform. Both presidential candidates in the 1976 election campaign promised that an effort would be made at some type of regulatory reform. Subsequent to being elected, President Carter has made some efforts in this direction. This past June, in a speech delivered at a meeting of the American Association for the Advancement of Science, Frank Press for the first time addressed the scientific community on the Carter Administration's regulatory reform policy. He is the President's Science Adviser and the Director of the Office of Science and Technology Policy in the Executive Office of the President. According to Dr. Press, we have a regulatory structure which is highly segmented, very aggressive and almost totally uncoordinated. To improve that structure is a major concern of the Administration, the Congress, and the whole nation. Dr. Press told the audience that, without altering his strong commitment to the environment, health, safety and other social goals, President Carter has undertaken a number of initiatives to improve the federal government's regulatory apparatus.

These initiatives are aimed at two objectives: first, to ensure that the regulators and the public are informed about the economics, the costs and benefits of regulations; and second, to bring as much coordination, consistency, and quality into the total regulatory system as possible. The basic component of the Carter Administration reform effort is interagency organization and cooperation (Figure 1).

The Regulatory Council is a recent initiative, and it is to ensure that regulations achieve their statutory goals in the most economical manner. It is to continually identify government-wide programs, resources, and policies that are needed to improve the regulatory process. President Carter announced the formation of the Council, headed by Douglas Costle, Administrator of the Environmental Protection Agency (EPA), on Oct. 31, 1978.

Another interagency activity is the IRLG, the Interagency Regulatory Liaison Group, which is composed of EPA, the Food and Drug Administration (FDA), the Occupational Safety and Health Administration, the Consumer Product Safety Commission, and the Food Safety and Quality Service Agency of the Department of Agriculture. This group is to coordinate the various agencies' regulatory activities and the research programs supporting their missions. The IRLG was founded in August of 1977.

A third effort is the establishment of the National Toxicology Program which involves the FDA, the National Cancer Institute and the environmental health and occupational health and safety research agencies of HEW. This program is to set priorities for the testing and evaluation of toxic chemicals. This operation was established in November of 1978.

And the last effort I will mention is the Toxic Substances Strategy Committee (TSCA) that was established by President Carter in 1977. This interagency group, through coordination by the Council on Environmental Quality, is to develop a program that will serve to implement the President's policy of prevention of hazards as the primary basis for controlling toxic substances. The program also is aimed at coordinating efforts in data collection, research, and regulatory action. Eighteen agencies or departments of the federal government are involved. Their recent draft report is being heavily criticized by industry.

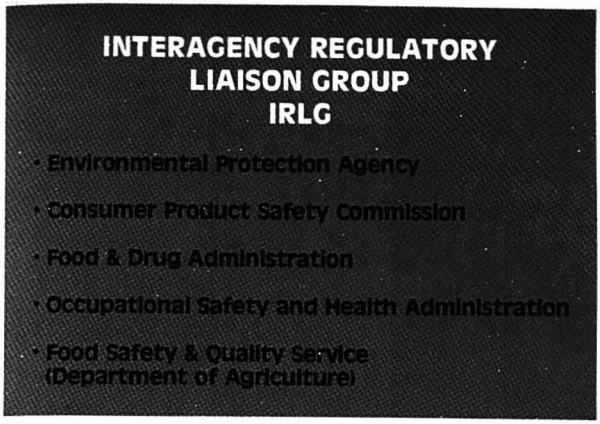

Figure 2.

Dr. Press has made a strong case for more involvement in the regulatory process by professional societies as well as individual scientists and engineers. Their contributions are needed for two reasons: to provide the soundest scientific knowledge upon which regulatory policies can be based; and to enhance the public confidence that is necessary for the implementation of those policies. I assess this situation as an opportunity for a new level of involvement that will allow the scientific and technical communities, including analytical chemists, to become an effective force in regulatory affairs.

Is there a need for regulatory reform, that is, improved quality in the analytical chemical measurement aspects of regulation? Let's consider the IRLG and its activities (Figure 2). The Department of Public Affairs has attempted to determine what activities are underway in the IRLG involving analytical chemical measurements, but we have not been able to identify any major effort in this regard.

There is a need for an interagency group that would deal with questions of policy involving analytical chemical measurements and strive for cooperation among agencies, consistency, and favorable cost/benefit relationships in regulations. A good example of where an interagency effort on analytical chemistry should be active right now is in the writing of good laboratory practices (GLP's) for the health effects section of TSCA. Later there will be GLP's for the environmental effects under TSCA as well. By EPA's own admission, its GLP's are more stringent than FDA's. Are these differences essential? These GLP's have many analytical chemical aspects, including the type of testing data to be generated, that should be worked out carefully and agreed upon by the entire analytical chemical community so that the best regulations are written.

Should the IRLG be the group to address analytical chemical measurement issues? I believe the answer is "yes." The IRLG is a combination of five agencies that deal with 25 laws, many of which turn or pivot on analytical chemical data. This also is the group which has received the charge to eliminate waste, duplication and inconsistencies in regulations; to develop compatible testing guidelines and a common approach to risk assessment; and to coordinate research as well as public information activities. The incorporation of analytical chemical measurements is compatible with these charges, and should not prove to be a formidable task for the IRLG.

Thus, it seems reasonable that the IRLG could establish a specific working group, or whatever is appropriate, to deal with the policy aspects concerning the use of analytical chemical measurements in the regulatory process. Also, this group could coordinate analytical chemistry research efforts, and the use of analytical data in compliance and enforcement.

How can the scientific and technological communities, including analytical chemists, get more involved in regulatory matters? The answer to this question brings me to my third point in these remarks, the role of the Division of Analytical Chemistry in regulatory matters.

In my opinion, the analytical chemistry community, through the ACS and this Division, should call for the establishment of an interagency group to deal with all matters involving analytical chemical measurements, and call for the establishment of specific advisory groups in analytical chemistry for all the regulatory agencies that are members of the interagency group. The IRLG could serve as the parent organization.

One mechanism the ACS can consider to develop interest in the establishment of an interagency group on analytical chemical measurements is to seek cosponsorship of a forum with the Office of Science and Technology Policy and the IRLG to further define the problem and develop goals, objectives and definitive action plans.

In addition to calling for the establishment of an interagency group on analytical chemical measurements, I also think that the analytical chemistry community should become much more involved in the specific regulatory activities of the various agencies. You can do this as individuals, as a Division, or as the National ACS.

Over the past year your Division's *ad hoc* Committee on Regulations and the Department of Public Affairs have made some progress. The REGULATIONS column in ANALYTICAL CHEMISTRY has been established as an important vehicle through which the analytical community can communicate to its own members as well as the government. It must be maintained at its current level of high quality.

The Department of Public Affairs has provided staff support in addressing the analytical chemical aspects of EPA's proposed pesticide testing guidelines, and is assisting the Committee on Environmental Improvement in its efforts to write a set of principles for environmental analysis. The Department of Public Affairs, as a matter of standard operating procedure, alerts your Committee on Regulations to proposed regulatory activities. Very recently I participated in a project of the Office of Science and Technology Policy which was to draw up a research agenda concerning the analytical chemical measurements connected with hazardous waste. This level of effort, in my opinion, is not enough. Clearly, more needs to be done.

I would like to make some suggestions that, if followed, should bring the Division and the National ACS into a good working partnership to deal with federal regulations:

- Give your Committee on Regulations permanent standing in the Division.
- Give the Committee a charter that allows it to develop policy for the Division in regulatory matters and to formulate this policy for consideration as Society policy. The charter should also spell out that the Committee will take the responsibility of reviewing proposed regulations. In order to make the regulatory program work, the Department of Public Affairs staff needs input as to what the issues and

problems are in proposed regulations. This holds true for any area of chemistry as well as analytical chemistry.

- The Committee needs to be enlarged, so we have all the bases covered and thereby reduce the probability of having something fall through the cracks.
- You need, and we need, a roster listing people and their areas of expertise so that we can call upon them when needed.
- At each national meeting the Division should have a forum that deals with regulations so that you can have an informal exchange on your problems, concerns, ideas, and needs, and hear a report given by the Committee. The forum setting could be simply an open meeting of the Committee on Regulations.

Finally, I want to briefly address my last point. ACS's participation in regulatory affairs over the past several years. Before 1977 and the creation of the Subcommittee on Regulatory Practices of the Committee on Chemistry and Public Affairs (CCPA), the Society's involvement in the regulatory area was very limited. During the period from 1972 to April 1977 only five of the 50 policy statements issued by the ACS were directed at the executive branch or its independent agencies.

The CCPA Subcommittee's first involvement in the regulatory area, via its Task Force on Priority Testing, was in April 1977 when it commented upon EPA's draft document, "Assessment and Control of Chemical Problems." Since this time, a total of 39 statements by the ACS has been released with 18 of them involving regulatory issues. Of these 18, 12 were developed by this CCPA Subcommittee. The overwhelming majority of statements in the regulatory area have been directed at EPA and the implementation of TSCA. The other groups within ACS that worked on the remaining statements were the Committee on Chemical Safety, the Committee on Chemistry and Public Affairs, the Committee on Environmental Improvement, an *ad hoc* group of pesticides experts, and the Committee on Analytical Reagents.

As you can see, the ACS is getting more involved with position-taking on regulatory issues. Our increased involvement in this area has provided a chance for a better rapport between the Society and the executive branch of the government.

There is much to be done, and we are capable of the task. All we need is your help.

Based on a presentation at a symposium on "The Analytical Chemists' Stake in Federal Regulations: A Survey" at the ACS National Meeting in Washington, DC, Sept. 11, 1979.

HPLC News:

A variable UV detector with outstanding performance

LDC's new SpectroMonitor III is all you have been asking for. Advanced optics give true dual beam operation for exceptional stability and low noise (1.5% peak to peak at 195 nm)

Sensitivity to 0.005 AUFS

Wavelength range 190 to 350 nm

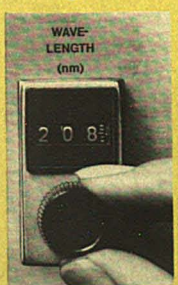

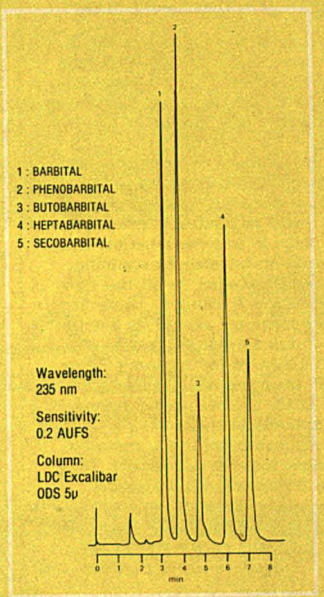

Actual SpectroMonitor III chromatogram demonstrates low noise and exceptional stability.

LDC liquid chromatography

Easy inspection, with the cell and liquid connections easily removed from the front for inspection and servicing.

Price: $3890.

Write for brochure with complete technical data.

LABORATORY DATA CONTROL
Division of Milton Roy
P.O. Box 10235,
Riviera Beach, FL 33404
305/844-5241 telex 513479

CIRCLE 159 ON READER SERVICE CARD

TAKING THE WRAPS OFF A NEW SERIES OF GILFORD RESEARCH INSTRUMENTATION PACKAGES.

For you who were waiting, NOW is that "better time."

In a day when everything except the dollar is going up, you have the opportunity to acquire a complete Gilford system at yesterday's prices. Eight Gilford Research Instrumentation Packages with dozens of applications and a performance-to-price ratio that translates to real value in today's economy.

An example? Our Wavelength Scanning/Kinetic System, at a price that was good last year, and which is even a better bargain today. The ideal instrumentation package for the researcher who recognizes the value of high sensitivity and a 3A range in enzyme kinetics, and who also requires high-resolution wavelength scanning.

You get the same performance/value in all the new Gilford Research Instrumentation Packages. There are two systems for wavelength scanning, others for kinetic assays. Yet another for automatic sample processing with an aspirating cuvette. And a system for scanning 20cm gels, as well as one which uses precise thermoelectric heating and cooling for DNA thermal denaturation - renaturation assays of exceptional quality.

Find out how these systems can benefit your research. Our instrumentation packages make it convenient. And accurate. And reliable. Our prices make it a pleasure.

Gilford Research Spectrophotometers:
Every job easier, every result more accurate.

CIRCLE 78 ON READER SERVICE CARD

gilford® INSTRUMENT

Oberlin, Ohio 44074
(216) 774-1041 Telex: 98-0456
Paris (Evry 91), France
Düsseldorf, W. Germany
Teddington, Middx., England

Cancer—The Outlaw Cell

Richard E. LaFond, *Editor*

An estimated 390,000 Americans will die of cancer this year alone and one out of every four will develop some form of this dread disease within their lifetime.

Statistics such as these show the need for a book that will explain our current state of the art in cancer research using simple, straightforward, non-medical language. *Cancer — The Outlaw Cell* successfully fulfills this need by making the latest advances in cancer research available to the general public in a clear, non-technical style that can be read and understood by both the professional scientist and non-scientist.

Written by leading experts at the forefront of their specialties and profusely illustrated in color, this collection of articles covers the great strides that have been made in understanding the causes of cancer, how this disease is spread, cancer as a biochemical problem, and non-surgical modes of therapy.

CONTENTS

192 pages (1978) clothbound $15.00
LC 78-2100 ISBN 0-8412-0405-5
192 pages (1978) paperback $8.50
LC 78-2100 ISBN 0-8412-0431-4

SIS/American Chemical Society
1155 16th St., N.W./Wash., D.C. 20036

Please send _____ copies of *Cancer — The Outlaw Cell*.

☐ cloth $15.00 (ACK 0405-5) ☐ paper $8.50 (ACK 0431-4)

☐ Check enclosed for $_____. ☐ Bill me. Postpaid in U.S. and Canada, plus 75 cents elsewhere.

Name _____

Address _____

_____ State Zip _____

NO POSTAGE NECESSARY IF MAILED IN THE UNITED STATES

BUSINESS REPLY CARD

FIRST CLASS Permit #27346 Philadelphia, Pa.

POSTAGE WILL BE PAID BY ADDRESSEE

analytical chemistry

P.O. BOX #7826
PHILADELPHIA, PA 19101

NOVEMBER 1979

VALID THROUGH MARCH 1980

ADVERTISED PRODUCTS:										
7	8	9	10	11	12	13	14	15	16	17
18	19	20	21	22	23	24	25	26	27	28
29	30	31	32	33	34	35	36	37	38	39
40	41	42	43	44	45	46	47	48	49	50
51	52	53	54	55	56	57	58	59	60	61
62	63	64	65	66	67	68	69	70	71	72
73	74	75	76	77	78	79	80	81	82	83
84	85	86	87	88	89	90	91	92	93	94
95	96	97	98	99	100	101	102	103	104	105
106	107	108	109	110	111	112	113	114	115	116
117	118	119	120	121	122	123	124	125	126	127
128	129	130	131	132	133	134	135	136	137	138
139	140	141	142	143	144	145	146	147	148	149
150	151	152	153	154	155	156	157	158	159	160
161	162	163	164	165	166	167	168	169	170	171
172	173	174	175	176	177	178	179	180	181	182
183	184	185	186	187	188	189	190	191	192	193
194	195	196	197	198	199	200	201	202	203	204
205	206	207	208	209	210	211	212	213	214	215
216	217	218	219	220	221	222	223	224	225	226
227	228	229	230	231	232	233	234	235	236	237
238	239	240	241	242	243	244	245	246	247	248
249	250	251	252	253	254	255	256	257	258	259

NEW PRODUCTS:										
408	409	410	411	412	413	414	415	416	417	418
419	420	421	422	423	424	425	426	427	428	429
430	431	432	433	434	435	436	437	438	439	440
441	442	443	444	445	446	447	448	449	450	451
452	453	454	455	456	457	458	459	460	461	462
463	464	465	466	467	468	469	470	471	472	473
474	475	476	477	478	479	480	481	482	483	484
485	486	487	488	489	490	491	492	493	494	495

READER SURVEY:										
308	309	310	311	312	313	314	315	316	317	318
319	320	321	322	323	324	325	326	327	328	329
330	331	332	333	334	335	336	337	338	339	340
341	342	343	344	345	346	347	348	349	350	351

TO VALIDATE THIS CARD, PLEASE CHECK ONE ENTRY FOR EACH CATEGORY BELOW:

Intensity of product need:
- ☐ 1. Have salesman call
- ☐ 2. Need within 6 mos.
- ☐ 3. Future project

Primary field of work:
- ☐ A. Energy
- ☐ B. Environmental
- ☐ C. Medical/Biological
- ☐ D. Drug/Cosmetic
- ☐ E. Forensic/Narcotic
- ☐ F. Textile/Fiber
- ☐ G. Metals
- ☐ H. Pulp/Paper/Wood
- ☐ I. Soaps/Cleaners
- ☐ J. Paint/Coating/Ink
- ☐ K. Electrical/Electronic
- ☐ L. Instrument Dev./Des
- ☐ M. Plastic/Polymer/Rub
- ☐ N. Agricultural/Food
- ☐ O. Inorganic Chemicals
- ☐ P. Organic Chemicals

Primary area of employment:

INDUSTRIAL
- ☐ A. Research/Development
- ☐ B. Quality/Process Control

MEDICAL/HOSPITAL
- ☐ C. Research/Development
- ☐ D. Clinical/Diagnostic

GOVERNMENT
- ☐ E. Research/Development
- ☐ F. Regulate/Investigate

COLLEGE/UNIVERSITY
- ☐ G. Research/Development
- ☐ H. Teaching

INDEPENDENT/CONSULTING
- ☐ I. Research/Development
- ☐ J. Analysis/Testing

This copy of Analytical is:
- ☐ 1. Personally addressed to me in my name.
- ☐ 2. Addressed to other person or to my firm.

NAME: _____

TITLE: _____

FIRM: _____

STREET: _____

CITY: _____

STATE: _____ ZIP: _____

PHONE: (___) _____

New Products

pH Monitor/Recorder

The portable pH monitor/recorder system contains a pH electrode, a pH standard, and an intermediate solution to protect the pH standard from the process solution. The pH electrode, the standard electrode and the differential electronics comprise a differential pH system. The standard electrodes do not require filling solutions or crystals and will not contaminate a process since there is no flow out of the electrode. The signal can be sent over 3000 feet. The rugged portable electronics package can be used indoors or out. It contains its own batteries and recharger. A 5 inch meter and $2\frac{1}{2}$ inch strip chart recorder provide the displays. Oceanography International **412**

Quantitative Photodensitometer

Model RFT photodensitometer features three monochromatic lighting modes—reflectance, fluorescence, and transmission. The modified Czerny-Turner monochromator has a range extending from 190 nm to 740 nm, narrowly defining either the tungsten or deuterium lamp to a specified wavelength by means of a 50 × 50 mm replica grating. The instrument offers over 100 different slit configurations, six scanning speeds, automatic zeroing, and automatic baseline adjustment. The computing integrator computes up to 64 fractions in area, percent, and percent multiplied by a three digit keyboard-entered normalization factor. V-tech Corp. **413**

LSD-100 light scattering detector is a low angle laser light scattering photometer designed for gel permeation chromatography. The instrument features absolute molecular weight determinations and molecular weight distribution determinations of synthetic or biopolymers. It incorporates a He-Ne laser source, fixed angle annulus, dual-beam optical design, high pressure GPC flow cell and choice of output signals for auxiliary recorder. Gain and output signal selection of P_o, P_oX10, and P_o as well as LED indicators of gain and laser source status are included. Chromatix **401**

Chart Recorder

Model 156 is a single channel recorder with 22 selectable speeds. The 125 mm recorder has controls which can be set to record a wide range of input voltages and signal responses. A crystal oscillator times the low-power CMOS chart drive system. Linear Instruments Corp. **427**

Combination pH-Temperature Meter

Model PA-21 performs pH, temperature in °C or battery voltage tests with push button switch actuation. Accuracies are 0.01 pH over the range of pH 0–14 and 0.1 °C from 0–100 °C. Response time is 10–12 s. A nonrefillable plastic-encased pH probe with gold plated connectors is standard. This pocket-sized instrument has $\frac{3}{10}$ inch digital LED's. Presto-Tek Corp. **420**

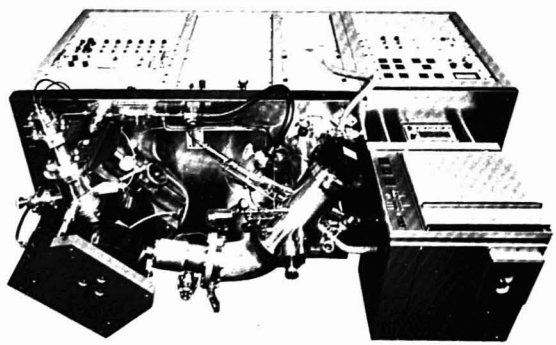

The 70-70H high resolution mass spectrometer has a resolution of 25 000 and a mass range of 2 to 700 at 4kV. The 70-70H is capable of scan rates of up to 0.3 sec./decade. The scan cycle time over the mass range 500 to 25 is 0.8 sec., so the 70-70H is suitable for high resolution capillary GC/MS. A data system which includes extensive control facilities can be supplied. VG-Micromass **402**

Bandpass Filter

Model 751A-02 Brickwall Filter is a 1 Hz to 100 kHz programmable high-pass/low-pass signal-processing filter. The design employs a 7th-order Elliptic filter with design values of 0.3 dB peak-to-peak passband ripple, and 85 dB stopband attenuation above 1.7 × cutoff frequency (low pass) and below 0.6 × cutoff frequency (high pass). The roll-off rate is better than 115 dB per octave on both sides of the passband. Both center frequency and bandwidth can be set anywhere in the 100 kHz band. The built-in IEEE STD 488/1978 Instrumentation Bus Interface provides the following functions: acceptor handshake, basic listener with listen only, and device trigger. Rockland Systems Corp. **421**

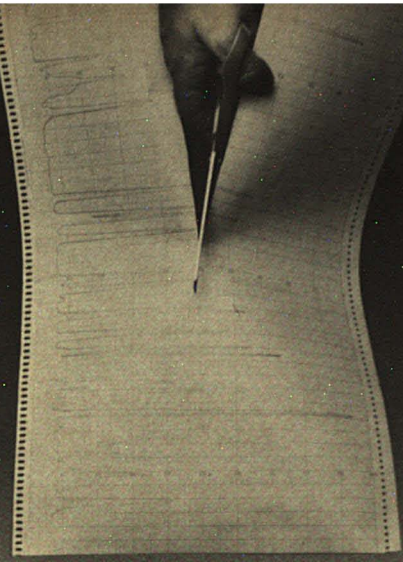

How to Cut Your Recording Costs.

Here's how to cut your recording budget down to size ...with the Linear 156. It offers an outstanding array of standard features, many only optional on other recorders, at a lower than standard price.

A PERFECT WAY TO CUT CORNERS.

When it comes to saving critical lab space, the 156 cuts down on valuable shelf space. Our recorder is only 9" wide... half the bench space occupied by most standard recorders.

DESIGNED FOR FULL PERFORMANCE.

The tighter your testing standards are, the more reason to consider a Linear 156. All 156 recorders are sprocket driven to deliver full-sized accuracy, with a ±1% overall limit of error. And with 5 input ranges (1 mV-10 V), 22 chart speeds, and 100% full scale suppression...we're as versatile as most recorders twice the size.

WE DIDN'T CUT ON THE GUARANTEE.

We pack a lot of quality and pride into our 156, and back it up with an airtight one year parts and labor guarantee. To find out how the Linear 156 "cuts it," write for a free brochure to Linear Instruments, 17282 Eastman Ave., Irvine, CA 92714.

Linear

A PRECISE SENSE OF VALUE.

CIRCLE 128 ON READER SERVICE CARD

New Products

Light Detector

Model 403B Photodiode features a rise-time of under 50 ps and FWHM delta function response of less than 80 ps. The spectral response of the detector ranges from 340 nm to 1100 nm. Signal levels of up to 500 mV (in to 50 ohms) can easily be obtained from inputs of less than 5 mW. The damage threshold is greater than 100 mW. The output signal has a peak ringing/overshoot of less than 25% of the main pulse amplitude. Applications include the monitoring of mode-locked ion lasers, pulsed ruby lasers and mode-locked Nd-Yag lasers. Spectra-Physics **411**

Potentiometric Blood Analysis Method

The analysis of electrolytes in serum takes about three minutes with a potentiometric slide. This self-contained, single-use slide is essentially a small disposable battery-like cell. It has a silver/silver chloride electrode which accepts a patient sample and a second identical electrode for deposition of a reference fluid of known electrolyte concentration. When 10 μl drops of the two fluids are placed on identical small strips of the flat electrodes, a liquid junction is formed by capillary flow through a small bridge. The small electrical current which is generated, when measured with an electrometer, gives a precise measure of the amount of the electrolyte in the sample. Eastman Kodak Co. **414**

On-Line Chemical Analyzers

New analyzers for specific purpose monitoring and control applications are available. Alkalinity analyzers provide a direct measurement of caustic carbonate (model 3218), hydroxide (model 3214), hardness-in-brine (model 3216) and 2P-M alkalinity (model 3212). On-line analyses are made, using microprocessor-controlled digital sampling, reagent and diluent techniques. Combined with spin-cell technology, this permits measurements of equilibrium reactions initiated by a digital delivery system. Model 3441 ammonia analyzer operates free from bound ammonia interference. The digitally-controlled, multiple reagent dispensing system and the design provide the user with the choice of either standard addition, standard depletion, or direct selective ion analysis technique. Ionics, Inc. **419**

Spectrofluorometer Accessories

The Digital Autoranging Photometer offers digital readout, an autoranging feature which automatically selects the proper photometer range and positions the decimal point, and both BCD and analog output. It will upgrade the company's SPF-125 and Aminco-Bowman spectrofluorometers and the filter fluorometric analyzers. A calculator accessory consisting of a Hewlett-Packard desk-top computer and graphics plotter is programmed for use with the company's SPF-500 Spectrofluorometers. It performs 19 different functions, and stores up to 40 spectra on a single tape. American Instrument Co. **418**

PW 1600/10 is a microprocessor-controlled simultaneous X-ray fluorescence spectrometer. It provides fixed channel simultaneous measurement of up to 28 elements, while scanning channels allow the identification and measurement of nonroutine elements. It can be used either as a stand-alone system or as an integrated element in an automatic process control analysis line. A universal interface allows for connection to any type of mini- or mainframe computer. Philips **403**

AA Double Feature!

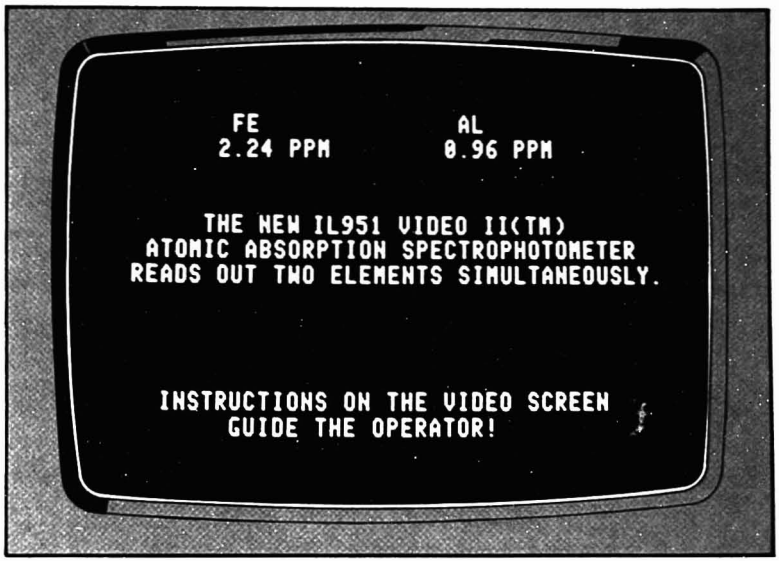

IL presents a unique, two-channel AA. Beginners can use it easily. Spectroscopists can use it brilliantly.

It's the new IL951 Video II, first AA spectrophotometer combining two double-beam channels with a video screen and a microcomputer.

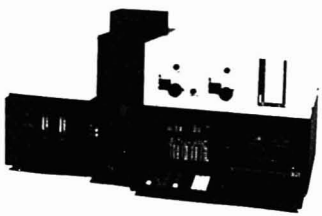

Easy enough for entry-level personnel.

Any technician can learn to run the IL951. Instructions on the video screen—in English, not computerese—guide the operator step by step. Even the analytical "Cookbook" is displayed. The microcomputer is controlled by just twelve functions keys (see below). Complete methods, including calibration, can be stored for 10 pairs of elements and re-entered at the touch of three keys.

Versatile enough for the most demanding spectroscopist.

The IL951 can perform wonders in the hands of an inventive scientist. You can determine two elements simultaneously, with flame or furnace atomizer. You can use an internal standard to improve accuracy, remove the effect of dilution errors, or even avoid weighing the sample. Ratios between two elements can be read directly. The instrument can be used as a dual-wavelength, UV-Vis. spectrophotometer. Flame emission can be done with excellent resolution.

Explicit graphics add protection from errors.

With its graphics option, IL's new AA shows you the shapes of working curves, and details of absorbance peaks. Background absorbance is shown simultaneously. And there's much, much more.

See it now! Phone toll-free for a demonstration in any of our 6 U.S. labs: 800-225-4040 (Ask for "A.I.D. Customer Service.")

Instrumentation Laboratory Inc.
Analytical Instrument Division
Wilmington, MA 01887

Instrumentation Laboratory

CIRCLE 132 ON READER SERVICE CARD

Moles's applications w

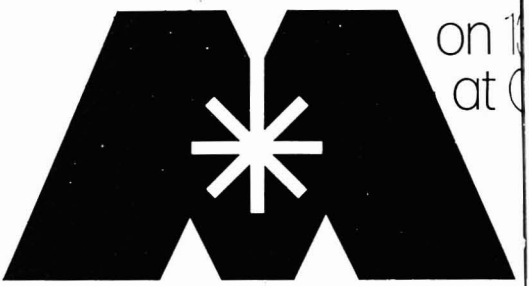

on 1
at (

Sponsored by :

- Laboratoire de Spectrochimie IR et Raman du C.N.R.S.
- Société de Chimie-Physique
- G.A.M.S.
- Instruments S.A., Jobin-Yvon Division.

Presided over

by Professor M. Delhaye

Provisional program

These two days will be dedicated to lectures and discussions on the Raman Microprobe Mole.

13th december

11:00	Introduction G. Payan - General Manager of Instruments S.A.
11:15	Inaugural Lecture Professor M. Delhaye - Director of the IR and Raman Spectroscopy Laboratory CNRS
12:00	Lectures
13:00	Lunch
14:30	Lectures
18:00	Closer

14th december

9:00	Lectures
12:00	Posters Cessions
13:00	Lunch
14:30	Lectures
16:00	Discussion
17:00	Closing Lecture J.Ch. Lefebvre - General Marketing Manager of Jobin-Yvo
18:00	Cocktail.

orkshop

h and 14th december 1979
N.R.S. - Thiais - France

Application Fields

Micropaleontology • Geology • Cements •
Medicine • Biology • Mineralogy •
Pollution and Industrial Materials Control • Polymers.

Shuttle service organized between
porte de Versailles
and C.N.R.S. Thiais.

Booth
JOBIN YVON
Salon
Mesucora/Physique
153 GH
Porte
de Versailles

JOBIN YVON
DIVISION INSTRUMENTS S.A.

16-18, rue du Canal
91160 Longjumeau
Tél. (1) 909.34.93
Télex JOBYVON 692882 F

Reply coupon to be sent to Instruments S.A. Jobin-Yvon

Name ..... Christian Name .....
Firm ..... Laboratory .....
Address .....
Phone ..... Extension .....

I would like to participate in the Mole's Application Workshop and I send you 150 FF for registration fee. (included lunches and shuttle service).

CIRCLE 88 ON READER SERVICE CARD

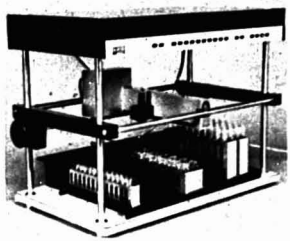

MultiRac is a microprocessor-controlled fraction collector suitable for use even with organic solvents and radioactive liquids. Collection can be made according to time, drop, or precise volume. Volume size can be varied from 10 μL to 3500 mL. Trays accept both funnels and spring-loaded racks which accommodate a variety of vessels from 12 mm diameter test tubes to 28 mm diameter scintillation vials. Data show on a red LED display. $2995. LKB Instruments, Inc. **404**

Filter

The Acrodisc CR, a disposable chemically resistant filter, is used to filter small volumes of solutions which are difficult to handle. Used on the tip of a syringe or teamed with an in-line filter system, the filter removes all particles larger than 0.45 μm. It is autoclavable or may be ETO sterilized. The filter is 25 mm in diameter, has an effective filtration area of 2.77 cm^2 and withstands pressures up to 4.2 kg/cm^2. $75/box of 50, nonsterile. Gelman Sciences, Inc. **429**

Reporting Integrator

The HP 3388A dual channel integrator is a microprocessor-based integrator for chromatographs. The two independent channels allow the user who has the optional second printer/plotter to execute two runs simultaneously with results appearing on individual printer/plotters. BASIC programming enables the terminal to operate as a live calculator keyboard and provides for off-line programming. For post-run calculations, BASIC controls the integrator, auto samplers, external events and all report information. The integrator also features keystroke programming and long-term data storage. Hewlett-Packard Co. **410**

For more information on listed items, circle the appropriate numbers on one of our Readers' Service Cards

Build a titration system that fits you.

Mettler's modular approach to titration lets you create a system that meets your requirements exactly.

You can choose a very basic system that includes a Mettler DV11 Burette Drive, a DK11 Rate and End Point Control, a DK14 Electrode Potential Amplifier and a DV103 Command Module.

Perhaps photometric end point indication is what you need. In that case, the Mettler DK18 and DK19 titration instruments are ideal. And, for "smart" keyboard control of operating parameters, there's the DK25 microprocessor system, the very latest concept for wet chemical analysis.

Or you can get even more sophisticated and choose a Mettler SR10 system in which most of the titration can be carried out automatically.

The point is, Mettler can put together the right combination of any type of titration instruments. It's your kind of system.

For complete information on titration, contact Mettler Instrument Corporation, P. O. Box 71, Hightstown, NJ 08520.

Mettler

CIRCLE 154 ON READER SERVICE CARD

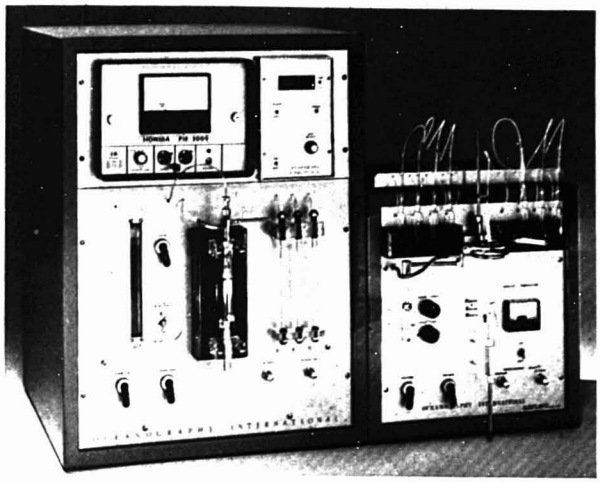

Horiba PIR-2000 is a system for measuring total organic carbon using glass ampules and wet oxidation technique. Up to 10 mL of sample are placed into a borosilicate ampule with an oxidizing agent and phosphoric acid. Inorganics are purged, and the ampule is sealed and then autoclaved to convert the organics to CO_2. The CO_2 is measured with an infrared analyzer. Sensitivity is 100 ppb. Precision is ±5% of actual value at 1 ppm, and approximately 2% of actual value at 5 ppm and above. Oceanography International **405**

Dual Bed Gas Purifier

The DBP-25 dual bed hydrogen purifier combines the function of an oxygen/hydrogen recombiner and a molecular sieve dryer in a single chamber. At flows below 25 SCFH, the unit will reduce 1% oxygen in hydrogen to less than 1 ppm. Water vapor is removed to below 1 ppm by a bed of molecular sieve below the catalyst. Under normal circumstances, a fresh DBP purifier will treat 12 to 25 200 SCF hydrogen tanks containing 100 ppm total oxygen and water before it requires regeneration or replacement. Resource Systems, Inc. **428**

Sample Introduction in Flame AA

Automated multiple flow injection analysis (AMFIA) entails insertion of discrete micro volumes of liquid sample into a constantly flowing solvent stream which is pumped directly into the nebulizer of a flame atomic absorption spectrometer. This allows analysis of discrete micro volume samples and a speed of 120 to 180 samples per hour. The modular-type units of the AMFIA MARK CHEM. FAAS can be adapted to your present AA. Mark Instrument Co. **422**

UV-VIS Spectrophotometer

The microcomputer controls all functions of the Model 559 UV-VIS spectrophotometer. Repetitive scan, wavelength programming and 1st and 2nd derivative are standard. The built-in flowchart recorder automatically positions to the paper grid line and allows for accurate serial and overlay presentation. A holographic grating is utilized by both the high performance version and the standard version, which have stray light of less that 0.002%T and less than 0.05%T, respectively, at 220 nm. Perkin-Elmer Corp. **408**

Microelectrode

The pulsed microelectrode features interchangeable solid gold, platinum, and glass carbon tips to permit polarographic analysis of materials with differing overpotentials. The piston action electrode also allows modeling of electrochemical processes, including electro-organic synthesis. The microelectrode, which fits any vessel with a 14/20 joint, is pulsed ¼ inch into the test solution at rates of 0.1 to 6 pulses/s with variable intensity control. A pulse controller is available optionally. Pulsed microelectrode, $521; pulse generator, $521. ECO, Inc. **417**

The last digit makes the difference!

sartorius
Weighing and filtration worldwide.

New Sartorius Super Balances.

Sartorius and the new balances 1264 MP and 1265 MP have once again set new standards in weighing technology: a consistent development towards larger weighing ranges, higher accuracy, and greater ease of weighing.

Optimal resolution with controlled standard deviation.
Model 1264 MP: 3000 g/10 mg (300000 digital steps)
Model 1265 MP: 400 g/1 mg (400000 digital steps)

Such a measuring scope could up to now be offered by dual range balances. The disadvantages of this design – switching the weighing range and continuing with the accuracy loss of 1 place – are now relegated to history.

- Microprocessor as standard, providing storage of special weighing functions
- Data output for connection to the economical Sartorius line of peripheral systems and commercially available data equipment
- Instant weight results
- Overload stop
- Digital stability control
- Electronic damping of vibrations.

For details, please write or call:

Sartorius GmbH
P.O. Box 19
D-3400 Göttingen/West Germany
Telephone: (0551) 308-1
Telex: 09 6 830

CIRCLE 189 ON READER SERVICE CARD

High Vacuum System

Model BAE 080 T laboratory high vacuum system is a portable system designed for biological and nonbiological specimen preparation in electron microscopy and for general vacuum investigations. The unit comes with standard turbomolecular pumping. It offers conventional resistance heating or electron beam evaporation, and is available with T- or cross-shaped vacuum chambers. Balzers Corp. **415**

Vacuum Recording Balance

Model 1000 Electrobalance is a fully electronic vacuum recording balance with a capacity of 100 g, a sensitivity of 0.5 μg, a precision of $\pm 10^{-5}$ of total load, and a maximum weight change of 10 g. The instrument is designed to measure mass and force changes under ambient conditions as well as in high vacuum and other controlled environments. The electronic control unit is compatible with any 1, 10 or 100 mV strip chart recorder, digital voltmeter or other device for monitoring weight changes. The unit features electrical taring and up to 10 g of weight suppression. The instrument has an automatic range expander and a "percent of sample" feature. A wide variety of accessories is available. $11 600. Cahn Instrument Co. **424**

Recorder

The Gila 1-6 channel Flat-Bed Recorder has module technic. The different modules increase the number of possible applications. The recorder has 1-6 channels for 250 mm chart width. It offers 18 selectable sensitivities from 0.05 mV to 40 V, and 20 switchable chart speeds from 600 mm/min. to 3 mm/h. A wide range of function modules is available. Netzsch Brothers, Inc. **426**

Chemicals

Gel Filtration and Chromatography Media

Five new additions to the company's line of media are available. HA-Ultrogel is an "alloy" of hydroxyapatite microcrystals in agarose, crosslinked with epichlorohydrin, for adsorption chromatography. It can concentrate substances from very dilute solutions, and is resistant to denaturing agents and to extremes of pH and temperature. Ultrogel AcA-202 is an agarose-polyacrylamide type, very high in polyacrylamide and with a linear fractionation range of 1000 to 15 000 and an exclusion limit for globular proteins of about 22 000. Grades A-6, A-4 and A-2 are straight agarose type Ultrogels for gel filtration and affinity chromatography. Linear fractionation ranges for the three types are, respectively, 25 000 to 2 400 000; 55 000 to 9 000 000; and 120 000 to 25 000 000. Globular protein exclusion limits are 4 000 000; 20 000 000 and 50 000 000. All Ultrogel grades are preswollen. LKB Instruments, Inc. **432**

Fluorescent Reagent

Many fluorogenic substrates can be prepared using 7-amino-methylcoumarin, a highly fluorescent reagent. Substrates prepared using this chemical are specific and sensitive. The high degree of fluorescence permits detection of microgram quantities of chymotrypsin, trypsin, elastase and urokinase. Chemical Dynamics Corp. **433**

Hewlett-Packard introduces a flexible fused

AN IMPORTANT BREAKTHROUGH IN CAPILLARY COLUMN

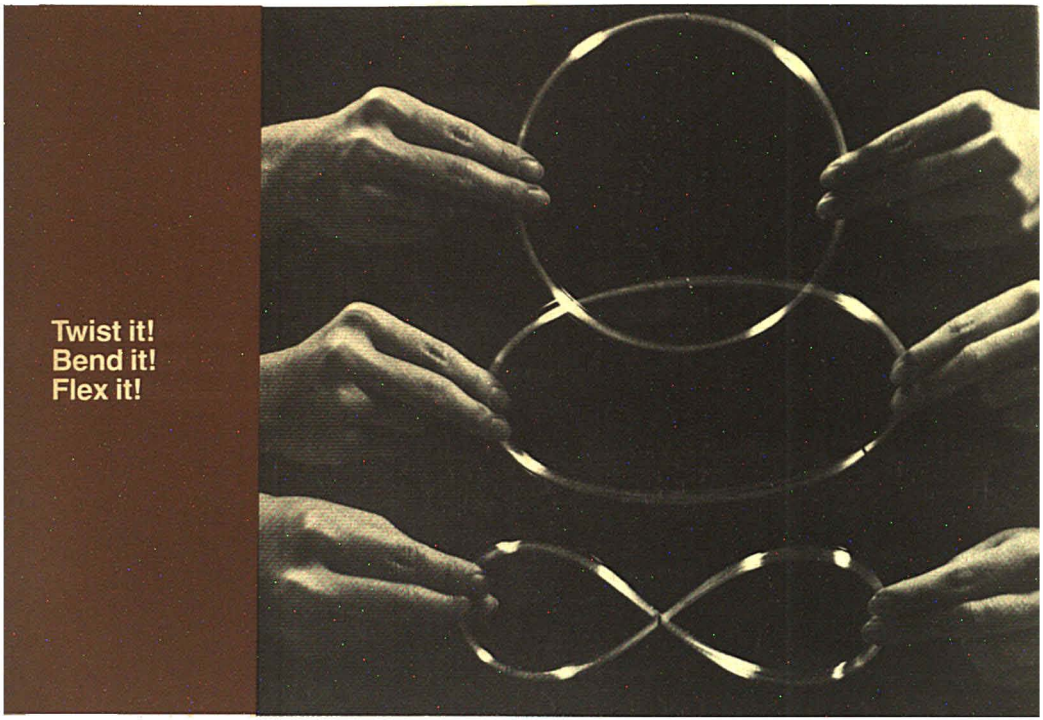

Four important advantages to enhance your chromatographic capabilities

A BREAKTHROUGH IN FLEXIBILITY . . . reduced breakage and easier installation. The columns are inherently straight permitting direct column connections for maximum performance. Note in the photographs how easily they can be twisted and configured to almost any shape required.

A BREAKTHROUGH IN INERTNESS . . . there are virtually no metal oxides to cause sample adsorption and column deterioration, thus enabling you to perform what might previously have been difficult or impossible analyses.

EXCELLENT THERMAL STABILITY . . . the upper temperature limit for the methyl silicone fluid (SP-2100) column is 280°C, and 220°C for the Carbowax® 20M.

HIGH EFFICIENCY . . . greater than 4000 theoretical plates per meter at k=5 (I.D.=0.20-0.21 mm) for methyl silicone column.

*Chemically identical to quartz but not crystalline.
® Registered Trademark of Union Carbide Corp.

revolutionary new silica* capillary column

TECHNOLOGY WITH DRAMATIC CHROMATOGRAPHIC PERFORMANCE

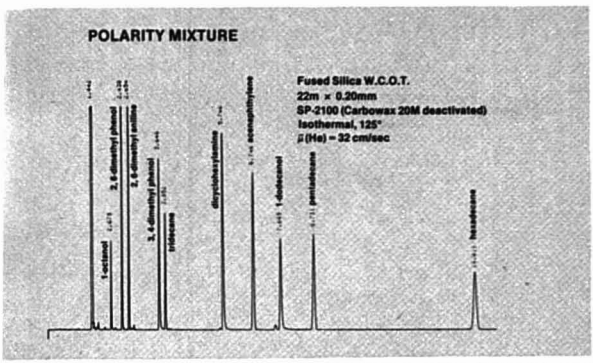

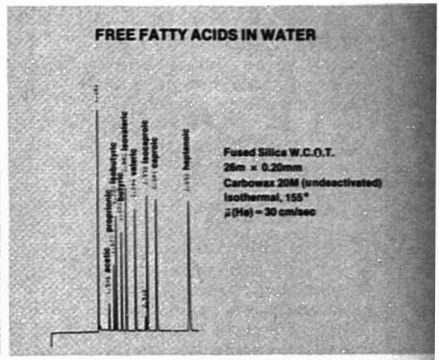

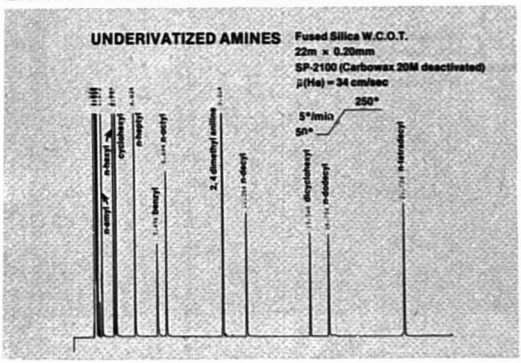

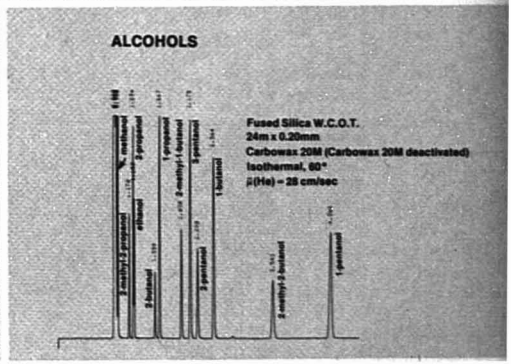

Above are a few of the GC analyses performed using HP fused silica capillary columns

ORDERING INFORMATION . . .

PART NO.	LENGTH	COLUMN TYPE	PRICE**
19091-60010	12 Meter	Methyl Silicone Column	$100
19091-60110	12 Meter	Carbowax* Column	100
19091-60210	12 Meter	Volatile Fatty Acid Column	100
19091-60025	25 Meter	Methyl Silicone Column	175
19091-60125	25 Meter	Carbowax* Column	175
19091-60225	25 Meter	Volatile Fatty Acid Column	175
19091-60050	50 Meter	Methyl Silicone Column	275
19091-60150	50 Meter	Carbowax* Column	275
19091-60250	50 Meter	Volatile Fatty Acid Column	275
19091-20050	50 Meter	Fused Silica Capillary Tubing	155

For larger quantities of fused silica capillary tubing contact factory for price and availability.

**U.S. price only. Subject to change without notice.

CONTACT YOUR LOCAL SALES REPRESENTATIVE FOR MORE TECHNICAL INFORMATION

The new Hewlett-Packard flexible silica capillary columns are available from stock. To place your order—call our toll-free number **800-523-7133** (8 A.M. - 5 P.M. EST)
PA residents call collect—215-268-2077

HEWLETT hp PACKARD

1507 Page Mill Road, Palo Alto, California 94304
For assistance call the HP regional office nearest you: Eastern 301 258-2000
Western 213 877-1282 Midwest 312 255-9800
Southern 404 955-1500 Canadian 416 678-9430
Ask the operator for analytical sales.

43908

CIRCLE 90 ON READER SERVICE CARD

Du Pont's new 1090 Thermal Analyzer collects, processes, stores, and reports the data you want, the way you want it.

The DuPont 1090 Thermal Analyzer/Data System combines speed and versatility with expanded data manipulation capabilities in a sophisticated instrument for research and product development.

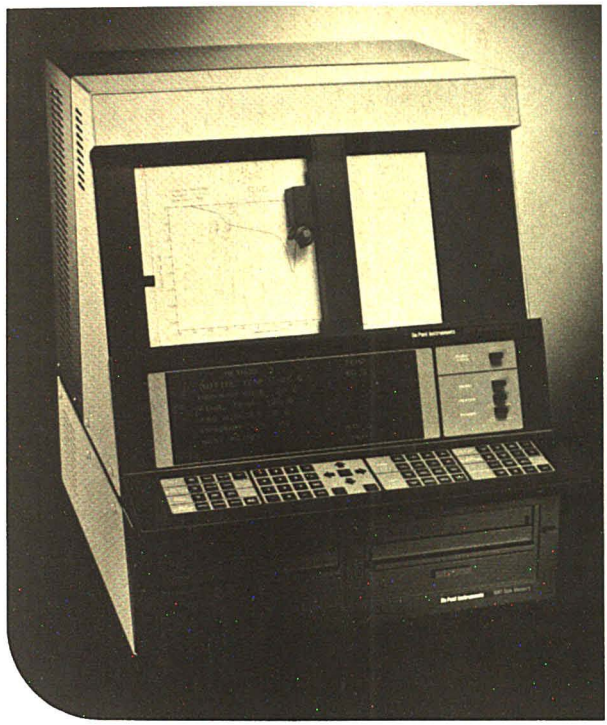

Microcomputer Data Analysis

The 1090 System microcomputers free personnel from time-consuming data computations and provide more complete reports than ever before. Minor transitions can be expanded and specific portions of the thermogram can be selected for data analysis. You can even analyze data from one scan while a second run is in progress.

Multiple Reporting System

In addition to the thermogram, the 1090 System can provide a printout of test conditions and analytical results. A bright alphanumeric display continuously indicates sample temperature and system status. Other program parameters are instantly displayed on command. All experimental data is stored on disks for recall at any time. You decide what to save or discard.

Expanded and Simplified Programming

Two-way conversational interaction between operator and instrument via the display makes programming easy. Increased versatility provides 12 linkable methods, heating rate selection in 0.1°C increments, and temperature scale expansion capability to 0.2°C/cm. Internal computer diagnostics inform you of errors in programming or circuitry.

Get Our New Literature

The 1090 system is compatible with all current DuPont modules. For details on the 1090 and other DuPont Thermal Analysis Systems, phone(302)772-5388 or write to DuPont Thermal Analyzers, Room 37359, Wilmington, DE 19898.

Thermal Analyzers

Scientific & Process Instruments Division

DUPONT

CIRCLE 54 ON READER SERVICE CARD

Manufacturers' Literature

Sampler. Discusses the design features and performance of the HP 7675A purge and trap sampler and use of the sampler in the analysis of trihalomethane, a slightly soluble volatile organic compound. 4 pp. Hewlett-Packard Co. **441**

Safety Manual. Covers OSHA requirements, a laboratory safety program, accident prevention, first aid, fires and firefighting, handling of toxic fumes, working with gases and acids, and disposal techniques. Catalogs a wide range of laboratory safety products. 80 pp. Fisher Scientific Co. **442**

Hazardous Compounds. Wall chart lists all of the OSHA concentrations for gases and vapors and notes analytical methods for the measurement of these 320 compounds. 11″ × 20″ Analytical Instrument Development, Inc. **444**

Gas Detector. Describes the principle of operation and specifications of a portable hazardous gas detector, Model 105, which uses photoionization to detect the presence of arsine and phosphine. 4 pp. Airco Industrial Gases **445**

Varian Instrument Applications. Vol. 13, No. 2 features articles on automated HPLC, measurement of acrylonitrile in industrial air by GC, user-generated pulsed NMR experiments, and fluorometric determination of Vitamin E compounds by HPLC. 15 pp. Varian Associates, Inc. **446**

The Liquid Chromatographer. No. 2 (Aug. 79) contains articles on an organic acids analysis HPLC column, HPLC columns for carbohydrate analysis, guard column systems, and reverse phase columns. 8 pp. Bio-Rad Laboratories **447**

Chromatography Newsletter. Vol. 7, No. 2 (Aug. '79) features articles on: determination of valproic acid using reversed phase LC; LC determination of phenytoin and phenobarbital; open tubular columns with thick liquid-phase films for low boiling compounds; LC separation of tricyclic antidepressant drugs; and polymer characterization by GPC using on-line data processing. 40 pp. Perkin-Elmer Corp. **440**

Chart Recorders. Details two Rustrak 4 inch chart trend recorder lines, the Series 7000 galvanometric recorders and the Series 6400 potentiometric recorders. 2 pp. Gulton Industries, Inc. **443**

Organophosphate Determination. Demonstrates that ion chromatography is the method of choice for the determination of dibutylphosphoric acid in nuclear fuel reprocessing streams. 2 pp. Dionex Corp. **450**

Manufacturers' Literature

Lead in Blood. Describes a method for the determination of lead in blood by means of an AA spectrophotometer, a furnace atomizer, and an autosampler. Ninety-five samples can be analyzed in 90 minutes. 4 pp. Instrumentation Laboratory **448**

pH Meters. Describes, illustrates, and provides comparative specifications for the company's pH and specific ion meters. Gives concentration ranges for 23 electrodes. 5 pp. Orion Research **449**

Catalogs

Liquid Chromatography. Contains LC and HPLC columns, pumps, detectors, gradient elution apparatus, fittings and valves. 60 pp. Glenco Scientific, Inc. **453**

Chemicals. Alphabetically lists inorganic and organic products, biochemicals, and biological stains which are available in quantities generally in the range of 0.01–20 g. 124 pp. Chem Service, Inc. **454**

NMR Products. Features sections on sample preparation, sample handling, sample tubes, microcell assemblies, EPR-ESR, special tubes and accessories. 12 pp. Kontes **455**

Research Chemicals. The 1979/1980 edition contains over 30 000 listings of organic and inorganic chemicals. 353 pp. Pfaltz & Bauer, Inc. **456**

Fluid Control. Information on the line of valves and filters includes applications and technical operating data. 16 pp. Hoke Inc. **457**

Oscillographic Recorders. Fixed range and plug-in signal conditioner chart recorders are described and illustrated. 6 pp. Gulton Industries, Inc. **458**

Biochemicals. The 1979–80 edition describes 980 products including immunochemicals, blood proteins, electrophoresis apparatus and reagents, and nucleic acids. 150 pp. Miles Laboratories, Inc. **459**

Pesticides. Includes defoliants, fumigants, insecticides, repellants, fungicides, herbicides and many others. 80 pp. Chem Service, Inc. **460**

For more information on listed items, circle the appropriate numbers on one of our Readers' Service Cards

DO ANY OR ALL!

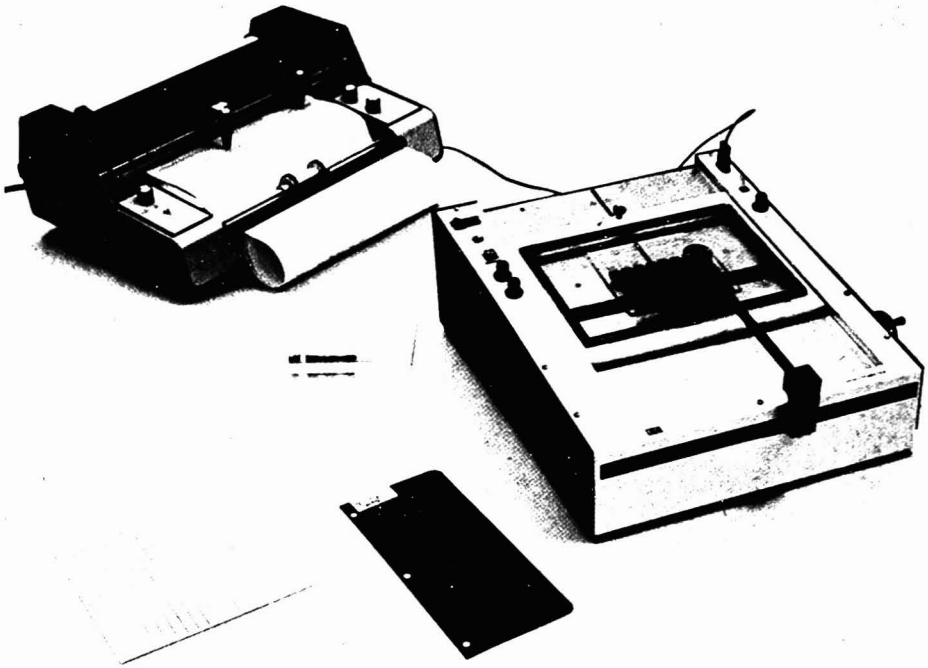

Autoradiograms, TLC plates, electrophoregrams. With one E-C Densitometer, do any or all!

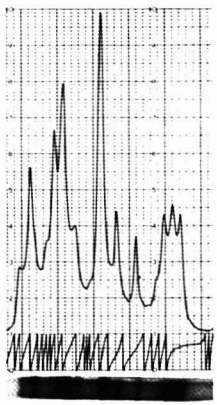

Scan and integration of DNA sequence autoradiogram.

The EC 910 Transmission Densitometer offers the most versatility at the lowest cost of any densitometer scanning in the visible light range. Only $1695* complete with electronic integrator, dielectric filter, and the support medium template of your choice.

With it you can scan and integrate *intact* gel slabs and columns, X-ray film, cellulose acetate and chromatography strips, and other patterns on selected support media. Scanning area 18cm X 25cm eliminates need for cutting.

Interchangeable light slits and optical filters enable precise quantitation regardless of stain characteristics.

Compatible with all millivolt recorders, the EC 910 Densitometer is lightweight, compact, and takes little bench space. Reliability assured by solid state electronics.

Like more information? Call E-C Technical Service collect at 813-344-1644 or write:

E-C Apparatus Corporation
3831 Tyrone Blvd. N.
St. Petersburg, Florida
33709

E-C

*Recorder additional but calibrated with Densitometer if ordered at the same time

CIRCLE 63 ON READER SERVICE CARD

Automatic Nitrogen Analyzer mod.1400

The first choice for micro and macro nitrogen determination

Feeds, soils, processed foods, coal, fertilizers, tobacco, fibers, polymers, lubricating oils, biological samples, organic compounds

- ☐ Fully automatic sample and data processing
- ☐ 50 nitrogen determinations in 4 hours
- ☐ Accuracy: ± 0,3%
- ☐ Reproducibility: ± 0,2%
- ☐ No digestion problems
- ☐ Low cost per analysis

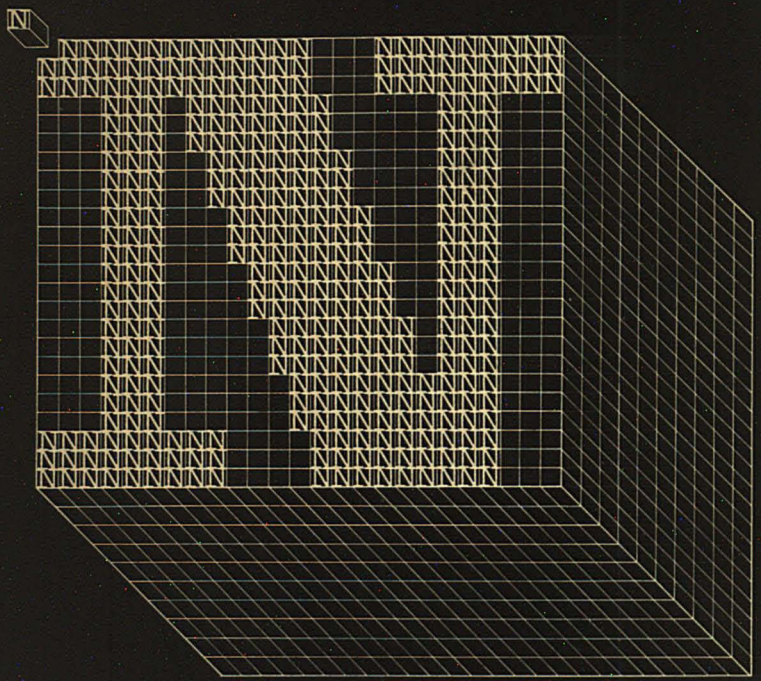

For further information in Europe and USA please contact our local Subsidiary or Distributor.

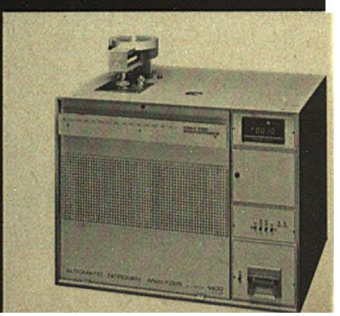

MONTEDISON GROUP
FARMITALIA CARLO ERBA

CARLO ERBA STRUMENTAZIONE

P.O. BOX 4342 I - 20100 MILANO

CIRCLE 37 ON READER SERVICE CARD

Statistics in Analytical Chemistry

Evaluation and Optimization of Laboratory Methods and Analytical Procedures: A Survey of Statistical and Mathematical Techniques. D. L. Massart, A. Dijkstra, and L. Kaufman. xvi + 596 pages. Elsevier North-Holland, Inc., 52 Vanderbilt Ave., New York, N.Y. 10017. 1978. $57.75

Reviewed by Harry L. Pardue, Department of Chemistry, Purdue University, W. Lafayette, Ind. 47907

This book is recommended to my colleagues in analytical and clinical chemistry with full confidence that it will be useful to all except those who are already expert in statistical methods and optimization procedures. The principal strength of the text is in the breadth of coverage; to the best of this reviewer's knowledge, there is no other single volume that includes all the topics in this text.

The book is presented in five parts, namely: evaluation of the performance of analytical procedures; experimental optimization; combinatorial problems; requirements for analytical procedures; and systems approach in analytical chemistry. There are 10 chapters in Part I, five chapters in Part II, nine chapters in Part III, three chapters in Part IV, and three chapters in Part V. Most of the rigorous material is in the first four sections; the last section is somewhat philosophical in content. Some specific topics included in the text are categories of errors, frequency distributions, parametric and nonparametric statistical tests, the method of least-squares, analysis of variance, noise and drift, optimization methods, factorial designs, the simplex method, steepest ascent methods, multivariate statistical methods, clustering procedures, factor and principal component analysis, operational research, the diagnostic value of a test, cost-benefit considerations, process monitoring, process control, analytical chemistry and systems theory, the analytical procedure, and the analytical laboratory. This is a selected, incomplete listing intended to convey in minimal space the breadth of coverage in the text; many important topics contained in the text are not included in the listing.

Another attractive feature of the book is the manner in which the more quantitative topics are presented. These topics are introduced with substantive general discussions that are followed by more rigorous mathematical treatments. This format aids in the presentation of some rather formidable material.

The principal weakness of the text is that in some cases extent and depth of coverage have been sacrificed for breadth. Although the text includes some examples, this reviewer does not consider it a "how-to-do-things" text because many details are left to the reader's interpretation. However, this potential shortcoming is largely offset by the liberal use of carefully selected references that provide details not included in the text.

This survey of statistical and mathematical techniques used in analytical chemistry is a valuable addition to the analytical literature.

Ion-Molecule Reactions, Part 1: Kinetics and Dynamics. J. L. Franklin, Ed. xiv + 399 pages. Academic Press, 111 Fifth Ave., New York, N.Y. 10003. 1979. $38

Reviewed by R. G. Cooks, Department of Chemistry, Purdue University, W. Lafayette, Ind. 47907

Several areas of science are being treated to volumes of "benchmark papers" in which a prominent specialist selects and comments upon key papers in an area of research. The concept is good, especially for an established investigator entering a new field: A beachhead into the area is provided, in the form of a single volume containing material culled from a variety of original sources over a period of time. This is a very considerable convenience, as is the organization by subject matter and the linking of topics by means of explanatory comments provided by the editor. Best of all, the original investigators are left to speak for themselves in this format.

J. L. Franklin has edited a two-volume set of benchmark papers on ion-molecule reactions. In this, the first volume, he covers the fundamentals of the subject, tracing its beginnings, treating theory and dynamics through 1977, dealing with the effects of energy on rates, and covering some thermochemical determinations. His selections have produced an exciting set of papers. Editorial comments are quite brief (less than 20 pages total) and serve as a set of guideposts, rather than assaying any critical interpretation. Particularly impressive is the coherent development of the subject through the volume. Some multiauthored texts don't flow as smoothly.

The second volume will include ion cyclotron resonance and chemical ionization and may, therefore, be more immediately relevant to analytical chemists. Nevertheless, the material covered here underlies such applications, and this book provides a successful approach for acquainting readers with ion-molecule reactions.

ESCA and AUGER Spectroscopy. D. M. Hercules. 6 audiotape cassettes (5.9 hours) + 152 page manual. Dept. of Educational Activities, American Chemical Society, 1155 16th St., N.W., Washington, D.C. 20036. 1979. $165

Reviewed by G. E. McGuire, Analytical Chemistry Laboratory, Tektronix Inc., Beaverton, Ore. 97077

The rapid proliferation of surface analytical techniques such as Auger and photoelectron spectroscopy in academic and industrial laboratories justifies the effort put forth in creating an audiocourse and related manual providing the background and development of these techniques. The audience for which this audiocourse was intended is the advanced undergraduate or graduate level scientist but not the expert in this field. In addition the course would be useful for anyone just entering the field or for anyone who wants to know about analytical applications of the techniques. Very little prior knowledge about the techniques is required. The material in the course is somewhat dated (none later than 1974) and is slanted more toward photoelectron spectroscopy (ESCA) than Auger spectroscopy (AES). The basic principles of these techniques are well presented even though the author obviously is not as familiar with AES.

The audio portion of the course is clear and precise. It progresses at a pace which is easily followed yet which requires the alert attention of the audience because it is heavily loaded with technical information. The manual follows very closely the audio por-

tion of the course and will make an excellent reference for the student to use at a later date.

The course has a good balance between the fundamentals of the technique, the instrumentation that is required, the common practices of the techniques, and analytical applications of ESCA and AES to a wide variety of systems. There is not a major area that is not discussed. The field is growing at such a rapid rate it would be hard to go into greater detail than the author has in a reasonable amount of time. Minor areas that could have received greater attention are UPS as a complement to XPS for looking at the valence band structure of solids and the use of X-ray analysis as a means of analysis to complement AES. Electron excited X-ray analysis is mentioned in passing at one point, and later one is left with the impression that the sensitivity of the technique is no better than 5%. Actually both AES and X-ray could be done simultaneously with about the same sensitivity for many elements.

The author has referenced his material well so that further study in specific areas is easily achieved. There are a number of good texts listed in the general bibliography that may be used as recent resource material. Most of the other references refer to literature published before 1975. The author has chosen some of the most appropriate references from that time period but perhaps overlooks the major applications and directions this field is taking today.

The figures used for illustration are clean and the majority are easy to follow. The author has made a judicious selection of material to illustrate his comments. This does not mean there could not be some improvement. However, since the author has presented most of the material just as it appeared in the literature, he has generally selected the best material available.

There are only two areas that this reviewer finds disconcerting. First, I find the author has slanted the material more toward ESCA than AES as would be expected due to his own experience and background. However, in doing so, one gets the impression he is not thoroughly familiar with AES and may misrepresent some aspects of the technique. For example, the mode of presenting AES data has historically been in derivative form. There is no physical barrier to prevent one from plotting the data directly in the N(E) mode, and recently this has become more widely accepted because the N(E) mode is more quantitative. Another area that is not thoroughly explained is the analyzer design for AES. Most Auger spectrometers were designed for high transmission and low resolution since many AES peaks were broader than the corresponding ESCA peaks, and historically the chemical shifts in Auger spectra were not widely recognized.

The second somewhat related area of discussion that I disagree with is that of C contamination. The author implies that C appears on every sample in an unavoidable fashion. At least in the semiconductor industry, where sources of contamination can be critical, there are many samples that appear C free. An inert or unreactive surface will not readily pick up C from the air if handled properly. Historically, Auger spectrometers have had much better vacuum systems than photoelectron spectrometers and have been used in a manner much more conducive to clean surface conditions.

These surface techniques and many others have opened new frontiers in materials science and have rapidly gained in popularity. This audiocourse does a good job of identifying some of those areas and is a valuable source for an introduction into this field.

Applications of High Performance Liquid Chromatography. A. Pryde and M. T. Gilbert. xii + 255 pages. John Wiley & Sons, Inc., 605 Third Ave., New York, N.Y. 10016. 1979. $29.95

Reviewed by Howard G. Barth, Analytical Division, Hercules Research Center, Hercules Inc., Wilmington, Del. 19899

Like most books of its genre, this HPLC application book contains a section on HPLC theory, equipment, and practice in addition to an applications section. Although the theory and equipment chapters are well-written and relatively free of errors, they offer little new information except to novice chromatographers. The remaining chapters in this section on the practice of HPLC and modes of chromatography contain some informative comments of interest to practicing chromatographers. This section contains adequate literature coverage with 233 references. However, topics are not treated in any significant depth, and many are just glossed over.

Only one serious error was found in this section. In discussing column packing materials, the authors state that it is desirable for particles to have fairly wide pores because "otherwise solute molecules can become trapped in the small pores thereby giving rise to tailed peaks." If this were true, gel

permeation chromatography would be in serious trouble! What happens, of course, is that the solute will be excluded from the smallest pores which will result in a lower capacity factor.

The application section covers pharmaceuticals (antibiotics, antibacterials, antidepressants, CNS depressants, analgesics, anti-inflammatory drugs, diuretics, drugs of abuse, alkaloids, miscellaneous drugs), biochemicals (lipids, steroids, prostaglandins, tricarboxylic acid cycle compounds, carbohydrates, biogenic amines, amino acids, proteins, nucleosides, nucleotides, nucleic acid bases, porphyrins, bile pigments, vitamins), environmentally important compounds (pesticides, carcinogens, industrial pollutants), plant and food products, organometallic and inorganic complexes, and separation of optically active compounds. These chapters are lucidly written and informative, although most of the 633 references in this section are pre-1977 (52 are from 1977).

For each compound there is a thorough discussion of HPLC methodologies and, as stated in the preface, there are sufficient details of chromatographic conditions to convey an idea of the method's potential. In the drug chapter, analysis of drugs in body fluids as well as in pharmaceutical formulations is presented. In addition, the degradation and metabolic products of many compounds are reviewed. The book contains a compound index as well as a subject index.

Of the nine appendixes in this book, four are tables of commercially available HPLC packing materials; although several years old they are still useful. However, the listing of GPC packing materials is practically useless because it is incomplete and does not include pore-size ranges of each support. I see no reason why an appendix describing the Wilke-Chang equation for calculating diffusion coefficients is included in an applications book. Similarly, the appendix on calculating surface coverage of bonded phases is out of place in this book. The appendix concerning the use of reverse phase HPLC to measure partition coefficients and to predict biological activity could have been expanded into a full chapter.

As a practically-oriented text on HPLC applications this book has the limitations cited; however, the chapters dealing with drugs and biochemicals are particularly useful. Thus, it is recommended to pharmaceutical chemists and biochemists who would like a comprehensive survey of most of the early literature.

New Books

Todd-Sanford-Davidsohn Clinical Diagnosis and Management by Laboratory Methods, 16th ed., Vol. I. J. B. Henry, Ed. xxiv + 1170 pages. W. B. Saunders Co., W. Washington Square, Philadelphia, Pa. 19105. 1979. $49

The 16th edition is divided into six parts, with three parts in each of two volumes. The first part (16 chapters) covers chemical pathology and clinical chemistry. Among the topics included are sources of variation in laboratory measurements, reference values, theory and practice of laboratory technique, and therapeutic drug monitoring and toxicology. The chapter on principles of instrumentation covers spectrophotometric and photometric

Selection guide to Swagelok® QUICK-CONNECTS

. . . the easy way to add versatility to your gas and fluid systems

- Reliable, leak-free service with vacuum or pressure
- Fast operation—no twisting
- Combinations of body and stem assemblies to suit your system requirements
- 360° swivel action
- Pressure ratings to 10,000 psi
- Brass and 316SS in sizes from 1/16" to 1" tubing or pipe connections
- Available from local distributor stocks

CRAWFORD FITTING COMPANY
29500 Solon Road, Solon, Ohio 44139
Crawford Fittings (Canada), Ltd., Ontario

MINIATURE "QM" SERIES

Finger-tip operation, low dead space, 1/16" male and female NPT, 1/16" and 1/8" tube connections.

STEMS **BODIES**

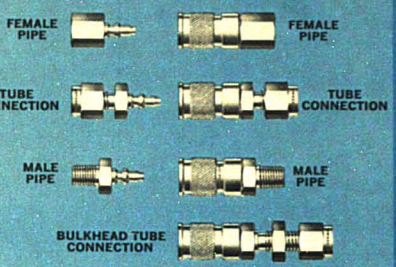

Patented

FULL FLOW "QF" SERIES

No orifice restrictions, 1/4" to 1" male and female pipe ends or tube connections.

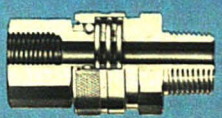

STEMS **BODIES**

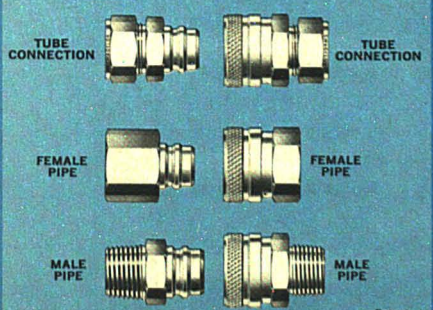

Patented

STANDARD "QC" SERIES

All stems available in single end or double end shut off, 1/8" to 1/2" sizes.

STEMS

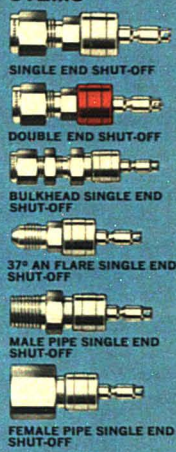

BODIES

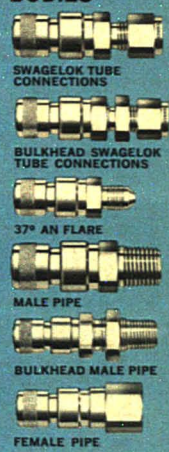

Patented

ACCESSORIES Special devices are available to prevent damage or contamination in the disconnected position.

"KEYED QC" SERIES

"Keyed" and color coded *(positive mechanical lockout system)* to prevent unmatched stems and bodies from coupling, eliminating accidental mixing of gases and fluids in multi-line systems. Eight different "Keys" available.

Patented

CIRCLE 32 ON READER SERVICE CARD

measurements, flame photometry, AA spectrophotometry, and eight other types of approaches. Radioimmunoassay and related techniques are the topic of another chapter.

The Chemistry of Silica: Solubility, Polymerization, Colloid and Surface Properties, and Biochemistry. R. K. Iler. xxiv + 866 pages. John Wiley & Sons, Inc., 605 Third Ave., New York, N.Y. 10016. 1979. $65

Chapter 5 covers silica gels and powders in 159 pages. Among the topics included are sources of silica gel, factors controlling gel characteristics, forming and shaping of gel particles, and special gel structures. Short sections are devoted to silica gels with ion-exchange surfaces, commercial silica gels, and chromatographic column packings. There are over 600 references, some as recent as 1977.

Physicochemical Measurement by Gas Chromatography. J. R. Conder and C. L. Young. xix + 632 pages. John Wiley & Sons, Inc., 605 Third Ave., New York, N.Y. 10016. 1979. $75

This text was written for those wishing to use GC in physicochemical investigations. However, four of the 13 chapters would be useful for those concerned with chemical analysis by GC. Principles, advantages, precision and accuracy of the GC method are covered in the first chapter. The chapter on basic theory and method for infinite dilution includes retention parameters, nonlinearity and concentration-dependent effects, and operating conditions for good measurements. Apparatus and experimental procedures, including finite concentration techniques and medium pressure GLC, are detailed in chapter 3. The supported liquid and its interfaces are the topic of chapter 11.

Continuing Series

GLC and HPLC Determination of Therapeutic Agents. Vol. 9, Part 3. Kiyoshi Tsuji, Ed. xiv + 528 pages. Marcel Dekker, Inc., 270 Madison Ave., New York, N.Y. 10016. 1979. $45

This volume is the last of three parts of Vol. 9, and Part 3 continues the full-scale exploration of Part 2 into the major drug classes. It contains detailed methodology and also provides a critical review of the literature. The 16 chapters are divided into two parts: metabolic disease and endocrine function agents, continued from Part 2, (11 chapters) and nutritional agents and others (5 chapters). Many chapters contain summary tables of drugs with details on chromatographic conditions.

U.S. Government Publications

Order copies of the following PREPAID at the price shown by SD Cat. No. from Superintendent of Documents, U.S. Government Printing Office, Washington, D.C. 20402. Foreign remittances must be in U.S. exchange and include an additional 25% of the publication price to cover mailing costs

A Reference Method for the Determination of Potassium in Serum. R. A. Velapoldi, R. C. Paule, Robert Schaffer,

John Mandel, L. A. Machlan, and J. W. Gramlich. 104 pages, 1979. $3.75. SD Cat. No. 003-003-20068-1

A reference method for the determination of serum potassium based on flame atomic emission spectroscopy is described. Results from 12 laboratories show that the standard error for a single laboratory's performance of the procedure ranged from 0.049 to 0.063 mmol/L with a maximum bias of 0.065 mmol/L over the range in concentrations from 1.319 to 7.326 mmol/L.

Rate Coefficients for Ion-Molecule Reactions. L. W. Sieck. 27 pages. 1979. $1.30. SD Cat. No. 003-003-02027-3

A compilation is presented of all experimentally determined biomolecular and termolecular rate coefficients for the reactions of organic ions (other than those containing only C and H) with neutral molecules in the vapor phase. The literature covered is from 1960 to the present, and both positive and negative ions are considered.

A Guide to Undergraduate Science Course and Laboratory Improvements. National Science Foundation, Science Education Directorate. 1979. Free. Order No. SE 79-40 from Forms and Publications, National Science Foundation, Washington, D.C. 20550

This book reports activities carried out at colleges and universities from 1976–80 with support from the National Science Foundation's Local Course Improvement and Instructional Scientific Equipment Programs. The complete project roster of 961 awards is arranged first by state and then by institution. The subject index with 11 273 entries contains project descriptions and titles, key subject terms, and equipment names for 804 projects.

ASTM Publications

The following are available from the American Society for Testing and Materials, 1916 Race St., Philadelphia, Pa. 19103 (U.S.A., Canada, and Mexico, add 3% shipping charges. Other countries, add 5%).

Part 31 of the Annual ASTM Standards. 1304 pages. 1979. $38

Part 31 contains all of the ASTM standards on water analysis (a total of 152), including many new additions. Among the contents are sampling and flow measurement, inorganic and organic constituents, radioactivity, and water-formed deposits. New standards include tests for: antimony in water; volatile alcohols in water by direct aqueous injection GC; and barium in brackish water, seawater, and brines.

Part 42 of Annual ASTM Standards. 618 pages. 1979. $21

Part 42 contains 78 standards on emission, molecular, and mass spectroscopy; chromatography; resinography; microscopy; computerized systems; and surface analysis. New standards as well as standards which have been revised or changed in status are included. New standards include: AA analysis, definitions relating to surface analysis, LC terms and relationships, approximate determination of the current density of large-diameter ion beams for depth profiling of solid surfaces, and testing fixed wavelength photometric detectors for use in LC.

Nanograde® Solvents– Provide Chemical Purity

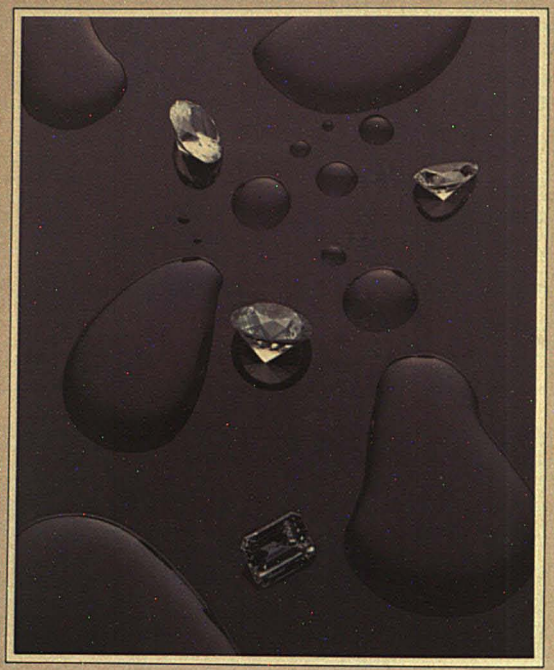

No solvent can be free of all possible impurities. But, like gem-quality diamonds, Nanograde® Solvents are made to be free of contaminants that would diminish their value in their intended use.

Performance in pesticide residue analysis.
All Nanograde products are essentially free of pesticide-like impurities and non-volatile substances are held to less than 5 ppm. They are closely controlled for impurities which can interfere with pesticide analysis by TLC or GLC with electron capture detection.

Maximum interferring peaks are guaranteed no greater than that produced by 10 nanograms/liter of heptachlor epoxide or 100 nanograms/liter of Parathion.

Nanograde Solvents: Acetone/Acetonitrile/Benzene/n-Butyl Acetate/Chloroform/Cychlohexane/Dichloromethane/Ether/Ethyl Acetate/Hexane/Isopropyl Alcohol/Methyl Alcohol/Pentane/Petroleum Ether/Toluene/2,2,4-Trimethylpentane

Nanograde Solvents are conveniently available from a nationwide network of Mallinckrodt distributors. Contact us today for more information and the name of the distributor nearest you.

Mallinckrodt® **Call the:**

Hot Line

(800) 325-7840

When you need something special

Mallinckrodt, Inc.
Science Products Division
P.O. Box 5840/St. Louis, Missouri 63134

CIRCLE 157 ON READER SERVICE CARD

Editors' Column

FACSS Meets in Philadelphia

The 6th Meeting of the Federation of Analytical Chemistry and Spectroscopy Societies (FACSS), held in Philadelphia, Sept. 16–21, 1979, was well attended, despite the fact that the fall American Chemical Society National Meeting had been held in Washington, D. C. the preceding week. Approximately 1400 people participated in this meeting where there were eight competing sessions at any one time! Sessions devoted to the latest techniques, such as inductively coupled plasmas, photoacoustic spectroscopy, and field flow fractionation, competed with more applied sessions dealing with forensic science, clinical chemistry, and steel analysis. Plenary lectures and award addresses lent balance to the technical program.

Looking to the future, C. Th. J. Alkemade of the Netherlands gave a plenary lecture "To Catch a Single Atom" in which he reviewed the latest work in detection of a single or a few atoms. He discussed both resonance and nonresonance optical methods and optical/electrical methods such as opto-galvanic, photoionization, and field ionization. E. Bright Wilson of Harvard University, in his award address as Lippincott Medal Winner, painted a rosy future for infrared spectroscopy based primarily on the development of tunable infrared lasers. In fact, Dr. Wilson predicted that we are on the edge of a revolution in infrared spectroscopy and that infrared will follow nuclear magnetic resonance in its development. These predictions are based on the availability of high power and coherence in sources which will produce very rich spectra. As the information provided will be much more complicated, more theoretical information is needed, and the computer will be absolutely essential to deal with the large amounts of data produced.

In his Anachem Award address, J. J. Kirkland of Du Pont, described his work with sedimentation field flow fractionation (SFFF) which turns out to be a useful separation method for macromolecules and for use in particle size determinations. SFFF, a retention chromatographic technique based on differential migration rates, uses a continuous mobile phase and yields a "fractogram." Dr. Kirkland showed through his work that the method also has potential for use as a preparative technique and can be used for biopolymer separations such as virus separations.

On a more practical level Joseph L. Peterson of the Dept. of Criminal Justice, at the University of Illinois summarized the status and problems of forensic science. This field is primarily a service and therefore must demonstrate its usefulness and its cost effectiveness. Currently it is used mainly by the prosecution, and the field is challenged to take the offensive in securing data which may be of value to either the prosecution or the defense.

Similar problems exist in clinical chemistry and in drug monitoring. That is, the techniques and instrumentation used must be shown to be of benefit to patients and to physicians treating patients. Before any regular drug monitoring program is instituted, it must be demonstrated that the level of drug(s) in the blood correlates in some way with the patient's condition. Arthur Karmen of the Albert Einstein College of Medicine described some of his work in following the concentration of therapeutic drugs in patient serum through drug therapy of epileptics. Any successful program such as this must be able to provide answers, for instance, while clinical patients are still in the clinic. Does it help a physician to know drug levels in serum of patients? When does he (she) need to know this? These are the questions faced in possible drug monitoring.

There were general application poster sessions on Wednesday in the exhibition hall. There were also two tutorial audiovisual sessions on Tuesday, morning and afternoon, put on by H. Sloane of SAVANT, Inc., Fullerton, Calif. The morning program dealt with atomic absorption and the afternoon program with high performance liquid chromatography. These well-done education aids attracted sizeable numbers of people. Each program consists of four 45-minute slide presentations with audio explanations. Information is carefully and clearly presented. Programs such as these should help in training people—the lack of well-trained chemists familiar with the principles of modern instrumentation is a constant complaint heard from those concerned with analytical problem-solving.

FACSS will meet again in Philadelphia in 1980 and '81. For next year's meeting, Sept. 28–Oct. 3, Sidney Flemming of Du Pont is Arrangements Chairman and Ted Rains of NBS is Program Chairman.

Josephine M. Petruzzi

Ohaus Brainweigh 300

Never before, for so little, could you get so much.

The Ohaus Brainweigh 300 costs only $1,195 and gives you a capacity of 300g with a readability of 0.01g. (If you want to find out how much that price is going to save you, just check what our competitors are charging for balances with similar capabilities.)

And we didn't stop with just economy. We went on to design in features that would be costly "extras" on any other balance on the market—if you could even get them.

Like extended visibility

Stand up, sit down, go to the back of the room. The display on the Ohaus 300 is still easy to read. That's because the no-glare window with the big, easy-to-read digits is deliberately angled for maximum visibility wherever you are. And that can save a lot of headaches whether you're in a lab, or on the line or in a classroom.

It tells you when it's ready—and when you've goofed

No more guessing whether the balance has settled down; no more annoying digit flutter. When the "g" appears beside the digits—in 3 seconds or less—it's your guarantee that the reading is stable.

And if the pan is overloaded or dislodged, you'll get an error sign in the window.

The 300 is a new generation balance

This new, low-profile balance is only a little larger than an ordinary desk phone. But packed inside is enough advanced technology to make the Ohaus 300 a generation ahead of any other balance on the market. Its state-of-the-art electronic components are almost entirely plug-in for easy service. And there are fewer of them—for better reliability and more dependable performance.

Want a BCD interface now—or later?

You don't have to worry about it. Unlike other electronic balances, every Ohaus Brainweigh comes equipped to handle a BCD option. You can add a BCD interface right away—or whenever you come to need it.

Parts and service are as near as your dealer

The Ohaus 300 is made right here in the U.S. And although its built-to-take-it die-cast case and solid state components put maintenance at a minimum, when the balance finally needs a little attention, it's nice to know your local dealer can do the job.

Get all the facts

If you'd like to see the rest of the reasons why the Ohaus Brainweigh 300 outclasses the competition, and the many ways it can make your operation faster, easier and more accurate, just return the coupon.

THE OHAUS BRAINWEIGHS™

The weigh of the future.

OHAUS ®Ohaus Scale Corporation, Dept. 11-119
29 Hanover Road, Florham Park, N.J. 07932
(201) 377-9000

☐ Yes, show me the weigh of the future. Send me the full-color catalog on the Ohaus Brainweighs.

☐ I'm ready to see a demonstration. Please have a dealer sales rep call me.

Name _____

Title _____

Organization _____

Address _____

City _____ State _____ Zip _____

Phone Number _____

CIRCLE 160 ON READER SERVICE CARD

The Problem:
Inadequate resolution

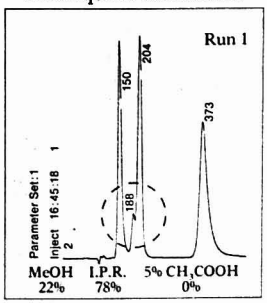

The Solution:
Optimized separation

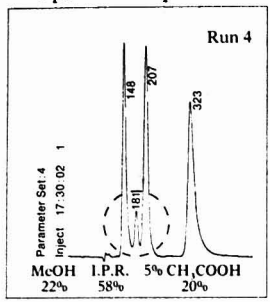

The ternary solvent generator of the SP 8000B automatically varies the ion pairing reagent independently of the methanol concentration to improve resolution of four peaks in this typical sample. ***Set-up time was only 10 minutes for a 1-1/2 hour automatic run.*** *(For more details, ask for our Ternary Solvent Applications Brief on automatic methods development; we'll also send you the latest issue of our quarterly* Chromatography Review.*)*

The New SP 8000B Improves Your Ability to Do Creative Chromatography.

Easier-than-ever programmed methods development.

We've added a CRT, injection delay, detector auto-zero and other important features to the SP 8000, the first truly automatic HPLC. The new CRT makes it really easy for you to interact with the SP 8000B. You can observe operating parameters anytime, whether you are doing methods development or routine analysis. Combine these features with SP 8000B's three patented processes–three-solvent mixing, helium degassing, and flow feedback control for pulse-free operation–and you have the best price/performance in the business. And good news for owners of our SP 8000–all these new features can be retrofitted in the field. Call or write us for details.

Easier to use! Just what you'd expect from Spectra-Physics, the leader in automated chromatography.

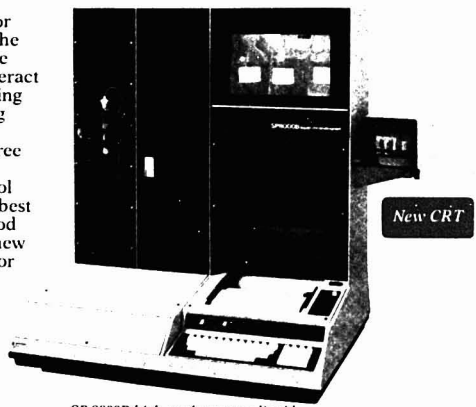

SP 8000B high-performance liquid chromatograph includes CRT, alphanumeric keyboard and printer/plotter for combined chromatogram and data reports.

USA headquarters: Spectra-Physics
2905 Stender Way, Santa Clara, CA 95051
European headquarters:
Spectra-Physics GmbH
Alsfelder Strasse 12, 6100 Darmstadt
West Germany
Telephone: 6151-7081 Telex: 419471
Or call one of our regional US sales offices: Midwest: 800-323-0583
In Illinois, (312) 956-0882
Mid-Atlantic: (301) 345-7333
East: 800-631-5693
In New Jersey, (201) 981-0390
South: 800-231-3567
In Texas, (713) 688-9886
West: 800-538-8118
In California, (408) 249-0105

Spectra-Physics
Innovators in Chromatography

CIRCLE 201 ON READER SERVICE CARD FOR PRODUCT INFORMATION.
CIRCLE 202 ON READER SERVICE CARD FOR APPLICATIONS BRIEF ON PROGRAMMED METHODS DEVELOPMENT.

Nonlinear Parameter Estimation

Thomas A. Brubaker
Department of Electrical Engineering
Colorado State University
Fort Collins, Colo. 80523

Kelly R. O'Keefe
Department of Chemistry
Colorado State University
Fort Collins, Colo. 80523

This is a second paper in a two-part sequence on the application of parameter estimation in analytical chemistry. Linear parameter estimation was treated in the first paper (1), and this will serve as background for the present discussion. In this paper nonlinear parameter estimation is described with emphasis given to gradient methods for the actual estimation process. Two examples, one from spectroscopy and one from kinetics, are used to demonstrate how nonlinear parameter estimation can be applied.

As mentioned previously, the paramount problem in successfully using parameter estimation in chemistry is the development of a parametric analytical model or a valid experimental data model for the chemistry being studied. For the linear case, the model is linear in the parameters and for scaler measurements the model output as a function of the independent variables, possibly past dependent variables, and the parameters is given as

$$\omega[x_k,\beta] = M[x_k]\beta. \qquad (1)$$

In (1) x_k is the kth vector of independent and dependent variables and β is the parameter vector. The term $\omega[x_k\beta]$ is the model output for a specific vector x_k which implies known or measured values for the independent and dependent variables. The term $M[x_k]$ is a one row matrix whose elements are the independent and dependent variables or are functions of these variables. Carefully note that we can also consider vector measurements where each measurement vector consists of two or more individual measurements taken at the same time.

For the nonlinear case, the model becomes a function of the parameters and this is denoted as the scaler quantity

$$\omega[x_k\beta] = f[x_k,\beta]. \qquad (2)$$

In both (1) and (2) the vector notation is simply a shorthand way of saying the model is a function of a set of independent and dependent variables and a set of parameters. An example is an output that is the sum of two exponential decays, such as might be observed for the phosphorescence of a binary mixture, where the model is given by

$$\omega[k\Delta t,\beta] = \beta_3 e^{-\beta_1 k\Delta t} + \beta_4 e^{-\beta_2 k\Delta t} \qquad (3)$$

where Δt is the increment of observation time.

For both the linear and nonlinear models, the most common error criterion describing how well the model fits the data is least squares where the summed square error is given as

$$S = \sum_{k=1}^{m} |y[x_k] - \omega[x_k,\beta]|^2. \qquad (4)$$

In (4), $y[x_k]$ is the measurement for the known or measured values of the kth vector of independent and dependent variables. In vector form the summed square error is given by

$$S = (y - \omega)^t(y - \omega) \qquad (5)$$

where y is a vector of all m measurements and ω is a vector of all model outputs. As shown in the previous paper, for the linear case

$$\omega = H\beta \qquad (6)$$

where H is a matrix of all of the M's given in (1). The resulting optimal estimate found by minimizing (5) is

$$\hat{\beta} = (H^tH)^{-1}H^ty. \qquad (7)$$

Note that for the linear model, (5) is quadratic in the parameter vector β and if S is plotted versus m parameters, S has the shape of an m-dimensional bowl with single minimum.

For the nonlinear model, S is not quadratic in the parameters and the shape of S in parameter space is generally unknown. Here local minima and maxima can occur, and as a result the procedure to find the set of parameters that minimizes S must be approached with caution. Probably the most viable tool in this work is interactive computer graphics that allow the chemist to interact with the estimation process as the computation proceeds. By experience we have found that the knowledge of the chemist coupled with the computer implementation of the algorithm to find the best $\hat{\beta}$ eliminates many of the problems associated with applying nonlinear parameter estimation to chemical problems.

Given the model for the chemistry, the problem is to find the values for the parameters that minimize the summed square error S. The most obvious solution is to simply search the parameter space; however, this method is very time consuming even for only a few parameters. Another alternative is to use a simplex approach which is a well-known algorithmic procedure for reaching a minimum. In the chemistry literature, simplex has been described by Deming and Morgan (2). Given the summed square error surface, a broad class of algorithms generally classified as gradient methods attempts to iteratively operate on the gradient of the error surface to force the summed square error rapidly toward a minimum. Well-known procedures are Newton's method, the Marquardt algorithm and Fletcher-Powell variable metric method. A more expanded list of gradient methods is given by Bard (3).

While no method for nonlinear parameter estimation has been shown to

0003-2700/79/A351-1385$01.00/0

be best, the gradient methods often are good choices in that convergence is proven and the rate of convergence is reasonably fast. However, most of the gradient algorithms, as well as many other methods, were designed for the solution of sets of nonlinear equations and not for parameter estimation where the measurements are corrupted by noise. As a result, the impact of the noise will usually lead to biased estimates, and the noise may have an effect on the convergence.

Because of space, emphasis in this paper will be placed on the gradient approach. Given the summed square error as defined by (5), the basis of these methods is to set up an iterative scheme of the form

$$\hat{\beta}_{i+1} = \hat{\beta}_i + P_i V_i \tag{8}$$

where V_i is a vector in the direction of the proposed ith step and P_i is a scaler selected such that $S_{i+1} < S_i$. In essence, then, V_i determines the direction of the new step and P_i determines its size so as to reduce the summed square error. An important theorem states that V_i is an acceptable direction if and only if there exists a positive definite matrix R_i such that

$$V_i = -R_i q_i \tag{9}$$

where q_i is the gradient vector. This now means the iterative expression given by (8) is following the gradient down toward a minimum value for the summed square S. This minimum can be a local minimum. The gradient methods vary in terms of the selection of a method for choosing R_i, q_i and P_i and with methods for calculating their values.

An approach to understanding the behavior of the algorithms is based on expanding the summed square error given by (5) using the model given by (2) in a Taylor series about a point β_i in parameter space. Doing this yields

$$S = S(\beta_i) + \left[\frac{\partial S}{\partial \beta_i}\right]^t (\beta - \beta_i) + \frac{1}{2}[(\beta - \beta_i)^t H_i (\beta - \beta_i)] + \ldots \tag{10}$$

In (10) the term $\partial S/\partial \beta_i$ is the gradient vector now denoted by

$$\frac{\partial S}{\partial \beta_i} = q_i \tag{11}$$

and H_i is the Hessian matrix of second partial derivatives whose elements are

$$H_{ij} = \frac{\partial^2 S}{\partial \beta_i \partial \beta_j} \tag{12}$$

where i and j range over the m parameter values. Given (10), suppose we truncate the series and let

$$Q_i = S(\beta_i) + (q_i)^t(\beta - \beta_i) + \frac{1}{2}(\beta - \beta_i)^t H_i (\beta - \beta_i). \tag{13}$$

Since Q_i is quadratic in β about the point β_i, Q_i is bowl-shaped and has a single minimum. Since $S(\beta_i)$ is a constant, taking the derivative of Q_i with respect to β and setting the result to zero will give the bowl minimum. Doing this yields

$$\frac{\partial Q_i}{\partial \beta} = q_i + H_i(\beta - \beta_i) = 0. \tag{14}$$

Assuming $\hat{\beta}_i$ is the ith estimate and letting $\beta_{i+1} = \beta$ = ith plus one estimate (14) now gives

$$\hat{\beta}_{i+1} = \hat{\beta}_i - (H_i)^{-1} q_i. \tag{15}$$

Equation (15) is known as the Newton or Newton-Raphson method. This method of gradient selection is effective as long as H_i is positive definite so that we know the algorithm is pointing toward a minimum. This is generally true if one is close to the minimum. However, over the total parameter space there is no guarantee that H_i is positive definite so the algorithm often is not viable.

Most other gradient methods deal with ways to force R_i in (9) to be positive definite. A well-known algorithm is a Marquardt-type algorithm where R_i is chosen to be

$$R_i = [A_i + \lambda_i I]^{-1} \tag{16}$$

where A_i is the Hessian or an approximation and λ_i is a constant chosen so that R_i is always positive definite. The Levenberg-Marquardt algorithm is a slight modification where A_i is chosen to be

$$A_i = J_i^t J_i \tag{17}$$

where J_i is a matrix of first derivatives with elements

$$J_{i(jk)} = \frac{\partial f_j(x;\beta)}{\partial \beta_k}. \tag{18}$$

This selection of A_i is useful for chemical parameter estimation because it is relatively easy to compute on an iterative basis. In addition, if the model chosen is correct, $J_i^t J_i$ is proportional to the Hessian as the error approaches the minimum, thus, in this region the algorithm behaves in a theoretic manner.

Examples. In the first example, we will demonstrate nonlinear parameter estimation using the simple sampled process

$$x(k\Delta T) = e^{\frac{-k\Delta T}{\tau}} \tag{19}$$

where τ is the time constant of the observed signal and ΔT is the sampling interval. Such signals commonly occur in time-resolved fluorescence and phosphorescence spectroscopy and the task is to estimate τ when the data are corrupted by noise. Using this model with the collected data y_i at intervals ΔT, the summed square error is

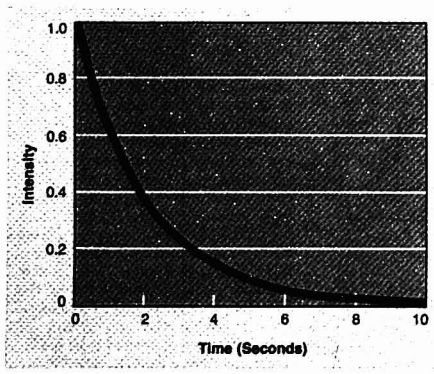

Figure 1. Ideal single exponential decay

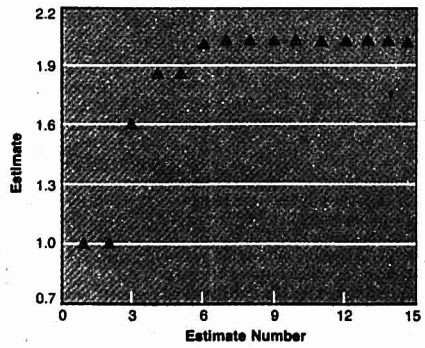

Figure 2. Convergence of estimates for time constants of single exponential decay

THE QUALITY REVERSE PHASE HPLC COLUMN

GUARANTEED!

Bio-Sil® ODS-10—the perfect combination of quality and price. Look at the price tag. Hard to believe only $195* for a 250 x 4 mm reverse phase column? As for quality, we guarantee top performance:

- 20,000 plates/meter minimum
- Asymmetry less than 1.5 at 10% peak height
- Low back pressure

Every Bio-Sil ODS-10 column comes with a test chromatogram and a test solution sample so you can verify performance yourself. This great combination is available from stock.

*U.S. domestic price only.

For a complete description of all Bio-Rad HPLC columns, request Bulletin 1056.

Contact:

BIO-RAD *Laboratories*

2200 Wright Avenue
Richmond, CA 94804
Phone (415) 234-4130
Telex 335 358

Also in Austria, England, Germany, The Netherlands, Italy and Switzerland.

CIRCLE 30 ON READER SERVICE CARD

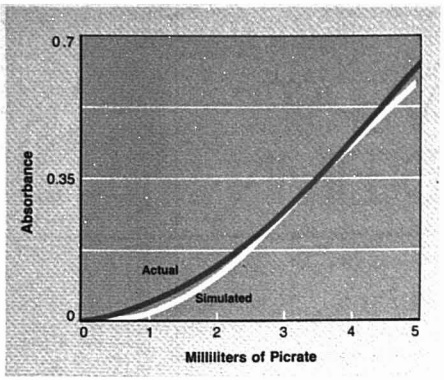

Figure 3. Actual and simulated photometric titration curves with kinetic complications

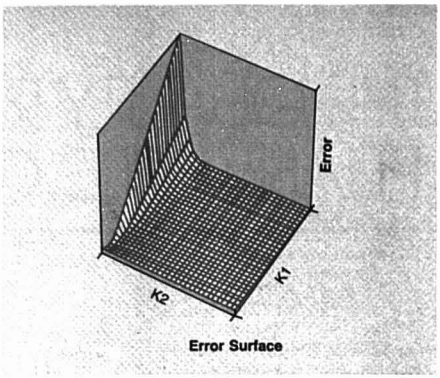

Figure 4. Global error surface for estimate of kinetic parameters

$$S = \sum_{i=1}^{m} (y(i\Delta T) - e^{-i\Delta T/i})^2. \quad (20)$$

For the case of $\tau = 2$ seconds, the ideal data is given in Figure 1. The parameter estimate is 2.015 seconds with additive noise with zero mean and variance 0.1. This corresponds to a signal to noise ratio of about 3. The convergence of the Marquardt Algorithm for an initial guess of 1.0 seconds is shown in Figure 2. Note that the convergence is dependent on the initial guess and the amount of noise power, but that in this case, convergence to a final estimate occurs in less than 9 iterations.

The second example involves the estimation of kinetic parameters from a photometric titration curve. If a titrand, A, is titrated at a constant rate with titrant T to produce a product, P, it is the sole absorbing species at the measurement wavelength, and in addition the titration reaction is

$$A + T \underset{k_2}{\overset{k_1}{\rightleftharpoons}} P. \quad (21)$$

The differential equation that describes the rate of reaction at any time in the titration is

$$\frac{d[A]}{dt} = -k_1[A]\{rC_t t/V - C_a V_i/V + [A]\} + k_2\{C_a V_i/V - [A]\} - r[A]/V \quad (22)$$

where r is the rate of titrant addition in Lsec^{-1}, V_i is the initial volume of the titrand in L, C_t and C_a are the titrant and titrand concentrations, respectively, in mol L^{-1}, V is the volume at time t, and d[A]/dt is the rate of appearance of species A. If all of these parameters in a titration are known, digital or analog techniques may be used to simulate the titration curve, i.e., produce an absorbance versus time plot. If, on the other hand, the kinetic parameters are unknown, our task is to estimate k_1 and k_2 so as to obtain good agreement between simulated titration curves and those experimentally measured.

When 3.70×10^{-4} mol L^{-1} creatinine was titrated with 1.19×10^{-2} mol L^{-1} picrate, both in 0.200 mol L^{-1} NaOH, the data labeled actual in Figure 3 were obtained. Pairs of initial guesses for k_1 in the range of 0 to 30 L mol^{-1} sec^{-1} and for k_2 in the range 0 to 3 sec^{-1} were supplied to the simplex parameter estimation algorithm; the differential equation was simulated for the guesses; and summed square errors were calculated using equation 4. Upon convergence, values of k_1 and k_2 were obtained that yield the titration curve labeled simulated in Figure 3. Repeated titration/estimation gave estimates of 4.67 ± 0.11 L mol^{-1} sec^{-1} for k_1 and 0.00172 ± 0.00012 sec^{-1} for k_2.

Figure 4 shows the summed square error surface for pairs of k_1 and k_2 in the parameter space. The complex nature of this surface results from the nonlinearity of the model and estimation structure.

References

(1) T. Brubaker, R. Tracy, and C. Pomernacki, "Linear Parameter Estimation," *Anal. Chem.*, **50**, 1017A–1024A (1978).
(2) S. N. Deming and S. L. Morgan, "Simplex Optimization of Variables in Analytical Chemistry," *Anal. Chem.*, **45**, 278A–283A (1973).
(3) Y. Bard, "Nonlinear Parameter Estimation," Academic Press, New York, N.Y., 1974.
(4) D. Marquardt, "An Algorithm for Least-Squares Estimation of Nonlinear Parameters," *J. Soc. Ind. Appl. Math*, **11**, No. 2 (1963).

This work was supported by Contract 8403203 between Lawrence Livermore Laboratory and Colorado State University.

Thomas A. Brubaker received his Ph.D. in Electrical Engineering in 1963 from the University of Arizona. Since that time he has taught at the University of Missouri, Columbia, and is presently a professor of electrical engineering at Colorado State University. His research interests are digital systems, digital signal processing, and their applications to instrumentation areas such as chemistry.

Kelly R. O'Keefe received his Ph.D. in Analytical Chemistry from the University of Illinois in 1975. He joined the faculty of Colorado State University in the same year. His research interests are in the areas of multielement atomic absorption spectrometry, kinetic methods of analysis, and applications of parameter estimation methods in analytical chemistry.

This $7.00* book can help you increase your productivity in pharmaceutical analyses

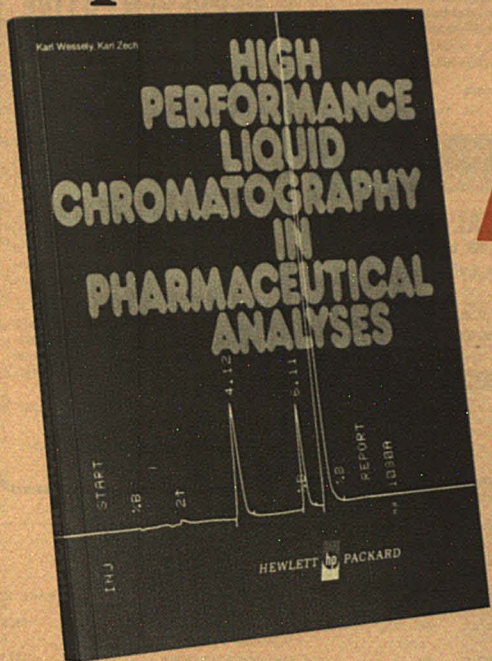

NEW

Just off the press from Hewlett-Packard, here is a user's handbook that provides

methodology for application of automated HPLC to a wide range of pharmaceutical analyses.

Here is a 157-page "digest" size compilation of information, so thorough and well-organized, that it makes one of the most valuable reference tools available to pharmaceutical industry chemists today.

A WEALTH OF INFORMATION AT YOUR FINGERTIPS

The information on the analyses includes chromatographic conditions, representative UV-Visible Spectra, chromatograms and complete reports. Major areas of HPLC applications such as isolation of natural compounds, pharmacokinetics and drug metabolism are described with text, sample chromatograms and illustrative figures.

Sections on methodology explain sample preparation procedures, HPLC separation system, detectors and quantitative analysis.

HERE ARE A FEW EXAMPLES OF THE ANALYSES:

- 13 digitalis glycosides by reverse phase HPLC
- Microbiological processes during penicillin production
- Decomposition study on benzodiazopine capsules
- Morphine alkaloids in raw opium
- Water soluble vitamins in pharmaceutical preparations
- Tablet formulation reproducibility study
- Theophilline assay by HPLC

AN INCLUSIVE BIBLIOGRAPHY INDEXED BY COMPOUND NAME

The bibliography references the pharmaceutical HPLC literature from 1974-1977 covering information useful in pharmaceutical separations.

USEFUL IN SOLVING SEPARATION PROBLEMS DURING ANALYSES

Each reference lists the column, mobile phase, detector and comments regarding the separation.

RELIABLE ANSWERS FOR CHEMISTS IN LESS TIME

The descriptions of improved separations, automated methods development and automatic sampling techniques can save the chemist valuable time.

HOW TO ORDER YOUR COPY

Send your check or money order to:

Hewlett-Packard Co.
Attn: D. Banks
Rt. 41, Avondale, PA 19311

*($7.00 plus other applicable taxes -- if any, plus $1.50 mailing cost) U.S. price only

Or, for more information, circle reader service number.

HEWLETT hp PACKARD

1507 Page Mill Road, Palo Alto, California 94304

For assistance call the HP regional office nearest you: Eastern 301/258-2000; Western 213/877-1282; Midwest 312/255-9800; Southern 404/955-1500; Canadian 416/678-9430

Ask the operator for analytical sales.

43910

CIRCLE 92 ON READER SERVICE CARD

LABORATORY SERVICE CENTER

CLASSIFIED SECTION
POSITIONS OPEN

INDEX TO ADVERTISERS IN THIS ISSUE

INDEX TO ADVERTISERS IN THIS ISSUE

Ten great reasons to choose KONTES...

1 TISSUE GRINDERS
- Duall®
- Dounce
- Potter-Elvehjem
- Micro Scale
- Ultrasonic

2 CHROMATOGRAPHIC APPARATUS
- Chromaflex® Columns
- TLC Densitometer
- Precoated TLC Plates
- Spotter & Tanks

3 SAMPLE PREPARATION
- Sweep Co-Distillation
- Extraction
- Kuderna-Danish
- Microflex® Systems
- Kjeldahl Systems

4 LABORATORY GLASSWARE
- Flasks
- Stopcocks
- Ground Joints
- Volumetrics

5 CRYOGENIC APPARATUS
- LNg Dewars
- Helium Dewars
- Cryostats
- Union Carbide Dewars
- Heli-Dewars®
- Poly-Dewars®

6 VACUUM APPARATUS
- Diffusion Pumps
- Mechanical Pumps
- Hi-Vac Valves
- McLeod Gages
- Cold Cathode Gages

7 FLOWMETERS
- Acrylic Purge Meters
- Variable Area Rotometers
- Differential Pressure Meters
- Process Meters
- Flow Indicators

8 DISTILLATION SYSTEMS
- Bench Scale
- Pilot Plant
- Adiabatic Columns
- Reactors

9 NMR SUPPLIES
- 5mm Sample Tubes
- Large Volume Tubes
- Microcells
- Filters

10 SEMI-MICRO GLASSWARE
- Bantam-ware® Organic Systems
- Microflex® Sample Prep Systems
- Airlessware® Systems
- Kem-Kits®

Outstanding Quality and Service are two more reasons.

...in one great TG-50 catalog. Ask for it.

KONTES
SCIENTIFIC GLASSWARE/INSTRUMENTS
Vineland, NJ 08360 (609) 692-8500

®T.M. Kontes

Exclusive Distributors: **KONTES OF ILLINOIS,** Evanston, Illinois • **KONTES OF CALIFORNIA,** San Leandro, California
KONTES (U.K.) LTD., Carnforth, England
CIRCLE 97 ON READER SERVICE CARD

ENJOY YOUR OWN MONTHLY COPY OF

Analytical Chemistry

1979

Toll Free: New Orders: 800-638-2000/Md. only 301-949-1551

	U.S.	Canada**	Foreign**
ACS Members*	☐ $12.00	☐ $21.00	☐ $21.00
Nonmembers	☐ $16.00	☐ $25.00	☐ $33.00

☐ Bill Me ☐ Bill Company ☐ Payment Enclosed
(Make payable to American Chemical Society)

RENEWAL?
☐ *Check here and attach your mailing label. Payment must be enclosed.* (E7)

Name

Position

Your Employer
☐ Home
Address ☐ Business

City State Zip
Employer's Business ☐ Manufacturing ☐ Academic
☐ Government ☐ Other

If manufacturing, type of products produced

*Subscriptions at ACS member rates are for personal use only.
**Payment must be made in U.S. Currency, by international money order, UNESCO coupons, U.S. bank draft, or through your book dealer.

Allow 60 days for your first copy to be put in the mail. 9998G

MAIL THIS POSTAGE FREE CARD TODAY

ENJOY YOUR OWN MONTHLY COPY OF

Analytical Chemistry

1979

Toll Free: New Orders: 800-638-2000/Md. only 301-949-1551

	U.S.	Canada**	Foreign**
ACS Members*	☐ $12.00	☐ $21.00	☐ $21.00
Nonmembers	☐ $16.00	☐ $25.00	☐ $33.00

☐ Bill Me ☐ Bill Company ☐ Payment Enclosed
(Make payable to American Chemical Society)

RENEWAL?
☐ Check here and attach your mailing label. Payment must be enclosed. (E7)

Name

Position

Your Employer
☐ Home
Address ☐ Business

City State Zip
Employer's Business ☐ Manufacturing ☐ Academic
☐ Government ☐ Other

If manufacturing, type of products produced

*Subscriptions at ACS member rates are for personal use only.
**Payment must be made in U.S. Currency, by international money order, UNESCO coupons, U.S. bank draft, or through your book dealer.

Allow 60 days for your first copy to be put in the mail. 9998G

MAIL THIS POSTAGE FREE CARD TODAY

NO POSTAGE
NECESSARY
IF MAILED
IN THE
UNITED STATES

BUSINESS REPLY CARD

FIRST CLASS PERMIT NO 10094 WASHINGTON D C

POSTAGE WILL BE PAID BY ADDRESSEE

AMERICAN CHEMICAL SOCIETY
Attn: Gayle Hebron
1155 Sixteenth Street, N.W.
Washington, D. C. 20036

NO POSTAGE
NECESSARY
IF MAILED
IN THE
UNITED STATES

BUSINESS REPLY CARD

FIRST CLASS PERMIT NO 10094 WASHINGTON D C

POSTAGE WILL BE PAID BY ADDRESSEE

AMERICAN CHEMICAL SOCIETY
Attn: Gayle Hebron
1155 Sixteenth Street, N.W.
Washington, D. C. 20036

analytical chemistry

Published by the
AMERICAN CHEMICAL SOCIETY
1155 16th Street, N.W.
Washington, D.C. 20036

Books and Journals Division
Director: D. H. Michael Bowen
Journals: Charles R. Bertsch
Magazine and Production: Bacil Guiley
Research and Development: Seldon W. Terrant
Circulation Development: Marion Gurfein

Manuscript requirements are published in the January 1979 issue, page 171. Manuscripts for publication (4 copies) should be submitted to ANALYTICAL CHEMISTRY at the ACS Washington address.

The Essence of Modern Analytical Chemistry

Every chemist would agree that modern-day analytical chemistry differs radically from that of fifty years ago, and most would no doubt point to the introduction of a variety of instrumental measurements as the major difference. As striking as this difference is, it fails to get to the essence of what makes the modern approach different from the classical.

Fifty years ago, the only question analysts sought to answer was the composition of matter, expressed as percentages of elements or compounds in a sample. Even today, one occasionally encounters such a narrow perception as to the goals of analysis, especially among those remote from the modern-day science. The fact is that as the capabilities of analytical science have improved, the demands placed upon it have correspondingly increased. The first change was toward increasingly demanding limits of detection and estimation of elements and compounds. But when the newer methods also proved capable of yielding information about oxidation state, crystal structure, coordination state, etc., this further depth of information soon became a requirement in special cases. When methods of high spatial resolution became available, the demands for such information grew. When methods of detecting transient, unstable, or unstable species in dynamic systems became available, the need for such information at once emerged. Analysis of living systems, including complex organisms, is at a research frontier today, but no doubt will be a routine demand some day. Thus instrumental approaches are merely the means to an end, namely for more detailed information in more complex systems, rather than being the heart of the analytical process.

What, then, marks the essential change from the relatively simple past of years ago? Analysis can now be more accurately described as being applied to a problem, rather than to a sample. To be sure, sampling is an important and often neglected part of the analytical process, but we really are interested in the problem the sample represents rather than the sample itself. To achieve these new goals of information, analytical chemists need increasingly detailed understanding of the system under observation as well as the measurement devices. The essence of the modern approach is a quest for fundamental understanding of a problem rather than an empirical determination of composition.

Time and Spatially Resolved Atomic Absorption Measurements with a Dye Laser Plume Atomizer and Pulsed Hollow Cathode Lamps

R. M. Manabe[1] and Edward H. Piepmeier*

Department of Chemistry, Oregon State University, Corvallis, Oregon 97331

Time and spatially resolved atomic absorption measurements were made using a 1-μs dye laser beam to atomize solid samples of Cu, Al, and Pb alloys, steel, and graphite. Pulsed hollow cathode lamps with pulses as short as 1 μs were used as primary sources for the atomic absorption measurements. The influences of sample chamber pressure were studied. The time-integrated, absorption spectral line profile of Cu in the plume was observed during the first 60 μs of the plume.

Intense focused laser beams have been used as atomizers for atomic absorption spectroscopic analysis of solid samples by several investigators (*1–7*). Mossotti et al. (*1*) and Piepmeier (*2*) used Q-switched lasers to atomize the sample, and flash lamps as the primary light source. Karyakin and Kaigorodov (*3*) took advantage of the intense radiation emitted from the laser plume itself as the primary source and used the widths of self-reversed lines produced on film as an analytical signal. Osten and Piepmeier (*4*) and Vul'fson et al. (*5*) used pulsed hollow cathode lamps as primary sources. Hollow cathode lamps operated in the dc mode have been used as primary light sources by Matousek and Orr (*6*), who used a graphite furnace to aid atomization by a CO_2 TEA laser, and by Ishizuka et al. (*7*), who swept the atomized sample into an auxiliary observation chamber by a rapid flow of argon gas. The graphite furnace (*6*) and the auxiliary observation chamber (*7*) were designed to mask emission signals from the plume, which interfere with the observation of the absorption signal. The masking effectively reduced the plume emission signals relative to the dc hollow primary source signals, but did not entirely eliminate sample emission in all cases.

Piepmeier and Osten (*8*) predicted from theoretical considerations that the intense continuum emission from the plume could be reduced by using a long laser pulse [of the same energy], and by using a laser with a shorter wavelength to reduce inverse Bremsstrahlung absorption of the laser energy in the plume, which tends to result in intense plasma emission. This study reports the results of using such a laser to atomize solid samples, and using long and short-pulse hollow cathode lamps as primary sources. The influence of the pressure of the gas in the sample chamber is studied.

EXPERIMENTAL

Laser Microprobe. The laser used in these experiments was a Chromabeam 1070 dye laser (Synergetics Research, Inc.). The lasing dye solution (1×10^{-4} M Rhodamine 6B in 95% ethanol) was circulated through the 1-cm bore of a coaxial flash lamp. The maximum energy for the 1-μs laser pulse was 0.1 J. The maximum repetition rate was 3 pulses per min.

The original laser trigger used an electromechanical relay in the primary circuit of a high voltage pulse transformer, similar to that used in a conventional automobile ignition system. The secondary circuit of the transformer was connected to the trigger (third) electrode of a spark gap which discharged a 0.3-μF capacitor through the lamp. The jitter time of this trigger circuit was 5 ms, much too long for these experiments. The relay in the primary of the high voltage pulse transformer was replaced by a silicon-controlled recitifier (GE C20D) which switched a 1.6-μF capacitor charged to 350 V through the primary of the transformer. This reduced the jitter time to 10 μs. During later experiments it was found that a continuous flow of nitrogen through the spark gap reduced the delay time before firing to 10 μs, with a jitter time of 1 μs.

The rectangular sample chamber had inside dimensions of 1.5 × 1.5 × 4 in. Quartz windows were mounted on five sides. The sample chamber was mounted on an XY micrometer adjustment stage similar to the one used by Piepmeier and Osten (*8*) so that the laser plume could be easily moved in the plane perpendicular to the optical axis of the atomic absorption detection system for spatial mapping. Additional micrometer translation stages were positioned to allow the sample chamber to be moved with respect to the laser beam so that any part of the sample surface could be sampled (*9*).

Detection System. The emission studies used an *f*/11, 1-m over-and-under research Czerny Turner spectrograph–spectrometer described by Osten (*10*). The first-order reciprocal linear dispersion was 0.83 nm/mm. At the focal plane, either photographic or photoelectric readout modules were fitted. A 4 × 5-in. sheet-film Polaroid photographic module was used for these studies. The photoelectric module consisted of two 1P28 photomultiplier tubes to allow dual channel readout for simultaneous monitoring of an analyte line and nearby background. This spectrometer was also used for atomic absorption measurements. Side-by-side 25-cm focal length parabolic mirrors were used to focus the light from the plume into the spectrograph–spectrometer. The mirrors were positioned to compensate for the astigmatism of the spectrograph so that a point source at the plume was correctly focused as a point at the focal plane of the spectrograph (*11*). A 200-μm horizontal slit was positioned 6 mm behind the entrance slit for spatially resolved studies. This arrangement produced maximum light transfer (*12*) and provided the spatial resolution vital to these experiments. Two 1-m focal length spherical mirrors in an over-and-under configuration were used to direct the hollow cathode radiation through the laser plume and spectrometer entrance optics.

The monochromator used in the atomic absorption spectral line profile studies was a Heath Model EU-700 equipped with a EU-701 photomultiplier tube module. This monochromator was employed as a variable band-pass filter to eliminate interfering lines from the interferometer. The interferometer (Tropel Model 242) system was essentially the same one used by DeJong and Piepmeier (*13*) with a 0.5-mm scanning aperture. The plates had a nominal reflectivity of 97.5% between 300 and 330 nm.

A He–Ne laser was used to aid in the initial alignment of the UV interferometer plates. A pin hole aperture was placed at the exit of the He–Ne laser to cause the laser to diverge and fill the working aperture of the interferometer. Four reflection spots were observed, due to the surfaces of the two interferometer plates. One of the four possible ways of superimposing two spots upon each other was arbitrarily chosen, and the plates were adjusted until a series of fringes was observed in the region of the superimposed reflection. The adjustments were fine tuned until the fringe spacing was a maximum. A low-pressure Hg lamp was then placed on the axis of the interferometer. Corning Glass 3-72

[1] Present address: Rockwell Hanford Operation, Richland, Wash. 99352.

0003-2700/79/0351-2066$01.00/0

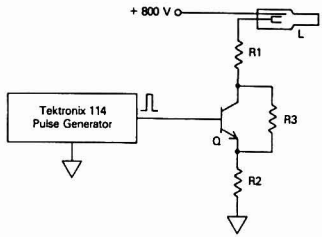

Figure 1. Electronic circuit used to pulse the hollow cathode lamp, L. R1 = 100 Ω; R2 = 0.7 Ω; R3 = 500 kΩ; Q = SK-3111

and 4-68 filters were placed in front of the Hg lamp to allow the green line of Hg (546.0 nm) to pass. Although the surfaces were not highly reflective at this wavelength, when the proper two surfaces of the plates were chosen, a series of concentric fringes was visible to the naked eye when the eye was focused at infinity. The alignment achieved by this technique was sufficient to observe the profile of the Cu(I) 324.8-nm line with the interferometer, and only final tuning with the piezoelectric drives was necessary to obtain maximum finesse. The interferometer was enclosed in a box with a 0.25-m thickness of styrofoam pellets surrounding it for thermal insulation. Alignment stability was greatly improved by leaving the power to the tuning piezoelectric drives on continuously. The gross alignment of the interferometer was stable over a 2-month period, during which time only fine adjustments of the piezoelectric drives were required to maintain maximum finesse.

The finesse of the interferometer was determined to be better than 18 from observations of a monoisotopic ^{198}Hg electrodeless discharge lamp. The 312.6-nm Hg(I) line was used because of its proximity to the 324.8-nm Cu(I) line.

The integrator for the electronic charge from the photomultiplier anode was built by using the circuit designed by Piepmeier (*14*). Because of the long integration times, R2 and C2 in this circuit (*14*) were not necessary, and slower operational amplifiers (MP 1039, McKee Pedersen, Inc.) were used. The diodes D1 and D2 were reversed to accept the negative signals from the photomultiplier.

The hollow cathode pulsing circuit, Figure 1, used a 1000-V transistor (SK-3111) as a switch in series with the hollow cathode lamp and a 100-Ω current limiting resistor. The emitter of the npn SK-3111 transistor was connected to common (ground) through a 0.7-Ω resistor. A 500-kΩ resistor was connected in parallel with the transistor (between the collector and emitter) so that a 1-mA background current continually flowed through the hollow cathode lamp. This background current prevented the hollow cathode from electrically floating when the transistor switch was off and thereby provided more reproducible pulsing characteristics for the lamp. A dc power supply of 800 V was needed to produce the fast response times for the lamp. Lower voltages produced slower response times for the lamp. Pulses as short as 0.5 μs were observed.

The base of the transistor was driven directly by the output of a Tektronix Model 114 pulse generator. The magnitude of the current pulses was controlled by the 100-Ω series resistor when the transistor was saturated (completely turned on). When the transistor was not saturated, the transistor acted as a current amplifier; the pulse current was controlled by the transistor, whose current was in turn controlled by the output current of the pulse generator. The current from the pulse generator was determined by the output voltage of the generator, the 50-Ω internal output resistance of the generator, and the input characteristics of the transistor circuit.

When the transistor is saturated, the output voltage of the pulse generator also influences the duration of the pulse, by increasing the duration of the hollow cathode pulse by up to 25 μs longer than the input pulse to the transistor base. Therefore, a 1-μs pulse into the base must have an amplitude small enough not to saturate the transistor if the hollow cathode pulse is to be as short as 1 μs. An input pulse of larger amplitude that causes the transistor to turn completely on (identified by a collector–emitter voltage

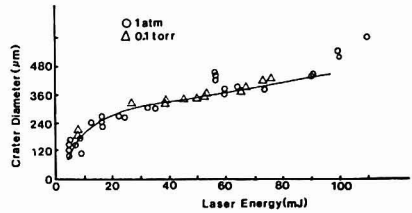

Figure 2. Crater diameter vs. laser energy at atmospheric pressure and 0.1 Torr for a pure copper target

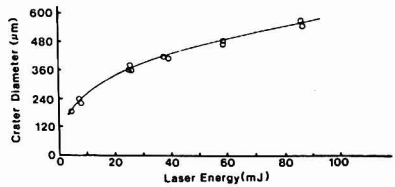

Figure 3. Crater diameter vs. laser energy at atmospheric pressure for a NBS 461 steel sample

of only a few tenths of a volt) will saturate the base region of the transistor with electrical charge. The excess charge will remain for a short time (up to 25 μs) after the input pulse had ceased, allowing current to continue to flow from collector to emitter and therefore through the hollow cathode lamp for this additional storage time. This storage time can be controlled from zero to 25 μs by the input pulse amplitude and by the input pulse duration. Since both the amplitude and duration of the input pulse can affect the storage time, the amount of charge injected into the base is an important factor in determining the storage time.

RESULTS AND DISCUSSION

Emission. Figure 2 shows the dependence of crater diameter upon laser energy of the flash lamp pumped dye laser for a copper target at atmospheric pressure in air and at 0.1 Torr (13 Pa). Figure 3 shows a similar variation in crater diameter with laser energy at atmospheric pressure for a steel sample (NBS 461 steel). For both pressures, the crater diameter for the copper sample increases with increasing laser energy, and pressure makes little difference in the shape of the curve. However, over the same range of laser energies, Piepmeier and Osten (*8*) found for a Q-switched Nd laser that the crater diameters increased for a pressure of 1.0 Torr, but remained constant with increasing energy at atmospheric pressure.

Time integrated photographs, taken with the same spectrograph, showed a heavy spectral continuum emission in the central region of the plume at atmospheric pressure for the Q-switched Nd laser (*8*), and relatively little continuum emission when the dye laser was used. There was negligible continuum in the plume (except at the surface spot) for both lasers at low pressure.

The differences in the crater and spectral results may be due to the decreased irradiance caused by the flash lamp pumped dye laser compared with the irradiance caused by the Q-switched Nd laser, and also to the shorter wavelength of the dye laser. The maximum energy flux at the focal point was 2×10^{11} W/cm^2 for the 60-ns Q-switched laser and 2×10^9 W/cm^2 for the 600-ns dye laser (using the minimum crater area observed as the focal spot area). The results of Piepmeier and Osten (*8*) indicate that a minimum irradiance of 5×10^9 W/cm^2 is needed in order to form a radiation supported shock wave or atmospheric plasma that absorbs a major fraction of the energy in the laser pulse, preventing all of the laser energy

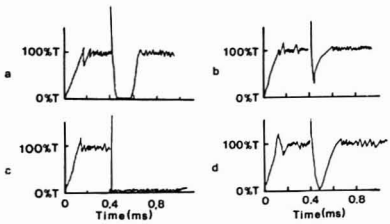

Figure 4. Time resolved atomic absorption at a height 2 mm above the sample surface for the Ca(II) 393.3-nm line at (a) 0.2 Torr and (b) 760 Torr; and for the Ca(I) 422.7-nm line at (c) 0.2 Torr and (d) 760 Torr

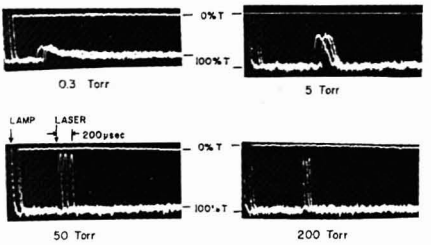

Figure 5. Oscilloscope tracings of time resolved atomic absorption for the Mn(I) 403.1-nm line at various pressures. Observation height = 2 mm. Steel sample: NBS 461

from reaching the sample surface. The presence of a radiation supported shock wave at atmospheric pressure could explain the essentially constant crater diameter for the Q-switched laser results and the intense spectral continuum. At the lower pressure, the shock wave does not form, or is relatively insignificant because of the greatly reduced concentration of the atmosphere. The irradiance caused by the dye laser is too low to form a shock wave at either pressure, and the crater diameters are therefore the same for both high and low pressures.

The absorption coefficient of a radiation supported shock wave is directly proportional to the wavelength of the laser radiation being absorbed (*8*). The shorter wavelength of the dye laser, 590 nm compared with 1060 nm for the Nd laser, should further reduce the likelihood of forming a radiation supported shock wave.

Time integrated photographic spectra of the dye laser plume were observed for copper, aluminum, and Mg-doped (10% w/w) graphite samples. The spectral band-pass of the spectrograph was 0.04 nm. The 327.4- and 324.8-nm Cu(I), the 309.3- and 308.2-nm Al(I), and the 285.2-nm Mg(I) lines were completely self-reversed at atmospheric pressure. The Cu and Al lines extended 2 mm above the surface of the sample. The Mg line and its self-reversal extended 5 mm above the surface, indicating that relatively unexcited Mg atoms are widely distributed in the outer regions of the plume even to a height of 5 mm.

The width of the darkened centers of the lines varied smoothly from 0.4 nm at the surface to 0.1 nm at a height of 2 mm. The wider emitting wings of these lines varied in a similar manner going from the surface to a height of 2 mm.

At low pressure (0.1 Torr), the lines were as narrow as the image of the entrance slit of the spectrograph, except within 0.5 mm of the surface of the sample. Emission line widths of 0.3 nm were observed within 0.5 mm of the sample surface, less than the corresponding broadening observed at atmospheric pressure. No self-reversal was observed.

At both high and low chamber pressures the broadening near the surface may be caused by relatively high Doppler and collisional broadening due to the initial high pressure of the plume before significant expansion has taken place. The increase broadening throughout the plume at high chamber pressure could be caused by increased collisional broadening with the atmospheric species and by increased collisional broadening within the plume caused by atmospheric confinement of the plume.

Atomic Absorption. The presence of self-reversed emission lines indicated that atomic absorption would be a better way to observe the analyte than atomic emission for this laser microprobe. A Ca-pulsed hollow cathode lamp was used as the primary source to observe absorption of the 422.7-nm Ca(I) line and the 393.3-nm Ca(II) ion line. Ca was chosen because there was a strong ion line in the pulsed hollow cathode lamp. Ca metal was used as the sample. Figure 4 shows the time resolved neutral atom and ion absorption signals at a low pressure (0.2 Torr) of the sample chamber and at atmospheric pressure. Observations were made at a height of 2 mm above the sample surface. In Figure 4, the lamp pulse began 0.4 ms prior to firing the laser. At 0.4 ms the laser fires and an emission pulse from the plume sends the signal off the top of the scale. As the emission subsides, and absorption becomes significant, the signal comes back on scale and drops below 100% T. At 0.2 Torr, the absorption of the neutral atom extends beyond the hollow cathode pulse, while the ion line absorption becomes negligible 0.25 ms after the beginning of the plume. At atmospheric pressure, the neutral atom absorption lasted for 0.25 ms, while the ion line absorption lasted for only 0.2 ms. The depth of the absorption peak for the ion line is distorted by the relatively long 15-μs RC time constant (chosen to reduce shot noise) of the coaxial cable and load resistor connected to the anode of the photomultiplier tube.

It appears from these results that the recombination rate for Ca ions is rapid compared with the time required for depletion of the free atom population, and that the recombination rate is slower at lower pressures as would be expected due to lower collisional rates caused by lower densities.

The influence of sample chamber pressure upon the sensitivity and character of the atomic absorption signal was studied by using a minor constituent, (0.3% w/w), Mn in a NBS 461 reference steel sample. The steel sample was chosen because it is certified to be homogeneous on the 1-μm level, and Mn was chosen because the peak absorption signals did not approach too close to 0% T.

Figure 5 shows oscilloscope photographs of representative pressures. Each photograph shows three traces. The traces are displaced in time from one another because of the jitter time of the spark gap of the laser triggering mechanism for these runs. The magnitude of the peak absorbance reached a maximum value at 50 Torr. Increases in sample chamber pressure result in decreases in the time duration of the absorption signal. Figure 6 shows how the width of the absorption peak at first becomes narrower as the pressure increases and then tends to level off above 100 Torr.

Three factors could conceivably contribute to the observed changes in absorption peak amplitude and peak width: the relationship of the spectral profile of the hollow cathode lamp to the absorption spectral profile of the atoms in the plume; the RC time constant of the coaxial cable and load resistor connected to the anode of the photomultiplier tube; and the spatial expanse of the plume.

The spectra profiles of the 403.1-nm Mn(I) line have been observed in a hollow cathode lamp and a flame (*15*). Even though the temperatures and pressures of these sources were quite different from each other, the width of the spectral profiles differed from each other by only 30% because of the

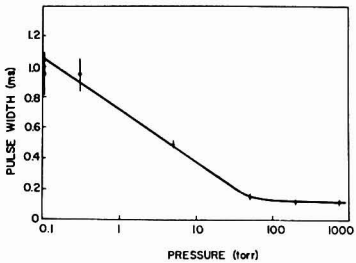

Figure 6. Absorption pulse width (ms) measured at 10% of maximum absorption vs. pressure for Mn atomic absorption in a NBS 461 steel sample

complex hyperfine structure of the lines. The individual peaks of the hyperfine components, though relatively narrow themselves at the low hollow cathode pressure, heavily overlap each other to form a relatively wide overall emission peak, not much narrower than the absorption peak in the atmospheric pressure flame. Therefore, the relatively small changes in spectral profiles caused by the pressure differences in the plume experiments (similar to the pressure differences between a hollow cathode lamp and an atmospheric flame) would account for only a small fraction of the large changes in peak absorption observed with changes in sample chamber pressure. This leaves two other considerations.

The absorption peaks in Figure 5 for low pressures reach their peak values well after the response-time delay caused by the RC time constant. The response time is only delayed on the rising or leading side of the absorption peak where the light is rapidly decreasing. On the falling or trailing side of the absorption peak, the light signal is rapidly increasing and the low-output-impedance photomultiplier is rapidly charging the capacitance of the coaxial cable, causing negligible distortion of the shape of that part of the peak. Evaluations of the photographs show that the RC time constant delays in the leading edges of the pulses could cause the observed widths to be shorter than the true width by 0.02–0.06 ms depending upon the magnitude of the initial emission spike which shoots the trace off scale prior to the absorption peak. Therefore, this time constant distortion could account for only a small portion of the change in pulse width with pressure, especially at the lower pressures. The time constant distortion could account for a large part of the decrease in absorption peak amplitude at pressures higher than 50 Torr, but does not distort the peak amplitude at lower pressures where the peak occurs well after any significant time constant delays. Therefore, the decrease in peak width and the increase in absorption peak amplitude with increased pressure at low pressure must have other causes. One such cause (the third factor considered) might be the influence that the chamber pressure has upon the size of the plume (*8*).

Therefore, atomic absorption measurements were made with 0.2-mm square cross section resolution up to heights 6 mm above the surface and out to 3 mm to the side of the plume, the physical limits imposed by the sample chamber. At 0.2 Torr, the peak absorbances at heights between 1 mm and 2 mm were constant from the center of the plume out to a radial distance 3 mm away from the center. However, at atmospheric pressure, absorption decreased with radial distance and was detectable only to a distance of 2 mm from the center. At low pressure, absorption was detected up to 6 mm above the surface, but at high pressure, absorption was not detected at or above 4 mm. For Cu and in a Cu sample, absorption was not detected beyond 1.3 mm radial distance at atmospheric pressure.

These observations show that the presence of the atmosphere has a confining effect upon the size of the plume; that is, upon the distances that free neutral atoms are allowed to reach after they are ejected from the surface of the sample. Two mechanisms may be at work. First, the atmosphere may act as a sort of outer shell which only slowly enlarges and actively confines most of the atoms ejected from the sample. The confining effect would cause an increase in concentration within the confined region, which would result in an increase in the peak absorption amplitude as the sample chamber pressure increased, as is observed for pressures up to 50 Torr. Secondly, the increased collision rate caused by the presence of the atmosphere may cool down the translational energy of the sample atoms and cause them to more quickly condense or chemically combine among themselves or with the air species, shortening the life of the absorption peak, as observed throughout the pressure region studied.

Precision. The relative precision of the atomic absorption measurements varied between 10 and 20% as the sampling site was moved to a fresh part of the surface for each laser shot. In order to try to improve the precision of the Mn atomic absorption measurement, the same spot on the NBS 461 steel sample was repetitively sampled. A height of 2 mm was chosen to allow the plume to expand and become more homogeneous before the atomic absorption peak occurred. A pressure of 0.2 Torr was chosen because of the observed increase in residence time of the atoms in the observation region. The peak absorbances of the first three shots were 0.49, 0.25, and 0.21, respectively. The next 16 shots produced a relatively constant absorbance of 0.18 with a relative standard deviation of 6%. Calculations indicated that this was the relative standard deviation expected due to shot noise. Therefore, better analytical measurements would be expected if a tunable, narrow-band laser were used instead of a pulsed hollow cathode lamp to eliminate shot noise.

The change in absorbance during the first few laser shots, and the improvement in precision of the measurements when the sample is not moved between successive laser shots, indicates the importance of reproducible surface preparation in obtaining reproducible analytical measurements. One cause of this initial change in absorbance during the first few laser shots may be adosrbed gases on the sample surface (*6*).

Short-Pulse Observations. Oscilloscope readout of absorption peaks is inconvenient for routine analytical work. Electronically time integrated readout of the emission signal from a short-pulse hollow cathode lamp would be easier to work with, and a short enough pulse would improve time resolution. A shorter hollow cathode pulse that was on only during the measurement time could be made more intense and thereby reduce shot noise. A copper hollow cathode lamp was used because spectral line profiles were available for this lamp (*13*). A 1-μs, 1-A pulse was used because it should exhibit even less self-absorption than the 10-μs pulses published by Piepmeier and de Galan (*16*). A 1-μs pulse also provides much better time resolution for both diagnostic and analytical studies.

The relative standard deviation for the time integrated 1-μs atomic absorption measurements for Cu in Pb foil at 1 Torr and a height of 2 mm was 5%. The hollow cathode pulse was triggered off of the laser pulse to avoid time jitter inherent in the laser spark gap trigger. The shortest time between the laser pulse and the hollow cathode pulse was 2 μs, due to delays inherent in the hollow cathode circuitry and the delay time after initiating the pulse in the lamp before the lamp emitted radiation.

At 2 μs after the laser pulse, the absorbance was 0.4. The absorbance rapidly decreased to 0.2 at 5 μs, and remained at 0.2 until 100 μs. From 100 μs the absorbance gradually

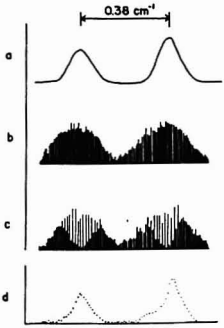

Figure 7. Emission spectral profile of the Cu(I) 324.8-nm line for a hollow cathode lamp operated in the dc mode (a), and in the pulsed mode (b). (c) Shows the spectral profile of the laser pulse for Cu in Pb foil at 1 Torr. (d) Shows the spectral profile obtained from c by smoothing and converting to absorbance

decreased to 0.16 at 1000 μs. The constant absorbance between 5 and 100 μs would tend to correlate with the photographic observations of Scott and Strasheim (*17*) who observe similar laser plumes to "hang as a nebula" for 1–100 μs after their initiation.

The possibility that nonspecific absorption could be causing the initially high absorbances was checked by using a 6-μs flash lamp continuum in place of the hollow cathode lamp. No absorption was detected above a noise level of 10%. Consequently, the initially high absorbance at 2 μs must be due to Cu atoms. These results show that the 1-μs pulsed hollow cathode lamp is a better light source for Cu in Pb than the long-pulse hollow cathode lamp that could not accurately respond to absorbances at 2 μs (because of the 15-μs RC time constant needed to reduce shot noise).

Spectral Profiles. The absorption spectral profile of Cu in the plume from a Pb foil sample was observed by using a Fabry–Perot interferometer and a pulsed hollow cathode lamp as the light source. The lamp emission pulse was time integrated. A lamp pulse current of 500 mA was used for maximum instantaneous intensity. The spectral profiles of the lamp were observed for several pulse durations. The spectral profile for a pulse duration of 60 μs represented the best compromise between a non-self-reversed emission spectral profile, consistent with sufficient signal-to-noise ratio. Longer pulse durations exhibited self-reversal and did not increase the integrated intensity signal to significantly reduce shot noise. Shorter pulses increased shot noise to unacceptable levels.

Figure 7 shows the data from a typical run. Figure 7a shows the emission profile for the 324.8-cm Cu(I) line from a Cu hollow cathode lamp operated in the dc mode. The two peaks are due to the hyperfine structure of the line (*18*). Figure 7b shows the emission profile of the lamp operating in the pulsed mode. Each vertical line represents one pulse. Figure 7c shows the profiles obtained when the laser fired with every other pulse of the lamp for a sample chamber pressure of 1 Torr. This alternating mode of operation allowed the 100% T curve to be obtained during the same run as the absorption profile of the plume. This profile represents the time integrated Cu absorption profile in the plume during the first 60 μs following the firing of the laser.

Figure 7d shows the absorbance profile that was calculated after manually passing smooth lines through the 100% T and absorption peaks in Figure 7c. The odd shape may be due to uncertainties in the data points and smoothing routine, or to actual changes in the absorption and emission spectral profiles during the 60-μs pulse (*16*, *19*, *20*). The relatively narrow shape of the profiles compared with those of the dc hollow cathode profiles indicates that the plume has cooled to a Doppler temperature of less than 1000 K during the 60-μs pulse, which occurs before the absorption signal at that pressure begins to decrease. Absorption profiles for sample chamber pressures of 50 Torr and above produced poorer results because the central regions of the profiles were totally absorbed.

To summarize the results of this study, the flash lamp pumped dye laser microprobe craters are independent of sample chamber pressure, indicating that very little of the laser energy is absorbed in the atmosphere, in contrast to the results obtained by using a Q-switched laser microprobe of similar energy. Lower pressures produce narrower emission spectral line widths. Low pressures also eliminate self-reversal of the very broad lines still present at the sample surface. The atmosphere shortens the lifetime of atoms and ions in the plume, which tends to decrease absorption. The atmosphere also has a confining effect upon the size of the plume which tends to increase absorption. The net result is a maximum absorption signal that occurs at a sample chamber pressure near 50 Torr. At 1 Torr, absorption spectral profiles indicate that a translational temperature of less than 1000 K is reached during the first 60 μs of the plume.

LITERATURE CITED

(1) Mossotti, V. G.; Lagua, K.; Hagenah, W. D. *Spectrochim Acta* **1967**, *23B*, 197.
(2) Piepmeier, E. H. Ph.D. Thesis, University of Illinois, Urbana, 1966.
(3) Karyakin, A. V.; Kalgorodov, V. A. *J. Anal. Chem. USSR* (*Engl. Transl.*) **1968**, *23*, 807.
(4) Osten, D. E.; Piepmeier, E. H. *Appl. Spectrosc.* **1973**, *27*, 165.
(5) Vul'fson, E. K.; Karyakin, A. V.; Shidlovskii, A. I. *Zavod. Lab.* **1974**, *40*, 945.
(6) Matousek, J. P.; Orr, B. J. *Spectrochim. Acta* **1976**, *31B*, 475.
(7) Ishizuka, T.; Uwamino, Y.; Sunahara, H. *Anal. Chem.* **1977**, *49*, 1339.
(8) Piepmeier, E. H.; Osten, D. E. *Appl. Spectrosc.* **1971**, *25*, 642.
(9) Manabe, R. M. Ph.D. Thesis, Oregon State University, Corvallis, 1977.
(10) Osten, D. E. Ph.D. Thesis, Oregon State University, Corvallis, 1972.
(11) Goldstein, S. A.; Walters, J. P. *Spectrochim. Acta* **1976**, *31B*, 201, 295.
(12) Salmon, S. G.; Holcombe, J. A. *Anal. Chem.* **1978**, *50*, 1714–1716.
(13) DeJong, G. J.; Piepmeier, E. H. *Spectrochim. Acta* **1974**, *29B*, 159.
(14) Piepmeier, E. H. *Appl. Spectrosc.* **1972**, *26*, 100.
(15) Wagenaar, H. C.; de Galan, L. *Spectrochim. Acta* **1973**, *28B*, 157.
(16) Piepmeier, E. H.; de Galan, L. *Spectrochim. Acta* **1975**, *30B*, 263.
(17) Scott, R. H.; Strasheim, A. *Spectrochim. Acta* **1970**, *25B*, 311.
(18) Brix, P.; Humbach, W. *Z. Phys.* **1950**, *128*, 506.
(19) Piepmeier, E. H.; de Galan, L. *Spectrochim. Acta* **1976**, *31B*, 163.
(20) Piepmeier, E. H.; de Galan, L. *Spectrochim. Acta* **1975**, *30B*, 211.

RECEIVED for review May 2, 1979. Accepted July 13, 1979. The authors thank the National Science Foundation for their support and award of Grant MPS-7305031.

Inductively-Coupled Argon Plasma as an Excitation Source for Flame Atomic Fluorescence Spectrometry

M. S. Epstein,[1] S. Nikdel, N. Omenetto,[2] R. Reeves,[3] J. Bradshaw, and J. D. Winefordner*

Department of Chemistry, University of Florida, Gainesville, Florida 32611

An inductively-coupled argon plasma (ICAP) is used as a narrow line radiation source for the excitation of atomic fluorescence in several analytically useful flames (nitrogen-separated air/acetylene and nitrous oxide/acetylene). Detection limits for 14 elements are compared to atomic fluorescence detection limits using other radiation sources and to those of other atomic spectrometric techniques. Dominant noise sources which limit measurement precision at low and high concentrations and the significance of and correction for the scatter problem are discussed. The reduction of spectral interference observed in ICAP emission is demonstrated for the determination of zinc in unalloyed copper (NBS SRM-394 and -396). The technique is also applied to the determination of zinc in fly ash (NBS SRM-1633), cadmium and zinc in simulated fresh water (NBS SRM-1643), and copper and zinc in orange juice.

The inductively-coupled argon plasma (ICAP) has been demonstrated (*1*) to be an excellent source for emission spectrometry. However, the spectral characteristics of the emission from this source, such as high intensity, excellent short and long term stability, narrow linewidth, and freedom from self-reversal, make it an ideal radiation source for the excitation of atomic fluorescence in flames.

The first reported use of a radio-frequency, induction-coupled plasma (36 MHz, 2 kW, Model SC15, Radyne Ltd., U.K.) as an excitation source for flame atomic fluorescence spectrometry (AFS) by Hussein and Nickless (*2*) resulted in relatively poor detection limits (*3*) (Table I) which probably contributed to the absence of further development of the ICAP as a source for AFS. However, the tremendous growth in the use of the ICAP for emission in the last decade has resulted in significant improvement in sample introduction and plasma stability (*4*), which now makes the ICAP an excellent source for AFS (*5*).

The advantage of the ICAP compared to other AFS sources *is its flexibility with respect to the availability of intense atomic and ionic line radiation for many elements.* Changing from one element to another is simply a matter of aspirating a different solution into the plasma, taking less than one minute. The availability of many intense nonresonance and ionic lines allows scatter correction to be easily performed using the two-line technique (*6*).

ICAP-excited AFS can also offer an alternative to ICAP emission when spectral interferences which are observed with monochromators of medium resolution (>0.01-nm spectral bandpass) significantly limit emission analysis. Interferences in emission due to changes in the plasma background radiation (which require a background correction procedure) are not observed using AFS. Line spectral interferences which cannot be resolved may also be reduced or eliminated because of the spectral selectivity of flame AFS. This selectivity results from: (a) differences in atomization, excitation, and ionization properties of the flame and plasma; (b) differences in quantum efficiencies between analyte and interferent lines; and (c) the property of the flame as a resonance detector with an effective spectral bandwidth equivalent to the width of the absorption transition.

We have investigated the application of the ICAP as an excitation source for atomic fluorescence using a simple optical setup, low resolution monochromator, and nitrogen-separated air/acetylene and nitrous oxide/acetylene flames. Detection limits obtained for 14 elements are compared to AFS detection limits using other excitation sources and to detection limits of other atomic spectrometric techniques, such as flame atomic absorption and ICAP emission. The noise sources limiting precision at low and high concentrations are delineated and the effect of various instrumental parameters such as spectral bandpass and ICAP nebulizer pressure on signal-to-noise ratios is described. The scatter problem is evaluated and the two-line method is applied for scatter correction. ICAP emission and ICAP-excited AFS are applied to the analysis of zinc in unalloyed copper (NBS SRM-394 and -396) and the AFS technique is employed to correct for a zinc–copper spectral interference at the 213.9 nm line in ICAP emission. ICAP-excited AFS is also employed for the analysis of copper and zinc in orange juice, zinc in fly ash (NBS SRM-1633), and cadmium and zinc in simulated fresh water (NBS SRM-1643).

EXPERIMENTAL

Instrumentation. The instrumentation used in this study is described in Table II and a diagram of the arrangement of experimental components is shown in Figure 1. Radiation from aqueous solutions of the analyte element aspirated into the ICAP is modulated at 600 Hz and focused by spherical quartz lenses on the separated flame. A reflector is placed behind the flame to provide a double-pass system. The fluorescence monochromator is placed 4 cm from the flame center and the viewing area is centered 2 cm above the burner head. A light trap is placed opposite the flame from the monochromator to reduce stray light and scatter effects. Once optical alignment is attained, the only ICAP parameters that must be optimized for different elements are the argon pressure to the nebulizer and the concentration of the solution nebulized. Torch position is not critical, since the entire emission area above the coils is focused on the area of the flame viewed by the fluorescence monochromator.

Emission measurements from the ICAP were performed as described previously (*7*).

Excitation Source (ICAP) Solutions. The solutions used for excitation of analyte emission from the ICAP contained 10 to 20 mg/mL of the analyte. Whenever possible, these "excitation" solutions were prepared by acid dissolution of the high purity metal or metal oxide, although other compounds (nitrates, chlorides, etc.) were employed when the former were not available. The selectivity of the fluorescence technique using line source excitation (i.e., its ability to discriminate against spectral interferences) depends on the spectral purity of the line source and, if significant interferent contamination exists in the excitation solution, interferent emission will be excited in the ICAP

[1] On leave from the Center for Analytical Chemistry, National Bureau of Standards, Washington D.C.
[2] On leave from the Institute of Inorganic and General Chemistry, University of Pavia, Pavia, Italy.
[3] Present address: Department of Chemistry, Biochemistry and Biophysics, Massey University, Palmerston North, New Zealand.

0003-2700/79/0351-2071$01.00/0

Table I. Limits of Detection (ng/mL)

element	λ, nm[a]	flame[b]	ICAP-excited AFS[c,d] this work	ICAP-excited AFS[c,d] ref. 2	ICAP emission same line[e]	ICAP emission commercial[f]	ICAP emission best[g]	AFS line[h]	AAS[i]
Al	308.2	S-NOA	1000	-	23	15	1	120	30
	309.3								
As	235.0	S-AA	5000	-	142	25	25	70	100
Ca	422.6	S-AA	4	100	10	4[j]	0.0005	0.3	1
Cd	228.8	S-AA	0.8	80	2.7	1	0.3	0.2	1
Co	240.7	S-AA	11	-	>23	2	0.4	1.5	10
	241.1								
	241.4								
	242.5								
Cr	357.8	S-AA	2	-	23	4	1	0.3	3
	359.3								
	360.5								
Cu	324.7	S-AA	2	50	5.4	2	0.3	0.3	2
	327.4								
Fe	248.3	S-AA	6	-	>20	2	0.2	0.6	10
	248.8								
	249.0								
Mg	285.2	S-AA(fr)	0.09	5	1.6	20[j]	0.01	0.09	0.1
Mn	279.5	S-AA	2	100	12	0.5	0.06	0.5	2
	279.8								
	280.1								
Mo	313.3	S-NOA	400	-	>37	5	0.5	750	30
	315.8								
Pb	283.3	S-AA	800	-	142	20	10	10	20
V	318.5	S-NOA	400	-	>17	2	0.2	88	60
	318.4								
	318.3								
Zn	213.9	S-AA	0.5	80	1.8	2	0.3	0.2	2

[a] Wavelengths of major fluorescence line(s) contributing to the fluorescence spectral intensity. Since the spectral bandpass of the monochromator is 16 nm, other lines may contribute some intensity (3). [b] Flame type: S-AA = nitrogen-separated air/acetylene; (fr) = fuel-rich; S-NOA = nitrogen-separated nitrous oxide/acetylene. [c] Detection limits from this work correspond to an analyte fluorescence signal equal to 3 times the standard deviation of the base line (SNR = 3) calculated from either sixteen 1-s integrations or from ³/₄ the peak-to-peak noise on the base line using a 3-s time constant. [d] From ref. 2, 3 (SNR = 2). [e] Predicted ICAP-emission limits of detection (12) for the same line(s) used to excite AFS. [f] Commercial multielement limits of detection (26) based on SNR = 2 for ICAP emission. [g] State-of-the-art limits of detection for ICAP emission using pneumatic nebulization (SNR = 2) (25). [h] Line source atomic fluorescence detection limits in a similar flame (SNR = 2) (3). [i] Atomic absorption detection limits (SNR = 2) (24). [j] Limit of detection based on the normal analytical line, not the most sensitive line (26).

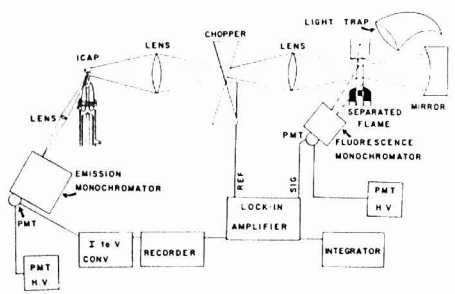

Figure 1. Diagram of experimental layout of components for measurement of ICAP-excited AFS and ICAP emission

which may degrade the selectivity. The effect of such contamination is discussed more fully for the analysis of zinc in unalloyed (high-purity) copper.

The use of solutions of such high concentrations does not significantly degrade the ICAP performance by clogging the sample orifice of the torch or the nebulizer during an 8-h working day. However, to prevent such degradation on prolonged use, which would result in source intensity drift, the torch is cleaned after a day's use in a solution of 1:3 v:v HNO_3/HCl.

Fluorescence Standards. Standards for AFS measurements were prepared from the same solutions used for excitation in the ICAP using serial dilution with deionized water and sub-boiling distilled acids prepared in this laboratory (8).

Sample Preparation. The samples analyzed by ICAP-excited AFS and ICAP emission were prepared as follows:

(1) Orange juice—dry ashing procedure is described by McHard et al. (7).

(2) Fly ash (NBS SRM-1633)—wet ashing procedure is described by Epstein et al. (9).

(3) Unalloyed copper (NBS SRM-394 and -396)—dissolution of 1 g of copper is carried out in 10 mL of sub-boiling distilled HCl with dropwise addition of sub-boiling distilled HNO_3 until complete, reduction in volume after dissolution by evaporation to 2 mL, and finally the solution is diluted to a volume of 100 mL.

(4) Simulated Fresh Water (NBS SRM-1643)—direct analysis is performed.

RESULTS AND DISCUSSION

Limits of Detection. As shown in Table I, limits of detection for many of the elements examined using ICAP-excited AFS approach, equal, or even exceed in one case (Mo) the best conventional atomic fluorescence detection limits (i.e., nonlaser source) ever obtained in similar flames (i.e., nitrogen-separated air/acetylene or nitrogen-separated nitrous oxide/acetylene) using a relatively conservative time constant (3 s) or integration time (1 s) and a rigorous (SNR = 3) definition of detection limit. While the fluorescence detection system for ICAP-excited AFS is well optimized for a background shot-noise limited, dispersive system, using double-pass optics, light traps, and a very low resolution (spectral bandpass = 16 nm) monochromator, the optical transfer of the ICAP emission to the flame *can be improved by at least an order of magnitude by the use of an ellipsoidal reflector (10, 11)*

Table II. Instrumentation and Operating Parameters

component	description	operating parameters
ICAP	PT-1500 torch assembly and HFP-1500D RF generator (Plasma Therm Inc., Kresson N.J.)	1.5-kW power, 15 mL/min argon coolant flow rate
nebulizer	concentric-ring glass neublizer T-220-A2 (J. E. Meinhard Assoc., Santa Anna, Calif.)	nebulizer pressure optimized for individual elements—from 15 to 35 psi; solution flow rates = 0.75 to 1.75 mL/min; argon flow rate < 0.5 L/min
emission monochromator	EU-700 monochromator (Heath Company, Benton Harbor, Mich.), 0.35-m focal length, f/6.8 aperture, 1180 groves/mm, grating blazed for 250 nm, adjustable slits, 2 nm/mm reciprocal linear dispersion	1-mm slit height, 25-μm slit width (effective 0.05-nm spectral bandpass)
fluorescence monochromator	H-10 monochromator (UV-V) (JY Instruments, Metuchen, N.J.) 0.1-m focal length, f/3.5 aperture, 8 nm/mm reciprocal linear dispersion, holographic grating with 1200 groves/mm, with 0.05-, 0.5-, 1-, 2-mm slits providing spectral bandpasses of 0.4, 4, 8, and 16 nm, respectively	2-mm slit width except where noted in text; 1-cm slit height
emission photomultiplier	R-928, (Hamamtasu TV Corp Ltd., Middlesex, N.J.)	1000 V
fluorescence photomultiplier	1P28, (RCA Copr., Harrison N.J.)	600 to 900 V, depending on background emission from flame
current-to-voltage converter	Keithley 427 (Keithley Instrument Company, Cleveland, Ohio)	
lock-in amplifier	Keithley 840 Autoloc amplifier, wideband	1- or 3-s time constant
recorder	Texas Instruments, Houston, Tex.	
chopper	Model 125, (Princeton Applied Research Corp., Princeton, N.J.)	600 Hz
nebulizer and mixing chamber for flame	Perkin-Elmer adjustable nebulizer and mixing chamber with flow spoiler (Perkin-Elmer Corp, Norwalk, Conn.)	5-8 mL/min aspiration rate
burner heads	circular stainless steel capillary burner head with auxiliary sheath	
lenses	Spectrosil, 5-cm diameter, 9-cm focal length	
mirror	5-cm aluminum-coated spherical with 5-cm focal length (Klinger Scientific Corp., Jamaica, N.Y.)	

placed off-axis or behind the plasma to collect a much larger solid angle of emission. This should improve detection limits by the increase in the light gathering power, assuming scatter does not become a significant noise source. We are presently collecting only about 2% of the source radiation using 5-cm spherical lenses with a focal length of 9 cm. Detection limits can also be improved by increasing the integration time or time constant and the concentration of analyte in the ICAP. The former will result, of course, in an increase in sample consumption and the latter can be used only for short periods of time to prevent clogging of the nebulizer or plasma torch sample orifice, but an order of magnitude improvement may be obtained in some cases by increasing both concentration in the ICAP and the integration time by a factor of 10.

The ICAP-excited AFS detection limits are a function of the atomic emission intensity from the ICAP and the flame background emission intensity. Shot-noise induced by the flame background emission is the limiting noise source at the detection limit using the 16 nm spectral bandpass with both separated air- and nitrous oxide/acetylene flames. The effect of spectral bandpass on the signal-to-noise ratio (SNR), and thus on the detection limit, is shown in Figure 2 for cadmium in an air/acetylene and vanadium in a nitrous oxide/acetylene flame. In the former flame, the SNR shows a slight decrease upon changing from a 16-nm spectral bandpass (2-mm slits) to a 4-nm spectral bandpass (0.5-mm slits), which is consistant with the changes in solid angle observed using the H-10 monochromator without focusing optics. Geometrical considerations show that over 2 cm of flame height are observed by the collimator although the vignetted region (i.e., the region in which the fluorescence radiation does not fill the collimator completely) is considerably extended, owing to the small

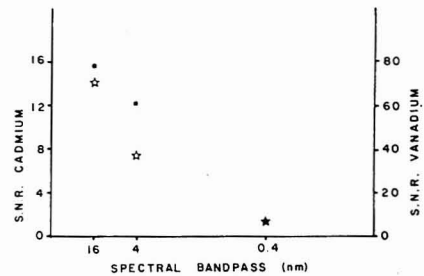

Figure 2. Effect of spectral bandpass on the ICAP-excited AFS signal-to-noise ratio from (■) cadmium in a nitrogen-separated air/acetylene flame and (☆) vanadium in a nitrogen-separated nitrous oxide/acetylene flame (20 ng/mL Cd; 100 μg/mL V)

effective aperture (2.86 cm) of the collimator. In all cases, the slit width is such that the overall width of the flame is viewed by the collimator. The considerable decrease in SNR upon a further 10-fold decrease in spectral bandpass is due to a change of the dominant noise from flame background-induced shot-noise to photomultiplier dark-current shot-noise and/or electronic noise. In the case of vanadium in the nitrous oxide/acetylene flame, the more significant decrease in SNR for the decrease in spectral bandpass from 16 to 4 nm is likely due to the exclusion of fluorescing lines from the bandpass which decreases the signal more than the case of cadmium, which involves one fluorescing line. The less significant decrease in SNR observed in the change from 4 nm to 0.4 nm

is also due to the exclusion of fluorescing lines and geometrical considerations, since the flame background-induced shot-noise is still limiting at the smaller bandpass.

For some elements, the ICAP-excited AFS detection limits are within an order of magnitude of the best reported ICAP-emission detection limits (Zn, Cr, Cd, Mg, Cu) listed in Table I. Furthermore, the ICAP-excited AFS detection limits are better than or equal to the detection limits obtainable on a commercial ICAP spectrometer for these same elements. These detection limits are representative of what we can obtain using our medium resolution monochromator (0.04-nm spectral bandpass) for ICAP emission.

Of further interest is a comparison of detection limits for ICAP-excited AFS and ICAP emission *using the same line.* A recent publication by Winge et al. (*12*) estimated detection limit capabilities for the prominent lines of 70 elements emitted in an ICAP excitation source. Their estimated detection limits using the lines with the best signal-to-background ratio are very close to the experimentally determined detection limits for a commercial ICAP instrument which were presented in Table I. The predicted ICAP-emission detection limits for the atomic resonance lines which we used to excite fluorescence (*12*) are also presented in Table I. It is interesting to note that for every element (except Pb and As) determined in a nitrogen-separated air/acetylene flame, the ICAP-excited AFS detection limits are from two to twenty times better than the predicted ICAP-emission detection limits for the same lines.

When detection limits are determined at the same line, the factors which must be considered are the solid angle of the ICAP emission focused on the flame vs. the solid angle viewed by the emission monochromator, the emission intensity of the excitation solution (10 mg/mL) in the ICAP vs. the emission intensity of the solution used to determine the ICAP-emission detection limit, the noise sources limiting detection for each technique, and the efficiency of emission and fluorescence excitation, collection, and detection. Although the signal in ICAP-excited AFS will suffer with respect to factors such as the fluorescence quantum efficiency (typically 0.01–0.05 in an air/acetylene flame) (*13*) and monochromator collection efficiency (since only a small percentage of fluorescence radiation is collected), ICAP-excited AFS will gain based on the solid angle of collection of ICAP emission and relative background emission intensities of the ICAP and the nitrogen-separated air/acetylene flame. The qualitative significance of these factors is illustrated by the improvement of the "same line" ICAP-emission detection limits using ICAP-excited AFS as a detection system, as shown in Table I.

Precision and Linearity. In Figure 3A, a typical ICAP-excited AFS analytical growth curve is shown, in this case for zinc, which is linear over slightly less than 4 orders of magnitude. In Figure 3B, a precision plot is shown for this same element, based on sixteen 1-s integrations at each data point and repeated twice. The analytical precision at high concentrations is on the order of 1 to 2% and is primarily limited by the source (ICAP) stability. This is in agreement with other researchers (*4*, *14*), who have reported the ICAP precision to be limited primarily by fluctuations in the nebulization and sample transport system to about 1%.

The long term stability of the ICAP emission is excellent (*14*), on the order of a few percent over long time periods, and thus its use to excite fluorescence represents a considerable advantage over many previous sources used for AFS such as electrodeless discharge lamps, which must be carefully thermostated (*15*) under certain conditions, and the Eimac short-arc xenon lamp (*16*), which has a much lower intensity in the ultraviolet.

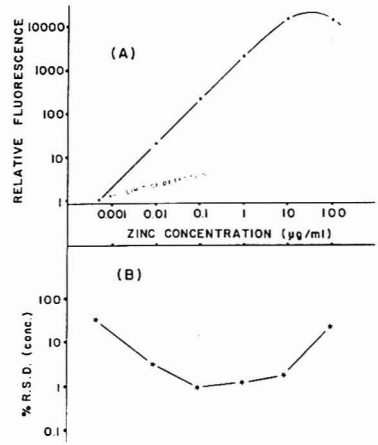

Figure 3. ICAP-excited AFS analytical growth curve (A) and precision curve (B) for zinc in a nitrogen-separated air/acetylene flame at 213.9 nm

Scatter. The problem of scattered radiation is perhaps the most significant interference in AFS when resonance transitions are employed. Scatter can occur from environmental sources, such as reflections off mirrors and burner heads, but this type of scatter is significant only when it becomes a dominant noise source due to either source-induced shot-noise or flicker. The latter is a problem with some pulsed dye lasers (*17*), where pulse to pulse variations may be 10% at a minimum. In ICAP-excited AFS, we observed environmental scatter to be significant only for those elements with detection limits less than about 5 ng/mL, and even in the case of magnesium, with a detection limit of 0.09 ng/mL, the scatter signal was not a significant noise source.

The other type of scattered radiation is that due to undissociated matrix particulates in the analytical flame. This scatter has been catagorized as primarily being of the Mie variety (i.e., due to particulates much larger than the wavelength of scattered radiation) (*6*, *18*) and does not have an easily defined relationship to wavelength as Rayleigh scatter does ($I \propto \lambda^{-4}$). A loss in accuracy will result from this type of scatter, since it may be mistaken for atomic fluorescence. The scatter interference is much more severe using continuum excitation sources than line sources, because of the greater spectral width of the former.

The primary method for correction using line excitation sources, the two-line technique (*6*, *19*), is based on the narrow linewidth of the atomic fluorescence and the assumption that the scatter signal does not change appreciably in the wavelength vicinity of the atomic fluorescence line. Another line from the source, which does not excite significant analyte *or* matrix fluorescence, is found near to the analyte line and the scatter signal is measured at that line, corrected for the relative intensities of the two lines, and subtracted from the signal excited by the analyte source line.

The ICAP is the ideal source for scatter correction using the two-line technique because of the great number of intense ion lines excited by the plasma. The ionic population of air/acetylene and electron-buffered (1 mg/mL K as KCl) nitrous oxide/acetylene flames is insignificant for most elements and thus these ion lines are available for scatter correction along with many other nonresonance transitions. These lines are equally as useful for the correction for broad

Table III. Sample Analysis Using ICAP-Excited AFS and ICAP Emission

sample	element	certified value, μg/g[a]	analyzed values, μg/g[b] ICAP-excited AFS	ICAP emission
unalloyed copper (SRM-394)	Zn	375 ± 38	376 ± 3	325 ± 25
unalloyed copper (SRM-396)	Zn	4.7 ± 0.3	4.8 ± 0.1	*c*
fresh water (SRM-1643)	Zn	0.065 ± 0.003	0.0656 ± 0.0008	*d*
	Cd	0.008 ± 0.001	0.0079	*d*
fly ash (SRM-1633)	Zn	210 ± 20	219 ± 4	*d*
orange juice	Cu	*e*	0.57	0.60
	Zn	*e*	0.45	0.46

[a] Office of Standard Reference Materials, National Bureau of Standards, Washington D.C. 20234. [b] ± one standard deviation of analytical results where multiple samples were analyzed. [c] Cannot be analyzed by ICAP emission with our experimental setup. [d] Analysis capability of ICAP emission for this element in this matrix already established. [e] Not a standard reference material.

band molecular fluorescence interferences although such interferences would be expected to be more severe with a continuum source than a line source.

The magnitude of the matrix-scatter interference in ICAP-excited AFS was investigated for the zinc 213.9-nm line using a 5% high-purity lanthanum solution. The scatter signal was equivalent to a concentration of 60 ng/mL Zn and could be corrected for completely using the Cd II line at 214.4 nm generated by 10 mg/mL Cd in the ICAP. It should be noted that any solutions used for production of "scatter-correction" radiation in the ICAP must be significantly free of analyte or an overcorrection may result. Comparison of analyte emission line intensity and scatter correction emission line intensity from the ICAP is made experimentally using a 5% high-purity lanthanum solution (*6*, *20*). The presence of analyte contamination in the scatter correction solution aspirated into the ICAP can be evaluated by observing if any signal is generated by an analyte standard in the flame. In general, care must be taken that the "scatter correction" solution does not emit spectral components capable of exciting fluorescence *within the spectral bandpass* of the monochromator.

Another possible method for scatter correction using the ICAP is based on the shape of the "excitation" curve of growth (*5*). The technique is similar to the method described by Haarsma et al. (*21*), which takes advantage of the self-absorption of the source at high concentrations. In the concentration range on the plateau region of the excitation curve of growth, the fluorescence intensity will not appreciably increase while the emission intensity and thus the scatter will increase. Aspirating two different high concentrations of the element being determined into the plasma and knowing the effect of the two different concentrations on the fluorescence and the emission signals, one can calculate the scatter signal and subtract it out.

Applications. *Zinc in Unalloyed Copper (NBS SRM-394 and -396).* The determination of trace zinc in high purity copper is a difficult analytical problem using either atomic absorption or ICAP emission. The major zinc resonance line at 213.856 nm is subject to a direct spectral interference by the copper 213.853-nm nonresonance transition (11 203–57 949 cm^{-1}). This interference has been reported (*6*) for flame atomic absorption analysis and requires an electrodeposition of the copper from solution (*22*) or a high-resolution atomic absorption technique employing wavelength modulation and line-nulling (*23*) before accurate analysis can be performed. The problem using ICAP emission is illustrated in Figure 4 by a scan of the wavelength region of the zinc 213.856-nm line for the unalloyed copper SRM 396. While the majority of the copper lines are easily resolved, the 213.853-nm line cannot be with the resolution available in spectrometers typically used for ICAP emission. Even with an echelle spectrometer (spectral bandpass = 0.003 nm), this line pair has been shown

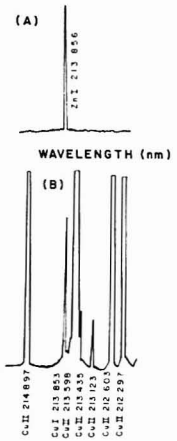

Figure 4. Wavelength scans of (A) 20 μg/mL zinc and (B) 10 000 μg/mL copper as SRM 396 (unalloyed copper) illustrating the spectral interferences observed in ICAP emission for zinc analysis in copper

to exhibit an overlap (*23*). The emission from this line at a concentration of 10 mg/mL copper is equivalent to the emission from approximately 20 μg/mL of zinc, making analysis impossible without the use of zinc-free copper for matrix-matching. The Zn II line at 206.2 nm can be used for the determination of zinc by ICAP emission without line spectral interference from copper, although background correction by scanning over the wavelength region of the line is still required to correct for a change in the background level caused by either stray light due to copper emission or changes in the plasma background. The zinc detection limit for this line was found to be approximately 4× worse than at the 213.9-nm line, in agreement with the results of Winge et al. (*12*). While SRM 394 was analyzed (375 μg/g certified value), SRM 396 (4.7 μg/g certified value) could not be analyzed because of its low zinc concentration, the poorer detection limit, and the continuum background in the vicinity of the 206.2-nm Zn II line generated by the copper matrix. The background was equivalent to approximately 1 μg/mL zinc at this wavelength. The analysis values for SRM 394 were approximately 10% less than the certified value, indicating a slight interference by ICAP emission.

The determination of zinc in both SRM 394 and 396 by ICAP-excited AFS is summarized in Table III along with the ICAP-emission results. The AFS results agree well with the certified values. There is no significant fluorescence excited

at the 213.853-nm copper line in the flame, owing to a combination of the relatively low thermal population in the air/acetylene flame of the 11203 cm^{-1} energy level and low quantum efficiency of the fluorescence process. This combination effectively minimizes copper spectral interference in ICAP-excited AFS by more than a factor of 10^4 compared to the ICAP-emission case. The effect of the flame as a resonance monochromator is not significant in this example, since even 10 mg/mL Cu in the ICAP did not excite any fluorescence from the Cu 213.853-nm line.

When the 16-nm spectral bandpass is used on the fluorescence monochromator, several resonance copper lines at 216.5, 217.8, and 218.2 nm are included. Although no spectral interference is observed when a pure zinc solution (20 mg/mL) is used for excitation in the ICAP, we found that our supposedly 99.99+ zinc standard contained about 5 μg/mL copper, indicating a purity of less than 99.98. This was enough copper to excite fluorescence at the resonance copper lines and, although no interference was observed for the analysis of SRM 394 in the part-per-million concentration range, a slightly higher value (approximately 20% greater) than the certified value for SRM 396 was obtained using the 16-nm spectral bandpass. The enhancement due to the copper fluorescence from the resonance lines, equivalent to approximately 10 ng/mL zinc, was completely eliminated by using the 0.4-nm spectral bandpass. A scatter signal of approximately 4% for SRM 396, equivalent to 2 ng/mL zinc, was observed and corrected for using the Cd II 214.4-nm line.

Fly Ash (NBS SRM-1633) and Trace Elements in Water (NBS SRM-1643). Zinc was determined in fly ash and cadmium and zinc in simulated fresh water by ICAP-excited AFS. No chemical interferences were observed in either case, and the results are presented in Table III. Excellent agreement with the certified values was obtained.

Orange Juice. The determination of copper and zinc in Florida orange juice was performed using both ICAP-excited AFS and ICAP emission. The optical arrangement for the former was as described in reference 5. Agreement of results between the two techniques was good, as illustrated in Table III. Matched-matrix standards were employed so that background correction by wavelength scanning was not required.

In the analysis of orange juice for zinc by ICAP emission, a series of wavelength scans through the vicinity of the 213.9-nm zinc line showed not only the gradually increasing continuum background from the argon plasma but also superimposed on this background were bands of the γ system of NO ($A^2\Sigma^+ \rightarrow X^2\Pi$) degraded to shorter wavelengths, resulting from the entrainment of the ambient air (27), with bandheads at 214.91 and 215.49 nm. Furthermore, the phosphate present in the matrix blanks and in the orange juice produced a strong emission at 213.620 nm. However, the monochromator resolution was sufficient to eliminate the effect of these spectral interferences.

For the copper analysis by ICAP emission, the wavelength scans from 323 to 326 nm showed several lines of argon (323.45, 323.681, 324.369, and 325.76 nm) and strong OH bands (323.5 and 325.7 nm) with some less intense OH peaks at other wavelengths (323.7, 324.1, 324.4, and 324.7 nm). Under our experimental conditions, the argon lines and OH bands caused no problems in the copper analysis at the 324.7-nm line.

CONCLUSION

Several conclusions can be derived from our experimental evaluation of the characterization of the ICAP as an excitation source in atomic fluorescence spectrometry.

(i) The ICAP has been confirmed to be an extremely versatile and intense excitation source for the atomic fluorescence determination of all the elements investigated.

(ii) The ICAP combines the versatility of a continuum source with the high spectral irradiance of a line source.

(iii) The excellent multielement excitation capability of the ICAP simplifies the application of the 2-line method of correcting for scattering problems using resonance transitions because of the many neutral as well as ionic lines available.

(iv) The spectral selectivity of the atomic fluorescence technique is shown to be advantageous in certain analytical applications where the emission technique is plagued with spectral interferences.

In addition to this, several promising areas of application for this source can be envisaged.

(i) Because of the high excitation power and freedom from interelement interferences, the ICAP emission of several elements aspirated simultaneously in it will result in little, if any, degradation of the detection limits obtained in atomic fluorescence, provided that no spectral interferences will result. Therefore, the use of a programmable slew-scan monochromator would permit the sequential determination of several elements in one sample.

(ii) The shape of the "excitation" curve of growth (5) should allow the possibility of scatter correction by taking advantage of the differences in the source emission intensity and excited-fluorescence intensity dependence on concentration due to self-absorption in the source.

(iii) Relatively high concentrations of the element investigated in a given matrix can be analyzed directly by aspirating the sample in the ICAP rather than in the flame, and using the flame as a resonance detector by monitoring the fluorescence from a high concentration of analyte in the flame. The flame fluorescence excited by the analyte in the ICAP will exhibit the linearity at high concentrations characteristic of an emission source with negligible self-absorption. This avoids the necessary dilution of the sample solution, should the analysis be performed in the conventional manner by AFS.

(iv) The system may also prove useful for electrothermal atomization techniques or hydride generation techniques, where the low background emission levels of these atomization cells may further improve detection limits.

(v) Although, in principle, the ICAP could also be advantageously used as a primary source in atomic absorption analysis, especially for elements which exhibit low hollow cathode lamp intensity, this application does not seem to offer any advantage as compared to the emission technique, not even for specific applications as in the case of atomic fluorescence.

In conclusion, it is our opinion that the ICAP-excited AFS technique *is an ideal adjunct to an ICAP-emission spectrometer, capable of solving many specific analytical problems.* An increase in: (a) the collection efficiency of the ICAP emission focused on the flame; (b) the concentration of analyte solution aspirated into the ICAP; (c) the time constant or integration time; and (d) the power applied to the ICAP, should considerably improve the already impressive detection limits. Investigations into this and several other above-mentioned possibilities are presently underway in this laboratory.

LITERATURE CITED

(1) V. A. Fassel and R. N. Kniseley, *Anal. Chem.*, **46**, 1110A (1974).
(2) Ch. A. M. Hussein and G. Nickless, paper presented to the 2nd ICAAS, Sheffield, England, 1969.
(3) V. Sychra, V. Svoboda, and I. Rubeska, "Atomic Fluorescence Spectroscopy", Van Nostrand, London, 1975, p 106.
(4) P. W. J. M. Boumans, "Inductively-Coupled Plasmas: State-of-the-Art in Research and Routine Analysis", paper presented at the 20th CSI and 7th ICAS, Prague, Czechioslovakia, 1977.
(5) N. Omenetto, S. Nikdel, J. D. Bradshaw, M. S. Epstein, R. D. Reeves, and J. D. Winefordner, *Anal. Chem.*, **51**, 1521 (1979).
(6) P. L. Larkins and J. B. Willis, *Spectrochim. Acta, Part B*, **29**, 319 (1974).
(7) J. M. McHard, S. J. Foulk, S. Nikdel, A. H. Ullman, B. D. Pollard, and J. D. Winefordner, *Anal. Chem.*, **51**, 1613 (1979).
(8) J. M. Mattinson, *Anal. Chem.*, **44**, 1715 (1972).

(9) M. S. Epstein, T. C. Rains, and O. Menis, *Can. J. Spectrosc.*, **20**, 22 (1975).
(10) M. Shull and J. D. Winefordner, *Anal. Chem.*, **43**, 799 (1971).
(11) P. Benetti, N. Omenetto, and G. Rossi, *Appl. Spectrosc.*, **25**, 57 (1971).
(12) R. K. Winge, V. J. Peterson and V. A. Fassel, *Appl. Spectrosc.*, **33**, 206 (1979).
(13) D. R. Jenkins, *Spectrochim. Acta, Part B*, **25**, 47 (1970).
(14) P. W. J. M. Boumans and F. J. DeBoer, *Spectrochim. Acta, Part B*, **32**, 365 (1977).
(15) R. F. Browner, B. M. Patel, T. H. Glenn, M. E. Rieita, and J. D. Winefordner, *Spectrosc. Lett.*, **5**, 311 (1972).
(16) R. L. Cochran and G. M. Hieftje, *Anal. Chem.*, **49**, 2040 (1977).
(17) Instruction Manual, CMX-4 Tunable Flashlamp Excited Dye Laser, Chromatix, Sunnyvale, Calif.
(18) N. Omenetto, L. P. Hart, and J. D. Winefordner, *Appl. Spectrosc.*, **26**, 612 (1972).
(19) K. J. Doolan and L. E. Smythe, *Spectrochim. Acta, Part B*, **32**, 115 (1977).
(20) T. C. Rains, M. S. Epstein, and O. Menis, *Anal. Chem.*, **46**, 207 (1974).
(21) J. P. S. Haarsma, J. Vlogtman, and J. Agterdenbos, *Spectrochim. Acta, Part B*, **31**, 129 (1976).
(22) T. C. Rains, National Bureau of Standards, private communication.
(23) A. T. Zander, T. C. O'Haver, and P. N. Keliher, *Anal. Chem.*, **49**, 838 (1977).
(24) G. F. Kirkbright and M. Sargent, "Atomic Absorption and Fluorescence Spectroscopy", Academic Press, London, 1974, p 462.
(25) P. W. J. M. Boumans and R. M. Barnes, *ICP Inf. Newsl.*, **3**, 445 (1978).
(26) "Detection Limits in Water", Jarrell-Ash Plasma AtomComp Direct-Reading Spectrometer System, Jarrell-Ash Division, Fisher Scientific Company, Waltham, Mass., 1978, p 7.
(27) R. M. Barnes and S. Nikdel, *Appl. Spectrosc.*, **29**, 477 (1975).

RECEIVED for review June 6, 1979. Accepted July 23, 1979. Work supported by AF-AFOSR-F44620-78-C-0005 and by WPAFB Contract number F33615-78-C-2036.

Lophine Chemiluminescence for Metal Ion Determinations

Allan MacDonald, Kenneth W. Chan,[1] and Timothy A. Nieman*

School of Chemical Sciences, University of Illinois, Urbana, Illinois 61801

The chemiluminescent reaction of lophine with H_2O_2 in alkaline solution has been investigated for use in determination of trace concentrations of metal ions and other inorganic species. The observed emission intensity is found to be a function of the reduction potential of the analyte. By varying reagent concentrations, it is possible to make dramatic changes in the relative sensitivity for a given analyte. Detection limits were found to be: OCl^-, 1×10^{-6} M; Co(II), 8×10^{-7} M; Cr(III), 5×10^{-6} M; Cu(II), 5×10^{-6} M. Relative standard deviations are in the range of 2–5%. The intensity of the observed emission for a mixture of analytes is less than the sum of the signals for the separate analytes, and is generally suppressed below the signal for either analyte alone.

Solution chemiluminescence (CL) methods are very sensitive for a variety of organic and inorganic analytes. CL determinations of trace concentrations of metal ions have received most attention, and have been performed using either luminol (*1*, *2*) or lucigenin (*3*, *4*). A major weakness of metal ion determinations via CL has been a lack of selectivity. There are, for example, at least 30 different species that cause enhanced light emission with the luminol system and at least 20 with the lucigenin system (*5*).

We have been interested in this selectivity problem in CL analysis, and have used two approaches. The first approach is to investigate alternate CL reactions to determine if they are useful for different sets of metal ion analytes. The second approach is to manipulate the experimental conditions for a given CL reaction to selectively enhance its sensitivity toward certain analytes. Logical CL reactions to investigate for metal ion determinations are those which occur under conditions similar to the well known luminol and lucigenin systems—reaction with H_2O_2 in strongly basic solution. Two such reactions that we have studied have been gallic acid (*5*, *6*) and lophine (*7–9*).

[1] Present address, Department of Chemistry, University of Arizona, Tucson, Ariz. 85721.

The CL oxidation of lophine (2,4,5-triphenylimidazole) was first reported by Radziszewski (*10*). The mechanism is thought to involve attack by H_2O_2 to form a hydroperoxide, conversion to a dioxetane intermediate, and cleavage of the peroxide bond resulting in light emission (*11–13*). Similar peroxide decomposition steps have been proposed for the luminol and lucigenin reactions (*14*).

This paper presents the results of our work to investigate the analytical utility of the lophine reaction, and particularly to examine the possiblity of selectivity control via variation in reagent concentrations.

EXPERIMENTAL

Instrumentation. All measurements were made in an inert, modular flow cell (*15*) with a stopped flow reagent delivery and mixing system (*6*) as previously described.

Reagents. All reagents were commercially available, and used without further purification: lophine (Aldrich); potassium hydroxide from standard volumetric solutions (Anachema); unstabilized 30% H_2O_2 (Mallinckrodt); reagent grade sodium hypochlorite (Baker); AR or ACS certified metal salts (generally chlorides or nitrates). Lophine has limited solubility in water; all lophine solutions were prepared in ethanol. All other solutions were prepared with water that was deionized (house supply) and then distilled in glass. The cleaning procedure for volumetric glassware included soaking in dilute nitric acid.

Procedure. The four syringes of the stopped flow device are filled with the four solutions (1.5 mL each) required for the reaction: lopine, KOH, H_2O_2, and analyte. All concentrations reported are for the solutions in the syringes. When the solutions are delivered to the cell, the data acquisition system is triggered. The signal is recorded as the maximum observed light emission intensity following initiation of the reaction and is termed the "peak height". A blank signal is determined by using water in place of the analyte. The analytical signal is taken as the difference in observed peak heights for the analyte and the blank. All signals are reported as photomultiplier current in nanoamperes. Periodically the entire system is cleaned by rinsing with HNO_3 followed by water. All measurements were made at room temperature.

RESULTS AND DISCUSSION

Survey of Enhancing Species. Preliminary work (*7*) involving a simplex optimization using $Fe(CN)_6^{3-}$ as the

0003-2700/79/0351-2077$01.00/0

Table I. Lophine Chemiluminescence Relative Response to Various Aqueous Ions at 10^{-3} M[a]

species	relative intensity	species	relative intensity	species	relative intensity
$AuCl_4^-$	1992.7	Al(III)	0	Mg(II)	0
OCl^-	686.2	As(V)	0	Mn(II)	0
MnO_4^-	80.4	Ba(II)	0	Mo(VI)	0
$Fe(CN)_6^{3-}$	57.1	Cd(II)	0	Ni(II)	0
Cr(III)	35.0	CrO_4^{2-}	0	Pr(III)	0
Ag(I)	14.8	Fe(II)	0	Pt(IV)	0
Co(II)	12.8	Fe(III)	0	Sb(III)	0
VO^{2+}	10.3	I_3^-	0	Se(VI)	0
Cu(II)	4.0	In(III)	0	Sr(II)	0
Mo(VI)	2.0	Ir(III)	0	Sn(IV)	0
Pb(II)	0.6	Ga(III)	0	Tl(III)	0
		Hg(II)	0	Zn(II)	0
				Sn(II)	quenches

[a] Conditions: lophine = 3.25×10^{-4} M, H_2O_2 = 0.020 M, KOH = 0.20 M. Relative intensities are given as signal above background (in nA).

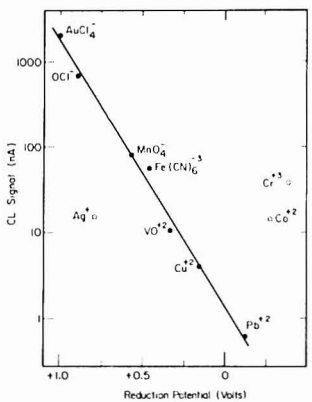

Figure 1. Correlation of the CL signal and the reduction potential of the analyte. The line is the least-squares fit to the solid data points

analyte (or enhancing species) had indicated appropriate concentrations for lophine, H_2O_2, and KOH. Table I gives the observed enhancement for 36 ions tested as potential analytes. Zero enhancement corresponds to the same response as the blank (within twice the relative standard deviation (RSD) of repetitive trials). All species were tested at 10^{-3} M. Repeating the experiment at lower analyte concentrations gives lower intensity signals, but the same relative ranking (with the exception of $AuCl_4^-$). The signal due to $AuCl_4^-$ drops very sharply with decreasing concentration.

Only 11 species show enhancement; thus lophine has greater selectivity than luminol or lucigenin, but less selectivity than gallic acid. The behavior of Sn(II) was quite interesting. In the presence of Sn(II), the observed signal was less than the blank; at the concentration tested, there was no signal observed above the dark current. Sn(II) does not suppress the blank emission in the luminol, lucigenin, or gallic acid systems (*5*); however, Sn(II) does cause significant suppression of the analytical signal due to Co(II) with gallic acid (*6*). The species which cause enhancement in the lophine system are generally species which cause enhancement in the luminol or lucigenin systems. However, several species for which these systems are particularly sensitive (Fe(II), Fe(III), Mn(II), and Ni(II)) cause no light emission in the lophine system.

Table II. Effect of Buffer Systems[a]

buffer	concn M	pH	relative CL signal, analyte = Cr(III), 1 × 10^{-4} M	relative CL signal, analyte = OCl^-, 1 × 10^{-4} M
none (KOH)	0.2	12.82	100	100
phosphate	0.2	12.76	73	81
salicylate	0.2	12.86	57	15
borate	0.2	12.86	54	18
$Ca(OH)_2$	0.001	12.90	8	14

[a] Conditions: lophine = 3.25×10^{-4} M, H_2O_2 = 0.18 M.

Several of the ions that cause the most intense light emission from lophine are fairly strong oxidents. Figure 1 gives a plot of the log of the CL signal vs. the standard reduction potential of the analyte (*16*). With the exception of Co(II), Cr(III), and Ag(I), the log of the CL signal is proportional to the reduction potential. The high degree of correlation is rather surprising ($r = 0.9958$). This type of behavior has been observed by Schuster (*17*) for CL reactions of organic peroxides in the presence of various aromatic hydrocarbons by a mechanism described as chemically initiated electron exchange luminescence. The least-squares fit to the lophine data gives a value of 3.13 decades change in CL signal for a change of 1 V in reduction potential. The class of reaction that has been examined by Schuster gives nearly 5 orders of magnitude change for a 1-V change. The strong correlation between CL intensity and analyte reduction potential suggests that the rate limiting step in the mechanism involves the analyte (M) acting as an oxidant. Two possibilities are

$$HO_2^- \xrightarrow{M} O_2^{-}\cdot + H^+ \quad (1)$$

$$\text{lophine} \xrightarrow{M} \text{lophine}^+\cdot \quad (2)$$

A step similar to Equation 2 has been proposed for the luminol reaction with cobalt (*18*). As will be discussed later, relative sensitivities can be influenced by reagent concentrations. However, the relative sensitivities for $AuCl_4^-$, OCl^-, MnO_4^-, $Fe(CN)_6^{3-}$, VO^{2+}, and Pb^{2+} (and therefore the observed correlation with reduction potential) show only slight variation with reagent concentrations.

Matrix Effects. We wanted to determine if it would be possible to replace the KOH reagent solution by a buffer solution of appropriate pH to reduce the sensitivity to the pH of the analyte solution. Buffer solutions were prepared from phosphate, salicylate, borate, and $Ca(OH)_2$. All of these solutions were in the pH range of 12.78 to 12.90. Each buffer was at a total concentration of 0.2 M (as was the unbuffered KOH) except for $Ca(OH)_2$; owing to solubility considerations the $Ca(OH)_2$ concentration was limited to 10^{-3} M. The experiments were run with a metal (Cr(III)) and a nonmetal (OCl^-) analyte. Table II summarizes the results. It can be seen that in every case, the CL signal is suppressed in the presence of a buffer. In addition, the magnitude of suppression is different for the two analytes. If buffering is necessary, these studies indicate phosphate buffer to be the best choice. All work reported in this paper, however, was done in unbuffered KOH solutions.

In a real sample, the analyte of interest will be in the presence of other species. These other species, although they themselves have no apparent effect on the CL reaction of lophine, may suppress or enhance the signal due to the analyte. We examined the effect of several ions and complexing agents on the lophine–Cr(III) and lophine–OCl^- systems. These

Table III. Species Tested for Matrix Effects on the Lophine System[a]

interfering species, 1×10^{-4} M	relative CL signal: analyte = Cr(III), 1×10^{-4} M	analyte = OCl^-, 1×10^{-4} M
none	100	100
NH_3	16	99
CO_3^{2-}	43	104
CN^-	20	101
I_3^-	138	---
EDTA	98	1
Se(VI)	116	99
As(V)	95	99
OCl^-	238	---
Cr(III)	---	31
Cu(II)	43	95

[a] Conditions: lophine = 3.25×10^{-4} M, H_2O_2 = 0.18 M, KOH = 0.20 M.

experiments used the same conditions as the buffer experiments, except that the analyte solutions were made 10^{-4} M in the enhancing species and 10^{-4} M in the interfering species. The analyte solutions were allowed to stand for 12 h to allow any complexation reactions to go to completion. (All solutions were pH 7–8 except for NH_3, CN^-, CO_3^{2-}, and OCl^- at pH 9–10.) Table III summarizes the results for the species examined. With Cr(III) as the analyte, the species NH_3, CO_3^{2-}, and CN^- cause significant suppression; the suppression with NH_3 or CN^- is expected in terms of their complexation properties. Similar results are seen with the gallic acid–Co(II) system (*6*). EDTA does not suppress the signal, but the Cr(III)–EDTA complex is known to be slow to form. I_3^- caused increased CL even though it does not cause CL by itself with lophine. The most dramatic effect on the signal due to OCl^- came with addition of EDTA. A redox reaction between EDTA and OCl^- is unlikely because in such a strongly basic solution, OCl^- is not a strong enough oxidant to oxidize EDTA (*16*, *19*). However, it is likely that a dialkyl chloramine is formed (*20*).

It is particularly interesting to note the results involving mixtures of OCl^-, Cr(III), and Cu(II) since each of these alone causes CL with lophine. As a result, one might expect the signal for a mixture of two of these species to be equal to the sum of the signals for the species alone. That is observed not to be the case. A mixture of Cu(II) and Cr(III) gives a signal less than that observed with Cr(III) alone. A mixture of Cr(III) and OCl^- gives a signal intermediate between those observed for Cr(III) and OCl^- alone. This behavior will be examined in more detail later.

Optimization of Reagent Concentrations. We wanted to locate the optimum conditions for determination of the potential analytes indicated in Table I; OCl^-, Cr(III), Co(II), VO^{2+}, and Cu(II) were selected for this procedure. The experiment was planned to give a picture of the CL response surface for each analyte (as a function of lophine, base, and H_2O_2 concentrations). The procedure was to develop the surface in slices by holding two of the reagent concentrations constant, and measuring the CL signal as a function of the concentration of the third reagent (at a constant analyte concentration of 10^{-4} M).

Figure 2 shows the CL signal as a function of H_2O_2 concentration. It is notable that no two of the analytes give the same curve. Each of the analytes has a range of H_2O_2 concentrations that maximize sensitivity, but those ranges are different for each analyte. Figures 3 and 4 show the CL signal as a function of KOH concentration. Figure 3 gives the results with 10^{-3} M peroxide (where Cu(II) shows maximum sensitivity). Figure 4 gives the results with 10^{-1} M peroxide (where

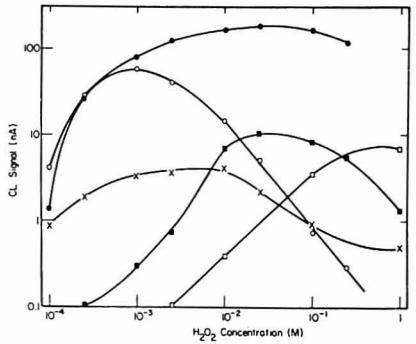

Figure 2. Variation of CL signal with H_2O_2 concentration. Lophine = 3.25×10^{-4} M; KOH = 0.20 M. OCl^- (●), Cu(II) (○), Cr(III) (■), Co(II) (□), VO^{2+} (×)

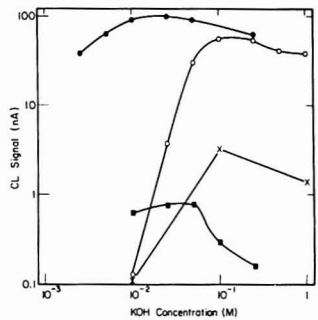

Figure 3. Variation of CL signal with KOH concentration. Lophine = 3.2×10^{-4} M; $H_2O_2 = 1.0 \times 10^{-3}$ M. OCl^- (●), Cu(II) (○), Cr(III) (■), Co(II) (□), VO^{2+} (×)

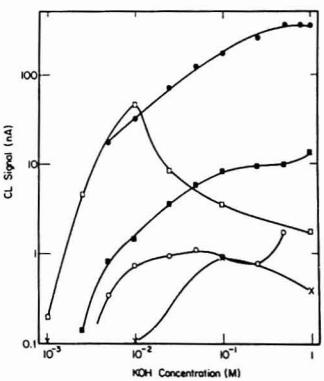

Figure 4. Variation of CL signal with KOH concentration. Lophine = 3.25×10^{-4} M; $H_2O_2 = 1.0 \times 10^{-1}$ M. OCl^- (●), Cu(II) (○), Cr(III) (■), Co(II) (□), VO^{2+} (×)

Co(II) and Cr(III) give higher response than Cu(II)). In general, the signal decreases as the KOH concentration decreases below 10^{-1} M, regardless of the analyte or the H_2O_2 concentration. The only exception is the peak in the Co(II)

Table IV. Optimum Reagent Concentrations[a]

analyte	H_2O_2, M	KOH, M
OCl^-	1.0×10^{-3}	1.0×10^{-2}
Co(II)	1.0×10^{-1}	1.0×10^{-2}
Cr(III)	1.0×10^{-1}	1.0×10^{-1}
Cu(II)	1.0×10^{-3}	1.0×10^{-1}
VO^{2+}	1.0×10^{-3}	1.0×10^{-1}

[a] Lophine concentration is 3.25×10^{-4} M in all cases.

signal at 10^{-2} M KOH (Figure 4). Similar curves were prepared for the CL signal as a function of lophine concentration; the CL signal increases monotonically with increasing lophine concentration (up to the solubility limit).

The results of this study indicate that distinctly optimum reagent concentrations exist for each of these analytes, and that these optima are separated from each other on the CL response surface. Table IV gives the reagent concentrations selected for each analyte. A few minor compromises were made in order to limit the total number of solutions required. The indicated reagent concentrations were used for the remainder of this work. The H_2O_2 concentration is the most critical, and the OH^- and lophine concentrations provide "fine tuning". Quite a degree of variation in the relative sensitivities is possible. The Cr(III)–Cu(II) situation is typical. At the Cu(II) optimum, the Cu(II) signal is 200 times the Cr(III) signal; at the Cr(III) optimum, the Cr(III) signal is 11 times the Cu(II) signal. So going from the Cu(II) optimum to the Cr(III) optimum, the ratio of relative sensitivities changes by over 2000.

Working Curves and Detection Limits. Working curves were prepared for each analyte (using the conditions in Table IV) from 10^{-3}M down to near the detection limit. The curves for OCl^- and Cu(II) are typical and are shown in Figure 5. The curve for Co(II) is similar to the Cu(II) curve and the curve for Cr(III) is similar to the OCl^- curve (with only slight curvature at high and low analyte concentrations). The sharp change in slope (at about 10^{-4} M) in the Cu(II) and Co(II) curves is quite interesting. The lophine concentration is only 3.25×10^{-4} and could be the limiting factor in the rate of reaction at higher analyte concentrations. (However no such sharp break occurs in the Cr(III) and OCl^- curves). Alternatively, one could postulate a lophine–metal complex is formed, with stoichiometry indicated by the concentrations at the break in the curve, although the formation constants for Cu(II)–imidazole ($\log k_1 = 3.76$, $\log k_2 = 3.39$, $\log k_3 = 3.03$, $\log k_4 = 2.66$) and Co(II)–imidazole ($\log k_1 = 2.42$, $\log k_2 = 1.95$, $\log k_3 = 1.58$, $\log k_4 = 1.2$) complexes are small (*21*, *22*). Similar evidence for formation of luminol–metal complexes has been reported (*23*).

Table V summarizes the results from the working curves for all the analytes. Detection limits are given as the concentration for which the analytical signal is twice the standard deviation of the blank. The relative standard deviation of the CL signal is in the range of 2–5% for each analyte over the linear range of the working curves. Similar detection limits for Cr(III) and Cu(III) have been reported using lucigenin CL (*4*). Lower detection limits for Co(II) and OCl^- have been reported with luminol CL (*2*, *24*). Atomic absorption detection limits for Co(II), Cr(III), and Cu(II) are generally somewhat lower than those observed with lophine CL.

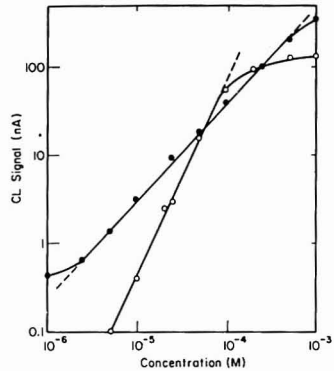

Figure 5. Working curves for OCl^- (●) and Cu(II) (○). Reagent concentrations given in Table IV

Multicomponent Determinations. Because the reagent concentrations have such a marked influence on the relative sensitivities for the different analytes, we were interested in investigating the use of such sensitivity control for determination of the concentrations of two (or more) analytes in a mixture without prior separation. The CL emission intensity from the analyte mixture would be measured at the reagent optima for each of the components. To determine the concentrations of the components, one needs to know (1) the working curves for each analyte at each reagent optimum used and (2) the relationship between the total CL signal (for the analyte mixture) and the CL signal due to each analyte separately.

The simplest case is when the total signal is the sum of the separate signals. The approach could then be similar to using UV-visible absorbance, and Beer's law, at n wavelengths for a mixture of n components. (Because the slopes of the log–log working curves are not unity, concentration terms in the simultaneous equations will have nonunity exponents) The absence of additive behavior does not necessarily preclude the determination, however.

Several binary mixtures of Co(II), Cr(III), and Cu(II) were prepared and tested. In each case the observed CL signal was not the linear sum of the CL signals for the separate components. As noted earlier (Table III), the response for the mixture was usually intermediate between the separate responses. To further characterize the situation, we again studied the CL response surface; this time binary mixtures of analytes were used. Figure 6 shows the CL signal as a function of H_2O_2 concentration for the three binary mixtures of Co(II), Cr(III), and Cu(II) with each component at 10^{-4} M. For comparison, the response curves for the separate components (also at 10^{-4} M) are included (from Figure 2). The results are totally intriguing. The response curves for the mixtures don't at all resemble the sum of the curves for the separate components. In fact, the response curves are all much lower than the curves for either of the separate species.

Table V. Working Curves and Detection Limits

analyte	linear range, M, log–log graph	slope $\pm\sigma$	standard error estimate	correlation coefficient	detection limit, M
OCl^-	2×10^{-6}–5×10^{-4}	1.095 ± 0.014	0.0244	0.9996	1×10^{-6}
Co(II)	8×10^{-7}–7×10^{-5}	1.108 ± 0.049	0.0501	0.9990	8×10^{-7}
Cr(III)	1×10^{-5}–5×10^{-4}	1.499 ± 0.042	0.0426	0.9992	5×10^{-6}
Cu(II)	5×10^{-6}–7×10^{-5}	2.101 ± 0.063	0.0661	0.9982	5×10^{-6}

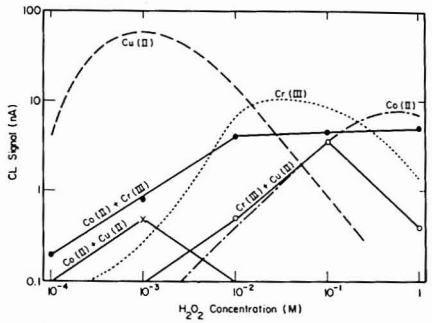

Figure 6. Variation of CL signal for equimolar analyte mixtures with H_2O_2 concentration. Lophine = 3.25 × 10^{-4} M; KOH = 0.20 M. Cr(III) and Co(II) (●), Cr(III) and Cu(II) (○), Co(II) and Cu(II) (×). The curves for the separate species (from Figure 2) are included for reference

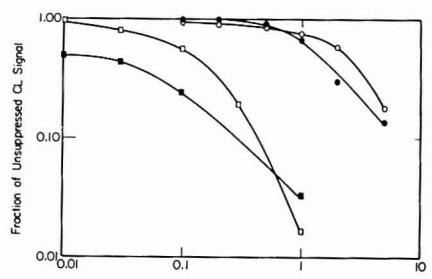

Figure 7. Suppression of the analytical CL signal as a function of the ratio of the concentrations of the interfering species and the analyte. All analytes are at 10^{-4} M. The reagent concentrations are chosen from Table IV for the analyte. Cu(II) analyte, Cr(III) interference (○); Cr(III) analyte, Cu(II) interference (●); Cu(II) analyte, Co(II) interference (□); Co(II) analyte, Cu(II) interference (■)

To quantitate this signal suppression, we examined the CL signal for a constant concentration (10^{-4} M) of analyte (at the optimum reagent conditions for that analyte) as a function of the concentration of a second analyte (or "interfering species").

Figure 7 gives the results for binary mixtures of Co(II), Cr(III), and Cu(II). As the concentration of the second analyte increases, the observed signal monotonically decreases. For example, with a constant amount of Cu(II) present, as Cr(III) is added, the observed signal continually decreases, provided the reaction is run with the reagent conditions optimized for Cu(II). If the same experiment (constant Cu(II) concentration and increasing Cr(III) concentration) is run with the reagent conditions optimized for Cr(III), the observed signal will increase with increasing Cr(III) concentration.

This second experiment amounts to construction of a calibration plot for one analyte in the presence of a given concentration of a second analyte. In the cases we have examined, the slope of the log working curve for a given analyte is not changed in the presence of a fixed concentration of a second analyte; the entire curve is shifted to lower intensities. Therefore, with knowledge of the working curves, and the mutual suppression data (Figure 7) it is possible to perform the multicomponent determination. However, because the relationship between the total signal and the signals for the analytes separate is one of suppression rather than addition, the experimental procedure and calculation (best handled by iteration) is more complex. As a result, actual determinations of mixtures were not undertaken in this investigation. In similar studies involving gallic acid (*5*, *25*) and lucigenin (*26*), we have found the total signal for mixtures to be given by the sum of the signals for the separate components. It is not clear at this point why these very similar systems should behave so differently in this respect.

The interpretation of the suppression data yields insight into the selectivity changes with reagent concentration. In the presence of two analytes (A_1 and A_2) the lophine CL reaction could be considered to proceed as in Equations 3 and 4;

$$\text{lophine} + A_1 \xrightarrow{k_1} P^* \rightarrow P + h\nu \quad (3)$$

$$\text{lophine} + A_2 \xrightarrow{k_2} P^* \rightarrow P + h\nu \quad (4)$$

where k_1 and k_2 are pseudo-constants containing the reagent concentrations and efficiencies of CL excitation and fluorescent emission. However, from the studies on selectivity control and on mixtures it seems important to also consider steps such as Equations 5 and 6 that proceed directly to ground state product without light emission.

$$\text{lophine} + A_1 \xrightarrow{k_1'} P \quad (5)$$

$$\text{lophine} + A_2 \xrightarrow{k_2'} P \quad (6)$$

k_1' and k_2' are again pseudo-constants. Operating under reagent conditions optimized for A_1 will give a low signal for A_2, which means that k_2 is small. However the overall rate of reaction between lophine and A_2 need not be small if k_2' is not decreased. In fact, for this particular reaction, a possible explanation for our experimental results is that with reagent conditions optimized for a particular analyte, the maximum fraction of the reaction is proceeding through the "light" path (via k); at reagent conditions that are far from optimum, a large portion of the reaction proceeds through the "dark" path (via k').

In general, the intensity changes that we observe could be due to a change in the reaction rate, a change in the CL excitation efficiency, a change in the fluorescence efficiency of the emitter, or some combination of these factors. Further study is needed to explain the role of metal ions in this reaction.

ACKNOWLEDGMENT

We thank Mitchell Newman and Susan Rivken for experimental work in the early stages of this project.

LITERATURE CITED

(1) Hartkopf, A.; Delumyea, R. *Anal. Lett.* **1974**, *7*, 79.
(2) Seitz, W. R.; Hercules, D. M. In "Chemiluminescence and Bioluminescence", Cormier, M. J., Hercules, D. M., Lee, J., Eds.; Plenum Press: New York, 1973; pp 427–49.
(3) Babko, A. K.; Dubovenko, L. I.; Terletskaya, A. V. *Ukr. Khim. Zh.* **1966**, *32*, 1326.
(4) Montano, L. A.; Ingle, J. D. *Anal. Chem.* **1979**, *51*, 919.
(5) Stieg, S. W. Ph.D Thesis, University of Illinois, Urbana, Ill., 1979.
(6) Stieg, S.; Nieman, T. A. *Anal. Chem.* **1977**, *49*, 1322.
(7) Newman, M. A. Unpublished work, University of Illinois, Urbana, Ill., 1976.
(8) Chan, K. W. B.S. Thesis, University of Illinois, Urbana, Ill., 1977.
(9) Rivkin, S. B. B.S. Thesis, University of Illinois, Urbana, Ill., 1978.
(10) Radziszewski, Br. *Ber.* **1877**, *10*, 70.
(11) Cottman, E. W.; Moffett, R. B.; Moffett, S. M. *Proc. Ind. Acad. Sci.* **1937**, *47*, 124.
(12) White, E. H.; Harding, M. J. C. *Photochem. Photobiol.* **1965**, *4*, 1129.
(13) McCapra, F.; Richardson, D. G.; Chang, Y. C. *Photochem. Photobiol.* **1965**, *4*, 1111.
(14) McCapra, F. In "Progress in Organic Chemistry", Carruthers, W., Sutherland, J. K., Eds.; Wiley: New York, 1973; Vol. 8, pp 231–77.
(15) Stieg, S. W.; Nieman, T. A. *Anal. Chem.* **1978**, *50*, 401.
(16) Bard, A. J., Ed. "Encyclopedia of Electrochemistry of the Elements", Marcel Dekker: New York, 1973.
(17) Koo, J. Y.; Schuster, G. B. *J. Am. Chem. Soc.* **1978**, *100*, 4496.

(18) Burdo, T. G.; Seitz, W. R. *Anal. Chem.* **1975**, *47*, 1639.
(19) Meites, L.; Zuman, P. "Electrochemical Data", Part I, Vol. A.; John Wiley: New York, 1974; p 454.
(20) Higuchi, T. *U.S. Dep. Commer., Off. Tech. Serv.*, 1962, AD 412,343; *Chem. Abstr.* **1964**, *60*, 9115g.
(21) Edsall, J. T.; Felsenfeld, G.; Goodman, D. S.; Gurd, F. R. N. *J. Am. Chem. Soc.* **1954**, *76*, 3054.
(22) Martin, R. B.; Edsall, J. T. *J. Am. Chem. Soc.* **1958**, *80*, 5033.
(23) Delumyea, R. Ph.D. Thesis, Wayne State University, Detroit, Mich., 1974.
(24) Nau, V.; Nieman, T. A. *Anal. Chem.* **1979**, *51*, 424.
(25) Stieg, S.; Nieman, T. A. *Anal. Chem.* submitted for publication.
(26) Veazey, R.; Nieman, T. A. *Anal. Chem.* **1979**, *51*, in press.

RECEIVED for review May 18, 1979. Accepted August 13, 1979. Acknowledgment is made to the donors of the Petroleum Research Fund, administered by the American Chemical Society, to Research Corporation, and to the National Science Foundation (Grant CHE-78-01614) for support of this research.

Enzyme Amplification Laser Fluorimetry

T. Imasaka[1] and R. N. Zare*

Department of Chemistry, Stanford University, Stanford, California 94305

Laser fluorimetry has been applied to the detection of enzyme reaction products at ultra-low concentrations using the 325-nm line of a He–Cd laser as an excitation source and liquid filters to isolate the fluorescence. In one direct enzyme reaction, glucose-6-phosphate is converted to 6-phosphogluconolactone as NADP is reduced to NADPH. Measurement of the fluorescence from NADPH permits quantitation of glucose-6-phosphate with a detection limit of 2 nM. In another direct enzyme reaction, α-ketoglutaric acid is converted to L-glutamic acid as NADPH is oxidized to NADP. Fluorescence from the alkaline-treated NADP is used to quantitate the α-ketoglutaric acid with a detection limit of 4×10^{-12} mol. By combining these two enzyme reactions, an enzyme cycle results in which both enzyme reaction products increase in concentration. After a fixed period of time, the enzyme cycle is stopped and the initial concentration of NADP is determined by measuring the final concentration of 6-phosphogluconolactone, using yet another direct enzyme reaction. This enzyme amplification method allows determination of 1×10^{-14} mol of NADP, which is about 30 times more sensitive than previously reported results.

Most enzyme reactions are monitored by measuring the coenzyme concentration of reduced nicotinamide adenine dinucleotide, NADH, or reduced nicotinamide adenine dinucleotide phosphate, NADPH (*1–3*). The low oxidation–reduction potential of these compounds (0.32 V) allows the enzyme reaction to proceed under moderate conditions. The most interesting property of NADPH or NADH might be its amplification capacity through enzyme cycles, as shown in Figure 1. In the presence of enzymes 1 and 2, NADP is reduced to NADPH and then oxidized to NADP repeatedly (cycle) as substrates 1 and 2 are transformed to products 1 and 2 (Figure 1a). After some fixed period of time, the enzyme cycle is stopped by destroying the enzymes. Then the concentration of product 1 or product 2 is measured by another enzyme reaction (Figure 1b) which converts NADP to NADPH. In our experiment, product 1 or 2 is quantitated by measuring the fluorescence from NADPH. Each enzyme cycle transforms one substrate molecule into a product molecule. By letting many cycles occur, the original NADP concentration is amplified.

Absorption measurements at 340 nm ($\epsilon = 6270$) provide the most common means for determining the concentration of NADPH or NADH (*2, 3*). However, fluorescence measurements may be used to advantage especially for low concentration samples where more than a hundred-fold improvement in detection sensitivity is realized (*4, 5*). Since NADPH or NADH does not fluoresce strongly, use of a conventional fluorescence spectrophotometer suffers from low sensitivity at reasonable spectral resolution. At the lowest concentrations it is recommended that the fluorescence spectrophotometer should be replaced by a tungsten lamp and filters. In this case, the detection limit is determined by the background signal, which is composed of the scattered light from the excitation source, slight fluorescence from the filters and impurities in the sample, and the Raman signal from water (*2, 3*).

The technique of laser fluorimetry can provide high sensitivity in the analysis of trace species (*6–9*). The detection of 0.02 parts-per-trillion of fluorescein dye is readily demonstrated using dye laser excitation and pulse-gated photon counting (*10*). Laser fluorimetry is so sensitive that the detectable concentration is limited by the background signals from the Raman spectrum of water and contaminant fluorescence in the solvent, even under good spectral resolution. For the detection of still lower concentrations, some "amplification procedure" becomes attractive, in which the concentration of the trace species is amplified without changing the background level (*11*). An example is the detection of 1×10^{-18} mol of ornithine δ-aminotransferase by enzyme amplification (*12*).

Our strategy for the measurement of NADP (NADPH) is the use of a He–Cd laser (325-nm line) to induce fluorescence, nonfluorescent inorganic liquid filters to reduce the background signal, and enzyme amplification to increase the signal intensity from the sample under study. We show here that laser fluorimetry is able to detect NADP (NADPH) at lower concentrations than previously reported, and that this technique may be applied to the sensitive detection of glucose-6-phosphate and α-ketoglutaric acid. Through the use of an enzyme cycle, the concentration of NADP (NADPH) is measured at levels of 1×10^{-10} M.

EXPERIMENTAL

Fluorescence Detection System. Figure 2 presents a schematic drawing of the experimental apparatus. The 325-nm output of a helium–cadmium laser (Liconix model 405 UV) passes

[1] Present address: Department of Applied Chemistry, Faculty of Engineering, Kyushu University, Hakozaki, Fukuoka, 812 Japan.

0003-2700/79/0351-2082$01.00/0

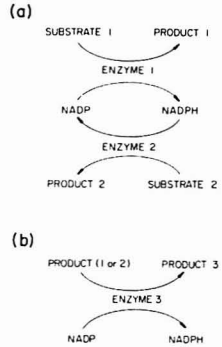

Figure 1. Enzyme amplification. In (a) enzymes 1 and 2 convert substrates 1 and 2 into products 1 and 2 while the coenzyme NADP is repeatedly reduced and reoxidized. After a set incubation time, enzymes 1 and 2 are destroyed stopping the reaction cycle. Then enzyme 3 is added which converts product 1 or 2 into product 3 while NADP is reduced to NADPH. After completion of reaction (b) the fluorescence from NADPH is measured

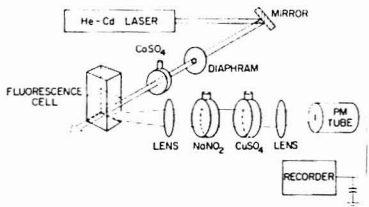

Figure 2. Laser fluorimeter

through a diaphragm and a $CoSO_4$ (300 g/L, 1.0-cm path length) liquid filter before entering a quartz cell (1 cm^2 in cross section) that contains the sample under study. The diaphragm and liquid filter combination reduces to a negligible level the visible background light from the laser discharge tube, particularly the 442-nm Cd emission line. Fluorescence from the sample is collected by an optical system that focuses an image of the fluorescent line onto the face of a photomuliplier (Centronic model Q4249 BA). The optical train consists of an $f/1$ lens, a $NaNO_2$ filter (133 g/L, 1.0-cm path length), a $CuSO_4$ filter (saturated solution, 1.8-cm path length), and an $f/3$ lens. The $NaNO_2$ filter removes the scattered light from the He–Cd laser and the Raman bands of water; the $CuSO_4$ filter reduces contaminant fluorescence at wavelengths longer than 530 nm. The filter combination is quite effective in isolating the NADPH fluorescence since the latter has a 7800 cm^{-1} Stokes shift. The output power (4 mW) of the He–Cd laser is well regulated (~0.5% rms noise). The experiment is limited by the background signal from the sample when no NADPH is present. The dark current from the photomultiplier is less than 1% of this signal. The dc output of the photomultiplier is displayed on a stripchart recorder using a 1-s time constant.

Figure 3a illustrates the transmission curves of the excitation filter (Corning 5840) and the fluorescence filter (Corning 4303 and 3387) typically used in conventional detection systems for NADPH. Also shown in this figure is the spectral profile of the Raman bands of water excited by light passing through the broadband excitation filter. There are three major problems with this excitation–detection system: (1) the Raman signal is only poorly suppressed; (2) the maximum transmission of the emission filter does not coincide with the fluorescence maximum of NADPH (460 nm); and (3) the Corning 3387 filter is fluorescent when irradiated by light passing through the excitation filter. Figure 3b illustrates the location of the laser line, the transmission curve

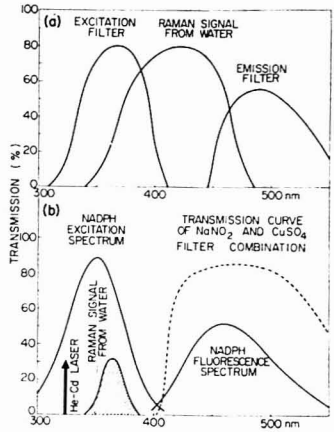

Figure 3. Transmission curves: (a) for a conventional fluorimeter; and (b) for the laser fluorimeter. The excitation and fluorescence spectra of NADPH are shown in (b). The Raman signal for each setup is also presented

of the detection filters used in this study, and the excitation and fluorescence spectra of NADPH. Note that the nonfluorescent liquid filter combination completely blocks the scattered light of the laser and the Raman signal from water. Moreover, this filter system has high transmission at the fluorescence maximum of NADPH.

Reagents. The enzymes (glucose-6-phosphate dehydrogenase, glutamate dehydrogenase, and 6-phosphogluconate dehydrogenase), coenzymes (NADP and NADPH), and substrates (glucose-6-phosphate and α-ketoglutaric acid) are obtained from Boehringer and are used without further purification. The imidazole is nonfluorescent grade (Sigma). Doubly-distilled water and 6 M sodium hydroxide are used after exposure to sunlight (1 day). This photobleaching procedure reduces the background fluorescence significantly (by a factor of about five).

Procedure. The experimental procedures described in ref. 2 and 3 are followed closely. Because the coenzyme and the buffer solution have fluorescent contaminants, care is taken to use as little of either as is needed. The sample volume is adjusted to 1 mL for comparison with conventional fluorescence measurements. Because of photobleaching effects caused by the 325-nm output of the He–Cd laser, the fluorescence intensity from the sample is recorded only for several seconds. The sample recovers in the dark after about 30 s. Typically the fluorescence intensity is measured twice.

The detection limit is calculated from the results of several (usually four) measurements of samples having identical concentrations. The signal-to-noise ratio, S/N, is calculated from the expression:

$$S/N = \frac{n_S - n_N}{\sqrt{\sigma_S^2 + \sigma_N^2}}$$

where n_S and n_N are signal and background intensities, σ_S and σ_N are their standard deviations. The detection limit is defined as $S/N = 2$ in this study.

RESULTS

Background Signal. The performance of the present instrument was determined by measuring the fluorescence from NADPH solutions at different concentrations (Figure 4). The high sensitivity of the instrument and the excellent rejection of the Raman bands from water and unwanted fluorescence and scattered light in this laser fluorescence system allow the detection of NADPH at concentrations in

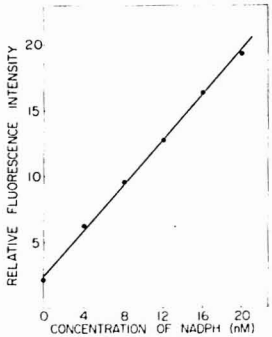

Figure 4. Analytical curve for the quantitation of NADPH

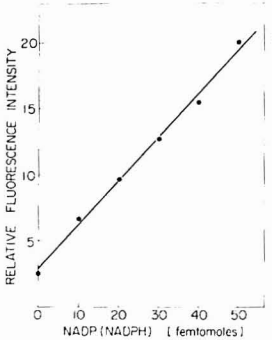

Figure 5. Analytical curve for the quantitation of NADP (NADPH) by enzyme amplification laser fluorimetry. The cycling volume is 100 μL. The detection limit is 10 fmol (0.1 nM)

the nanomolar range. Most of the background signal comes from distilled water. The background signal, corresponding to 2 nM of NADPH, slightly varies from day to day and depends on the water container and the extent of photobleaching. This fact shows that the contribution from Raman bands of the water is much less important than that from impurities in the distilled waters. The low background signal of the laser fluorimeter implies that laser fluorescence analysis may be quite promising for the measurement of enzyme reactions at low concentrations.

Glucose-6-phosphate. The concentration of glucose-6-phosphate is determined using the enzyme reaction

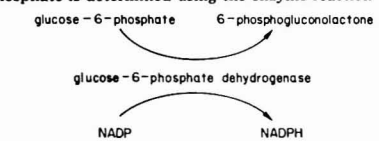

(1)

the fluorescence intensity from NADPH is used to quantitate the glucose-6-phosphate. The analytical curve is linear over the range 0–80 nM. The detection limit is 2 nM, corresponding to 2×10^{-12} mol of glucose-6-phosphate in the 1-mL sample volume. The detection limit is set by fluctuations in the background signal from distilled water and NADP. Reactions are quite reproducible; the scatter in the data is about 5%.

Alkaline Development of NADP. The NADP is itself nonfluorescent, but it may be converted to a strongly fluorescent molecule by adding concentrated alkaline solution (*2, 3, 5*). The spectral properties of alkaline-treated NADP are similar to NADPH, and the same detection system is used in conventional fluorimetry. The analytical curve using our detection system is linear over the range 0–25 nM with a detection limit of 4 nM, corresponding to 4×10^{-12} mol. The long incubation time (10 min) at elevated temperature (60 °C) with concentrated alkaline solution (6 M NaOH) damaged the quartz cell through repeated use. Consequently, disposable Pyrex test tubes were used instead for incubation. However, the background fluorescence from contaminants then could not be subtracted for the individual samples. The background signal corresponds to 1×10^{-11} mol of NADP. Although alkaline-treated NADP can be detected with high sensitivity by this method, the detection limit is not so low as expected. The reason appears to be that maximum in the excitation spectrum shifts from 350 nm for NADPH to 375 nm for alkaline-treated NADP. Consequently, the 325-nm line of the He–Cd laser is more than ten times less effective in exciting fluorescence.

α-Ketoglutaric Acid. The application of the alkaline development of NADP is demonstrated by the quantitation of α-ketoglutaric acid using the enzyme reaction

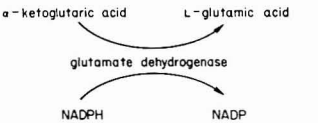

(2)

After the enzyme reaction proceeds at room temperature for 20 min, 0.3 M HCl is added to decompose the fluorescent NADPH that remains. Following alkaline development, a linear analytical curve is obtained over the range $0–20 \times 10^{-12}$ mol with a detection limit of 4×10^{-12} mol. One third of the background signal originates from the distilled water, while the rest comes from the alkaline development.

Detection of NADP by Enzyme Amplification. By combining reactions 1 and 2, an enzyme cycle is obtained (see Figure 1a, where substrate 1 = glucose-6-phosphate, enzyme 1 = glucose-6-phosphate dehydrogenase, product 1 = 6-phosphogluconolactone, substrate 2 = α-ketoglutaric acid, enzyme 2 = glutamate dehydrogenase, and product 2 = L-glutamic acid). The sample is incubated for 2 h at 38 °C. During this period several thousand cycles are expected to occur if the enzymes have full activity (*2, 3*). The sample is then heated to 85–90 °C for 3 min to destroy the enzymes. Next 6-phosphogluconate dehydrogenase is added which reduces NADP to NADPH at the same time that 6-phosphogluconolactone is converted to ribulose-5-phosphate (see Figure 1b).

In this enzyme amplification procedure, the concentration of NADP and NADPH is determined unspecifically, and thus both are measured to the same sensitivity. If it is desired to measure only one of them, then the other must be decomposed before measurement by the addition of acid or alkaline solution (*2, 3*). Figure 5 shows the analytical curve for the detection of NADP (NADPH) by enzyme amplification laser fluorimetry. The detection limit of 1×10^{-14} mol is set by the fluctuations in the enzyme reaction rates occurring in the individual incubation tubes. This fluctuation is found to be very sensitive to the cleanliness of the glassware.

DISCUSSION

The use of enzyme reactions combined with laser fluorimetry offers many advantages for trace analysis of biomedical species. Table I summarizes the detection limits obtained in this study and compares them to previous literature values.

Table I. Comparison of Detection Limits

substance	present work	literature value	ref.
glucose-6-phosphate	2 nM	200 nM	2, 3
α-ketoglutaric acid	4 pmol	20 pmol	2, 3
NADP	0.1 nM	1 nM	2
	10 fmol	300 fmol	3

The background signal of our laser fluorimeter corresponds to a 2 nM concentration of NADPH. This value is 50 times lower than that obtained using a conventional fluorescence detection system (*2, 3*). Thus the laser excitation source and nonfluorescent filter system provides a very effective means of reducing the background signal. The present excitation–detection system allows the quantitation of glucose-6-phosphate by a direct enzyme reaction to concentrations of 2 nM. This detection limit is 100 times better than that measured by the usual fluorescence detection system. It is noteworthy that the sensitivity of the direct measurement of NADPH in this study almost equals that of the enzyme amplification technique in a conventional system (1 nM). The present method using direct enzyme reaction is quite simple and requires only 10 min incubation time while the use of enzyme amplification is not so straightforward and requires long incubation times. However, when enzyme amplification is combined with laser fluorimetry, it is possible to measure as little as 10 femtomoles of NADP. This amount is 30 times smaller than previously reported results.

Only a small improvement is obtained by using the alkaline treatment of NADP for the quantitation of the latter. The detection limit in the present study is equal to or slightly better than the literature values. The use of the 364-nm line of the argon ion laser, for example, might enhance the fluorescence intensity of the alkaline-treated NADP by more than an order of magnitude compared to that of the 325-nm line of the helium–cadmium laser, since the 364-nm line nearly coincides with the absorption maximum of the alkaline-treated NADP.

The present detection system is versatile because it may be applied not only to the quantitation of NADPH but also to NADH, since the spectral properties of NADH are almost identical to those of NADPH. The detection of NADPH and NADH is quite general for monitoring enzyme reactions. Even if the enzyme reaction is not a redox reaction, the reaction products may undergo a subsequent redox reaction so that NADPH or NADH can be used (*13*). The quantitation of NADPH (NADH) may also be used in the analysis for inorganic substances, such as for phosphate (*2, 3*) or nitrate (*14*) by using appropriate enzyme reaction systems.

In this study the sample volume is adjusted to 1 mL so that the results can be readily compared to other studies. However, because laser light can be focused easily to a small spot size without loss of intensity, microanalysis may be possible. This would permit the measurement of microliter samples, for example, without the need for dilution. Care should be taken to avoid or minimize photodecomposition of the sample. With the use of a quartz cell, this problem can become severe. However, it may be possible to use flow injection and immobilized enzymes, in which the sample is continuously passed over the enzymes which are bound to some solid support structure (*15*). For the detection part, the use of a flowing droplet might provide high sensitivity since cell wall fluorescence is avoided (*16*).

When fluorescence from contaminants in the sample becomes too strong, some separation procedure may be necessary, such as centrifugation or chromatography. High-pressure liquid chromatography (HPLC) is increasingly being used in biomedical applications. For example, a reverse phase μBondapak C_{18} column separates NADH from contaminants on the basis of polarity (*17, 18*). The application of laser fluorimetry as a detection system for HPLC (*19*) may offer advantage in this case. However, while alkaline development is useful for conventional fluorescence analysis, in HPLC this procedure may not be practical because the proper pH level is difficult to maintain. For example, the fluorescence from alkaline treated NADP decreases to 50% of its value at pH 9.6 and falls to zero at pH 6 (*5, 20*).

An alternative for overcoming the fluorescence interference from contaminants is to use enzyme amplification since the latter technique has the potential for dramatically increasing the signal-to-noise because typically several thousand enzyme cycles occur per hour. Recently many researchers have reported the use of enzyme-linked immunoassay as a replacement for radioimmunoassay in biomedical studies (*21, 22*). In enzyme-linked immunoassay, each enzyme produces typically several thousand NADPH (NADH) coenzyme molecules. The concentration of NADPH (NADH) can then be amplified by use of an enzyme cycle, as described in this study. Thus by using enzyme-linked immunoassay together with enzyme amplification laser fluorimetry, it may be possible to detect and quantitate hormones at very low concentrations.

LITERATURE CITED

(1) Fishman, M. M. *Anal. Chem.* **1978**, *50*, 261R–73R.
(2) Lowry, O. H.; Passonneau, J. V., "Flexible System of Enzymatic Analysis"; Academic Press: New York, 1972.
(3) Anan, K.; Konno, K.; Tamura, Z.; Matsuhashi, M.; Matsumoto, J. "Kiso-Seikagaku-Jikkenho"; Maruzen, 1976.
(4) Greengard, P. *Nature (London)* **1959**, *178*, 632–4.
(5) Lowry, O. H.; Roberts, N. R.; Kapphahn, J. I. *J. Biol. Chem.* **1957**, *224*, 1047–64.
(6) Smith, B. W.; Plankey, F. W.; Omenetto, N.; Hart, L. P.; Winefordner, J. D. *Spectrochim. Acta, Part A* **1974**, *30*, 1459–63.
(7) Bradley, A. B.; Zare, R. N. *J. Am. Chem. Soc.* **1976**, *98*, 620–21.
(8) Richardson, J. H.; Wallin, B. W.; Johnson, D. C.; Hrubesh, L. W. *Anal. Chim. Acta* **1976**, *86*, 263–7.
(9) Imasaka, T.; Kadone, H.; Ogawa, T.; Ishibashi, N. *Anal. Chem.* **1977**, *49*, 667–8.
(10) Ishibashi, N.; Ogawa, T.; Imasaka, T.; Kunitake, M., *Anal. Chem.*, in press.
(11) Blaedel, W. J.; Bagusloski, R. C. *Anal. Chem.* **1978**, *50*, 1026–32.
(12) Kato, K.; Hamaguchi, Y.; Okawa, S.; Ishikawa, E.; Kobayashi, K.; Katunuma, N. *Lancet* **1977**, (1), 40.
(13) Lloyd, B.; Burrin, J.; Smythe, P.; Alberti, K. G. M. M., *Clin. Chem.* **1978**, *34*, 1724–9.
(14) Kiang, C. H.; Kuan, S. S.; Guilbault, G. G. *Anal. Chem.* **1978**, *50*, 1323–5.
(15) Betteridge, D. *Anal. Chem.* **1978**, *50*, 832A–46A.
(16) Diebold, G. J.; Zare, R. N. *Science* **1977**, *196*, 1439–41.
(17) Loshorn, C. A.; McComb, R. B.; Bond, L. W.; Bowers, G. N., Jr.; Coleman, W. H.; Gwynn, R. H., *Clin. Chem.* **1977**, *23*, 1576–80.
(18) Margolis, S. A.; Howell, B. F.; Schaffer, R., *Clin. Chem.* **1977**, *23*, 1581–84.
(19) Lidofsky, S. D.; Imasaka, T.; Zare, R. N. *Anal. Chem.* in press.
(20) Kaplan, N. O.; Colowick, S. P.; Barnes, C. C. *J. Biol. Chem.* **1951**, *191*, 461–72.
(21) Ishikawa, E. *J. Biochem.* **1973**, *73*, 1319–21.
(22) Yoshioka, M.; Taniguchi, H.; Kawaguchi, A.; Kobayashi, T.; Murakami, K.; Seki, M.; Tsutou, A.; Tamagawa, M.; Minoda, H.; Baba, S. *Clin. Chem.* **1979**, *25*, 35–8.

RECEIVED for review May 29, 1979. Accepted July 30, 1979. The support of the National Cancer Institute under grant NIH 2R01 CA23156-03 is gratefully acknowledged.

Microdetermination of Manganese in Animal Tissues by Flameless Atomic Absorption Spectrometry

David I. Paynter[1]

Department of Animal Science and Production, University of Western Australia, Nedlands, Western Australia 6009

A method is described for the microdetermination of manganese in animal soft tissues. Plasma and homogenates of tissues were acidified with HCl, followed by heating at 60 °C and centrifugation. This treatment effectively liberates the manganese into the supernatant fraction where its concentration was determined using flameless atomic absorption spectrometric methods. Optimal instrument operating parameters are discussed for both the Varian model 63 and model 90 carbon rod atomizers. Matrix interferences were not detected, and the use of background correction and manganese standard additions was found to be unnecessary. Using a number of liver samples, good agreement was obtained between the proposed flameless method and results obtained using complete wet digestion followed by conventional flame atomic absorption analysis. Relative standard deviation for a sample of plasma extract, containing 2.07 ng Mn/mL, was 3.5%.

Manganese is an essential trace element in animals. In tissues, it is involved in a number of enzyme reactions as an activator, and in a limited number of enzymes as an integral bound metal ion (*1*, *2*). The low concentrations of manganese present in plasma and most soft tissues have in the past presented problems in analysis. Neutron activation methods, while offering the required sensitivity (*3*), are not generally applicable to routine use. Other methods previously used including colorimetric (*4*) and conventional flame atomic absorption spectrometry (*5*), although relatively free from interference, lack the sensitivity required for many tissues, and entail relatively time-consuming sample preparation. The development of flameless (furnace) atomic absorption spectrometry has considerably lowered detection limits for manganese, and methods have now been reported for the determination of this element in biological material such as serum (*6*, *7*) cerebrospinal fluid (*6*), and tissue fractions (*8*, *9*).

Matrix interferences have been found to occur in the flameless determination of manganese (*10*). In methods involving biological samples, these interferences have been at least partially compensated for by using standard additions of manganese and/or background correction (*6–9*).

The small final sample size actually used in the determination in flameless methods, and the relative heterogeneity of some tissues, necessitates some form of tissue digestion or homogenization. In the present study, a method involving tissue homogenization, followed by acid treatment, permitted the determination of manganese in a variety of animal tissues by flameless atomic absorption spectrometry. Matrix interferences were not encountered in the present method and neither standard additions or background correction were necessary.

[1]Present address: Attwood Veterinary Research Laboratories, Mickleham Road, Westmeadows, Victoria, Australia 3047.

EXPERIMENTAL

Apparatus. An AA-375 double beam atomic absorption spectrophotometer with simultaneous deuterium arc background correction facilities, equipped with either a CRA-63 or CRA-90 carbon rod atomizer, an ASD-53 autosampler, chart recorder, and digital printout recorder (all Varian Techtron products) was used for these studies. The manganese hollow-cathode lamp was operated at 5 mA, with the AA-375 set at 279.8 nm, using CRA slit and peak height modes. For 10-μL sample sizes, internally threaded graphite rods were used; for smaller sample sizes (2 and 5 μL), the normal nonthreaded rods were used. All rods were pyrolytically coated, and during use were purged with nitrogen at a flow rate of 6 L/min. The work head was equipped with a single beam mask with a 3-mm aperture.

Sample Preparation. Plasma was obtained from rat heparinized whole blood. Tissues from the same animals were washed in cold 0.9% (w/v) NaCl after removal, then stored at 4 °C or −20 °C prior to analysis. Tissues were homogenized with an aqueous 0.2% (v/v) Triton X-100 solution, using all-glass tissue homogenizers (Kontes). Homogenates of 10% (w/v) were prepared, using 0.5 or 1.0 g (wet weight) samples of tissue. To aliquots of these homogenates (in 3-mL snap cap tubes) HCl appropriately diluted with water was added, to give the required final concentration of manganese, in 2 M HCl. The acid treated samples were then heated at 60 °C for 1 h in a water bath, cooled, and then centrifuged. The clear supernatants, without further treatment, were used for injection into the carbon rod atomizer. With plasma, HCl was added directly to the sample, followed by heating and centrifugation as described for tissue homogenates. All samples were diluted with HCl such that total manganese in the 2-μL sample (or 10 μL in the case of plasma) applied to the carbon rod atomizer was in the range of 5–60 pg.

For flame atomic absorption spectrophotometric analysis of livers, 1.0-g samples were wet ashed with 10 mL of a 9:1 mixture (by volume) of nitric and perchloric acids until the digestion had been at white fumes for 30 min. Digest volumes were then adjusted to 10 mL with water and analyzed for manganese using an oxidizing air–acetylene flame.

Chemicals. A manganese standard solution, containing 1000 μg Mn/mL (as the chloride) was obtained from BDH. Dilutions in water or HCl from a 10-μg Mn/mL stock to working concentrations were prepared on the day of use. Nitric acid was distilled before use; all other chemicals were of analytical reagent grade.

RESULTS AND DISCUSSION

Preliminary Experiments. Attempts to determine manganese in untreated tissue homogenates by the flameless atomization method were unsuccessful. A considerable proportion of manganese in these samples was associated with the particulate fraction, and settling of the fraction occurred with standing of samples in the autosampler. This and the small sample size applied to the rod (2 μL) contributed to the poor reproducibility encountered. Difficulties were also found with untreated plasma samples. While a previous report has indicated the successful determination of manganese in untreated serum samples using a flameless atomization method (*6*), we encountered difficulties with spluttering and foaming of plasma samples during the drying stage, even with a 2-μL sample size. Addition of Triton X-100 (0.1 to 1.0% (v/v) final concentration) alleviated this problem, but created

0003-2700/79/0351-2086$01.00/0

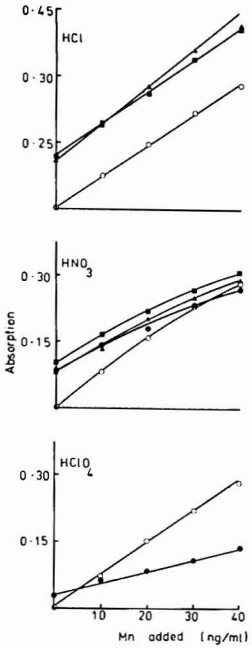

Figure 1. Effect of acid treatments on recoveries of manganese from heart homogenates. Standards in H_2O only, ○; standards in homogenate with final acid concentrations of 10% (v/v), ●; 25% (v/v), ▲; 50% (v/v) ■

others. Creepage on the rod occurred, with the degree of creepage being related to the previous history of the rod being used. Standard additions were required to obtain accurate results. To overcome these matrix effects and to ensure homogenous samples, further sample treatment was desirable.

Proposed Method. Several acids, including trichloroacetic, hydrochloric, nitric, perchloric, and sulfuric, and one alkali (KOH) were added at several concentrations to samples of tissue homogenates, along with standard additions. After heating at 60 °C for 1 h, the samples were centrifuged, then assayed for manganese. The curves for homogenate with standard additions were then compared to curves of standards in water only. The results for three of these acids (HCl, HNO_3, and $HClO_4$) are shown in Figure 1. Only HCl treatment gave samples free of matrix interferences, as indicated by the similar slopes for standard additions of manganese to water only and to tissue homogenates treated with HCl. Similar results were obtained for both liver and heart homogenates. Other treatments led to either excessive manganese contamination (e.g., trichloroacetic acid, KOH) and/or matrix interferences, as occurred with nitric and perchloric acids.

In a previous study, significant matrix interferences by the nitrates and chlorides of both calcium and magnesium have been reported in the determination of manganese by flameless methods (*10*). In the present study, interferences due to chlorides of these elements, have not been observed with either tissue homogenates or plasma samples when the acid used is HCl. Significant suppression of the manganese signal was found to occur when HCl was replaced by HNO_3 for sample acid treatment. The differences in matrix effects observed between these studies relate to a number of factors, including

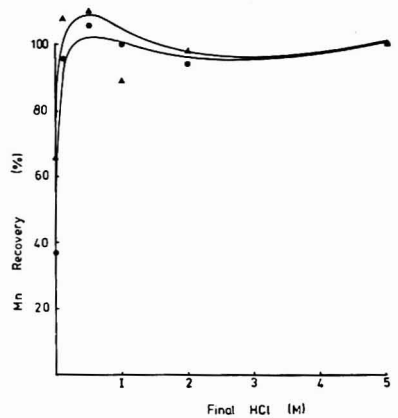

Figure 2. Effect of HCl concentration on recoveries of manganese from heart homogenate. Recovery from homogenates without manganese standard additions, ●; and with standard additions, ▲. Values for the 5 M HCl treatment value were used as the 100% recovery value

the types of carbon rod used, the sample sizes applied to these rods, and the relative concentrations of calcium and magnesium in the final sample.

As additions of HCl to homogenates and plasma did not completely digest these samples, the effect of HCl concentration on solubilizing the manganese fraction was investigated. At each of several acid concentrations (0 to 5 M HCl), recoveries of manganese in heart homogenate supernatants was determined after manganese standard additions to these samples of 0 and 13.5 ng Mn/mL, followed by heating (60 °C for 1 h) and centrifugation. The results are shown in Figure 2. Without acid treatment, only 37% of the manganese inherent in the sample, and 63% of the added manganese, was recovered in the supernatant fraction following centrifugation. In contrast, addition of HCl at concentrations of 0.1 M and greater gave near 100% recoveries in this fraction. The low concentration required to liberate manganese from the homogenate particulate fraction, suggests that manganese is released from this fraction by a pH rather than hydrolysis-type action.

Effect of Furnace Conditions on Results. In drying the sample on the rod, no problems were encountered with creepage or spluttering of the sample. In general the drying phase was very similar to that of aqueous standards, presumably owing to the removal of much of the matrix from these samples by treatment with HCl. For most samples a 2-μL sample size was used to minimize the drying time required, and avoid unnecessary sample dilution. For plasma, however, a 2-μL sample gave insufficient sensitivity. This was overcome by the use of internally threaded graphite tubes, on which the sensitivity was increased by using a 10-μL sample size. Drying parameters for both these sample sizes are shown in Table I.

In the ash cycle following drying, liver, heart, and kidney samples gave a single sharp ash peak which volatilized at <600 °C. Above this temperature no other background peaks were apparent and ash temperatures of up to 1500 °C for 10 s could be used before Mn volatilization became apparent (Figure 3), giving a relatively large range of satisfactory ashing temperatures for which background correction was unnecessary. For plasma derived samples, a second non-atomic ash fraction was present volatilizing at approximately 1100 °C. Failure

Table I. Operating Parameters for the Determination of Manganese, Using the Varian Carbon Rod Atomizers, and HCl Treated Samples

carbon rod atomizer furnace type	CRA-90 plain	CRA-90 threaded	CRA-63 plain	CRA-63 threaded
sample volume (μL)	2	10	2	10
dry	100 °C, 25 s	105 °C, 60 s	5.75, 25 s	5, 60 s
ash plasma		1300 °C, 10 s		6.75, 20s
ash homogenates	900 °C, 10 s		6.5, 15 s	
atomize	ramp rate 700 °C/s, final temp. 2500 °C, hold at final temp. 0.5 s		7, 2 s (step mode)	

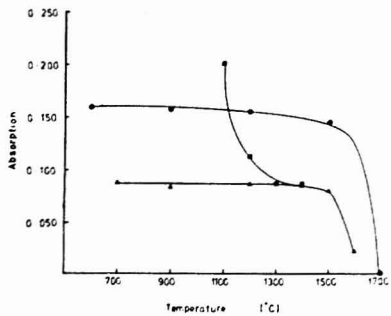

Figure 3. Effect of ashing temperatures on the manganese signal obtained in the atomize phase from HCl treated plasma and heart homogenate samples. Heart homogenate without background correction, ●; Plasma with background correction, ▲; and without background correction, ■

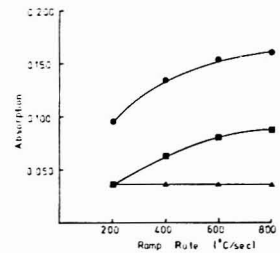

Figure 4. Effect of temperature ramp rate in atomize phase, on peak height and peak area of HCl treated samples. Peak height mode with plasma (10-μL sample size), ■; Peak height mode, ●; and peak area mode, ▲; for heart (2-μL sample size)

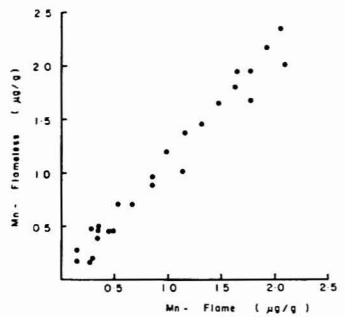

Figure 5. Comparison of liver manganese concentrations determined by the proposed flameless method and by the conventional flame method

to remove this peak resulted in considerable signal interference unless background correction was used (Figure 3).

The ash parameters listed in Table I are for measurement of plasma samples without the use of background correction. In practice, we have observed slightly better precision when this non-atomic peak in plasma is removed prior to atomization, rather than relying on background correction for its removal.

In the atomize phase, increasing the ramp rate (°C rise in temperature/s) considerably increased the peak height values for homogenate and plasma extracts without affecting the peak area (Figure 4). Atomize settings shown in Table I enable maximum peak heights and sensitivities to be obtained. The high ramp rate used with the CRA-90, is similar to that obtained using step-mode atomization available with the CRA-63 (approximately 800 °C/s); both atomizers gave similar final results at the settings shown in Table I. Only one peak (corresponding to the element peak) occurs in the atomize phase, using the ash parameters shown in Table I. At these atomize settings, rod life usually exceeds 100 firings.

Accuracy and Precision. Accuracy of the method was investigated by comparing results obtained by the proposed flameless method and by conventional flame atomic absorption spectrometry. In the latter, wet digestion of samples was performed in duplicate (see Experimental section). In the former method, a single homogenate and acid extract was prepared for each sample, with duplicate firings on the carbon rod. A total of 27 livers, obtained from rats fed diets containing 0.2 to 30 μg Mn/g diet, were assayed. Manganese content of these livers was distributed through the range of 0.25 to 2.5 μg Mn/g wet weight. No attempt was made to re-assay any sample, and the individual results are shown in Figure 5. The Mn content of these livers, determined by the flame method (x) and the proposed flameless method (y) were related according to the equation $y = 1.03x - 0.004$ μg/g wet weight, with a coefficient of determination of 0.96, showing good agreement between the two methods.

Relative standard deviations for 10 replicate determinations of manganese in liver and plasma extracts were 0.5% and 3.5%, respectively. For the liver extract, the final concentration of manganese after acid treatment was 26 ng/mL and 2 μL samples were applied to the rod. The plasma extract contained 2.07 ng Mn/mL final concentration and 10-μL samples were applied.

ACKNOWLEDGMENT

The author is indebted to B. S. Fleming for his technical assistance and to R. J. Moir for his discussions.

LITERATURE CITED

(1) M. C. Scrutton, *Biochemistry*, **10**, 3897–3904 (1971).
(2) E. J. Underwood, "Trace Elements in Human and Animal Nutrition", 4th ed., Academic Press, New York, London, 1977, pp 170–195.
(3) P. S. Papavasiliou and G. C. Cotzias, *J. Biol. Chem.*, **236**, 2365–2369 (1961).

(4) H. Fore and R. A. Morton, *Biochem. J.*, **51**, 594–598 (1952).
(5) M. Suzuki and W. E. C. Wacker, *Anal. Biochem.*, **57**, 605–613 (1974).
(6) D. J. D'Amico and H. L. Klawans, *Anal. Chem.*, **48**, 1469–1472 (1976).
(7) F. Bek, J. Janouskova, and B. Moldan, *At. Absorp. Newsl.*, **13**, 47–48 (1974).
(8) S. B. Gross and E. S. Parkinson, *At. Absorp. Newsl.*, **13**, 107–108 (1974).
(9) J. Smeyers-Verbeke, C. May, P. Drochmans, and D. L. Massart, *Anal. Biochem.*, **83**, 746–753 (1977).
(10) J. Smeyers-Verbeke, Y. Michotte, P. Van den Winkel, and D. L. Massart, *Anal. Chem.*, **48**, 125–130 (1976).

RECEIVED for review April 13, 1979. Accepted July 25, 1979. D.I.P. was the holder of an Australian Wool Corporation Postgraduate Scholarship.

Determination of Aluminum in Blood, Urine, and Water by Inductively Coupled Plasma Emission Spectrometry

Pierre Allain* and Yves Mauras

Laboratoire de Pharmacologie, C.H.U., 49036 Angers Cedex, France

A method is described for the determination of aluminum in water, urine, and blood by inductively coupled plasma using a concentric pneumatic nebulizer. Optimum working conditions are determined. Interferences are systematically studied using different metals and metalloids and especially those commonly found in biological samples. Some metals, particularly Ca, Li, Sr, Na, Fe increase background intensity and alkali metals and alkaline earth metals increase the net signal intensity of Al. The limits of detection are: 0.4 μg/L in water, 1 μg/L in urine, and 4 μg/L in blood. Sampling preparation for blood and urine is reduced to a simple dilution with demineralized water. Aluminum assays on 14 healthy subjects gave the following results: blood 12.5 ± 4 (std dev) μg/L, urine 4.7 ± 2.5 (std dev) μg/L.

Aluminum assays in body fluids and water have taken on considerable importance over the past few years, ever since the metal was first suspected of being involved in cases of encephalopathy in patients with renal insufficiency under dialysis.

Recent reports (*1* - *11*) show aluminum is commonly determined by graphite furnace atomic absorption spectrometry. Our experience with this technique often produced manifestly erratic results so that reliable assays could be obtained only by frequently repeated measurements. These difficulties have led us to carry out aluminum assays by inductively coupled plasma emission spectrometry as described below.

EXPERIMENTAL

Apparatus. Plasma emission spectrometry was carried out using a Jobin Yvon Elemental Analyzer JY 38 P, consisting of a Plasmatherm source inductively coupled to a high frequency (27.12 MHz) magnetic field operating at 1.5 kW, a thermoregulated monochromator H-R 1000, and an electronic readout console. The monochromator in Czerny-Turner configuration includes a holographic grating with 2400 grooves/mm. The focal length is 1 m, wavelength range 190–700 nm, dispersion 0.4 nm/mm. The gas used as coolant and carrier was argon and the samples were introduced into the plasma by means of a concentric pneumatic nebulizer.

Atomic absorption spectrometry was carried out using a Perkin-Elmer HGA 2100 graphite furnace mounted on an Instrumentation Laboratory IL 151 spectrophotometer with correction for nonspecific absorption.

Reagents. The calibration for aluminum and the evaluation of spectral interference were based on standard Merck Titrisol metal solutions of 1 g/L. All solutions were prepared in plastic laboratory ware with water demineralized after reverse osmosis.

Working Conditions. The influence of wavelength, excitation level, nebulization, and height above load coil on the signal intensity and the background intensity was studied using a 1 mg/L solution of aluminum in water, in order to determine optimum working conditions for the best signal/background ratio.

Evaluation of Interference. Spectral interference was studied by nebulizing 1 g/L solutions of different metals and recording the spectra for wavelength sweeps about 394.40 and 396.15 nm.

The effect on the signal intensity and on the background intensity was studied by adding increasing concentrations of different metals to a 1 mg/L solution of aluminum and measuring the signal strength at the wavelength of aluminum, 396.15 nm, and the background level at a lower value, 396.09 nm.

The effect of anions was studied by comparing the results obtained with 1 mg/L solutions of aluminum in sodium chloride, nitrate, sulfate, phosphate, and EDTA solutions at appropriate concentrations so that each sample contained 0.5 g/L of sodium.

Procedure. Water, urine, and blood aluminum assays were carried out at 396.15 nm. Urine samples were diluted to $^1/_4$, blood samples to $^1/_{10}$ while water samples were examined pure or diluted in the case of concentrated solutions such as used in dialysis. The calibration was carried out using an additive technique: each sample was successively added to using standard solutions in appropriate concentrations so as to obtain standard additions of 31.25, 125, and 500 μg/L. After centrifugation, each tube was measured by taking five readings of 5 s each. The background intensity, measured after a wavelength displacement of 0.06 nm, was subtracted from each measurement. The standard addition lines were calculated by the method of least squares, and the concentration of the samples was determined by extrapolation.

RESULTS

Optimum Working Conditions. Among the various known lines of aluminum, only two, 394.40 and 396.15 nm, produce a signal strong enough to allow aluminum determinations at concentrations of less than 1 mg/L. For each of these lines, the best working conditions were obtained at 1 kW, at a height of 25 mm above the load coil, with nebulization at a pressure of 30 psi and argon flow at 1 L/min corresponding to a nebulization speed of about 6 mL/min. The coolant gas (argon) flow was adjusted to 13 L/min. Under these conditions, a 1 mg/L solution of aluminum gave an overall signal–background ratio of 40 at 396.15 nm and 20 at 394.40 nm.

Interference. Interference was evaluated using different metals and metalloids, especially those commonly found in biological samples. The interaction of the matrix elements on aluminum determination can be classified under three headings: spectral interference, modification of background

0003-2700/79/0351-2089$01.00/0

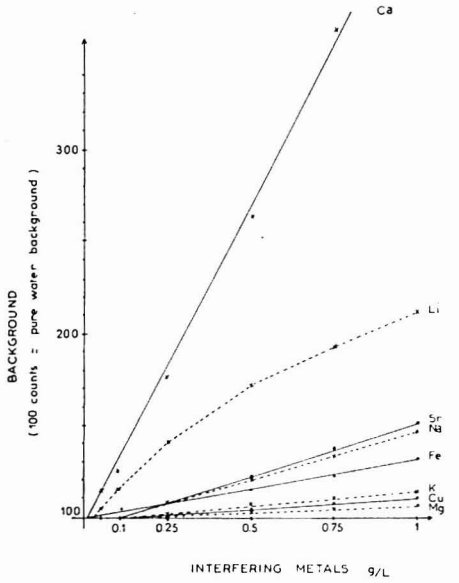

Figure 1. Action of different metals on the background measured at the peak base of aluminum line: 396.09 nm

level, and modification of signal strength.

Spectral Interference. No spectral interference was observed with Na, K, Mg, Sr, Li, and Tl. With Ca, Fe, Pb, Zn, Hg, Cu, Bi, La, and Rb, signals of identical relative intensity obtained at exactly the wavelength of aluminum 394.40 and 396.15 nm, were attributed to aluminum impurities in concentrations less than 20 μg/L.

The only element which gave several peaks around 394.40 and 396.15 nm was boron at 1 g/L and may therefore possibly introduce errors in aluminum determination. However, these peaks disappear at boron concentrations of less than 1 mg/L.

Calcium produced an emission at 396.8 nm, but this could easily be separated from the aluminum line by the high resolution of the monochromator.

Modification of Background Level. Some metals in solution can increase the background level of demineralized water. In Figure 1, signal counts are plotted against concentrations of interfering metals, with 100 counts as the base value of demineralized water for background correction at 396.09 nm under the working conditions described.

Among the metals, Ca, Li, Sr, Na, Fe, K, Cu, and Mg, calcium provoked the greatest modification of background level, a fourfold increase at a concentration of 1 g/L. Figure 2 shows that, as mentioned above, the interference is not due to the presence of a calcium line but to an increase in background around 396 nm. At biological concentrations, and taking into account the dilutions necessary for blood and urine assays, Na, K, Ca, and Fe are the only metals likely to lead to increase in background. When several of these metals are involved, the increase in background is roughly equal to the sum of the component increases.

The metals, Pb, Bi, Zn, and Rb, and the anions, chloride, sulfate, nitrate, phosphate, and EDTA, showed no action on background intensity.

Similar results were obtained for aluminum determination at 394.40 nm.

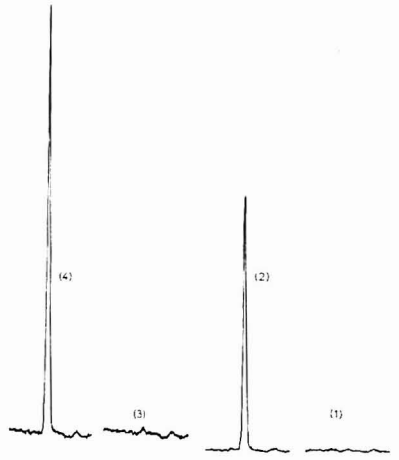

Figure 2. Spectra obtained for wavelength sweeps from 395.90 to 396.35 nm with pure water (1), pure water containing 250 μg/L Al (2), 250 mg/L Ca (3), 250 μg/L Al + 250 mg/L Ca (4)

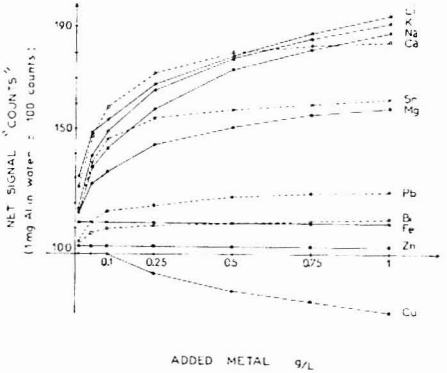

Figure 3. Action of different metals on 1 mg/L Al signal intensity

Modification of Signal Strength. Figure 3 shows signal counts, with background intensity subtracted, plotted against concentrations of added metals, with 100 counts as the base level for a 1 mg/L aluminum solution in demineralized water. It can be seen that the aluminum line intensity at 396.15 nm is modified by the presence of other metals in solution.

Alkali metals and alkaline earth metals increase the signal strength by 20–30% at a concentration of 0.01 g/L and by almost 100% at 1 g/L. Copper is the only element tested which reduced the signal intensity. When several metal ions are present, the increase in signal strength is roughly equal to that of the element producing the highest increase on its own.

The anions, chloride, sulfate, nitrate, phosphate, and EDTA, showed no action on signal strength.

Similar results were obtained for aluminum determination at 394.40 nm.

Blood, Urine, and Water Aluminum Determinations. The calibration graphs for aluminum in blood, urine, and water are remarkably linear. Over a wide range of concen-

Table I. Reproducibility of 20 Day-to-Day Replicate Determinations

	mean $\bar{x}$ μg/L	standard deviation	coefficient of variation
water	12.6	1.1	8.7
	374	16.3	4.4
urine	21	1.5	7.1
	394	12.4	3.1
blood	40	2.7	6.8
	483	23.5	4.9

trations (0–2000 μg/L) linear regression coefficients are 0.9999 in blood, 0.9999 in urine, and 0.9998 in water. The detection limit was calculated as the concentration corresponding to twice the standard deviation of background noise (*12*, *13*). With the dilutions used, we find 0.4 μg/L for water, 1 μg/L for urine, and 4 μg/L for blood.

Table I indicates the reproducibility of the method used. The same measurements were repeated each day for 20 days. The coefficient of variation is 6–9% at low concentrations and 3–5% at high concentrations.

Aluminum assays on 14 healthy subjects of both sexes gave the following results: blood, 12.5 ± 4.0 (std dev) μg/L; urine, 4.7 ± 2.5 (std dev) μg/L.

Aluminum assays on some patients under dialysis sometimes indicate concentrations as high as 500 μg/L or even higher.

Ordinary tap water from our town supply contains less than 30 μg/L of aluminum.

The results of 16 blood samples routinely assayed using plasma spectrometry and graphite furnace atomic absorption techniques show a good correlation between the two methods (r = 0.991).

DISCUSSION

The study of spectral interference showed that only the presence of boron at concentrations higher than 1 mg/L could introduce an error in aluminum assays. Boron, at such concentrations, is very rare in biological samples and could be easily dealt with by identification at 249.6 nm, a wavelength at which there is no interference with aluminum. The signal count at 396.15 nm could then be corrected for the concentration of boron in the sample.

Aluminum assays could also be carried out at 394.40 nm, but this wavelength has the disadvantage of lower sensitivity although the interference and the interaction due to other metals in the matrix remain unchanged. Besides, it should be noted that the interaction on the background and on the signal intensity vary with working conditions: height above load coil, nebulization and plasma torch characteristics. Thus the values indicated in Figures 1 and 3 are mean values obtained under the defined conditions.

The matrix of the individual samples, especially in the case of urine and water, is unknown and may vary considerably causing changes in signal intensity and in background level. This is why it is better to calibrate for each sample by using the additive technique and measuring the background at peak base by wavelength shifts. For blood samples, however, we observed almost no differences in background intensity, which may be explained by their relatively constant viscosity and their similar Na, K, Ca, and Fe content.

During the nebulization of blood, the main problem encountered was due to the presence of high concentrations of organic compounds which burn in the neighborhood of the induction coils and clog the central orifice of the plasma torch. Increasing the dilution of the samples to 1/15 or 1/20 produced only slight improvement while the sensibility fell sharply. To overcome this difficulty, we had new torches constructed, with a larger diameter for the upper orifice of the central tube, which allow several hundreds of blood samples, diluted to 1/10, to be assayed for aluminum without clogging and without loss of sensitivity compared to standard equipment.

The nebulization of undiluted urine raised no special problems, although it was found preferable to dilute the samples so as to dissolve minerals precipitated during storage at 4 °C as well as to decrease background level.

One of the main advantages of the plasma torch is to allow blood and urine aluminum assays without modification of samples, thus decreasing the risk of loss or contamination which easily occurs with techniques based on mineralization, precipitation, or extraction. Centrifugation after dilution, destined to prevent clogging of the nebulizer, does not alter the signal strength.

The only disadvantage of the present technique is that it requires fairly large test samples of at least 2 mL but we have not yet had any experiences with the ultrasonic nebulizer. We are currently experimenting with the introduction of microsamples using a graphite furnace.

The sensitivity of aluminum assays in water samples corresponds to that indicated by Boumans and Barnes (*14*). The linearity of the calibration graphs extends to very high aluminum concentrations so that practically all blood and urine samples can be directly assayed. For the same reason, in routine assays on large numbers of biological samples, it is possible to use a single addition for calibration. Our aluminum assays on healthy subjects are in good agreement with those obtained by other authors (*1*, *11*, *15*) using atomic absorption spectrometry. However, the reproducibility of results is far more satisfactory with the plasma torch method. Our experience with graphite furnace absorption spectrometry in routine aluminum assays showed the appearance of frequent erratic peaks in spite of all the modifications we attempted in the graphite tube as well as in the techniques of sample preparation. The poor consistency of the method sometimes obliged us to inject each sample, three or even five times over as did Crapper (*16*). Having encountered no difficulties of this kind during hundreds of blood, urine, and water assays with the plasma torch, we have finally decided to drop graphite furnace atomic absorption spectrometry in favor of inductively coupled plasma spectrometry for aluminum determination.

LITERATURE CITED

(1) J. P. Clavel, M. C. Jaudon, and A. Galli, *Ann. Biol. Clin.*, (*Paris*), **36**, 33 (1978).
(2) C. Fuchs, M. Brashe, K. Pashen, H. Nordbeck, and E. Quellhorst, *Clin. Chim. Acta*, **52**, 71 (1974).
(3) K. Garmestani, A. J. Blotcky, and E. P. Rack, *Anal. Chem.*, **50**, 144 (1978).
(4) J. E. Gorsky and A. A. Dietz, *Clin. Chem.* (*Winston-Salem, N.C.*), **24**, 1485 (1978).
(5) K. Julshamn, K. J. Andersen, Y. Willassen, and O. R. Braekkan, *Anal. Biochem.*, **88**, 552 (1978).
(6) M. T. Kovalchik, W. D. Kaehny, A. P. Hegg, J. T. Jackson, and A. C. Alfrey, *J. Lab. Clin. Med.*, **92**, 712 (1978).
(7) F. J. Langmyhr, and D. L. Tsalev, *Anal. Chim. Acta* **92**, 79 (1977).
(8) G. R. Legendre and A. C. Alfrey, *Clin. Chem.*, (*Winston-Salem, N.C.*), **22**, 53 (1976).
(9) Y. Pegon, *Anal. Chim. Acta*, **101**, 385 (1978).
(10) J. A. Persson, W. Frech, and A. Cedergren, *Anal. Chim. Acta*, **92**, 95 (1977).
(11) S. Ranisteano-Bourdon, F. Proullet, and R. Bourdon, *Ann. Biol. Clin.* (*Paris*), **36**, 39 (1978).
(12) P. W. J. H. Boumans, F. J. De Boer, *Spectrochim. Acta*, *Part B*, **32**, 365 (1977).
(13) S. Greenfield, *ICP Inform. Newsl.*, **4**, 199 (1978).
(14) P. W. J. M. Boumans and R. M. Barnes, *ICP Inform. Newsl.*, **3**, 445 (1978).
(15) W. D. Kaehny, A. C. Alfrey, R. E. Holman, and W. J. Shorr, *Kidney Int.*, **12**, 361 (1977).
(16) D. R. Crapper, S. S. Krishnan, and S. Quittkat, *Brain*, **99**, 67 (1976).

RECEIVED for review April 2, 1979. Accepted July 25, 1979.

Chemiluminescent Determination of Clinically Important Organic Reductants

Robert L. Veazey and Timothy A. Nieman*

School of Chemical Sciences, University of Illinois, Urbana, Illinois 61801

The chemiluminescent (CL) reaction of lucigenin with reducing agents in alkaline solution has been investigated for determination of certain clinically important organic species. Detection limits (in mg/L) were found to be: ascorbic acid, 0.17; creatinine, 4.7; uric acid, 0.64; glutathione, 1.0; glucuronic acid, 9.1; lactose, 5.2; glucose, 21. The relative standard deviation of the CL signal is in the range of 0.5–5%. Certain metal ions (Fe(III), Mn(II), Cu(II)) interfere with the determination. The observed emission intensity for a mixture of analytes is equal to the sum of the emission intensities for the separate analytes.

The chemiluminescent (CL) reaction of lucigenin (Luc) (*N,N*-dimethyl-9,9′-biacridinium dinitrate) with hydrogen peroxide was first reported in 1935 by Gleu and Petsch (*1*). Since that time the reaction has received considerable mechanistic study (*2–4*). This reaction has been shown to be useful for determination of a variety of metal ions based on their enhancing or inhibiting effect on the CL emission (*5–7*). Despite the attention paid to the Luc CL reaction, the details of the reactions remain subject to debate. It is probable that the mechanism involves both oxidation and reduction steps (*8, 9*). Totter found that the reductants ascorbate, hydroxylamine, creatinine, and fructose were effective in producing CL from alkaline solutions of Luc in the absence of hydrogen peroxide (*9*). These results suggested the possibility of using the Luc reaction to develop CL methods of analysis for organic reducing agents of clinical significance—those commonly analyzed for in blood and urine.

CL determination of organic compounds has unfortunately received much less attention than has determination of metal ions. The only published determinations by direct reaction have been for hydralazine using $Ru(bipy)_3^{3+}$ (*10*) and for fluorescent compounds with the peroxyoxalate reaction via energy transfer (*11*). Indirect determinations for glucose (*12–15*), NADH (*16*), amino acids (*17*), and glycerides (*18*) involve enzymatic conversion of the analyte into a species (typically H_2O_2) which can be determined via CL reaction. A limited number of organics can be determined via their enhancement of emission in reactions of H_2O_2 with CL reagents. The most sensitive analyses are possible with compounds containing a metal; examples are heme compounds (containing Fe(III)) (*8, 19*) and vitamin B_{12} (containing Co(III)) (*20*). Formaldehyde can be determined by enhancement of CL emission in the gallic acid–H_2O_2 system (*21*). Surveys of many organic compounds for enhancement of CL emission in the luminol–H_2O_2 system (*22–25*) have not resulted in any analytical applications. Organic complexants such as EDTA (*26*), 8-hydroxyquinoline (*27*), and amino acids (*28*) have been determined by their inhibition of CL from metal-enhanced systems.

We have investigated the CL reaction of Luc with the organic reducing agents found at significant levels in blood and urine. Table I indicates the species of interest and their normal concentration ranges (*29*). Because these components are seen to be present in a large range of concentrations, the low detection limits and wide working ranges routinely offered by CL analytical methods could be advantageously applied to determinations involving these reductants.

Table I. Reductants Found in Biological Fluids

reductant	blood, 95% range, mg/L	urine, 95% range, mg/24 h
ascorbic acid	2–14	10–100
creatine	1.6–7.9	11–270
creatinine	5–18	1000–2500
glucuronic acid	20–44	193–591
glutathione	270–415	- - -
sugars		
glucose	600–1200	16–132
galactose	3–28	3–25
lactose	- - -	0–91
uric acid	16–76	80–976

EXPERIMENTAL

Reagents. Lucigenin (Aldrich Chemical Company) was used as obtained with no further purification to prepare 1×10^{-3} M stock solutions. One molar potassium hydroxide stock was prepared from Acculute solution (Anachemia Chemicals, Ltd.). Unstable reducing solutions were prepared within two hours of use. Uric acid stock was prepared by adding 1 M potassium hydroxide dropwise until dissolved, yielding a final pH of approximately 8. All solutions were prepared using deionized, glass distilled water.

Apparatus and Procedure. All measurements were made on a house-built inert stopped flow instrument described by Stieg and Nieman (*30*). Basically the instrument consists of three glass-barrelled syringes driven by an air piston. The syringes deliver solution through inert Teflon tubing and Kel-F and sapphire check valves into a four-way manifold mixer and then to the measurement cell. The measurement flow cell used (Figure 1) is a modification of the one used by Stieg and Nieman (*31*). Several improvements have been made to make the cell simpler, easier to machine, and to provide a smaller volume. The cell itself is machined into the back Teflon plate in the threaded cell holder (thus eliminating the original variable depth flow spacer), and is sealed by the presser screw to a glass window which serves as the entire front of the cell. The volume of the cell is kept to about 100 μL while still exposing a large surface area to the adjacent photomultiplier. The cell is mounted inside a GCA/McPherson modular sample compartment, which is then mounted on an optical rail with GCA/McPherson PMT module. This arrangement gives a very short cell-to-PMT distance, while retaining the advantages of modularity.

Figure 2 is a block diagram of the apparatus, illustrating the data collector/controller interface. A house-built microcomputer system based on the Intel 8080 microprocessor is interfaced to the stopped flow to allow software control of sampling and data collection.

Upon beginning a measurement cycle, (see Figure 3) the microcomputer controller causes the three stopped flow syringes to fill with solutions of Luc, base, and analyte, respectively, and to deliver solution a total of four times in order to rinse the cell thoroughly. After the last delivery is completed, a microswitch on the syringe driver triggers the beginning of data collection. The light output from the reaction in the flow cell is detected

0003-2700/79/0351-2092$01.00/0

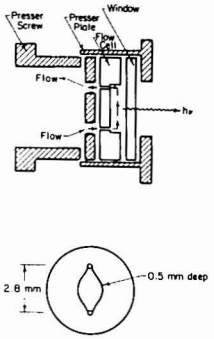

Figure 1. Flow cell; top figure is side view; bottom figure is front view

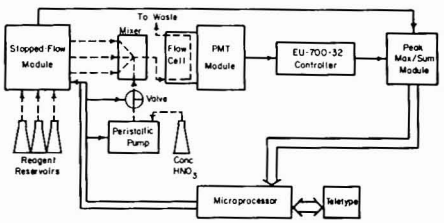

Figure 2. Block diagram of apparatus

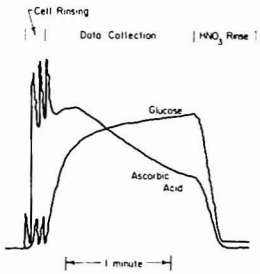

Figure 3. Typical data and measurement cycle

with a 1P28 photomultiplier tube. A GCA/McPherson EU-700-32 controller is used to amplify and signal average the PMT output and to digitize the encoded information. The digital output from the controller is fed into a hardwired data handler (*32*) which collects a preselected number of data points from the EU-700-32, and performs the tasks of summing the data points and of latching the maximum value obtained during a given measurement. This allows two methods of evaluating data: one on the basis of a signal integrated over an entire peak and one based on the peak height of the emission signal; or, in the case of a measurement being stopped before a slowly changing signal peaks, the data are the sum of the emission intensities from the beginning of the measurement period (the end of reactant delivery) up to a set time after mixing, and the maximum intensity obtained during that same period.

A PMT voltage of 900 V was used in all cases except for very concentrated ascorbic acid solutions, in which case the results obtained at a reduced voltage were normalized to a PMT voltage of 900 V. The EU-700-32 controller was adjusted to signal average 500 ms for each datum digitized and sent to the peak max/sum handler. A total of 150 signal averaged points constituted one measurement.

Table II. Relative Intensities[a]

reductant	intensity
ascorbic acid	10 000
creatinine	152
uric acid	143
fructose	73
glutathione	30
glucuronic acid	28
lactose	25
glucose	12
galactose	9
creatine	0
sucrose	0

[a] Conditions: Luc = 10^{-3} M, KOH = 0.5 M, reductants = 0.60 mM.

When the chosen number of data points have been summed, the sum and peak height information are strobed to the microcomputer which prints them out on the teletype. The microcomputer then opens an auxiliary valve to the flow cell and turns on a perstaltic pump to deliver concentrated nitric acid. After each measurement approximately 4 mL of nitric acid are flushed through the mixer and cell in a period of 30 s. This acid rinse is necessary to remove reaction products such as *N*-methylacridone which are insoluble in the alkaline reaction mixture. The measurement routine is then repeated three times for a total of four measurements with each sample. After the fourth sample, the microcomputer signals through the teletype for the operator to change the analyte solution. Normal procedure was to alternate sample solutions with blank solutions. The analytical signal was the average of the four sample measurements minus the average of eight blank measurements, four previous to and four after the true sample measurement.

RESULTS AND DISCUSSION

The reaction conditions were not optimized for each reductant in the normal sense; instead, a set of four conditions of Luc and base concentrations (combinations of 10^{-3} M and 10^{-1} M Luc with 0.5 M and 1.0 M base) were used with each reductant to determine which of these conditions gave the highest signal-to-noise ratio (SNR). The concentrations used were determined from early experiments with glucose to be good starting points for optimization, yielding a reasonable signal without undue background reaction. At higher Luc and/or base concentrations, the background reaction yielded a high emission signal without a corresponding SNR increase, and these conditions caused heavy precipitation of reaction products in the cell, making rinsing difficult.

Figure 3 shows the typical peak shapes obtained for glucose and for ascorbic acid, superimposed on each other, showing the measurement time period and illustrating the need for a reproducible sample mixing and data timing sequence, which is achieved through using a microcomputer for timing and controlling the experiment.

Relative Responses. Table II lists the responses obtained from the reducing agents (plus sucrose as a comparison of a nonreductant) all measured under the same Luc and base concentrations of 10^{-3} and 0.5 M, respectively, and at the same reductant concentration of 0.6 mM. This concentration is within the ranges for real clinical sample concentrations and was chosen to obtain an easily measured response from each reactant. The results are normalized to an ascorbic acid response of 10 000. As would be expected, there is a different relative response for each reducing agent, and thus the detection limits for each will be different. There is no obvious correlation between the relative response and the reduction potential for a given analyte; such a relationship has been noted in certain metal–ion CL analyses (*33*). With the exception of ascorbic acid (for which this method is very sensitive) and creatine (which produces significant response only at much higher concentrations), the range of relative responses

Table III. Working Curves (Log Intensity vs. Log Concentration)

reductant	slope ± σ	intercept ± σ	standard error of estimate	correlation coefficient	limit of detection, mg/L, SNR = 2
ascorbic acid[a]	1.413 ± 0.046	1.690 ± 0.024	0.06899	0.99587	0.17
creatinine[b]	1.091 ± 0.023	0.230 ± 0.044	0.04081	0.99896	4.7
uric acid[c]	0.796 ± 0.012	1.158 ± 0.023	0.02179	0.99888	0.64
glutathione[b]	0.187 ± 0.027	1.821 ± 0.054	0.02395	0.96023	1
glucuronic acid[b]	1.0280 ± 0.024	-0.230 ± 0.053	0.02124	0.99915	9.1
lactose[b]	0.738 ± 0.054	0.110 ± 0.105	0.05093	0.96950	5.2
glucose[c]	0.905 ± 0.019	-0.907 ± 0.049	0.03224	0.99769	21

[a] KOH = 1 M, Luc = 10^{-4} M; [b] KOH = 0.5 M, Luc = 10^{-3} M; [c] KOH = 1 M, Luc = 10^{-3} M.

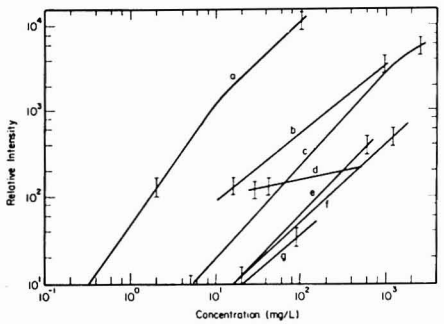

Figure 4. Composite of working curves. Bars on each line indicate the upper and lower limits of the normal clinical concentration range. (a) Ascorbic acid, (b) uric acid, (c) creatinine, (d) glutathione, (e) glucuronic acid, (f) glucose, (g) lactose

for these analytes is fairly narrow.

Note by comparison to Table I that the response rank of a given compound is not the same as the concentration rank for that compound—thus the reaction will be more easily amenable to measuring some compounds in preference to others: a compound such as ascorbic acid, although present in small quantities, should be easily detectable owing to its large relative response. Additionally, there may be different optimum reaction conditions for the various analytes (*33*, *34*).

Analytical Results. Working curves of response vs. concentration were prepared for each of the reductants listed in Table III, which gives the chosen reaction conditions, least-squares parameters of the working curves, and calculated detection limits. All working curves were plotted on a log-log basis.

Figure 4 is a plot of all of the working curves on the same graph, illustrating the great differences in responses and concentration ranges for the various reductants. Bars indicate the clinical working range for each compound. Note that the ascorbic acid curve has a region in which there is a definite change in slope. This is possibly due to achieving an ascorbic acid concentration where the reaction kinetics are no longer limited by the reducing agent, but by one of the chemiluminescent reagents. Note also the small slope of the glutathione curve, which will cause small uncertainties in the determination of the chemiluminescent response to grossly affect the glutathione concentration as determined from the working curve. For most of the reductants, the detection limit is clearly sufficiently small to be able to measure the clinical samples. The RSD of the CL signal is in the range of 0.5–5% for each analyte over the range of the working curves. The extent of the working range is sufficient in most cases, and in those in which it is not, simple dilution will bring the sample down to a measurable region. Further optimization of reaction conditions for each reductant may be possible in order to make this dilution unnecessary.

Table IV. Expected Levels of Certain Metals in Serum

metal	mean, mg/L	95% range, mg/L
Fe	1.90	0.50–3.30
Cu	1.10	0.50–1.41
Zn	1.09	0.69–1.49
Al	0.17	0.16–0.19
Mn	0.04	up to 0.10
Pb	0.03	up to 0.04
Sn	0.02	up to 0.03

Table V. Effect of Metals on Glucose CL[a]

species added	% of glucose signal
Fe(III)	161
Zn(II)	106
Sn(IV)	100
Al(III)	97
Pb(II)	96
Mn(II)	27
Cu(II)	-224
all metals	301
all metals + EDTA	-181

[a] Conditions: Luc = 10^{-3} M, KOH = 1M, glucose = 1.4×10^{-3} M, EDTA = 2×10^{-3} M, metals at maximum clinical concentrations (Table IV).

Metal Ion Interference. Chemiluminescent reactions in solution are characteristically sensitive to the presence of certain metals which can inhibit or enhance the chemiluminescence process, or act in synergy with another impurity or analyte to affect the quantity measured. Table IV lists most of those metals normally found in body fluids, and their range of concentrations in serum (*29*). To determine if these metals would interfere with the CL determination of reducing agents, the reaction with glucose was evaluated under the presence of different metals at the maximum concentrations found in blood serum. Although the effect of the metals may be different in conjunction with one of the other reductants, this study does yield information as to the amount of interference to be expected from these low levels of contaminants.

The metals were added to the glucose solutions and the data was taken within 3 h of mixing. Table V shows the results of this study, as percent response compared to that of 250 mg/L glucose. A value of 100% would indicate no change in the glucose signal; a value of 0% would indicate the background CL level. It can be seen from the table that under the experimental conditions employed, Zn, Sn, Al, and Pb should not pose a problem in the analysis since the results obtained for glucose solutions containing these ions do not deviate significantly from that of glucose alone. Copper(II) might be expected to reduce the signal since in alkaline Cu(II)

Table VI. Mixture Analysis

ascorbic acid, mg/L	glucose, mg/L	predicted intensity[a]	measured intensity
1.0	400	262	255
2.0	250	358	322
2.5	100	385	368
3.0	600	668	678

[a] Predicted values from:
$I = 98.97\ (C_{\text{Ascorbic acid}})^{1.3421} + 0.7117\ (C_{\text{Glucose}})^{0.9074}$.
Conditions: Luc = 10^{-3} M, KOH = 0.5 M.

solutions, glucose is oxidized to a mixture of its sugar acids. The measured response for the glucose–Cu(II) solution is much less than the glucose signal alone, and the presence of Cu(II) causes almost complete inhibition of the background signal (no glucose) itself. Mn(II) also inhibits the reaction, to the extent of removing the glucose enhancement completely. If the reaction mechanism for the background reaction is different from the mechanism for the glucose enhancement reaction, it is of course possible that the Mn(II) could block the enhancement but not the background reaction. Fe(III) is apparently an enhancer of the reaction, its contribution to the total signal approximately equalling the observed signal due to glucose.

A mixture of all of the metals plus glucose significantly enhances the signal to a level approximately 3 times that of glucose alone. There is apparently a synergistic effect of certain of the metals in the mixture: the degree of enhancement from the metal mixture would not be predicted from the results for the individual species.

The analytical CL signal for glucose was not altered by the presence of EDTA, so addition of EDTA was attempted as a solution to the metal ion interference. EDTA was added in 10-fold excess to a solution containing glucose plus the mixture of metal ions. The result was to decrease the CL signal to well below the glucose background level. Apparently, certain of the metal–EDTA complexes are inhibitors of the reaction. (It has been previously shown that certain metal–EDTA complexes enhance light emission in the luminol CL system (*35*).) This result leads us to believe that it would be necessary to physically separate the analytes from any metal ion interferences prior to CL determination.

Mixtures of Analytes. An important point in the characterization of a CL reaction for analysis is the relationship between the total CL signal (for a sample containing several analytes) and the CL signals due to each analyte separately. In some CL systems this relationship is extremely nonlinear (*33*).

We studied this relationship in the Luc–reductant system using binary mixtures of ascorbic acid and glucose. The mixtures contained between 1.0 to 3.0 mg/L of ascorbic acid and 100 to 600 mg/L glucose. The observed CL intensity for each analyte mixture is equal to the sum of the observed CL intensities for ascorbic acid and glucose alone, at the same concentration as in the mixture. The observed intensity is then given by Equation 1

$$I = I_{AA} + I_G = a[AA]^b + a'[G]^{b'} \qquad (1)$$

where AA stands for ascorbic acid; G stands for glucose; a, b, a', and b' are the least squares parameters from the working curves. Table VI gives a comparison, for four mixtures, of the measured signal and the predicted signal. The average deviation of the measured signal from the predicted signal is 4.6%. Figure 5 is a plot of measured intensity vs. predicted intensity for 4 binary mixtures, 3 glucose samples, and 4 ascorbic acid samples. The prediction accuracy for mixtures is seen to be comparable to the prediction accuracy for single components.

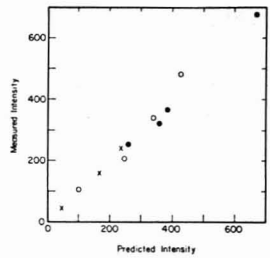

Figure 5. Measured vs. predicted emission intensities for glucose and ascorbic acid (O), glucose (×), mixtures of ascorbic acid and glucose (●). Table VI gives the composition of the mixtures and the equation used to generate the predicted intensities

CONCLUSION

The lucigenin–base–reducing agent CL system has been shown to be applicable to certain compounds of clinical interest. Detection limits and working ranges are satisfactory for the analysis of real samples. For a real application, however, possible interferences in a sample must be removed prior to the CL analytical reaction. In addition, since the reaction does not differentiate reductants, the analysis would be most direct if the analytes were separated from each other. Thus, a major strength of this CL reaction could lie in its application as a detector for HPLC. Preliminary work in this direction has been promising, and will be reported at a later date. An additional application planned for investigation is the determination of certain polysaccharides by conversion to the reductants which can be determined with this CL reaction.

ACKNOWLEDGMENT

We thank Susan Rivken for experimental work in the early stage of this project.

LITERATURE CITED

(1) Gleu, K.; Petsch, W. *Angew. Chem.* **1935**, *48*, 57.
(2) McCapra, F. *Q. Rev., Chem. Soc.* **1966**, 485.
(3) McCapra, F. In "Progress in Organic Chemistry", Vol. 8; Carruthers, W., Sutherland, J. K., Eds.; John Wiley & Sons: New York, 1973; pp 231–77.
(4) Gundermann, K.-D. *Top. Curr. Chem.* **1974**, *46*, 61.
(5) Babko, A. K.; Dubovenko, L. I., Terletskaya, A. V. *Ukr. Khim. Zh.* **1966**, *32*, 1326.
(6) Babko, A. K.; Dubovenko, L. I.; Lukovskaya, N. M. "Chemiluminescent Analysis" (in Russian); Teknika: Kiev, 1966.
(7) Montano, L. A.; Ingle, J. D. *Anal. Chem.*, **1979**, *51*, 919.
(8) Isacsson, U.; Wettermark, G. *Anal. Chem. Acta* **1974**, *68*, 339.
(9) Totter, J. R. *Photochem. Photobiol.* **1975**, *22*, 203.
(10) Nonidez, W. K.; Leyden, D. F. *Anal. Chim. Acta* **1978**, *96*, 401.
(11) Curtis, T. G.; Seitz, W. R. *J. Chromatogr.* **1977**, *134*, 343.
(12) Bostick, D. T.; Hercules, D. M. *Anal. Chem.* **1975**, *47*, 447.
(13) Auses, J. P.; Cook, S. L.; Maloy, J. T. *Anal. Chem.* **1975**, *47*, 244.
(14) Williams, D. C.; Huff, G. F.; Seitz, W. R. *Clin. Chem.* **1976**, *22*, 372.
(15) Williams, D. C.; Huff, G. F.; Seitz, W. R. *Anal. Chem.* **1976**, *48*, 1003.
(16) Williams, D. C.; Seitz, W. R. *Anal. Chem.* **1976**, *48*, 1478.
(17) Lowery, S. N.; Carr, P. W.; Seitz, W. R. *Anal. Lett.* **1977**, *10*, 931.
(18) Hercules, D. M.; Sheehan, T. L. *Anal. Chem.* **1978**, *50*, 22.
(19) Chapelle, E. W.; Piccolo, G. L., Eds., "NASA Special Publication, Vol. 388: Analytical Applications of Bioluminescence and Chemiluminescence"; NASA: Washington, D.C., 1975.
(20) Sheehan, T. L.; Hercules, D. M. *Anal. Chem.* **1977**, *49*, 446.
(21) Slawinska, D.; Slawinski, J. *Anal. Chem.* **1975**, *47*, 2101.
(22) Yurrow, H. W.; Sass, S. *Anal. Chim. Acta* **1974**, *68*, 203.
(23) Yurrow, H. W.; Sass, S. *Anal. Chim. Acta* **1975**, *77*, 324.
(24) Yurrow, H. W.; Sass, S. *Anal. Chim. Acta* **1976**, *81*, 203.
(25) Yurrow, H. W.; Sass, S. *Anal. Chim. Acta* **1977**, *88*, 389.
(26) Babko, A. K.; Dubovenko, L. I.; Mikhailova, L. S. *Zh. Anal. Khim.* **1966**, *21*, 548.
(27) Babko, A. K.; Lukovskaya, N. M. *Ukr. Khim. Zh.* **1969**, *35*, 1060.
(28) Pantel, S.; Weisz, H. *Anal. Chim. Acta* **1975**, *74*, 275.
(29) Diem, K.; Lentner, C. "Scientific Tables"; Geigy Pharmaceuticals: Ardsley, N.Y., 1970; pp 561–676.
(30) Stieg, S.; Nieman, T. A. *Anal. Chem.* **1977**, *49*, 1322.
(31) Stieg, S.; Nieman, T. A. *Anal. Chem.* **1978**, *50*, 401.
(32) Nieman, T. A., *Anal. Chem.*, submitted for publication.
(33) MacDonald, A.; Chan, K. W.; Nieman, T. A. *Anal. Chem.*, **1979**, *51*, in press.

(34) Stieg, S.; Nieman, T. A. *Anal. Chem.*, submitted for publication.
(35) Seitz, W. R.; Suydam, W. W.; Hercules, D. M. *Anal. Chem.* **1972**, *44*, 957.

RECEIVED for review May 5, 1979. Accepted July 31, 1979.

This research was supported by the donors of the Petroleum Research Fund, administered by the American Chemical Society; by Research Corporation; and by the National Science Foundation (CHE 78-01614).

Laser Fluorometry of Fluorescein and Riboflavin

Nobuhiko Ishibashi,* Telichiro Ogawa, Totaro Imasaka, and Mikio Kunitake

Faculty of Engineering, Kyushu University, Fukuoka 812, Japan

The detection limits of fluorescein and riboflavin are determined to be 0.02 and 0.6 parts-per-trillion, respectively, with the use of a very sensitive fluorometric system (a nitrogen-laser-pumped dye laser and a pulse-gated photon counter). The dependences of the *S/N* ratio and the detection limit of the excitation and emission wavelengths are calculated and expressed in the figures for convenient determination of the optimal condition for ultratrace analysis. The results show that the Stokes shift of the sample molecule as well as the molecule's absorptivity, fluorescence quantum yield, and fluorescence bandwidth influence the detection limit significantly. The present system incorporates an emission monochromator, and this is especially useful for the analysis of a molecule with a small Stokes shift.

Ultratrace analysis of fluorescing molecules has made great progress by the use of laser sources for excitation. The unique properties of the nitrogen-laser-pumped dye laser can give rise to substantial gains in improving detection limits (*1*, *2*). The previously reported detection limits of fluorescein with a laser source and a monochromator (*3*–*5*) were in the order of 30–100 ppt (ppt = 10^{-12}) and are approximately identical to that of a conventional fluorescence spectrophotometer. Recently, however, the fluorescein detection limit, as determined by laser fluorometry, has been reported to be 2 ppt (*1*).

The detection limit of a very sensitive fluorometric system is not always determined by the sensitivity of the instrument. The detection of fluorescein at the concentration of 1×10^{-15} M would be possible with an instrument which is capable of detecting the molecular fluorescence at $A\phi = 5 \times 10^{-11}$ (A, absorbance; ϕ, quantum yield) (*6*). However, residual fluorescence from the solvent impurities, which cannot be removed by any practical purification methods, interferes with the determination of such weak molecular fluorescence.

The signal-to-noise (S/N) ratio is defined as the ratio of the fluorescence intensity of the sample molecule to the fluctuation of the background signal. The excitation wavelength has a great influence on the fluorescence intensity and the profile of the background signal. However, the excitation wavelength has no influence on the profile of the fluorescence band. It is useful to know the effect of the excitation and emission wavelengths on the minimum detectable concentration and to choose the optimal wavelengths for detection with the highest S/N ratio.

In this paper an application of the very sensitive laser fluorometric system (*6*) for the ultratrace analysis of fluorescein and riboflavin is described. The optimal experimental condition for the fluorometry is discussed in terms of the analysis of the S/N ratio.

EXPERIMENTAL

The spectroscopic apparatus consists of a dye laser and a pulse-gated photon counter, and has been described in detail elsewhere (*6*). The fluorescence cell is cylindrical, 6 cm in height and 4 cm in diameter. Fluorescence was observed with a double monochromator (JASCO CT-40D) equipped with an HTV R928 photomultiplier. The photoelectron signal was gated and counted. The gatewidth was adjusted to 0–200 ns. The integration time of the photoelectron signal was 50 s for each point in the spectrum, and four runs measured under identical conditions were accumulated. In the measurement of an analytical curve, the intensity of the fluorescence signal of the sample and that of the Raman signal of water were measured 10 times (50 s × 10), respectively, and the ratio of fluorescence signal to the Raman signal was plotted. This ratioing is useful to improve reproducibility when the sample cell is exchanged. The drift of signal is negligibly small during ratioing (*6*).

The fluorescein (Wako, chemically pure grade), and riboflavin (Tokyo Kasei, guaranteed grade) were recrystallized from water. The water was deionized, passed through activated charcoal, and filtered (MF-Millipore, GS). Further distillation did not reduce the background signal in the solution blank. The glassware was thoroughly washed with soap, NaOH, and a chromic acid mixture by using an ultrasonic cleaner and then rinsed with copious amounts of water. The pH of the sample solution of fluorescein was adjusted to 13 with NaOH, and that of riboflavin to 6–7 with acetic acid and sodium acetate.

ANALYSIS

The proper selection of excitation and emission wavelengths is important for ultrasensitive fluorometry. Calculation and visualization of the dependences of the S/N ratio and of the detection limit on wavelength will be useful for this purpose.

In the presence of a background signal, n_b (n, number of photoelectrons), the actual fluorescence, n_f, can be obtained by subtracting n_b from the signal of the sample, n_s.

$$n_f = n_s - n_b \tag{1}$$

The background signal consists of the scattered light of the source radiation, source-induced background, and source-independent background. In the present study the source-independent backgrounds such as dark counts of the photomultiplier and electrical noise from the nitrogen laser were negligible.

Then the S/N ratio is expressed as (*7*)

$$S/N = n_f / \sqrt{n_s + n_b} \tag{2}$$

Since the S/N ratio depends on the number of photoelectrons

0003-2700/79/0351-2096$01.00/0

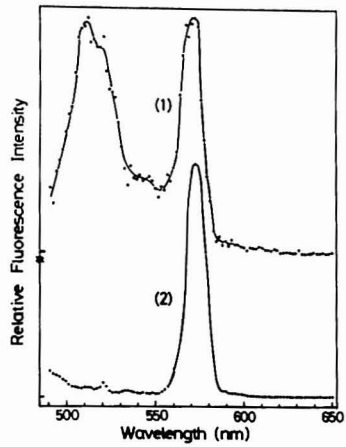

Figure 1. Fluorescence spectrum of fluorescein (pH 13, 5×10^{-11} M) (1) and background spectrum of solvent water (2). Excitation source: esculin dye laser (λ_{ex} = 480 nm, $\Delta\lambda_{ex}$ = 0.3 nm)

coming from the sample fluorescence and the background photoemission, the S/N ratio varies as a function of the excitation and fluorescence wavelengths.

The detection limit (DL) of the fluorometry is defined with respect to the concentration at which $S/N = 2$. From Equation 2,

$$n_f(\mathrm{DL}) = 2(1 + \sqrt{1 + 2n_b}) \tag{3}$$

where $n_f(\mathrm{DL})$ is the number of photoelectrons of the actual fluorescence at the detection limit. Thus, the concentration at the detection limit, $c(\mathrm{DL})$, is expressed as follows;

$$c(\mathrm{DL}) = k\,\frac{2(1 + \sqrt{1 + 2n_b})}{I \cdot \epsilon(\lambda_{ex}) \cdot \phi(\lambda_{em})} \tag{4}$$

where ϵ is the absorptivity, ϕ the quantum yield, I the intensity of the exciting laser, and k a proportionality constant.

The S/N ratio and the detection limit can be plotted as a function of the fluorescence wavelength at a specified excitation wavelength, and this figure is useful for the selection of the optimal experimental condition for fluorometry.

RESULTS

Fluorescence Spectrum. The fluorescence spectrum of fluorescein (5×10^{-11} M, pH 13) excited by an esculin dye laser is shown in Figure 1, together with the background spectrum from the solution blank; these spectra have been improved in comparison with the previous result (*1*) by using the double monochromator and the pulse-gated photon counter. The fluorescence band of fluorescein appears at 514 nm; the Raman bands of water appear at 521 and 570 nm. The fluorescence peak height of the 5×10^{-11} M sample is nearly equal to that of the Raman band of water. The absorption maximum of fluorescein is located at 491 nm, and its Stokes shift is about 910 cm^{-1} (23 nm), which is considerably smaller than typical organic molecules. The fluorescence bandwidth is 35 nm.

The fluorescence spectrum of riboflavin and the background spectrum excited at 377 nm are shown in Figure 2. Riboflavin has maxima at 266, 377, and 445 nm, in the absorption and excitation spectra (*8*) and has a fluorescence maximum at 526 nm. The separations of the absorption and fluorescence

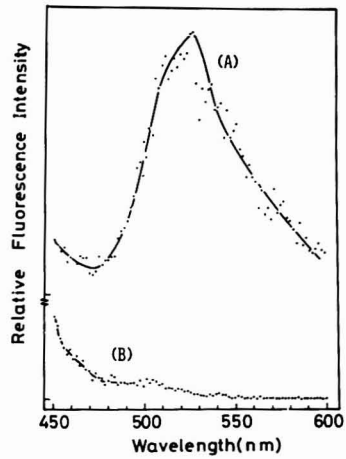

Figure 2. Fluorescence spectrum of riboflavin (pH 6–7), 1×10^{-8} M) (A) and background spectrum of solvent water (B). The Raman band of water is located at 431 nm (not shown). Excitation source: PBD dye laser (λ_{ex} = 377 nm, $\Delta\lambda_{ex}$ = 0.4 nm)

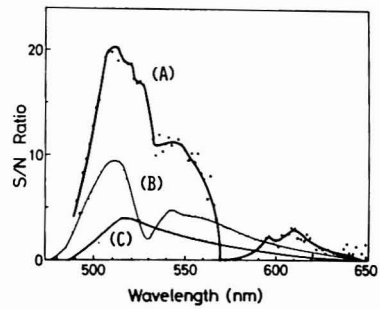

Figure 3. S/N ratio of fluorescein (pH 13, 5×10^{-11} M). Excitation source: (A) esculin dye laser (480 nm), (B) 4-MU dye laser (450 nm), (C) Al–Calcein Blue chelate laser (420 nm)

maxima are 19000 cm^{-1} (260 nm), 7500 cm^{-1} (149 nm), and 3500 cm^{-1} (81 nm), respectively, and the last one coincides with the Raman shift of water. The bandwidth of the fluorescence is 85 nm.

Wavelength Dependences of S/N Ratio and Detection Limit. The S/N ratios of fluorescein excited at 420, 450, and 480 nm were calculated from Equation 2 and are shown in Figure 3. It can be seen that excitation at 480 nm gives the highest S/N ratio. The most preferable analytical condition thus exists when the excitation is at this wavelength and the observation of the emission is at 510 nm. The decrease of the S/N ratio at 570 nm is due to the presence of the Raman band of water. In the longer wavelength region, the fluorescence is weak, and the S/N ratio decreases. When the excitation wavelength was adjusted to 420 nm, the background signal of the impurity and of the Raman band of water decreased. However, the larger decrease of the fluorescence intensity of fluorescein reduced the S/N ratio.

The detection limit of fluorescein calculated from Equation 4 (Figure 4) shows that the most preferable observation wavelength for the ultratrace analysis is in the 510–530 nm

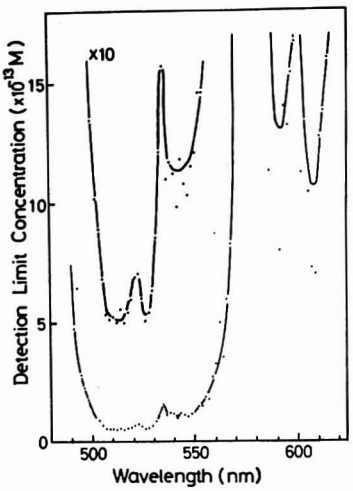

Figure 4. Detection limit of fluorescein (pH 13). Excitation source: esculin dye laser (480 nm)

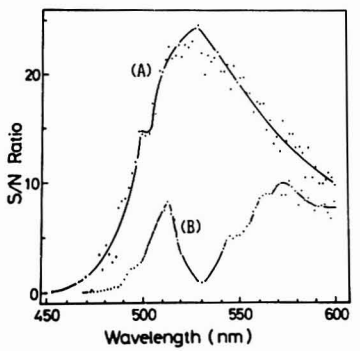

Figure 5. S/N ratio of riboflavin (pH 6–7, 1×10^{-9} M). Excitation source: (A) PBD dye laser (377 nm), (B) 4-MU dye laser (450 nm)

region, and the minima of the detection limit appears on both sides of the weak Raman band of water. The steep increase at 570 nm is due to the strongest Raman band of water, and the increase at above 620 nm is due to the weak fluorescence.

The excitation of riboflavin at 377 nm gives a higher S/N ratio than that at 450 nm, as shown in Figure 5. This is due to the smaller background signal when excited at the shorter wavelength. Furthermore, the overlapping of the fluorescence and the Raman bands reduced the S/N ratio when excitation occurred at 450 nm.

The detection limit of riboflavin is shown in Figure 6. The minimum detectable concentration can be measured with emission at 526 nm. A wide region (500–600 nm) is open for ultratrace analysis, since there is a concomitant decrease of the background signal with the decrease of the fluorescence intensity in this region.

Analytical Curve and Detection Limits. The dependence of the fluorescence intensity of fluorescein on concentration is measured. The analytical curve of fluorescein

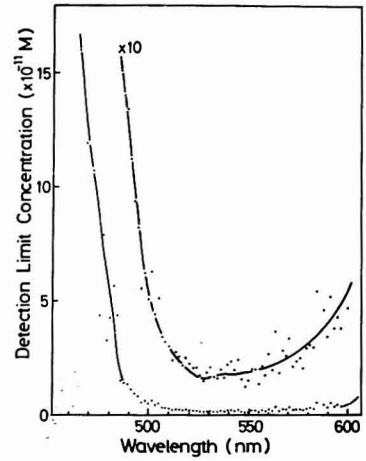

Figure 6. Detection limit of riboflavin (pH 6–7). Excitation source: PBD dye laser (377 nm)

is straight. The observed detection limits of fluorescein and riboflavin are 5×10^{-14} M (0.02 ppt) and 1.5×10^{-12} M (0.6 ppt), respectively.

DISCUSSION

Factors Affecting the Detection Limit. In ultratrace analysis, spectroscopic parameters such as the absorptivity, the fluorescence quantum yield, and the half-width of the fluorescence band have a great influence on the detection limit. Furthermore, the analysis of the S/N ratio indicates that the Stokes shift of the fluorescing molecule can profoundly influence the detection limit, since it depends on the overlapping between the fluorescence of the sample and the Raman band of the solvent (see Figures 4 and 6).

Fluorescent molecules can be categorized into three groups according to the relative magnitude of the Stokes shift (λ_S) of the molecule and the Raman shift (λ_R) of the water.

(*a*) $\lambda_S < \lambda_R$ (*e.g., Fluorescein*). The excitation and emission wavelengths should be carefully adjusted, since the highest S/N ratio, hence, the lowest detection limit, can be obtained in the limited wavelength region (Figures 3 and 4). In this case the double monochromator is especially useful to reduce the scattered light of the laser.

(*b*) $\lambda_S \simeq \lambda_R$ (*e.g., 450-nm Excitation of Riboflavin*). The bandwidth of the fluorescence of many organic molecules in the condensed phase is larger than that of the Raman band of water, and there two peaks appear in the S/N ratio as shown in Figure 5.

(*c*) $\lambda_S > \lambda_R$ (*e.g., 377-nm Excitation of Riboflavin*). A wide spectral region is available for utlratrace analysis (Figures 5 and 6), since the fluorescence maximum is located at longer wavelength than the Raman band of water, and since the background signal decreases with increasing separation of the excitation and observing wavelengths.

Since it is important to select the optimal condition for ultratrace analysis, the illustrations of the S/N ratio and the detection limit as shown before will be very useful, especially for cases *a* and *b*.

Comparison of an Emission Monochromator with a Filter. As shown above, the monochromator is very useful for ultratrace analysis in case *a*, since the emission wavelength can be adjusted to the most preferable position. An optical

Table I. Detection Limits of Fluorescein

exciting source	detection apparatus	λ_{ex}, nm	$\Delta\lambda_{ex}$, nm	λ_{em}, nm	$\Delta\lambda_{em}$, nm	detection limit, ppt	ref.
dye laser	pulse-gated photon counter	480	0.3	510	0.5	0.02	*a*
dye laser	averager	470	10	514	1.6	2	(*1*)
Xe lamp	dc amplifier	470	10	514	1.6	70	(*1*)
dye laser	boxcar integrator	480	0.4	514	---	100	(*3*)
dye laser	boxcar integrator	470	0.1	514	---	40	(*4*)
N_2 laser	boxcar integrator	337	<0.1	514	---	30	(*4*)
dye laser	charge-to-count data converter	469	0	522	4	70	(*5*)

[a] Present work.

Table II. Detection Limits of Riboflavin

exciting source	detection apparatus	λ_{ex}, nm	$\Delta\lambda_{ex}$, nm	λ_{em}, nm	$\Delta\lambda_{em}$, nm	detection limit, ppt: monochromator	detection limit, ppt: filter	ref.
dye laser	pulse-gated photon counter	377	0.4	526	1	0.6		*a*
Xe lamp	dc amplifier	---	---	---	---	100		(*12*)
Hg lamp	photon counter	365	<0.1	filter			40	(*11*)
dye laser	boxcar integrator	375	---	540	8	38		(*13*)
dye laser	boxcar integrator	375	---	filter			0.47	(*13*)

[a] Present work.

filter can be more useful for the measurement of weak photoemission in case *c*. Notably, the sub-parts-per-trillion detections of rhodamine B (*2*) and rhodamine 6G (*9*) were carried out with filters. Another advantage of a monochromator is that the Raman band of water can be used as an internal standard of the analytical curve. This procedure improves reproducibility of the data.

Detection Limit. The detection limits of fluorescein determined by various exciting sources thus far reported are shown in Table I. The detection limit in the present system is two orders of magnitude lower than that previously reported. In the previous study (*1*), the major sources of noise at the detection limit were the dark current of the photomultiplier and the background signals caused by impurities in the solvent. In the present study, the reduction of the dark current by the gated electronics, repeated purifications of the solvent, careful adjustment of the experimental conditions with the aid of the S/N ratio and detection limit analyses allowed the ultratrace analysis of fluorescein.

The detection limit of riboflavin is shown in Table II along with previous results. The low absorptivity ($\epsilon = 1.06 \times 10^4$ (*10*)) and the low quantum yield ($\phi = 0.26$ (*7*)) of riboflavin restricted the detection limit to 0.6 ppt, although this value is much smaller than the previous value in a similar (monochromator) detection system. The excitation spectrum of riboflavin has three maxima. Excitation at 450 nm has difficulty in resolving fluorescence from the Raman line. Excitation at 377 nm has been satisfactory for the ultratrace analysis. If second harmonic generation is possible, excitation at 266 nm may be more preferable because of the higher absorptivity and the lower background signal at 526 nm. Riboflavin has a large Stokes shift and has a wide bandwidth, so that the filter detection would be useful; Richardson et al. detected 0.47 ppt with filters (*13*).

CONCLUSION

The statistical variation of the number of the photoelectron pulses from the solution blank places a limitation on the minimum detectable concentration. Thus, the use of a still higher-output-power dye laser will not provide a large reduction of the detection limits. Still, there are two promising methods for the detection of even lower levels. One is the further purification of the solvent. The other is to make use of temporal discrimination to reject unwanted signals.

ACKNOWLEDGMENT

The authors thank S. D. Lidofsky of Stanford University for his critical reading of the manuscript.

LITERATURE CITED

(1) Imasaka, T.; Kadone, H.; Ogawa, T.; Ishibashi, N. *Anal. Chem.* **1977**, *49*, 667–8.
(2) Richardson, J. H.; George, S. M. *Anal. Chem.* **1978**, *50*, 616–20.
(3) Smith, B. W.; Plankey, F. W.; Omenetto, N.; Hart, L. P.; Winefordner, J. D. *Spectrochim. Acta, Part A* **1974**, *30*, 1459–63.
(4) Geel, T. F. V.; Winefordner, J. D. *Anal. Chem.* **1976**, *48*, 335–8.
(5) Harrington, D. C.; Malmstadt, H. V. *Anal. Chem.* **1975**, *47*, 271–6.
(6) Imasaka, T.; Ogawa, T.; Ishibashi, N. *Anal. Chem.* **1979**, *51*, 502–4.
(7) Tobin, M. C. *J. Opt. Soc. Am.* **1968**, *58*, 1057–61.
(8) Anacreon, R. E.; Ohnishi, Y. *Appl. Opt.* **1975**, *14*, 2921–26.
(9) Bradley, A. B.; Zare, R. N. *J. Am. Chem. Soc.* **1976**, *98*, 620–21.
(10) Whitby, L. G. *Biochem. J.* **1953**, *54*, 437–42.
(11) Aoshima, R.; Iriyama, K.; Asai, H. *Appl. Opt.* **1973**, *12*, 2748–50.
(12) Aaron, J. J.; Winefordner, J. D. *Talanta* **1972**, *19*, 21–29.
(13) Richardson, J. H.; Wallin, B. W.; Johnson, D. C.; Hrubesh, L. W. *Anal. Chim. Acta* **1976**, *86*, 263–7.

RECEIVED for review February 28, 1979. Accepted July 27, 1979. This research was supported by Grants-in-Aids for Special Project Research (Grant No. 112004, 211204, and 310503), for Scientific Research (Grant No. 347054), and for Environmental Science (Grant No. 303046) from the Ministry of Education of Japan.

Flame Photometric Determination of Carbon Disulfide in Air after Specific Preconcentration

Jean Godin,* Jean-Louis Cluet, and Claude Boudène

INSERM U 122, Laboratoire de Toxicologie, UER des Sciences Pharmaceutiques, 92290 Chatenay-Malabry, France

A new technique for determining carbon disulfide in air has been developed. It is based on concentrating this contaminant on a chromatographic support treated with sodium azide and hexamethylphosphorotriamide (HMPT) and then applying a headspace technique followed by flame photometry. This method is simple, accurate and allows analysis of a large number of samples. Among the different factors affecting quantitative determination of CS_2 in air which were studied, temperature-dependent partial hydrolysis of CS_2 leading to the formation of H_2S and COS is the most important.

The use of large quantities of carbon disulfide by the chemical industry necessitates monitoring of this compound both in industrial and ambient atmospheres. It is therefore of interest to develop simple and rapid methods for sampling and determination of this pollutant. Colorimetry based on copper diethyldithiocarbamate formation has been extensively used for many years but is not very suitable for field measurement (*1*, *2*). Methods involving the trapping of CS_2 on solid phases, like active charcoal sampling (*3*) and subsequent analysis with the flame photometric detector (FPD) are increasingly used because of their greater sensitivity and feasibility (*4*). The ambient air concentration of CS_2 has also been determined by cryogenic trapping at −196 °C (*5*).

The aim of this work is to describe a new method for CS_2 sampling and determination, both in industrial areas and in ambient air. This method is sufficiently easy and quick and requires only commercially available material, i.e., a Tracor HM 270 analyzer fitted with a septum injector, and reagents.

Carbon disulfide is first specifically retained on a treated support of high efficiency. The support is then placed in a headspace flask and the gas phase thus released is used for CS_2 measurement by a flame photometry detector.

EXPERIMENTAL

Reagents. The absorbing reagent was prepared as follows: 10 mL of HMPT (Prolabo, France), 10 mL of distilled water, 2 g of NaN_3 (Prolabo), and 50 mL of ethanol (96% v/v) were successively placed in a 200-mL flask.

The flask was gently stirred until the sodium azide had completely dissolved. Ten grams of acid-washed Chromosorb W (60–80 mesh) were then added. Ethanol and a large quantity of water were eliminated under vacuum in a rotary evaporator. The mixture can be stored without deterioration for long periods in tightly-capped vessels.

Apparatus. Absorption cartridges were prepared by placing 80 to 100 mg (about 1 cm) of treated support in glass tubes 4 cm long (i.d., 0.4 cm). The support was maintained by two glass wool plugs. For storage, cartridges must be capped at both ends by glass stoppers and small pieces of PTFE tubing.

For release of CS_2, 40-mL headspace flasks were used (Pierce Chemical Co., Rockford, Ill.). They can be replaced by inexpensive 60-mL flasks fitted with Bakelite screw caps (Sovirel, France). The cap was lined with a PTFE disk 0.2 mm thick. A silicone rubber spacer was placed between the PTFE disk and the Bakelite cap. Both cap and spacer had a syringe bore of 5-mm diameter.

CS_2 determinations were performed with a Tracor HM 270 analyzer fitted with two chromatography columns, the first for total sulfur estimation and the second (poly(phenyl ether), H_3PO_4) for separation of sulfur compounds (*6*). For H_2S and COS separation, the second column was replaced by a special silica gel column (Tracor) (*7*).

To assess the efficiency of CS_2 trapping by different absorbent mixtures, an automatically controlled injection device (Intersmat, France) was connected to the gas valve of the analyzer, allowing injection of a fresh gas sample every 3 min.

For headspace determinations, a septum injector was placed in front of the column; the temperature was maintained at 60 °C.

Gas syringes of 0.1- to 1-mL volume (type A2, Precision Sampling Corp., USA) were used throughout the study.

Atmospheres contaminated with known amounts of CS_2 were prepared with a permeation tube maintained in a thermostated chamber (Tracor 412) as described previously (*8*). In this experiment, the mean CS_2 permeation flow was 7.75 μg/h.

Procedure. *Sampling.* Air contaminated with CS_2 was drawn through the absorbent cartridge at a flow rate of 150 mL/min. Flow rate, sampling time, and absorbent weight can all be modified.

Analysis. The content of one cartridge was poured into a headspace flask containing 2 mL of 58% AR hydriodic acid (Prolabo). The flask was promptly capped and placed in a water bath at 40 °C. Two hours later an aliquot of the gas (usually 0.1 to 1 mL) was injected into the analyzer.

Calibration. Calibration curves were constructed by running cartridges containing known amounts of CS_2 in exactly the same way as the samples. Daily standardization of the analyzer was simple and consisted of treated standard solutions of sodium diethyldithiocarbamate AR (Carlo Erba, Italy) which, under these conditions, produce known quantities of CS_2.

RESULTS AND DISCUSSION

In the first part of this work, we tested the CS_2 trapping efficiency of several mixtures. Air samples containing small amounts of CS_2 were drawn through cartridges and injected into the analyzer every 3 min by means of an automatic gas valve. The time interval was measured between CS_2 entry at the inlet of the cartridge and its exit at the outlet. The best results were obtained with a mixture containing either sodium azide or a secondary amine (e.g., piperazine) and HMPT on Chromosorb W. HMPT greatly improved the capacity of the absorbent. Sodium azide was chosen because of its instability and because of the lability of the azide–carbon disulfide addition product.

The efficiency of this trapping mixture was very high. As an example, CS_2 at a concentration of 174 μg/L air, was drawn through 100 mg of treated Chromosorb at a flow rate of 4.5 L/h for 6 h, 45 min before any trace of CS_2 could be detected at the outlet of the cartridge.

In the second part of this work, we attempted to determine CS_2 in the form of $N_3CS_2^-$. Spectrophotometric determinations was not used because of insufficient sensitivity (*9*). Further, extraction of the addition product by organic solvents prior to chromatographic analysis is not satisfactory because of the presence of sodium azide and HMPT and also because these solvents usually prolong chromatography and require a back-flush system to avoid detector flame extinction.

For all these reasons, we chose a technique involving the destruction of the azide–CS_2 addition product in acid medium and the volatilization of CS_2. Among the different compounds

0003-2700/79/0351-2100$01.00/0

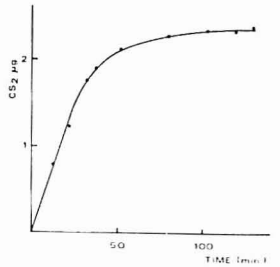

Figure 1. CS_2 generation from $N_3CS_2^-$ in a headspace flask

Table I. Precision Study[a]

	within a set of samples drawn from same cartridge	within a set of samples drawn from different cartridges on different days
determination of CS_2 without conversion into COS and H_2S	5.342 ± 0.131 (20) 0.645 ± 0.016 (22)	3.833 ± 0.125 (16) 1.291 ± 0.065 (14)
determination of CS_2 after complete conversion into COS and H_2S	—	1.563 ± 0.193 (18)

[a] Mean and standard deviation (number of determinations), results expressed in µg.

tested hydriodic acid completely released CS_2 within 2 h at 40 °C (Figure 1) whereas acetic acid, iodine + acetic acid, *o*-phosphoric acid and hydrochloric acid released only small amounts of CS_2 during the same period. At higher temperature (80 °C), regeneration of CS_2 was completed in less than 30 min, but under these conditions, condensations in syringes increased the variability of the results. This is why all incubations were performed at 40 °C. The volume of hydriodic acid had little effect on the results in the 2- to 6-mL range.

Table I shows the results of reproducibility experiments with fresh samples. The detection limit may be improved by using smaller headspace flasks or increasing injected sample volume to several milliliters. Using 40-mL headspace flasks and 1-mL gas phase injections, the CS_2 detection limit per cartridge was 1.2 ng or twice the background noise. However, since the reagents in the flasks contained CS_2, it was not possible to attain this limit (mean of eight experimental determinations: 1.97 ng, s = 0.434). Great care was taken to avoid contamination of flasks or syringes.

A standard curve can be made by injecting 0.1 mL of gas phase coming from the headspace flasks. So, the CS_2 quantity in cartridges is determined by the relation:

$$\log \text{ng } CS_2 = 0.495 \log R + 1.339$$

where R = height of the peak (mm) × FPD attenuation (range: 10^{-7}).

Large variations in experimental conditions such as sampling time, air flow rate, flask volume, size of the sample injected, and the detector attenuation enabled determination of a wide range of CS_2 concentrations in air. Another advantage of the method used is the possibility of making repeated determinations in a short time (less than 2 min per chromatographic measurement).

A single peak appeared on chromatograms when cartridges were treated immediately after sampling; however, when they were kept at room temperature for several hours, this peak decreased, forming a second peak. Judging by the retention times on the poly(phenyl ether)-H_3PO_4 column, the second peak might correspond to carbonyl sulfide and/or hydrogen sulfide. These compounds were readily identified on a silica gel column.

COS and H_2S formation may result from partial hydrolysis of the azide–carbon disulfide addition product in accordance with following scheme:

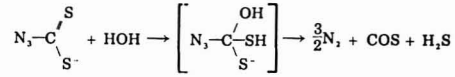

Thus, according to this scheme, measurement of the amount of COS and H_2S formed by CS_2 hydrolysis should permit determination of the amount of CS_2 initially present in the cartridges before its conversion. However, we observed that only the COS chromatogram peak was usable, since the response to H_2S varied considerably for the same sample, probably because of the losses in H_2S from the flask, and during its gas phase transfer by syringe.

We also noted that for a given quantity of CS_2, the response was much greater when CS_2 was not converted into COS. This can certainly be explained by the different number of S atoms in these two molecules. We therefore found that 1 µg CS_2 converted into COS produced a response equal to about 0.5 µg CS_2.

Tubes stoppered at both ends can be stored for more than a month at room temperature without loss of COS. Nevertheless, the variability of the results obtained under these conditions is greater than the results for CS_2. After total transformation of CS_2 into COS, a calibration curve has been obtained according to the relation:

$$\log \text{ng } CS_2 = 0.493 \log R + 1.635$$

COS and H_2S retention times in cartridges were very brief. Thus when a COS–H_2S–air mixture was passed through the cartridges, followed by a CS_2–air mixture of similar concentration (0.86 µg/L, 9 L/h), only a small fraction of the COS and H_2S was retained for a few minutes, whereas CS_2 was bound to the absorbent for many hours.

Since, COS and H_2S were not retained on the absorbent in the presence of an air current, we feared that during prolonged sampling, the COS and H_2S produced by CS_2 hydrolysis might be eliminated from the sampling tube. Therefore, in order to create the most unfavorable conditions for sampling CS_2 in air, tubes containing 1.94 µg CS_2 were subjected to a 150 mL/min air current at ambient temperature for different periods. The resulting measurements were compared to determinations made from freshly taken samples. Losses of CS_2 were then 5% after 30 min, 10% after 1 h, and 38% after 4 h. At the last time, the COS remaining in the cartridge was approximatively 1% of the CS_2 initially present. Cooling the cartridges to 0 °C almost completely prevented losses after 4 h, and kept them below 10% after 24 h.

Stability of cartridges after sampling was excellent at −20 °C for over one month. At ambient temperature, however, degradation occurred after several hours and, at 50 °C, was complete in less than 2 h.

Cartridge absorption capacity was satisfactory when sampling tubes were used in ambient air with normal humidity. Thus, for 50 to 60% relative humidity, 100 mg of support remained effective for more than 6 h with a CS_2 current in air of 800 µg/h. On the other hand, for the same amount of support, the same CS_2 flow rate, and the relative humidity of 90 to 100%, the absorbent was effective for only a few minutes. Nevertheless, with maximum humidity and the same air flow rate, the cartridges retained CS_2 for several hours when the amounts of CS_2 were much smaller. When the water and CS_2 content of air are high, humidity can be

eliminated by using a prefilter containing magnesium perchlorate, which does not retain CS_2; but in most cases, such elimination is unnecessary.

LITERATURE CITED

(1) Hunt, E. C.; McNally, W. A.; Smith, A. F. *Analyst (London)*, **1973**, *98*, 585–92.
(2) Truhaut, René; Boudène, Claude; Nguyen-Phu-Lich; Baquet, André. *Arch. Mal. Prof. Med. Trav. Secur. Soc.* **1972**, *33*(7–8), 341–46.
(3) Smith, Darrell B.; Krause, Leonard A. *Am. Ind. Hyg. Assoc. J.* **1978**, *39*(12), 939–44.
(4) McCammon, Charles S.; Quinn, Patricia M.; Kupel, Richard E. *Am. Ind. Hyg. Assoc. J.* **1975**, *36*(8), 618–25.
(5) Sandalls, F. J.; Penkett, S. A. *Atmos. Environ.* **1977**, *11*, 197–99.
(6) Baumgardner, R. E.; Clark, T. A.; Stevens, R. K. *Anal. Chem.* **1975**, *45*, 563–66.
(7) Pearson, David C.; Hines, W. J. *Anal. Chem.* **1977**, *49*, 123–26.
(8) Godin, Jean; Boudène, Claude. *Anal. Chim. Acta* **1978**, *96*, 221–23.
(9) Franco, Douglas W.; Neves, E. A.; de Andrade, J. P. *Anal. Lett.* **1977**, *10*(3), 243–49.

RECEIVED for review April 16, 1979. Accepted August 10, 1979.

Quantitative Electron Spectroscopy for Chemical Analyses of Bitumen Processing Catalysts

G. M. Bancroft and R. P. Gupta[1]

Department of Chemistry, University of Western Ontario, London, Ontario, Canada

A. H. Hardin* and M. Ternan

Energy Research Laboratories, Department of Energy, Mines and Resources, Ottawa, Ontario, Canada

X-ray photoelectron spectroscopy (XPS or ESCA) has been used to analyze a large number of Mo/Al_2O_3 hydrodesulfurization catalysts containing nickel and cobalt as promoters. Results were obtained from conventional 3.2-nm diameter pressed or extruded pellets. Results were also obtained from four extruded catalysts which were ground and repressed in an infrared sample press. We thus obtain external pellet surface and pellet interior (or "bulk") ESCA analyses, respectively, from the above two sample types. Oxidation states of the metals have been assigned from the chemical shifts, while the computed areas of the deconvoluted ESCA bands have enabled quantitative determinations. The ESCA external pellet surface and ESCA interior "bulk" analyses are generally in good agreement with each other, and with the bulk chemical compositions. One commercial Ketjen catalyst, however, yielded an apparent exterior surface Mo concentration which is almost five times that of the chemical bulk and ESCA "bulk" compositions. The catalyst preparation method has a strong effect on the surface chemical composition. The surfaces of the gel impregnated metal oxide catalysts are more or less the same as their bulk, but this is not true for catalysts prepared by impregnation of calcined γ-Al_2O_3.

X-ray photoelectron spectroscopy (XPS) or ESCA (electron spectroscopy for chemical analysis) recently has been used widely to study molybdenum compounds (*1*, *2*) and Mo/Al_2O_3 hydrodesulfurization catalysts (*3–9*), usually containing Co as a promoter. The Mo 3d binding energies have been very useful in assigning the oxidation state and coordination environment of Mo in the oxidized and sulfided catalysts. However, the interpretation of the Co binding energies is less clear cut (*8*, *9*). ESCA studies of such catalysts with Ni promoters have not yet been reported.

In the past few years it has become clear that ESCA intensities can be used, with certain assumptions, to obtain quantitative analyses of surfaces (*10*, *11*). For example, Adams et al. (*11*) have concluded that atom ratios for the principal constituents of homogeneous inorganic compounds and minerals can be obtained with an accuracy, on average, of 5%. The most important factors affecting quantitative XPS determinations of homogeneous samples have been discussed, for example, by Wagner (*12*). However, in previous ESCA studies of heterogeneous catalysts, there has been no report of a fully satisfactory attempt to obtain quantitative elemental analyses of the catalyst surfaces. The problems of photoelectron attenuation by surface segregated and/or sintered metal particles have been discussed in detail for Ni/Al_2O_3 (*13*), Rh/C (*14*) and M/SiO_2 (*15*) catalysts, for example. In these cases the segregated, reduced metal particles, having thicknesses which are significant fractions of the photoelectron mean-free paths, directly attenuate the transmission of photoelectrons from both the metal and other, anterior atoms. The intensities of selected photoelectrons from the active, reduced metal and the support are thus incorrect, the degree of attenuation being a function of the low degree of metal dispersion and particle size.

Neglecting the effects of mass transfer limitations, it is evident that the catalytic activity will depend on the average composition of the total surface area (external and interior of pellets) rather than the average macroscopic bulk chemical composition. It is not clear that the concentrations of Mo, Ni, and Co on the particle surfaces in the pellet interiors of these catalysts are directly equivalent to, or even related to, their true bulk or macroscopic concentrations.

The prior quantitative ESCA studies on the external surfaces of reduced metal catalysts (*13–15*) have shown that considerable caution must be used in interpreting those ESCA results because of the metal atom segregation. However, for impregnated and unreduced metal-oxide catalysts it is accepted (*16*, *17*) that segregation of the catalyst from the support does not occur in the same way. Nor is it evident that external surface ESCA compositions need necessarily vary from the chemical, bulk compositions.

We have undertaken a detailed ESCA study of over 30 Mo/Al_2O_3 catalysts in the oxide and sulfide states to determine the oxidation states of the metals, the concentrations

[1] Present address: Division of Mechanical Engineering, National Research Council of Canada, Ottawa, Ontario, Canada.

0003-2700/79/0351-2102$01.00/0 Published 1979 by the American Chemical Society

of the metals on the surfaces, and on pellet interior, "bulk", surfaces. We report representative spectra which show that ESCA can be a very powerful, routine technique for such analyses. Detailed results are contained in a Departmental Contract report (*18*).

EXPERIMENTAL

The catalysts were prepared by a gel impregnation technique as discussed previously (*19*) and were examined in both oxided and H_2S presulfided forms (*20*). Average macroscopic chemical compositions were determined by atomic absorption. Surface areas were measured by a conventional N_2 BET method. Surface morphologies, particle types and sizes were examined by transmission electron microscopy, energy dispersive X-ray analysis, and X-ray diffraction.

The ESCA analyses of both oxided and sulfided catalysts were obtained on extruded pellets of 1-cm length and 3-mm diameter. In four cases, the pellets were ground and reformed into 0.5-mm thick disks in an infrared sample press. The analyses of these pellet interior surfaces should better approximate the average macroscopic compositions and we label these four ESCA analyses "bulk" in this paper.

Spectra were obtained using a McPherson ESCA 36 spectrometer with a Mg or Al anode. The angle between the incident photons and analyzed electrons was 90°. Eight samples were mounted on the sample carrousel. A number of extruded pellets were aligned in parallel across a sampling plate to give the maximum sensitivity. As a result of the relatively high concentration of physisorbed matter, sample degassing was quite considerable. The samples were not dehydrated prior to mounting in the ESCA chamber to avoid contamination by carbonaceous impurities. Consequently the chamber was pumped down overnight for each loaded set of samples.

Broad scans for all samples were obtained from 1000 to 0 eV binding energies with a channel width of 1 eV. Narrow scans (10–30 eV) for all the peaks of importance (Al 2p, C 1s, Mo 3d, O 1s, Ni 2p, and Co 2p) were obtained to high statistics where practicable.

The irregularity of the extruded pellet (essentially nonconducting) surfaces resulted in considerable charging (3 eV) and substantial differential charging which increased line widths to close to 3 eV. The line widths in the two, infrared style, pressed disks were considerably smaller because of the smoother, flatter surfaces of these disks. Binding energies were calibrated relative to the C 1s contaminant peak at 284.5 eV. This peak value was set at the value for graphitic C 1s obtained on the McPherson 36 spectrometer. However, since the C 1s binding energy shifts for different carbon chemical species, there is some potential uncertainty in the determinations of changing corrections. Confidence in the method used can be derived from the fact that, relative to C 1s, the corrected binding energies of both O 1s (531.1 eV) and Al $2p_{3/2}$ (73.8 eV) are constant to within ±0.1 eV over the whole series of samples. This suggests that our charging error correction method does not introduce errors of more than ±0.2 eV. However, both the O 1s and Al 2p values are 0.4 eV lower than typical literature values (O 1s 531.6 eV and Al 2p 74.3 eV (avg. of 7) relative to C 1s at 284.6 eV)(*21*).

The complex bands were deconvoluted using a program written by L. L. Coatsworth (*22*), and modified by one of us (R.P.G.) so that the splittings and areas of spin-orbit doublets could be constrained to their observed and/or theoretical values. Each spectrum was fitted with an analytical function consisting of Gauss–Lorentz functions and a linear base-line correction. The Co and Ni 2p peaks have substantial shake-up intensities associated with them, and we have included this shake-up intensity in the Co and Ni areas.

RESULTS

Qualitative Analyses. The familiar, typical broadscan is shown in Figure 1, and the major primary peaks are identified. It was important and pleasing that the C 1s contamination peak in this and other spectra was small. The spectrum clearly demonstrates that the attenuating effects of contaminant carbon on all photoelectrons of interest in this work should be minimal. From the narrow scans, the ranges

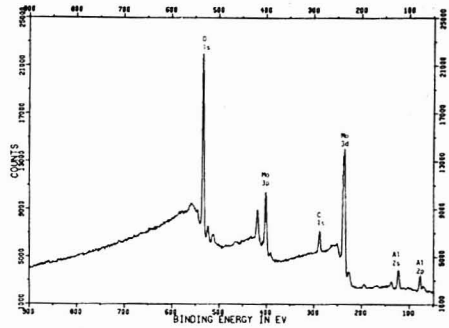

Figure 1. Widescan ESCA spectrum of the unused catalyst number 317 (Ketjen). The major primary peaks are noted

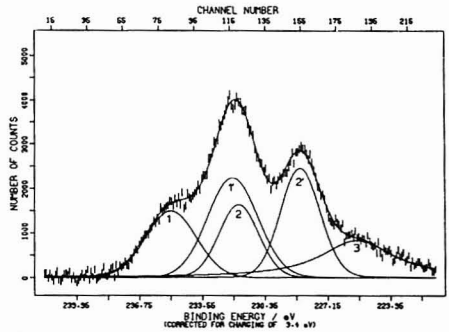

Figure 2. ESCA spectrum of the Mo 3d region in sulfided catalyst number 236. Peaks 1 and 1′ are assigned to MoO_3, peaks 2 and 2′ to MoS_2, and peak 3 to the S 2s peak

Table I. Binding Energies for the Major Species in Catalyst Samples[a]

peak	binding energy, eV[b]
Mo^{VI} $3d_{5/2}$	232.0 ± 0.5
Mo^{IV} $3d_{5/2}$	228.5 ± 0.2
Al $2p_{3/2}$	73.8 ± 0.2
O 1s	531.2 ± 0.2
S^{VI} $2p_{3/2}$	167.7 ± 0.2
S^{2-} $2p_{3/2}$	161.4 ± 0.2
Co^{II} $2p_{3/2}$	786.8 ± 0.5
satellite	786.8 ± 0.5
Ni^{II} $2p_{3/2}$	856.4 ± 0.4

[a] All binding energies are determined with C 1s at 284.5 eV as a reference. [b] The range of binding energies for all samples is given.

of binding energies for the most intense peak of each element were obtained (Table I). The oxided samples gave simple spectra with Mo $3d_{5/2}$ binding energies characteristic of MoO_3 (*1*, *2*), and Al 2p binding energies characteristic of Al_2O_3 (*23*). The Co and Ni binding energies, and shakeup satellite positions and intensities point to Co^{2+} (*8*, *24*) and Ni^{2+} (*23*, *25*) in oxide environments. The sulfided samples give two Mo doublets (Figure 2), mainly due to MoS_2 and MoO_3 (*7*). The sulfur 2p spectra contain both S^{2-} and S^{VI} (presumably SO_4^{2-}) (*23*). Figure 2 shows line widths, separations, and band shapes obtained for the peak area determinations by deconvolution. As well, error bars show the statistical uncertainty for the

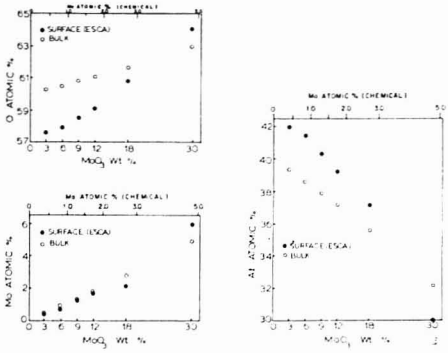

Figure 3. Variation of bulk (chemical analyses) and surface (ESCA) atomic percent for O, Mo, and Al as a function of MoO_3 wt % for the six Mo/Al_2O_3 test catalysts. The Mo at. % is shown on the top scale

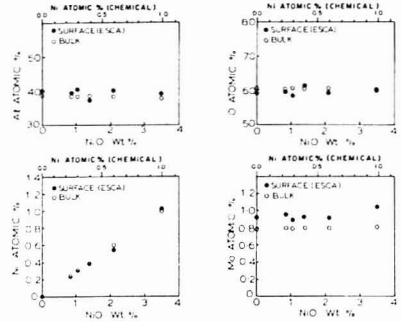

Figure 4. Variation of bulk (chemical analyses) and surface (ESCA) atomic percent for Al, O, Ni, and Mo as a function of NiO wt % in the six $Ni/Mo/Al_2O_3$ test catalysts. The Ni at. % is also shown on the top scale

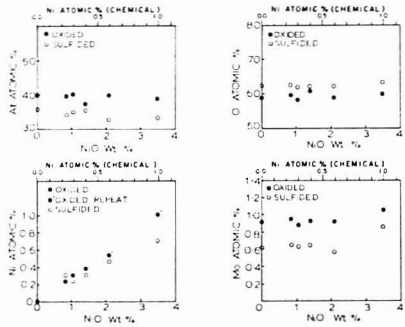

Figure 5. Variation of surface (ESCA) atomic percent in oxided and sulfided samples as a function of NiO wt %

electron counts for each channel analyzed. For any given catalyst there was no noticeable change in the Co $2p_{3/2}$ or Ni $2p_{3/2}$ binding energies on sulfiding. There are, however, noticeable binding energy trends as a function of catalyst concentration within a series of catalysts, but discussion of these trends will be reserved for another paper.

Quantitative Analysis. A number of workers have used ESCA band areas to obtain quantitative analyses of surfaces, and Wagner's recent article summarizes this important use of ESCA (*10*). In our treatment, we neglect the attenuating effect of the small C contamination layer, Figure 1, and the β asymmetry values (*10, 11, 26*). We can then write for a peak area, A_x, determined by this spectrometer:

$$A_x \propto n_x \sigma_x (\text{K.E.})_x^{1.7} \tag{1}$$

where n_x is the number of x atoms, σ_x is the probability of exciting a photoelectron—the so-called cross section (*27*), and K.E. is the kinetic energy of the outgoing photoelectron.

The transmission of the analyzer is linear with the kinetic energy, and Wagner (*10*) has shown that the mean free path or escape depth is proportional to $(\text{K.E.})^b$ for $0.68 < b < 0.82$. We take the escape depth dependence to be proportional to $\text{K.E.}^{0.7}$, and combine the transmission and escape depth functions to obtain $(\text{K.E.})^{1.7}$ in Equation 1.

The exact proportionality function in Equation 1 depends on such experimental parameters as the X-ray source power and X-ray source/sample/slit geometry, and is not known. However, the proportionality factor is constant for given instrumental settings, and thus, the *ratio* of two n's can be written as:

$$\frac{n_x}{n_y} = \frac{\sigma_y}{\sigma_x} \frac{(\text{K.E.})_y^{1.7}}{(\text{K.E.})_x^{1.7}} \frac{A_x}{A_y} \tag{2}$$

From Scofield's cross sections (*27*) and the measured peak areas and kinetic energies, we can determine in the usual way, first, the ratio of n's for all elements on the surface (excluding carbon) and, finally, the elemental compositions in atomic per cent.

We then can compare the ESCA results with the chemical compositions, Figures 3–5 and Table II. To obtain the chemical composition in atom per cent for this comparison we use the practical nominal weight per cent values from preparation, Table II (right column). If we use actual atomic absorption values, very similar atomic per cents are obtained. For example, the following atomic per cents are obtained from the preparative (and atomic absorption) values for catalyst 244: O, 62.8 (62.6); Al, 32.1 (32.8); and Mo, 4.88 (4.65). The results in Figures 3 and 4 show that for both the Mo and Ni/Mo oxide test catalyst series, the ESCA external pellet surface and macroscopic average chemical compositions are remarkably close—in nearly all cases within 5%. Another indication of the close agreement comes from plots (*18*) of external surface ESCA vs. macroscopic chemical analysis values for Al, O, and Mo. As a result of the layering of surface MoO_3 for loadings of less than 13 wt %, the four catalysts having 3, 6, 9, and 12 wt % MoO_3 are expected to give the best behavior. Linear least-squares correlations of data for these four samples yield correlation coefficients (R) of 0.992, 0.997, and 0.975, respectively. These R values indicate that the pellet external surface compositions determined by ESCA have relatively small uncertainties.

Despite our simplifying assumptions, we believe that the *differences* between the ESCA external pellet surface and chemical analyses, Figure 3, are not due to systematic errors. The results in Figure 3 show that these ESCA external pellet surface results are within 5% of the average macroscopic values and have considerably more precision than that.

The atomic absorption chemical analyses of the nonsulfided catalysts reported in this paper are given in Table II. In spite of the fact that the chemical compositions varied from 0 to 30 wt % MoO_3, the BET N_2 surface areas do not differ remarkably, Table II. We would normally expect the measured areas to have a precision of ±5%. For four catalysts we measured the areas 2 or 3 times. The variation in areas is

Table II. Chemical Analyses of the Catalysts

catalyst no.	atomic absorption analysis, wt % ± 5%				wt % of total		nominal wt % from preparation		N_2 Bet area
	Al_2O_3	MoO_3	NiO (CoO)	total[a]	MoO_3	NiO (CoO)	MoO_3	NiO (CoO)	M_2 g^{-1}
164	78.34	4.32	3.00	85.66	5.04	3.50	5.4	3.5	226 ± 5%
165	77.86	4.32	1.82	84.00	5.14	2.17	5.4	2.1	178 ± 5%
166	78.78	4.28	1.25	84.31	5.08	1.48	5.4	1.4	213 ± 5%
167	77.88	4.19	0.73	82.80	5.06	0.88	5.4	0.84	216 ± 5%
185	81.16	4.55	0.01	85.72	5.31	0.01	5.4	nil	179 ± 5%
188	77.99	4.41	0.92	83.32	5.29	1.10	5.4	1.05	-
233	91.48	2.90	--	94.38	3.07	--	3	--	193 ± 6%
234	89.59	5.30	--	94.89	5.59	--	6	--	189 ± 7%
235	85.55	8.60	--	94.15	9.13	--	9	--	215 ± 4%
236	84.55	10.90	--	95.45	11.42	--	12	--	215 ± 2%
244	67.45	25.40	--	92.85	27.36	--	30	--	198 ± 5%
245	80.18	16.70	--	96.88	17.24	--	18	--	183 ± 5%
314	74.18	10.52	(4.70)	89.40	11.76	(5.26)	12	(4)	
315	72.45	11.22	(4.20)	87.87	12.77	(4.78)	12	(4)	
316	74.52	10.61	(3.89)	89.02	11.92	(4.37)	12	(4)	
317	70.93	14.45	2.51	87.89	16.44	2.85	15	3	
318	71.46	13.56	(5.17)	90.19	15.03	(5.73)	16	(5)	

[a] It is assumed that the balance is H_2O.

somewhat better than ±5%, Table II. The similarities of areas indicates that the average microparticle size does not vary greatly from catalyst to catalyst. However, since MoO_3 external to the support is present in monolayer form (*16, 17*), we expect little of the surface areas to be derived from this MoO_3.

Conventional powder X-ray diffraction patterns of the two series of test catalysts indicated that the support phase is γ-Al_2O_3 having very small particle sizes or a high degree of microcrystallinity. Transmission electron microscopy did not indicate the formation of large crystallites of MoO_3 in the most heavily loaded catalyst. However, energy dispersive X-ray analysis of particles from the catalyst with 30 wt % MoO_3 indicated that the Mo/Al ratio varied from 1:2 to 2:1 depending on the individual particle studied. A more careful X-ray diffraction study of the 30 wt % MoO_3 catalyst, using a Guinier camera, identified a clear MoO_3 phase. However, no distinct Al_2O_3 pattern was found, as before. This might be due to the formation of an amorphous solid of Al_2O_3 incorporating part of the MoO_3 in the bulk. Subsequent particle size determinations gave a mean MoO_3 particle size of 4.0 nm for the 30 wt % MoO_3 sample.

From these characterizations and the previous work (*16, 17*), we conclude that the catalysts having less than 10–15 wt % oxide loadings, yield surface MoO_3 in highly dispersed, monolayer form. Only at very high loading is there evidence for MoO_3 crystallite formation. This is in stark contrast to the observed formation of aggregated metal particles in supported, reduced metal catalysts (*13–15*).

ESCA results for gel impregnated, mixed metal-oxide catalysts are in contrast to the ESCA results for supported, reduced metal catalysts (*13–15*). In the latter cases aggregation of the reduced metal atoms into metal particles leads to low degrees of dispersions (relative to a monolayer). The consequent anomalies in the ESCA determinations have been discussed in detail (*13–15*).

For Co-Mo-Al_2O_3 catalysts, however, it is generally accepted (*16, 17*) that MoO_3 occurring near the support surfaces is highly dispersed, most probably as partial monolayers on the Al_2O_3 spherulites. (For catalysts of about 200 m^2 g^{-1}, a full monolayer corresponds to about 13 wt %.) Above about 10–15 wt % molybdenum oxide, particles are believed to form, in addition to the monolayer, giving an increasing ratio of particulate and monolayered molybdenum oxides. At loadings below 13 wt % MoO_3, segregated monolayers are generally expected to exist (*16, 17*).

Photoelectrons scattered from such metal-oxide catalysts would not be attenuated in the same ways as for particulate, reduced metal catalysts. Within the error of the method, forward scattered photoelectrons from Al and O in anterior layers, as well as photoelectrons from Mo and O in the superior layers should all escape subject only to relatively normal depth attenuations. Thus the atom ratios determined by Equation 2 should be valid for gel impregnated, mixed metal-oxide catalysts. However, such ratios for catalyst made by impregnation of precalcined aluminas might be expected to yield less satisfactory results, especially at high coverages.

Figure 4 shows as well that for the Ni(Co)Mo series the external surface ESCA and macroscopic chemical values are very similar—even for Ni which is present in small amounts in these samples. However, the Mo ESCA values are systematically higher than the macroscopic chemical values by about 0.15 at. %. At the same time Al and O are, respectively, too high and too low compared to the chemical values. Since the differences extend to zero nickel content they could not be considered Ni induced. These trends are entirely consistent with the behavior of the MoO_3/Al_2O_3 series of catalysts, Figure 3.

The important quantitative ESCA results to be drawn from Figure 4 is that for constant MoO_3 content one can analyze for Ni, O, and Al with some confidence. Preparation of suitable standards within a family of catalysts is thus feasible.

For sulfided Co-Mo-Al_2O_3 catalysts, monolayer distributions of MoS_2 similar to those of MoO_3 are believed to predominate (*17*). However, the monolayer domains are expected to shrink upon reduction (*16*) from oxide to sulfide. The effect of sulfiding on the external surface ESCA composition is shown in Figure 5 for the Ni/Mo series of test catalysts. The differences between oxided and sulfided catalysts were usually small for Al and O (3–4% abs.). However, the sulfided catalysts usually had systematically lower Al, Mo, and Ni values (up to 50%, relative, for Mo). At the same time the determined oxygen content in the sulfided catalysts was systematically higher than in the oxides!

These systematic shifts can be explained on the basis of relative atomic populations in transforming from MoO_3/Al_2O_3 to MoS_2/Al_2O_3 to $xMoS_2/yMoSO_4/Al_2O_3$ during sulfiding and partial re-oxidation.

Quantitative ESCA and average macroscopic chemical analysis results for the series of five commercial catalysts are

Table III. Constituent Atomic % by Chemical Analyses and ESCA for the Unused Commercial Catalysts

	sample number											
	314		315		316			317			318	
element	chemical[a]	ESCA "bulk"[b]	chemical	ESCA "bulk"[b]	chemical	ESCA surface[c]	ESCA "bulk"[b]	chemical	ESCA surface[c]	ESCA "bulk"[b]	chemical	ESCA surface[c]
Al	36.2	31.6	36.2	31.7	36.2	31.4	31.2	35.6	14.8	34.0	34.8	29.8
Mo	1.83	1.87	1.83	2.39	1.83	2.43	2.29	2.31	12.67	2.72	2.49	2.90
O	60.8	65.1	60.8	64.3	60.8	64.6	64.9	61.2	72.0	63.3	61.2	65.2
Co(Ni)	1.17	1.48	1.17	1.59	1.17	1.60	1.56	0.89	0.54 Ni	not determined	1.50	2.06

[a] Determined average macroscopic composition by atomic absorption. [b] Determined from the extrudates by grinding and reforming as infrared style disks. [c] Determined from the original extrudates external surfaces.

given in Table III. Some of these catalysts were observed in the ground/reformed, pellet interior, or "bulk", form. With the exception of catalyst 317, the (i) chemical, (ii) external pellet surface ESCA, and (iii) interior pellet "bulk" ESCA results are in reasonable agreement. Thus, for catalyst 316, the ESCA "bulk" and external surface ESCA results are within 0.3% of each other. However, the ESCA results are not in as good agreement with the macroscopic chemical values as they were for the previous two series of test catalysts. For example, the indicated ESCA Mo contents average about 25% higher than the chemical value. At the same time one sees that the indicated ESCA Co(Ni) contents average 33% higher and the Al contents average 13% lower than the bulk chemical analyses, Table III. This type of discrepancy between quantitative ESCA analyses and chemical composition has been observed before (*13–15*). These differences in the commercial catalysts may well be caused by real differences between the average chemical composition and the surface structure.

However, one should also examine them on the basis of inhomogeneities in surface atom distribution, aggregation of metal atoms, and growth of particle size as a function of sintering. Each of these situations leads to a preferential escape of near surface photoelectrons over the attenuation of sub-surface photoelectrons. As well, in cases where catalysts were reduced to yield segregated metal particles, the ratios of photoelectron mean-free-paths to particle sizes determines the degree of overall and self-attenuation by the atoms (*13–15*).

The ESCA results given in Table III are more consistent with such inhomogeneities, i.e., aggregation of Mo and Co(Ni) oxide particles distinct from the Al_2O_3 support. (There is no ESCA peak consistent with the formation of molybdenum metal.) In such a case, one would expect high Mo and Co(Ni) ESCA values with lowered, attenuated Al content apparent. An extreme example of this effect was detected for commercial catalyst 317, Table III. The ESCA analyses of the exterior pellet surface gave Mo contents (12.67%) about 5 times that of both the pellet interior "bulk" ESCA results (2.72%) as well as the average macroscopic chemical analysis (2.51%). These results were verified several times on several portions of MB 317.

To determine if Ni in catalyst 317 (as contrasted to Co in all other samples in the 314–318 series) was related to the excessive exterior surface Mo concentration, we scanned two other catalysts, MB 132 and 143. The former contained 1 at. % Co, and the latter contained 1 at. % Ni. The ESCA external pellet surface Mo concentrations (1.3 at. %) were very similar in both samples, and in good agreement with the chemical compositions.

The successful analyses of the six MoO_3/Al_2O_3 and six $NiO/MoO_3/Al_2O_3$ test catalysts, compared to the less satisfactory analyses of the five commercial catalysts, can be attributed to the two different methods of preparation. Our test catalysts were prepared by dispersion of the catalyst and promoter precursors in AlOOH gels followed by dehydration, decomposition, and calcining to 500 °C. On the other hand the five commercial catalysts (Ketjencats, Akzo Chimie) give ESCA results entirely consistent with the impregnation preparation described by Moné and Moscow (*28, 29*) of Akzo Chimie. They describe catalysts similar to 314–318 that have very similar bulk chemical compositions. The commercial extrudates of γ-alumina were doubly impregnated with, first, ammonium molybdate and, second, cobalt or nickel nitrate solutions. In those cases, diffusion of Co(Ni) into the bulk is known to be very dependent on calcining temperature (*29*).

Based on the ESCA results, and corroborated by the X-ray diffraction results described above, the two series of MoO_3/Al_2O_3 and $Co/Mo/Al_2O_3$ test catalysts analyzed in this work are apparently relatively (ESCA) homogeneous.

ACKNOWLEDGMENT

We extend our thanks to J. Z. Skulski for A.A. determinations, to E. E. Laufer for transmission electron microscopic studies, to C. M. Mitchell for particle size determinations, and to R. A. Packwood for helpful suggestions and discussions.

LITERATURE CITED

(1) Swartz, W. E.; Hercules, D. M. *Anal. Chem.* **1971**, *43*, 1774.
(2) Tenret-Noel, C.; Verbist, J.; Gobillon, Y. *J. Microsc. Spectrosc. Electron.* **1976**, *1*, 255.
(3) Friedman, R. M.; Declerck-Grimee, R. I.; Fripiat, J. J. *J. Electron Spectrosc.* **1974**, *5*, 437.
(4) Cimino, A.; de Angelis, B. A. *J. Catal.* **1975**, *36*, 11.
(5) Ratnasamy, J. *J. Catal.* **1975**, *40*, 137.
(6) Stevens, G. C.; Edmonds, T. *J. Catal.* **1975**, *37*, 544.
(7) Stevens, G. C.; Edmonds, T. *J. Catal.* **1976**, *44*, 488.
(8) Walton, R. A. *J. Catal.* **1976**, *44*, 335.
(9) Declerck-Grimee, R. I.; Canesson, P.; Friedmann, R. M.; Fripiat, J. J. *J. Phys. Chem.* **1978**, *82*, 889.
(10) Wagner, C. D. "Quantitative Surface Analysis of Materials ASTM STP 643", McIntyre, N. S. Ed., ASTM, 1978; pp 31–46 and references.
(11) Adams, J. M.; Evans, S.; Reid, P. I.; Thomas, J. M.; Walters, M. J. *Anal. Chem.* **1977**, *49*, 2001.
(12) Wagner, C. D. *Anal. Chem.* **1977**, *49*, 1282.
(13) Shalvoy, R. B.; Reucroft, P. J. *J. Electron Spectrosc.* **1977**, *12*, 351.
(14) Brinen, J. S.; et al. *J. Catal.* **1975**, *40*, 295.
(15) Briggs, D.; *J. Electron Spectrosc.* **1976**, *9*, 487.
(16) Fransen, T.; van der Meer, O.; Mars, P. *J. Catal.* **1976**, *42*, 79.
(17) Massoth, F. E. *J. Catal.* **1977**, *50*, 190.
(18) Gupta, R. P.; Bancroft, G. M. "ESCA Analysis of Bitumen Processing Catalysts", CANMET Contract Report ERP7-9067, Department of Energy, Mines and Resources, Ottawa, 1978.
(19) Parsons, B. I.; Ternan, M. "Proc. Sixth Int. Congr. on Catalysis", Bond, G. C., Wells, P. B., Tompkins, F. C., Eds.; Chem. Soc.: London, 1977; Vol. 2, p 965.
(20) Ternan, M.; Whalley, M. J. *Can. J. Chem.* **1976**, *54*, 642.
(21) Wagner, C. D.; et al. "Handbook of X-ray Photoelectron Spectroscopy", 1st ed.; Perkin-Elmer: Eden Prairie, Minn., 1979.
(22) Coatsworth, L. L.; et al. *Anal. Chem.* **1975**, *47*, 586.
(23) Carlson, T. A. "Photoelectron and Auger Spectroscopy", 1st ed.; Plenum: New York, 1975.
(24) Chuang, T. J.; Brundle, C. R.; Rice, D. W. *Surf. Sci.* **1976**, *59*, 413.
(25) McIntyre, N. S.; Cook, M. G. *Anal. Chem.* **1975**, *47*, 2205.
(26) Reilman, R. F.; Msezane, A.; Manson, S. T. *J. Electron Spectrosc.* **1976**, *8*, 389.
(27) Scofield, J. H. *J. Electron Spectrosc.* **1976**, *8*, 129.
(28) R. Moné and L. Moscow, "Hydrocracking and Hydrotreating", *ACS Symp. Ser.* **20**, 150 (1975).
(29) R. Moné "Preparation of Catalysts", Delmon, B., Jacobs, P. A., Porncelet, G., Eds.; Elsevier, Amsterdam, 1976; p 381.

RECEIVED for review February 22, 1979. Accepted July 11, 1979. This work was supported by the Department of Energy, Mines and Resources and in part by DSS contract numbers 23440-7-9067 and 23375-8-7524.

Determination of Elemental Concentration Maps from Digital Secondary Ion Images

Wolfgang Steiger and Friedrich G. Rüdenauer*

SGAE, Lenaugasse 10, A-1082 Vienna, Austria

Contrast in secondary ion micrographs from topographically structured surfaces may include artifacts, i.e., intensity variations not related to proportional variations of local elemental concentration. Removal of artifact contrast is attempted by applying a numerical correction routine in each picture element of the digitized ion micrograph. Thus, elemental concentration maps may be obtained from ion micrographs of all elements present in the sample. In addition the microdistribution of concentration for at least one internal standard element has to be known. At present, image correction can be performed at a rate of approximately 0.2 s/pixel on a PDP 11 minicomputer.

Space resolved secondary ion mass spectrometry is a powerful technique for the compositional analysis of solids on a microscale. Instrumentation developed for this purpose, e.g., the scanning ion microprobe (*1*) and the ion microscope (*2, 3*) offer lateral resolution in the micron and submicron range and depth resolution of the order of 100 Å for the mass resolved secondary ion signal. It must however be realized that extreme care has to be taken when interpreting the secondary ion micrograph of a particular element as being representative for the quantitative distribution of that element across the sample surface (*4–9*). It has been demonstrated that "artifact contrast" in secondary ion micrographs, i.e., contrast not related to local variations of elemental concentrations can be created owing to phenomena inherent to the physical processes involved in secondary ion emission and detection. The most important of these contrast effects have been identified in previous papers (*6, 9*). On flat surfaces, artifacts may be produced by:

(a) Matrix contrast, i.e., local variations in absolute and relative ion yield due to local variations in matrix composition or locally variable presence of adsorbed reactive gas species (e.g., oxygen).

(b) Crystallographic contrast, i.e., variations in ion yield due to locally variable orientation of microcrystallites with respect to the sample surface (*10, 11*).

On rough surfaces additional artifacts may be introduced by:

(c) Topographic contrast, i.e., local variations in secondary ion collection efficiency due to topographic microstructure (*6, 9*).

(d) Chromatic contrast, i.e., element-dependent ion collection efficiency due to element-dependent ion emission energies (*6, 8*).

In addition to the sample-related effects (a–d) the ion detector itself may cause distortions of the contrast in secondary ion images. Detector-related discrimination appears to be particularly important in instruments of the ion microscope type. Fassett et al. (*5*) have taken into account nonhomogeneous detector response and detector nonlinearity due to the blackening of photographic film, when the ion micrograph is recorded by direct film exposure in the converter section of the ion microscope and digitized in a scanning microdensitometer.

Further attempts to remove artifact contrast from secondary ion micrographs include the application of a relative sensitivity factor correction (*7*), simplified 2-parameter LTE correction of every pixel of the digitized elemental ion images (*8*) and

0003-2700/79/0351-2107$01.00/0

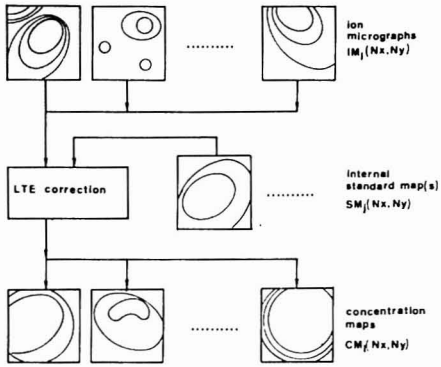

Figure 1. Quantitative image correction, using LTE algorithm (schematic)

fast analog referencing of the mass-selected to the total emitted ion current (total current monitoring (*4*)). With exception of the LTE approach, these procedures can only correct for a proportional variation of the signal level in all elemental images and therefore should be mainly useful for removal of topographic contrast. The 2-parameter LTE approach described in (*6*, *9*) generally provides for nonlinear local variations of relative secondary ion yields which have to be expected when matrix and chromatic contrast are present. It is, however, a computationally not very fast algorithm. Owing to the great amount of multidimensional data representing corresponding digitized secondary ion micrographs of a number of different elements, computational speed is of utmost importance when one considers removal of artifact contrast by digital methods. We have therefore developed a fast correction algorithm which is based on a 1-parameter LTE procedure similar to that developed by Morgan and Werner (*12*).

Quantitative Correction of Secondary Ion Micrographs. Quantitative correction of a set of corresponding ion micrographs is equivalent to performing a complete quantitative elemental point analysis in each pixel (= picture element) of a digitized "scene" of a selected sample area. Here the term "scene" is used to designate the set of locally registered ion micrographs of all elements present in a certain sample area. Quantitative elemental point analysis by means of simplified 2- or 1-parameter LTE (local thermal equilibrium) (*12–14*) requires monatomic elemental ion currents of all elements present in the analytical sample point as well as absolute atomic concentration values for one or more internal standard elements as input data. Extending this to LTE analysis of a 2-dimensional sample area, the following input data are needed (see Figure 1):

(a) Registered ion micrographs of all elements present in the imaged sample area ("input scene"). These should be already available in digitized form, i.e., a digitized ion current (ion count) value per element in each of the $N(x)\cdot N(y)$ pixels and should be corrected for detector distortion;

(b) Absolute concentration values for one or more internal standard elements in each pixel; these values may be thought of being arranged in 2-dimensional "internal standard maps". These maps should already be registered with respect to the ion micrographs.

Now, in each of the $N(x)\cdot N(y)$ pixels corresponding ion currents and concentration values from the set of input micrographs and internal standard maps are sent through a LTE correction routine, yielding absolute concentration values for all elements for which ion micrographs are available. Thus, computed elemental "concentration maps" are obtained showing the "true" 2-dimensional distribution of elements across the imaged sample area.

Two problem areas, however, warrant further discussion: the question of how to obtain internal standards and the capability of LTE to compensate for the local contrast effects described in the previous section. Obviously correction of secondary ion micrographs generally requires "local standards" on a microscale as compared to the "global standards" used in conventional LTE analysis of flat, compositionally homogeneous samples. There, internal standard concentrations may be derived from a bulk analysis of the sample by other standardized analytical techniques. Such an approach may be taken in image correction only if it can be assumed that the element selected as global internal standard is homogeneously distributed within the imaged sample area so that contrast in the ion micrograph of that standard element is "artifact contrast" in the sense discussed above. In all the other cases, local standards have to be defined in each pixel. New techniques obviously have to be envisaged for this purpose, e.g., application of multiple space resolved analytical techniques on the same sample (electron microprobe, Auger microprobe, etc.).

A more basic question, however, is the applicability of LTE to quantitative correction of secondary ion micrographs of topographically structured surfaces. At present it is acknowledged that LTE gives useful semiquantitative analytical results on flat samples although there is considerable disagreement concerning the existence of a plasma in local thermal equilibrium (LTE) at the ion-bombarded sample surface (*12–15*).

In this paper the acronym "LTE" simply is used to designate a mathematical correction algorithm (which incidentally can be derived from hypothetical equilibrium assumptions). Considering specifically 2-parameter LTE (where two fitting parameters T and η_e are used), it has been shown that Andersen's original computer code CARISMA (*15*) can be considerably simplified (*13*) without noticeably affecting analytical accuracy (*16*). The 1-parameter LTE approach recently developed by Morgan and Werner (*12*) (using only one fitting parameter T) has also been shown to yield satisfactory analytical accuracy although considerably less experimental data are available. Accepting the viability of 2- or 1-parameter LTE for analysis of flat surfaces immediately leads to the consequence that these models should also be capable of correcting for topographic and matrix contrast on rough surfaces. Pure topographic contrast is a geometrical effect and leads to proportional variations of secondary ion signals for all detected elements. Since ion current ratios only enter into LTE, a common factor of proportionality does not influence analytical results. Matrix contrast elimination of course is also an inherent feature of LTE, due to the freedom in fitting the model parameters T, η_e, or T alone to known (local) internal standard concentrations. Chromatic contrast compensation is not immediately obvious. It has been pointed out in (*6*) and (*9*) that the electrostatic microfields in front of local surface structures affect an energy preselection of secondary ions before they enter the mass analyzer. It has been demonstrated for 1-parameter LTE that very similar analytical results can be obtained irrespective of the energy bandpass setting of the mass analyzer (*12*). However, consistently higher values for the fitting parameter T ("temperature") were obtained for higher transmitted initial ion energies. No satisfactory theoretical explanation can yet be offered for this finding. Accepting however the experimentally verified phenomenon, it appears very likely that chromatic contrast conpensation should be within the capabilities of 1-parameter LTE since it should not matter whether ion energy selection is performed by surface microstructure or the ESA setting.

Very little is known about the physics of crystallographic contrast, particularly as far as variations of relative secondary ion intensities with crystal orientation are concerned; consequently, no conclusions may be drawn with respect to contrast compensation by LTE correction.

EXPERIMENTAL

We have applied the 1-parameter LTE image correction method to ion micrographs obtained from a fracture surface of a 5-component glass sample. Such a surface is topographically strongly structured and exhibits ridges and crevices of up to 20-μm height. Consequently, artifact contrast may be expected. Positive ion micrographs of the main isotopes of the constituent elements were taken on a UHV Scanning Ion Microprobe described elsewhere (*17*) in a frame-interlaced rather than in an element-interlaced mode (i.e., a complete frame for one element was recorded, after which the spectrometer was set to the next element and the next frame was recorded). Detector ion currents were digitized in a 23 × 23 square raster and stored on magnetic disk. The scanned target area was 1 × 1 mm^2, spot resolution was of the order of 10 μm and resolution in the digitized image 40 μm (due to the large sampling interval).

Since in this particular sample no isotopic or molecular overlap was detected for the main isotopes, these five isotopic ion micrographs were sufficient to define the input scene in the sense of Figure 1. The evaluation of this particular scene using a 2-parameter LTE correction routine has been described previously (*9*). This computer routine had a running time of about 10 s/pixel so that a full scene correction needed almost 2 h of computer time on a PDP 11/34 minicomputer. In this paper we want to report on the results of a fast 1-parameter LTE routine allowing correction of the same scene in less than 2 min.

Basically, Morgan and Werner's approach, described in detail in (*12*), was taken with two modifications which are essential to increase computation speed and avoid divergences of the algorithm in single image points. Their approach consists of an iterative fit of the parameter T to the mass spectral input data and the internal standard concentration(s) until successive T steps differ in amounts less than an arbitrary value (1%). We are using a starting "temperature" for the iteration which is identical to the optimum fit temperature of the neighboring pixel, thus considerably reducing the number of iterations needed. The overall fit of all elements contained in a sample to the exponential "Saha–Eggert line" (*12*) is influenced very little by a large misfit of a single trace element (such as As). Therefore, the convergence condition of a constant T fraction is changed to a more stringent constant T difference (ΔT = 30 K) since a detailed analysis of the convergence behavior of the algorithm has shown that the fit of a trace element to the Saha–Eggert line is considerably improved when the convergence value of T is approached as closely as possible.

This modified algorithm now is sequentially applied to each pixel of the input scene in a row oriented sequence. The resulting concentration maps (see Figure 1) are stored on magnetic disk. In addition, distribution maps for the parameter T and the error of fit (of calculated concentration values to observed ion currents) are included in the output file. In the calculations described here, oxygen was used as a "global" internal standard with the bulk value for the oxygen concentration. From other information available, good elemental homogeneity of the bulk sample may be expected (*18*). In addition elemental inhomogeneities which might be present near the surface or near inner voids (bubbles) should be much less pronounced for the matrix oxygen than for the oxide cations.

The computer program package was developed to perform image correction, image handling, and display functions. The programs are written in FORTRAN IV and have the following capabilities:

(1) The input scene may consist of an arbitrary number of lines and number of columns; nonsquare images may also be accepted.

(2) The input scene may contain up to 10 elemental micrographs, up to 4 molecular ion maps (not used in the image correction routine), and up to 3 internal standard maps. In addition, up to 10 global standards may be specified.

Table I. Computation Times for Various LTE Image Correction Procedures, Implemented on a PDP 11 Minicomputer

algorithm/configuration	time/pixel	time/image, 64 × 64
CARISMA (*20*)	20 s	23 h
simplified 2-parameter LTE (*14*)	10 s	11 h
fast 1-parameter LTE/ no floating point processor (this work)	0.15 s	10 min
fast 1-parameter LTE/ float. point proc.	0.03 s[a]	2 min[a]
fast 1-parameter LTE/ array processor	2 ms[a]	8 s[a]

[a] Estimated values

(3) Quantitative correction may be performed on the full input scene or on an arbitrary subscene (defined by first and last pixel and pixel jump for both axes).

(4) Elements, for which a corrected concentration map is stored, may be individually specified; this feature serves to conserve storage space.

(5) A factor representing the spatial dimensions of the scanned sample area (in μm) may be specified; this "scale factor" is automatically adapted when a subimage is corrected or displayed.

(6) For display purposes, low resolution single images or full scenes may be 2-dimensionally interpolated to a finer image raster.

(7) Square images may be interpolated from a small number of horizontal high resolution linescans which are taken at equidistant vertical line spacings and cover a square image field.

(8) Display of ion micrographs, concentration maps, and standard maps is possible using lines of equal concentration (or equal intensity) or intensity-modulated display on the screen of a storage oscilloscope (in the latter case point density modulation techniques are used).

(9) In the intensity modulation mode, contrast stretch or contrast modification may be performed.

(10) Zooming or subimage display is possible.

(11) Full screen or split screen (quadrant) display of multiple images may be selected;

The programs are implemented on a PDP 11/34 minicomputer with 48-k words of core memory and two 1,2-Mword magnetic disks, operating under RSX 11-M control. No hardware floating point processor is installed. A Tektronix 613 storage scope, driven by a DEC LPS11 interface, is used as an image display.

RESULTS AND DISCUSSION

The results of the image correction procedures described above are shown in Figures 2 and 3. In Figure 2, a–c, uncorrected ion micrographs are shown in the top rows, the corresponding LTE-corrected elemental concentration maps in the bottom rows of intensity modulated split-screen storage scope displays. Also shown in Figure 2c are the distribution of the fitting parameter (T) and the error of fit (ERRFAC) across the analyzed sample area. In these figures, the input scene of 23 × 23 pixels has been interpolated to size 64 × 64 for better display appearance before being LTE-corrected. The images are displayed using brightness levels equally spaced between zero and maximum image intensity. Figure 2d illustrates some of the image handling features which can be easily software-implemented when a digitally stored image is available. All four subimages show a zoomed subsection of the corrected concentration map of silicon; different contrast functions are used in the first three subimages (clockwise from lower left), isoconcentration lines are shown in the fourth subimage. Note that the length scale displayed has been adjusted to give the correct spatial dimensions of the zoomed image section. The zooming and contrast modification feature of course can also be implemented in the iso-intensity line display mode as shown in Figure 3, a and b.

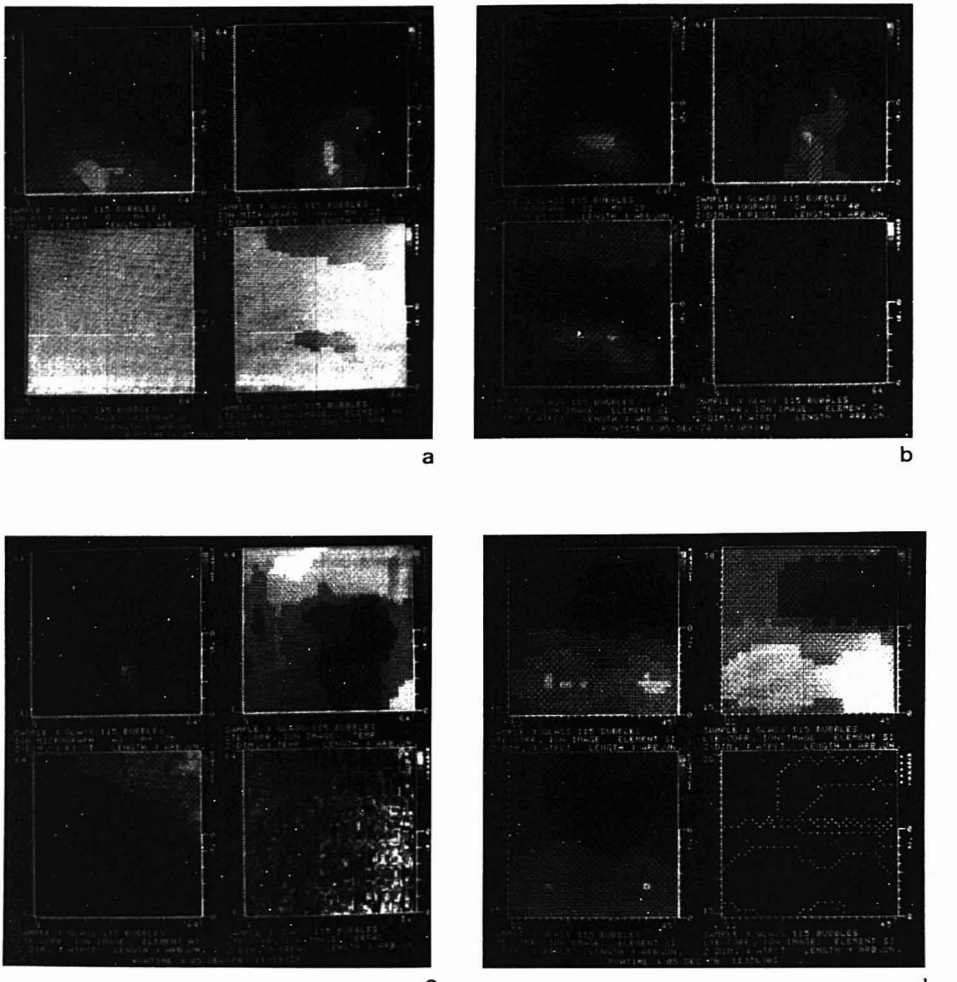

Figure 2. Ion micrographs and LTE-corrected concentration maps from a glass fracture surface; if not stated otherwise, linear equidistant intensity levels between 0 and maximum ion count I_{max} and maximum concentration c_{max}, respectively. (a) O . . . I_{max} = 1988 PIXCT, c_{max} = 58.34 ATPCT; Na . . . I_{max} = 6659 PIXCT, c_{max} = 39.86 ATPCT. (b) Si . . . I_{max} = 32793 PIXCT, c_{max} = 12.33 ATPCT; Ca . . . I_{max} = 4964 PIXCT, c_{max} = 10.55 ATPCT. (c) As . . . I_{max} = 2626 PIXCT, c_{max} = 4.61 ATPCT; *T* . . . linear equidistant levels, 11000–14272 K, ERRFAC . . . linear equidistant levels between 1.000–1.003. (d) Zoomed image, concentration map of Si; equidistant levels 1.08–12.33 ATPCT (upper left); logarithmic equidistant levels (upper right); high range expanded 2.0, 7.0, 11.0, 12.0, 13.0 ATPCT (lower left); logarithmic equidistant isoconcentration lines as in upper right (lower right)

The analytical accuracy of the corrected elemental maps displayed in Figures 2 and 3 primarily of course depends on the correctness of the assumption of a homogeneous oxygen concentration. As has been stated in the previous section this assumption appears to be reasonably justified. Furthermore, average concentration values as determined from the LTE-corrected concentration maps are in good agreement with bulk analyses of the same glass sample (*18*); the range of concentrations in the corrected map for As agrees within a factor of about 1.5 with maximum and minimum As concentrations obtained in selective analyses of As-enriched and undisturbed bulk zones respectively (*19*); and the contrast range in the concentration maps shown in Figure 2 is generally decreased compared to the corresponding ion micrographs. Such a behavior may be expected when artifact contrast is dominating in the ion micrographs. The use of the 1-parameter LTE approach does not appear to introduce additional analytical error when compared to the more frequently used 2-parameter approach. This is demonstrated in Figure 4 where for a single line of the Ca^+ image the corrected concentration data are

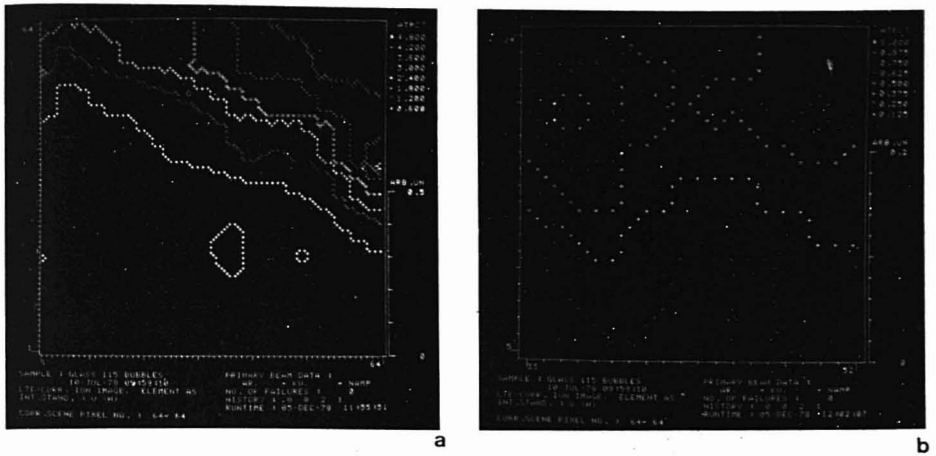

Figure 3. Iso-concentration line display of LTE-corrected As map; (a) full scene, equidistant linear concentration levels, (b) subscene, expanded concentration levels

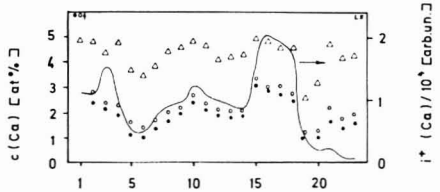

Figure 4. Line scan data for calcium, corrected by different LTE algorithms; (——) uncorrected data for $^{40}Ca^+$; (●) 1-parameter, internal standard O; (○) 1-parameter, internal standards O, Ca; (△) 2-parameter, internal standards O, Ca

shown for two different versions of the 1-parameter and the simplified 2-parameter approach (*14*). It can be seen that relative contrast for the two correction methods is very similar but that the average computed concentration levels differ by about 40%. This however is the same order as the generally accepted accuracy level of the LTE algorithm (*12–14, 16*).

Because of the inherent properties of the LTE algorithm, the relative correction factors which have to be applied to the elemental ion currents to obtain absolute concentration figures depend exponentially on the fit parameter T. The observed variation of T across the scanned area (Figure 2c) shows that in this sample the correction factors exhibit strong local variations. Therefore, neither the total ion current ratioing method (*4*) nor the relative sensitivity factor method (with RSFs constant across the sample (*7*)) would yield correct results on this particular sample, because none of these methods provides for locally varying correction factors. Since, from the contrast effects previously described, only topographic contrast can be eliminated by normalization to the total secondary ion current, the observed local variation in T also shows that the contrast in the ion micrographs of Figure 2 cannot be caused by topography alone.

Compared to the original CARISMA version of LTE, the computation time has been considerably reduced in our version of the model (see Table I). It can be seen that an order of magnitude saving in computation time may be expected when using state of the art commercially available array processors.

CONCLUSION

Quantitative correction of secondary ion micrographs from a topographically structured fracture surface of a glass sample has been attempted, using a fast 1-parameter LTE routine. Strong indications are offered for the capability of this method to remove artifact contrast from uncorrected ion images. Much work however still needs to be done in the definition and evaluation of local internal standards and in a basic investigation of contrast mechanisms in secondary ion micrographs before quantitative image correction can be thought of as a standard analytical technique. When these problems can be satisfactorily solved, state of the art computer hardware would allow one to obtain corrected elemental concentration maps quasi on-line to ion microprobe analysis of a solid sample.

LITERATURE CITED

(1) H. Liebl, *J. Appl. Phys.*, **38**, 5277 (1967).
(2) G. H. Morrison and G. Slodzian, *Anal. Chem.*, **47**, 932A (1975).
(3) J.-M-Gourgout, *Mikrochim. Acta*, in press.
(4) H. Kobayashi, K. Suzuki, K. Yukawa, H. Tamura, and T. Ishitani, *Rev. Sci. Instrum.*, **48**, 1298 (1977).
(5) J. D. Fassett, J. R. Roth, and G. H. Morrison, *Anal. Chem.*, **49**, 2322 (1977).
(6) F. G. Rüdenauer, W. Steiger, and H. W. Werner, *Proc. 7th Intern. Vac. Congr. and 3rd Int. Conf. Solid Surf. (Vienna, 1977)*, R. Dobrozemsky et al., Eds.
(7) J. H. Schilling and P. A. Büger, *Int. J. Mass Spectrom. Ion Phys.*, **27**, 238 (1978).
(8) A. Breth, R. Dobrozemsky, F. G. Rüdenauer, and W. Steiger, SGAE-Report No. 2673, Oct. 1976, available from Dr. H. W. Werner, Philips Research Labs., Eindhoven, The Netherlands.
(9) F. G. Rüdenauer, W. Steiger, and H. W. Werner, *Mikrochim. Acta*, in press.
(10) M. Prager, Ph.D. Thesis; Universität Tübingen, West Germany, 1975.
(11) G. J. Scilla and G. H. Morrison, *Anal. Chem.*, **49**, 1529 (1977).
(12) A. E. Morgan and H. W. Werner, *Mikrochim. Acta*, **II**, 169 (1978).
(13) D. S. Simons, J. E. Baker, and C. A. Evans, *Anal. Chem.*, **48**, 1341 (1976).
(14) F. G. Rüdenauer and W. Steiger, *Vacuum*, **26**, 537 (1976).
(15) C. A. Andersen and J. R. Hinthorne, *Science*, **175**, 853 (1972).
(16) D. S. Smith and W. H. Christie, **ORNL/TM-5728** (1977).
(17) F. G. Rüdenauer and W. Steiger, *Jpn. J. Appl. Phys., Suppl. 2*, Pt. 1, 33 (1974).
(18) F. Meijer, Philips Research Labs, private communication, 1977.
(19) A. Breth, R. Dobrozemsky, F. G. Rüdenauer, and W. Steiger, SGAE-Report No. 2926, May 1978; available from H. W. Werner, Philips Research Labs, Eindhoven, The Netherlands.
(20) D. E. Newbury, National Bureau of Standards, Washington, D.C., 1978, private communication.

RECEIVED for review December 18, 1978. Accepted June 14, 1979.

Processing Elemental Microanalytical Data

Bruno Colombo and Guido Giazzi

Carlo Erba Strumentazione, Rodano, Milan, Italy

Ermes Pella*

Farmitalia Carlo Erba, Ricerca e Sviluppo Chimico, Milan, Italy

A method of simultaneous CHNS microdetermination, based on combustion and gas chromatography, is used with an aim at establishing the mutual atomic ratio of the four elements without having to weigh the samples. Thus firstly the reproducibility of the four integrated TC signals in the sample weight range of 0.2–1.5 mg is checked by comparing integral binary ratios; then the relationship between integral binary ratios and atomic binary ratios is experimentally determined and found linear. After having worked out the three relevant linear equations, since they are permanently valid for the same analytical method and the same type of analyzer, they can be introduced into the CPU memory of a data processing unit, which processes the data from the unweighed analyzed samples and calculates the corresponding CHNS ratios with no need for references substances. Moreover, when the sample weight is known, the data processing unit is able to carry out the probabilistic analysis of the percentage remainder, providing information on the components of the molecule other than CHNS.

Over the past few years some papers (*1–4*) have appeared concerning the possibility of elemental analysis of organic substances without weighing the sample, obtaining the analytical results in the form of atomic ratios. Clearly, the more elemental indications that are obtained from the same sample during one analytical process, the more valid this approach will be. Since a multielement determination method which simultaneously determines C-H-N-S has been set up recently by us (*5*), we tried to develop a new calculation method to relate digital data obtained from integration of thermal-conductimetric signals with the elemental composition of the sample, without knowing the amount of substance analyzed.

Moreover, when the sample weight was known, we tried to obtain analytical indications not only on the elements analyzed directly but also on unknown constituents which make up the rest of the molecule.

The analyzer was coupled to a data processing unit which integrated and processed the data, made the necessary calculations, and printed out the results as atomic ratios, or as percentages of the analyzed elements, with the percentage remainder expressed as atomic mass units.

Principle of the Method for Calculating Atomic Ratios. In usual microanalytical practice, it is customary to express the concentrations of several elements as percentage values, but this means the weight of the sample must always be known in advance.

For relative analysis methods such as combustion-GC, besides the weight of the sample, one must also know a calibration factor, obtained by combusting a known amount of reference compound. Mathematical calculation of the percentages is then done using Equation 1 to determine the calibration factor K, then Equation 2:

$$K = \frac{\%\mathrm{X}_{\mathrm{ref}} W_{\mathrm{ref}}}{I_{\mathrm{ref}}} \quad (1)$$

$$\%\mathrm{X} = \frac{I_{\mathrm{x}} K}{W_{\mathrm{x}}} \quad (2)$$

where X is the element determined, W its weight and I the peak area integral of the relevant combustion gas.

From the percentage values, one can then mathematically work out the ratio of the atoms detected, and—provided all the elements of the molecule have been detected—the empirical formula.

On the basis of this method of calculating atomic ratios, Häberli (*2*) set up a mathematical procedure to obtain the atomic ratio of the elements detected without needing to know the weight of the sample. His method requires only the integration values of the CO_2, N_2, and H_2O peaks produced by combusting unknown amounts of the sample and reference substance. Häberli's method has been applied by others (*3, 4*) and also modified (*3*).

We maintain, however, that a method aimed at obtaining atomic ratios without weighing the sample must rely simply on the assumption that for an unknown compound the ratio between its atoms can be established directly on the basis of the resulting combustion gases, and therefore from measurements of their thermoconductivity in a helium stream. Obviously there must be a linear relation between TC measurements and combustion gases, which was already demonstrated by us (*5, 6*). In the GC-combustion method described (*5*), therefore, for an unknown, unweighed sample, four integration values are obtained for N_2, CO_2, H_2O, and SO_2. Singly these values mean nothing, but taken as binary ratios they can provide a decipherable analytical response.

We considered only the following three of the various binary integral ratios: I_{CO_2}/I_{N_2}, I_{CO_2}/I_{H_2O}, and I_{CO_2}/I_{SO_2}.

Integration values are taken in relation to I_{CO_2} since carbon is always present and is usually detectable with the greatest accuracy.

The constancy of the binary ratios for a given sample in the method described has been checked by analyses with variable amounts of a reference sample containing CHNS (Table I).

The binary integral ratios remained constant despite weight differences. Prerequisites for obtaining good values are an accurate blank determination and high purity of the tin containers and the analytical reagents. The upper limit of weighing can be reasonably established at 1.5 mg whereas some variations can be seen for weighings smaller than 0.2 mg.

The binary integral ratios clearly start to change whenever the elemental composition differs. Nevertheless the integral ratios can be seen to be linearly related to the corresponding atomic ratios when the former are plotted against the latter in a diagram. Such a graph can be drawn exactly only after several analytical measurements have been made with test substances showing different but known elemental composition, aimed at establishing the greatest possible number of

0003-2700/79/0351-2112$01.00/0

Table I. Binary Integral Ratios for Cystine

weight, mg	I_{CO_2}/I_{N_2} ratio	I_{CO_2}/I_{H_2O} ratio	I_{CO_2}/I_{SO_2} ratio
0.1230	7.11	1.96	2.74
0.1695	7.12	1.92	2.65
0.1750	7.20	1.89	2.67
0.2920	7.28	1.88	2.61
0.3024	7.21	1.84	2.60
0.4981	7.17	1.90	2.55
0.5807	7.23	1.85	2.63
0.6091	7.25	1.85	2.57
0.7274	7.21	1.87	2.56
0.7966	7.24	1.84	2.57
0.8546	7.15	1.84	2.57
0.9018	7.21	1.86	2.56
1.0005	7.18	1.83	2.54
1.0721	7.19	1.84	2.56
1.1468	7.17	1.87	2.53
1.2603	7.24	1.84	2.54
1.4152	7.16	1.80	2.56
1.6112	7.10	1.78	2.53

Table II. Establishment of the Linear Relationship C/N against I_{CO_2}/I_{N_2}

reference substance	atomic ratio	integral ratio[a]	slope
urea	0.5	1.197	0.418
adenine	1	2.400	0.417
picric acid	2	4.850	0.412
2-thiouracile	2	4.820	0.415
cystine	3	7.190	0.417
nicotinamide	3	7.214	0.416
sulfapyridine	11/3	8.810	0.416
S-benzylthiouronium chloride	4	9.612	0.416
diphenylguanidine	13/3	10.45	0.415
sulfanilic acid	6	14.50	0.414
acetanilide	8	19.28	0.415
$C_{20}H_{18}N_2O_3$	10	24.15	0.414
benzanilide	13	31.44	0.414
atropine	17	40.82	0.416

[a] Average values.

points where the coordinates meet. The line drawn appears to fulfil a straight-line relationship whose equation is obtained by the least squares method.

An example of the study of the linear function for atomic ratios C/N against binary ratios I_{CO_2}/I_{N_2} is shown in Table II.

The line obtained is straight and the linear relationship is represented by the following equation:

$$y = -0.0006 + 0.415x \quad (3)$$

This procedure was applied in other cases too. The atomic ratio C/S being known, we experimentally worked out the I_{CO_2}/I_{SO_2} ratios. Again, a straight line was obtained, passing next to the zero point, and giving the following equation:

$$y' = 0.0005 + 1.13\,x' \quad (4)$$

The equation for C/H ratios against I_{CO_2}/I_{H_2O} was similarly established, taking care of reducing to a minimum the blank of water when the greatest I_{CO_2}/I_{H_2O} values are worked out. The corresponding equation is:

$$y'' = 0.0095 + 0.2608x'' \quad (5)$$

We could also supply the values for the other linear functions referring to the N/H and N/S ratios, but we consider these equations of no use for our calculation method.

When Equations 3, 4, and 5 are known, any unknown substance can be analyzed using the GC-combustion method described, without the sample needing to be weighed. Four integration values will be obtained, giving three integral ratios from which three binary atomic ratios can be obtained, and hence the partial empirical formula. The C/H ratio is the most difficult to establish, since C/H can have many slightly differing values; however the y'' value from Equation 5 is reliable and can be used by itself.

An example of atomic ratio calculation without sample weighing is as follows:

Integration values after blank subtraction from I_{N_2} and I_{H_2O}:

$$I_{N_2} = 29563$$
$$I_{CO_2} = 211968$$
$$I_{H_2O} = 113960$$
$$I_{SO_2} = 82476$$

Integral binary ratios:

$$I_{CO_2}/I_{N_2} = \frac{211968}{29563} = 7.17$$

$$I_{CO_2}/I_{H_2O} = \frac{211968}{113960} = 1.86$$

$$I_{CO_2}/I_{SO_2} = \frac{211968}{82476} = 2.57$$

	deduced atomic ratios:
From Equation 3: $y = 0.415 \times 7.17 = 2.98$	C_3N_1
From Equation 4: $y' = 1.13 \times 2.57 = 2.90$	C_3S_1
From Equation 5: $y'' = 0.01 + 0.261 \times 1.86 = 0.496$	C_nH_{2n}

Partial empirical formula: $(C_3H_6N\,S)_n$

The straight-line relationships achieved by us with one instrument are clearly obtainable with all instruments based on TC measurements and a similarly efficient combustion principle. What is more, the relationships remain constant regardless of the type of sample analyzed and of differences in analysis conditions (reactor and GC-oven temperature, carrier gas flow rate). They are affected only by incomplete combustion and adsorption phenomena.

The amount of calculation required starting from the four original integration values in order to determine the partial empirical formula calls for time and effort if done manually. If possible, it should be done by a data processing unit which can integrate peak areas, acquire, compare, and process data, and display the final value. The method of coupling the analytical instrument to a data processing unit is described below.

EXPERIMENTAL

Figure 1 shows the scheme of the elemental analyzer coupled to a data processing unit. This coupling, working now as a prototype, will be commercially produced in the near future. The samples, in tin capsules, are loaded into a multiplace sample holder, then dropped sequentially into the reactor at 1050 °C to coincide with oxygen enrichment of the helium carrier gas. A combustion mixture forms which, after going through suitable oxidative and reductive catalytic layers, enters the GC column. The individual components are separated, eluted in the sequence N_2–CO_2–H_2O–SO_2, and measured by the TC detector.

The electrical signals arrive at the control unit which in turn feeds a potentiometric recorder and the data processing unit. The control unit sets and monitors the analytical program; the recorder gives a chromatogram for visual check of the combustion process, as shown in Figure 2.

The data processing unit comprises an analog/digital converter, an I/O interface, three units, ROM, CPU, and RAM, and the calculation unit. At the outlet there is a keyboard and a display panel for exhibiting and printing the data.

The data processing unit can be fed either by the TC signals from the detector or the signals referring to sample weight coming from balance through the relevant interface.

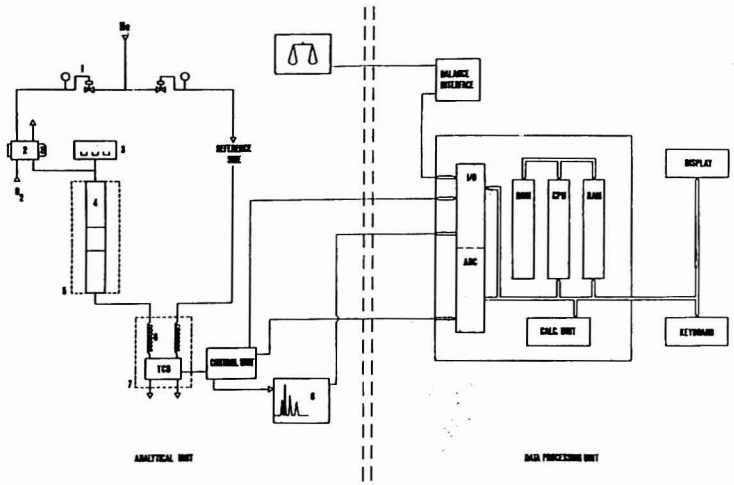

Figure 1. Schematic of coupling elemental analyzer–data processing unit. (1) Flow controller, (2) oxygen injection valve, (3) sample holder, (4) reactor, (5) furnace, (6) GC column, (7) thermostatic oven, and (8) recorder

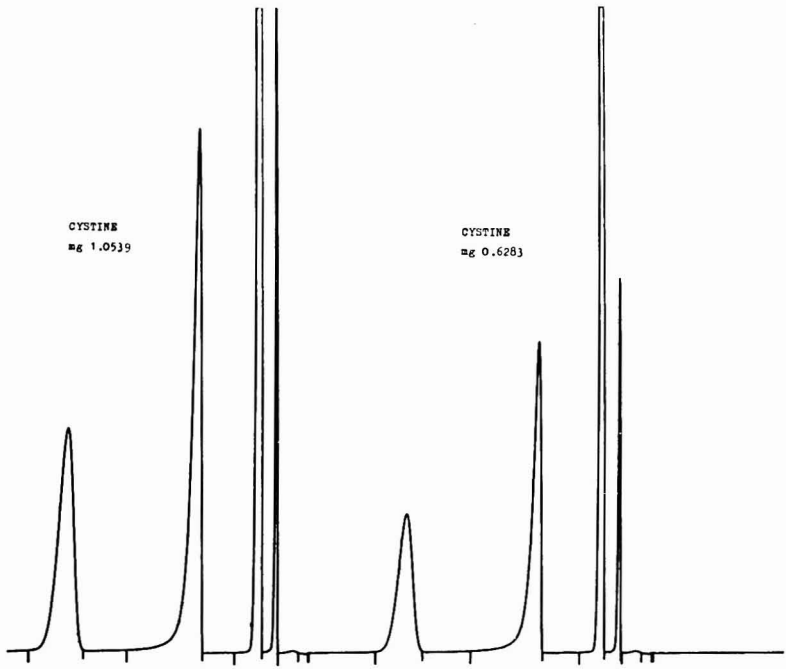

Figure 2. Analysis chromatograms

The data processing unit's first step is to integrate the signals for the peaks for the four gases on the basis of certain parameters such as blank level, retention time window, and slope sensitivity.

A blank can, if necessary, be determined automatically, subtracting it from the integral value obtained for each combustion gas eluted.

When the data processing unit has integrated the above signals, it starts mathematical treatment of the data, calculating the binary ratios for the integration values to determine the atomic ratios when the sample has not been weighed, or calculating—by means of the calibration factor—the elemental percentages and then, following a preset program, the percentage remainder. The

Table III. Probabilistic Determination of % Remainder

% remainder in amu	inferences	% remainder in amu	inferences
16	O	66.42	PCl
19	F	67	O_2F
23	Na	67.45	O_2Cl
30.97	P	70	F_2O_2
32	O_2	70.90	Cl_2
35	OF	71	O_4Na
35.45	Cl	76	F_4
38	F_2	77.94	P_2O
39	ONa	78	O_2Na_2
46.97	PO	78.97	PO_3
48	O_3	79.91	Br
51	O_2F	83	O_4F
51.45	OCl	83.45	O_3Cl
54	OF_2	86	O_3F_2
54.45	ClF	86.91	OCl_2
55	O_2Na	87	O_4Na
57	F_3	89.90	FCl_2
58.45	NaCl	93.90	Cl_2Na
62.97	PO_2	93.94	P_2O_2
64	O_4	94.97	PO_4

straight-line relationship between atomic ratios and binary integral ratios, established experimentally as described before, is introduced into the CPU memory, which thereafter processes the data each time, calculating the atomic ratio desired on the basis of the specific linear function.

To determine atomic ratios, the amount of substance sampled should not exceed the oxidation capacity of the system; on the other hand, it must not be so small (sample weight not <0.2 mg) that analysis is affected by adsorption phenomena.

The application of this GC calibration response method is easily checked by carrying out analysis without weighing the sample, using reference test substances whose empirical formula is known.

Probabilistic Analysis of the Percentage Remainder. The multielement determination method described gives atomic ratios without sample weighing, or percentage values for four constituents of the molecule when the sample is weighed, but it cannot give information on the other elements in a molecule's composition. A simple mathematical procedure, however, can be carried out by the data processing unit coupled to the analyzer, to provide general indications on the part of the molecule that has not been directly analyzed.

Naturally, in this case it is necessary to know the sample weight in order to express the percentage remainder (%R) in atomic mass units.

The procedure consists of calculating the precentages of the four elements, from which it is easy to work out the %R, which is 100 − $\Sigma\%_{C,H,N,S}$. Then the partial empirical formula is calculated, from which it is possible to add the atomic weights (AW) for the four elements in the molecule, that is $\Sigma AW_{C,H,N,S}$.

At this point, the following simple equation can be solved:

$$\%R{:}100 = x{:}(\Sigma AW_{C,H,N,S} + x)$$

as follows:

$$\%R{:}(100 - \%R) = x{:}\Sigma AW_{C,H,N,S}$$

and x can be obtained.

This mathematical development is followed by the data processing unit and the remainder, which is MW − $\Sigma AW_{C,H,N,S}$, is given in atomic mass units.

This figure has then to be interpreted in terms of elemental composition using Table III which shows the simple, most frequent combinations of organic elements other than C, H, N, and S. For simplicity's sake, only binary, not multiple, couplings of common elements are considered here.

The smaller the value of x but not <8, the more reliable is the information obtained from this method, which is valid only for pure substances. High x values are difficult to interpret and often indicate an inorganic residue in the sample. In any event, the analyst must critically assess the indications obtained from probabilistic analysis of the percentage remainder.

Table IV. Examples of Atomic Ratio Calculation

sample name	area integrals, I_{CO_2}, I_{H_2O}, I_{N_2}, I_{SO_2}	found atomic ratio	theoretical empirical formula
sulfanilamide	469059 166591 65324 87051	$C_6H_8N_2S_1$	$C_6H_8N_2SO_2$
thiobarbituric acid	272740 71892 56736 77574	$C_4H_4N_2S_1$	$C_4H_4N_2SO_2$
research compound	258153 203640 106563 289122	$C_1H_3N_1S_1$	$C_6H_{16}N_6S_6Cl_2Ni$
research compound	921634 290745 42603 58882	$C_{18}H_{21}N_2S_1$	$C_{18}H_{21}N_2SO_2Cl_3$
thiourea	73145 76902 60862 83672	$C_1H_4N_2S_1$	CH_4N_2S
methionine	512048 303933 42487 116208	$C_5H_{11}N_1S_1$	$C_5H_{11}NSO_2$
research compound	605540 175350 13290 363060	$C_{19}H_{21}N_1S_1$	$C_{19}H_{21}NSO_3$
research compound	774860 153091 66 55713	$C_{14}H_{12}S_1$	$C_{14}H_{12}SO_3$
dibenzyldisulfide	455091 119233 60 73856	$C_7H_7S_1$	$C_{14}H_{14}S_2$
research compound	1314370 546706 32085 87230	$C_{17}H_{27}N_1S_1$	$C_{17}H_{27}NSO$

An example of percentage remainder calculations is as follows:

Probabilistic determination of %R in sulfanilic acid

Found % C = 41.58
Found % H = 4.05
Found % N = 8.10
Found % S = 18.45

% Σ = 72.18

Percentage remainder: 100 − 72.18 = 27.82
$27.82{:}100 = x{:}(\Sigma AW_{C,H,N,S} + x)$
$27.82{:}(100 - 27.82) = x{:}\Sigma AW_{C,H,N,S}$

Partial empirical formula, calculated according to the usual method is C_6H_7NS, from which $\Sigma AW_{C,H,N,S}$ = 125.197.
Then, $27.82{:}(100 - 27.82) = x{:}125.197$ and x = 48.2
MW − $\Sigma AW_{C,H,N,S}$ = 48 amu

RESULTS AND DISCUSSION

Table IV shows some examples of atomic ratio calculation for reference test substances and unknown compounds. A calculation program with the aim of obtaining only whole numbers was used.

Calculated atomic ratios appear to be affected neither by instrumental parameters such as carrier flow rate, column

temperature, and detector current nor by analytical variables such as type of catalyst, composition, type, and weight of samples.

Clearly an oxidative method has to be used in which the original elements are quantitatively converted to their combustion gases with physical and chemical adsorption phenomena (the latter due to alkaline impurities in catalysts) kept to a minimum.

When conversely we calculated the O/N ratio directly from area measurements of CO and N_2 peaks by oxygen determination (*7*), the results were unsatisfactory in the case of high O/N ratios because of partial nitrogen adsorption.

Precise integration of signals from the detector is another prerequisite to keep the straight-line relationships between atomic and binary integral ratios constant; slight variations are noted in Equations 3, 4, and 5 when the integration system is changed.

This method of operation and of presenting the data (patent pending) offers undeniable advantages over the traditional procedure. Apart from the most obvious advantage of eliminating the need for weighing, it also cancels out errors deriving from weighing, especially in the case of liquids or hygroscopic substances. The analytical response is valid even in presence of inorganic residue in the sample, data handling is entirely avoided, and finally by this procedure an elemental analyzer can be calibrated once and for all, with no need to use reference substances thereafter.

The GC response calibration method described does not correspond to any of the three main methods used in gas chromatography, i.e., normalization, internal standardization, and external standardization, but can be considered an absolute normalization method. It uses binary area ratios without either internal or external standards; the measured ratio of peak areas makes it possible then from a preestablished calibration curve, to find the corresponding atomic ratio and, thus, the partial empirical formula.

Incidentally, binary atomic ratios are often used in the petrochemical and agricultural industries. Moreover, the comparison between preestablished slopes (Equations 3, 4, and 5) and slopes experimentally determined by means of unweighed reference samples offers a criterion to check the correct working of the analyzer.

When it is preferable to have the analytical response in percentage values rather than the atomic ratio, the probabilistic determination of the percentage remainder can supply useful information on the remaining part of the molecule, not directly analyzed.

LITERATURE CITED

(1) Terentieva, E. A.; Fedorova, M. V.; Malolina, T. M. *J. Anal. Chem. USSR* **1968**, *23*, 1370.
(2) Häberli, E. *Mikrochim. Acta* **1973**, 597.
(3) Stoffel, R.; Gade, K. H. *Pharm. Ztg.* **1974**, *33*, 1286.
(4) Rezl, V. *Mikrochim. Acta* **1978**, 493.
(5) Pella, E.; Colombo, B. *Mikrochim. Acta* **1978**, 271.
(6) Pella, E.; Colombo, B. *Mikrochim. Acta* **1973**, 697.
(7) Pella, E.; Colombo, B. *Anal. Chem.* **1972**, *44*, 1563.

RECEIVED for review March 30, 1979. Accepted June 28, 1979.

Sensitivities and Interferences in Activation Analysis of Thin Samples by means of 25-MeV to 30-MeV Protons

P. Priest

Laboratoire de Chimie Inorganique et Nucléaire, Université Catholique de Louvain 2, Chemin du Cyclotron, B-1348 Louvain-la-Neuve, Belgium

G. Desaedeleer*

Service de Radioprotection, Université Catholique de Louvain, 2, chemin du Cyclotron, B-1348 Louvain-la-Neuve, Belgium

Activation properties of Na, Mg, Cl, Ca, Ti, Cr, Mn, Fe, Ni, Cu, Zn, As, Br, Sr, Cd, Sn, Sb, and Pb through bombardment of thin samples by 25-MeV to 30-MeV protons for routine analysis are considered. In the investigation of airborne particulate matter, interferences between competitive reactions can be solved. Under normal nonlimitative irradiation and counting conditions, limits of detection are in the nanogram to microgram levels according to the element considered.

Analysis of samples of very complex or poorly defined matrix through destructive methods may be subject to errors due to contamination and losses of volatile compounds and trace elements by coprecipitation on insoluble residues or container walls. Therefore nondestructive atomic or nuclear methods have been successfully applied to the determination of many elements in various matrices. Among atomic methods, X-ray fluorescence is the most popular; quantitative determinations require, however, cautious corrections for the self-absorptions of X-rays. Among nuclear methods, instrumental neutron activation analysis (INAA) is the most widely used because of the availability of nuclear reactors and the wide range of elements investigated. However, INAA is not capable of analysis for all elements; for those apparently beyond the scope of INAA, alternative methods are needed. Fast-neutron and photo activation provide alternatives; however their sensitivities are generally less adequate and experimental facilities are rare. Charged-particle activation analysis has not been extensively used in the past, in part because of the scarcity of sources of energetic particles. The proliferation of more and more cyclotrons for medical purposes, however, now makes readily available these new sources for routine analysis by charged-particle activation.

In the past, charged-particle activation with protons, deuterons, helium-3, and helium-4 have been used mostly for the determination of light elements and trace impurities in refractory metals (*1–4*). Most of these works were performed with thick targets, requiring each sample to be irradiated individually and being so far rather irradiation time-consuming. Instead, the method proposed here is aimed toward routine analysis of thin samples. The incident particles

0003-2700/79/0351-2116$01.00/0

selected for this purpose are protons, because of their high penetrability; 50 MeV proton activation has already been used for the determination of lead in aerosols (5).

Samples and standards are stacked together in a pile and irradiated simultaneously. Corrections have to be made for variations in activity induced in the samples with proton energy. The scope of this work is to determine the ability of proton activation as a multielement method for routine analysis of thin samples. The composition of the matrix determines and affects the identification and quantitative analysis of the samples. Our main goal being toward the characterization of the elemental composition of aerosols, we developed this work considering a matrix of airborne particulates supported on a filter paper.

EXPERIMENTAL

Sample Preparation. Inhomogeneous and homogeneous standards may be used. Inhomogeneous standards are made through punctual spot impregnation of Whatman 41 cellulose filter paper. Sartorius membrane filters (SM 11302), or Nuclepore polycarbonate filters (No. 40 CPR02500) with a 1.0–3.0 μL calibrated standard solution. Thicknesses of the filter support are 4.0, 1.0, and 0.3 mg/cm², respectively. Elemental content of standards ranges from 10 ng to 10 μg according to the element considered. Homogeneous standards are prepared by uniform impregnation of the filter paper with standard solution. Filters are, in the latter case, analytically determined by classical methods for retention efficiency.

Irradiations. Irradiations are carried out with the external beam of the isochronous cyclotron of Louvain-la-Neuve. Fifteen to twenty thin samples are stacked in a pile and mounted in a target holder, each sample being sandwiched between aluminum foils of 15-μm thickness. The target holder is fixed in a carrier for pneumatic transfer into the irradiation position. The target holder is water-cooled, and heat dissipation is aided by diffusion of helium gas along the targets. The surface irradiated ranges from a few mm² to a couple of cm² with the aid of appropriate collimating systems. The irradiations are performed with 30-MeV incident protons and under beam intensities of 200–300 nA for 15 to 150 min. Integrated currents are measured in a Faraday cup coupled to an integrator, and are typically in the range of 1 to 3 mC for elemental analysis.

Counting. Radionuclides are identified by γ spectrometry using a Phillips APY40AIN Ge(Li) detector with a useful volume of 80 cm³, 16% relative efficiency, and a resolution of 2.09 keV at 1333.0 keV. The detector signal is fed into a Northern Econ II multichannel analyzer through a Canberra 2011 amplifier. The samples are counted after at least 4 h cooling time to allow sufficient decay of the short-lived β^+ emitters induced in the filter paper. Counting intervals range from 400 s for short-lived radionuclides to 4000 s for longer-lived ones. Aluminum foils are removed before counting. Recoil of radionuclides from the sample to the aluminum foils or from impurities of the aluminum foil into the sample are not significant.

RESULTS

The present investigation was aimed toward the characterization of airborne particulate matter. Therefore, only selected elements, major constituents of aerosols, were taken into consideration. Among these, Na, Mg, Cl, Ca, Ti, Cr, Mn, Fe, Ni, Cu, Zn, As, Br, Sr, Cd, Sn, Sb, and Pb are elements also having appropriate proton activation properties. Other elements, e.g., Sc, V, and Se have also been considered, but owing to their low abundance in aerosols or their poor activation characteristics, such elements are not analytically determined and are considered only on an interference basis.

Production Rates of Radionuclides. Pertinent information on the production and properties of radionuclides produced by irradiation of the selected elements with 30-MeV protons are reported in Table I. Available compilations and tables were used to select *Q*-values (6), excitation functions (7), isotopic abundances in natural elements (8) and spectrometric data (9). Only analytically favorable and interfering reactions leading to adequate γ emitters are listed.

The analytical radionuclides together with their γ peaks and the measured activities for three decay intervals are reported in Table II. These are expressed as counts under the most appropriate γ peak, accumulated in a 1000-s counting interval, after irradiation of 1.0 μg of natural element with an integrated beam charge of 1.0 mC. Activities for a zero decay time are calculated by extrapolation of the measured area. The reproducibility of the measured activities is better than 20% for different irradiations.

For light elements, proton activation leads to radionuclides induced through (p,pn) reactions, e.g., Cl and Sc. For heavier elements, (p,3n) reactions are more favored, e.g., As, Cd, Sn, and Pb, whereas intermediate elements activate most favorably through (p,2n) reactions, e.g., Fe, Cu, Zn, and Sr.

Activation Curves for the Production of Radionuclides. A second important factor we have to consider, for routine analysis of a large number of samples, is the variation of activity induced as a function of the energy of the incoming proton. In order to make proton activation analysis as suitable as, for example, neutron activation, one has to be able to irradiate simultaneously a rather large number of samples and standards; however, with the difference that going through the pile of samples the energy of the proton varies and so does the cross section. If in the literature excitation functions for quite a variety of reactions occurring on various elements are reported or can be evaluated by extrapolation, the present study requires for the elements under investigation (a) that we know the excitation functions of production of radionuclides, rather than for specific reactions, and (b) that we test the linearity of the excitation function in the energy range considered, such linearity allowing easy interpolation between activities induced in the pile of samples.

Activation curves for the various elements under investigation are presented in Figure 1. The activity induced in the pile of samples is normalized to the activity in the first sample (30 MeV). Losses of energy in each of the samples are typically of the order of 0.1–0.3 MeV, which corresponds to a loss of approximately 5 MeV in the total pile of samples. An energy range of 25 to 30 MeV was investigated and compared with additional data at 21 MeV. Neglecting the cross-section value at 21 MeV, one could characterize the elements into two different groups, one presenting a slight or zero slope in the excitation function, e.g., Na, Cr, Mn, Mg, Ni, Cd, and Pb, and the other with much larger variations, e.g., As and Br. Linear and nonlinear fits of the data of the activation curves have been performed, and using the proposed fit, the reproducibility is better than ±15%.

Element-to-Element Discussion. Interferences encountered in charged-particle activation analysis are of two kinds: (a) one associated with different reactions occurring on contiguous elements and leading to the production of the same radionuclide, and (b) the other associated with overlapping of peaks in the γ spectra. Both interferences are independent on an evaluation basis; however, since they occur simultaneously, it is more appropriate to examine them at the same time. Of course, the possibility of these interferences is strongly related to the composition of the matrix and the sample support; in the present case, the samples are airborne particulates collected on filter paper. The present discussion is limited to elements where interferences can be apparent.

Sodium. Activity of ^{22}Na due to the activation of Mg is not appreciable as compared to activation of Na. Determination of Na is unambiguous as long as the Mg concentrations are of the same order of magnitude as Na concentrations.

Chlorine. The only interference may arise from sulfur, through the ^{34}S(p,n)^{34m}Cl reaction. However, the data of Table II imply that sulfur concentrations a hundred-fold times the

Table I. Data on Production and Properties of Radionuclides Observed after 30-MeV Proton Irradiation of Standards

element to be determined	major reactions[a]	isotopic abundance, %	Q-value, MeV	E_{max}, MeV[b]	FWHM[b]	σ_{max}, mb[b]	half-life	major γ rays, keV	intensity (%)
$_{11}$Na	→ ^{23}Na(p,pn)^{22}Na	100	−12.4	28	41	122	2.6 yr	1274 (90)	
$_{12}$Mg	^{24}Mg(p,2pn)^{22}Na	79.0	−24.1	47.5	-	65	2.6 yr	1274 (90)	
	→ ^{25}Mg(p,2p)^{24}Na	10.0	−12.1	29.1	-	52	15.0 h	1368 (100)	2754 (99)
$_{16}$S	^{34}S(p,n)^{34m}Cl	4.2	−6.3	14.4	10.4	62	32 min	146 (36)	2128 (48)
$_{17}$Cl	→ ^{35}Cl(p,pn)^{34m}Cl	75.8	−12.6	28*	23*	170*	32 min	146 (36)	2128 (48)
$_{20}$Ca	→ ^{44}Ca(p,2p)^{43}K	2.1	−12.2	30*	14*	40*	22 h	372 (82)	616 (65)
	→ ^{44}Ca(p,n)^{44}Sc	2.1	−4.4	13*	10*	400*	3.92 h	1157 (99)	
	^{44}Ca(p,2n)^{43}Sc	2.1	−14.1	28*	14*	200*	3.89 h	372 (22)	
	^{46}Ca(p,2n)^{45}Sc	0.19	−8.7	23*	14*	600*	3.42 d	159 (70)	
$_{21}$Sc	^{45}Sc(p,pn)^{44}Sc	100	−11.3	22.0	23.0	600	3.92 h	1157 (99)	
	^{45}Sc(p,p2n)^{43}Sc	100	−21.0	39*	23*	300*	3.89 h	372 (22)	
$_{22}$Ti	^{46}Ti(p,2pn)^{44}Sc	7.93	−21.7	-	-	-	3.92 h	1157 (99)	
	^{47}Ti(p,α)^{44}Sc	7.28	−2.3	13*	10*	70*	3.92 h	1157 (99)	
	→ ^{46}Ti(p,αn)^{44}Sc	73.9	−13.9	30*	15*	70*	3.92 h	1157 (99)	
	^{46}Ti(p, 2p)^{45}Sc	73.9	−11.4	28*	15*	50*	3.42 d	159 (70)	
	^{49}Ti(p,2pn)^{47}Sc	5.51	−19.6	-	-	-	3.42 d	159 (70)	
	^{50}Ti(p,α)^{47}Sc	5.34	−2.2	13*	10*	50*	3.42 d	159 (70)	
	→ ^{46}Ti(p,n)^{46}V	73.9	−4.8	12*	10*	350*	16.0 d	983 (100)	1312 (98)
$_{24}$Cr	^{50}Cr(p,2pn)^{46}V	4.3	−21.1	-	-	-	16.0 d	983 (100)	1312 (98)
	→ ^{52}Cr(p,pn)^{51}Cr	83.8	−12.0	27*	20*	1000*	27.7 d	320 (10)	
	^{52}Cr(p,n)^{52}Mn	83.8	−5.5	12.3	10*	485	5.7 d	744 (85)	936 (93)
									1434 (100)
	^{53}Cr(p,2n)^{52}Mn	9.5	−13.4	26*	14*	600*	5.7 d	744 (85)	936 (93)
$_{25}$Mn	→ ^{55}Mn(p,pn)^{54}Mn	100.0	−10.2	26*	20*	550*	312.5 d	835 (100)	
$_{26}$Fe	→ ^{54}Fe(p,2pn)^{52}Mn	5.8	−20.9	-	-	-	5.7 d	744 (85)	936 (93)
	^{56}Fe(p,2pn)^{54}Mn	91.7	−20.4	-	-	-	312.5 d	835 (100)	
	→ ^{56}Fe(p,2n)^{55}Co	91.7	−15.5	29*	11*	150*	17.9 h	477 (16)	931 (73)
$_{28}$Ni	→ ^{58}Ni(p,pn)^{57}Ni	67.8	−12.2	28.5	17.8	220	36.0 h	127 (15)	1378 (85)
$_{29}$Cu	→ ^{63}Cu(p,p2n)^{61}Cu	69.1	−19.7	37.5	16.6	330	3.3 h	283 (13)	656 (10)
	→ ^{63}Cu(p,2n)^{62}Zn	69.1	−13.3	26*	14*	180*	9.3 h	548 (14)	597 (23)
$_{30}$Zn	^{64}Zn(p,p2n)^{62}Zn	48.9	−21.0	-	-	-	9.3 h	548 (14)	597 (23)
	→ ^{67}Zn(p,2n)^{66}Ga	4.1	−13.0	27*	14*	900*	9.3 h	1039 (37)	
	→ ^{68}Zn(p,3n)^{66}Ga	18.6	−23.2	38*	17*	200*	9.3 h	1039 (37)	
	→ ^{68}Zn(p,2n)^{67}Ga	18.6	−12.0	26*	14*	500*	78.1 h	93 (38)	185 (20)
$_{33}$As	→ ^{75}As(p,3n)^{73}Se	100	−21.7	37*	16*	350*	7.2 h	361 (99)	
$_{34}$Se	^{74}Se(p,pn)^{73}Se	0.9	−12.1	28*	20*	250*	7.2 h	361 (99)	
	^{76}Se(p,n)^{76}Br	9.0	−5.9	14*	9*	600*	15.9 h	559 (66)	657 (13)
	^{77}Se(p,2n)^{76}Br	7.5	−13.3	26*	12*	900*	15.9 h	559 (66)	657 (13)
	^{77}Se(p,n)^{77}Br	7.5	−2.1	10*	10*	850	56.0 h	239 (26)	521 (24)
	^{78}Se(p,2n)^{77}Br	23.5	−12.6	26*	13*	550*	56.0 h	239 (26)	521 (24)
$_{35}$Br	→ ^{79}Br(p,p2n)^{77}Br	50.7	−19.0	39*	19*	350*	56.0 h	239 (26)	521 (24)
	^{81}Br(p,pn)^{80m}Br	49.3	−10.2	30.3	22*	230	4.4 h	617 (7)	
$_{38}$Sr	^{88}Sr(p,3n)^{86}Y	82.6	−25.6	39	15.8	500	14.7 h	628 (33)	1077 (82)
	→ ^{88}Sr(p,2n)^{87}Y	82.6	−13.8	25.5	12.0	1200	80.3 h	388 (80)	485 (96)
	→ ^{88}Sr(p,2n)^{87m}Y	82.6	−13.8	-	-	-	14.0 h	381 (74)	
$_{48}$Cd	→ ^{110}Cd(p,2n)^{109}In	12.4	−12.7	25*	12*	900*	4.2 h	204 (68)	
	→ ^{111}Cd(p,3n)^{109}In	12.8	−19.7	35*	15*	700	4.2 h	204 (68)	
	^{110}Cd(p,n)^{110m}In	12.4	−4.7	13.0	8*	870	4.9 h	658 (99)	885 (95)
	^{111}Cd(p,2n)^{110m}In	12.8	−11.7	24*	12*	900*	4.9 h	658 (99)	885 (95)
	^{113}Cd(p,3n)^{110m}In	24.0	−21.1	31.7	15*	780	4.9 h	658 (99)	885 (95)
	→ ^{111}Cd(p,n)^{111}In	12.8	−1.6	13.0	8*	530	2.83 d	171 (91)	245 (94)
	→ ^{112}Cd(p,2n)^{111}In	24.0	−11.0	21.0	12.5	1000	2.83 d	171 (91)	245 (94)
	→ ^{113}Cd(p,3n)^{111}In	12.3	−17.5	33*	15*	900*	2.83 d	171 (91)	245 (94)
$_{50}$Sn	→ ^{118}Sn(p,2n)^{117}Sb	24.1	−11.9	25*	12*	900*	2.8 h	158 (88)	
	→ ^{119}Sn(p,3n)^{117}Sb	8.6	−18.3	33*	14*	900*	2.8 h	158 (88)	
	→ ^{119}Sn(p,2n)^{118m}Sb	8.6	−11.0	24*	12*	900*	5.1 h	254 (8)	1229 (10)
	→ ^{120}Sn(p,3n)^{118m}Sb	32.8	−20.1	35*	14*	700*	5.1 h	254 (8)	1229 (10)
$_{51}$Sb	→ ^{121}Sb(p,3n)^{119m}Te	57.3	−19.3	34*	15*	900*	4.68 d	153 (62)	1213 (67)
$_{82}$Pb	→ ^{206}Pb(p,3n)^{204}Bi	24.1	−20.6	34*	12*	1000*	11.3 h	375 (75)	899 (99)
	→ ^{207}Pb(p,2n)^{206}Bi	22.1	−11.2	20.4	9.4	910	6.24 d	803 (100)	881 (67)
	→ ^{208}Pb(p,3n)^{206}Bi	52.4	−18.5	30.8	12.4	990	6.24 d	803 (100)	881 (67)

[a] → Most appropriate nuclear reactions. [b] * Data obtained by extrapolation (7).

chlorine concentrations are needed to lead to a significant contribution to ^{34m}Cl.

Among these elements we have been looking at, chlorine is the only one with a half-life shorter than 2 h, leading eventually to some problems in the routine analysis of a larger number of samples.

Calcium, Scandium, and Titanium. Proton activation of these three elements leads mainly to the production of scandium radionuclides; therefore they are considered simultaneously and interferences have to be considered cautiously.

To avoid these interferences, Ti can be determined from ^{48}V (Cr interferes and its contribution must be subtracted) and Ca is determined unambiguously from ^{43}K; Sc is finally evaluated from ^{44}Sc, after the deduction of the contribution of Ti and Ca to this radionuclide.

This procedure is, however, unappropriate in the analysis of airborne particulate matter, because the γ peaks of ^{43}K are

Table II. Analytical Radioisotopes and Induced Activities

element to be determined	radioisotope (half-life)[a]	γ-ray selected, keV	activity measured, counts × μg^{-1} × mC^{-1} × $(1000\ s)^{-1}$			
			t_d = 0	4 h	15 h	10 d
Na	^{22}Na(2.6 yr)•	1274	4.0	4.0	4.0	4.0*
Mg	^{24}Na(15.0 h)•	1368	230.0	191*[b]	115	-
Cl	^{34m}Cl(32.0 min)•	146	80000	440*	-	-
Ca	^{41}K(22 h)•	372	14	12	10*	
		616	7.2	6.35	4.49*	-
	^{43}Sc(3.89 h)•	372	100	49.0*	6.91	-
	^{44}Sc(3.92 h)	1157	37	18.2*	2.61	-
	^{47}Sc(3.42 d)	159	11	10.6	9.69*	1.45*
Sc	^{43}Sc(3.89 h)	372	1300	640*	89.8	-
	^{44}Sc(3.92 h)	1157	28000	13805.*	1975	-
Ti	^{44}Sc(3.92 h)•	1157	3500	1725*	247	-
	^{47}Sc(3.42 d)	159	570	551	502*	75.1*
	^{46}V(16.0 d)•	983	32	32	31	16*
Cr	^{48}V(16.0 d)	983	44	44	43	29*
	^{51}Cr(27.7 d)•	320	150	150	150	117*
	^{52}Mn(5.7 d)	744	29	28	27*	8.6*
Mn	^{54}Mn(312.5 d)•	835	35	35	35	34*
Fe	^{54}Mn(312.5 d)	835	7.5	7.5	7.5	7.3*
	^{52}Mn(5.7 d)•	744	85	83	79*	25*
	^{55}Co(17.9 h)•	931	400	343	224*	-
Ni	^{57}Ni(36.0 h)•	127	1000	926	750*	10
		1378	600	555	450*	6
Cu	^{61}Cu(3.3 h)•	283	3200	1380*	137	
	^{62}Zn(9.3 h)•	597	320	237	105*	-
Zn	^{62}Zn(9.3 h)	597	300	223	98*	-
	^{66}Ga(9.3 h)•	1039	350	260	115*	-
	^{67}Ga(78.1 h)•	93	250	241	219*	30*
As	^{73}Se(7.2 h)•	361	20000	13610*	4720*	-
Se	^{73}Se(7.2 h)	361	300	200*	71*	-
	^{76}Br(15.9 h)	559	750	630	390*	-
	^{77}Br(56.0 h)	239	250	238	208*	13
Br	^{77}Br(56.0 h)•	239	240	228	199*	12
	^{80m}Br(4.4 h)	617	170	90*	16	-
Sr	^{87}Y(80.3 h)•	388	1700	1640	1490*	214*
	^{87m}Y(14.0 h)•	381	7700	6320	3665*	-
Cd	^{109}In(4.2 h)•	204	16000	8270*	1350	-
	^{110m}In(4.9 h)	658	3700	2100*	443	-
	^{111}In(2.83 d)•	171	1700	1630	1450*	145
		245	1400	1345	1200*	120
Sn	^{117}Sb(2.8 h)•	158	37000	13750*	905	-
	^{118m}Sb(5.1 h)•	254	8500	4940*	1110	-
Sb	^{119m}Te(4.68 d)•	153	2300	2245	2100*	525*
Pb	^{204}Bi(11.3 h)•	375	3700	2895	1475*	-
		899	1800	1410	717*	-
	^{206}Bi(6.24 d)•	803	300	295	280*	100*

[a] • Most appropriate analytical radionuclide. [b] * Most appropriate decay interval.

rarely observed in a routine determination, and because ^{48}V is not a sensitive radionuclide for titanium.

Scandium radionuclides must then be used: an aid to resolve the inherent interferences is to consider the ratios Ca/Ti/Sc which are usually 1000/100/1 in an aerosol. Ca is now determined from ^{43}Sc, since the contribution of Sc to this radionuclide is negligible; the γ peak at 372 keV is close to the 374-keV γ peak of ^{204}Bi, and this contribution must be subtracted.

Another problem arises from ^{43}K, which also has a γ peak at 372 keV.

Ti is determined from ^{44}Sc, since the contribution of calcium and scandium to this radionuclide is low in an aerosol sample. Finally, because of its low abundance in airborne particulate matter, Sc cannot be evaluated.

Chromium. ^{51}Cr is the most pertinent radionuclide for the determination of Cr; the contribution to ^{51}Cr from vanadium, through the ^{51}V(p,n)^{51}Cr reaction is negligible.

Manganese can be determined from ^{54}Mn; this radionuclide is also produced from Fe, but with lower yield. Correction factors for the contribution of iron may be evaluated, and Mn can be determined in a matrix with a Fe/Mn ratio of up to 10.

Iron is best determined via the 931-keV γ ray of ^{55}Co; this element can also be evaluated via ^{52}Mn (which is also produced from Cr) in a matrix with a low Cr/Fe ratio.

Copper is best determined via the ^{61}Cu radionuclide; the contribution to ^{61}Cu from Ni, through the ^{62}Ni(p,2n)^{61}Cu reaction is very small. Copper can also be evaluated from ^{62}Zn, but Zn interferes through the ^{64}Zn(p,p2n)^{62}Zn reaction. This interference is rather important at 30 MeV, but very low at 25 MeV (see Figure 1).

Arsenic, Selenium, and Bromine. These three elements interfere with each other and, according to the matrix and sample composition, their determination will be more or less accurate and possible. Se can be determined unambiguously via ^{76}Br. Contribution of ^{77}Br from the activation of selenium can be evaluated, and the subsequent determination of Br through the ^{79}Br(p,p2n)^{77}Br reaction can be carried out. Since activities of ^{77}Br induced on Se and Br are of the same order of magnitude, the corrections are valid as long as Se concentrations are lower or equal to the Br concentrations. Arsenic can be determined via ^{73}Se through the ^{75}As(p,3n)^{73}Se reaction. However, since ^{73}Se is also produced from Se, but with a much lower yield, determinations of As are unambiguous only as long as Se concentrations are not higher than

Table III. Sensitivities of Instrumental Proton (IPAA) and Neutron (INAA) Activation Analysis

element	limit of detection, ng IPAA	limit of detection, ng INAA	element	limit of detection, ng IPAA	limit of detection, ng INAA
Na	1600	200	Cu	190	50
Mg	340	3000	Zn	190	100
Cl	470	500	As	50	40
Ca	130	1000	Se	260	10
Sc	3	3	Br	430	20
Ti	270	200	Sr	15	-
Cr	60	20	Cd	25	-
Mn	180	3	Sn	30	-
Fe	160	1500	Sb	54	30
Ni	60	1500	Pb	20	-

As concentration by an order of magnitude.

CONCLUSION

Analytical Considerations. Our limitations to Na, Mg, Cl, Ca, Se, Ti, Cr, Mn, Fe, Ni, Cu, Zn, As, Br, Sr, Cd, Sn, Sb, and Pb are due (a) to the composition of the matrix considered: airborne particulates collected on filter paper, and (b) to adequate activation properties of these elements. Extension to other elements is feasible considering the extension to other incident particles and energies. For routine analysis of thin samples, the proton is the most appropriate particle, because of its high penetrability; 30-MeV activation is a middle choice between high and low energies. Higher energies of incident particles create more exotic reactions, and subsequently more elements could potentially be determined. However, in complex matrices more interfering reactions would occur simultaneously and the complexity of the γ spectra would make analytical determinations rather difficult. Therefore, and also because of the availability of sources of low-energy particles, activation with lower-energy particles is more common. Activities induced with 20-MeV and 30-MeV protons are comparable for most elements within a factor of 2 (Figure 1); 30-MeV proton activtion being more appropriate for the determination of As, Br, and Sb. However for lower proton energies, the larger loss of energy through the pile of samples makes it less adequate for routine analysis.

In Table III, limits of detection are reported. Calculations are based upon background levels encountered after irradiation with 30-MeV protons of a 4 mg cm^{-2} filter support and a 200 μg cm^{-2} airborne particulate-matter sample with an integrated beam current of 1 mC. Limits of detectability are calculated from $N = 4.65 \times B^{1/2}$, where B is the number of counts in the background and N is the minimum number of counts under the γ peak (*11*).

Subsequent evaluation of minimum detectable amounts is done through Table II and is reported in Table III. In the same table, and for comparison purposes, sensitivities obtained for routine analysis of aerosols by neutron activation are reported (*12*) (flux of neutrons: 2×10^{12} n/cm^2·s during 5 min for short-lived radionuclides or 10^{13} n/cm^2·s during 5 h for long-lived radionuclides). In both cases, the counting times are comparable, i.e., from 400 to 4000 s, according to the half-life of the radionuclides. Sensitivities for IPAA as defined in Table IV could be improved, one of the limiting factors being the thermal resistance of the samples. Indeed, most of the energy loss by the incident particle while penetrating the pile of samples is dissipated in heat. In the present case, since a large number of nonthermal-conducting materials are piled up, we have a stringent restriction on beam intensities. According to the thermal resistance of the samples, beam

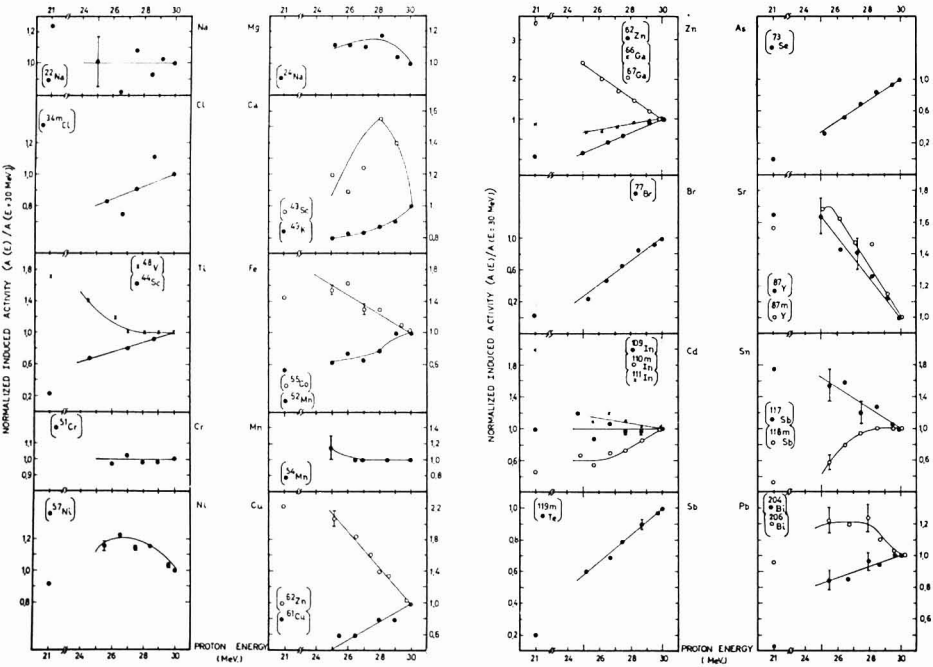

Figure 1. Relative excitation functions for the production of radionuclides from irradiation of natural elements with 21 to 30 MeV protons

Table IV. Analytical Determinations on Airborne Particulates in Belgium Performed by Neutron (INAA) and Proton (IPAA) Activation[c]

	Dourbes		Mechelen		Brussels		Ghent residential		Ghent industrial		Charleroi		Liege		IPAA/INAA, $\bar{x} \pm \sigma_x$
	INAA	IPAA	INAA	IPAA	INAA	IPAA	INAA	IPAA	INAA	IPAA	INAA	IPAA	INAA	IPAA	
Na	1270	1320	920	1070	950	1490	1520	1620	1130	1320	2340	2420	1930	1900	1.14 ± 0.20
Mg+[b]	680	940	490	550	330	900	800	960	500	670	610	1960	830	930	(1.73 ± 0.86)
Ca*[a]	3700	1900	1700	1000	3200	3300	3500	1900	3200	1100	6000	6600	12700	7800	(0.68 ± 0.28)
Ti	110	120	100	140	100	150	240	220	110	110	410	360	260	260	1.11 ± 0.24
Cr	20	-	12	15	14	12	13	-	10	9	38	35	61	56	0.97 ± 0.16
Mn	120	130	60	90	90	120	300	220	90	90	200	240	340	340	1.12 ± 0.25
Fe	2600	2300	2100	2700	2600	2800	2600	2800	1800	1600	6200	5400	7300	7400	1.01 ± 0.15
Ni+	32	11	42	24	<70	22	35	44	25	14	<70	18	85	55	(0.68 ± 0.34)
Cu*	52	110	101	90	53	150	54	70	40	50	83	108	270	280	(1.53 ± 0.69)
Zn	750	720	500	500	830	920	420	390	330	300	3270	3070	5260	5100	0.97 ± 0.07
As	14	14	22	35	27	34	15	24	17	18	25	24	21	22	1.22 ± 0.28
Br	85	110	200	240	200	350	150	250	125	150	210	330	380	650	1.48 ± 0.25
Sr	-	11	-	8	-	14	-	10	-	10	-	22	-	33	
Cd+	16	18	17	7	10	15	10	13	<7	9	13	25	270	280	(1.22 ± 0.50)
Sn	-	5	-	23	-	1	-	9	-	10	-	28	-	35	
Sb	8	11	250	-	44	49	19	-	16	15	13	25	13	15	1.30 ± 0.38
Pb	-	250	-	390	-	560	-	330	-	240	-	550	-	870	

[a] * Errors associated with IPAA (see text). [b] + Errors associated with INAA (See text). [c] Units expressed in ng/m³.

intensities up to several μA could be used, and consequent improvements in sensitivities achieved.

Applicability to Elemental Analysis of Aerosols. Aerosols collected at various locations in Belgium are routinely analyzed for their elemental compositions. In Table IV we present a comparison of results of determinations performed by instrumental neutron (INAA) and proton (IPAA) activation analysis. Airborne particulates were collected by filtration of approximately 200 m³ of air on a 66 cm² Whatman 41 filter paper. The filter paper is folded, and a 2 cm² aliquot is taken for analysis by IPAA, of which approximately 1 cm² was bombarded in the irradiation chamber. Analyses by INAA were performed at the University of Ghent.

It is not our purpose here to give an interpretation of the data, but rather to point out the analytical aspects. The concordance between the two methods is usually good: within ±20% for Na, Ti, Cr, Mn, Fe, Zn, As, Br, and Sb. For Mg, Ni, and Cd, uncertainties associated with the INAA values are much larger, but within these limits agreement is good. The IPAA determination of Ca is a little more ambiguous, due to the correction associated with the activation of Ti and Sc. The same problem arises with Cu, due to the activation of Zn.

ACKNOWLEDGMENT

We are indebted to C. Ronneau for his helpful assistance, interest and discussion, to D. Apers for his guidance, and to J. Cara, M. Cogneau, N. Jacob, G. Michotte, J. L. Navarre, and P. Negmegeer for their support and technical assistance. We thank D. Schuykens and M. Devillers, for their help in different phases of this work, and R. Dams of the University of Ghent (Rijksuniversiteit Gent, Belgium) for providing samples and analytical determinations by instrumental neutron activation analysis.

LITERATURE CITED

(1) R. S. Tilbury, "Activation Analysis with Charged Particles", NAS-NS 3110, USAEC.
(2) V. Krivan, *Anal. Chem.*, **47**, 469 (1975).
(3) J. N. Barrandon, S. Benaben, J. L. Debrun, and M. Vallandon, *Anal. Chim. Acta*, **73**, 39 (1974).
(4) K. Strijckmans, C. Vandecasteele, and J. Hoste, *Anal. Chim. Acta*, **89**, 255 (1977).
(5) G. Desaedeleer, C. Ronneau, and D. Apers, *Anal. Chem.*, **48**, 572 (1976).
(6) K. A. Keller, H. Münzel, and H. Lange, "Q-values for Nuclear Reactions", Landolt-Börnstein, New Series, Group I, Vol. 5, Part a, Springer, Berlin, 1973.
(7) K. A. Keller, H. Lange, H. Münzel, and G. Pfennig, "Excitation Functions for Charged-Particle Induced Nuclear Reactions", Landolt-Börnstein, New Series, Group I, Vol. 5, Part b, Springer, Berlin, 1973.
(8) W. Seelmann-Eggebert, G. Pfennig, and H. Münzel, Nuklidkarte, Kernforschungszentrum, Karlsruhe, 1974.
(9) G. Erdtmann and W. Soyka, Die γ-Linien der Radionuklide, Kernforschungsanlage Jülich, 1973.
(10) K. A. Keller, H. Lange, and H. Münzel, "Estimation of Unknown Excitation Function and Thick-Target Yields for Nuclear Reactions Induced by p, d, ^{3}He and α-particles", Landolt-Börnstein, New Series, Group I, Vol. 5, Part c, Springer, Berlin, 1974.
(11) L. A. Currie, *Anal. Chem.*, **40**, 586 (1968).
(12) R. Dams, J. A. Robbins, K. A. Rahn, and J. W. Winchester, *Anal. Chem.*, **42**, 861 (1970).

RECEIVED for review December 11, 1978. Accepted July 9, 1979. The study was conducted with financial assistance from the Centre National d'Etude de la Pollution Atmosphérique par la Combustion and the Institut Interuniversitaire des Sciences Nucléaires.

Thermometric Titrations of Polyprotic Acids

Maurice A. Bernard and Jean-Louis Burgot*[1]

Laboratoire de Chimie Minérale B, Groupe de Cristallographie et Chimie Solide, L.A. 251, Universite de Caen, 14032 Caen Cedex, France

The authors formulate n equivalent equations for the thermometric titration curve of a polyprotic acid H_nA, the pK values of which are comparable, neutralized by a strong base. The main term of the pth equation corresponds to a line segment with slope proportional to the enthalpy of neutralization ΔH_p of the pth acidity. Terms which are numerically small justify the roundoff sections connecting these segments to the base lines and to each other. These equations have been experimentally checked with a diacid, glutaric acid, and with a triacid, citric acid. In the case of a diacid, the deviation between the experimental curve and the theoretical lines, at the point corresponding to semi-neutralization, is evaluated as a function of the acidity constants and enthalpies of neutralization. A rapid graphic method is used to estimate the ratio of the two acidity constants.

In most monographs devoted to thermometric titrations (*1–7*), the authors stress two basic differences between these titrations and those followed by potentiometry.

First, while potentiometric titrations take advantage of the Gibbs free energy variation ΔG (or the equilibrium constant K) involved in the titration, thermometric titrations use the corresponding enthalpy variation ΔH, which can, in some cases, provide a significant advantage as in the often-quoted titration of orthoboric acid by a sodium hydroxide solution (*1, 8, 9*).

Second, thermometric methods produce linear titration curves, whereas potentiometric methods lead to logarithmic curves. As a rule, a thermogram representing the heat $-q(t)$ developed in the reaction vessel, as a function of time consists of a number of line segments. These segments are connected to each other by curves of variable size, reflecting, among other phenomena, the reversibility of the reactions involved. The parameters on which the roundoff due to this reversibility depend have been identified by various authors (*1–10*), especially Tyrrel (*10*), who investigated the reactions represented by the equilibrium:

$$A + B \rightleftharpoons C$$

This rounding off, which may hinder the detection of the equivalent point, is, however, valuable for more or less accurate determinations of the equilibrium constant K and thus of variations in the entropy and Gibbs free energy functions (*11–15*).

In the case of a polyprotic acid, or more generally of a polyfunctional compound, the titration curve is, as a rule, formed by the linking of the successive titration curves of the various functions of the compound analyzed.

In point of fact, this can only be achieved for a potentiometric titration if the successive dissociation constants of the test compound have sufficiently different orders of magnitude. For example, it is generally acknowledged that potentiometric identification of the two successive acidities of a diacid H_2A is only possible if $\Delta pK = pK_2 - pK_1 \geq 4$, corresponding to a maximum distribution coefficient for HA^- approaching one (*16*).

The application of thermometric titration to exploit the enthalpy variation ΔH (and not the Gibbs free energy variation ΔG, hence of the equilibrium constant K) and the linearization of the corresponding curves, provides hope for a lowering of the detection limits of the functions for the successive stages of thermometric titration of a polyfunctional compound.

Using thermometric titration in aqueous solution with a sodium hydroxide solution, Harries (*17*) showed that phthalic acid ($\Delta pK = 2.47$) (*18*), oxalic acid ($\Delta pK = 2.96$) (*19, 20*), malonic acid ($\Delta pK = 2.86$) (*21, 22*), and succinic acid ($\Delta pK = 1.45$) (*23, 24*) produce thermograms which exhibit two breaks for the successive neutralization of the two acid groups, even though for these acids, the maximum coefficient for HA^- is much less than one. On the other hand, he observed no slope change for the neutralization of the following diacids: glutaric ($\Delta pK = 1.08$) (*21*), adipic ($\Delta pK = 0.99$) (*21*), maleic ($\Delta pK = 4.42$) (*25*), fumaric ($\Delta pK = 1.51$) (*25*), and tartaric ($\Delta pK = 1.27$) (*18*).

Using equipment described elsewhere (*26, 27*), with sufficient sensitivity and suitable recording speed, we clearly identified the slope changes corresponding to the successive neutralizations of these diacids. We also, contrary to the results in the literature (*28*), obtained three obviously distinct line segments with slightly different slopes in the case of a triacid (citric acid). These results prompted us to develop a theoretical framework in order to justify and discuss these experimental data.

This study has been conducted for a polyprotic acid H_nA with, as experimental support, application to the particular instances of glutaric and citric acids.

EXPERIMENTAL

Reagents. The sodium hydroxide solutions are prepared by extemporaneous dilution of standard solutions with distilled water. The glutaric acid solution is prepared from the Fluka commercial product, the purity of which is checked by testing its melting point, 95–96 °C. The citric acid solution is prepared from the Fluka commercial product, labeled "puriss".

Apparatus. The thermometric titration apparatus is described elsewhere (*27*). Characteristics: at maximum sensitivity, a change of 10^{-2} °C corresponds to 1 cm on the recorder chart ordinate or 0.25 °C per full scale deflection. Variation of 0.1 cm corresponds to 0.6 J. The chart ordinate can be read with an accuracy of ±0.05 cm corresponding to $\pm 5.10^{-4}$ °C or ±0.3 J. Accordingly, the minimum temperature difference which can be estimated with relative accuracy (within 1%) is 0.05 °C; the minimum heat variation with the same relative accuracy is 30 J.

For potentiometric titrations, we used a Tacussel measurement and titration unit of the "titrimat" type, and a Tacussel digital reading pH-meter of the "Minisis" type, both equipped with a glass electrode and a calomel reference electrode.

Process of Thermometric Titrations. An accurately measured volume $V_0 = 10^{-1}$ L of the acid solution of fixed concentration C_A ($C_A = 115 \times 10^{-4}$ mol L^{-1} for the glutaric acid solution and 7.20×10^{-3} mol L^{-1} for the citric acid solution) is introduced into the reaction vessel. The agitator, the Wheatstone bridge in which the thermistors are incorporated, and the recorder are connected. The bridge is balanced. After 5 to 10 min, the bridge is rebalanced and the automatic buret started. The titration curve is recorded. The invariability in the flow rate of the buret $v = 2 \times 10^{-3}$ L min^{-1} is checked by systematically determining the volume discharged within a given interval, before and after each series of measurements. The concentration of the sodium hydroxide solution is $C_B = 1.91$ mol L^{-1}. The recorder paper speed is fast: 30 cm min^{-1}. All the titrations are carried

[1] Present address: Laboratoire de Chimie Analytique, U.E.R. du Medicament, 2, avenue du Professeur Léon Bernard, 35043 Rennes Cedex, France.

0003-2700/79/0351-2122$01.00/0

out at ambient temperature (23 ± 2 °C).

Process of Potentiometric Titrations. In this case, the same volume $V_0 = 10^{-1}$ L of acid solution is determined using the same sodium hydroxide solution as above. The pH values as a function of the volume of sodium hydroxide added are read directly from the recorded curve and confirmed by the digital-reading pH meter. The initial pH values are 3.11 for the glutaric acid solution and 2.80 for the citric solution.

Constants Employed.

Enthalpy of ionization of water:

$H^+ + HO^- \rightarrow H_2O \qquad \Delta H_0$: −55 740 J mol^{-1} (*29,30*)

Enthalpies of neutralization of glutaric acid:

$H_2A + HO^- \rightarrow HA^- + H_2O \qquad \Delta H_1$: −56 246 J mol^{-1} (*18*)

$HA^- + HO^- \rightarrow A^{2-} + H_2O \qquad \Delta H_2$: −58 169 J mol^{-1} (*18*)

Enthalpies of neutralization of citric acid:

$H_3A + HO^- \rightarrow H_2A^- + H_2O \qquad \Delta H_1$: −51 556 J mol^{-1} (*18*)

$H_2A^- + HO^- \rightarrow HA^{2-} + H_2O \qquad \Delta H_2$: −53 313 J mol^{-1} (*18*)

$HA^{2-} + HO^- \rightarrow A^{3-} + H_2O \qquad \Delta H_3$: −59 087 J mol^{-1} (*18*)

THEORETICAL

Polyprotic Acid H_nA. We assume that only the first acidity of H_nA is sufficiently great, so that, before the beginning of addition, the aqueous solution contains only the H^+ of concentration $(H^+)_0$, H_nA and $H_{n-1}A^-$ entities. The dilution is taken into account in the calculation but the concentrations are not explicitly corrected for the activity coefficients.

The following notations are used for the successive enthalpies of neutralization of the n acids H^+, $H_nA \ldots HA^{(n-1)-}$.

$$H^+ + HO^- \rightarrow H_2O \qquad \Delta H_0$$

$$H_nA + HO^- \rightarrow H_{n-1}A^- + H_2O \qquad \Delta H_1$$

$$H_{n-(p-1)}A^{(p-1)-} + HO^- \rightarrow H_{n-p}A^{p-} + H_2O \qquad \Delta H_p$$

$$HA^{(n-1)-} + HO^- \rightarrow A^{n-} + H_2O \qquad \Delta H_n$$

For the remainder of the calculations, it is useful to introduce an auxiliary notation for the concentrations of the various species which may be present in solution a time t.

$$C_0 = (H_nA) + (H_{n-1}A^-) + \ldots\ldots\ldots\ldots + (A^{n-})$$

$$C_1 = (H_{n-1}A^-) + \ldots\ldots\ldots\ldots + (A^{n-})$$

$$C_p = (H_{n-p}A^{p-}) + \ldots\ldots + (A^{n-}) = \sum_{i=p}^{n} (H_{n-i}A^{i-})$$

$$C_n = (A^{n-})$$

We also consider:

$$\bar{C}_1 = C_0 - C_1$$

$$\bar{C}_p = C_0 - C_p = C_0 - \sum_{i=1}^{n} (H_{n-i}A^{i-})$$

$$\bar{C}_n = C_0 - C_n$$

This notation can be easily condensed using the matrix form (details are available on request).

In these conditions the calorimetric balance (assuming heat losses and heat of dilution to be negligible: the thermogram becoming with this assumption, an enthalpogram (*10*)) expresses at time t, the heat corresponding to:

Neutralization of the H^+ ion (the strongest acid in solution) or $[(H^+)_0V_0 - (H^+)(V_0 + vt)]\,\Delta H_0$

Effective formation of the compound $H_{n-1}A^-$ by reaction with sodium hydroxide, or: $[(H_{n-1}A^-)(V_0 + vt) - (H^+)_0 V_0]\Delta H_1$

Formation of compounds $H_{n-2}A^{2-} \ldots H_{n-p}A^{p-}, \ldots A^{n-}$ or:

$$(H_{n-2}A^{2-})(V_0 + vt)(\Delta H_1 + \Delta H_2)$$
$$+ \ldots (H_{n-p}A^{p-})(V_0 + vt)(\Delta H_1 + \Delta H_2 + \ldots \Delta H_p)$$
$$+ \ldots (A^{n-})(V_0 + vt)(\Delta H_1 + \Delta H_2 + \ldots \Delta H_p + \ldots \Delta H_n)$$

Hence, after finding a common factor for the ΔH_p terms and after using the above notation:

$$-q = (H^+)_0V_0\,(\Delta H_0 - \Delta H_1) - (H^+)(V_0 + vt)\,\Delta H_0 + (V_0 + vt)\sum_{i=1}^{n} \Delta H_i C_i \quad (1)$$

By introducing the electroneutrality and mass conservation Equations 2 and 3

$$\sum_{i=1}^{n} C_i = (H^+) - (HO^-) + \frac{C_B vt}{V_0 + vt} \quad (2)$$

$$C_0 = \frac{C_A vo}{V_0 + vt} \quad (3)$$

and considering that, at time t, among the concentrations of the $(n + 1)$ species in solution (H_nA), $(H_{n-1}A^-)$, etc. . . ., two are numerically greater than the others, i.e.,

$H_{n-(p-1)}A^{(p-1)-}$ and $H_{n-p}A^{p-}$, with:

$$H_{n-(p-1)}A^{(p-1)-} + HO^- \rightarrow H_{n-p}A^{p-} + H_2O \quad \Delta H_p$$

we arrive at Equation 4 (detailed calculations are available on request from the authors).

$$-q = C_B\,vt\,\Delta H_p + (H^+)_0\,V_0\,(\Delta H_0 - \Delta H_1) + C_A\,V_0 \sum_{i=1}^{n} (\Delta H_i - \Delta H_p) - (H^+)(V_0 + vt)\,\Delta H_0 + [(H^+) - (HO^-)]\,(V_0 + vt)\,\Delta H_p - \sum_{i=1}^{p} \bar{C}_i(\Delta H_i - \Delta H_p)(V_0 + vt) + \sum_{i=p+1}^{n} C_i(\Delta H_i - \Delta H_p)(V_0 + vt) \quad (4)$$

In this equation, owing to the hypotheses made, the first three terms are the only ones which are numerically great in relative value. In coordinates $-q = f(t)$ or $-q = f(vt)$, the equation is thus that of a line with the slope $C_B v \Delta H_p$ or $C_B \Delta H_p$ and with the intercept: $(H^+)_0V_0(\Delta H_0 - \Delta H_1) + C_A\,V_0 \sum_{i=1}^{P} (\Delta H_i - \Delta H_p)$ independent of time, with a series of corrective terms. This line is the support of the segment relative to the pth neutralization of the polyacid.

The corrective terms are of two types:

(a) terms directly dependent on the solution pH

$$(H^+)\,(\Delta H_p - \Delta H_0)\,(V_0 + vt) - (HO^-)\Delta H_p(V_0 + vt)$$

(b) terms dependent on the concentrations

$$\sum_{i=1}^{P} \bar{C}_i\,(\Delta H_i - \Delta H_p)\,(V_0 + vt) + \sum_{i=p+1}^{n} C_i(\Delta H_i - \Delta H_p)(V_0 + vt)$$

These corrective terms may be considered as numerically small, except at the ends of the segment in question, where they may justify connection curves with neighboring segments.

Remark: an equation similar to 4, but slightly more complex, can be derived for the case of a polyacid H_nA, the i first acidities of which are sufficiently strong to be dissociated in the initial solution (Detailed calculations are available on request).

Monoprotic Acids. For a monoacid ($p = n = 1$), Equation 4 giving the calorimetric balance becomes, for the overall reaction:

$$HA + HO^- \rightarrow A^- + H_2O \qquad \Delta H$$

$$-q = C_B\, vt\, \Delta H + (H^+)_0\, V_0\, (\Delta H_0 - \Delta H) + [(H^+) - (HO^-)]\, (V_0 + vt)\, \Delta H - (H^+)\, \Delta H_0\, (V_0 + vt)$$

The recorded thermogram $-q = f(vt)$ is a line with the slope $C_B\Delta H$ and with the intercept $(H^+)_0\, V_0(\Delta H_0 - \Delta H)$ if the terms involving variable concentrations can be ignored. This equation reproduces the conditions advanced by Tyrell (*10*) in the case of a reaction of the form $A + B \rightleftharpoons C$.

Symmetrical Diprotic Acids. (*a*) *General Equations.* If $p = 1$ (first neutralization) and $n = 2$, Equation 4 becomes:

$$-q = C_B vt\Delta H_1 + (H^+)_0\, V_0\, (\Delta H_0 - \Delta H_1) + [(H^+) - (HO^-)]\, (V_0 + vt)\, \Delta H_1 - (H^+)\, \Delta H_0\, (V_0 + vt) + (A^{2-})(\Delta H_2 - \Delta H_1)(V_0 + vt) \qquad (5)$$

and for $p = 2$ (second neutralization) and $n = 2$:

$$-q = C_B vt\Delta H_2 + (H^+)_0 V_0(\Delta H_0 - \Delta H_1) + C_A V_0(\Delta H_1 - \Delta H_2) + [(H^+) - (HO^-)]\, (V_0 + vt)\, \Delta H_2 - (H^+)\, \Delta H_0\, (V_0 + vt) - (H_2A)(\Delta H_1 - \Delta H_2)\, (V_0 + vt) \qquad (6)$$

(*b*) *Simplified Equations.* Equations 5 and 6 both represent the heat balance during the entire titration. If all terms which include a concentration $(H^+)_0$ are ignored, Equations 4 and 5 can each be considered as the equation of a line experimentally representing the two successive neutralization stages of H_2A. The justification of this simplification will be given subsequently.

During the first part of the neutralization of the diacid H_2A whose balance is expressed by:

$$H_2A + HO^- \rightarrow HA^- + H_2O$$

Equation 5 can thus be written:

$$-q = C_B vt\Delta H_1 - (H^+)_0 V_0(\Delta H_1 - \Delta H_0) \qquad (5')$$

corresponding to the equation of a line segment with slope $C_B v\Delta H_1$ in a system of $(-q, t)$ coordinates or of slope $C_B\Delta H_1$ in a system of $(-q, vt)$ coordinates corresponding to the recorded thermogram, and with the q intercept

$$-(H^+)_0\, V_0\, (\Delta H_1 - \Delta H_0)$$

Similarly, during the second part of the neutralization of the same diacid, taken as a whole:

$$HA^- + HO^- \rightarrow H_2O + A^{2-}$$

Equation 6 becomes:

$$-q = C_B\, vt\, \Delta H_2 + C_A\, V_0\, (\Delta H_1 - \Delta H_2) + (H^+)_0\, V_0\, (\Delta H_0 - \Delta H_1) \qquad (6')$$

corresponding to a line equation with slope $C_B\Delta H_2$ and a q intercept

$$C_A V_0\, (\Delta H_1 - \Delta H_2) + (H^+)_0\, V_0\, (\Delta H_0 - \Delta H_1)$$

(*c*) *Discussion.* Qualitatively, for the portion corresponding to the first neutralization, one can, at the start of the addition, ignore the (HO^-) and (A^{2-}) concentrations appearing in Equation 5. The only corrective terms are, therefore, the terms:

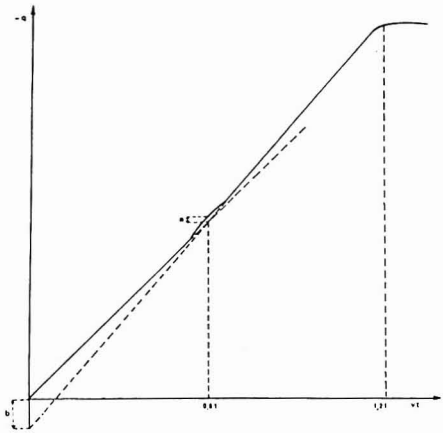

Figure 1. Typical enthalpogram obtained during neutralization of a glutaric acid solution (C_A = 115 10^{-4} mol L^{-1}, $V_0 = 10^{-1}$ L) by a sodium hydroxide solution (C_B = 1.91 mol L^{-1})

$$a_0 = -(H^+)_0\, V_0\, (\Delta H_1 - \Delta H_0)$$

and

$$a = (H^+)\, (V_0 + vt)\, (\Delta H_1 - \Delta H_0)$$

a_0 and a only act, as a rule, at the very beginning of the reaction and justify an initial rounding off, which is, in fact, only slight.

At the end of the neutralization reaction of the first acidity, if (H^+) and (HO^-) are negligible, (A^{2-}) is not, in spite of its weakness. For the portion corresponding to the second neutralization, the corrective terms are:

$$(HO^-)\, (V_0 + vt)\, \Delta H_2$$

and

$$(H_2A)\, (V_0 + vt)(\Delta H_2 - \Delta H_1)$$

equal to

$$(A^{2-})\, (V_0 + vt)(\Delta H_2 - \Delta H_1)$$

at the junction of the two line segments represented by Equations 5′ and 6′. It is, moreover, easy to check that the junction corresponds to the semi-neutralization of the diacid.

According to the foregoing qualitative discussion, the experimental curve corresponding to the titration period properly speaking must successively exhibit a curve portion, a line segment, a new curve, followed by another line segment and possibly a final curve connecting it to the base line. This is confirmed by the experiment (Figure 1). It may be observed that the curve obtained can be "fitted" on two lines. These two lines have the following equations:

$$-q = C_B\, vt\, \Delta H_1$$

and

$$-q = C_B\, vt\, \Delta H_2 + C_A\, V_0\, (\Delta H_1 - \Delta H_2)$$

The experimental data at the start and the known values of neutralization enthalpies (cf. Experimental) make it possible to calculate the differents corrective terms of expressions 5 and 6 in relation to the respective values $C_B vt\Delta H_1$ and

$C_B v t \Delta H_2 + C_A v_0 (\Delta H_1 - \Delta H_2)$. The term $(H^+)_0 V_0 (\Delta H_0 - \Delta H_1)$ equal to 0.039 J is always negligible. Up to the semi-neutralization point, all the corrective terms of expression 5 are negligible. (These terms were computed with the results of a parallel potentiometric experiment with the same experimental conditions according to classical calculations (*31*)). The only exception is the term $(A^{2-})(V_0 + vt)(\Delta H_2 - \Delta H_1)$ which at the first neutralization point has a value of 0.42 J, a value lying within the measurement limits of our apparatus. This also applies to the corrective terms of expression 6 except at the semi-neutralization point where the term is $(H_2A)(V_0 + vt)(\Delta H_2 - \Delta H_1)$ is also equal to 0.42 J, and near the complete neutralization point (1.20×10^{-3} L sodium hydroxide added) for which the term in $(HO^-)(V_0 + vt)\Delta H_2$ takes the value of 0.6 J. At the end of the first neutralization, we experimentally ascertained for glutaric acid in the experimental conditions used, a small "hump" (Figure 1) which can be explained by the corrective terms $(A^{2-})(V_0 + vt)(\Delta H_2 - \Delta H_1)$ and $(H_2A)(V_0 + vt)(\Delta H_2 - \Delta H_1)$. This equation is explored further in the following paragraphs.

At the end of the first neutralization, we have (*31*):

$$(H_2A) = (A^{2-}) = \frac{C_A}{2 + \sqrt{K_1/K_2}}$$

K_1 and K_2 being the first and second acidity constants of the diacid. Hence, at this point, the ratio δ of the deviation from the theoretical line $-q = C_B v t \Delta H_1$, due to the corrective term $(A^{2-})(\Delta H_2 - \Delta H_1)(V_0 + vt)$, to the intercept $C_A v_0 (\Delta H_2 - \Delta H_1)$ of the support line of the second segment is equal to:

$$\delta = \frac{d}{b} = \frac{(A^{2-})(\Delta H_2 - \Delta H_1)(V_0 + vt)}{C_A V_0 (\Delta H_2 - \Delta H_1)} = \frac{1}{2 + \sqrt{K_1/K_2}}$$

since $vt \ll V_0$. Thus:

$$\frac{K_1}{K_2} = \left(\frac{1}{\delta} - 2\right)^2$$

In the same line, the relative deviation δ' from the theorical line due to the same corrective term as above amounts to:

$$\delta' = \frac{a}{c} = \frac{(A^{2-})(\Delta H_2 - \Delta H_1)(V_0 + vt)}{C_B v t \Delta H_1}$$

$$= \frac{(A^{2-})(\Delta H_2 - \Delta H_1)}{C_A \Delta H_1} \quad \text{since } C_B v t = C_A V_0$$

$$= \frac{1}{2 + \sqrt{K_1/K_2}} \left(\frac{\Delta H_2}{\Delta H_1} - 1\right) = \delta \left(\frac{\Delta H_2}{\Delta H_1} - 1\right)$$

These relations reveal the extent to which the parameters ΔH_1, ΔH_2, K_1, and K_2 act at the end of the first neutralization.

With glutaric acid the computed values are: $\delta \simeq 0.18$ and $\delta' \simeq 0.006$. These values are approximately the same as those obtained from the diagram (Figure 1). Unfortunately, the deviation ("hump") is very small and is at the borderline of the resolution power of our apparatus, so that we obtain with this graphic method only an order of magnitude of the ratio K_1/K_2.

Triprotic Acids. In this case ($n = 3$), the equations giving the calorimetric balances of the successive reactions:

$$H_3A + HO^- \rightarrow H_2A^- + H_2O \qquad (p = 1)$$

$$H_2A^- + HO^- \rightarrow HA^{2-} + H_2O \qquad (p = 2)$$

$$HA^{2-} + HO^- \rightarrow A^{3-} + H_2O \qquad (p = 3)$$

are written:

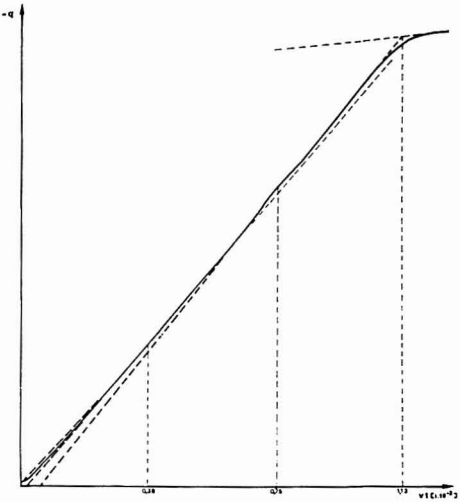

Figure 2. Typical thermogram obtained during neutralization of a citric acid solution ($C_A = 7.20 \times 10^{-3}$ mol L^{-1}, $V_0 = 10^{-1}$ L) by a sodium hydroxide solution ($C_B = 1.91$ mol L^{-1})

Table I. Errors Committed in Compiling the Calorimetric Balance by Using Only Equations 10, 11, and 12[a]

$vt \times 10^{-3}$ L	deviation from line, J, Eq 10	deviation from line, J, Eq. 11	deviation from line, J, Eq 12
0.04	+0.57		
0.08	+0.48		
0.20	+0.17		
0.36	−0.11		
0.40	−0.21	−0.10	
0.44		0	
0.60		−0.10	
0.76		−0.61	
0.80		−0.90	−0.31
0.84			−0.20
1.00			0
1.12			0
1.16			0
1.20			+3.32

[a] Note. The values calculated from Equations 7 and 8 on the one hand, and Equations 8 and 9 on the other, do not coincide perfectly. In our opinion, this must be considered as a result of the relative uncertainty concerning calculated concentration values and the enthalpy values employed.

$$-q = C_B v t \Delta H_1 + (H^+)_0 V_0 (\Delta H_0 - \Delta H_1) - (H^+)\Delta H_0 (V_0 + vt) + [(H^+) - (HO^-)](V_0 + vt)\Delta H_1 + (HA^{2-})(\Delta H_2 - \Delta H_1)(V_0 + vt) + (A^{3-})(\Delta H_3 + \Delta H_2 - 2\Delta H_1)(V_0 + vt) \quad (7)$$

$$-q = C_B v t \Delta H_2 + (H^+)_0 V_0 (\Delta H_0 - \Delta H_1) + C_A V_0 (\Delta H_1 - \Delta H_2) - (H^+)\Delta H_0 (V_0 + vt) + [(H^+) - (HO^-)](V_0 + vt)\Delta H_2 - (H_3A)(\Delta H_1 - \Delta H_2)(V_0 + vt) + (A^{3-})(\Delta H_3 - \Delta H_2)(V_0 + vt) \quad (8)$$

$$-q = C_B vt\Delta H_3 + (H^+)_0 V_0 (\Delta H_0 - \Delta H_1) + C_A V_0(\Delta H_1 + \Delta H_2 - 2\Delta H_3) - (H^+)\Delta H_0(V_0 + vt) + [(H^+) - (HO^-)](V_0 + vt)\Delta H_3 - (H_3A)(\Delta H_1 + \Delta H_2 - 2\Delta H_3)(V_0 + vt) - (H_2A^-)(\Delta H_2 - \Delta H_3)(V_0 + vt) \quad (9)$$

The recorded thermogram $-q = f(vt)$ must be based on three line segments, the respective equations of which are:

$$-q = C_B vt\Delta H_1 + (H^+)_0 V_0 (\Delta H_0 - \Delta H_1) \quad (10)$$

$$-q = C_B vt\Delta H_2 + (H^+)_0 V_0 (\Delta H_0 - \Delta H_1) + C_A V_0 (\Delta H_1 - \Delta H_2) \quad (11)$$

$$-q = C_B vt\Delta H_3 + (H^+)_0 V_0(\Delta H_0 - \Delta H_1) + C_A V_0 (\Delta H_1 + \Delta H_2 - 2\Delta H_3) \quad (12)$$

The deviations from linearity are justified by nonnegligible values of one or more terms which we have not taken into account in writing these line equations.

The experimental thermogram of citric acid (Figure 2) shows that one can effectively plot three line sections which intersect each other for added volumes of sodium hydroxide corresponding to the successive neutralization of the three acidities.

Table I shows, for successive volumes vt of sodium hydroxide added, the differences between the heat calculated from the complete Equations 7, 8, and 9 and the heat calculated from Equations 10, 11, and 12 of the corresponding line sections. (Here again the heat was computed with the results of a parallel potentiometric experiment with same experimental conditions using classical calculations (*31*)).

It can be seen that, within the range of accuracy of our equipment (cf. Experimental), the only glaring deviations from the lines are located:

At the start of the titration, where the term in $(H^+)(V_0 + vt)(\Delta H_1 - \Delta H_0)$ in Equation 7 is not negligible;

On both sides of the point equivalent to the neutralization of the second acidity for which the term in $(A^{3-})(\Delta H_3 - \Delta H_2)(V_0 + vt)$ is not negligible in Equation 8 and for which the term in $-(H_2A^-)(\Delta H_2 - \Delta H_3)(V_0 + vt)$ is not negligible in Equation 9;

At the very end of the determination, where the term in $-(HO^-)(V_0 + vt)\Delta H_3$ becomes great.

These results coincide perfectly with the thermogram obtained (Figure 2).

LITERATURE CITED

(1) J. Jordan, *Rec. Chem. Prog.*, **19**, 193 (1958).
(2) J. Jordan, in I. M. Kolthoff and P. J. Elving, "Treatise on Analytical Chemistry", Part I, Vol. 8, Interscience, New York, 1968, p 5175.
(3) L. D. Hansen, R. M. Izatt and J. J. Christensen, in J. Jordan, "New Developments in Titrimetry", Dekker, New York, 1974, p 1.
(4) H. J. V. Tyrrell and A. E. Beezer, "Thermometric Titrimetry", Chapman and Hall, London, 1968.
(5) L. S. Bark and S. M. Bark, "Thermometric Titrimetry", Pergamon, Oxford, 1969.
(6) G. A. Vaughan, "Thermometric and Enthalpimetric Titrimetry", Van Nostrand Reinhold, New York, 1973.
(7) J. Barthel, "Thermometric Titrations", John Wiley, New York, 1975.
(8) F. J. Miller and P. F. Thomason, *Talanta*, **2**, 109 (1959).
(9) J. Jordan, *Chimia*, **17**, 101 (1963).
(10) H. J. V. Tyrrell, *Talanta*, **14**, 843 (1967).
(11) J. Jordan, *J. Chem. Educ.*, **40**, 15 (1963).
(12) J. J. Christensen, R. M. Izatt, L. D. Hansen, and J. A. Partridge, *J. Phys. Chem.*, **70**, 2003 (1966).
(13) J. Barthel, F. Becker, and N. G. Schmahl, *Z. Phys. Chem.*, **29**, 58 (1961).
(14) F. Becker, J. Barthel, and N. G. Schmahl, *Z. Phys. Chem.*, **37**, 33 (1963).
(15) R. J. Raffa, M. J. Stern, and L. Malspeis, *Anal. Chem.*, **40**, 70 (1968).
(16) G. M. Fleck, "Equilibria in Solution", Holt, Rinehart and Winston, New York, 1966.
(17) R. J. N. Harries, *Talanta*, **15**, 1345 (1968).
(18) J. J. Christensen, R. M. Izatt, and L. D. Hansen, *J. Am. Chem. Soc.*, **89**, 213 (1967).
(19) L. S. Darken, *J. Am. Chem. Soc.*, **63**, 1010 (1941).
(20) G. D. Pinching and R. G. Bates, *J. Res. Natl. Bur. Std.*, **40**, 412 (1948).
(21) R. Gaue and C. K. Ingold, *J. Chem. Soc.*, 2158 (1931).
(22) W. J. Hawer, J. O. Burton, and S. F. Acree, *J. Res. Natl. Bur. Std.*, **24**, 290 (1940).
(23) G. D. Pinching and R. G. Bates, *J. Res. Natl. Bur. Std.*, **40**, 412 (1948).
(24) G. D. Pinching and R. G. Bates, *J. Res. Natl. Bur. Std.*, **45**, 327 (1950).
(25) G. Dalgren, and F. A. Land, *J. Am. Chem. Soc.*, **82**, 1306 (1960).
(26) J. L. Burgot, *Talanta*, **25**, 233 (1978).
(27) J. L. Burgot, *Talanta*, **25**, 339 (1978).
(28) J. Barthel, F. Becker, and N. G. Schmahl, *Z. Phys. Chem.*, **29**, 58 (1961).
(29) J. D. Hale, R. M. Izatt, and J. J. Christensen, *J. Phys. Chem.*, **67**, 2605 (1963).
(30) C. E. Vanderzee and J. A. Swanson, *J. Phys. Chem.*, **67**, 2608 (1963).
(31) J. H. Ricci, "Hydrogen Ion Concentration, New Concepts in a Systematic Treatment", Princeton University Press, Princeton, N. J., 1952.

RECEIVED for review May 11, 1978. Accepted March 12, 1979.

Cathodic Stripping Voltammetric Determination of Organic Halides in Drug Dissolution Studies

Ian E. Davidson*

Wyeth Laboratories, Huntercombe Lane South, Taplow, Maidenhead, Berkshire, SL6 0PH, England

W. Franklin Smyth

Department of Chemistry, Chelsea College, University of London, Manresa Road, London SW3, England

A method has been developed to analyze therapeutically active organic hydrochlorides and hydrobromides in drug dissolution studies by cathodic stripping voltammetry. Results on tablets are accurate at concentrations of 10^{-5} and 5×10^{-6} M for hydrochlorides and hydrobromides with coefficients of variation of 3.1 and 2.9%, respectively. Problems associated with halide monolayer formation on hanging mercury drop electrodes are discussed, and by presaturating the supporting electrolyte with mercurous halide limits of detection of 10^{-6} and 2×10^{-7} M for chloride and bromide, respectively, are obtained in 0.05 M nitric acid/potassium nitrate. The effects of 17 common pharmaceutical excipients are studied and the method is shown to be an order of magnitude more sensitive than UV spectrophotometry for drugs with molar extinction coefficients of 2000 m^2 M^{-1}. Applications of dc polarography, cyclic voltammetry, and a mercury-coated glassy carbon electrode are also discussed.

An important aspect in the development of a new drug formulation is the determination of its bioavailability. In addition to determination of drug and metabolite levels in body fluids such as blood and urine, the testing of in vitro formulation dissolution is of importance. This method determines the dissolution profile of a drug from tablets, capsules, suppositories, etc. The general nature of dissolution testing is well documented (*1–4*), normally involving measurement of drug levels released into a dissolution medium, usually water, at set time intervals. Measurement is commonly carried out by sampling an aliquot of the solution and determining the drug content by UV spectrophotometry. Either discrete sampling or automated flow analysis can be used. UV spectrophotometric analysis does depend however on a relatively high extinction coefficient for the compound since concentrations are usually of the order of 1–10 μg mL^{-1} (about 10^{-6} M for many drugs). Problems are encountered when compounds involved in dissolution studies either (a) are present in low concentrations or (b) possess low extinction coefficients. Other more sensitive but time-consuming techniques, such as solvent extraction/concentration, gas chromatography, high pressure liquid chromatography, fluorescence, etc., need to be considered in these situations.

Many drugs are formulated as halide salts of weak organic bases (*3, 5*). At present, of the FDA-approved commercially marketed salts, 43% are hydrochlorides, 4% are chlorides, 2% are hydrobromides, 5% are bromides, and 2% are iodides, i.e., a total of 56% are possible candidates for halide analysis.

Many methods exist for the determination of chloride ion in a variety of media. Most are applicable satisfactorily at levels of 10^{-2}–10^{-3} M. These are well-documented and include titration with silver or mercury salts with visual (*6, 7*) or potentiometric (*8*) end-point detection. A wide range of methods for the chloride ion in biological fluids has been summarized (*9*) including electrochemical methods such as polarography, coulometry, and conductimetry. The coulometric method is widely used (*10*) and ion selective electrodes have also been used (*11*). Bromide analysis is less well documented although most of the above techniques can be used for its determination. It has been determined in clinical situations by complexation with ferric thiocyanate (*12*).

A seldom exploited though sensitive analytical technique for halide measurement is cathodic stripping voltammetry (CSV). Several workers have applied CSV to the determination of halides in a variety of media. Work to date has been summarized in two recent monographs (*13, 14*) and has been limited mainly to inorganic analysis. The determination of halide ions in aqueous solution in the range 2×10^{-5}–10^{-3} M (*15*) and the determination of bromide and chloride in airborne particulate matter have been described (*16*). Exchange reactions involving electrogenerated mercurous halide films have been studied by CSV, as has the simultaneous determination of bromide and chloride (*17, 18*). Using this method, sensitivities of 10^{-5}, 10^{-6}, and 10^{-7} M for Cl^-, Br^-, and I^-, respectively, have previously been claimed by other workers (*19*). This paper attempts to show that the technique is particularly applicable to samples at about the 10^{-6} M level and to organic halide salts with low extinction coefficients. Organic hydrochlorides and hydrobromides are considered in this paper and the two model compounds used to display the application of CSV are compounds I and II, i.e., (−)-*cis*-2-(α-dimethylamino-*m*-hydroxybenzyl)cyclohexanol hydrochloride and (−)-13β-amino-5,6,7,8,9,10,11,12-octahydro-5α-methyl-5,11-methanobenzocyclodecen-3-ol hydrobromide, respectively.

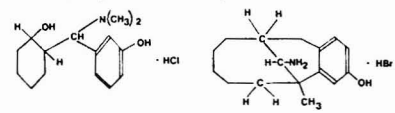

I II

EXPERIMENTAL

Apparatus. All experiments were performed using a Princeton Applied Research Model 174A polarograph with a Metrohm E410 hanging mercury drop electrode (HMDE). Voltammograms were recorded on an Advance Instruments X–Y plotter type LC100. The three-electrode system was utilized with a platinum wire auxiliary electrode and a saturated calomel reference electrode separated from the sample cell via a fritted glass salt bridge tube containing saturated potassium nitrate solution. Sample solutions were stirred using a 1-cm bar magnet rotating at 120 rpm.

Accurate additions of standards to samples were made using a 100-μL syringe micropipet.

Dissolution equipment used was similar to that described in "United States Pharmacopoeia XIX", 1975; p 651, using distilled water as the dissolution medium.

A Beckman DB spectrophotometer was used for UV spectrophotometric analysis.

0003-2700/79/0351-2127$01.00/0

Reagents. Compounds I and II, named above, were prepared in Wyeth Laboratories, and purities were checked by thin-layer chromatography. Both had purities above 99%.

Doubly distilled water was obtained by fractionally distilling water containing 1 g of silver nitrate and 20 mL of concentrated nitric acid per liter. The purified water was stored in glass containers.

Supporting electrolyte solutes were an Analar grade.

Mercurous bromide was supplied by Pfaltz and Bauer, Stamford, Conn., and mercurous chloride by British Drug Houses Ltd., Poole, England.

Triply distilled mercury was used in the HMDE.

Pharmaceutical excipients were of pharmacopoeial monograph grade where such a specification existed for the substance.

Procedure. Mercurous chloride (or mercurous bromide) saturated supporting electrolyte, 2.5 mL, containing 0.1 M potassium nitrate and 0.1 M nitric acid (prepared as described below) was added to a 2.5-mL sample (containing up to 2×10^{-5} M chloride or 5×10^{-6} M bromide) in the sample cell. The solution was degassed by bubbling oxygen-free nitrogen through the solution for 5 min after which a flow of nitrogen was maintained over the solution. A five-division mercury drop was dialed on the working electrode and maintained at a potential of −0.70 V for 5 min. This negative potential preconditioning allowed adsorbed impurities to be removed from the mercury surface. The potential was then scanned in a positive direction to +0.35 V for chloride (or +0.30 V for bromide) and electrolysis performed for 2 min with stirring followed by a 15-s quiescent period. A potential scan at 5 mV s^{-1} towards negative potentials was then employed to obtain the stripping voltammogram. A reverse scan to the electrolysis potential was then employed and the electrolysis/stripping process repeated.

At the end of the second scan, the potential was held at −0.70 V, 0.05 mL of standard solution added (concentrations up to 2×10^{-3} M chloride or 5×10^{-4} M bromide, depending on sample concentration) and a reverse scan back to the electrolysis potential performed with stirring, and the electrolysis/stripping process repeated in duplicate. Sample concentrations were calculated as described later in the text.

Blank scans were run on mercurous halide saturated electrolyte diluted ×2 with distilled water with subsequent standard addition to determine any blank correction to be made to the determination of the concentration.

The polarograph was normally operated using the 5-μA current range, and all experiments were performed at ambient room temperature (22 °C).

RESULTS AND DISCUSSION

Dc Polarographic Behavior of Compounds I and II. Anodic waves corresponding to the formation of insoluble mercury salts such as halides have previously been studied polarographically (*20*). Theoretically, the shape of the polarographic wave should commence discontinuously and the half-wave potential is given by the Nernst equation,

$$E_{1/2} = E'^0 - \frac{RT}{F} \ln \frac{(A^-)}{2}$$

where the symbols have their usual meaning and (A^-) is the molar concentration of halide in solution. However, in practice, departures from this ideal behavior are seen for halides with the appearance of a small adsorption prewave prior to the main wave, due to monolayer salt formation. Figures 1, a and b, show the anodic waves obtained for compounds I and II (5×10^{-4} M in 0.1 M HNO_3/KNO_3) where Hg_2Cl_2 and Hg_2Br_2, respectively, are the products of electrochemical oxidation. In each curve, process 1 represents the adsorption prewave and 2 the main wave, shifted to more positive potentials by virtue of the extra resistance to oxidation imposed by the adsorbed monolayer. The importance of this monolayer formation and its effect on the application to stripping analysis is considered below.

For compound I, $E_{1/2}$'s for the prewave and main wave are respectively +0.24 and +0.27 V, while the respective values

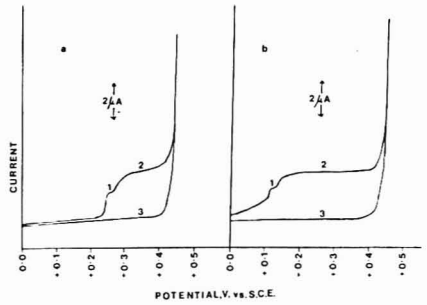

Figure 1. Dc polarography of 5×10^{-4} M solutions of (a) compound I and (b) compound II in 0.1 M KNO_3/HNO_3. 1 represents adsorption prewave; 2 is the main wave; 3 is the residual current due to the electrolyte alone

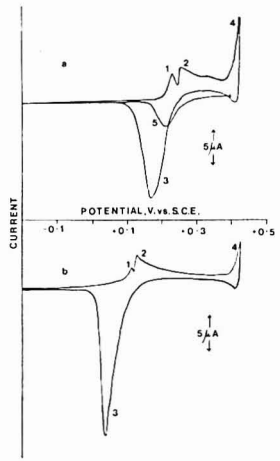

Figure 2. Cyclic voltammetry of 5×10^{-4} M solutions of (a) compound I and (b) compound II in 0.1 M KNO_3/HNO_3. See text for details

for compound II are +0.10 and +0.13 V in 0.1 M HNO_3/KNO_3.

The above work was performed using a conventional dropping mercury electrode.

Cyclic Voltammetry of Compounds I and II. The anodic oxidation processes with subsequent reversed stripping are best demonstrated by cyclic voltammetry at the hanging mercury drop electrode. Figures 2, a and b, show the voltammograms for compounds I and II; processes 1, 2, and 3 correspond respectively to monolayer formation, bulk deposition of mercurous halide, and cathodic stripping, while process 4 shows the oxidation and reduction of the mercury contained in the hanging mercury drop electrode. Experiments were performed in quiescent solution with a scan rate of 50 mV s^{-1}. For compound I, potentials were (1) +0.24 V, (2) +0.27 V, (3) +0.17 V while for compound II, potentials were (1) +0.12 V, (2) +0.13 V, and (3) +0.04 V. Concentrations of 5×10^{-4} M in 0.1 M HNO_3/KNO_3 were used.

The area under the reduction peak is greater than that for the sum of the oxidation peaks, i.e., apparently Q stripping is greater than Q deposition where Q represents the quantity of electricity involved in the process. However the reason for this is that after processes 1 and 2 the plating process con-

tinues through the remainder of the positive going scan, back through the negative going scan to the point at which stripping commences, leading to a concentration of mercurous halide throughout the sequence 1 → 2 → 4 → 3. This confirms data presented by other workers (*15*). Figure 2a, scan 5, shows an immediate direct scan of 5×10^{-4} M compound I under similar conditions, from +0.40 V. The peak is due to the stripping of Hg_2Cl_2 plated in scanning from +0.40 V to commencement of stripping. The phenomenon is even more marked for compound II, where a longer time period elapses between initial anodic reaction and subsequent cathodic stripping. The importance of accurate and reproducible timing of electrolysis and stripping is therefore evident.

This preliminary study indicated the possibility of cathodic stripping voltammetric analysis using electrolytic plating for chloride and bromide at potentials more positive than +0.30 and +0.20 V, respectively.

Cathodic Stripping Voltammetry of Compounds I and II. *Choice of Indicator Electrode for Cathodic Stripping Voltammetry.* Two types of electrode were considered for the CSV studies, viz., (a) a hanging mercury drop electrode as described above, and (b) a mercury-coated glassy carbon electrode (MCGCE). The latter was a Princeton Applied Research epoxy-sealed electrode supplied with planar impervious "glass" carbon surface (approximate surface area 28 mm^2) polished to a mirror finish and subjected to electrolysis with a 10^{-5} M solution of $Hg(NO_3)_2 \cdot H_2O$ at–0.55 V vs. the saturated calomel electrode.

Stirring was carried out for the 30-min duration of the electrolysis. Several alternative mercury plating techniques have been reported previously (*21–24*). Figures 3, a and b, show the peak shapes obtained for approximately 10^{-5} M solutions of compounds I and II for each type of electrode. Although higher sensitivities could be achieved using a plated electrode, peak shape was better and total analysis time shorter using the HMDE, so this electrode was used in all subsequent work.

Efficiency of Electrolysis/Stripping Process. Previous workers (*17*) have reported that in 1.8 M sulfuric acid at a scan speed of 50 mV/s and Cl^- concentration of 3.3×10^{-5} M several scans were required for the complete removal of the plated compound. Under the conditions of our experiments, we have not observed such an effect. Repeat scans after identical plating conditions have given reproducible stripping peaks, with complete removal of the plated mercurous halide. However, a much slower scan speed (5 mV/s) is used in the present work. The effect of scan speed on peak height and shape is discussed below.

Effect of Scan Rate on Stripping Current and Peak Shape. Scanning at rates of 2, 5, 10, and 20 mV s^{-1} gave stripping peak heights in the ratio 14:32:58:75 (10 units ≡ 0.5 μA) at a concentration of 2.5×10^{-5} M compound I in 0.1 M HNO_3/KNO_3 after 1.5-min stirred, 15-s quiescent electrolysis at +0.35 V. Approximate linearity is therefore obtained between scan rate and peak height up to 10 mV s^{-1}. Recovery of plated material was shown to be complete at each of these scan rates by performing replicate electrolyses. Peak shape was improved the lower the scan rate with 5 mV s^{-1} providing the optimum compromise between speed of analysis and sensitivity.

Choice of Supporting Electrolyte. Small amounts of impurities and surfactants in distilled water have a distinctly adverse effect on chloride CSV, but affect bromide analysis to a much lesser extent. For CSV studies it is recommended that the purification process referred to above, i.e., refluxing with silver nitrate and nitric acid before final distillation, is adopted.

A supporting electrolyte of 0.05 M potassium nitrate/nitric acid (pH 1.5) was chosen after a brief investigation of other possible combinations, i.e., (a) 0.1 M KNO_3/HNO_3, (b) 0.1 M HNO_3, (c) 0.1 M KNO_3/HNO_3 in 50% ethanol. Minimum background current was exhibited by 0.05 M HNO_3/KNO_3. This electrolyte contained HNO_3 to avoid the possible formation of mercury oxides/hydroxide at neutral or alkaline pH.

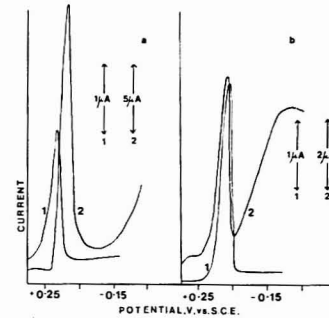

Figure 3. Comparison of performances of (1) hanging mercury drop electrode and (2) mercury-coated glassy carbon electrode for (a) compound I and (b) compound II. Concentrations are (1a) 3×10^{-5} M; (2a) 6×10^{-3} M; (1b) 2×10^{-5} M; (2b) 10^{-5} M in 0.05 M KNO_3/HNO_3. Current ranges as shown

Although greater sensitivity can be achieved by lowering the temperature and using an electrolyte containing alcohol (the solubility of the plated product is lowered), this advantage is outweighed by losses due to evaporation on degassing and maintaining an accurate temperature. The use of room temperature with an aqueous supporting electrolyte was found to be more practical.

Presaturation of Supporting Electrolyte with Mercurous Halide. Electrolytic plating can be achieved only if (a) the solubility product of the mercurous halide in the electrolyte is exceeded and (b) the minimum concentration for salt nucleation and growth is achieved. Below a certain concentration plating cannot be achieved and this concentration is temperature dependent. Figure 4 shows the dependence of the peak current/sample concentration graphs on temperature for the stripping of Hg_2Cl_2 produced from compound I. Limits of detection using a supporting electrolyte not saturated with mercurous chloride at 0, 19, and 40 °C were about 5×10^{-6}, 10^{-5}, and 3×10^{-5} M, respectively.

In order to overcome the problem of minimum threshold sample concentration for plating, the supporting electrolyte was presaturated with the relevant mercurous halide and samples were added to this electrolyte. The effect is shown for Hg_2Cl_2 in Figure 5. Prior to saturation, a nonlinear relationship between stripping peak height and concentration was obtained. After saturation at 70 °C, with subsequent cooling, additions of chloride ion to this electrolyte led to a linear graph passing through the origin. For accurate work near the limit of detection this presaturation process is considered essential.

The behavior of bromide is similar although the concentration threshold is lower. Presaturation ensures that all sample concentration is used in plating and none in overcoming the solubility product and salt growth threshold problems.

Greater sensitivity is possible in the case of bromide since the solubility products of Hg_2Cl_2 and Hg_2Br_2 are respectively 1.1×10^{-18} and 1.3×10^{-21} at room temperature (*25*). Using mercurous saturated supporting electrolyte, limits of detection of samples at 22 °C of 10^{-6} M chloride and 2×10^{-7} M bromide could be achieved, approximately an order of magnitude lower than without presaturation.

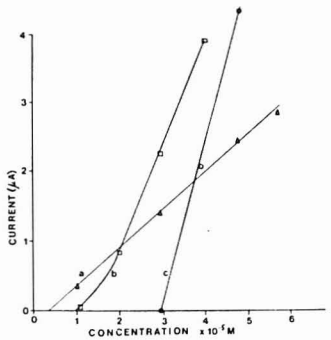

Figure 4. Variation of stripping current with temperature for compound I in the concentration range (1–5) × 10^{-5} M in 0.05 M KNO_3/HNO_3: (a) 0 °C, (b) 19 °C, (c) 40 °C

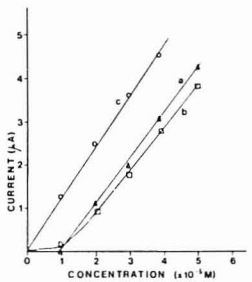

Figure 5. Cathodic stripping of compound I with electrolyte (0.05 M KNO_3/HNO_3) presaturated with mercurous chloride. Electrolyte (a) with no mercurous chloride; (b) presaturated cold with mercurous chloride; (c) presaturated at 70 °C with mercurous chloride

The procedure used to obtain accurate concentrations of halide in the electrolyte was to presaturate 0.1 M HNO_3/KNO_3 with the relevant halide by heating at 70 °C with excess mercurous halide for 1 h with stirring, cooling, and testing by CSV. Generally, supersaturation led to a small stripping peak being obtained. This supersaturated solution was diluted with 0.1 M HNO_3/KNO_3 until the peak almost disappeared on plating/stripping. This diluted solution was then taken as the supporting electrolyte for subsequent determination of organic halides, and any slight peak obtained subtracted from added samples and standards in calculations. Linearity of sample concentration vs. peak height was obtained using this presaturated supporting electrolyte technique over the range 10^{-6} M to at least 4 × 10^{-5} M for chloride and 2 × 10^{-7} M to at least 5 × 10^{-6} M for bromide.

In the above work, plating was performed under stirred conditions with a minimum quiescent period prior to stripping, as explained below.

Electrode Monolayer Formation and Effect of Stirring during Electrolysis Step. Under quiescent conditions of electrolysis the subsequent stripping peak occurs in two processes, corresponding to the removal of bulk mercurous halide followed by a more strongly held monolayer. The phenomenon of monolayer formation has previously been studied for mercury salts at mercury electrodes by a number of workers (*20*, *26*, *27*). Figures 6, a and b, show the difference between quiescent and stirred electrolysis of compound I. At approximately a concentration of 5 × 10^{-5} M in quiescent solution two peaks are produced with maxima at +0.20 and

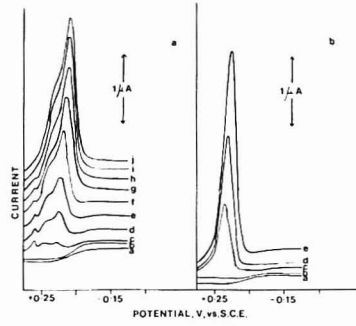

Figure 6. Cathodic stripping of compound I: effect of stirring on peak shape. (a) Unstirred solution: 10-min electrolysis at +0.35 V. (b) Stirred solution: 2-min stirred, 15-s quiescent electrolysis at +0.35 V. Concentrations are: (a) 0.0, (b) 0.99, (c) 1.96, (d) 2.91, (e) 3.84, (f) 4.75, (g) 5.64, (h) 6.54, (i) 7.41, (j) 8.26 × 10^{-5} M in 0.05 M KNO_3/HNO_3

+0.10 V while in stirred solution; only a single peak is produced at +0.20 V, showing that the less positive monolayer peak has been eliminated and only a peak due to bulk deposition is in evidence. A similar though less marked effect occurs for bromide, where two peaks with maxima +0.15 and +0.07 V are seen in unstirred solution and a single peak at +0.10 V in stirred solution, at the 10^{-5} M concentration level (electrolyte 0.05 M KNO_3/HNO_3 for both chloride and bromide).

For practical analysis, the sample solution must be stirred. Figures 7, a and b, show the peak current vs. concentration relationships for chloride in unstirred (less positive peak measured) and stirred solutions. Linearity is achieved for the stirred solution, not for the quiescent. Graphs do not pass through the origin since a nonsaturated supporting electrolyte was used with the most dilute solutions being below the threshold level of Hg_2Cl_2 at which plating occurs. Stirring at 120 rpm using a small bar magnet was found to be adequate for practical purposes.

During electrolysis, a minimum quiescent period is required after stirring, sufficient only to allow the sample solution to settle; otherwise distorted type monolayer/bulk stripping peaks result. Stirring for 2 min followed by a 15-s quiescent period was found to be ideal.

Effect of Plating Potential. The half-wave potentials for the anodic waves of chloride and bromide are +0.31 and +0.19 V, respectively, at the 10^{-4} M level, in 0.05 M KNO_3/HNO_3. Optimum potentials for electrolysis were shown to be +0.35 and +0.30 V, respectively. An important factor is that for a particular concentration, electrolysis is carried out on the plateau of the dc curve since $E^1/_2$ varies with concentration. At points on the rising portion, alterations in concentration would alter the efficiency of electrolysis.

A study of the electrocapillary curve in the chosen electrolyte for both chloride and bromide was undertaken after problems of easy dislodgment of the hanging mercury drop occurred at potentials more positive than +0.36 V and more negative than −1.5 V. Using a normal dropping mercury capillary, the drop rate was measured against potential, with the results shown in Figure 8 for supporting electrolyte alone (0.05 M KNO_3/HNO_3) and containing 10^{-4} M compounds I and II. Drop time is proportional to surface tension (*28*) and with a HMDE the drop is most stable at the electrocapillary maximum (about −0.5 V). Surface tension falls suddenly between +0.25 and +0.40 V, explaining the tendency for easy drop dislodgement above +0.36 V.

Effect of Common Pharmaceutical Excipients. Various

Table I. Effect of the Addition of (a) 500 μg and (b) 1 mg of Excipients on the Stripping Currents and Potentials of a 5-mL Solution of Compound I at a Concentration of 3×10^{-5} M in 0.05 M KNO_3/HNO_3 (9 μg/mL)

	before excipient addition		after excipient addition		
	peak current,		peak current, μA		
excipient	μA	E_p, V[a]	a	b	E_p, V[a]
lactose USP	2.23	+0.20	2.10	2.00	+0.20
talc USP	2.15	+0.20	2.18	2.18	+0.20
povidone USP	2.08	+0.20	1.50	1.65	+0.19
maize starch BP	2.78	+0.20	2.73	2.58	+0.20
Avicel	2.28	+0.20	2.33	2.05	+0.20
Solka Floc	3.28	+0.20	2.88	3.75	+0.21
Amijel	2.75	+0.20	3.00	2.68	+0.17
Celacol 20M	3.00	+0.20	3.28	4.00	+0.16
Amberlite IRP 88	2.45	+0.20	2.75	1.35	+0.20
magnesium stearate USP	2.35	+0.20	2.58	2.55	+0.20
dibasic calcium phosphate	2.10	+0.20	2.10	2.18	+0.20
sodium starch glycolate	2.55	+0.20	>>5.0	>>5.0	+0.20
sodium lauryl sulfate BP	3.45	+0.20	complete signal removal		
soft gelatin mix 1	1.80	+0.20	1.43	1.43	+0.15
soft gelatin mix 2	2.75	+0.20	2.55	2.80	+0.14
soft gelatin mix 3	1.73	+0.20	1.98	2.00	+0.15
hard gelatin mix	2.10	+0.20	1.93	1.95	+0.15

[a] Vs. SCE.

Table II. Effect of the Addition of (a) 500 μg and (b) 1 mg of Excipients on the Stripping Currents and Potentials of a 5-mL Solution of Compound II at a Concentration of 3×10^{-5} M in 0.05 M KNO_3/HNO_3 (10 μg/mL)

	before excipient addition		after excipient addition		
	peak current,		peak current, μA		
excipient	μA	E_p, V[a]	a	b	E_p, V[a]
lactose USP	2.18	+0.08	2.40	2.35	+0.08
talc USP	1.67	+0.08	1.68	1.73	+0.08
povidone USP	2.75	+0.08	2.75	2.58	+0.08
maize starch BP	2.35	+0.08	2.68	2.73	+0.08
Avicel	2.63	+0.08	2.88	2.95	+0.08
Solka Floc	4.30	+0.08	3.75	3.68	+0.08
Amijel	3.10	+0.08	3.75	3.93	+0.05
Celacol 20M	3.25	+0.08	4.25	3.70	+0.08
Amberlite IRP 88	2.35	+0.08	2.93	3.08	+0.07
magnesium stearate USP	3.35	+0.08	3.23	2.95	+0.08
dibasic calcium phosphate	3.05	+0.08	3.13	2.88	+0.08
sodium starch glycolate	2.68	+0.08	>>5.0	>>5.0	+0.20
sodium lauryl sulfate BP	2.65	+0.08	complete signal removal		
soft gelatin mix 1	3.38	+0.08	3.95	4.18	+0.03
soft gelatin mix 2	3.23	+0.08	4.35	4.63	+0.03
soft gelatin mix 3	2.68	+0.08	2.85	3.63	+0.03
hard gelatin mix	2.60	+0.08	2.75	3.63	+0.03

[a] Vs. SCE.

excipients including fillers, binders, lubricants, and capsule shells were tested at levels in excess of those likely to be present compared with drugs and shown to have the effects shown in Tables I and II for compound I and compound II at the 3×10^{-5} M concentration level. In general, peak shapes were less affected in the case of bromide than chloride, as expected from previous literature notes on problems with chloride analysis (*13*), but no real practical analytical problems were encountered for either moiety except in the cases of sodium lauryl sulfate, a strong surfactant which completely removed stripping peaks from both halides and sodium starch glycolate which contains chloride as a high level impurity and completely masks both halide peaks. Slight peak shifts, usually about −0.01 to −0.05 V were observed for certain excipients, as detailed in Tables I and II. Overall, excipients had little effect on the practical application of the method to tablet and capsule analysis. The procedure was as given in the Experimental section above.

Comparison of Results by Measuring Both Peak Current and Quantity of Electricity. Results have been calculated by two methods: (a) measurements of peak current, I_p, (i.e., height of peak from starting current to peak top), and (b) measurement of area beneath the stripping curve by graphical triangulation (giving a measure of Q stripping, the quantity of electricity involved in the process). Since peaks are very symmetrical, after stirred electrolysis, no advantage appears to be gained by measuring Q rather than I_p. Results of the two methods of calculation are given in Table III. However, in any experimental situation where quiescent deposition was required resulting in peaks containing monolayer distortions, it is considered that electronic means of measuring quantity of electricity (integration, coulometry) would need to be used to obtain concentration dependent linearity.

Application of CSV to Dissolution Studies and Comparison with UV Spectrophotometry. Tablets containing 200 mg of maize starch, 200 mg of Avicel, 200 mg of Amijel, 4 mg of magnesium stearate, and respectively nominally 20 mg of compound I (19.6 mg actual) and 16 mg of compound II (16.4 mg actual) were prepared and dispersed

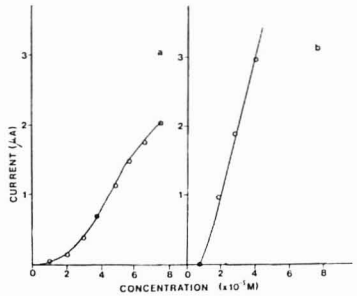

Figure 7. Cathodic stripping of compound I: effect of stirring on calibration curve. (a) Unstirred solution: 10-min electrolysis at +0.35 V. (b) Stirred solution: 2-min stirred, 15-s quiescent electrolysis at +0.35 V

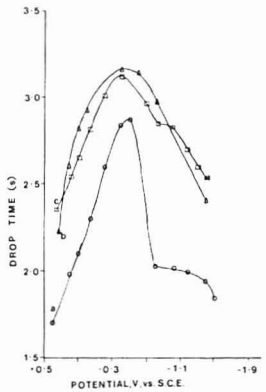

Figure 8. Electrocapillary curves for compounds I and II in 0.05 M KNO_3/HNO_3: (a) electrolyte along; (b) electrolyte + 9.9 × 10^{-5} M compound I; and (c) electrolyte + 9.4 × 10^{-5} M compound II

in the dissolution apparatus described above (containing 1 L of water at 37 °C) for 30 min. Samples were then withdrawn for analysis. In the case of compound I no dilution was required prior to CSV analysis, while sample II was diluted ×2 to obtain the optimum concentration. Results for CSV analysis are shown in Table III and compared with UV spectrophotometric analysis. For dissolution testing using spectrophotometry it was required to use 2 tablets of compound I and 5 tablets of compound II per liter to obtain a concentration sufficient for accurate analysis. Relative concentration levels of measured solutions are given in Table III. Cathodic stripping voltammetry therefore provides equally accurate results to UV spectrophotometry at a concentration of an order of magnitude lower, with little loss in precision.

Detection Limits of Other Polarographic Methods. Using 0.1 M KNO_3/HNO_3 as supporting electrolyte, limits of detection of about 5 × 10^{-4} and 10^{-4} M for dc and 5 × 10^{-5} and 10^{-6} M for differential pulse polarography were obtained for compounds I and II, respectively. Sensitivity is limited by the difficulty of accurate wave height and peak measurement due to the proximity of the half-wave potentials to the electrolyte cut-off potential. Stripping voltammetry therefore offers a great improvement in sensitivity over these polarographic modes. The anodic oxidation of compounds I and II at the glassy carbon electrode has recently been used

Table III. Comparison of Stripping Voltammetric and UV Spectrophotometric Results for Dissolution of Compounds I and II from Tablets

	cathodic stripping voltammetry			UV spectrophotometry		
	concentration of drug in original tablet		concentration level in voltammetric cell, M	molar extinction coefficient in water, m^2 M^{-1}	concentration of drug in original tablet	concentration level measured, M
compd	measurement method a[a]	measurement method b[a]				
I	calculated 19.7 mg (mean of 9 results) coefficient of variation 3.1% actual content 19.6 mg (100.5% recovery)	calculated 19.7 mg (mean of 9 results) coefficient of variation of 3.5% actual content 19.6 mg (100.5% recovery)	2×10^{-5}	2174 (276 nm)	calculated 20.6 mg (mean of 10 results) coefficient of variation 1.7% actual content 20.7 mg (99.5% recovery)	2×10^{-4}
II	calculated 16.5 mg (mean of 7 results) coefficient of variation 2.9% actual content 16.4 mg (100.5% recovery)	calculated 16.0 mg (mean of 7 results) coefficient of variation 2.5% actual content 16.4 mg (97.5% recovery)	5×10^{-6}	2073 (280 nm)	calculated 16.6 mg (mean of 10 results) coefficient of variation 1.0% actual content 16.6 mg (100.0% recovery)	2.5×10^{-4}

[a] Method a, measuring peak height from starting current to peak top; method b, measuring peak area by triangulation.

for the determination of the compounds in tablets (29). Sensitivities of about 10^{-6} M were obtained; however the method was not applicable to dissolution studies since a 98% ethanolic electrolyte was required for the process.

LITERATURE CITED

(1) "United States Pharmacopoeia XIX", 1975; p 651.
(2) "Remington's Pharmaceutical Sciences", 15th ed.; Mack Publishing Co.: Easton, Pa., 1975; p 1368.
(3) Berge, S. M.; Bighley, L. D.; Monkhouse, D. C. *J. Pharm. Sci.* **1977**, *66*, 1–19.
(4) Wagner, J. G. "Biopharmaceutics and Relevant Pharmacokinetics", 1st ed.; Drug Intelligence Publications: Hamilton, Ill., 1971; p 133.
(5) "British Pharmacopoeia", Pharmaceutical Society of Great Britain; 1973.
(6) Volhard, J. *J. Prakt. Chem.* **1874**, *9*, 217.
(7) Isaacs, M. L. *J. Biol. Chem.* **1922**, *53*, 17.
(8) Kolthoff, I. M.; Furman, N. H. "Potentiometric Titrations", 2nd ed.; Wiley: New York, 1931, pp 154–158.
(9) "Clinical Chemistry–Principles and Technics", 2nd ed.; Henry, R. J., Cannon, D. C., Winkelman, J. W., Eds.; Harper and Row: New York, 1974.
(10) Cotlove E. In "Standard Methods of Clinical Chemistry", D. Seligson, Ed.; Academic Press: New York, 1961; Vol. 3, p 81.
(11) Orion Research Inc., "Analytical Methods Guide", May 1975.
(12) Schales, O. In "Standard Methods of Clinical Chemistry", Reiner, M., Ed.; Academic Press: New York, 1953; Vol. 1, p 37.
(13) Brainina, Kh. Z. "Stripping Voltammetry in Chemical Analysis", Wiley: New York and Toronto, 1974; pp 142–151.
(14) Vydra, F.; Stulik, K.; Julakova, E. "Electrochemical Stripping Analysis", Wiley: New York, 1976; pp 219–223.
(15) Manandhar, K.; Pletcher, D. *Talanta* **1977**, *24*, 387–390.
(16) Dennis, B. L.; Wilson, G. S.; Moyers, J. L. *Anal. Chim. Acta* **1976**, *86*, 27–34.
(17) Colovos, G.; Wilson, G. S.; Moyers, J. L. *Anal. Chem.* **1974**, *46*, 1045–1050.
(18) Colovos, G.; Wilson, G. S.; Moyers, J. L. *Anal. Chem.* **1974**, *46*, 1051–1054.
(19) Perchard, J. P.; Buvet, M.; Molina, R. *J. Electroanal. Chem.* **1967**, *14*, 57–74.
(20) Armstrong, R. D.; Fleischmann, M. *J. Polarogr. Soc.* **1965**, *11*, 31–40.
(21) Petrie, L. M.; Baier, R. W. *Anal. Chem.* **1978**, *50*, 351–357.
(22) Matson, W. R.; Roe, D. K.; Carritt, D. E. *Anal. Chem.* **1965**, *37*, 1594–1595.
(23) Schieffer, G. W.; Blaedel, W. J. *Anal. Chem.* **1977**, *49*, 49–53.
(24) Joyce R. J.; Westcott, C. C. From "Trace Characterization–Chemical and Physical", *Natl. Bur. Stand. (U.S.), Monogr.* **1967**, No. 100.
(25) Vogel, A. I. "Quantitative Inorganic Analysis", 3rd ed.; Longmans Ltd.: London, 1966; p 1166.
(26) Kolthoff, I. M.; Miller, C. S. *J. Am. Chem. Soc.* **1941**, *63*, 1405–1411.
(27) Vicek, A. A. *Collect. Czech. Chem. Commun.* **1954**, *19*, 221–233.
(28) Meites, L. "Polarographic Techniques", 2nd ed.; Interscience: New York, 1965; p 135.
(29) Chan, H. K.; Fogg, A. G. *Anal. Chim. Acta* **1979**, *105*, 423–428.

RECEIVED for review February 6, 1979. Accepted July 2, 1979.

Pseudopolarographic Determination of Metal Complex Stability Constants in Dilute Solution by Rapid Scan Anodic Stripping Voltammetry

Steven D. Brown[1] and Bruce R. Kowalski*

Department of Chemistry, University of Washington, Seattle, Washington 98195

The theory of anodic stripping voltammetry states that at any deposition potential, the deposition current will either be the limiting current or a fraction of the limiting current, depending on the deposition potential with respect to the metal deposition potential. By using a computer controlled anodic stripping voltammeter with automatic background correction, pseudopolarograms can be obtained by plotting the peak area vs. the deposition potential for a series of stripping voltammetric runs. With ASV as a method of amplification, the ligand number and stability constants are determined for metal complexes at concentration ranges expected of natural water systems. Results for lead and cadmium with chloride and carbonate are in excellent agreement with those of less sensitive methods used at higher concentrations. No complexation of lead and cadmium was found with glycine at pH 4.68. The structure of arsenic(III) at 1.0 ng/mL in acidic solutions was determined to be $As(OH)_3$ using a gold film electrode. Finally, the speciation of lead in a geothermal water was examined by pseudopolarography and a shift consistent with a $PbCl^+$ complex was observed.

The evaluation of the complexing properties of metals in solution has long been of interest to analytical chemists, who have developed a variety of techniques suited to the assignment of metal complexation in solution. These techniques, which include visible absorption spectrometry, isotopic exchange methods, and, in a few cases, vibrational (Raman) spectroscopy as well as more exotic methods, have been used by a variety of groups to study the kinetics of ligand exchange.

For dilute solutions, in the millimolar range, however, these techniques lack the sensitivity needed to evaluate metal complexation. Polarographic techniques based on the shift of the half-wave potential ($E_{1/2}$) with ligand concentration were first used by Heyrovsky (*1*) and Lingane (*2, 3*) to investigate metal complexation in dilute solution; these and similar determinations via ion-selective electrodes (*4, 5*) do not extend to metal concentration ranges below about 10^{-5} M. Thus, neither technique is directly applicable to evaluations of metal complexation at concentrations approximating those found in dilute natural waters, typically 10^{-8}–10^{-10} M.

To extend the sensitivity of polarography, a number of techniques have been employed, including differential pulse (*6, 7*) and square wave polarography (*8, 9*), various alternating current polarography-based techniques (*10–12*), and stripping voltammetry (*13–18*), but these techniques have not seen extensive use in studies of metal complexation in dilute natural waters.

Most recent work has been aimed at the classification of metal complexation in natural waters. A number of schemes (*13–15*) based on anodic stripping voltammetry have been developed to classify metal complexes as "free" or "bound". Florence (*16–18*) has devised a system which classifies metal

[1] Present address: Department of Chemistry, University of California, Berkeley, Calif. 94720.

0003-2700/79/0351-2133$01.00/0

complexes as (1) free ions, (2) ASV labile complexes, (3) dissociable complexes, (4) nondissociable complexes. These systems have been called "coarse" speciation (*19*).

Direct identification of the metal complex in dilute solution via determination of the ligand number and complex stability constant has only been attempted quite recently, and most studies have used relatively large metal concentrations compared to levels found in dilute natural systems. This "fine" speciation (*19*) has not involved ASV, because many runs are needed to establish peak shifts, and ASV peak positions are known to be sensitive to factors such as ionic strength and scan rate (*20*).

Because metal reduction has been demonstrated to be sensitive to metal complexation through changes in the amount of metal deposited as a function of deposition potential (*21*), coupling reproducible plating at various potentials with a sensitive ASV technique will allow measurements of deposited metal charge (or, here, as peak currents derived from the ASV stripping peak) as a function of deposition potential. Two recent papers use linear scan ASV in this fashion (*22, 23*) to obtain stability constants in dilute solutions. We report here the application of this technique to thin, glassy carbon-supported mercury and gold films using rotating disk electrodes and minicomputer-controlled background-subtracted anodic stripping voltammetry. The system is capable of generating automated Q vs. E_d plots, called pseudopolarograms, with either linear scan or staircase stripping ASV. We also describe the theoretical basis of the technique.

THEORY

At any deposition potential E_d, the deposition current $i(t)$ is given by either the limiting current of the deposition process at the rotating disk electrode, or some fraction thereof. For constant plating time, the material deposited also will vary with E_d, and the individual stripping steps will merely analyze the material preconcentrated in the electrode.

For a rotating disk electrode, the instantaneous current $i(t)$ is given by:

$$i(t) = \frac{nFAD_{OX}}{\delta_{OX}}[C_{OX}^{\circ} - C_{OX}(0,t)] \quad (1)$$

where C_{OX}° is the bulk concentration of analyte ion, $C_{OX}(0,t)$ is the surface concentration of analyte ion at time t, δ is the thickness of the diffusion layer, and the other symbols have their usual meaning.

De Vries and Van Dalen (*24-26*) have shown for thin mercury film electrodes the surface activity of the amalgam as a function of plating time is:

$$C_{RED}(0,t) = \frac{i(t)}{nFA}\left(\frac{t}{l} + \frac{1}{3D_{RED}}\right) \quad (2)$$

Here t is the plating time and l is film thickness; this equation is suitable for $t \geq 20$ s.

For an electrode process

$$i(t) = nFA[k_{fn}C_{OX}(0,t)\gamma_O - k_{bh}C_{RED}(0,t)\gamma_R] \quad (3)$$

where k_{fn} and k_{bh} are the forward and backward hetrogeneous rate constants for the metal reduction. Combining Equations 1-3 yields:

$$i(t) = nFAk_{fn}\gamma_{OX}\left(C_{OX}^{\circ} - \frac{i(t)\delta_{OX}}{nFAD_{OX}}\right) - k_{bh}\gamma_r i(t)\left(\frac{t}{l} + \frac{1}{3D_{RED}}\right) \quad (4)$$

Since we desire charge, we integrate Equation 4 with respect to time to get:

$$Q = \frac{k_{fn}\delta_{OX}}{D_{OX}}(Q_{LIM} - Q)\gamma_{OX} - k_{bh}\left(\frac{t}{2l} + \frac{1}{3D_{RED}}\right)Q\gamma_r \quad (5)$$

where

$$Q_{LIM} = \int_0^t i_{LIM}dt = \int_0^t \frac{nFAC_{OX}^{\circ}}{\delta_{OX}} D_{OX}dt \quad (6)$$

$$Q = \int_0^t i(t)dt \quad (7)$$

Rearrangement of Equation 5, and substitution of

$$k_{fn} = k_{fh}^{\circ}\, e^{(-anF/RT)E_d} \quad (8)$$

and

$$\frac{k_{bh}}{k_{fh}} = \exp\left\{\frac{nF}{RT}(E_d - E^{\circ})\right\} \quad (9)$$

gives

$$E_d - E^{\circ} = \frac{RT}{nF}\ln\left[\left(\frac{Q_{LIM} - Q}{Q}\right) - \frac{D_{OX}}{\delta_{OX}k_f^{0}\gamma_{OX}}\exp(\alpha nFE_d/RT)\right] - \frac{RT}{nF}\ln\left(\frac{\delta_{OX}}{D_{OX}} - \frac{\gamma_{OX}}{\gamma_R}\right) - \frac{RT}{nF}\ln\left(\frac{1}{3D_{RED}} + \frac{t}{2l}\right) \quad (10)$$

where $\alpha(E_d)$ is the transfer coefficient for the reduction and k_f° is the heterogeneous rate constant for reduction at E°.

Equation 10 is the general equation for the pseudopolarographic reduction and stripping of a free model ion under quasi-reversible conditions. Various techniques including ASV (*27*) and stripping chronoamperometry (*28*) can be used to strip the metal ions out of the film and monitor the charge, so this and subsequent equations are left in terms of charge, rather than peak stripping current.

When $k_f^{\circ} \to \infty$, the reaction at the electrode surface is reversible and Equation 10 reduces to:

$$E_d - E^{\circ} = \frac{RT}{nF}\ln\left(\frac{Q_{LIM} - Q}{Q}\right) + \frac{RT}{nF}\ln\left(\frac{\delta_{OX}\gamma_{OX}}{D_{OX}\gamma_{RED}}\right) - \frac{RT}{nF}\ln\left(\frac{1}{3D_{RED}} + \frac{t}{2l}\right) \quad (11)$$

Equation 11 is similar to that obtained by Zirino and Kounaves (*29*), but differs from their result as we use the exact expression for C_r and integrate.

For complexes, we consider the equilibria:

$$M^{n+} + L \rightleftharpoons ML^{n+} \quad (12)$$

$$ML^{n+} + L \rightleftharpoons ML_2^{n+}$$

$$\vdots$$

$$ML_{j-1}^{+} + L \rightleftharpoons ML_j^{+}$$

where complex formation is presumed rapid and reversible, and the stability constant β_j is defined as:

$$\beta_j = \frac{[ML_j^{\eta+}]}{[M^{n+}][L]^j} \cdot \frac{\gamma_{ML_j}}{\gamma_M\gamma_L{}^j} \quad (13)$$

Using the method of DeFord and Hume (*30*), which presumes only M^{n+} is reducible, all $D_{OX} = D$, excess L, and all activity

constants do not vary with distance from the electrode, Equation 14 is obtained for a quasi-reversible system:

$$E_d = E^\circ + \frac{RT}{nF}\ln\left[\left(\frac{Q_{LIM}-Q}{Q}\right) + \frac{D}{k^0\delta_{OX}}\sum_{j=0}^{N}\left(\frac{\beta_j[L]^j\gamma^j_i}{\gamma_{ML_j}}\right)e^{(\alpha nF/RT)E_d}\right] - \frac{RT}{nF}\ln\left[\frac{\gamma_r D}{\delta_{OX}}\left(\frac{t}{2l}+\frac{1}{3D_{RED}}\right)\right] - \frac{RT}{nF}\ln\left[\sum_{j=0}^{N}\left(\frac{\beta_j[L]^j\gamma^j_L}{\gamma_{ML_j}}\right)\right] \quad (14)$$

For reversible cases, this is reduced to:

$$E_d = E_0 + \frac{RT}{nF}\ln\left(\frac{Q_{LIM}-Q}{Q}\right) - \frac{RT}{nF}\ln\frac{\gamma_r D}{\delta_{OX}}\left(\frac{t}{2l}+\frac{1}{3D_{RED}}\right) - \frac{RT}{nF}\ln\left[\sum_{j=0}^{N}\left(\frac{\beta_j(L)^j\gamma^j_i}{\gamma_{ML_j}}\right)\right] \quad (15)$$

from which:

$$E^*_{1/2,\,comp} = E_0 - \frac{RT}{nF}\ln\frac{\gamma_r D}{\delta_{OX}}\left(\frac{t}{2l}+\frac{1}{3D_{RED}}\right) - \frac{RT}{nF}\ln\sum_{j=0}^{N}\left(\frac{\beta_j[L]^j\gamma_i{}^j}{\gamma_{ML_j}}\right) \quad (16)$$

results. For constant values of l, δ_{OX}, γ_r, and t:

$$\Delta E^*_{1/2} = (E^*_{1/2,\,free} - E^*_{1/2,\,comp}) = -\frac{RT}{nF}\ln\left(\frac{D}{D_{OX}}\cdot\gamma_M\right) + \frac{RT}{nF}\ln\left[\sum_{j=0}^{N}\left(\frac{\beta_j[L]^j\gamma_i{}^j}{\gamma_{ML_j}}\right)\right] \quad (17)$$

or, for a single complex with $\gamma_M \approx \gamma_{ML}$, $D \approx D_{OX}$

$$\Delta E^*_{1/2} \approx \frac{RT}{nF}\ln\beta_j + j\frac{RT}{nF}\ln a_L \quad (18)$$

where a_L is the ligand activity.

Equation 17 is exactly analogous to that obtained by DeFord and Hume for polarographic reduction of metal complexes where many complexes are possible, and Equation 18 is analogous to the Lingane equation (3), suited for analysis of single complex systems. Thus, plots of $\Delta E^*_{1/2}$ vs. A_L provide metal complexation information through analyses similar to those used in classical polarographic studies.

Here, because stripping peak heights are directly proportional to total charge (26), we use ASV peak heights in our evaluations of $E^*_{1/2}$.

Davison has examined (31) the limitations on conventional polarographic and voltammetric schemes used to monitor speciation, and finds for conventional ASV that, for a kinetic current equal to 10% of the limiting current:

$$Q = \frac{\beta^{3/2}[L]}{k_1{}^{1/2}}(1+\beta[L])^{1/2} = \frac{9\delta}{D^{1/2}} \quad (19)$$

where k_1 is the second-order rate constant for the rate of substitution of the active form of the metal, here M^{n+}. For $D = 10^{-5}$ cm^2 s^{-1}, Q values of 10^4–10^6 result for δ between 10^{-4} and 10^{-2} cm. For ligand concentrations in the 10^{-3} M range, and for $k_1 = 10^9$ L mol^{-1} s^{-1}, limiting β values of about 10^5 are obtained.

The same argument can be applied to the pseudopolarographic determination of stability constants, since the technique relies on the measurement of charge passed during the plating period. There are some differences, however. Because plating times should be kept short, to avoid altering the composition of the solution, normal ASV with long plating times cannot be used, as serious metal depletion results. With the ASV method using background subtraction, sensitivities are such that a 5-min plating period allows detection of pg/mL levels of metals (27); this allows the observation of small kinetic currents, approximately 1% of the diffusion current in the absence of complexer. The β values easily observable would then extend to about 10^{-6} for ligand concentrations in the 10^{-3} M range. The precision of the determination suffers slightly here, though, with kinetic currents on the order of 1% of the diffusion currents, because the entire pseudo-polarogram is simply reduced in height proportionally, making the error in determining the half-wave potential somewhat larger. The possibility of decreasing the rotation rate, thus increasing δ, also exists.

EXPERIMENTAL

Equipment and Apparatus. The rapid-scan, background-subtracted ASV apparatus described in ref. 27 was used for these studies. Modifications were made to the software to allow a sequence of scans to be performed automatically, with each run differing by a fixed value in the plating potential, but otherwise having identical parameters. Runs were stored sequentially on the disk to allow easy processing.

Measurements of pH were made with a Beckman 4500 digital pH meter, calibrated with pH 4.008 solution.

Electrodes and Cell. Both mercury and gold film electrodes were used in this study, the gold electrode being used for studies of arsenic speciation. Preparation of the electrodes has been discussed (27). A saturated KNO_3 bridge was used between the SCE reference electrode and test solution to avoid contamination of the solution with trace amounts of complexer. The cell (27) was cleaned thoroughly with 5 N citric acid between runs to avoid any transfer of complexer. This is particularly necessary in the case of arsenic, as arsenic species strongly absorb on the cell, and later interfere.

Reagents. The standards used in the work reported in ref. 27 were also used as standards for this work. Arsenic standards were prepared by dissolving ultrapure As_2O_3 (Alpha) in ultrapure $NaHCO_3$ (Baker) and adjusting the pH with Ultrex HCl.

Dilute perchloric acid (0.1 N) was made by diluting the reagent grade acid (Mallinckrodt) with distilled water. Dilute sodium hydroxide (0.3 N) was made from reagent grade pellets (Mallinckrodt) and distilled water.

The ionic strength of all solutions was adjusted with KNO_3 solutions.

Trace metal content of solutions was adjusted by addition of 100 mL of 1–2 μg/mL standards. The transfer was performed with Eppendorf pipets.

Procedure. *Data Acquisition.* A series of solutions of ligand was prepared from the stock solution of the ligand. These solutions were spiked to obtain a final trace metal content of 1–5 ng/mL, the ionic strength was adjusted with KNO_3 and the pH with either $HClO_4$ or NaOH.

A portion (75 mL) of each solution was subjected to analysis by the pseudopolarographic process. This consisted of a 5-min deaeration of the solution, with rotation of the preplated electrode, after which a series of ASV experiments was performed on the solution, each at a different plating potential. The ASV run consisted of plating for a specified time, usually 150 s, at the deposition potential. The potential is switched to the rest potential when 2 s remain of plating time. Stirring at a specified rate was performed until 15 s of plating time remained, after which the solution was allowed to become quiescent before the scan. A single scan, using either the linear ramp or staircase waveform, was then performed, using multiple point averaging (typically 16 points). Stirring at the cleaning potential was then performed for 20 s., after which a 10-s quiescent perod was provided. With 2 s remaining, the potential was again switched to the rest potential,

Table I. Shift of $E^*_{1/2}$ with Chloride Concentration for Cadmium[a]

$E^*_{1/2}$	[Cl^-]	log [Cl^-]
−745 ± 5	0.0050	−2.3
−758 ± 5	0.010	−2.0
−775 ± 5	0.050	−1.3
−789 ± 5	0.10	−1.0
−725 ± 5	0	--

[a] I = 0.10, pH 5.00.

and another scan, exactly like the first, was used to monitor the background. Current measurements were subtracted, point by point, and the result was plotted on the Tektronix 4012 screen, and stored on disk. The deposition potential was redefined, and another run was automatically performed, exactly like the first, but at a different deposition potential. This process was continued, until a specified number of runs was performed. The resultant file of ASV runs could be used to generate a pseudopolarogram for each peak present in the voltammogram. A pseudopolarogram run, like that described above, was performed for each solution. The electrode film was maintained between solutions to ensure that uniform conditions applied within a series of runs; it was washed with distilled water between analyses of different solutions to prevent carryover of ligand.

Data Reduction. The ASV peak heights were measured with an interactive graphics routine. The potentials and peak heights were plotted for each solution, resulting in a series of pseudopolarograms for each metal.

Because for ASV the peak current is directly proportional to charge stripped, the pseudopolarograms were examined for reversibility by plotting the deposition potential E_d vs. log $[(i_L - i)/i]$, where the limiting current, i_L, was estimated from the top of the step-shaped wave, and i was the peak current monitored for the metal of interest on the ASV run where the deposition potential E_d was used. A straight line, with slope of approximately $59.1/n$ mV resulted for a reversible system; nonlinear relationships, or slopes drastically different from the $59.1/n$ value expected, were treated as irreversible systems.

For reversible systems, the least squares best estimate was used to calculate $E^*_{1/2}$ from log $[(i_L - i)/i] = 0$. The error in this value is estimated at 1% relative. For irreversible systems, estimates were made of $E^{*irr}_{1/2}$ by extrapolating the foot of the wave upward, estimating the limiting current, and evaluating the potential for a current value equal to one-half the limiting current. The error in this value is somewhat larger, about 3–5% relative.

Values for $E^*_{1/2}$ (or $E^{*irr}_{1/2}$) were then plotted vs. the log of ligand concentration, and the slopes of the resultant linear relationships were evaluated via linear regression analysis.

Intercepts were also calculated. The errors in $E^*_{1/2}$ were used to obtain an estimate of the errors in the ligand number, p, and the stability constant, log β, calculated from the slope and intercept, respectively. The more exact method of DeFord and Hume (*30*) as modified by Varga and others (*32, 33*) was not used here, as the scope of such a study (which would require at least 10–20 pseudopolarograms) was beyond this work, whose intent is to demonstrate the feasibility of the technique. Instead, the simpler method of Lingane (*2, 3*) was used. Future experimentation, involving sufficient runs to use the DeFord and Hume procedure, is planned.

RESULTS AND DISCUSSION

Cadmium and Lead Complexation by Chloride. A series of KCl solutions of fixed 0.10 M ionic strength and pH 5.00 were examined with the pseudopolarographic technique. A staircase scan with τ = 10.0 ms was used in the ASV runs, with 150-s plating times used for deposition. Twenty ASV experiments, differing in plating potential by 40 mV, were run. The rest potential was −1200 mV (SCE) and the plating potentials ranged from −1000 to −200 mV (SCE). Both the Pb and Cd pseudopolarograms were observed to behave reversibly, with slopes from −30 to −33 mV (theoretical −29.8 mV). Table I lists the $E^*_{1/2}$ values obtained for cadmium as a function of chloride concentration. From the table, a least-squares fit gives a ligand number p of 1.1 ± 0.1 and an equilibrium constant of log β = 3.2 ± 0.2.

Table II. Shift of $E^*_{1/2}$ with Chloride Concentration for Lead[a]

$E^*_{1/2}$	[Cl^-]	log [Cl^-]
−480 ± 5	0.005	−2.3
−485 ± 5	0.01	−2.0
−495 ± 5	0.05	−1.3
−499 ± 5	0.1	−1.0
−475 ± 5	0	--

[a] I = 0.10, pH 5.00.

Table III. Comparison of Results for Cadmium and Lead Chloride Species

metal	P	I	log β	ref.
Cd	1	1.0	1.7–2.2	54
Cd	1	0.1	3.2	this work
Pb	1	0.1	1.0–1.6	54
Pb	1	0.1	1.4	this work

Table IV. Shift of $E^*_{1/2}$ with Carbonate Concentration for Lead[a]

$E^*_{1/2}$	[HCO_3^-]	log [CO_3^{2-}]	[CO_3^{2-}]
−623 ± 5	5.2×10^{-3}	−1.02	0.095
−595 ± 5	2.6×10^{-3}	−1.3	0.047
−551 ± 5	5.2×10^{-4}	−2.0	0.0095
−545 ± 5	2.6×10^{-4}	−2.3	0.0047
−501 ± 5	0	--	

[a] I = 0.1, pH 7.87.

For lead, shifts were much smaller, as shown in Table II. From the table, a least-squares fit gives a ligand number of 0.7 ± 0.2 and a stability constant of log β = 1.4 ± 0.3. Values for the lead–chloride system are much less precise because of the small shifts, combined with the error in locating $E^*_{1/2}$. More ASV runs would better define the curve, and better locate $E^*_{1/2}$ values here, resulting in less error.

Results here agree reasonably well with previous literature values, as shown in Table III.

Cadmium and Lead Complexation by Carbonate. A series of Na_2CO_3 solutions at pH 7.87 were prepared with fixed ionic strength (0.1 M) by addition of KNO_3. Metal concentration was nominally 2 ng/mL for both Cd and Pb. An experiment, identical to the one used for the chloride studies, was performed. Neither the Cd, nor the Pb polarogram was totally reversible, slopes being greater than −38 mV.

Table IV lists the shifts in the half-wave potential for lead. Using these values, a ligand number of 0.9 ± 0.1 and a stability constant of log β = 6.1 ± 0.1 may be calculated.

It should be noted that a plot of $E^*_{1/2}$ vs. log [HCO_3^-] also gives a linear relation, with a slope indicating a ligand number of 0.9 as well. Stumm (*34*) has shown, however, that all reported bicarbonate complexes may be better interpreted as carbonate complexes. Thus, the data reported here are regarded as indicative of carbonate, rather than bicarbonate species.

Results for lead agree quite well with published values, as shown in Table V.

Results for cadmium are listed in Table VI. The observed shifts are quite small, within even the error attributed to the assignment of $E^*_{1/2}$ At this pH, cadmium is apparently not signficantly complexed by carbonate. Similar results were obtained by differential pulse polarography and ASV of more concentrated Cd–CO_3^{2-} systems (*35*). $CdCO_3$ was observed at higher pH values, however (*34*).

Cadmium and Lead Complexation by Glycine. A series of solutions of glycine, adjusted to pH 4.68, was made up, again

Table V. Comparison of Results for Lead Carbonate Species

method	I	Pb[a]	pH	log β	ref.
ASV	0.1	200	7.3-10.3	6.4	34
DPP	0.1	200-50	5.0- 9.1	6.1	34
polarography	1.7	20000	10.9	8.2[b]	55
DPASV	0.1	500	-	6.3	56
cyclic voltammetry	0.7	10	7.2	6.21	57
pseudo-polarography	0.1	2	7.87	6.1	this work

[a] In ng/mL. [b] Value is log β_2.

Table VI. Shift of $E^*_{1/2}$ with Carbonate Concentration for Cadmium[a]

$E^*_{1/2}$	$[CO_3^{2-}]$
−728 ± 5	5.2×10^{-3}
−722 ± 5	2.5×10^{-3}
−725 ± 5	5.2×10^{-4}
−725 ± 5	2.6×10^{-4}
−720 ± 5	0

[a] I = 0.1, pH 7.87.

Table VII. Shift of $E^*_{1/2}$ with Glycine Concentration for Cadmium and Lead[a]

$E^*_{1/2}$ (Cd)	$E^*_{1/2}$ (Pb)	[glycine]
−720 ± 5	−537 ± 5	0.005
−715 ± 5	−539 ± 5	0.01
−715 ± 5	−539 ± 5	0.05
−715 ± 5	−545 ± 5	0.1
−715 ± 5	−537 ± 5	0

[a] I = 0.1, pH 4.68.

with a total ionic strength of 0.1 M. Pseudopolarographic analysis was performed as described previously, using the same conditions as before. Table VII shows the shifts in $E^*_{1/2}$ for Pb and Cd as a function of the glycine concentration. Again, shifts are within the error of the experiment, and no complexation has resulted for either the Pb or the Cd. The interaction of glycine with Pb and Cd has been studied by ASV and DPP analysis of more concentrated solutions, where no complexation of Cd or Pb was observed (*35*), although glycine complexes of Cd have been claimed (*36*), but this work is in question (*37*).

Structure of Arsenic(III) in Aqueous Solution. Arsenic has received a considerable amount of attention in the past, primarily owing to the analytical difficulties associated with its relative insolubility in mercury (*38*, *39*). A variety of electrochemical techniques have been applied in efforts to improve the detection limit values for arsenic analyses (*40–46*). No concerted effort has been applied to studies of As speciation in dilute solution using electrochemical methods, however. Recent advances in the field, brought about by the use of gold wire (*43*) or gold film (*47*) electrodes combined with ASV, suggested that an attempt was feasible.

A solution of As(III) in 0.1 M KNO_3 was prepared. The pH was adjusted to a series of values with dilute $HClO_4$ and dilute NaOH. The nominal As concentration was 1.0 ng/mL. The effects of pH on the $E^*_{1/2}$ value for the As stripping peak on an Au film electrode were briefly investigated by obtaining pseudopolarograms for As at several pH values.

The pseudopolarograms were obtained using 300-s plating time, followed by background subtracted staircase ASV, with a step height of 3.66 mV and a delay time of 16.7 ms. Total scan time was 5 s. It was observed here that linear scan ASV gave much poorer peaks as well as less effective removal of

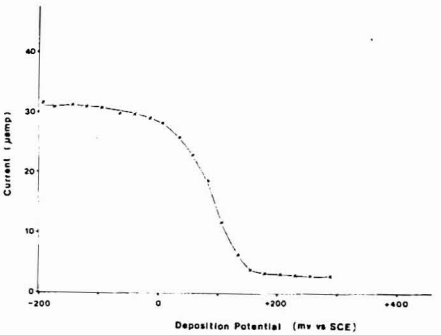

Figure 1. Pseudopolarogram for arsenic on gold

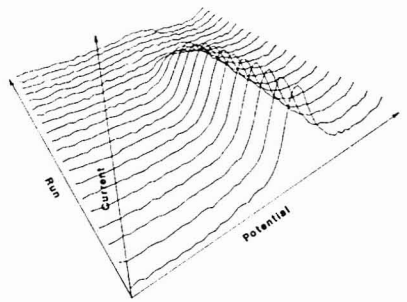

Figure 2. Sequence of runs used to generate pseudopolarogram

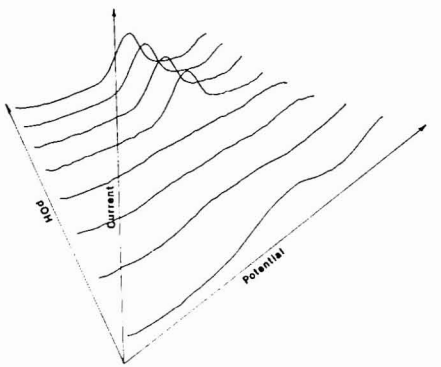

Figure 3. Dependence of arsenic peak on pOH

background, while for other pseudopolarograms, little difference (other than sensitivity) was observed. The same film was used for all runs. Plating potentials varied between −200 ms and +300 mV vs. the SCE, with a rest potential of −200 mV (SCE). Solution volumes were 75 mL.

A typical pseudopolarogram obtained at pH 2.85 and 1.0 ng/mL As(III) is shown in Figure 1. The sequence of ASV runs generating this pseudopolarogram is depicted in Figure 2, where the decay in peak height shows along the y axis. The peak potential for the As peak remains constant. A logarithmic analysis of the pseudopolarograms give slopes near those expected for a reversible system (theoretical −19.8 mV);

Table VIII. Shift of $E^*_{1/2}$ with Hydroxide Concentration for Arsenic[a]

$E^*_{1/2}$	pH	pOH
−42 ± 3	6.65	8.35
−33 ± 2	4.26	9.74
86 ± 1	3.56	10.44
108 ± 1	2.85	11.15

[a] I = 0.1 M (KNO_3).

the values observed were −20, −18, −19, and −18 mV for the four pseudopolarograms.

The peak heights for As on Au films drastically decrease with decreasing pOH, as shown in Figure 3. The runs performed in basic solution gave broad, distorted peaks indicating that the As is converted into a highly irreversible form in basic solution. An analysis of runs in acidic solution with data given in Table VIII, gives a ligand number of 3.0 ± 0.1 and an intercept of −548.3 mV. The intercept cannot be converted, as was done before, to a log β value as (1) no $E^*_{1/2,free}$ value could be obtained for As(III), and (2) values of D_{As} are certainly not comparable to $D_{As(OH)_3}$, owing to the large collection of water molecules expected for the "free" As(III) ion (*48*). Thus, no convenient route to a stability constant for the complex predicted, $As(OH)_3$, exists. Support for such a complex is found in the Raman spectra of dilute solutions of As_4O_6; in acid solutions, the only detectable species is $As(OH)_3$. $As(OH)_2O^-$, $As(OH)O_2^{2-}$ and AsO_3^{3-} also appear in basic solutions (*49*). Such a result is consistent with the ligand number of 3 in acidic solution, and with the degradation of the As peak in basic solution, as the amount of $As(OH)_3$ decreases.

Estimation of Lead Species in Geothermal Water. A sample of air-exposed geothermal water obtained from the Lawrence Livermore Laboratory (Department of Energy) project in the Imperial Valley, Calif., was filtered under air through a 0.45-μm filter. The pH was 1.99. The pH was adjusted to 5.00, and the filtrate was diluted by a factor of 40 to obtain an approximate ionic strength, mostly as NaCl, of 0.1 M. Nominal concentration of minor elements were Pb (7 μg/mL), Cu (25 ng/mL), Fe (6 μg/mL), and Sn (1 μg/mL). A pseudopolarographic scan at low sensitivity was performed, and is plotted for Pb in Figure 4. The half-wave potential, of −501 mV, is consistent with the shift observed above for $PbCl^+$ in 0.1 M KCl at pH 5.00. It is reasonable to assume that the Pb exists primarily as $PbCl^+$ in this solution. An attempt was made to examine data for cadmium, but the much larger Pb wave obscured the Cd wave. In view of the high Pb concentration, simple ligands present, and convenient ionic strength, this solution must be regarded as only a model system, and many more ligands and systems must be studied to ascertain direct speciation like that approximated above, but it certainly seems feasible. Work is underway to demonstrate this feasibility in natural systems with metal concentrations in the low ppb range. Thus direct assessment of chemical models (e.g., 50) seems feasible. This is particularly useful in view of the drastically different effects of different complexes in natural systems, especially as regards bioavailability and toxicology (*51–53*).

CONCLUSIONS

Pseudopolarography has been shown to provide a rapid, sensitive means of performing measurements in very dilute solution (ng/mL or less). Because the theoretical treatment is so closely related to classical polarography, the considerable literature on the polarographic analysis of solutions may be applied to the problem of analysis of pseudopolarographic waves. Results identical to those obtained by other, less sensitive, means were obtained for the Cd–Cl, Pb–Cl, and

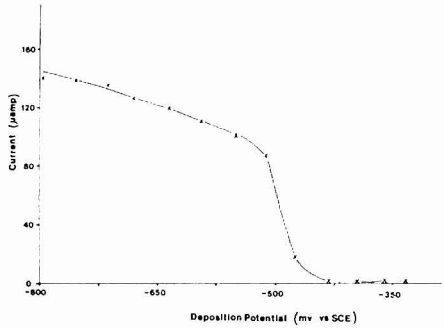

Figure 4. Pseudopolarogram of lead species in geothermal water

Pb–Co_3 systems. Cd–CO_3, Cd–glycine, and Pb–glycine were found not to interact in the pH ranges studied.

The speciation of As(III) in acid solution was examined using the new technique. The complex $As(OH)_3$ was identified as the dominant electrochemically-active species, consistent with Raman results.

The speciation of Pb in a geothermal water was examined by pseudopolarography. A shift consistent with a $PbCl^+$ complex was observed.

The new technique of pseudopolarography, performed with rapid-scan ASV instrumentation, appears to be a major advance in the area of chemical speciation.

ACKNOWLEDGMENT

The authors are pleased to acknowledge the assistance of Robert M. Corn. The authors also acknowledge J. Harrar, Lawrence Livermore Laboratory, for providing the geothermal water sample, and the Department of Energy for support associated with the speciation of geothermal waters.

LITERATURE CITED

(1) J. Heyrovsky and D. Ilkovič, *Collect. Czech. Chem. Commun.*, **7**, 198 (1935).
(2) J. M. Kolthoff and J. J. Lingane, *Chem. Rev.*, **24**, 1 (1939).
(3) J. J. Lingane, *Chem. Rev.*, **29**, 1 (1941).
(4) M. J. Stiff, *Water Res.*, **5**, 171 (1971).
(5) H. Gardiner, *Water Res.*, **8**, 23 (1974).
(6) G. C. Barker, *Anal. Chim. Acta*, **18**, 118 (1958).
(7) G. C. Barker and A. W. Gardner, *Fresenius' Z. Anal. Chem.*, **173**, 79 (1960).
(8) G. C. Barker and J. L. Jenkins, *Analyst (London)*, **77**, 685 (1952).
(9) P. E. Sturrock and R. J. Carter, *Crit. Rev. Anal. Chem.*, **5**, 201 (1975).
(10) B. Breyer and H. H. Bauer, "Alternating Current Polarography and Tensammetry", Interscience, New York, 1963.
(11) D. E. Smith, in "Electroanalytical Chemistry", A. J. Bard, Ed., Vol. 1, Dekker, New York, 1966, p 1.
(12) D. E. Smith, *Crit. Rev. Anal. Chem.*, **2**, 247 (1971).
(13) R. Clem, *Anal. Chem.*, **50**, 102 (1978).
(14) M. Whitfield, in "Chemical Oceanography", 2nd ed., Vol. 4, Academic Press, London, 1975, p 1.
(15) W. R. Matson, Dissertation, Massachusetts Institute of Technology, Cambridge, Mass., 1968.
(16) T. M. Florence and G. E. Batley, *Talanta*, **22**, 201 (1975).
(17) T. M. Florence and G. E. Batley, *Talanta*, **23**, 179 (1976).
(18) G. E. Batley and T. M. Florence, *Anal. Lett.*, **9**, 397 (1976).
(19) W. Davidson and M. Whitfield, *J. Electroanal. Chem.*, **75**, 763 (1977).
(20) Z. Galus, "Fundamentals of Electrochemical Analysis", Wiley, London, 1976.
(21) P. Delahay, "New Instrumental Methods in Electrochemistry", Interscience, New York, 1964.
(22) S. Bubic and M. Branica, *Thalassia Jugosl.*, **9**, 47 (1973).
(23) H. Nürnberg, P. Valenta, L. Mart, B. Raspor, and L. Sipos, *Fresenius' Z. Anal. Chem.*, **282**, 357 (1976).
(24) W. T. DeVries and E. Van Dalen, *J. Electroanal. Chem.*, **8**, 366 (1964).
(25) W. T. DeVries, *J. Electroanal. Chem.*, **9**, 448 (1965).
(26) W. T. DeVries and E. Van Dalen, *J. Electroanal. Chem.*, **14**, 315 (1967).
(27) S. D. Brown and B. R. Kowalski, *Anal. Chim. Acta*, **107**, 13 (1979).
(28) G. Mamantov, P. Papoff, and P. Delahay, *J. Am. Chem. Soc.*, **79**, 4034 (1957).
(29) A. Zirino and S. Kounaves, *Anal. Chem.*, **49**, 56 (1977).
(30) D. D. DeFord and D. N. Hume, *J. Am. Chem. Soc.*, **73**, 5321 (1951).
(31) W. Davison, *J. Electroanal. Chem.*, **87**, 395 (1978).

(32) L. P. Varga, *Anal. Chem.*, **41**, 323 (1969).
(33) L. N. Klatt and R. L. Rouseff, *Anal. Chem.*, **42**, 1234 (1970).
(34) H. Bilinski, R. Huston, and W. Stumm, *Anal. Chim. Acta*, **84**, 157 (1976).
(35) R. Ernst, H. E. Allen, and K. H. Mancy, *Water Res.*, **9**, 969 (1975).
(36) J. H. Smith, A. M. Cruikshank, J. T. Donoghue, and J. F. Pysz, Jr., *Inorg. Chem.*, **1**, 148 (1962).
(37) K. Momoki, H. Sato, and H. Ogawa, *Anal. Chem.*, **39**, 1072 (1967).
(38) F. Vydra, K. Stulik, E. Julakova', "Electrochemical Stripping Analysis", Halstead Press, London, 1976.
(39) J. P. Arnold and R. M. Johnson, *Talanta*, **16**, 1191 (1969).
(40) K. Hagiwara and T. Murase, *Bunseki Kagaku*, **14**, 757 (1960).
(41) G. C. Whitnack and R. G. Brophy, *Anal. Chim. Acta*, **48**, 123 (1969).
(42) L. F. Trushina and A. A. Kaplin, *Zh. Anal. Khim.*, **25**, 1616 (1970).
(43) G. Forsberg, J. W. O'Laughlin, R. G. Megargle, and S. R. Koirtyohann, *Anal. Chem.*, **47**, 1586 (1975).
(44) A. A. Kaplin, N. A. Velts, N. M. Mordvinova, and G. G. Glukhov, *Zh. Anal. Khim.*, **32**, 687 (1977).
(45) D. J. Myers and J. Osteryoung, *Anal. Chem.*, **45**, 267 (1973).
(46) F. T. Henry, T. O. Kirch, and T. M. Thorpe, Abstract No. 180, 29th Pittsburgh Conference on Analytical Chemistry and Applied Spectroscopy, Cleveland, Ohio, 27 Feb.–3 Mar., 1978.
(47) P. H. Davis, G. R. Dulude, R. M. Griffin, W. R. Matson, and E. W. Zink, *Anal. Chem.*, **50**, 137 (1978).
(48) F. A. Cotton and G. Wilkinson, "Advanced Inorganic Chemistry", 3rd ed., Interscience, New York, 1972.
(49) T. M. Loehr and R. A. Plane, *Inorg. Chem.*, **7**, 1708 (1968).
(50) D. T. Long and E. A. Angino, *Geochem. Cosmochim. Acta*, **41**, 1183 (1977).
(51) I Bremner, *Proc. Anal. Div. Chem. Soc.*, **14**, 218 (1977).
(52) T. L. Coombs, *Proc. Anal. Div. Chem. Soc.*, **14**, 219 (1977).
(53) G. Topping, *Proc. Anal. Div. Chem. Soc.*, **14**, 222 (1977).
(54) L. G. Sillén and A. E. Martell, "Stability Constants of Metal Complexes", Spec. Pub. No. 17, The Chemical Society, London, 1964.
(55) J. Faucherre and J. Bonnaire, *C. R. Hebd. Seances* Acad Sci., **248**, 3705 (1959).
(56) A. Zirino and S. Yamamoto, *Limnol. Oceanogr.*, **17**, 661 (1972).
(57) L. M. Petrie and R. W. Baier, *Anal. Chem.*, **50**, 351 (1978).

RECEIVED for review October 17, 1978. Accepted July 24, 1979. This work was partially supported by the Office of Naval Research. S.D.B. gratefully acknowledges the support, during the 1977–78 year, of an ACS Analytical Division Fellowship, sponsored by the Perkin-Elmer Corp. This work was abstracted in part from the dissertation of S.D.B., submitted in partial fulfillment of requirements for the Ph.D. degree, University of Washington.

Potassium Titanium(IV) Oxalate as a Reagent for Automated Pulse Polarographic Determination of Seromucoids

P. W. Alexander* and M. H. Shah

Department of Analytical Chemistry, University of New South Wales, P.O. Box 1, Kensington, N.S.W., Australia 2033

A new reagent, potassium titanium(IV) oxalate, is reported for quantitative polarographic determination of the seromucoid fraction of human serum. The reagent is shown to be sensitive to seromucoids without significant interference from the albumin or globulin content of serum, and is used for automated determination of seromucoids in a continuous-flow polarographic system in the differential pulse operational mode. The system is shown to operate at 60 samples/h with approximately ±0.5% precision and less than 2% carry-over for determinations in the range 1–30 mg L^{-1}. Interferences from amino acids, vitamins, and antibiotics are shown to occur but at tolerance limits below the levels in normal serum.

The role of glycoproteins in medical diagnostic applications has been reviewed by several authors (*1–3*) and it is clear that the serum level of this particular class of proteins is as yet of undecided value. The serum levels vary considerably with different types of pathological conditions, but also may depend greatly on the analytical method chosen for the determination.

The important analytical methods for determination of serum glycoproteins have been reviewed by Winzler (*1*), Toro et al. (*2*), and Searcy (*3*). The acid soluble seromucoid fraction of serum is commonly determined in serum filtrates after precipitation of the major protein components with perchloric acid. After filtration of the protein precipitate, the seromucoid content of the filtrate is precipitated by addition of phosphotungstic acid and determined either by turbidimetry (*4*) or by treatment of the precipitate with various reagents for colorimetric determination (*2*). An alternative approach is to determine the carbohydrate content of the seromucoid fraction with orcinol reagent (*2*).

Polarographic methods for determination of glycoproteins have also been reported. Brdicka's hexammine cobalt(III) chloride reagent is sensitive to glycoproteins, but other serum proteins interfere and separation of interfering proteins by acid precipitation is required. Polarographic behavior of proteins and analytical applications of Brdicka's method have been reviewed (*5–7*). Recently in addition, an automated method for Brdicka's determination of proteins by differential pulse polarography has been reported (*8*), and a new type of reagent, a Rh(III) substituted ethylenediamine complex, has been used for highly sensitive determination of serum proteins including glycoproteins (*9*), and applied for accurate determination of total serum proteins (*10*). This reagent again cannot be applied for glycoprotein determinations without separation steps because of interference from other proteins.

To date, therefore, a simple automated method for determination of glycoproteins does not appear to have been reported because of the separation steps required for the various methods. We describe a new sensitive and automated procedure for this purpose. The reagent, potassium titanium(IV) oxalate, is highly sensitive to glycoproteins in the presence of albumin and γ-globulins, and detection limits and quantitation by automated differential pulse polarography are described. Interferences from other components of normal serum are investigated in detail and the method is then applied to the determination of the range and standard deviation of glycoproteins in serum from 120 normal samples. Results are then compared to the data of de La Huerga et al. (*4*) obtained by the turbidimetric method.

EXPERIMENTAL

Reagents and Solutions. A stock solution of 0.1 M potassium titanium(IV) oxalate (BDH Analar) was made up in distilled water after dissolving in warm water. Working solution concentration 5×10^{-2} M was then prepared by dilution in 0.1 M oxalic acid (BDH). To study the pH effect in the range pH 1–4, the concentration of oxalic acid was varied while the concentration of potassium titanium(IV) oxalate was maintained constant in the solution. Human glycoproteins (Cohn Fraction VI), human γ-globulins (Fraction II), human albumin (Fraction V), all from

0003-2700/79/0351-2139$01.00/0

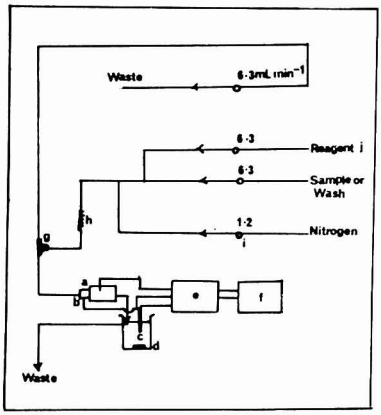

Figure 1. Schematic diagram of the polarographic flow system. (a) Flow-through cell; (b) Pt auxiliary electrode; (c) SCE; (d) waste electrolyte solution; (e) PAR model 174; (f) recorder; (g) debubbler; (h) mixing coil; (i) proportioning pump; (j) potassium titanium oxalate reagent (5.0×10^{-2} M) in 4.0×10^{-2} M oxalic acid at pH 1.67

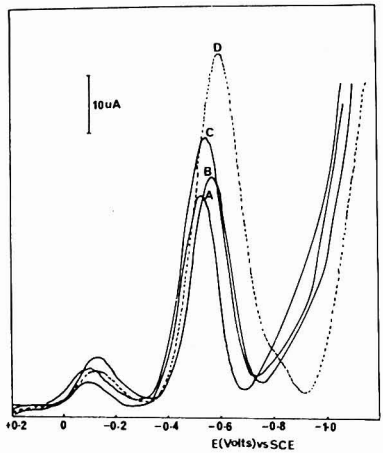

Figure 2. Continuous-flow differential pulse scans of the reagent, potassium titanium oxalate (5.0×10^{-2} M) with varying glycoprotein concentrations. (A) 0, (B) 20, (C) 100, (D) 300 mg L^{-1}

Miles Laboratories Inc., were used in this work. Stock solutions of 1 mg mL^{-1} were prepared in distilled water, and appropriate dilutions were freshly made when required to obtain concentrations in the range of 5–100 mg L^{-1}.

Instrumentation. A Princeton Applied Research Model 174 polarographic analyzer equipped with a drop timer (Model 174/70) and a Mace Laboratory recorder (FBQ 100) was used for polarographic analysis with differential pulse operation. The controls were set as follows. Current range 200 μA, modulation amplitude 100 mV, drop time 1 s, fixed potential -0.55 V, potential scan rate 5 mV s^{-1} (when required), chart speed 250 mm h^{-1}. Polarographic waves were measured with a three-electrode system consisting of Pt-metal, a saturated calomel reference electrode (SCE), and a dropping mercury electrode, DME, as the indicator electrode. Electrode characteristics were $m = 1.2$ mg s^{-1}, $t = 5$ s at a mercury column height of 56.8 cm measured in 5×10^{-2} M potassium titanium oxalate at -0.55 V. All measurements were made at room temperature.

The DME was inserted in an air tight flow-through glass cell (*8*). The cell contained a Pt auxiliary electrode situated upstream from the DME, and allowed operation in the differential pulse mode with a 3-electrode system and with accurately controlled droptimes. The reference electrode (SCE) was situated downstream from the cell in the waste solution as shown in the schematic diagram, Figure 1. For automated pumping of the reagents through the flow cell, a Desaga multichannel peristaltic pump, type No. 131900, was used. The required flow rate was obtained by use of a speed controller and pump tubes varying from 1.0–3.0 mm in internal diameter.

Procedure. With the flow system shown in Figure 1, the reagent and wash solutions were pumped initially through the flow cell and scanned in the differential pulse mode from +0.2 V to -1.8 V. A constant flow rate of 7.4 mL min^{-1} was maintained by use of the Desaga pump. The reagent solution consisted of potassium titanium(IV) oxalate, at a concentration of 5×10^{-2} M, prepared in 0.1 M oxalic acid to obtain a pH value of 1.67, with distilled water as the wash solution. The reagent and wash solutions were continuously deaerated with nitrogen gas, which was also used for segmentation in the flow system. Individual protein solutions were then aspirated continuously for 3–4 min in place of the wash solution and the range from +0.2 V to -1.8 V was rescanned to search for changes in peak voltages.

After choosing an appropriate fixed potential, the reagents and wash solutions were pumped through the cell continuously at a flow rate of 7.4 mL min^{-1} to establish a base line and suitable current range at which the noise level in the base line was low. At the chosen fixed potential, protein solutions were then manually aspirated into the system, followed by a water wash after each sample. The sample to wash ratio was kept constant at 1:1 throughout with 30-s sampling and 30-s wash times being accurately controlled with a stop watch. Current response to various protein sample solutions was continuously recorded in the 0.2-mA current range with 100-mV amplitude in the differential pulse mode and a 1-s controlled drop time. A calibration curve for glycoprotein was constructed in the concentration range of 5–100 mg L^{-1} at a sampling rate of 60 per hour and a flow rate of 7.4 mL min^{-1}.

RESULTS

Studies of the polarographic behavior of the reagent, potassium titanium(IV) oxalate, indicated significant shifts in half-wave potential on addition of glycoprotein to the reagent solution.

Figures 2 and 3 show the results of the differential pulse scan for the reagent at a concentration of 5.0×10^{-2} M and indicate a shift in potential of the second TiO^{2+} peak at -0.51 V, with increasing glycoprotein concentration. The peak shifted from -0.51 V to -0.81 V on increasing the glycoprotein concentration from 5 to 1000 mg L^{-1}, together with a marked increase in peak height.

For fixed potential determination of glycoprotein, the voltage was set at -0.55 V, where the most sensitive response to glycoprotein was observed. If the potential was set at the higher value of -0.81 V, positive response to glycoprotein was not observed for low concentrations of glycoprotein below 500 mg L^{-1}.

Other proteins tested were albumin and γ-globulin. Shifts in the TiO^{2+} peak potential were not observed with these proteins since it was found that both albumin and γ-globulin precipitated in the flow-system on mixing with the acidified reagent stream. Precipitation of these proteins apparently prevented any reaction with the reagent.

Effect of pH and Reagent Concentration. The sensitivity of the TiO^{2+} reagent to glycoprotein was measured as a function of pH, and reagent concentration, all of which were interdependent. The effect of pH was studied by varying the oxalic acid concentration at fixed reagent and glycoprotein concentrations, as shown in Figure 4. Maximum sensitivity was found to be independent of glycoprotein concentration and occurred at pH 1.67.

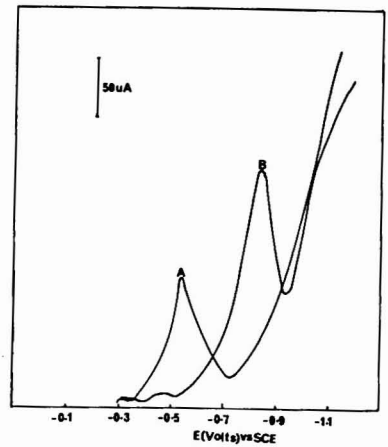

Figure 3. Effect of high glycoprotein concentration on the continuous-flow differential pulse scan of potassium titanium oxalate reagent solution. (A) Reagent alone (5.0×10^{-2} M); (B) reagent with added glycoprotein (1000 mg L^{-1})

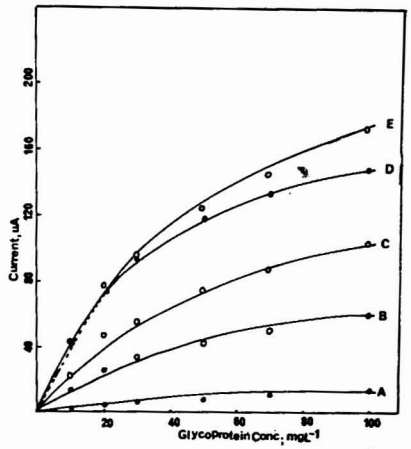

Figure 5. Glycoprotein calibrations at pH 1.67 in the DPP mode at 60 $S\,h^{-1}$ with varying TiO^{2+} reagent concentrations: (A) 2.0×10^{-2}, (B) 3.0×10^{-2}, (C) 4.0×10^{-2}, (D) 5.0×10^{-2}, (E) 6.0×10^{-2} M

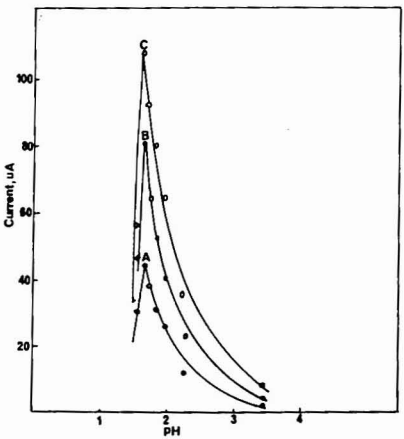

Figure 4. Effect of pH on the continuous-flow peak heights for glycoprotein at fixed TiO^{2+} and oxalic acid concentrations. TiO^{+} (5.0×10^{-2} M), oxalic acid (4.0×10^{-2} M) with glycoprotein concentrations of: (A) 10, (B) 20, and (C) 70 mg L^{-1}

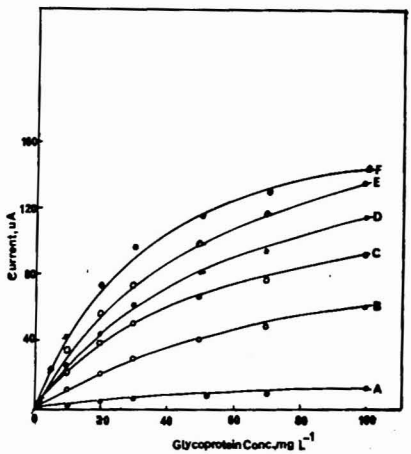

Figure 6. Glycoprotein calibrations at various pH values in the DPP mode at 60 $S\,h^{-1}$ with TiO^{2+} reagent concentrations at 5.0×10^{-2} M: (A) pH 3.48, (B) 2.25, (C) 1.99, (D) 1.83, (E) 1.73, (F) 1.67

The sensitivity for glycoprotein determination was also markedly dependent on the TiO^{2+} reagent concentration. Figure 5 shows the effect of the reagent concentration on glycoprotein response. Optimum sensitivity was achieved between 5.0×10^{-2} M and 6.0×10^{-2} M TiO^{2+} with pH kept constant at 1.67 by varying the oxalic acid concentration. Response to glycoprotein was not detectable below 2.0×10^{-2} M concentration. All subsequent measurements were made with these optimum pH and reagent concentrations while keeping the oxalic acid concentration constant at 4.0×10^{-2} M.

Calibrations. Using the optimum fixed voltage of −0.55 V, glycoprotein calibration plots were measured in the continuous flow system with the dpp operational mode at various pH values, as shown in Figure 6. The calibration plots were not linear, but calibration plot F, constructed at optimum conditions of pH and reagent concentration, was used as a working curve.

Figure 7 shows a typical automated readout for protein peak measurements. In automated analysis, carryover contributes significantly toward accuracy and precision of the system. As the carryover (i.e., the % interaction between minimum and maximum calibration concentrations) increases, accuracy is expected to decrease. The impact of carryover on accuracy can be evaluated by running random sampling. Table I shows data on the accuracy of the system determined by random sampling. An error of up to 4% is expected in the results for calibration in the range 1–30 mg L^{-1}.

The detection limit for glycoprotein was calculated to be 0.6 mg L^{-1} based on the definition of twice the standard deviation of a peak near the blank reading.

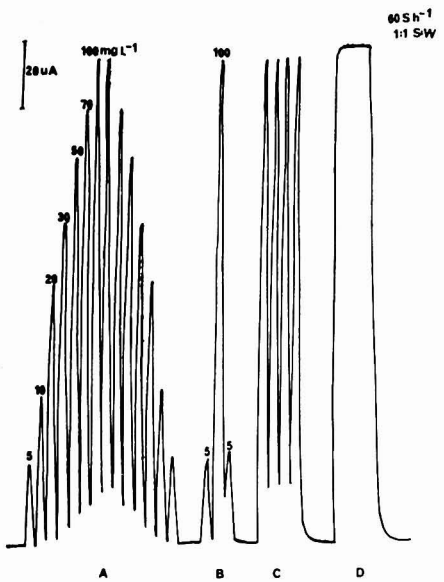

Figure 7. Continuous recording of glycoprotein sample peaks at a fixed potential of −0.55 V. (A) Calibration for the concentration range 5–100 mg L^{-1}. (B) Carryover between sequential samples of 5, 100, and 5 mg L^{-1} glycoprotein. (C) Replicates for 100 mg L^{-1} glycoprotein; (D) steady-state reading at 100 mg L^{-1}

Table I. Relative Errors in Random Glycoprotein Determinations under Continuous-Flow Conditions

glycoprotein concn, mg L^{-1}	current, μA	calcd concn from calibration, mg L^{-1}	% error
30	96	29	3.3
70	140	76	8.5
20	78	20	0
50	116	48	4
10	44	10	0

At a sampling rate of 60 per hour, the % of steady state obtained was 96% with a precision of 0.5% RSD for replicate samples at a total solution flow rate of 7.4 mL min^{-1}. Carryover was 1.7%. Precision is quite independent of accuracy in a continuous-flow system. Excellent precision as obtained here (±0.5%) can be obtained while accuracy may be very poor owing to carryover and interference problems.

Determination og Glycoproteins in Serum. The reagent potassium titanium(IV) oxalate has a dual function. On the one hand, it acts as a precipitating agent for albumin and γ-globulins, while on the other hand, it is sensitive to glycoproteins. Because of these characteristics of the reagent, it is possible to measure glycoprotein levels in serum samples without interference from albumin and γ-globulins on glycoproteins. Table II shows the effect of albumin and γ-globulins on glycoproteins. Albumin affects the glycoprotein peak at a concentration of 500 mg L^{-1}, whereas γ-globulin up to 500 mg L^{-1} concentration does not have any effect on glycoproteins. Precipitation of albumin and γ-globulin occurred in the flow system but did not affect the DME or the sensitivity of the system. A voltage scan with diluted normal serum from +0.2 to −1.80 was also carried out before analysis

Table II. Interference Effects of Proteins on Glycoprotein[a] Continuous-Flow Determinations

concn of albumin, mg L^{-1}	glycoprotein peak height, μA	concn of γ-globulin mg L^{-1}	glycoprotein peak height, μA
0	44	0	44
50	44	50	44
100	42	100	44
500	30	500	44

[a] For glycoprotein in concentration of 10 mg L^{-1}.

Table III. Interference Effects on the Glycoprotein[a] Continuous-Flow Peak Height

type of interference concn, mg/L	peak height, μA 0.5	1.0	2.0
tyrosine	44	44	44
arginine	44	44	48
histidine	46	49	60
tryptophan	48	50	70
vitamin B_1	59	66	96
vitamin B_6	44	52	66
ascorbic acid	44	42	42
glutamine	44	44	44
glutamic acid	44	44	44
bicillin	44	46	54
penicillin G	44	42	38

[a] Concentration of glycoprotein is 10 mg/L.

of the samples at the fixed potential of −0.55 V. An increase in peak height along with a shift from −0.51 V to −0.55 V was observed, similar to the response by the standard glycoprotein, Cohn Fraction VI.

Studies have been made on the determination of glycoprotein by analyzing 120 serum samples from normal subjects obtained from the N.S.W. State Blood Bank. The serum samples were diluted by a factor of 1:40 and the diluted samples were fed through the flow system at the rate of 60 per hour. The seromucoid concentrations were calculated from the calibration curve obtained above in Figure 6 with Cohn Fraction VI glycoprotein as the standard.

The results gave a mean value of 740 ± 160 mg L^{-1} and a range of 400–1200 mg L^{-1}. The range for 95% of the samples was 420–1080 mg L^{-1}. These results compare favorably with those of de La Huerga et al. (4) who found a value of 812 ± 180 mg L^{-1} for normal adults by analysis of perchloric acid filtrates and turbidimetric measurement after precipitation with phosphotungstic acid.

Interference Effects. Table III shows the effect of a range of possible interferences on the peak height of glycoprotein Fraction VI at a concentration of 10 mg L^{-1}. Most of the molecules tested interfered at or above a concentration of 1 mg L^{-1}.

Of the amino acids tested, histidine and tryptophan interfered most seriously at concentrations as low as 0.5 mg L^{-1}, but simpler amino acids such as glycine, alanine, and valine had no effect. Vitamins B_1 and B_6 also increased the glycoprotein peak height and of the antibiotics tested bicillin and penicillin G had opposite effects. The former increased but the latter decreased the peak height. It seems likely that competitive complexing of TiO^{2+} by these interfering molecules must play some part in the mechanism of these interference effects, as discussed in the following section.

DISCUSSION

Previous polarographic methods with the Brdicka's Co(III) reagent (8) or the Rh(III)-sdmen (9) complex reagent lack specificity for glycoproteins, require a separation step and have

not as yet been completely automated. The use of the Ti(IV) oxalate reagent proposed here overcomes these problems to a large extent. Acid precipitation of albumin and globulins occurred in the flow system and little interference was observed from these proteins when in large excess of glycoprotein as in normal serum since the electrode did not respond to precipitated solids. Hence a separation step was not required and the function of the DME was not affected.

It was therefore possible to directly automate the method without treatment of the serum samples except for dilution. Samples were analyzed in the continuous-flow system at the rate of 60 per hour with acceptable precision and little carryover The method is therefore rapid and useful for screening of large numbers of serum samples for clinical studies.

The electrochemical reduction of tetravalent titanium has been studied by Lingane and Kennedy (*11*), and Habashy (*12*). Reduction of the tetravalent titanium ion was found to occur in acidic solution in the form of TiO^{2+} according to the reaction:

$$TiO^{2+} + 2H^+ + e \rightarrow Ti^{3+} + H_2O$$

which is accompanied by high overvoltage. The polarography of tetravalent titanium in oxalate supporting media has been investigated by Vandenbosch, (*13*), as a function of pH. Tetravalent titanium under these conditions behaves reversibly at the DME over certain pH ranges. The half-wave potential of the tetravalent titanium ion, as recorded by us, was −0.51 V.

The electrode reaction of TiO^{2+} in the presence of glycoprotein and other interfering molecules is uncertain. It appears that differences in the degree of complex formation affect the reduction of TiO^{2+}, resulting in a shift of voltage. In the case of albumin and γ-globulin, because of precipitation in the acid reagent, complexing does not occur and no shift in the voltage of the TiO^{2+} peak is observed. It is likely that the differences in values of the isoelectric point (*14*) of these classes of proteins is responsible for this difference in reactivity, and hence glycoprotein can be selectively determined in the presence of other proteins. Smaller molecules which do not precipitate in acid medium may, however, complex TiO^{2+} and cause interference.

The effects of pH and reagent concentration have been studied to optimize sensitivity of the method, and are clearly interdependent. The pH was varied by changing the oxalic acid concentration with the TiO^{2+} reagent concentration held constant, and hence the ionic strength also changed. Because of this large number of interdependent variables, the optimum pH of 1.67 obtained in Figure 2 is somewhat arbitrary due to our choice of experimental conditions, but represents the optimum we were able to find in our studies of reagent effects.

Despite this problem of complex formation of smaller molecules with the TiO^{2+} reagent, the method has been applied to the determination of serum samples from blood bank donors. The normal range for glycoprotein concentration in serum was arbitrarily defined (*14*) as the range of values that would encompass 95% of a population of clinically normal persons, and a mean value and standard deviation were calculated. From our results, for glycoprotein in serum, the normal range was found to be similar to the value obtained by de La Huerga et al. (*4*) by the turbidimetric method. Possible interferences to our method have been shown to be negligible in normal serum in our interference studies.

However, we have not attempted a direct correlation study of the two methods for two reasons. First, the standards used in the original method, either mucoprotein fraction MP-1 or albumin as a secondary standard, were different from glycoprotein Fraction VI used in this study. Secondly, the seromucoid values obtained are known (*1*) to depend greatly on the particular type of analytical method used, because each method may yield an estimate of only certain fractions of the total glycoprotein concentration in serum. Our method has been shown to be a rapid procedure for quantitative determination of the serum glycoprotein fraction which is capable of reacting with the TiO^{2+} reagent.

Possible interference problems we have found are from certain vitamins, antibiotics, and amino acids including tyrosine, tryptophan, phenylaniline, arginine, histidine, and methionine. However, the free concentration of these amino acids in normal serum is in the range 8–33 mg L^{-1} and is therefore too low in our diluted serum sample (50 μL in 2.0 mL water) to interfere seriously despite the high sensitivity of the TiO^{2+} reagent to these molecules. After dilution of the sample in our method, the tryptophan content for example is expected to be in the range from 0.4–0.6 mg L^{-1}. We have shown the tryptophan tolerance limit to be approximately 1 mg L^{-1} before interference begins for 10 mg L^{-1} glycoprotein. The levels of other molecules shown in Table III and present in normal serum are too low to cause interference to glycoprotein determinations.

The automated Ti method therefore has been shown to be useful for rapid screening of total acid-soluble glycoproteins in serum with few interference problems. This is of particular interest concerning the role of glycoproteins in various pathological conditions as reviewed by Searcy (*3*). But further work may also be of interest in this method for determination of amino acids and other molecules which may complex TiO^{2+} and cause shifts in peak potentials.

ACKNOWLEDGMENT

We gratefully acknowledge the assistance from a Colombo Plan Fellowship for M.H.S. and the supply of serum samples from K. Kenrick, N.S.W. State Blood Bank.

LITERATURE CITED

(1) R. J. Winzler, "Methods of Biochemical Analysis", Vol. II, David Glick, Ed., Interscience, New York, 1955, p 279.
(2) G. Toro and Philip G. Ackerman, "Practical Clinical Chemistry", Little, Brown and Company, Boston, Mass., 1975, p 214.
(3) R. L. Searcy, "Diagnostic Biochemistry", McGraw-Hill, New York, 1969, p 258.
(4) J. de. la Huerga, A. Dubin, D. S. Kushner, H. A. Dyniewicz, and H. Popper, *J. Lab. Clin. Med.*, 47(3), 403 (1956).
(5) R. Brdicka, *Collect. Czech. Chem. Commun.*, 5, 1 (1936).
(6) M. Brezina, "Advances in Polarography", I. S. Langmuir, Ed., Pergamon Press, Oxford, 1960, 3933 pp.
(7) J. Homolka, "Methods of Biochemical Analysis", Vol. 19, David Glick, Ed., Interscience, New York, 1955, p 435.
(8) P. W. Alexander and M. H. Shah, *Talanta*, 26, 97 (1979).
(9) P. W. Alexander, R. Hoh and L. E. Smythe, *J. Electroanal. Chem.*, 80, 143 (1977).
(10) P. W. Alexander, R. Hoh and L. E. Smythe, *J. Electroanal. Chem.*, 81, 152 (1977).
(11) James J. Lingane and John H. Kennedy, *Anal. Chim. Acta*, 15, 294 (1956).
(12) G. M. Habashy, "Advances in Polarography", Vol. 3, I.S. Langmuir, Ed., Pergamon Press, New York, 1960, p 833.
(13) V. Vandenbosch, *Bull. Soc. Chim. Belg.*, 58, 532 (1949).
(14) N. W. Tietz, "Fundamentals of Clinical Chemistry", W. B. Saunders Co., London, 1970, p 235.

RECEIVED for review October 25, 1978. Accepted July 13, 1979.

Amperometric Membrane Electrode for Measurement of Ozone in Water

John H. Stanley and J. Donald Johnson*

Department of Environmental Sciences and Engineering, School of Public Health, University of North Carolina at Chapel Hill, Chapel Hill, North Carolina 27514

An amperometric membrane electrode has been developed for the selective measurement of molecular ozone in water. The membrane electrode system consists of a gold cathode, a double junction reference electrode (10% KNO_3/SCE), a potassium sulfate electrolyte (0.5 M, pH 3.7), and a Teflon membrane (3.3×10^{-3} cm thickness). A current sensitivity of 0.484 $\mu A \cdot (mg/L)^{-1} \cdot (cm)^{-2}$ was observed at an applied voltage of +0.6 V (vs. SCE) at 22 °C. A detection limit of 62 $\mu g/L$ is predicted at twice the observed residual current. Less than 2% interference was observed from bromine, hypobromous acid, chloride dioxide, hydrogen peroxide, trichloramine, and hypochlorous acid.

A drawback to the use of ozone as a chemical disinfectant and/or oxidant for water treatment is the lack of a selective and reproducible analytical technique for monitoring residual ozone concentrations. Present methods are influenced by the chemical instability of the ozone molecule in water and are subject to interferences from oxidizing agents that may be present.

Amperometric membrane electrodes have been used successfully for dissolved oxygen and halogen analysis (*1*, *2*). More recently, the use of these electrode systems for the measurement of molecular ozone dissolved in aqueous solution has been demonstrated (*3–5*). This work indicates that membrane electrodes possess the required detection sensitivity and potentially the selectivity for the measurement of molecular ozone. Also, membrane electrodes may be particularly suitable for ozone analysis since in situ measurements are possible.

A new amperometric membrane electrode design has been developed for the measurement of ozone in water. This design has evolved from the original amperometric ozone electrode proposed earlier by Dunn and Johnson (*3*) and voltammetric studies of the ozone reduction process to optimize the electrolytic media and applied voltage. A homogeneous Teflon membrane was chosen in place of the microporous film from the earlier design because the diffusion transport properties of the former aid in the selective measurement of gaseous molecules like ozone. Operational characteristics of the membrane electrode and potential interferences in water treatment have also been examined.

EXPERIMENTAL

Apparatus. A Delta Scientific (now National Sonics Corporation) model no. 8324 HOCl amperometric electrode has been modified using an Orion model No. 09-02 double junction reference electrode and a Teflon membrane (Delta Scientific No. 824110) of 3.3×10^{-3} cm thickness (See Figure 1). A 0.38-cm^2 gold button serves as the working cathode. The electrochemical circuit is completed using a 0.5 M potassium sulfate supporting electrolyte (pH 3.7, 0.1 M NaOAc/HAc buffer system).

The membrane is applied over the gold surface and a capillary film of electrolyte. The membrane is held in position using Teflon tape and a plastic ring collar. The electrolyte layer between the cathode and the membrane is replenished through wicks located around the electrode tip leading to an electrolyte reservoir in which the reference anode is immersed. When the membrane is mounted over the cathode, a primary concern is the avoidance of tears or creases in the membrane which affect diffusion processes and the reproducibility of the current response.

Voltammetric studies were conducted using a three-electrode arrangement consisting of a gold-plated E. H. Sargent model no. S-30421 platinum hook working electrode, an identical platinum hook auxiliary electrode, and a saturated calomel reference electrode. The rotating gold electrode was mounted in an E. H. Sargent model no. S-76985 synchronous rotator (600 rpm).

Voltages were impressed and current was monitored using a McKee-Pedersen Instruments MP-1502 Electroanalyzer equipped with an MFE model 715 X-Y Recorder. The electrode potential was monitored using a Fisher Scientific model no. 420 pH/ion meter.

Ozone was produced from oxygen using a W. R. Grace model LG-2-L1 Corona generator. The generator output was varied from 0 to 1.5% by wt in O_3 by controlling the applied voltage across the electrical discharge tube and the oxygen gas flow rate.

Amperometric titrations were conducted using the above equipment with the Sargent rotating platinum hook electrode, synchronous rotator, and a saturated calomel reference electrode. A voltage of +0.2 V (vs. SCE) was applied to the working electrode.

Procedures. All reagents and test solutions were prepared using distilled and deionized water. Chemical reagents were prepared according to standard procedures (*6*) with Fisher ACS Certified, Malinckrodt, or Baker Analyzed chemical reagents. Two buffers were used, pH 6.0 (0.1 M KH_2PO_4, Na_2HPO_4), and pH 3.7 (0.1 M HAc, NaOAc).

Current-potential relationships were developed at 5 °C at an electronic sweep rate of 25 mV $(min)^{-1}$ in the anodic then the cathodic direction. Ozone concentration measurements were made at 300- to 500-mV intervals to normalize the current measurements, expressed as $\mu A\ (mg/L)^{-1}$, for ozone losses during the experiment. Voltammograms were also developed in oxygen saturated electrolyte solutions to establish the base-line current response.

Amperometric measurements were made with the membrane electrode positioned in a cylindrical Plexiglas contactor (13 cm × 6 cm). Ozone was contacted in the test solution with a circular glass fritted diffuser inserted through the top plate of the Plexiglas reactor. The contactor was placed on a magnetic stirrer to accomplish stirring at the electrode tip. After ozonation and complete mixing was accomplished, a steady-state current response was achieved. After observing this current for approximately 30 s, the current response was recorded as a sample was collected for analysis. Water column and electrode temperature were controlled using an external Plexiglas jacket. Temperature equilibrium was attained after approximately an hour.

Current potential relationships were also developed using the Delta Scientific electrode in a two-electrode system in the Plexiglas contactor. These voltammograms were developed in a manner similar to the three-electrode studies except the stirring rate was 1000 rpm. The desired electrolyte was ozonated directly in the contactor and samples were again periodically analyzed to account for ozone loss.

The iodometric procedure (*6*, *7*) was chosen as the reference technique for ozone analysis in the absence of interferences. End-point detection for direct and back titration procedures using either sodium thiosulfate or phenylarsine oxide was accomplished amperometrically.

Oxidants considered possible interferences were prepared by known procedures (*8*, *9*) and analyzed by standard methods (*6*).

0003-2700/79/0351-2144$01.00/0

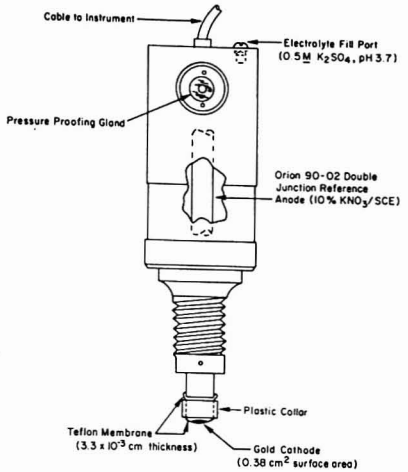

Figure 1. Schematic view of the membrane electrode system

The membrane electrode was lowered into a concentrated solution of the particular oxidant and the current response was noted. Identical measurements were made with the membrane applied over the cathode and with the membrane removed.

RESULTS AND DISCUSSION

A principal concern was improving the selectivity of the membrane electrode for molecular ozone in the presence of other oxidants. Along with the selectivity, a linear and reproducible current response with a detection sensitivity comparable to or exceeding that observed with other designs (*3–5*) was desired. Several design factors were examined in an effort to optimize both the current sensitivity and selectivity of the system.

Design Features. Dunn (*3*) used a potassium chloride (1.6 M, pH 6.0) supporting electrolyte and measured reduction currents at an applied voltage of +0.35 V (vs. Ag/AgCl). Voltammograms developed in this electrolyte illustrate that the application of more anodic voltages is limited to the potential range less positive than +0.4 to 0.5 V (vs. Ag/AgCl) because the observed current is affected by a competing oxidation reaction at more positive voltages. This results in a reduced current response from ozone and a more significant residual current signal. Gaur and Schmid (*10*) first observed this oxidation current in the presence of chlorine, which they report results from the anodic dissolution of the gold cathode due to the formation of a gold chloride complex. Voltammograms developed in studies with other electrolytes (*4, 11, 12*) are limited by oxygen evolution at much more positive voltages. The use of one of these electrolytes would allow for the application of more anodic voltages. Since the use of a more positive voltage at the gold cathode restricts electron flow, selectivity is improved because reduction reactions occur only for the most powerful oxidizing agents like ozone. The choice of a supporting electrolyte thus directly affects the selectivity of the system for ozone.

This was confirmed by studying the reduction of ozone in several electrolytic media: potassium chloride (1.6 M, pH 6.0), sulfuric acid (0.05 M, pH 1.3), and perchloric acid (0.1 M, pH 1.2). As is illustrated in Figure 2, the use of chloride electrolyte restricts the accessible anodic potential range at which the ozone reduction processes can occur when compared with the use of sulfate electrolyte. Reduction currents for ozone were

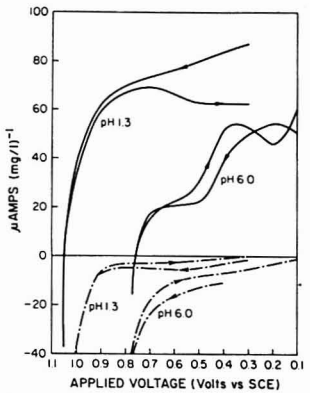

Figure 2. Current–voltage relationship at the rotating gold electrode in 0.05 M H_2SO_4 (pH 1.3) and 1.6 M KCl (pH 6.0). Solid lines are for ozone reduction current and dashed lines are residual current

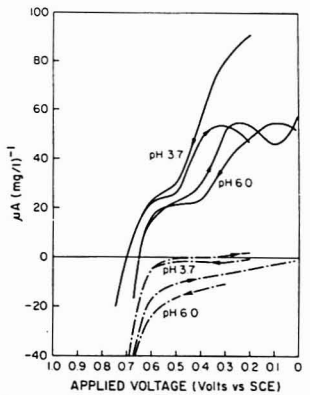

Figure 3. Current–voltage relationship at the rotating gold electrode in 1.6 M KCl (pH 6.0) and 0.5 M KCl (pH 3.7). Solid lines are for ozone reduction current and dashed lines are residual current

observed up to an applied voltage of +1.05 V (vs. SCE) in sulfuric acid. In the potassium chloride media, reduction currents were observed at potentials at or below +0.65 V (vs. SCE) only. A similar result was observed in perchloric acid. In addition, the increased stability of the O_3 molecule in the acidic media resulted in a greater reduction current response and a more electrochemically reversible process. The residual current was also much less significant in the sulfate media even at the more anodic voltages. A low and reproducible residual current is essential for maximizing the current detection sensitivity of the system.

The effect of the pH of the supporting electrolyte on the reduction current was examined more closely using sulfate and chloride media. In Figure 3, an oxidation current is again observed in the more acidic chloride media. Figure 4 shows improved electrochemical reversibility and an increase in the magnitude of the reduction current of ozone in sulfate media at lower pH values.

Based on these results, potassium sulfate (0.5 M, pH 3.7) was selected as the supporting electrolyte. The effect of chloride on the reduction current response also required the

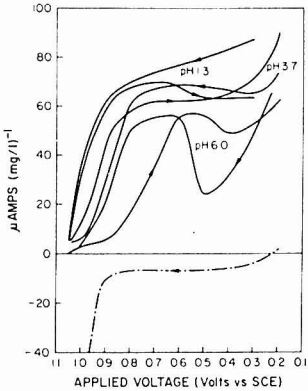

Figure 4. Current–voltage relationship at the rotating gold electrode in 0.05 M H_2SO_4 (pH 1.3), 0.5 M K_2SO_4 (pH 3.7), and 0.5 M K_2SO_4 (pH 6.0). Solid lines are for ozone reduction current and dashed lines are residual current

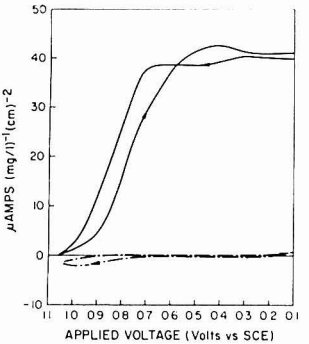

Figure 5. Current–voltage relationship at the uncovered Delta gold button cathode in 0.5 M K_2SO_4 (pH 3.7). Solid line is for ozone reduction current and dashed line is residual current

use of a double junction reference electrode.

For amperometric or steady-state measurements with the new modified Delta electrode system, an applied voltage of +0.6 V (vs. SCE) was selected based on the voltammogram developed with this two-electrode system in Figure 5. The current response observed with this stationary electrode was less ideal than the voltammetric relationship obtained with the rotating gold electrode. But the current response is a more realistic appraisal of the steady-state membrane electrode performance. The selection of an applied voltage of +0.6 V (vs. SCE) represents a compromise between additional selectivity (by the application of more anodic voltages) and a concomitant loss of current range and sensitivity. Application of the membrane over the cathode to complete the design further reduces the current sensitivity of the system but defines the steady-state current and greatly improves selectivity.

Current Sensitivity. A typical current response of the membrane electrode system at +0.6 V (vs. SCE) is 0.484 with a standard deviation of ±0.007 μA $(mg/L)^{-1}$ $(cm)^{-2}$ and an r value of 0.995 at 22 °C in an ozone test solution at pH 4.9. Residual currents at this voltage range from −2 to −15 nA. A detection limit of 62 μg/L is predicted at twice the residual

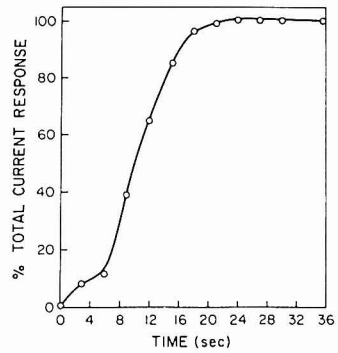

Figure 6. Response time to step change from 0 to 1 mg/L ozone at stirring rate of 1000 rpm

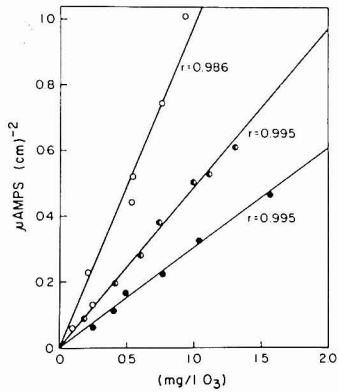

Figure 7. Current sensitivities at 13 °C (●), 22 °C (◐), and 32 °C (○) at +0.6 V (vs. SCE)

current of 15 nA. The high correlation and low residual current shows the current response is linear and reproducible.

The current response is only slightly affected by stirring. A 98% current response is observed at a stirring rate of 600 rpm with a 2.5-cm stirring bar located 1.4 to 1.6 cm below the electrode tip. Since the effect is highly dependent on membrane structure and thickness, the use of this Teflon membrane is advantageous since only minimal stirring is required to achieve the maximum current response.

Response Time. The response time of the membrane electrode to a step change in the dissolved ozone concentration is illustrated in Figure 6. A 95% response was observed in 18 s when the electrode was transferred from air saturated water to a sample containing approximately 1 mg/L of ozone. The response time is dependent on the membrane permeability for ozone and the thickness of the electrolyte film. The initial lag in the response has been observed before (*13*) but no explanation is given for this experimental peculiarity.

Temperature Effects. The current response of the system is highly dependent on temperature as illustrated in Figure 7. Current sensitivities (ϕ) range from 0.316 to 0.992 μA $(mg/L)^{-1}$ $(cm)^{-2}$ at 13 and 32 °C with an average variation at normal temperatures of 5.8% per °C. Since the current response of a given membrane at steady-state conditions is solely dependent on the rate of transport from the test solution

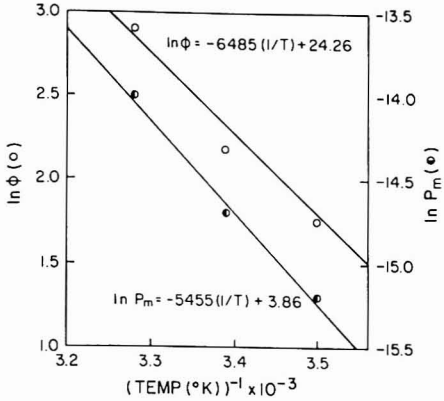

Figure 8. ln ϕ (O) vs. $1/T$ (K) × 10^{-3}, ln Pm (●) vs. $1/T$ (K) × 10^{-3} at 13, 22, and 32 °C

Table I. Current Response to Interferences

chemical compound	current response: μA (mg/L)$^{-1}$	current response: μA (mequiv/L)$^{-1}$	% interference in measurement of ozone[a]
Br_2	5×10^{-4}	0.080	1.8
HOBr	3×10^{-4}	0.048	1.1
HOCl	3×10^{-5}	0.001	0.03
NCl_3	2×10^{-5}	2×10^{-4}	0.01
H_2O_2	0	0	-
ClO_2	5×10^{-3}	0.068	1.5

[a] Based on current response to ozone at 22 °C = 0.184 μA (mg/L)$^{-1}$ = 4.416 μA (mequiv/L)$^{-1}$

to the cathode, the high temperature coefficient is mainly attributable to the permeability characteristics of the membrane. If the permeability coefficient is directly proportional to the current sensitivity, ϕ should also exhibit a similar temperature dependence. In Figure 8, the temperature dependence of the experimental current sensitivities and membrane permeabilities to ozone is demonstrated to be in adherence with the classical laws governing an activated diffusion process as first suggested by Mancy (*14*).

Interferences. The current response of the membrane electrode to several oxidants considered to be possible interferences was examined as shown in Table I. Other oxidizing and reducing agents commonly found in water and wastewaters were excluded from the study based on their observed lack of polarographic behavior (*8*, *15*). Trichloramine, hypobromous acid, bromine, hypochlorous acid, hydrogen peroxide, and chlorine dioxide exhibited less than a 2% interference in the measurement of ozone. With the membrane removed, the response to all the compounds except hydrogen peroxide increased. Presumably, the membrane selectivity prevents the transfer of polar species such as hypochlorous acid in favor of gaseous molecules like chlorine dioxide. However, only those compounds which are powerful oxidants are capable of being reduced at the cathode surface even though diffusion through the membrane is possible.

ACKNOWLEDGMENT

The authors gratefully acknowledge the assistance of R. Smart in obtaining reference material.

LITERATURE CITED

(1) I. Fatt, "Polarographic Oxygen Sensor", CRC Press, Cleveland, Ohio, 1976.
(2) J. D. Johnson, J. W. Edwards, and F. K. Keeslar, *J. Am. Water Works Assoc.*, **70**, 341 (1978).
(3) J. F. Dunn and J. D. Johnson, "Ozone Amperometric Membrane Electrode" in "Second International Symposium on Ozone Technology", Ozone Press International, Jamesville, N.Y., 1976, pp 132–141.
(4) R. Smart and K. H. Mancy, unpublished report, Department of Environmental and Industrial Health, University of Michigan, Ann Arbor, Mich., 1977.
(5) J. H. Stanley and J. D. Johnson, "A Molecular Ozone Membrane Electrode", Paper presented at the 175th National Meeting of the American Chemical Society, Anaheim, Calif., March 1978.
(6) American Public Health Association, "Standard Methods for the Examination of Water and Wastewater", 13th ed., Washington, D.C., 1971, pp 107–143, 271–275.
(7) D. L. Flamm, *Environ. Sci. Technol.*, **11**, 978 (1977).
(8) F. K. Keeslar, "A Selective Amperometric Membrane Electrode for Measurement of Chlorine and Bromine Residuals in Water", Technical Report, Submitted to Dept. of Environmental Sciences and Engineering, University of North Carolina, 1975, ESE publication no. 605.
(9) J. R. Knechtel, E. G. Janzen, and E. R. Davis, *Anal. Chem.*, **50**, 202 (1978).
(10) N. Gaur and G. M. Schmid, *J. Electroanal. Chem. Interfacial Electrochem.*, **24**, 279 (1970).
(11) D. C. Johnson, D. T. Napp, and S. Bruckenstein, *Anal. Chem.*, **40**, 482 (1968).
(12) A. A. Rakov and V. I. Veselovskii, *Russian J. Phys. Chem.*, **35**, 1134 (1961).
(13) A. Berkenbosch, *Acta Physiol. Pharmacol. Neerl.*, **14**, 300 (1967).
(14) K. H. Mancy, D. A. Okun, and C. N. Reilley, *J. Electroanal. Chem.*, **4**, 65 (1962).
(15) D. T. Sawyer, R. S. George, and R. C. Rhodes, *Anal. Chem.*, **31**, 2 (1959).

RECEIVED for review September 11, 1978. Accepted August 20, 1979. This work was supported by a grant to J.D.J. from the Environmental Protection Agency (Program IBC-611). This paper was presented at the 175th National Meeting of the American Chemical Society, Division of Environmental Chemistry, Anaheim, Calif., March 12, 1978, from a thesis submitted to the Graduate School, University of North Carolina, Chapel Hill, N.C., in partial fulfillment of requirements for a Master of Science in Environmental Sciences. ESE Publication No. 534.

Copper Ion-Selective Electrode for Determination of Inorganic Copper Species in Fresh Waters

Renato Stella and M. T. Ganzerli-Valentini

Laboratorio di Radiochimica e Centro di Radiochimica ed Analisi per Attivazione del C.N.R., Istituto di Chimica Generale ed Inorganica, Università di Pavia, Viale Taramelli 12, 27100 Pavia, Italy

A method is described for determination of soluble copper inorganic species in fresh waters. Assuming that OH^- and CO_3^{2-} are the most important ligands, the presence and the distribution of $CuOH^+$, $Cu_2(OH)_2^{2+}$, $CuCO_3(aq)$, $Cu(CO_3)_2^{2-}$ are deduced by measuring Cu^{2+} concentration as a function of pH in controlled media. The cupric ion-specific electrode is used. The procedure devised for copper speciation in natural waters requires that, beside free cupric ion concentration $[Cu^{2+}]$, only total carbonate carbon C_T and pH be known. Some examples of application to actual samples are given.

Copper toxicity toward aquatic life is dependent on chemical forms and hence the knowledge of chemical species distribution is of primary interest (*1*) in the studies concerning copper transport and biological interaction in natural waters.

The copper ion-selective electrode has commonly been applied to distinguish between free and bound copper ion (*2, 3*). In the present work this technique was exploited to study copper behavior in weakly basic and hydrocarbonate solutions, following the line traced by Stiff (*4*). The investigated concentration range simulated natural systems. This research was part of an interdisciplinary investigation on the ecosystems of the Po and Ticino rivers in Northern Italy. To minimize any possible interference or change in chemical equilibria, the standard addition method was discarded and the direct use of the electrode was extended down to 10^{-10} M Cu^{2+}. As the hydrogen ion, H_3O^+, is competitive with copper toward the ligands OH^- and CO_3^{2-}, accurate pH measurements were simultaneously made with Cu^{2+} activity determination, thus allowing a more precise identification of all complexation and precipitation equilibria involved.

EXPERIMENTAL

Electrode Calibration. Before examining simulated Cu(II)/OH^- and Cu(II)/HCO_3^-–CO_3^{2-} systems, the Orion 94-20 A copper ion-selective electrode was carefully calibrated (*5–7*). The following set of operational conditions was selected:

(1) Ionic strength. In all tested solutions, this was fixed at 0.05 M by adding KNO_3.

(2) Dissolved oxygen interference. Before running any measurement, formaldehyde up to 10^{-3} M was added to prevent the CuS membrane oxidation. Bubbling a N_2 gaseous stream through the solution was avoided as CO_2 also was carried off, thus altering carbonate–hydrocarbonate equilibria.

(3) Stirring speed and electrode distance. These were both kept constant through all the measurements.

(4) Operational details. A total volume of 100 cm^3 was used for all solutions undergoing copper measurement, all the equipment being screened from incident light.

(5) TPX plastic containers were always used as this plastic showed little or no adsorption and release of trace metals. Glass- or polytheneware were prevented from coming in contact with diluted copper solutions.

A 9.95×10^{-2} M copper solution was prepared by dissolving the appropriate "Suprapure" $Cu(ClO_4)_2 \cdot 6H_2O$ amount in tridistilled water and the titer was made by EDTA complexometric titration, both visual and potentiometric. From this solution more diluted ones, up to 10^{-5} M, were prepared by stepwise dilution. Still more diluted ones were prepared according to Hansen (*8*) as copper ion buffers with nitrilotriacetic acid (NTA) at buffered pHs. Calibration graphs resulted as straight lines down to 10^{-12} M Cu^{2+}.

The cupric ion-selective electrode response was measured with a high impedance electrometer using a single junction Orion 90-01 reference electrode. A tenfold change in activity yielded an electrode response change of about 29.5 ± 0.5 mV as expected. Concentration instead of activity was plotted vs. the mV electrode response as the concentration is directly known.

Procedure. The effect of copper complexation by the OH^- ligand (or cupric ion hydrolysis) was studied as a function of ligand concentration in a selected pH range (pH 6 to 9).

Measured amounts of copper standard solution and "Suprapure" 40% carbonate free NaOH, properly diluted, were added to a stock solution containing formaldehyde and KNO_3, 10^{-3} M and 5×10^{-2} M, respectively. To avoid CO_2 absorption a N_2 atmosphere was constantly kept over the solution up to the end of the experiment. "Suprapure" diluted $HClO_4$ was added stepwise to lower pH from initial 9.7 to 6 and electrode responses were correspondingly recorded. After each addition at least 10 min was required to reach constancy of the electrode response.

Interactions between copper and CO_3^{2-} anions were also studied using a copper solution at a total concentration lower than 4.97×10^{-4} M to which a $NaHCO_3$ or $Ca(HCO_3)_2$ solution was added. Concentrations of the ligands, CO_3^{2-} and OH^-, are obviously related to the pH of the system. Therefore pH was continuously changed from 9 to 6 by stepwise addition of "Suprapure" $HClO_4$ and the electrode responses were correspondingly recorded.

In the first case, a 0.105 M Na_2CO_3 solution in known aliquots was added to the copper solution containing formaldehyde and KNO_3. In the second case, a standard $Ca(HCO_3)_2$ solution was prepared by bubbling a CO_2 stream through a $CaCO_3$ suspension in water for 1 h. After the excess $CaCO_3$ was filtered off, pH was measured and the filtrate potentiometrically titrated to evaluate the alkalinity which corresponds to $[HCO_3^-]$ at pHs ≃ 8.

The total carbonate, C_T, was deduced from the $[HCO_3^-]$ using the diagram reported by Stumm (*9*) or the following formula:

$$C_T = \left[\frac{[H^+]^2 + [H^+]K_1 + K_1K_2}{[H^+]K_1} \right] \times [HCO_3^-]$$

The value of C_T determined this way was 1.63×10^{-2} M, which was only 5% higher than $[HCO_3^-]$.

RESULTS AND DISCUSSION

Cu(II)/OH^- System. Results are shown in Figure 1 where a −2 slope of the log $[Cu^{2+}]$ vs. pH curve indicates the presence of the $Cu(OH)_2$ precipitate. Over the straight portion (up to the lowest pH value allowing precipitation) log $*K_{so}$ for the following equilibrium may be calculated:

$$Cu(OH)_2(s) + 2H^+ \rightleftarrows Cu^{2+} + 2H_2O \qquad (1)$$

A value of log $*K_{so} = 9.58 \pm 0.12$ ($I = 0.05$) is obtained, which is very close to the 9.60 value that is calculated, for both CuO and $Cu(OH)_2$, from Schindler's formula (*10*) when the influence of the molar surface, and hence the precipitate particle size as a function of pH, is taken into account. At lower pH

0003-2700/79/0351-2148$01.00/0

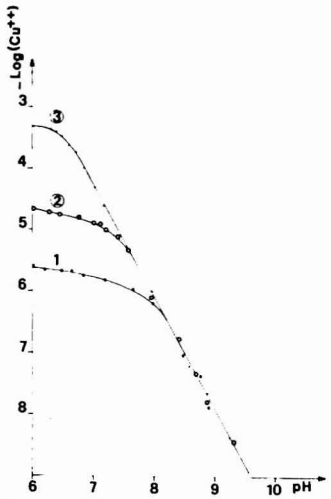

Figure 1. Cupric ion concentration (log) as a pH function (carbonate free solutions). (1) $Cu_T = 1.55 \times 10^{-6}$ M; (2) $Cu_T = 3.88 \times 10^{-5}$ M; (3) $Cu_T = 9.95 \times 10^{-4}$ M

values, where no precipitate is formed, the curves fit the predicted Cu^{2+} concentrations relative to the following acid–base (or hydrolysis) equilibrium:

$$Cu^{2+} + H_2O \rightleftarrows CuOH^+ + H^+ \qquad (2)$$

$$\log {}^*K_1 = -7.52 \ (I = 0.05) \ (9)$$

The influence of the latter equilibrium is strongly evidenced at the lowest total copper concentrations. Figure 1 also shows that the higher the total copper concentration, the lower the pH at which the precipitate disappears.

A complete description of the $Cu(II)/OH^-$ system should include also the second hydrolysis product $Cu(OH)_2(aq)$, but a lack of convincing data on the ${}^*\beta_2$ constant of the following equilibrium:

$$Cu^{2+} + 2H_2O \rightleftarrows Cu(OH)_2(aq) + 2H^+ \qquad (3)$$

makes the problem still open.

In a recent paper Vuceta and Morgan (*11*) suggested, on the basis of potentiometric titrations, a value of $\log {}^*\beta_2 = -13.7$ in agreement with those previously reported by Quintin (*12*) and by Spivakovskii and Makovskaya (*13*) and discarded the hypothesis suggested by Mesmer and Baes (*14*) of $\log {}^*\beta_2 = -17.3$. The measured $[Cu^{2+}]$ as a function of pH suggests a $\log {}^*\beta_2$ value of about −16. This may easily be derived from the displacement of the reported curves in a position intermediate between those theoretically calculated by Vuceta and Morgan (*11*). A more recent work by W. G. Sunda and P. J. Hanson (*15*) suggests a value very close to −16. As the problem of ${}^*\beta_2$ value is not solved, the second hydrolysis product $Cu(OH)_2(aq)$ was not taken into an account. Anyway it seems to add a contribution much lower than could be predicted on the basis of Vuceta and Morgan results.

$Cu(II)/CO_3^{2-}$, HCO_3^- System. The variation of −log $[Cu^{2+}]$ vs. pH is reported in Figures 2 and 3: they show that no relevant difference exists when calcium instead of sodium hydrocarbonate is used.

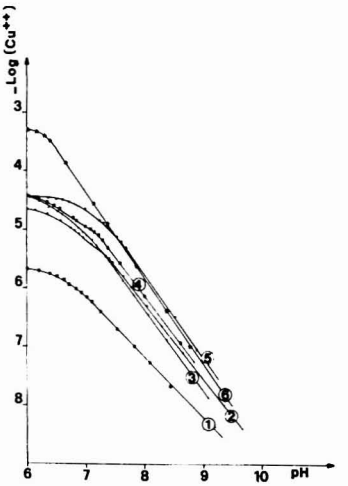

Figure 2. Cupric ion concentration (log) as a pH function in the presence of $NaHCO_3$. (1) $Cu_T = 2.49 \times 10^{-6}$ M, $C_T = 2.63 \times 10^{-3}$ M; (2) $Cu_T = 1.94 \times 10^{-5}$ M, $C_T = 2.63 \times 10^{-3}$ M; (3) $Cu_T = 3.88 \times 10^{-5}$ M, $C_T = 5.25 \times 10^{-3}$ M; (4) $Cu_T = 3.88 \times 10^{-5}$ M, $C_T = 2.60 \times 10^{-3}$ M; (5) $Cu_T = 3.88 \times 10^{-5}$ M, $C_T = 1.10 \times 10^{-3}$ M; (6) $Cu_T = 4.98 \times 10^{-4}$ M, $C_T = 2.60 \times 10^{-3}$ M

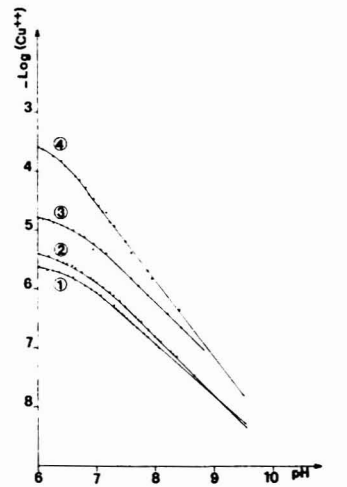

Figure 3. Cupric ion concentration (log) as a pH function in the presence of $Ca(HCO_3)_2$. (1) $Cu_T = 2.62 \times 10^{-6}$ M; (2) $Cu_T = 4.98 \times 10^{-6}$ M; (3) $Cu_T = 1.94 \times 10^{-5}$ M; (4) $Cu_T = 4.98 \times 10^{-4}$ M. $C_T = 1.23 \times 10^{-3}$ M in all samples

Part of the total inorganic carbon is subtracted by the formation of the following calcium species (*1*):

$$Ca^{2+} + CO_3^{2-} \rightleftarrows CaCO_3(aq) \qquad \log K_{eq} = 3.2 \qquad (4)$$

$$Ca^{2+} + H^+ + CO_3^{2-} \rightleftarrows CaHCO_3^+ \qquad 11.6 \qquad (5)$$

The amounts of $CaCO_3(aq)$ and $CaHCO_3^+$ thus formed may be calculated; they were not higher than 1% of the total

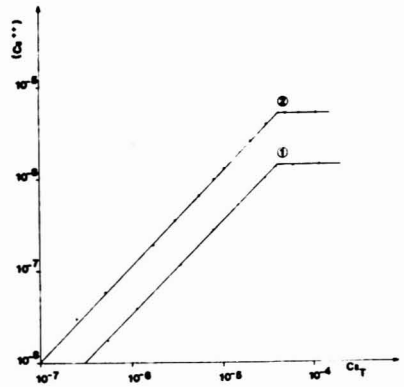

Figure 4. Cupric ion concentration as a function of total added copper concentration—malachite precipitation. (1) $C_T = 2.65 \times 10^{-3}$ M, pH 7.88; (2) $C_T = 2.49 \times 10^{-3}$ M, pH 7.70

calcium and for this reason both equilibria were neglected in this work.

The upper curves, for which $Cu_T \geq 1.94 \times 10^{-5}$ M in Figure 2 and $Cu_T = 4.98 \times 10^{-4}$ M in Figure 3, show, for the straight portion, a −1.5 slope which may be related to the presence of precipitated malachite $Cu_2(OH)_2CO_3$ undergoing the following reaction:

$$^1/_2Cu_2(OH)_2CO_3 + {}^3/_2\,H^+ \rightleftarrows Cu^{2+} + {}^1/_2HCO_3^- + H_2O \quad (6)$$

$$\log {}^*K_{so} = 3.54 \; (I = 0.05) \; (16)$$

For lower total-copper concentration, the curve slope is close to −1, thus indicating that the ion pair $CuCO_3$(aq) is the predominant species; CO_3^{2-} concentration shows in fact a similar pH dependence in the range between the two pK values of the carbonic acid, 6.3 and 10.25. The following equilibrium takes place:

$$Cu^{2+} + CO_3^{2-} \rightleftarrows CuCO_3(aq) \quad (7)$$

$$\log K_1 = 6.04 \; (I = 0.05) \; (9)$$

Equilibrium 7 obviously does not prevent the simultaneous occurrence of equilibrium 2 but the former is certainly predominant owing to the higher equilibrium constant value, not considering any effect due to a favorable ligand concentration; this view is supported by the fact that curve bending is displaced toward lower pH values. For the malachite precipitation equilibrium

$$CuOH(CO_3)_{1/2} \rightleftarrows Cu^{2+} + OH^+ \; 1/2 \; CO_3^{2-} \quad (8)$$

the calculated $-\log K_{so} = 14.42 \pm 0.09$ ($I = 0.05$) is surprisingly lower than 15.94, the corresponding value obtained from Schindler's data (*10*). The measured value was confirmed by checking $[Cu^{2+}]$ and pH on the same malachite saturated solution for 7 days; ageing did not result in any change. The $[Cu^{2+}]$ measurements were repeated in a modified precipitation experiment where copper was added and all other parameters were kept constant: results reported in Figure 4 were consistent with $pK_{so} = 14.42$. Such a remarkable discrepancy cannot be ascribed to a lack of precision in the experimental data, but it may be due to a particle size effect similar to the one already reported for $Cu(OH)_2$ or CuO. According to Hepburn (*17*) the formation of basic cupric carbonate (malachite) is due to an absorption process; to an extent which is a continuous function of both particle size and concentration of CO_2 in solution, the absorbent and the

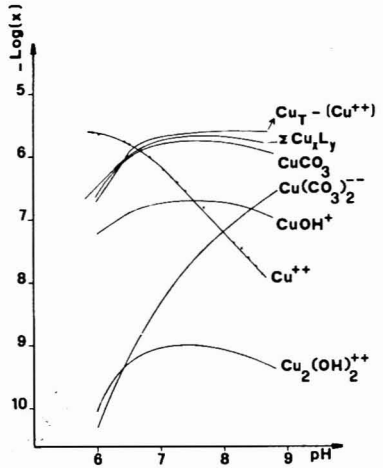

Figure 5. Copper carbonate and hydroxo complex distribution as a pH function. $Cu_T = 2.50 \times 10^{-6}$ M; $C_T = 2.62 \times 10^{-3}$ M ($NaHCO_3$); L = OH^- or CO_3^{2-}; $x = 1$ or 2; $y = 1$ or 2

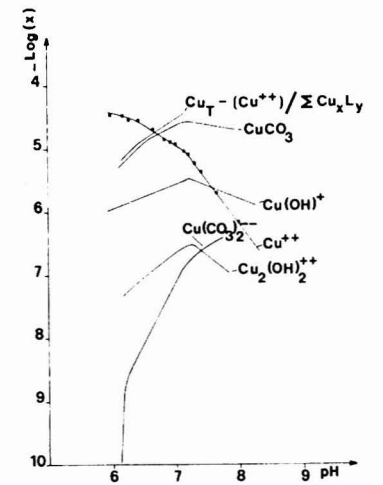

Figure 6. Copper carbonate and hydroxo complex distribution as a pH function. $Cu_T = 3.88 \times 10^{-5}$ M; $C_T = 2.62 \times 10^{-3}$ M ($NaHCO_3$); L = OH^- or CO_3^{2-}; $x = 1$ or 2; $y = 1$ or 2

absorbed materials being, respectively, cupric oxide and un-ionized carbonic acid.

To calculate the distribution of the most probable copper species in fresh waters at carbonate–hydrocarbonate natural levels, the following equilibria, besides equilibria 2 and 7, were considered:

$$2Cu^{2+} + 2H_2O \rightleftarrows Cu_2(OH)_2{}^{2+} + 2H^+ \quad \log K_{eq} \; (I = 0.05) \; (9, 10, 16) \; -10.54 \quad (9)$$

$$Cu^{2+} + 2CO_3^{2-} \rightleftarrows Cu(CO_3)_2{}^{2-} \quad 9.28 \quad (10)$$

To check the reliability of the assumed set of equilibria, the

Table I. Copper Hydroxide and Carbonate Species Distribution in Natural Waters[a]

samples	natural pH	C_T	Cu_T[b]	$[Cu^{2+}]$	$[CuOH^+]$	$[Cu_2(OH)_2^{2+}]$	$[CuCO_3]$	$[Cu(CO_3)_2^{2-}]$
Po A1	7.63	1.71×10^{-3}	4.72×10^{-8}	3.70×10^{-10}	3.79×10^{-10}	4.50×10^{-15}	2.43×10^{-9}	2.53×10^{-11}
Po C1	7.59	1.85×10^{-3}	3.79×10^{-8}	1.00×10^{-11}	9.33×10^{-12}	2.76×10^{-18}	6.38×10^{-11}	6.46×10^{-13}
Po F1	7.86	2.74×10^{-3}	1.39×10^{-7}	3.23×10^{-10}	5.62×10^{-10}	9.95×10^{-15}	5.95×10^{-9}	1.73×10^{-10}
Ticino 2	7.62	2.08×10^{-3}	4.25×10^{-8}	1.80×10^{-9}	1.80×10^{-9}	1.02×10^{-13}	1.40×10^{-8}	1.72×10^{-8}

[a] All concentrations in moles per liter. [b] By atomic absorption including organically bound copper.

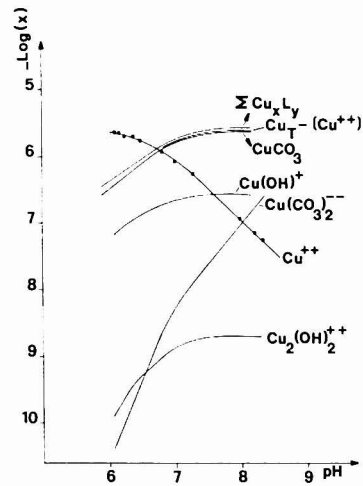

Figure 7. Copper carbonate and hydroxo complex distribution as a pH function. $Cu_T = 2.62\ 10^{-8}$ M; $C_T = 2.47 \times 10^{-3}$ M $[Ca(HCO_3)_2]$; $L = OH^-$ or CO_3^{2-}; $x = 1$ or 2; $y = 1$ or 2

sum of all calculated concentrations is also reported in Figures 5, 6, and 7 for a comparison with the amount directly obtained as $Cu_T - [Cu^{2+}]$ at different pH values. In Figure 6 this comparison is limited to pH 7.2 as malachite precipitation occurs beyond this point. The close similarity of the two curves means that the whole system is sufficiently described by the proposed equilibria. In Figure 5 the discrepancy observed for pH values higher than 7.8 may be due to the fact that the $Cu(OH)_2(aq)$ reaches the highest concentration in this region; even if its contribution could be exactly calculated, this should make available a reliable value for its equilibrium constant $*\beta_2$.

Application to River Samples. Water samples of the Ticino and Po Rivers were collected and immediately filtered through a Millipore HA filter (0.45-μm pore size). The filtered water still contains all colloids holding trace metals and may be fractionated using the ultrafiltration technique. The soluble copper distribution among the most probable hydroxy and carbonate species may however be calculated. It is sufficient to measure the natural pH value, the corresponding free cupric ion concentration, and to calculate the total carbonate carbon concentration C_T from the measured alkalinity. Several examples of these calculations are reported in Table I.

CONCLUSIONS

Though natural surface waters are very complicated systems which cannot be easily simulated, the simplified speciation model described here allows one to obtain useful informations at least for the most commonly soluble inorganic copper species.

Other inorganic ligands such as phosphate and chloride may, in fact, interfere, as suggested by Stiff (4), but because of the low formation constants of the complexes and the relative low concentration of the ligands their contribution may be neglected.

ACKNOWLEDGMENT

The authors are grateful to S. Meloni for valuable discussion concerning this work.

LITERATURE CITED

(1) G. K. Pagenkopf, R. C. Russo, and R. V. Thurston, *J. Fish. Res. Board Can.*, **31**, 462 (1974).
(2) S. Ramamoorty and D. J. Kushner, *J. Fish. Res. Board. Can.*, **32**, 1755 (1975).
(3) Y. K. Chau and K. Lum Shue Chan, *Water Res.*, **8**, 383 (1974).
(4) M. J. Stiff, *Water Res.*, **5**, 585 (1971).
(5) D. Midgley, *Anal. Chim. Acta*, **87**, 7 (1976).
(6) M. J. Smith and S. E. Manahan, *Anal. Chem.*, **45**, 836 (1973).
(7) W. J. Blaedel and D. E. Dinwddie, *Anal. Chem.*, **46**, 873 (1974).
(8) E. H. Hansen, C. G. Lamm, and J. Ruzicka, *Anal. Chim. Acta*, **59**, 403 (1972).
(9) W. Stumm and J. J. Morgan, "Aquatic Chemistry, an Introduction Emphasizing Chemical Equilibria in Natural Waters", Wiley-Interscience, New York, 1970, Chap. 4, 5, and 6, pp 118–299.
(10) P. Schindler, M. Reinert, and H. Gamsjager, *Helv. Chim. Acta*, **51**, 1845 (1968).
(11) J. Vuceta and J. J. Morgan, *Limnol. Oceanogr.*, **22**, 742 (1977).
(12) M. Quintin, *C. R. Hebd. Seances Acad. Sci.*, **204**, 968 (1937).
(13) V. B. Spivakovskii and G. V. Makovskaya, *Russ. J. Inorg. Chem.*, **13**, 815 (1968).
(14) R. E. Mesmer and C. F. Baes Jr., ORNL-NSF-EATC-3 (1974).
(15) W. G. Sunda and P. J. Hanson, "Chemical Modeling in Aqueous Systems: Speciation, Sorption, Solubility, and Kinetics", E. A. Jenne, Ed.; *ACS Symp. Ser.*, **93**, 179.
(16) L. G. Sillen and A. E. Martell, "Stability Constants of Metal-Ion Complexes", *Chem. Soc. Spec. Publ.* No. 17 (1964); No. 25 (1971).
(17) J. R. Irons Hepburn, *J. Chem. Soc.*, 2883 (1927).

RECEIVED for review March 12, 1979. Accepted July 24, 1979. This work was supported by the ENEL (Italian Electrical Energy Agency) which also gave permission for publication.

Quantitative Examination of Thin-Layer Chromatography Plates by Photoacoustic Spectroscopy

S. L. Castleden,* C. M. Elliott, G. F. Kirkbright, and D. E. M. Spillane

Department of Chemistry, Imperial College, London SW7 2AY, U.K.

A technique is described for the nondestructive quantitative determination of materials on thin-layer chromatography plates utilizing photoacoustic spectroscopy with minimal sample preparation and without the need for solvent extraction. Linear calibration is obtained for the determination of fluorescein in the range 0.2–2 μg following development of separated fluorescein spots on silica gel substrates, supported on aluminum and glass plates. A limit of detection of 20 ng of fluorescein in 4.5 mg of silica gel is reported; relative standard deviations on the measurements made were in the range 0.08–0.1.

A number of techniques exist for the quantitative determination of analyte species separated on thin-layer chromatograms (*1*, *2*). These methods may be divided into two distinct types, those which involve measurements being made in situ and techniques by which the material is removed from the TLC plate and then determined by, for example, gas chromatography, UV-visible spectrophotometry, gravimetry, or titrimetry. Difficulties are commonly encountered when either type of technique is used. Deviant spots and the stringent control of conditions required to produce reference standards make in situ densitometric determinations exacting (*3*). Nonquantitative recovery of eluted fractions and the pre-treatment required before measurements can be made complicate further any determinations carried out upon material removed from TLC plates (*1*).

One of the reasons for the current interest in photoacoustic spectrometry (PAS) is the usefulness of the technique for samples, such as opaque or light-scattering solids and turbid liquids, which are difficult to determine satisfactorily using conventional spectrophotometric techniques (*4*, *5*). The light-scattering nature of TLC substrates suggests that PAS might have advantages over other techniques for qualitative and quantitative determinations. Rosencwaig and Hall (*6*) have shown that absorption spectra may be obtained from thin-layer chromatograms and qualitative identification achieved using PAS. This paper reports the application of PAS in the quantitative determination of analyte species on TLC plates with the minimum of sample pre-treatment, excepting that necessary to remove the sample from the plate and place it in the PAS cell.

EXPERIMENTAL

Instrumentation. The double-beam photoacoustic spectrometer used in this study has been described in detail elsewhere (*7*). A pyro-electric detector (Eltec type 404CM, Rofin Ltd., Egham, U.K.) was used in the reference channel of the spectrometer to correct for the variation of the output power of the source with wavelength. The source used was a 300-W compact xenon arc lamp (Varian-Eimac, type VIX-300). The signals from the microphone (Brüel and Kjaer, type 4166), fitted with a type 4169 pre-amplifier, and from the pyro-electric detector were taken to lock-in amplifiers (Model 124A, Princeton Applied Research Corporation; and Model 9502, Brookdeal Electronics Ltd., Bracknell, U.K., respectively). The two outputs from the lock-in amplifiers were taken to a ratiometer (Brookdeal, Model 5047) and the normalized output was displayed on a digital voltmeter or chart recorder.

An aluminum insert was made to fit the sample cell described in earlier work (*7*). The insert was polished and contained a central depression (diameter 10 mm, depth 1 mm), which was used to contain the small samples (ca. 10 mg) scraped from TLC plates. The use of the insert achieved the two objectives of reducing the dead volume of the cell and positioning the sample reproducibly when the sample material available was insufficient to cover the whole of the base of the cell.

Chromatography. Studies were carried out using glass-backed and aluminum foil-backed thin-layer chromatography plates. The aluminum-backed plates (20 cm × 20 cm Silica gel 60 F_{254}, TLC aluminum sheets, Merck type 5554, BDH Chemicals Ltd., Pool, U.K.) were used by cutting out a 20-mm diameter disk containing the analyte spot at its center. The disk was then placed directly into the PAS cell.

The glass-backed plates (20 cm × 20 cm Silica gel 60, Merck type 5721) were used by removing the analyte spot from the developed plate. A circle (diameter 9.5 mm) was marked out containing the analyte spot and the material within this area removed using a vacuum collection device of the type described by Mulhern (*8*). This consisted of a glass probe, containing a sintered disk, attached to a vacuum line. The sample from the TLC plate was collected on the sintered disk and then transferred to the PAS cell. The average weight of sample removed from the plate by this method was 9 mg.

Procedure. Aluminum-backed and glass-backed TLC plates were cleaned by development with ether followed by activation by heating for 2 h in an oven at 120 °C. Solutions of fluorescein were spotted onto the TLC plates using a microsyringe.

Development of the chromatograms was carried out using a solvent mixture containing ethyl acetate (33% v/v) in acetone. After development the chromatograms were allowed to dry in a desiccator.

RESULTS

Figure 1 shows the PAS spectrum obtained for 1 μg of fluorescein developed under the conditions described above on a silica gel TLC plate and the corresponding spectrum for the silica gel substrate. The maximum PAS signal is observed at 447 nm for fluorescein; the signal at 600 nm is the same for both fluorescein and the silica gel blank and the difference in the signal amplitudes at 600 and 447 nm may be employed to determine the mass of fluorescein present in the samples.

A calibration graph for the mass of fluorescein present on disks cut from aluminum-backed TLC plates was prepared by placing on the plate 1-μL aliquots of a series of standard solutions containing fluorescein in the concentration range 0.2 μg μL^{-1} to 2 μg μL^{-1}. The calibration graph was found to be linear over the weight range studied and reproducibility studies yielded a relative standard deviation on each point of 0.1. On cutting an aluminum-backed plate into a series of strips and placing a 1-μL aliquot of one of a series of the standard fluorescein solutions upon each strip, it was found to be possible to obtain a linear calibration graph by developing each strip separately without any precise control of the development time.

A calibration graph for the weight of fluorescein present in scrapings obtained from silica coated glass-backed TLC

0003-2700/79/0351-2152$01.00/0

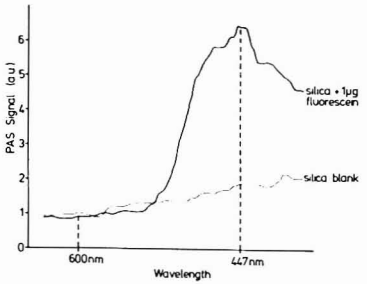

Figure 1. Spectrum of fluorescein on a silica gel-coated aluminum-backed TLC plate

plates was obtained by spotting a 1-μL aliquot of each of a series of standard fluorescein solutions, having concentrations in the range 0.2 $\mu g\ \mu L^{-1}$ to 1.2 $\mu g\ \mu L^{-1}$. Under these conditions the area of the spot obtained on the TLC plate was maintained approximately constant as the mass of fluorescein present was varied. This technique resulted in a linear calibration graph being obtained for weights of fluorescein in the range 0.2 to 1.2 μg. The reproducibility of the results obtained using material removed from glass-backed TLC plates was investigated and the relative standard deviation was found to be 0.08. A limit of detection of 20 ng of fluorescein in a sample of silica gel weighing 4.5 mg was obtained. This result corresponds to a fluorescein concentration in silica gel of 4.4 $\mu g\ g^{-1}$.

DISCUSSION

The relative standard deviations of measurements made in the determination of fluorescein using both glass-backed and aluminum-backed TLC plates have been found to be in the range 0.08–0.1. The majority of the errors incurred in the results appear to be caused by problems in transporting the sample from the TLC plate to the PAS cell. It was found to be difficult to remove a 20-mm diameter disk from aluminum-backed plates without some silica gel becoming detached from the perimeter of the disk. Any exposed aluminum produced in this way was found to have a considerable enhancement effect upon the magnitude of the PAS signal observed.

As a result of some spatial variation in the intensity of the radiation illuminating the sample holder in the PAS cell, the location of the analyte spot on the disk cut from a TLC plate was found to require careful identification and reproducible sample positioning in the cell.

In the case of sample spots being removed from glass-backed TLC plates, difficulty was experienced initially in preventing loss of analyte material during the transfer process involved. This problem became less severe as the experience of the operator increased.

It has been shown that the square root of the area of the sample spot, after development, is a linear function of the logarithm of the weight of the material it contains (*9*). Although this implies that the area of the eluted spot is only a very weak function of the weight of silica present, nevertheless this function was not found to affect the linearity of calibration graphs over the range of weights of fluorescein studied.

The amount of silica gel containing the analyte spot was found to be an important parameter. Importance is, therefore, attached to the thickness of the silica gel coating being uniform over the whole of the plate. An increase in the amount of silica gel transferred with the analyte spot has a dilution effect upon the sample and consequently reduces the magnitude of the PAS signal obtained. All the points on the calibration graphs presented in this paper were obtained from a single TLC plate.

CONCLUSIONS

The technique employed with the glass-backed TLC plates is superior to the use of disks cut from aluminum-backed plates. With a chromatogram containing several different spots, it is unlikely that adjacent analyte spots would be sufficiently well separated to allow a disk to be cut containing only one spot at its center.

The current wavelength range of the PAS system employed is from the UV (250 nm) to the near-IR (2.5 μm). The method described in this paper for the quantitative and nondestructive determination of substrates on thin-layer chromatograms is potentially applicable to the determination of a wide range of analyte species with absorption bands in this range.

The plate-to-plate reproducibility for quantitative measurements is no less than for any densitometric technique and may be overcome simply by adequate standardization. The immunity to interference effects caused by light-scattering solids, such as silica gel, and the capability of the technique for the examination of opaque substrates makes the quantitative study of thin-layer chromatograms a particularly promising application for PAS.

LITERATURE CITED

(1) "Chromatography", 3rd ed., E. Heftmann, Ed., Van Nostrand-Reinhold, New York, 1975, pp 164–186.
(2) "Quantitative Thin Layer Chromatography", J. C. Touchstone, Ed., Wiley Interscience, New York, 1973.
(3) S. Samuels, *J. Chromatogr.*, **1**, 1 (1974).
(4) A. Rosencwaig, *Anal. Chem.*, **47**, 592A (1975).
(5) W. R. Harshbarger and M. B. Robin, *Acc. Chem. Res.*, **6**, 329 (1973).
(6) A. Rosencwaig and S. S. Hall, *Anal. Chem.*, **47**, 548 (1975).
(7) M. J. Adams, B. C. Beadle, and G. F. Kirkbright, *Analyst (London)*, **102**, 569 (1977).
(8) B. M. Mulhern, *J. Chromatogr.*, **34**, 558 (1968).
(9) S. J. Purdy and E. V. Truter, *Analyst (London)*, **87**, 802 (1962).

RECEIVED for review May 7, 1979. Accepted July 23, 1979. We are grateful to the Laboratory of the Government Chemist (Department of Industry) and to EDT Research Limited, U.K., for the provision of studentships for two of us (C.M.E. and D.E.M.S., respectively).

Mass Spectrometric Tracer Pulse Chromatography

J. F. Parcher* and M. I. Selim

Chemistry Department, The University of Mississippi, University, Mississippi 38677

Mass spectrometric tracer pulse (MSTP) chromatography measures vapor–liquid or vapor–solid equilibrium data. The technique is based on normal tracer pulse chromatography, but utilizes stable isotopes and a mass specific detection system. The procedure was used to measure partition isotherms of propane and carbon dioxide in *n*-hexadecane over the range of 25 to 50 °C and 400 to 1200 Torr. The agreement of the MSTP data with the literature data is excellent for the $CO_2/C_{16}H_{34}$ system at all three temperatures. There is a discrepancy in the literature for the $C_3H_8/C_{16}H_{34}$ system. The MSTP data are in excellent agreement with one data set and 3–10% lower than two other compilations.

There is a tremendous need for a fast, accurate technique to measure vapor–liquid or vapor–solid equilibrium data over a wide range of temperature and pressure. The usual vapor pressure or equilibrium still methodology is accurate, but time consuming; and there are few data available at temperatures and pressures other than 25 °C and 1 atmosphere.

The potential applications of gas–liquid and gas–solid chromatography in this area have been recognized for many years, but never fully exploited. Normal elution chromatography, with the solute at infinite dilution, has been used successfully for these measurements, and there are many advantages to this technique. The method, however, is limited to systems which obey Henry's law and to solutes which are significantly retained by the stationary phase. The uncertainty in the determination of the dead time or void volume of the column limits the accuracy of elution data for systems in which the solubility is low, i.e., systems with a Henry's law constant greater than 10^3.

Several methods have been suggested for measuring equilibrium systems chromatographically at finite concentrations, and these methods have been thoroughly reviewed and evaluated (*1–3*). Presently, none of these techniques have been used extensively for several reasons. The theory of mass transport through a fixed bed reactor or column is very complex. The differential equations describing a normal chromatographic column cannot be solved analytically (*4*), and numerical solutions require extensive computer time and facilities. Simplifying assumptions have been used to reduce the mathematical complexity of the problem to reach an analytical solution. These assumptions are often unrealistic, such as zero pressure drop, constant flow rate, or constant gas phase viscosity. This limits the accuracy and applicability of the simpler frontal techniques.

There is yet another chromatographic technique for obtaining finite concentration equilibrium data. This method is tracer pulse chromatography (*5–8*) and is probably the most commonly used type of frontal chromatography (*9–18*). In this technique, the solute vapor is introduced into a packed column as the carrier gas or as a component of the carrier gas at a known partial pressure. The column is saturated with the carrier gas so that a vapor–liquid or vapor–solid equilibrium is established. A small elution sample of a radioactive isotope of the solute vapor can be used as a probe to determine the amount of solute vapor which is absorbed or adsorbed on the liquid or solid stationary phase. The number of moles of solute, n_i, condensed on or in the stationary phase is directly proportional to the corrected retention time, t_{Ri}', of the tagged solute, i (*8*).

$$n_i = Mt_{Ri}' \tag{1}$$

M is the mass flow rate (moles/min) of the solute vapor in the column. This result is obtained with no assumptions concerning the shape of the isotherm, effect of diffusion, constancy of the void volume, or heat of sorption. The one necessary assumption in normal tracer pulse theory is that there is no isotope effect on the equilibrium properties of the system.

Tracer pulse chromatography does not require special chromatographic instrumentation and the method is simple and elegant. The major disadvantage of the method is the necessary detection and handling of radioactive isotopes in the gas phase. The solutes usually contain ^3H or ^{14}C isotopes which must be trapped out of the gas stream. The sample size of the eluted isotopes must be small to avoid perturbation of the equilibrium and these small samples are hard to detect with ionization detectors.

Tracer pulse chromatography does not inherently require the use of radioactive isotopes. Any distinguishable isotope, such as ^{13}C or ^2H, would be satisfactory with the proper detection system. This paper describes the use of stable isotopes and a mass spectrometric detector to extend and improve the capabilities of tracer pulse chromatography.

EXPERIMENTAL

The GC/MS system used for this investigation was a Hewlett-Packard Model 5985A. This is a quadrapole instrument with a high pumping capacity and real-time selected ion monitoring capabilities. The gas chromatograph was modified for variable outlet pressure operation by the addition of a microneedle valve (Scientific Glass Engineering Pty. Ltd. Model MNVU-100) at the outlet. Subatmospheric pressures were obtained by venting the outlet of the valve to vacuum.

The flow sensor on the gas chromatograph was calibrated for each carrier gas over a range of flow rates. The molar flow rate for each experiment was obtained from the sensor output and the calibration factors.

The inert gases were all Linde Research grade and the carrier gases were Linde Instrument grade. The specified minimum purities were 99.99% for carbon dioxide and 99.5% for propane. The stable isotope solutes, 2,2-d_2 propane (98% *D*) and ^{13}C labeled carbon dioxide (90% ^{13}C) were obtained from Merck and Co.

The *n*-hexadecane (Altech Associates) was used as the stationary liquid phase. This was coated on 60/80 mesh Chromosorb-P which had been deactivated with dimethyldichlorosilane (Johns-Manville). The columns were made of 0.25-in. o.d. copper tubing of various lengths from 200 to 350 cm. The liquid loading for the three columns used in this investigation ranged from 24–32%.

The accurate measurement or calculation of the retention time, t_0, of a truely unretained solute is a critical factor in tracer pulse chromatography. The standard use of an air peak or a single inert gas peak is totally inadequate because all of these gases are soluble in hexadecane to some extent at the temperatures and pressures used in this investigation.

Several methods have been proposed for the accurate determination of t_0. All of these methods are based on some form of linearization scheme for an equation of the form

$$\ln (t_{Ri} - t_0) = \alpha + \beta\psi_i \tag{2}$$

0003-2700/79/0351-2154$01.00/0

Table I. Solubility (Mole Fraction) of Propane and Carbon Dioxide in *n*-Hexadecane at One Atmosphere

vapor	temp., °C	this work	King and Al-Najjar (*30*)	Chappelow and Prausnitz (*29*)	Hayduk et al. (*28, 31*)	Lenoir et al. (*32*)
propane	25	0.128	0.139*	0.124* 8.05	0.137	0.135 7.41
	35	0.104	0.114*	0.104* 9.96	0.109	---
	45	0.087	0.095*	0.087* 11.46	0.0896	---
carbon dioxide	25	0.0142	0.142	---	0.0138	0.016 62.5
	40	0.0123	0.0123*	---	0.0121	
	50	0.0114	0.0113	---	0.0113	

* Interpolated from measured values at other temperatures.

α and β are constants and ψ_i represents some extrapolation parameter for solute i.

A flame ionization detector will not respond to an air sample, so chromatographers have developed a method for determining t_0 based on the use of the carbon number of a series of *n*-alkanes (*19–21*) or other homologs (*22*) for ψ_i. This is a popular method, but is not acceptable for solutes with small $t_{Ri} - t_0$ values because Equation 2 is often not valid for the lower members of a homologous series when carbon number is used for the ψ_i parameter. If higher members of a series are used, the procedure involves a long extrapolation and a small uncertainty in the t_{Ri} values causes a large uncertainty in t_0 (*21*).

Other workers have used the inert gas series of solutes and various physical parameters for ψ_i. Heats of adsorption (*23*), polarizability (*13, 16*), the square root of the Lennard-Jones potential (*14*), and the Kirkwood-Muller potential parameter (*17*) have all been used for ψ_i. We found the Kirkwood-Muller potential function (*17*) to give the best straight line fit with nonlinear least squares regression of Equation 2. This technique was used throughout the investigation to determine t_0 based on the retention of neon, argon, krypton, and xenon.

The mass spectrometric detection system has the advantage over ionization chambers or conventional detectors that the chromatograph can be operated at low pressures (*24*) with no deleterious effects on the sensitivity of the detection system. The effect of reduced pressure on the efficiency of the chromatographic column is less certain. Shellier and Guiochon (*25*) concluded that vacuum outlet operation had little or no effect on the plate height. Hatch and Parrish (*24*) showed that under other conditions there is a large effect on the efficiency. In general, atmospheric pressure operation yielded a lower plate height, but the optimum flow rate was always larger for the vacuum conditions.

The effect of column pressure on the solute plate height was not systematically investigated; however, there was no significant loss of efficiency observed at subatmospheric pressures.

The use of a mass specific detection system obviates the assumption that there is no isotope effect on the equilibrium measurements. In our studies, we found that there was no measurable difference in the solubilities of CO_2 and $^{13}CO_2$ in hexadecane. On the other hand, there is a significant difference between the solubility of natural propane and dideuterated propane in hexadecane. The heavier isotope is less soluble by 1–2%. This type and magnitude of an isotope effect has been observed previously (*26, 27*) and must be taken into account for accurate measurements by tracer pulse chromatography.

The relative retention times of eluted samples of natural and isotopic solutes were used as correction factors to determine the retention time of a natural solute from the observed retention time of a isotopic solute.

RESULTS AND DISCUSSION

The experimental isotherms for propane and carbon dioxide in *n*-hexadecane are shown in Figures 1 and 2. Comparison of the experimental data with previous nonchromatographic studies at a single pressure (1 atm) are given in Table I, where the data marked with * are interpolated from measured values at other temperatures. In some cases, the experimental results were presented as Henry's law constants and these values are given in the second row.

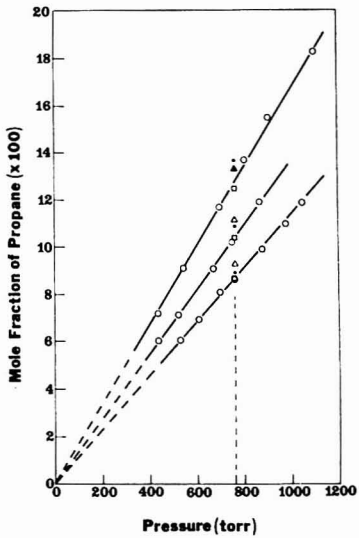

Figure 1. Partition isotherms for propane in *n*-hexadecane at 25, 35, and 45 °C. Literature data at 760 Torr. (*) Hayduk et al. (*28, 31*). (Δ) King and Al-Najjar (*30*). (□) Chappelow and Prausnitz (*29*)

The MSTP data for carbon dioxide agree well with the literature values except for the data of Lenoir et al. (*32*). This measurement was carried out by elution chromatography at the limit of $P = 0$ and the extrapolation to atmospheric pressure may be questionable, although our data over a range of pressure indicate that the Henry's law constant is independent of pressure up to 1200 Torr.

The propane measurements agree with those of Chappelow and Prausnitz (*29*) within 2% but are 3–10% lower than the other literature values (*26, 30–32*).

The data reported here were all measured at a constant molar flow rate with variable inlet and outlet pressures and volume flow rate. Extensive measurements were also carried out with a constant outlet pressure and variable flow rates and inlet pressure. There was no measurable difference in data obtained under these two sets of conditions. The liquid mole fraction of propane was a function of the mean pressure of propane in the column and the temperature, and was independent of flow rate, inlet and outlet pressures, and the amount of hexadecane in the column.

MSTP chromatography can be used to measure solubility data with accuracy comparable to established methods and

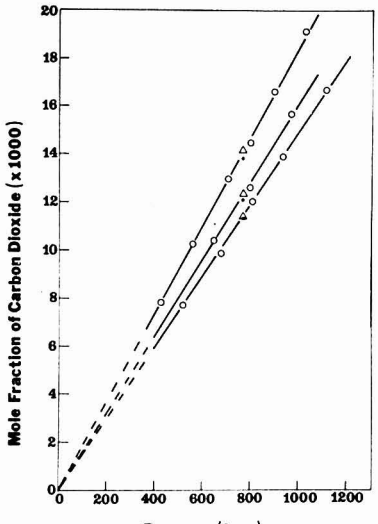

Figure 2. Partition isotherms for carbon dioxide in *n*-hexadecane at 25, 40, and 50 °C. Literature data at 760 Torr is the same as Figure 1

has all the advantages of normal chromatographic techniques, such as speed, simplicity, and wide temperature and pressure ranges.

The use of a mass specific detection system allows the use of nonradioactive isotopes, subatmospheric pressures, and quantitative evaluation of any possible isotope effects.

One of the significant disadvantages of the static volumetric or gravimetric techniques is the excessively long times required to ensure complete equilibration in the system. A commonly quoted figure is 2–4 h (*28*, *29*) and the procedures require extensive degassing of the solvent. In a chromatographic column the solvent is present as a very thin film spread over a large surface area and all of the solvent is continuously in contact with the solute vapor, so the equilibration time is essentially the time required for the solute front to pass through the column. In one experiment, the retention time of a tagged sample of propane was measured at intervals of 10–15 min for the system of propane/hexadecane at 45 °C. The retention time was constant within 2% for the time interval from 5 to 110 min. The required equilibration time varied with flow rate and pressure but was always less than 10 min after the vapor front reached the outlet of the column.

The major disadvantage of the procedure is the requirement of a mass spectrometer as a mass specific detector. This is complex and expensive instrumentation; however, the simplest form of quadrapole mass spectrometer is adequate for this procedure. The experiment does not require modification of the mass spectrometer and can be used on any GC/MS system.

As with any chromatographic technique, the solvents are limited to those with low vapor pressure at the operating temperatures. This is a restriction; however, the technique is applicable to high molecular weight solvents and polymers, and these are precisely the types of systems which are not amenable to other techniques.

The tracer pulse method requires large amounts of vapor for the carrier gas. This can be introduced as the carrier alone or as a component of a mixture of gases. The solute can be used alone as the carrier if the vapor pressure is sufficient at room temperature. The solute vapor can also be introduced by bubbling an inert gas through a saturator containing liquid solute, or the solute can be pumped into the system as a liquid and vaporized ahead of the column.

The equilibrium data obtained by this procedure or any chromatographic method, must be an average value. The inlet of a column must be at a higher pressure than the outlet and the solubility can only be given at the mean column pressure.

Probably the most significant potential for the technique is in the study of multicomponent systems. The mass specific detection system can differentiate components of a mixture even if the chromatographic resolution is inadequate for a separation. Vapor–liquid equilibrium data for multicomponent systems cannot be obtained readily by any other nonchromatographic technique.

LITERATURE CITED

(1) Laub, R. J.; Pecsok, R. J. "Physiochemical Applications of Gas Chromatography", Wiley Interscience: New York, 1978.
(2) Parcher, J. F. In "Advances in Chromatography", Giddings, J. C., et al., Eds.; Marcel Dekker: New York, 1978; Vol. 16, Chapter 5.
(3) Locke, D. C. In "Advances in Chromatography", Giddings, J. C., et al., Eds.; Marcel Dekker: New York, 1976; Vol. 14, Chapter 4.
(4) Parcher, J. F.; Ho, T. H.; Haynes, H. W. *J. Phy. Chem.* **1976**, *80*, 2656–2661.
(5) Helfferich, F.; Peterson, D. L. *Science*. **1963**, *142*, 661–663.
(6) Stalkup, F. I.; Deans, H. A. *AIChE J.* **1963**, *9*, 106–108.
(7) Gilmer, H. B.; Kobayashi, R. *AIChE J.* **1965**, *11*, 702–705.
(8) Peterson, D. L.; Helfferich, F. *J. Phys. Chem.* **1965**, *69*, 1283–1293.
(9) Asano, K.; Nakahara, T.; Kobayashi, R. *J. Chem. Eng. Data* **1971**, *16*, 16–18.
(10) Peterson, D. L.; Helfferich, F.; Carr, R. J. *AIChE J.* **1966**, *12*, 903–905.
(11) Haydel, J. J.; Kobayashi, R. *Ind. Eng. Chem., Fundam.* **1967**, *6*, 546–554.
(12) Masukawa, S.; Kobayashi, R. *J. Chem. Eng. Data*. **1968**, *13*, 197–199.
(13) Masukawa, S.; Kobayashi, R. *J. Gas Chromatogr.* **1968**, *6*, 461–465.
(14) Hori, Y.; Kobayashi, R. *J. Chem. Phys.* **1971**, *54*, 1226–1236.
(15) Khoury, F.; Robinson, D. B. *J. Chromatogr. Sci.* **1972**, *10*, 683–690.
(16) Masukawa, S.; Alyea, J. I.; Kobayashi, R. *J. Gas Chromatogr.*, **1968**, *6*, 266–269.
(17) Nakahara, T.; Chappelear, P. S.; Kobayashi, R. *Ind. Eng. Chem., Fundam.* **1977**, *16*, 220–228.
(18) Everett, A.; Kobayashi, R. *AIChE J.* **1978**, *24*, 745–747.
(19) Guardino, X.; Albaiges, J.; Firpo, G.; Rodriquez-Vinals, R.; Gassiot, M. *J. Chromatogr.* **1978**, *118*, 13–22.
(20) Garcia Dominguex, J. A.; Garcia Munoz, J.; Fernandez Sanchez, E.; Molera, M. J. *J. Chromatogr. Sci.* **1977**, *15*, 520–527.
(21) Haken, J. K.; Wainwright, M. S.; Smith, R. J. *J. Chromatogr.* **1977**, *133*, 1–6.
(22) Ashes, J. R.; Mills, S. C.; Haken, J. K. *J. Chromatogr.* **1978**, *166*, 391–396.
(23) Masukawa, S.; Kobayashi, R. *J. Gas Chromatogr.* **1968**, *6*, 257–265.
(24) Hatch, F. W.; Parrish, M. E. *Anal. Chem.* **1978**, *50*, 1164–1172.
(25) Sellier, N.; Guiochon, G. *J. Chromatogr. Sci.* **1970**, *8*, 147–150.
(26) Bruner, F.; Cartoni, G. P.; Liberti, A. *Anal. Chem.* **1966**, *38*, 298–303.
(27) Cartoni, G. P.; Liberti, A.; Pela, A. *Anal. Chem.* **1967**, *39*, 1618–1622.
(28) Hayduk, W.; Walter, E. B.; Simpson, P. *J. Chem. Eng. Data* **1972**, *17*, 59–61.
(29) Chappelow, C. C.; Prausnitz, J. M. *AIChE J.* **1974**, *20*, 1097–1104.
(30) King, M. B.; Al-Naljar, H. *Chem. Eng. Sci.* **1977**, *32*, 1241–1246.
(31) Hayduk, W.; Castaneda, R. *Can. J. Chem. Eng.* **1973**, *51*, 353–358.
(32) Lenoir, J. R.; Renault, P.; Renon, H. *J. Chem. Eng. Data* **1971**, *16*, 340–342.

RECEIVED for review June 5, 1979. Accepted August 13, 1979. This work was supported by grant number CHE-7809918 from the National Science Foundation.

Effect of Temperature on the Separation of Conformational Isomers of Cyclic Nitrosamines by Thin-Layer Chromatography

Haleem J. Issaq,* Mario M. Mangino, George M. Singer, David J. Wilbur, and Nelson H. Risser

Chemical Carcinogenesis Program, Frederick Cancer Research Center, Frederick, Maryland 21701

The separation of conformational isomers of cyclic nitrosamines which did not separate at room temperature was possible when the thin-layer chromatography (TLC) plate was developed at −77 °C. Effects of temperature and continuous development on the separation and resolution were studied. The results show better separation at lower temperatures and improved resolution with continuous development. NMR spectra of the separated compounds support the TLC data which indicated that the separated compounds are conformational isomers.

Separations by thin-layer chromatography (TLC) are normally carried out at room temperature. However, in certain cases it may be necessary to develop the plate at lower or higher temperatures than room temperature in order to achieve a separation.

It has been shown that lower temperatures affect the separation of compounds by TLC. Abbott et al. (*1*) studied the effect of temperature (+40 °C to −20 °C) on development times and R_f values of 12 chlorinated pesticides. They found that the migration rates of all compounds studied were temperature dependent. Compounds with R_f values above 0.40 at room temperature showed the greatest variation; compounds with R_f values of less than 0.20 showed almost no variation at higher temperatures although their R_f values dropped at −20 °C. Separation was least effective at −20 °C.

Abbott et al. (*1*) and Stahl (*2*) observed that development of the plates at low temperatures was not only faster but also that more compact spots were obtained, which resulted in better resolution. Stahl (*3*) was able to separate a mixture of geranyl acetate, asarone, carotol, and hydroxycaryophyllene at −10 °C, which is otherwise difficult. Henderson and Clayton (*4*) used ultra cold chromatography to separate saturated phosphoglycerides.

Lieberek et al. (*5*) used TLC at 0–2 °C to separate *E* and *Z* isomers of *N*-nitroso-*N*-alkyl-amino acids. They also reported that TLC at 0–2 °C offers a more sensitive method of checking the conformational purity of isomers than does NMR spectroscopy, since small contamination of one by the other can be detected more easily by TLC than by NMR spectroscopy.

In our work it was necessary to develop a method for the separation of conformational isomers of heterocyclic nitrosamines which are in equilibrium at room temperature owing to rotation about the *N*–*N* bond of the nitrosamine function. It seemed likely that if the rate of rotation could be slowed by reducing the temperature, then the difference in polarities of the conformers might allow separation by TLC. This paper describes a cryogenic apparatus used for the separation of conformational isomers at −77 °C. NMR and TLC data show that the separated compounds are conformational isomers. To our knowledge, this is the first instance of a separation of nitrosamine conformers in which the equilibrium is free from the influences of hydrogen bonding (*5, 6*) or steric effects (*7*).

EXPERIMENTAL

Apparatus. Standard glass tanks were used for plate development at room temperature and −5 °C. The cryogenic apparatus (Figure 1) was used for plate development at −77 °C. A viewing cabinet with long (366 nm) and short (254 nm) ultraviolet (UV) lamps (Brinkmann, Westbury, N.Y.) was used to locate the spots on the plate. A Varian XL-100 NMR Spectrometer with a Nicolet TT-100 Fourier transform unit was used for the NMR spectra. Streaks on the plate were made using a De Saga Autoliner (Brinkmann, Westbury, N.Y.).

Reagents. All solvents used were glass-distilled (Burdick and Jackson, Muskegon, Mich.). Deuterated solvents were obtained from Merck & Co., Inc. (Rahway, N.J.). Nitrosamines were synthesized at the Frederick Cancer Research Center. Drummond micropipets were used for spotting the sample solutions on silica gel plates, EM silica gel 60F-254 (Brinkmann, Westbury, N.Y.).

Procedure. Solutions of the nitrosamines (5 mg/mL) were made in ethyl acetate. Plates were spotted (streaked) at room temperature after which they were cooled to the development temperature before they were developed for approximately 12 cm in a saturated tank or cryogenic apparatus (Figure 1) which had been equilibrated at the required temperature. The solvent systems used were diethyl ether or hexane/tetrahydrofuran (3:1).

After development, the plate was taken out and covered with a clear glass plate to shield the sample from UV light. A 1-cm channel at the edge of the plate was left uncovered. The plate was then viewed under short UV and the bands were marked with a pencil. While still wet, the bands were scraped off the plate, one at a time, as fast as possible to avoid plate warmup and transferred to a cold flask which was kept at −77 °C in an acetone–dry ice bath. The flask was capped to prevent acetone contamination. The separated conformers were extracted from the silica gel by adding cold methylene chloride and the flask was shaken for 5 min. After settling for a few minutes, the methylene chloride extract was transferred to test tubes which were kept at −77 °C. The test tubes were evacuated under reduced pressure (0.1–0.005 mm Hg) until the solvents were removed. The residue was then dissolved in cold deuterated chloroform and an NMR spectrum was obtained at −20 °C or −40 °C.

RESULTS AND DISCUSSION

TLC of 1,4-dinitrosopiperazine (DNPZ) and its *cis*-2,6-dimethyl-(2,6-DMDNPZ), *trans*-2,5-dimethyl-(2,5-DMDNPZ), and 2-methyl (2-MDNPZ) derivatives yielded one spot each at room temperature and at −5 °C when spotted on silica gel plates and developed in either diethyl ether or hexane/tetrahydrofuran (3:1). Published NMR data indicate the presence of two isomers for DNPZ (*8*) and 2,6-DMDNPZ (*8*), three isomers for 2,5-DMDNPZ (*8*), and four isomers for 2-MDNPZ (*9*). No separation of the isomers occurred even at −20 °C, so the plates were then continuously developed at −77 °C, obtained by using a dry ice–acetone bath in a cryogenic apparatus developed in our laboratory (Figure 1). The cryogenic apparatus is a closed unit to prevent water from the atmosphere from condensing on the plate, which would make evaporation of the solvent from the plate difficult, and thus interfere with the separation. Initially, the separation of 2,6-DMDNPZ and 2-MDNPZ at −77 °C under continuous development in tetrahydrofuran–hexane (1:3) gave two spots for 2,6-DMDNPZ and three spots for 2-MDNPZ after 2 h. In another experiment, the four compounds 2-MDNPZ, 2,6-

0003-2700/79/0351-2157$01.00/0

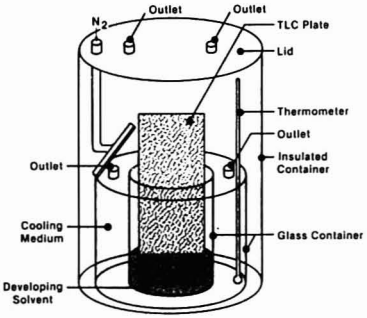

Figure 1. Cold/continuous development apparatus

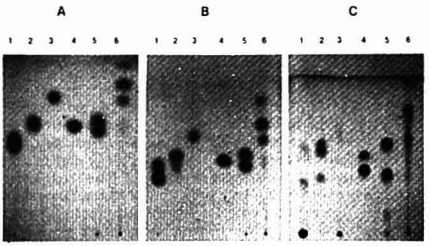

Figure 2. Comparison of the separation of nitrosamines: (1) DNPZ, (2) 2-MDNPZ, (3) 2,5-DMDNPZ, (4) 2,6-DMDNPZ, (5) NMEPO, and (6) 3,5-DMN4P at (A) room temperature, (B) −5 °C, and (C) −77 °C

DMDNPZ, 2,5-DMDNPZ, and DNPZ were each spotted on three plates and the plates were developed once in diethyl ether at room temperature, −5 °C, and −77 °C. Separation of the isomers was achieved only at −77 °C (Figure 2). Continuous development at −77 °C for 2 h improved the resolution. It is apparent, therefore, that continuous development at low temperatures significantly improved the separation of these compounds.

In certain cases it may not be necessary to use low temperatures. For example, *N*-nitroso-3-methyl-4-piperidone (NMEPO) was separated into two spots ($R_f \times 100 = 38$ and 50) when chromatographed on silica gel plates and developed in petroleum ether–ethyl acetate (3:2) at −5 °C. Two experiments were carried out to establish that the two resolved spots are conformational isomers. First, a solution of NMEPO was spotted onto a cold (−5 °C) TLC plate and developed as described above to give two spots (lower temperatures were found to give a better separation). The plate was then left at room temperature for 10 min after which it was cooled in the refrigerator, placed in the cold tank, and developed at 90° to the first development. After development, each spot was resolved into two spots which had the same relative R_f values as initially found. This suggested that the individual conformers re-equilibrated at room temperature to the two conformational isomers. When the solution was spotted and developed in both directions at a cold temperature, only two spots were observed. Proton NMR spectra at −20 °C of the two isolated compounds, eluted off the plate at low temperature (Figure 3), indicated that each spot contained a single isomer of NMEPO and not decomposition products.

Relative intensities of the methyl doublets at $\delta = 1.14$ and 1.22 (Figure 3) clearly show that each sample is 80–90% conformationally pure. Figure 3D indicates that the isomers re-equilibrate at room temperature with a half-life of 20 to

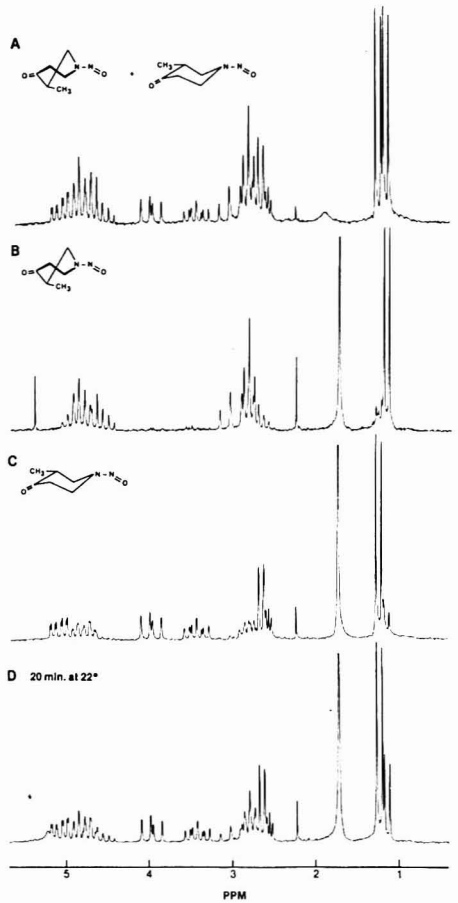

Figure 3. 100-MHz ^{1}H NMR spectra of *N*-nitroso-3 methyl-4-piperidone at −20 °C in $CDCl_3$. (A) Equilibrium mixture of two isomers. (B) Low R_f isomer isolated by cryogenic TLC. (C) High R_f isomer isolated by cryogenic TLC. (D) Same sample as C, after warming to 22 °C for 20 min. Impurity peaks at δ = 1.8, 2.1, and 5.3 are water, acetone, and methylene chloride, respectively

30 min. Each of the samples whose spectra are shown in Figure 3B and 3C gave spectra indistinguishable from Figure 3A when allowed to equilibrate to room temperature for several hours.

The spectrum in Figure 3C indicated that this is the anti-3-equatorial-methyl isomer in a fairly normal chair conformation. The resonances of the α protons can be separated into four distinct multiplets, centered at $\delta = 3.4$, 3.9, 4.8, and 5.1. On the basis of the relative chemical shifts of α protons in other cyclic nitrosamines (*10*), we assigned the multiplet at $\delta = 4$ to an axial proton, anti to the nitroso. This proton is clearly coupled to only two other protons, with coupling constants of 13.3 and 10.6 Hz, which are typical values for germinal and axial–axial coupling constants, respectively (*11*). This proton must, therefore, be adjacent to the proton bearing the methyl group, and the methyl must

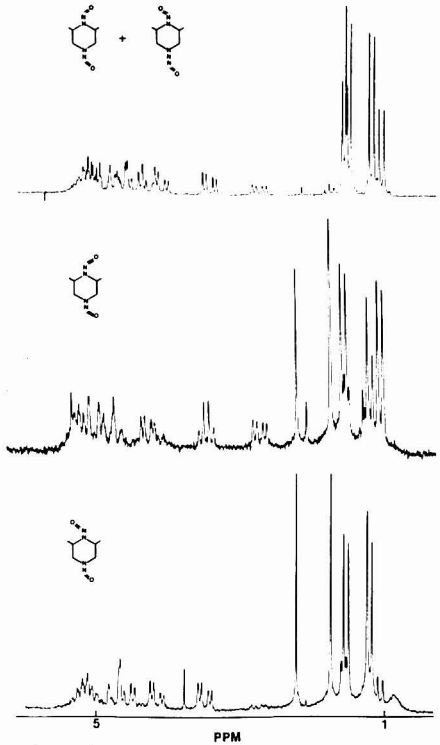

Figure 4. 100-MHz ^{1}H NMR spectra of dinitroso-2,6-dimethylpiperazine. (A) Equilibrium mixture at 25° C. (B) High R_f isomer at −40 °C, isolated by cryogenic TLC. Impurity peaks are acetone at δ = 2.1, water δ = 1.8, and diethyl ether (developing solvent) at δ = 3.4 and 1.2. (C) Low R_f isomer at −40 °C, isolated by cryogenic TLC. Impurity peaks are acetone at δ = 2.1 and water at δ = 1.8

be equatorial. The spectrum, Figure 3B, is not so readily analyzed, but we believe that the nitroso group is anti to the nitroso with the ring in a flexible twist conformation. A full discussion of the spectra and factors causing the increased barriers to ring inversion as well as nitroso group rotation will be published separately.

For the four piperazines, DNPZ, 2-MDNPZ, 2,5-DMDNPZ, and 2,6-DMDNPZ which were separated at −77 °C, TLC indicated that the component conformers re-equilibrated at room temperature. When the plate was turned 90° and developed again, each spot separated into the same number of spots as obtained in the first development. Figure 4 shows the proton NMR spectra of the two isomers of 2,6-DMDNPZ along with a spectrum of the equilibrium mixture. The four methyl doublets in the region δ = 1.0–1.6 show that good separation of the isomers was achieved at −77 °C, although some diethyl ether, used as developing solvent, remained in one of the samples (Figure 4B). The chemical shifts of the methyl signals indicated that the isomer with high R_f (Figure 4B) has the two nitroso groups cis to each other (*10*), while the bottom spot (Figure 4C) has the two nitroso groups trans to each other (*8*).

When the separated isomers were warmed up to −16 °C for 20 min, the proton NMR spectrum showed that the isomers had nearly equilibrated.

It is apparent from the above results that cryogenic TLC is a practical way to separate cyclic nitroso conformational isomers. Better resolution is achieved when cryogenic/continuous development is used. Combination of cryogenic TLC and NMR spectroscopy would make possible kinetic studies of nitroso group rotations in cyclic nitrosamines.

LITERATURE CITED

(1) D. C. Abbott, H. Egan, and J. Thomson, *J. Chromatogr.*, **16**, 481 (1964).
(2) E. Stahl, *Angew. Chem. Int. Ed. Engl.*, **3**, 784 (1964).
(3) E. Stahl, *Arch. Pharmaz.*, (*Weinheim, Ger.*), **297**, 500 (1964).
(4) R. F. Henderson and M. H. Clayton, *Anal. Biochem.*, **70** 440 (1976).
(5) B. Liberek, J. Augustyniak, J. Clarkowski, K. Plucinska, and K. Stachowiak, *J. Chromatogr.*, **95**, 223 (1974).
(6) W. T. Iwaoka, T. Hansen, S. T. Hsieh, and M. C. Archer, *J. Chromatogr.*, **103**, 349 (1975).
(7) A. Manschrak, H. Munch, and A. Mattus, *Angew. Chem.*, **78**, 751 (1966).
(8) D. Hofner, D. S. Stephenson, and G. Birnsch, *J. Magn. Reson.*, **32**, 131 (1978).
(9) G. Singer, unpublished results.
(10) Y. L. Chow and C. J. Colon, *Can. J. Chem.*, **46**, 2827 (1968).
(11) L. M. Jackson, and S. Sternhell, "Applications of Nuclear Magnetic Resonance Spectroscopy to Organic Chemistry", Pergamon Press, Elmsford, N.Y., 1969.

RECEIVED for review July 9, 1979. Accepted August 17, 1979. Presented in part at the 30th Pittsburgh Conference on Analytical Chemistry and Applied Spectroscopy, Cleveland, Ohio, 1979. This work was supported by Contract N01-CO-75380 with the National Cancer Institute, NIH, Bethesda, Md. 20205.

Thin Layer Chromatographic Separation of Pesticides, Decachlorobiphenyl, and Nucleosides with Micellar Solutions

Daniel W. Armstrong* and Robert Q. Terrill

Department of Chemistry, Bowdoin College, Brunswick, Maine 04011

The use of micellar solutions as mobile phases in thin layer chromatography (TLC) is described for the first time. The possible advantages of micellar solutions over traditional pure and mixed solvent systems are described. *p,p'*-DDT; *p,p'*-DDD; *p,p'*DDE and decachlorobiphenyl were chromatographed using aqueous solutions of sodium dodecyl sulfate (SDS) with polyamide and alumina thin layer sheets. A reversed micellar solution was shown to separate the nucleosides adenosine, cytidine, guanosine, and uridine using a reversed phase TLC sheet. Possible mechanisms to account for the observed chromatographic behavior are discussed.

In liquid chromatography, one attempts to choose a solid or liquid stationary phase and a liquid mobile phase that will produce the optimum separation of the substances being analyzed. If a chromatographic separation is not satisfactory (even after adjusting physical parameters), one must either change the stationary phase or utilize a solvent system (for the mobile phase) that has a more appropriate polarity. In this paper we introduce a new type of mobile phase, that of solutions of surfactant aggregates or micelles. The highly selective partitioning of many solutes to micelles cannot be duplicated by any pure or mixed solvent system (*1–4*). The fact that aqueous micellar systems can mimic certain properties of organic solvents (i.e., solubilizing nonpolar solutes) could, in some cases, eliminate the need to use potentially harmful or toxic solvents (benzene for example). In addition, micellar solutions are very inexpensive. To change the "apparent polarity" of a micellar mobile phase, one simply alters the concentration of surfactant in solution.

This first in a series of studies reports the use of surfactant solutions in thin layer chromatography. The pesticides 1,1-bis(*p*-chlorophenyl)-2,2,2-trichloroethane (*p,p'*-DDT), 2,2-bis(*p*-chlorophenyl)-1,1-dichloroethane (*p,p'*-DDD), 2,2-bis(*p*-chlorophenyl)-1,1-dichloroethylene (*p,p'*-DDE), and the pollutant decachlorobiphenyl (DCB) were separated on silica gel, alumina, and polyamide thin layer sheets. The effects of different surfactants and surfactant concentration on the separations are analyzed. Reversed micelles (surfactant aggregates in nonpolar organic solvents) were used in a *reverse phase* chromatographic separation of the nucleosides: adenosine, guanosine, cytidine, and uridine. We have previously reported a transfer RNA purification using aqueous micellar solutions and gel filtration chromatography (*5*).

To understand some of the advantages of using surfactant solutions as the mobile phase in liquid chromatography, it is necessary to understand some of the pertinent physical and chemical properties of micelles. Micelles are spherical or possibly ellipsoidal association colloids that form when the critical micelle concentration (CMC) of any given surfactant is exceeded. Micelles are not static species. The monomers which compose the micelle (about 25–160 monomers/micelle) are in dynamic equilibrium with a smaller number of "free" monomers in solution. A solute can partition to an aqueous micelle generally in one of three ways. (a) *Via Electrostatic Interactions*: Micelles composed of ionic surfactants have a fraction of charge on their surface (i.e., Stern Layer). Thus micelles composed of anionic surfactants have a negative fraction of charge and tend to attract positively charged substances to its surface. Conversely, micelles composed of cationic surfactants would tend to attract negatively charged substances. (b) *Hydrophobic Interactions*: Nonpolar substances that often have low or negligible solubility in water easily partition to the hydrophobic core of the aqueous micelle. (c) *Via Electrostatic and Hydrophobic Interactions*: Amphiphilic substances such as amino acids or other surfactants would partition to the micelle so that the polar portion of the substance is in proximity to the hydrophylic surface and the hydrophobic portion of the solute is directed toward the core of the micelle.

Surfactant aggregates in nonpolar organic solvents are often referred to as reversed micelles. It should be understood, however, that the aggregational behavior and thermodynamics of formation of reversed micelles are not analogous to those of aqueous micelles (*6*). In reversed micelles, the hydrophilic head groups are located in the core of the aggregate and the hydrophobic tails are directed outward in contact with the organic solvent (*1, 6*). One can solubilize appreciable quantities of water in the core of a reversed micelle. In general, the greater the amount of water present, the larger the reversed micelle. Hydrophilic substances would tend to partition to the aqueous core of a reversed micelle. Thus solutions of reversed micelles can be used to great advantage in reverse phase chromatography. As will be demonstrated, varying the water content of a reversed micelle can alter the partitioning of a substance to it.

If desired, partition coefficients of substances to micelles can be measured in a variety of ways (*1, 3, 4*). It should be noted that the use of micelles in chromatographic separations is only one of a number of uses of micelles in analytical chemistry. Many innovative investigators are now using the unique properties of micelles in a wide variety of techniques (*7–10*).

EXPERIMENTAL

Materials. Gold label 99+% pure *p,p'*-DDT; *p,p'*-DDD; *p,p'*-DDE and decachlorobiphenyl were obtained from Aldrich Chemical Co., as was sodium dioctylsulfosuccinate and cetyltrimethylammonium bromide (CTAB). These reagents were used without further purification. Adenosine, cytidine, guanosine, uridine, and sodium dodecylsulfate (SDS) were obtained from Sigma Chemical Co. and analyzed for impurities as previously described (*3*). Igepal CO-710 (a nonionic surfactant) was obtained from GAF Corporation and used as received. Silica gel 60 F_{254}, aluminum oxide F_{254} and silanized silica gel 60 F_{254} thin layer sheets were obtained from VWR Scientific Co. Polyamide-6 UV_{254} thin layer sheets were obtained from Brinkmann Instruments, Inc. Distilled water and/or spectral grade cyclohexane were used to make the stock surfactant solutions.

Methods. The following solutions of surfactant were made and utilized as the mobile phase in the appropriate TLC: 1.0×10^{-1}, 2.0×10^{-1}, 3.0×10^{-1}, and 4.0×10^{-1} M aqueous solutions of SDS were used for TLC on silica gel, alumina, and polyamide sheets; 5.0×10^{-2}, 6.0×10^{-2}, 7.0×10^{-2}, 8.0×10^{-2}, 9.0×10^{-2}, and

0003-2700/79/0351-2160$01.00/0

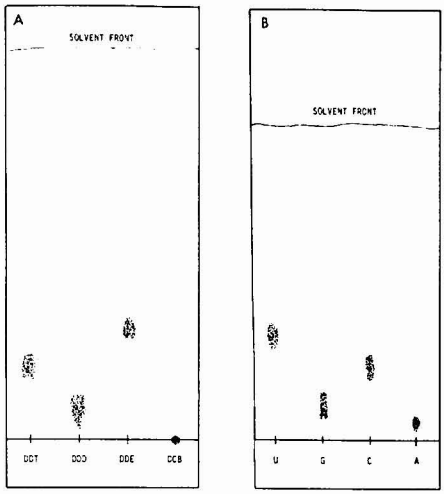

Figure 1. Tracing of developed chromatograms. Chromatogram A consists of a polyamide stationary phase developed with a 4.0×10^{-1} M SDS_{aq} solution. Chromatogram B shows the separation of uridine (U), guanosine (G), cytidine (C), and adenosine (A) using reverse phase TLC. The mobile phase consisted of 1.5 M sodium dioctylsulfosuccinate and 4.44 M H_2O in cyclohexane

1×10^{-1} M aqueous solutions of CTAB were used for TLC on silica gel, alumina, and polyamide sheets; 0.68, 2.00, 5.00, 10.00, and 20.00% aqueous solutions of Igepal CO-710 were used for TLC on silica gel, alumina, and polyamide sheets. For reverse phase chromatography (on silanized silica gel sheets), various amounts of water were solubilized in cyclohexane containing 1.5 M sodium dioctylsulfosuccinate. Solutions were made containing 0.0, 0.11, 0.56, 1.11, 2.22, 3.33, 4.44, 5.56, and 11.11 M H_2O. All ascending TLC were run in air tight containers. The size of all TLC sheets was 8 × 20 cm. All reported R_f values are an average of four identical runs. Development times were 2 to 3 h when using aqueous micellar solutions. All spots were detected by illuminating the chromatograms with a 254_{max} nm mineral light. The spots were carefully outlined and shaded. Typical chromatograms are shown in Figure 1. It should be noted that sodium dodecyl sulfate from different companies can give solutions that produce different R_f values. For example, solutions of SDS from Bio-Rad Laboratories gave higher R_f values for the pesticides than did analogous solutions of SDS obtained from the Sigma Chemical Co. Consequently, one must be careful to indicate the source of ones surfactant and/or indicate in detail the purification procedure, many of which have been published (*1*).

RESULTS AND DISCUSSION

Aqueous solutions of SDS and CTAB proved to be effective mobile phases when chromatographing the hydrophobic pesticides on polyamide and alumina thin layer sheets. These compounds moved as distinct spots and their R_f values were dependent on the concentration of surfactant used. Generally speaking, the greater the concentration of surfactant, the greater the R_f value. Aqueous solutions of the nonionic surfactant were ineffective in TLC regardless of the type of stationary phase used. This was because all species tended to smear along the length of the chromatogram rather than move as discrete spots. Silica gel stationary phases were also of little use in micellar chromatography as they tended to bind the pesticides too strongly.

Figure 2, a–d, illustrates how a change in surfactant concentration affects the R_f of various chlorinated hydrocarbon pollutants. In all cases the change in R_f is a linear function of surfactant concentration. Using these plots, one can determine the optimum surfactant concentration to achieve separation. As will be shown in a separate paper, one can also determine the partition coefficient of solutes to micelles using analogous plots. Optimum separation generally, but not always, occurs at higher surfactant concentration. There is an upper limit to the concentration of surfactant one can use.

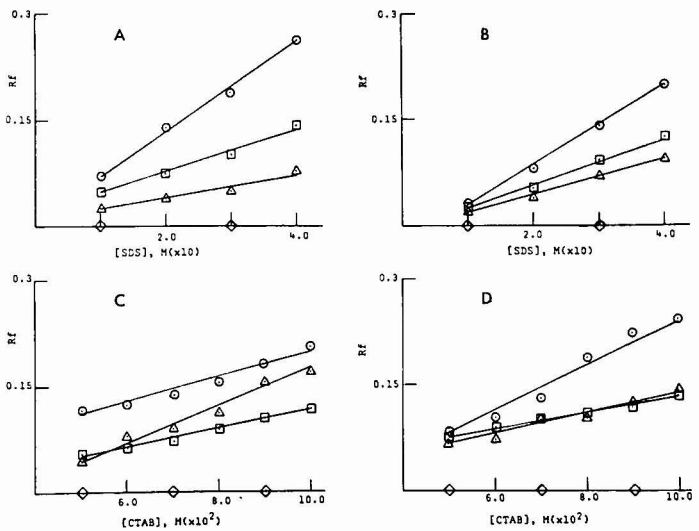

Figure 2. Plots of R_f value vs. surfactant concentration for DDE (⊙), DDT (⊡), DDD (△), and DCB (♦). In A, the stationary phase is polyamide and the surfactant is SDS. In B, the stationary phase is alumina and the surfactant is SDS. In C, the stationary phase is polyamide and the surfactant is CTAB. In D, the stationary phase is alumina and the surfactant is CTAB

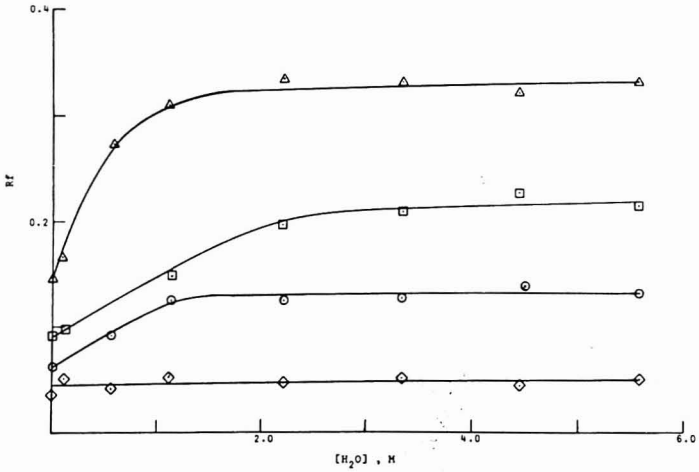

Figure 3. A plot of R_f value vs. concentration of water (in the sodium dioctylsulfosuccinate reversed micelle) for uridine (△), cytidine (□), guanosine (○), and adenosine (◇)

Above 0.6 M SDS and 0.2 M CTAB, the surfactant solutions are too viscous to be used for TLC. It is interesting to note that the order of R_f values (using polyamide as the stationary phase) of the pesticides is different depending on which surfactant is used. For CTAB solutions, relative R_f's are: *p,p'*-DDE > *p,p'*-DDD > *p,p'*-DDT; while for SDS solutions; *p,p'*-DDE > *p,p'*-DDT > *p,p'*-DDD. This indicates that there are electrostatic interactions that must be taken into consideration, in addition to the hydrophobic interactions, between the pesticides and the micelle. In all cases the DCB did not move from the origin; thus it is easily separated from the chlorinated pesticides.

Reversed micellar solutions (of sodium dioctylsulfosuccinate) effectively separate nucleosides using reverse phase chromatography. In this technique the substances being chromatographed partition to the hydrophilic core of the reversed micelle. By altering the amount of water in the hydrophilic core of the micelle one can alter the nature of the mobile phase and thereby the R_f of a substance. Figure 3 illustrates this behavior for three of the four nucleosides. Adenosine, oddly enough, is not affected by the amount of water in the core of the reversed micelle. The R_f of the other nucleosides tends to increase with increasing water concentration up to a point after which there is no further change in R_f. It should be noted that the nucleosides showed absolutely no movement when neat cyclohexane was used as the mobile phase. Thus the reversed micelle (and the water therein) is solely responsible for the movement of these substances.

The fact that the adenosine R_f value is independent of the water content of the reversed micelle indicates that partitioning may largely be due to an electrostatic interaction between the charged head groups of the surfactant and the nucleoside. Electrostatic interactions of this type have previously been shown to occur through the nucleoside base (*3*). The behavior of cytidine, guanosine, and uridine was somewhat analogous. The fact that these nucleosides move at zero concentration of water in the reversed micelle, indicates that there is an electrostatic interaction between the polar head groups of the reversed micelle and these nucleosides (similar to that of adenosine). However, the increasing R_f values with increasing water content of the reversed micelle indicates that the ability to become solubilized in the "water pool" is a more important factor for cytidine, guanosine, and uridine. The leveling off of the R_f values at higher water concentrations is very interesting. Although the exact reason for this behavior is not known, we offer one possible explanation. As one gradually adds water to the reversed micellar mobile phase, a point will eventually be reached where the concentration of water is very large compared to the concentration of the solute one is chromatographing. At this point the solute will move along the chromatogram as if the mobile phase were pure water. In other words, if it were possible to run the reverse phase chromatography with water as the mobile phase (which cannot be done since >20% H_2O destroys the chromatograms), one would obtain R_f values close to those indicated by the horizontal lines in Figures 1b, c, and d. Since the R_f values of cytidine, guanosine, and uridine have reached this maximum value by the time the water concentration is ~2.0 M, increasing the concentration of water still further would not be expected to produce any significant change. At very high water concentration (>6.0 M) the R_f values of the nucleosides will begin to decrease. This is probably due to physical factors such as very high solution viscosity and/or possible microemulsion formation. Except at very low water concentrations where some smearing occurs, the nucleosides moved as distinct spots using the reversed micellar mobile phase.

CONCLUSIONS

For normal phase TLC (using aqueous micellar solutions), it was found that SDS was the best surfactant as solutions of nonionic surfactant produced smears rather than spots. CTAB, while satisfactory, appeared to bind somewhat to the stationary phases. Polyamide stationary phases produced the best separations when using aqueous micellar mobile phases. Silica gel was virtually useless as a stationary phase while alumina was somewhat less satisfactory than polyamide.

In reverse phase TLC (using a reversed micellar solution as mobile phase), the optimum separations were achieved when 2.0 to 4.0 M water was solubilized in the hydrophilic core of the aggregate. Partitioning of substances to the reversed micelle involved both electrostatic interactions with the polar head groups of the surfactant and solubilization by

the "water pool" in the hydrophylic core.

LITERATURE CITED

(1) Fendler, J. H.; Fendler, E. J., "Catalysis in Micellar and Macromolecular Systems"; Academic Press: New York, 1975.
(2) Cordes, E. H.; Gitler, C. *Prog. Bioorg. Chem.* **1973**, *2*, 1–53.
(3) Nagyvary, J.; Harvey J.; Nome, F.; Armstrong, D.; Fendler, J. H. *Precambrian Res.* **1976**, *3*, 509–516.
(4) Armstrong, D. W.; Sequin, R.; Fendler, J. H. *J. Mol. Evol.* **1977**, *10*, 241–250.
(5) Armstrong, D. W.; Fendler, J. H. *Biochim. Biophys. Acta* **1977**, *478*, 75–80.
(6) Fendler, J. H., *Acc. Chem. Res.* **1976**, *9*, 153–165.
(7) Hinze, W. L. "Colloid and Interface Science", Kerker, M., Ed.; Academic Press: New York, 1976; Vol., p 425.
(8) Spurlin, S.; Hinze, W. L.; Armstrong, D. W. *Anal. Lett.* **1977**, *10* (12), 997–1008.
(9) Chang, S.; Spurlin, S.; Hinze, W. L. *Sci Ciencia* **1976**, *6* (1), 54–56.
(10) Hinze, W. L. "Solution Chemistry of Surfactants", Mittal, K. L., Ed.; Plenum Press: New York, 1979; Vol. 1, p 79.

RECEIVED for review June 21, 1979. Accepted August 27, 1979. This work was supported by a grant from the Research Corporation.

N,N'-Bis(*p*-phenylbenzylidene)-α,α'-bi-*p*-toluidine as Stationary Phase in a Packed and in a Micropacked Column

F. Janssen

Chemistry Department, KEMA Laboratories, Utrechtseweg 310, Arnhem, The Netherlands

The chromatographic behavior of a synthetic mixture of polycyclic aromatic hydrocarbons (PAH) was studied on two columns: a packed column (1.80 m, 2-mm i.d., 6-mm o.d., glass) and a micropacked column (3.00 m, 0.6-mm i.d., 2-mm o.d., glass). The columns were packed with 2.8% (w/w) *N,N'*-bis(*p*-phenylbenzylidene)-α,α'-bi-*p*-toluidine (BPhBT) on Chromosorb WHP 80–100 mesh. BPhBT was chosen in this study as stationary phase because of its low bleed level, high efficiency, and its excellent properties in the resolution of PAH. The measurements were carried out with a GC-MS system of Varian Mat. Scanning electron microscopy and thermal analyses (DSC and TG) were applied to study the behavior of BPhBT during thermal treatment and before and after the use in the gas chromatograph. The highest separation power for the BPhBT as stationary phase was achieved at a column temperature of 275–280 °C.

In environmental studies, there is a growing interest in the determination of polycyclic aromatic hydrocarbons (PAH). These compounds, a number of which have mutagenic and carcinogenic activities (*1–19*), occur in dusts from highways and urban centers, light fuel oils, in the emissions from paraffin domestic heaters and flue gases, tobacco smoke, smoke-dried food, etc.

Their formation can be ascribed to the combustion of fossil fuels such as oil and coal. Because of the dangers they present, it is necessary to analyze environmental samples qualitatively and quantitatively. Many investigations of environmental and artificial blends of PAH have been carried out on gas chromatographs equipped with a flame-ionization detector (*2–6, 8–17*). The most suitable feature for this analytical purpose, however, is the combination of gas chromatograph/mass spectrometer (*7, 9, 16–18, 20–27*).

The interface of the gas chromatograph mass spectrometer is the jet separator (*21, 24*), but also the direct coupling is employed in the case of capillary columns (*17, 26, 27*). In addition to the GC-MS measurements used, high-resolution low-voltage mass spectrometry has been applied (*19, 20*). Various workers have investigated the separation of the PAH isomers on packed (*2–16*) and capillary columns (*16–27*). As liquid phase OV-101 (*2, 4, 8, 16, 24*), OV-17 (*5*), OV-7 (*14, 21*), OV-1 (*26*), SE-52 (*5, 13, 17, 22, 25*), SE-30 (*18*), BBBT (*3, 4, 10*), BPhBt and BHxBT (*9, 12*), BMBT (*11*), and Dexsil 300 (*5, 20, 23, 27*) are used. With a number of these phases, it is possible to separate extremely complex environmental mixtures. Nevertheless, with the apolar phases, base-line separation of PAH with the same molecular weight cannot be achieved. If there is any separation at all, for instance on the polysiloxanes, than the sequence of eluation in case of the $C_{20}H_{12}$ molecules is 1,2-benzopyrene, 3,4-benzoperylene, and perylene. In case of capillary columns, this sequence changes in, on, i.e., the phase SE-52, 3,4-benzopyrene, 1,2-benzopyrene, and perylene. The shape and the size of a molecule is probably a decisive factor.

Investigation of nematic liquid crystals as stationary polar phases in packed, columns, fully explained by Janini and other workers (*3, 4, 9–12*), showed the sequence of 3,4-benzopyrene, perylene, and 1,2-benzopyrene. The cause of this effect is probably the influence of the size of the molecules whereby the role of the support in case of packed columns is not unimportant. Also other aspects contribute to it like the symmetry, the charge distribution and deformation of the π-systems of the polycyclic aromatic hydrocarbon molecules, and interaction between the different compounds during the separation of mixtures.

This paper describes the gas chromatographic behavior of polycyclic aromatic compounds on two columns; one packed and one micropacked (*28, 29*). The micropacked column combines to a certain extent the advantages of packed and open tubular columns. The micropacked column is compatible with the GC-MS combination, because it yields high efficiency, high column capacity, and high column loading. It functions with low flow rates and possesses low bleeding characteristics in comparison with packed columns.

EXPERIMENTAL

Materials. The liquid crystal BPhBT was prepared as described by Janini et al. (9) with a 90% yield and was recrystallized five times from boiling ethanol. The starting reagents: α,α'-bi-*p*-toluidine (Eastman Kodak) and *p*-phenylbenzaldehyde (Aldrich) were purified by recrystallization from a water–ethanol solution. The reagents as well as the end product were submitted in our laboratories to infrared spectroscopy (Perkin-Elmer model 183) and solid probe mass spectrometry (Varian Mat 112) to check

0003-2700/79/0351-2163$01.00/0

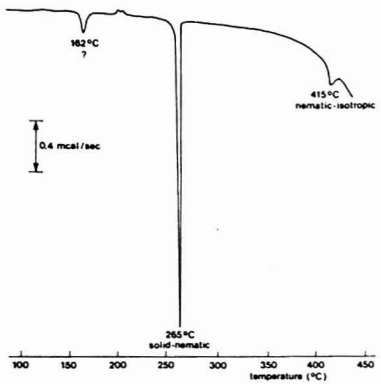

Figure 1. DSC scan of BPhBT, scan rate 10 °C/min, helium flow rate 50 mL/min

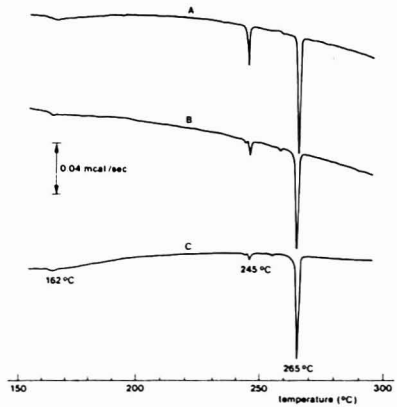

Figure 2. DSC scans of BPhBT on Chromosorb WHP of one sample

the purity and structure of the compounds.

Standard polycyclic aromatic hydrocarbons, purchased from Fluka, ICN, and Merck, were used without further purification and were dissolved in glass distilled benzene. The sample bottles were wrapped up in aluminum foil, to prevent photolysis. The compound 3,4-benzopyrene contained 11,12-benzofluoranthene and 1,2-benzopyrene.

Columns. Two types of glass columns were employed in this study; a packed column (1.80 m, 2-mm i.d., 6-mm o.d.) and a high-performance micropacked column (3 m, 0.6-mm i.d., 2-mm o.d.). The packing 2.3% BPhBT 80–100 mesh Chromosorb WHP was prepared from a solution of BPhBT in benzene (solubility 0.15 g per 100 mL. boiling benzene). This solution was contacted with Chromosorb WHP (conditioned at 500 °C for 5 h) into a rotary evaporator and the solvent slowly evaporated. The amount of stationary phase was measured by thermogravimetry before and after the use in the column.

The packing was resieved to 80–100 mesh and placed in the column. The columns were previously silanized by HMDS (hexamethyldisilazane) in benzene (10% solution) followed by drying with high-purity nitrogen. A 1–2 cm plug of 5% SE-30 on Chromosorb WHP was packed on both sides of the column to retard deterioration and to protect the column during storage. The coating efficiency of the phase was checked by thermogravimetry (DuPont) before and after the measurements in the gas chromatograph. The phase transitions and thermostability were measured by differential scanning calorimetry (DuPont).

Scanning electron microscopy (Jeol JSM 35) was applied to study the coating of the liquid crystal BPhBT on the solid support Chromosorb WHP.

The packed column was installed via Vespel ferrules and the micropacked column via low dead volume connections with graphite ferrules.

The columns were conditioned overnight, 10 °C above the operating temperature.

Apparatus. The measurements were performed on a Varian 1440 gas chromatograph coupled via a slit separator (Brunee) and glass-lined tubing with a Varian Mat 112 mass-spectrometer equipped with two turbo molecular pumps (200 L/s).

The temperature settings of the injector, slit separator, the tubing and the ion source were 250, 300, 350, and 300 °C, respectively; the temperatures were those on the instrument dials. Ultra-high purity helium was used as carrier gas. The flow was regulated by a calibrated constant flow controller (Porter, Hatfield).

The micro-packed column was used in the splitless injection mode. Injections were made with the aid of an all-glass solid injector (moving needle).

All the glass-ware, used in this investigation, such as columns, 10-μL syringes, and sample bottles were silanized by a 10% HMDS solution in benzene.

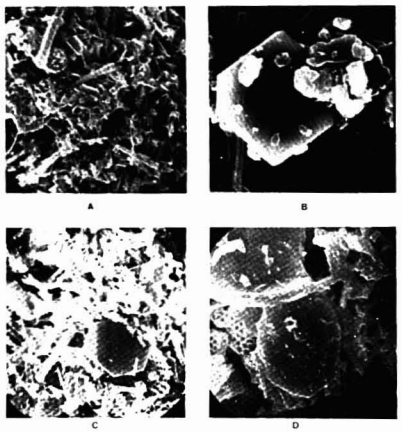

Figure 3. Scanning electron micrographs of: (A) Chromosorb WHP 80-100 mesh (1000×), (B) *N,N'*-Bis(*p*-phenylbenzylidene)-α,α'-bi-*p*-toluidine (1500×), (C) BPhBT on Chromosorb (1000×) before use in the column, (D) BPhBT on Chromosorb (2000×) after use in the column

DISCUSSION AND RESULTS

Thermal Analysis. Phase transition temperatures of pure BPhBT, BPhBT as stationary phase before and after use in the column, were measured with differential scanning calorimetry. The pure BPhBT shows five transitions on the DSC scan (Figure 1): An exotherm doublet at 200–210 °C and three endotherm peaks at 162, 265 and 415 °C. Janini et al. (*9*) measured for the solid–nematic transitions and for the nematic–isotropic transition a temperature of 257 °C and 415 °C, respectively. After the coating procedure of the BPhBT on the Chromosorb, a new peak appears at 245 °C and the doublet at 200–210 °C disappears (Figure 2).

The intensity of this new peak as well as the peak at 265 °C decreases after use in the column.

Electron-microscope photographs (Figure 3C) show the existence of BPhBT crystals between the skeletons of the Chromosorb. After use in the gas chromatograph the peak at 245 °C is no longer present and no free and pure crystals

Table I. Heat of Solution on BPhBT[a]

compound	ΔH,[b] kJ·mol^{-1}	C[c]	r^2[d]
11,12-benzofluoranthene	−69.0	−8.40	0.99
1,2-benzopyrene	−69.3	−8.43	0.99
perylene	−73.5	−8.90	0.99
3,4-benzopyrene	−74.1	−8.90	0.99

[a] Column: 6 ft, 2.0-mm i.d., glass; packing: 2.8% (w/w) BPhBT on Chromosorb WHP 80–100 mesh; flow rate 20 mL/min.; column temperature, 280–300 °C. [b] Calculated from $\log_e t_r - 1/T$ plot. [c] Last term of equation $\log_e(t_r - t_0) = -(\Delta H/RT) + C$. [d] r^2 = coefficient of determination.

(Figure 3B) are found with the electron microscope. Instead there are crystals enclosed among Chromosorb particles (Figure 3D). The surface tension and the polarity of the nematic liquid is probably high enough to effect the formation of small drops on the support. The growing droplets effect a decrease of the specific surface of the physically adsorbed BPhBT-phase. Consequently both resolution and selectivity of the column decrease.

The phenomenon of the disappearance of the peak at 245 °C could be imitated by using DSC.

The sample was put in a hermetically closed pan, which was in a helium atmosphere. The pan was placed in the DSC and the programmed heating started (10 °C/min). After the heating (300 °C), the sample was cooled down to 25 °C and the heating restarted (Figure 2B). The same process was repeated (Figure 2C). Hereby the intensity of the peak decreased at 245 °C and a peak appears on the left side of the peak.

The peak at 245 °C is probably a recrystallization of physically adsorbed BPhBT.

Hence it follows that the stationary phase BPhBT is rather a dynamic phase. During the use of the column, such processes take place as recrystallization, evaporation and condensation, and deterioration of the BPhBT.

Gas Chromatography. The plot of $\log_e(t_r - t_0)$ vs. $1/T$ in the temperature range of 300–280 °C for each of the compounds 1,2-benzopyrene is linear and the slope is proportional to the heat of solution (within a accuracy of 5%).

The calculations of the approximate ΔH_{sol} for four members of the $C_{20}H_{12}$ molecule are summarized in Table I. The separation factors (Table II) slightly increase with increasing temperature while the resolution and the net retention time decrease.

The plots of $\log_e(t_r - t_0)$ vs. $1/T$ in Figure 4 can be divided into three regions: the graphical representation of $\log_e(t_r - t_0)$ vs. $1/T$ in region 1 ($T > 551$ K) is in accordance with the equation in Ref. 5.

In region 2 ($553 < T < 551$ K) the transition solid–nematic takes place; the plots are not linear anymore.

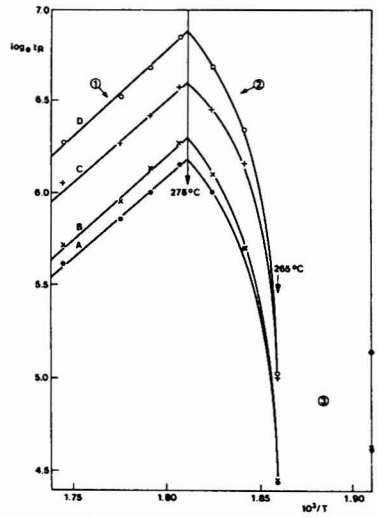

Figure 4. $\log_e t'_R - 1/T$ plots. (A) 11,12-benzofluoranthene, (B) 1,2-benzopyrene, (C) perylene, (D) 3,4-benzopyrene. Column: 6 ft, 2-mm i.d., helium flow 20 mL/min

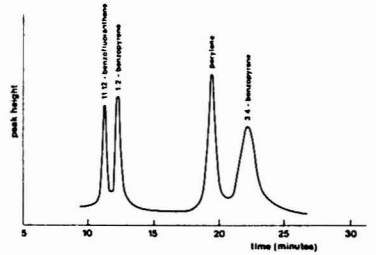

Figure 5. Resolution of PAH on a packed column. Column conditions: 8 ft, 1.8-mm i.d., helium flow 20 mL/min

In this region the resolution for the pairs 11,12-benzofluoranthene/1,2-benzopyrene and perylene/3,4-benzopyrene is very low and becomes zero, while the retention time drastically decreases. In region 3, where the BPhBT is in the solid state, the retention times increase again.

In Figure 4 there are two striking temperatures at 278 and 265 °C, determined by graphical extrapolation. The tem-

Table II. Separation Factors[a] on BPhBT[b] in the Nematic Region

column temperature, °C	separation factors: 11,12-benzofluoranthene	1,2-benzopyrene	perylene	3,4-benzopyrene min.	R[c]
270	0.541	0.541	0.859	9.2	1.00
275	0.513	0.565	0.792	13.2	1.00
280	0.508	0.567	0.766	15.5	1.03
285	0.512	0.567	0.768	13.2	1.03
290	0.516	0.568	0.777	11.3	1.00
300	0.522	0.577	0.788	8.8	0.95

[a] Separation factor = $t'_{r,compound}/t'_{r,3,4\text{-benzopyrene}}$. [b] Column conditions as in Table I. [c] Resolution for perylene and 3,4-benzopyrene.

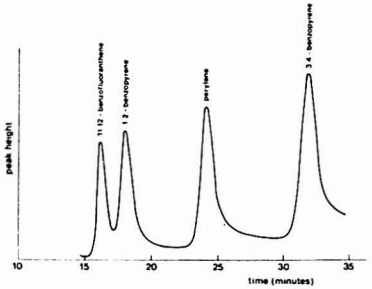

Figure 6. Resolution of PAH on a micropacked column. Column: 3 m, 0.6-mm i.d., flow rate 2 mL/min, temperature 280 °C

Table III. Difference between a Packed and a Micropacked Column

	packed	micropacked
column length	1.80 m	3.00 m
inside diameter	2.0 mm	0.6 mm
outside diameter	6.0 mm	2.0 mm
plate-number	1100	2700
plate-height	1.6 mm	1.1 mm
resolution[a]	1.0	2.9
separation factor[a]	1.1	1.3
relative retention time		
anthracene	0.018	0.005
2-methylanthracene	0.022	0.010
9-methylanthracene	0.033	0.020
pyrene	0.059	0.046
3,4-benzophenanthrene	0.106	0.088
chrysene	0.272	0.257
1,2-benzoanthracene	0.435	0.386
perylene	0.767	0.798
3,4-benzopyrene	1.000	1.000
ret. time 3,4-benzopyrene	1246 s	1519 s

[a] Resolution and separation factor for perylene and 3,4-benzopyrene.

perature 265 °C corresponds with the phase transition solid–nematic as measured by DSC (Figure 1). Janini (9) found with differential scanning calorimetry 257 °C and with gas chromatography 270 °C.

The discrepancy between the measurements with GC and with DSC can be ascribed to the dynamic character of the DSC method. Figures 5 and 6 and Table III illustrate the difference between a packed and a micropacked column.

There is also a relationship between the composition of a mixture and the retention time of the respective compounds (Figure 7). This figure shows the plots of the net retention time vs. the composition of a mixture of 3,4-benzopyrene and perylene. During each measurement the total concentration of 3,4-benzopyrene and perylene was 500 ng per μL benzene (injection volume 1 μL). When the mole fraction of perylene increases, the retention time of both perylene and 3,4-benzopyrene will decrease. There is a tendency that the decrease of the retention times becomes more obvious as the column temperature is lowered.

Many more investigations are necessary to study this important effect of the influence exerted by the concentration on the retention time of PAH.

Hence, identification of peaks of PAH mixtures by retention time measurements alone is doubtful. The identification should always be accompanied by GC-MS measurements.

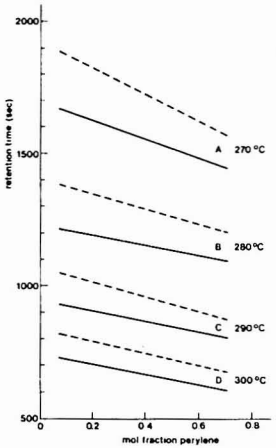

Figure 7. Retention time vs. mole fraction perylene in a mixture of 3,4-benzopyrene and perylene. Mole fraction 0.2 means 0.2 × 500 = 100 ng perylene and 400 ng 3,4-benzopyrene per μL benzene. The dotted line is the retention behavior of 3,4–benzopyrene

ACKNOWLEDGMENT

The author is grateful to C. Wenneker and J. Sijben, H. Cillessen and Th. v. d. Bosch for technical assistance; A. Noothout and J. Kanij for helpful discussions; and the KEMA laboratories for permission to publish this work.

LITERATURE CITED

(1) A. Herlan, *Zentralbl. Bakteriol. Hyg, Abt. 1: Orig., Reihe B*, **165** 174 (1977).
(2) G. Grimmer, H. Böhnke, and H. Borwitzky, *Fresenius Z. Anal. Chem.*, **289**, 91 (1978).
(3) J. W. Strand and A. W. Andren, *Anal. Chem.*, **50**, 1508 (1978).
(4) A. Radecki, H. Lamparczyk, J. Grzybowski, and J. Halkiewicz *J. Chromatogr.*, **150** 527 (1978).
(5) L. S. Lysyuk and A. N. Korol, *Chromatographia*, **10** 712 (1977).
(6) H. H. Hill, K. W. Chan, and F. W. Karasek *J. Chromatogr.*, **131** 245 (1977).
(7) P. W. Jones, R. D. Giammar, P. E. Strup, and T. B. Stanford, *Environ. Sci. Technol.*, **10**, 806 (1976).
(8) G. Grimmer and H. Böhnke, *Chromatographia*, **9** 30 (1976).
(9) G. M. Janini, G. M. Muschik, J. A. Schroer, and W. L. Zielinsky, *Anal. Chem.*, **48**, 1879 (1976).
(10) G. M. Janini, G. M. Muschik, and W. L. Zielinsky, *Anal. Chem.*, **48**, 809 (1976).
(11) G. M. Janini, K. Johnston, and W. L. Zielinsky, *Anal. Chem.*, **47**, 679 (1975).
(12) G. M. Janini, B. Shaikh, and W. L. Zielinsky, *J. Chromatogr.*, **132**, 136 (1977).
(13) R. Guerrini and A. Pennacchi, *Riv. Combust.*, **7**, 349 (1975).
(14) D. A. Lane, H. K. Moe, and M. Katz, *Anal. Chem.*, **45**, 1776 (1973).
(15) L. E. Strömberg and G. Widmark, *J. Chromatogr.*, **49**, 334 (1970).
(16) G. Grimmer and H. Böhnke, *Erdöl Kohle, Erdgas*, **31**, 272 (1978).
(17) W. Giger and C. Schaffner, *Anal. Chem.*, **50**, 243 (1978).
(18) R. W. Schimberg, P. Pfäffli, and A. Tossavainen, *Staub-Reinhalt. Luft*, **38**, 273 (1978).
(19) A. Herlan, *Staub-Reinhalt. Luft*, **38**, 276 (1978).
(20) A. Herlan and J. Mayer, *Staub-Reinhalt. Luft*, **38**, 134 (1978).
(21) H. Tausch and G. Stehlik, *Chromatographia*, **10**, 350 (1977).
(22) M. L. Lee, G. P. Prado, J. B. Howard, and R. A. Hites, *Biomed. Mass. Spectrom.*, **4**, 182 (1977).
(23) W. Cautreels and K. van Cauwenberghe, *J. Chromatogr.*, **131**, 253 (1977).
(24) W. Bertsch, E. Anderson, and G. Holzer, *J. Chromatogr.*, **126**, 213 (1976).
(25) M. L. Lee and R. A. Hites, *Anal. Chem.*, **48**, 1890 (1976).
(26) U. Rapp, U. Schröder, S. Meier, and H. Elmenhorst, *Chromatographia*, **8**, 474 (1975).
(27) A. Herlan, *Erdöl Kohle, Erdgas*, **27**, 138 (1974).
(28) C. A. Cramers and J. A. Rijks, *J. Chromatogr.*, **65** 29 (1972).
(29) J. A. Rijks, C. A. Cramers, and P. Bocek, *Chromatographia*, **8**, 482 (1975).

RECEIVED for review March 5, 1979. Accepted July 5, 1979.

Interactive Effects of Temperature, Salt Concentration, and pH on Head Space Analysis for Isolating Volatile Trace Organics in Aqueous Environmental Samples

Stephen L. Friant

Academy of Natural Science, Philadelphia, Pennsylvania 19104

Irwin H. Suffet*

Department of Chemistry, Environmental Studies Institute, Drexel University, Philadelphia, Pennsylvania 19104

A systematic approach is presented for the isolation and quantification of volatile trace organics from aqueous solutions by head space analysis. Fundamental information is obtained on the partition process for a multiple solute system consisting of model compounds under varying aqueous matrix conditions, i.e., pH, temperature, and salt addition. Interactive effects between parameters are quantitatively shown by the use of the thermodynamic equilibrium partition coefficient. A general optimum head space isolation methodology is obtained from statistical evaluation of the effect of parameter variation on the partition coefficient. The optimum head space analysis sampling conditions of pH 7.1, 50 °C and 3.35 M sodium sulfate were determined from a statistical design. At the optimum conditions of this design, enrichment factors of the vapor phase of up to 66 times were achieved as compared to a reference state of pH 7.1, 30 °C, without electrolyte addition. Under optimum head space analysis conditions, river and drinking water can be routinely profiled for volatile trace organics.

Two different analytical approaches are utilized to determine organic compounds in water (*1*). The first consists of quantitative analysis of one pollutant such as bis(2-chloroethyl) ether (*2*), a group of chemically related pollutants such as the trihalomethanes (*3*), or a pollutant and its related breakdown products such as an organophosphorus pesticide, fenthion, and its oxons, sulfoxides, and sulfones (*4*).

The second approach is a general "screening" procedure for organic compounds. This consists of a qualitative analysis with semiquantitative evaluation of the constituents found. An example of a general screening procedure would be the analysis of volatile organics responsible for taste and odor incidence in drinking water (*5*).

The isolation method used to collect trace organic compounds from water is the primary basis of any analysis as it defines the type of compounds to be analyzed, the maximum recovery of a compound, the precision and accuracy of the method, and possible co-extractives that may interfere with a subsequent quantitative analytical step. Each isolation technique has a selective efficiency for specific compounds as reviewed by Suffet and Radziul (*1*). Thus the analytical problem is to define the parameters involved in an isolation method to enable optimization for a specific purpose.

Vapor phase isolation of trace organics present in aqueous samples can be divided into two areas: dynamic volatile organic analysis and equilibrium head space analysis as discussed by Weurman (*6*). Two commonly used dynamic organic analyses are the gas stripping (purge and trap) procedure of Bellar and Lichtenberg (*3*) and the closed looped stripping procedure of Grob and Zurcher (*7*). The purge and trap method is used primarily for analysis of volatile organics of less than 2% solubility and boiling points below 150 °C (*3*).

Head space analysis (head gas analysis) is the static sampling of the vapor phase in thermodynamic equilibrium with the aqueous phase. The initial liquid phase concentration is determined from the measurement of the equilibrated vapor phase concentration and the equilibrium partition coefficient. Trace organics which favor the vapor phase are easily determined at the microgram per liter concentration level by head space analysis. Examples of these trace organics are hydrocarbons and chlorinated hydrocarbons (*8*). McAuliffe (*8*) found that vapor phase partitioning for the following chemical classes followed the order: alkanes > olefins > cycloalkanes > aromatics. It was also shown that within each chemical class an increased vapor partition was observed as the molecular weight increased. Head space analysis can selectively separate nonpolar volatiles from more water soluble alcohols and acids whereas purge and trap analysis can remove more of these polar compounds (*7*).

Enhancement of vapor phase partitioning has been achieved by both the addition of an electrolyte and increased temperatures (*9*, *10*). Quantification of the interactive effects of temperature and salt addition on the vapor phase partitioning process is of interest for both types of vapor phase trace organic isolation methods.

This study was undertaken to investigate the quantitative effects of salt addition, temperature, and pH on the vapor phase partitioning of selected compounds utilizing an ANOVA analysis of an experimental design. The ultimate goal was to understand how to increase the vapor concentration of organics. Model compounds of high polarity and solubility were studied to investigate the limits of the ability of head space analysis to partition these materials into the vapor phase.

Model Compound Selection for Characterization of the Air:Water Partitioning Process. Criteria for the selection of the four model compounds (Table I) were based on several factors. These included (1) ability for simultaneous GC analysis, (2) aqueous solubility, and (3) volatility. In addition, the compounds should represent industrial process chemicals and should be representative of several major chemical classes. The choice of model compounds that represent major chemical classes was determined using the concept of the solubility parameter (δ_T). The solubility parameter is a measure of a compound's polarity in a pure state; the square root of the cohesive energy density (*11*). It was felt that the selection of compounds based on this concept would yield results that could be generalized since the solubility parameter is not solely dependent on functional groups but is a measure of the compound's total polarity.

The major applications of the solubility parameter theory have been in chromatography, reverse osmosis membrane rejection predictions, and polymer chemistry (*11*). The solubility parameter approach applied to the chromatographic

0003-2700/79/0351-2167$01.00/0

Table I. Model Compounds and Experimental Conditions

polarity (11)	δ_T (14)	compound	initial aqueous phase concn, mg/L
dipole orientation	9.5	methyl ethyl ketone	5.64
dipole orientation	11.0	nitroethane	20.90
proton donor	12.0	*n*-butanol	40.49
proton acceptor	10.1	*p*-dioxane	93.30

General Experimental Conditions

equilibration time	5 h
vapor volume	1100-1200 mL
liquid volume	1000-1040 mL
volume of vapor samples	5.0 mL
pH	7.1
sodium sulfate concentration	0.00-3.35 M
ionic strength	0.00-10.02
orthophosphate buffer (15)	0.20 M

partitioning process is described by functional probes (methyl ethyl ketone, *n*-butanol, nitroethane, and dioxane) (*11-14*). The polarity probes are representative of ketones, alcohols, nitro groups, and ethers. These functional groups are representative of the intramolecular forces of dispersion, dipole orientation, and proton donor and acceptor capabilities (*11*). Keller (*12*) emphasized that nitromethane is an excellent probe for classical polarity (dipole orientation) with little acid–base function. The same appears to hold true for nitroethane (δ_T = 11.0) except at alkaline pH where an aci-nitrogen effect becomes important. Methyl ethyl ketone (δ_T = 9.5) was considered to be more of a combined polarity by Hartkopf et al. (*13*) than of specifically dipole orientation as originally described. Dioxane (δ_T = 10.1) and butanol (δ_T = 12.0) have predominant proton acceptor and donor forces, respectively. The total solubility parameter values of these compounds ranged from 9.4 to 11.6 on a scale of 6 for nonpolar alkanes to 23.5 for very polar water (*14*).

EXPERIMENTAL

Apparatus. All chromatography was conducted on a Tracor MT-550 gas chromatograph equipped with dual flame ionization detectors. The chromatographic column was 8 feet × $^1/_8$ inch i.d. stainless steel packed with 20% SE-30 on 80/100 mesh Gas Chrom Q. The column temperature was maintained isothermally at 130 °C. Inlet, outlet, and detector temperatures were 180, 200, and 200 °C, respectively.

Glassware in contact with both water and vapor phases was silanized to minimize surface absorption. First, the glassware was washed with detergent. This was followed by rinsing with distilled water and air drying. The dry surface was treated with Glas-treet (Alltech Associates) and rinsed with anhydrous methanol.

The sampling bottle used for laboratory test conditions was a modified 2-L Pyrex reagent bottle. The neck was reformed by using #30 glass O-ring joints and the top was rounded and sealed. The two joints were sealed by a Buna rubber O-ring and a compression clamp. To allow syringe sampling of the vapor two ($^1/_4$-inch diameter) glass sidearms were attached. A stainless steel ($^1/_4$ to $^1/_8$ inch) Swagelok reducing union was attached to the glass sidearms by $^1/_4$-inch rubber O-rings and a Swagelok nut. The sampling port was sealed by a chromatographic silicon septum (*15*). The gas syringe was a Precision Scientific (Baton Rouge, La.) pressurizable Series A-2 10.0-mL gas syringe equipped with sideport needle and stop/go valve. The valve permitted the sampling of larger vapor volumes by allowing compression of the sample prior to injection, thereby reducing peak broadening. The syringe also permits easier injections since the pressure in the syringe can be equal to the GLC column head pressure.

Table II. Statistical Design (3 × 3 × 2) for the Investigation of Salt, pH, and Temperature Effects on the Partitioning Process

run no.	salt concn *M*	pH	temperature, °C	code
1	0.00	4.5	30	111
2	0.00	7.1	30	121
3	0.00	9.1	30	131
4	0.00	4.5	50	112
5	0.00	7.1	50	122
6	0.00	9.1	50	132
7	1.41	4.5	30	211
8	1.41	7.1	30	221
9	1.41	9.1	30	231
10	1.41	4.5	50	212
11	1.41	7.1	50	222
12	1.41	9.1	50	232
13	3.35	4.5	30	311
14	3.35	7.1	30	321
15	3.35	9.1	30	331
16	3.35	4.5	50	312
17	3.35	7.1	50	322
18	3.35	9.1	50	332

Table III. Three-Dimensional Presentation of the Experimental Results for the Analysis of Variance of Methyl Ethyl Ketone, $K \times 10^{-3}$

	temperature, °C					
	30			50		
	salt concentration, M					
pH	0.00	1.41	3.35	0.00	1.41	3.35
4.5	4.19	21.3	118	21.3	39.8	234
7.1	3.90	20.0	109	20.0	37.6	260
9.1	4.56	18.7	105	18.7	35.0	229

All experiments were run isothermally in a constant temperature air bath controlled to ±0.5 °C. All samples were stirred on a magnetic stirrer.

Reagents and Chemicals. All chemicals used were reagent grade or better. Solvents were pesticidal quality.

Procedures. Table I shows the group of four model compounds studied, aqueous phase concentrations, and experimental conditions. The ionic strength and pH of all experiments were adjusted first to 0.2 M with orthophosphate buffers (*16*). Ionic strength was subsequently adjusted with Na_2SO_4 as desired. All sample and standard solutions were prepared based on the density of the pure solute. Sample solutions were prepared by individually pipeting with a microsyringe a known volume of solute into a 1-L volumetric flask filled with the appropriate buffer solution. Standards were prepared (by density) in carbon disulfide. The vapor phase concentration of the solutes was determined by comparison of the area of the vapor phase injections to standard curve areas of the solutes in carbon disulfide.

Experiments requiring the addition of an electrolyte were completed by placing the salt (anhydrous sodium sulfate) in a clean sample bottle at the required experimental temperature 16 h prior to the study period to reduce the time required to dissolve the salt. Samples and standard solutions were prepared daily. A saturated solution of Na_2SO_4 was used that contains 475 g/L (3.35 M) when dissolved in 0.2 M orthophosphate buffer. A solution of Na_2SO_4 containing 200 g/L (1.4 M) when dissolved in 0.2 M orthophosphate buffer was also used.

A maximum sampling temperature of 50 °C was chosen to minimize water vapor condensation in the syringe during pressurization and enable ease of sample handling. A minimum temperature of 30 °C was chosen to maintain the temperature of equilibration of the head space bottle above ambient room temperature.

Vapor samples were withdrawn through the sidearm sampling port of the sample bottle with a gas syringe. The syringe was flushed with the vapor phase prior to withdrawing the sample. After sampling the vapor, the syringe valve was closed and the

Table IV. ANOVA Table for Methyl Ethyl Ketone

SOURCE	SS	DF	MS	F CALC	PROB OF F	
A	0.0248535	1.0000000	0.0248535	249.0214	1.0000	1
B	0.1930203	2.0000000	0.0965102	966.9896	1.0000	2
AB	0.0271621	2.0000000	0.0135810	136.0759	1.0000	3
C	0.0002594	2.0000000	0.0001297	1.2997	0.7029	4
AC	0.0001816	2.0000000	0.0000908	0.9096	0.5770	5
BC	0.0003457	4.0000000	0.0000864	0.8659	0.4953	6
ABC	0.0004975	4.0000000	0.0001244	1.2462	0.6729	7
ERROR	0.0017965	18.0000000	0.0000998			
TOTAL	0.2481166	35.0000000				

GROUP MEANS		A. Temperature	B. Salt Concentration	C. pH
		1. 0.046506	1. 0.011533	1. 0.073397
GRAND MEAN IS	0.072781	2. 0.099056	2. 0.031092	2. 0.075717
			3. 0.17572	3. 0.069228
CORRECTION FACTOR	0.19069			

Table V. Two-Factor Interaction of Significances for Methyl Ethyl Ketone[a]

	K			
	salt concentration (A)			
temperature, °C	A_1 (0.00 M)	A_2 (1.41 M)	A_3 (3.35 M)	mean
C_1 (30 °C)	0.421×10^{-2}	2.47×10^{-2}	11.1×10^{-2}	4.66×10^{-2}
C_2 (50 °C)	2.00×10^{-2}	3.75×10^{-2}	24.6×10^{-2}	10.1×10^{-2}
mean	1.21×10^{-2}	3.11×10^{-2}	17.9×10^{-2}	7.39×10^{-2}

[a] Notes: Means of partition coefficients at levels specified are averaged over pH 4.5, 7.1, and 9.1. The 90% confidence interval for A_3C_2 is: $23.8-25.4 \times 10^{-2}$. Conclusions: Statistically significant maximum yield two-factor interaction occurs for A_3C_2 (3.35 M salt concentration at 50 °C).

volume reduced to $^1/_{10}$ sample volume followed by direct injection into the chromatographic column.

Calculations. The basis for the evaluation of the magnitude of parameter effects was the partition coefficient (K):

$$K = \frac{[A]_v}{[A]_w} \text{ as } \frac{\gamma_v}{\gamma_w} \rightarrow 1 \quad (1)$$

where $[A]_v$ and $[A]_w$ are the equilibrium vapor and water phase concentrations of a solute A, respectively. The terms γ_v and γ_w are the corresponding activity coefficients. At equilibrium the activity terms are equal and in dilute solutions they approach unity. Equation 1 can then be rewritten in terms of solute equilibrium weights and volumes:

$$K = \frac{W_v/V_v}{W_w/V_w} = \frac{W_v}{W_w} \times \frac{V_w}{V_v} \quad (2)$$

where W_v, W_w and V_v, V_w are the equilibrium weights and volumes for the solute in the vapor and water phase, respectively. If W_T is the weight of the total solute in the system, $W_w = W_T - W_v$. Substituting for W_w in Equation 2 and defining the equilibrium volume ratio V_v/V_w as α yields:

$$K = \frac{W_v}{\alpha(W_T - W_v)} \quad (3)$$

In a head gas experiment, if the initial volume of water and vapor are changed owing to the addition of an electrolyte, the initial α value must also be changed as the water volume increased the vapor volume decreases. The correction factor (CF) can be used:

$$CF = V_v/V_{v_i}$$

where V_{v_i} is the initial vapor volume. Therefore the initial α is multiplied by CF to obtain the new experimental α value. If no electrolyte is added, the CF term is unity while the addition of salt decreases CF to less than 1.

Sampling Parameters. From preliminary work, the parameters shown to influence the partitioning process most significantly were pH, temperature, and the addition of an electrolyte (*16*). A quantitative investigation of these parameters for the vapor–water partitioning process was completed by a statistical design using an analysis of variance (ANOVA) to evaluate interactive results. The experimental design investigated the effects of parameter variation on the partitioning process by a 3 × 3 × 2 analysis of variance, Table II. The 18 experiments and replicates were completed using a random order (*17*). Results of the design were reported as the equilibrium partition coefficient, K, and were used as input data to an IBM 370/168 computer using available APL statistical package ANOVA (*18*).

RESULTS AND DISCUSSION

Statistical Design. Table III is a three-dimensional presentation of the results obtained from the 3 × 3 × 2 statistical experiments. Methyl ethyl ketone data are shown as an example. The computer results of the analysis of variance summarizing main effects are shown in Table IV where A, B, and C represent temperature, salt concentration, and pH, respectively. As indicated in Table IV by the large probability of F, a significant two-factor interaction exists between salt concentration and temperature. Table V shows a two-factor interaction of significance existed at both 1.41 and 3.35 M sodium sulfate and 50 °C.

The results drawn from the statistical design are:

(a) pH had no effect on methyl ethyl ketone, butanol, and dioxane. The optimum pH for nitroethane was either 4.5 or 7.1; both were found to be equivalent.

(b) The optimum salt concentration for all compounds was 3.35 M sodium sulfate.

(c) The optimum sampling temperature for all compounds was 50 °C.

(d) For all two-factor interactions, the maximum K occurred for either pH 4.5, or 7.1, 50 °C and 3.35 M sodium sulfate.

From the above statistical approach the general head space analysis conditions for the optimum isolation of volatile trace organics was pH 7.1, 50 °C, and 3.35 M sodium sulfate.

The partition coefficients are shown in Table VI for all compounds investigated at the optimum and reference state conditions. The order of increasing partition coefficients at all experimental conditions is dioxane < butanol < nitroethane < methyl ethyl ketone. A plot of the partition coefficients is shown in Figure 1 for methyl ethyl ketone under the various conditions of salt and temperature.

Table VI. Partition Coefficient of Model Compounds at the Optimum and Reference States

compound	$K \times 10^{-3}$ optimum conditions, pH 7.1, 50 °C 3.35 M[a]	$K \times 10^{-3}$ reference condition, pH 7.1, 30 °C, no salt[a]
methyl ethyl ketone	260	3.90
nitroethane	72.5	2.89
butanol	44.3	0.746
dioxane	13.7	0.278

[a] 0.2 M orthophosphate buffer.

Analysis of the Effects of Salt and Temperature on the Partitioning Process. An advantage of employing the statistical design approach for the selection of optimum head space analysis conditions is that interactions or main effects of interest can be factored from the design to enable a more comprehensive data evaluation. Salt and temperature effects expressed as enrichment factors are shown in Table VII for all compounds. Enrichment factors are defined as the ratios of the partition coefficients at the condition of interest to the reference conditions of pH 7.1, 30 °C, without the addition of salt. From Table VII the dominant force responsible for the partitioning process is salt addition at the 3.35 M level, ranging from 2.7 to 5.2 times larger than the temperature effect. The effect of salt addition at the 1.41 M level yielded enrichment factors approximately equal to the effect of temperature although the salt–temperature interactions were significantly greater.

The total enrichment factors shown represent the interactive effects of salt (3.35 M) and temperature (50 °C) over the reference conditions. Total enrichment factors ranged from 25 to 67 for the model compounds. The order of increased total enrichment factors is nitroethane < dioxane < butanol < methyl ethyl ketone. It is worth noting that the magnitude of enrichment is not the same for all compounds. This is in agreement with the work of Kepner et al. (*19*) and Nawar and Fagerson (*20*). They found that enrichment increased the vapor phase concentration but the relative proportion of each compound recovered was considerably altered. Table VII shows that the increased partition coefficients and enrichment factors are not in agreement. The order of increased partition coefficients also does not agree with the vapor pressure–temperature relationships of the pure solute (*15*). This qualitative discrepancy between pure vapor pressure trends and enrichment factors supports Dravnieks and O'Donnell (*21*) who indicated that vapor phase partitioning of anything but the pure solute is not only a function of vapor pressure but also of activity coefficients, presence of salt, complexing ability of the solute, and pH.

Analysis of the Effect of pH on the Partitioning Process. The results of the analyses of variance showed that methyl ethyl ketone, dioxane, and butanol were not affected by pH. They apparently do not exhibit significant acid or base intramolecular bonding forces in the aqueous environment. Nitroethane showed maximum and equivalent vapor phase concentration at pH 4.5 and 7.1. This was expected since nitro substituted compounds in aqueous solution can form aci-nitrogen complexes; hence, solute–solvent interaction would be at a minimum in acid or neutral solutions. The pH effect exhibited by nitroethane is discussed by Gould (*22*). An addition of base to an aliphatic nitro compounds—e.g., nitroethane—consumed an equimolar quantity of base. This indicates a neutralization reaction. The reaction of the nitro group and base is due to the ionization of the C–H bond and causes a delocalization of the negative charge in the resulting anion.

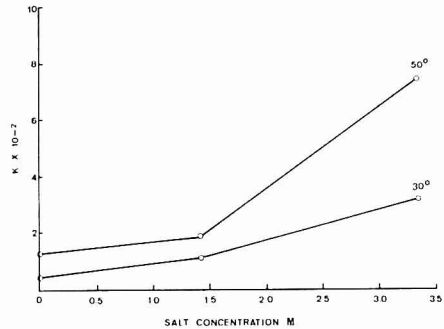

Figure 1. Partition coefficients for methyl ethyl ketone vs. salt concentration for varying temperatures

Henry's Law of Dilute Solution. The effect of varying the initial solute concentration on the partition coefficient was determined for the model compounds. The water phase concentrations were simultaneously varied over 100-fold from low concentrations of methyl ethyl ketone (0.051 mg/L), nitroethane (0.187 mg/L), *n*-butanol (0.363 mg/L), and dioxane (0.834 mg/L). The study was completed at the optimum analysis conditions of pH 7.1, 50 °C, and 3.35 M sodium sulfate.

The partition coefficients were found to be independent within experimental error of initial water phase concentrations over a 100-fold change of the initial concentration. This was found to hold for all compounds except nitroethane where a large variance was noted at the lowest concentration investigated while at the two higher concentrations excellent agreement was obtained. This adherence to Henry's law for a multiple solute system implies that all compounds were sufficiently dilute to minimize intra-solute–solute interaction.

According to Henry's law, the initial water phase solute concentration can be determined for a constant volume system from a knowledge of the equilibrium partition coefficient and an experimental determination of the equilibrium vapor phase concentration (Equation 3). This is particularly useful for the isolation and quantification of a specific solute.

Detection Limits of Head Space Analysis. The calculated theoretical detection limits for the four model compounds are shown plotted against the reciprocal of the partition coefficient ($1/K$) in Figure 2. The theoretical limits were determined by assuming a nominal flame ionization detector limit of 50 ng absolute amount injected and calculating the initial water phase concentration by Equation 3. For head space analysis this is the amount in 5.0 mL of injected vapor. The detection limits ranged from 50 μg/L for methyl ethyl ketone to 740 μg/L for dioxane. The smaller $1/K$ is, the lower the detection limit. Figure 2 can be used to determine the theoretical detection limits for any solute from the measured partition coefficient under comparable conditions.

The head space analysis detection limits can be further enhanced by decreasing the equilibrium vapor to liquid volume ratio. Equations 3 and 4 can be used to determine the effect of varying the vapor to liquid volume ratio, α, on the percent solute concentration in the vapor $((A)_v)/(A)_i$. Figure 3 shows the curves obtained by solving Equation 3 for W_v and varying the α ratios and partition coefficients. The total solute weight (W_T) is held constant and at a concentration of 100 μg/L for varying partition coefficients of 0.2 to 1.0 and varying α ratios of 0.19, 0.65, and 1.00. The total volume of the system, V_T,

Table VII. Individual and Total Effects of Salt Concentration and Temperature on the Partition Coefficient

	enrichment factors—ratio of K values			
	A	B		total
compound	salt, 0.00 to 3.35 M	temperature, 30 to 50 °C	A/B	0.00 to 3.35 M plus 30 to 50 °C
methyl ethyl ketone	28.0	5.1	5.2	66.7
nitroethane	10.8	4.0	2.7	25.1
butanol	18.4	5.4	5.4	56.1
dioxane	19.3	4.7	4.1	49.3

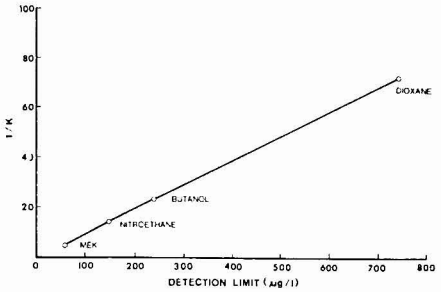

Figure 2. Theoretical detection limits for model compounds plotted vs. the reciprocal of the partition coefficients. The nominal FID detection limit is 50 ng and the amount in 5.0 mL of injected vapor is calculated

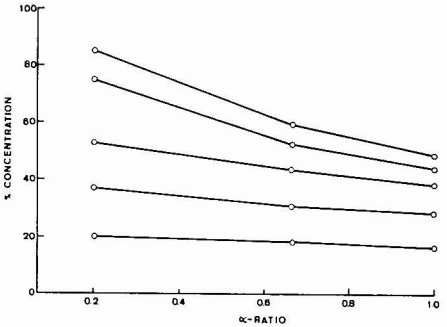

Figure 3. Calculated percent concentration ratio vs. the vapor to liquid volume ratio (α) for theoretical partition coefficients. The initial aqueous phase concentration in the system is set to 100 μg/L and the total volume of the head gas container is 2.0 L

was 2.0 L. In all cases, for a decreasing α ratio the solute percent concentration in the vapor phase increased. This is equivalent to an increase in sensitivity of head space analysis by injecting into the GC a larger percentage of the solute. The change in percent solute concentration in the vapor is greatest for larger partition coefficients. An α ratio change from 1.00 to 0.19 will increase solute concentration by 2.7-fold for a partition coefficient of 1.00. For a partition coefficient of 0.2, the increase is 1.8-fold. The effect of α on the vapor phase enhancement of compounds with partition coefficients less the 0.2 is minimal. This analysis assumes that the total vapor volume is sufficiently large to maintain the head gas equilibrium upon sampling.

Comparison of Experimental Partition Coefficients to Literature Values. Table VIII compares the partition coefficients obtained in this study vs. literature values. The literature values for *n*-butanol and dioxane were found to be within the 95% confidence limits of the experimental values found in this study. Other experimental values were greater than literature values. This could be due to the fact that experimental values were run under a constant ionic strength, pH, and temperature of 30 °C. Literature values were completed under a constant temperature of 25 °C while pH and ionic strength were not controlled. The second value shown for butanol was in a saturated solution of sodium sulfate (475 g/L) at 30 °C, while the partition coefficients obtained by Nelson and Hoff (*9*) were 600 g/L sodium sulfate solution at 28 °C. The excellent agreement between partition coefficients, although salt concentrations differ significantly, was probably due to the fact that once the salt saturation concentration was exceeded no further salting out effect would be observed.

An underlying assumption of this work is that each solute molecule in a mixture acts independently of all other solute present in dilute aqueous solution (Henry's law). This assumption is demonstrated when one compares partition coefficients obtained by this research to the available literature values. All literature values were obtained with only one solute in solution. In this study, all partition coefficients were obtained in a multisolute solution. If solute–solute interaction was present, it would be expected that the partition coefficient would decrease as a function of the most volatile solute present. This is not the case, as all values obtained are comparable literature values obtained in a single solute solution.

Applications of Head Space Analysis. The head space approach to quantitatively determine organic compounds has been demonstrated in this paper. Specific conditions can be set for the specific analytical purpose. The standard deviations of the partition coefficients that were determined are reported in Table VIII. Analysis can be improved by the addition of an internal standard (*19*). To calculate the initial water concentrations of volatile solutes, all that is needed is the solute K and a measure of the equilibrium vapor concentration. This work suggests that salt addition is more effective in increasing vapor phase partitioning of moderately polar compounds than just temperature although the interactive effects are far superior to salt addition and temperature individually. This also applies to purge and trap analysis which can utilize the same approach to increase the efficiency of analysis.

The general "screening" procedure for qualitative analysis with semiquantitative evaluation has been utilized for taste and odor profiling in the food industry. In this case the head gas composition is much more meaningful that purge and trap analysis as has been clearly described in a recent ACS symposium book, "Analysis of Food and Beverages, Headspace Technique" (*25*). A primary reason for the investigation of head space analysis was to subsequently develop a method that would isolate volatile organics causing taste and odor in drinking water. Isolation of possible taste and odor organics under the enhanced conditions allows determination of the initial water phase concentrations. These concentrations can then be used to determine the vapor phase concentrations of the organic compounds presented to the consumer of drinking water. All that is needed is the partition coefficients of the

Table VIII. Comparison of Experimental and Literature Partition Coefficients

compound	K experimental[a]	K literature[b]	ref.
methyl ethyl ketone	$3.90 \pm 0.01 \times 10^{-3}$	2.13×10^{-3}	(23)
		$3.57 \pm 0.03 \times 10^{-3}$	(24)
nitroethane	$2.89 \pm 0.13 \times 10^{-4}$	N.F.[f]	
butanol	$7.46 \pm 0.57 \times 10^{-4}$	$3.6 \pm 0.4 \times 10^{-4}$	(23)
butanol[c] (sodium sulfate saturation)	$13.7 \pm 0.1 \times 10^{-3}$	13.3×10^{-3}[d,e]	(9)
dioxane[d]	$2.78 \pm 0.54 \times 10^{-4}$	1.85×10^{-4}[e]	(23)

[a] Experimental conditions: pH 7.1, 0.00 M salt concentration at 30 °C. [b] Experimental conditions: not reported other than temperature of 25 °C. [c] Experimental condition this study: pH 7.1, 3.35 M salt concentration at 30 °C. [d] Experimental condition this study: 4.23 M salt concentration at 28 °C, pH not reported. [e] Literature values within 95% confidence limits of experimental data. The remaining values do not fall within the 95% confidence limits. [f] N.F. = No value found.

organic compound at the enhanced and drinking water conditions, respectively.

Application of the method of head space analysis as described was utilized for GC/MS of a drinking water sample in Philadelphia. The results of mass spectral identification of the compounds found in the drinking water showed the presence of toluene, two C-2 benzene isomers, $CHCl_3$, $CHClBr_2$, $CHCl_2Br$, and 1,1,2,2-tetrachloroethane. The quantitative effect of salt and temperature was also studied. The optimized head space conditions of 50 °C with a saturated salt solution was compared to 24 °C without salt addition. An increase in peak response was observed of 8- and 22-fold for chloroform and bromodichloromethane, respectively. The analysis was completed in a 125-mL bottle containing 100 mL of tap water. A 50-μL gas sample was injected onto the GC using a ^{63}Ni electron capture detector. Thus the methodology should be capable for analysis of microgram/liter quantities of organics in drinking water.

LITERATURE CITED

(1) I. H. Suffet and J. V. Radziul, *J. Am. Water Works Assoc.*, **68**, 520 (1976); Erratum, **69**, 174 (1977).
(2) I. H. Suffet and P. R. Cairo, *J. Environ. Sci. Health*, **A13**, 117 (1978).
(3) T. A. Bellar and J. J. Lichtenberg, *J. Am. Water Works Assoc.*, **66**, 739 (1974).
(4) I. H. Suffet, G. Dozsa, and S. D. Faust, *Water Res.*, **5**, 473 (1971).
(5) I. H. Suffet and S. Segall, *J. Am. Water Works Assoc.*, **63**, 605 (1971).
(6) C. Weurman, *J. Agr. Food Chem.*, **17**, 370 (1969).
(7) K. Grob and F. Zurcher, *J. Chromatogr.*, **117**, 285 (1976).
(8) C. D. McAuliffe, "Marine Pollution Monitoring (Petroleum)", *Natl. Bur. Stand. (U.S.), Spec. Publ.*, **409**, Dec. 1974.
(9) P. E. Nelson and J. E. Hoff, *J. Food Sci.*, **33**, 479 (1968).
(10) W. G. Jennings, *J. Food Sci.*, **27**, 366 (1972).
(11) A. F. M. Barton, *Chem. Rev.*, **75**, 731 (1975).
(12) R. A. Keller, *J. Chromatogr. Sci.*, **11**, 49 (1973).
(13) A. Hartkopf, S. Grunfeld, and R. Delumyea, *J. Chromatogr. Sci.*, **12**, 119 (1974).
(14) B. L. Karger, L. R. Snyder, and C. Eon, *J. Chromatogr.*, **125**, 71 (1976).
(15) G. D. Christian and W. C. Purdy, *J. Electroanal. Chem.*, **3**, 363 (1962).
(16) S. L. Friant, Ph.D. Thesis, Drexel University, Philadelphia, Pa., 1977.
(17) O. L. Davies, "Design and Analysis of Industrial Experiments", 2nd ed., Hafner, New York, 1971.
(18) J. Prins, "Statistical Program Package in APL", 5th ed., State U. College of New York, 1973.
(19) R. E. Kepner, H. Maarse, and J. Strating, *Anal. Chem.*, **36**, 77 (1964).
(20) W. W. Nawar and I. S. Fagerson, *Food Technol.*, **16**(11), 107 (1962).
(21) A. Dravnieks and A. O'Donnell, *J. Agr. Food Chem.*, **19**, 1049 (1971).
(22) E. S. Gould, "Mechanism and Structure in Organic Chemistry", Holt, Rinehart & Winston, New York, 1959.
(23) A. G. Vitenberg, B. V. Toffe, Z. St. Dimitrova, and I. L. Butaeva, *J. Chromatogr.*, **112**, 319 (1975).
(24) L. Rohrschneider, *Anal. Chem.*, **45**, 1241 (1973).
(25) "Analysis of Food and Beverages, Headspace Technique", G. Charalambous, Ed., Academic Press, New York, 1978.

RECEIVED for review November 15, 1978. Accepted July 30, 1979. Presented before the Division of Analytical Chemistry, 176th National Meeting of the American Chemical Society, Miami Beach, Fla., Sept. 15, 1978. This research was supported by the Philadelphia, Pa., Water Department under the leadership of Water Commissioner Carmen F. Guarino.

Determination of Alkoxyl Substitution in Cellulose Ethers by Zeisel-Gas Chromatography

K. L. Hodges,* W. E. Kester, D. L. Wiederrich, and J. A. Grover

The Dow Chemical Company, Midland, Michigan 48640

An improved Zeisel gas chromatographic technique has been developed for the determination of molar substitution in cellulose ether derivatives. The method utilizes adipic acid to catalyze the hydriodic acid cleavage of the substituted alkoxyl groups quantitatively to their corresponding alkyliodides. An in-situ xylene extraction of the alkyliodides in a sealed vial allows for the determination of methoxyl, ethoxyl, hydroxyethoxy, or hydroxypropoxy substitution in mixed or homogeneous cellulosic ethers.

Cellulose ethers are used extensively as thickeners, binders, lubricants, emulsifiers, and film formers. Their capability to perform this large variety of tasks depends on the number of moles of ether (alkoxyl) substituted per anhydroglucose unit, molar substitution; and on the number of hydroxy groups substituted, degree of substitution. The ability to quantitatively determine the molar substitution is therefore important in adjusting the solubility, thermal gelation point, viscosity, and other physical properties associated with solutions of these cellulose ethers.

A wide variety of analytical methods have been developed over the years for the determination of molar substitution, largely owing to the variety of ethers being marketed.

The classical Zeisel distillation method (*1*) has been combined with gas chromatography (*2–10*) to obtain the selectivity needed for the analysis of mixed cellulose ethers.

0003-2700/79/0351-2172$01.00/0

These techniques work well for either homogeneous or mixed *O*-methyl or *O*-ethyl substituted cellulose. However, the formation of ethylene and propylene (*9*), in the cleavage of hydroxyethyl and hydroxypropyl ethers, respectively, leads to low substitution values, which severely limits their utilization.

Other methods have been described which provide selectivity through a different approach. These include a chromic acid oxidation and distillation (*11*) which has also been combined with gas chromatography (*12*), a spectrophotometric method based on the ninhydrin colorimetric technique (*13*), and the formation of the alditol acetates of methyl and ethyl cellulose which are suited for gas chromatography (*14*). The increased selectivity shown by these techniques, however, has caused losses in precision and reproducibility.

Proton NMR (*15*, *16*) provides perhaps the most detailed information concerning degree of substitution as well as molar substitution; however, the precision and accuracy is critically dependent on the measurement of the intensity of a group of bands which are fairly weak relative to other bands in the spectrum. As a result, signal-to-noise enhancement through multiple scanning with computer data acquisition makes the technique undesirable as a routine quality control test.

The described method uses a catalyst, adipic acid, which allows the Zeisel cleavage reaction to proceed quantitatively for the four types of cellulose ethers described without the formation of ethylene or propylene. An in-situ extraction of the resulting alkyliodides with *o*-xylene allows for the gas chromatographic determination of substitution in either homogeneous or mixed difunctional substituted cellulose ethers in a single 1.5-h analysis without elaborate distillation equipment or complicated apparatus.

EXPERIMENTAL

Apparatus. A Hewlett-Packard Model 5700 gas chromatograph equipped with a thermal conductivity detector was used. The column was 10 ft × 1/8 in. stainless steel packed with 10% UCW 98, methyl silicone on 100/120 mesh Chromosorb WHP, available from Applied Science Laboratories State College, Pa. 16801. The oven temperature was 100 °C; injection port and detector temperatures, 200 °C. The carrier gas was helium at a flow rate of 20 mL/min. The detector current was 170 mA.

A Hewlett-Packard 3380 reporting integrator was used to facilitate data handling and improve method precision.

Reactivials, 5 mL, capped with Mininert valves available from Pierce Chemical Co., Rockford, Ill. 61105, were used to contain the Zeisel cleavage reaction and a Reactitherm heating module was used to control the reaction temperature. Three-dram, soft glass vials, 10-mL capacity, capped with smaller Mininert valves were used for preparation and storage of the standards.

Reagents. Hydriodic acid, specific gravity 1.7, containing 57% HI (Matheson Coleman and Bell) and adipic acid, mp 151–153 °C (Matheson Coleman and Bell) were used. The *o*-xylene and toluene were ACS reagent grade. Iodomethane (99% min), iodoethane (97% min), and 2-iodopropane (97% min), available from Aldrich Chemical Company, were assayed under the stated chromatographic conditions and appropriate corrections were made in the preparation of the calibration standard.

An internal standard stock solution containing 25 mg toluene/mL *o*-xylene was prepared by weighing 2.50 ± 0.01 g into a 100-mL volumetric flask and diluting to volume with *o*-xylene.

Procedure. A 60–70 ± 0.1 mg sample of dried cellulose ether was weighed into a 5.0-mL Reactivial. An amount of apidic acid equal to or as much as twice the sample weight was added. Two milliliters of the internal standard stock solution was pipeted to the Reactivial and 2 mL of hydriodic acid added. The vial was immediately tightly capped with the Mininert valve top and weighed before insertion into the hot heating block. Samples were reacted for 1 h at 150 °C with agitation by shaking after 5 and 30 min. Since the glass vials were under pressure during the reaction, the manual agitation was conducted with caution behind a safety shield in a fume hood. Chemical workers goggles and insulated gloves were worn to prevent exposure to hydriodic acid in case any accidental release of reaction contents occurred.

After 1 h the vial was removed from the block, cooled for approximately 45 min and reweighed to determine any loss due to leakage.

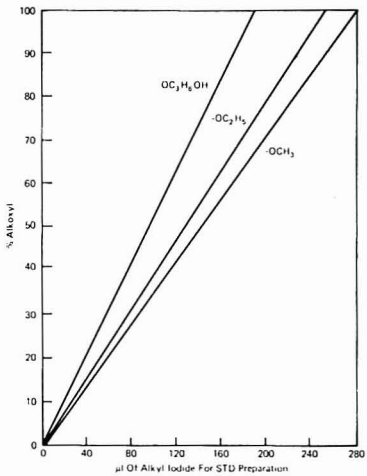

Figure 1. Alkyl iodide – alkoxyl equivalency

CALIBRATION

Two calibration standards were prepared using the following procedure and the average component response factor determined to calibrate the integrator. Four milliliters of hydriodic acid were pipetted into a 3-dram vial containing 120–140 mg of adipic acid. Two 2.0-mL aliquots of the internal standard stock solution were added with the same pipet used for the preparation of the samples and the vial was capped tightly with a Mininert valve cap using Teflon tape as a sealant for the vial threads. Based on the percent alkoxyl substitution anticipated in the prepared samples, the quantity of each respective alkyliodide needed for calibration was determined according to the graph in Figure 1.

Each alkyliodide was introduced to the tared vial through the Mininert valve top with a 100-μL syringe and the vial weighed to the nearest 0.1 mg after each addition. The equivalent weight of alkoxyl added in mg was determined according to the following equations:

$$\text{mg } OCH_3 = \text{g } CH_3I \left(\frac{\text{mol wt } OCH_3 \times 1000}{\text{mol wt } CH_3I} \right)$$

$$\text{mg } OC_2H_5 = \text{g } C_2H_5I \left(\frac{\text{mol wt } OC_2H_5 \times 1000}{\text{mol wt } C_2H_5I} \right)$$

$$\text{mg } OC_3H_7O = \text{g } C_3H_7I \left(\frac{\text{mol wt } OC_3H_7O \times 1000}{\text{mol wt } C_3H_7I} \right)$$

Two microliters of the upper (xylene) layer of each prepared standard was injected into the gas chromatograph (Figure 2) and the component response factor was determined by programming the integrator. The following equations can be used if a data acquisition device is not available.

$$\text{response factor} = \frac{\text{mg alkoxyl in std}}{\text{alkyliodide peak area}} \times \frac{\text{toluene peak area}}{\text{mg toluene in std}}$$

A variance of greater than 5% relative between two component factors was considered unacceptable and a third standard was prepared to resolve the difference. The integrator was pro-

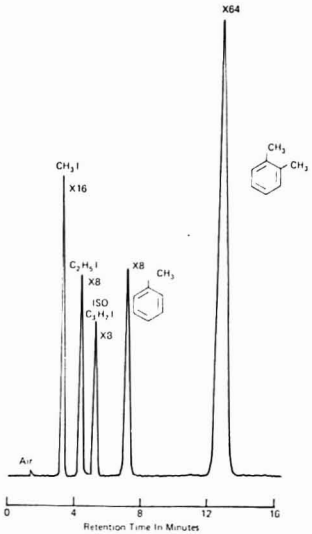

Figure 2. Chromatogram of alkyliodides. Column 10-ft UC W98 methyl silicone; helium 20 mL/min. Temperature 100 °C: 170 mA

grammed to report weight percent alkoxyl by entering the internal standard and sample weights.

Two microliters of the upper (xylene) layer of the sample was injected and the weight percent alkoxyl substitution was determined. See Equation 1.

RESULTS AND DISCUSSION

The success of the new Zeisel gas chromatographic method depends on the quantitative conversion of the substituted alkoxyl unit to the corresponding iodide by reaction with hydriodic acid. This conversion proceeds through a postulated vicinal 1,2-diiodo intermediate (I).

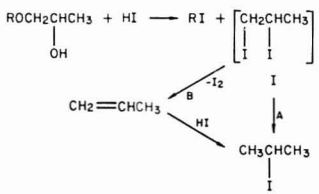

Its existence is presumed to be transitory since it has never been isolated or prepared synthetically.

The intermediate proceeds through two routes to the desired alkyliodide. The first route (A) is the direct conversion to 2-propyl iodide through a biomolecular iodine elimination reaction. This reaction is acid catalyzed (*17*) and quantitative conversion is achieved by using organic acids such as adipic, succinic, formic, acetic, citric, or valeric.

In the absence of an acid catalyst, the reaction with hydriodic acid proceeds through an alternative route (B) resulting in the quantitative conversion of alkoxyl unit to propylene and isopropyl iodide. Reactions performed at temperatures between 130 and 170 °C in the absence of adipic acid yielded low, reproducible, hydroxy propoxy values but quantitative methoxyl values (Table I).

Support for this mechanism was obtained when the off gas from acid catalyzed reactions showed appreciable lower propylene levels than nonacid catalyzed reactions. If adipic acid was catalyzing the addition of hydriodic acid to propylene, there would also be a significant reduction in the propylene content in the reactor off gas. This was not found to be true since the addition of a measured quantity of propylene to hydriodic acid with and without adipic acid at a constant rate yielded the same quantity of 2-iodopropane.

Table I. Adipic Acid as Catalyst for Determination of Methoxy and Hydroxy Propyl Substitution

Propylene Glycol Monomethyl Ether (Theor. 34.4% OCH_3, 65.6% OC_3H_7)		
method	% OCH_3	% OC_3H_7
Zeisel-GC	33.8, 33.6	29.2, 28.9
Zeisel-GC with adipic acid	33.9, 33.9	63.9, 63.7

Propylene Glycol (Theor. 76.4% OC_3H_7)	
method	% OC_3H_7
Zeisel-GC	44.5, 44.6
Zeisel-GC with adipic acid	75.0, 74.8

According to Morgan (*18*), the fate of propylene thus formed should be similar as long as the reaction takes place in a sealed tube and propylene is kept in constant contact with hydriodic acid. It has been reported (*19–25*), however, that the addition of hydriodic acid to ethylene in the gas phase is kinetically faster than the addition to propylene. This then could explain why the propylene generated from the Zeisel reaction of propylene glycol and propylene glycol monomethyl ether does not react quantitatively as does ethylene in ethylene glycol monomethyl ether.

The presence of xylene during the course of a reaction is an important factor in obtaining quantitative 2-iodopropane values due to the elimination of the reported disproportionation reaction (*24*). This reaction occurs when the iodide is not extracted from the hydroiodic acid thus:

$$2C_3H_7I \rightarrow C_3H_8 + C_3H_6 + I_2$$

Support for this disproportionation step was obtained by heating 2-iodopropane in the presence of hydroiodic acid with and without *o*-xylene being present. Without xylene, both propane and propylene were present in the reaction headspace and a loss of 2-iodopropane was noted.

With *o*-xylene no propane was observed and essentially 100% of the 2-iodopropane was recovered.

Earlier studies by Merz (*24*) on the hydriodic acid cleavage of polypropylene oxide oligomers indicated the formation of significant quantities of propionaldehyde. In the current method, there is no evidence for the formation of propionaldehyde. Samples of the xylene and hydroiodic acid layers of reactions performed with and without adipic acid were analyzed by proton NMR. No evidence for components other than 2-iodopropane, which was larger in the adipic catalyzed reactions, was observed.

Quantitative conversion was somewhat dependent on structure. Model compounds containing ethoximer or propoximer content greater than 2 such as tetraethylene glycol or tetrapropylene glycol required higher temperatures, more catalyst, and longer reaction times to obtain quantitative recovery. Alkoxyl groups substituted on aromatic rings also required more severe conditions.

Most substitutions evaluated, however, would react quantitatively at temperatures between 130–180 °C. Some hydroxypropoxy determinations would be accompanied by the

$$\% \text{ alkoxyl} = \frac{\text{alkyliodide peak area} \times \text{average component response factor} \times \text{mg toluene in sample}}{\text{toluene peak area} \times \text{mg sample}} \times 100 \quad (1)$$

Table II. Validation and Precision

method	% OCH_3	% rel 2σ	(# runs)	% OC_3H_6OH	% rel 2σ	(# runs)
Hydroxypropyl Methylcellulose Sample A						
ASTM D-2363-72	29.45	1.4	(8)	7.71	8.0	(10)
Zeisel-GC	30.17	1.7	(10)	8.17	4.3	(10)
Sample B						
ASTM D-2363-72	27.45	1.1	(7)	4.59	21.2	(8)
Zeisel-GC	27.28	1.2	(8)	4.37	0.8	(8)
Sample C						
ASTM D-2363-72	21.27	1.04	(8)	12.69	6.4	(10)
Zeisel-GC	21.32	1.8	(11)	13.52	2.7	(11)
Methyl Cellulose Sample D						
ASTM D-2363-72	30.09	0.72	(5)	-	-	-
Zeisel-GC	30.06	0.80	(7)	0.39	10.2	(7)

method	% OC_2H_5	% rel 2σ	(# runs)
Ethyl Cellulose Sample E			
ASTM D-2363-72	46.20	0.96	(5)
Zeisel-GC	46.35	0.54	(12)
Ethyl Cellulose Sample F			
ASTM D-2363-72	49.01	1.61	(8)
Zeisel-GC	48.79	0.42	(14)

Table III. Different Cellulose Ethers by Zeisel-Gas Chromatography Using Adipic Acid Catalyst

sample	cellulose type[a]	Zeisel-GC % OCH_3	Zeisel-GC % OC_2H_5	Zeisel-GC % OC_3H_6OH	equiv. % OCH_3	ASTM D-2363-72 % OCH_3
Henkel	MC	25.9	0.6	0.4	26.3	26.7
Brit. Cellanese	MC	26.7	<0.1	<0.1	26.7	26.9
Shin Etsu	HPMC	28.0	<0.1	9.0	31.8	31.8
Natl. Starch	no sub.	<0.1	<0.1	<0.1	<0.1	0.8
Stein Hall	no sub.	0.1	<0.1	0.1	0.2	1.0
Stein Hall	HP	<0.1	<0.1	12.7	5.2	5.3
Hercules	HP	0.2	<0.1	67.3	36.8	37.4
Stein Hall	CMHP	<0.1	<0.1	14.6 (14.5)	-	-
Dow	HEHPMC	10.4 (10.4)	24.1 (24.1)	14.4 (14.1)	-	-
Dow	HEMC	0.6 (0.5)	31.1 (31.0)	<0.1 (<0.1)	-	-
Hoechst	HEMC	24.6 (25.1)	(1.8) (1.8)	<0.1 (<0.1)	-	-
ICI	MCET	3.9 (4.1)	14.1 (14.9)	<0.1 (<0.1)	-	-

[a] MC = methoxyl, ET = ethoxyl, CM = carboxymethyl, HE = hydroxyethyl, HP = hydroxypropyl, (-) = duplicate determinations.

formation of *n*-propyliodide when the reaction temperatures were outside these limits. In general its appearance served as an innate indicator that the reaction had not gone to completion.

The standards were prepared over hydriodic acid and adipic acid to negate the partition coefficient of the alkyl iodides in the acid layer. While the ethyl and propyl iodides partition less than 1% relative, methyl iodide losses can be as large as 3% relative. Standards prepared in this fashion had a shelf life of 2–3 months, when stored at 0 °C.

VALIDATION, PRECISION

The results of analyzing four samples of hydroxypropylmethyl cellulose containing significantly different amounts of methoxyl and hydroxypropyl substitution by the new Zeisel-GC technique, standard Zeisel distillation, and chromic acid oxidation distillation (26) are shown in Table II.

The relative precision at the 95% confidence level for the GC method was found to range from ±0.8 to ±1.8% for methoxyl substitution and 1.8 to 4.3% for hydroxypropyl.

Similar methoxy values in terms of both precision and quantity were found using the two techniques but considerably worse precision, ±20% relative, was experienced for the chromic acid oxidation. Comparative ethoxyl values obtained on samples of *O*-ethyl cellulose show similarly good agreement.

The ability of the method to analyze a wide variety of substituted cellulose ethers is shown in Table III.

The absence of a blank and the selectivity of the Zeisel gas chromatographic technique provide a more precise definitive analysis than can be accomplished with the two distillation techniques, especially when low levels of one type of alkoxyl substitution is present in another type of substituted cellulosic ether.

Because of its speed and versatility, this procedure should provide useful information in the characterization of butoxy or even phenoxy substituted ethers as well as acrylate and maleate esters.

ACKNOWLEDGMENT

The authors thank L. Piper and R. Graunke for their advice

and direction as well as D. L. Lock and Sue Arters for their aid in the method development, and Bill Kracht for his NMR and mass spectral interpretation.

LITERATURE CITED

(1) "Methods In Carbohydrate Chemistry", Vol. III; Whistler, R. L., Ed.; Academic Press: New York, 1963, pp 305–314.
(2) Martin, F.; Vertalier S. XV International Congress on Pure and Applied Chemistry (Analytical Chemistry), Lisbon, September 8 to 16, 1956.
(3) Haslam, J.; Hamilton, J. B.; Jeffs, A. R. *Analyst (London)* **1958**, *83*, 66.
(4) Cobler, J. G.; Samsel, P. E.; Beaver, G. H. *Talanta* **1962**, (9), 473–481.
(5) Miller, D. L.; Samsel, E. P.; Cobler, J. G. *Anal. Chem.* **1961**, *33*, 677.
(6) Sproek, K. F.; Danyi, M. D., *Anal. Chem.* **1962**, *34*, 1957.
(7) Misui, T.; Kitamura, Y. *Microchem. J.* **1963**, *7*, 141.
(8) Karnisin, A. A. *Fresenius' Z. Anal. Chem.* **1968**, *23*, 1072.
(9) Merz, W. *Fresenius' Z. Anal. Chem.* **1967**, *232*, 82.
(10) Ehrenberger, F. *Fresenius' Z. Anal. Chem.* **1965**, *210*, 424.
(11) Lemieux, R. V.; Purves, C. B. *Can. J. Res., Sect. B* **1947**, *25*, 485.
(12) Jacin, H.; Slamski, J. M. *Anal. Chem.* **1970**, *42*, 801.
(13) Henkel and Cie, *Fresenius' Z. Anal. Chem.* **1974**, *271*(1), 31.
(14) Ivannikova, L. B.; Tropina, V. A.; Vasilenko, A. M.; Prokofeva, M. V. *Khim. Drev.* **1975**, (6), 22–5 (Russ.).
(15) Ho, F.; Kohler, R. R.; Ward, G. A. *Anal. Chem.*, **1972**, *44*, 178.
(16) Clemett, C. J. *Anal. Chem.* **1973**, *45*, 166.
(17) Shriner, R. L.; Fuson, R. C.; Curtin, D. Y. "The Systematic Identification of Organic Compounds", Vol. 4; John Wiley and Sons: New York; p 116.
(18) Morgan, P. W. *Ind. Eng. Chem., Anal. Ed.*, **1946**, *18*, 500.
(19) Benson, S. W.; et al. *J. Chem. Phys.*, **1964**, *40*, 2946.
(20) Benson, S. W.; et al. *J. Chem. Phys.* **1962**, *37*, 1081.
(21) Benson, S. W.; et al. *J. Chem. Phys.* **1963**, *39*, 132.
(22) Benson, S. W.; et al. *J. Chem. Phys.* **1963**, *38*, 882.
(23) Benson, S. W.; et al. *J. Chem. Phys.* **1963**, *38*, 1945.
(24) Holmes, J. L.; Maccoll, A. *J. Chem. Soc.* **1963**, 5919.
(25) Merz, W. *Anal. Chim Acta* **1967**, *232*, 82.
(26) Standard Methods of Testing Hydroxypropyl in Hydroxypropyl Methylcellulose, ASTM-D-2363-72.

RECEIVED for review October 27, 1978. Accepted August 3, 1979.

Reduction in Sample Foaming in Purge and Trap Gas Chromatography/Mass Spectrometry Analyses

M. E. Rose and B. N. Colby*

Chemistry and Chemical Engineering, Systems, Science and Software, P.O. Box 1620, La Jolla, California 92038

In the determination of volatile organic compounds in industrial effluent waters and process streams by purge and trap GC/MS, foaming of the sample has been a serious problem. The foam tends to enter the transfer line leading to the sorbent trap and may actually reach the trap itself. This has several negative effects on the current and subsequent determinations, including deactivation of the trap and introduction of thermal decomposition products from labile, nonvolatile materials. Two methods to reduce foaming are evaluated, one employing a silicone surfactant and a second involving heat dispersion of the foam. The qualitative and quantitative aspects of these two foam-reduction methods are described for volatile priority pollutants in spiked pure water and soap solutions.

As a result of the "Consent Decree", the United States Environmental Protection Agency (EPA) has undertaken a major sampling and analysis effort to determine a group of materials, called priority pollutants, in industrial waste waters. In order to achieve their goals, a screening protocol (*1*) was established for laboratories to use as a guide in carrying out the investigations. With this protocol, the volatile organic priority pollutants are determined using a Purge and Trap (PAT) sample preparation procedure and combined gas chromatographic/mass spectrometric (GC/MS) analysis. The PAT methodology was developed by EPA personnel (*2, 3*) and has proved extremely effective for the analysis of drinking water (*4–6*). With the PAT technique, volatile, slightly soluble molecules in the water sample are entrained by a stream of pure inert gas as it is purged through the sample. The purge gas is then passed through a sorbent trap where the entrained molecules are retained. Once this purge and trap process is complete, the trap is backflushed and the contents are thermally desorbed into a GC/MS for analysis. For most samples, this process is straightforward and determinations proceed with little difficulty. Occasionally, however, a series of samples will be encountered which foam excessively when purged. If foam is allowed to traverse the gas transfer lines and enter the sorbent trap, several negative effects on the current and subsequent analyses can be expected if the trap is not replaced and the transfer line thoroughly cleaned. These negative effects include deactivation of the trap and introduction of thermal decomposition products from nonvolatile labile materials. For samples which do not form a highly persistent foam, it is possible to reduce foaming by reducing the purge gas flow rate slightly and/or by inserting a mechanical barrier to the foam, such as a bundle of capillary tubes, just past the purge tube. For other samples, these steps are insufficient and alternative means are required. One alternative is the addition of surfactants such as silicone antifoaming agents and a second is to apply heat to dissipate the foam. The purpose of the studies presented here was to qualitatively and quantitatively evaluate these two approaches to foam reduction for the determination of volatile priority pollutants.

EXPERIMENTAL

Apparatus. A Tekmar Model LSC-1 purge and trap unit, incorporating the manufacturer's recommended modifications, was used throughout the study. The desorbed sample gases were transferred through an 0.028-i.d. stainless steel line directly onto the head of the GC column in a DuPont Model 321 GC/MS. The 8 ft long × 2 mm i.d. glass column was packed with Carbopak C (60/80 mesh) coated with 0.2% Carbowax 1500. The column oven was programmed from 50 to 185 °C at 8 °C per min after a 4-min hold. The mass spectrometer was scanned from 45 to 300 amu at 4 s per scan; emission current was 500 μA and electron energy was 73 eV. Data acquisition and processing was done automatically by a Finnigan/INCOS data system.

Reagents. Two series of standard solutions were prepared from unchlorinated distilled water (Arrowhead, Los Angeles, Calif.) which had been purged until analysis indicated it to be free of volatile organic compounds. Both series of solutions were identically prepared except that the second series of solutions contained approximately 0.5% (v/v) of dishwashing detergent (Purex Balsom Trend). Aliquots of commercially prepared (Supelco, Bellefonte, Pa.) priority pollutant standards were added to the pure water using a Hamilton microsyringe. The resulting solutions contained priority pollutants at concentration levels of 1, 3, 10, 30, 100, 300, and 1000 μg/L. The samples were analyzed

0003-2700/79/0351-2176$01.00/0

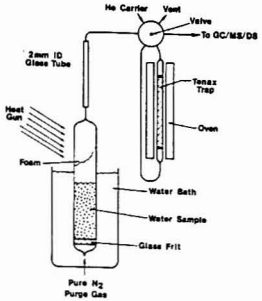

Figure 1. Apparatus configuration for heat dispersion of foam

Table I. Quantitation Masses

compound name	quantitation mass	internal standard
benzene	78	BCM[a]
carbon tetrachloride	117	BCM
chlorobenzene	112	DCB[b]
1,2-dichloroethane	98	BCM
1,1,1-trichloroethane	97	BCM
1,1-dichloroethane	63	BCM
1,1,2-trichloroethane	97	DCB
chloroform	83	BCM
1,1-dichloroethylene	96	BCM
1,2-*trans*-dichloroethylene	96	BCM
1,2-dichloropropane	112	BCM
ethylbenzene	106	DCB
methylene chloride	84	BCM
bromoform	173	DCB
dichlorobromomethane	127	BCM
trichlorofluoromethane	101	BCM
chlorodibromomethane	127	DCB
tetrachloroethylene	164	DCB
toluene	92	DCB
trichloroethylene	130	BCM

[a] Bromochloromethane (BCM), quantitation mass = 128. [b] 1,4-Dichlorobutane (DCB), quantitation mass = 55.

in order of concentration, starting at 1 μg/L.

For those soap solutions analyzed using the silicone antifoaming agent, 1 μL of the agent (Dow, Antifoam A) was added to the purge tube immediately following the 5-mL sample. The surfactant was used as supplied; no attempts at purification were made.

Procedure. Five-milliliter sample aliquots were purged with pure nitrogen at atm cm³ per min. After a 12-min purge interval, a 180 °C desorb cycle was activated for 3 min with a helium carrier gas flow rate of 20 mL per min.

With the heat dispersion method, the purge tube was placed in a small water bath at ambient temperature (Figure 1). When purging was initiated, foam would rise in the tube and, as it neared the top of the tube, a hair dryer-style gun was used to direct a stream of hot air at the top of the sample tube. The heat causes the foam to break down before it can enter the transfer line leading to the trap. A 6-in. section of a 2-mm i.d. glass tube was placed just above the purge tube to act as a condenser for water vapor generated during the heating process. When droplets could be detected visually in this condenser, it was replaced. The condenser helped to reduce the quantity of water vapor entering the sorbent trap.

An automatic GC/MS data reduction procedure was employed throughout the study to identify priority pollutants and to determine relative response values used for quantitation. Relative response values were calculated by dividing mass chromatogram areas for the quantitation masses of the priority pollutants by those of the internal standards (Table I). Calibration curves were prepared by carrying out logarithmically weighted linear regressions of relative response vs. concentration.

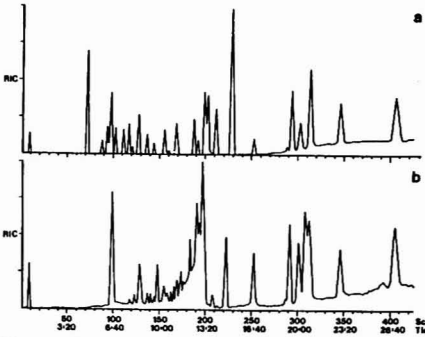

Figure 2. Reconstructed gas chromatograms for (a) 100 μg/L pure standard mixture and (b) 100 μg/L standard mixture containing soap when foam was allowed to enter the sorbent trap

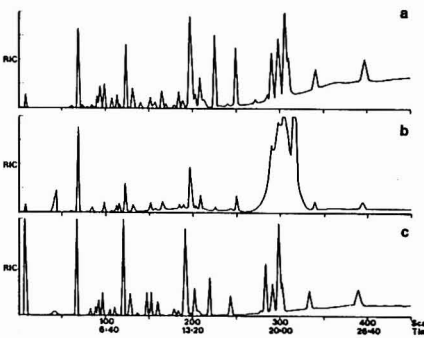

Figure 3. Reconstructed gas chromatograms for 10 μg/L pure standard mixture (a) with/without soap, (b) using a silicone antifoaming agent, and (c) heat dispersion to reduce foaming

RESULTS AND DISCUSSION

The significance of keeping foam from entering the sorbent trap is illustrated in Figure 2 for two 100 μg/L samples; one a pure standard solution and the second a soap solution. A small amount of foam from the soap solution sample was allowed to enter the trap. Several of the early eluting components detected in the pure standard solution are not readily detected when foam has entered the trap. It is believed that this is due to a modification of sorbent surfaces which makes it less effective as a sorbent. However, it could also be due to an alteration in thermal desorption characteristics. Second, note that several spurious peaks are present in Figure 2b which are not present in Figure 2a. These are believed to be decomposition products of thermally labile nonvolatile materials present in the foam. However, it is possible that they could be due to volatile, water-soluble compounds which are not effectively entrained by the purge gas under normal operating conditions. Irrespective of the reasons, when foam enters the trap, both qualitative and quantitative analyses for priority pollutants are severely interfered with.

A qualitative comparison of chromatograms obtained using the two foam reduction methods is given in Figure 3 for 10 μg/L samples. Note that the silicone antifoaming agent, although it eliminates the foaming problem, results in the addition of spurious peaks to the chromatogram. The severity of these interferences increases with each additional analysis

Table II. Correlation Coefficients of Calibration Curves

compound name	correlation coefficients: pure standard	silicone antifoaming agent	heat dispersed foam
benzene	0.994	0.994	0.992
carbon tetrachloride	0.991	0.986	0.995
chlorobenzene	0.994	0.999	0.995
1,2-dichloroethane	0.993	0.994	0.991
1,1,1-trichloroethane	0.996	0.996	0.998
1,1-dichloroethane	0.993	0.994	0.997
1,1,2-trichloroethane	0.994	0.995	0.998
chloroform	0.919	0.930	0.936
1,1-dichloroethylene	0.981	0.956	0.994
1,2-*trans*-dichloroethylene	0.992	0.998	0.997
1,2-dichloropropane	0.992	0.987	0.994
ethylbenzene	0.995	0.990	0.995
methylene chloride	0.999	0.994	0.997
bromoform	0.991	0.998	0.990
dichlorobromomethane	0.990	0.989	0.983
trichlorofluoromethane	0.992	0.995	0.997
chlorodibromomethane	0.994	0.998	0.999
tetrachloroethylene	0.995	0.998	0.995
toluene	0.999	0.999	0.999
trichloroethylene	0.993	0.993	0.995
mean	0.989	0.989	0.992

Table III. Error Factors for Data Compared to the Regression Line through That Set of Data

compound name	error factor: pure standard	silicone antifoaming agent	heat dispersed foam
benzene	1.24	1.23	1.24
carbon tetrachloride	1.24	1.36	1.16
chlorobenzene	1.25	1.05	1.23
1,2-dichloroethane	1.21	1.19	1.22
1,1,1-trichloroethane	1.17	1.19	1.13
1,1-dichloroethane	1.23	1.22	1.13
1,1,2-trichloroethane	1.24	1.21	1.13
chloroform	2.16	1.84	1.79
1,1-dichloroethylene	1.45	1.77	1.25
1,2-*trans*-dichloroethylene	1.27	1.12	1.14
1,2-dichloropropane	1.27	1.29	1.20
ethylbenzene	1.23	1.25	1.24
methylene chloride	1.06	1.13	1.17
bromoform	1.24	1.11	1.34
dichlorobromomethane	1.24	1.25	1.21
trichlorofluoromethane	1.25	1.18	1.15
chlorodibromomethane	1.17	1.10	1.09
tetrachloroethylene	1.22	1.08	1.20
toluene	1.09	1.08	1.10
trichloroethylene	1.26	1.22	1.17
mean	1.27	1.24	1.22

employing the silicone antifoaming agent, and it ultimately became necessary to dismantle the PAT system, replace the sorbent trap, and bake clean transfer lines and flow directing valve. This cleaning process was necessary after approximately every tenth run using the antifoaming agent if all priority pollutants were to remain identifiable at concentrations down to 10 μg/L. It is possible that by using less of the antifoaming agent, contamination would be reduced. However, all attempts to find a suitable solvent in which to dilute it were unsuccessful; 1 μL was the minimum volume which could be handled.

Contamination did not result when using the heat dispersion method; the chromatograms remained qualitatively identical to those of nonfoaming samples for indefinite periods. In excess of 60 foaming samples were analyzed using the heat foam dispersion method with no noticeable change in detection limits and zero incidence of interferences. It is possible, however, that the use of elevated temperatures could lead to sample degradation in some instances. Although this did not appear to be the case with priority pollutants in soap solutions, it should be considered a possibility with other compounds and with other matrices.

Both approaches to foam reduction had some effect on relative peak areas and, as a consequence, the accuracy of the determinations. This can be seen in the chromatograms shown in Figure 3. In order to evaluate the precision and accuracy provided by the two foam reduction methods, data obtained for the three sets of standard solutions were compared. Table II shows that the correlation coefficients for the priority pollutant calibration curves obtained from pure standard solutions and soap solutions, using either of the foam reduction methods, are essentially equivalent. The correlation coefficient for chloroform was the only one found to be uniformly less than 0.99. The problem with the chloroform data is the result of nonlinear response; the relative response drops off more rapidly at low concentration than at high concentration. In other purge and trap experiments performed in this laboratory, nonlinearity for the relative response of chloroform has not been obvious and no reason for the phenomenon is known. If chloroform values below 10 μg/L are rejected, the correlation coefficients for chloroform in all three sets of data are greater than 0.995. However, because the statistical evaluations performed in this study were for the sole purpose of evaluating the data rather than rejecting potential outliers, the lower values for correlation coefficients were included in Table II.

In screening industrial waste waters and process streams for priority pollutants using the EPA protocol, the intent has been to provide data with accuracy sufficient to place each data point, x, within a window defined by −50% and +100%. That is:

$$\frac{1}{2}x \leq x \leq 2x$$

or

$$x \leq 2^{\pm 1}x$$

That is; the data should be "within a factor of two". Because of the geometrical nature of this goal, it is convenient to consider errors in terms of the factor by which a data point deviates from the calibration curve or regression line. For the purpose of this presentation, error is defined as:

$$\text{error factor} = \left(\frac{\text{known concentration}}{\text{calculated concentration}}\right)^{\pm 1} \geq 1$$

Thus, a +100% deviation from the calibration curve is numerically equivalent to a −50% deviation.

When the error factors for each of the priority pollutants in each of the three sets of data are determined using the regression line through that set of data as a reference or calibration curve, the values shown in Table III are produced. The similarity in the mean values is consistent with the correlation coefficients already mentioned. Of the priority pollutants investigated, only chloroform failed to meet the "factor of two" criteria; all others fell well within the window. It should be pointed out that this approach to evaluating accuracy involves an implicit correction for matrix effects which might alter purging and/or trapping efficiencies. Consequently, the error factors in Table III should be considered as best case values.

If the pure standard data are used as the calibration or working curves, and the soap solution data treated as if it were

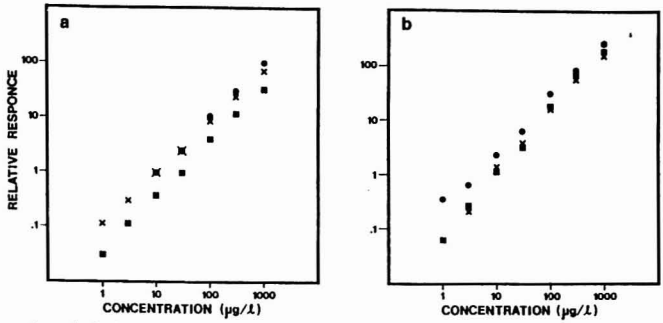

Figure 4. Comparison of acquired relative response values for (a) toluene and (b) 1,1,1-trichloroethane plotted for samples analyzed (x) without soap and with soap using (●) a silicone antifoaming agent and (■) heat dispersion to reduce foaming

Table IV. Error Factors Using Pure Standard Solution Data as a Calibration Curve

compound name	error factors: silicone antifoaming agent	error factors: heat dispersion
benzene	1.22	1.51
carbon tetrachloride	1.49	1.20
chlorobenzene	1.41	2.59
1,2-dichloroethane	1.29	1.32
1,1,1-trichloroethane	1.99	1.15
1,1-dichloroethane	1.29	1.85
1,1,2-trichloroethane	1.71	1.89
chloroform	1.96	2.40
1,1-dichloroethylene	2.00	1.75
1,2-*trans*-dichloroethylene	1.36	1.44
1,2-dichloropropane	2.21	1.59
ethylbenzene	1.34	2.34
methylene chloride	1.15	3.16
bromoform	2.08	2.25
dichlorobromomethane	1.45	1.39
trichlorofluoromethane	1.42	1.17
chlorodibromomethane	1.84	2.69
tetrachloroethylene	1.34	4.04
toluene	1.38	2.71
trichloroethylene	1.22	1.47
mean	1.56	2.00

unknown, the error factors shown in Table IV are obtained. Even though these are within the factor-of-two window on the average, there are several compounds which fall outside that window. This is believed to be the result of matrix effects which alter the relative purging efficiencies of priority pollutants and internal standards. These relative differences could be due to solubility changes or perhaps alterations in purge gas bubble size which might affect entrainment. Figure 4 illustrates examples of these matrix effects for toluene and 1,1,1-trichloroethane. Note that the relative response values for toluene obtained using the silicone antifoaming agent, correspond fairly well with those of the pure standard while those acquired using the heat dispersion method do not. It seems that soap solution lowers the purging efficiency of toluene relative to the internal standard, whereas soap solution plus silicone antifoaming agent results in approximately equivalent purging efficiencies for the two. In fact, all the priority pollutants referenced to the second internal standard and determined using heat dispersion, gave low relative response values compared to those of pure standards. If only those priority pollutants determined using the first internal standard were used to calculate the mean error factor for the heat dispersion method, a value of 1.61 is produced. This is comparable, on the average, with that of the silicone antifoaming agent approach. Essentially, the opposite situation to toluene is encountered with 1,1,1-trichloroethane, which exhibits an increased relative response with soap solution treated with silicone antifoamant and essentially no change with heat dispersion. Although matrix effects are believed to be the major reason for apparent differences in relative purging efficiencies, it is possible that thermal effects could have some influence on the data acquired, using the heat dispersion method. Thermally induced enhancement of purging efficiency has been reported for several ketones from an aqueous salt solution at 50 °C compared to 23 °C (*6*). In the studies reported here, however, the majority of the sample volume was at ambient temperature surrounded by the water bath.

It is interesting to note that there is no clear relationship between the relative magnitude of matrix effect, i.e., error factor in Table IV, and structural similarities of the priority pollutants. This is clearly illustrated for di- and trichloroethanes. 1,1- and 1,2-dichloroethane have fairly small error factors with the silicone antifoaming agent and soap, while 1,1,1- and 1,1,2-trichloroethane have larger error factors. However, with heat dispersion, it is the 1,2-di- and 1,1,1-trichloroethanes which have small error factors. Apparently, compounds which behave similarly in one instance, may not in the next. This tends to suggest that a universally good internal standard for any given compound may not exist. Because of this, it seems likely that standard additions, rather than the working curve approach to quantitation, would result in more accurate results. Standard additions accuracy should approach that represented by the error factors given in Table III or about 15 to 25%.

In comparing the two foam reduction procedures, the heat dispersion method is superior qualitatively because it does not introduce interfering substances into the analyses. It is also better in a practical sense because it does not necessitate dismantling and cleaning of the purge and trap apparatus after several successive runs. The silicone antifoaming agent provides more accurate quantitation when the soap solution was referenced to pure standards; however, both approaches to foam reduction exhibited matrix effects. Because of these matrix effects, standard additions or some other matrix compensation approach should be employed for accurate quantitation. Alternative approaches are currently being investigated and will be reported on in the future.

LITERATURE CITED

(1) U.S. Environmental Protection Agency, "Sampling and Analysis Procedures for Screening of Industrial Effluents for Priority Pollutants"; Environmental Monitoring and Support Laboratory: Cincinnati, Ohio, April 1977.

(2) Bellar, T. A.; Lichtenberg, J. J. J. Am. Water Works Assoc. 1974, 66, 739.
(3) Bellar, T. A.; Lichtenberg, J. J.; Kroner, R. C. J. Am. Water Works Assoc. 1974, 66, 703.
(4) Brass, H. J.; Feige, M. A.; Holloran, T.; Mello, J. W.; Munch, D.; Thomas, R. F. "The National Organic Monitoring Survey: Samplings and Analyses for Purgeable Organic Compounds", in "Drinking Water Quality Enhancement Through Source Protection", Pojasek, Robert, Ed.; Ann Arbor Science Publishers: Ann Arbor, Mich., 1977.
(5) Kopfler, F. C.; Melton, R. G.; Lingg, R. D.; Coleman, W. E. "GC/MS Determination of Volatiles for the National Organics Reconnaissance Survey (NORS) of Drinking Water", in "Identification and Analysis of Organic Pollutants in Water", Keith, L. H., Ed.; Ann Arbor Science Publishers: Ann Arbor, Mich., 1977.
(6) Mieure, J. P.; Mappes, G. W.; Tucker, E. S.; Dietrich, M. W. "Separation of Trace Organic Compounds from Water", in "Identification and Analysis of Organic Pollutants in Water", Keith, L. H., Ed.; Ann Arbor Science Publishers: Ann Arbor, Mich., 1977.

RECEIVED for review June 4, 1979. Accepted August 13, 1979.

Trace Enrichment with Hand-Packed CO:PELL ODS Guard Columns and Sep-Pak C_{18} Cartridges

William A. Saner,* J. Richard Jadamec, and Richard W. Sager

U.S. Coast Guard Research and Development Center, Avery Point, Groton, Connecticut 06340

Timothy J. Killeen

Statistics Department, University of Connecticut, Storrs, Connecticut 06368

CO:PELL ODS-packed guard columns were used for the trace enrichment (TE) of seawater-soluble fractions of a bunker-C oil. Extracted compounds showed predominantly nonlinear accumulation rates with respect to sample volume. In addition, Sep-Pak C_{18} cartridges were also used for trace enrichment and displayed decreases in extraction efficiency with increasing sample volumes for five model compounds in seawater. An equation defining the decrease in extraction efficiency of benzene with sample volume was used to predict the sampling volume at which the amount of benzene present on the Sep-Pak cartridge would be maximal.

Various adsorbents have been demonstrated as effective matrices for the removal of organic compounds from water. Many of these adsorbents are polymers and/or copolymers of styrene/divinylbenzene and include XAD-2 (*1*, *2*), XAD-4 (*3*, *4*), IRA-93 (*5*), and Porapak Q (*6*). In addition, the slightly less hydrophobic acrylic ester polymers such as XAD-7 (*7*), and XAD-8 (*8*) have been used to adsorb more polar compounds from water. Both XAD-4 and XAD-8 (50:50) were used in the same column to extract organics of varying polarities from drinking water (*9*). Spheron-SE has also been used to analyze trace amount of impurities in water (*10*); it represents both the acrylic ester and the styrene-type adsorbents since it is a copolymer of styrene and ethylene dimethacrylate. In addition, polyurethane, (amide ester polymer) (*11*), and Tenax-GC (phenylene oxide polymer) (*12*) have also been shown capable of adsorption of trace levels of organics from water.

More recently (after 1975), reverse-phase ODS liquid chromatographic packing has also been used to extract and concentrate trace levels of organics from water. Kirkland first proposed the possibility of preconcentration on the head of an ODS packed column from large volume aqueous injections in 1974 (*13*). Creed (*14*) and Chisler et al., (*15*) were among the first to demonstrate the potential of ODS as a means of trace enrichment (TE) of aqueous samples (the extraction and concentration of organics from large injection volumes onto ODS packing). Other workers have utilized the trace enrichment technique for the adsorption of organics from various aqueous samples including distilled water (*16*), drinking water (*17*, *18*), urine (*19*), chlorinated water (*20*), natural water (*21*), wastewater (*22*), and seawater (*23*).

The technique of trace enrichment affords a means of concentration and collection of sample in the same step. Because of its intrinsic simplicity, it would seem to allow easy on-site collection of samples. However, since recovery of compounds from water increases as an inverse function of their solubility in water (*15*), then accurate quantification can be carried out for an organic compound in water only by first measuring extraction efficiency for that model compound to correct for compound-to-compound recovery ("extraction") differences. For those specialized applications where only one or a very limited number of compounds are sought, use of this model compound approach is feasible. However, when one is dealing only with unknowns, accurate quantification, for determining extent of spillage after accidental discharge dictates some other approach. Thurman et al. (*8*) used water solubility to predict k', and consequently calculated extraction efficiency (breakthrough volume) for 20 test solutes on XAD-8 resin. Alternatively, k' values could be used to predict water solubilities and, as a result, extraction efficiencies for unknown solutes trace enriched on ODS.

The problem of variable extraction efficiency from solute to solute was recognized. Any dependence of extraction on sampling volumes or on the presence of other solutes, either already adsorbed on the ODS prior to extraction, or coextracted as multiple solutes present in the same water sample, would be necessary in order to use the technique of trace enrichment quantitatively. Further, if the mechanism of decreased extraction efficiency for the more polar solutes could be determined, then perhaps the effect of inefficient extraction could be counterbalanced. Finally, the accurate mapping of a toxic, unknown hazardous spill using trace enrichment on-scene for sample collection, necessitates that the preconcentration technique maintains constant extraction efficiency over many orders of magnitude in solute concentration. These aspects are addressed in the present study.

EXPERIMENTAL

Both pellicular and porous reverse-phase ODS packings were used, but not for the purpose of comparison. CO:PELL ODS (pellicular, ~30-μm particle) was dry packed by hand into small

0003-2700/79/0351-2180$01.00/0

guard columns. Bondapak C_{18} (porous ~70-μm particle) was factory packed into small disposable cartridges under the trade name Sep-Pak. The study began using the CO:PELL ODS material, but later, after Sep-Pak cartridges became available, they were used exclusively. The Sep-Pak cartridges obviated hand-packing of the nondisposable guard columns, and thus reduced any accidental contamination and packing variations due to this procedure. More importantly, the Sep-Pak cartridges allowed the use of a hand-held syringe instead of electrical pumps to apply the water samples for extraction by the ODS packing, considerably improving portability for on-scene sampling.

Instrumentation. Both a Perkin-Elmer Series 3 and a Waters liquid chromatograph were used. Detection was by UV absorption employing a Waters 440 Absorbance Detector at 254 nm. Data recording was done on Perkin-Elmer Model 56 recorders. A Waters U6-K injector was used with both chromatographs.

Reagents. Milli-Q system water and spectroquality methanol (MCB), filtered through 0.5-μm pore Fluoropore filters (FH P04700) were used in the chromatographs. The same methanol (unfiltered) and spectroquality acetonitrile (MCB) were used to pre-rinse the Sep-Pak cartridges (with tap water rinses sandwiched in between). Isopropanol and acetone (spectroquality MCB) were used in some applications as final rinses (in place of methanol) of Sep-Paks prior to trace enrichment. *m*-Cresol and acetophenone standards were obtained from Fluka Chemical; the acetone, benzene, and toluene standards were spectroquality MCB solvents.

TE Using CO:PELL ODS Guard Columns. *TE Procedures.* CO:PELL ODS stationary phase was dry packed into Whatman column-survival kit pre-columns (0.21 × 7 cm). This provided a surface area of ~2 m^2/pre-column.

The water-soluble fraction from a petroleum oil was obtained by carefully layering a bunker-C oil onto the surface of seawater contained in a 3-L glass jug. (The seawater was collected from an idle dock on Fisher's Island Sound off Avery Point, Groton, Conn., into a clean 3-L brown solvent jug.) The water was not filtered and was maintained at room temperature for the duration of the oil/water contact time from 1 to 35 days. A glass tube extended through the oil layer to the bottom of the jug into which a Teflon line was inserted for removal of "clean" water samples from under the oil layer. A Waters 6000A pump was used to apply the water samples to the guard columns. Each guard column was used only once for TE, then cleaned out, detergent washed, and repacked.

HPLC Separation of Adsorbates. After loading, the guard columns were first rinsed with 15 mL of Milli-Q System water to remove inorganic salts prior to chromatographic analysis. The outlet of the rinsed guard column was then connected to the head of the analytical column (ES Industries Chromegabond C_{18}, 0.46 × 15 cm) for desorption and chromatographic separation. A two-segment, linear gradient from 0% to 50% methanol in water in 20 min followed by 50% to 100% methanol in 50 min was used for separation of the water-soluble oil components at a flow rate of 1 mL/min at room temperature. The same bunker-C oil extracted into seawater was also extracted into acidified methanol (*24*), and this methanolic extract was chromatographed using a linear gradient from 50% methanol/water to 100% methanol (50 min).

TE Using Sep-Pak Cartridges. *TE Procedure.* The Sep-Pak cartridges were used as supplied directly from the manufacturer. (Since each cartridge contains ~0.35 g of packing and the Bondapak C_{18} material presents 400 m^2/g of surface area, there are 140 m^2 of surface area per cartridge.)

The Sep-Pak cartridges were rinsed prior to use by means of a hand-held glass (10-mL) syringe. (The Sep-Paks are made specifically with an entrance port to fit a luer-lock tipped syringe for manual introduction of solutions and solvents.) Ten-milliliter rinses, each of methanol followed in sequence by tap water, then acetonitrile, then a second tap water, and, finally, a second methanol rinse, served to both desorb any organic impurities and also to wet the packing prior to trace enrichment. Methanol in the void volume of the cartridge was removed by plunging 10 mL of room air through the packing using the syringe. The cartridge was then connected to an all glass (100-mL) syringe arranged vertically in a ring stand. Solutions of known concentrations of standard compounds in seawater were plunged through the cartridges at a rate of flow (~100 mL/min) resulting in a very fast drip, but not a steady stream, of seawater from the cartridge outlet. Standard compounds were added either as concentrated solutions in methanol or as the undiluted liquid directly to the seawater contained within the barrel of the syringe or into a beaker (for sampling volumes greater than the 100-mL syringe capacity). After one or two exchanges of the charged seawater solutions between syringe and beaker to ensure thorough mixing, the solutions were plunged through the cartridge as described. Residual seawater was removed from the cartridge by passing ~100 mL of room air through it prior to desorbing adsorbed components with 2 mL of methanol.

HPLC Separation of Adsorbates. Adsorbates were removed from the Sep-Pak cartridges after TE with 2 mL of methanol which was then filtered by means of a Millipore Sample Clarification Kit to remove inorganic salt precipitates. (A distilled water rinse would have removed these salts also, and obviated the need for filtering; however, some loss of adsorbate, particularly those with low k' values, i.e., benzene, was experienced using this approach).

A Whatman guard column (0.21 × 7 cm) packed with CO:PELL ODS was used with a Dupont Zorbax ODS analytical column for chromatographing the methanol rinses from the cartridges. All separations, except those where acetone was used, were carried out isocratically using methanol at 1 mL/min flow rate, at room temperature. The acetone injections were done isocratically at 90% methanol in water in order to retain the acetone peak long enough as to separate it from a large, quickly eluting, unidentified compound which was extracted in all instances from the seawater by the Sep-Pak cartridges.

Calculation of Recovery Efficiency. Undiluted standard (or a concentrated solution of the standard) was added to seawater and extracted using a Sep-Pak cartridge. The same volume of standard was then diluted with 2 mL of methanol for comparison (desorption of Sep-Pak-retained components was with 2 mL of methanol, hence the dilution). Since injection volumes were held constant, the recovery (extraction) efficiency was simply determined by the peak-height ratios from chromatograms of these two injections.

RESULTS

TE of Water-Soluble Oil Components Using CO:PELL ODS Guard Columns. *Packing Wettability.* Some preliminary experiments were carried out to determine the need for pre-wetting the packing and/or the need to add an organic solvent modifier to the seawater samples. This would ensure that the ODS material became and remained wetted during the trace enrichment process. For these experiments, a bunker-C oil was allowed to contact 3 L of seawater for 22 days without agitation, as previously described. One-hundred-milliliter volumes of the seawater were loaded at the same flow rate (9.9 mL/min) across both a dry and a methanol (15-mL) pre-rinsed guard column. Pre-wetting had virtually no effect as both chromatograms were nearly identical.

The effect of different methanol concentrations in the seawater samples on the efficiency of extraction was also investigated. TE from a 5% methanol in seawater solution resulted in a chromatogram nearly identical in overall profile as that obtained from 100% seawater, although a general decrease in UV absorbance for the chromatogram of the 5% methanol/seawater sample was noted. An increase to 10% methanol for the trace enrichment produced a chromatogram showing further reduction in UV absorption intensities for late eluting peaks, and nearly a complete loss of early eluting peaks. A 50% methanol in seawater solution resulted in no retention by the guard column whatever. It appeared, therefore, that the CO:PELL ODS material was wetted by 100% seawater, and the addition of the methanol modifier served only to lower extraction efficiency, particularly affecting adversely those compounds with low k' values.

Although use of a methanol pre-rinse had no effect on the TE efficiency (primarily because the packing is apparently wetted by 100% seawater), it could serve to desorb any

Table I. Absorbances[a] for Ten Peaks from Trace Enrichment of Bunker-C Oil-Contaminated Seawater at Loading Rates of 5 mL/min and 10 mL/min

peak	5 mL/min, 325 mL	10 mL/min, 300 mL
1	0.014	0.014
2	0.007	0.006
3	0.006	0.007
4	0.006	0.011
5	0.006	0.009
6	0.016	0.016
7	0.006	0.008
8	0.007	0.007
9	0.020	0.019
10	0.003	0.002

[a] Standardized to 325 mL loading volume.

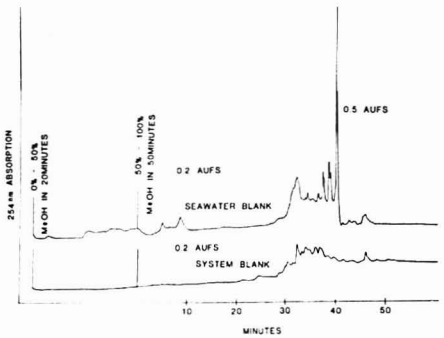

Figure 1. Comparison of liquid chromatographic system blank and trace enrichment chromatogram of 250 mL of uncontaminated seawater

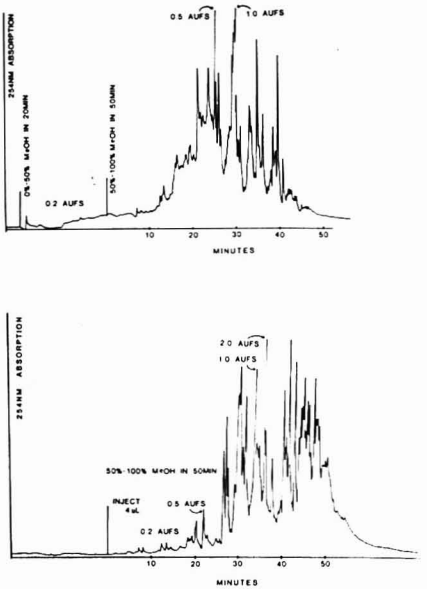

Figure 2. Trace enrichment chromatogram (upper) of 250 mL of Bunker-C oil-contaminated seawater (24-h oil/water contact time) and chromatogram of a 4-μL injection of a methanolic extract of the same Bunker-C oil

impurities prior to the extraction process. No presence of impurities, however, was evident. For these reasons, the guard columns were not pre-wet, nor was any organic modifier added to the seawater samples prior to extraction.

Loading Rate. Two flow rates, i.e., 5.0 and 9.9 mL/min, were investigated to determine any effects of these loading rates on extraction efficiency. Slower loading rates were not considered since it was felt that any improvements in extraction efficiency at low loading rates would be more than offset by increases in loading times, which could compromise synoptic coverage of an aqueous spill site. Further, the faster flow rates would allow greater sampling volumes in the same unit time which could provide more representative samples.

Table I lists the absorbances for ten peaks eluting between 24 and 42 min from the gradient elution chromatograms of two trace enrichments at loadings of 5 mL/min (325 mL) and 9.9 mL/min (300 mL) of bunker-C oil-contaminated seawater. Absorbances for the 300-mL sample were standardized to 325 mL, and the seawater/oil contact time was 14 days. Because the absorbance intensities show minimal differences, the efficiencies of removing these organic compounds from seawater are very similar at these loading rates. Apparently, the efficiency of extraction vs. loading rate curve is flat over this pumping range. Consequently, twice as much material can be trace-enriched and recovered at the faster flow rate without having to compromise on the loading time.

Effect of Sampling Volume on Extraction Efficiency. Figure 1 shows both a chromatographic system blank (no intentional trace enrichment) and a sample blank consisting of 250 mL of seawater trace-enriched at 9.9 mL/min loading rate. A trace enrichment chromatogram of 250 mL of bunker-C oil-contaminated seawater, after a 24 h oil/water contact time, is shown in Figure 2 along with one of a 4-μL injection of a methanolic extract of the same bunker-C oil. Two-segment, linear gradient elution was used for all trace-enriched samples, as previously described; only the second segment of the linear gradient was used for the separation of the injected methanol extract. Very minor contribution of contamination is evidenced by the system blank chromatogram. Similarly, only minor UV absorption from naturally occurring compounds in seawater sampled in February is apparent in the sample blank chromatogram, with the presence of only one peak necessitating attenuation (Figure 1). Of particular interest in the trace enrichment chromatogram of oil contaminated seawater is the 26 to 42 min elution range where the relative peak-to-peak variations in height are basically the same as those in the methanol injection chromatogram. This indicates a similar solubilization (extraction) of these compounds directly into methanol on the one hand and into seawater (thence onto C_{18} reverse-phase) on the other. The quickly eluting polar compounds show an increase in the trace-enriched chromatogram whereas the very large organic compounds of very limited water solubility are drastically reduced.

An additional trace enrichment of the same oil contaminated seawater is shown in Figure 3; however, the loading volume was reduced to 25 mL while the oil/water contact time increased to 22 days. Some differences between this and the same trace enrichment after 24 h (Figure 2) are evident, and could be partially attributable to microbial action, increased solubilization of certain components, and/or extraction differences induced by sampling size differences (250 vs. 25 mL).

Various volumes of the same seawater, in contact with the bunker-C oil for four weeks were extracted (9.9 mL/min loading rate). Extraction volumes ranged from 10 to 100 mL.

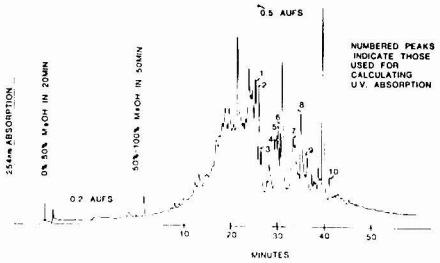

Figure 3. Trace enrichment chromatogram of 25 mL of Bunker-C oil-contaminated seawater (three-week oil/water contact time)

Table II. Peak Height Ratios for Ten Peaks Trace Enriched from 10, 20, 40 and 100 mL of Oil-Contaminated Seawater (4 weeks oil/water contact time)

	sampling volume ratios					
peak	10:20	20:40	40:100	10:40	20:100	10:100
1	1.58	2.26	0.97	3.57	2.19	3.45
2	1.76	2.22	1.10	3.90	2.43	4.29
3	1.88	2.00	1.25	3.75	2.50	4.71
4	1.60	2.25	2.07	3.72	4.67	7.72
5	2.03	2.28	2.43	4.61	5.40	10.95
6	2.00	2.31	2.31	4.61	5.33	10.67
7	2.16	1.92	2.35	4.14	4.50	9.73
8	2.32	2.16	2.65	4.96	4.47	10.38
9	2.34	2.20	4.30	5.15	9.45	22.13
10	2.50	2.56	3.41	6.32	8.54	21.36
$\bar{x}$	2.02	2.21	2.28	4.48	4.95	10.54
expected ratio	2.00	2.00	2.50	4.00	5.00	10.00

Table II lists (in order of elution) peak height ratios for ten selected peaks eluting between 24 and 42 min for the various extraction volumes. The peaks are designated by number on the chromatogram in Figure 3. Although the expected linear increases in peak heights with sampling volumes are approached quite closely in the averages, a general trend from much below the expected value progressing, with increasing peak number (i.e., elution time) to ratios much above the expected, is obvious in examining any column. The expected ratios are encountered only through the middle of the 24 to 42 min elution range, namely from peaks 5 to 7; prior eluting peaks show a depressed rate of growth with increasing sampling volume slower than expected (for a linear increase with sampling size), while late eluting peaks (8 to 10) show an enhanced growth faster than expected.

The rate of change in UV absorption with increasing sampling volumes (growth curves) for each of these ten peaks is plotted against volumes of seawater trace-enriched in Figure 4. Curves of peaks 1 through 6 generally display decreasing convexity with volume, indicating a tendency to increase in peak height linearly with volume. Growth curves of peaks 1 and 2 indicate that growth is minimal, and perhaps even negative, after a certain volume of water is sampled. Peaks 7 and 8 show linear increases in peak heights with volume over the sampling volume range. Unlike convex peaks 1 and 2, peaks 9 and 10 are concave, and their inordinate growth increases with sampling volume could be due, at least partially, to mutual zone solubility effects. Such an effect can occur when a component has substantially different solubility in or affinity for an adsorbed component than it has with respect to the original stationary phase. As a compound becomes adsorbed onto the column, the packing material becomes

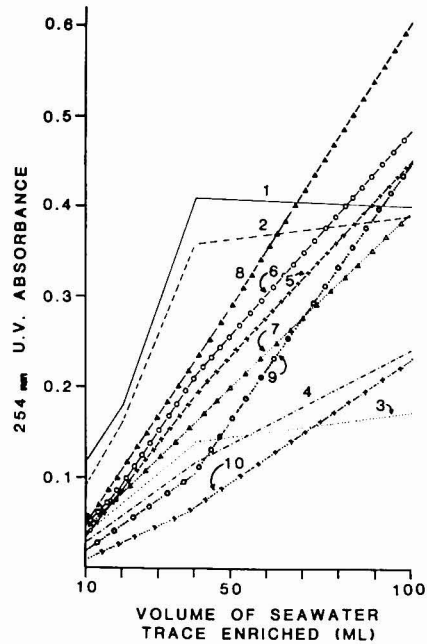

Figure 4. Rates of change in UV absorption for ten chromatographic peaks (See Figure 3 for peak locations) trace enriched from various volumes of Bunker-C oil-contaminated seawater (four weeks oil/water contact time)

chemically altered. The alteration can offset the adsorption of other components in a negative or positive manner, depending on their attraction to the "new" packing material. The inordinate increase in adsorption of late eluting peaks (9 and 10) could represent a stationary phase change which renders it more attractive to, and therefore more efficient at, removing these compounds with relatively large k's. On the other hand, the same stationary phase changes causing this enhancement of extraction, could conversely produce a less attractive medium for extracting the more polar components, resulting in decreased extractability of these components (peaks 1 and 2 in particular).

In addition to mutual zone solubility, these growth curves can also be due, in part, to an effect discussed in a following section on the optimization of sampling volume for recovery of adsorbate. This effect is actually the result of a shift in the adsorption/desorption equilibrium favoring increased desorption from the packing causing a net loss of adsorbate from the C_{18} packing with increased sampling volumes, particularly for small k' value compounds.

Trace Enrichment of Model Compounds Using Sep-Pak C_{18} Cartridges. *Reproducibility of Cartridge Extraction.* In order to determine the reproducibility of extraction efficiency of the Sep-Pak cartridges, independent of the variations caused by hand measurement of peak heights and the injection process itself, repeated injections of standards and samples were made. Table III lists the standard deviations and percents relative standard deviation (in peak height cm.) for repeated injections of a toluene standard and of benzene and toluene samples which were repeatedly trace enriched from 100-mL volumes of seawater.

Table III. Reproducibility of Peak Height (cm) for Standard Injections and Sep-Pak C_{18} Cartridge Extractions from 100-mL Seawater Volumes of Benzene and Toluene @ 25 ppm

	standard (toluene)	extracted toluene	extracted benzene
	12.78	11.10	3.62
	12.50	10.90	3.78
	12.90	10.88	3.80
	12.90	10.80	3.65
	12.80	11.80	3.90
	12.60	9.60	3.40
	12.40		
$\bar{x}$	12.70	10.85	3.70
σ	0.20	0.66	0.176
σ^2	0.04	0.436	0.031
rel σ	1.6%	6.1%	4.6%
	corrected σ	0.64	0.164
	corrected rel σ	5.9%	4.43%
av extraction efficiency		84.9%	22.0%

Results showed a 1.6% relative standard deviation due to injection and hand measurement of peak height, and 4.6% and 6.1% relative standard deviations for benzene and toluene trace enrichment samples. The reproducibility of cartridge extraction is independent of the efficiency of extraction since the extraction efficiencies for benzene and toluene (22% and 85%, respectively) are distinct while the percents relative standard deviation are about the same. The lack of reproducibility of the toluene and benzene trace enrichment samples is due, in small part, to the injection and peak height measurement process, but is mostly due to cartridge-to-cartridge variations, and variations in their use (application of the water samples and desorption of the absorbed components). [*Note 1*: Extraction efficiency (%) based on a one-injection standard will not be as reproducible as that based on an average from multiple injections of the standard. Furthermore, all reproducibility data are for the same lot of Sep-Paks. A different lot provided significantly different extraction efficiencies for the same compound (probably attributable to silanization differences), in addition to producing different cartridge-to-cartridge (intra-lot) reproducibility.] [*Note 2*: Since the standards are independent of the cartridge extraction samples, then the contribution to noise from hand measurements of peak height and injection can be corrected for. But since the magnitude of the standard deviation is peak-height proportional, differences in peak heights, i.e., $\bar{X}$'s, must be considered prior to subtracting out this noise contribution. This was done by taking the ratio of the average sample peak height to the average standard peak height and multiplying this times the standard injection standard deviation, i.e., from Table II, the ratio of $\bar{X}_s$ for toluene (10.85) to $\bar{X}_s$ for the standard (12.70) provides the proportional contribution (0.85) from hand injection and peak-height measurement noise. The corrected standard deviations thus represent the noise contributions caused by variations in the cartridges themselves and in their usage. Negligible contribution from hand injection and peak height measurement is evident comparing corrected and uncorrected σ values listed in Table III.]

Recently, Scott and Kucera (25) examined the solute–solvent–stationary phase interaction for a number of reverse phases. They showed that for solutes with a k' of 10 or less, under conditions where the stationary phase is wetted, solute molecules interact with the adsorbed solvent layer, and not directly with the C_{18} hydrocarbon moiety itself. In light of this, it was felt that some selectivity differences for the extraction of toluene from seawater might be demonstrable by Sep-Pak C_{18} cartridges simply by substituting different water-miscible organic solvents for methanol as the final cartridge rinse prior to trace enrichment. In this way, different adsorbed solvent layers could be substituted on the C_{18} packing for interacting with toluene during the extraction from seawater. Table IV lists extraction efficiencies and peak heights for repeated extractions of toluene by the Sep-Paks after preparing the cartridges by substituting the final methanol rinse with isopropanol, acetonitrile, and acetone. Taking the uncorrected % relative standard deviation of 6.1% for toluene (Table III), then 95% of all individual observations will be within 12%. From Table IV, the average extraction efficiencies for the isopropanol, acetonitrile, and acetone rinsed cartridges are 85.7%, 81.5% and 85.8%, respectively. Since these values are not significantly different from the methanol-washed cartridge efficiency of 84.9%, any real effects these solvents may have on the extraction of toluene from seawater are not directly measurable owing to the system noise. On the other hand, there is a definite effect resulting in enhancement of extraction of benzene from seawater by pre-loading the cartridge with toluene; the reverse is true, i.e., lessened toluene extraction efficiency, when the cartridge is pre-loaded with benzene. This mutual zone solubility effect arises from a stationary phase alteration caused by an adsorbed layer on the C_{18} packing which alters packing selectivity.

Table IV. Effect of Various Solvent Final Rinses of Sep-Pak C_{18} Cartridges on Extraction of 25 ppm Toluene from 100 mL Seawater Volumes (peak height, cm)

	isopropanol	acetonitrile	acetone
	10.45	10.1	11.00
	10.70	9.8	10.90
	10.83	10.2	10.77
	10.50	8.8	11.90
	11.00	9.6	9.90
			10.95
$\bar{x}$ smpl.	10.70	9.7	10.92
σ	0.23	0.56	0.64
rel σ	2.1%	5.7%	5.9%
$\bar{x}$ std	12.48	11.9	12.73
extraction efficiency ($\bar{x}$ spml/ $\bar{x}$ std)	87.5%	81.5%	85.8%

Mutual Zone Solubility on Sep-Pak Cartridges. From Table III, the average efficiency of extraction of toluene (@ 25 ppm) from a 100-mL seawater sample is 84.9%, while that for a 25 ppm benzene solution is only 22.0%. However, a 36% increase in benzene extraction efficiency can be realized by first loading a Sep-Pak cartridge with toluene (i.e., 84.9% of a total of 2.5 μL of toluene extracted from 100 mL of seawater) followed by 100 mL of a 25 ppm benzene solution in seawater. This results in a 30% extraction efficiency for benzene, and a simultaneous decrease in toluene recovery, from 84.9% to 35%. This is not an active displacement of toluene by benzene on the C_{18} packing, since a nearly identical loss in toluene recovery (to 37%) is also caused by a 100-mL seawater rinse of the cartridge after the initial toluene loading. This loss apparently arises from a chemical/physical interaction between an adsorbed component and the water stream forced through the cartridge causing a desorption of adsorbate both during the extraction process itself and particularly during any follow-up rinses of previously loaded cartridges. This phenomenon is addressed in more detail in a following section on the loss of adsorbate from Sep-Pak cartridges to seawater.

Extraction of Model Compounds from Various Volumes of Seawater by Sep-Pak C_{18} Cartridges. The extraction from various volumes of seawater of five model compounds, i.e.,

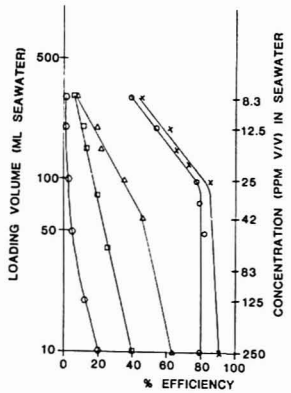

Figure 5. Change in extraction efficiency with sampling volume during the trace enrichment of five model compounds from seawater. (○) Acetone, (□) benzene, (△) *m*-cresol, (◇) acetophenone, (X) toluene

acetone, benzene, *m*-cresol, acetophenone, and toluene was studied. Since the extraction efficiencies were expected to be inversely proportional with respect to the water solubilities, these five standards were chosen on the basis of their wide range in solubilities, from completely miscible to less than 0.05% (by weight) soluble. Furthermore, although such compounds as halogenated pesticides could have been selected as representative of a low solubility compound, problems with adsorption on the walls of the container during extraction would have made choice of such a compound questionable. Furthermore, in order to ensure solubility in seawater at all concentrations utilized (as was provided for), then the use of such minimally soluble compounds would have necessitated using prohibitively large sampling volumes in order to provide sufficient adsorbate to permit good detectability.

Figure 5 shows the change in extraction efficiency against sampling volume for the five model compounds. In all cases, 2.5 μL of the model compound was added to volumes of seawater ranging from 10 to 300 mL. Consequently, concentrations varied from 250 ppm for the 10-mL sample volume to 8.3 ppm for the 300-mL sample volume. Adsorption onto the glass walls of the syringe during extraction was not a problem since the seawater solutions were immediately extracted and all model compounds were completely soluble in seawater over the concentration range utilized.

All compounds show a loss in extraction efficiency with increasing sampling volumes. This loss could be dependent on either decreasing concentrations of the model compounds in seawater or dependent directly on sampling volume. The water solubilities of the compounds are a rough approximation to their relative extraction efficiencies regardless of any effect due to sample volume increase or concentration decrease. Table V lists water solubilities, extraction efficiencies from 100-mL seawater volumes, and k' values for the five model compounds. (Sep-Pak C_{18} material was dry packed into a 0.21 × 7 cm column for determination of k's.) The water solubility is not perfectly inversely correlated to k' since the k' value for benzene (18.3) is less than the expected (i.e., between 30.3 and 66.5). In addition, the expected direct proportionality between k' and extraction efficiency is also not perfectly followed since the extraction of benzene (22%) is much lower than expected (i.e., between 77.5 and 84.9%). The occurrence of this exception, encountered within such a limited model compound set, makes the occurrence of other exceptions highly probable such that the use of the k' value of an unknown for correcting extraction efficiency for calculation of concentration is highly suspect. For this reason, the actual compound should be used for experimentally determining extraction efficiency for those spill situations which are known, and where model compounds can be attained.

Table V. Comparison of k', Water Solubility,[a] and Extraction Efficiency Using Sep-Pak C_{18} Cartridges for Five Model Compounds

	k', 10% MeOH/H_2O	water solubility, % by weight	extraction efficiency, %
acetone	0.4	∞	3.1
m-cresol	14.8	1.9–2.5	34.6
acetophenone	30.3	0.55	77.5
benzene	18.3	0.18	22.0
toluene	66.5	0.05	84.9

[a] From Coast Guard Chemical Hazard Response Information System (Commandant Instruction M 16465.12, October 1978).

Loss of Adsorbate from Sep-Pak Cartridges to Seawater. In order to determine if the drop in extraction efficiency with increasing sampling volumes was, in fact, representative of a loss in extraction capability due to displacement (and loss) of the solvent layer (methanol) from the cartridge packing (methanol was used as the final solvent rinse prior to trace enrichment), a series of seawater rinses of various volumes from 10 to 300 mL was applied to the cartridges before trace-enriching toluene (@ 250 ppm) from 10-mL seawater samples.

The extraction efficiency remained constant, independent of pre-loading (pre-extraction) rinse volumes applied to the cartridges, as evidenced in Figure 5 by the vertical plot. These data suggest that the pre-rinses cause no physical/chemical changes to the packing material since its extraction characteristics do not change with pre-rinses.

On the other hand, when the cartridges are first loaded by trace-enriching 10 mL of 250 ppm toluene in seawater (~90% efficiency under these conditions), and subsequently (post-loading) rinsed with various seawater volumes, a significant loss of adsorbed toluene occurs which is proportional to the square root of the post-loading rinse volume. This loss is reflected in depressed efficiency of extraction from 90% (no loss) with no rinse to 3% efficiency with a 300-mL rinse. This loss in efficiency actually reflects an inability of the cartridges to retain adsorbed toluene during the rinse. The least-squares plot of the post-loading rinse curve is also shown in Figure 6.

The third curve included in Figure 6 is that of the efficiency of toluene extraction from various sampling volumes (no seawater rinses). These data are the same as those shown previously, in Figure 5, and are included in the present Figure in order to show that they lie between the curve of pre-loading rinses (no loss in efficiency) and the curve of post-loading rinses (maximum loss in efficiency).

[*Note 3*: The no-rinse data are plotted in Figure 6 as the least-squares curve, disregarding the 10-mL loading point, which is plotted on the least-squares post-loading rinse curve at zero rinse volume. Since this point could have been validly plotted on either curve, it was plotted only for the one as described above since there is apparently no loss of adsorbed toluene from a 10-mL loading volume, while all other data points (100-mL and larger loading volumes) for the no-rinse (variable volume loading) curve have appreciable loss of adsorbed toluene (during the loading process). This is evidenced by the nearly identical slopes of −0.187 and −0.190.]

Both adsorption and desorption processes are related to the extraction volume as a square function. The y intercept of 16.94 indicates that a post-loading rinse of 287 mL of seawater

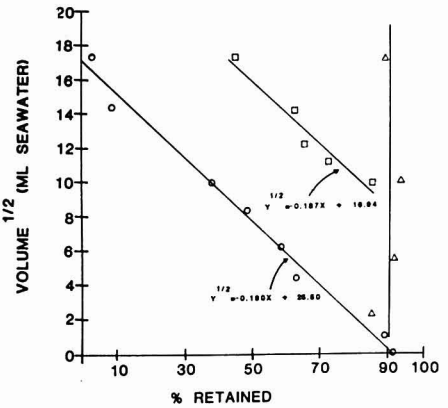

Figure 6. Adsorption and retention of toluene from seawater by Sep-Pak C_{18} cartridges as a function of pre- (Δ) and post-sampling rinses (O) (constant 10-mL sampling volume) and variable sampling volumes (□), (no rinses)

is sufficient to totally remove any pre-absorbed toluene from the Sep-Pak cartridges. Similarly, the y intercept of the equation for the no-rinse curve of 25.5 indicates that a volume of 625 mL of seawater (containing 2.5 μL of toluene) would result in no retention of toluene on the cartridge. (These y intercepts are useful only for comparison purposes since both curves, in reality, are asymtotic to the y axis.) The different y intercepts (for the linear portions of the curves shown in Figure 6) arise, on the one hand, from loading the toluene all at once, followed by toluene-free seawater for the post-loading rinse data and, on the other hand, from loading the toluene in various seawater volumes for the no-rinse curve. For the latter case, loss of adsorbed toluene is less severe than for the former. Although no post-loading rinses were applied to the cartridges for the no-rinse data points, portions of the loading volumes themselves act as rinses for already adsorbed toluene, but these rinses are: (1) actually toluene solutions and (2) this loading solution/(rinse) can affect losses upon only that proportion of total toluene in the system which is in an adsorbed condition.

In addition, Figure 7 plots the post-loading rinse and no-rinse least-squares curves for benzene adsorption and loss to/from seawater by Sep-Paks. Although the slopes are very small, they are significantly different from zero (t-test on smaller slope, i.e., −0.0449, $P < 0.01$). The adsorption/desorption processes are related to the extraction volume as the $\log_{10}$ of the volume.

Extraction Efficiency of Acetophenone as a Function of Concentration Using Sep-Pak C_{18} Cartridges. Acetophenone was used to study linearity of extraction from various concentrations in seawater since its high molar absorptivity allowed detectability (254-nm absorption) at low concentrations. Since the extraction efficiencies for both benzene and toluene are highly dependent on the volume of seawater extracted, this was held constant at 100 mL, although three extraction volumes of 10 mL were also utilized for comparison purposes. The acetophenone concentration was varied from 1 ppt to 1 ppb. Although the acetophenone from a 1 ppb, 100-mL seawater sample was detectable (~15 pg injected into the chromatograph), accurate quantification was not possible owing to co-elution of natural interferences from the extracted seawater. Table VI lists the extraction efficiencies for acetophenone vs. its concentration in seawater. All concentrations, except for 1000 ppm, produced comparable extraction

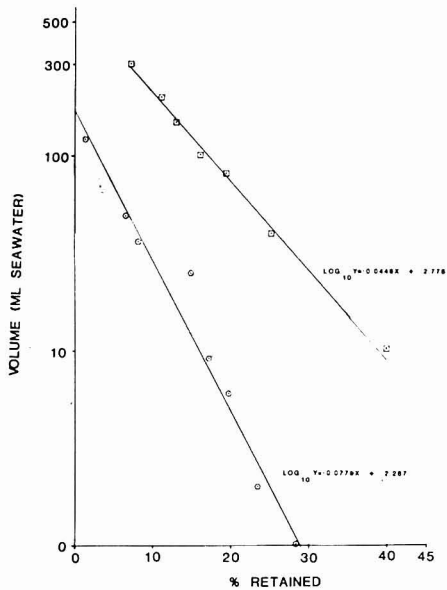

Figure 7. Adsorption of benzene from seawater by Sep-Pak C_{18} cartridges as a function of post-sampling rinses, ⊙ (constant 10-mL sampling volume) and variable sampling volumes, ⊡ (no rinses)

Table VI. Extraction Efficiency of Acetophenone at Various Concentrations in Seawater by Sep-Pak C_{18} Cartridges (100-mL sampling volume)

concn, ppm	volume acetophenone added, μL	efficiency of extraction, %
1000	100	27.1
1000[a]	10	85.1
250	25	73.1
250[a]	2.5	72.8
100	10	71.5
52[a]	0.52	72.8
50	5.0	74.8
10	1.0	76.8
1.0	0.1	79.6
0.1	0.01	77.1
0.01	0.001	75.0

[a] 10-mL sampling volume.

efficiencies indicating that the adsorption efficiency of acetophenone is constant for variations over six orders of magnitude in concentration. Since the acetophenone was completely soluble in seawater at all experimental concentrations, except at 1000 ppm, the drop in extraction efficiency to 27.1% for the 100-mL, 1000 ppm sample, could be due to partial loss of acetophenone via adsorption onto the inner walls of the glass syringe, so that a portion of acetophenone was never exposed to the cartridge.

[*Note 4*: A definite adsorption problem onto container walls was particularly accentuated by the lower solubilities of some larger molecular weight aromatic standards investigated. For example, while the average extraction efficiency ($n = 4$) for 1,3-dimethylnaphthalene was only 54.4%, the average ($n = 2$) for 1-methyl naphthalene was 65.6%. Even if steric hindrance prevents effective interaction between a methyl

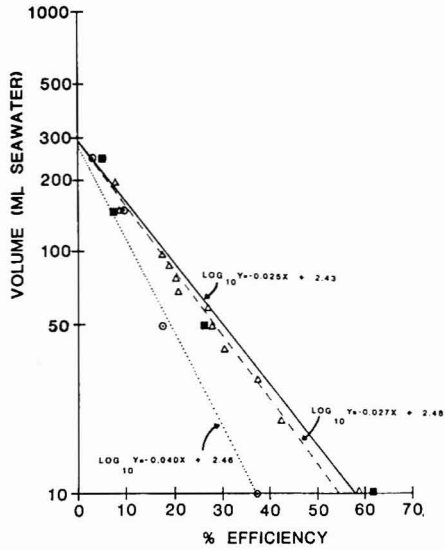

Figure 8. Adsorption of benzene from 50 (⊙....), 100 (Δ---), 150 ppm (■——) seawater solutions by Sep-Pak C_{18} cartridges as a function of sampling volume

group on the dimethylnaphthalene and the Sep-Pak C_{18} material, the extraction efficiencies should have at least been comparable for these naphthalenes (if adsorption on container walls were also comparable for each).]

The drop in extraction efficiency for the 1000 ppm solution to 27.1%, however, could also be partly due to saturation of the Sep-Pak cartridge. A second 1000 ppm solution, but in a total volume of 10 mL, provided 85.1% efficiency; however, this 1000 ppm solution contained a total of 10 μL of acetophenone, while the previous 1000 ppm solution in 100 mL contained 100 μL of acetophenone. (All other determinations contained 25 μL or less of acetophenone.)

Optimization of Sampling Volume for Recovery of Adsorbate. The detectability of an adsorbed compound can be improved, in some cases, particularly for poorly extracted (significantly water-soluble) compounds, by sampling a volume of seawater maximized for recovery of that compound, which does not necessarily mean extracting the maximum available or practicable volume of contaminated water.

The equations defining the loss in extraction efficiency of benzene and toluene from seawater with increasing sampling volumes (Figures 6 and 7) are applicable only for variable concentration sampling volumes and do not indicate the relationship between extraction efficiency and sampling volumes at constant concentration. Furthermore, the actual amounts of adsorbate extracted showed a constant decrease with increasing sampling volume for benzene and toluene (the actual amounts are proportional to the percent extraction efficiency since a constant 2.5 μL of benzene or toluene was added for all determinations). For any constant sampling concentration, however, the actual amounts of compound present in different extraction volumes are variable such that the extraction efficiencies will not be directly proportional to actual extracted amounts. Although the extraction efficiencies would be expected to decrease with increasing sampling volumes, inefficient adsorption could be offset by sampling very large volumes. However, if either for the situation where

Table VII. Effect of Sampling Volume on Total Adsorbed Benzene and Efficiency of Benzene Extraction from a 100 ppm Seawater Solution Using Sep-Pak C_{18} Cartridges

volume, mL	N	efficiency, %	adsorbed benzene, μL: $\bar{x}$	adsorbed benzene, μL: two-point running $\bar{x}$
10	2	58.7	0.59	
				}0.72
20	4	42.2	0.84	
				}0.98
30	3	37.2	1.12	
				}1.17
40	4	30.2	1.21	
				}1.30
50	3	27.7	1.39	
				}1.50
60	4	26.9	1.61	
				}1.53
70	5	20.6	1.44	
				}1.53
80	3	20.1	1.61	
				}1.65
90	4	18.7	1.68	
				}1.72
100	3	17.6	1.76	
				}1.61
150	4	9.7	1.46	
				}1.58
200	3	8.7	1.70	
				}1.45
250	3	4.8	1.20	
				}1.32
300	3	4.8	1.44	

the rate of adsorption from seawater reaches equilibrium with the desorption rate or for the situation where the rate of loss can exceed the rate of adsorption, then there will exist an optimum sampling volume for which larger sampling volumes will not increase the net amount of adsorbate (former case) or will actually decrease the amount of adsorbate (latter case).

Various sampling volumes of 50, 100, and 150 ppm solutions of benzene in seawater were applied to Sep-Pak C_{18} cartridges. Figure 8 plots the least-squares curves defining the decreases in efficiency of extraction with increasing sampling volumes for these three concentrations.

It can be seen that the effect of decreasing extraction efficiency with volume can be accentuated by lower concentrations of benzene in seawater, i.e., as the concentration of benzene decreased in order from 150 to 100 to 50 ppm, the negativity of the slopes increased for the least-squares curves (−0.025 to −0.027 to −0.040). Lower concentrations apparently accelerate this loss in extraction efficiency since the lowest (50 ppm) concentration effected a large change in slope relative to the minor slope change effected by a concentration reduction from 150 to 100 ppm. It is interesting to note, that the y intercepts are the same for all three curves, regardless of benzene concentration in the seawater. Although the rates of loss in efficiency are concentration-dependent, the volume at which extraction efficiency becomes zero is concentration-independent.

Table VII lists the sampling volumes, extraction efficiencies, and amounts (μL) of adsorbed benzene for the 100 ppm curve in Figure 8.

For the equations of the regression lines in Figure 7, [(x)·(y)·(concentration)] defines the amount of cartridge-extracted benzene and [(x)·(y)] defines relative amounts of extracted benzene at any constant concentration.

Solving the least-squares equations in Figure 8 for [(x)·(y)] gives:

$$\left[\frac{\log y - b}{m}\cdot y\right] = [(x)\cdot(y)] \tag{1}$$

For maximum [(x)·(y)], set $[d(xy)]/[d(y)] = 0$,

$$d(xy) = \frac{\log y - b + (1/\ln 10)}{m} = 0 \tag{2}$$

Solving for y_{max} (volume y at maximum [(x)(y)]) gives

$$\log (y_{max}) = b - \frac{1}{\ln 10} = b - 0.434 \tag{3}$$

The slopes of the regression lines have no effect on this (y max)

calculation; only the y intercepts affect it. Solving (y_{max}) for the least-squares curves in Figure 8 gives:

$$y_{max} @ 150 \text{ ppm} = 99 \text{ mL}$$

$$y_{max} @ 100 \text{ ppm} = 111 \text{ mL}$$

$$y_{max} @ 50 \text{ ppm} = 106 \text{ mL}$$

These volumes are not significantly different. They agree well with the experimental y_{max} of ~100 mL from the moving two-point average in Table VII for the 100 ppm benzene solution. Although the extraction efficiency decreases with sampling volume, and does so at a faster rate for the lower concentrations, the volume at which the amount of adsorbed benzene is maximal is independent of concentration. Generally, as the water solubility of a compound decreases (as k' on C_{18} increases), not only would extraction efficiency for any given sampling volume be expected to increase, but so also will the y_{max} value.

CONCLUSION

CO:PELL ODS liquid chromatographic packing can be used in guard columns to extract seawater-soluble fractions of petroleum oils by trace enrichment of large sample volumes. Extracted compounds show predominantly nonlinear accumulation rates with volume. This is partially due to mutual zone solubility, particularly for compounds with large k' values (resulting in faster than expected accumulation) and also due to desorption of adsorbed compounds, particularly those with small k' values (resulting in actual loss or diminished net accumulation rates).

Sep-Pak C_{18} cartridges offer significant improvements in portability and simplicity of use in addition to the convenience of being disposable, over dry-packing of nondisposable guard columns by hand. The efficiency of extraction of five model compounds is roughly proportional to their respective k' values on RP-18 and inversely proportional to their water solubilities.

Increasing the sampling volume caused decreases in the extraction efficiencies for all five compounds, regardless of whether the concentration of compound in seawater was variable or held constant, i.e., regardless of whether the amount of model compound was held constant for variable volumes (concentration variable) or whether the concentration was held constant (total amount of compound varied with sampling volume).

The extraction efficiency for acetophenone remained constant for constant sampling volume (100 mL), while its concentration ranged from 1000 ppm through 0.01 ppm in seawater.

Equations defining the loss in extraction efficiency as a function of sampling volume for benzene at three different concentrations in seawater were used to predict the sampling volume, y_{max}, at which a maximum amount of benzene would be present on the Sep-Pak C_{18} cartridge. This volume (~100 mL) is independent of the sample concentration over the range used (50 to 150 ppm); however, the lower concentrations caused faster extraction efficiency losses with increasing sampling volumes. These y_{max} values are compound specific; consequently, for the recovery of maximum adsorbate, variable sampling volumes should be employed.

Since extraction efficiency is dependent on both sampling volumes and water solubilities (and/or k' values) of compounds to be trace enriched, these factors must be considered when doing quantitative extraction from water. Further, cartridge lot-to-lot variability must also be accounted for. (Extraction efficiencies for toluene and benzene averaged 85% and 22%, respectively, for sampling 100-mL volumes, using one lot, while a second cartridge lot provided respective efficiencies of only 57% and 17%.) Consequently, the cartridges have limited potential when used for quantitative trace-enrichment applications, particularly when used to extract water samples of unknown composition where the mutual-zone solubility effect could alter extraction efficiency. Further, in those situations where two or more components are present and each must be analyzed, multiple discrete sampling volumes may have to be extracted if maximum recovery of each is desired or necessary.

The Sep-Pak cartridges should prove useful when a specific contaminant is being sought since efficiencies at various volumes and concentrations can be experimentally derived. This would permit much improved accuracy in the quantitative mapping of aqueous spill sites. The simplicity of use of the cartridges makes them particularly appropriate for performing extractions in the field and allows fast turn-around time for following the movement and dilution of some of the more toxic organic pollutants. Nevertheless, additional extraction procedures will still be necessary, such as those using methylene chloride as an extracting solvent (*26*, *27*). Such a liquid/liquid extraction step cannot be circumvented since it can minimally provide a more effective extraction of the more polar (water-soluble) compounds for which the Sep-Paks provide poor extraction efficiency and very limited concentrating capability.

LITERATURE CITED

(1) Rohm and Haas technical bulletin, Amberlite XAD-2, August 1975.
(2) J. T. Walsh, R. C. Chalk, and C. Merritt, *Anal. Chem.*, **45**, 1215 (1973).
(3) Rohm and Haas technical bulletin, Amberlite XAD-4, February 1978.
(4) J. P. Ryan and J. S. Fritz, *J. Chromatogr. Sci.*, **16**, 488 (1978).
(5) W. Van Ryswyk, *J. Chromatogr.*, **103**, 259 (1975).
(6) R. M. Cassidy, M. T. Hurteau, J. P. Mislan, and R. W. Ashley, *J. Chromatogr. Sci.*, **14**, 444 (1976).
(7) A. K. Burnham, G. Y. Calder, J. S. Fritz, G. A. Junk, H. J. Svec, and R. Willis, *Anal. Chem.*, **44**, 139 (1972).
(8) E. M. Thurman, R. L. Malcolm, and G. R. Aiken, *Anal. Chem.*, **50**, 775 (1978).
(9) A. D. Thurston, *J. Chromatogr. Sci.*, **16**, 254 (1978).
(10) E. Brizova, M. Popl, and J. Coupek, *J. Chromatogr.*, **139**, 15 (1977).
(11) J. D. Navratil, R. E. Sievers, and H. F. Walton, *Anal. Chem.*, **49**, 2260 (1977).
(12) V. Leoni, G. Puccetti, R. J. Colombo, and A. M. D'Ovidio, *J. Chromatogr.*, **125**, 399 (1976).
(13) J. Kirkland, *Analyst (London)*, **99**, 859 (1974).
(14) C. G. Creed, *Res./Dev.*, **27**, 40 (1976).
(15) *Natl. Bur. Stand. (U.S.), Tech. Note*, **889**, 30 (1976).
(16) F. Eisenbeiss, H. Hein, R. Joester, and G. Naundorf, *Chromatogr. Newsl.*, **6**, 8 (1978).
(17) K. Ogan, E. Katz, and W. Slavin, *J. Chromatogr. Sci.*, **16**, 517 (1978).
(18) Waters Associates technical bulletin H63, November 1976.
(19) R. W. Frei, *Int. J. Environ. Anal. Chem.*, **5**, 143 (1978).
(20) A. R. Oyler, D. L. Bodenner, K. J. Welch, R. J. Liukkonen, R. M. Carlson, H. L. Kopperman, and R. Caple, *Anal. Chem.*, **50**, 837 (1978).
(21) R. Kummert, E. Molnar-Kubica, and W. Giger, *Anal. Chem.*, **50**, 1637 (1978).
(22) Waters Associates technical bulletin H91, October 1977.
(23) W. E. May, S. Chesler, S. Cram, B. Gump, H. Hertz, D. Enagonio, and S. Dysezel, *J. Chromatogr. Sci.*, **13**, 535 (1975).
(24) W. A. Saner, G. E. Fitzgerald, and J. P. Welsh, *Anal. Chem.*, **48**, 1747 (1976).
(25) R. Scott and P. Kucera, *J. Chromatogr.*, **142**, 213 (1977).
(26) L. Sheldon and R. Hites, *Environ. Sci. Technol.*, **12**, 1188 (1978).
(27) G. Jungclaus, V. Lopez-Avila, and R. Hites, *Environ. Sci. Technol.*, **12**, 88 (1978).

RECEIVED for review February 16, 1979. Accepted July 9, 1979.

Survey of Carbon-13 Chemical Shifts in Aromatic Hydrocarbons and Its Application to Coal-Derived Materials

C. E. Snape and W. R. Ladner*

National Coal Board, Coal Research Establishment, Stoke Orchard, Cheltenham, Glos. GL52 4RZ, England

K. D. Bartle

Department of Physical Chemistry, University of Leeds, Leeds LS2 9JT, England

A survey of ^{13}C chemical shifts of aromatic hydrocarbons is used to derive an assignment scheme which should be applicable to the majority of coal-derived materials and also to other hydrocarbons such as crude oils and aromatic resins. This scheme is used to derive structural information on four extracts prepared from low-rank British coals.

^{13}C nuclear magnetic resonance (NMR) spectrometry is playing an increasingly valuable role in the characterization of products from coal liquefaction processes (see for example references 1 and 2). It enables direct structural information to be obtained about the carbon groups present, especially those not containing hydrogen such as internal aromatic carbon, carbonyl, and aromatic ether and which thus cannot be observed by ^1H NMR. For coal-derived materials, the major separation in ^{13}C NMR spectra is between aromatic and aliphatic carbon; this separation enables the fraction of aromatic carbon or aromaticity (*3*) to be determined directly and important structural information, particularly about the aliphatic carbon groups present, can be derived (*4*, *5*).

As early as 1966, the potential of ^{13}C NMR to give a direct estimate of the aromaticity was recognized by Friedel and Retcofsky, who recorded the rapid passage, dispersion mode spectra of neutral oils from high-temperature carbonization products (*6*). However, because of proton coupling, the aliphatic carbon band was not resolved and the aromatic carbon signal appeared as a doublet due to the large aromatic ^{13}C–^1H coupling constants. Knight obtained ^{13}C spectra of aromatic petroleum fractions (*7*) which showed similar features to those observed by Friedel and Retcofsky in the neutral oils from coal. Later, Retcofsky and co-workers (*8*) recorded the ^{13}C proton coupled spectra of a variety of coal-derived materials and compared the aromaticity values with those obtained indirectly from ^1H NMR by the Brown–Ladner method (*9*).

The advent of pulsed Fourier transform NMR (*10*) and proton decoupling (*11*) has made it possible to obtain well-resolved bands in both the aromatic and aliphatic regions of the spectra of coal-derived materials. The improved resolution on proton decoupling has led to important structural information being obtained; for example, the presence of long alkyl side chains as major aliphatic substituents in extracts of sub-bituminous coals (*4*, *12*). However, variable nuclear Overhauser enhancements and long thermal relaxation times (T_1) can make quantitative measurements unreliable, and can also result in some carbon atoms with a long T_1, such as bridgehead aromatic carbon, not being observed unless special precautions are taken (*13*, *14*).

The detailed assignment of ^{13}C chemical shifts in the spectra of coal-derived materials has been hampered until recently by the lack of data on suitable model structures. This paper proposes a scheme for the assignment of ^{13}C chemical shifts which is based on published data and which should be applicable to the majority of coal-derived materials: consideration is given to the chemical shifts in a variety of structures including alkyl aromatics, hydroaromatics, and heterocyclics. The assignment scheme is used to derive structural information on coal extracts for which reliable quantitative results have been obtained.

SURVEY OF CHEMICAL SHIFTS

The data on the chemical shifts of aromatic and aliphatic structures relevant to coal-derived materials has been obtained from references (*3*, *10–12*, *14*, and *15–21*). The data relate to tetramethylsilane as internal standard and, where possible, to chloroform-*d* as solvent, but it must be remembered that the chemical shifts can alter by up to ±0.5 ppm with solvent, concentration, and paramagnetic effects (*11*).

Aromatic Structures. The chemical shifts of a variety of mono-, di-, and polyaromatics are given in Tables IA and IB; those for aromatic carbon joined to groups other than hydrogen in Table IA (123–160 ppm) and those for aromatic carbon joined to hydrogen in Table IB (110–140 ppm). The tables show that the chemical shift range for alternant hydrocarbons, which are the major structural units in coal-derived materials, is approximately 120 to 150 ppm. For mono- and diaromatics not containing heteroatoms, there is a fairly marked separation (shown hatched in Tables IA and B) at 129.5 ppm between C_{AR}–H and C_{AR}–C groups. The exceptions indicated in Table IB are for C_{AR}–H in *o*-xylene and 1–8-octahydroanthracene where the ortho chemical shift effects from the alkyl and hydroaromatic ring substituents are greater than 1 ppm from benzene (δ_c = 128.7 ppm). Table IA shows that the α shifts for substituted mono- and diaromatics are between +5 and +20 ppm from benzene so that all the C_{AR}–C values occur within the range 129.5–150 ppm.

The introduction of heteroatoms into mono- and diaromatic species widens the aromatic range to approximately 110 to 160 ppm and also results in exceptions to the separation at 129.5 ppm between C_{AR}–H and C_{AR}–C groups. Table IA shows that alkyl groups ortho to C_{AR}–OH groups give C_{AR}–C resonances at higher field than 129.5 ppm as do internal aromatic carbons in nitrogen-containing rings, while Table IB shows that aromatic carbon para to basic nitrogen (pyridine and quinoline) and meta to C_{AR}–OH groups resonates at lower field than 129.5 ppm. The increased chemical shift range of phenols in relation to alkyl benzenes results from C_{AR}–OH resonances between 153 and 156 ppm and C_{AR}–H resonances ortho to C_{AR}–OH, between 115 and 118 ppm. Similarly, for bases, neutral nitrogen compounds and aromatic ethers, the increased chemical shift range in relation to alternant hydrocarbons is due to C_{AR}–O and C_{AR}–N resonances between 147 and 160 ppm and C_{AR}–H resonances α or β to C_{AR}–N groups between 100 and 118 ppm.

The chemical shift range for polyaromatic species (phenanthrenes, anthracenes, benzanthracenes, fluoranthenes, and pyrenes) is no larger than that for mono- and diaromatic species, but Table IB indicates that there are some C_{AR}–C resonances at higher field than 129.5 ppm, e.g. $C_{15,16}$ in pyrene and C_{12} in 2 methyl phenanthrene, while there are virtually no C_{AR}–H resonances at lower field than 129.5 ppm.

0003-2700/79/0351-2189$01.00/0

Table IA ^{13}C shifts of aromatic groups other than CAR-H (123 - 160 ppm)

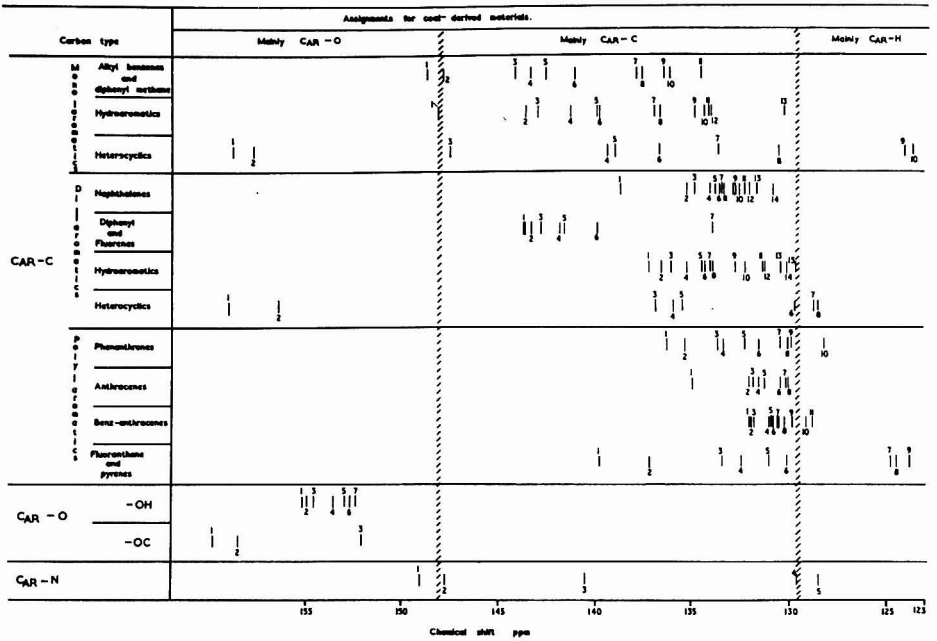

Key to Table IA

Monoaromatics
Alkyl bz. + diph.m.
1. isopropyl bz.
2. cyclohexyl bz.
3. ethyl bz.
4. butyl bz.
5. propyl bz.
6. diph. m.
7. toluene
8. p-xylene
9. o-xylene
10. mesitylene
11. m-xylene
Hydroaromatics
1. 1,3 dime. indan
2. indan
3. C5a 4,7 dime. indan
4. C8a 1 hex. 7 but. tet.
5. C7 7 bu. tet.
6. C7 1 hex. 7 but. tet.
7. tet.
8. C8a 7 bu. tet.
9. C10a 1-8 anph.
10. 1-8 chan.
11. C4a 1-8 ahph. and C4a 7 bu. tet.
12. C4a 1 hex. 7 but. tet.
13. C4 4,7 dime. indan

Heterocyclics
1. Dee. pyridine
2. 2,6 time. pyridine
3. 4 me. pyridine
4. m-cresol
5. 1,5 xylenol
6. p-ethyl phl.
7. 3 me. pyridine
8. p-cresol
9. o-cresol
10. 2,6 xylenol
Di-aromatics
Naphthalenes
1. C8b acenaph.
2. C2 2 me. naph.
3. C3 1,3 dime. naph.
4. C1 1 me. naph.
5. C1, C4a 1,3 dime. naph.
6. C8a 2 me. naph.
7. C4a 1 me. naph.
8. naph.
9. C2, C8a, 1,2 dime. naph.
10. C8a 1 me. naph.
11. C4a 1,2 dime. naph.
12. C5a acenaph.
13. C4a 2 me. naph.
14. C8a 1,3 dime. naph. and C1 1,2 dime. naph.

Diph. and fluorenes
1. C9a, C5a 4 me. fluorene
2. C4a fluorene
3. C4a 4 me. fluorene
4. C4a fluorene
5. diph.
6. C4b 4 me. fluorene
7. C4 4 me. fluorene
Hydroaromatics
1. C4a, 9, 10 dihyrh.
2. 9, 10 dihyan.
3. C5a, 1-3 9, 10, 10a hhpy.
4. C10a, 4, 5, 9, 10 thpy.
5. C10a, 9, 10 dihyph.
6. C5a 1-3, 9, 10, 10a hhpy.
7. C10a 1-3, 6-8 hhpy.
8. C10a thph.
9. C4a thph.
10. C8a thph. and C10b 1-3, 9, 10, 10a hhpy.
11. C8a 1-3, 9, 10, 10a hhpy.
12. C4b thnh.
13. C10b 4,5,9,10 thpy.
14. C10b 1-3,6-8 hhcy.
15. C10c 1-3 9,10,10a hhpy.
Heterocyclics
1. C9a quinoline
2. 2, 2' bipyridyl
3. C4a 2 me. indole.
4. C8a indole.
5. C7 2 me. indole.
6. C7a " "
7. C4a quinoline
8. C7a indole

Poly-aromatics
Phenanthrenes
1. C2 2 me. ph. and C3 3 me. ph.
2. C4 4 me. ph.
3. C10a " "
4. C3a " "
5. C10a or C9a 2 and 3 me. phs.
6. C4b 4 me. ph.
7. C4b 2 me. ph.
8. C4a or C4b 3 me. ph.
9. C4a 4 me. ph.
10. C4a 2 me. ph.
Anthracenes
1. C2 2 me. an.
2. C4a "
3. C10a "
4. an.
5. C8a 2 me. an. and C9a, C8a 9 me. an.
6. C9a 2 me. an.
7. C4a, C10a 9 me. an.
8. C9a, 9 me an.

Benzanthracenes
1. C4a, dibenzan.
2. C4a benzan.
3. C7a "
4. C7 7 me. benzan.
5. C12 "
6. C7a dibenzan.
7. C12a, C12b benzan.
8. C7b dibenzan.
9. C7a, 7 me. benzan.
10. C6a dibenzan.
11. C11a benzan.
Pyrenes and flu.
1. C10a fl.
2. C10b fl.
3. C4 4 me. py.
4. C10c fl.
5. C10a py.
6. C3a fl.
7. C10b 3 me. py.
8. C10b py.
9. C10c 3 me. py.
C_{AR}–OH
1. phenol
2. m-cresol
3. 3,5 xylenol
4. o-cresol
5. p-ethyl phl.
6. p-cresol.
7. 2,6 xylenol
C_{AR}–OC
1. methoxy bz.
2. diphenylene oxide
3. xanthene
C_{AR}–N
1. C8a quinoline
2. aniline
3. acridan
4. C7a 2 methyl indole
5. C7a indole

Abbreviations: ar = aromatic; m = methane; me = methyl; but = butyl; hex = hexyl; bz = benzene; diph = diphenyl; tet = tetralin; phl = phenol; naph = naphthalene; oh = octahydro; hh = hexahydro; th = tetrahydro; dihy = dihydro; an = anthracene; ph = phenanthrene; py = pyrene; fl = fluoranthene

Aliphatic Structures. The aliphatic chemical shifts for a variety of alkyl, hydroaromatic, and naphthenic substituents are given in Tables IIA and IIB. Where literature values were not available, the shifts have been predicted as follows.

(a) Alkyl aromatics, by an extension of the Grant and Paul (*20*) additivity rule for alkanes where a phenyl ring results

Table IB ^{13}C shifts of aromatic C_{AR}-H groups (110-140ppm)

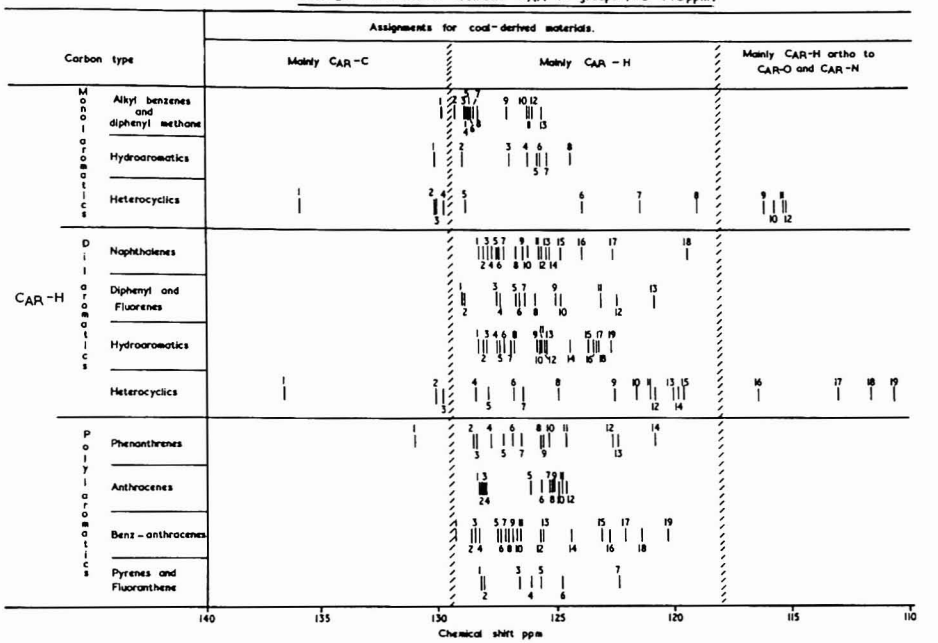

Key to Table IB

Mono-aromatics

Alkyl bz.• diph. m.

1. C3 p-xylene
2. C2 toluene
3. p-xylene
4. C2 diph. m.
5. bz.
6. C3 cyclohexyl bz.
7. C3 toluene
8. C3 diph. m.
9. C2 cyclohexyl bz.
10. C4 " "
11. C4 p-xylene
12. C4 diph. m.
13. C4 toluene

Hydroaromatics

1. 1-8 ohan,
2. C5 tet.,C5,C5,7 butyl tet
3. 4,7 dime indan
4. 1-8 obph
5. C5 indan
6. C6 7 butyl tet.
7. C6 tet.
8. C4 indan

Heterocyclics

1. C4 pyridine
2. C3 p-cresol
3. C3 phl.
4. C3 aniline
5. C3 p-ethyl phl.
6. C3 pyridine
7. C4 phl.
8. C4 aniline.
9. C2 "
10. C2 phl.
11. C2 p-cresol
12. C2 p-ethyl phl.

Di-aromatics

Naphthalenes

1. C5 1 me. naph.
2. C3 acenaph.
3. C3 2 me. naph.
4. C1 naph.
5. C5 2 me. naph.
6. C8 " "
7. C4 " "
8. C1 " "
9. C2 1 me naph.
10. C4 " "
11. C7 2 me. naph.
12. C2 naph.
13. C7 1 me.naph.
14. C3, C6 "
15. C6 2 me. naph.
16. C8 1 me. naph.
17. C4 acenaph.
18. C2 "

Diph. and fluorenes

1. C3 diph.
2. C3 4 me. fluorene
3. C4 diph.
4. C2 " "
5. C7 fluorene
6. C6 4 me. fluorene
7. C7 " "
8. C7 " "
9. C1 fluorene
10. C8 4 me. fluorene
11. C5 "
12. C1 "
13. C4 fluorene

Hydroaromatics

1. C10 1-4 thph.
2. C8 "
3. C3 9,10 dihyph.
4. C4 1-3, 9,10,10a hhpy.
5. C1, C2 9,10 dihyan.
6. C1 9,10 dihyph.
7. C2, 4,5,9,10 thpy.
8. C2 9,10 dihyph.
9. C1 4,5,9,10 thpy.
10. C7 1-3, 9,10,10a hhpy.
11. C8 " "
12. C6 1-4 thph.
13. C7 "
14. C9 "
15. C4 9,10 dihyph.
16. C4 1-3 6-8 hhpy.
17. C5 1-3, 9,10,10a hhpy
18. C6 " "
19. C5 1 - 4 thph.

Heterocyclics

1. C4 quinoline
2. C8 "
3. C7 "
4. C5 "
5. C1 acridan
6. C6 quinoline
7. C3 acridan
8. C2 indole
9. C5 "
10. C3 quinoline
11. C4 indole
12. C5 2 me. indole
13. C6 indole
14. C4 2 me. indole
15. C6 " "
and C2 acridan
16. C4 xanthene
17. C4 acridan
18. C7 indole
19. C7 2 me. indole
" "

Poly-aromatics

Phenanthrenes

1. C3 4 me. ph.
2. C1 ph.
3. C8 4 me. ph.
4. C10 "
5. C1, C5 "
6. C9 ph.,C9 4 me.ph.
7. C2, C3 ph.
8. C2 4 me. ph.
9. C7 " "
10. C6 " "
11. C8 " "
12. C4 ph.
13. C4 3 me. ph.
14. C4 1 me. ph.

Anthracenes

1. C3, C8 2 me. an.
2. C1 an.
3. C5 2 me. an.
4. C4 " "
5. C9 an.
and C1 2 me an.
6. C10 " "
7. C2 9 me. an.
8. C2 an.
and C3 9 me. an.
9. C7, C9 2 me. an.
10. C6 " "
11. C10 9 me. an.
12. C1 " "

Benzanthracenes

1. C11 7 me.benzan,
2. C4 dibenzan,
3. C4 benzan,
4. C8 "
5. C11 "
6. C6 dibenzan,
7. C7 benzan,
8. C5 dibenzan,
9. C2 "
and C5, C6 benzan,
10. C3 dibenzan,
and C2 benzan,
11. C3 "
12. C10 "
13. C9 "
14. C8 7 me. benzan,
15. C6 " "
16. C1 benzan,
and C1 dibenzan,
17. C7 "
18. C12 benzan,
19. C12 7 me. benzan,

Pyrenes and fla.

1. C7 fl.
2. C2 "
3. C3 "
4. C8 "
5. C2 py.
6. C1 "
7. C1 fl.

Abbreviations: ar = aromatic; m = methane; bz = benzene; me = methyl; diph = diphenyl; tet = tetralin; phl = phenol; naph = naphthalene; oh = octahydro; hh = hexahydro; th = tetrahydro; dihy = dihydro; an = anthracene; ph = phenanthrene; py = pyrene; fl = fluoranthene

in an α shift of +23 ppm, a β shift of +9.5 ppm, and a γ shift of −2 ppm.

(b) Hydroaromatic rings (tetralin and indan type structures), from the literature values of tetrahydrophenanthrene, tetralin, and indan and from the α and β equatorial shifts for alkyl substituents derived from literature values for methyl indans (*3*) and alkyl tetralins (*16*).

(c) 1-4,4a,9,10,10a-Octahydrophenanthrene and 1,4,4a,-

Table IIA Summary of ^{13}C shifts of aliphatic CH_2 and CH_3 groups

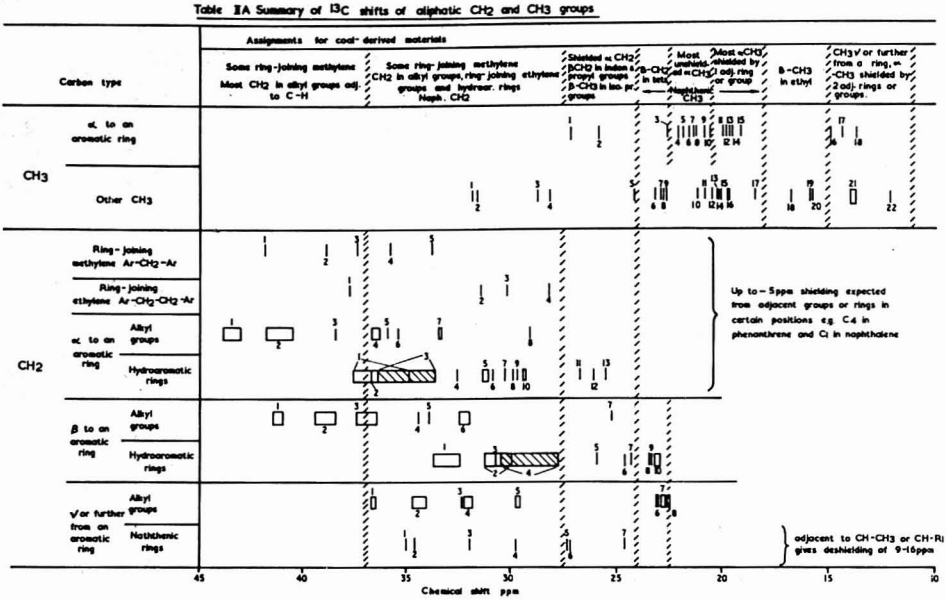

Key to Table IIA

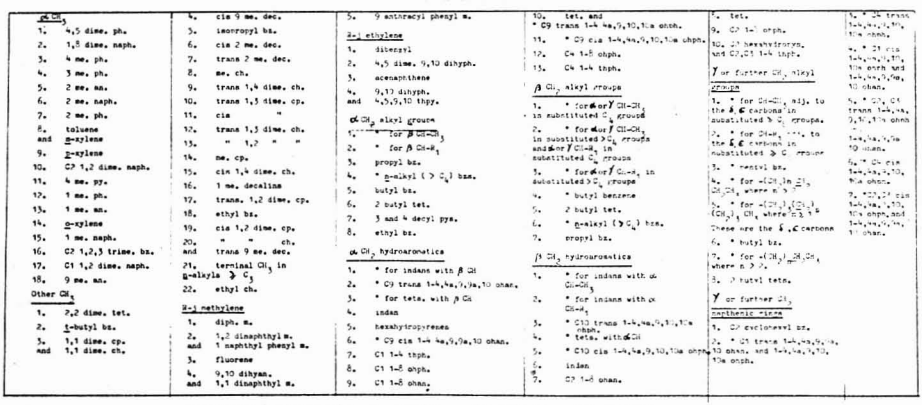

α CH_3

1. 4,5 dime. ph.
2. 1,8 dime. naph.
3. 4 me. ph.
4. 3 me. ph.
5. 2 me. an.
6. 2 me. naph.
7. 2 me. ph.
8. toluene and p-xylene
9. p-xylene
10. C7 1,2 dime. naph.
11. 4 me. py.
12. 1 me. ph.
13. 1 me. an.
14. p-xylene
15. 1 me. naph.
16. C2 1,2,5 trime. ba.
17. C1 1,2 dime. naph.
18. 9 me. an.

Other CH_3

1. 2,2 dime. tet.
2. t-butyl ba.
3. 1,1 dime. cp. and 1,1 dime. ch.
4. cis 9 me. dec.
5. isopropyl ba.
6. cis 2 me. dec.
7. trans 2 me. dec.
8. me. ch.
9. trans 1,4 dime. ch.
10. trans 1,3 dime. cp.
11. cis " "
12. trans 1,3 dime. ch.
13. " 1,2 " "
14. me. cp.
15. cis 1,4 dime. ch.
16. 1 me. decalins
17. trans. 1,2 dime. cp.
18. ethyl ba.
19. cis 1,2 dime. cp.
20. " " ch.
and trans 9 me. dec.
21. terminal CH_3 in n-alkyls $\geq C_3$
22. ethyl ch.

R-j methylene

1. diph. m.
2. 1,2 dinaphthyl m. and 1 naphthyl phenyl m.
3. fluorene
4. 9,10 dihyan.
and 1,1 dinaphthyl m.
5. 9 anthracyl phenyl m.

R-j ethylene

1. dibenzyl
2. 4,5 dime. 9,10 dihyph.
3. acenaphthene
4. 9,10 dihyph.
and 4,5;9,10 thpy.

α CH_2 alkyl groups

1. * for β CH_3
2. * for β CH-R_1
3. propyl ba.
4. * n-alkyl (> C_3) ba.
5. butyl ba.
6. 2 butyl tet.
7. 3 and 4 decyl pya.
8. ethyl br.

α CH_2 hydroaromatics

1. * for indans with β CH
2. * C9 trans 1-4,4a,9,9a,10 ohan.
3. * for tets. with β Ca
4. indan
5. hexahydropyrenes
6. * C9 cis 1-4 4a,9,9a,10 ohan.
7. C1 1-4 thph.
8. C1 1-5 ohph.
9. C1 1-8 ohan.
10. tet. and
* C9 trans 1-4,4a,9,10,10a ohnh.
11. * C9 cis 1-4,4a,9,10,10a chph.
12. C4 1-8 ohph.
13. C4 1-4 thph.

β CH_2 alkyl groups

1. * for α or γ CH-CH_3 in substituted $C_{\geq 3}$ groups
2. * for α or γ CH_2-CH_3 in substituted $\geq C_4$ groups and α or γ CH-R_1 in substituted $C_{\geq 3}$ groups
3. * for α or γ CH_2-$R_{\geq 2}$ in substituted $\geq C_4$ groups
4. * butyl benzene
5. 2 butyl tet.
6. * n-alkyl ($\geq C_4$) bza.
7. propyl ba.

β CH_2 hydroaromatics

1. * for indans with α CH_2-CH_3
2. * for indans with α CH_2-R_2
3. * C10 trans 1-4,4a,9,9a,10a ohph.
4. * tets. with α CH_2
5. * C10 cis 1-4,4a,9,10,10a ohph.
6. indan
7. C2 1-8 ohan.
* tet.
9. C2 1-4 ohph.
10. C7 hexahydropyrs. and C7,C8 1-4 thpt.

γ or further CH_2 alkyl groups

1. * for CH_2-CH_3 adj. to the β,ε carbons in substituted $\geq C_3$ groups.
2. * for CH_2-$R_{\geq 2}$ adj. to the β,ε carbons in substituted $\geq C_4$ groups
3. * butyl ba.
4. * for $-(CH_2)_n$-CH_3 where $n \geq 3$
5. * for $-(CH_2)_n$-CH_3 where $n \geq 4$
These are the β,ε carbons
6. * butyl bz.
7. * for $-(CH_2)_n$-R_1 where $n \geq 2$
8. p butyl tets.

γ or further CH_2 naphthenic rings

1. C2 cyclohexyl bz.
2. * C1 trans 1-4,4a,9,9a, 10 ohan. and 1-4,4a,9,10, 10a onph.
1. * 2H trans 1-4,4a,9,10, 10a ohnh.
2. * 2H cis 1-4,4a,9,10, 10a ohnh.
3. C4 trans 1-4,4a, 9,10,10a ohnh and 1-4,4a,9,9a, 10 ohan.
4. * C4, C4 trans 1-4,4a, 9,10,10a ohnh
5. * C4 cis 1-4,4a,9,9a 10 ohan.
6. * C4 trans 1-4,4a,9,10, 10a ohnh and 1-4,4a,9,9a, 10 ohan.

Abbreviations! * = predicted value; adj = adjacent; R-j = ring-joining; R_1 = n-alkyl > methyl; ba = benzene; m = methane; me = methyl; ch = cyclohexane; cp = cyclopentane; naph = naphthalene; dinh = dinhenyl; tet = tetralin; dihy = dihydro; th = tetrahydro; oh = octahydro; dec = decalin; ph = rhenanthrene; py = pyrene; an = anthracene

9,9a,10-octahydroanthracene, from consideration of the effect of a phenyl ring on the chemical shifts of *cis*- and *trans*-dekalin (22) by the differences in chemical shift between tetralin and cyclohexane. Saturates have not been included in Tables IIA and B because in virtually all characterization work on products from coal liquefaction processes these are removed by column chromatography.

The chemical shifts of aliphatic groups are governed mainly by whether they, and their adjacent aliphatic groups, are methyl, methylene, or methine. Methyl groups have a chemical shift range of 12 to 32 ppm, methylene groups of 22.5 to 44 ppm (for one adjacent methine group), and methine groups of 27 to 57 ppm for no adjacent methine groups. Quaternary aliphatic carbons, which are not considered by the authors to be major groups in coal extracts, have not been included in Tables IIA and B, but their chemical shifts are expected to overlap to a large extent with those of methine groups. Some workers, such as Farcasiu (22), consider that quaternary aliphatic carbons are major constituents in their liquefaction products.

Table II B Summary of ^{13}C shifts of aliphatic methine groups

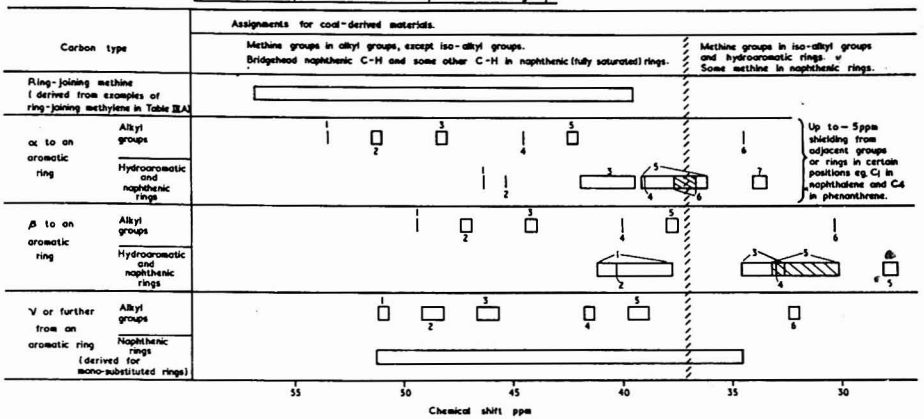

Key to Table IIB

alkyl groups	Hydroaromatic and naphthenic rings	alkyl groups	Hydroaromatic and naphthenic rings	or further alkyl groups
1. * - $CH(C_2H_5)_2$	1. * Cis-trans 1-4, 4a,5,8,8a-ohah	1. * - $CH(C_2H_5)_2$	1. * for indans with CH-R_1	1. * - $CH(C_2H_5)_2$ * -
2. * - $CH(C_2H_5)R$	2. Cis cyclohexyl benzene	2. * - $CH(C_2H_5)R$	2. * Cis-trans 1-4, 4a,9,9a-10 ohan. and C10a " " 4a,5,8,8a-ohahn.	2. * - $CH(C_2H_5)R$
3. * - CHR_2	3. * for indans with CH-R_1	3. * - CHR_2	3. * for indans with CH - CH_3	3. * - CHR_2
4. * - $CH(CH_3)(C_2H_5)$	4. * Cis-cis 1-4, 4a,5,8,8a-ohah.	4. * - $CH(CH_3)(C_2H_5)$	4. * Cis-cis 1-4, 4a,4,9a-10 ohan. and C10a " " 4a,5,8,8a-ohahn.	4. * - $CH(C_2H_5)CH_3$
5. * - $CH(CH_3)R$	5. * for tetralins with CH-R_1	5. * - $CH(CH_3)R$	5. * for tetralins with CH-R_1	5. * - $CH(CH_3)R$
6. isopropyl benzene	6. * for indans with CH-CH_3	6. isobutyl benzene	6. * for tetralins with CH-CH_3	6. * - $CH(CH_3)_2$
	7. * for tetralins with CH-CH_3			

Abbreviations:

* = predicted value

R = n-alkyl ethyl

R_1 = n-alkyl methyl

ohan = octahydroanthracene

ohph = octahydrophenanthrene

Note:

Compounds with 2 adjacent methine groups are not included, but it is estimated that for these the shifts will be increased by about 5-10 ppm. Quarternary aliphatic carbon shifts are also excluded. It is estimated that with the exception of t-butyl benzene (34.5 ppm), the majority of these occur between 37 and 40 ppm.

Methyl. The majority of methyl groups likely to be present in coal-derived materials have chemical shifts at higher field than 24 ppm. Methyl groups with chemical shifts between 24 and 32 ppm are generally sterically hindered, such as in 1,8-dimethylnaphthalene and 2,2-dimethyltetralin, and are less likely to be present. From the evidence presented in Table IIA, the chemical shift range 12–24 ppm can be subdivided as follows: (a) 22.5–24 ppm, attributed to methyl in some naphthenic and hydroaromatic rings; (b) 20.5–22.5 ppm, attributed to methyl α to an aromatic ring not shielded by any adjacent groups or rings (e.g., 2-methylnaphthalene) plus some on naphthenic and hydroaromatic rings; (c) 18–20.5 ppm, attributed to methyl α to an aromatic ring shielded by 1 adjacent group or ring (e.g., 1-methylnaphthalene) plus some CH_3 on naphthenic rings; (d) 15–18 ppm attributed to methyl in ethyl groups and in *cis*-1,2-disubstituted five- and six-membered rings, and (e) 12–15 ppm, attributed to terminal methyl in alkyl chains $\geq C_3$ and to CH_3 α to an aromatic ring shielded by 2 adjacent groups or rings (e.g., 9-methylanthracene).

Methylene. Table IIA shows that for methylene groups the range of chemical shifts possible for most of the environments considered is significantly less than the overall chemical shift range of 22.5 to 44 ppm. For example, ring-joining methylene groups have chemical shifts between 34 and 42 ppm, with the values moving toward higher field as the shielding from adjacent rings and groups increases. There is a division at 37 ppm between ring-joining methylene groups shielded by one or no adjacent ring or group and those shielded by more than one adjacent ring or group. Ring-joining ethylene resonances can occur between 28 and 37 ppm; those shielded by more than one adjacent ring or group occurring mainly between 28 and 32 ppm.

For methylene in alkyl groups α or β to an aromatic ring, Table IIA suggests that there is a reasonable separation at approximately 37 ppm between methylene adjacent and not adjacent to methine. An exception is the α methylene in propyl benzene at 38.5 ppm. Methylene in hydroaromatic rings α to an aromatic ring has a chemical shift range of 25 to 37.5 ppm, with a separation at 33 ppm between the predicted values for methylene adjacent to CH, and the observed values for methylene in unsubstituted hydroaromatic rings. This range is larger than the 23–33 ppm range used by Seshadri et al. (23) to calculate hydroaromatic carbon in

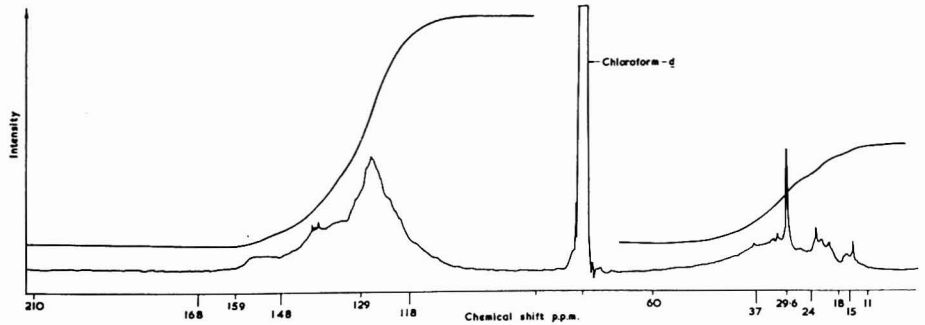

Figure 1. ^{13}C spectrum of asphaltenes from a hydrogen donor solvent extract (extract a)

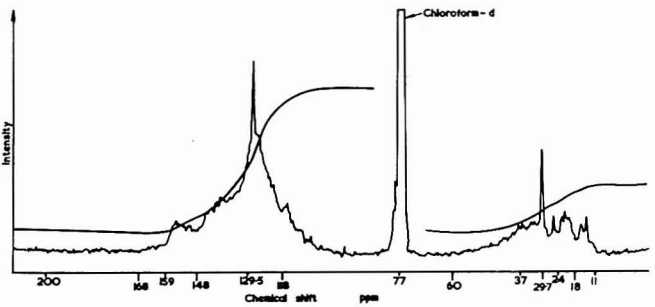

Figure 2. ^{13}C spectrum of asphaltenes from a supercritical gas extract (extract b)

hydrogenated anthracene oil and will include α-CH_2 adjacent to methine groups. It is interesting to note that the hydroaromatic methylene groups α to an aromatic ring with resonances between 25 and 27.5 ppm, such as C_4 in 1-4-tetrahydrophenanthrene, are in positions shielded by an adjacent aromatic ring. A comparison of the chemical shifts of C_1 in 1-8-octahydroanthracene and 1-8-octahydrophenanthrene at 29.9 and 29.7 ppm, respectively, with that of C_4 in 1-8-octahydrophenanthrene (26.1 ppm), which is shielded by an adjacent ring, shows that the additional shielding in 1-8-octahydrophenanthrene produces an upfield shift of nearly 4 ppm. Therefore from the chemical shift of 29.1 ppm for ethylbenzene, it is likely that methylene in ethyl groups at positions which are shielded by an adjacent ring, such as C_4 in phenanthrene and fluorene, will have chemical shifts between 25 and 26 ppm. β-CH_2 groups in unsubstituted 6-membered hydroaromatic rings, e.g., tetrahydrophenanthrene and tetralin, give resonances between 22.5 and 24 ppm, and those in substituted hydroaromatic rings give resonances between 27 and 35 ppm.

Methylene groups γ or further from an aromatic ring in *n*-alkyl groups, as for *n*-alkanes, have resonances at 29.6–29.8, 31.8–32.4, and 22.5–23 ppm for positions respectively δ, ϵ, or further, γ and β from the terminal methyl group.

Methine. Table IIB indicates that methine resonances in alkyl groups, ring-joining groups, and many naphthenic and hydroaromatic rings occur at lower field than 37 ppm. Methine resonances occurring at higher field than 37 ppm are isopropyl, isobutyl, and other iso-alkyl groups and α-CH–CH_3 and β-CH–R (R ≥ methyl) in tetralin, β and some α-CH–CH_3 in indan, C_{10a} in *cis*-1-4,4a,9,10,10a-octahydrophenanthrene and C_{9a} in *cis*-1-4,4a,9,9a,10-octahydroanthrene. These resonances include a substantial number of hydroaromatic methine groups.

APPLICATION TO COAL EXTRACTS

Coal Extracts. The extracts chosen were: (a) the asphaltenes from an extract of a low-rank coal (National Coal Board, Coal Rank Code 702) prepared at 400 °C with a hydrogen donor solvent; (b) the asphaltenes from a supercritical gas (SCG) extract of a low-rank coal (NCB, CRC 902) prepared at 400 °C (*5*); (c) the aromatic fraction of the *n*-pentane solubles from a SCG extract of a low-rank coal (NCB, CRC 802) prepared at 400 °C in the presence of hydrogen and catalyst (*5*); and (d) the residue of a product oil from hydrogenation of a SCG extract.

^{13}C NMR Spectra. The ^{13}C spectra of the extracts were recorded on a Bruker WH 180 WB instrument using 3 g of sample for the asphaltenes, 0.7 g for the *n*-pentane soluble SCB extract and 2.2 g for the hydrogenated SCG extract residue, each in 15 mL of chloroform-*d*. To obtain reliable quantitative results (*14*), 200 mg of chromium acetylacetonate was added to the asphaltenes and hydrogenated SCG extract residue and 100 mg was added to the *n*-pentane soluble SCG extract. A delay period of 4 s after each 35° pulse (10-μs duration) and a 0.335-s data acquisition period was used in the gated decoupling sequence. Reference 14 demonstrates that these conditions have given accurate aromaticity values for a mixture of model compounds and extract (c).

The ^{13}C NMR spectra of the four extracts investigated are shown in Figures 1–4 and the data obtained from these spectra are given in Table IIIA together with the aliphatic H/C ratios derived from ^1H and ^{13}C NMR and ultimate analysis. The analytical results for ^1H NMR, ultimate analysis, phenolic

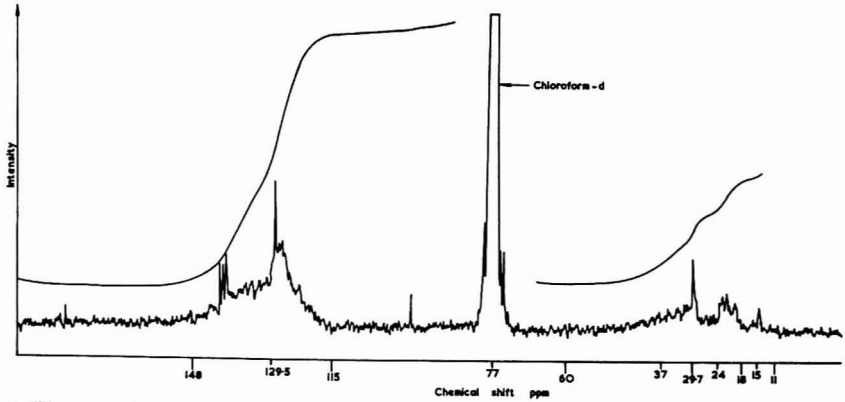

Figure 3. ^{13}C spectrum of aromatic fraction of the *n*-pentane solubles from a supercritical gas extract prepared in the presence of hydrogen and catalyst (extract c)

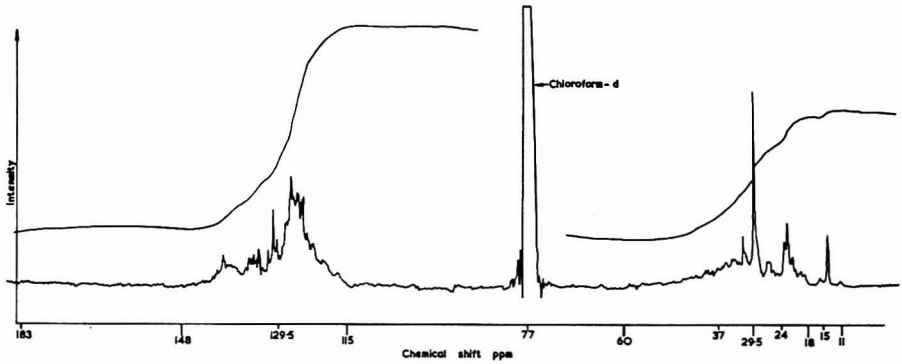

Figure 4. ^{13}C spectrum of residue from a product oil of hydrogenated supercritical gas extract (extract d)

–OH and molecular weight, of the extracts are summarized in Table IIIB.

Aromatic Carbon–Oxygen Groups. Carbonyl resonances (170–210 ppm) were not observed in any of the spectra, although two extracts (a and b) contain 5.1 and 8.6% oxygen. The absence of carbonyl groups in these extracts appears at first sight somewhat surprising since some of the oxygen in coals is believed to be present as carbonyl. However, the carbonyl groups in the asphaltenes of the extract prepared using a hydrogen donor solvent (extract a) may have been reduced by the solvent in a similar way to that found by Benjamin et al. (*24*) using tetralin. Their absence in the SCG extract b may be associated with the nature of supercritical gas extraction in that the coal could have been separated into a carbonyl lean extract and an insoluble carbonyl-rich solid residue.

The chemical shift range 148–168 ppm mainly contains resonances from aromatic carbon joined to hydroxyl and ether oxygen, while the range 100–115 ppm contains those C_{AR}–H ortho to these groups. Extracts a and b show resonances in both these regions (see Figures 1 and 2 and Table IIIA), with the bulk of resonances between 148 and 159 ppm. This supports the analytical evidence in Table IIIB which indicates that there are many more phenolic hydroxyl than aromatic ether groups: the resonances of the latter are more likely to be spread between 148 and 168 ppm. There is good agreement in Table IIIA between the oxygen by ultimate analysis and by ^{13}C NMR (C_{AR}–O). As expected extracts c and d which have low oxygen contents, do not show any resonances in these regions, and none of the extracts displayed resonances in the region between 60 and 75 ppm assigned to aryl alkyl ethers.

Aromatic Carbon–Hydrogen and Other Aromatic Carbon Groups. As has already been mentioned, there should be a reasonable separation at 129.5 ppm between C_{AR}–H groups and other aromatic carbon groups when the numbers of aromatic ring systems containing more than 2 rings and heterocyclic groups are small. This, in fact, appears to be the case for extracts b and c because Table IIIA shows that reasonable agreement is obtained between the percentage of carbon in C_{AR}–H groups calculated from ^{13}C NMR and from ^{1}H NMR plus the H/C ratio.

These extracts are known to have open aromatic structures consisting largely of aromatic systems with 1 or 2 rings (*5*). Further, the heteroatom content (see Table IIIB) of extract c is low and, although extract b contains a significant number of heteroatoms, this does not appear to have a significant effect on the separation at 129.5 ppm.

The situation is somewhat different for extracts a and d where the agreement between the C_{AR}–H groups by ^{13}C and ^{1}H NMR and H/C ratio is poor. However, these extracts are

Table IIIA. Carbon Distributions Derived from the ^{13}C Spectra of the Coal Extracts (* = value from ultimate analysis. ** = value from ^{1}H NMR + H/C ratio)

assignments	chemical shift, ppm	(a) asphaltenes from a hydrogen donor solvent extract		(b) asphaltenes from a supercritical gas extract		(c) aromatic fraction of *n*-pentane sols. from a supercritical gas extract prepared in the presence of H_2 and catalyst		(d) residue from a product oil of hydrogenated supercritical gas extract	
		% of total carbon	% of aliphatic carbon	% of total carbon	% of aliphatic carbon	% of total carbon	% of aliphatic carbon	% of total carbon	% of aliphatic carbon
carbonyl	170-210	-	-	-	-	-	-	-	-
aromatic C-O	148-168	4.4 (*4.4)	-	8.0 (*7.8)	-	-	-	-	-
Mainly aromatic C-C and aromatic C-NH	129.5-148	28.6	-	32.3	-	33.4	-	21.8	-
Mainly aromatic C-H with aromatic C-H ortho to C-OH between 100 and 115 ppm	100-129.5	37.4 (**25.6)	-	33.3 (**30.7)	-	35.0 (**31.6)	-	37.7 (**28.8)	-
Ring joining methylene (32-43 ppm) CH_2 in alkyl groups (except iso-alkyls) and naphthenic rings. CH_2 in alkyl groups adjacent to CH	37-60	7.6	25.7	5.9	22.3	6.0	19.0	7.2	17.8
CH_2 in alkyl groups not adjacent to CH (except some α-CH_2 and CH_2 adjacent to terminal CH_3 in alkyl groups $>C_4$ CH_2 in ring joining ethylene groups. α-CH_2 and CH, β-CH in hydroaromatic rings. Naphthenic CH_2	27.5-37	11.3	38.2	9.3	35.2	12.4	39.2	19.2	47.4
Naphthenic CH_2. Shielded α-CH_2 groups, β-CH_2 in indan and propyl groups. β-CH_3 in isopropyl	24-27.5	2.4	8.1	2.1	8.0	2.7	8.5	3.5	8.6
CH_2 adjacent to terminal CH_3 in alkyl groups $>C_4$. β-CH_2 in unsubstituted tetralin structures. CH_3 on hydroaromatic and naphthenic rings (18-24 ppm)	22.5-24	2.2	7.4	1.2	4.5	2.4	7.6	4.6	11.4
α-CH_3 not shielded by any adjacent rings or groups	20.5-22.5	1.5	5.0	2.4	9.1	2.9	9.2	1.9	4.7
α-CH_3 shielded by 1 adjacent ring or group	18-20.5	1.7	5.7	1.8	6.8	2.4	7.6	1.6	4.0
β-CH_3 in ethyl groups	15-18	1.5	5.0	1.9	7.1	1.3	4.1	0.5	1.2
CH_3 γ or further from an aromatic ring + α-CH_3 shielded by 2 adjacent rings or groups	11-15	1.5	5.0	1.9	7.1	1.5	4.7	2.1	5.2
Aromaticity		0.70		0.74		0.68		0.60	
Aliphatic H/C ratio		2.0		2.5		2.5		2.1	

Table IIIB. Other Analytical Data of the Coal Extracts

		(a) asphaltenes from a hydrogen donor solvent extract	(b) asphaltenes from a supercritical gas extract	(c) aromatic fraction of *n*-pentane solubles from a supercritical gas extract in presence of H_2+ catalyst	(d) residue from product oil of a hydrogenated supercritical gas extract
%	C	86.1	82.2	91.0	90.0
	H	6.5	6.6	8.4	8.7
	O	5.1	8.6	0.8	1.5
	N	1.8	1.2	0.25	0.3
	S	0.35	1.2	<0.1	<0.1
average molecular weight		610	430	280	260
% OH		5.0	6.2	0.5	<0.1
% nonphenolic oxygen		0.4	2.8	0.3	>1.4
H/C atomic		0.90	0.96	1.10	1.15
% of total hydrogen from ^{1}H NMR	$H_{AR,OH}$ (5–9 ppm)	33.1	37.4	28.4	26.0
	$H_{\alpha,2}$ (3.3–4.5 ppm)	4.7	6.0	4.3	1.6
	H_α* (2–3.3 ppm)	25.4	28.2	34.0	23.1
	H_N (1.5–2 ppm)	9.1		8.7	12.4
	H_β** (1.0–1.5 ppm)	16.8	22.0	17.2	24.5
	H_γ (0.5–1.0 ppm)	10.8	6.4	7.4	12.4

* 1.9–3.3 ppm for SCG extract asphaltenes. ** 1.0–1.9 ppm for SCG extract asphaltenes. Hydrogen types: $H_{AR,OH}$ = aromatic and phenolic, $H_{\alpha,2}$ = ring-joining methylene, H_α = α to an aromatic ring, H_N = CH_2 and CH β to an aromatic ring in hydroaromatic and alkyl groups, H_β = CH_2 and CH further than β from an aromatic ring (further than α from an aromatic ring for SCG extract asphaltenes), H_γ = CH_3 γ or further from an aromatic ring.

believed to contain much larger peri- and cata- condensed systems (5) which will result in some C_{AR}–C resonances at higher field than 129.5 so that the percentage of C_{AR}–H groups by ^{13}C NMR is overestimated.

Aliphatic Groups. The aliphatic H/C ratios of the extracts are listed in Table IIIA. The value of 2.5 for extracts b and c is significantly larger than those of 2.0 and 2.1 for extracts a and d, respectively. Figures 1–4 show that this can be attributed to the latter two extracts containing more CH_2 and CH resonances (22.5–60 ppm) and fewer methyl resonances (11–22.5 ppm). For example, extract a has 79.4% of the aliphatic carbon resonances between 22.5 and 60 ppm compared to 70% for extract b.

All four extracts may contain naphthenic structures (37–60 ppm). This region contains resonances from bridgehead and other CH naphthenic carbons, some methylene bridge carbon (between sites with a total of one or no adjacent ring or group), alkyl CH other than in iso-alkyl groups and alkyl CH_2 adjacent to alkyl CH. If it is assumed that the numbers of the last two groups are small, because the fraction of hydrogen α to an aromatic ring from ^{1}H NMR (Table IIIB) indicates that the average size of alkyl and naphthenic groups is approximately 2 carbon atoms, then subtraction of the percentage of carbon in methylene bridges (derived from ^{1}H NMR), gives a rough estimate of the number of bridgehead and other CH naphthenic carbon. In this way it can be estimated that the extracts contain between 3–6% bridgehead and other CH naphthenic carbon. The percentage of carbon in methylene bridges derived from ^{1}H NMR is probably an overestimate for that in the 37–60 ppm range because Table IIIA shows that the region between 33 and 37 ppm contains methylene bridge carbon between sites with a total of two or more adjacent rings or groups.

The region between 27.5 and 37 ppm contains the resonances of methylene groups in several different environments and also of methine groups in hydroaromatic rings. The most prominent signal in this region is a sharp peak at 29.5–29.7 ppm which is attributed to methylene ε or further from the end of the chain, and γ or further from an aromatic ring in alkyl chains at least 8 carbon atoms long. Except for extract d, the area under this peak is relatively small. A column chromatographic separation on silica gel showed extract d to contain some long chain alkyl aromatics. The peak between 31.7 and 32 ppm is attributed to methylene in the γ position from the end of an alkyl side chain.

The band between 24 and 27.5 ppm accounts for about 8% of the aliphatic carbon in the extracts: the main contributors are thought to be α-CH_2 groups shielded by adjacent rings or groups, some naphthenic CH_2, β-CH_2 in propyl and indan groups and β-CH_3 in isopropyl groups. It is likely that these groups are present in different proportions in extracts b and d to extracts a and c because in Figures 2 and 4 peaks at 26.5 ppm are observed while in Figures 1 and 3 there are no distinctive peaks between 24 and 27.5 ppm.

The signals between 22.5 and 24 ppm are less pronounced in extract b (Figure 2) than in the other extracts, which together with the fact that there is no distinctive ^{1}H band between 1.5 and 2.0 ppm (see Table IIIB), indicates that hydroaromatic substituents are not major structural types in this extract. Apart from β-CH_2 in unsubstituted 6-membered hydroaromatic rings, CH_2 β to the terminal methyl group in long alkyl side chains (≥C_4) is thought to be the other major contributor to the 22.5–24 ppm band. Table IIIA shows that this band accounts for more aliphatic carbon in extract d than in the other extracts, probably because it contains the most long alkyl side chain resonances as well as a considerable number from hydroaromatic groups. Methyl groups in hydroaromatic and naphthenic rings are also likely to contribute

to the 22.5–24 ppm band as well as the 18–22.5 band.

The 18–20.5 and 20.5–22.5 ppm bands, attributed respectively to methyl α to an aromatic ring adjacent to one (e.g., 1-methylnaphthalene) or no ring or group (e.g., 2-methylnaphthalene) are of similar intensity for all the extracts. This fact should be taken into account when average structures are constructed to represent the large number of individual compounds in these complex materials (*5*).

The band between 15 and 18 ppm has been assigned to β-CH_3 in ethyl groups, although methyl groups, for example, in disubstituted hydroaromatic and naphthenic rings may also contribute. The intensity of this band accounts for less than 50% of that of the 18–22.5 ppm band for all the extracts and therefore it is likely that there are at least twice as many methyl as ethyl groups.

The band between 11 and 15 ppm has been assigned to methyl α to an aromatic ring shielded by 2 adjacent groups or rings (e.g., 9-methylanthracene) and to terminal methyl in alkyl side chains ($\geq C_3$). The intensity of this band for extract d is far larger than that of the 15–18 ppm ethyl band, and it is thought that the major contributor is terminal methyl because this extract probably contains the most long alkyl chain aromatics. For the other extracts, the intensity of the 11–15 ppm band is similar to that of the 15–18 band and it is thought that in these the 11–15 ppm band contains similar amounts of shielded methyl and terminal methyl.

CONCLUSIONS

A detailed consideration of the ^{13}C chemical shifts in model compounds has been made which has enabled a ^{13}C chemical shift assignment scheme to be developed for proton decoupled spectra of coal-derived materials. This scheme has yielded valuable structural information on the oxygen groups and on the distribution of aliphatic substituents in extracts from low-rank British coals.

ACKNOWLEDGMENT

The authors thank I. Stenhouse of the PCMU, Harwell, for the ^{13}C spectra and T. G. Martin and W. F. Wyss for providing the extracts.

LITERATURE CITED

(1) I. Schwager, P. A. Farmanion, and T. F. Yen, *Prepr., Div. Pet. Chem., Am. Chem. Soc.*, **22**(2), 677 (1977).
(2) K. D. Bartle, T. G. Martin, and D. F. Williams, *Chem. Ind. (London)*, 313, (1975).
(3) H. L. Retcofsky and R. A. Friedel "Spectrometry of Fuels", Plenum, New York, 1970, Chapter 8.
(4) R. J. Pugmire, D. M. Grant, K. W. Zilm, L. L. Anderson, A. G. Oblad, and R. E. Wood, *Fuel*, **56**, 295 (1977).
(5) K. D. Bartle, W. R. Ladner, C. E. Snape, T. G. Martin, and D. F. Williams, *Fuel*, **56**, 413 (1979).
(6) R. A. Friedel and H. L. Retcofsky, *Chem. Ind. (London)*, 455 (1966).
(7) S. A. Knight, *Chem. Ind. (London)*, 1923 (1967).
(8) H. L. Retcofsky, F. K. Schweighardt, and M. Hough, *Anal. Chem.*, **49**, 585 (1977).
(9) J. K. Brown and W. R. Ladner, *Fuel*, **39**, 87 (1960).
(10) J. K. Stothers, "^{13}C NMR Spectroscopy", Academic Press, New York, 1972, Chapter 3.
(11) E. Breitmaier, and W. Voelter, "^{13}C NMR Spectroscopy", Verlag Chemie, Weinheim/Bergst, Germany, 1974.
(12) K. D. Bartle, A. Calimli, D. W. Jones, R. S. Matthews, A. Olcay, H. Pakdel, and T. Tugrul, *Fuel*, **58**, 423 (1979).
(13) J. N. Shoolery and W. L. Budde, *Anal. Chem.*, **48**, 2146 (1976).
(14) W. R. Ladner and C. E. Snape, *Fuel*, **57**, 658 (1978).
(15) K. S. Seshadri, R. G. Ruberto, D. M. Jewell, and H. P. Malone, *Fuel*, **57**, 111 (1978).
(16) D. K. Dalling, K. H. Ladner, D. M. Grant, and W. R. Woolfenden, *J. Am. Chem. Soc.*, **99**, 7142 (1977).
(17) R. S. Ozubko and G. W. Buchanan, *Can. J. Chem.*, **52**, 2493 (1974).
(18) J. B. Stothers, C. T. Tan, and N. K. Wilson, *Org. Magn. Reson.*, **9**, 408 (1977).
(19) D. M. Grant and E. G. Paul, *J. Am. Chem. Soc.*, **86**, 2984 (1964).
(20) D. K. Dalling and D. M. Grant, *J. Am. Chem. Soc.*, **89**, 6612 (1967).
(21) D. K. Dalling and D. M. Grant, *J. Am. Chem. Soc.*, **95**, 3718 (1973).
(22) M. Farcasiu, *Fuel*, **56**, 9 (1977).
(23) K. S. Seshadri, R. G. Ruberto, D. M. Jewell, and H. P. Malone, *Fuel*, **57**, 549 (1978).
(24) B. M. Benjamin, V. F. Raaen, P. H. Maupin, L. L. Brown, and C. J. Collins, *Fuel*, **57**, 269 (1978).

RECEIVED for review March 8, 1979. Accepted July 11, 1979. Permission to publish this work is given by the National Coal Board, United Kingdom, and the views expressed are those of the authors and not necessarily those of the Board.

Error Estimates for Finite Zero-Filling in Fourier Transform Spectrometry

Melvin B. Comisarow* and Joe D. Melka

Chemistry Department, University of British Columbia, Vancouver, British Columbia Canada V6T 1W5

A systematic procedure is developed for estimating the maximum peak height error and the maximum frequency error which results from Fourier transformation of a zero-filled, truncated, exponentially damped sinusoid. The errors are functions of the number of zero-fillings and the ratio of the acquisition period to the relaxation time of the sinusoid. The error estimates are given in both analytical form and graphical form for both absorption mode and magnitude mode Fourier transform spectra. It is concluded that four zero-fillings for the absorption mode and three zero-fillings for the magnitude mode will usually suffice to reduce the peak height error to less than 2%. Applications to Fourier transform nuclear magnetic resonance spectrometry and Fourier transform ion cyclotron resonance spectrometry are briefly discussed.

Within the past 15 years, a new method called the Fourier transform (FT) method has been developed for obtaining spectral data (*1*). In the FT method as applied to nuclear magnetic resonance (NMR) spectrometry (*2–5*), microwave spectrometry (*6*), and ion cyclotron resonance (ICR) spectrometry (*7–16*), the motion of the entire sample is excited at once and a time domain signal which is a composite signal from all of the excited motion is sampled and stored. In this manner the FT method can produce a time domain transient signal, which is characteristic of the entire spectrum, in the amount of time which a conventional scanning spectrometer would require to observe just a single peak in the spectrum (*1, 17*). The experiment may be repeated several times to produce a time domain signal of increased signal to noise ratio (*1*). The conventional frequency spectrum is derived from the transient time domain signal by the mathematical process called Fourier transformation (*17–21*). Since for any linear system the Fourier transform of the time domain response is identical with the frequency spectrum (*20*), the above procedure provides a powerful technique for either producing spectra very quickly or for producing spectra of high sig-

0003-2700/79/0351-2198$01.00/0

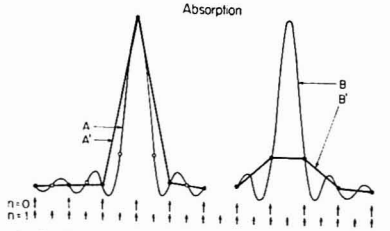

Figure 1. Continuous and discrete absorption mode spectral peaks. Curves A and B are continuous spectral peaks of identical line shape and intensity which were calculated from Equation 7 with a value of $T/\tau = 1.0$. The maximum of curve A falls exactly on one of the frequencies of the discrete frequency spectrum labeled $n = 0$. The maximum of curve B falls exactly half way between two points of the discrete frequency spectrum labeled $n = 0$. Curves A′ and B′ are discrete frequency spectral line shapes formed by straight line connection of the points in the discrete spectrum labeled $n = 0$. The discrete frequency spectrum labeled $n = 1$ has twice the resolution of the $n = 0$ discrete spectrum. The open circles are the values of curve A in the $n = 1$ discrete spectrum

nal-to-noise ratio (*1*). In actual experimental practice, however, the *continuous* time domain response is not *analytically* transformed to produce a *continuous* frequency spectrum. Rather, the continuous time domain response is sampled at a finite number of particular instants of time to yield a *discrete* time domain response. The discrete time domain response is then *numerically* transformed to produce a *discrete* frequency spectrum. This discrete frequency spectrum is defined at M specific frequencies, f, given by

$$f = m/T \text{ Hz}, m = 0, 1, 2 \ldots M - 1 \quad (1)$$

where T is the acquisition period of the time domain signal. Now unless the signal frequency to be determined happens to be exactly one of the particular discrete frequencies given by Equation 1, the intensities in the discrete frequency spectrum will not correspond to the peak maxima in the continuous frequency spectrum. This situation is illustrated in Figure 1. Figure 1 shows two continuous line shapes, A and B, where the maximum of A is *exactly on* one of the discrete frequencies of a discrete frequency spectrum and the maximum of B is half way between two discrete frequencies. Straight line connnection of the amplitudes in the discrete frequency spectrum leads to the *discrete* line shapes A′ and B′. It is obvious that A′ provides an exact estimate of the amplitude and the frequency of A. A′ also provides a reasonable approximation to the line width of A. However, the peak height, frequency, and line shape of B are poorly estimated by B′.

With experience, the distorted line shapes and incorrect amplitudes occurring in FT spectrometry can be recognized. However, the occurrence of this distortion can be obscured by the manner in which the data system indicates peak maxima and locations. The peak heights and the peak locations in FT spectrometry are usually determined with a "peak peaking" algorithm run under computer control. If this algorithm examines only the values of the discrete spectrum, the output intensities and frequencies from the algorithm will usually not correspond to the (true) maxima and frequencies in the continuous spectrum. Furthermore, the discrete graphical spectra produced by straight line connection of the points in the discrete frequency spectrum will usually not give an accurate description of the continuous line shape (cf. Figure 1).

The problem illustrated by Figure 1 has been well recognized in the literature. One solution (*4, 18, 21–28*) is to extend the time domain data table by adding zeros to the end of the sampled transient signal prior to Fourier transformation. Usually zeros are added until the data table length has been extended by a factor of 2^n, where $n = 1, 2, 3 \ldots$, but the procedure is valid for any positive value of n. Since the effective "zero-filled acquisition time", T_z, is now longer,

$$T_z = (T)2^n \quad (2)$$

the spacing in the discrete frequency spectrum is now reduced to $1/T_z$ from $1/T$. In the limit, $n \to \infty$, the numerical Fourier transform becomes identical with the analytical Fourier transform and the discrete frequency spectrum becomes identical to the continuous frequency spectrum. A further advantage of this particular interpolation method is that the first set of added zeros increases the signal-to-noise ratio of the final absorption spectrum (*24*). Further zero-fillings, however, will only interpolate to the continuous line shape.

Another solution to the problem illustrated by Figure 1 is to use an interpolating procedure which fits three or more points from a discrete line shape to an assumed analytic line shape. For cases in which the continuous line shape is known in advance and is analytically simple (i.e., Gaussian, Lorentzian, etc.), this procedure has the advantage of shorter computation time when compared with extended zero-filling. These curve fitting procedures will give the peak height and the peak maximum and addition will provide the complete continuous line shape if desired. For cases where the line shape is more complicated, the discrete line shape can be fitted to a simpler analytical form. For example, the experimental line shapes in high resolution FT–NMR spectrometry, whose analytical form is given by Equation 7 of this work, may be fitted to a parabolic equation. Fitting the discrete points from a complex line shape to a simple analytical function yields interpolated peak maxima and peak frequencies, which, while closer to the true maxima, are still in error because of the mismatch between the (complex) continuous line shape and the (simple) fitting function. A significant advantage of the extended zero-filling method of interpolation is that the method will always produce the true continuous line shape whatever that line shape may be.

While the effect of zero-filling has been known for some time, we are unaware of any quantiative criteria for determining the number of zero-fillings which are required to achieve a particular accuracy. These criteria are required because the computation time for the fast Fourier transform (FFT) rapidly increases with increasing length of the data table being transformed (*21*). It is thus advantageous to zero-fill only until the desired accuracy is achieved. More extended zero-filling merely increases the computation time.

The error resulting from finite zero-filling of Fourier transform faradaic admittance data and quantitative criteria for reducing this error have recently been studied by Smith (*29*). Closely related to the objective of the present work is the study of Horlick (*27*) which examined the error in peak maximum measurement as a function of the number of points above the half-maximum for a number of different line shapes. The residual error for finite zero-filling of a Lorentzian line shape (as is found in pressure-broadened Fourier transform infrared (FT-IR) spectrometry) can be readily derived from the tables in ref 27.

In the following section, the maximum *frequency* error resulting from finite zero-filling is given. The continuous frequency spectrum of a truncated exponentially damped sinusoid is given in two forms: the absorption spectrum (the cosine transform of the time domain signal) and the magnitude spectrum (the square root of the sum of the squares of the cosine transform and the sine transform). A systematic procedure is developed for estimating the maximum error in *peak height* which results after a specific number of zero-fillings. The procedure is applied to both absorption mode

spectra and magnitude mode spectra for different values of T/τ, where T is the acquisition period and τ is the relaxation time of the time domain signal. The error estimates are presented in both analytical and graphical form. Use of the error equations and the error graphs as well as applications to FT-NMR spectrometry and FT-ICR spectrometry are discussed.

ERROR ESTIMATES FOR ZERO-FILLED FT SPECTRA

(a) Frequency Errors. It follows from Equations 1 and 2 that the only allowed values, Δf, for the distance between the points in the discrete frequency spectrum are given by

$$\Delta f = \frac{1}{T} \text{ Hz} \tag{3}$$

if no zero-filling is done prior to Fourier transformation, and

$$\Delta f = \frac{1}{T_z} = \frac{1}{2^n T} \text{ Hz}; \; n = 0, 1, 2 \ldots \tag{4}$$

if the time domain signal is zero-filled n times prior to Fourier transformation. The maximum error in frequency determination will occur when the maximum for the *continuous* line shape falls exactly *half way* between two adjacent points in the *discrete* spectrum. Since the spacing in the discrete spectrum is halved for every power of 2 of zero-filling (Equation 4), the maximum error in frequency determination as a function of the number zero-fillings may be stated by Equation 5.

max frequency error in Hz after n zero fillings =

$$\frac{\pm 1}{T 2^{n+1}} \qquad n = 0, 1, 2 \ldots \tag{5}$$

Equation 5 gives the maximum error in determination of the frequency of a peak maximum as a function of acquisition period T, and n, the number of zero-fillings. The error may be positive or negative.

(b) Intensity Errors. Consider a continuous time domain signal of the form

$$F(t) = \exp(-t/\tau) \cos \omega t \qquad 0 < t < T \tag{6}$$

The *continuous* absorption mode frequency spectrum (i.e., the *analytical* Fourier transform) of Equation 6 is (*29*)

$$A(\Delta\omega) = \frac{\tau}{1 + (\Delta\omega)^2\tau^2}(1 + \exp[-T/\tau](\Delta\omega)\tau \sin((\Delta\omega)T) - \cos((\Delta\omega)T)) \tag{7}$$

The continuous magnitude mode frequency spectrum of Equation 6 is

$$C(\Delta\omega) = \left(\frac{\tau^2}{1 + (\Delta\omega)^2\tau^2}\right)^{1/2}(1 - 2\exp[-T/\tau]\cos((\Delta\omega)T) + \exp[-2T/\tau])^{1/2} \tag{8}$$

In Equations 6–8, τ is the relaxation time of the oscillation in seconds, $\Delta\omega$ is the frequency distance from the peak maximum in radians/second, and T is the time period in seconds over which the damped oscillation (Equation 6) was observed. Equations 6–8 are very general equations characteristic of any damped oscillation. They are applicable to many forms of spectrometry and in particular NMR spectrometry and ICR spectrometry. The line shape described by Equation 7 is sometimes called a "convolved sinc function", but the phrase "Lorentzian convolved with a sinc" is probably more apt. Now when Equation 6 is sampled at a series of discrete times, the discrete frequency spectrum resulting from Fourier transformation will only exist at the particular frequencies given by Equation 1. The only allowed values for the distance between the points in the discrete frequency spectrum are given by Equation 3 if no zero-filling is done prior to Fourier transformation, and Equation 4 if the time domain signal is zero-filled n times prior to Fourier transformation. For a continuous spectral peak which happens to fall *exactly on* one of the discrete frequencies of the discrete frequency spectrum, as, for example, curve A in Figure 1, the intensity of the line shape will be defined only at the discrete frequency values given by

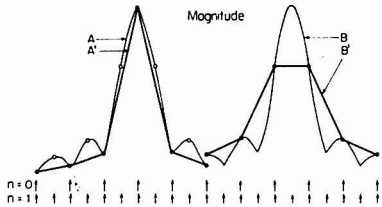

Figure 2. Continuous and discrete magnitude mode spectral peaks. Curves A and B are continuous spectral peaks of identical line shape and intensity which were calculated from Equation 8 with a value of $T/\tau = 1.0$. The maximum of curve A falls exactly on one of the frequencies of the discrete frequency spectrum labeled $n = 0$. The maximum of curve B falls exactly half way between two points of the discrete frequency spectrum labeled $n = 0$. Curves A' and B' are discrete frequency spectral line shapes formed by straight line connection of the points in the discrete spectrum labeled $n = 0$. The discrete frequency spectrum labeled $n = 1$ has twice the resolution of the $n = 0$ discrete spectrum. The open circles are the values of curve A in the $n = 1$ discrete spectrum

$$\Delta\omega = \frac{2\pi}{2^n T}P \qquad P = 0, \pm 1, \pm 2 \ldots \tag{9}$$

where n is the number of zero-fillings. For a value of $P = +1$, the intensity of the peak at the first discrete frequency above the peak maximum will be obtained. Substituting Equation 9 with a value of $P = +1$ into Equation 7 and Equation 8, gives

$$A(\Delta\omega) + \tau\left(1 + \frac{Y}{X}\right)^{-1}\left(1 + e^{-Y}\left[\frac{Y}{X}\sin(Y) - \cos(Y)\right]\right) \tag{10}$$

and

$$C(\Delta\omega) = \tau[1 + (Y/X)^2]^{-1/2}[1 - 2e^{-X}\cos(Y) + e^{-2X}]^{1/2} \tag{11}$$

where

$$X = T/\tau \tag{12}$$

and

$$Y = 2\pi/2^n \tag{13}$$

Equation 10 gives the discrete intensity value for the first discrete frequency above the peak maximum (i.e., $P = 1$), for an absorption mode line shape as a function of τ, the relaxation time of the time domain signal, X, the ratio of the acquisition period T to the relaxation time τ, and n, the number of zero-fillings. Equation 11 is the corresponding equation for a *discrete* magnitude mode line shape.

Examination of Figure 1 or 2 leads to a systematic procedure for determining the maximum amplitude error due to the finite frequency resolution of a discrete frequency spectrum. Curve A in Figure 1 (Figure 2) is a continuous absorption mode (magnitude mode) line shape calculated from Equation 7 (Equation 8) for $T/\tau = 1.0$. Curve B in Figure 1 or 2 is a continuous line shape which is identical with Curve A but is located at a different frequency. Now if the spectral peak A were obtained by sampling a time domain signal (Equation 6) and Fourier transformation, and if the maximum of curve

A was exactly on one of the points in the discrete frequency spectrum, the *discrete* magnitude mode line shape obtained by connecting the points in the discrete frequency spectrum would be curve A′. If the sampling conditions were appropriate for curve A, then the maximum of curve B will be incorrectly indicated by the *discrete* magnitude line shape, curve B′. Since the maximum for the continuous peak B falls exactly half way between two of the discrete frequencies of the nonzero-filled (n = 0) discrete frequency spectrum, measurement of spectral peak B′ will lead to the worst possible estimate for the frequency and amplitude of curve B. If peak B were less than half way between two frequencies of the n = 0 discrete spectrum, B′ would have an amplitude *closer* to that of peak B.

If the sampled transient which leads to curve A′ were zero-filled once (n = 1) prior to Fourier transformation, the points indicated as open circles in Figure 1 or 2 would be obtained for spectral peak A. Comparison of curve B′ with the open circles of curve A leads to the following conclusion: The *minimum* amplitude for a discrete peak which falls between two points of a non-zero-filled spectrum will be equal to the amplitude of the first (i.e., P = 1) point away from the maximum of the "zero-filled once" (n = 1) spectrum of a peak whose maximum falls *exactly on* one of the frequencies of the non-zero-filled (n = 0) spectrum. The fractional error after no zero-filling is given by 1.0 less the peak maximum in the discrete, n = 0 spectrum divided by the maximum in the continuous spectrum. Since the (true) continuous spectrum maximum is obtained after an infinite number of zero-fillings, the maximum fractional error after no zero-filling is given by the formulas

$$\begin{pmatrix}\text{max fractional error}\\ \text{obtained after no}\\ \text{zero-filling}\end{pmatrix} = \left(1.0 - \frac{\text{Equation 10 } (n = 1)}{\text{Equation 10 } (n = \infty)}\right) \quad (14)$$

$$\begin{pmatrix}\text{max fractional error}\\ \text{obtained after no}\\ \text{zero-filling}\end{pmatrix} = \left(1.0 - \frac{\text{Equation 11 } (n = 1)}{\text{Equation 11 } (n = \infty)}\right) \quad (15)$$

Equation 14 gives the maximum fractional error for a discrete absorption mode line shape which was obtained after no zero-filling as a function of the ratio X (Equation 12). Equation 15 is the corresponding equation for the magnitude mode line shape. Note that Equations 14 and 15 are dependent upon the ratio X but, unlike Equations 10 and 11, are independent of the absolute values of the acquisition period, T, and the relaxation time, τ. The preceding ideas may be generalized to

$$\begin{pmatrix}\text{max fractional error}\\ \text{obtained after}\\ n \text{ zero-fillings}\end{pmatrix} = \left(1.0 - \frac{\text{Equation 10 } (n = n + 1)}{\text{Equation 10 } (n = \infty)}\right) \quad (16)$$

and

$$\begin{pmatrix}\text{max fractional error}\\ \text{obtained after}\\ n \text{ zero-fillings}\end{pmatrix} = \left(1.0 - \frac{\text{Equation 11 } (n = n + 1)}{\text{Equation 11 } (n = \infty)}\right) \quad (17)$$

Equation 16 gives the maximum fractional error for an absorption mode line shape as a function of n, the number of zero-fillings, and X, the ratio of the acquisition period to the relaxation time of the time domain signal, which when Fourier transformed, gives the absorption mode line shape. Equation 17 is the corresponding equation for the magnitude mode line shape. Equations 16 and 17 like Equations 14 and 15 depend upon the ratio X but, unlike Equations 10 and 11, are independent of the absolute magnitudes of T and τ.

The residual error calculated from Equations 16 and 17 for various values of n are graphically displayed in Figures 3 and 4. Figure 3 shows the percentage amplitude error resulting from finite zero-filling for the absorption mode line shape. As expected, extended zero-filling prior to Fourier transformation rapidly reduces the error. As the time domain signal is relaxed during the acquisition period (increasing T/τ), the error for fixed n also becomes less. Figure 4 shows the same information as Figure 3 but for the magnitude mode line shape. The general dependence of the error is the same as for the absorption mode but the error is less for any given values of n and T/τ. This lower error for the magnitude mode arises because of the broader line shape of the magnitude mode (*3*, *12*, *29*); cf. Figures 1 and 2.

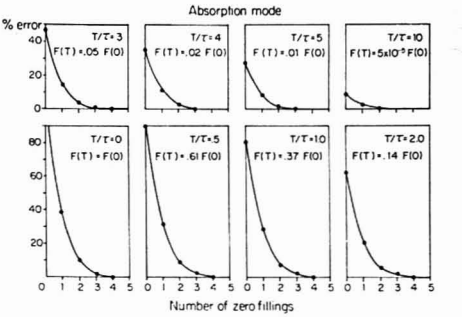

Figure 3. Relative error due to noninfinite zero-filling for an absorption mode line shape. Each curve gives the *maximum* percentage error for a particular ratio of T/τ as a function of the number of zero-fillings. The value of the time domain function (Equation 6) at the end of the acquisition period is indicated on each graph. The errors at integral values of n are the most important but the curves are valid for nonintegral values of n also. The curves were calculated from Equation 16. Note that the error scale is different than that of Figure 4

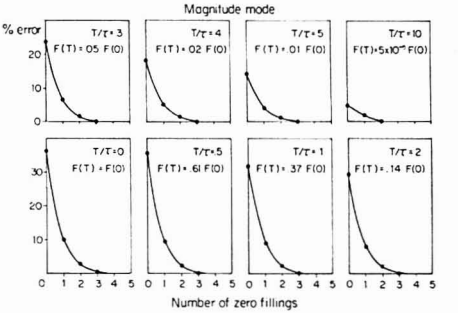

Figure 4. Relative error due to noninfinite zero-filling for a magnitude mode line shape. Each curve gives the *maximum* percentage error for a particular ratio of T/τ as a function of the number of zero-fillings. The value of the time domain signal (Equation 6) at the end of the acquisition period is indicated on each graph. The errors at integral values of n are the most important but the curves are valid for nonintegral values of n also. The curves were calculated from Equation 17. Note that the error scale is different than that of Figure 3

The peak maximum in the discrete frequency spectrum is always less than the peak maximum in the continuous spectrum. The *amplitude* errors described by Equations 16 and 17 and Figures 3 and 4 are therefore always negative. On the other hand, the *frequency* error resulting from measurement of the peak frequency in a discrete spectrum may be positive or negative (Equation 5).

DISCUSSION

The treatment of the previous section shows that the maximum error in the determination of both the location and amplitude of a spectral peak described by a discrete frequency spectrum occurs when the maximum of continuous peak falls exactly half way between two adjacent points in the discrete frequency spectrum. This simple statement for the occurrence of worst case allows the derivation of the simple analytical expressions, Equations 16 and 17, for the maximum amplitude error. The derivation of the error expressions, Equations 16 and 17, shows that the amplitude error in a discrete frequency spectrum depends upon the T/τ but not the absolute values of T or τ. As a consequence, the errors described by Equations 16 and 17 and displayed in Figures 3 and 4 can be presented as functions of only two independent variables: n, the number of zero-fillings and the ratio T/τ. This is very convenient because the relatively few graphs in Figures 3 and 4 can be applied to a very wide range of experimental values of T and τ.

Usually, provision is made in the FT experiment for display of the (accumulated) time domain signal prior to Fourier transformation and the ratio T/τ can be visually obtained from this signal by noting the initial and final values, $F(0)$ and $F(T)$, of the time domain signal. The final value, $F(T)$ as a function of the initial value, $F(0)$, is indicated on the appropriate graphs of Figure 3 and 4. Once the ratio T/τ is known and the desired error limit is chosen, the required number of zero-fillings can be determined quickly from the appropriate graph in Figure 3 or 4. One conclusion which follows directly Figures 3 and 4 is that four zero-fillings for the absorption mode and three zero-fillings for the magnitude mode are sufficient to reduce the peak height error to less than 2%.

In most experimental practice, the time domain signal will consist of a sum of components of the form, Equation 6. These spectral components could have differing relaxation times and differing errors associated with their spectral peaks. Determination of an overall T/τ ratio for the composite signal will not necessarily give the correct T/τ ratio for any particular spectral component. However, it follows from Figures 3 and 4 that, after three or four zero-fillings, the error is essentially independent of the ratio, T/τ. Thus even for cases where the relaxation time differs from peak to peak, Figures 3 and 4 provide a useful guide to the required number of zero-fillings. Of course the occurrence of differing relaxation times is readily apparent in zero-filled spectra from the differing line widths of the various spectral components. For cases where one line is much narrower than others it is probably best to repeat the zero-filling procedure with more zero fillings to ensure that no significant errors remain.

As noted above, the error resulting from finite zero-filling depends upon the ratio T/τ. This ratio is often under control of the experimentalist and deserves some comment. In general it is desirable to make the acquisition time T as long as possible as this maximizes the inherent resolution of the FT experiment. In practice, however, this is not always possible because of limitations in the size of the available memory. According to the Nyquist criterion, the transient signal must be sampled as a rate which exceeds twice the highest frequency in the signal. For a sampling rate of S, the acquisition period will be given by

$$T = N/S \tag{18}$$

where N is the number of words of available computer memory. For example, for a transient signal which contained frequency components from dc to 1 kHz, the sampling rate must exceed 2 kHz. With a computer data memory of 16 384 words, the memory will be filled up in 8 s (Equation 18). If the relaxation time τ was, for example, 1 s, the ratio T/τ would be 8 and only two zero-fillings would be required to reduce the error to less than 2%. On the other hand, if the transient signal contained components up to 20 kHz, a computer memory of 16 384 words would be filled up in only 0.41 s. For the same value of τ as the above example the ratio T/τ is 0.41 and four zero-fillings are required to achieve an error of less than 2%. In general then, as the band width increases and as the relaxation time increases, more zero-filling will be required to achieve any particular error minimization.

The data table length to be transformed is of course limited by the size of the total memory (semiconductor plus magnetic disk) in the data system. The access time of disk memory is such that the maximum rate at which data can be written onto the disk is about 20 kHz and the band width for a "direct to disk data acquisition" is therefore limited by the Nyquist criterion to less than 10 kHz. The access time of semiconductor memory is much shorter and acquisition rates to semiconductor memory can be as high as 100 MHz. For wide spectral band widths then, the acquisition time T will be limited by the size of the available semiconductor memory as described in the previous paragraph, but the number of zero-fillings will be limited by the size of the total (semiconductor plus disk) memory.

In NMR spectrometry it is most common to present frequency data in the absorption mode (*3*). This is true for both scanning and Fourier transform NMR spectrometry. The most common FT–NMR procedure is to zero-fill the sampled transient once ($n = 1$) to obtain the maximum possible absorption mode sensitivity as originally recommended by Berthodi and Ernst (*24*). However, it follows from Figure 3 that, for cases where the transient signal has not decayed significantly during the acquisition time, significant amplitude errors will be still present unless the data are further treated by, for example, curve fitting. For example, it is not until the transient has been sampled for greater than four relaxation times (Figure 3) that the finite resolution of the $n = 1$ discrete frequency spectrum is great enough to reduce the amplitude error to less than 5%.

In FT–ICR spectrometry, the most common spectral presentation is the magnitude mode (*12, 13*). The spectral band width is large and the Nyquist criterion requires high sampling rates (*14*). For example, a band width of 1 MHz (corresponding to a mass range of 30 to ∞ at a magnetic field of 20 kG) requires a sampling rate of at least 2 MHz, and a computer memory of 16 384 words will be filled in only 8 ms. Since FT–ICR transient signals often last for several tens of milliseconds (*12*), wide mass range FT–ICR signals are characterized by values of T/τ which are less than 1.0. For these cases several zero-fillings are necessary to reduce the frequency and amplitude errors accruing from the finite resolution of the FT–ICR spectrum.

LITERATURE CITED

(1) P. R. Griffiths, "Transform Techniques in Chemistry", Plenum Press, New York, 1978.
(2) R. R. Ernst and W. A. Anderson, *Rev. Sci. Instrum.*, **37**, 93 (1966).
(3) D. Shaw, "Fourier Transform NMR Spectroscopy", Elsevier, Amsterdam, 1976.
(4) T. C. Farrar, Chapter 8 in ref 1.
(5) J. W. Cooper, Chapter 9 in ref 1.
(6) J. C. McGurk, T. G. Schmalz, and W. H. Flygare, *Adv. Chem. Phys.*, **25**, 1, 1974.
(7) M. B. Comisarow, Chapter 10 in ref 1.
(8) M. B. Comisarow, *Adv. Mass Spectrosc.*, **7**, 1042 (1978).
(9) C. Wilkins, *Anal. Chem.*, **50**, 493A (1978).

(10) M. B. Comisarow and A. G. Marshall, *Chem. Phys. Lett.*, **25**, 282 (1974).
(11) M. B. Comisarow and A. G. Marshall, *Chem. Phys. Lett.*, **26**, 489 (1974).
(12) M. B. Comisarow and A. G. Marshall, *Can. J. Chem.*, **52**, 1977 (1974).
(13) M. B. Comisarow and A. G. Marshall, *J. Chem. Phys.*, **62**, 293 (1975).
(14) M. B. Comisarow and A. G. Marshall, *J. Chem. Phys.*, **64**, 110 (1976).
(15) M. Comisarow, G. Parisod, and V. Grassi, *Chem. Phys. Lett.*, **57**, 413 (1978).
(16) M. B. Comisarow, *J. Chem. Phys.*, **69**, 4097 (1978).
(17) A. G. Marshall and M. B. Comisarow, Chapter 3 in ref 1.
(18) J. W. Cooper, Chapter 4 in ref 1.
(19) Charles T. Foskett, Chapter 2 in ref 1.
(20) D. C. Champeney, "Fourier Transforms and Their Applications", Academic Press, New York, 1973.
(21) E. O. Brigham, "The Fast Fourier Transform", Prentice-Hall, Englewood Cliffs, N.J., 1974.
(22) R. D. Larsen, Chapter 13 in ref 1.
(23) P. R. Griffiths, Chapter 5 in ref 1.
(24) E. Bertholdi and R. Ernst, *J. Magn. Reson.*, **11**, 9 (1973).
(25) P. R. Griffiths, *Appl. Spectrosc.*, **29**, 11 (1975).
(26) R. T. Pajer and I. M. Armitage, *J. Magn. Reson.*, **21**, 485 (1976).
(27) G. Horlick and W. K. Yuen, *Anal. Chem.*, **48**, 1643 (1976).
(28) P. C. Kelly and G. Horlick, *Anal. Chem.*, **45**, 518 (1973).
(29) R. J. O'Halloran and D. E. Smith, *Anal. Chem.*, **50**, 1391 (1978).
(30) A. G. Marshall, M. B. Comisarow, and G. Parisod, *J. Chem. Phys.*, in press.

RECEIVED for review January 22, 1979. Accepted July 23, 1979. This research was supported by the Natural Sciences and Engineering Research Council of Canada and by the Research Corp.

Simulation of Nuclear Magnetic Resonance Spin Lattice Relaxation Time Measurements for Examination of Systematic and Random Error Effects

T. Phil Pitner* and Jerry F. Whidby*

Philip Morris USA Research Center, P.O. Box 26583, Richmond, Virginia 23261

Systematic and random errors in NMR spin lattice relaxation time (T_1) measurements are investigated by simulating relaxation data using various experimental parameters: pulse width, recovery delay, waiting times, and signal-to-noise. T_1's are calculated from the hypothetical data by linear least squares, two-parameter exponential, three-parameter exponential, and four-parameter exponential analyses to explore the suitability of these analyses. The computed T_1's and standard deviations are discussed in terms of random and systematic errors. Experimental data are presented to illustrate the applicability of the calculations.

When faced with measuring spin lattice relaxation times (T_1), the NMR spectroscopist is confronted by a myriad of confusing opinions, almost amounting to myth and folklore, as to the proper choice of measurement method, experimental parameters, and data analysis method. Several studies have appeared in the literature, aimed at delineating and clarifying this problem (*1–19*). The need in this laboratory for accurate and reproducible T_1 measurements led us to investigate some of the various methods by simulating experimental relaxation data and subjecting these data to several analyses to determine how well the calculated T_1's compare with T_1's used in generating the data. We hope the results presented in this paper will aid and give insight to experimentalists who desire to have a reasonable degree of confidence in the T_1's they measure.

EXPERIMENTAL

^2H (12.29 MHz) NMR spectra were obtained with a Bruker WP-80 spectrometer at ambient probe temperature. T_1's were measured for the ^2H resonance of a 5% solution of D_2O (Merck & Co.) in H_2O doped with a trace of copper sulfate.

RESULTS AND DISCUSSION

The most common method of measuring T_1's involves applying a perturbing rf pulse to the nuclear spins, waiting for a range of times τ to allow the spins to relax, and sampling the extent of relaxation with an observing pulse. The peak intensity A_τ after waiting time τ is given for steady-state conditions by

$$A_\tau = A_\infty \sin\beta \frac{1 - [1 - \cos\alpha\,(1 - e^{-D/T_1})]\, e^{-\tau/T_1}}{1 - [\cos\alpha\cos\beta\, e^{-D/T_1}]\, e^{-\tau/T_1}} \quad (1)$$

(*2*, *14*, *18*) where A_∞ is the equilibrium intensity; α, the perturbing pulse flip-angle; β, the observing pulse flip-angle; and D, the recovery delay between the observing pulse and the next perturbing pulse. For the standard inversion–recovery experiment $\alpha = 180°$ and $\beta = 90°$ (*1*, *2*). Equation 1 assumes rf homogeneity, no offset effects (i.e., (pulse width) << (spectral width)$^{-1}$), and no refocusing effects. These complications will be mentioned later. Equation 1 is used to simulate relaxation data for a hypothetical T_1 of 100 s and for various values of α, β, and D. The additional variable of signal-to-noise ratio (S/N) is introduced by adding to each A_τ a random number between $-0.5\,N$ and $0.5\,N$ (the S/N reported is the raw signal to noise, A_∞ divided by peak-to-peak noise).

With commercial spectrometers, the experimentalist can easily control four instrumental variables which affect the systematic and random errors in T_1 measurements: the flip-angles α and β, the recovery delay (D), the number of scans, and the waiting times (τ). In addition, the method used to fit the experimental data to a relaxation time can introduce appreciable systematic error if unsuitable experimental parameters are chosen for the measurement. Because of the intimate relationship between experimental method and data analysis method, we examine the effect of altering each of the experimental parameters on T_1's determined with the fitting methods (*18*, *20*, *21*) used most commonly:

Linear least squares fit

$$\ln(A_\infty - A_\tau) = \kappa - \tau/T_1 \quad (2)$$

where $1/T_1$ is the slope and κ the intercept;

Two-parameter exponential fit

$$A_\tau = B\,(1 - 2\,e^{-\tau/T_1}) \quad (3)$$

0003-2700/79/0351-2203$01.00/0

Table I. Calculated T_1's Reflecting Systematic Errors Resulting from Missett Pulses[a]

	T_1 (SD)		
flip-angles	linear fit	2-parameter fit	3-parameter fit
120, 60	99.1 (0.05)	56.1 (6.81)	100.1 (0.01)
140, 70	99.1 (0.05)	79.8 (4.01)	100.1 (0.01)
160, 80	99.0 (0.05)	94.5 (1.26)	100.1 (0.00)
180, 90	99.0 (0.05)	99.4 (0.13)	100.0 (0.00)
200, 100	98.9 (0.04)	94.5 (1.22)	99.9 (0.00)
220, 110	98.9 (0.04)	79.8 (3.96)	99.9 (0.01)

[a] T_1 = 100 s; $S/N = \infty$; 5 T_1 recovery delay; τ = 0, 7.28, 15.14, 23.66, 32.98, 43.26, 54.72, 67.66, 82.53, 500 s.

Table II. Calculated T_1's Reflecting Systematic Errors Resulting from Short Recovery Delay[a]

	T_1 (SD)		
recovery delay	linear fit	2-parameter fit	3-parameter fit
5 T_1	99.0 (0.05)	99.4 (0.13)	100.0 (0.00)
4 T_1	97.2 (0.12)	98.5 (0.32)	100.0 (0.00)
3 T_1	92.4 (0.34)	95.8 (0.71)	100.0 (0.00)
2 T_1	79.0 (0.93)	88.5 (1.23)	100.0 (0.00)
1 T_1	39.1 (2.67)	68.2 (1.32)	100.0 (0.00)

[a] T_1 = 100 s; $S/N = \infty$; $\alpha = 180°$; $\beta = 90°$; τ = 0, 7.28, 15.14, 23.66, 32.98, 43.26, 54.72, 67.66, 82.53 s. Last τ = recovery delay.

where the constants B and T_1 are optimized in an iterative manner;

Three-parameter exponential fit

$$A_\tau = B(1 - C\,e^{-\tau/T_1}) \tag{4}$$

where B, C, and T_1 are optimized.

For completeness we also present the four-parameter exponential fit

$$A = B\,\frac{(1 - C\,e^{-\tau/T_1})}{(1 - E\,e^{-\tau/T_1})} \tag{5}$$

where B, C, E, and T_1 are optimized.

Since Equation 5 is of the same form as Equation 1,

$$B = A_\infty \sin\beta$$

$$C = (1 - \cos\alpha\,(1 - e^{-D/T_1}))$$

$$E = \cos\alpha\,\cos\beta\,e^{-D/T_1}$$

the four-parameter fit should be exact for high S/N. The important experimental parameters accompany each of the tables.

Table I illustrates the errors obtained for misset pulses. The two-parameter fit calculates T_1's which deviate unacceptably from 100 s for pulses misset by only 10%, since the pre-exponential factor is not equal to 2 as assumed in Equation 3 when $\alpha \neq 0$ (compare Equations 1 and 3). Although the linear fit exhibits little error attributable to misset pulses, an appreciable systematic error is observed since the magnetization has not fully recovered to A_∞ in 5 T_1. The three-parameter fit is acceptable even for severely misset pulses, although some systematic error is observed due to the increasing importance of E. The four-parameter fit is, of course, exact. The magnitudes of the systematic errors depend on the range of delay times (τ); however, the errors in Table I could not be improved significantly for a wide variety of delay ranges tried, and in many cases worse errors were encountered. Note that the standard deviations obtained with the two-parameter fit are deceptively low and do not reflect the severe systematic error obtained for misset pulses.

The influence of recovery time (D) on fitted T_1's is shown in Table II. The systematic error in the linear fit reflects errors in A_∞ for short values of D. The two-parameter fit, as before, suggests deviation of the parameter C from 2. The three-parameter fit is exact since $E = 0$ for $\cos\beta = 0$.

Table III illustrates the effect of S/N on T_1's determined by the four methods. Average results of 100 simulations are shown in the table. Each simulation results in a $T_1 \pm SD$, and the averages of 100 T_1's and 100 SD's yield T_1 ($\pm$ sd$_{T_1}$) and SD ($\pm$ sd$_{SD}$). Even though the linear fit is a two-parameter fit, the systematic errors which result from errors in A_∞ produce a sd$_{T_1}$ value twice that obtained for the two-parameter exponential fit. The SD's obtained for the linear and two-parameter exponential fits are essentially identical. The three-parameter and four-parameter fits exhibit correspondingly greater SD's reflecting the requirement of multiparameter fits for higher S/N data. In fact, the four-parameter fit will not converge consistently for $S/N \lesssim 10$.

Choice of delay times (τ) is complicated by the interrelationships among the range of delay times (DR), the distribution of τ values within this range, the recovery time (D), and the standard deviation of the calculated T_1. Tables IV and V are assembled with the hope that general trends can be illustrated in a finite number of simulations. Unless otherwise indicated, the 10 delay times are spaced exponentially within the delay range. When specified, the last τ (LT) is replaced by the time indicated. The S/N is adjusted for each simulation to represent the same total experimental time; thus, if the sum of all delays and all recovery times is equal to TT then, $S/N = (\text{const} \times TT)^{-1/2}$. To avoid clutter, the tables show only the three-parameter fit SD's of 100

Table III. Calculated T_1's.[a] Effect of Signal-to-Noise Ratio on Standard Deviation

	T_1 (sd$_{T_1}$) SD(sd$_{SD}$)			
S/N	linear fit	2-parameter	3-parameter	4-parameter
50	98.85 (0.78)	99.45 (0.43)	99.89 (0.74)	99.87 (5.79)
	0.53 (0.11)	0.42 (0.08)	0.74 (0.15)	5.59 (1.37)
20	98.70 (1.89)	99.40 (0.97)	99.77 (1.84)	101.34 (14.96)
	1.28 (0.30)	0.99 (0.20)	1.79 (0.31)	14.38 (6.14)
10	99.48 (4.13)	99.75 (2.29)	100.44 (3.84)	****
	2.66 (0.58)	2.08 (0.38)	3.78 (0.74)	****
5	98.98 (8.08)	98.56 (3.78)	99.72 (7.68)	****
	5.02 (1.29)	3.95 (0.79)	7.18 (1.74)	****
2	96.61 (20.08)	99.24 (10.97)	98.50 (21.74)	****
	11.72 (4.57)	10.30 (2.84)	18.92 (7.67)	****

[a] T_1 = 100 s. $\alpha = 180°$; $\beta = 90°$. τ = 0, 7.28, 15.14, 23.66, 32.98, 43.26, 54.72, 67.66, 82.53, 500 s. Recovery delay = 5 T_1.

Table IV. Average Standard Deviations of Calculated T_1's[a]

delay range	recovery time 1 T_1	2 T_1	3 T_1	4 T_1	5 T_1	6 T_1	7 T_1
0-0.5 T_1	9.3	5.2	4.4	4.4	4.8	4.9	5.5
0-1 T_1	10.2	4.6	3.7	3.6	3.6	3.8	4.2
0-2 T_1	6.5	5.0	3.7	3.6	3.6	3.9	4.2
0-3 T_1	4.9	4.8	3.9	3.8	3.8	4.0	4.1
0-5 T_1	4.2	4.5	4.0	3.7	3.7	4.0	4.2
0-7 T_1	4.2	4.3	3.9	3.8	3.8	4.1	4.2

[a] $\alpha = 180°$; $\beta = 90°$; recovery time = last τ; three-parameter fit.

Table V. Average Standard Deviations of Calculated T_1's[a]

delay range	last τ 3 T_1	4 T_1	5 T_1	6 T_1	7 T_1
0-0.5 T_1	3.2	3.1	3.0	3.1	3.2
0-1 T_1	2.8	2.6	2.5	2.5	2.6
0-2 T_1	3.6	3.4	2.9	2.8	2.9
0-3 T_1	4.0	3.7	3.4	3.4	3.3

[a] $\alpha = 180°$; $\beta = 90°$; recovery time = delay range; three-parameter fit.

Table VI. Average Standard Deviation of Calculated T_1's for 90°-τ-90° Sequence[a]

delay range	last τ 3 T_1	4 T_1	5 T_1	6 T_1	7 T_1
0-0.5 T_1	3.5	3.3	3.3	3.3	3.6
0-1 T_1	2.9	2.8	2.8	2.8	3.0
0-2 T_1	3.5	3.1	3.1	3.1	3.3

[a] $\alpha = 180°$; $\beta = 90°$; recovery delay = 2 s (acquisition time); three-parameter fit.

simulations for each set of conditions.

Tables IV and V illustrate the interplay between two mutually exclusive factors which determine the final standard deviation: the increase in kinetic dynamic range due to longer D and/or longer LT, and the increase in spectral sensitivity resulting from a larger number of scans. The upper left-hand corner of each table illustrates the errors encountered for limited kinetic dynamic range; the low values of D limit the intensity of early data points, whereas the low values of LT limit the intensity of the last data point. The lower right-hand corner of each table illustrates errors resulting from loss in sensitivity due to fewer scans within the allotted time. Note in Table IV that for D, $LT \geq 3\ T_1$, the SD's in a given column are very similar for $DR \geq 1\ T_1$; therefore, for these parameters and a fixed total experimental time, the errors in calculated T_1's are affected only marginally by the range of delay times. Also, we have found that spacing the values linearly in time rather than exponentially has little effect for the same delay range, unless, of course, very large delay ranges are chosen. The lowest SD was obtained (Table V) for D,$DR \sim 1\ T_1$ and $LT \sim 5$-$6\ T_1$. We tried a considerably wider variety of D,DR, and LT, than shown in Tables IV and V and did not obtain significantly lower SD values.

For comparison, Table VI presents simulations with the widely used 90°-τ-90° sequence (9). The SD's are slightly higher than those in Table V. The increase in spectral sensitivity due to more scans in the 90°-τ-90° sequence is more than offset by the increase in kinetic dynamic range resulting from a 1 T_1 recovery time in the 180°-τ-90° sequence. It is important to emphasize that the three-parameter fit must be used when the recovery time is short compared to T_1 as in the optimal cases in Tables V and VI; otherwise

Table VII. Effect of Misset Pulses on Experimentally Measured T_1's

flip-angles	$T_1/T_{1_{ref}} \times 100$ ($SD/T_{1_{ref}} \times 100$)[a] linear fit	2-parameter fit	3-parameter fit
120, 60	99.4 (0.7)	58.3 (6.7)	100.4 (0.8)
140, 70	98.5 (0.6)	81.3 (3.7)	99.6 (0.8)
160, 80	99.2 (0.5)	92.5 (1.7)	100.2 (0.5)
180, 90	99.4 (0.2)	95.4 (1.2)	100.4 (0.2)
200, 100	99.3 (0.2)	89.9 (2.2)	100.3 (0.3)
200, 110	98.1 (0.5)	77.6 (4.2)	99.0 (0.7)

[a] Recovery delay = 2.356 s, $S/N > 300/1$, $\tau = 0.0$, 0.034, 0.071, 0.111, 0.155, 0.203, 0.257, 0.318, 0.388, 2.356 s. $T_{1_{ref}}$, 0.4738 (0.0005) s, was measured for the same solution with 20 τ values over the same delay range.

Table VIII. Effect of Short Recovery Delay on Experimentally Measured T_1's

recovery delay	$T_1/T_{1_{ref}} \times 100$ ($SD/T_{1_{ref}} \times 100$)[a] linear fit	2-parameter fit	3-parameter fit
5 T_1 (2.356 s)	99.4 (0.2)	95.4 (1.2)	100.4 (0.2)
4 T_1 (1.893 s)	98.3 (0.2)	96.6 (1.0)	101.1 (0.1)
3 T_1 (1.420 s)	92.4 (0.5)	90.6 (1.5)	99.5 (0.6)
2 T_1 (0.946 s)	81.0 (0.9)	83.6 (1.9)	101.0 (0.4)
1 T_1 (0.473 s)	48.6 (3.0)	64.7 (1.9)	106.3 (1.9)

[a] Experimental parameters are the same as those in Table VII except $\alpha = 180°$, $\beta = 90°$, last τ = recovery delay.

systematic errors as in Table II will occur.

Although the simulations in this paper have assumed rf homogeneity, very short pulses and no refocusing effects, Equation 1 can be modified to include these effects. However, if a homospoil (*1*, *3*) pulse is applied immediately before and after the perturbing pulse, leaving magnetization only along the field direction, or if pulse phase alternation (*11*, *15*) technqiues are used, then these effects become equivalent to misset pulses, and errors of the type shown in Table I will result. Although the same fractional error in perturbing and observing pulses was assumed in Table I, this would not be true for peaks offset significantly from the carrier frequency. It would also not necessarily be true for spectrometers on which the perturbing pulse is automatically set to a value twice that of the observing pulse. In these cases the magnitude of the errors obtained for the two-parameter fit vary somewhat from those in Table I; however, the same qualitative trends are observed, with minimal errors in the linear and three-parameter fits.

Tables VII and VIII present ^2H_2O relaxation data to demonstrate experimentally the results of Tables I and II and simultaneously to provide verification for the simulation model used here. For convenience in comparing the tables, we have presented the ^2H T_1 (SD)'s in terms of percentage of a reference T_1 ($T_{1_{ref}}$) determined under more exacting conditions for the same sample. The finite S/N is reflected in SD values for the three-parameter fit, and will also contribute to the SD's for the other two fits. In addition, the systematic error in the two-parameter fit, even for long recovery delay and pulses supposedly set to 180° and 90°, as well as the error in the three-parameter fit (Table VIII) for recovery delay = 1 T_1, both suggest that the settability of the pulses is not as accurate as might be desired. So that, if errors of the types in Tables I and II are made simultaneously, the systematic errors in linear and two-parameter fits may be magnified. Even so, the three-parameter fit results in a systematic error of only ≃6% for the extreme case of 1 T_1 recovery delay. It has recently

been pointed out (22) that systematic errors resulting from misset pulses with short recovery delay can be cancelled by using a constant total cycle time ($\tau + D$ = constant) and the three-parameter fit (this makes the denominator of Equation 1 a constant). Although this option is not available on most spectrometers in current use, it is desirable and should not be difficult to implement. However, using this approach places an upper limit on the last τ value, so that the optimum trade off between kinetic dynamic range and spectral sensitivity (Table V) cannot be achieved, an important consideration for low S/N samples.

Before using the T_1 calculation routine in the computer programs supplied by NMR spectrometer manufacturers, the spectroscopist should determine whether or not this routine employs a three-parameter fit. As long as the spectroscopist uses a three-parameter fit, he can be confident that he will obtain similar standard deviations for a wide range of experimental parameters. However, if he has a good estimate of the T_1, he can choose the optimal conditions (Table V) and decrease the standard deviation by a significant factor, or decrease the experimental time by an even greater factor.

ACKNOWLEDGMENT

The authors thank Charles N. Reilley for very helpful discussion of this manuscript.

LITERATURE CITED

(1) Vold, R. L.; Waugh, J. S.; Klein, M. P.; Phelps, D. E. *J. Chem. Phys.* **1968**, *48*, 3831.
(2) Freeman, R.; Hill, H. D. W. *J. Chem. Phys.* **1969**, *51*, 3140.
(3) Redfield, A. G.; Gupta, R. K. *Advan. Magn. Reson.* **1971**, *5*, 81.
(4) Freeman, R.; Hill, H. D. W. *J. Chem. Phys.* **1971**, *54*, 3367.
(5) Markley, J. L.; Horsley, W. J.; Klein, M. P. *J. Chem. Phys.* **1971**, *55*, 3604.
(6) Jones, D. E. *J. Magn. Reson.* **1972**, *6*, 191.
(7) Freeman, R.; Hill, H. D. W.; Kaptein, R. *J. Magn. Reson.* **1972**, *7*, 82.
(8) Mehring, M.; Waugh, J. S. *Rev. Sci. Instrum.* **1972**, *43*, 649.
(9) McDonald, G. C.; Leigh, J. S., Jr. *J. Magn. Reson.* **1973**, *9*, 358.
(10) Meakin, P.; Jesson, J. D. *J. Magn. Reson.* **1973**, *10*, 290.
(11) Demco, D. E.; VanHecke, P.; Waugh, J. S. *J. Magn. Reson.* **1974**, *16*, 467.
(12) Christensen, K. A.; Grant, D. M.; Schulman, E. M.; Walling, C. *J. Phys. Chem.* **1974**, *78*, 1971.
(13) Canet, D.; Levy, G. C.; Peat, I. R. *J. Magn. Reson.* **1975**, *18*, 199.
(14) Levy, G. C.; Peat, I. R. *J. Magn. Reson.* **1975**, *18*, 500.
(15) Cutnell, J. D.; Bleich, H. E.; Glasel, J. A. *J. Magn. Reson.* **1976**, *21*, 43.
(16) Leipert, T. K.; Marquardt, D. W. *J. Magn. Reson.* **1976**, *24*, 181.
(17) Harris, R. K.; Newman, R. H. *J. Magn. Reson.* **1976**, *24*, 449.
(18) Sass, M.; Ziessow, D. *J. Magn. Reson.* **1977**, *25*, 263.
(19) Wehrli, F. W., Varian Application Note, Number NMR-77-2, 1977.
(20) Draper, N. R.; Smith, H. "Applied Regression Analysis"; John Wiley and Sons: New York, 1966; Chapter 10.
(21) Patt, S. L., private communication.
(22) Pearson, G. A., 20th Experimental NMR Conference, Asilomar, Calif., 1979.

RECEIVED for review March 19, 1979. Accepted July 27, 1979.

Detection of Small Quantities of Photochemically Produced Oxygen by Reaction with Alkaline Pyrogallol

I. A. Duncan,* A. Harriman, and G. Porter

Davy Faraday Research Laboratory of The Royal Institution, 21 Albemarle Street, London W1X 4BS England

A procedure is described for quantitative estimation of small amounts of oxygen produced by photochemical reaction. The procedure involves continuous removal of evolved oxygen in a stream of carrier gas to avoid inhibitory side reactions and subsequent chemical trapping of the oxygen with alkaline pyrogallol. The concentration of oxygen can be measured indirectly by absorption spectrometry of the highly colored oxidation product of pyrogallol. The reagent solution is stable over the experimental time scale and the change in absorbance at 450 nm gives a good measure of the concentration of oxygen present in the solution. Under the experimental conditions, the minimum amount of oxygen that can be detected is 3.5×10^{-7} mol which corresponds to a minimum quantum yield for oxygen production of 1×10^{-3}.

The photodissociation of water into hydrogen and oxygen is a subject of great interest since it can provide a means of collection and storage of solar energy (*1*). The most commonly used methods for detection of gaseous products from such reactions are mass spectrometry (*2*), electrochemistry (*3–5*), and gas chromatography (*6*). These techniques provide simple but sensitive analytical methods, especially for hydrogen. However, oxygen is a notorious inhibitor of photochemical reactions (*7*) and must be removed immediately upon its evolution. This means that, at any given time, the concentration of oxygen is often too low for accurate detection by the above techniques. In the present method, a flow system is described in which oxygen is removed from an aqueous solution and quantitatively trapped by reaction with alkaline pyrogallol (*8*). The concentration of evolved oxygen is then measured indirectly by spectrophotometry since the oxidation product is highly colored.

EXPERIMENTAL

The carrier gas was oxygen-free nitrogen (British Oxygen Company) further purified by passing over hydrogen reduced copper powder (British Drug Houses) (BDH) at 350 °C and through two consecutive solutions of alkaline pyrogallol (*9*). These scrubbing solutions contained pyrogallol (BDH, AR grade, 2 g) in aqueous potassium hydroxide (BDH, 60 mL, 9 M) and were renewed each day. The detection solution comprised pyrogallol (4 g) in potassium hydroxide (100 mL, 9 M) and was freshly prepared in situ in the apparatus after outgassing with the carrier gas. For the photolysis experiments, potassium permanganate (*10*) (BDH, General Purpose grade) was used as received. Oxygen saturated water (1.3×10^{-3} M) was prepared by bubbling pure oxygen (BOC) through distilled water (20 °C) for 45 min.

Apparatus. The flow system was constructed entirely from glass and all joints (ground glass) were smeared with vacuum grease, held together by clips and, where necessary, liberally coated with poly(vinyl alcohol) to seal further against atmospheric oxygen. The photolysis cell was made of cylindrical quartz with two optical windows giving a path length of 5 cm. The total volume of the

0003-2700/79/0351-2206$01.00/0

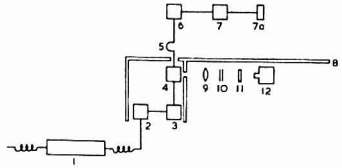

Figure 1. Schematic representation of the apparatus. (1) Copper powder furnace to remove oxygen, (2) and (3) alkaline pyrogallol gas scrubbers, (4) irradiation cell, (5) cold finger, (6) detection cell in spectrometer, (7) silicone oil gas bubbler to stop suck-back, (7a) gas flow meter, (8) blackened support board, (9) lens, (10) filters, (11) water cooled filter, (12) xenon-arc lamp, 250 W

cell was 150 mL and the contents were stirred by a well dispersed flow of carrier gas. A septum seal at the top of the cell facilitated removal of photolysate for analysis and allowed injection of oxygen-saturated water for calibration purposes. For the 254-nm irradiation experiments, a slightly modified photolysis cell was employed. The low-pressure mercury-arc lamp in a quartz envelope was immersed in the solution to be photolyzed in order to give a good incident photon density. The total volume of the cell was 125 mL.

The detection cell was of square cross-section, total volume 100 mL, with optical windows giving a path length of 3 cm. Solid pyrogallol was contained in a side arm while the potassium hydroxide solution was outgassed by purging with carrier gas for about 1 h. After mixing, the absorbance of the solution was allowed to stabilize. The contents of the cell were stirred throughout the experiment with a small magnetic stirrer. The cell was mounted in the beam of a Perkin-Elmer 114 spectrometer, set to display absorbance changes at 450 nm on a pen recorder. The whole system was mounted onto a solid support (Figure 1).

The light source was a 250-W xenon arc lamp for visible irradiation or a low pressure mercury arc for the 254-nm photolysis studies. The xenon-arc light beam was passed through 2 cm of cold, running tap water and then through glass filters to isolate the wavelength region required, before being focused so as to pass through the optical windows of the photolysis cell. The low pressure mercury-arc light was filtered through a 1-cm jacket of cold, running tap water.

The light intensity was calibrated for each wavelength region by ferrioxalate actinometry (*11*). Typical light intensities were in the range $3.5–6 \times 10^{18}$ photons/min for the xenon-arc lamp and 1.6×10^{19} for the low-pressure mercury-arc lamp. The system was calibrated by injection of known volumes of oxygen saturated water (20 °C, 1 atm of pure gas) into the photolysis cell. Changes in absorbance at 450 nm, caused by the absorption of oxygen by the detection solution, were continuously displayed on a chart recorder.

Throughout the experiment the carrier gas flow rate was maintained at 14 ± 2 mL/min. A cold finger between the photolysis and detection cells ensured that no volatile substances were transported by the carrier gas.

The photochemical decomposition of potassium permanganate in aqueous solution was studied with the above system. The photolysis solution (1–2.5 mM), adjusted to pH 9 with dilute sodium hydroxide solution, was thoroughly purged with carrier gas for 2 h before irradiation. Irradiation was intermittent so that oxygen was evolved in a series of steps. Sufficient time was allowed between each step for the carrier gas to transport completely the oxygen produced in the photolysis cell to the detection cell. Blank experiments were carried out to ensure that the system was stable toward stray heat and over long periods of time.

RESULTS AND DISCUSSION

The oxidation of pyrogallol in alkaline solution provides a simple but sensitive method for quantitative detection of oxygen (*8*). The reaction involves formation of a highly colored product from a colorless reagent so that the extent of reaction can be followed easily by absorption spectrometry. However, the mechanism for aerial oxidation of pyrogallol in alkaline aqueous solution is quite complex and involves a number of

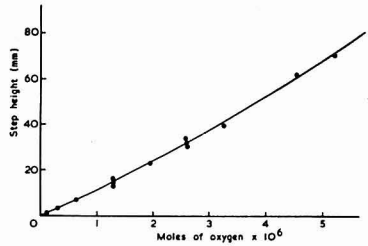

Figure 2. Calibration curve. Plotted as step height against moles of O_2 (10 mm ≡ 0.01 o.d.)

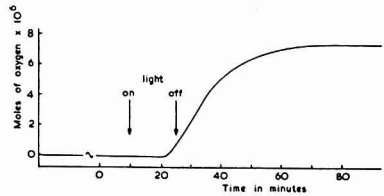

Figure 3. Typical record of oxygen production from irradiation of permanganate showing the response time. The response time between oxygen evolution and absorbance change is about 10 min

intermediates (*12*). These intermediates, although not well characterized, have different absorption profiles while their stability and reaction with oxygen depend upon the experimental conditions. Therefore the use of pyrogallol as a quantitative determinant for oxygen concentrations requires careful choice of experimental conditions to avoid such problems.

Fortunately, by running a series of absorption spectra at different O_2 concentrations, it was found that at any one concentration the absorbance at 450 ± 20 nm remains stable over at least 5 h and the absorbance at this wavelength was almostly linearly sensitive to oxygen. Therefore despite possible interconversion of the intermediates, this wavelength is suitable for monitoring oxygen concentrations, provided that the measurement is made within this period.

At 450 nm, a calibration graph (Figure 2) shows an almost linear relationship between absorbance and concentration of oxygen. The sensitivity of the reactant solution at this wavelength is such that injection of 1 mL of oxygen-saturated water, i.e., 1.3×10^{-6} mol oxygen gives an absorbance change of 0.014 ± 0.002 corresponding to a pen response of 14 ± 2 mm. Repeating the calibration experiment several times over a number of weeks gave a reproducibility of about 10% for the calibration graph. Over 4 h the stability of the pen recorded base line is generally better than ±2 mm. Thus, during an experiment, a pen deflection of 4 mm can be detected, corresponding to the minimum concentration of oxygen that can be measured by the experimental arrangement of about 3.5×10^{-7} mol. The time required for the carrier gas to completely transport small quantities of oxygen from the reaction cell to the detection cell is about 50 min. A typical oxygen detection trace is shown in Figure 3.

The concentration of hydroxide used for the detection solution is unimportant provided it is in excess of about 2 M (*13*). At very high hydroxide concentrations the solution is viscous and there are problems with achieving a suitable rate of mixing. We have found that a 9 M solution gives satisfactory results as regards speed of oxidation, ease of mixing, stability of absorbance at 450 nm over prolonged standing, high extinction coefficient of products, and reproducibility

Table I. Quantum Yields of Oxygen from Permanganate Irradiation

λ irradiation, nm	Φ_{O_2}	Φ_{O_2} Zimmerman (*10*)
254	0.026	0.055
330–400	0.002	-
365	0.0024	0.0023
405	-	0.0011
420–480	<0.0002	-
436	-	0.00016
546	-	$<10^{-5}$

of calibration curve. However, the concentration of pyrogallol is quite important with a 4% solution giving the best results (*8*).

The above system has been developed to determine the amount of oxygen produced during photochemical reactions. Zimmerman (*10*) has shown that the photodecomposition of potassium permanganate in aqueous solution gives rise to the production of oxygen. The quantum yield of oxygen formation is wavelength dependent, slightly dependent upon temperature at longer wavelengths, independent of pH (in the range 7–13) and concentration. Thus, this reaction provides a useful calibration source of oxygen, in low amounts, as would be expected for subsequent studies of the photodissociation of water.

For a typical 1-h irradiation, the photon density was about 5×10^{18} photon/min so that the minimum quantum yield for oxygen formation which can be measured by this pyrogallol method is 1×10^{-3}. This level of sensitivity is sufficient for most photochemical processes, especially systems aimed at the practical photodissociation of water, and in fact the method provides a suitable detection system for the photodecomposition of permanganate ions. As shown in Table I, the quantum yield for oxygen formation can be estimated when it exceeds 10^{-3}. The Φ_{O_2} values obtained in this work are in reasonable agreement with those determined by Zimmerman using the much more elaborate technique, developed by Pringsheim et al. (*14*), of phosphorescence quenching of the dye acriflavine by oxygen. Zimmerman's technique is highly sensitive to oxygen and hence can be used only for irradiations of short duration or of low light intensity; otherwise the phosphor becomes insensitive. However, a problem with the present system is that the extent of photodecomposition needs to be quite high (~1%) in order to produce a sufficient concentration of oxygen for accurate estimation. This gives rise to an inner filter effect, due to precipitated MnO_2, a reaction product. Since the MnO_2 absorbs throughout the wavelength region, it will affect all wavelengths. However, it is only at 254 nm that the effect is clearly seen since, at this wavelength, the Φ_{O_2} value is an order of magnitude higher than for other wavelengths. Thus the measured Φ_{O_2} values at 254 nm are dependent upon irradiation time, since photodecomposition is high (>3%), whereas the values determined by Zimmerman for low extents of decomposition (<0.1%) are independent of irradiation time.

LITERATURE CITED

(1) G. Porter, and M. D. Archer, *Interdisciplinary Sci. Rev.*, **1**, 119 (1976).
(2) G. Sprintschnik, H. W. Sprintschnik, P. P. Kirsch, and D. G. Whitten, *J. Am. Chem. Soc.*, **98**, 2337 (1976).
(3) I. A. Duncan, A. Harriman, and G. Porter, *J. Chem. Soc., Faraday Trans 2*, **74**, 1920 (1978).
(4) P. Joliot, and A. Joliot, *Biochem. Biophys. Acta*, **153**, 625 (1968).
(5) P. Joliot, G. Barbieri, and R. Chabaud, *Photochem. Photobiol.*, **10**, 309 (1969).
(6) S. J. Valenty, *Anal. Chem.*, **50**, 669 (1978).
(7) O. L. J. Gijzeman, F. Kaufman, and G. Porter, *J. Chem. Soc., Faraday Trans. 2*, **69**, 708 (1973).
(8) D. D. Williams, C. H. Blachly, and R. R. Miller, *Anal. Chem.*, **24**, 1819 (1952).
(9) A. J. Gordon, and R. A. Ford, "The Chemist's Companion", Wiley-Interscience, New York, 1972.
(10) G. Zimmerman, *J. Chem. Phys.*, **23**, 825 (1955).
(11) J. G. Calvert, and J. N. Pitts, "Photochemistry", Wiley, New York, 1966.
(12) R. L. Tuve, U.S. Patent 2440315 (1948).
(13) K. Fujinawa, *J. Chem. Soc. Jpn.*, **54**, 31 (1951).
(14) M. Pollack, P. Pringsheim, and D. Terwood, *J. Chem. Phys.*, **12**, 295 (1944).

RECEIVED for review May 22, 1979. Accepted August 7, 1979. We thank the S.R.C., the E.E.C., and G.E. Schenectady, for support of this work.

Neutron-Capture Prompt γ-Ray Activation Analysis for Multielement Determination in Complex Samples

M. P. Failey,[1] D. L. Anderson, W. H. Zoller, and G. E. Gordon*

Department of Chemistry, University of Maryland, College Park, Maryland 20742

R. M. Lindstrom

Center for Analytical Chemistry, National Bureau of Standards, Washington, D.C. 20234

Gamma-ray spectra were taken up to 11 MeV from a wide range of samples and elemental standards while under neutron irradiation to determine the elements whose prompt γ rays are observable and can be used for analytical measurements. Up to 17 elements from among the set H, B, C, N, Na, Mg, Al, Si, P, S, Cl, K, Ca, Ti, V, Mn, Fe, Cd, Nd, Sm, and Gd are measurable in samples of coal, fly ash, orchard leaves, and bovine liver by neutron-capture prompt γ-ray activation analysis (PGAA). The combination of PGAA and instrumental neutron activation analysis (which uses the same equipment) can be used to measure concentrations of 40 to 50 elements in individual samples of many types of material. Concentrations are reported for the elements measurable by PGAA in National Bureau of Standards Standard Reference Materials: coals (SRMs 1632, 1632a, 1635), fly ashes (1633, 1633a), orchard leaves (1571), and bovine liver (1577).

There is continuing need for improved methods for nondestructive multielement analyses of complex samples encountered in the study of environmental, geochemical, and biomedical problems. Instrumental nuclear methods of analysis have been very useful in these applications, especially instrumental neutron and photon activation analysis (INAA and IPAA, respectively) (*1–3*). For these techniques, both the nuclear projectiles and the emitted γ rays have such long ranges in materials that there are rarely significant problems of self-shielding or -absorption by samples. As the methods are instrumental, there is no need for chemical manipulation of the samples, which could allow coprecipitation of trace elements on insoluble residues or container walls, or contamination of samples by impurities in the reagents. Capabilities of INAA and IPAA were demonstrated in a four-laboratory analysis of National Bureau of Standards (NBS) Standard Reference Materials (SRMs) coal and fly ash (*4*). Concentrations of about 40 elements were determined in the SRMs, with results in better agreement between laboratories and with NBS certified values than achieved by laboratories using other methods in a blind, round-robin analysis of the standards.

Despite the strengths of INAA and IPAA in the analysis of complex samples, further improvements are needed. First, measurements of some key elements (e.g., B, Cd, S) are impossible or marginal in many samples. Second, electron accelerators needed for IPAA are not widely available. Third, INAA studies of biological and marine samples are not as successful as for more "crustal" samples (coal, fly ash, rocks) because of interference from high levels of Na, K, and Cl. The interference can be partly overcome by chemical removal of these elements, but this eliminates many advantages of nuclear methods. Fourth, some samples have restrictions that make it impossible to insert them into reactors, e.g., they might decompose or explode, they are physically too large, or the heating, radiation damage, and residual activity are undesirable. Fifth, both INAA and IPAA have two-week or greater turn-around times for complete analyses.

To overcome some of these problems, yet take advantage of the beneficial aspects of instrumental nuclear methods, we investigated the use of neutron-capture prompt γ-ray activation analysis (PGAA). In PGAA, one observes γ rays emitted while the sample is being irradiated with neutrons. Nuclei formed in capture have excitation energies equal to the binding energy of the added neutron, from 5 to 11 MeV. The excitation energy is released by emission of one or several "prompt" γ rays over times $<10^{-14}$ s. Thus, nearly every neutron capture yields γ rays that are potentially usable for analysis for the capturing element.

By contrast, neutron capture does not necessarily form a radioactive species that can be used in INAA. The resulting product may be stable, have a very short or long half-life, or emit no intense γ radiation. For example, Cd has an enormous neutron-capture cross section, but most of the cross section is for the $^{113}Cd(n,\gamma)$ reaction, which forms stable ^{114}Cd, which is of no help in INAA. [Cadmium can sometimes be observed by the reaction $^{114}Cd(n,\gamma)$, which produces 2.3-day ^{115m}Cd.] But in PGAA, one may observe prompt γ rays from capture by ^{113}Cd.

Several papers on PGAA appeared over the past decade (*5–10*). These studies demonstrated the potential of PGAA by calculations or by analyses for one or two elements in several samples. The only multielement applications to complex samples are recent reports of concentrations of nine elements in several NBS and U.S. Geological Survey standards (*11*) and of three elements in several standards (*12*). In order fully to exploit PGAA, one must identify the species responsible for each of the hundreds of lines in prompt γ-ray spectra (*13–15*) and irradiate pure standards of each observable element to determine inter-element interferences of γ-ray lines in the spectra.

We have constructed a facility at the NBS Reactor to irradiate samples in an external thermal neutron beam and observe prompt γ rays with a high resolution γ-ray detection system. This setup was used to identify species observable by PGAA of various types of samples, to determine the best lines of each element, and to identify significant interferences between lines of similar energies of different elements. Applications of the method have been demonstrated by analysis of several classes of NBS Standard Reference Materials.

EXPERIMENTAL

Irradiation Facility. One can either place samples inside the reactor, where the flux is large, and observe the γ rays outside of the reactor, or bring a neutron beam outside to a sample mounted close to the detector. The former has a high neutron flux, but poor counting geometry and the latter is just the opposite.

[1] Present address: Babcock and Wilcox, Lynchburg, Va.

0003-2700/79/0351-2209$01.00/0

Gladney et al. (9) chose the former and we have chosen the latter. Flux and geometry factors balance out to about the same overall efficiency, but the external setup has several advantages: (1) samples are subjected to no heating, little radiation damage, and have very little residual activity; (2) one can use samples that are too large or fragile to be inserted into a reactor; (3) one can put filters in the neutron beam to remove the γ-ray flux from the beam or neutrons of certain energy ranges; and (4) one has greater flexibility in the sample and detector setup, e.g., one can do coincidence counting with two or more detectors.

A vertical beam port was installed on top of the NBS research reactor, a 10-MW D_2O-cooled and -moderated reactor with internal fluxes up to 10^{14} n/cm^2-s. The internal beam tube extends 5.8 m into the reactor. It is made of Al in the lower portion and steel near the top and contains neutron and γ-ray collimators of decreasing diameter up the tube. The external beam tube, which provides shielding around the beam between the top of the reactor vessel and a beam stop, is designed to be purged with helium if desired to prevent neutron scattering by air molecules and neutron capture in N_2 near the target. Boron carbide (B_4C) in paraffin and natural Li_2CO_3 in paraffin are used to thermalize and absorb scattered neutrons to reduce the background in the detectors. A Plexiglas sample box, 1.1 m above the floor, is surrounded by plates of B_4C in polystyrene to absorb neutrons scattered by the sample. A beam stop, consisting of $^6Li_2CO_3$ in polystyrene surrounded by natural Li_2CO_3 in polystyrene with Pb shielding surrounding the latter, is mounted at the top of the beam tube.

The mass of material placed near the sample must be kept small to minimize neutron and γ-ray scattering into the detector and must have small capture cross sections to keep the capture γ-ray background low. We seal most samples in 0.0025-cm Teflon film which is suspended in the beam with nylon fish line. The carbon and fluorine of Teflon have low capture cross sections.

At the sample position, the beam has a 4.5-cm diameter, with a flux constant to about 3% over the central 3 cm. The thermal neutron flux is about 2×10^8 n/cm^2-s, with an integrated flux over the entire beam of 3×10^9 n/s and a gold–cadmium ratio of thermal/fast neutrons of about 55 (16). Additional details on the beam tubes are given elsewhere (16, 17).

Detection System. The detection system must span energies from 100 keV to nearly 11 MeV with good resolution, especially up to about 2 MeV, as the spectra have a high density of lines below that point. The detector is a true coaxial Ge(Li) detector of 24% efficiency (relative to a 7.6 × 7.6 cm NaI crystal) yielding a peak with full-width at half-maximum of 1.9 keV at 1332 keV. The Ge(Li) detector is mounted inside a large NaI crystal that will be used for Compton suppression and pair spectra.

The detection system must be well shielded from γ rays and neutrons, the latter to reduce the prompt γ-ray background from capture in the detector during experiments and to prevent long-term activation and radiation degradation of the detector. The detection system is surrounded by 5 to 10 cm of Pb, and a 2.5-cm thick layer of B_4C in polystyrene, all sealed in an Al shell. A Pb collimator, 15-cm long with a 2.5-cm i.d. is placed between the sample position and the Ge(Li) detector. A 1.3-cm thick, fused $^6Li_2CO_3$ plug is placed in front of the collimator to absorb neutrons. These measures have not entirely removed backgrounds, but have reduced them to acceptable levels (see below).

To take full advantage of the resolution of the Ge(Li) detector, events must be sorted into a large number of channels. The data-handling system is a Tennecomp TP-5000 analyzer whose central component is a Digital Equipment Corporation PDP-11/34 computer with a 128K-word memory. The system has inputs from six 8192-channel analog-to-digital converters (ADCs). For spectra reported here, we used two ADCs, one covering the 0- to 4-MeV range and the second, with input from a biased amplifier, covering the region from 3.2 to 11 MeV.

Irradiation Procedures. For most samples and standards, we use about 1 g of material, formed into a 1.3-cm diameter pellet in a press, sealed in 0.0025-cm Teflon film and suspended in the central, uniform portion of the beam, oriented at 45° to the beam. For elements with very high cross sections (B, Cd, Sm, and Gd), calculations and experiments show that much smaller standards must be used to avoid self-shielding of the neutron beam. For Gd, for example, surface densities of <150 μg/cm^2 must be used to keep self-shielding to <1%. Standards of strongly absorbing materials are made by pipetting dilute solutions, drop by drop, over a large area of a Whatman 541 filter paper and forming the filter into a pellet.

During these exploratory experiments, most complex samples were left in the beam for 12 to 24 h to build up good statistics for weak lines. Most standards were run for 1 to 2 h. A Cr standard was frequently run to check on flux variations and geometry. The flux is constant to <1% over many-hour periods when the reactor has been running for more than several hours at constant power, as it normally does for six-week periods between scheduled shutdowns. When shutdowns occur, the external beam tube and detection system must be moved to provide access to the top of the reactor. When the system is repositioned and aligned, efficiency changes of up to 5% can occur because of alignment of the detectors, collimators, etc. Use of the Cr standard allows us accurately to correct runs from one fuel cycle to another.

Several elements with products of short half-lives can be measured more sensitively from γ rays emitted in decay of the products than by observing prompt γ rays. For species of a few minutes half-life (2.3-min ^{28}Al and 3.8-min ^{52}V), the samples are irradiated for several half lives to ensure saturation before starting the count. For species with longer half lives (2.6-h ^{56}Mn and 15-h ^{24}Na), irradiation time is accurately monitored and the data corrected by the integral of the saturation factor, $(1\text{-}e^{-\lambda t})$. This procedure was checked by running known amounts of these elements for 24 h and storing spectra at intermediate times.

Data Handling. During each experiment, 8192-channel spectra are accumulated in the computer memory and stored on magnetic disk and tape. During another experiment, data from tapes or disks are read into the memory for analysis. Several programs were developed for use with the system. One program selects peaks of elements of interest, analyzes them using an established energy calibration curve, and displays the results on a CRT. The user can accept the result or use a light pen to indicate a different background for subtraction from the peak. Another program integrates areas under all peaks in the spectrum and can be used for preliminary scanning of new samples. A Decwriter prints all observed peaks with the assigned energies, peak areas, and associated errors.

One is greatly aided in the identification of peaks by using the excellent resolution of the Ge(Li) detector to determine the energies corresponding to the peak centroids as accurately as possible, to within ±0.5 keV. The energy scale can be calibrated to an accuracy of about ±0.1 keV up to 3.5 MeV with radioactive sources. From 3.5 to 10.8 MeV, we calibrated the energy scale mainly with the use of accurately measured lines from neutron capture in nitrogen (18).

Prompt γ-Ray Spectra. Portions of the prompt γ-ray spectrum produced by irradiation of NBS standard fly ash (SRM 1633a) are shown in Figures 1 to 4. The region from 70 to 520 keV in Figure 1 has a rather low density of lines, but a large continuous background at low energy from scattered γ radiation from the beam and Compton events. It will be possible to reduce this background about fourfold by Compton suppression (i.e., operating the surrounding NaI crystal in anti-coincidence with the Ge(Li) detector) and further by absorbing γ rays from the neutron beam with a single crystal of Bi in the beam shutter. The peak from B at 477 keV is Doppler-broadened as it is emitted from ^{7}Li, which is moving with random direction with respect to the detector following the $^{10}B(n,\alpha)^7Li$ reaction.

The region between 500 and 900 keV has a great density of lines as shown in Figure 2. Much of the complexity is caused by Sm and Gd, which have enormous capture cross sections (5900 and 39 100 b, respectively) and complex prompt spectra. The high density of lines continues up to about 2 MeV.

At high energy (Figures 3 and 4), the spectrum is less complex than at low energies. In this region, each γ ray produces three peaks: the full energy peak and two additional peaks displaced downward by 511 and 1022 keV, corresponding to the loss of one and two 511-keV annihilation photons following pair production by the high energy γ rays in the detector, the so-called single- and double-escape peaks, respectively. Because of the relative simplicity of the high energy region, it is desirable to use high energy lines for analyses if possible.

Portions of the spectrum of NBS Bovine Liver (SRM 1577) are shown in Figures 5 to 7. The low energy portion is much

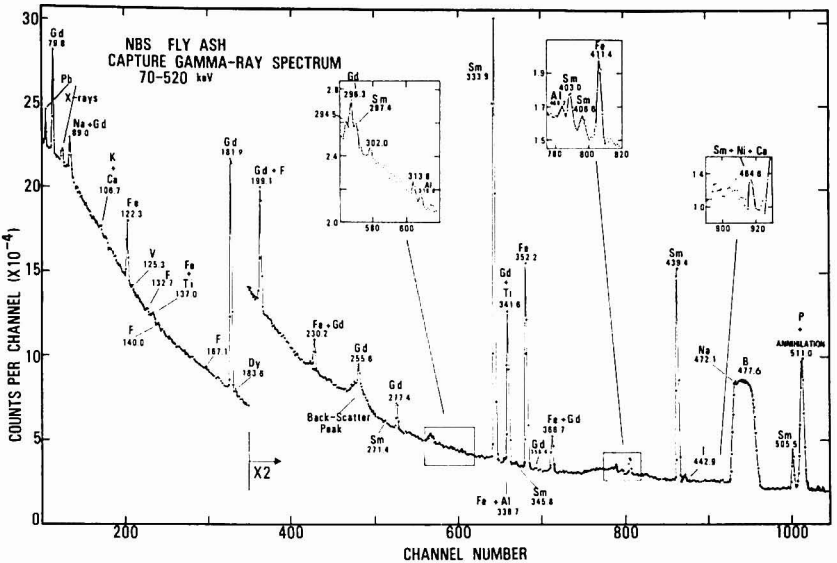

Figure 1. Prompt γ-ray spectrum of NBS Fly Ash (SRM 1633a) in the region of 70 to 520 keV observed by irradiating an 0.82-g sample for 20 h in the external thermal-neutron beam from the NBS reactor. Peaks are labeled by energies in keV and the element of origin

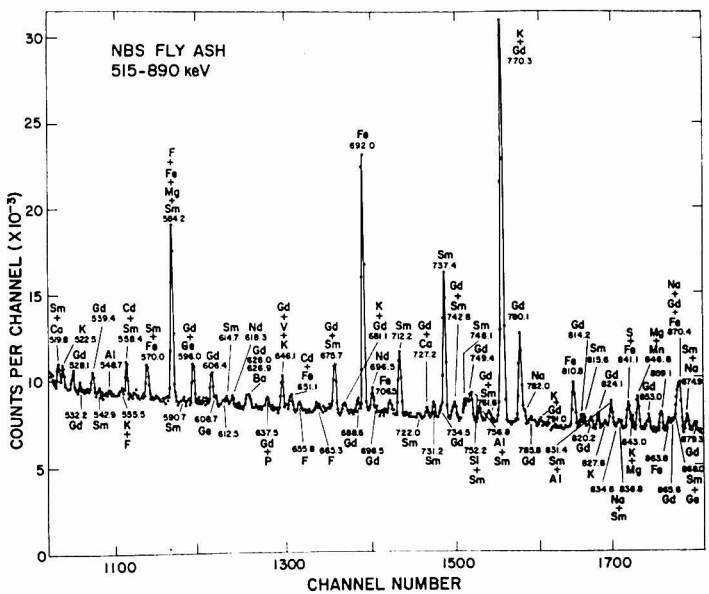

Figure 2. Prompt γ-ray spectrum of NBS Fly Ash (SRM 1633a) in the region of 515 to 890 keV

simpler than for Fly Ash, in part because of lower concentrations of elements that produce many lines in the Fly Ash spectrum, notably Sm and Gd. In fact, Sm lines are so weak in the Bovine Liver spectrum that its concentration could not be measured reliably. Some Gd lines are barely observable, but too weak for analysis. The B/Na ratio is smaller in Bovine Liver than in Fly Ash, so the 472-keV line of Na is distinct in the B 477-keV Doppler-broadened peak in the Bovine Liver spectrum. The region near the 558-keV Cd peak is less cluttered in the Bovine Liver spectrum.

High energy portions of the spectra are also quite different. Whereas the Fly Ash spectrum is dominated by lines from major

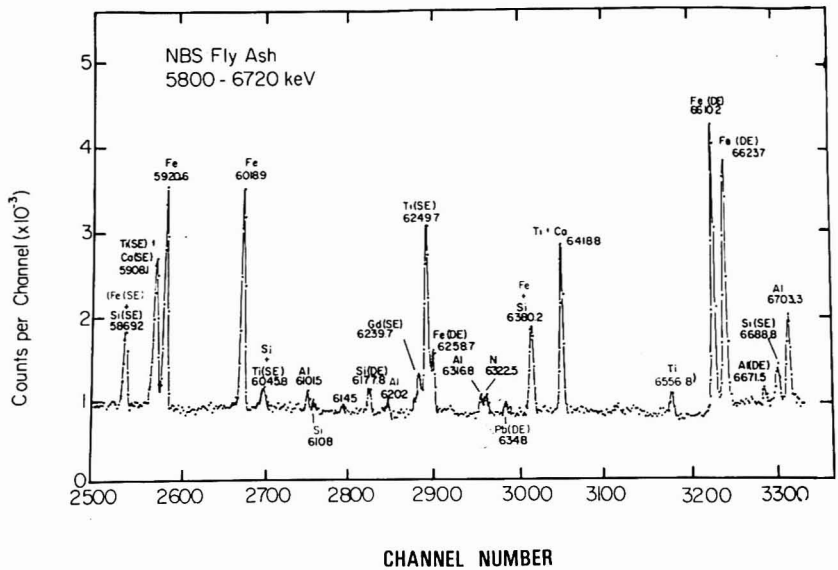

Figure 3. Prompt γ-ray spectrum of NBS Fly Ash (SRM 1633a) in the region of 5800 to 6720 keV. Note that this spectrum was taken simultaneously with the data for Figure 1 and 2, but the channel number scale for this portion (and that of Figure 4) is different from those of Figure 1 and 2, as signals for the former were taken via a biased amplifier covering the range from 3.2 to 11 MeV which were run into a separate 8K analog-to-digital converter. Single- and double-annihilation-photon escape peaks are designated SE and DE, respectively

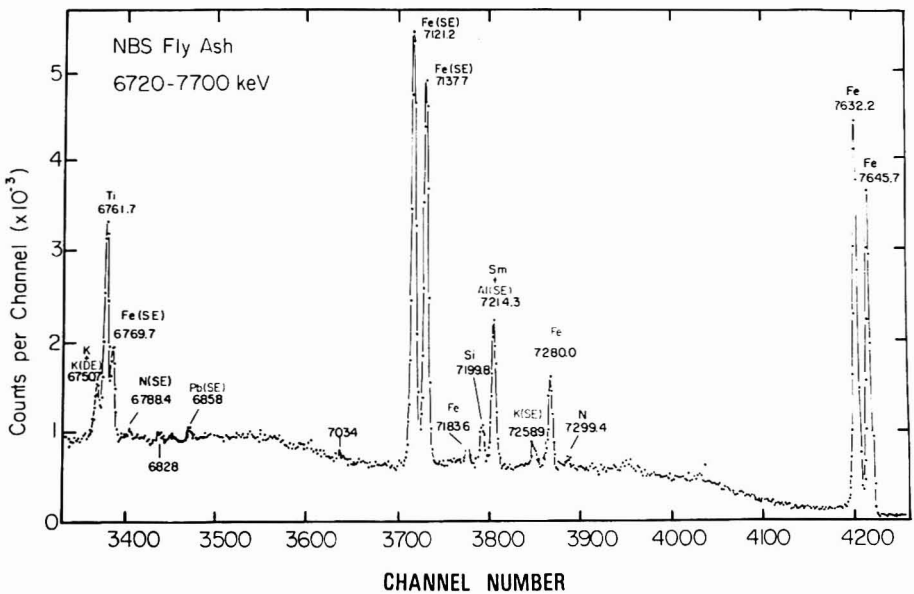

Figure 4. Prompt γ-ray spectrum of NBS Fly Ash (SRM 1633a) in the region of 6720 to 7700 keV. See caption of Figure 3

and minor crustal elements such as Fe, Si, Ti, and Al, the Bovine Liver spectrum is dominated by lines from Cl, N, S, and K. A major problem in the application of INAA to biological and marine samples is the enormous activities of ^{24}Na, ^{42}K, and ^{38}Cl produced that make it difficult to observe other elements with products of half-lives less than a few days. In PGAA, interference by Na and K is rather small, but the Cl prompt spectrum contains many strong lines spread over the entire energy spectrum.

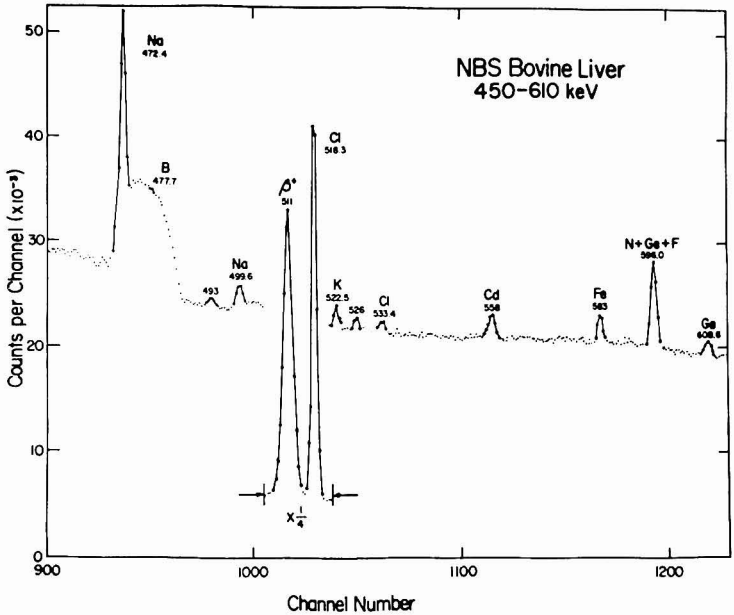

Figure 5. Prompt γ-ray spectrum of NBS Bovine Liver (SRM 1577) in the region of 450 to 610 keV observed by irradiating a 1.3-g sample for 24 h in the external thermal-neutron beam of the NBS reactor. Peaks are labeled by energies in keV and the element of origin

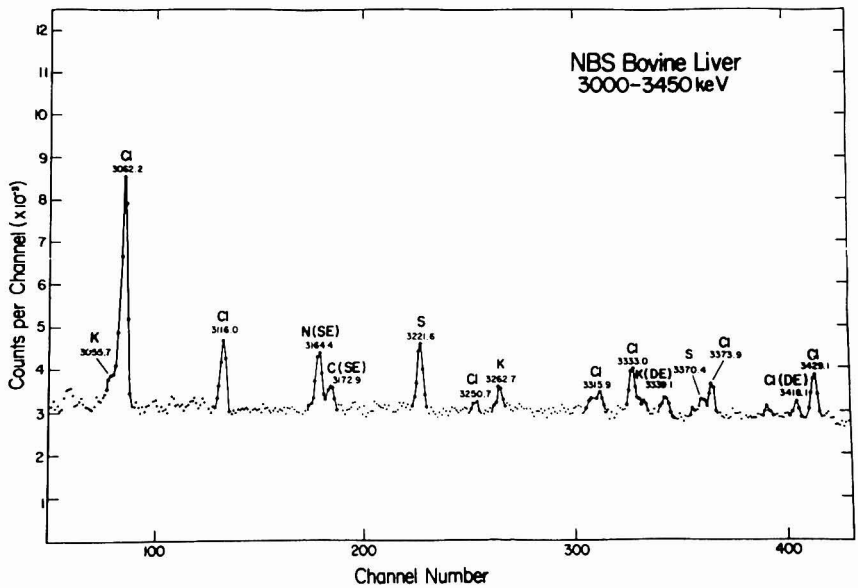

Figure 6. Prompt γ-ray spectrum of NBS Bovine Liver (SRM 1577) in the region of 3000 to 3450 keV. Note that this portion of the spectrum was taken at the same time as that of Figure 5, but the channel number scale is not the same because of the use of a biased amplifier for this and Figure 7. (See caption of Figure 3)

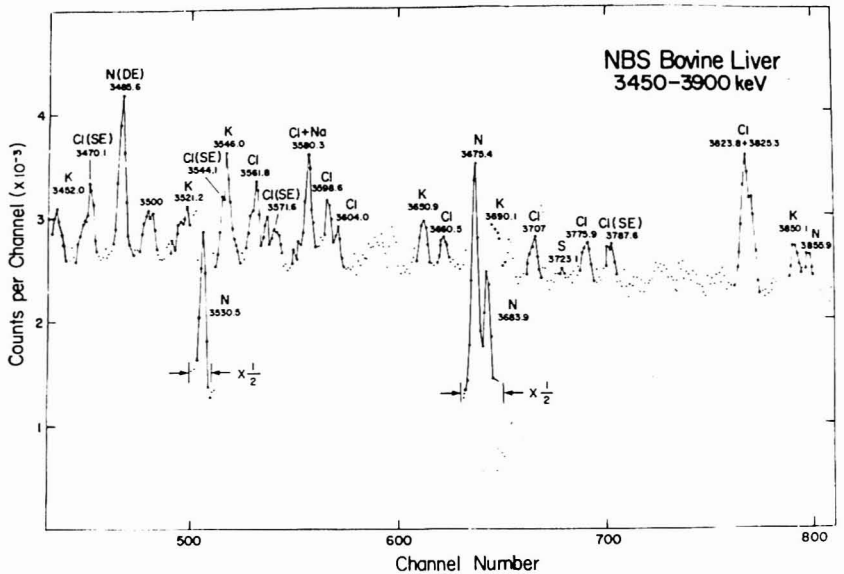

Figure 7. Prompt γ-ray spectrum of NBS Bovine Liver (SRM 1577) in the region of 3440 to 3870 keV. See caption of Figure 6

Identification of Prompt γ-Ray Lines. Energies of significant peaks were determined to ±0.5 keV accuracy. Preliminary identifications were made using compilations of prompt γ-ray spectra of individual elements (*13–15*). Identifications were checked by irradiating a standard of the pure element or simple compounds. Confirmation of identities of lines was essential because of deficiencies in compilations; some listed γ-ray energies are wrong by up to 5 keV. Tabulations for many elements contain lines belonging to other elements, probably arising from trace impurities in the elemental standards, especially Cd, Sm, and Gd, which have such large cross sections that trace quantities can produce sizeable peaks. In one compilation, the γ-ray lists for 38 elements contain a line near 558 keV (*13*). Many of these seem to result from Cd contamination of the elemental standard.

We also observe contaminant lines in spectra of the highest purity samples obtainable. We have identified and removed contaminant lines from internal compilations by running standard materials of each element obtained from two or more quite different sources, in some cases the pure element and a simple compound of it. Ratios of intensities of lines associated with the element are constant, but lines from the contaminant are absent from one of the spectra or, if present, the relative intensities are different from that of lines belonging to the element. As we know the entire spectra of most contaminant species, we can note their presence on the basis of several lines in a familiar intensity pattern and use prominent lines, along with the known spectrum of the contaminant, to subtract its contributions.

We have identified most lines in the spectra whose intensities are great enough for possible use in quantitative measurements. We selected the best lines for quantitative determinations based on their intensities and freedom from interference. Recommended lines for each element, along with interferences, are listed in Table I. For each species, we have taken the absolute intensity of one major line from the literature and used relative intensities of the other lines from our own work. The latter were determined with a photopeak efficiency curve established up to 10.8 MeV from capture spectra of elements that yield a wide range of photopeaks in known intensity ratios (*17*).

Quantitative Determinations. Elemental concentrations were measured by irradiating approximately 1-g samples as described above. Concentrations relative to standards were determined from the ratios of areas under the peaks produced by the lines listed in Table I, after subtraction of significant interferences.

Table II lists count rates for significant peaks in the background. Two types of backgrounds are shown: one with the upper beam tube purged with helium and sealed and the other, with air left in the tube. Although the latter background is higher for some peaks (especially ^{41}Ar and N), it is more constant with time than those obtained with He flushing. Thus, it is preferable to run without flushing except when analyzing low-nitrogen samples to obtain accurate N values. The major background lines are from capture in H, B, N, C, Fe, and Pb. Capture in H and C occurs in the Plexiglas beam tubes and that in B occurs in the B_4C around the sample box. Capture lines of Pb and Fe and the decay line of ^{28}Al are from construction and shielding materials. Capture in N occurs in the air beyond the sample box and, when not He-flushed, in air in the beam tube. Argon-41 is always present in the air near a reactor.

Before computing net areas of the peaks, one must subtract contributions of interfering lines. Those contributions are determined from clean lines of the interfering species with the use of the spectrum of the species. For example, the strongest line of Cd, at 558 keV, contains interferences from several species that must be removed to obtain reliable Cd analyses. The Sm interference is determined from the intensities of Sm lines at 333, 439, 505, and 736 keV, using the ratio of the intensity of the 558-keV peak to those lines in the spectrum of Sm_2O_3. For the fly ash spectrum of Figure 2, about 15% of the 558-keV peak is due to Sm interference. If the peak is not resolved from one at 556 keV, interferences from K, F, and Ni must be removed if those elements are present at percent levels. Although the removal of interferences sounds rather cumbersome, it can be done easily and accurately with a library of reliable spectra of interfering species.

RESULTS

The PGAA method was tested by analyzing several types of NBS standards: Coals (SRM 1632, 1632a, and 1635), Fly Ashes (SRM 1633 and 1633a), and biological samples, Orchard Leaves (SRM 1571) and Bovine Liver (SRM 1577). Concentrations observed in five irradiations of each standard are given in Tables III, IV, and V, along with NBS values and

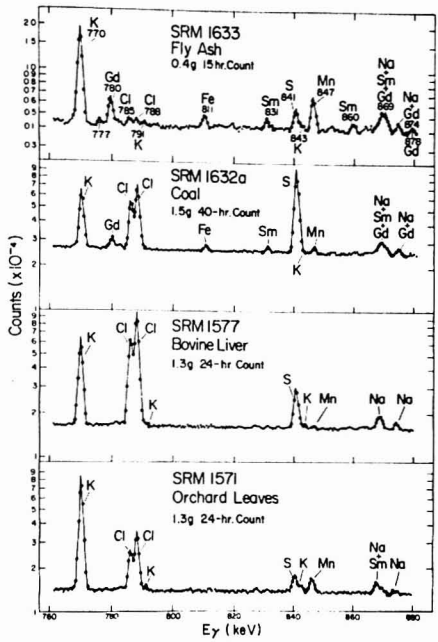

Figure 8. Expanded plots of the prompt γ-ray spectra of NBS standards in the vicinity of the 841-keV S line

other reported values. The data under "Other Values" are not exhaustive compilations as have been summarized in Ref. 28 for Coal, Ref. 29 for Coal and Fly Ash, and Ref. 33 for the biological samples.

Concentrations of about 16 elements are measurable in a range of typical coals (see Table III). In most cases for which PGAA values can be checked against other data, the agreement is quite good. A possible exception is our Ti value in SRM 1632a, which may be slightly too low. For both SRM 1632 and Fly Ash (Table IV), our values for B are consistently lower than those measured by PGAA at Los Alamos (*9*). We believe our values are correct, as they agree better with some other values reported, especially the charged-particle-track measurements by Carpenter in Fly Ash (*31*). There is good agreement with the Los Alamos group for B in Orchard Leaves. Within the quoted limits of error, there is agreement between this work and that of Los Alamos on the Cd values for SRMs 1632 and 1633.

Although not in disagreement outside of quoted limits of error (except for Orchard leaves), the Los Alamos values (*10*) for S are usually somewhat larger than ours. As sulfur is very important for environmental measurements, we show expanded plots of the spectra from several types of samples in Figure 8 around the 841-keV line of S used in the Los Alamos analyses. The 843-keV line of K appears as a shoulder on the 841-keV S line and must be subtracted to obtain accurate S values. When this is done, we obtain good agreement with the S determinations based on the higher energy lines (see Table I and Figure 6). Although the higher energy lines are more free of interference, the 841-keV peak gives better statistics. In addition, there is a well-separated peak from decay of ^{56}Mn at 847 keV, which is not shown in the Los Alamos spectrum. We use the line for Mn determinations, but the Los Alamos count may have been so short that ^{56}Mn had not grown in appreciably. Their spectrum shows a larger 843/841 peak area ratio than ours and they may not have subtracted enough 843 from the 841-keV peak. As noted recently by Curtis et al. (*34*), there is a possible interference of Cr with the 841-keV S peak in samples with large Cr/S ratios, e.g., meteorites. The Cr peak at 835 keV would be cleanly separated from the 841-keV peak unless the former were enormous.

For Si in SRM 1633, there are two sets of values: 21–22% from our group and 17–18% for the Los Alamos values (*11*, *27*). There are no independent values that might resolve the discrepancy. The PGAA values for Mg are not in agreement with those from INAA, as our value is too low and the LASL value, too high. Instrumental neutron activation analysis is probably more accurate than PGAA for Mg (as well as V) in fly ash. Our values for Na, Ca, and Fe agree well with results from other methods, but the Los Alamos values (*11*) for Na and Fe are somewhat too high and for Ca, too low.

With our present system, P can be determined most sensitively via the 637-keV line. The P concentration in Fly Ash 1633 is below our detection limit for that line (see Table VI below). Gladney et al. (*11*) report a value for P of 0.3%, as compared to a value of 0.088% from another group at Los Alamos (*27*). The PGAA value is based on a line at 2154 keV (*11*). We observe a doublet in the P standard consisting of 2152- and 2157-keV lines of comparable intensity, but have not used them because of possible interferences by γ rays of Cl (2156 keV) and K (2154 keV).

For the remaining elements in SRM 1633 Fly Ash in Table IV, there is good agreement between the PGAA values and those obtained by other techniques. The Certificate of Analysis was recently issued for SRM 1633a. Except for Ca, for which our value is slightly too high, there is agreement within limits of error for all certified values. There appears also to be good agreement with the information values except, possibly, for V.

The PGAA technique is much more sensitive to analysis for major elements than INAA, which is mainly a trace element method. In the Fly Ashes of Table IV, note that PGAA measures nearly all major elements that are traditionally measured by geochemists in rocks, the main exceptions being Na and Mg, which are marginal by PGAA, but easily measured by INAA. In fact, if one uses the traditional geochemical method and sums the weights of common oxides of the elements (e.g., Na_2O, Al_2O_3, CaO, etc.) and puts in values for Na, Mg, and P where necessary, the sums obtained for SRM 1633 and 1633a are 102% and 95%, respectively. This suggests that, if one had measured oxygen values, one could account for essentially the entire mass of the fly ash. Applying this approach to the coals, with the inclusion of C, H, and N, one accounts for 90% and 97% of the mass of SRM 1632 and 1632a, respectively, but only 68% of that of SRM 1635. The reason for the larger discrepancy in the latter case is probably that the oxygen content of the coal is related to the degree of alteration between cellulose and anthracite. The 1635 Coal, a western coal, would be expected to have a higher oxygen content than the other standards, which are eastern coals.

Because of the lower concentrations of most elements from Tables III and IV in the biological samples, we are able to measure far fewer elements in Orchard Leaves and Bovine Liver (see Table V). For the elements reported, there is generally good agreement with other values if known, the major exception being Na. Both Na and Mn are barely measurable by PGAA in these types of samples, so the uncertainties are large for both elements.

Limits of Detectability. In Table VI are listed the sensitivities and limits of detectability for one or more major

Table I. Recommended Lines for Elemental Determinations by Neutron-Capture Prompt γ-Ray Activation Analysis

element	cross section for th.-neutron cap.,[a] barns	E_γ,[b] keV	I_γ,[c] γ rays/100 cap.	interferences[d]
H	0.33	1201.2 DE	4.4	Cl, Mg
		1712.2 SE	6.9	Cl
		2223.2[e]	100[f]	
B	760	477.6[g]	94[h]	Na, P, Cl, Gd, Sm, Fe
C	0.0034	1261.9[i]	26	Gd, Sm, Si, Fe
		3683.8[i]	32	P, S, Si, Fe
		3923.4 DE	24	P, Cl, S, Si
		4434.4 SE	39	Cl, Al, S, Si
		4945.4[i]	67[j]	P, Cl, F, S, Si
N	0.075	1884.8[k]	18	Fe, Sm
		3677.7[k]	14	Ca
		5269.1[k]	31[l]	Gd
		5297.8[k]	30	
		9807.1 DE	14	
		10318.1 SE	23	
		10829.1[k]	13	
F	0.0096	655.9[m]	13	
		665	10	Sm
	^{19}F, 100%, 0.0096b, 11-s ^{20}F	1633.7 D[i]	100[i]	Na, Ti, Sm, V
Na	0.53	472.3[i]	69[h]	B, P, Gd
		869.1[i]	23	Sm, Gd
		874.4[i]	15	
	^{23}Na, 100%, 0.53b, 15-h ^{24}Na	1368.5 D	100[h]	Gd
Mg	0.064	585.1[i]	26	F, Sm, Fe
		1808.7[m]	23	P, Cl, Sm
		2829[m]	31	Fe, Cl
		3917	41[j]	C, Si
Al	^{27}Al, 100%, 0.23b, 2.24-min ^{28}Al	1778.8 D[h]	100[i]	N, C
	0.23	6701.9 DE	21	Sm
		7212.9 SE	30	Sm
		7723.9[n]	26[n]	
Si	0.165	1273.3[i]	12	Sm
		2093	16	Fe, Cl
		3539	63	Fe, P, C, S
		4422.2 SE	40	C, Cl, Al, Si, Sm
		4933.2[i]	71[j]	C, Cl
		5869.0 SE	11	Fe
		6380.0[i]	12	Fe
P	0.18	636	11	Sm, Gd, Cl
		1071	12	Cl, Si
		3523	14	Sm
		3900	18[i]	
S	0.51	840.4[i]	35	Gd, K
		2380	29	Fe, Cl
		2933.7[m]	12	Fe
		3219.9[m]	18	Fe
		4910 SE	29	P, Al, Sm
		5421	42[j]	Si, Al
Cl	33.1	516.7[m]	9.5	
		786.3[m]	5.1	Al, Gd
		788.4[i]	7.5	
		1164.7[i]	16	
		1950.9[n]	13	
		1959.1[n]	8.5	
		2863.9[n]	4.5	P
		5089.0 DE	6.7	
		5600.0 SE	15	Si
		6111.0[n]	19.8[n]	Si
K	2.1	770.5[i]	31[j]	Sm, Gd, S
		1159.0[m]	6.2	Gd, Sm
		1618.9[m]	4.7	Al
		2073	6.2	Fe, Cl
		4360	7.2	P
Ca	0.43	519.4[i]	4.5	Sm
		1942.6[i]	52.5[i]	Fe, P, Al, F
		2001.2[i]	10	Fe, Cl
		2009.8[i]	6.3	Cl
Ti	6.1	341.9[i]	14	Fe, Cl, Sm, Gd
		1381.4[i]	65.5[i]	Sm, Al
		5397 DE	14	Ca
		5730 DE	23	Fe, Cl
		5908 SE	23	Ca
		6251 SE	39	Fe, Cl
		6417	24	Ca
		6762	39	Fe, Cl

Table I. (*Continued*)

element	cross section for th.-neutron cap.,[a] barns	E_γ,[b] keV	I_γ,[c] γ rays/100 cap.	interferences[d]
V	5.0	645.7[f]	12[f]	
	^{51}V, 99.75%, 4.9b, 3.75-min ^{52}V	1434.3 D[f]	100[f]	
		6517	19[f]	
		7163	14[f]	
Mn	^{55}Mn, 100%, 13.3b, 2.6-h ^{56}Mn	846.8 D[f]	99[f]	Gd
Fe	2.6	352.3[f]	6.1	S, Gd
		692.3[f]	3.9	Si
		1725.0[n]	7.8	Cl, Sm
		7120.1 SE	30	
		7134.5 SE	27	
		7631.1[n]	28[m]	
		7645.5[n]	23	
Cd	2420	558.3[f]	80[f]	F, Sm
		651.0[f]	16	Fe
		725.0[f]	5.2	Fe, Cl
		805.9[f]	6.4	Fe
Nd	49	6180[f]	22.9	
		6965[f]	62.1	Gd
Sm	5900	333.9[f]	83[f]	Gd
		439.4[f]	55	Cl
		505.5[h]	11	Si, Gd
		737.5[f]	13	Gd
		1170.6[f]	5.8	Gd, Cl, ^{60}Co bkgd
Gd	39 100	181.9[o]	14.9[f]	
		944.1[o]	9.4	Cl, Sm, Al
		962.1[o]	6.4	Cl
		977.1[o]	4.5	
		1107.6[o]	5.6	Fe, Sm
		1184.0[o], 1187.1[o]	13.3	Fe, Al

[a] Unless otherwise noted, data are from Ref. 19. Cross sections are for the natural isotopic mixture except for lines observed from short-lived decay products, in which case, the target isotope, its isotope abundance, and cross section and the half live of the product nuclide are given. [b] Energies based on this work unless otherwise noted. SE and DE indicate single and double escape peaks and D indicates a γ ray emitted by radioactive decay. Energies are accurate to better than ±0.2 keV if energy listed to 0.1 keV; otherwise to ±0.5 keV. [c] Absolute γ-ray intensities in terms of γ rays per 100 neutron captures. Absolute intensities of one or more lines for each species were obtained from indicated references and the remainder are based on observed relative intensities of this work. Note that relative intensities of SE and DE peaks are valid only for our detection system. [d] From 0 to 4 MeV, interferences are listed if the interfering line is within ±3 keV of the line in question and, from 4 to 11 MeV, if within ±10 keV. [e] Ref. 20. [f] Ref. 15. [g] Doppler broadened (to about 15 keV) by motion of ^{7}Li following ^{10}B (n, α) reaction. [h] Ref. 21. [i] Ref. 19. [j] Ref. 13. [k] Ref. 18. [l] Ref. 22. [m] Ref. 23. [n] Ref. 24. [o] Ref. 25.

Table II. Comparison of Intensities of Background Peaks with Those of Same Peaks in the Spectrum of Standard Coal (SRM 1632a) and Bovine Liver (SRM 1577)

		peak area count rate (c/s)			
				background	
E_γ, keV	source element	SRM 1632a Coal, He-flushed	SRM 1577 Bovine Liver, He-flushed	He-flushed	not flushed
477	B	51.0 ± 0.2	2.35 ± 0.02	0.22 ± 0.01	0.41 ± 0.01
511	β^+ annihilation	6.78 ± 0.05	3.84 ± 0.01	1.96 ± 0.05	2.93 ± 0.05
1173	^{60}Co decay	0.034 ± 0.009	0.025 ± 0.008	0.070 ± 0.004[a]	0.043 ± 0.002
1294	^{41}Ar decay	0.050 ± 0.009	0.037 ± 0.009	0.017 ± 0.004	0.043 ± 0.002
1333	^{60}Co decay	0.056 ± 0.010	0.059 ± 0.009	0.091 ± 0.004[a]	0.051 ± 0.002
1779	^{28}Al decay	1.34 ± 0.02	0.053 ± 0.011	0.006 ± 0.003	0.012 ± 0.003
1885	N	0.17 ± 0.01	0.31 ± 0.01	0.079 ± 0.003	0.115 ± 0.004
2223	H	64.8 ± 0.1	60.2 ± 0.1	2.5 ± 0.1	3.1 ± 0.1
4945	C	0.192 ± 0.004	0.129 ± 0.003	0.006 ± 0.001	0.008 ± 0.001
5269	N	0.085 ± 0.004	0.178 ± 0.003	0.047 ± 0.002	0.066 ± 0.001
5533	N	0.058 ± 0.003	0.099 ± 0.003	0.027 ± 0.002	0.041 ± 0.001
5562	N	0.028 ± 0.003	0.054 ± 0.003	0.015 ± 0.001	0.023 ± 0.001
6322	N	0.046 ± 0.003	0.081 ± 0.002	0.020 ± 0.001	0.035 ± 0.001
7299	N	0.011 ± 0.002	0.025 ± 0.002	0.005 ± 0.001	0.011 ± 0.001
7368	Pb	-	-	0.0032 ± 0.0006	0.0020 ± 0.0005
7632	Fe	0.105 ± 0.002	0.0056 ± 0.0013	0.0051 ± 0.0006	0.0058 ± 0.0006
7646	Fe	0.087 ± 0.002	0.0052 ± 0.0014	0.0042 ± 0.0015	0.0049 ± 0.0005
10830	N	0.0117 ± 0.0005	0.0238 ± 0.0006	0.0055 ± 0.0004	0.0089 ± 0.0004

[a] Increase due to improperly shielded ^{60}Co in vicinity.

lines of species observable in various types of samples. Here we have used definitions by Jaklevic and Walter (*35*) based on work by Currie (*36*). The sensitivity S is the net count rate under the peak of interest (counts/s) per unit mass of the element in question (mg) after subtraction of general background. The sensitivity for a given element for the particular

Table III. Concentrations of Elements in NBS Standard Coals (μg/g unless % indicated)

	SRM 1632 (old coal standard)			SRM 1632a (Bituminous)			SRM 1635 (Subbituminous)		
element	this work[a]	NBS[b]	other values	this work[a]	NBS[b]	other values[c]	this work[a]	NBS[b]	other values[c]
H (%)	4.02 ± 0.05	-	4.3 ± 0.1[d]	3.7 ± 0.1	-	-	3.96 ± 0.03	-	-
B	42.1 ± 0.7	-	47.0 ± 1.6,[e] 30 ± 1,[f] 43[g]	52.7 ± 1.8	-	-	104.5 ± 2.6	-	-
C (%)	70 ± 5	-	73 ± 3,[d] 69.6 ± 2.1[f]	71 ± 4	-	-	59 ± 3	-	-
N (%)	1.3 ± 0.2	-	1.2 ± 0.2[d]	1.27 ± 0.08	-	-	1.0 ± 0.1	-	-
Na	-	-	414 ± 20[h]	-	-	850 ± 45	2700 ± 50	-	2440 ± 200
Al (%)	1.68 ± 0.04	-	1.85 ± 0.13,[h] 1.74 ± 0.04[i]	3.01 ± 0.13	(3.07)	2.91 ± 0.32	0.34 ± 0.04	(0.32)	0.30 ± 0.02
Si (%)	2.95 ± 0.06	(3.2)	3.92[j]	5.8 ± 0.1	-	-	0.52 ± 0.02	-	0.56 ± 0.07
S (%)	1.29 ± 0.03	-	1.32 ± 0.07[k]	1.59 ± 0.02	(1.64)	1.8 ± 0.4	0.32 ± 0.01	(0.33)	-
Cl	895 ± 15	-	890 ± 125,[h] 844 ± 35[i]	784 ± 17	-	780 ± 40	26 ± 2	-	26 ± 4
K (%)	0.275 ± 0.010	-	0.28 ± 0.03,[h] 0.30 ± 0.02[i]	0.42 ± 0.02	-	0.42 ± 0.02	0.0097 ± 0.0006	-	0.0117 ± 0.0015
Ca (%)	0.33 ± 0.05	-	0.43 ± 0.05,[h] 0.35 ± 0.03[i]	0.24 ± 0.02	-	0.24 ± 0.02	0.54 ± 0.02	-	0.55 ± 0.08
Ti	890 ± 35	(800)	1100 ± 100,[h] 890 ± 50[i]	1550 ± 40	(1750)	1620 ± 70	190 ± 20	(200)	205 ± 20
Mn	43.5 ± 2.4	40 ± 3	43 ± 4,[h] 41 ± 4[i]	29 ± 5	28 ± 2	32 ± 3	24 ± 7	21.4 ± 1.5	22 ± 3
Fe (%)	0.842 ± 0.024	0.87 ± 0.03	0.84 ± 0.04[h]	1.11 ± 0.06	1.11 ± 0.02	1.15 ± 0.03	0.22 ± 0.01	0.239 ± 0.005	0.22 ± 0.02
Cd	0.18 ± 0.02	0.19 ± 0.03	0.2 ± 0.05[e]	0.21 ± 0.03	0.17 ± 0.02	-	-	0.03 ± 0.01	-
Nd	11.3 ± 2.0	-	8.7 ± 1.0,[i] 10 ± 7[j]	11.8 ± 0.4	-	12 ± 3	-	-	1.4 ± 0.2
Sm	1.53 ± 0.02	-	1.7 ± 0.2,[h] 1.38 ± 0.10[i]	2.10 ± 0.07	-	-	0.25 ± 0.01	-	-
Gd	1.43 ± 0.05	-	-	1.95 ± 0.03	-	-	0.23 ± 0.01	-	-

[a] Based on five separate irradiations for most elements. [b] NBS Office of Standard Reference Materials Certificate of Analysis. Values in parentheses are information values, not certified. [c] Ref. 26. [d] Ref. 12. [e] Ref. 9. [f] Ref. 27. [g] Ref. 28. [h] Ref. 4 [i] Ref. 29. [j] Ref. 30. [k] Ref. 10.

Table IV. Concentrations of Elements in Standard Fly Ashes (μg/g unless % indicated)

element	SRM 1633 this work[a]	SRM 1633 NBS[b]	SRM 1633 other values	SRM 1633a this work[a]	SRM 1633a NBS[b]
B	433 ± 4	-	434 ± 9,[c] 493 ± 14,[d] 500 ± 29[e]	39.2 ± 0.7	-
Na (%)	0.30 ± 0.02	-	0.32 ± 0.04,[f] 0.283 ± 0.014,[g] 0.36[h]	0.21 ± 0.06	0.17 ± 0.01
Mg (%)	1.5 ± 0.2	-	1.8 ± 0.4,[f] 1.78 ± 0.20,[g] 2.4[h]	-	0.455 ± 0.010
Al (%)	12.6 ± 0.2	-	12.7 ± 0.5,[f] 12.35 ± 0.25,[g] 12.3[h]	14.0 ± 0.2	(14)
Si (%)	21.8 ± 0.3	-	21 ± 2,[f] 17.7,[h] 17[e]	22.2 ± 0.4	22.8 ± 0.8
P (%)	-	-	0.3,[h] 0.088[e]	~0.2	-
S (%)	0.39 ± 0.04	-	0.44 ± 0.07[i]	0.27 ± 0.02	-
K (%)	1.76 ± 0.05	(1.72)	1.61 ± 0.15,[f] 1.80 ± 0.13,[g] 1.69,[h] 1.75[e]	1.97 ± 0.04	1.88 ± 0.06
Ca (%)	4.75 ± 0.08	-	4.7 ± 0.6,[f] 4.69 ± 0.14,[g] 3.8[h]	1.29 ± 0.11	1.11 ± 0.01
Ti (%)	0.72 ± 0.02	-	0.74 ± 0.03,[f] 0.70 ± 0.03,[g] 0.696[h]	0.84 ± 0.01	(0.8)
V	190 ± 50	214 ± 8	235 ± 13,[f] 237 ± 20[g]	360 ± 40	(300)
Mn	480 ± 25	493 ± 7	496 ± 19,[f] 488 ± 14[g]	190 ± 15	(190)
Fe (%)	6.1 ± 0.1	-	6.2 ± 0.3,[f] 6.7[h]	9.7 ± 0.2	9.40 ± 0.10
Cd	1.50 ± 0.07	1.45 ± 0.06	1.6 ± 0.2[d]	1.07 ± 0.05	1.0 ± 0.15
Nd	62.1 ± 2.4	-	57.8 ± 1.6,[g] 81[j]	65.6 ± 5.4	-
Sm	12.1 ± 0.4	-	12.4 ± 0.9,[f] 11.4 ± 1.6[g]	16.0 ± 0.2	-
Gd	11.4 ± 0.2	-	-	15.3 ± 0.2	-

[a] Based on five separate irradiations. [b] NBS Office of Standard Reference Materials Certificate of Analysis. Values in parentheses are information values, not certified. [c] Ref. 31. [d] Ref. 9. [e] Ref. 27. [f] Ref. 4. [g] Ref. 29. [h] Ref. 11. [i] Ref. 10. [j] Ref. 30.

Table V. Concentrations of Elements in Standard Orchard Leaves and Bovine Liver (μg/g unless % indicated)

element	SRM 1571 Orchard Leaves this work[a]	SRM 1571 NBS[b]	SRM 1571 other values	SRM 1577 Bovine Liver this work[a]	SRM 1577 NBS[b]	SRM 1577 other values
H (%)	5.54 ± 0.08	-	6.1 ± 0.1[c]	6.8 ± 0.3	-	7.0 ± 0.1[c]
B	33.2 ± 0.1	33 ± 3	33 ± 2,[d] 23.7-38[e]	3.2 ± 0.2	-	-
C (%)	46 ± 2	-	47 ± 5,[c] 45.8 ± 1.3[f]	52 ± 2	-	51 ± 2,[c] 49.6 ± 1.5[f]
N (%)	2.70 ± 0.09	2.76 ± 0.05	2.5-2.86,[e] 2.7 ± 0.4,[c] 2.76[f]	10.35 ± 0.30	10.6 ± 0.6	10.4 ± 0.8,[c] 10.6[f]
Na	-	82 ± 6	71-90[e]	3100 ± 600	2430 ± 130	2000-2670[e]
Mg (%)	0.63 ± 0.07	0.62 ± 0.02	0.40-0.71[e]	-	-	0.060-0.061[e]
S (%)	0.17 ± 0.02	(0.19)	0.23 ± 0.02[g]	0.72 ± 0.02	-	0.72 ± 0.04[d]
Cl	730 ± 30	(700)	790[e]	3000 ± 100	(2600)	2542 ± 300[h]
K (%)	1.49 ± 0.04	1.47 ± 0.03	1.11-1.62[e]	1.00 ± 0.03	0.97 ± 0.06	0.756-0.99[e]
Ca (%)	2.13 ± 0.11	2.09 ± 0.03	2.052-2.125[e]	-	-	0.0117-0.0125[e]
Mn	98 ± 20	91 ± 4	52-144[e]	13 ± 6	10.3 ± 1.0	9.1-28[e]
Cd	-	0.11 ± 0.02	<0.1-0.45[e]	0.27 ± 0.06	0.27 ± 0.04	<0.1-0.35[e]
Sm	0.11 ± 0.03	-	-	-	-	-

[a] Based on five separate irradiations. [b] NBS Office of Standard Reference Materials Certificate of Analysis. Values in parentheses are information values, not certified. [c] Ref. 12. [d] Ref. 9. [e] Ranges covered by literature values from many groups as compiled by Becker et al. (32). [f] Ref. 27. [g] Ref. 10. [h] Ref. 33.

flux and geometry of the facility is independent of the sample. The minimum detection limit, C(mdl), is given by:

$$C(\text{mdl}) = 3.29\ (R_b/t)^{1/2}/S$$

where R_b is the background counting rate (counts/s) under the peak area and t is the duration of the count (s). We have calculated the C(mdl) values for two samples, SRM 1632a Coal and SRM 1577 Bovine Liver, based on the assumption of a 20-h irradiation of 1 g of sample. Values are similar for the two samples, but there are some differences because of different background rates in the spectra. In general, we can measure elements whose concentrations exceed the limits of Table VI. However, in a few cases, we could not measure elements present at levels above the calculated detection limit, e.g., Na and Mg in Coals SRM 1632 and 1632a, because of inter-element line interferences not included in the equation for C(mdl).

It is not necessary to observe lines of an element in the spectrum in order to calculate a C(mdl) in that material. It is necessary only to obtain sensitivities for various lines of the element from a standard and the background rates in the appropriate regions of the sample spectrum. Thus, we have listed limits of detectability for several elements that are not measurable in these samples, but which could be measured in comparable samples having higher levels of the elements in question (e.g., atmospheric particulate material). We have observed most of the elements of Table VI in one or more other types of samples not discussed here (e.g., Cu ores, rocks, atmospheric particles).

As shown in Table VI, low energy lines for many elements give the highest sensitivities, but the limit of detectability is often lower for a higher energy line (e.g., N, Si) because of the generally lower backgrounds at higher energies. Thus, to achieve optimum limits of detectability, one should have a counting system that can handle both low and high energy γ rays. If possible, we use three or more γ rays, preferably in different energy regions for determination of an element. Unfortunately, some elements (e.g., Cd) have no intense γ rays at high energy, so we must use low energy lines.

From the above equation, we see that C(mdl) varies as $1/t^{1/2}$. In checking the capabilities of PGAA, we have used very long counting times for complex samples and the C(mdl)s in Table VI are based on 20-h irradiations. To handle large numbers of samples routinely, we will use shorter counting times, so there will be an increase of the C(mdl) values, eliminating the possibility of measuring some marginally

Table VI. Sensitivity and Limits of Detectability of PGAA for Various Elements in Coal and Bovine Liver

element	E_γ, keV	sensitivity, counts/mg/s	minimum detection limit, mg/g[a] Coal (SRM 1632a)	Bovine Liver (SRM 1577)
H	2223	0.86	0.012	0.033
B	477	530	4.9×10^{-5}	6.7×10^{-5}
C	1261	4.0×10^{-4}	27	37
	4945	2.4×10^{-4}	16	24
N	1885	0.0030	3.4	6.5
	5269	0.0017	2.0	3.5
	10829	2.5×10^{-4}	0.92	1.9
Na	472	0.15	0.28	0.13
	1368D	0.036	0.27	0.27
F	1633	0.0016	6.1	7.9
Mg	585	0.0085	1.2	1.9
Al	1779D	0.024	0.45	0.53
	7724	0.0013	0.86	1.4
Si	1273	0.0036	2.4	3.2
	3539	0.0066	0.61	0.83
	4934	0.0042	1.1	1.9
P	637	0.0062	1.3	2.6
S	841	0.054	0.18	0.28
	2380	0.015	0.28	0.33
	3221	0.0067	0.59	0.64
	5421	0.0090	0.34	0.44
Cl	516	1.5	0.0072	0.012
	785 + 788	1.2	0.0093	0.015
	1164	1.0	0.0096	0.016
K	770	0.13	0.069	0.12
Ca	1942	0.022	0.49	0.98
Ti	342	0.38	0.037	0.041
	1382	0.39	0.027	0.027
V	1433D	0.33	0.025	0.035
Mn	212	0.53	0.049	0.053
	847D	1.05	0.0086	0.010
Fe	352	0.046	0.34	0.35
	7120 + 7135	0.015	0.41	0.59
	7631 + 7645	0.013	0.16	0.18
Cu	278	0.12	0.17	0.18
Zn	1077	0.019	0.44	0.58
As	165 (+ 163)	0.17	0.23	0.24
Se	239	0.31	0.083	0.084
Br	244	0.18	0.12	0.19
	315	0.036	0.44	0.59
Mo	778	0.11	0.088	0.094
Cd	558	174	6.1×10^{-5}	9.3×10^{-5}
In	162	2.9	0.014	0.014
	186	2.6	0.013	0.014
	273	2.7	0.0081	0.0079
Nd	697	1.3	0.0074	0.0082
Sm	334	639	2.7×10^{-5}	3.1×10^{-5}
Gd	182	688	4.7×10^{-5}	5.3×10^{-5}
	1185	108	8.6×10^{-5}	1.5×10^{-4}
Pb	7368	3.9×10^{-4}	5.1	5.6

[a] Calculated for 20-h count.

observable species. However, we can increase the geometry of the counting system about 10-fold for "singles" counting, which was used for these experiments. The Ge(Li) detector is located inside of the large NaI(Tl) Compton-suppression shield. As a consequence, the Ge(Li) detector is about four times as far from the samples as it would need to be if used alone and the γ-ray beam is strongly collimated, so we don't take advantage of the full size of the detector. By moving the detector closer and relaxing the collimation, an approximately 10-fold increase in count rates should be possible.

SUMMARY AND CONCLUSIONS

The PGAA method can be used to analyze for an interesting mixture of elements. Unlike INAA, the new method observes many matrix elements, e.g., most elements traditionally measured in rocks by geochemists and, for organic matrices, the major elements C, H, N, and S. On the other hand, PGAA is also quite sensitive for four trace elements with large capture cross sections: B, Cd, Sm, and Gd.

At present, PGAA can measure concentrations of about 15 elements in many types of samples. This is fewer than the 30 or so that can usually be measured by INAA. However, one should view PGAA as a complement to INAA, as any laboratory equipped to do PGAA has the reactor and detection system needed for INAA. Since PGAA leaves almost negligible residual activity in the samples, the same samples can be re-irradiated in the reactor for INAA measurements. The combination of methods allows one to measure about 45 elements in "crustal" samples such as rocks, soil, coal, fly ash, and probably 30 elements in biological samples. The former is illustrated in Figure 9, which shows the elements usually measurable in coals by the two methods.

The PGAA method has several advantages relative to off-line methods such as INAA and IPAA. First, if samples are placed outside of the reactor, samples are subjected to no heating and to such a small neutron flux that there is virtually

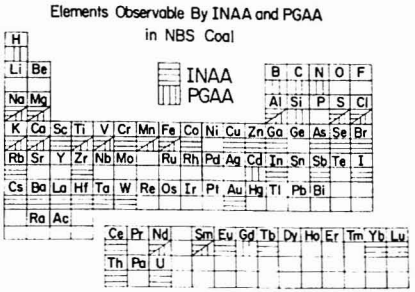

Figure 9. Periodic chart showing elements measurable by PGAA and INAA in coal

no radiation damage or residual activity left in the samples. Thus, one can analyze samples that are too fragile, dangerous, or irreplaceable to be subjected to intense fluxes of neutrons or photons. Second, the turn-around time is much shorter for PGAA, as the data are ready for analysis at the end of the irradiation, whereas one must wait two weeks or so before observing long-lived products in INAA and IPAA. Third, the reproducibility and accuracy of PGAA determinations of many elements seem to be better than for the off-line methods, in part because of the several peaks that can be used for determination of most elements. Also, PGAA eliminates errors of timing encountered in INAA for few-minute activities (e.g., corrections for decay during counts, change of dead-time fraction during count). On the other hand, the absence of decay for most elements in PGAA means that one cannot take advantage of decay to identify species, observe contaminants, or avoid interferences. Another advantage of PGAA is that the prompt γ rays are emitted before the product has any chance to migrate out of the sample. This avoids any possibility of losses of volatile species as a result of Szilard–Chalmers processes following prompt γ-ray emission that sometimes cause losses of elements such as Hg or Br prior to off-line counting.

Although PGAA is quite useful as presently developed, many improvements are possible. Additional elements may become measurable, or detection limits lower for presently observable elements, when backgrounds (Comptons, single- and double-escape peaks) are reduced by the use of the NaI shield detector. Further improvements may be made by removing γ-ray and fast-neutron components of the beam, such as by placing a single crystal of Bi in the beam (*37*) or by bending the thermal neutron beam away from the other components with a neutron beam guide (*7*).

ACKNOWLEDGMENT

We thank Robert Carter, Jack Sturrock, James Torrence, and the operations staff of the NBS reactor for their considerable help on the design, construction, and installation of the beam tube. We are grateful to William Walters for his help in design of the counting system and to Paul Solomon for his help in early phases of the technique development. We thank Dick Duffey for his continued interest and helpful suggestions about the project.

LITERATURE CITED

(1) Zoller, W. H.; Gordon, G. E. *Anal. Chem.* **1970**, *42*, 257–265.
(2) Aras, N. K.; Zoller, W. H.; Gordon, G. E.; Lutz, G. J. *Anal. Chem.* **1973**, *45*, 1481–1490.
(3) Olmez, I.; Aras, N. K.; Gordon, G. E.; Zoller, W. H. *Anal. Chem.* **1974**, *46*, 935–937.
(4) Ondov, J. M.; Zoller, W. H.; Olmez, I.; Aras, N. K.; Gordon, G. E.; Rancitelli, L. A.; Abel, K. H.; Filby, R. H.; Shah, K. R.; Ragaini, R. C. *Anal. Chem.* **1975**, *47*, 1102–1109.
(5) Lombard, S. M.; Isenhour, T. L.; Heintz, P. H.; Woodruff, G. L.; Wilson, W. E. *Int. J. Radiat. Isot.* **1968**, *19*, 15–22.
(6) Lombard, S. M.; Isenhour, T. L. *Anal. Chem.* **1968**, *40*, 1990–1994.
(7) Comar, D.; Crouzel, C.; Chasteland, M.; Riviere, R.; Kellershohn, C. In "Modern Trends in Activation Analysis", DeVoe, J. R., Ed.; *Natl. Bur. Stand. (U.S.), Spec. Publ. No. 312*, **1969**; Vol. 1, pp 114–127.
(8) Henkelmann, R.; Born, H. J. *J. Radioanal. Chem.* **1973**, *16*, 473–481.
(9) Gladney, E. S.; Jurney, E. T.; Curtis, D. B. *Anal. Chem.* **1976**, *48*, 2139–2142.
(10) Jurney, E. T.; Curtis, D. B.; Gladney, E. S. *Anal. Chem.* **1977**, *49*, 1741–1743.
(11) Gladney, E. S.; Curtis, D. B.; Jurney, E. T. *J. Radioanal. Chem.* **1978**, *96*, 299–308.
(12) Gladney, E. S.; Curtis, D. B.; Jurney, E. T. *Anal. Chim. Acta*, in press.
(13) Rasmussen, N. C.; Hukai, Y.; Inouye, T.; Orphan, V. J. "Thermal Neutron Capture Gamma-Ray Spectra of the Elements", Scientific Report No. 2, Contract No. AF19(682)5551, Mass. Inst. of Technology, Jan. 1969.
(14) Duffey, D.; El-Kady, A.; Senftle, F. E. *Nucl. Instrum. Methods* **1970**, *80*, 149–171.
(15) Bartholomew, G. A.; Doveika, A.; Eastwood, K. M.; Monaro, S.; Groshev, L. V.; Demidov, A. M.; Pelekov, V. I.; Sokolovskii, L. L. *Nucl. Data* **1967**, *A3*, 367.
(16) Gordon, G. E.; Anderson, D. L.; Failey, M. P.; Zoller, W. H.; Lindstrom, R. M. "Prompt Gamma-Ray Neutron Activation Analysis", in *Proc. of the 3rd Int. Conf. on Nucl. Methods in Environmental and Energy Research*, Vogt, J. R., Ed.; University of Missouri, Columbia, Mo.; 1978 TID Document CONF 771072, pp 83–89.
(17) Failey, M. P.; Anderson, D. L.; Zoller, W. H.; Walters, W. B.; Lindstrom, R. M. submitted to *Nucl. Instrum. Methods*.
(18) Greenwood, R. C.; Chrien, R. E. In "Neutron Capture Gamma-Ray Spectroscopy", Chrien, R. E., Kane, W. R., Eds.; Plenum: New York, 1979; pp 621–623.
(19) Lederer, C. M.; Shirley, V. S.; Browne, E.; Dairki, J. M.; Doebler, R. E. "Table of Isotopes", 7th ed.; Wiley-Interscience: New York, 1978.
(20) Greenwood, R. C.; Chrien, R. E. In "Neutron Capture Gamma-Ray Spectroscopy", Chrien, R. E., Kane, W. R., Eds.; Plenum: New York, 1979; pp 618–620.
(21) Lauritson, T.; Ajzenberg-Selove, F. *Nucl. Phys.* **1966**, *78*, 1.
(22) Thomas, G. E.; Batchley, D. E.; Bollinger, L. M. *Nucl. Instrum. Methods* **1967**, *56*, 325.
(23) Endt, P. M.; VanderLeun, C. *Nucl. Phys.* **1978**, *A310*, 1.
(24) Stelts, M. L.; Chrien, R. E. *Nucl. Instrum. Methods* **1978**, *155*, 253.
(25) Greenwood, R. C.; Reich, C. W.; Baader, H. A.; Roch, H. R.; Breitig, D.; Schult, O. W. B.; Fogelberg, B.; Backlin, A.; Mampe, M.; Von Egidy T.; Schreckenbach, K. *Nucl. Phys.* **1978**, *A304*, 327.
(26) Germani, M.; Gokmen, I.; Sigleo, A. C.; Kowalczyk, G. S.; Olmez, I.; Small, A.; Anderson, D. A.; Failey, M. P.; Gulovali, M. C.; Choquette, C. C.; Lepel, E. A.; Gordon, G. E.; Zoller, W. H., submitted to *Anal. Chem.*
(27) Waterbury, G. R. Group CMB-1, Los Alamos Scientific Laboratory, cited as private communication in Refs. (*10*–*12*).
(28) Gluskoter, H. J.; Ruch, R. R.; Miller, W. G.; Cahill, R. A.; Dreher, G. B.; Kuhn, J. K. "Trace Elements in Coal: Occurrence and Distributions", Ill. State Geological Survey Circular 499, 1977.
(29) Steinnes, E.; Rowe, J. J. *Anal. Chim. Acta* **1976**, *87*, 451–462.
(30) Millard, H. T.; Swanson, V. E. *Trans. Am. Nucl. Soc.* **1975**, *21*, 108.
(31) Carpenter, B. S. National Bureau of Standards, private communication, 1979.
(32) Becker, D. A.; Rook, H. L.; LaFleur, P. D. "High Purity Materials, Standards and Reference Materials", Chap. 5; Sect. IV of "Instrumental Neutron Activation Analysis", Amiel, S., Ed., to be published, 1979.
(33) Zikovsky, L.; Schweikert, E. A. *J. Radioanal. Chem.* **1977**, *37*, 571.
(34) Curtis, D. B.; Gladney, E. S.; Jurney, E. T. *Anal. Chem.* **1979**, *51*, 158.
(35) Jaklevic, J. M.; Walter, R. L. In "X-Ray Fluorescence Analysis of Environmental Samples", Dzubay, T. G., Ed.; Ann Arbor Science: Ann Arbor, Mich., 1977; Chapter 5.
(36) Currie, L. A. In "X-Ray Fluorescence Analysis of Environmental Samples", Dzubay, T. G., Ed.; Ann Arbor Science: Ann Arbor, Mich., 1977; Chapter 25.
(37) Rustad, B. M.; Als-Nielsen, J.; Bahnsen, A.; Christensen, C. J.; Nielsen, A. *Rev. Sci. Instrum.* **1965**, *36*, 48.

RECEIVED for review June 21, 1979. Accepted August 9, 1979. This work was supported in part by the U.S. Department of Energy under Contract No. EY-76-S-05-5173. Certain commercial equipment, instruments, or materials are identified in this paper in order to adequately specify the experimental procedure. In no case does such identification imply recommendation or endorsement by the National Bureau of Standards, nor does it imply that the material or equipment identified is necessarily the best available for the purpose.

Frequency Modulated Correlation Chromatography

Dan C. Villalanti and M. F. Burke*

Analytical Division, Department of Chemistry, University of Arizona, Tucson, Arizona 85721

J. B. Phillips

Department of Chemistry and Biochemistry, Southern Illinois University, Carbondale, Illinois 62901

Cross correlation chromatography experiments up till now have assumed a linear system. However, the use of multiple injections needed for these types of experiments often drives the system into nonlinearity. By frequency modulating a signal, the change in the amount of solute on the column at any time can be restricted to a small range. Thus each injection experiences a nearly identical environment. This enables one to work in nonlinear areas of an isotherm and still take advantage of signal processing techniques, such as correlation and deconvolution.

In a benchmark article by Reilley et al. (*1*), the response of a chromatographic column to any sample input profile was discussed. The use of input profiles other than the usual step and spike functions, and their output responses were predicted for analytical work and for studying fundamental properties of chromatographic systems. To date, multiple injection profiles appear the most promising.

Correlation chromatography has been proposed as a method for continuous monitoring of process streams (*2*) and as a means of increasing signal-to-noise ratios for lower detection limits (*3–5*). Annino (*6*) proposed the use of a pseudo-random binary sequence (PRBS) as the input function for correlation chromatography. This function was chosen because it was simple to generate, its code length was easily varied, and most importantly, it contributed no correlation noise when one entire code length sequence was used. A deconvolution approach to eliminating correlation noise by Phillips and Burke (*7*) allowed other input regimes to be used since correlation noise was removed in data reduction.

However, in each of these cases an inherent problem, first pointed out by Annino (*2*) exists. Since correlation assumes a linear system, extreme base-line irregularities are created when the sample concentration is high enough to reach into the nonlinear regions of the isotherm. For that reason, successful correlation experiments required dilute streams to keep the partition coefficient constant, or working in a comparison mode in which the two streams are of similar concentration. The latter solution seems impractical since concentration is the parameter that we propose to measure.

Frequency modulated correlation chromatography is a novel multiple injection technique which involves modulating an input signal a small amount around some fixed carrier frequency. This method is similar to standard FM radio broadcasting. A frequency modulated signal resulting from the convolution of the input signal with the impulse response function (transfer function) of the chromatographic system is then recorded at the detector output. The input signal is then deconvolved from the output signal to compute the impulse response of the chromatographic system. This impulse response is equivalent to a normal chromatogram. Alternatively, the input and output signals may be demodulated and cross-correlated to give the same chromatogram.

The main advantage of the frequency modulated approach is that the amount of solute on the column at any time is almost constant, this being set by the carrier frequency. The input signal is impressed on the system by making small changes around the carrier frequency. By maintaining the solute concentration at an almost constant value, partition coefficients also remain constant even when working in a nonlinear region of an isotherm (see Figure 1).

THEORY

A frequency modulated signal can be input to a chromatographic column by slightly modifying a constant frequency multiple injection signal. Before each injection, a random number is generated to determine the magnitude and sign of the deviation from the carrier frequency for the next injection time. The next injection may come a little earlier or later than the time dictated by the carrier frequency.

The amount of deviation allowed from the carrier frequency (i.e., degree of modulation) is a theoretically important parameter. As it is increased, the bandwidth and information carrying capacity of the signal also increase. However, as the degree of modulation is decreased, the deviations from linearity inherent in a chromatographic system become less important because each cycle of the carrier experiences a more similar environment. A very large degree of modulation causes correlation noise in the computed chromatogram while a small modulation reduces the information content of the signal to the point where all but the carrier frequency is lost in the noise. Thus, there is some optimum degree of modulation which gives the best S/N ratio for a particular chromatographic system. The previously employed pseudo-random input signals have high degrees of modulation and therefore suffered from correlation noise unless sample sizes were small to minimize nonlinearity.

The carrier frequency should be high enough to cause severe peak overlap. A low frequency carrier offers no advantages and can slow the experiment by limiting the frequency of the modulating pseudo-random signal. A high frequency carrier is desirable because it gives a more uniform sample distribution minimizing nonlinearity. Beyond some frequencies, however, the remaining nonlinearity is caused by the degree of modulation and changing the carrier will have no effect.

The impulse response or transfer function (H) can be derived directly from a deconvolution procedure or can be approximated by computing the cross-correlation. The correlation method is described first with the deconvolution procedure following.

The output signal is demodulated by subtracting it from itself with a delay of one cycle of the carrier signal

$$Y'(T) = Y(T + \tfrac{1}{2}F) - Y(T - \tfrac{1}{2}F) \qquad (1)$$

where $Y(T + {}^1/_2 F)$ is the output signal at a time T plus one half a carrier cycle and $Y(T - {}^1/_2 F)$ is the output signal one cycle earlier.

Similarly, the input signal, X, is demodulated by:

$$X'(T) = X(T + \tfrac{1}{2}F) - X(T - \tfrac{1}{2}F) \qquad (2)$$

where $X'(T)$ is the demodulated input signal and $X(T + {}^1/_2 F)$ and $X(T - {}^1/_2 F)$ are the input signals separated by one carrier cycle.

The top portion of Figure 2 shows a frequency modulated FID signal followed by pure carrier frequency. This carrier

0003-2700/79/0351-2222$01.00/0

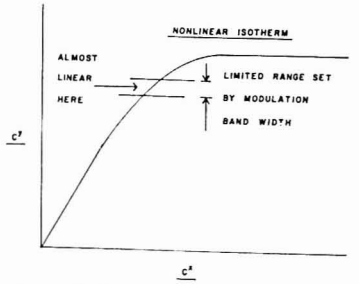

Figure 1. An example of a nonlinear distribution isotherm approximating a linear system by restricting the change in concentration by frequency modulation

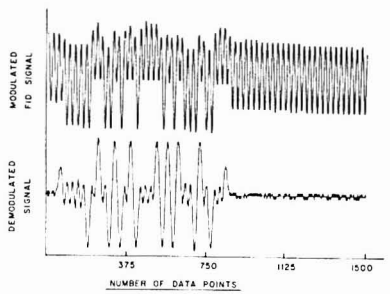

Figure 2. Detector output and demodulated signal of hexane on Durapak-*N*-octane at 60 °C. PRBS code length = 31. Data acquisition rate = 10 Hz. Carrier frequency = 0.400 Hz. Flow rate = 40 cm^3/min. Column head pressure 18 psi. Modulation bandwidth = 0.416–0.384 Hz. or ±4.0%

wave is the result of overlapped peaks. The demodulated signal, calculated from Equation 1, appears on the lower portion from about 75–850 and the demodulated carrier is essentially reduced to zero from 850–1500 on the abscissa.

The demodulated input and output signals are then cross-correlated in the usual way to approximated the transfer function or impulse response of the system

$$\phi_{xy}(\tau) = 1/T \sum_{T=1}^{n} X(T)^* Y(T-\tau) \qquad (3)$$

where τ is the delay time and T is a data point. Figure 3 summarizes the important steps in a frequency modulated correlation type experiment.

The transfer function H can also be solved by the Fourier transform deconvolution method (*8–10*). This not only saves computation time but also simplifies boundary problems encountered when using Equation 3.

$$\begin{array}{ccccc} Y(T) & = & X(T) & \circledast & H(T) \\ \downarrow & & \downarrow & & \downarrow \\ \text{FT} & & \text{FT} & & \text{FT} \\ \downarrow & & \downarrow & & \downarrow \\ Y(F) & = & X(F) & * & H(F) \end{array} \qquad (4)$$

$$(5)$$

Solving for $H(F)$:

$$\begin{array}{ccccc} H(F) & = & Y(F) & / & X(F) \\ \uparrow & & \uparrow & & \uparrow \\ \text{IFT} & & \text{IFT} & & \text{IFT} \\ \downarrow & & \downarrow & & \downarrow \\ H(T) & = & Y(T) & \circledast^{-1} & X(T) \end{array} \qquad (6)$$

$$(7)$$

or overall:

$$H(T) = \text{IFT}(FT[Y(T)]/FT[X(T)]) \qquad (8)$$

where: X = input, Y = output, H = transfer function, $\circledast$ = correlation, $\circledast^{-1}$ = inverse correlation, T = time domain, F = frequency domain, FT = Fourier Transform, and IFT = Inverse Fourier Transform.

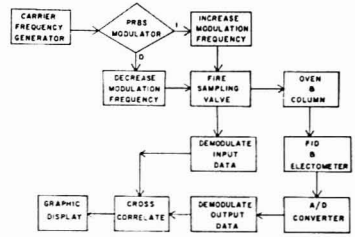

Figure 3. Flowchart diagram summarizing the basic steps of a frequency modulated (FM) correlation type experiment

Thus the entire demodulation and cross-correlation procedure is reduced to a mere division operation in the frequency domain. With a sufficiently high carrier frequency and a limited modulation bandwidth, the input signal can be limited to a small region of the isotherm of a nonlinear system which will then behave as if it were linear.

EXPERIMENTAL

A Varian model 1700 gas chromatograph with a FID detector and a Linear model 261 recorder were used throughout these experiments. The column was a 30 cm by $^1/_8$ in. copper tube, packed with 80/100 mesh Porapak P. The carrier gas was filtered dry nitrogen. The solutes were hexane and acetone. Sampling was done via a sample loop type, Seiscor model VIII sampling valve with variable resistance (Nupro model SG fine metering valve) to match sample loop and column head pressures. Total switching time was specified to be 10 ms by the manufacturer. The sample loop was shortened from 24 to 2.4 in. to reduce the sample volume approximately 50 μL. This maximized the frequency response of the valve by shortening the sweep and refill times of the sample loop. These times, at a carrier flow of 30 cm^3/min, are approximately 100 ms. Although other sampling methods have been proposed (*11*), the Seiscor valve provided the speed, accuracy, and reliability needed for these experiments.

Data acquisition and experimental control were under the reign of a dedicated Hewlett-Packard 2115A computer, with an integrating digital voltmeter (HP 2401C), and a digital voltage source (HP 6131B). Programming for the experimental side of the computer network was written in Fortran and HP assembly language. User selected experimental parameters included: data acquisition rate, pseudo-random binary sequency (PRBS), code length, carrier frequency, and modulation bandwidth.

Briefly, the experiment begins by the user inputting the desired operating parameters to the computer. When finished, the computer then starts generating injections at the carrier frequency. This brings the concentration up to a stable level and maintains it there. After a specified time period, the program jumps to the PRBS subroutine which returns with a 0 or a 1. With this number the computer will begin frequency modulating the input signal to the chromatograph. This was accomplished by sending out a pulse via the digital voltage source to an EXACT model 128 function generator with a variable pulse width, which then fired a Clippard Minimatic model EOV-3 nitrogen powered solenoid connected to the Seiscor sampling valve. Table I shows this procedure for a PRBS code length of 7, carrier frequency of 0.400 Hz, and 25% modulation. Figure 4 is a graphical representation of this procedure.

Every 64 data points, input and output data were sent to a larger disk-operating system over a high-speed communications network. When the entire PRBS code was cycled, the carrier frequency reappears for a short time and the experiment is terminated (see Figure 5).

RESULTS AND DISCUSSION

The first correlation chromatograms using the frequency modulated scheme were essentially pure noise. The reasons

Table I. Generation of an FM Signal for Multiple Injection Chromatography Using a Pseudo-Random Binary Sequence

N	output from PRBS	deviation	ΔT between injections, s	current frequency, Hz
N-1	–	0	2.500	0.400
N	–	0	2.500	0.400
N+1	1	+	3.125	0.320
N+2	1	+	3.125	0.320
N+3	1	+	3.125	0.320
N+4	0	–	1.875	0.533
N+5	1	+	3.125	0.320
N+6	0	–	1.875	0.533
N+7	0	–	1.875	0.533
end of cycle	–	0	2.500	0.400
	–	0	2.500	0.400

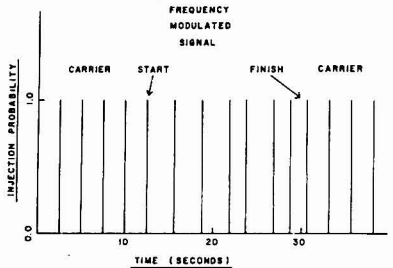

Figure 4. Input profile of a simple frequency modulated experiment. PRBS code length = 7. Carrier frequency = 0.400 Hz. Modulation bandwidth = 0.320–0.533 Hz or ±25.0%

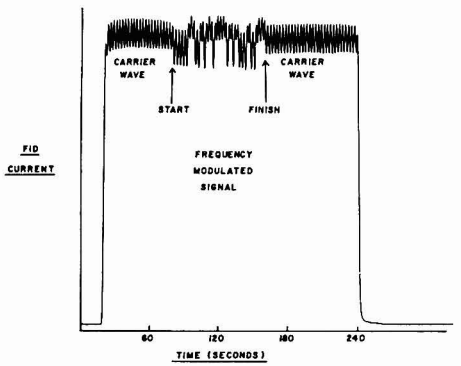

Figure 5. Entire detector output for an FM experiment (carrier > FM > carrier). Same conditions as Figure 2

for this were numerous and a systematic evaluation of the signal processing at every step of the experiment was undertaken.

Initial experiments used a PRBS code length of 31 and a 0.400-Hz carrier frequency. With a data acquisition rate of 10 Hz, the total number of data points in one cycle of the PRBS was 31/0.400 Hz times 10 Hz or 775 data points. Because of memory limitations on the computer, we were forced to use an even power of two in the Fourier routines. However, by using 2^9 or 1024 points, about one and one-third PRBS code lengths were covered. These results are seen in

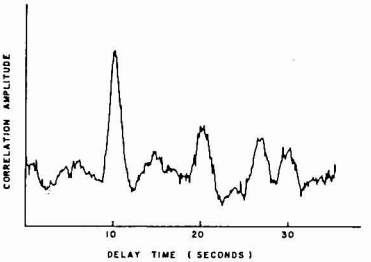

Figure 6. Example of correlation noise due to PRBS cycle length. Column was a 50-cm long, 2-mm i.d. copper tubing packed with 100/120 mesh Porapak P. Solute = acetone at 120 °C. $k' = 2.5$. Other parameters were the same as in Figure 2, except for ±20% modulation

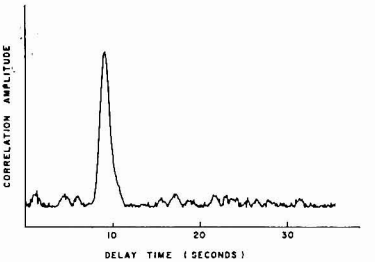

Figure 7. Same correlation chromatogram as in Figure 6, except that carrier frequency was reduced to 0.303 Hz. Correlation noise is greatly reduced because one complete PRBS code is used

Figure 6. Although the major correlation peak at 10.5-s delay corresponds to the correct retention time, spurious peaks and a jagged base line result because of the code length not matching the Fourier matrix dimensions. Although the PRBS code was not used to inject samples directly, it was used to modulate the carrier frequency and therefore complete cycles must be used to avoid correlation noise. By slightly reducing the carrier frequency to 0.303 Hz or 33 points per PRBS call, 31/0.303 Hz times 10 Hz of 1023 data points were collected. This was very close to the 1024 points which the fast Fourier transform routine must use. Figure 7 shows a well defined base line with a much better signal-to-noise ratio than Figure 6. These improvements are the result of using one entire PRBS code length sequence. Another solution to this problem would be to zero fill the Fourier matrix (*12*) in the above case from data point 776 to 1024, although this solution is wasteful of computer time and memory.

The second source of noise in these first experiments with FM chromatography involved the input scheme mentioned earlier. That was applying a carrier frequency, then modulating a cycle, and then returning to the carrier, (i.e., carrier > FM > carrier). This scheme wasted some of the data points in the beginning, until the breakthrough time of the first injection, and at the end; that is, all data after the last injection were lost. These boundary problems are not peculiar to FM type experiments, but also exist for other correlation experiments.

The solution to this problem was to run through two cycles of the PRBS, i.e., (FM > FM), and then grab only the output during the last cycle. The time that was wasted until the breakthrough was now filled with the data that were missed after the last injection. Thus the entire output for one complete cycle of the PRBS was collected.

One other pitfall that was encountered occasionally involved the use of Equation 6, the division of the output by the input in the frequency domain. This was done sequentially starting at dc and moving to the higher frequencies. The problem occurred when the input contained only very small amounts of those higher frequencies. The division then caused an overflow in the program. This was corrected by dividing only the lower frequencies, with no sacrifice in accuracy because all of the chromatographic information was concentrated in this area of the frequency domain. Once the above problems had been solved, frequency modulated experiments could be run in a routine manner.

The concept of information encoding and subsequent decoding, which allows frequency modulated experiments is summarized in Equation 8. It is impressive in its simplicity and conciseness. From this equation any input to a chromatograph can be used to solve for the transfer function of the column, i.e., the spike elution response. Frequency modulation has been shown to expand the scope of potential applications of multiple injection chromatographic experiments by allowing finite concentration systems. Other encoding techniques such as pulse and phase modulation (*13*) appear to have similar advantages. Work in these areas is currently being investigated.

ACKNOWLEDGMENT

The authors thank B. Keller of the Seiscor Division of the Seismograph Service Corporation for the use of the sampling valve, and also thank L. Schooley, M. Trandal, and D. McCaughey of the Electrical and Systems Engineering Departments at the University of Arizona and G. Horlick of the University of Alberta for their consultation in signal processing.

LITERATURE CITED

(1) C. N. Reilley, G. P. Hildebrand, and J. W. Ashley, Jr., *Anal. Chem.*, **34**, 1198 (1962).
(2) R. Annino, and L. E. Bullock, *Anal. Chem.*, **45**, 122 (1973).
(3) G. C. Moss, J. P. Kippling, and K. R. Godfrey, "Application of Statistical Correlation Techniques and Pseudo Binary Sequences to Trace Chromatographic Analysis", in "Gas Chromatography 1972", S. G. Perry and E. R. Adlard, Eds., Applied Science Publishers, London, 1973.
(4) H. C. Smit, *Chromatographia*, **3**, 515 (1970).
(5) H. Clough, T. C. Gibb, and A. Littlewood, *Chromatographia*, **5**, 351 (1972).
(6) R. Annino and E. Grushka, *J. Chromatogr. Sci.*, **14**, 205 (1976).
(7) J. B. Phillips and M. F. Burke, *J. Chromatogr. Sci.*, **14**, 495 (1976).
(8) R. N. Bracewell, "The Fourier Transform and Its Applications", 2nd ed., McGraw-Hill, New York, 1978.
(9) A. B. Carlson, "Communication Systems", 2nd ed., McGraw-Hill, New York, 1975.
(10) G. Horlick and G. M. Hieftje, "Correlation Methods in Chemical Data Measurements", in "Contemporary Topics in Analytical and Clinical Chemistry", Vol. 3, Plenum Press, New York, 1978, p 153.
(11) R. Annino, M. F. Gonnard, and G. Guiochon, *Anal. Chem.*, **51**, 379 (1979).
(12) P. R. Griffins, "Transform Techniques in Chemistry", Plenum Press, New York, 1978.
(13) D. Obst, *J. Chromatogr.*, **32**, 8 (1968).

RECEIVED for review May 18, 1979. Accepted August 20, 1979.

Inductively Coupled Plasma Emission Spectrometric Detection of Simulated High Performance Liquid Chromatographic Peaks

David M. Fraley, Dennis Yates,[1] and Stanley E. Manahan*

Department of Chemistry, University of Missouri, Columbia, Missouri 65211

Because of its multielement capability, element-specificity, and low detection limits, inductively coupled plasma optical emission spectrometry (ICP) is a very promising technique for the detection of specific elemental species separated by high performance liquid chromatography (HPLC). This paper evaluates ICP as a detector for HPLC peaks containing specific elements. Detection limits for a number of elements have been evaluated in terms of the minimum detectable concentration of the element at the chromatographic peak maximum. The elements studied were Al, As, B, Ba, Ca, Cd, Co, Cr, Cu, Fe, K, Li, Mg, Mn, Mo, Na, Ni, P, Pb, Sb, Se, Sr, Tl, V, and Zn. In addition, ICP was compared with atomic absorption spectrometry for the detection of HPLC peaks composed of EDTA and NTA chelates of copper. Furthermore, ICP was compared to UV solution absorption for the detection of copper chelates.

One of the major challenges remaining in the area of trace element analysis is the measurement of trace element-containing species (*1*). In addition, matrix effects and instrumental interferences still cause problems in the analysis of elements in some samples by techniques such as neutron activation analysis and furnace atomic absorption. Separation of sample species by high performance liquid chromatography (HPLC) and detection with an element-specific detector can enable analysis of species and help eliminate interferences in elemental analysis.

Conventional flame atomic absorption spectrometry (AAS) was one of the first element-specific techniques applied to HPLC (*2*, *3*) and was used to detect copper chelates separated by HPLC. Chromium organometallics separated by use of an organic mobile phase were subsequently detected by AAS (*4*). In these investigations the HPLC column outlet was interfaced directly to the AAS nebulizer inlet. Ion-exchange HPLC with AAS detection has been employed for the analysis of Cr(III) and Cr(VI) complexes (*5*), Mn(II) and Mn(VII) (*6*), and mixtures of Cu(gly), Cu(EDTA), and Cu(trien) species (*7*). Gel permeation chromatography has been employed for the analysis of condensed phosphate complexes of Mn(II) (*8*) and zinc compounds in plant extracts (*9*). Affinity HPLC has been employed for the analysis of alkyl and aryl zinc organometallics in lubricating oils (*10*), metals bound by amino acids (*11*), and alkyllead compounds in gasoline (*12*). A number of other applications are cited in a review article dealing with the subject (*13*).

Inductively coupled plasma optical emission spectrometry (ICP) is developing as an excellent tool for the analysis of a

[1] Spectroscopy Group Leader, University of Missouri Environmental Trace Substances Center.

0003-2700/79/0351-2225$01.00/0

Table I. Experimental Conditions for AAS and ICP Detectors Employed to Monitor Copper Chelate Peaks

parameter	AAS	ICP
instrument	Perkin-Elmer 403	Jarrell-Ash 975
source	Cu hollow cathode lamp	plasma
wavelength	3247 A	3247 A
spectral bandpass	7 A	1.7 A
flame	acetylene/air 4in. single-slot burner	argon plasma
sample introduction rate	2.0 mL/min	2.0 mL/min
incident power (rf signal)	- - -	1.2 kW
reflected power	- - -	<5 W
viewing height above coil	- - -	14 mm
sample gas flow	- - -	0.50 L/min
plasma gas flow	- - -	0.75 L/min
coolant gas flow	- - -	25 L/min
air flow rate	21 L/min	- - -
acetylene flow rate	6 L/min	- - -

number of elements, and is particularly attractive for its simultaneous multielement analysis capability (*14*). Because of this capability, element-specificity, and low detection limits, ICP is a very promising mode of detection for elemental species separated by HPLC using an aqueous mobile phase. Furthermore, the analyte atoms in the hot argon plasma tend to behave as an optically thin emitting source (*15*). This phenomenon fortunately provides a linear emission signal for each analyzable element over several orders of magnitude concentration, a virtually necessary characteristic for chromatographic detectors.

This investigation was conducted to determine the operating parameters of the ICP as a detection device for HPLC separation of elemental species. The major objectives of the study were (1) to determine the optimum hardware and operating parameters for the ICP–HPLC interface, (2) to evaluate the ICP as a detector for HPLC and to compare the ICP to AAS in that application, and (3) to evaluate the sensitivities and detection limits for the ICP as a detector for HPLC. Because of the importance of the last objective in this application, it was emphasized in this study.

EXPERIMENTAL

The HPLC system consisted of a Waters Model 6000A constant flow rate pump, a Valco constant volume injector equipped with a 10-μL sampling loop (Alltech), and associated columns. Most studies were conducted employing a "dummy" column that did not retain any analyte species and which yielded a uniform Gaussian peak for all species injected. Peak spreading in this column was due to diffusion and not retention of the species by the column material. The column packing consisted of 230–320 mesh glass spheres deactivated by silanization to eliminate nucleophilic hydroxyl surface groups. Silanization was effected by refluxing a 5% solution of dichloromethylsilane (Aldrich Chemical Co.) in toluene with dried glass beads for 4 h (*16*). The treated beads were packed into a 15 cm × 3.2 mm o.d. × 2.1 mm i.d. stainless steel column (Alltech and Assoc.). Separation of copper chelates was accomplished on a column of 10 cm × 3.2 mm o.d. × 2.1 mm i.d. dimensions packed with Aminex A-14 anion-exchange resin (Bio-Rad Laboratories).

The ICP instrument used in this study was a Jarrell-Ash 975 Atom-Comp direct-reading spectrophotometer equipped with a Plasma-therm HFD-2000D 27-MHz RF generator power supply capable of delivering 2.0 kW forward power. The spectrometer employed was a Rowland circle type, which had the capability to monitor 32 selected elements both separately and simultaneously. An integrated PDP/8 computer acted to store and implement operational parameters, as well as storing, processing, and reporting output data from the detector system. Data were displayed on a teletype, Decwriter II terminal (Digital Equipment Corp.) or Perkin-Elmer Model 56 strip-chart recorder. The

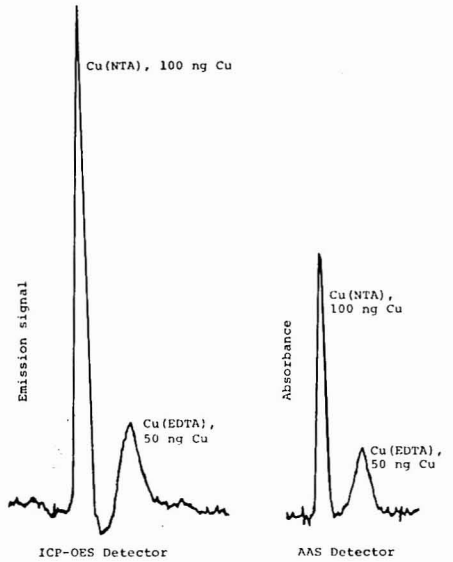

Figure 1. HPLC separation of copper chelated by NTA (100 ng Cu) and EDTA (50 ng Cu) injected as a 10-μL sample in a 0.05 M $(NH_4)_2SO_4$ aqueous mobile phase on an Aminex A-14 anion-exchange resin. For ICP detection of Cu(NTA), peak height/noise, 39; fwhm, 0.50 cm; peak area, 11.8 cm^2; detection limit, 5.1 ng. For ICP detection of Cu(EDTA), peak height/noise, 7.2; fwhm, 0.89 cm; peak area, 5.6 cm^2; detection limit, 15 ng. For AAS detection of Cu(NTA), peak height/noise, 27; fwhm, 0.45 cm; peak area, 5.4 cm^2; detection limit, 7.5 ng. For AAS detection of Cu(EDTA), peak height/noise, 6.8; fwhm, 0.84 cm; peak area 2.6 cm^2; detection limit 15 ng

instrument also had a single-channel capability through a 0.5-m Ebert Monochromator. Ultraviolet absorption detection data were taken with a Lab Data Control Duo Monitor HPLC detector system operating at 254 nm.

The HPLC column outlet was connected to the ICP nebulizer by means of a 3-cm length of $^1/_{16}$-in. o.d. narrow-bore Teflon flexible capillary tubing (Lab Data Control) fastened to the column exit by a $^5/_{16}$-in. stainless steel Swagelok fitting. This interface is crucial in that it must provide a flexible connection with minimum dead volume.

The EDTA and NTA chelates of copper(II) were prepared by precipitating excess copper(II) as the hydroxide from solutions of the chelating agent (*3*). Solutions of elements examined in the detection limit study were prepared by diluting certified atomic absorption reference solutions (Fisher Scientific) of each element in 1 F acetic acid. Aqueous 0.05 M $(NH_4)_2SO_4$ was employed as a mobile phase in the separation of the EDTA and NTA chelates of copper(II) on the Aminex A-14 column. The mobile phase used in the multielement detection limit studies consisted of 1 F acetic acid titrated to pH 3.0 with 0.1 N NaOH.

Samples of the elements for which detection limits were determined were introduced into the dummy column in 10-μL quantities through the constant volume injector system. The resulting chromatographic peaks for each element were monitored by the ICP and displayed on the strip chart recorder. In addition, solutions of each element were introduced at a steady rate under continuous nebulization conditions to give experimental values of detection limits under nonchromatographic conditions. Both the chromatographic peak and continuously aspirated samples were introduced to the ICP nebulizer by a pump at a constant flow rate of 1.0 mL/min. Less than approximately 5% of the sample introduced into the nebulizer ultimately reaches the plasma; the remainder is lost as drainage from the nebulizer chamber.

Table II. Comparison of Detection of Copper-Containing Species by ICP and UV Absorption at 254 nm

	Cu^{2+}	$Cu(NTA)^-$	$Cu(EDTA)^{2-}$
mode of detection	ICP	UV	UV
Cu concentration, ppm	2.0	10.0	10.0
peak height, mV	6.42	3.50	2.70
peak half-width, mL	0.12	0.097	0.095
peak area, mV·mL	0.770	0.340	0.256
detector sensitivity, (mV·mL)/ng	3.85×10^{-2}	3.40×10^{-3}	2.56×10^{-3}
noise, mV	0.14	0.030	0.030
detection limit, ng of Cu	6.9	18	24

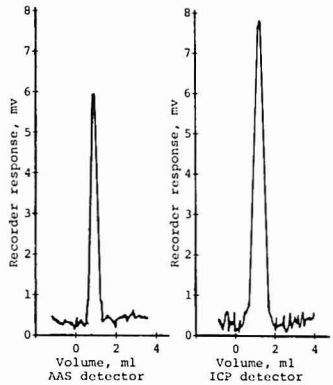

Figure 2. AAS and ICP detector response to 100 ng Cu chelated to NTA in a 10-μL sample run through the dummy HPLC column. For AAS, peak height/noise, 26.6; fwhm, 0.40 cm; peak area, 5.3 cm^2; noise, 0.50 cm. For ICP, peak height/noise, 23.1; fwhm 0.55 cm; peak area, 10.6 cm^2; noise, 0.85 cm

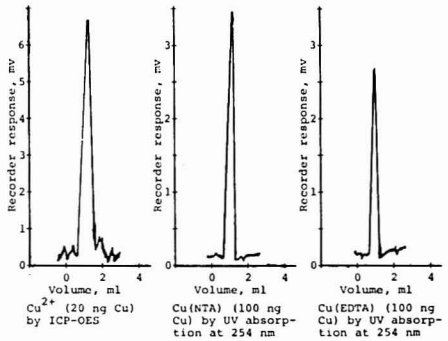

Figure 3. ICP response to 20 ng Cu^{2+} and UV absorption response to 100 ng Cu chelated to NTA and EDTA in a 10-μL sample run through the dummy HPLC column. For ICP, peak height/noise, 23; fwhm 0.12 mL; detectability, 6.9 ng/mL. For UV detection of Cu(NTA) peak height/noise, 58; fwhm, 0.095 mL; detectability, 18 ng/mL. For UV detection of EDTA, peak height/noise, 45; fwhm, 0.095 mL; detectability, 24 ng/mL

RESULTS AND DISCUSSION

Comparison of Detection of Copper Chelates by ICP and AAS. Nitrilotriacetate (NTA) and EDTA chelates of copper(II) were separated on an Aminex A-14 column according to a procedure previously published (*3*). Copper was monitored in these peaks with both AAS and ICP under conditions given in Table I. The peaks obtained are shown in Figure 1. The first peak in each chromatogram is due to the NTA chelate of copper(II) and the second peak is due to the EDTA chelate. It is seen that the two modes of detection are comparable.

Figure 2 is a comparison of ICP and AAS detectors for identical Cu(NTA) chelate peaks generated on the dummy column. It is seen that generally similar peaks are obtained by the two modes of detection.

Comparison of ICP and UV Detection. A comparison was made between ICP and ultraviolet solution absorption for the detection of HPLC peaks of copper species in an attempt to determine peak broadening in the nebulizer. The peaks were derived from the dummy column as described in the Experimental section. A solution of copper(II) acetate was monitored by ICP, and solutions of copper(II)–NTA chelate and copper(II)–EDTA chelate were monitored by UV absorption of the organic chelating agent at 254 nm. In all three cases, well defined sharp peaks were obtained as shown in Figure 3. Pertinent parameters for these peaks are given in Table II. A somewhat greater half-width of the ICP peak is due to mixing effects in the ICP nebulizer manifested as apparent peak spreading. Significantly, however, the detection limit for Cu is considerably better with the ICP than with the UV detector (at 254 nm). This illustrates that the ICP is competitive with one of the more commonly used HPLC detection techniques in sensitivity for at least one significant species. Of course, ultraviolet solution spectrometry does not provide the element-specificity possible with atomic spectrometry. Furthermore, atomic spectrometric methods enable quantization of elements, which may be desirable in some cases.

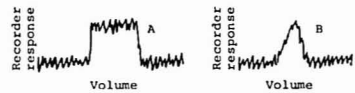

Figure 4. ICP signal from an element introduced (A) continuously at a steady rate and (B) as a chromatographic peak at concentrations near the detection limit

Detection Limits. A commonly used definition of detection limit is, *that quantity or concentration of analyte that will yield a scale deflection on the recording device equal in amplitude to twice the height of the random base-line noise.* For ICP detection of HPLC peaks, this definition stipulates that the concentration at the detection limit is equal to the maximum concentration of the analyte in the peak at the point of peak maximum. This concept is illustrated in Figure 4. Figure 4A shows the ICP signal from an element introduced into the instrument at a continuous steady rate at a concentration near the detection limit. Figure 4B shows introduction of the same analyte in the form of a chromatographic peak. Although the detection limits might be expected to be almost the same in both cases, in practice introduction of the analyte as a chromatographic peak requires a higher concentration for detection.

The determination of detection limit is crucial in the evaluation of ICP as a detector for HPLC. Detection limits were determined for 25 elements for which the direct reader was designed on the basis of general analytical interest,

Table III. Concentrations and Wavelengths of Lines Monitored for Elements in Standard Solutions Employed for Continuous Aspiration and Chromatographic Detection Limit Studies

element	designation and elemental concentrations (mg/L) of solutions used to determine detection limits in Table IV				wavelength, nm
1 *F* acetic acid solvent	1A blank				all
	2A	2B	2C	2D	
Ca	1.0	2.0	5.0	10.0	317.9
Cd	0.20[a]	0.50[a]	1.0	10.0	228.8 (II)[b]
Co	0.50[a]	1.0	2.0	10.0	228.6
Cu	0.50	1.0	2.0	10.0	324.7
Mg	0.05[a]	0.10[a]	0.20[a]	10.0	383.2
Mn	0.10	0.20	0.50	10.0	257.6
Pb	4.0	7.5	15.0	10.0	220.3
Zn	0.20[a]	0.50	1.0	10.0	213.8
	3A		3B	3C	
Al	10.0		20.0	40.0	309.2
Ba	2.0		0.50	1.0	493.4
Fe	1.0		2.0	4.0	259.9
Li	1.0		2.0	4.0	670.7
Mo	2.5		5.0	10.0	202.0
Na	2.0		5.0	10.0	589.0
Ni	4.0		8.0	15.0	231.6 (II)
Sb	15.0[a]		30.0[a]	50.0	217.5
Sr	0.25		0.50	1.0	421.5
Ti	1.0		2.0	5.0	334.9
	4A		4B	4C	
As	15.0[a]		30.0[a]	50.0	193.6
B	2.0		5.0	10.0	249.7
Cr	2.0		5.0	10.0	267.7
P	30		50	100	214.9 (II)
Se	15		30	50	196.0
	5A		5B	5C	
K	25		50	200	766.5
V	2.0		5.0	10.0	292.4

[a] Concentration too low to give a meaningful response. [b] (II) denotes detection at second-order loci.

environmental importance, and uniquity of analysis by ICP. These elements were contained at different concentrations in five different solutions as shown in Table III.

Under conditions of continuous analyte nebulization, as in Figure 4A, the detection limit is improved by displaying the emission intensity as a composite signal that has been measured and integrated by computer over a 4–50 s time span. For detection of the transient signal from a chromatographic peak, however, a time constant of only about 1 s is desired. Therefore, to compare detection limits from a chromatographic peak with those from continuous aspiration, it was necessary to determine the detection limits at an RC constant of 1 s under continuous aspiration.

As noted in the Experimental section, samples of elements for which chromatographic detection limits were determined were introduced into the injector system in 10-μL aliquots, from which they passed through the dummy column to the ICP for measurement of the emission of the element in question. Passage of the solution through the dummy column results in the formation of an idealized Gaussian chromatographic peak because of diffusion processes in the column. Some additional peak spreading occurs in the ICP nebulizer. The concentration of analyte at the peak maximum was calculated for each peak. Linear extrapolation of this concentration vs. the signal intensity at the peak maximum

Table IV. Minimum Detectable Concentration (MDC) Values for the ICP under Time-Resolved Continuous Aspiration Conditions and for Sample Introduction as a Chromatographic Peak

element	MDC at continuous aspiration, μg/L[a]	MDC as a chromatographic peak, μg/L[b]
Al	2.2×10^2	1.2×10^2
As	(did not give meaningful results)	
B	39	64
Ba	1	1.5
Ca	2.1	9.2
Cd	46	89
Co	17	21
Cr	19	20
Cu	3.3	6.8
Fe	15	28
K	7.5×10^2	6.3×10^2
Li	4.2	6.4
Mg	15	1.8×10^3
Mn	1	1.3
Mo	26	62
Na	5.7	82
Ni	34	43
P	1.6×10^2	2.9×10^2
Pb	2.1	2.3×10^2
Sb	1.3×10^2	4.1×10^2
Se	4.3×10^2	2.8×10^2
Sr	1	7.2
Ti	0.7	2.1
V	10	11
Zn	14	19

[a] See Figure 4A. [b] See Figure 4B. Concentrations in this column are concentrations at the peak maximum of the smallest detectable peak for that element, i.e., a peak with an amplitude equal to 2 *N*.

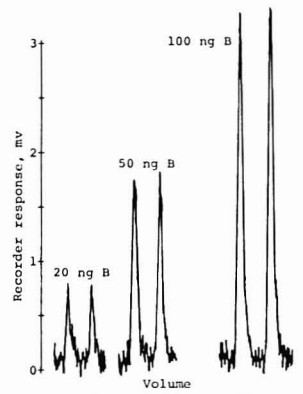

Figure 5. ICP detection of boron peaks at three different concentrations (two peaks for each concentration)

enabled calculation of the detection limit, denoted as *minimum detectable concentration* (MDC), given in Table IV. Duplicate peaks for each of three different concentrations of boron are given in Figure 5.

In order for the results to be independent of peak width, the chromatographic detectability of each element of interest was expressed as the concentration of analyte at peak maximum. This is necessitated by the fact that in practice, the width of chromatographic peaks, i.e., the mobile phase volume over which the peaks are integrated, may vary substantially. The calculation of absolute detection limits, however, is dependent upon peak areas. This requires incorporation of the mobile phase volume encompassed by each

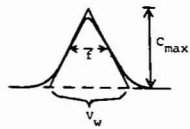

Figure 6. Approximation of a chromatographic peak as a triangle, where C_{max} is the peak height, f is the peak half-width, and V_w is the base width. For purposes of illustration, the peak width shown is exaggerated relative to height in comparison to the peaks actually obtained

peak, as detailed below. Therefore, the absolute detection limit would be unique to the particular separations to which the technique might be applied.

The calculation of analyte concentration at peak maximum is performed with knowledge of analyte concentration in the 10-μL aliquot injected and of the peak size and shape recorded from the ICP signal. The analysis of the chromatographic peak is illustrated in Figure 6. The peaks obtained in this study may be approximated rather accurately as triangles as shown in Figure 6. Treating the peak as a triangle, C_{max} is the peak height, f is the peak half-width, and V_w is the base width obtained by extrapolating the lines tangent to the peak sides to the base line. From purely geometric considerations the area of the peak, A, is given by the following two equations:

$$A = \frac{1}{2} C_{max} V_w \tag{1}$$

$$A = C_{max} f \tag{2}$$

It is readily seen that in terms of the physical quantities actually involved in formation of the peak, V_w is the volume of eluent over which the peak is eluted, C_{max} is the maximum concentration of analyte, and A is the total quantity of analyte. If V is used to designate the volume of eluent at any point since the peak first began to elute and C is the concentration of analyte at that particular volume, the following relationship holds:

$$A = \int_0^V C \cdot dV \tag{3}$$

The treatment described above enables the concentration of analyte at the peak maximum, C_{max}, to be evaluated readily. The total amount of analyte in the peak, A, is known from the concentration of analyte in the 10-μL aliquot injected into the system, and V_w is evaluated from the time recorded on the recorder chart and the known flow rate of mobile phase. Where N is the signal strength corresponding to the noise level, extrapolation of C_{max} down to a value of 2 N yields the detection limit designated as MDC in Table IV.

For the peaks actually observed in the detection limit studies, the values of V_w fell within a range of 250–333 μL, compared to a volume of 10 μL for the analyte sample injected. This means that for a peak with V_w equal to 250 μL, C_{max} is only 8% of the original concentration. Such a dilution effect of course occurs with any chromatographic detection system.

Several elements listed in Table IV are worthy of special mention. Arsenic gave a very poor performance because of the extremely high background arising from carbon emission (from C in the acetate medium) at 193.6 nm, a wavelength which is very close to the vacuum ultraviolet range. High background levels were also observed on the aluminum, selenium, and antimony channels. The MDC obtained for magnesium with this system was anomalously high because the optimum wavelength was not programmed on the system used. That is because magnesium is normally present at relatively high levels in the samples analyzed with the ICP system available.

A less favorable detection limit can be due to either increased noise or decreased sensitivity. In general, sensitivity is the ability of a measuring and recording system to convert sample concentration or quantity to an electrical signal. In the case of chromatographic detectors sensitivity is commonly expressed in millivolts (mV) of recorder response divided by concentration (C) in μg/L. Thus, C is given by the equation,

$$C = E/S \tag{4}$$

where E is the potential recorded by the recorder and S is the sensitivity. At the detection limit,

$$E = 2N \tag{5}$$

where N is the noise level in mV, and

$$C = \text{MDC} \tag{6}$$

where MDC is the minimum detectable concentration, or "detection limit". Substitution of Equations 5 and 6 into Equation 4 gives the equation,

$$\text{MDC} = 2N/S \tag{7}$$

expressing detection limit in terms of noise and sensitivity.

Examination of Equation 7 shows that the detection limit is increased (i.e., is less favorable) with increased N and/or decreased S. In the cases of each element studied in this investigation, the value of N was found to be the same under conditions of continuous aspiration and under chromatographic conditions. Therefore, differences in MDC for these two conditions were due to differences in S. It should be kept in mind that under some circumstances, however, noise can be introduced from chromatographic pumps, contributing to a less favorable detection limit.

In conclusion, the utility of inductively coupled plasma optical emission spectrometry as an element-selective detector for high performance liquid chromatography has been investigated. The investigation has been concerned with the direct applicability of the ICP detector for the detection of copper chelates separated by HPLC, as well as the potential for extending the technique to the detection of species of other elements of interest, including some not analyzed well by atomic absorption spectrometry. The method is readily applicable to those chromatographic techniques which employ essentially aqueous phases. These techniques include ion exchange high performance ion-pair chromatography, and reverse phase liquid chromatography. The uses of organic eluting agents and gradient solvent systems are suggested for future investigations.

LITERATURE CITED

(1) Manahan, S. E. "Environmental Chemistry", 3rd ed.; Willard Grant Press: Boston, Mass., 1979.
(2) Manahan, S. E.; Jones, D. R. *Anal. Lett.* **1973**, *6*, 745.
(3) Jones, D. R.; Manahan, S. E. *Anal. Chem.* **1976**, *48*, 502.
(4) Jones, D. R.; Manahan, S. E. *Anal. Lett.* **1975**, *8*, 569.
(5) Pankow, J. F.; Janaver, G. E. *Anal. Chim. Acta* **1974**, *69*, 97.
(6) Van Loon, J. C.; Radzuik, B. Paper presented at the Federation of Analytical Chemistry and Spectroscopy Societies, Philadelphia, Pa., Nov. 15–19, 1976.
(7) Van Loon, J. C.; Radzuik, B. *Can. J. Spectrosc.* **1976**, *21*, 46.
(8) Yoza, M.; Kouchiyama, K. *Anal. Lett.* **1975**, *8*, 641.
(9) Umebayashi, M.; Kitagishi, K. Paper presented at the Fifth International Conference on Atomic Spectroscopy, Melbourne, Australia, Aug. 25–29, 1975.
(10) Van Loon, J. C.; Radzuik, B.; Kahn, N.; Lichwa, J.; Fernandez, F. J.; Kerber, J. D. *At. Absorpt. Newsl.* **1977**, *16*, 4.
(11) Van Loon, J. C.; Radzuik, B.; Kahn, N.; Fernandez, F. J.; Kerber, J. D. Paper presented at the 28th Pittsburgh Conference on Analytical Chemistry and Applied Spectroscopy, Cleveland, Ohio, Feb. 28–Mar. 4, 1977.
(12) Botre, C.; Cacace, F.; Cozzani, R. *Anal. Lett.* **1976**, *9*, 825.
(13) Fernandez, F. J. *At. Absorpt. Newsl.* **1977**, *16*, 2.
(14) Fassel, V. A.; Knisely, R. N. *Anal. Chem.* **1974**, *46*, 1110A–1120A.
(15) Fassel, V. A.; Knisely, R. N. *Anal. Chem.* **1974**, *46*, 1155A–1164A.
(16) Fraley, D. M. M.A. Thesis, University of Missouri, Department of Chemistry, Columbia, Mo., 1979.
(17) Jones, D. R. Ph.D. Thesis, University of Missouri, Department of Chemistry, Columbia, Mo., 1976.

RECEIVED for review February 26, 1979. Accepted August 31, 1979. This research was supported by a National Science Foundation Grant No. MPS75-03330.

Selective Electrocatalytic Method for the Determination of Nitrite

James A. Cox* and Anna F. Brajter

Department of Chemistry and Biochemistry, Southern Illinois University at Carbondale, Carbondale, Illinois 62901

The reduction of Mo(VI) at −0.48 V vs. SCE in a pH 2.1 solution of 0.1 mM Na_2MoO_4, 0.1 M KCl results in a deposit on mercury and graphite electrodes which selectively catalyzes nitrite reduction. With linear potential scan voltammetry, a peak is developed at −0.88 V in direct proportion to nitrite concentration over the range 0.01–1 mM. Nitrate does not interfere until it reaches about a 100-fold excess at which point it causes an increase in the analytical current. Neither chloride nor sulfate interfere. Dissolved oxygen causes a correctable increase in the base-line current. The electroactive species was shown to be HNO_2. Under the recommended conditions, chemical decomposition was insignificant for at least 30 min, but sparging the pH 2.1 solution with N_2 to remove dissolved oxygen must not exceed 10 min to prevent significant volatility loss.

Nitrite is known to be electroactive under a wide variety of conditions, but few are suitable for quantitative determinations, particularly in the presence of nitrate. Many of the electrocatalytic methods for nitrate (*1*) are also responsive to nitrite, but only the total concentration of these ions can be determined. Nitrite can be electrochemically reduced in strong acid solutions, but the volatility of HNO_2 and its chemical instability in such solutions complicates obtaining precise analytical data (*2, 3*). At a cadmium electrode, nitrite and nitrate are also simultaneously reduced (*1, 4*).

A method for the polarographic determination of nitrite in citrate buffer has been reported (*5*). The applicability is hampered by a narrow concentration range, 10–60 μM NO_2^-, over which the current is directly proportional to concentration (*5*).

A quantitative method for determining nitrite using controlled potential coulometry with oxidation at a Pt electrode has been reported (*6*). The process is strongly influenced by the extent of oxidation of the electrode surface (*6*) but is otherwise uncomplicated.

Recently reported potentiometric methods which involve enzyme-catalyzed reactions permit the selective determination of nitrite in the range 5×10^{-5}–10^{-2} M (*7, 8*). These methods have the drawback of pH sensing (*9*).

The present study was undertaken to develop a selective method for the determination of nitrite in the presence of nitrate. Compatibility to our voltammetric ion selective electrode design (*10*) was also a consideration. The approach reported herein involves reduction at a mercury electrode which has been modified by deposition of a Mo-catalyst.

EXPERIMENTAL

Linear scan (LSV) and cyclic voltammetry (CV) experiments were performed with a conventional three-electrode potentiostat, Wavetek Model 114 function generator, and Hewlett-Packard 7004B x-y recorder. A Metrohm microburet hanging mercury drop assembly and vitreous graphite (Atomergic Chemicals Corp.) which was sealed into a glass tube with Torrseal epoxy (Varian Associates, Vacuum Division) served as indicator electrodes. The Hg and graphite electrode areas were 0.0185 and 0.12 cm^2, respectively. The graphite electrode was polished in several steps ending with diamond paste and a water-Gamal (Fisher Scientific Co.) suspension of 0.1-μm mesh.

All chemicals used were ACS Reagent Grade. The solutions were prepared with doubly deionized water with Cole-Parmer research grade cartridges used in the final stage. All potentials are reported vs. SCE.

Unless otherwise stated, the analytical experiments were performed by first adjusting a nitrite-containing solution of 10^{-4} M Na_2MoO_4, 0.1 M KCl to pH 2.1 with dilute HCl or KOH and then sparging with H_2O-saturated N_2 for 5–10 min. The indicator electrode was inserted and equilibrated for 0.5–5 min at 0.0 V. A negative potential scan of 70 $mV \cdot s^{-1}$ was applied; this value was found to yield the highest signal-to-background ratio without causing the nitrite reduction peak to be shifted too close to the potential at which the discharge of the supporting electrolyte occurs. The peak current at −0.88 V was measured from a base line obtained by extrapolation of the current decay of the −0.48 V molybdate reduction peak out to −0.88 V. The peak current linearly correlated to the nitrite concentration as discussed below.

RESULTS AND DISCUSSION

As illustrated in Figure 1, the product of the reduction of MoO_4^{2-} in pH 2.1 solution at a mercury electrode can catalyze the reduction of nitrite. Comparison of the LSV data in Figure 1 permits assignment of the peaks at −0.17 and −0.48 V to the reduction of Mo species and the peak at −0.88 V to nitrite reduction. The development of a separate nitrite reduction peak, as opposed to the presence of that ion merely enhancing the other peaks, is indicative that the present analytical method is not based upon a catalytic regeneration reaction in which nitrite is chemically reduced. Methods based upon the latter mechanism (*3*) often have a narrow linear working range and an inherently low signal-to-background ratio.

Under the conditions of Figure 1, the peak current, i_p, at −0.88 V is directly proportional to nitrite concentration in the range 0.01–1 mM. A linear least squares fit with a forced zero intercept of 10 points over that range has a slope of 8.18 ± 0.04 nA/μM and a 0.9997 correlation coefficient. At 5×10^{-5} M nitrite, 5 replicate experiments have a standard deviation of 1.6% in the peak current. Above 1 mM nitrite, the working curve has a negative deviation from linearity; however, if the MoO_4^{2-} concentration is increased to 1 mM, the linear response range becomes 1–7 mM nitrite (slope, 2.4 ± 0.1 μA/mM; correlation coefficient, 0.998; 5 data points).

In order to obtain precise analytical results, some control of the contact of the Hg electrode to the molybdate-containing solution prior to initiation of the LSV experiment must be exercised. For example, with a 0.0 V initial potential and a solution which consists of 10^{-4} M MoO_4^{2-} and 0.1 M KCl at pH 2.1, a 70 $mV \cdot s^{-1}$ scan results in a 0.95 μA peak at −0.48 V if the LSV experiment is initiated immediately upon extruding the Hg electrode drop. If the drop is contacted to the solution for 0.5 min at 0.0 V prior to scanning the potential, the peak current increases to 1.80 μA; lengthening the contact time to 10 min yields no further change in the −0.48 V peak. As shown in Figure 2, equilibration of the electrode also affects the height of the nitrite reduction peak and its resolution from the discharge of the supporting electrolyte.

0003-2700/79/0351-2230$01.00/0

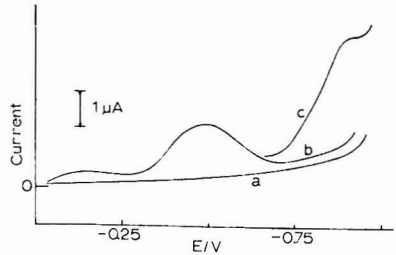

Figure 1. Linear potential scan voltammetry of nitrite at Hg in the catalytic medium. (a) 0.1 M KCl; pH 2.1 (presence or absence of nitrite). (b) 0.1 mM MoO_4^{2-}; 0.1 M KCl; pH 2.1. (c) 0.3 mM NO_2^- in b. (Curves b and c superimpose in region not shown. Scan rate, 70 mV·s^{-1}. The pH was adjusted with dilute HCl

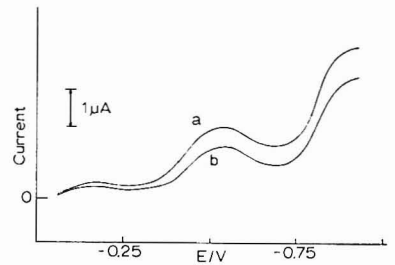

Figure 2. Effect of electrode–solution contact time on the generation of the catalyst. (a) 0.5 min of Hg–solution contact at 0.0 V prior to LSV. (b) LSV scan initiated immediately after contact of the Hg electrode to the solution. All other conditions the same as in Figure 1c

Hence, in all analytical experiments and other subsequent work, at least 0.5 min was allowed for equilibration.

The above results are consistent with previous reports of Mo(VI) adsorption at Hg (*11*, *12*). In 0.5 min under our conditions, the maximum surface coverage at 0.0 V is apparently attained. This subsequently yields a limiting quantity of the catalytic species.

The sensitivity of the method is dependent upon pH. Variation over the pH range 1.5–2.6 yielded a maximum sensitivity at pH 2.1. At higher values, log i_p is inversely proportional to pH which attests to HNO_2 rather than NO_2^- being the actual electroactive species, which is in accordance with other reports (*13*, *14*). Below pH 2.1, i_p is not only diminished but is also quite erratic. Apparently these observations are a result of solution instability. Both the volatility of HNO_2 and the chemical decomposition of $H_2NO_2^+$, which may form at low pHs, have been reported to affect analytical results (*5*, *6*, *13*).

At the recommended value of pH 2.1, the primary source of instability is the volatility of HNO_2. For example, when a deaerated Mo(VI), KCl, HCl solution is made 0.3 mM in KNO_2, repeated LSV experiments yield $i_p = 2.6 \pm 0.1$ μA for up to 30 min. If, however, a freshly prepared solution which contains the nitrite is continuously sparged with N_2, except for interruptions for performing the LSV experiments, after 15 min an i_p decrease which is significant relative to the standard deviation is observed.

An important characteristic of the present method is that over a wide concentration range nitrate does not interfere. As shown in Table I, i_p for nitrite reduction is independent of nitrate concentration up to about a 100-fold excess of the latter ion. At that point nitrate causes an increase in i_p. It should be noted that experiments in the absence of nitrite show no

Table I. Effect of Nitrate on the Nitrite Peak Current

NO_2^-/ M × 10^5	NO_3^-/ M × 10^5	i_p/μA	$(i_p/[NO_2^{-1}])$/ μA (LM^{-1}) × 10^5
5	0	0.42	0.084
5	5	0.43	0.086
5	50	0.43	0.086
5	200	0.46	0.092
5	500	0.79	0.158
10	500	0.93	0.093
20	500	1.70	0.085
30	500	2.53	0.084

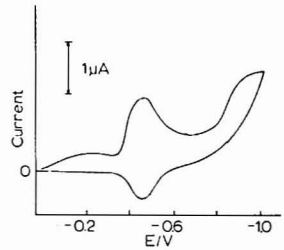

Figure 3. Cyclic voltammetry of nitrite at a Hg electrode modified by prior Mo–catalyst deposition. Electrode modification by electrolysis at −0.5 V in 0.1 mM MoO_4^{2-}, 0.1 M KCl at pH 2.1. Reported CV obtained with the modified electrode in 0.3 mM NO_2^-, 0.1 M KCl at pH 2.1. Scan rate, 70 mV·s^{-1}

peak in the region −0.5 to −1.0 V even when 10 mM NO_3^- is present; hence, the interference is due to neither NO_3^- reduction nor an impurity in the KNO_3 reagent. If a large nitrate excess is suspected, standard additions of nitrite can be made; a linear i_p response will establish the veracity of the determination (see Table I).

Other common anionic interferences in voltammetric methods for nitrite are sulfate and chloride. With the present procedure, sulfate up to at least 10^{-2} M did not affect i_p, and chloride certainly does not interfere as it was the supporting electrolyte anion. Dissolved oxygen increases the background current and should be removed for optimum measurements. Reducible metals would likewise interfere and may also influence the catalysis; they were not investigated as the former problem alone would require preliminary separation from such cations.

A factor in determining whether the Mo-catalyzed nitrite reduction can be used with voltammetric methods other than LSV is the physical nature of the catalytic species. Based upon previous reports it was anticipated that the catalyst was a surface film of either $MoO_2 \cdot 2H_2O$ (*15*, *16*) or a HMo(VI) species (*17*). A medium transfer experiment verified that the reduction at −0.48 V yields a catalytic film. In this case a mercury electrode was first put into a pH 2.1 solution of 0.1 mM Na_2MoO_4, 0.1 M KCl. After 1 min at −0.5 V, the electrode was removed and rinsed. Upon insertion into a pH 2.1 solution of 0.3 mM KNO_2, 0.1 M KCl, the CVs shown in Figure 3 were obtained.

The presence of the symmetrical peaks at about −0.5 V, which are sustained even after 5 min of continuous cycling, demonstrates that both the oxidized and reduced forms of Mo exist as surface species under the present conditions.

Beyond 5 min a significant loss of the catalyst occurs. For example, the area under the cathodic peak at −0.48 V immediately after medium transfer is 3.50×10^{-6} C; after 15 min and 1 h the areas are 1.21×10^{-6} C and 3.26×10^{-7} C, respectively. A commensurate decrease in the nitrite peak occurs. That the deposit is stable for at least enough time

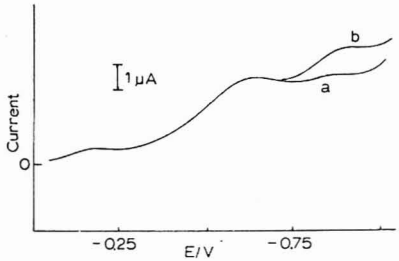

Figure 4. Linear potential scan voltammetry of nitrite at vitreous graphite in the catalytic medium. Conditions the same as in Figure 1b and 1c for a and b, respectively. Curves a and b superimpose in region not shown

to make a LSV measurement is important in that it may be possible to construct a nitrite probe based upon this system. In addition, the catalytic deposit is suitable for inclusion in a voltammetric ion selective electrode similar to our recent design for nitrate (*10*).

For either of the above proposed applications, a solid indicator substrate would be superior to Hg. Preliminary results obtained by LSV at a vitreous graphite electrode are depicted in Figure 4. The overall results are similar to those obtained at Hg (Figure 1); however, the onset of the supporting electrolyte discharge partially obscures the analytical peak. Presently other forms of graphite are being tested to alleviate this problem.

LITERATURE CITED

(1) R. J. Davenport and D. C. Johnson, *Anal. Chem.*, **45**, 1979 (1973).
(2) I. M. Kolthoff and J. J. Lingane, "Polarography", Vol. II, 2nd ed., Interscience, New York, p 533.
(3) D. T. W. Chow and R. J. Robinson, *Anal. Chem.*, **25**, 1493 (1953).
(4) D. C. Johnson and R. J. Davenport, *Anal. Chem.*, **46**, 1971 (1974).
(5) R. Annino and J. E. McDonald, *Anal. Chem.*, **33**, 475 (1961).
(6) J. E. Harrar, *Anal. Chem.*, **43**, 143 (1971).
(7) C. H. Kiang, S. S. Kuan, and G. G. Guilbault, *Anal. Chim. Acta*, **80**, 209 (1975).
(8) C. H. Kiang, S. S. Kuan, and G. G. Guilbault, *Anal. Chem.*, **50**, 1319 (1978).
(9) J. Ruzicka, E. H. Hansen, A. K. Ghose, and H. A. Mattola, *Anal. Chem.*, **51**, 199 (1979).
(10) J. A. Cox and G. Litwinski, *Anal. Chem.*, **51**, 554 (1979).
(11) M. Lamach and P. Souchay, *J. Chim. Phys.*, **70**, 384 (1973).
(12) M. N. Hull, *J. Electroanal. Chem.*, **51**, 57 (1974).
(13) D. L. Ehman and D. T. Sawyer, *J. Electroanal. Chem.*, **16**, 541 (1968).
(14) B. Keilin and J. W. Otvos, *J. Am. Chem. Soc.*, **68**, 2665 (1946).
(15) P. Lagrange and J. P. Schwing, *C. R. Acad. Sci., Ser. C*, **263**, 848 (1966).
(16) P. Lagrange and J. P. Schwing, *Bull. Soc. Chim. Fr.*, **536** (1968).
(17) K. Ogura and Y. Enaka, *J. Electroanal. Chem.*, **95**, 169 (1979).

RECEIVED for review June, 29, 1979. Accepted August 28, 1979. This work was supported in part by the Water Resources Center, University of Illinois, Project A-087-ILL, in the OWRT Allotment Program. AFB received partial support from the Eastern European Universities Exchange Program, Grant 6-21983 from the U.S. State Department. This work was presented in part at the 178th National Meeting of the American Chemical Society, Washington, D.C., Sept. 9–14, 1979.

Hydroxyl Anion Chemical Ionization Screening of Liquid Fuels

L. Wayne Sieck

National Bureau of Standards, National Measurement Laboratory, Division 543, Washington, D.C. 20234

K. R. Jennings and P. D. Burke

Department of Chemistry and Molecular Sciences, University of Warwick, Coventry CV4 7AL, England

The use of OH^- as a reagent ion for chemical ionization screening of the aromatic components in liquid fuels is discussed. The hydroxyl anions were generated by the reactions of O^-, from N_2O, with hexane, which also served as the solvent for the fuel samples. The resulting mass spectra were characterized by the absence of measurable signals from aliphatic components. The method requires no prior fractionation or separation, as well as a 2–3 minute turn-around time between successive analyses. Some preliminary data pertinent to determinations of actual molecular weight distributions by this technique are also presented.

Recently (*1*) it was shown that cyclohexane could be used as a source of cationic reagent ions in chemical ionization (CI) mass spectrometry for purposes of screening and fingerprinting fossil fuels. Cyclohexane also acted as the solvent for the fuel samples, and no prior fractionations or separations were required to achieve discriminatory CI charge exchange spectra of the aromatic components. As an extension of these studies, we wish to report our findings concerning the possible use of aliphatic solvents as a source of anionic reagent ions for similar screening of petroleum products. This effort was prompted by the fact that OH^- is known to be unreactive toward saturated hydrocarbons (*2*), but to react efficiently by proton abstraction (*2–4*) with molecules having strongly acidic hydrogen atoms, such as alkyl substituted aromatics;

$$OH^- + M \rightarrow (M - H)^- + H_2O \quad (1)$$

(M = aromatic with acidic sites). The hydroxyl anion, OH^-, can be conveniently generated (*5*) in N_2O/hydrocarbon mixtures by the sequential reactions

$$e^- + N_2O \rightarrow O^- + N_2 \quad (2)$$

$$O^- + RH \rightarrow OH^- + R \quad (3)$$

where RH denotes a paraffin serving as the solvent. In this article we discuss the negative ion spectra observed in N_2O/hexane/liquid fuel mixtures, and give some preliminary results relating to possible future quantitation of aromatic components by this technique.

EXPERIMENTAL

All measurements were taken with a KRATOS MS 1073 mass spectrometer modified for negative ion operation. (Manufacturers' names are used only to define the nature of the technique. Their usage does not imply endorsement of their products by the National Bureau of Standards.) The 1073 is a fast scanning, dou-

0003-2700/79/0351-2232$01.00/0

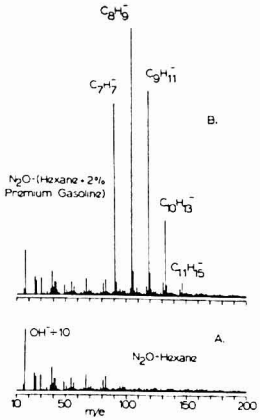

Figure 1. OH^- spectrum of hexane (A) and a 2% solution of a gasoline in hexane (B)

ble-focusing instrument with a resolving power of approximately 1000. The combined EI/CI chamber and the associated sample introduction systems were maintained at 175 °C, and all spectra were recorded using analog data acquisition. Repellers were maintained at nominally zero volts with respect to the chamber, and the ionizing electron energy was adjusted to give maximum signals (usually 50–100 eV). Fuel samples, as well as calibration standards, were derived from a variety of sources and used without further treatment. The procedure used to generated OH^- spectra was as follows. A steady-state flow of N_2O corresponding to static pressures of 0.02 to 0.05 Torr in the CI chamber was first established. The composite mass spectrum obtained under these conditions typically contained 50–60% O^-, 40–50% NO^- (from the reaction $O^- + N_2O \rightarrow NO^- + NO$), as well as minor peaks (less than 5% total) at m/e 26 (CN^-), 32 (O_2^-), 42 (NCO^-). Ten-μL liquid samples containing 0.1 to 5% by volume of the fuels dissolved in hexane (obtained from Fisons, Ltd., and labeled "Hexane Fraction from Petroleum") were then syringe-injected into a sample reservoir inlet and the leak rate adjusted to provide total pressures of 0.08 to 0.1 Torr (N_2O + hexane + fuel) in the CI chamber. The instrument was then scanned magnetically from m/e 400 to m/e 16 at the range of 10 s/decade, and the resulting spectrum recorded as an oscillographic tracing. The reservoir volume was then evacuated, followed by another syringe injection. Turn-around times between successive samples were typically less than 3 min when only 3–4 CI spectra of a given mixture were recorded by repetitive scanning.

RESULTS AND DISCUSSION

Figure 1A gives the negative ion spectrum obtained from a N_2O–hexane mixture without any additives (~0.02 Torr N_2O, ~0.08 Torr hexane). As anticipated, the major peak is OH^- produced via the reaction

$$O^- + C_6H_{14} \rightarrow OH^- + C_6H_{13} \quad (4)$$

Minor peaks are also evident at m/e 25 (C_2H^-), 26 (CN^-), 30 (NO^-), 39 ($C_3H_3^-$), and so forth. No background of any significance is evident above m/e 83 ($C_6H_{11}^-$?) except for a succession of low level periodic multiplets apparently resulting from e^- attachment to high molecular weight free radical species produced by pyrolytic reactions on the filament. Since the major components in the fuel samples of interest have molecular weights ≥90 amu, it would therefore appear that hexane provides a suitably clean source of reagent ions for screening purposes.

Figure 1B gives the OH^- CI spectrum of a 2% solution of a premium leaded gasoline in hexane recorded under the same conditions as Figure 1A. The major ions observed are associated exclusively with the aromatic components, and result from proton abstraction;

$$OH^- + M \rightarrow (M - H)^- + H_2O \quad (1)$$

where M, in this case, is an alkyl-substituted benzene. The signals at m/e 91, 105, 119, 133, and 147 can be ascribed to toluene (mol wt = 92), xylenes and ethylbenzene (mol wt = 106), trimethyl-, methylethyl-, and propyl-benzenes (mol wt = 120), etc. Minor peaks are also indicated at m/e 117, 131, and 145. Noteworthy is the absence of measurable signals from heptanes, octanes, and nonanes, and their unsaturated analogues, even though these compounds comprise more than 85% of the total hydrocarbon content of typical premium gasolines (the minor peak at m/e 109 could be due to reaction of OH^- with an octadiene or empirically equivalent ring compound, but the fractional intensity is <1% of the total signal due to aromatics). Comparison of Figures 1A and 1B also indicates that ions such as C_2H^-, CN^-, and NO^- react extremely slowly, if at all, with the components present in this particular sample. Variations in the sample dilution factor in hexane from 0.1% to 5.0%, or in the total pressure of the hexane solutions from ~0.01 to ~0.1 Torr, had no discernible effect on the resulting spectra except for substantially influencing the total signal level. It is appropriate at this stage to point out that other laboratories (2, 6) have reported condensation and elimination reactions involving certain organic anions and N_2O which could give a distorted or complicated overall CI spectrum. A major channel observed for aromatic derivatives is condensation followed by loss of H_2O to give an $(M + 25)^-$ anion; i.e.,

$$C_6H_5CH_2^- \text{ (from toluene, M = 92)} + N_2O \rightarrow C_6H_5CN_2^- \ (m/e\ 117) + H_2O \quad (5)$$

As mentioned above, the gasoline spectrum given in Figure 1B exhibits peaks at m/e 117, 131, and 145 which, in the absence of further information, could be assigned to secondary reactions of this general type involving $C_7H_7^-$, $C_8H_9^-$, and $C_9H_{11}^-$. In order to clarify this aspect of the measurements, a number of alkyl benzenes, thiophenes, and naphthalenes were diluted with hexane (~1000:1 v/v) and introduced separately into the CI chamber under the same conditions as the diluted fuel samples. Although the overall response or sensitivity varied somewhat among structural isomers (see last portion of Results), no peaks amounting to >1% of the $(M - 1)^-$ base peaks were detected at higher or lower m/e values for any of the molecules chosen. The absence of significant secondary reaction can be attributed to the fact that we initially (and arbitrarily) chose to use the lowest possible N_2O pressures consistent with an acceptable overall instrumental sensitivity (estimated to be in the range 0.02–0.03 Torr). Indeed, other measurements with synthetic mixtures taken at elevated N_2O pressures (>0.06–0.08 Torr) sometimes yielded substantial $(M + 25)^-$ peaks, particularly for the xylenes, ethylbenzene, and dimethylcumene. However, all of the spectra discussed here were recorded under conditions where secondary condensation reactions were negligible; therefore the m/e 117, 131, and 145 peaks shown in Figure 1B can be ascribed to substituted benzenes having olefinic side chains, or indan and tetralin (fused ring) derivatives present in the gasoline.

Figure 2 reproduces the OH^- CI spectrum derived from a No. 4 Fuel Oil (1% dilution in hexane). The rather complex composite spectrum can be resolved into the individual patterns from two series; substituted benzenes and substituted naphthalenes. These separated spectra are given in Figure 3, where the integer indicated on the mass scale denotes the total number of carbon atoms on the side chains; i.e., toluene is designated as 1, xylenes plus ethylbenzene as 2, etc.

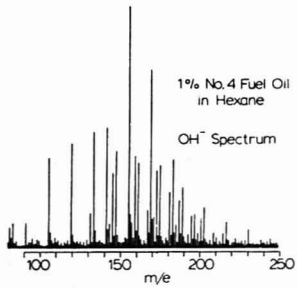

Figure 2. OH^- spectrum of a No. 4 Fuel Oil in hexane

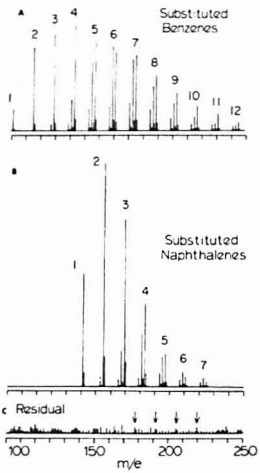

Figure 3. Resolved substituted benzene and naphthalene profiles for the No. 4 Fuel Oil spectrum given in Figure 2. See text for description of residual spectrum

Calculated isotope peaks (multiple ^{13}C excluded) are also included, as well as those associated with molecules having unsaturated side chains. When these family patterns are subtracted from the composite spectrum given in Figure 2 only the low-level signals given as Figure 3C, remain, most of which are due to the background pattern observed in pure N_2O–hexane mixtures (compare with Figure 1A, especially below m/e 140). Some of the residual peaks may also arise from other trace aromatic derivatives. For example, those indicated by arrows in Figure 3C occur at m/e values appropriate for naphthalenes with tri-olefinic or naphthenic (fused ring) side chains, or alkylated anthracenes and phenanthrenes. However, these assignments are purely speculative. In any event, the substituted benzene and naphthalene series given in Figures 3A and 3B account for 91% of the integrated mass spectrum of this fuel oil between m/e 130 and m/e 250. As before, nonaromatic components appear to be virtually absent in the OH^- spectrum, and the mass spectrum was again insensitive to the dilution factor in hexane over the range of concentrations studied (0.1 to 5.0% by volume).

The OH^- spectra of four other oils (2% by volume in hexane) are reproduced in Figure 4. The distributions correspond to the 35 most intense peaks occurring within the mass range 80 to 240 amu. For purposes of comparison, the composite spectra have been normalized to give equal signals

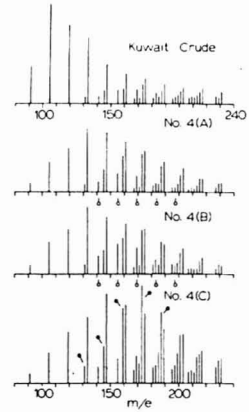

Figure 4. OH^- spectrum of a Light Kuwait Crude, as uncontaminated (A) and contaminated (B) sample of a No. 4 Fuel Oil, and an uncontaminated No. 4 Fuel Oil from a different manufacturer (C). See text for meaning of the open and darkened circles

at m/e 133 ($C_{10}H_{13}^-$ from alkylbenzenes having the empirical formula $C_{10}H_{14}$). The spectra designated A and B are of the same No. 4 fuel oil, with the exception that sample B had been deliberately contaminated with a lubricating oil. Signals corresponding to alkylnaphthalenes, which increase only slightly in relative intensity after contamination, are indicated in the mass scale by open circles (lubricating oils are typically ≥80% paraffinic). Spectrum C is from a neat No. 4 Fuel Oil derived from a different manufacturer than A, and the distribution obtained from a light Kuwait crude is also included for comparison. Note the higher concentrations of naphthenoor olefinic benzenes in oil C relative to A (indicated on C by darkened circles) and the fact that the unrefined crude is very rich in low molecular weight aromatics, as would be expected for a virgin sample.

Although the patterns shown in Figures 1–4 are discriminatory in the sense that one could, for example, presumably distinguish between fuel samples from different sources, there are two factors which must be considered before any attempt can be made to interpret rigorously the mass distributions in terms of actual molecular weight profiles. We have already shown that the anions produced by the reaction of OH^- with the aromatic components do not react further with N_2O or hexane under our low pressure conditions to give ions of higher m/e. Accepting that the negative ion spectrum is "clean", an equally important consideration for determinations of molecular weight profiles is the fact that little, if anything, is known concerning the relative reactivity of OH^- toward the various structural isomers which are certainly present in these complex fuel samples. Prepared mixtures of known composition were used to investigate qualitatively this aspect of the screening technique. Table I gives the relative $(M-1)^-$ signal levels observed for equimolar concentrations of several low molecular weight aromatics normalized to m/e 119 from mesitylene (1,3,4-trimethylbenzene, M = 120) = 1.0. These measurements were taken from mixtures of two or more of the components at various relative concentrations to develop an overall pattern. In agreement with Smit and Field (2), no product ions were obtained from benzene, naphthalene, or *tert*-butylbenzene, confirming the inertness of aromatics lacking acidic hydrogens toward OH^-. Although the values quoted have a precision of ~20%, it would appear that the reactivity reflects somewhat both the number of acidic hy-

Table I. Relative $(M - 1)^-$ Peak Heights Obtained from the Reaction of OH^- with Equimolar Mixtures of Aromatic Compounds[a,b]

molecule	peak ht.	molecule	peak ht.
toluene	0.4	ethylbenzene	0.5
m-xylene	0.8	isopropylbenzene	0.2
mesitylene	1.0	*n*-propylbenzene	0.8
2-methylthiophene	0.4	*sec*-butylbenzene	0.5
2,5-dimethylthiophene	0.5	*n*-butylbenzene	0.9
thionaphthene	0.2	3,4-dimethylcumene	0.9

[a] All values ± 20%. [b] Normalized to *m/e* 119 from mesitylene = 1.0.

drogens for any homologous series and the length of the alkyl side chain, at least for the first few family members. For example, compare the series toluene/*m*-xylene/mesitylene, isopropyl- and *sec*-butylbenzene with *n*-propyl- and *n*-butylbenzene, the series ethyl, *n*-propyl-, *n*-butylbenzene, etc. It must be emphasized that the MS 1073 is not designed for competitive kinetic studies, so that these preliminary data can be considered only qualitative at best. However, they do indicate that the relative sensitivities for low-boiling aromatics essentially do not differ by more than a factor of two or three, and there is some evidence that the response may flatten out as the molecular weight increases, probably reflecting a collision efficiency for proton abstraction approaching unity. A comprehensive study of the rates and mechanisms of OH^- reactions with heavy aromatic derivatives is being undertaken at NBS using ion cyclotron resonance mass spectrometry, and hopefully these future results will provide definitive information concerning possible quantitation of fuel samples by the OH^- CI technique.

CONCLUSION

The use of N_2O–hexane mixtures to generate OH^- reagent ions provides a very useful and rapid method for screening and characterizing the aromatic compounds in fuel samples. When measurements are taken at low partial pressures of N_2O, the resulting spectra are undistorted by secondary reactions, and the patterns appear to afford the same type of information provided by low voltage electron impact with the exception that benzene and naphthalene are not detected. An advantage of the technique is the fact that the fuel samples can presumably be dissolved directly in any aliphatic solvent, without any loss of low-boiling components, and immediately analyzed without any pre-separation of the saturate fraction. Extension of the method to compound classification will require a more thorough examination of the relative rates of reaction of OH^- with substituted aromatics and heterocyclics.

LITERATURE CITED

(1) L. W. Sieck, *Anal. Chem.*, **51**, 128 (1979).
(2) A. L. C. Smit and F. H. Field, *J. Am. Chem. Soc.*, **99**, 6471 (1977).
(3) J. I. Brauman and L. K. Blair, *J. Am. Chem. Soc.*, **92**, 5986 (1970).
(4) D. F. Hunt, S. K. Sethi, and J. Shabanowitz, paper MF-1 presented at the 26th Annual Conference on Mass Spectrometry and Allied Topics, St. Louis, Mo., 1978.
(5) D. K. Bohme and F. C. Fesenfeld, *Can. J. Chem.*, **47**, 2717 (1969).
(6) V. M. Bierbaum, C. H. DePuy, and R. H. Shapiro, *J. Am. Chem. Soc.*, **99**, 5800 (1977).

RECEIVED for review June 19, 1979. Accepted August 21, 1979. This research was supported by the Office of Environmental Measurement, National Bureau of Standards, Washington, D.C. 20234, and the Office of Basic Energy Sciences, Department of Energy, Washington, D.C. 20545. Additional support for the Warwick group was provided by the Science Research Council and Shell Research, Ltd., of Britain.

Interlaboratory Study of the Determination of Polychlorinated Biphenyls in a Paper Mill Effluent

Joseph J. Delfino*

Laboratory of Hygiene, 465 Henry Mall, University of Wisconsin—Madison, Madison, Wisconsin 53706

Dwight B. Easty

The Institute of Paper Chemistry, P.O. Box 1039, Appleton, Wisconsin 54912

Six laboratories collaboratively studied a method for determining polychlorinated biphenyls (PCBs) in paper mill effluent. In preliminary studies, the recovery and relative standard deviation (RSD) for the PCB Aroclor 1242 added to and extracted from distilled water were 95.6% and 14.7%, respectively. Because the RSD of data from direct injection of Aroclor 1242 solutions into the gas chromatograph was of similar magnitude, 15.6%, gas chromatographic analysis appeared to provide the principal source of variation in the overall determination. Participating laboratories achieved an average 93.7% recovery of Aroclor 1242 added to a paper mill effluent; their data had a RSD of 16.0%. The results indicate that the method is satisfactory for use with paper mill effluents having PCB concentrations above 2 μg/L and it compares favorably with findings from studies in other environmental matrices. Greater variation might be expected from effluents containing significant interferences.

Polychlorinated biphenyls (PCBs) were formerly used in carbonless copy papers, but this practice was terminated in 1971 (*1*, *2*). Small amounts of PCBs, particularly the Aroclor 1242 mixture, are still entering paper mills which recycle used paper fibers as part of their manufacturing process. It has not been logistically nor economically feasible to completely separate carbonless copy paper from the other waste papers that are being recycled (*1*). Thus, until all of the PCB-containing papers still in circulation cease to appear in recycled fiber, small quantities of PCBs will continue to be discharged in the mills' aqueous effluents. The amounts of PCBs discharged can be lowered by reducing the suspended solids in the effluent from the mill (*3*).

A procedure for determining PCBs in industrial effluents has been issued by the Environmental Protection Agency (EPA) (*4*). In our collaborative investigation, we modified the EPA method to apply specifically to paper mill effluents and

0003-2700/79/0351-2235$01.00/0

aimed to document the precision of the modified method when used in several laboratories. However, the modified method described here has not been submitted to the EPA for approval—an action that would be necessary if the data were to be included in an EPA-required monitoring program. Participants in the study included industry, universities, independent laboratories, and government agencies.

The promulgated EPA method for determining PCBs in industrial effluents involves liquid–liquid extraction, Florisil cleanup (Florisil is a registered Trade Mark of the Floridin Company, Pittsburgh, Pa. 15235), and electron capture gas chromatography. Previous work has revealed deficiencies when this procedure is used on in-mill process streams containing large amounts of cellulose fibers (*2*). Complete removal of the PCBs from cellulose fiber suspensions required alcoholic KOH reflux of the isolated fibers subsequent to liquid–liquid extraction. Samples of paper mill effluent for PCB monitoring are typically taken following waste treatment. Because a large percentage of the suspended fibers is removed in the treatment system, these samples should not require PCB isolation procedures beyond those specified in the EPA method (*4*). Therefore, the procedure used in this investigation retained many features of the EPA method (*4*) and was judged suitable by the collaborators for the purposes of this study. As described below, some modifications were incorporated to make the method easier to use on effluents in which organochlorine pesticides were not expected or generally observed in previous analyses.

EXPERIMENTAL

The interlaboratory study was performed in two parts. Phase 1 was designed to determine the comparability of PCB methodologies in use in each laboratory and to assess the ability of the participating analysts to perform the basic operations employed in PCB determinations. Phase 2 consisted of application of the modified method to determination of Aroclor 1242 in a paper mill effluent.

Phase 1. Each participating analyst was provided with septa-sealed vials containing acetone solutions of Aroclor mixtures. Each laboratory was asked to analyze the PCB mixture by (a) direct injection into a gas chromatograph (GC) employing an electron capture detector, and (b) addition of 1 mL of the unknown to 1000 mL of distilled water followed by solvent extraction, concentration, and then injection into the GC. Procedures for these operations were left to the discretion of the analysts.

Phase 2. *Validation of Sample Preparation Procedure.* Prior to collection of paper mill effluent samples to be used for the PCB determinations, a separate study was performed to evaluate the study coordinator's ability to provide equivalent effluent samples to each participant. Because PCBs tend to sorb onto suspended solids, samples for collaborative study must contain equivalent suspended solids contents. A large volume of paper mill effluent was placed in a metal container and was mechanically stirred. Aliquots (250 mL) were removed and sequentially added to each of ten separate 2.5-L glass containers. (Bottles were rinsed with hexane several times to remove possible contaminants before being used for paper mill effluent samples. The hexane was drained and the bottles air dried prior to use. Aluminum foil was used to line the bottle caps.) The process was repeated ten times until each 2.5-L container was filled. Suspended solids were determined on the contents of each container.

Instructions to Analysts. Each analyst received two 2.5-L paper mill effluent samples and three sealed glass ampules containing Aroclor 1242. Two of the three ampules contained Aroclor 1242 in isooctane; one ampule was designated a "known" and contained 13.6 μg/10 mL; the second ampule was an "unknown" and contained 35.2 μg/10 mL. Participants were asked to analyze each solution by direct injection into the GC. The third ampule contained an unknown concentration of Aroclor 1242 in methanol and was to be added directly to one of the two paper mill effluent sample bottles. The ampule was designed to deliver 6.8 μg of Aroclor 1242 directly into the paper mill effluent sample bottle.

The study plan called for each participant to divide the contents of one of the paper mill effluent samples into two equal portions. Then, each portion was to be extracted and the Aroclor 1242 concentration of each portion determined by GC. Each analyst was also instructed to add the ampule containing the 6.8 μg of Aroclor 1242 to the second 2.5-L sample container, break the ampule inside the container, mix well, and let this "spiked" sample stand for 24 h before beginning extraction and analysis by GC. As before, this "spiked" effluent sample was also to be analyzed in duplicate by dividing the 2.5-L sample into two equal portions with each one being analyzed separately.

Determination of PCBs in Paper Mill Effluent. In the promulgated method for PCBs in industrial effluents (*4*), PCBs and organochlorine pesticides are coextracted from the sample by liquid–liquid extraction. A silica gel microcolumn procedure and standard Florisil column cleanup are prescribed for separating PCBs from pesticides and for dividing the pesticides into subgroups. Because pesticides are unlikely constituents of paper mill effluents and were not of concern here, the EPA method (*4*) was modified for use in this study by removing from the procedure those steps necessary for extraction, separation, and determination of pesticides. The features of the EPA method (*4*) which were modified for application to paper mill effluent in this investigation are:

(1) Hexane and petroleum ether (30–60 °C) were independently shown by the collaborators to be suitable alternates to 15% methylene chloride in hexane for separatory funnel extraction of effluent. Hexane extraction has been shown to recover PCBs almost quantitatively from effluents with low fiber contents (*2*). Solvents of higher polarity, such as methylene chloride in hexane, extract excessive amounts of non-PCB materials without improving PCB recovery.

(2) To assure consistent performance of the electron capture detector and to minimize down time for detector cleaning, all extracts were subjected to Florisil column cleanup prior to gas chromatographic analysis.

(3) In addition to the specifications for Florisil columns (*4*), other column sizes and amounts of Florisil and eluting solvent were acceptable for PCB determination provided that (a) all PCBs were completely eluted, and (b) chromatogram quality signified that samples had been adequately cleaned up. Elution of PCBs from the Florisil column with hexane or petroleum ether as well as with 6% ethyl ether in petroleum ether was permitted. Use of petroleum ether alone for elution is standard practice in determining PCBs in paper and paperboard (*5*).

(4) The silica gel microcolumn procedure for separating PCBs from pesticides was deleted from the method.

(5) Gas chromatographic column liquid phases specified in the EPA method (*4*) include SE-30 or OV-1, and OV-17/QF-1. Other silicone liquid phases used successfully for determining PCBs in Phase 1 of this study included OV-17, OV-210, DC-200, OV-101, OV-225, and equivalent SP phases. An earlier collaborative study has indicated that several column materials are useful for PCB determinations (*6*). Therefore, the phases listed above were considered acceptable for this study. Also accepted were stainless steel as well as glass columns.

(6) Unknown Aroclors were identified by matching retention times and relative peak heights with peaks in reference Aroclors. To ensure valid quantitation, amounts were injected such that the size of the peaks from the sample and the standard were within ±25%. When quantitation was based upon peak heights, at least four peaks were used.

RESULTS AND DISCUSSION

Phase 1. The results of the GC analyses of Aroclor 1242 in acetone are presented in Table I. The average PCB concentration (as Aroclor 1242) based on direct injection into the GC was 1.47 ng/μL, representing an average recovery of 98% of the 1.5 ng/μL present in the acetone solution. Therefore, on the average, the results indicated that the eight participants in Phase 1 had good GC technique and could quantify PCBs.

While the results of the direct injection experiment were good, some variation among the analysts was evident as shown by the standard deviation (0.23 ng/μL), relative standard deviation (RSD) (15.6%) and range (1.05–1.76 ng/μL). While

Table I. Determination of PCBs as Aroclor 1242 in Acetone Solution by Direct Injection and Extraction from Distilled Water (Phase 1)

analyst	PCB by direct injection, ng/μL[a]	PCB extraction from distilled water, %
1	1.52	90.0
2	1.41	99.3
3	1.46	89.6
4	1.70	>100[c]
5	1.59	114
6	1.26	106
7	1.76	70.1
8	1.05	100
average	1.47 ng/μL[b]	95.6%[d]
range	1.05-1.76 ng/μL	70.1-114%
standard deviation	0.23 ng/μL	14.1%
rel. std. deviation	15.6%	14.7%

[a] Concentration of Aroclor 1242 = 1.50 ng/μL. [b] Represents average finding by direction injection = 98%. [c] Treated as outlier as analyst was unable to quantitate recovery except as reported. [d] Data from analyst no. 4 excluded in statistical calculations.

Table II. Test for Determining Suspended Solids Concentrations in Representative Samples

run	suspended solids, mg/L
1	73.2
2	80.8
3	74.8
4	74.8
5	75.6
6	73.6
7	77.6
8	77.6
9	74.4
10	72.4
average	75.5 mg/L
range	72.4-80.8 mg/L
std. deviation	2.53 mg/L
rel. std. dev.	3.3%

this indicated more variation than might be desired in an interlaboratory study, it is shown later that a RSD of 15.6% is typical for PCB determinations involving environmental matrices.

The extraction of Aroclor 1242 added to distilled water resulted in an average recovery of 95.6%. This was satisfactory, although the variation was again relatively high as indicated by the RSD (14.7%) and the range (70–114%). Because this sample was free from interferences, the precision represents that which is attainable under unusually favorable analytical conditions.

The RSDs obtained in the direct injection experiment and in determination of Aroclor 1242 added to distilled water were of similar magnitude. This suggests that GC analysis provided the major sources of between-laboratory variation in the overall analytical scheme. Likely contributors to this variation included: (a) use of different Aroclor 1242 standards with slightly different PCB isomeride composition, and (b) use of different quantitation methods, including measurement of peak heights, peak areas, or weight percentages of individual peaks (*7–9*). The contribution of different GC columns and conditions is difficult to assess, although it was possibly advantageous for the analysts to use their own columns which produced familiar Aroclor chromatograms.

Phase 2. This phase of the study again involved determination of Aroclor 1242 by direct injection of solvent solutions into the GC and, of greater importance, also included determination of Aroclor 1242 in a paper mill effluent. The effluent was studied as collected and after addition of a known amount of an Aroclor 1242 standard.

The ability of the proposed sample collection procedure to supply equivalent mill effluent samples for collaborators was tested by determining if the procedure could provide samples of equivalent suspended solids content. Results are given in Table II. One analyst removed aliquots from each of ten different 2.5-L sample bottles, filled as described earlier, and performed the standard suspended solids measurement (*10*). The data indicate that representative suspended solids distribution could be achieved by the sampling technique, since the RSD experienced was 3.3%. The published RSD for suspended solids determinations ranges from 0.76 to 33% depending on the actual suspended solids concentration present in the sample (*10*).

Known and unknown Aroclor 1242 concentrations were determined by direct GC injection from glass ampules. The results are shown in Table III. The known solution allowed participating analysts to check their in-house standards with one prepared by the coordinating laboratory and also provided a reference standard to be used for the spiking, extraction, and recovery experiment involving the paper mill effluent sample.

The determination of the known and unknown PCB concentrations by direct injection into the GC yielded essentially the same average calculated recovery data, i.e., 98% and 97%, respectively (Table III). However, the variation among seven reporting analysts was somewhat greater for the unknown standard solution (RSD = 12.6%) than for the known standard solution (RSD = 7.5%). There is no im-

Table III. Determination of PCBs as Aroclor 1242 in Isooctane Solution by Direct Injection (Phase 2)

	PCB concentration as Aroclor 1242			
	known (13.6 μg/10 mL)		unknown (35.2 μg/10 mL)	
analyst	concn reported, μg/10 mL	calcd recovery, %	concn reported, μg/10 mL	calcd recovery, %
1	14.2	104	37.0	105
2	13.6	100	34.0	97
3	12.5	92	36.0	102
5	12.5	92	27.3	78
6	12.8	94	31.0	88
7	15.0	110	40.7	116
8	12.5	92	33.4	95
average	13.3 μg/10 mL	98%	34.2 μg/10 mL	97%
range	12.5-15 μg/10 mL	92-110%	27.3-40.7 μg/10 mL	78-116%
std. dev.	1.0 μg/10 mL	7.2%	4.3 μg/10 mL	12.2%
rel. std. dev.	7.5%		12.6%	

Table IV. Determination of PCBs as Aroclor 1242 in a Paper Mill Effluent (Phase 2)

analyst	replicate, μg/L no. 1	replicate, μg/L no. 2	average PCB concn reported by each analyst, μg/L
1	2.70	2.09	2.40
2	3.48	3.88	3.36
3	2.45	2.89	2.67
6	2.26	2.32	2.36[a]
7	2.33	2.73	2.53[a]
8	2.98	2.84	2.95[a]
average (n = 12)		2.74 μg/L	2.71 μg/L[b]
range		2.09-3.88 μg/L	2.36-3.36 μg/L
std. dev.		0.52 μg/L	0.39 μg/L
rel. std. dev.		19.0%	14.4%

[a] Includes small additional amount of PCB obtained by rinsing sample bottle with solvent after removal of sample. [b] Statistics developed by considering only the average PCB concentration reported by each analyst.

mediate explanation for this except that the unknown solution was ca. 2.5 times more concentrated than the known solution. This resulted in an additional dilution step to keep the unknown Aroclor on scale. This could have introduced additional error and the slightly higher RSD.

The PCB concentration in the paper mill effluent was determined in duplicate by six analysts according to the modified analytical procedure. The results are given in Table IV. The paper mill effluent was also analyzed in duplicate following addition of a methanol-based Aroclor 1242 standard. These data appear in Table V. Relative standard deviations of the PCB determinations performed on the effluent as collected and following addition of Aroclor 1242 were 19.0% and 16.0%, respectively.

The variations in the results for the determination of Aroclor 1242 in the paper mill effluent among the six analysts who completed Phase 2 were not very different from the variations noted for the direct GC injection of Aroclor 1242 solutions (Tables I and III). This suggests, as did the Phase 1 findings, that only small additional errors were introduced by the sample extraction and Florisil cleanup steps.

As indicated in Table V, the average recovery of the added Aroclor 1242 was 93.7%. This average is slightly misleading since three results clustered near 100% and the remainder ranged from 84 to 88%.

Following Florisil cleanup of the paper mill effluent used in this study, all collaborators obtained characteristic Aroclor 1242 chromatograms. Some other paper mill effluents contain interfering materials that cannot be removed on Florisil and which produce badly distorted chromatograms (*11*). Between-laboratory variation in PCB determinations conducted on effluents containing intractable interferences would undoubtedly be greater than that experienced in the current investigation.

Other observations reported by the collaborators in Phase 2 included (a) formation of emulsions during solvent extraction of the effluent, and (b) small differences in peak ratios between the individual laboratory's Aroclor 1242 standards and the standard provided by the coordinating laboratory. Emulsions were broken by centrifugation or addition of Na_2SO_4. The problem of variations in PCB standards could be obviated by providing Aroclor standards from a common source to all laboratories conducting PCB determinations.

Considering the nature of the paper mill effluent matrix, the results of this interlabortory study were good. This can be substantiated by comparison of the RSDs reported in this study with those reported for PCB collaborative studies involving other complex environmental matrices (Table VI). It is clear, however, that analysts desiring to compare their results for the determination of PCBs in environmental samples must anticipate variations within the range of 15–20% expressed as the RSD.

Table VI. Some Examples of Interlaboratory Variation Based on Collaborative Studies Involving PCBs

sample matrix	rel. std. dev., %	no. of analysts	ref.
paperboard	15-22	11	(*6*)
milk	18-31[a]	10	(*9*)
chicken fat	6-16[a]	10	(*9*)
marine wildlife	21	14	(*12*)
shark liver homogenate	27	6	(*13*)
marine sediments	22	10	(*14*)
fish	27-37	7-13	(*15*)
paper mill effluent	15-19	6	this study

[a] RSD varied with method used for GC quantitation.

CONCLUSIONS

Based on this interlaboratory study, the method described herein for PCBs in paper mill effluents appeared satisfactory. However, the statistics developed in this work were derived from determination of Aroclor 1242 mixtures in the concentration range of 2–6 μg/L and on an effluent from which interferences were readily removed. Different precision and accuracy findings could occur when the method is applied to paper mill effluents having different contents of PCBs and of materials which interfere in the determination. Gas chromatographic standards and techniques appear to have been the principal sources of variation in this study. It is

Tavle V. Determination of PCBs as Aroclor 1242 in a Paper Mill Effluent to Which a Standard Solution of Aroclor 1242 Was Added

analyst	replicate, μg/L no. 1	replicate, μg/L no. 2	average PCB concn reported by each analyst, μg/L	calcd recovery of std. PCB,[b] %
1	4.30	4.90	4.60	88
2	6.26	5.95	6.10	100
3	6.56	4.50	5.53	103
6	4.32	4.15	4.32[a]	84[a]
7	5.80	4.96	5.42[a]	101[a]
8	4.64	5.17	4.96[a]	86[a]
average (n = 12)		5.13 μg/L	5.16 μg/L[a]	93.7%[c]
range		4.15-6.56 μg/L	4.32-6.10 μg/L	84-103%
std. dev.		0.82 μg/L	0.63 μg/L	8.53%
rel. std. dev.		16.0%	12.2%	9.1%

[a] Includes small additional amount of PCB obtained by rinsing sample bottle with solvent after removal of sample. [b] Based on average PCB concentration reported by analysts in Table IV. [c] Statistics developed by considering only the average PCB concentration reported by each analyst.

important that regulatory officials seeking to establish effluent standards for PCBs in discharge media such as paper mill effluent take the findings of this and other related studies into consideration, so that the standards may be enforced rationally in light of analytical variability.

ACKNOWLEDGMENT

The efforts of the participating analysts in this study are greatly appreciated, as is the cooperation of the paper manufacturer that assisted in the collection of the effluent used for the comparison study. S. Kleinert and T. B. Sheffy of the Wisconsin Department of Natural Resources (DNR) and D. J. Dube of the Wisconsin Laboratory of Hygiene assisted in the establishment and coordination of the program.

LITERATURE CITED

(1) Ayer, F. A., Ed.; "Proceedings, National Conference on Polychlorinated Biphenyls, November 1975, Chicago". EPA-560/6-75-004; Environmental Protection Agency: Washington, D.C., 1976.
(2) Easty, D. B., Wabers, B. A. *Tappi* **1978**, *61*(10), 71–74.
(3) Ball, J.; Gibson, T.; Priznar, F.; Delfino, J.; Dube, D.; Peterman, P. "Investigation of Chlorinated and Nonchlorinated Compounds in the Lower Fox River Watershed". EPA-905/3-78-004; Environmental Protection Agency: Chicago, Ill., 1978.
(4) *Fed. Regist.* **1973**, *38*(199), Part II, 28758.
(5) Young, S. J. V.; Finsterwalder, C. E.; Burke, J. A. *J. Assoc. Off. Anal. Chem.* **1973**, *56*(4), 957–961.
(6) Finsterwalder, C. E. *J. Assoc. Off. Anal. Chem.* **1974**, *57*(3), 518–521.
(7) Webb, R. G.; McCall, A. C. *J. Chromatogr. Sci.* **1973**, *11*, 366–373.
(8) Sawyer, L. D. *J. Assoc. Off. Anal. Chem.* **1978**, *61*(2), 272–281.
(9) Sawyer, L. D. *J. Assoc. Off. Anal. Chem.* **1978**, *61*(2), 282–291.
(10) "Standard Methods for the Examination of Water and Wastewater", 14th ed.; American Public Health Association: Washington, D.C., 1975; p 94.
(11) Easty, D. B.; Wabers, B. A. *Anal. Lett.* **1977**, *10*(11), 857–867.
(12) Holden, A. V. *Pestic. Monit. J.* **1973**, *7*, 37.
(13) Harvey, G. R.; Miklas, H. P.; Bowen, V. T.; Steinhauer, W. G. *J. Mar. Res.* **1974**, *32*, 103.
(14) Pavlou, S. P.; Hom, W. *Mar. Chem.* **1976**, *4*, 155.
(15) van Hove Holdrinet, M. "Preliminary Results of an Interlaboratory PCB Check Sample Program". In "Pesticides, Environmental Quality and Safety", Suppl. Vol. III, Coulston, F., Korte, F., Eds.; Georg Thieme Publ.: Stuttgart, 1975; pp 51–56.

RECEIVED for review May 31, 1979. Accepted August 9, 1979.

Quaternized Porous Beads for Exclusion Chromatography of Water-Soluble Polymers

C. P. Talley and L. M. Bowman*

Research and Development, Calgon Corporation, Post Office Box 1346, Pittsburgh, Pennsylvania 15230

The novel approach of using ion-exchange chromatographic supports for size exclusion chromatography of neutral and cationic water-soluble polymers is presented. A quaternary ammonium group, a strong anion exchanger, has been bonded to the surface of porous silica glass in the pore size range from 40 to 25 000 Å. Chromatograms are shown of poly(2-vinylpyridine) and dextran molecules using acidic salt solutions as eluents. Molecular weight calibration graphs, theoretical plate height plots, and concentration effects are discussed in detail.

Gel permeation chromatography (GPC), originated in 1965 by J. Moore (*1*), has primarily focused on nonaqueous applications and many advances have been achieved. However, progress in the area of aqueous exclusion has not been as rapid owing to the many experimental difficulties encountered (*2*). Aqueous GPC has been confined to neutral and anionic polymers since commercially available supports work favorably for a number of these materials (*3*). Cationic polymers have not been chromatographed because porous silica glasses and cross-linked copolymer resins tend to be anionic in nature leading to solute–support interactions. G. B. Butler (*4*), in 1976, chromatographed cationic polyelectrolytes on quaternized styrene/divinylbenzene supports with limited success. Some of the disadvantages observed were: (1) the swelling of the resin which was a function of ionic strength; (2) the support compression as the flow rate increased; (3) the limited porosity of these supports. The porous silica glass supports were felt to serve as the ideal substrate if adsorption could be eliminated. They have a fixed pore and particle size and can be used at the high flow rates needed for microparticulate high resolution chromatography. Attempts to deactivate the surface by silanization (*3*) and by the addition of cationic surfactants to the eluent (*5*, *6*) have been unsuccessful. In this paper, we are introducing the concept of using ion-exchange supports on glass to reduce solute–glass interactions (*7*).

The ion-exchange support chosen to chromatograph cationic polymers must be a strong anion exchanger. The quaternary ammonium ion is an excellent choice since it creates a positively-charged surface to repel the positively-charged polyelectrolyte. The support was prepared by reacting 3-aminopropyltriethoxysilane with the glass followed by reaction of the terminal NH_2 group with 3-chloro-2-hydroxytrimethylammonium chloride. The procedure was similar to those described in the literature for the silanization of glasses (*2*, *8*, *9*) and is illustrated in the equations below:

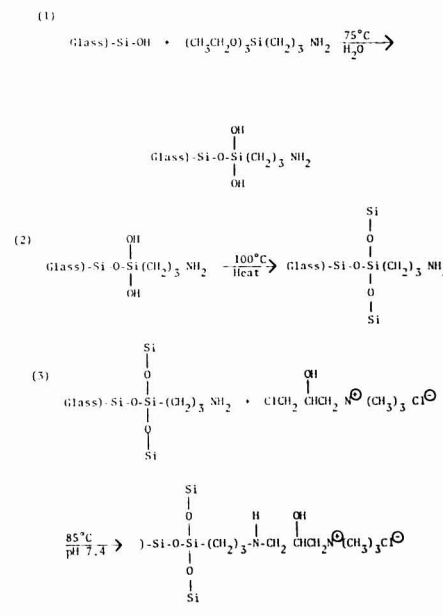

Table I. Quaternized Supports

sample	nominal pore size, Å	particle size, μm
40 porous silica	40	39–75
CPG-75	75	39–75
CPG-170	170	39–75
CPG-350	350	39–75
CPG-1400	1 400	39–75
BIO-2500	2 500	39–75
EM-GEL 5,000	5 000	79–125
EM-GEL 10,000	10 000	79–125
EM-GEL 25,000	25 000	79–125
CPG-1500	1 500	5–10

Supports were prepared with Electro-Nucleonics Porous Silica Glass of pore size 40 Å, Corning Controlled Pore Glass (CPG) of pore size 75 Å to 3000 Å, Bio-Rad Bio-Glas of pore size 2500 Å, and E. Merck EM-Gel of pore size 5000 to 25 000 Å. The actual pore sizes of the quaternized supports are dependent on the percentage of the surface covered and the charge repulsion between polymer and surface. Furthermore, these effects should be more pronounced in the smaller pores than in the larger ones.

EXPERIMENTAL

Apparatus. The gel permeation chromatograph consisted of a Waters Model 301 Refractive Index Detector, a Laboratory Data Control Constametric I liquid pump, and a DuPont Model 834 Automatic Liquid Sampler. All columns were made using 91-cm lengths of 0.952-cm o.d. stainless steel tubing. All connecting fittings were 0.952 cm to 0.158 cm low dead volume Swageloks with 5-μm porous frits. The aqueous GPC eluent was 0.1 N in HNO_3 and 0.1 N in $NaNO_3$. Elution volumes were measured with a Waters Liquid Volume Indicator whose count volume was 3.6 mL. A Hewlett-Packard 3354A Lab Data System was used in data acquisition and reduction. All samples were made up at 0.2 wt % based on active polymer, and the injection volume was varied from 0.25 to 2.0 mL.

Materials. The Na_3PO_4, K_3PO_4, $NaNO_3$, HCl, and HNO_3 were ACS grade purchased from Fisher Scientific Company; the 3-aminopropyltriethoxysilane from PCR, Inc.; and the 3-chloro-2-hydroxytrimethylammonium chloride from Story Chemical Company. All porous silica glasses described were purchased from either Electro-Nucleonics or Sigma Chemical Company and the EM-Gel supports from Scientific Products Company. All support data are listed in Table I. Dextran standards were purchased from Pharmacia and poly(4-vinylpyridine) from Polysciences, Inc. The poly(2-vinylpyridine) standards were synthesized by Pressure Chemical Company. Poly(*N,N*-diallyldimethylammonium chloride) is a standard product of Calgon Corporation. The quaternized poly(4-vinylpyridine) and *N,N*-dimethylpiperidinium chloride were prepared at the Calgon Research Laboratories.

Procedure. The bare glass supports were activated at room temperature for 24 h in 6.0 N HCl, washed with deionized water, filtered, and dried (*9*). To 125 cm^3 of activated support was added 150 cm^3 of a 10% aqueous solution of 3-aminopropyltriethoxysilane. The solution was evacuated until the cessation of bubbling and placed in an oven at 75 °C for 2 h. After cooling, the silanized support was washed exhaustively with water on a Buchner funnel and dried in an oven for 12 h at 100 °C. The dried support was added to 400 cm^3 of a 5 wt % solution of 3-chloro-2-hydroxytrimethylammonium chloride and buffered at pH 7.4 by a standard phosphate buffer. This solution was held at 85 °C for 12 h and the quaternized support was filtered, washed with H_2O, and dried. The columns were prepared by standard dry packing techniques (*8*). Characterization of the glass after Step I of the reaction by elemental analysis showed that 95% of the surface had been covered. Upon completion of Step III, a quaternary ammonium titration indicated that 80% of the surface had been quaternized.

POLYMER CHARACTERIZATION

The anionically polymerized, isotactic poly(2-vinylpyridine) samples synthesized by Pressure Chemical Company were characterized in our laboratory. A Brice Phoenix Model 3200 Light Scattering Photometer was used to determine weight average molecular weights at 546 nm. The weight average molecular weights were determined in benzene at 25 °C from a Zimm plot using the angular dependence from 35° to 135°. The dn/dc value, measured with a Brice Phoenix Model 5000 refractometer at 546 nm, was found to be 0.075 mL/g. The number average molecular weights were determined in benzene at 25 °C with a Hewlett-Packard Model 502 membrane osmometer equipped with a nonaqueous membrane (18527A) and a nonaqueous capillary (18551A). All molecular weight data are listed in Table II.

Table II. Molecular Weights of Poly(2-vinylpyridine)

sample	$\bar{M}_w \times 10^4$	$\bar{M}_n \times 10^4$	$\bar{M}_w/\bar{M}_n$
PVP-2	3.1	2.9	1.07
PVP-3	9.2	8.9	1.04
PVP-4	46.0	44.0	1.05
PVP-5	23.0	20.0	1.15
PVP-6	2.2	2.0	1.10
PVP-7	60.0	5.2	1.15

Table III. Plate Counts

column	particle size, μm	flow rate, mL/min	initial count, plates/meter
700 Å CPG	39–75	1.12	1900
5000 Å EM-GEL	75–125	1.04	1150
1500 Å CPG	5–10	1.10	5180

RESULTS AND DISCUSSION

Quaternized supports were prepared from each of the porous substrates described in the Experimental section. The coating procedure appeared to work equally well for all of the supports as based on initial theoretical plate counts using *N,N*-dimethylpiperidinium chloride in the aqueous 0.1 N HNO_3 + 0.1 N $NaNO_3$ eluent. Examples of initial column plate counts are shown in Table III.

The different values of plate counts listed in Table III can be attributed to the different particle sizes (*10*). In all samples chromatographed on these columns, no peaks were noted after total penetration with the exception of an anion-exchange peak resulting from the polymer counterion. In the first 3 months of usage, all columns showed a decreased plate count followed by a leveling off value. For example, a column packed with quaternized CPG-75 and run at a flow rate of 1.08 mL/min exhibited plate counts/meter of 1680 initially, 790 after 3 months, and 780 after 9 months. The reason(s) for this decrease is currently under investigation.

The aqueous eluent chosen for use in this system was 0.1 N HNO_3 + 0.1 N $NaNO_3$. The acid was necessary to protonate the secondary amine functionality resulting from Reaction 3 and/or the residual primary amine group remaining due to any failure of Reaction 3 to go to completion. The highly acidic medium also tended to suppress the ionization of free silicon hydroxyl groups on the support surface which may have escaped silanization. A salt concentration of the order of 0.1 N or greater was necessary to reduce the polyelectrolyte effects (*12, 14*) exhibited by the highly-charged cationic polymers chromatographed on this system. The salt concentration was held at a minimum to prevent salting out of the polymeric solute (*15*) during chromatography.

Figures 1, 2, and 3 are chromatograms of a poly(2-vinylpyridine), a dextran, and a quaternized poly(4-vinylpyridine), showing some polymers which can be chromatographed on these supports. To determine whether these quaternized

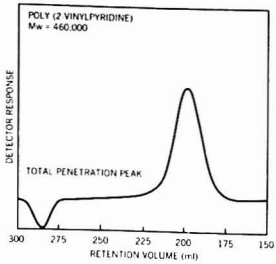

Figure 1. Chromatogram of a 460 000 mol wt poly(2-vinylpyridine) in 0.1 N HNO_3 + 0.1 N $NaNO_3$ on an 8-column set of quaternized supports varying in porosity from 75 to 25 000 Å. Flow rate = 2 mL/min

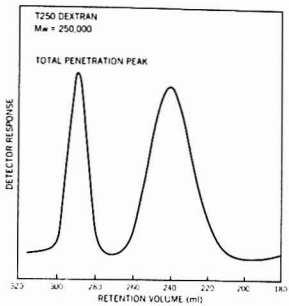

Figure 2. Chromatogram of a 250 000 mol wt dextran in 0.1 N HNO_3 + 0.1 N $NaNO_3$ on an 8-column set of quaternized supports varying in porosity from 170 to 25 000 Å. Flow rate = 2 mL/min

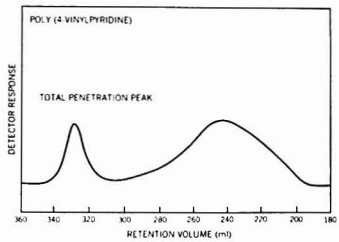

Figure 3. Chromatogram of a quaternized poly(4-vinylpyridine) in 0.1 N HNO_3 + 0.1 N $NaNO_3$ on a 10-column set of quaternized supports varying in porosity from 40 to 25 000 Å. Flow rate = 2 mL/min

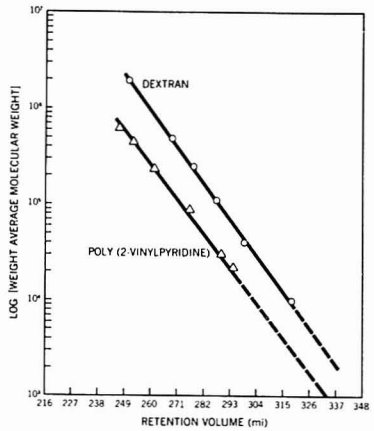

Figure 4. Calibration curves for poly(2-vinylpyridine) and dextran in 0.1 N HNO_3 + 0.1 N $NaNO_3$ on a 10-column set of quaternized supports varying in porosity from 40 to 25 000 Å. Flow rate = 2 mL/min

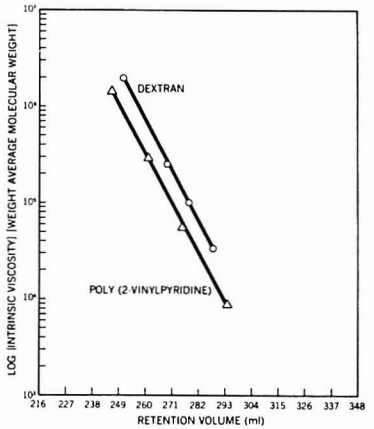

Figure 5. Log (hydrodynamic volume) vs. retention volume for poly(2-vinylpyridine) and dextran in 0.1 N HNO_3 + 0.1 N $NaNO_3$ on a 10-column set of quaternized supports varying in porosity from 40 to 25 000 Å. Flow rate = 2 mL/min

supports were operating by the exclusion mechanism, the series of narrow molecular weight distribution poly(2-vinylpyridine) samples and a series of dextran standards from Pharmacia (*16*) were chromatographed. Figure 4 is the plot of log (weight average molecular weight) vs. retention volume for these polymers. Both series gave a linear relationship with retention volume which was an indication that separation by size was occurring. As expected, the two calibration curves are parallel rather than superpositioned. Poly(2-vinylpyridine) is charged, leading to a more extended structure (*11*, *17–19*) in solution, whereas dextran would conform to a more compact structure. In other words, a particular molecular weight poly(2-vinylpyridine) eluted before the same molecular weight dextran.

Furthermore, a plot of the log (hydrodynamic volume) vs. retention volume for poly(2-vinylpyridine) and dextran does not superimpose as shown in Figure 5. If the universal calibration (*20*) is to hold for these polymers in this chromatographic system, the two lines should coincide. Since the lines are parallel, it can be concluded that the universal calibration does not hold for comparison of neutral to charged polymers. However, the validity of the concept has not been established when comparing polyelectrolyte to polyelectrolyte or neutral polymer to neutral polymer in this system.

The effectiveness of the coating procedure was determined by measuring theoretical plate height as a function of eluent velocity for a cationic polymer, poly(*N*,*N*-diallyldimethylammonium chloride), and monomer, *N*,*N*-dimethylpiperidinium chloride. Figure 6 is a plot of plate height vs. velocity for these species. In both cases, the plate height decreased with velocity obeying a typical plate height vs. velocity plot for polymer and monomer (*21*). Furthermore, the elution volumes of the polymer and monomer did not vary with velocity.

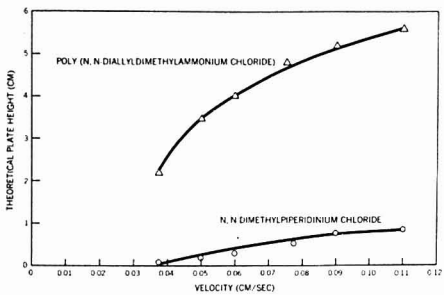

Figure 6. Plate height vs. velocity for poly(*N,N*-diallyldimethylammonium chloride) and *N,N*-dimethylpiperidinium chloride in 0.1 N HNO_3 + 0.1 N $NaNO_3$ on a 10-column set of quaternized supports varying in porosity from 40 to 25 000 Å

Table IV. Concentration vs. Retention Volume

Concn., wt %	retention volume, mL
0.1	270
0.2	272
0.3	271
0.4	270
0.5	271

The effect of polymer concentration on chromatographic behavior was determined by measuring the elution volumes and relative areas of a poly(*N,N*-diallyldimethylammonium chloride) sample over a range of concentrations. Figure 7 is a plot of relative area as a function of concentration and Table IV lists retention volume as a function of concentration. These data indicate that retention volume is independent of concentration up to 0.5 wt %. In addition, the detector response is linear with concentration up to ~0.3 wt %. Therefore, in a normal operating range, the chromatographic system is essentially independent of concentration. The reproducibility of the system was assessed by injecting a sample of poly(*N,N*-diallyldimethylammonium chloride) 5 times at 0.25 wt %. The total area and retention volume varied ±6% at the 95% confidence level.

The initial data obtained with these quaternized supports indicate that a variety of cationic and neutral polymers can be chromatographed on silica glass deactivated by converting it to an ion-exchange support. The size exclusion mechanism appears to work with minimal solute–substrate interaction. A number of authors (*11–13*) have stated that, since polyelectrolyte size is dependent upon salt concentration, the true molecular weight and molecular weight distribution must be carefully evaluated if determined from aqueous size exclusion chromatography. The ionic quaternary ammonium groups lining the pore surface may serve to significantly increase the ionic strength of the environment felt by a solute molecule as it enters a pore, particularly if it can come into intimate contact with the pore surface. The effect becomes more pronounced as the pore size decreases. The effect of ionic strength on elution, the chromatography of other cationic polyelectrolytes, and the range of application of the universal calibration need further investigation. It should also be

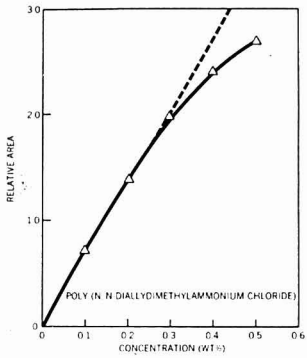

Figure 7. Relative area vs. concentration for poly(*N,N*-diallyldimethylammonium chloride) in 0.1 N HNO_3 + 0.1 N $NaNO_3$ on a 10-column set of quaternized supports varying in porosity from 40 to 25 000 Å. Flow rate = 2 mL/min

mentioned that although a broad range of pore sizes was used here, other authors (*22*) have shown this not to be the optimum case.

CONCULSIONS

In this paper, we have found that silica-based ion-exchange supports can be used for the size exclusion chromatography of cationic polyelectrolytes. After initial equilibration, these supports appear to be stable for several months in an acidic medium. For poly(2-vinylpyridine) and dextran molecules, the log molecular weight vs. retention volume relation appears to hold. This novel approach should be applicable to anionic polymers using a suitable cation-exchange support such as a sulfonic acid.

LITERATURE CITED

(1) J. C. Moore, *J. Polym. Sci., Part A*, **2**, 835 (1964).
(2) F. E. Regnier and R. Noel, *J. Chromatogr. Sci.*, **14**, 316 (1976).
(3) A. R. Cooper and D. P. Matzinger, *Am. Lab.*, **9**, 13 (1977).
(4) G. B. Butler, U.S. Patent 3,962,206, June 8, 1976.
(5) A. L. Spatorico, *J. Appl. Polym. Sci.*, **19**, 1601 (1975).
(6) A. L. Spatorico and G. L. Beyer, *J. Appl. Polym. Sci.*, **19**, 2933 (1975).
(7) C. P. Talley et al., U.S. Patent 4,118,316, October 3, 1978.
(8) M. Lynn and A. M. Filbert, in "Bonded Stationary Phases in Chromatography", E. Grushka, Ed., Ann Arbor Science Publishers, Ann Arbor, Mich., 1974, p 1.
(9) S. H. Chang and F. E. Regnier, U.S. Patent 4,029,583, June 14, 1977.
(10) J. C. Giddings and K. L. Mallik, *Anal. Chem.*, **38**, 997 (1966).
(11) T. K. Yamashita, *Polym. J.*, **4**, 262 (1973).
(12) B. Stenlund, *Adv. Chromatogr.* **14**, 37 (1976).
(13) K. G. Forss and B. G. Stenlund, *J. Polym. Sci., Polym. Symp.*, **42**, 951 (1973).
(14) J. C. Giddings, G. Lin, and M. N. Myers, *J. Liquid Chromatogr.*, **87 1**, 1 (1978).
(15) S. Fundano and K. Konishi, *J. Chromatogr.*, **87**, 117 (1973).
(16) Pharmacia Fine Chemicals, Product Bulletin, August 1971, p 14.
(17) A. J. Hyde and R. B. Taylor, *Polymer*, **4**, 1 (1963).
(18) K. Matsuzaki, T. Matsubara, and T. Kanai, *J. Polym. Sci., Polym. Chem. Ed.*, **15**, 1573 (1977).
(19) S. Arichi, *Bull. Chem. Soc. Jpn.*, **41**, 548 (1968).
(20) H. Benoit, Z. Grubisic, P. Rempp, D. Decker, and J. G. Zilliox, *J. Chim. Phys.*, **63**, 1507 (1966).
(21) J. C. Giddings, L. M. Bowman, and M. N. Myers, *Anal. Chem.*, **49**, 243 (1977).
(22) W. M. Yau, C. R. Ginnard, and J. J. Kirkland, *J. Chromatogr.*, **149**, 465 (1978).

RECEIVED for review February 5, 1979. Accepted August 15, 1979.

Electrochemical Studies of the Oxidation Pathways of Apomorphine

H.-Y. Cheng, E. Strope, and R. N. Adams*

Department of Chemistry, University of Kansas, Lawrence, Kansas 66045

The oxidative reaction mechanisms of apomorphine in aqueous buffer are reported, based on electrochemical data and product analysis. In the absence of strong nucleophiles, an irreversible chemical reaction follows the initial $2e^-/2H^+$ oxidation of apomorphine and eventually produces a new redox couple. This new redox couple adsorbs irreversibly on the Nujol-carbon paste electrode surface and exhibits properties of electrocatalysis on the oxidation of ascorbic acid. In the presence of excess glutathione, a strong nucleophile, other reactions predominate.

Apomorphine (I) was synthesized from naturally occurring morphine over a century ago and was soon recognized for its powerful emetic effect in animals and humans (*1*, *2*).

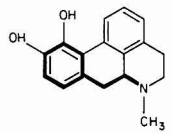

I, APM

Recently a number of research developments, mainly the work on dopamine which led to the introduction of treatment for Parkinson's disease, have caused a great deal of interest in this compound (*3*). The dopamine backbone may be traced in the structure (heavier lines, structure I), and it is thought to derive its pharmacological activity from this sub-structure.

Aqueous solutions of apomorphine rapidly undergo spontaneous oxidative decomposition and turn green. This process is accelerated by oxygen and high pH, but little is known of its mechanism. There have been conflicting reports on the qualitative and quantitative changes of pharmacological activity by the development of color in old solutions (*4*, *5*). The chemical identity of the oxidation products has been studied by several workers (*6–8*). The oxidation of aqueous solutions of apomorphine with O_2 or $HgCl_2$ at about neutral pH all resulted in a similar product. Structure II was postulated, based on spectroscopic data of UV-vis, IR, NMR, and mass spectrometry. These workers also found that at higher pH (*10–14*), various other products were formed.

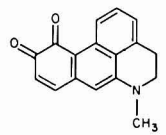

II, oxo-APM

No work has been reported on the electrochemistry of apomorphine. This study investigates the redox behavior of apomorphine in aqueous solutions of near physiological pH with an underlying intention of better understanding its biological interactions in brain. Major efforts are on the elucidation of the reaction mechanism, the identification of products, and the probing of interactions between a reactive intermediate and glutathione. Preliminary results on the electrochemistry of an irreversibly adsorbed product on the Nujol-carbon paste electrode are also included.

EXPERIMENTAL

Instrumentation. Cyclic voltammograms of moderate scan rate were obtained using the Princeton Applied Research (PAR) model 174 polarographic analyzer and a Houston Omnigraphic X-Y recorder. Coulometry and bulk electrolysis were performed utilizing the PAR model 173 polarographic analyzer equipped with a model 179 digital coulometer. A home-built potentiostat interfaced to the Hewlett-Packard 2100A minicomputer was employed for fast electrochemical experiments and thin-layer coulometry.

A Cary 14 spectrophotometer was used to obtain UV-visible spectra.

Electrodes and Cells. Cyclic voltammetry was run on the conventional Nujol–graphite (30/70 w/w) paste electrode with a surface area of ~2 mm^2. Unless otherwise specified, the electrode was freshly packed for each cyclic voltammetric run to minimize the undesirable electrochemical signals which arise from surface-adsorbed species. Bulk electrolysis utilized either the platinum gauze or carbon cloth electrode. The hanging mercury drop electrode (HMDE) was used in the fast cyclic voltammetric experiment to estimate the rate of the follow-up reaction. The reference electrode was a SCE and the auxiliary electrode was a piece of platinum wire.

Thin-layer coulometric experiments were done in a cell fashioned from a 10-mL beaker and two $1 \times 1 \times {}^1/_{10}$ inch quartz plates. A $1{}^1/_2 \times {}^3/_{16}$ inch length of Au grid (100 lines/inch), positioned between the quartz slides, serves as the working electrode. This cell is basically the same design as Heineman's thin-layer electrode; detailed procedures for cell construction are available (*9*). The volume of solution around the Au grid was calibrated with standard solutions of 4-methylcatechol in pH 6.0 buffer and with solutions of hydroquinone in 0.1 N H_2SO_4.

Chemicals. Apomorphine was obtained from Mallinckrodt as the hydrochloride (USP) and was used without further purification. Glutathione, in reduced form, was purchased from Sigma. All other chemicals were reagent grade and were used as received.

Oxidation Product. Several bulk electrolysis experiments of apomorphine in pH 6.0 or 7.4 McIlvaine buffer were done to obtain enough electrochemical oxidation product. The potential was set at 0.6 V vs. SCE and the electrolysis was interrupted several times to allow the blue-green product covering the Pt gauze electrode to be washed off with $CHCl_3$. The crude extract was washed with 0.5 M HCl and filtered to remove traces of H_2O, then evaporated down on a rotary evaporator. The yields of crude oxidation product from these electrolyses varied from 24% to 55%, with pH 6.0 solutions giving higher yields. The crude electrolysis product was recrystallized from hot benzene. Thin-layer chromatography was used to check for purity. Elemental analysis was performed by Micro-Tech Laboratories.

RESULTS AND DISCUSSION

Reaction Mechanism. Figure 1 is a cyclic voltammogram of apomorphine in phosphate buffer at pH 7.4. Two anodic

0003-2700/79/0351-2243$01.00/0

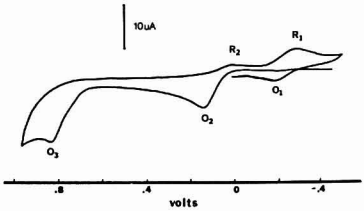

Figure 1. Cyclic voltammetry of apomorphine in pH 7.4 phosphate buffer. Scan rate, 3 V/min; [APM] $\simeq 10^{-3}$ M. Applied potential vs. SCE

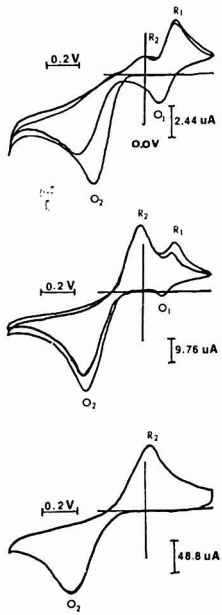

Figure 2. Fast scan cyclic voltammetry of $\sim 10^{-3}$ M apomorphine in pH 6.0 buffer. Scan rates, from top to bottom: 5 V/min, 100 V/min, 1000 V/min

waves (O_2,O_3) appear at +0.15 and +0.82 V vs. SCE, respectively, on the first scan in the positive direction. Upon scan reversal, only one corresponding reduction peak (R_2) is visible, while a new redox couple (O_1,R_1) appears at −0.2 V on subsequent scans. The ratios of R_2/O_2 and R_1/O_1 depend greatly on scan rates, as shown in Figure 2, indicating a rate-limiting chemical reaction following the initial oxidation. The formation of the follow-up product, R_1, which appears at less positive potential than its parent compound, can be eliminated by scanning at 1000 V/min in a pH 6 solution. The rate of this follow-up reaction is also pH-dependent, as evidenced by the gradual disappearance of R_1/O_1 in more acidic solutions. In acid solution (see, for example, Figure 3a, run in 1.2 M HCl), there is no sign of follow-up reactions.

The voltammetric peak O_3 (see Figure 1) starts to merge into background as the scan rate increases to greater than 6 V/min or at pH below 6, making electrochemical investigation difficult. However, within the limited window of available experimental manipulation, one can correlate the magnitude

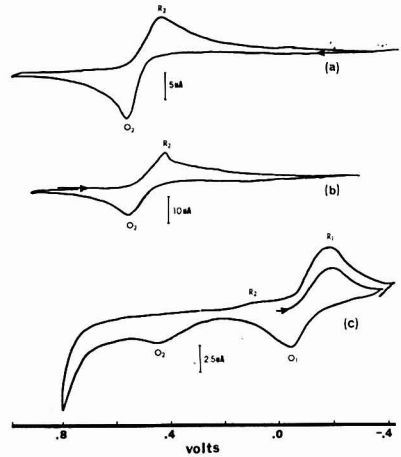

Figure 3. Fate of oxidized apomorphine at pH 4.5. Cyclic voltammograms were taken: (a) Before electrolysis, 4.37 mg apomorphine-HCl in 10 mL 1.2 M HCl. (b) After 2 e^- electrolysis, oxidized apomorphine in 1.2 M HCl. (c) Immediately after adequate amount of buffer was added to allow the pH to reach 4.5. 1:1 ratio of apomorphine:oxo-apomorphine

of O_3 with the production of the peaks O_1/R_1, particularly in the presence of external nucleophiles. This will be discussed in detail later.

The redox potential of apomorphine shifts toward more positive direction as the solution becomes more acidic. Both anodic and cathodic peak potentials show E_p vs. pH variations with linear slopes of −75 mV/pH and −61 mV/pH, respectively, in the pH range 2–6. In spite of the serious distortion of the voltammetric peak due to absorption occurring at the carbon paste electrode, one can safely assume a 2-electron–2-proton process for the initial oxidation of apomorphine. The peak separation between O_1 and O_2 is approximately 300 mV and remains constant at this pH region.

Coulometric experiments utilizing a precalibrated thin-layer cell were run on solutions of apomorphine in 0.1 N H_2SO_4, and 2.07 ± 3% electrons/molecule was obtained for the initial oxidation process. The resulting solution was yellowish brown.

The electrolysis of apomorphine in 1.2 M HCl was stopped after 2 electrons per molecule had passed into the solution. An adequate amount of buffer was then added to the remaining yellowish brown solution to allow the pH to reach about 4.5. The solution very quickly turned bluish green, resembling the color developed in old solutions of apomorphine. Figure 3 shows the cyclic voltammograms taken before the electrolysis, after the electrolysis, and after the buffer was added. Notice that the initial potentials and scan directions are different in Figure 3a, b, and c. It is concluded that at higher pH 1 mol of the oxidized apomorphine (Figure 3b) will rapidly product $^1/_2$ mol of the reduced APM and $^1/_2$ mol of the final product. (In Figure 3c, O_2 corresponds to the oxidation of the reduced APM and R_1 corresponds to the reduction of the final product.) The drawn-out voltammetric peaks and slightly larger than 1:1 ratio of O_1:O_2 are the consequence of strong adsorption of the final product on the electrode.

Identification of this electrochemical oxidation product in neutral pH solution was carried out as follows: apomorphine (11–16 mM) was electrolyzed in pH 6 or 7.4 buffer using a Pt gauze electrode. The blue-green oxidation product, adsorbed

on the electrode surface, was washed off with $CHCl_3$ and recrystallized from hot benzene. This product exhibited the same voltammetric behavior and adsorption pattern as the redox couple O_1/R_1. The UV-visible spectrum in isoamyl acetate was identical with that of the chemical oxidation product (II), oxo-APM (*6*). Elemental analysis of this dark purple electrochemical oxidation product yielded the following data: Calculated: C, 77.53; H, 4.98; N, 5.32; O, 12.16. Found: C, 77.66; H, 4.77; N, 5.23; O, 12.33. Calculation based on molecular formula ($C_{17}H_{13}NO_2$).

A plausible mechanism can thus be concluded based on the positive identification on oxo-APM as the final product. An

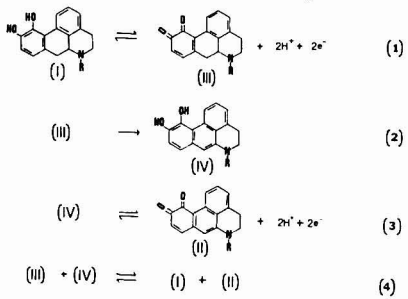

initial $2e^-/2H^+$ oxidation of apomorphine (I) to *o*-quinone (III) (reaction 1) is followed by a rate-limiting chemical reaction 2. The product IV, which is easier to oxidize than I, can either oxidize directly at the electrode (reaction 3) or react with III to form the final product II, oxo-apomorphine. The redox potential of oxo-APM is about 300 mV more negative than that of APM, therefore one would expect reaction 4 to favor the direction of products. Owing to complications arising from the electrode adsorption process, electrochemical kinetic data are not sufficient to determine the nature of reaction 2. However, a rough estimation of the half-life of III was done by fast scan cyclic voltammetry utilizing a hanging mercury drop electrode. Assuming an irreversible first-order reaction, a rate constant of 1.6 s^{-1} for reaction 2 was obtained in pH 7.4 phosphate buffer of 0.5 mM apomorphine solution. The measurements were made at two different scan rates (30 and 10 V/min).

Interaction with Glutathione. Voltammetric peaks O_3 and O_1/R_1 can be eliminated by adding excess nucleophiles such as glutathione (GSH) to the solutions. As shown in Figure 4, in the presence of 1 mM GSH there is no appreciable change from that of Figure 1, while 5 mM GSH wiped out all peaks except O_2. No reducible species can be detected in the time scale of medium scan rate cyclic voltammetry (60 V/min). The unusually sharp peaks and the shifting of the peak positions are believed to result from adsorption of products and extensive filming on the electrode surface. Evidently, GSH reacts with the initial oxidation product III irreversibly, and this reaction competes with reaction 2 to form products which are not reducible or oxidizable at this potential range. The identities of these products are yet to be determined.

Glutathione was used previously as a model nucleophile to illustrate potentially neurotoxic actions of the important drug 6-hydroxydopamine. It was shown that when 6-hydroxydopamine was injected into brain tissue, an appreciable percentage was quickly oxidized to the 6-hydroxydopamine quinone (6-Q) and the latter underwent rapid nucleophilic interaction with brain constituents (*10, 11*). The second-order rate constant for the reaction between 6-Q and GSH was 22.5 M^{-1} s^{-1} at pH 7.4 and in the presence of 5 mM GSH, the pseudo first-order rate constant would be 0.11 s^{-1} (*12*). Note

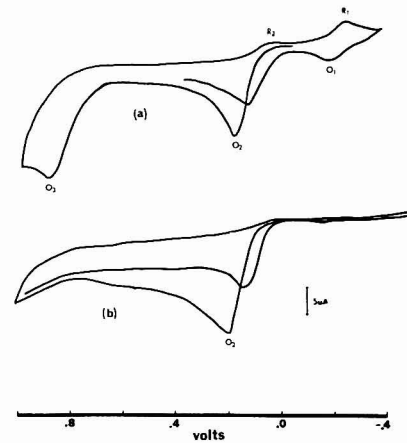

Figure 4. Interaction of oxidized apomorphine with glutathione. Apomorphine ~1 × 10^{-3} M in pH 7.4 phosphate buffer, scan rate 3 V/min. Glutathione concentrations: (a) 1.0 × 10^{-3} M; (b) 5.0 × 10^{-3} M

that in Figure 4b the reaction of GSH with oxidized APM is faster than the rearrangement of reaction 2; this reaction has an estimated rate constant of 1.6 s^{-1}. Under these experimental conditions, interaction between GSH and oxidized APM is much faster than that between GSH and 6-Q.

Since APM is a widely used pharmacological agent in small animal studies, we were concerned that it also might act as a neurotoxin via the above rapid nucleophilic interaction of its oxidized form with thiol constituents of brain tissue. Fortunately, however, APM is sufficiently more difficult to oxidize at pH 7.4 ($E^{0\prime}$ ~ +0.2 V vs. SCE) in comparison to 6-hydroxydopamine (+0.08 V vs. SCE) that little or no oxidized APM is formed in the brain redox environment and hence neurotoxic actions similar to those of 6-hydroxydopamine are quite unlikely.

Adsorption on Electrode Surfaces. The new redox couple (R_1/O_1), structures II and IV, formed during the cyclic voltammetry potential sweep of apomorphine solution, adsorbs irreversibly and tenaciously on the Nujol/carbon paste electrode. The filmed electrode has interesting characteristics as a "chemically modified" surface as depicted in Figure 5. A cyclic voltammogram of apomorphine is shown in Figure 5a. If the positive scan does not go over +0.8 V, the adsorption peaks at −0.2 V grow as the follow-up reaction proceeds, while the oxidation peak of apomorphine remains approximately the same for subsequent scans. The electrode can now be taken out of the solution, washed with distilled water, and put into fresh buffer containing no apomorphine; the new redox couple is still evident, while the initial redox couple (R_2/O_2) is absent (Figure 5b). This surface-modified electrode can now be inserted in solutions of other redox components to see if their redox reactions are affected by the surface modification. Figure 5d demonstrates a case of electrocatalysis of ascorbic acid by this "chemically modified" electrode. The peak potential of ascorbate oxidation shifted about 350 mV more negative than that at a bare carbon paste electrode (Figure 5c), while the redox couple corresponding to the adsorbed species was virtually unchanged. The surface-modified electrode can partially differentiate dopamine from ascorbate in linear sweep voltammetry in vitro. Interestingly enough, the oxo-apomorphine-adsorbed electrode did not alter volt-

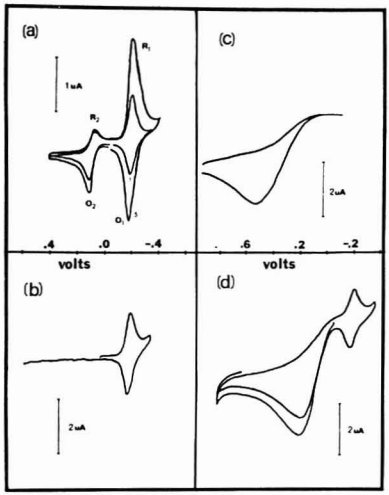

Figure 5. Oxo-apomorphine-modified carbon paste electrode. Buffer, pH 6.8 phosphate; scan rate, 3 V/min. (a) Fresh carbon paste electrode after 1st and 5th scans, immersed in 1×10^{-4} M apomorphine; (b) "chemically modified" electrode immersed in buffer only; (c) fresh carbon paste electrode immersed in 1×10^{-3} M ascorbic acid; (d) "chemically modified" electrode, as in (b), immersed in 1×10^{-3} M ascorbic acid

ammetric characteristics of species such as dopamine and NADH at pH 7.

Anson and co-workers have recently reported the electrochemistry of the surface-adsorbed 9,10-phenanthroquinone electrode (*13*, *14*); their surface-modified electrode is intended for electrocatalysis of solution species. The oxidation peak potential of 9,10-dihydroxyphenanthrene at pH 6.9 phosphate buffer is −0.20 V, very close to that of (O_1). Closer examination of the structure of oxo-APM (structure II) revealed that the 3,4-phenanthroquinone substructure of II could be responsible for the adsorption process. Desorption occurred at +0.83 V vs. SCE in pH 7.4 solution and yielded a well-defined peak. This voltammetric peak was assigned as O_3 in Figure 1. The nature of the desorption process is not clear; however, O_3 can probably be correlated with further oxidation of oxo-APM.

Kuwana et al. have demonstrated that quinones chemically attached to graphite surfaces can catalyze oxidation of ascorbic acid and NADH in solutions (*15*, *16*), and have suggested a surface E–C catalytic mechanism. The thermodynamic requirement for such a mechanism is that the reversible redox potential of either ascorbic acid or NADH be less positive than that of the surface attached species. Current findings of the "oxo-apomorphine-adsorbed" electrode catalyses do not fit this picture, since oxo-APM oxidizes at less positive potential than ascorbic acid.

Continuing investigation of the electrochemistry of surface-adsorbed oxo-apomorphine can be very beneficial for studies involving chemically modified electrodes. First, the amount to be adsorbed on the electrode surface can be well controlled by manipulating the rate of the follow-up reaction and electrolysis time. Second, the comparisons of electrochemical behavior of different surface-adsorbed species with various arrangements of quinoidal functions may reveal structure-conformation dependence of electrocatalysis. Third, this chemically modified electrode can partially differentiate dopamine and ascorbate electrochemically. Lane and Hubbard have reported an iodine-treated Pt electrode for in vivo detection of ascorbic acid and dopamine in rat brain (*17*, *18*). Their electrode suffered from instability which did not allow quantitative information to be obtained. The oxo-apomorphine-adsorbed carbon paste electrode is quite stable in solutions and may have important applications for in vivo electrochemistry.

LITERATURE CITED

(1) A. Matthiessen and C. R. A. Wright, *Anal. Chem.*, Suppl. 7, 170 (1870).
(2) E. L. Mayer, *Chem. Ber.*, **4**, 121 (1871).
(3) T. L. Sourkes and S. Lal, in "Advances in Neurochemistry", Vol. 1, B. W. Agranoff and M. H. Aprison, Eds., Plenum, New York, 1975.
(4) J. E. Gorrell and P. L. Gray, *Proc. Soc. Exptl. Biol. Med.*, **25**, 619 (1928).
(5) A. M. Burkman, *J. Pharm. Pharmacol.*, **15**, 461 (1963).
(6) H. H. A. Linde and M. S. Ragab, *Helv. Chim. Acta*, **51**, 638 (1968).
(7) J. H. Preininger, Jr., Z. Samek, and F. Santavý, *Arch. Pharm.*, **302**, 808 (1969).
(8) K. Rehse, *Arch. Pharm.*, **302**, 487 (1969).
(9) W. R. Heineman, B. J. Norris, and J. F. Goetz, *Anal. Chem.*, **47**, 79 (1975).
(10) Y.-O. Liang, R. M. Wightman, P. Plotsky, and R. N. Adams, in "Chemical Tools in Catecholamine Research", Vol. I, G. Jonsson, T. Malmfors, and Ch. Sachs, Eds., North-Holland Publishing Co., Amsterdam, 1975.
(11) Y.-O. Liang, P. M. Plotsky, and R. N. Adams, *J. Med. Chem.*, **20**, 581 (1977).
(12) Y.-O. Liang, Ph.D. Dissertation, University of Kansas, 1977, p 48.
(13) A. P. Brown, C. Koval, and F. C. Anson, *J. Electroanal. Chem.*, **72**, 379 (1976).
(14) A. P. Brown and F. C. Anson, *J. Electroanal. Chem.*, **92**, 133 (1978).
(15) J. F. Evans and T. Kuwana, *J. Electroanal. Chem.*, **80**, 409 (1977).
(16) D. C.-S. Tse and T. Kuwana, *Anal. Chem.*, **50**, 1315 (1976).
(17) R. F. Lane and A. T. Hubbard, *Anal. Chem.*, **48**, 1287 (1976).
(18) R. F. Lane, A. T. Hubbard, K. Fukunaga, and R. J. Blanchard, *Brain Res.*, **114**, 346 (1976).

RECEIVED for review July 5, 1979. Accepted September 4, 1979. The support of the National Science Foundation via Grant CHE77-11855 and the National Institutes of Health via Grant RO1 NS08740 is gratefully acknowledged.

Determination of Urinary Ammonia by Osmometry

Man S. Oh,* Kenneth R. Phelps, Ruth L. Lieberman, and Hugh J. Carroll

Department of Medicine, State University of New York, Downstate Medical Center, Brooklyn, New York 11203

Osmometry replaces the cumbersome titration technique in this new, accurate, and simple method for measuring urinary ammonia. Ammonia liberated from urine by addition of saturated K_2CO_3 is trapped as $(NH_4)_2SO_4$ in 0.3 N H_2SO_4 through an aeration train. One milliliter of 0.4 N NaOH is added to 1 mL of the trapping solution and the osmolality of the mixture is measured. Sufficient NaOH is present in the mixture to titrate completely H_2SO_4 and $(NH_4)_2SO_4$ to Na_2SO_4 and NH_3. Since NH_3 remains in solution unless it is agitated vigorously, the osmolality of this solution is greater, by the quantity of ammonia trapped, than the osmolality of a blank consisting of a mixture of the H_2SO_4 and NaOH.

The technique of osmometry lends itself to the measurement of the concentration of any chemical substance which can be caused to alter the osmolality of a given solution. We have previously described a simple and accurate method for the measurement of total CO_2 concentration in biological fluids. In that system CO_2 is trapped in a solution of NaOH, the osmolality of which is lowered in proportion to the quantity of CO_2 trapped (*1*). Among the methods commonly used for measurement of urinary NH_3 (*2–6*) are titration technics, which require alkalinization of the sample, trapping of NH_3 in acid either by aeration (*2*) or by microdiffusion (*3*), and finally back-titration of the trapping solution. The principle of the technique described here is that NH_3 trapped by an acid solution as NH_4^+ and converted back to NH_3 by addition of strong alkali, remains in solution and is readily measured as an osmotically active substance.

EXPERIMENTAL

An aeration train driven by vacuum draws air in series through a solution of 1.0 N H_2SO_4, the urine sample, and the trapping solution of 0.3 N H_2SO_4. Multiple sets of sample tubes and tubes containing trapping solution can be placed in series between the vacuum line and the first trapping solution (Figure 1). The 1.0 N H_2SO_4 traps NH_3 contained in atmospheric air before the air passes through the urine sample. A drop of antifoam is added to the urine sample before the sample tube is closed with its rubber stopper. Saturated K_2CO_3 is then added to the urine sample through a needle piercing the stopper, and the vacuum line is opened. The NH_3 formed in the alkalinized urine is driven off by vigorous aeration and is carried into the tube containing 0.3 N H_2SO_4, H_2SO_4, where it is trapped as $(NH_4)_2SO_4$. When liberation and trapping of ammonia are complete, after 10–15 min of vigorous airflow, 1 mL of trapping solution is withdrawn and mixed with 1 mL of 0.4 N NaOH in an osmometer tube (a). In a separate osmometer tube (b), 1 mL of the same NaOH solution is mixed with 1 mL of the blank trapping solution (0.3 N H_2SO_4). The osmolalities of tubes a and b are determined.

The reaction in tube a is:

$$H_2SO_4 + (NH_4)_2SO_4 + \text{excess NaOH} \rightarrow Na_2SO_4 + NaOH + NH_3$$

The reaction in tube b is:

$$H_2SO_4 + \text{excess NaOH} \rightarrow Na_2SO_4 + NaOH$$

The excess NaOH is sufficient for complete titration of NH_4^+ to NH_3, and unless the tube is vigorously agitated, the loss of NH_3 between mixing of the solution and measurement of osmolality is negligible. The difference in osmolality between tubes a and b is equal to the concentration of NH_3 in tube a. Since osmolality of the tube b is relatively constant over a few days, one value can be used for the measurement of NH_3 in multiple urine samples. With time, however, exposure of the stock NaOH solution to the atmosphere leads to trapping of CO_2 as Na_2CO_3 and lowering of the osmolality, so that tube b should be prepared and its osmolality determined every few days.

The concentration of NH_3 in the original sample of urine is calculated as:

$$NH_3(\text{mmol/L}) = \frac{V_2}{V_1} \times 2 \times \Delta\text{Osm (mOsm/L)}$$

where V_1 and V_2 are the volumes of the urine sample and the trapping solution, and ΔOsm is the difference in osmolality between tubes a and b. The factor 2 reflects dilution of NH_3 concentration upon mixing of H_2SO_4 trapping solution with NH_3 solution.

The technique was applied to the measurement of standard solutions made from dried $(NH_4)_2SO_4$, and also to measurement of recovery of standard solutions from different urine samples. To determine the specificity of the technique, the results by osmometric measurement of NH_3 concentration of a known standard and 5 urine samples were compared to those measured by titration. In the latter method, H_2SO_4 solution containing trapped NH_4^+ was titrated, using a pH meter, with a standard solution of NaOH to an end point of pH 6.5. NH_3 concentration then was calculated from the normality of the H_2SO_4 solution before the trapping of NH_3 and the quantity of NaOH required to titrate H_2SO_4 after trapping NH_3.

Osmolality was measured with an Advanced Osmometer (Advanced Instrument, Inc., Newton Highlands, Mass. 02161) and titration was carried out with a Beckman Expandomatic SS-2 pH meter (Beckman Instruments, Inc., Fullerton, Calif. 92634).

Table I. Recovery of NH_3 from Urine Samples

sample no.	expected, mmol/L	recovery, mmol/L	% recovered
1	58.3	57.3	98.3
2	60.7	57.6	94.9
3	85.5	85.9	100.5
4	122.5	125.0	102.0
5	70.8	70.3	99.3
6	70.8	73.1	103.2
7	70.0	74.6	106.4
8	70.0	73.1	104.4
9	70.0	73.6	105.1
			101.5 mean
			1.2 SEM

RESULTS

The measured concentration of NH_3 in standard solutions agreed well with predicted values, with a correlation coefficient of 0.99.

The average recovery of NH_3 from 9 urine samples was 101.5 ± 1.2 (Table I). Results of osmometric determinations and of titrations were in close agreement (Table II). This indicates that negligible loss of NH_3 occurred between the mixing of NaOH solutions with trapping solutions and the measurement of osmolality. It also appears that NH_3 was the only substance

0003-2700/79/0351-2247$01.00/0

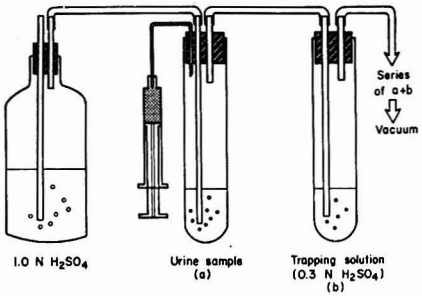

Figure 1. Schematic diagram of the aeration train. The syringe attached to the sample tube contains saturated K_2CO_3, which is to be injected into the sample

Table II. Comparison of Titration Technique to Osmometric Technique

sample no.[a]	osmometric technique, mmol/L	titration technique, mmol/L
1	57.6	58.5
2	29.5	27.9
3	36.8	35.9
4	8.0	6.0
5	23.7	23.9
6	35.5	33.0

[a] No. 1 is an ammonia standard at 57.5 mmol/L. Nos. 2 to 6 are samples of urine.

extracted from urine and trapped in H_2SO_4 in significant quantities.

DISCUSSION

NH_3 formed by the alkalinization of the trapping solution is not readily released into the environment, presumably because of its extraordinarily high solubility coefficient; 10 to 15 min of vigorous aeration are required to drive NH_3 from alkalinized urine. The agreement between the osmometric method and the titration method (Table II) proves that NH_3 loss prior to the measurement of osmolality is negligible.

The concentration of H_2SO_4 and NaOH need not be exact, provided that NaOH is present in excess when the two solutions are mixed; NH_4^+ is completely converted to NH_3 when the solution pH is 12 or greater. The quantity of ammonia that can be trapped is limited by the concentration of H_2SO_4; for a solution of 0.3 N H_2SO_4 the maximal concentration of NH_3 in the solution will be 300 mmol/L. For urine containing higher concentrations of NH_3, smaller volumes of urine or larger volumes of trapping solution can be used. It is also possible to use trapping solutions with a greater acid concentration and proportionally greater concentrations of NaOH, provided that the final osmolality of the mixture of the trapping solution and NaOH is within the range of the osmometer. If the concentration of NH_3 in the urine is very low, the use of a larger volume of urine will enhance the accuracy of the technique. Vigorous aeration is very important in ensuring complete recovery of NH_3 within a given time period; incomplete recovery of NH_3 results from insufficient release of NH_3 from the alkalinized sample rather than from incomplete trapping in the H_2SO_4 solution. However, overly vigorous aeration may cause the H_2SO_4 solution to coat the sides of the tube, and a spuriously high NH_3 concentration may be obtained. This difficulty may be obviated by the use of tubes of larger diameter for trapping and also by inversion of the tube at the end of trapping to allow complete mixing of the H_2SO_4 solution. By using test tubes of 2.3-cm diameter, complete release and trapping of NH_3 was possible in 10–15 min of aeration, whereas 20–30 min of aeration were needed with tubes of 1.5-cm diameter.

Cunarro et al. concluded that the ammonia electrode provides the most accurate and rapid determination of urinary ammonia concentration (*6*). However, potential disadvantages of the ammonia electrode include its expense and short life span (average, 3 months). These disadvantages make the electrode method primarily suitable for laboratories doing large numbers of determinations. If an osmometer is available, ordinary laboratory supplies can be utilized to complete the aeration for the method described herein. The method is technically simple and rapid. The ease with which ammonia can be extracted and trapped and the precision of osmometry provide for accurate results.

LITERATURE CITED

(1) Oh, Man S.; Whang, Edmund M. S.; Carroll, Hugh J. *Kidney Int.* **1975**, *8*, 56–59.
(2) Sobel, Albert E.; Hirschman, Albert; Besman, Lottie. *Ind. Eng. Chem.* **1947**, *49*, 927–929.
(3) Conway, E. J.; O'Malley, E. *Biochem. J.* **1942**, *36*, 655–661.
(4) Jorgensen, K. *Scan. J. Clin. Lab. Invest.* **1957**, *9*, 287–291.
(5) Wilcox, Alan A.; Carroll, Wallace E.; Sterling, Rex E. *Clin. Chem.* **1966**, *12*, 151–157.
(6) Cunarro, Julia A.; Weiner, Michael W. *Kidney Int.* **1974**, *5*, 303–305.

RECEIVED for review July 9, 1979. Accepted September 4, 1979.

Ligand Exchange Chromatography of Alkyl Phenyl Sulfides

Vaclav Horak,* Mercedes De Valle Guzman, and George Weeks

Department of Chemistry, Georgetown University, Washington, D.C. 20057

Chromatographic behavior of eight alkyl phenyl sulfides (R–S–Ph; R = Me, Et, Pr, *i*-Pr, Bu, *sec*-Bu, *i*-Bu, and *t*-Bu) was examined using Hg^{2+}, Ag^+, Cd^{2+}, and Pb^{2+} impregnated silica gel plates. Very efficient separation was achieved with Hg^{2+} and Ag^+ ions in solvents of medium polarity (chloroform, ethyl acetate). The contribution of polar (σ^*), molecular weight (MW), and steric effects E_S to R_M values was determined. For Hg^{2+} and Ag^+ impregnated plates, respectively, the following equations were calculated:

$$R_{M(Hg^{2+})} = -1.933\sigma^* - 0.0061\ MW + 0.077\ E_S + 0.679$$

$$R_{M(Ag^+)} = -2.397\sigma^* - 0.0077\ MW + 0.156\ E_S + 1.152$$

Recently, numerous selective separations have been achieved with compounds carrying either π- or n-electrons using ligand exchange chromatography. Chromatographic separations of organic sulfides on stationary phases with anchored Hg^{II} (*1*, *2*), Zn^{II} (*3*), and Cu^{II} (*4*) have been reported in the literature. For some of the chromatographic systems

0003-2700/79/0351-2248$01.00/0

Table I. Physical Constants of Alkyl Phenyl Sulfides

R-S-Ph, R =	bp/50 mm, °C	n_D^{20}
(1) methyl[a]	-	1.5852
(2) ethyl	100	1.5660
(3) *n*-propyl	120	1.5563
(4) isopropyl	108-114	1.5488
(5) *n*-butyl	155	1.5472
(6) *tert*-butyl	117	1.5293
(7) *sec*-butyl	136-137	1.5440
(8) isobutyl	141	1.5483

[a] Methyl phenyl sulfide (thioanisole) was supplied by Aldrich Chemical Co. (99% purity and bp 188 °C).

the retention of sulfides was so strong that sulfides were recovered (*2, 4*) by backwashing. Earlier, one of us reported on studies of nonchromatographic partition of sulfides between a saturated mercuric acetate solution in aqueous acetic acid and *n*-heptane (*5*). Whereas all of the reported methods offered some practical applications, the last reference included structure vs. partition coefficient relationship study as well.

The study reported in this paper is a continuation of our investigations of properties and separation of organic sulfides such as the study mentioned above and similar investigations (*6, 7*) (reviewed in (*8*)). The present ligand exchange chromatographic study involves eight alkyl phenyl sulfides serving as electron donors (Ph-S-R: 1, R = Me; 2, R = Et; 3, R = Pr; 4, R = *i*-Pr; 5, R = Bu; 6, R = *t*-Bu; 7, R = *sec*-Bu; 8, R = *i*-Bu) and four cations Hg^{II}, Ag^{I}, Cd^{II}, and Pb^{II} serving as electron acceptors. The selected ions represent both strong and weak acceptors with respect to the sulfide ligand allowing searching for selective chromatographic system. The sulfide series allows for examination of structural effects controlling the ligand strength and, thus, the chromatographic process as well.

EXPERIMENTAL

Apparatus. Refractive indexes were determined with a Bausch & Lomb Abbe type refractometer and the values were corrected to 20 °C (0.00045/°C). Ultraviolet spectra were recorded with a Cary 15 spectrophotometer using hexane as the solvent.

Chemicals. The following chemicals were used: thiophenol (97%, Aldrich Chemical Co.); bromoethane (98%, Aldrich Chemical Co.); 1-bromopropane (Matheson, Coleman and Bell); 2-bromopropane (Aldrich Chemical Co.); 1-bromobutane (97%, Aldrich Chemical Co.); 2-bromobutane (98%, Aldrich Chemical Co.); 1-bromo-2-methylpropane (Aldrich Chemical Co.); isobutylene (certified purity, Matheson Gas Products); silica gel 7GF (Baker TLC reagent, J. T. Baker Chemical Co.); mercury acetate (98.8%, Fisher Scientific Co.); cadmium acetate dihydrate (Baker analyzed reagent, J. T. Baker Chemical Co.); silver nitrate (99.9%, J. T. Baker Chemical Co.); lead acetate trihydrate (100.0%, Fisher Scientific Co.); disodium ethylenedinitrilotetracetate (EDTA, 100%, J. T. Baker Chemical Co.); Eriochrome Black T (indicator grade, Aldrich Chemical Co.); chloroform (0.75% ethanol as preservative, meets ACS specifications, J. T. Baker Chemical Co.); ethyl acetate (certified ACS, Fisher Scientific Co.); hexane (meets ACS specifications, J. T. Baker Chemical Co.); and ferric ammonium sulfate 12-hydrate (99–100%, J. T. Baker Chemical Co.).

Synthesis of Alkyl Phenyl Sulfides. Alkyl phenyl sulfides were prepared according to the general method from thiophenol and alkylhalide in 95% ethanol in the presence of potassium hydroxide (*9*), with the exception of *tert*-butyl phenyl sulfide which was prepared from thiophenol and isobutylene in 75% sulfuric acid (*9*). For final purification all sulfides were distilled under reduced pressure (50 mm Hg) using a short distillation column. Physical constants of phenyl sulfides are found in Table I.

Thin-Layer Chromatography. *Preparation of Plates.* The Stahl's applicator "Model S 11" was used for the preparation of 0.2-mm thin layers on standard glass plates (20 × 20 cm). A slurry was made by thoroughly mixing 30 g of silica gel 7GF (Baker TLC reagent) and 80 mL of the aqueous solution of the particular metal salt in a 250-mL Erlenmeyer flask (shaken strongly for about 40 s). The following solutions of salts were used for preparing TLC plates: (i) 25% mercury acetate, (ii) 5% silver nitrate, (iii) 25% lead acetate, and (iv) 5% and 25% cadmium acetate, respectively. For the preparation of control silica gel plates, the slurry was prepared with 80 mL of water. The plates were air dried for about 1 h and activated plates were stored for a short period of time in a well-closed TLC carrying case under anhydrous $CaSO_4$. However, the plates were reactivated at 100–110 °C for 1 h if they were not used for several days.

Spotting of the Samples. The samples were spotted as 0.5% solution in chloroform (about 50 μL/10 mL of chloroform) by means of a 2-μL microcap (Drummond Scientific Co.). The starting line was drawn about 2.5 cm from the bottom. A distance of 1.5 cm between each spot was maintained by using a Spotting Guide (Arthur H. Thomas Co.) leaving a 2-cm margin on each side. The spots were about 2 mm in diameter. Once spotted, the plates were left to air-dry for 5 min.

Developing Procedure. Plates were developed by the ascending technique at room temperature (23 ± 2 °C) to a distance of 15–18 cm. The chromatographic chamber was lined with filter paper and allowed to equilibrate for a period of at least 1 h prior to use. The developed plates were air dried for 5 min before being sprayed for detection. In one experiment a plate was developed at 7 °C. For this purpose the chamber was placed in a refrigerator.

Detection. For detection the plates were sprayed with potassium permanganate reagent (*10*) (1:1 solution of 0.1 M $KMnO_4$ and 2 M CH_3COOH). The sulfides visualized as yellow spots on dark violet background were marked immediately. The limit of detection is approximately 1 μg. UV light was used for detection on cadmium-impregnated plates. R_f values are reported in Tables II to VII.

Determination of the Metal Content. The metal content of impregnated plate which was already used in the experiment was determined using standard analytical procedures after scraping off the silica gel (0.1–0.3 g) and extracting the metal with acidic solution (dil. HNO_3). Mercury and silver were titrated with ammonium thiocyanate solution using Fe(III) as the indicator (*11*). Cadmium and lead were titrated with EDTA using Eriochrome Black T as the indicator (*12*). The determined metal contents are given in each Table of R_f values.

Table II. R_f Values on Mercury Acetate-Impregnated Layers[a] and Chloroform[b] as Mobile Phase

R-S-Ph, R =	R_f						
	a	*b*	*c*	*d*	*e*	*f*	$\bar{R}_f$
(1) methyl	0.480	0.585	0.557	0.560	0.529	0.494	0.535 ± 0.041
(2) ethyl	0.400	0.511	0.494	0.491	0.454	0.426	0.463 ± 0.044
(3) *n*-propyl	0.443	0.565	0.546	0.520	0.517	0.471	0.501 ± 0.060
(4) isopropyl	0.348	0.460	0.554	0.474	0.420	0.414	0.445 ± 0.069
(5) *n*-butyl	0.486	0.582	0.552	0.586	0.546	0.520	0.545 ± 0.038
(6) *tert*-butyl	0.300	0.395	0.420	0.454	0.385	0.388	0.390 ± 0.051
(7) *sec*-butyl	0.414	0.511	0.506	0.537	0.506	0.474	0.491 ± 0.043
(8) isobutyl	0.491	0.602	0.575	0.600	0.575	0.540	0.562 ± 0.047
(9) benzyl sulfide	-	-	0.300	0.306	0.286	0.274	0.292 ± 0.014

[a] Mercury content 20%. [b] Commercial chloroform containing 0.75% ethanol was used. Pure chloroform yielded elongated spots.

Table III. R_f Values on Mercury Acetate-Impregnated Layers and Chloroform[a] as Mobile Phase at Two Different Temperatures

	7 °C		26 °C	
R-S-Ph, R =	R_f	R_M	R_f	R_M
(1) methyl	0.583	−0.146	0.451	0.085
(2) ethyl	0.576	−0.133	0.389	0.196
(3) *n*-propyl	0.523	−0.040	0.451	0.085
(4) isopropyl	0.400	0.176	0.323	0.321
(5) *n*-butyl	0.606	−0.187	0.411	0.156
(6) *tert*-butyl	0.363	0.244	0.251	0.475
(7) *sec*-butyl	0.486	0.024	0.343	0.282
(8) isobutyl	0.636	−0.242	0.450	0.087

[a] See Table II.

Determination of Adsorption Isotherm (*13*) for *n*-Butyl Phenyl Sulfide in Mercury Acetate Impregnated Silica Gel. Five milliliters of a solution of *n*-butyl phenyl sulfide in hexane (concentration S) and 0.2 g of exactly weighed adsorbent containing 20% Hg were added to a stoppered vial. The vial was shaken for 10 min to establish equilibrium and centrifuged for 5 min to separate the phases. In the top layer the concentration of organic sulfides was determined from reading of the λ_{max} in the range 250–260 mm and using a calibration graph. Table VIII shows concentration of the free sulfide S_F and calculated amount of the adsorbed sulfide S_A (per 1 mL of the solution) for four original concentrations of *n*-butyl phenyl sulfide (S). Plot of log S_F vs. log S_A is a straight line with a correlation coefficient r = 0.994.

DISCUSSION

In order to obtain maximum reproducibility, the plates were prepared from silica gel and solution of the respective metal salt using the same quantities, concentrations, and procedures. Fluctuation in R_f values resulted primarily from fluctuations in temperature since the plates were developed without temperature control. Only in an experiment in which temperature dependence of R_f values was examined (Table III) the chromatographic chamber was kept at a constant temperature. However, by using benzyl sulfide as a standard using R_S or $R_{f(corr)}$ (for definition see Table IX) such fluctuation is substantially reduced; e.g., in the Hg^{2+}–chloroform system, the standard deviation of R_f values is about ±10%, for $R_{f(corr)}$ about ±2.5%. However, this method does not increase the accuracy for the Ag^+–ethyl acetate sufficiently for meaningful correlation. Here, the use of Dean and Dixon's method (*14*) increases the accuracy to about 2.5%.

The strength of the respective metal to complex the sulfide ligand is measured by the increased sulfide retention compared to the retention on untreated (plain) silica gel. This effect expressed as $R_{f(metal)}/R_{f(plain)}$ gives for butyl phenyl sulfide the following values: $AgNO_3$(EtAOc) 0.51, $Hg(OAc)_2$(chloroform) 0.85, $Pb(OAc)_2$(chloroform) 0.9, $Cd(OAc)_2$(5%, chloroform) 0.99, $Cd(OAc)_2$(25%, chloroform) 1.08. Whereas the first three metals increase the retention of the butyl phenyl sulfide, low content of cadmium has no effect and large content decreases the activity of the stationary phase indicating no interaction of the sulfides with this metal. However, this ratio differs from sulfide to sulfide.

The strong dependence of the equilibrium constant on the polarity of the solvent is evident from the comparison of R_f = 0.0 value for butyl phenyl sulfide in the Hg^{2+}/hexane system and R_f = 0.545 in the Hg^{2+}/chloroform system.

The range of R_f values which reflects the susceptibility of the chromatographic medium to structural differences of the sulfide molecules varies quite markedly for systems under examination. Whereas silica gel as well as Pb^{2+} and Cd^{2+} ions are unable to differentiate among individual molecules I–VIII, Hg^{2+} and, particularly, Ag^+ ions show remarkable discriminating power and, thus, suggest practical applications.

The effect of temperature on chromatographic data involving the Hg^{2+}–chloroform system was tested in correlation of $R_{M(7°)}$ data (calculated from R_f at 7 °C) and $R_{M(26°)}$ data (calculated from R_f at 26 °C). The plot is a straight line (correlation coefficient 0.883 for n = 8, significant at 1% probability level) with parameters: intercept = 0.238, slope = 0.707. From this resulting $\Delta R_{M(t)} = R_{M(j°C)}/R_{M(j+1°C)} = 0.0372$.

In order to characterize the ligand exchange chromatographic processes, the metal–sulfide interactions were examined quantitatively in a nonchromatographic experiment. For this purpose four different concentrations of butyl phenyl sulfide were distributed between Hg^{2+}-impregnated silica gel (same quantities, scraped from a TLC plate) and hexane, and the concentration of the free sulfide was determined by UV. The linear $\log[\text{sulfide}]_{free}$ vs. $\log[\text{sulfide}]_{adsorb}$ plot suggests a Freundlich isotherm controlled adsorption process.

The effect of the molecular structure on the chromatographic mobility of sulfide I–VIII was examined in some detail for data obtained in both the Hg^{II}–chloroform system and the Ag^+–ethyl acetate system. For this purpose, averaged $\bar{R}_S$, $\bar{R}_{f(corr)}$, and $\bar{R}_{M(corr)}$ data were calculated from the experimental R_f values using the following relationships:

$$\bar{R}_S = \frac{1}{n}\sum_j R_{Sj} = \frac{1}{n}\sum_j \frac{R_{f(\text{R-S-Ph})j}}{R_{f(\text{benzylsulfide})j}}$$

$$\bar{R}_{f(corr)} = \frac{1}{n}\sum_j R_{Sj} R_{f(\text{benzylsulfide-standard})}$$

$$\bar{R}_{M(corr)} = \log\,(1/\bar{R}_{f(corr)} - 1)$$

The "correction" of R_f values ($R_{f(corr)}$) makes it possible to substantially reduce effects of those factors (e.g., temperature, plate activity, etc.) which are responsible for R_f differences observed in different experiments. The benzylsulfide standard is chosen arbitrarily (in Table II represented data was R_f value from column c).

Table IV. R_f Values on Silver Nitrate-Impregnated Layers[a] and Ethyl Acetate as Mobile Phase

	R_f					
R-S-Ph, R =	*a*	*b*	*c*	*d*	*e*	$\bar{R}_f$
(1) methyl	0.395	0.392	0.438[b]	0.407	0.412	0.409 ± 0.018
(2) ethyl	0.260[b]	0.313	0.301	0.311	0.333[b]	0.304 ± 0.027
(3) *n*-propyl	0.395	0.392	0.411	0.412	0.440[b]	0.410 ± 0.019
(4) isopropyl	0.310	0.326	0.384[b]	0.316	0.322	0.332 ± 0.030
(5) *n*-butyl	0.407[b]	0.369[b]	0.445	0.430	0.443	0.419 ± 0.032
(6) *tert*-butyl	0.319	0.307	0.390[b]	0.316	0.327	0.332 ± 0.033
(7) *sec*-butyl	0.344[b]	0.375	0.459[b]	0.373	0.390	0.388 ± 0.043
(8) isobutyl	0.500	0.466	0.541[b]	0.480	0.503	0.498 ± 0.028
(9) benzyl sulfide	0.243	0.250	0.308	0.288	0.282	0.274 ± 0.027

[a] Silver content 2.4%. [b] Values which were rejected (using method 17) in calculation. $\bar{R}_f$ values in Table XI.

Table V. R_f Values on Cadmium Acetate-Impregnated Layers[a] and Chloroform[b] as Mobile Phase

	layers prepared with solution containing			
	5% $Cd(AcO)_2$		25% $Cd(AcO)_2$[a]	
R-S-Ph, R =	*a*	*b*	*c*	*d*
(1) methyl	0.669	0.682	0.716	0.710
(2) ethyl	0.693	0.680	0.727	0.710
(3) *n*-propyl	0.705	0.697	0.739	0.719
(4) isopropyl	0.687	0.691	0.722	0.727
(5) *n*-butyl	0.687	0.691	0.753	0.756
(6) *tert*-butyl	0.687	0.691	0.730	0.744
(7) *sec*-butyl	0.693	0.691	0.737	0.744
(8) isobutyl	0.687	0.691	0.737	0.744
(9) benzyl sulfide	0.687	0.691	0.767	0.764

[a] Cadmium content 14%. [b] 0.7% ethanol.

Table VI. R_f Values on Lead Acetate-Impregnated Layers[a]

	$R_{f(\text{hexane})}$		$R_{f(\text{chloroform})}$	
R-S-Ph, R =	*a*	*b*	*c*	*d*
(1) methyl	0.494	0.463	0.600	0.600
(2) ethyl	0.534	0.477	0.600	0.600
(3) *n*-propyl	0.557	0.503	0.600	0.600
(4) isopropyl	0.545	0.497	0.603	0.600
(5) *n*-butyl	0.537	0.503	0.600	0.600
(6) *tert*-butyl	0.545	0.520	0.603	0.603
(7) *sec*-butyl	0.545	0.508	0.603	0.603
(8) isobutyl	0.537	0.497	0.600	0.600
(9) benzyl sulfide	0.437	0.404	0.594	-

[a] Lead content 19%.

In order to determine the effect of electron donation by the sulfur atom on chromatographic behavior of individual alkyl phenyl sulfides the $R_{M(corr)}$ for Hg^{2+}–chloroform data were plotted against Taft σ^* substituent constants (Figure 1). The negative slope of the straight line $R_{M(corr,\ C_4H_9SPh)} = -1.400\ \sigma^* - 0.320$, ($r = 0.994$) provides an evidence of an increase in ligand strength of the sulfur atom with an increase in electron donation from alkyl groups in the series of four isomeric butyl phenyl sulfides. Another line is separated by an increment $\Delta R_{M(corr)}$ which corresponds to the contribution of one carbon atom to the migration of individual compounds within each homologous series of alkyl phenyl sulfides (e.g., *n*-alkyl-, *sec*-alkyl-, etc.). Thus, $R_{M(corr)}$ values of sulfides I–VIII are functions particularly of the polar and molecular weight effects. The minor role of steric effect compared to these two effects appears to be evident from the "normal" behavior of *tert*-butyl phenyl sulfide. Figure 2 visualizes the molecular

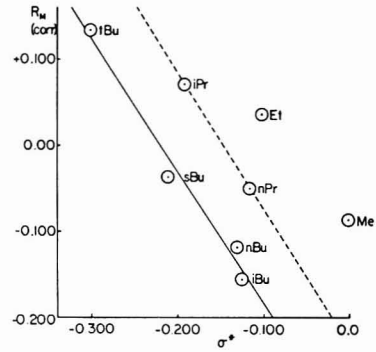

Figure 1. Plot of $R_{M(corr)}$ from Hg^{2+}/chloroform system vs. Taft σ^* constants for alkyl R in Ph–S–R (I–VIII)

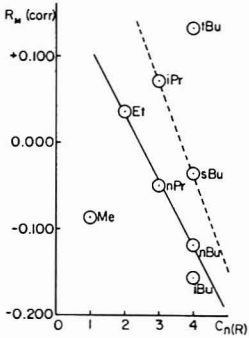

Figure 2. Plot of $R_{M(corr)}$ from Hg^{2+}/chloroform system vs. number of carbon atoms in alkyl R in Ph–S–R (I–V, VII)

weight effect on $R_{M(corr)}$ values. The straight line plotted through ethyl, propyl, and butyl phenyl sulfide points, $R_{M(CH_3(CH_2)_nSPh)} = -0.0777\ n + 0.111$, [$r = 0.999$, $n = 1, 2, 3$], suggests linearity for compounds from one and the same structural class, *n*-alkyl phenyl sulfides. Points for isopropyl phenyl sulfide and *sec*-butyl phenyl sulfide lie on a line comprising another structurally related class of compounds, *sec*-alkyl phenyl sulfides. In this diagram, the $\Delta R_{M(corr)}$ separating two isomeric sulfides reflects the difference in electron donation effect of an alkyl group attached through the primary and secondary carbon atom, respectively. These results are comparable with those obtained by one of us in a study mentioned earlier involving Hg^{2+}–sulfide complexation

Table VII. R_f Values on Nonimpregnated Silica Gel Layers

	hexane		ethyl acetate		chloroform[a]	
R-S-Ph, R =	*a*	*b*	*c*	*d*	*e*	*f*
(1) methyl	0.217	0.249	0.706	0.696	0.665	0.726
(2) ethyl	0.211	0.243	0.734	0.702	0.676	0.727
(3) *n*-propyl	0.221	0.254	0.751	0.713	0.686	0.727
(4) isopropyl	0.206	0.237	0.718	0.696	0.665	0.716
(5) *n*-butyl	0.223	0.271	0.728	0.713	0.665	0.727
(6) *tert*-butyl	0.194	0.220	0.712	0.685	0.665	0.716
(7) *sec*-butyl	0.211	0.260	0.700	0.690	0.665	0.716
(8) isobutyl	0.253	0.288	0.720	0.708	0.665	0.716
(9) benzyl sulfide	0.080	0.090	0.734	0.713	0.670	0.727

[a] See Table II.

Table VIII. Determination of Adsorption Isotherm for Butyl Phenyl Sulfide Using Mercury Acetate-Impregnated Silica Gel and Hexane

S, μg/mL[a]	S_F, μg/mL[b]	S_A μg/mL[c]
5.92	4.58	1.34
5.03	3.78	1.27
3.55	2.54	1.01
2.37	1.60	0.77

[a] S = original sulfide concentration. [b] S_F = equilibrium sulfide concentration. [c] S_A = amount of sulfide adsorbed.

Table IX. Calculated $\overline{R}_S$, $\overline{R}_{f(corr)}$, and $R_{M(corr)}$ Values for Mercury Acetate/Chloroform System

R-S-Ph, R =	$\overline{R}_S$[a]	$\overline{R}_{f(corr)}$[b]	$R_{M(corr)}$
(1) methyl	1.835 ± 0.024	0.550 ± 0.007	−0.0872
(2) ethyl	1.598 ± 0.038	0.479 ± 0.012	0.0365
(3) *n*-propyl	1.762 ± 0.060	0.529 ± 0.018	−0.0504
(4) isopropyl	1.510 ± 0.034	0.459 ± 0.016	0.0714
(5) *n*-butyl	1.891 ± 0.035	0.568 ± 0.010	−0.1189
(6) *tert*-butyl	1.412 ± 0.056	0.424 ± 0.017	0.1330
(7) *sec*-butyl	1.738 ± 0.029	0.521 ± 0.011	−0.0365
(8) isobutyl	1.964 ± 0.038	0.590 ± 0.011	−0.1563

[a] Average R_S values calculated using data in columns *c–f* in Table II. [b] Average $R_{f(corr)}$ values calculated using $R_{f(corr)}$ values from data in columns *d–f* and R_f value for benzylsulfide from column *c* as a standard value from Table II.

Table X. Calculated R_S, $R_{f(corr)}$, and R_M Values * for Silver Nitrate/Ethyl Acetate System

R-S-Ph, R =	R_S	$R_{f(corr)}$	$R_{M(corr)}$
(1) methyl	1.500 ± 0.094	0.364 ± 0.023	0.242
(2) ethyl	1.112 ± 0.106	0.270 ± 0.026	0.432
(3) *n*-propyl	1.504 ± 0.118	0.366 ± 0.029	0.239
(4) isopropyl	1.241 ± 0.088	0.296 ± 0.020	0.376
(5) *n*-butyl	1.532 ± 0.092	0.373 ± 0.022	0.226
(6) *tert*-butyl	1.213 ± 0.085	0.295 ± 0.021	0.378
(7) *sec*-butyl	1.417 ± 0.084	0.340 ± 0.017	0.288
(8) isobutyl	1.839 ± 0.173	0.444 ± 0.036	0.122

[a] R_S, $R_{f(corr)}$, and $R_{M(corr)}$ have meanings similar to those from Table IX.

(*5*). In the quoted paper, sulfides from a similar series were partitioned between a polar ligand phase ($AcOH/H_2O$) saturated with $Hg(OAc)_2$ and heptane and logarithms of the partition coefficient was plotted vs. *n* number of carbon atoms of the R substituent in the formulae R–S–Bu. The plot showed separation into classes: one in which R was *n*-alkyl and another in which R was *sec*-alkyl. Separation into structural classes has been observed in gas chromatography in log rV vs. n plots (rV is relative elution volume and n is number of carbon atoms) involving different homologous series of hydrocarbons (e.g., *n*-paraffins, 2-methyl paraffins, 2,2-dimethyl paraffins, etc.) (*15*). The structural effects on elution parameters are here associated with the differences in boiling points which exist for isomeric hydrocarbons.

"Anomalous" behavior of the methyl derivative (I), $R_{M(corr)}$ of which does not fit on the line of regression comprising *n*-alkyl phenyl sulfides (Figure 1), is similar to that observed for a methyl derivative in studies of the partition processes involving Hg^{2+}–sulfide complexation quoted above (*5*) as well as to other known examples (*16*). This apparent inconsistency is, however, clarified by applying linear equation in which R_M is expressed in terms of polar (σ^*), molecular weight (MW), and steric (*17*) (E_S) effects. Using a computer program by M. Charton (*18*) and the equation $R_M = a\sigma^* + b\mathrm{MW} + cE_S + d$,

Table XI. Calculated $\overline{R}_f'$ and R_M' Values[a] for Silver Nitrate/Ethyl Acetate System

R-S-Ph, R =	$\overline{R}_f'$	R_M'
(1) methyl	0.402 ± 0.010	0.1725
(2) ethyl	0.308 ± 0.006	0.3516
(3) *n*-propyl	0.402 ± 0.010	0.1725
(4) isopropyl	0.318 ± 0.007	0.3314
(5) *n*-butyl	0.439 ± 0.008	0.1059
(6) *tert*-butyl	0.317 ± 0.008	0.3334
(7) *sec*-butyl	0.379 ± 0.009	0.2071
(8) isobutyl	0.487 ± 0.017	0.0226

[a] $\overline{R}_f'$ values were derived by rejecting (using method 14) questionable values (marked with [b] in Table IV). R_M' values were calculated from $\overline{R}_f'$ values.

the $R_{M(corr)}$ for the Hg^{2+}–chloroform system and R_M' for the Ag^+–ethyl acetate system, respectively, is correlated producing the following information:

	Hg^{2+}–chloroform	Ag^+–ethyl acetate
a	−1.933 ± 0.132	−2.397 ± 0.254
b	−0.00611 ± 0.00059	−0.0077 ± 0.00114
c	+0.0774 ± 0.0231	+0.1559 ± 0.0445
d	+0.6792 ± 0.0816	+1.1518 ± 0.1575
	$r_{(n=8)} = 0.993$	$r_{(n=8)} = 0.983$

Interestingly, the R_M data from one set of data on non-impregnated plates and hexane as solvent analyzed using the same linear relationship reveal similar character with regard to the participation of polar, steric, and molecular weight effects as those from Hg^{2+} and Ag^+ impregnated plates: a = −0.833 ± 0.137, b = −0.00372 ± 0.00061, c = +0.0203 ± 0.0240, d = + 0.935 ± 0.085, $r_{(n=8)}$ = 0.969.

The large values of standard deviations in the various slopes are accounted for by both the experimental errors and the fact that the various factors (σ^*, MW, and E_S) are not mathematically independent; just coincidentally correlating vs. each other with a correlation coefficient r = 0.87.

Based on the above data average percent contribution of individual structural factors is calculated as follows: (for average σ^* contribution)

$$\frac{100\sum_i|a\sigma_i^*|}{\sum_i|a\sigma_i^*|+\sum_i|b\mathrm{MW}_i|+\sum_i|cE_{Si}|}$$

(similar formulations were used for MW and E_S) producing the following information:

	Hg^{2+}–chloroform	Ag^+–ethyl acetate	unimpregnated
σ^*	22%	21%	17%
MW	74%	73%	81%
E_S	4%	6%	2%

As a result of the above presented analysis of chromatographic behavior of alkyl phenylsulfides on Hg^{2+}- and Ag^+-impregnated silica gel plates based on the contribution of individual structural factors shows, the molecular weight is far more influential than polar and steric effects. However, the steric effect, the contribution of which to the R_M is generally the smallest, is a factor by which the behavior of the methyl derivative is explained. Finally, whereas the retention of sulfides with Ag^+ is much stronger than with Hg^{2+} the contribution of polar, molecular weight and steric factors to the R_M is identical.

Since the vast increase of retention on impregnated plates is evidently due to the interaction of the particular metal ion with the electron donating site of the sulfide molecule, it seems that plain silica gel interacts with the same site, probably the sulfur atom. However, in the latter case the energy of the

interaction is rather small resulting in much smaller retention and poor resolution.

The results presented in this paper demonstrate the efficiency of the ligand exchange chromatography for separation of alkyl phenyl sulfides using Hg^{2+} and Ag^{+} ion-loaded stationary phase and suggest analytical applications. Furthermore, the method may be appplicable to other types of sulfides as well. Resulting from our preliminary experiments, leaching of the metal salts from the stationary phase is a problem which should be solved to allow successful application of the method discussed in this paper in HPLC.

LITERATURE CITED

(1) L. R. Snyder, *Anal. Chem.*, **41**, 314 (1969).
(2) W. L. Orr, *Anal. Chem.*, **38**, 1558 (1966).
(3) W. L. Orr, *Anal. Chem.*, **39**, 1163 (1967).
(4) J. W. Vogh and J. E. Dooley, *Anal. Chem.*, **47**, 816 (1975).
(5) V. Horak and J. Pecka, *Collect. Czech. Chem. Commun.*, **32**, 3394 (1967).
(6) V. Horak and J. Pecka, *Collect. Czech. Chem. Commun.*, **32**, 3055 (1967).
(7) V. Horak, J. Pecka, and J. Jurjev, *Collect. Czech. Chem. Commun.*, **32**, 3386 (1967).
(8) V. Horak and J. Pecka, "Mechanisms of Reactions of Sulfur Compounds", Vol. 4, Intra-Science Research Foundation, Santa Monica, Calif., 1969, p 43.
(9) V. N. Ipatieff, H. Pines, and S. M. Friedman, *J. Chem. Soc.*, **60**, 2731 (1938).
(10) S. Stahl, "Thin Layer Chromatography", Academic Press, New York, 1965, p 494.
(11) I. M. Kolthoff and E. E. Sandell, "A Textbook of Quantitative Inorganic Analysis", 3rd ed., Macmillan, New York, p 461.
(12) K. A. Connors, "A Textbook of Pharmaceutical Analysis", Wiley, New York, 1967, p 49.
(13) R. Alger, H. Spitzy, and R. W. Frei, *Anal. Chem.*, **48**, 3 (1976).
(14) R. D. Dean and W. J. Dixon, *Anal. Chem.*, **23**, 636 (1951).
(15) A. T. James, A. J. P. Martin, and G. H. Smith, *Biochem. J.*, **52**, 238 (1952).
(16) I. E. Bush, "The Chromatography of Steroids", Pergamon Press, London, 1961, p 31.
(17) R. W. Taft, Jr., "Steric Effects in Organic Chemistry", M. S. Newman, Ed., John Wiley & Sons, New York, 1956.
(18) M. Charton, Pratt Institute, Brooklyn, New York.

RECEIVED for review May 2, 1979. Accepted August 7, 1979.

Observation of Electrochemical Concentration Profiles by Absorption Spectroelectrochemistry

Richard Pruiksma and Richard L. McCreery*

Department of Chemistry, Ohio State University, Columbus, Ohio 43210

A laser beam passing parallel to a working electrode surface was used to monitor an electrogenerated chromophore employing absorption spectrophotometry. By placing a 10-μm slit parallel to the electrode and intercepting the beam after passage by the electrode, a portion of the diffusion layer was sampled. Movement of the slit relative to the electrode allowed monitoring of concentration as a function of distance from the electrode surface. The resulting concentration profiles agree well with theory for both single- and double-step experiments for distances of 50–200 μm from the surface. Because of long optical path length (0.5 cm or greater), the present method is much more sensitive than previous spectroelectrochemical methods. In addition, spatial resolution of the diffusion layer provides both fundamental information about mass transfer and additional insight into reactions accompanying charge transfer.

The use of spectroscopic probes to monitor electrochemical events has become widespread and spectroelectrochemistry has been used for a variety of purposes (*1–3*). The majority of applications of spectroelectrochemistry involves light absorption, with the beam transmitted through the electrode or reflected off its surface. For the techniques used to examine solution species in the vicinity of the electrode, two major objectives have been realized, spectral characterization of electrogenerated materials and kinetic monitoring of reactive species. The most common techniques use optically transparent electrodes, with the spectrophotometric beam being perpendicular to the electrode plane. This approach yields an integrated absorbance throughout the entire diffusion layer, and the time course of this absorbance has been used to diagnose reaction mechanisms for electrogenerated species and to spectrally characterize reactive intermediates. Internal reflection spectroscopy (IRS) has been used for the same purposes, with the region of the diffusion layer within one wavelength of the electrode surface being sampled by the evanescent wave (*4*).

These previous spectroelectrochemical methods based on absorption suffer from two major drawbacks when applied to the monitoring of transient electrogenerated species. First, the optical path length is very short, being limited to the thickness of the diffusion layer or the length of the evanescent wave. Thus these techniques have been applied primarily to strong chromophores or species with relatively long lifetimes, allowing measurement of absorbance value vs. time transients with acceptable signal-to-noise ratios. Second, these techniques cannot supply information about the concentrations of electroactive species (or their reaction products) as a function of distance from the electrode surface. IRS can provide surface concentrations, and a transmission or reflection experiment can provide total concentration in the diffusion layer, but neither allows spatial resolution of the diffusion layer. Reflection spectroscopy at a glancing incidence angle (*5*) can greatly extend the optical pathlength but still does not resolve the concentration gradients of electroactive species. Despite the fundamental importance of concentration vs. distance profiles to electrochemistry, they have not been observed using absorption techniques.

Several experiments have been reported which make use of the refractive index gradient of a diffusion layer to construct a concentration vs. distance profile (*6–10*). While these interferometric techniques have succeeded in some cases, they lack both sensitivity and selectivity because they are based on refractive index changes accompanying electrochemical events. It is very difficult to monitor more than one solution component using changes in refractive index, and fairly large refractive index gradients are required to be measured interferometrically. Hence refractive index techniques have allowed observation of diffusion profiles only for fairly concentrated solutions (ca. 0.1 M) of single components (e.g., $CuSO_4$). Application of such techniques to reactive systems at millimolar levels would be extremely difficult.

The objective of the present work is to construct concentration vs. distance profiles for an electrogenerated species using absorption spectrophotometry. The light beam is or-

0003-2700/79/0351-2253$01.00/0

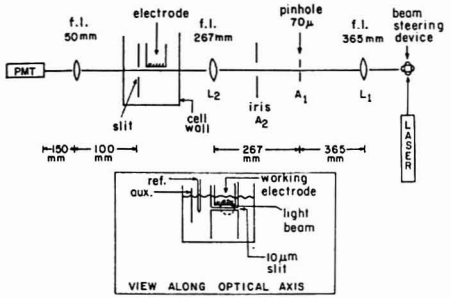

Figure 1. Schematic of experimental apparatus. Laser is a 0.5-mW He-Ne (Spectra Physics, Mountain View, Calif.), PMT is a 1P28. Beam was directed into L_1 by a beam steering device (Newport Research, Fountain Valley, Calif.). The long axis of the slit was oriented perpendicular to the plane of the figure, immediately to the left of the electrode. Insert shows details of cell, viewed along the optical axis, in the direction of light propagation

ienting parallel to the electrode plane, and portions of the beam are sampled by a slit with a dimension of 10 μm along the dimension perpendicular to the electrode plane. Absorbance vs. time curves are constructed using light passing through the slit, during generation and diffusion of an absorbing solution component. The use of absorption rather than refraction greatly improves sensitivity and selectivity, and the path length is limited only by the physical dimension of the electrode, not the diffusion layer thickness. Most importantly, movement of the slit along the dimension perpendicular to the electrode surface allows concentration vs. time curves to be obtained at various distances from the electrode, and therefore concentration vs. distance profiles may be constructed as a function of time.

EXPERIMENTAL

The experimental apparatus is shown in Figure 1; all components were mounted on a 4 ft × 6 ft optical table (Newport Research Corp., Fountain Valley, Calif.). The lenses and circular apertures (L_1, L_2, A_1, A_2) were used to spatially filter the laser beam (0.5 mW, 632.8 nm) and produce a collimated, gaussian beam lacking plasma discharge, etc. A_2 occluded light diffracted by the pinhole. The beam then passed through the first wall of the cell, and past a gold electrode with a dimension of 0.45 cm along the optical axis. The electrode was constructed from an optical flat (flat to λ/4) coated with Hanovia Liquid Bright Gold 61 BB (Englehard Industries, East Newark, N.J.), for adhesion purposes. This was followed by vapor deposition of gold to give a pure gold surface. The slit, which consisted of a razor-blade scratch on a front surface optical mirror coated with a clear acrylic spray to insulate the mirror electrically from the gold electrode, was placed immediately after the electrode, in the solution. It is important to place the slit as close as possible to the electrode, to minimize the intensity of scattered light passing through the slit. Clearly the ideal situation occurs when only collimated light which passes parallel to the electrode enters the slit. The electrode plane was oriented horizontally in the solution to minimize convection caused by density gradients.

The alignment of the beam with respect to the electrode is of critical importance, and was accomplished as shown in Figure 2. After the pentaprism P_1 deflected the beam by 90°, the beam was reflected off the electrode by two cornercube reflectors (P_2 and P_3), the cell and solution being temporarily removed. The electrode was then positioned with a multi-axis manipulator (David Kopf Instruments, Tujunga, Calif.) until the incoming beam was reflected back onto itself. Provided the distance (D) is long enough (130 cm in this case), this procedure will accurately align the electrode parallel to the beam. The beam covered a significant fraction of the electrode (ca. 50%), and no observable beam divergence was observed after reflection, indicating that

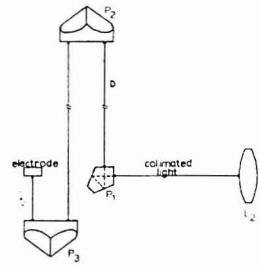

Figure 2. Method for aligning electrode plane parallel to filtered laser beam. P_1, pentaprism; P_2, P_3, cornercube reflectors; D = 1.3 m

the electrode flatness was not disturbed by the gold coating process. After removal of P_1 the laser beam will pass parallel to the electrode plane.

The cell was constructed from 1.6-mm quartz plate and had dimensions of 60 × 40 × 30 mm with the 30-mm dimension being along the optical axis. To ensure that its presence did not adversely affect the alignment of electrode and beam, it was positioned so that the reflection of the beam off its face was directed back onto the incoming beam. This process aligned the cell face perpendicular to the beam and assured that the cell and solution did not deflect the beam. The 10-μm slit was moved vertically (along a dimension perpendicular to the electrode) with a high resolution micrometer (Lansing Research, Ithaca, N.Y.) having resolution and readability of 0.13 μm. The light leaving the slit was collected by a small lens (focal length = 50 mm) and directed onto the active surface of a 1P28 photomultiplier tube. As much of the light transmitted by the slit as possible was used for absorbance measurements. Diffraction by the slit and any scattering by the cell wall on the exit side are unimportant, since the light has already passed the electrode and the slit has already selected a particular region of the diffusion layer.

A commercial potentiostat (Princeton Applied Research Model 173) driven by a laboratory computer (Hewlett-Packard 1000) controlled the potential using a Pt auxiliary electrode and SCE reference electrode. No particular care was taken with auxiliary and reference electrode placement, except to avoid the laser beam. The computer monitored the PMT output before and during a single or double potential step, and calculated the absorbance vs. time transients. Since the initial light intensity varied with slit movement, the PMT high voltage supply was adjusted to bring the PMT output voltage into the optimum range of the analog-to-digital converter.

The test system used for this work was the oxidation of *N,N,N',N'*-tetramethylparaphenylenediamine (TMPD) to its cation radical (Wurster's blue). The one-electron character of this oxidation is well established (*11*), but additional experiments were carried out to verify its suitability for the present work. At pH 7, TMPD exhibits a reversible voltammetric wave centered at +0.04 V vs. SCE. Potential step experiments from −0.2 to +0.2 V at a graphite paste electrode produced current transients which were linear with $t^{-1/2}$ for at least 15 s. The diffusion coefficient determined from chronoamperometry at pH 7 is 8.3×10^{-6} cm^2/s. Using reflectance spectroelectrochemistry with a normal incident angle (*5*), absorbance was linear with $t^{1/2}$ for a period from 0.2 to 15 s indicating a stable chromophore for this period. The radical was not sufficiently stable (i.e. a half-life of minutes) to determine its molar absorptivity by normal means, so the absorptivity was calculated from the reflection data to be 4200 M^{-1} cm^{-1} at 632.8 nm. It was assumed that the diffusion coefficients for the reduced and radical forms are equal. Thus for the time frame of the present work, TMPD is an appropriate test system, exhibiting an uncomplicated oxidation to a blue chromophore. The sensitivity of TMPD to air oxidation was controlled by careful degassing with argon which had been passed through a Cr^{2+} solution.

Theoretical concentration vs. time curves at various distances from the electrode were determined from standard digital simulation techniques (*12*). The effect of the 10-μm slit was

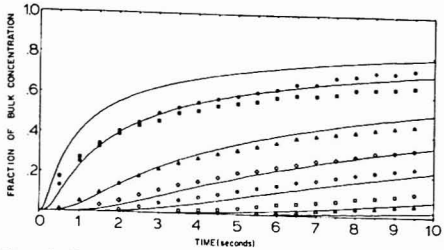

Figure 3. Fraction of bulk concentration vs. time at various distances from the electrode for a single-step experiment. Solid lines are theoretical curves (listed from top) at 25, 38, 70, 102, 133, 197, and 260 μm from the electrode. Points are experimental results: (●) 25 μm, (■) 38 μm, (▲) 70 μm, (◊) 102 μm, (○) 133 μm, (□) 197 μm, (△) 260 μm

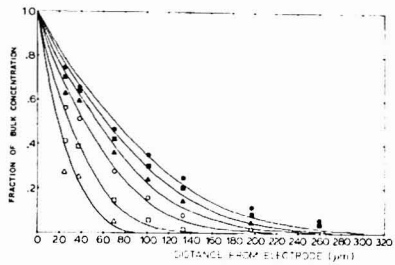

Figure 4. Fractional concentration as a function of distance for various times after a single-potential step. Solid lines are theoretical curves (listed from top) for 10, 8, 6, 4, 2, and 1 s. Points are experimental results: (●) 10 s, (■) 8 s, (▲) 6 s, (○) 4 s, (□) 2 s, (△) 1 s

incorporated by averaging the simulation "boxes" corresponding to this dimension.

RESULTS

Experimental absorbance vs. time curves were converted to concentration vs. time curves using the molar absorptivity for the radical cation and the geometric pathlength of the electrode (0.45 cm). Because of the long pathlength, absorbance values were large, ranging from 0.05 to 2.0 units. Concentrations were then divided by the bulk concentration of TMPD (1.0 mM) to obtain fractional concentration of radical vs. time. Theoretical curves of fractional concentration vs. time as a function of distance were determined from the simulated results and the values of the diffusion coefficient for TMPD. Experimental and theoretical plots of fractional concentration vs. time are shown in Figure 3, for a single step experiment to a potential on the diffusion limit for production of radical (0.2 V vs. SCE). As expected, the curves rise sharply at distances close to the electrode, since electrogenerated material reaches these distances rapidly.

The concentration vs. time plots at various distance may easily be converted to concentration vs. distance plots at various times, commonly referred to as diffusion profiles. These profiles for various times are shown in Figure 4. The solid lines represent theoretical diffusion profiles, and the points represent the experimental results.

Fractional concentration vs. time profiles for double-step experiments are shown in Figure 5. After 5 s of generation of radical at the diffusion controlled rate, the potential was returned to a value required for diffusion controlled reduction back to TMPD (–0.2 V vs. SCE). Note that the peak in the electrogenerated radical concentration occurs later at greater distances from the electrode. The concentration vs. time plots

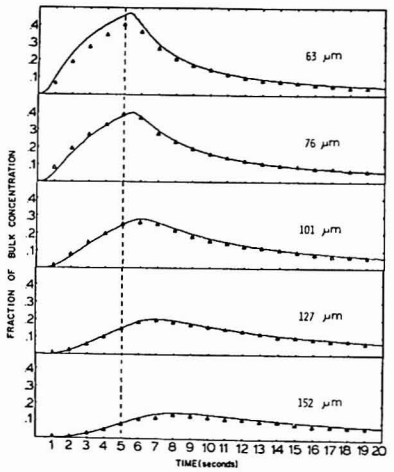

Figure 5. Fractional concentration vs. time at various distances for a double-potential step experiment. Numbers indicate distances from electrode. Solid lines are theoretical, points are experimental. Step from –0.20 to +0.20 V vs. SCE at $t = 0.0$ s. Step from +0.20 to –0.20 V vs. SCE at $t = 5.0$ s

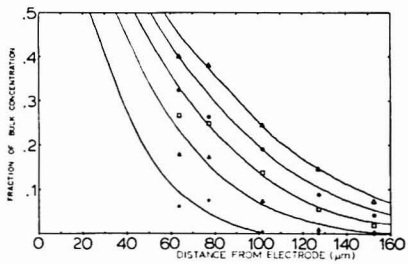

Figure 6. Concentration vs. distance for five times during forward step of double-potential step experiment. Theoretical curves from the top: 5, 4, 3, 2, 1 s. Experimental points: (△) 5 s, (○) 4 s, (□) 3 s, (▲) 2 s, (●) 1 s

were converted to concentration vs. distance plots, shown in Figures 6 and 7. Figure 6 includes five profiles before the potential switch while Figure 7 shows five profiles after the switch.

Figure 8 compares theoretical and observed concentration vs. time profiles at a distance very close to the electrode (13 μm). Not only is the correspondence poor, but the experimental results are quantitatively irreproducible.

DISCUSSION

While the quantitative agreement between theory and experiment for the single step shown in Figure 3 is not outstanding, the important qualitative features are apparent. As the distance increases, the concentration rises more slowly, as expected for electrogenerated material diffusing away from the electrode. In fact at 260 μm, more than 5 s elapse before any radical is observable. The concentration profiles of Figure 4 have the expected shape, and quantitative agreement again is good, although not outstanding. In both Figures 3 and 4, it is apparent that the quantitative disagreement is poorest at short (<50 μm) or long (≥200 μm) distances, and at long electrolysis times. Although significant improvement in

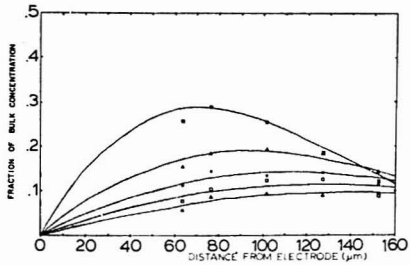

Figure 7. Fractional concentration vs. distance for reverse step of double-potential step experiment. Theoretical curves from top: 7, 9, 11, 13, and 15 s. Experimental points: (△) 15 s, (□) 13 s, (○) 11 s, (▲) 9 s, (■) 7 s

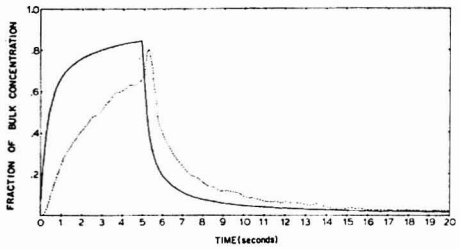

Figure 8. Fraction of bulk concentration vs. time for 13 μm from electrode surface. Double-step experiment. Solid line, theoretical; dashed line, experimental.

quantitation is anticipated with further development, it is possible that convection is a cause of error at long times and large distances. Solution convection will be greatest at large distances, and its effects will increase with time.

The concentration vs. time curves for the double-step experiment shown in Figure 5 agree very well with theory, at least at distances greater than about 60 μm. The diffusion profiles before the step (Figure 6) are similar to those in Figure 4, although at shorter times. After the potential reversal (Figure 7), the observed concentrations follow the expected behavior, again agreeing quite well with theory.

The results of Figures 3–7 clearly demonstrate that absorption spectroelectrochemistry can be used to observe electrochemical concentration gradients. Obviously variation in the wavelength will allow selection of different solution species, allowing selectivity which is not possible with methods based on refractive index. In addition, the long optical pathlength (0.45 cm in this case) allows high sensitivity, with absorbances of ca. 1.0 unit for conditions where a standard transmission spectroelectrochemical experiment would yield values two or three orders of magnitude lower.

The sources of error, particularly at short distances, remain to be elucidated, but can be classified into two categories. First, physical phenomena such as diffraction from the electrode surface or bending of the beam in the refractive index gradient will cause variations in light reaching the slit. Both these effects will be dependent on the presence of the diffusion layer (therefore will be time dependent) and both will be most pronounced near the surface, where the concentration gradient is largest. Calculations indicate that refractive index effects should be very small for the concentrations used here, but further work is necessary to determine their importance. The second category of potential errors stems from the technical aspects of the apparatus, particularly the alignment of beam, electrode, and slit. If

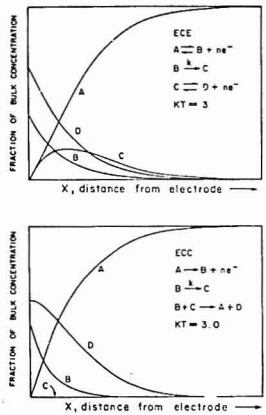

Figure 9. Simulated diffusion profiles for ECE and ECC mechanisms. The cross reaction for the ECC case is assumed to be fast, and "bulk concentration" refers to the starting material, A

either the beam or the slit is not parallel to the electrode plane, the resulting error will be largest near the electrode, where the gradient is steepest. A poorly aligned slit or beam will sample a range of distances, resulting in an absorbance which does not represent a particular distance, and is not reproducible from experiment to experiment. The behavior shown in Figure 8 may be due in part to this problem. Finally, any scattered light which passed through the slit but did not traverse the sampled region of the diffusion layer will be a source of error. The agreement with theory at the large absorbance values observed in this work (up to 2.0 units) indicates this problem is small, but should nevertheless be considered.

Even with the quantitative errors mentioned above, the technique in its present form has significant applications. The ability to monitor concentrations at various distances has important advantages. By using different wavelengths, it is possible to construct concentration profiles for different species involved in homogeneous reactions of electrogenerated materials. The shapes of these profiles are very sensitive to reaction mechanism, as shown in Figure 9, comparing the ECE and ECC mechanisms. While these two mechanisms differ only slightly in their faradaic responses (ca. 10–20%) (*13*), the differences in profiles (particularly for "C") are large. A conventional spectroelectrochemical experiment with the beam perpendicular to the electrode can supply only the total concentration of each species through the diffusion layer, thus not permitting the spatial resolution of the present method. Thus concentration vs. distance information is an additional probe of solution reactions, of potentially more value than the surface concentrations reflected in current measurements or the overall concentration obtained from conventional spectroelectrochemistry.

The aberrations of the technique in its present form at short distances would seem to limit the method to chromophores having lifetimes of several seconds. However, even if the minimum distance cannot be improved, which is unlikely, it should be possible to observe relatively short-lived intermediates because of the long optical pathlength. For example, an electrogenerated species with a diffusion coefficient of 10^{-6} cm^2/s will reach 1% of the bulk precursor concentration at a distance of 50 μm in 0.66 s. With a pathlength of several centimeters, this concentration would easily be detectable even for moderate chromophores.

Future efforts involving the technique presented here will involve improvement of resolution using a smaller slit, improvement in alignment between slit and electrode, and the use of diffracted light to examine events close to the electrode. In its present form, the technique allows direct observation of concentrations of electroactive materials as a function of both time and distance with unprecedented sensitivity and selectivity. The long pathlength, selectivity gained from wavelength selection, and spatial resolution will allow much greater definition of the solution adjacent to an electrode surface. In addition to observing fundamental aspects of electrochemical mass transport, the technique will allow improved characterization of homogeneous reactions accompanying charge transfer.

ACKNOWLEDGMENT

The authors thank Robert Fagan for helpful discussion.

LITERATURE CITED

(1) Winograd, N.; Kuwana, T. "Spectroelectrochemistry at Optically Transparent Electrodes", in "Electroanalytical Chemistry", Vol. 7, Bard, A. J., Ed.; Marcel Dekker: New York, 1974.
(2) Kuwana, T. *Ber. Bunsenges. Phys. Chem.* **1973**, *77*, 858.
(3) Heineman, W. R. *Anal. Chem.* **1978**, *50*, 390A.
(4) Winograd, N.; Kuwana, T. *J. Electroanal. Chem.* **1970**, *23*, 333.
(5) McCreery, R. L.; Pruksma, R.; Fagan, R. *Anal. Chem.* **1979**, *51*, 749.
(6) Müller, R. H. *Adv. Electrochem. Electrochem. Eng.* **1973**, *9*, 281.
(7) Srinivasan, V. S. Ref. 6, p 369.
(8) Obrien, R. N.; Dieken, P. *J. Electroanal. Chem.* **1973**, *42*, 25.
(9) Obrien, R. N., et al. *Can. J. Chem.* **1965**, *43*, 3304.
(10) Obrien, R. N.; Rosenfield, C. *J. Phys. Chem.* **1963**, *67*, 643.
(11) Michaelis, L.; Hill, E. S. *J. Am. Chem. Soc.* **1933**, *55*, 1481.
(12) Feldberg, S. W. In "Electroanalytical Chemistry", Bard, A. J., Ed.; Marcel Dekker: New York, 1970; Vol. 3.
(13) Adams, R. N. "Electrochemistry at Solid Electrodes"; Marcel Dekker: New York, 1969; p 254.

RECEIVED for review June 26, 1979. Accepted September 4, 1979. This work was supported by grants from NIMH (28412) and NSF (CHE-7828068).

Rotating-Ring-Disc Analysis of Iron Tetra(*N*-methylpyridyl)Porphyrin in Electrocatalysis of Oxygen

Armand Bettelheim and Theodore Kuwana*

Department of Chemistry, The Ohio State University, 140 West 18th Avenue, Columbus, Ohio 43210

When cyclic voltammetry and the rotating ring-disc electrode (RRDE) were used, the water soluble iron tetra(*N*-methylpyridyl)porphyrin (FeTMPyP) was found to catalyze O_2 electroreduction by ca. 400 mV and produce H_2O_2, at a yield of 95%, as the initial product. Using the RRDE method, the rate of removal of Fe(II)TMPyP by O_2 was estimated to be in the 10^7–10^8 $M^{-1}s^{-1}$ region. A mechanism involving an "iron(III)–superoxide ion" intermediate seems to be consistent with the above experimental results and with other data reported in the literature.

In a previous publication (*1*), it was proposed that the electrocatalytic reduction of O_2 occurred through an *ec* catalytic regeneration mechanism:

$$\text{Fe(III)TMPyP} + e^- = \text{Fe(II)TMPyP} \quad (1)$$

$$\text{Fe(II)TMPyP} + {}^1/_2O_2 + H^+ = \text{Fe(III)TMPyP} + {}^1/_2H_2O_2 \quad (2)$$

where the water soluble Fe(III) tetra(*N*-methylpyridyl)-porphyrin cation (abbreviated as Fe(III)TMPyP) was reduced at the electrode to Fe(II)TMPyP and reacted rapidly in a homogeneous reaction with dissolved oxygen. The stoichiometry of the reaction as deduced from the analysis of the cyclic voltammetric waves indicated hydrogen peroxide as the major product. In this paper, the rotating-ring-disc electrode was employed to assess the production of hydrogen peroxide as indicated by reactions 1 and 2, and to evaluate, if possible, the rate parameters for reaction 2. Also, additional cyclic voltammetric results on the O_2 concentration dependence and the effect of added catalase are presented to further characterize the iron porphyrin catalytic reduction of O_2.

EXPERIMENTAL

Iron III tetra(*N*-methylpyridyl)porphyrin as the sulfate salt (henceforth abbreviated as $Fe(III)TMPyP^{+5}$) was prepared in our laboratory (*2*). All other chemicals were analytical grade. Solutions were prepared with doubly distilled water. The concentration of the iron-porphyrin complexes in the solutions was determined by measuring the optical adsorption at the Soret band (at pH 1: $\lambda_{max} = 398$ nm, $\epsilon_{398} = 1 \times 10^5$ M^{-1} cm^{-1}) (*3*) using a Cary 15 spectrophotometer. Nitrogen 99.9% pure was used for deaeration of all solutions. Solutions were saturated with oxygen and with mixtures of oxygen and nitrogen using Matheson's analyzed gases. The stock solutions were stored refrigerated (5 °C) and in the dark.

Glassy carbon electrodes were obtained from Tokai Ltd. (Japan), Sigma (Germany), and Atomergic Chemetals (France). The electrodes were polished to a bright surface using alumina powder (final polish using 0.05-μm particle size, Buehler). The electrodes were then washed with 0.1 N H_2SO_4 and distilled water to remove any alumina. Elemental aluminum was found to be absent from the surface within limits of Auger and ESCA analysis.

The rotating-ring-disc electrode (RRDE, Pine Instrument Co.) consisted of a glassy carbon disc surrounded by a platinum ring. The area of the disc was 0.48 cm^2. The collection coefficient was determined to be 0.131 using the ferrocyanide–ferricyanide redox couple. Potentiostatic experiments were performed with a double potentiostat (RDE-3, Pine Instrument Co.). The RRDE was pretreated mechanically and electrochemically. The electrode was polished with alumina powder by rotating it on fine polishing cloth which was mounted on a glass disc. It was then washed with 0.1 N H_2SO_4 and doubly distilled water and introduced in a 0.1 N KCl nitrogen saturated solution. The potentials of the disc and the ring electrodes were then cycled in the range −0.6 to +0.2 V, and 0 to +1.0 V, respectively, until a minimum residual current density was obtained ($\approx$0.5 $\mu A \cdot cm^{-2}$).

Cyclic voltammetry was performed using a conventional three-electrode potentiostat.

All reported potentials are with respect to a Ag/AgCl (sat'r.) reference electrode. Experiments were conducted at room temperature (20 ± 1 °C).

RESULTS AND DISCUSSION

Cyclic Voltammetry. As previously reported (*1*), the presence of the water soluble porphyrin, Fe(III)TMPyP, greatly enhanced the rate of O_2 reduction at a highly polished

0003-2700/79/0351-2257$01.00/0

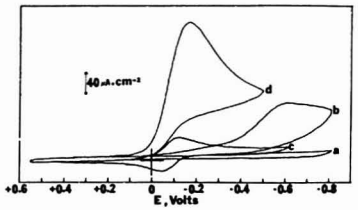

Figure 1. Cyclic voltammograms at a scan rate of 50 mV s^{-1} using glassy carbon as the working electrode (A = 0.66 cm^2) for: (a) a N_2 saturated 0.1 N N_2SO_4 solution; (b) an air saturated 0.1 N H_2SO_4 solution; (c) a nitrogen saturated 0.1 N H_2SO_4 solution containing 2.7 × 10^{-4} M FeTMPyP; (d) same solution as for curve c but air saturated

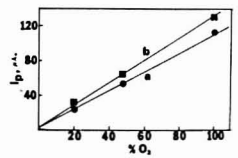

Figure 2. The cathodic peak current (A = 0.13 cm^2) as function of oxygen concentration for: (a) 10^{-4} M FeTMPyP in phosphate buffer at pH 6.8, (b) the same solution (volume: 20 mL) in the presence of 2 mg of catalase

glassy carbon electrode. (Similar results can be obtained at Pt, Au, or doped tin oxide electrodes.) Figure 1 shows typical current–potential (i–E) curves as obtained by cyclic voltammetry (CV) at glassy carbon: (1) Trace a is an electrode in 0.1 N H_2SO_4 aqueous solution after thoroughly purging and saturating with N_2; (2) Trace b is for air-saturated solution where O_2 concentration is ca. 2 × 10^{-4} M; (3) Trace c is for 2.7 × 10^{-4} M Fe(III)TMPyP in absence of O_2; and (4) Trace d is the same as conditions for trace c except after air-saturation (20 °C).

As may be seen from comparison of curves b, c, and d, the current is markedly enhanced and the overpotential is reduced by ca. 400 mV when O_2 is reduced in the presence of the iron porphyrin. Consistent with the *ec* mechanism, reactions 1 and 2, *the potential of the catalytic O_2 reduction is determined by the redox potential of the Fe(III/II)TMPyP couple* (see traces c and d of Figure 1). (Analysis of the potential vs. pH of the reaction will be discussed in a separate publication.) The peak current, i_p, was linearly proportional to the square root of the scan-rate, $V^{1/2}$, for both FeTMPyP and O_2 in the presence of FeTMPyP. The analysis of the i_p vs. $V^{1/2}$ was in agreement with previous results which were consistent with O_2 being reduced by a two-electron overall process to hydrogen peroxide. The i_p was found to be linearly dependent on the oxygen concentration as shown in Figure 2, trace a, for a 10^{-4} M FeTMPyP solution in phosphate buffer at pH 6.8. The choice of pH was dictated by our desires to test the effect of the catalase, a peroxide decomposing catalyst, on the height of the i_p. The i_p does increase slightly when catalase is present (trace b, Figure 2) consistent with a mechanism whereby more O_2 becomes available due to the increased rate of H_2O_2 dismutation:

$$H_2O_2 \xrightarrow{\text{catalase}} {}^1/_2O_2 + H_2O \qquad (3)$$

Rotating-Ring-Disc Electrode. To further assess the proposed reactions 1 and 2, rotating-ring-disc electrode experiments were conducted. In Figure 3, curves a, b, and c, are the disc currents, i_D, at different rotation speeds for air-saturated solutions of 10^{-4} M FeTMPyP at pH 9.0 (0.1 M KCl).

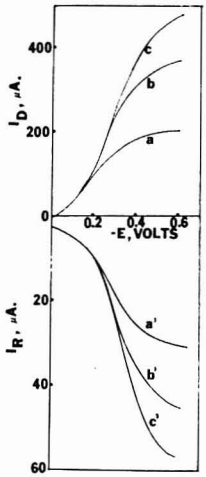

Figure 3. Polarization curves for the disc (a–c) and ring (a′–c′) electrodes for an air saturated solution of 0.1 M KCl and 10^{-4} M FeTMPyP (pH 9) at different rotation speeds: 225, 750, and 1225 rpm for curves a, b, and c, respectively. E_r = +1.0 V

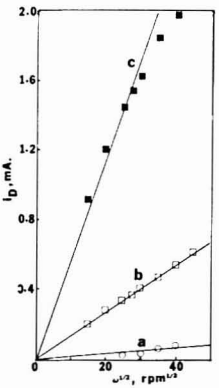

Figure 4. Limiting currents of the disc electrode as function of square root of rotation speed for a nitrogen, air, and oxygen saturated solution (curves a, b, and c, respectively) of 0.1 M KCl and 10^{-4} M FeTMPyP (pH 9)

A single reduction wave with a $E_{1/2} \simeq -0.25$ V is observed for the FeTMPyP–O_2 reduction at the disc. When the ratio of O_2:FeTMPyP becomes large so that the *ec* mechanism becomes pseudo-first-order in FeTMPyP, a second wave at more negative potentials may be observed due to the "excess" O_2 being reduced directly on the glassy carbon electrode. However, in the concentration range where only a single wave is found, the i_D depends linearly on the O_2 concentration and the square root of the rotation speed (see Figure 4).

The number of electrons, n value, involved in the reduction of O_2 was calculated to be 2 ± 0.1 using the limiting disc current, $(i_D)_L$, equation (ref. 4):

$$(i_D)_L = 0.62nFAD^{2/3}\, V^{-1/6}\, \omega^{1/2}\, C^b \qquad (4)$$

where V is the kinematic viscosity, (cm^2/s), ω is the rotation speed (rad/s), C_b is the bulk O_2 concentration (mol/cm^3), D

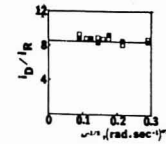

Figure 5. The ratio of disc and ring currents as function of $\omega^{-1/2}$ for an air saturated solution of 0.1 M KCl and 10^{-4} M FeTMPyP (pH 9). ■ $E_D = -0.3$ V, □ $E_D = -0.6$ V

is the diffusion coefficient for O_2 (2.6×10^{-5} cm^2/s), and the other variables have their usual meaning. The n value is consistent with hydrogen peroxide as the product of reactions 1 and 2.

Curves a′, b′, and c′ in Figure 3 correspond to the ring current, i_R, at a set potential of +1.0 V as a function of the time the disc is being scanned from 0 to −0.6 V. The ring potential is set to monitor only H_2O_2 as it is formed at the disc. A diagnostic plot which permits a distinction between reaction intermediates and the products in a parallel reaction path is obtained from the equation (ref. 5):

$$\frac{i_D}{i_R} = \frac{n_1 + Xn_4}{N_0 n_3} + \frac{n_1 + n_2 + Xn_4}{N_0 n_3} \frac{k'}{D} \beta\omega^{-1/2} \quad (5)$$

where N_0 is the collection coefficient, $\beta = 0.643\ V^{1/6} D^{1/3}$ and n_1–n_4 stands for the number of electrons in various possible reactions on the disc and the ring electrodes, namely, the scheme:

$$\text{Disc} \begin{cases} O_2 \xrightarrow{n_1} H_2O_2 \xrightarrow[k']{n_2} H_2O & (6) \\ O_2 \xrightarrow{n_4} H_2O & (7) \end{cases}$$

$$\text{Ring:} \quad H_2O_2 \xrightarrow{n_3} O_2 \quad (8)$$

A plot of i_D/i_R vs. $\omega^{-1/2}$ is shown in Figure 5. A line parallel to the $\omega^{-1/2}$ axis was obtained for the potential range used. From the intercept, the H_2O_2 yield was calculated to be 95%. Furthermore, the slope being zero indicates that $k' = 0$, i.e., that no further reduction of H_2O_2 to H_2O is taking place on the disc. However, thin cell coulometric experiments on the time scale of 5 min or more gave a n value of 4 for the FeTMPyP–O_2 reduction (6). This result was obtained in a cell using a Au minigrid as well as a glassy carbon working electrode. It can be concluded that H_2O_2 is the primary product of O_2 reduction and then it undergoes a slow chemical decomposition to water (probably dismutation to O_2 and H_2O, possibly catalyzed by FeTMPyP). The fate of H_2O_2 in various electrolyte solutions in the absence and presence of various metal porphyrins is presently being evaluated.

The RRDE was also used to estimate the kinetic rate for the *removal of Fe(II)TMPyP by* O_2. The disc electrode generates the Fe(II)TMPyP and the ring current monitors the amount of the Fe(II)TMPyP that survives the passage from the disc to the ring. This was achieved by adjusting the potential of the ring at a value at which only Fe(II)TMPyP (but not H_2O_2) was oxidized. E_R was set at +0.3 V.

Using the equation (ref. 7):

$$I_r(R_J = R_2) = \beta n F \pi R_2^2 D \omega^{3/2} \nu^{-1/2} k^{-1}_{obsd} \quad (9)$$

(Where R_J is the radical coordinate of the reaction front at the electrode surface, R_2 is the inner radius of the ring, $I_r(R_J = R_2)$ is the kinetic ring current, k_{obsd} is the pseudo-second-order rate constant of the homogeneous reaction, and β is a constant determined experimentally to be 210 when I_r is measured in μA.). The rate of the Fe(II)TMPyP removal by O_2 was calculated to be $4(\pm 5) \times 10^7$ M^{-1} s^{-1}. The measured ring currents were only slightly larger than background (≪0.5 μA) which precluded high precision and accuracy of the calculated rate. Further evaluation of the rate parameter is presently underway using spectroelectrochemical methods with optically transparent electrodes and will be reported in a future paper.

CONCLUSION

The results confirm the previous observation that the major product of the catalyzed oxygen reduction by the electrogenerated, *water soluble* Fe(II)TMPyP species is hydrogen peroxide. The rate of the Fe(II)TMPyP removal of O_2 is between 10^7 and 10^8 M^{-1} s^{-1}. With such a fast rate of reaction, the cyclic voltammetric i_p appears essentially diffusion-controlled in O_2. It is interesting to note that the oxygen reduction is occurring at a potential closely related to the redox potential of the iron porphyrin couple. The i–E curves of this couple, as examined by cyclic voltammetry and supported by chronocoulometry data (6) in the absence of O_2, exhibited no evidence of adsorption onto the electrode surface of either the iron(III) or iron(II) porphyrin species. Thus, the water-soluble Fe(III/II)TMPyP cation allows clear delineation of the general overall mechanism where all of the data are consistent with the earlier proposed *ec* catalytic regeneration mechanism.

If superoxide ion, $O_2^{\cdot-}$, is the initial species of the oxygen reduction by Fe(II)TMPyP, its concentration must be lowered to less than 10^{-12} to 10^{-14} M during the reduction since the $E°$ is −0.33 V (vs. NHE, ref. 18) for the reaction:

$$O_2 + e^- = O_2^{\cdot-} \quad (10)$$

Pasternack and Halliwell (9) have recently examined the thermodynamically favored reaction of superoxide ion and Fe(III)TMPyP and found the rate of $O_2^{\cdot-}$ removal to be 3×10^7 M^{-1} s^{-1}. The mechanism postulated was:

$$\text{Fe(III)TMPyP} + O_2 \cdot^- \rightarrow \text{Fe(II)TMPyP+}\ O_2 \quad (11)$$

$$\text{Fe(II)TMPyP} + O_2^{\cdot-} + 2H^+ \rightarrow \text{Fe(III)TMPyP} + H_2O_2 \quad (12)$$

If superoxide is to be implicated in the *ec* mechanism (reaction 2), it is the reverse of reaction 11. Furthermore, the forward and reverse rates of the reaction to be nearly identical is inconsistent with the thermodynamic considerations of reaction 11. There may be a common intermediate which can be formed by either Fe(III)TMPyP and $O_2^{\cdot-}$ or Fe(II)TMPyP + O_2. This intermediate would covalently bond at the axial position of the iron:

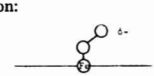

where the oxygen would have a partial negative charge (*10*). To call this intermediate an "iron(III) and superoxide ion" would be a formalism convenient for electron/charge balance purposes. Rapid protonation followed by another electron from either the electrode or another Fe(II)TMPyP would produce hydrogen peroxide. The redox potential of this intermediate is predicted to be a few hundred millivolts more positive than the FeTMPyP couple. At present, there is no experimental evidence to implicate an iron(IV) species. Such a species might be produced if the intermediate is protonated to yield a species resembling HO_2 which is considered a strong oxidant. ($E° = +1.42$ V vs. NHE, ref. 8).

ACKNOWLEDGMENT

The authors acknowledge assistance and discussions with P. Forshey and R. Chan. Communications received from R. Goddard are also appreciated.

LITERATURE CITED

(1) T. Kuwana, M. Fujihira, K. Sunakawa, and T. Osa, *J. Electroanal. Chem.*, 88, 299 (1978).
(2) R. J. H. Chan and T. Kuwana, to be published.

(3) R. F. Pasternack, H. Lee, P. Malek, and C. Spencer, *J. Organ. Nucl. Chem.*, **39**, 1865 (1977).
(4) H. R. Thirsk and J. A. Harrison, "A Guide to the Study of Electrode Kinetics", Academic Press, London and New York, 1972, p 84.
(5) W. J. Albery and M. L. Hitchman, "Ring-Disc Electrodes", Clarendon Press, Oxford, 1971, Chap. 6, p 73.
(6) P. A. Forshey and T. Kuwana, to be published.
(7) D. C. Johnson and S. Bruckenstein, *J. Am. Chem. Soc.*, **90**, 6592 (1968).
(8) D. T. Sawyer and E. T. Seo, *Inorg. Chem.*, **16**, 499 (1977).
(9) R. F. Pasternack and B. Halliwell, *J. Am. Chem. Soc.*, **101**, 1026 (1979).
(10) J. P. Collman, R. R. Gagne, C. A. Reed, T. R. Halbert, G. Lang, and W. T. Robinson, *J. Am. Chem. Soc.*, **97**, 1427 (1975).

RECEIVED for review June 14, 1979. Accepted August 30, 1979. This work was supported by a grant from the U.S. Air Force Office of Scientific Research (AFOSR-78-3672).

Radiation-Induced Surface Redox and Shake-Up Structure in X-Ray Photoelectron Spectra of Copper(II) Chelates

Michael Thompson,* R. Bruce Lennox, and Deborah J. Zemon

Department of Chemistry, University of Toronto, 80 St. George Street, Toronto, Ontario, Canada, M5S 1A1

X-ray photoelectron spectroscopy of the copper(II) complex of 1,8-bis(2′-pyridyl)-3,6-dithiaoctane in the S 2p and Cu $2p_{3/2}$ regions has confirmed that the chelate exhibits an X-ray-induced surface redox reaction. Oxidation of the sulfur moiety to the level of a sulfone is possible through a reaction with "spectrometer" oxygen-containing species. The beam-induced reaction has also been demonstrated in a variety of other Cu(II) chelates. Shake-up satellite peaks are discussed in terms of known optical absorption data.

The potential of X-ray photoelectron spectroscopy (XPS) as an analytical technique for the investigation of the nature of metal coordination in metalloproteins has attracted considerable interest in recent years (*1*). Much of this work has been directed toward the chemical shift effect with respect to core levels in both the metal and coordinating groups. Gray and co-workers (*2*, *3*) have reported on sulfur–copper coordination in the blue electron-carrying protein, plastocyanin, and in oxyhemocyanin. Although the plastocyanin study suggested that a 4–5 eV shift in the S 2p peak occurs on sulfur–copper coordination, one group proposed that the shift could be attributed to an oxidized sulfur impurity (*4*). In the view of Baker, Brisk, and Liotta (*5*) such an impurity could result from radiation damage. Using a model complex Thompson et al. (*6*) were able to reproduce the higher binding energy peak and indicated that it could be caused by a radiation-induced copper-catalyzed oxidation of ligated sulfur. A similar opinion has been offered by Walton and co-workers (*7*). Finally, the possibility that the peak is not associated with a shift effect but is caused by a shake-up transition has been raised by Larsson (*8*).

The shake-up satellite structure observed on the low kinetic energy side of the main peak or photoline in many XP spectra has been the subject of much recent study (*9*, *10*). In the case of transition metal complexes and certain other systems, the charge transfer transition has been implicated as the mode of electron promotion that occurs with the photoionization process (*11*). Others have argued that neither satellite energies nor satellite intensities are well predicted by the charge transfer model (*12*). The information yielded by interpretation of shake-up structure has great promise in the elucidation of the nature of metal–ligand bonding, such as coordination geometry and bond covalency (*13*). With regard to copper(II) complexes, an earlier suggestion that shake-up structure is related to 3d → 4s, 4p transitions (*14*) has apparently been re-interpreted in terms of charge transfer processes (*15*).

The present paper includes a report on further studies of the radiation-induced surface effect in a series of copper(II) complexes which encompasses biological analogues involving N, S, and O coordination. In addition, shake-up structure is discussed in terms of optical absorption data obtained from the literature.

EXPERIMENTAL

The copper(II) complexes of imidazole–$Cu(imi)_4Cl_2$ (system VI), ethylenediamine–$[Cu(en)_2]SO_4$ (VII) and $[Cu(en)_3]SO_4$ (VIII), σ-phenanthroline–$[Cu(phenan)_2(OAc)_2]$ (IX), 2,2′-biquinolyl-$[Cu(biq)Cl_2]$ (X), 8-hydroxyquinoline–$Cu(quinolato)_2$ (XI), pyridine–$[Cu(pyr)_2Cl_2]$ (XII) and $[Cu(pyr)_4(NO_3)_2]$ (XIII), thiosemicarbazide–$[Cu(tsc)_2Cl_2]$ (XIV), and diethylthiocarbamate–$Cu(detc)_2SO_4$ (XV) were synthesized according to standard procedures given in the literature. The complexes of 1,8-bis(2′-pyridyl)-3,6-dithiaoctane–$[Cu(C_{16}H_{20}N_2S_2](ClO_4)_2$ (I), 1,8-diamino-3,6-dithiaoctane and 1-methylimidazole-$[Cu(C_6H_{16}N_2S_2)(C_4H_8N_2)](ClO_4)_2$ (II), 1,9-diamino-3,7-dithianonane–$[Cu(C_7H_{18}N_2S_2)](ClO_4)_2$ (III), 1,11-diamino-3,6,9-trithiadecane–$[Cu(C_8H_{20}N_2S_3)](ClO_4)_2$ (IV) and *N*,*N*′-ethylene-bis(σ-hydroxybenzylamine)–$[Cu(C_{16}H_8N_2O_2)]$ (V) were available in this laboratory. Schematic representations of the systems (I to XV) are depicted in Figure 1.

X-ray photoelectron measurements were made on the samples pressed into graphite with a McPherson ESCA36 spectrometer using Mg Kα radiation. Spectra were recorded under conventional conditions and calibrated in the usual manner.

RESULTS AND DISCUSSION

The time-dependent Cu $2p_{3/2}$ and S 2p spectra of system I are shown in Figure 2, and representative Cu $2p_{3/2}$ spectra of remaining compounds containing Cu–S bonds and those with metal to N and/or O bonds are given in Figures 3 and 4, respectively. The peaks in each of the metal-core spectra can be divided into two categories. The first group consists of either a pair of peaks within 3 eV of each other or a single peak at approximately the expected position of the Cu $2p_{3/2}$ photoline. Where twin peaks are observed, the ratio of high binding energy peak to low binding energy component differs considerably among the various systems. The second group, often of weak intensity and containing more than one component, lies between 6 to 10 eV to the high binding energy side of the photoline(s). These peaks clearly relate to shake-up processes but the provenance of the first group is not immediately obvious.

Possible sources of low kinetic energy satellites close to the main photoline are the shake-up transition or multiplet splitting effects. Alternatively the twin-peak structure may

0003-2700/79/0351-2260$01.00/0

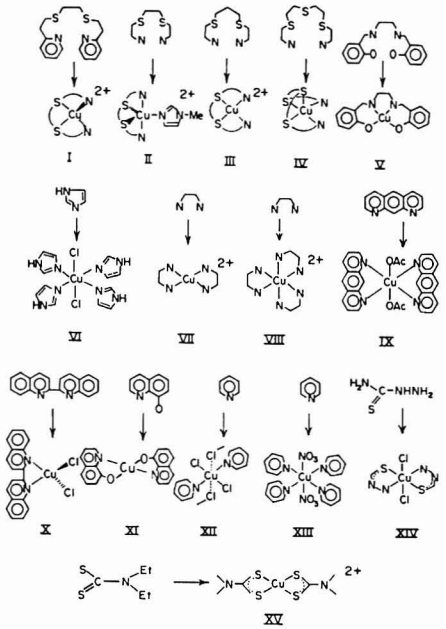

Figure 1. Suggested structures of the various ligand and complex systems

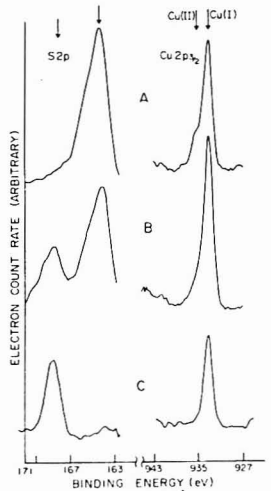

Figure 2. Sulfur 2p and Cu $2p_{3/2}$ XP spectra of the Cu(II) complex of 1,8-bis(2'-pyridyl)-3,6-dithiaoctane. (A) 20-min X-ray exposure, (B) 12-h exposure to X-ray beam, and (C) 10-s exposure to 10-μA argon-ion beam

relate to the valence condition or the chemical environment of the ligated copper atom. Such a result could only be explained by the presence of a sample impurity. The consensus of opinion among electron spectroscopists is that

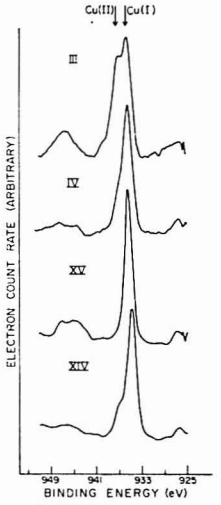

Figure 3. Representative XP Cu $2p_{3/2}$ spectra of chelates containing metal to sulfur bonds

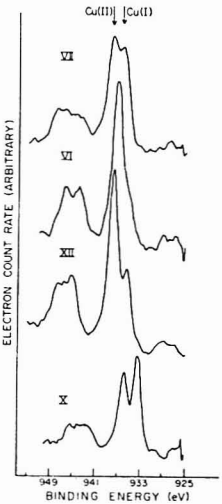

Figure 4. Representative XP Cu $2p_{3/2}$ spectra of chelates with N and/or O to metal bonds

multiplet splitting is not a significant source of satellite structure on transition metal 2p peaks, but it does appear to generate photoline broadening (*16*). In the case of Cu $2p_{3/2}$ the broadening effect has been set at approximately 1.3 eV. Clearly, the twin-peak structure obtained in this work is not compatible with the "no-peak" nature of multiplet splitting. It seems unlikely that the origin of the peaks lies in a shake-up process in the light of the variability in the ratio of peak intensities. Hence, the question of sample contamination has to be considered as the most likely explanation.

We have shown previously that the S 2p spectra of system I are time-dependent with respect to exposure to the source

Table I. XP Cu $2p_{3/2}$ Data and Optical Charge Transfer Assignments for Copper(II) Chelates

	XPS Cu $2p_{3/2}$				optical charge transfer	
compound	Cu(II), eV	Cu(I), eV	approx. Cu(II)/Cu(I) ratio	ΔE,[a] eV	band, cm^{-1} (eV)	assignment
I	935.2	933.5	0.5	9.1	28 000 (3.5)	$S(\sigma) \rightarrow Cu$
II	935.2	933.9	0.6	8.0	31 000 (3.8)	$S(\sigma) \rightarrow Cu$
					38 000 (4.7)	$N(\sigma) \rightarrow Cu$
III	936.7	935.3	0.3	9.4	31 000 (3.8)	$S(\sigma) \rightarrow Cu$ $(d_{x^2-y^2})$
					40 000 (5.0)	$N(\sigma) \rightarrow Cu$
IV	936.5	935.2	0.2	9.6	29 000 (3.6)	$S(\sigma) \rightarrow Cu$
					40 000 (5.0)	$N(\sigma) \rightarrow Cu$
V	935.1	*b*	>4	9.3	25 500 (3.2)	$Cu \rightarrow phen(\pi^*)$
					30 500 (3.8)	$Cu \rightarrow phen(\pi^*)$
VI	936.9	934.7	3	7.0	32 400 (4.0)	$N(\sigma) \rightarrow Cu$ and
				9.2		$Cu \rightarrow imi(\pi^*)$
VII	938.0	936.0	1	6.0	~40 000 (4.7)	$N(\sigma) \rightarrow Cu$
				9.2		
VIII	937.4	*b*	3	9.0	~40 000 (4.7)	$N(\sigma) \rightarrow Cu$
IX	936.2	934.2	0.8	8.4		
X	935.8	933.4	0.8	7.4	>20 000 (2.5)	$Cu \rightarrow biq(\pi^*)$
				9.4		
XI	936.0	*b*	3	9.2	23 000 (2.9)	$Cu \rightarrow phen(\pi^*)$
					28 000 (3.5)	$Cu \rightarrow phen(\pi^*)$
XII	937.8	935.6	2	7.5	~30 000 (3.7)	$Cl(\pi) \rightarrow Cu$
				9.5		
XIII	938.0	*b*	>4	7.0		
				9.1		
XIV	*b*	934.8	<0.2	~9.0	23 000 (2.9)	$Cl(\pi) \rightarrow Cu$
					29 000 (3.7)	$Cu \rightarrow tsc(\pi^*)$
XV	*b*	935.4	<0.2	~7.6	23 000 (2.9)	$Cu \rightarrow detc(\pi^*)$
				~9.6		

[a] Energy difference between Cu(II) photoline and satellite(s). [b] Shoulder not sufficiently resolved to assign a binding energy.

beam (*6*). The corresponding Cu $2p_{3/2}$ spectra are shown in Figure 2 for both source exposure of various periods of time and for short exposure to an argon-ion beam. The concomitant reduction in intensity of the high binding energy component of the pair of metal core-level peaks with exposure, and removal of this line by severe treatment can be rationalized in terms of the valence state of copper at the "surface" of the particulate sample. Convincing evidence has been presented in the literature to the effect that a shift of approximately 2 eV is expected between Cu(I) and Cu(II) 2 $p_{3/2}$ peaks, with the higher binding energy line associated with the latter (*17*). The relatively low intensity of the high binding energy peak for S 2p compared to that for the low binding energy component of Cu $2p_{3/2}$ strongly implies that a Cu(I)/Cu(II) condition occurs at the "surface" of the sample of system I, since the escape depth of the metal 2p photoelectrons (~320 eV) would be expected to be significantly lower than that for photoelectrons originating from the sulfur 2p level (~1086 eV).

These results confirm that a "surface" reduction of copper has occurred in system I. Although damage by natural light cannot be excluded as a contributing factor, it certainly appears that the effect is exacerbated by X-ray exposure. The photochemical reaction exhibited in system I is not surprising in the light of the large amount of data on photoreduction of copper(II) in the literature (*18*). It is interesting to note that with copper(II) systems in solution, visible light irradiation does not appear to cause a reaction but radiation corresponding to ligand-to-metal charge transfer bands induces reduction (*19*). Furthermore, it is apparent that the ligand radical produced in this type of reaction may undergo secondary reactions with the solvent or other species in solution. In view of this evidence, we postulate that the oxidized sulfur moiety in system I reacts with adsorbed oxygen-containing compounds producing a surface species of sulfur at the oxidation level of a sulfone. In this regard, it is interesting to note that Burness and co-workers (*20*) also suggested that X-ray promoted chemical change of an imine linkage occurs via "spectrometer" water.

With regard to the other systems described here the Cu(I)/Cu(II) system binding energies are given in Table I. Where a single peak is observed, the binding energy is assigned on the basis of peak width at half height (i.e. Cu(II) $2p_{3/2}$ exhibits multiplet splitting). Since the metal–core spectra were recorded under similar conditions, the relative severity of the beam-induced damage of the compounds requires comment, although it is clearly dangerous to arrive at specific damage-structure correlations. All the chelates containing Cu–S bonds (I to IV, XIV, XV) exhibit significantly greater photoreduction than those with N and/or O bonds to metal. Additionally, it appears that systems containing pyridine and imidazole rings are more resistant to the effect than those with conjugated rings such as biquinolyl. These results are entirely consistent with the accepted behavior of the appropriate donor species with respect to polarizability and relative electronegativity.

We now turn to the shake-up structure observed in the Cu $2p_{3/2}$ spectra. If the charge transfer model of the shake-up process is correct, it would seem reasonable to expect at least an empirical relationship to exist between charge transfer data obtained from optical spectroscopy and photoline-shake-up energy differences. In summary, the shake-up process is governed by monopole selection rules, viz. $\Delta J = \Delta L = \Delta S = \Delta m_j = \Delta m_s = 0$, whereas allowed transitions in optical spectroscopy are controlled by dipole rules ($\Delta 1 = \pm 1$, $\Delta S = 0$). Using optical charge transfer terminology Kim (*11*) suggested that allowed shake-up "channels" involve $L \rightarrow M$ or $M \rightarrow L$ electron transfers. This model has been employed to provide an argument for the preferential presence of satellite structure on the metal or ligand photolines depending on the contribution of the metal or ligand orbitals to the orbitals involved in the transition (*13*).

Optical charge transfer data gleaned from the literature and XPS shake-up data for compounds I–XV are summarized in Table I. Before attempting to delineate a correlation, several cautionary factors must be specified. First, solid-state broadening tends to merge shake-up structure. Second, much of the optical data have been obtained from experiments carried out in solution. In a sense, it is more desirable to compare shake-up structure (solid-phase) with reflectance spectra. A good case in point is system XIV, where the 23 000 cm^{-1} band due to a Cl → Cu transition is missing in solution spectra. Third, no detailed MO energy level picture exists for these compounds and therefore the optical assignments are often somewhat arbitrary. Fourth, since the compounds studied in this work are partially converted to species involving Cu(I), the intensity of the shake-up structure will be altered.

The optical charge transfer data of compounds I to XV is dominated by bands in the 30 000–40 000 cm^{-1} range (3.7–5.0 eV). In certain cases, more than one transition has been postulated; for example, convincing evidence has been presented for N(σ) → Cu d_{z^2,y^2} (40 000 cm^{-1}) and S(σ) → Cu d_{z^2,y^2} (30 000 cm^{-1}) assignments in the spectra of compounds I to IV, used as models for plastocyanin (*21*). Although equivalent shake-up processes should occur, because of broadening effects one would not expect to be able to distinguish the corresponding peaks in XP spectra. Shake-up structure in nearly all the chelate spectra is centered for the most part at 8 eV from the main photoline (Cu(II) $2p_{3/2}$). The apparent split of the structure into two peaks in some spectra is similar to observations made for other Cu(II) compounds (*22*). The central question in assigning the structure is whether the XP shake-up transition involves virtual orbitals which reflect the same levels given above for the corresponding optical transitions. If this is indeed the case, then the shake-up energies appear to be too high with the discrepancy being about 3–4 eV.

In order to assign the shake-up peaks, molecular relaxation effects that occur on photoionization must be considered. The creation of a positive hole will result in significant stabilization of a number of valence and virtual orbitals. Both contraction and molecular flow are expected to contribute to the relaxation process. To account for the high shake-up energies obtained in comparison to those predicted for a charge transfer process, increased separation of e_g-like bonding and e_g-like crystal-field orbitals must be considered. However, calculations have indicated that such energy differences are actually smaller in the core-ion state than in the ground-state (*12*). Such a model would necessitate assignment of the shake-up peaks to crystal-field orbital-to-conduction band transitions, although these are formally forbidden based on the monopole selection rules. On the other hand it is possible that the relaxation process does in fact widen the "gap" between orbitals participating in the shake-up promotion of electrons as is implied in calculations of relaxation effects with regard to molecular Auger spectra (*23*, *24*).

In the light of the propositions expressed above, the nature of shake-up transitions in Cu(II) compounds relative to those exhibited by Cu(I) species deserves comment. It has been suggested that interpretation of shake-up structure in terms of the charge transfer model rules out the possibility of such a process with Cu(I) compounds owing to its $(t_{2g})^6(e_g)^4$ configuration (*12*). However, peaks of weak intensity have in fact been observed in the spectra of Cu(I) samples, but they have been assigned to energy-loss processes. It is apparent that these peaks may indeed be due to genuine shake-up transitions. Since shake-up intensity is known to be related to the magnitude of charge redistribution in the core-ion state, it is possible that this would be minimal with Cu(I) species resulting in peaks of weak intensity.

CONCLUSIONS

The results presented in this work reveal the occurrence of photoinduced redox reactions at the "surface" of solid Cu(II) chelates. The possibility exists that such an effect has not been confirmed previously because the resulting Cu(I)–Cu(II) peak split has not been resolved sufficiently to allow appropriate spectral interpretation. It is clear that great care should be exercised in future in the assignment of shifts of coordinating group binding energy to metal ligation. Interestingly, the occurrence of a ligand group shift may imply ipso facto that the ligand is bonded to a metal.

In view of the uncertainty of assignment of shake-up peaks in the spectra of Cu(II) compounds, it appears that the potential of such transitions for the elucidation of the nature of metal-coordination sites in solid samples is limited until further definitive experimental and theoretical work is carried out. This is especially true for the analytical chemist who may be interested in structures of metalloproteins where the concentration of metal is inherently low.

ACKNOWLEDGMENT

We are indebted to B. Bosnich of the University of Toronto for the provision of samples of compounds I to V.

LITERATURE CITED

(1) H. Rupp and U. Weser, *Biochim. Biophys. Acta*, **446**, 151 (1976).
(2) E. L. Solomon, P. J. Clendening, H. B. Gray, and F. J. Grunthaner, *J. Am. Chem. Soc.*, **97**, 3878 (1975).
(3) J. A. Wurzbach, P. J. Grunthaner, D. M. Dooley, H. G. Gray, F. J. Grunthaner, R. R. Gay, and E. I. Solomon, *J. Am. Chem. Soc.*, **99**, 1257 (1977).
(4) J. Peeling, B. G. Haslett, I. M. Evans, D. T. Clark, and D. J. Boulter, *J. Am. Chem. Soc.*, **99**, 1025 (1977).
(5) A. D. Baker, M. A. Brisk, and D. C. Liotta, *Anal. Chem.*, **50**, 328R (1978).
(6) M. Thompson, J. Whelan, D. J. Zemon, B. Bosnich, E. I. Solomon, and H. B. Gray, *J. Am. Chem. Soc.*, **101**, 2482 (1979).
(7) V. Srinivasan, E. I. Stiefel, A. Elsberry, and R. A. Walton, *J. Am. Chem. Soc.*, **101**, 2611 (1979).
(8) S. Larsson, *J. Am. Chem. Soc.*, **99**, 7708 (1977).
(9) M. A. Brisk and A. D. Baker, *J. Electron Spectrosc. Relat. Phenom.*, **7**, 197 (1975).
(10) G. A. Vernon, G. Stucky, and T. A. Carlson, *Inorg. Chem.*, **15**, 278 (1976).
(11) K. S. Kim, *J. Electron Spectrosc. Relat. Phenom.*, **3**, 217 (1974).
(12) J. A. Tossell, *J. Electron Spectros. Relat. Phenom.*, **10**, 169 (1977).
(13) G. M. Bancroft, B. D. Boyd, and D. K. Creber, *Inorg. Chem.*, **17**, 1008 (1978).
(14) D. C. Frost, A. Ishitani, and C. A. McDowell, *Mol. Phys.*, **24**, 861 (1972).
(15) D. C. Frost, C. A. McDowell, and R. L. Tapping, *J. Electron Spectrosc. Relat. Phenom.*, **6**, 347 (1975).
(16) C. S. Fadley and D. A. Shirley, *Phys. Rev. A*, **2**, 1109 (1970).
(17) H. Rupp and U. Weser, *Bioinorg. Chem.*, **5**, 43 (1976).
(18) V. Balzani and V. Carassiti, "Photochemistry of Coordination Compounds", Academic Press, New York, 1970.
(19) H. D. Gafney and R. L. Lintvedt, *J. Am. Chem. Soc.*, **93**, 1623 (1971).
(20) J. Burness, L. Taylor, and J. Dillard, *J. Electron Spectrosc. Relat. Phenom.*, **8**, 483 (1976).
(21) A. R. Amundsen, J. Whelan, and B. Bosnich, *J. Am. Chem. Soc.*, **99**, 6730 (1977).
(22) M. S. Ioffe and Yu. G. Borod'ko, *J. Electron Spectrosc. Relat. Phenom.*, **11**, 235 (1977).
(23) R. H. A. Eade, M. A. Robb, I. G. Csizmadia, and G. Theodorakopoulos, *Chem. Phys. Lett.*, **52**, 526 (1978).
(24) M. Thompson, P. A. Hewitt, and D. S. Woolliscroft, *Anal. Chem.*, **48**, 1336 (1976).

RECEIVED for review July 23, 1979. Accepted August 22, 1979. Support for this work from the Natural Sciences and Engineering Research Council of Canada is gratefully acknowledged.

Analysis of Metal Alloys by Inductively Coupled Argon Plasma Optical Emission Spectrometry

Arthur F. Ward* and Louis F. Marciello

Jarrell-Ash Division, Fisher Scientific Company, 590 Lincoln Street, Waltham, Massachusetts 02154

A technique for analyzing metal alloys using a direct-reading inductively coupled argon plasma (ICAP) spectrometer is described in which samples are acid-dissolved before analysis. Because a concentration ratio method is used for analysis, dilution errors of up to ±40% can be tolerated without significant loss of accuracy. The ICAP technique is used to determine 17 elements in irons and steels, 14 elements in copper-based alloys, and 12 elements in aluminum alloys. The analytical accuracy of these determinations is verified by the analysis of standard reference materials for each sample matrix.

Routine analyses of metal alloys in quality control laboratories are performed most commonly by spark emission spectrometry or X-ray fluorescence because of rapid sample turnaround and ease of operation. The problem with both of these techniques is that the analytical signal is highly dependent on matrix composition. Precise matching of sample and standard matrices is required if accurate results are to be obtained. However, certified standards for calibration that match the samples to be analyzed often are difficult to find. Other alternatives, e.g., wet chemistry procedures, are unaffected by the certified standards problem because synthetic standards can be prepared readily, but such methods are time-consuming. Also, analytical determinations must be made sequentially, compounding the time factor. Atomic absorption spectrometry is a faster analytical technique than wet chemistry but, again, determinations are made sequentially. The inductively coupled argon plasma (ICAP) spectrometry technique has positive characteristics for application to metal alloy analysis, i.e., its simultaneous, multielement determination capability and its use of synthetic standards.

Fassel and Dickinson (*1*) described a method of analyzing arsenic and tin in solders that involved melting the sample, forming an aerosol by ultrasonic nebulization, and analyzing the aerosol by ICAP. Hoare and Mostyn (*2*) described a high frequency plasma method for determining boron and zirconium in nickel-based alloys following sample dissolution. Souilliart and Robin (*3*) described a method for determining hafnium in zirconium by ICAP. Kirkbright and Ward (*4*) compared the ICAP with flame emission using a separated nitrous oxide–acetylene flame for the determination of copper, zinc, iron, titanium, manganese, and magnesium in aluminum alloys and concluded that the ICAP gave better precision and offered simultaneous multichannel analytical capability.

Butler et al. (*5*) described a procedure for the determination of aluminum, chromium, copper, manganese, and nickel in steel samples using an ICAP spectrometer that had been calibrated with synthetic standards prepared in the presence of iron only. With this minimal matrix matching, these workers were able to analyze low alloy, high alloy, and stainless steels with the same calibration curve.

Other applications of the ICAP to metal alloy analyses in which several elements have been determined in various sample matrices also have been reported in the literature (*6–10*). However, none of these reports has covered the simultaneous multielement analysis of the metal alloy sample in a truly comprehensive fashion.

In this paper, we describe the analysis of iron-based, copper-based, and aluminum-based alloys in which the majority of the alloying components is determined and the concentration ratio method of analysis employed. The concentration ratio method offers a potential analytical advantage; only relative solution concentrations rather than absolute solution concentrations are required for analysis. Consequently, there is no need to weigh the initial sample or measure the final volume accurately, provided that the solution concentrations of both analyte and matrix are within the instrument's calibration range. The elimination of the need for accurate sample weighing not only speeds up sample preparation but also prevents any potential errors that may be caused by misreading or mistakes in arithmetic or transcription.

EXPERIMENTAL

Theory. Because the concentration ratio method of analysis is described fully elsewhere (*11*), only a brief discussion will be presented here.

If the concentration of the ith analyzed element in the original sample is C_i, the concentration of the jth unanalyzed element is C_j and the matrix element concentration is C_M, then

$$\sum_i C_i + \sum_j C_j + C_M = 100 \tag{1}$$

where all concentrations are in percentages. This equation then may be arranged to the form:

$$1 + \frac{\sum C_i}{C_M} = 1 + \sum_i B_i = \frac{100 - \sum_j C_j}{C_M} \tag{2}$$

where B_i is the concentration ratio of the ith element to the matrix element.

When the analytical technique exhibits a linear relationship between signal and concentration, then the ratio of the net line intensity of the ith element to the matrix element, R_i, may be described by Equation 3, where p_i and q_i are calibration constants:

$$R_i = p_i + q_i B_i \tag{3}$$

Given this, the concentration ratio technique should give equivalent data regardless of the absolute solution concentrations and hence be independent of the weight of solid used or the final dilution volume.

Once the concentration ratios and any residual concentration (C_j) have been determined, then Equation 2 may be solved to determine the matrix element concentration (C_M). From this value and the determined concentration ratio (B_i), the absolute concentration of the ith element in the original sample is calculated from Equation 4:

$$C_i = B_i C_M \tag{4}$$

If the relationship is not linear, however, this freedom from solution concentration and the concentration ratio technique are not valid. For example, if the analytical equation is second order, Equation 3 is modified to Equation 5, where p_i, q_i, and r_i are the

0003-2700/79/0351-2264$01.00/0

Table I. Elements and Analytical Wavelengths (nm) Employed

element	copper		iron		aluminum	
	line	bkgd[a]	line	bkgd[a]	line	bkgd[a]
Ag	328.068	328.102	...[b]	---	...[b]	---
Al	308.215	308.249	308.215	308.249	308.215[c]	---
As	193.696	193.730	193.696	193.730	...[b]	---
B	...[b]	---	249.773	249.807	...[b]	---
Cd	226.502	226.536	...[b]	---	...[b]	---
Co	...[b]	---	228.616	228.650	...[b]	---
Cr	...[b]	---	267.716	267.750	267.716	267.750
Cu	213.598[c,d]	---	324.754	324.788	324.754	324.788
Fe	259.940	259.974	238.863[c]	---	259.940	259.974
Mg	...[b]	---	...[b]	---	383.231[d]	---
Mn	257.610	257.644	257.610	257.644	257.610	257.644
Mo	...[b]	---	202.030	202.064	...[b]	---
Nb	...[b]	---	313.079	313.113	...[b]	---
Ni	231.604	231.621	231.604	231.621	231.604	231.621
P	253.565	253.599	214.914	214.931	...[b]	---
Pb	220.353	220.387	...[b]	---	220.353	220.387
Sb	217.581	217.615	...[b]	---	217.581	217.615
Si	288.158	288.192	288.158	288.192	...[b]	---
Sn	189.989	190.023	...[b]	---	189.989	190.023
Ta	...[b]	---	240.063[d]	---	...[b]	---
Ti	...[b]	---	334.941	334.978	334.941	334.978
V	...[b]	---	292.402	292.436	...[b]	---
W	...[b]	---	207.911	207.945	...[b]	---
Zn	206.200	206.217	...[b]	---	213.856	213.890
Zr	...[b]	---	339.198	339.222	...[b]	---

[a] Background measurement wavelength. [b] Signifies element not determined. [c] Signifies used as internal standard, no background correction employed. [d] Line selected on external monochromator.

Table II. Operating Conditions

ICAP	
Plasma torch	Quartz type, 1-mm nozzle diameter
Argon gas flows	Coolant—18 L/min Auxiliary—0.5 L/min Sample—0.7 L/min
Peristaltic pump	Gilson Minipuls II
Solution uptake rate (pumped)	0.95 mL/min
Forward RF power	1.2 kW
Reverse RF power	<5 W
Induction coil	Three-turn water-cooled copper tubing
Optics	
Focusing element	Separate off-axis front-surfaced concave mirrors for direct reader and monochromator
Magnification	×3.6 nominal
Height of observation plasma	18 mm above coil
Entrance slit aperture	3 mm
Direct reader	
Entrance slit	25 μm
Exit slits	50 μm
Grating	2360 gr/mm ruled concave
Blaze	270 nm
Direct reader	
Dispersion	0.53 nm/mm first order
Monochromator	
Entrance slit	10 μm
Exit slit	20 μm
Grating	1180 gr/mm ruled plain
Blaze	270 nm
Dispersion	1.6 nm/mm first order
Electronics	
PMT	Hamamatsu type R427—185-200 nm direct reader, R300—250-500 nm direct reader, R456—185-800 nm monochromator
Voltage	600-950 V
Read out	Central processing unit (PDP-8A, DEC, Maynard, Mass.), controlled individual op-amp analog integrators with multiplexed A/D converters
Integration period	14 s—line 7 s—background
CPU terminal	LA-36 DECwriter (DEC, Maynard, Mass.)
CPU mass storage	RX01 Dual Floppy Disks (DEC, Maynard, Mass.)

calibration constants and C'_i is the solution concentration of the ith element:

$$R_i = p_i + q_i B_i + r_i B_i C'_i \quad (5)$$

Since Equation 5 has two unknowns, B_i and C'_i, it is impossible to use the concentration ratio method from a single measurement. Reasonable approximations can be made if either, or preferably both, the terms r_i and C'_i are small, and the matrix element constitutes over 90% of the sample and remains fairly constant. If the matrix element is subject to large variations in concentration and constitutes only 50–70% of the sample, e.g., iron in stainless or high alloy steels, or copper in brass, then the likelihood for substantial error exists, especially for the major alloying elements.

Spectral Line Interference Corrections. In any emission spectroscopic technique, the possibility always exists of spectral line interferences from a concomitant species upon the analyte line. The ICAP technique is no exception to this condition. The high precision of the ICAP coupled with the ease with which synthetic standards can be prepared makes the correction of spectral interferences a much simpler task when compared with other emission techniques.

In the spectrometer data processing unit, corrections for spectral line overlap are made on the ith element from the kth element using Equation 6, where B_i is the corrected concentration ratio,

Table III. Linear Calibration Verification Standards

Copper

% w_a/w_m[a] in sample	mg/L in solution	elements
0, 0.05, 0.1, 0.2	0, 2.5, 5, 10	Ag, As, Cd, Mn, Ni, P, Sb, Si
0, 0.2, 0.5, 1.0, 2.0	0, 10, 25, 50, 100	Fe, Sn
0, 0.5, 1.0, 2.0, 5.0	0, 25, 50, 100, 250	Al, Pb
0, 1, 5, 10, 20, 50	0, 50, 250, 500, 1000, 2500	Zn
100	5000	Cu (added to all standards)

Iron

0, 0.05, 0.1, 0.2	0, 2.5, 5	As, B, P, Zr
0, 0.05, 0.1, 0.2, 0.5	0, 2.5, 5, 10, 25	Co, Cu, Nb, Ta, V, W
0, 0.2, 0.5, 1.0, 2.0	0, 5, 25, 50, 100	Al, Mn, Si
0, 0.5, 1.0, 2.0, 5.0	0, 25, 50, 100, 250	Mo, Ti
0, 1, 5, 10, 20	0, 50, 250, 500, 1000	Cr, Ni
100	5000	Fe (added to all standards)

Aluminum

0, 0.05, 0.1	0, 0.5, 1	Cr, P, Sb, Sn
0, 0.05, 0.1, 0.2, 0.5	0, 0.5, 1, 2, 5	Fe, Pb
0, 0.2, 0.5, 1.0, 2.0	0, 2, 5, 10, 20	Mn, Ni
0, 1, 2, 5, 10	0, 10, 20, 50, 100	Cu, Zn
0, 2, 5, 10, 25	0, 20, 50, 100, 250	Mg
100	1000	Al (added to all standards)

Multielement Standards

Copper based alloys

standard #	element	mg/L solution	$\%w_a/w_m$ in solid
1	Cu	5000	100
2	Cu	5000	100
	Zn	2500	50
3	Cu	5000	100
	Ag	5	0.1
	Pb	250	5.0
	Sn	50	1.0
4	Cu	5000	100
	Al	250	5.0
	Fe	10	0.2
	Mn	5	0.1
	Ni	5	0.1
5	Cu	5000	100
	As	5	0.1
	Cd	5	0.1
	P	5	0.1
	Sb	5	0.1
	Si	5	0.1

Iron based alloys

1	Fe	5000	100
2	Fe	5000	100
	Cr	1000	20
	Cu	100	2.0
	Mn	100	2.0
	Ni	1000	20
3	Fe	5000	100
	Al	100	2.0
	Co	100	2.0
	Mo	100	2.0
	Ti	100	2.0
4	Fe	5000	100
	Nb	10	0.2
	Ta	10	0.2
	V	10	0.2
	W	10	0.2
	Zr	10	0.2
5	Fe	5000	100
	As	10	0.2
	B	10	0.2
	P	10	0.2
	Si	10	0.2

Aluminum based alloys

1	Al	1000	100
2	Al	1000	100
	Cu	100	10
	Si	100	10
3	Al	1000	100
	Zn	100	10
4	Al	1000	100
	Mg	100	10
	Ni	100	10
5	Al	1000	100
	Cr	10	1
	Fe	10	1
	Mn	10	1
	Pb	10	1
	Sb	10	1
	Sn	10	1
	Ti	10	1
	Zr	10	1

[a] Weight of analyte elements/weight of matrix elements.

B'_i is the uncorrected concentration ratio, B_k is the concentration ratio of the interfering element and K_{ik} is the empirically determined interference factor:

$$B_i = B'_i - \sum_k K_{ik}B_k \quad (6)$$

These empirical interference factors are determined subsequent to the calibration routine and are applied automatically by the central processor prior to the output of the determined concentration ratios.

Interference corrections from the matrix element do not have to be determined empirically since the instrument is standardized by Equation 3, which automatically relates the concentration of the matrix element to the intensity ratio.

Instrumentation. A Model 96-986 (Jarrell-Ash Division, Fisher Scientific Company, Waltham, Mass. 02154) ICAP Atom-Comp Direct Reading Spectrometer programmed for the elements listed in Table I was used for this study. Automatic background correction provided by a Model 90-555 Spectrum Shifter attachment (Jarrell-Ash) was used for the lines designated in Table I. Lines not programmed into the unit were measured with a Model 96-978 N+1 Channel, a 0.5-m Ebert scanning monochromator (Jarrell-Ash). The operating conditions for the ICAP and spectrometers are shown in Table II.

Reagents. Stock calibration standards containing 1% w/v of the analyte were prepared from spectroscopically pure chemicals (Specpure grade, Johnson Matthey Co. Ltd., England) dissolved in high purity acids (Hipure grade, Fisher Scientific Co., Fair Lawn, N.J.). The same high purity acids were used to dissolve the samples.

Method. *Copper-Based Alloys.* About 250 mg of sample (usually chips or turnings) was transferred to a 2-oz plastic bottle. One milliliter of concentrated nitric acid was added. After the reaction subsided, 15 mL of concentrated hydrochloric acid was

Table IV. Correction Factors (K_{ik}) for Spectral Interferences

	element	interferent	factor
copper alloys	As	Al	0.00467
		Fe	0.00044
	P	Fe	0.87841
	Pb	Al	−0.00100
	Sb	Mn	0.00074
		Al	0.00199
		Pb	0.00417
		Fe	0.00112
		Zn	0.00016
	Sn	Zn	0.00200
iron alloys	Al	Mn	0.00086
		Mo	0.00731
		Co	−0.00640
		V	0.00579
	As	Mo	0.00091
		Ni	0.00085
		Cr	0.00088
		Al	0.00467
		W	−0.04979
		V	0.00142
	Co	Mo	−0.00258
		Ni	0.00004
		Cr	0.00021
		Ti	0.00164
	Cr	Ti	0.00018
		W	0.00102
		V	−0.00019
	Cu	Mo	0.00038
	Mn	Ni	0.00001
	Nb	Ni	−0.00010
		Cr	−0.00015
		Ti	0.06745
		V	0.00801
	Ni	Co	−0.00146
	P	Mo	0.00585
		Ni	0.00025
		Cr	−0.00258
		Cu	0.07717
	Si	Cr	−0.00856
	Ta	Ti	0.00158
		W	0.01358
		Co	0.01357
	Ti	Cr	0.00020
	V	Mo	−0.01069
		Cr	0.00010
		Ti	0.00049
	W	Mo	0.00053
		Cr	0.00007
		Cu	−0.01002
		V	−0.00167
	Zr	Mo	0.00050
		Ni	−0.00007
aluminum alloys	Sb	Mg	0.00013
		Ni	0.00635
		Cu	0.00226
	Zn	Ni	0.00307
	Sn	Zr	0.00200

Table V. Detection Limits (% w/w) for Alloying Elements

element	matrix: copper	matrix: iron	matrix: aluminum	element	matrix: copper	matrix: iron	matrix: aluminum
Ag	0.0005	–[a]	–[a]	Ni	0.0002	0.0004	0.0009
Al	0.0005	0.0003	–[b]	P	0.003	0.002	–
As	0.0004	0.0006	–	Pb	0.0009	–	0.004
B	–[a]	0.001	–	Sb	0.0008	–	0.004
Cd	0.0001	–	–	Si	0.0003	0.0003	–
Co	–	0.0002	–	Sn	0.0008	–	0.009
Cr	–	0.0002	0.0004	Ta	–	0.005	–
Cu	–[b]	0.0001	0.0003	Ti	–	0.0001	0.0002
Fe	0.0006	–[b]	0.0005	V	–	0.0004	–
Mg	–	–	0.016	W	–	0.0005	–
Mn	0.0001	0.0001	0.0001	Zn	0.003	–	0.0003
Mo	–	0.0006	–	Zr	–	0.0003	0.0003
Nb	–	0.0004	–				

[a] Element not determined. [b] Matrix element.

Table VI. Effect of Weight of Sample upon Measured Concentration Ratios for NBS SRM 1100[a]

element ratio	50	100	150	200	250[b]	300	350	400	500
Ag/Cu	0.992	0.989	0.993	0.997	1.000	0.999	1.006	1.008	1.004
	0.010	0.023	0.008	0.009	0.010	0.005	0.009	0.008	0.006
As/Cu	0.777	0.963	0.989	0.981	1.000	1.008	0.998	1.019	1.023
	0.085	0.047	0.024	0.025	0.013	0.032	0.018	0.027	0.021
Cd/Cu	1.016	1.005	1.002	1.002	1.000	0.997	0.991	0.992	0.997
	0.015	0.028	0.011	0.013	0.013	0.012	0.012	0.014	0.009
Fe/Cu	1.022	0.996	0.995	0.998	1.000	0.996	0.991	1.001	1.005
	0.015	0.018	0.007	0.013	0.012	0.013	0.011	0.018	0.013
Mn/Cu	1.046	0.996	0.997	0.994	1.000	0.998	0.991	0.995	1.003
	0.013	0.017	0.007	0.012	0.013	0.013	0.012	0.018	0.010
Ni/Cu	0.989	0.982	0.999	0.995	1.000	0.998	0.990	0.994	0.994
	0.010	0.020	0.007	0.013	0.015	0.012	0.013	0.013	0.009
Pb/Cu	1.01	1.06	1.03	1.04	1.00	0.95	0.95	1.02	0.97
	0.06	0.09	0.06	0.04	0.06	0.08	0.05	0.04	0.05
Sn/Cu	0.85	0.97	0.98	1.01	1.00	0.97	0.98	1.02	1.01
	0.07	0.03	0.09	0.06	0.05	0.08	0.07	0.03	0.02
Zn/Cu	1.060	1.008	1.004	0.996	1.000	1.002	0.985	0.998	0.990
	0.010	0.044	0.012	0.014	0.010	0.012	0.008	0.012	0.010

[a] Weight (mg) in 50-mL solution. [b] Normalization value.

Table VII. Copper Based Alloys (Values in % w/w)

SRM no.	type		Ag	Al	As	Cd	Cu	Fe	Mn
1100	cartridge brass	NBS	0.019	0.008	0.019	0.013	67.43	0.072	0.003
		ICAP	0.018	0.010	0.019	0.0136	67.3	0.068	0.0031
		limits	0.001	0.002	0.001	0.0004	0.4	0.004	0.0003
1101	cartridge brass	NBS	0.003	0.0006	0.009	0.0055	69.50	0.037	0.0055
		ICAP	0.0026	0.004	0.008	0.0060	69.2	0.036	0.0057
		limits	0.0008	0.002	0.001	0.0003	0.3	0.002	0.0002
1104	free cutting brass	NBS	-	-	-	-	63.33	0.088	-
		ICAP	<0.0005	0.003	0.0006	<0.0001	61.5	0.088	<0.0001
		limits	-	0.002	0.0004	-	0.2	0.002	-
1105	free cutting brass	NBS	-	-	-	-	63.7	0.044	-
		ICAP	<0.0005	0.006	0.0010	0.0006	63.7	0.042	0.0001
		limits	-	0.001	0.0005	0.0001	0.1	0.002	0.0001
1106	naval brass	NBS	-	-	-	-	59.08	0.004	0.005
		ICAP	<0.0005	0.012	<0.0004	0.0011	59.3	0.006	0.0046
		limits	-	0.002	-	0.0001	0.3	0.002	0.0004
1108	naval brass	NBS	-	-	-	-	64.95	0.050	0.025
		ICAP	<0.0005	0.046	<0.0004	<0.0001	65.0	0.049	0.025
		limits	-	0.003	-	-	0.1	0.002	0.001
1110	red brass	NBS	-	-	-	-	84.59	0.033	-
		ICAP	0.0011	0.0007	<0.0004	0.0003	84.6	0.032	0.0001
		limits	0.0006	0.0005	-	0.0001	0.1	0.002	0.0001
1114	gilding metal	NBS	-	-	-	-	96.45	0.017	-
		ICAP	0.0009	<0.0005	<0.0004	<0.0001	96.46	0.017	0.0001
		limits	0.0005	-	-	-	0.05	0.002	0.0001
1115	commercial brass	NBS	-	-	-	-	87.96	0.13	-
		ICAP	0.0018	0.0008	<0.0004	<0.0001	88.0	0.130	<0.0001
		limits	0.0006	0.0005	-	-	0.1	0.001	-
1118	aluminum bronze	NBS	-	2.80	0.007	-	75.1	0.065	-
		ICAP	<0.0005	2.78	0.0065	0.0001	75.3	0.064	0.0001
		limits	-	0.02	0.0007	0.0001	0.2	0.004	0.0001

SRM no.	type		Ni	P	Pb	Sb	Si	Sn	Zn
1100	cartridge brass	NBS	0.052	0.010	0.106	0.018	(0.010)	0.055	32.20
		ICAP	0.0524	0.012	0.103	0.017	0.0087	0.053	32.4
		limits	0.0008	0.003	0.003	0.001	0.0005	0.002	0.4
1101	cartridge brass	NBS	0.013	0.002	0.050	0.012	(0.005)	0.016	30.30
		ICAP	0.0131	<0.003	0.050	0.012	0.0047	0.017	30.6
		limits	0.0005	-	0.002	0.001	0.0002	0.001	0.3
1104	free cutting brass	NBS	0.070	0.005	2.77	-	-	0.43	35.3
		ICAP	0.070	0.008	2.72	<0.0008	0.0008	0.430	35.3
		limits	0.003	0.004	0.05	-	0.0003	0.006	0.2
1105	free cutting brass	NBS	0.043	0.003	2.0	-	-	0.21	34.0
		ICAP	0.044	0.003	1.96	<0.0008	0.0012	0.211	34.1
		limits	0.001	0.003	0.03	-	0.0004	0.006	0.1
1106	naval brass	NBS	0.025	-	0.032	-	-	0.74	40.08
		ICAP	0.0250	<0.003	0.032	<0.0008	0.0010	0.743	39.9
		limits	0.0007	-	0.002	-	0.0004	0.009	0.2
1108	naval brass	NBS	0.033	-	0.063	-	-	0.39	34.42
		ICAP	0.031	<0.003	0.066	<0.0008	0.0004	0.394	34.40
		limits	0.001	-	0.002	-	0.003	0.008	0.08
1110	red brass	NBS	0.053	-	0.033	-		0.051	15.20
		ICAP	0.052	<0.003	0.033	<0.0008	<0.0003	0.050	15.2
		limits	0.002	-	0.001	-	-	0.002	0.2
1114	gilding metal	NBS	0.021	0.009	0.012	-	-	0.027	3.47
		ICAP	0.0208	0.009	0.008	<0.0008	<0.0003	0.028	3.47
		limits	0.0007	0.003	0.002	-	-	0.001	0.05
1115	commercial brass	NBS	0.074	0.005	0.013	-	-	0.10	11.73
		ICAP	0.074	0.005	0.014	<0.0008	<0.0003	0.103	11.6
		limits	0.002	0.003	0.001	-	-	0.002	0.2
1118	aluminum bronze	NBS	-	0.13	0.025	0.010	0.0021	-	21.9
		ICAP	0.0005	0.129	0.019	0.008	0.0020	<0.0008	21.8
		limits	0.0003	0.009	0.006	0.002	0.0007	-	0.1

Statistical Analysis of Data

	Cu	Fe	Ni	P	Pb	Zn
n	10	10	9	6	10	10
m	0.9990	1.001	0.999	0.996	9.994	1.0003
b	0.1119	−0.0004	−0.0001	0.0008	0.0003	−0.0119
r	1.0000	0.9997	0.9992	0.9982	0.9994	1.0000
χ^2	0.78	0.85	1.28	0.17	2.47	1.12
p	<0.02	<0.02	<0.02	<0.02	<0.02	<0.02
t	0.41	−1.55	0.75	1.40	−1.13	0.36
p	<0.02	<0.02	<0.02	<0.02	<0.02	<0.02

Table VIII. Iron and Steel (Values in % w/w)

SRM no.	type		Al	As	B	Co	Cr	Cu
8i	plain	NBS	-	-	-	-	0.009	0.016
	carbon	ICAP	<0.0003	<0.0006	<0.001	<0.0002	0.0072	0.0136
		limits	-	-	-	-	0.0006	0.0006
19g	plain	NBS	0.031	-	-	0.012	0.374	0.093
	carbon	ICAP	0.030	<0.0006	<0.001	0.0109	0.377	0.093
		limits	0.004	-	-	0.0005	0.009	0.002
51b	plain	NBS	-	-	-	-	0.455	0.071
	carbon	ICAP	0.010	<0.0006	<0.001	<0.0002	0.455	0.072
		limits	0.001	-	-	-	0.008	0.002
65d	plain	NBS	0.059	-	-	-	0.049	0.051
	carbon	ICAP	0.058	<0.0006	<0.001	0.0054	0.049	0.050
		limits	0.003	-	-	0.0003	0.001	0.001
160a	stainless	NBS	-	-	-	0.071	18.74	0.174
	steel	ICAP	<0.0003	<0.0006	<0.001	0.067	18.6	0.175
		limits	-	-	-	0.002	0.2	0.002
344	high	NBS	1.16	-	-	-	14.95	0.106
	alloy	ICAP	1.16	<0.0006	<0.001	0.0591	15.04	0.105
		limits	0.01	-	-	0.0004	0.04	0.002
348	high	NBS	0.23	-	0.0031	-	14.54	0.22
	alloy	ICAP	0.226	<0.0006	0.003	0.127	14.54	0.219
		limits	0.004	-	0.001	0.001	0.05	0.002
1261	low	NBS	0.021	0.017	0.0005	0.030	0.69	0.042
	alloy	ICAP	0.022	0.017	<0.001	0.0302	0.690	0.042
		limits	0.002	0.002	-	0.0007	0.006	0.002
1262	low	NBS	0.095	0.092	0.0025	0.30	0.30	0.50
	alloy	ICAP	0.093	0.091	0.003	0.311	0.305	0.499
		limits	0.005	0.005	0.001	0.005	0.005	0.006
1263	low	NBS	0.24	0.010	0.00091	0.048	1.31	0.098
	alloy	ICAP	0.242	0.010	<0.001	0.046	1.31	0.098
		limits	0.008	0.002	-	0.001	0.01	0.002
1264	low	NBS	(0.008)	0.052	0.011	0.15	0.065	0.249
	alloy	ICAP	0.008	0.050	0.011	0.154	0.065	0.249
		limits	0.002	0.003	0.002	0.004	0.003	0.004
1265	electrolytic	NBS	(0.0007)	(0.0002)	0.00013	0.0070	0.0072	0.0058
	iron	ICAP	0.0005	<0.0006	<0.001	0.0068	0.0072	0.0058
		limits	0.0004	-	-	0.0004	0.0008	0.0007

SRM no.	type		Fe	Mn	Mo	Nb	Ni	P
8i	plain	NBS	-	0.511	0.003	-	0.009	0.080
	carbon	ICAP	99.18	0.515	0.004	<0.0004	0.010	0.081
		limits	0.01	0.006	0.001	-	0.001	0.009
19g	plain	NBS	-	0.554	0.013	0.026	0.066	0.046
	carbon	ICAP	98.29	0.555	0.012	0.0280	0.067	0.048
		limits	0.02	0.004	0.001	0.0008	0.003	0.008
51b	plain	NBS	-	0.573	0.014	-	0.053	0.013
	carbon	ICAP	97.32	0.574	0.014	<0.0004	0.054	0.014
		limits	0.02	0.006	0.001	-	0.002	0.004
65d	plain	NBS	-	0.073	0.025	-	0.060	0.015
	carbon	ICAP	98.35	0.071	0.025	<0.0004	0.060	0.017
		limits	0.02	0.006	0.002	-	0.001	0.004
160a	stainless	NBS	-	1.62	2.83	-	14.13	0.027
	steel	ICAP	61.7	1.62	2.84	0.010	14.18	0.031
		limits	0.2	0.01	0.04	0.001	0.09	0.004
344	high	NBS	-	0.57	2.40	-	7.28	0.018
	alloy	ICAP	72.76	0.567	2.41	0.004	7.31	0.014
		limits	0.03	0.005	0.03	0.001	0.02	0.004
348	high	NBS	53.3	1.48	1.3	-	25.8	0.015
	alloy	ICAP	53.28	1.481	1.30	0.020	25.73	0.014
		limits	0.09	0.007	0.01	0.002	0.08	0.004
1261	low	NBS	(95.6)	0.66	0.19	0.022	1.99	0.015
	alloy	ICAP	95.54	0.662	0.189	0.021	1.99	0.015
		limits	0.02	0.005	0.004	0.001	0.02	0.003
1262	low	NBS	(95.3)	1.04	0.068	0.29	0.59	0.042
	alloy	ICAP	95.74	1.05	0.069	0.078	0.59	0.044
		limits	0.02	0.01	0.005	0.008	0.01	0.009
1263	low	NBS	(94.4)	1.50	0.030	0.049	0.32	0.029
	alloy	ICAP	94.48	1.51	0.030	0.048	0.324	0.028
		limits	0.02	0.01	0.002	0.002	0.005	0.005
1264	low	NBS	(96.7)	0.255	0.49	0.157	0.142	0.018
	alloy	ICAP	96.75	0.255	0.49	0.157	0.142	0.018
		limits	0.02	0.005	0.01	0.008	0.002	0.003
1265	electrolytic	NBS	(99.9)	0.0057	0.0050	<0.00001	0.041	0.0025
	iron	ICAP	99.90	0.0058	0.0051	<0.0004	0.043	0.0039
		limits	0.01	0.0004	0.0008	-	0.002	0.0038

Table VIII. (*Continued*)

SRM no.	type		Si	Ta	Ti[a]	V	W	Zr
8i	plain	NBS	0.020	-	-	0.012	-	-
	carbon	ICAP	0.021	<0.005	<0.0011	0.013	<0.0005	<0.0003
		limits	0.001	-	-	0.002	-	-
19g	plain	NBS	0.186	-	0.027	0.012	-	-
	carbon	ICAP	0.186	<0.005	0.0266	0.013	<0.0005	<0.0003
		limits	0.004	-	0.0008	0.001	-	-
51b	plain	NBS	0.246	-	-	0.002	-	-
	carbon	ICAP	0.245	<0.005	0.0002	0.0019	<0.0005	<0.0003
		limits	0.007	-	0.0001	0.0006	-	-
65d	plain	NBS	0.370	-	-	0.002	-	-
	carbon	ICAP	0.366	<0.005	0.0012	0.0021	0.0008	<0.0003
		limits	0.077	-	0.0003	0.0008	0.0005	-
160a	stainless	NBS	0.605	-	-	0.051	-	-
	steel	ICAP	0.605	<0.005	0.0026	0.043	0.036	<0.0003
		limits	0.008	-	0.0003	0.002	0.002	-
344	high	NBS	0.395	0.002	0.076	0.040	-	-
	alloy	ICAP	0.396	<0.005	0.076	0.0429	0.0010	<0.0003
		limits	0.005	-	0.003	0.0009	0.0005	-
348	high	NBS	0.54	-	2.24	0.25	-	-
	alloy	ICAP	0.541	<0.005	2.24	0.245	0.029	<0.0003
		limits	0.007	-	0.01	0.005	0.002	-
1261	low	NBS	0.223	0.020	0.020	0.011	0.015	0.009
	alloy	ICAP	0.224	0.022	0.0199	0.013	0.018	0.0087
		limits	0.005	0.006	0.0006	0.001	0.001	0.0005
1262	low	NBS	0.39	0.20	0.084	0.041	0.21	0.19
	alloy	ICAP	0.38	0.023	0.038	0.041	0.217	0.194
		limits	0.01	0.004	-	0.002	0.008	0.008
1263	low	NBS	0.74	(0.053)	0.050	0.31	0.045	0.049
	alloy	ICAP	0.726	0.047	0.049	0.312	0.047	0.048
		limits	0.005	0.005	0.002	0.009	0.002	0.001
1264	low	NBS	0.067	0.11	0.24	0.105	0.10	0.068
	alloy	ICAP	0.068	0.091	0.244	0.107	0.101	0.068
		limits	0.002	0.009	0.009	0.002	0.004	0.002
1265	electrolytic	NBS	0.0080	-(<0.00005)	0.0006	0.0006	(-0.00004)	-(<0.00001)
	iron	ICAP	0.0079	<0.005	0.0001	0.0007	<0.0005	<0.0003
		limits	0.0008	-	0.0001	0.0005	-	-

Statistical Analysis of Data

	n	*m*	*b*	*r*	χ^2	*p*	*t*	*p*
Al	7	0.999	0.0001	1.0000	0.14	<0.02	-1.076	<0.02
Co	7	1.005	-0.0007	0.9992	2.90	<0.02	0.219	<0.02
Cr	12	1.0035	-0.0011	1.0000	2.35	<0.02	0.007	<0.02
Cu	12	1.006	-0.0011	0.9999	1.65	<0.02	-0.666	<0.02
Mn	12	1.0019	0.0001	1.0000	0.45	<0.02	1.978	<0.02
Mo	12	1.001	0.0000	1.0000	0.55	<0.02	1.502	<0.02
Ni	12	1.0006	0.0006	1.0000	1.28	<0.02	-0.110	<0.02
P	12	1.026	-0.0002	0.9894	0.61	<0.02	0.891	<0.02
Si	12	0.994	0.0006	0.9999	1.42	<0.02	-0.673	<0.02
Ti[a]	6	1.001	-0.0005	1.0000	0.27	<0.02	-1.334	<0.02
V	12	1.008	0.0004	0.9982	7.53	<0.02	0.111	<0.02

[a] Sample 1262 not used in statistical analysis for this element.

added. The solution was allowed to stand in a water bath at 40 °C for about 5 min until dissolution was complete. Deionized water then was added to bring the final solution volume to about 50 mL, and the solution analyzed using the ICAP.

Iron-Based Alloys. About 250 mg of sample (usually chips or turnings) was transferred to a 50-mL Teflon beaker. Twenty milliliters of aqua regia was added and, after the reaction subsided, the solution was boiled for 20 min. The cooled solution then was diluted to about 50 mL with water and analyzed by the ICAP after undissolved carbon particles were allowed to settle from solution.

Aluminum-Based Alloys. About 100 mg of sample (usually chips or turnings) was transferred to a 250-mL glass beaker. Ten milliliters of 6 M hydrochloric acid was added and the solution heated until no further dissolution occurred (about 15–20 min). At this point, black specks of silicon metal are visible in the solution. The solution then was cooled and diluted to about 100 mL with water, and allowed to stand so that undissolved silicon particles settled from solution before analysis by the ICAP.

Calibration Standards. The instrument was calibrated by using synthetically prepared standards. These were made up to represent original alloys that contained up to 50% of the analyte (relative to the weight of matrix element) in the presence of a constant concentration of the matrix element. The calibration range for each element in each matrix is shown in Table III. After the linearity of every analytical line investigated was established to be over the range shown in Table III, the instrument was standardized using the low standard and the high standard. In order to reduce the number of standard solutions required to calibrate the unit for routine operation, the multielemental standards listed in Table III were used.

Following instrument standardization, the empirical interference correction factors (K_{ik}) were determined. This was achieved by introducing the high, single element calibration standard into the ICAP and observing the apparent concentration of the affected analytes. The factors found to be significant at the analyte and interferent levels in the original samples are shown in Table IV. These factors were stored in the data processing unit and used to modify the apparent concentration ratios determined from the calibration curve into the "real" concentration ratios using Equation 6.

Concentration Calculations. Because the elements left undetermined in the copper alloys constituted less than 0.01% of the

Table IX. Aluminum Alloys (Values in % w/w)

BCS no.	type		Cr	Cu	Fe	Mg	Mn	Ni
181/2	copper	BCS	(0.008)	3.96	0.42	1.56	0.20	1.90
	aluminum	ICAP	0.0079	3.96	0.42	1.57	0.201	1.89
	alloy	limits	0.0008	0.03	0.01	0.02	0.006	0.03
182/2	silicon	BCS	-	0.045	0.47	0.075	0.21	0.055
	aluminum	ICAP	<0.0005	0.042	0.45	0.075	0.207	0.055
	alloy	limits	-	0.001	0.01	0.02	0.006	0.002
216/2	duralumin	BCS	-	4.56	0.28	0.75	0.71	0.17
	alloy	ICAP	0.0008	4.44	0.28	0.73	0.71	0.166
		limits	0.0005	0.06	0.01	0.02	0.02	0.004
262/2	magnesium	BCS	(0.002)	0.039	0.20	10.74	0.084	0.071
	aluminum	ICAP	0.0019	0.040	0.20	10.68	0.083	0.073
	alloy	limits	0.0006	0.001	0.02	0.09	0.002	0.002
263/2	magnesium	BCS	0.074	0.019	0.26	4.67	0.36	-
	aluminum	ICAP	0.075	0.019	0.263	4.69	0.354	0.0015
	alloy	limits	0.002	0.002	0.008	0.06	0.007	0.0009
268	silicon	BCS	-	1.34	0.39	0.56	0.22	0.12
	aluminum	ICAP	<0.0005	1.35	0.397	0.57	0.217	0.122
	alloy	limits	-	0.02	0.009	0.02	0.006	0.004
300/1	zinc	BCS	0.13	1.27	0.24	2.74	0.33	-
	aluminum	ICAP	0.133	1.26	0.241	2.72	0.329	0.0012
	alloy	limits	0.003	0.03	0.006	0.07	0.008	0.0008
380	aluminum	BCS	-	0.90	1.15	0.18	0.018	0.91
	alloy	ICAP	<0.0005	0.91	1.16	0.19	0.020	0.911
		limits	-	0.01	0.03	0.02	0.002	0.008

BCS no.	type		Pb	Sb	Sn	Ti	Zn	Zr
181/2	copper	BCS	0.040	-	0.028	0.019	0.074	-
	aluminum	ICAP	0.040	<0.004	0.027	0.0186	0.0739	<0.0003
	alloy	limits	0.004	-	0.009	0.0004	0.0009	-
182/2	silicon	BCS	0.050	-	0.025	0.11	0.100	-
	aluminum	ICAP	0.052	<0.004	0.028	0.109	0.095	<0.0003
	alloy	limits	0.004	-	0.009	0.001	0.003	-
216/2	duralumin	BCS	0.038	0.029	0.048	0.037	0.20	-
	alloy	ICAP	0.036	0.030	0.048	0.037	0.203	<0.0003
		limits	0.006	0.005	0.009	0.003	0.003	-
262/2	magnesium	BCS	(0.054)	-	(0.042)	0.005	0.084	-
	aluminum	ICAP	0.049	<0.004	0.035	0.0043	0.086	<0.0003
	alloy	limits	0.006	-	0.009	0.0004	0.007	-
263/2	magnesium	BCS	-	-	-	0.022	0.056	-
	aluminum	ICAP	<0.004	<0.004	<0.005	0.0225	0.056	<0.0003
	alloy	limits	-	-	-	0.0009	0.001	-
268	silicon	BCS	0.035	-	0.03	<0.02	0.05	-
	aluminum	ICAP	0.035	<0.004	0.033	0.0157	0.052	<0.0003
	alloy	limits	0.005	-	0.006	0.0005	0.003	-
300/1	zinc	BCS	-	-	-	0.09	5.87	0.18
	aluminum	ICAP	0.012	<0.004	<0.005	0.09	5.88	0.181
	alloy	limits	0.005	-	-	0.001	0.09	0.004
380	aluminum	BCS	-	-	-	0.22	0.011	-
	alloy	ICAP	<0.004	<0.004	<0.005	0.222	0.0108	<0.0003
		limits	-	-	-	0.02	0.0008	-

Statistical Analysis of Data

	Cu	Fe	Mg	Mn	Ni	Ti	Zn
n	8	8	8	8	6	7	8
m	0.998	0.992	0.997	0.982	0.997	1.006	0.998
b	−0.0008	0.0019	0.0026	0.0022	0.0010	−0.0005	−0.0000
r	0.9998	0.9982	0.9999	0.9998	1.0000	0.9999	0.9999
χ^2	3.42	1.30	0.58	0.60	0.16	0.75	0.69
p	<0.02	<0.02	<0.02	<0.02	<0.02	<0.02	<0.02
t	−0.855	0.000	−0.699	−0.693	−0.690	−0.926	0.553
p	<0.02	<0.02	<0.02	<0.02	<0.02	<0.02	<0.02

alloy, the final concentration calculations were performed on-line by the central processing unit, and direct concentration values were printed out. For the iron- and aluminum-based alloys, the concentration ratios only were printed. Final concentration calculations were performed off-line after concentrations of elements not determined above 0.02% (C_j values) had been merged with the ICAP data. In this study, values for carbon, sulfur, and nitrogen in iron-based alloys, and silicon in aluminum alloys were taken from the certificates of analysis supplied by NBS and BAS, respectively.

Effect of Sample Weight. In order to determine the effect of different sample weights, samples of NBS SRM 1100 Cartridge Brass were weighed on a milligram balance over the range 50–500 mg into Teflon beakers. Each sample then was treated with 1 mL of concentrated nitric acid and, after the reaction subsided, 15 mL of concentrated hydrochloric acid was added. After dissolution, the solutions were transferred to 50-mL Teflon volumetric flasks, diluted to volume with water, and analyzed by the ICAP.

RESULTS AND DISCUSSION

Detection Limits. The experimentally-determined detection limits for the copper, iron, and aluminum matrices ana-

lyzed are listed in Table V. The detection limits are defined as the concentration of analyte required to produce a signal equivalent to the 95% confidence limit (2.131 standard deviation) of the background variation as determined on a set of 16 measurements performed on the matrix blank interspersed randomly among the samples analyzed. Although the variation of detection limits with sample weight was not studied here, the confidence limits measured for the analysis of sample 1265, a high purity iron, are close to the detection limits measured on the blank iron standard.

Effect of Sample Weight Analyzed. The effect of sample weight on the determined concentration ratios of several elements in NBS SRM 1100 Cartridge Brass is shown in Table VI. The results normalized against the 250-mg sample in 50-mL value, are expressed as the mean and the 95% confidence level on a set of eight replicates at each solute concentration. Clearly, there is no significant difference in the determined concentration ratio for weights in the 150–500 mg range which represents the equivalent of a 40% weighing error. In practice, we decided to limit the weighing error to about ±20% by using a milligram balance to ensure a minimum sample size of 200 mg and a maximum sample size of 300 mg.

The volume error was kept to about ±10% by use of graduated glass beakers. When plastic containers were used, a simple batch calibration was performed by dispensing 50 mL of water from a graduate and marking a line on the outside of the container.

Copper-Based Alloys. Analytical data obtained from the analysis of NBS reference copper-based alloys including brasses, bronzes, and gilding metals are listed in Table VII. The ICAP values are expressed as the mean of a set of 16 replicate analyses for each element plus or minus the 95% confidence limit. In addition, for each element certified to be present in at least six alloys, the correlation coefficient, slope and intercept of the linear regression line of the form of Equation 7 between the NBS certified values and the experimentally determined ICAP values, weighted with respect to the 95% confidence limit for the determination, are shown:

$$(\text{ICAP}) = m(\text{NBS}) + b \qquad (7)$$

Both the chi-square value for the regression line and the Students' "t" value for the paired data points are consistent with the 98% confidence limit, indicating a lack of bias between the ICAP and the certified values.

Iron-Based Alloys. Analytical data obtained from 12 NBS reference iron and steel samples determined by the ICAP are listed in Table VIII. These data are expressed as the mean of the number of at least 16 replicate analyses for each sample together with the 95% confidence limit for each elemental determination. Analyses for carbon, nitrogen, and sulfur in these samples were taken from the NBS certificate prior to calculation of the final concentration for each element.

The statistical data tabulated for the iron-based alloy samples are determined in the same manner as were those for the copper-based alloys. The ICAP data were found to show no significant deviation ($p < 0.02$) from the referee data with the exception of sample 1262. It is believed that the low ICAP values from these samples are caused by the presence of niobium and titanium in the sample as carbides which are insoluble by this technique. The residue from the dissolution of sample 1262 analyzed by a dc arc in conjunction with a Mark IV 3.4-m Ebert Spectrograph (Jarrell-Ash) showed that high levels of niobium and titanium were present. Furthermore, calibration curves obtained for samples 1261–1265 using an electronically-controlled waveform spark source coupled to a Model 90-750 AtomComp Direct Reading Spectrometer (Jarrell-Ash) indicated that these elements were present in the sample at the certified values.

Aluminum-Based Alloys. Analytical data obtained from the determination of eight BCS aluminum alloys using the ICAP technique are shown in Table IX. Prior to calculation of the elemental concentration C_i from the determined concentration ratios, the silicon concentrations (C_j) listed on the certification of analysis sheet were used to solve Equation 2 for the aluminum concentration (C_M).

The statistical analyses presented in Table IX show that there is no significant difference ($p < 0.02$) between the ICAP data and the certified values.

CONCLUSIONS

The direct reading ICAP spectrometer coupled with the concentration ratio method of analysis has been demonstrated to produce analytically accurate data for the determination of alloying elements in metals. This is true over a concentration range exceeding four decades with a typical precision of better than 10% for trace and 1% for minor and major alloying components. The relative freedom from chemical interferences eliminates the matching of standards to samples that is required in other analytical techniques. Indeed, the only matrix matching required is the addition of the matrix element and acids to the calibration standards. With such minimal matching, it is possible to analyze samples in which the major matrix element extends over a wide range. The use of the concentration ratio procedure also permits significant dilution errors from the target dilution factor without any resultant loss of analytical accuracy. This permits very rapid sample preparation that requires a minimum of operator skill. Indeed, the tolerance of the procedure to dilution errors suggests that the automating of the entire sample preparation procedure might be practically and economically feasible.

The limitations of the concentration ratio method are that all elements present in significant concentrations (total non-analyzed elements should not exceed 0.1%) must be determined and that insoluble materials could produce a significant error. Furthermore, any error caused by insoluble material is compounded over all elements. However, only one among the 30 samples analyzed in this study exhibited this problem. In this case, the only significant errors observed were on those elements that had been incompletely dissolved.

ACKNOWLEDGMENT

The authors thank James G. Gardner for his assistance in performing the spark analysis of the low alloy steel samples.

LITERATURE CITED

(1) Fassel, V. A.; Dickinson, G. W. *Anal. Chem.* **1968**, *40*, 247.
(2) Hoare, H. C.; Mostyn, R. A. *Anal. Chem.* **1967**, *39*, 1153.
(3) Souilliart, J. C.; Robin, J. P. *Analusis* **1972**, *1*, 427.
(4) Kirkbright, G. F.; Ward, A. F. *Talanta* **1974**, *21*, 1145.
(5) Butler, C. C.; Kniseley, R. N.; Fassel, V. A. *Anal. Chem.* **1975**, *47*, 825.
(6) Greenfield, S.; Jones, I. Ll.; McGeachin, H.; Smith, P. B. *Anal. Chim. Acta* **1975**, *74*, 225.
(7) Borclonati, C.; Biancifiori, M. A.; Donato, A.; Morello, B. *Comit. Nazl. Energia Nucl.* **1969**, *69*, 16.
(8) Newland, B. T. N.; Mostyn, R. A. *Matl. Qual. Assur. Dir., Engl. Rep.* **1977**, R258.
(9) Scott, T. H.; Strasshein, A.; Oakes, A. R. *Colloq. Spectrosc. Int.* (*18th Proc.*) **1975**, *1*, 176.
(10) Ohls, K. *Pure Appl. Chem.* **1977**, *49*, 1485.
(11) "Methods for Emission Spectrochemical Analysis", 6th ed.; ASTM: Philadelphia, 1971; Recommended Practice E-158, Section 9.

RECEIVED for review November 22, 1978. Accepted July 20, 1979. This article is the extension of a paper presented at the 176th National ACS Meeting, Miami Beach, Fla., September, 1978.

Synthesis and Identification of the 22 Tetrachlorodibenzo-*p*-dioxin Isomers by High Performance Liquid Chromatography and Gas Chromatography

T. J. Nestrick,* L. L. Lamparski, and R. H. Stehl

Analytical Laboratory, Dow Chemical U.S.A., Midland, Michigan 48640

By controlled flow pyrolysis conditions, various combinations of di-, tri-, and tetrachlorophenols were reacted to form tetrachlorodibenzo-*p*-dioxins (TCDDs). These reaction products were separated by high performance liquid chromatography (HPLC) and were characterized by gas chromatography–mass spectrometry (GC-MS). This combination of HPLC and GC-MS allowed assignment of identity to all 22 isomers of TCDD. Applications of this selective analysis to determination of TCDD in a variety of samples are also discussed.

Recently considerable attention has been directed toward understanding the formation, distribution, and transport properties of chlorinated aromatic compounds in the environment. Polychlorinated dibenzo-*p*-dioxins (CDDs) are one class of such compounds that have been identified at trace concentrations in both commercial products and noncommercial materials (*1–3*). There are 75 possible CDD isomers ranging from mono- to octachlorinated species. Toxicological investigations have demonstrated a wide range of biological activity for CDDs, and also that this activity is highly dependent upon the number and ring position of chlorines present in the molecule (*4–10*). The chemical abstract numbering system for CDDs is shown in Figure 1.

Evidence to date concerning relative biological activity of CDDs indicates that peak toxicity is observed for 2,3,7,8-tetrachlorodibenzo-*p*-dioxin (2378-TCDD) (*11–13*). The consequences of toxicity, and large variations in biological activity between closely related CDD isomers, make the analytical task of isomer-specific identification and quantitation of 2378-TCDD in biological, environmental, and product matrices both important and formidable.

Problems involving quantitation of 2378-TCDD are largely related to the necessity of detecting very low concentrations, often in the range of 1–10 parts per trillion (ppt, 10^{-12} g/g). The development of a variety of sample clean-up technologies, which permit CDD isolation and concentration (~100 to 4000×), coupled with high-sensitivity mass spectrometric detectors can provide adequate detection and CDD identification capability (*14–17*).

The completely specific identification of 2378-TCDD has not been reported to date. Largely this can be attributed to the lack of availability of isomerically-pure TCDD standards. The technique involving high-resolution gas chromatography (GC), using wall coated open-tubular glass capillary columns, has been reported by Buser and Rappe for the separation of at least 12 different TCDD isomers. These authors indicate that capillary column efficiencies of 140 000 theoretical plates would still be far too low to accomplish the separation of all 22 TCDD isomers directly (*18, 19*). Although future work may result in the improved column efficiency and practicality required to use this technique, the sequential use of liquid and gas chromatographic separations can achieve an equivalent degree of specificity.

Recent publications have described the identification of a large variety of chlorinated dioxin isomers in environmental particulate samples associated with combustion processes (*18, 20–22*). Since these findings include both qualitative and quantitative information regarding the presence of several TCDDs, and were accomplished using analytical procedures whose ability to separate all 22 possible isomers has not been proved, then it must be concluded that such analyses are not unequivocal. One approach to improving the reliability of TCDD analyses is to prepare isomerically-pure standards of each individual TCDD. In this paper, we report the preparation of 22 TCDD isomers via pyrolytic condensation of their potassium chlorophenate precursors. Because such pyrolytic syntheses are well known (*23–25*) and generally do not produce isomerically pure products, critical to the synthesis of 22 TCDDs is our development of a combined chromatographic system which permits the isolation and identification of 22 discrete isomers. This system begins with a high performance liquid chromatography (HPLC) reverse-phase (RP) separation and collection of the neutral pyrolyzate products, followed by an HPLC normal-phase adsorption (silica) separation. The silica-HPLC TCDD fractions were examined by packed-column gas chromatography–low resolution mass spectrometry (GC-LRMS). Via multiple ion detection, TCDDs were identified by nominal mass (resolution 400), chlorine isotope pattern, and GC retention time (relative to ^{13}C-2378-TCDD). The combination of these three sets of retention time data confirmed the existence of 22 discrete TCDD isomers. The end result has been the isolation of 10–2000 ng quantities of each TCDD isomer, essentially free of other isomeric TCDD impurities.

EXPERIMENTAL

Caution. The procedures described herein permit the synthesis of all 22 TCDD isomers, including 2378-TCDD. In addition to expected products many pyrolyzates were found to contain 2378-TCDD; either as an expected byproduct when 245-TCP was present or as an unexpected byproduct. Persons attempting to prepare these substances should be experienced in the handling procedures for extremely toxic materials. Appropriate precautions should be taken so as to minimize the chances of either personal or environmental exposure to TCDDS. All waste materials, to include equipment washing solvents, should be carefully packaged and isolated until destroyed by appropriate incineration techniques.

Reagents. Chlorophenols were obtained from Aldrich (Milwaukee, Wis.) in the best available purity and were used as received except as noted: 2,4-dichlorophenol (24-DCP, 99%), 25-DCP (98%), 26-DCP (99%), 2,3,4-trichlorophenol (234-TCP, mp 77–79 °C), 235-TCP (mp 57–59 °C), 236-TCP (99%), 245-TCP (mp 63–65 °C), 246-TCP (98%), 2,3,4,5-tetrachlorophenol (2345-TeCP, 98%), 2356-TeCP (mp 114–116 °C), 2346-TeCP (recrystallized, unknown purity). Aqueous solutions were prepared using deionized water. Purge gas for the pyrolysis reactor was pre-purified nitrogen (Matheson, 99.995%), further purified by passage

0003-2700/79/0351-2273$01.00/0

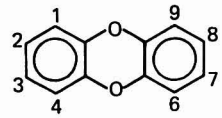

Figure 1. Dibenzo-*p*-dioxin structure and *Chemical Abstracts* Numbering System for substituents

through a General Electric "Go-Getter" before use. Silica, as 100/200-mesh Bio-Sil A (BioRad Laboratories, Richmond, Calif.), was used as supporting matrix in the pyrolysis reactor. Before use, the silica was exhaustively extracted with constant boiling hydrochloric acid for a period of approximately 48 h in a Soxhlet extraction apparatus. It was then elutriated with deionized water for a period of approximately 6 h at a flow rate sufficient to remove bulk fines and residual acid. The silica was then rinsed with methanol followed by methylene chloride (Burdick & Jackson, distilled-in-glass quality) and air dried. Final cleanup of the silica was accomplished by charging this material into a glass tube, and placing it in a temperature-controlled clam-shell tube furnace, heated to 180 °C for 1 h under nitrogen flow. After being cooled to ambient temperature, the tube was inverted and approximately three bed volumes each of methanol followed by methylene chloride were forced through using 10 psi nitrogen pressure. The silica was then returned to the tube furnace and step-programmed from 50 to 180 °C in 15 min, and held at 180 °C for a period of 1 h. The cooled silica was transferred to a clean glass bottle, equipped with a Poly-Seal top, and stored in a desiccator over phosphorus pentoxide until used. Silica treated in this manner is reasonably free of trace metal salts which could influence chlorophenate condensation reactions, and demonstrates a very low degree of trace organic contamination.

2:2 TCDD Isomer Synthesis (See Tables I and II). A diagram of the apparatus to be described is shown in Figure 2. A bed support of Pyrex glass wool was inserted into a glass reactor tube (1.3 cm i.d. × 70 cm, 24/40 end fittings). In a 30-mL vial, 3 g of silica followed by 1 g of 1 M potassium hydroxide were combined and manually shaken for several minutes to produce a uniform free-flowing powder (caustic-silica). This material was charged into the reactor tube and heated to 180 °C for approximately 20 min under 200 cm^3/min nitrogen flow to remove water. A potassium chlorophenate solution was prepared in a 10-mL vial by combining 30 mg (0.15 mmol) total TCP (15 mg each TCP for mixed reactions) and 1.5 mL of 1 M aqueous potassium hydroxide. The solution was extracted once with 8 mL of hexane (hexane extract discarded) and the potassium chlorophenate solution combined with 4 g of silica in a 40-mL vial. Several minutes of manual shaking produced a uniform free-flowing powder (K-phenate silica). After drying of the caustic-silica, the reactor tube was removed from the furnace and allowed to cool to ambient temperature. The K-phenate silica was then charged into the reactor tube, 200 cm^3/min nitrogen flow reestablished, and the system returned to the tube furnace (adjusted to a temperature of 130 °C) for 25 min. When dry (no condensate visible at the exit port), the nitrogen purge was reduced to 10 cm^3/min. The furnace temperature was then increased to 180 °C for approximately 10 min to remove the last traces of residual water, and then increased to 280 °C where it was maintained for 30 min. Upon completion of the pyrolysis reaction, the reactor tube was removed from the tube furnace and allowed to cool to ambient

Table I. TCDD Isomer Groups by Chlorine Substitution Pattern

2:2 isomers[a] = 13 total				3:1 isomers[b] = 8 total	
1267	1368	1469	2378	1236	1246
1268	1369	1478		1237	1247
1269	1378			1238	1248
1278	1379			1239	1249
1279					
1289					

4:0 isomer[c] = 1 total

1234

[a] 2:2 = two chlorine atoms in each carbon ring. [b] 3:1 = three chlorine atoms in one carbon ring and one chlorine atom in the other ring. [c] 4:0 = four chlorine atoms in one carbon ring.

temperature. TCDDs, adsorbed on the silica support matrix, were selectively removed by inverting the reactor tube (entrance port up) and eluting the system as a chromatographic column with 50 mL of methylene chloride. When drained to bed level, a second portion of 25 mL of methylene chloride was passed through the column. The combined effluents were collected in a 100-mL bottle. As a preliminary check on formation of TCDDs, a 4-μL aliquot of this effluent was injected into the gas chromatograph–low resolution mass spectrometer (GC-LRMS, conditions described in GC-LRMS section) operating in the multiple ion detection mode. Final processing prior to TCDD isomer separation involved evaporation of the methylene chloride under a stream of specially purified nitrogen. Approximately 10–15 mL of 1 M aqueous sodium hydroxide was added to the residue which was then extracted three times with hexane (10 mL, 5 mL, 5 mL); the combined hexane extracts were again evaporated to dryness under a stream of nitrogen. For each pyrolysis reaction (Table II) a white, crystalline residue was obtained at this point. These residues were protected from light and stored dry until further processed.

3:1 TCDD Isomer Syntheses (See Tables I and II). A diagram of the apparatus to be described is shown in Figure 3. Mixed potassium chlorophenate solutions were prepared by combining 15 mg DCP (0.092 mmol) and 21 mg TeCP (0.091 mmol) in a 10-mL vial to which was added 0.8 mL of 0.5 M methanolic potassium hydroxide (0.4 mmol). The mixture was gently swirled to produce a clear solution. It was then transferred to a 1.5–2.0 cm glass wool plug in the reactor tube, 200 cm^3/min nitrogen purge was established, and the treated glass wool plug slid into the tube furnace (adjusted to 120 °C) for a period of 15 min. During this operation the methanol and trace water present were vented to a fume hood, and when complete white-crystalline potassium chlorophenate salts were visible on the walls of the reactor tube and throughout the glass wool (K-phenate) plug. After cooling the reactor tube, a 3-g silica bed was inserted between glass wool bed supports at the exit end of the tube. The silica adsorbent bed was positioned such that it would be outside of the tube furnace when the K-phenate plug was inside the furnace. The glass tube support rod and exit port fitting were installed, the nitrogen purge was reestablished at 40 cm^3/min, and the system placed in the tube furnace such that the K-phenate plug was outside the heated zone. The furnace was then quickly heated

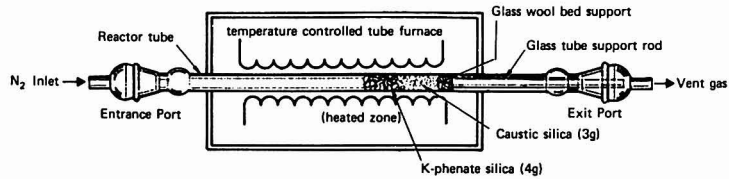

Figure 2. Pyrolysis reactor apparatus for 2:2 TCDD isomer syntheses

Table II. Potassium Chlorophenate Pyrolysis Reactions and Generalized TCDD Products by Direct Addition and Smiles Rearrangement

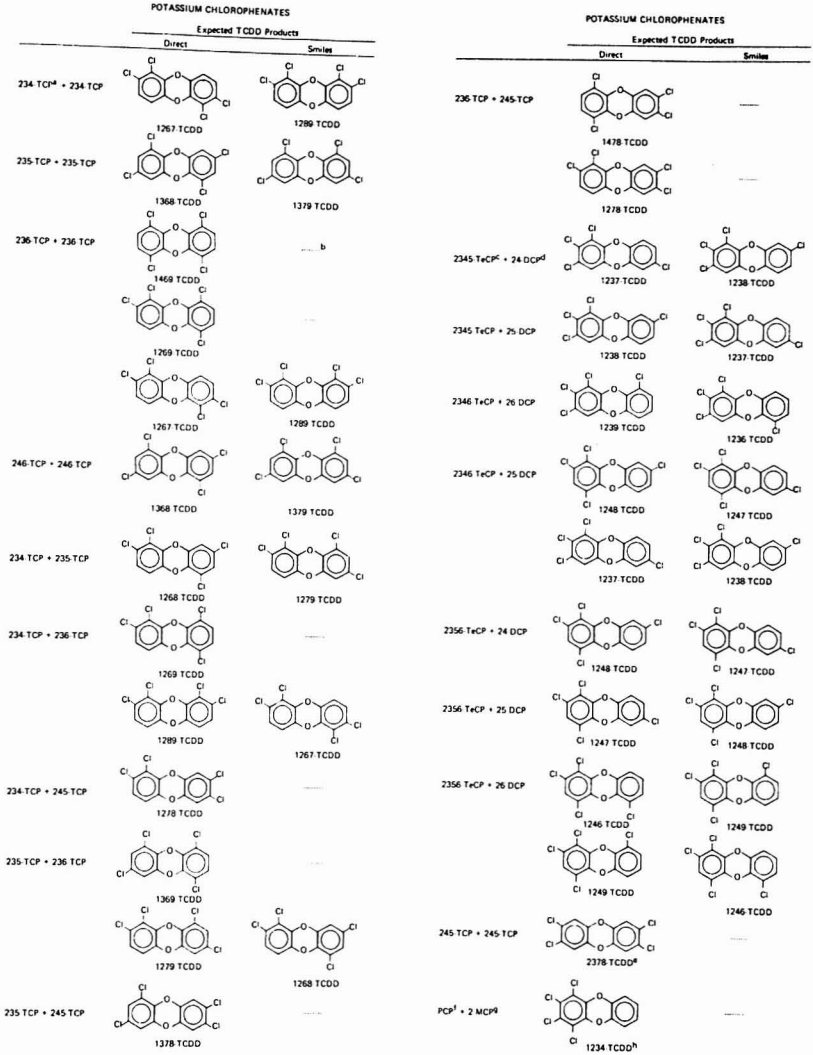

[a] TCP = trichlorophenol; [b] Smiles Rearrangement product same as direct addition; [c] TeCP = tetrachlorophenol; [d] DCP = dichlorophenol; [e] authentic standard available, obtained as byproduct from other pyrolyses; [f] PCP = pentachlorophenol; [g] MCP = monochlorophenol; [h] authentic standard available, pyrolysis reaction not conducted.

to 280 °C, and the reactor tube was slid into the furnace to position the K-phenate plug in the heated zone and a cool air flow was directed on the silica adsorbent bed for approximately 1 min to speed cooling to room temperature. After 15 min reaction time, the system was removed from the tube furnace and allowed to cool to ambient temperature. TCDDs, present in the reactor tube, were selectively removed via the chromatographic procedure described for the 2:2 TCDD isomer syntheses. The workup and preliminary analysis procedures were also the same. This procedure can be used to prepare 1234-TCDD (4:0 TCDD isomer); however this material is commercially available from Analabs (North Haven, Conn.) at a purity exceeding 99%.

Preliminary Gas Chromatography–Low Resolution Mass Spectrometry (GC-LRMS). Each crude pyrolyzate, dissolved in approximately 75 mL of methylene chloride, was qualitatively analyzed for TCDDs using a Hewlett-Packard Model 5992A GC-/LRMS operating in the multiple ion detection (MID) mode monitoring m/e^-: 320, 322, 324, and 332, at unit resolution.

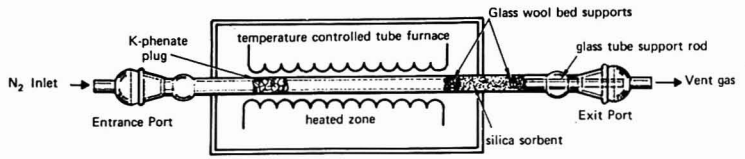

Figure 3. Pyrolysis reactor apparatus for 3:1 TCDD isomer syntheses, reactor tube shown in pyrolysis position

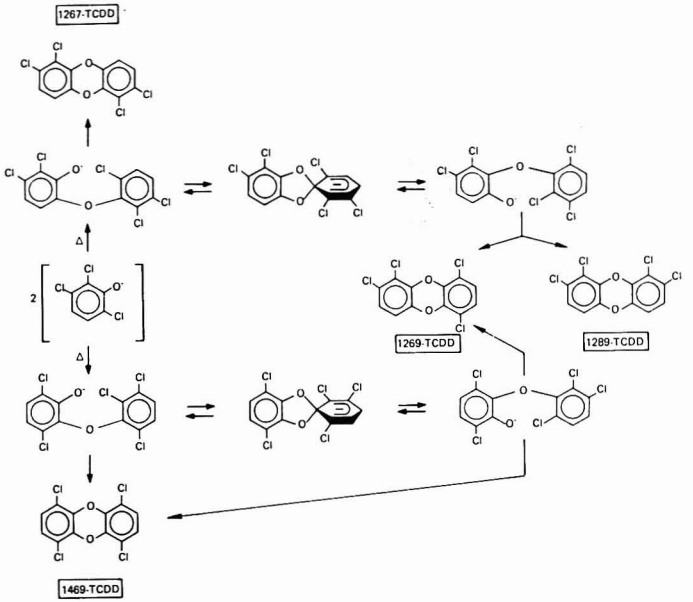

Figure 4. Reaction pathways for condensation of 236-TCP

Approximately 1 ng of ^{13}C-2378-TCDD was coinjected with each sample to provide a TCDD retention index, this species was monitored at m/e^- 332. GC-LRMS operating conditions were as follows: column, 2 mm id × 210 cm silylated glass; packing, 0.60% OV-17 silicone + 0.40% Poly S-179 on a specially deactivated high-temperature 80/100-mesh support (a recent development of the Dow Chemical Company which has been licensed to HNU Systems, Inc.); column temperature, programmed from 210 to 250 °C at 10 °C/min and held at maximum; injection port temperature, 280 °C; carrier gas, helium at 14 cm³/min; separator, single-stage glass jet operating at column temperature; electron energy, 70 eV.

Gas Chromatography with Electron-Capture Detection (GC-EC). Caustic extracted pyrolyzates were analyzed qualitatively for the presence of chlorinated species other than TCDDs, and semiquantitatively for a rough approximation of total TCDDs present, using a Varian Model 3700 gas chromatograph equipped with a ^{63}Ni pulsed electron capture detector (ECD). An average response factor for TCDDs was obtained by calibration of the instrument with a standard containing: 1368-TCDD, 1379-TCDD, 1378-TCDD, at 200 ng/mL each. A 1-μL injection of each sample, appropriately diluted in hexane, was made under the following instrumental conditions: column, 2 mm i.d. × 210 cm silylated glass; packing, 0.60% Poly S-179 on a specially deactivated high-temperature 80/100-mesh support; column temperature, 210 to 300 °C at 6 °C/minute and held at maximum; injection port temperature, 250 °C; carrier gas, nitrogen at 20 cm³/min; attenuation, 2560×.

Reverse Phase High Performance Liquid Chromatography (RP-HPLC). The first stage of TCDD isomers separation involved RP-HPLC using a Perkin-Elmer Model LC-65T liquid chromatographic column oven and variable wavelength UV detector. The instrumental operating parameters were: column, two 6.2 × 250 mm Zorbax-ODS (Dupont Instruments Division, Wilmington, Del.) columns in series; isocratic eluent, methanol at 2.0 mL/min; pump, Altex Model 110A; column temperature, 50 °C; UV detector, 0.32 aufs at 235 nm; injector, Rheodyne Model 7120 with 50-μL sample injection loop. The caustic extracted pyrolyzates were dissolved in chloroform such that 5 μL injected would contain approximately 2–4 μg total TCDDS. An authentic standard of 2378-TCDD demonstrated a retention time of 14.2 min under these conditions. During the course of each sample separation, fractions corresponding to each peak observed eluting between 10 and 18 min retention time were collected in 15-mL vials equipped with Poly-Seal caps. TCDDs were recovered from each fraction by addition of approximately 8 mL of 2% (w/v) aqueous sodium bicarbonate followed by two extractions with 2 mL of hexane. The combined extracts were evaporated to dryness under a stream of specially purified nitrogen in 4-mL vials (RP-HPLC fraction).

Normal Phase Adsorption (Silica) High Performance Liquid Chromatography (Silica-HPLC). Each RP-HPLC

fraction was dissolved in 500 μL of hexane. A 2-μL aliquot was coinjected with approximately 1 ng ^{13}C-2378-TCDD into the GC-LRMS, operating as previously described, with the exception that the column temperature was maintained at 246 °C isothermal. This procedure was used to determine which RP-HPLC fractions contained TCDDs. Selected RP-HPLC fractions were then evaporated to dryness, redissolved in 80 μL of hexane, and quantitatively injected into the following silica-HPLC system: Laboratory Data Control Model 1204 variable wavelength UV detector, 0.5 aufs at 235 nm; column, two 6.2 × 250 mm Zorbax-Sil (Dupont Instruments Division, Wilmington, Del.) columns in series; isocratic eluent, hexane at 2.0 mL/min; pump, Altex Model 110A; column temperature, ambient; injector, Rheodyne Model 7120 with 100-μL sample injection loop. Again during the course of each sample separation, fractions corresponding to each observed peak were collected in 4-mL vials and the hexane solvent was evaporated to dryness under a stream of specially purified nitrogen. It is important to note the Zorbax-Sil HPLC columns must be activated (residual water removed) before they can be used to separate TCDD isomers. These columns were activated in accordance with the procedure of Bredeweg et al. (26): approximately 250 mL of methylene chloride at 2.5 mL/min were pumped through the new columns as received from the manufacturer, followed by 60 mL of 2% 2,2-dimethoxypropane + 2% acetic acid in methylene chloride (v/v) at 2.5 mL/min, followed by 375 mL of methylene chloride at 2.5 mL/min, and finally the dried columns were reequilibrated by pumping approximately 350 mL of hexane through at 2.5 mL/min. Burdick & Jackson non-spectro hexane (distilled-in-glass quality) is normally used in this system and it typically contains between 0.003 and 0.009% water. Without any precautions to further dry the eluent, TCDD retention times demonstrate a very slow drift toward shorter retention times as the columns adsorb trace water from the eluent. The separation of TCDD isomers has been demonstrated to be adequate when an authentic standard of 2378-TCDD has an absolute retention time between 12.5 and 17.0 min. When the retention time becomes less than 12.5 min, the columns are redried. Normally 5–7 L of eluent can be passed through the system between dryings. Because of the described slow decrease in TCDD isomer retention times, relative retention times were computed for each TCDD fraction based upon the absolute retention time for an authentic 2378-TCDD standard. (During the course of this work, the 2378-TCDD retention time decreased from 15.35 to 14.30 min.)

Final GC-LRMS. The silica-HPLC fractions were redissolved in 500 μL of hexane and a 2.0-μL aliquot was coinjected into the GC-LRMS along with 1 ng ^{13}C-2378-TCDD. The instrument parameters were as previously described; however the column temperature was maintained at 246 °C isothermal. TCDD isomers were identified by their characteristic 4-chlorine isotope pattern monitored at m/e^-: 320, 322, and 324. Their gas chromatographic relative retention times were computed from the absolute retention time of coinjected ^{13}C-2378-TCDD which was assigned a value of 1.000.

TCDD Standards. The authentic standard of 2378-TCDD used for calibration purposes in this work was prepared by W. W. Muelder of the Dow Chemical Company (27). The structure of this material was determined by single crystal X-ray diffraction techniques, and its purity as determined by mass spectrometry was 98%. The ^{13}C-2378-TCDD was prepared by A. S. Kende of the University of Rochester (Rochester, N.Y.) and by mass spectrometry was shown to be 86 at. % ^{13}C. The 1368-TCDD, 1379-TCDD, and 1378-TCDD standards used for calibration of the gas chromatograph (ECD) were of the best quality available; however, their structures have not been thoroughly authenticated. The 1378-TCDD was prepared by A. S. Kende, and the 1368-TCDD and 1379-TCDD was prepared by T. Brady of the Dow Chemical Company.

RESULTS AND DISCUSSION

Since 1968 a large amount of research effort has been directed toward the synthesis of CDDs, in particular the more toxic homologues (*11, 12, 28, 29*). In general the goal has been to produce isomerically pure compounds for toxicological evaluation and for use as reference standards for analytical purposes. There are two basic approaches to this problem. The first involves regiospecific syntheses which are "designed" to yield isomerically pure CDD products. This procedure trades a difficult synthesis problem (i.e., requires preparation of regiospecific precursors (*28, 29*) and may suffer multiple product formation via Smiles rearrangement) for a simplified product separation and recovery. The second approach, described herein, employs very simple pyrolysis reactions based upon easily available starting materials (potassium chlorophenates) to produce limited mixtures of CDD isomers. In this case the simplified syntheses are exchanged for a highly sophisticated isomer-specific separation and recovery technique. Any, or all, of the 22 TCDD isomers can be isolated by this single procedure.

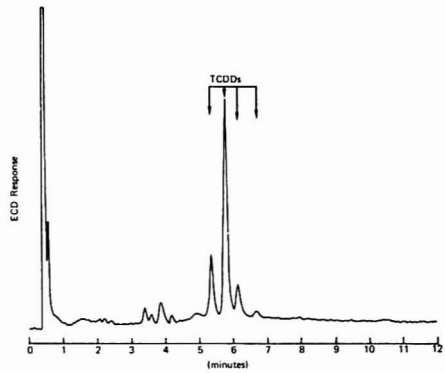

Figure 5. Temperature-programmed GC-ECD chromatogram for caustic extracted 2,3,6-TCP pyrolyzate, conditions in text.

Table III. Chromatographic Retention Indices for 236-TCP TCDDs

expected TCDDs	RP-HPLC, abs. RT, min[a]	silica-HPLC, rel. RT[b]	GC-packed column, rel. RT[c]
1469-TCDD	11.6–13.0	1.497	0.912
1269-TCDD	11.6–13.0	1.623	1.090
1267-TCDD	11.6–13.0	1.702	0.998
1289-TCDD	11.6–13.0	1.801	1.203

[a] Abs. RT = absolute retention time. [b] Rel. RT = relative retention time as computed from absolute retention time for 2378-TCDD = 1.000. [c] Rel. RT = relative retention time as computed from absolute retention time for coinjected ^{13}C-2378-TCDD = 1.000.

Application to 2,3,6-Trichlorophenate. In accordance with the current literature, pyrolytic condensation of chlorophenate salts is believed to proceed via the reaction pathways shown in Figure 4 for 236-TCP (*29*). Four possible TCDD isomers can be formed, and this particular reaction will be used to illustrate our technique.

The pyrolysis equipment shown in Figures 2 and 3 was designed to minimize the possibility of accidental exposure to CDD products. The incorporation of a silica support matrix permitted preliminary separation of CDDs, using the reactor tube as a liquid chromatography column; hence direct handling of the crude products (tars) was eliminated. The designation of different reactors for the 2:2 TCDD and 3:1 TCDD

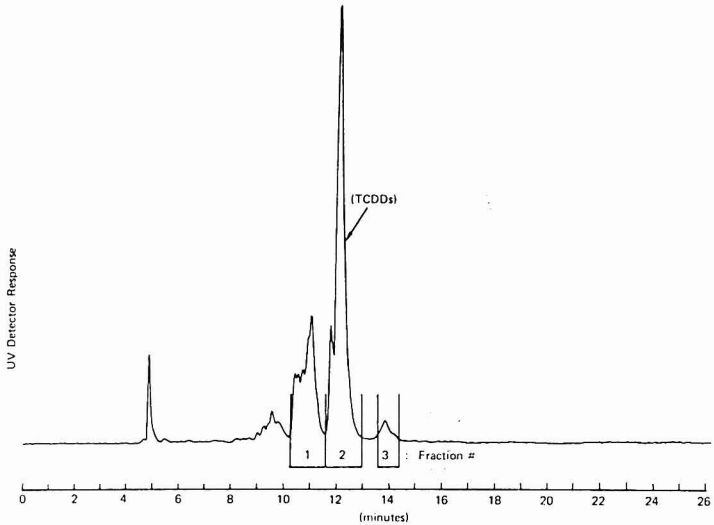

Figure 6. RP-HPLC chromatogram for caustic extracted 2,3,6-TCP pyrolyzate, conditions in text

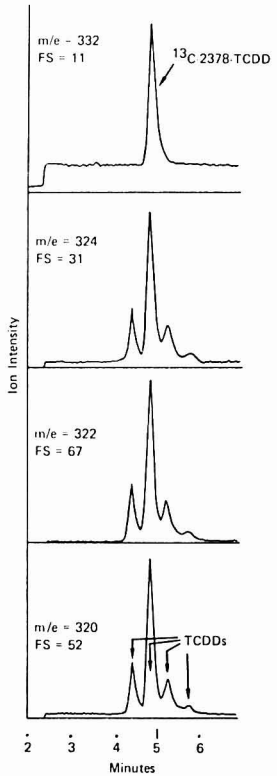

Figure 7. Packed column GC-LRMS mass chromatograms for RP-HPLC TCDDs fraction #2, conditions in text. FS is full scale factor applied to each ion

Table IV. TCDD Isomer Retention Indices

TCDD isomers	RP-HPLC, abs. RT, min[a]	silica-HPLC, rel. RT[b]	GC-packed column, rel. RT[c]
1267/1289	12.2-12.9	1.623	1.081
	12.2-12.9	1.795	1.200
1268/1279	13.3-13.9	1.238	0.956
	13.3-13.9	1.291	1.065
1269	11.6-13.0	1.702	0.998
1278	14.0-14.7	1.288	0.893
1368	15.9-16.8	0.977	0.729
1369/1478	13.3-13.9	1.220	0.802
	13.3-13.9	1.340	0.907
1378	14.9-15.7	1.000	0.858
1379	14.9-15.9	0.940	0.771
1469	11.6-13.0	1.497	0.912
2378	13.8-14.5	1.000	1.006[d]
1236/1239	13.8-14.4	1.356	1.037
	14.4-15.2	1.350	0.969
1237/1238	14.0-15.0	1.100	0.979
	14.0-15.0	1.128	0.990
1246/1249	13.7-14.5	1.328	0.896
	13.7-14.5	1.441	0.898
1247/1248	14.2-15.1	1.154	0.854
	14.2-15.1	1.199	0.857
1234	15.8-16.8	1.248	0.960

[a] Abs. RT = absolute retention time (±0.1 min). [b] Rel RT = relative retention time as computed from absolute retention time of 2378-TCDD = 1.000 (1.000 ± 0.010). [c] Rel. RT = relative retention time as computed from absolute retention time of ^{13}C-2378-TCDD = 1.000 (1.000 ± 0.005). [d] Native 2378-TCDD elutes slightly later than ^{13}C-2378-TCDD.

isomer groups is not intended to be necessary from a synthesis point of view. Our initial efforts centered on the preparation of the 13 2:2 TCDD isomers and were conducted according to the described procedure. Attempted preparation of the 3:1 TCDD isomers using this same procedure gave poor TCDD yields. The problem appeared to be related to dichlorophenate stability during the preliminary drying stages. Apparent hydrolysis of the dichlorophenate salt to free phenols led to severe losses due to their volatility at 180 °C. The 3:1 TCDD isomer reactor design eliminates this problem and provides

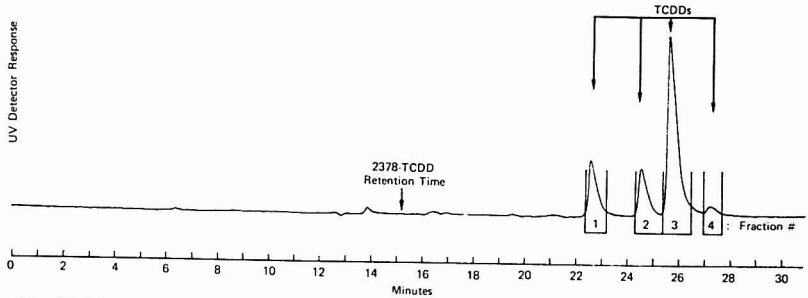

Figure 8. Silica-HPLC chromatogram for RP-HPLC TCDDs fraction #2, conditions in text

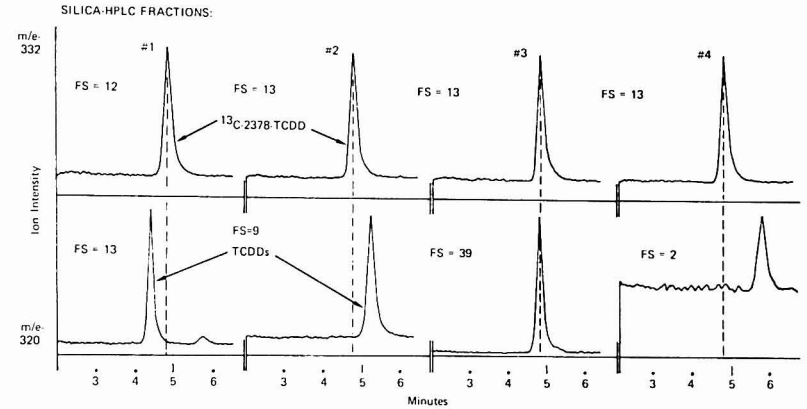

Figure 9. Composite mass chromatograms for silica-HPLC TCDD fractions #1 through #4, conditions in text. Ion $m/e^- = 332$ is ^{13}C-2,3,7,8-TCDD retention time marker

improved yields. We anticipate that this reactor would also be suitable for 2:2 TCDD isomers. However, use of the described 2:2 TCDD isomer reactor appears to favor only 2:2 TCDDs; hence the undesirable formation of 3:1 TCDDs resulting from impurities in the chlorophenol precursors may be significantly reduced.

When the separation technique described in the Experimental section (RP-HPLC fractionation, silica-HPLC fractionation, GC separation, and LRMS detection and identification) is applied to the pyrolysis products of 236-TCP, each of the four expected TCDD isomers (Figure 4) are isolated. The temperature-programmed GC-EC chromatogram of the caustic extracted product is shown in Figure 5. These particular TCDD isomers are well separated on the GC column. Figure 6 illustrates the RP-HPLC fractionation step. Three fractions were collected and each was analyzed by GC-LRMS to determine the presence of TCDDs. The major product TCDDs, observed by GC-LRMS analysis of the crude pyrolyzate, were found to be present in RP-HPLC fraction #2 (Figure 7). This material was then subjected to silica-HPLC fractionation, with the resulting chromatogram shown in Figure 8. Four fractions were collected and GC-LRMS analyses indicated the presence of a TCDD isomer in each one. Figure 9 is a composite of these mass chromatograms. The resultant chromatographic retention indices for 236-TCP products are listed in Table III. It is important to note that these data clearly indicate the presence of four distinct TCDD isomers; however, from these data alone, their identities cannot be determined.

Isomer Identification. In the same manner as described for 236-TCP, each of the pyrolysis reactions listed in Table II was conducted and the products were examined. Chromatographic retention time data were compiled for each major TCDD product observed, along with a list of expected TCDD isomers. Examination of all retention indices data demonstrated the existence of exactly 22 distinct sets. With the complete assemblage of these data, it became possible to characterize the retention indices observed with either single TCDD isomers, or pairs of isomers related via the Smiles rearrangements. The basic process involved compilation of recurring retention indices for TCDD isomers that could be formed by more than one set of chlorophenate precursors. The only exception to this case was 2378-TCDD which by virtue of its symmetry can be isolated, essentially as a pure isomer, from the pyrolysis of 245-TCP. In all other cases, either two TCDD isomers can be formed from the TCP precursor, or a mixed TCPs reaction is required which results in the formation of the desired mixed TCDD product plus those TCDDs associated with each individual TCP. The final results for TCDD isomer identification by this procedure are shown in Table IV. Figures 10 and 11 illustrate isomer elution sequence for RP-HPLC and silica-HPLC separations. Those cases where two TCDD isomers are listed represent situations where multiple TCP pyrolyses cannot provide sufficient information

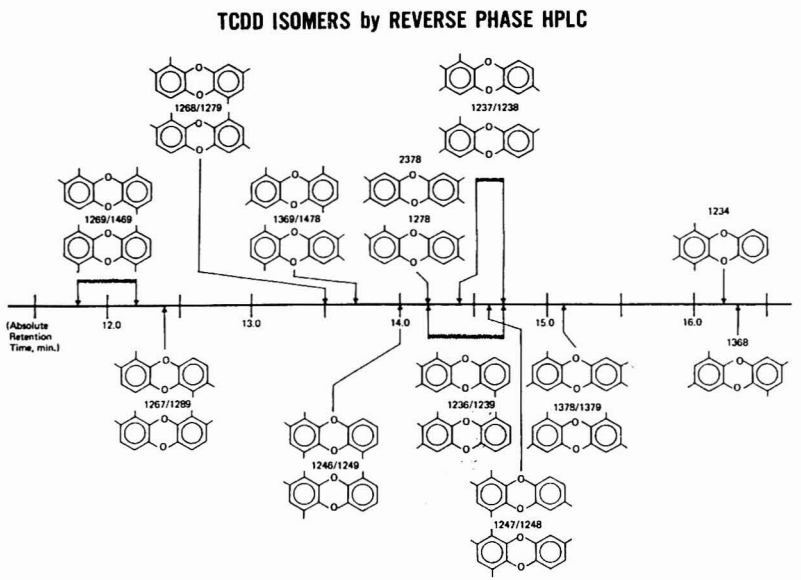

Figure 10. TCDD isomer elution sequence for RP-HPLC

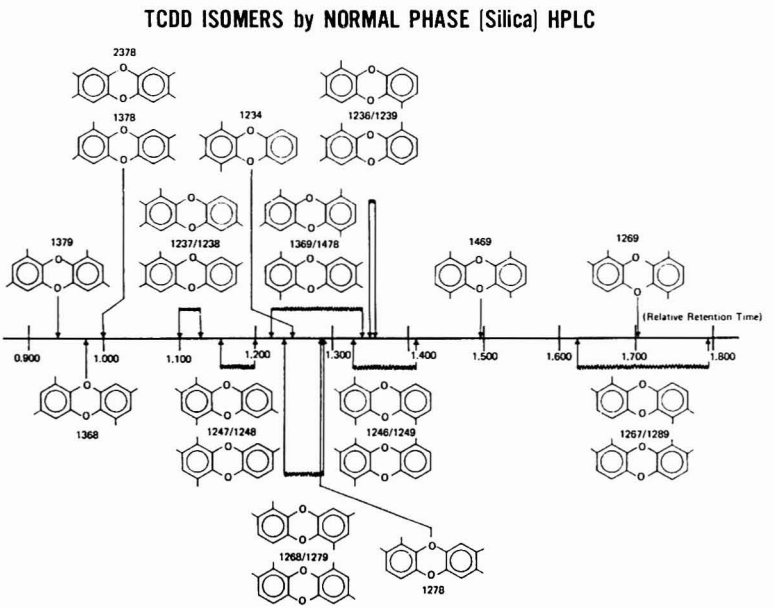

Figure 11. TCDD isomer elution sequence for silica-HPLC, approximate 2,3,7,8-TCDD absolute retention time is 14.70 min and is defined as 1.000; refer to text for description

to differentiate between isomers related via the Smiles rearrangement. Although these isomers can easily be separated, we cannot currently identify which set of retention indices go with what isomer. This problem could be solved by iso-

lating a quantity of one TCDD isomer from each pair sufficient to permit structural identification by other instrumental means.

CONCLUSIONS

CDDs represent a class of molecules whose parent structure is a relatively small fused aromatic ring. Substitutional positions are occupied by chlorine and hydrogen. The combination of small parent structure, and multiplicity of substitutional patterns by reasonably nonpolar functional groups, has severely taxed the limits of all single-approach forms of chromatographic isomer separation. Relative to CDDs in general, the separation problem appears to have peak intensity for the TCDD group, where there are a maximum number of possible isomers.

The application of three different forms of chromatography, whose mechanisms for achieving separation involve significantly different molecular parameters, has permitted the first documented separation of all 22 TCDD isomers. Although HPLC fractionations dictate limitations upon the total amount of material which can be processed at one time, the incorporation of automated injection and collection devices could permit the isolation of milligram quantities of individual isomers. Because of the variety of activity tests available, these amounts should be adequate for biological testing.

Perhaps the most valuable asset of HPLC fractionation of TCDDs is its amenability to a wide variety of sample matrices. This concept of multiple chromatographies allows CDDs to be fractionated into groups according to degree of chlorination, allows isomers within a group to be separated, and simultaneously permits separation of a wide variety of other environmentally important species (i.e., polychlorinated dibenzofurans, polychlorinated biphenyls, polychlorinated terphenyls, polybrominated biphenyls, DDTs, and phthalate esters). We are currently investigating such applications for biological, environmental, and product analyses as a means for trace contaminant monitoring and will report our findings in the near future.

LITERATURE CITED

(1) D. Firestone, J. Ress, N. L. Brown, R. P. Baron, and J. Damico, *J. Assoc. Off. Anal. Chem.*, **54**, 85 (1972).
(2) C. A. Nilsson and L. Renberg, *J. Chromatogr.*, **89**, 325 (1974).
(3) W. B. Crummett and R. H. Stehl, *Environ. Health Perspect.*, **5**, 15 (1973).
(4) B. A. Schwetz, J. M. Norris, G. L. Sparschu, V. K. Rowe, P. J. Gehring, J. L. Emerson, and C. G. Gerbig, "Chlorodioxins—Origin and Fate", E. H. Blair, Ed., American Chemical Society, Washington, D.C., 1973.
(5) E. E. McConnell, J. A. Moore, J. K. Haseman, and M. W. Harris, *Toxicol. Appl. Pharmacol.*, **37**, 146 (1976).
(6) A. Poland, E. Glover, and A. S. Kende, *J. Biol. Chem.*, **251**, 4936 (1976).
(7) G. R. Higginbotham, A. Huang, D. Firestone, J. Verrett, J. Ress, and A. D. Campbell, *Nature (London)*, **220**, 702 (1968).
(8) B. A. Schwetz, J. M. Norris, G. L. Sparschu, V. K. Rowe, P. J. Gehring, J. L. Emerson, and C. G. Gerbig, *Environ. Health Perspect.*, **5**, 87 (1973).
(9) R. L. Johnson, P. J. Gehring, R. J. Kociba, and B. J. Schwetz, *Environ. Health Perspect.*, **5**, 171 (1973).
(10) J. S. Cantrell, N. C. Webb, and A. J. Mabis, *Acta Crystallogr. Sect. B*, **25**, 150 (1969).
(11) A. P. Gray, S. P. Cepa, I. J. Solomon, and O. Aniline, *J. Org. Chem.*, **41**, 2435 (1976).
(12) A. S. Kende, J. J. Wade, D. Ridge, and A. Poland, *J. Org. Chem.*, **39**, 931 (1974).
(13) B. A. Schwetz, J. M. Norris, G. L. Sparschu, V. K. Rowe, P. J. Gehring, J. L. Emerson, and C. G. Gerbig, *Adv. Chem. Ser.*, **120**, 55 (1973).
(14) L. A. Shadoff and R. A. Hummel, *Biomed. Mass Spectrom.*, **5**, 7 (1978).
(15) N. H. Mahle, H. S. Higgins, and M. E. Getzendaner, *Bull. Environ. Contam. Toxicol.*, **18**, 123 (1977).
(16) L. L. Lamparski, N. H. Mahle, and L. A. Shadoff, *J. Agric. Food Chem.*, **26**, 1113 (1978).
(17) R. W. Baughman and M. Meselson, *Environ. Health Perspect.*, **5**, 27 (1973).
(18) H. R. Buser and C. Rappe, *Chemosphere*, **7**, 199 (1978).
(19) H. R. Buser, *Anal. Chem.*, **49**, 918 (1977).
(20) Dow Chemical Co., "Trace Chemistries of Fire", Nov. 1978.
(21) K. Olie, P. L. Vermeulen, and O. Hutzinger, *Chemosphere*, **6**, 455 (1977).
(22) H. R. Buser, H. P. Bosshardt, and C. Rappe, *Chemosphere*, **7**, 165 (1978).
(23) H. R. Buser, *J. Chromatogr.*, **114**, 95 (1975).
(24) O. Aniline, *Adv. Chem. Ser.*, **120**, 126 (1973).
(25) C. Rappe, S. Marklund, H. R. Buser, and H. P. Bosshardt, *Chemosphere*, **7**, 269 (1978).
(26) R. A. Bredeweg, L. D. Rothman, and C. D. Pfeiffer, submitted for publication in *Anal. Chem.*
(27) F. P. Boer, F. van Remoortere, and W. W. Mueider, *J. Am. Chem. Soc.*, **94**, 1006 (1972).
(28) A. E. Pohland and G. C. Yang, *J. Agr. Food Chem.*, **20**, 1093 (1972).
(29) A. S. Kende and M. R. DeCamp, *Tetrahedron Lett.*, **33**, 2877 (1975).

RECEIVED for review June 15, 1979. Accepted August 24, 1979.

CORRESPONDENCE

Diffusion Control in Linear Sweep Voltammetry

Sir: In many linear sweep voltammetry experiments, even if the charge transfer is irreversible or there are coupled chemical reactions, the current will become purely diffusion controlled at a potential sufficiently past the peak (*1*). Then the current-voltage curve obeys effectively a simple Cottrell equation: current–time curve (*2*) with $E = vt$, where E = potential, v = sweep rate, and t = time. In some cases a further electrode process will interrupt the diffusion control (*3*) but in many situations one can use this part of the curve to obtain chronoamperometric (i–t) data, obviating the necessity for separate potential step experiments. The Cottrell equation is (*2*)

$$i = \frac{nFSCD^{1/2}}{\pi^{1/2}} \cdot \frac{1}{t^{1/2}} \tag{1}$$

where i = current; n is the number of electrons involved in the process; F, the Faraday; S, the electrode area; C, the concentration of electroactive material; and D, its diffusion coefficient. In a potentiostatic experiment the initial time is obvious—it is the time at which the E_1 to E_2 pulse is applied (where $E_1 \ll E_p$ and $E_2 \gg E_p + (0.16/n)$ V). It is indicated experimentally by a sharp rise in current as in the solid curve in Figure 1a. However, the corresponding time (t_0) in a linear sweep experiment, such that the diffusion part of the curve past the peak matches the equivalent potentiostatic current-time curve, is not known a priori, and therefore needs to be included in the equation. Thus we can write

$$i = \frac{nFSCD^{1/2}}{\pi^{1/2}} \cdot \frac{1}{(t - t_0)^{1/2}} = \frac{K}{(t - t_0)^{1/2}} \tag{2}$$

Equation 2 becomes identical to Equation 1 if one puts $t_0 = 0$. In linear sweep voltammetry $t = E/v$ and therefore

$$i = \frac{G}{(E - E_0)^{1/2}} \tag{3}$$

where $E = vt$; $E_0 = vt_0$ and $G = v^{1/2}K$. (This is the form used by Ginzburg (*4*) with $G = A$ and $E_0 = B$).

Re-arranging Equation 3 gives

$$\frac{1}{i^2} = \frac{E}{G^2} - \frac{E_0}{G^2} \tag{4}$$

A plot of $1/i^2$ vs. E should give a straight line for pure diffusion control with slope = $1/G^2$ and intercept at $-E_0/G^2$. Hence E_0 = −intercept/slope.

Of major interest is G^2 from which n^2D may be obtained and hence values of n and D if a rough value of D is known and n is small and integral. We have used this empirical approach in the study of the electrochemical reduction of carbon dioxide under various conditions (*5*).

t_0 is a virtual zero time and can be more usefully expressed as a potential E_0 with respect to the half-wave potential ($E_{1/2}$) or the peak potential (E_p).

Ginzburg's (*4*) form of Equation 3 is

$$\bar{i} = \frac{A}{(E - B)^{1/2}} \tag{5}$$

B, the "zero time" potential is expressed with respect to E_p and the current is normalized so $\bar{i} = i/i_p$.

Ginzburg gives calculated values for A and B for both reversible and irreversible charge transfer. However the basis for his calculations is not clear, especially as he expresses surprise that constant

$$A = \left(\frac{RT}{nF}\right)^{1/2} \quad \text{(reversible)}$$

or

$$A = \left(\frac{RT}{\alpha nF}\right)^{1/2} \quad \text{(irreversible)}$$

We have compared the theoretical values for the current linear sweep voltammetry with the diffusion controlled current–time values. In order to do this we needed to calculate additional values of $\pi^{1/2}\chi(at)$ well into the region of pure diffusion control. We have done this for the simple reversible electron transfer process following Nicholson and Shain's procedure (*6*) with a slight modification.

From Equation 33 in ref. 6 normalized current function

$$\chi(at) = \frac{1}{\pi\sqrt{at}\,(1 + \gamma\theta)} + \frac{1}{4\pi} I \tag{6}$$

where

$$I = \int_0^{at} \frac{dz}{\sqrt{at - z}\,\cosh^2\left(\dfrac{\log \gamma\theta - z}{2}\right)}$$

Let $z = at \sin^2\phi$, then $dz/d\phi = 2\,at \sin\phi \cos\phi$, so

$$I = \int_0^{\pi/2} \frac{2\,at \sin\phi \cos\phi\, d\phi}{\sqrt{at(1 - \sin^2\phi)}\,\cosh^2\left(\dfrac{\log \gamma\theta - at \sin^2\phi}{2}\right)}$$

$$= 2\sqrt{at} \int_0^{\pi/2} \frac{\sin\phi}{\cosh^2\left(\dfrac{\log \gamma\theta - at \sin^2\phi}{2}\right)} d\phi$$

This integral was evaluated by Simpson's rule to six significant figures with $\log \gamma\theta = 6.5$ (ref. 6.) using a computer program. The data from these calculations, using $\pi\chi(at)$ for normalized dimensionless current at potentials given as $(E - E_{1/2})$ (as in ref. 6), was fitted by a linear least squares analysis computer program to Equation 4, where $i = \pi^{1/2}\chi(at)$. Values of $(E - E_{1/2})$ were taken from −0.2 to −1.0 V.

The regression analysis was repeated using more cathodic initial potentials and then some more sets with cathodic potentials between −1.0 and −2.0 V. Over this whole range the correlation coefficient was between 0.99999 and 1.00000. Standard deviations in G^2 were always better than ±0.1% and in E_0 better than ±2%. The values of G^2 slowly increased toward the theoretical value as the initial value of E was shifted cathodically. However from the practical point of view the lowest value of G^2 was only 0.7% less than theory.

At the same time the value of E_0 shifted from +25 mV toward zero, i.e., the point at which $E_0 = E_{1/2}$. Some data are shown in Table I. It will be noted that the values of G^2 and

0003-2700/79/0351-2282$01.00/0

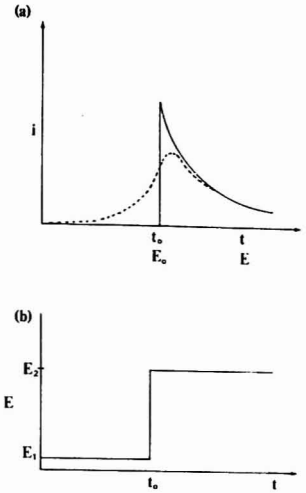

Figure 1. Comparison of potentiostatic *I/t* curve with linear sweep voltammetric *I/E* curve. (a) Potentiostatic *I/t* curve (—) compared with linear sweep voltammetric *I/E* curve (---) such that $E = vt$. (b) Potential step determining the initiation of the *I/t* curve

Table I. The Shift of E_e Values from +25 mV toward 0

range of E/mV	$G^2 \times 10^3$	E_e/mV	computed % error in E_e
−200 to −1000	8.1135	25.0	1.6
−300 to −1000	8.1323	19.6	0.9
−400 to −1000	8.1418	16.7	0.6
−600 to −1000	8.1519	13.5	0.2
−800 to −1000	8.1570	11.7	0.09
−920 to −1000	8.1609	10.3	0.03
−1000 to −2000	8.1676	2.3	
−1940 to −2000	8.1710	1.6	
theory	8.1740	0.0	

E_0 differ from Ginzburg's values of A and B (*4*).

The theoretical value of G^2 can be found from the point at which the linear sweep voltammetric current (i_v) becomes equal to the potential step chronoamperometric current (i_t). Now

$$i_t = \frac{nFSCD^{1/2}}{\pi^{1/2}(t - t_0)^{1/2}} \tag{7}$$

and

$$i_v = nFSCD^{1/2}\, a^{1/2}\, \pi^{1/2} \chi(at) \tag{8}$$

$$a = \frac{nFv}{RT}$$

When $i_t = i_v$

$$\sqrt{\pi}\chi(at) = \left(\frac{RT}{\pi nF}\right)^{1/2} \frac{1}{v(t - t_0)^{1/2}} \tag{9}$$

Now $v(t - t_0)$ can be replaced by $E - E_0$ and therefore

$$\sqrt{\pi}\,\chi(at) = \left(\frac{RT}{\pi nF}\right)^{1/2} \frac{1}{(E - E_0)^{1/2}} \tag{10}$$

Comparing Equations 3 and 10

$$G^2 = \frac{RT}{\pi nF} = 0.008174 \text{ at } 298 \text{ K}$$

Note Ginzburg's value for $A^2 = RT/nF = 0.02568$, as he has omitted the $\pi^{1/2}$ term from the Cottrell equation (*4*). Apart from that, his data are clearly accurate to ±1% as indicated in the condition for diffusion control that $i_t > 0.991$.

The dimensionless current ratio i_t/i_p used by Ginzburg does not however give the result he quotes, despite the $\pi^{1/2}$.

$i_p = i_v$ (max) =

$$nFSCD^{1/2}\, a^{1/2}\, \pi^{1/2}\, \chi(at) \text{ max} \quad \text{(ref. 6.)}$$

$$= nFSCD^{1/2} \left(\frac{nFv}{RT}\right)^{1/2} 0.4463 \text{ at } E = E_p \quad \text{(ref. 6.)}$$

therefore

$$i_t/i_p = \frac{nFSCD^{1/2}}{\pi^{1/2}(t - t_0)^{1/2}} \left(\frac{RT}{nFv}\right)^{1/2} \frac{1}{nFSCD^{1/2} \cdot 0.4463}$$

therefore

$$i^2 = \frac{RT}{nF\pi(0.4463)^2} \cdot \frac{1}{(E - E_0)}$$

Thus A^2 should be $= RT/(nF\pi(0.4463)^2)$. Ginzburg gives one value for $B = +0.0445$ V (ref. 4).

This is with respect to E_p. As $E_{1/2}$ is 0.0285 anodic of E_p this value is equivalent to $E_0 = +0.016$—which is within the range of values we obtained. Polcyn and Shain (*3*) give an empirical factor β (= 0.96 - 0.99) to adjust the theoretical G^2 factors to the computed values for some arbitrary ranges of potential given the calculated values of their equivalent of E_0, which is $E^1 - E^0$ which again fall within the range of values we obtained.

However a more systematic approach is needed extending farther out into the diffusion controlled region. The latter authors (*3*) confine themselves within the range 50 to 830 mV (rev) and 36 to 845 mV (irrev.)

Cyclic voltammetry of benzoquinone in acetonitrile yields two reversible one-electron waves (*7*). Analysis of tails of the first cathodic peaks for four scans at different scan rates and concentrations of quinone gave data from which values of the diffusion coefficient of benzoquinone were calculated using Equation 4. The mean value was 2.9 ± 0.3 cm^2 s^{-1} which is comparable with the value of 2.4 cm^2 s^{-1} obtain in ref. 7 using the Randles–Sevcik equation and with the value of 2.9 cm^2 s^{-1} obtained by potential step chronoamperometry (*8*).

LITERATURE CITED

(1) Adams, Ralph N. "Electrochemistry at Solid Electrodes"; Marcel Dekker: New York, 1969; p 125.
(2) Ref. 1, p 50.
(3) Polcyn, Daniel S.; Shain, Irving *Anal. Chem.* **1966**, *38*, 370–5.
(4) Ginzburg, Gregory. *Anal. Chem.* **1978**, *50*, 375–6.
(5) Eggins, Brian R.; McNeill, Joanne, Unpublished results, 1977.
(6) Nicholson, Richard S.; Shain, Irving. *Anal. Chem.* **1964**, *36*, 706–23.
(7) Eggins, Brian R. *Chem. Commun.* **1969**, 1267–8.
(8) Eggins, Brian R.; Chambers, James Q. *J. Electrochem. Soc.* **1970**, *117*, 186–92.

Brian R. Eggins*
School of Physical Science
Ulster Polytechnic
Shore Road
Newtownabbey
Co. Antrim, BT37 0QB, N. Ireland

Norman H. Smith
School of Mathematics
Ulster Polytechnic
Shore Road
Newtownabbey
Co. Antrim, BT37 0QB, N. Ireland

RECEIVED for review November 22, 1978. Accepted July 19, 1979. The financial support of The Chemical Society is gratefully acknowledged.

Direct Sample Insertion Device for Inductively Coupled Plasma Emission Spectrometry

Sir: The inductively coupled plasma (ICP) is currently the most effective source for simultaneous trace multielement analysis of solution samples by atomic emission spectrometry (*1–5*). However, more efficient solution sample introduction systems are required for the ICP and, as well, the analytical capability of the ICP would be greatly extended if other sample forms such as powders and solids could be directly introduced into the plasma and effectively analyzed. Although several workers have developed and investigated various approaches for introduction of such sample forms into the ICP (*3, 6–12*), no one system has yet been widely accepted or utilized. In this correspondence, a sample introduction system for the ICP is described that allows the direct insertion of small amounts of sample (powders, solids, or desolvated liquids) into the central core of the ICP. The sample container is a conventional undercut cup graphite electrode such as those used in dc arc emission spectrometry. The conventional ICP torch has been modified so that the electrode is held in a simple mechanical insertion system that replaces the normal central aerosol tube of the torch. Solid and powder samples ranging from 20 mg to less than 1 mg and liquid samples as small as 5 μL can be analyzed with this system.

A schematic drawing of the direct sample insertion system is shown in Figure 1. A torch essentially identical to the conventional design has been utilized except that it is constructed without the central aerosol tube and is mounted in a Teflon block. The graphite electrode sits on top of a solid quartz rod that is placed inside a central quartz tube. The rod extends completely through the Teflon block to a sliding platform. Several types of electrodes have been used including Ultra Carbon #781, Spex 4033, and Spex 4004 undercut graphite cup electrodes.

When igniting the plasma, the top of the electrode is set at a height that is identical to that of the top of a conventional aerosol injector tube. After the plasma is lit and the desired flow rates and power level are set, the electrode containing the sample is inserted into the plasma simply by raising the lower platform by hand. The electrode is inserted to a position just above the top of the load coil and the whole process takes less than 1 s. No problems have been encountered in maintaining the plasma either during electrode insertion or while the electrode is in the plasma. Little if any adjustment of the automatic matching network occurs when the electrode is inserted. The electrode appears to be almost white hot in about 2 s after insertion. Essentially no consumption of the electrode occurs, a consequence of the inert Ar atmosphere of the plasma.

Solid and powder samples, once placed in the electrode, can be inserted into the plasma with no further treatment; however, it is necessary to desolvate liquid (aqueous) samples before insertion. Liquid samples were placed in the cup using a 5-μL Eppendorf pipet. Desolvation was accomplished by inductively heating the electrode before igniting the plasma. The electrode containing the 5-μL aqueous sample is inserted to the center of the coil region and very low forward power is applied (~50 W). With a little practice, the sample can be quickly and effectively desolvated in about 1 min in this manner. Although not tested, inductive heating may also be useful for ashing samples directly in the cup. If the normal ignition level of forward power is applied to the system while the electrode is inserted in the coil region, it is quickly heated to a bright orange color and in 2 to 3 s the plasma will ignite. In fact, it was by inserting a graphite rod, that Reid ignited his plasma systems back in the early 60's. The normal procedure is, however, to lower the electrode containing the desolvated sample back to the starting position before starting the plasma and then insert the electrode as described previously.

A commercially available radiofrequency inductively coupled plasma source was used in this investigation (Plasma-Therm Inc., Kresson, N.J.). The source consisted of a Model HFP-2500D 2.5-kW RF generator (27.12 MHz), a Model ADC5-3 automatic power control, a Model AMN-2500E automatic matching network, and a Model PT-2500 plasma torch assembly. The source was operated at a forward power of 2 kW and a plasma gas (coolant) flow rate of 17 L/min. No auxiliary or central ("aerosol") gas flows were used. Several measurement systems were used including a computer-coupled photodiode array spectrometer (*13*), a single channel scanning monochromator (Heath EU-700)–photomultiplier tube system, and a Bausch & Lomb 2-meter dual grating spectrograph.

The spectrum resulting from a 5-μL aqueous sample (1 ppm Zn and Cd) as measured with the photodiode array spectrometer is shown in Figure 2. The sample was inductively desolvated before insertion and the spectral signal was integrated for 12.5 s after electrode insertion. The ICP spectral background was not subtracted for this spectrum; as a result the cadmium and zinc lines are seen superimposed on the NO bands and continuum that occur in this spectral region (*14*). The total spectral coverage of the photodiode array spectrometer is about 50 nm.

The 12.5-s integration of the spectral signal was achieved by the summation of 5 consecutive 2.5-s integration time cycles of the photodiode array measurement system. It was clear while observing the successive spectra on the photodiode array oscilloscope readout that Zn and Cd were not vaporizing at the same time. To determine the emission time behavior of these two species, the photodiode array integration time was set at 0.16 s and the intensities of Cd(II) 226.5 nm and Zn(II) 202.5 nm were monitored for 18 consecutive integration cycles (2.88 s) after electrode insertion. Plots of the intensities of these lines as a function of time are shown in Figure 3. From these results, it is clear that this sampling system will require extensive characterization in the time domain.

An analytical curve was measured for Zn concentrations from 1 to 100 ppm. The sample was added as a solution (5 μL) and inductively desolvated before electrode insertion. The curve was linear with a correlation coefficient of 0.98. The relative standard deviation for samples of the same concentration was 15%. The most likely sources of imprecision include reproducibly introducing a 5-μL sample to the electrode cup and manual control of the desolvation and electrode insertion steps.

The spectrum of a powder sample is shown in Figure 4. The sample was a commercial powder standard available from Spex Industries and normally used in dc arc analysis. This sample was one of the G-7 series standards and contained 0.0001% of 49 elements in a graphite matrix along with 0.1% indium for use as an internal standard where required. About 5 mg of this standard were added to the cup of the electrode. The spectrum was obtained about 1 s after insertion of the electrode and the spectral signal was integrated for 0.64 s.

The photodiode array spectrometer was set for the Zn–Cd region. At the particular point in time at which this spectrum was acquired, most of the Cd had already vaporized, although the Zn lines are still quite prominent. With a 5-mg sample

0003-2700/79/0351-2284$01.00/0

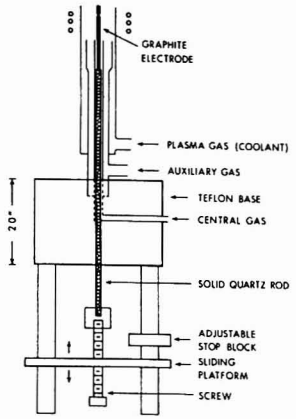

Figure 1. Schematic drawing of the direct sample insertion torch

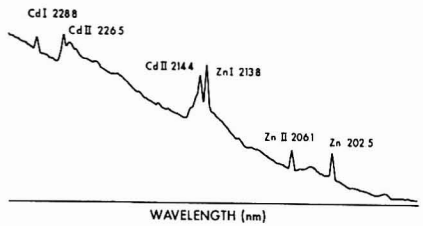

Figure 2. Spectrum of a 5-μL aqueous sample containing 1 ppm of Cd and Zn

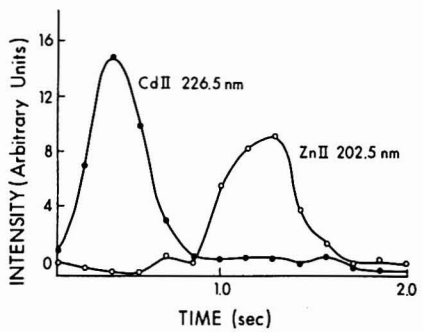

Figure 3. Time study plots for Cd and Zn

only about 5 ng of each element is present in this sample.

To test the quantitative capability of this sample introduction system for powdered samples, a set of 5 powdered samples containing Ag, Pb, B, and Zn were prepared in a graphite powder matrix. The samples were run in Spex #4004 electrodes complete with boiler caps. The use of boiler cap electrodes provided more reproducible time behavior. The sample size was about 15 mg and was weighed in all cases. The single channel monochromator measurement system was used and Zn was determined at the 213.8-nm line. The amount of Zn in the samples ranged from 1.8 ng to 12 μg. As can be seen in Figure 5, the analytical curve is linear up to about 1.3 μg. The slope of the line is 0.98 and the correlation coefficient

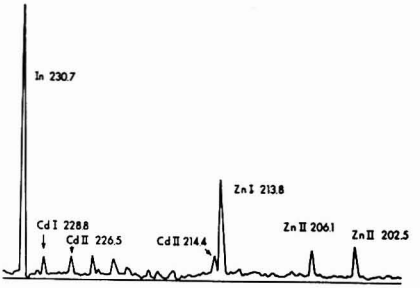

Figure 4. Spectrum of 0.0001% G-7 Spex Industries graphite matrix powder standard

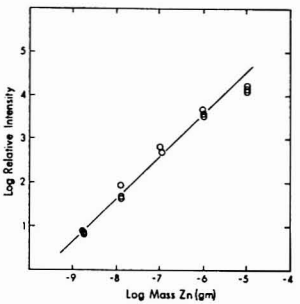

Figure 5. Analytical curve for Zn in powder samples with a graphite matrix

is 0.99. The detection limit (S/N = 2) is estimated to be about 0.1 ng. Finally it should be noted that this analytical curve was obtained without the use of an internal standard.

Because of the nature of the sample cup and the capability of analyzing powders directly, comparison of this system to a dc arc is inevitable. Thus a direct semiquantitative comparison was carried out using a Bausch & Lomb 2-meter dual grating spectrograph. The Spex G standards containing 49 elements but without the In internal standard (0.1, 0.01, 0.001, and 0.0001%) were run on this system using both a dc arc source and the direct sample insertion device (DSID)-ICP source. In both cases the samples were run in 781 Ultra Carbon electrodes. SA-1 plates were used and only the wavelength region from 240 to 340 nm was recorded. The results are summarized in Table I. Essentially equivalent detection limits were obtained for Ag, Be, Cd, Cr, Fe, Mg, Mn, Sb, and Sn. The DSID-ICP was better for As, Bi, Cu, Ga, In, Na, Pb, Tl, and Zn while the dc arc was better for B, Ca, Ge, Mo, Ti, and V. Certain elements were seen by only one or the other system. Co, Nb, Ni, and W were seen only with the dc arc and Hg, P, and Sr only with the DSID-ICP.

This brief study is by no means meant to be a definitive comparison, but was simply carried out to obtain a feeling for the capability of these two systems under reasonably identical conditions. In addition, it should be kept in mind that only the wavelength range from 240 to 340 nm was observed. For both techniques, more sensitive lines for several elements occur outside this region, particularly for the ICP (*15*). The main conclusion to be drawn both from the results shown in Table I and Figure 5 is not which technique is best but the fact that the ICP when coupled to the direct sample insertion system can be utilized directly for quantitative, semiquantitative, and

Table I. Semiquantitative Comparison of dc Arc and DSID-ICP Using the Spex G Standards (240-340) nm)

	dc arc		DSID-ICP	
element	% concn.	line	% concn.	line
Ag	0.0001	328.1	0.0001	328.1
As	0.1	278.0	0.01	278.0
B	0.001	249.7	0.01	249.7
Be	0.0001	249.5	0.0001	313.0
Bi	0.1	293.8	0.01	306.8
Ca	0.001	315.9	0.01	315.9
Cd	0.1	326.1	0.1	326.1
Co	0.1	245.0	NS[a]	
Cr	0.001	283.6	0.001	283.6
Cu	0.01	327.4	0.001	324.8
Fe	0.001	239.6	0.001	239.6
Ga	0.01	294.4	0.001	294.4
Ge	0.001	365.1	0.01	365.1
Hg	NS		0.01	253.7
In	0.01	325.6	0.001	325.6
Mg	0.0001	285.2	0.0001	285.2
Mn	0.0001	257.6	0.0001	257.6
Mo	0.001	284.8	0.1	284.8
Na	0.1	330.2	0.01	330.2
Nb	0.01	309.4	NS	
Ni	0.1	253.2	NS	
P	NS		0.1	255.3
Pb	0.1	283.3	0.01	283.3
Sb	0.01	326.8	0.01	287.8
Sn	0.01	303.4	0.01	326.2
Sr	NS		0.01	338.1
Ti	0.01	334.9	0.1	336.1
Tl	0.1	276.8	0.01	276.8
V	0.0001	310.2	0.01	310.2
W	0.1	263.5	NS	
Zn	0.1	330.3	0.01	328.2

[a] NS = Not seen at any concentration level.

Table II. Qualitative Analysis of NBS (SRM 1632) Coal (230-340 nm)

observed			not observed		
element	concn., ppm	line, nm	element	concn., ppm	best line, nm
Cu	18	324.8	As	6	193.7
Fe	8700	239.5	Cr	20	205.6
Mn	40	259.3	Ni	15	221.6
V	35	309.3	Pb	30	220.3
			Zn	37	213.9

qualitative analysis of powder samples with a capability at least equal to the dc arc.

Finally, some recent experiments indicate that it is possible to directly insert samples that have a predominantly organic matrix and carry out at least a qualitative analysis. Both NBS Coal and NBS Orchard Leaves can be packed into the cup and (without ashing) be inserted directly into the plasma. The elements and lines that have been spectrographically observed in the resulting emission from the plasma are summarized in Tables II and III along with those elements listed by NBS for these samples and not detected. In most of the undetected cases, the most sensitive line of the element was outside the observed wavelength range (<240 nm) in a region difficult to reach with the SA-1 emulsion.

Clearly this sample introduction system has the potential of significantly expanding the overall analytical capability of the inductively coupled plasma. Sample types and small solution volumes previously difficult to introduce into the ICP can now readily be studied. This direct sample insertion

Table III. Direct Qualitative Analysis of NBS (SRM 1571) Orchard Leaves (230-340 nm)

observed			not observed		
element	concn	line, nm	element	concn, ppm	best line, nm
Be	0.03 ppm	313.1	As	10	193.7
Ca	2%	315.8	B	33	249.8
Cr	2.6 ppm	284.3	Cd	0.11	2.4.4
Cu	12 ppm	324.7	Hg	0.15	194.2
Fe	300 ppm	239.4	Ni	1.3	221.6
K	1.5%	404.4	Mo	0.3	202.0
Mg	0.6%	285.2	Pb	45	220.3
Mn	91 ppm	259.4	Ru	12	240.3
Na	82 ppm	330.2	Sb	2.9	206.8
P	0.2%	255.3	Se	0.08	196.0
Zn	25 ppm	334.5	U	0.03	386.0

technique could supplement existing ICP sample introduction methods much as electrothermal atomizers have enhanced atomic absorption measurements. Just as clear is the need to carefully assess the analytical characteristics of each sample type, particularly in the time domain. The time behavior observed is similar to that which is observed with dc arc sources (*16*) and electrothermal atomizers. However, while analogies to the capabilities and characteristics of the dc arc and electrothermal atomizers are unavoidable, important differences exist. It is felt, for example, that selective volatilization and thermochemical reactions which may take place as the sample is vaporized from the electrode can be more reproducibly controlled in the ICP discharge, which is considerably more stable than the dc arc. In addition, the relative insensitivity of ICP emission characteristics to a variety of classic matrix effects is well documented. Further characterization of this ICP sample introduction system is continuing. In particular, plasma gas environment, sample matrix, electrode geometry, and plasma power are all being investigated as to their effects on analyte emission characteristics.

LITERATURE CITED

(1) Winge, R. K.; Fassel, V. A.; Knisely, R. N.; Hass, W. J., Jr. *Spectrochim Acta, Part B* **1977**, *32*, 327.
(2) Dahlquist, R. L.; Knoll, J. W. *Appl. Spectrosc.* **1978**, *32*, 1.
(3) Greenfield, S.; McGeachin, H. McD.; Smith, P. B. *Talanta* **1978**, *23*, 1.
(4) Boumans, P. W. J. M. *Mikrochim. Acta* **1978**, *1/3-4*, 383.
(5) Boumans, P. W. J. M.; Bastings, L. C.; deBoer, F. J.; van Kollenburg, L. W. J. *Fresenius' Z. Anal. Chem.* **1978**, *291*, 10.
(6) Scott, R. H. *Spectrochim. Acta, Part B* **1978**, *33*, 123.
(7) Human, H. G. C.; Scott, R. H.; Oakes, A. R.; West, C. D. *Analyst (London)* **1976**, *101*, 265.
(8) Dagnall, R. M.; Smith, P. J.; West, T. S.; Greenfield, S. *Anal. Chim. Acta* **1971**, *54*, 397.
(9) Hoare, H. C.; Mostyn, R. A. *Anal. Chem.* **1967**, *39*, 1153.
(10) Kniseley, R. N.; Fassel, V. A.; Butler, C. C. *Clin. Chem.* **1973**, *19*, 807.
(11) Greenfield, S.; Smith, P. B. *Anal. Chim. Acta* **1972**, *59*, 341.
(12) Nison, P. E.; Fassel, V. A.; Knisely, R. N. *Anal. Chem.* **1974**, *46*, 210.
(13) Horlick, Gary. *Appl. Spectrosc.* **1976**, *30*, 113.
(14) Horlick, Gary. *Ind. Res./Dev.* **1978**, *20*(8), 70.
(15) Winge, R. K.; Peterson, V. J.; Fassel, V. A. *Appl. Spectrosc.* **1979**, *33*, 206.
(16) Boumans, P. W. J. M. "Theory of Spectrochemical Excitation"; Hilger: London, 1966.

Eric D. Salin
Gary Horlick*

Department of Chemistry
University of Alberta
Edmonton, Alberta, Canada T6G 2G2

RECEIVED for review December 8, 1978. Accepted August 14, 1979.

Effects of Switching Potential and Finite Drop Size on Cyclic Voltammograms at Spherical Electrodes

Sir: The past two decades have seen cyclic voltammetry develop from a technique employed only by the specialist to one used by many non-electrochemists in the characterization of a wide variety of chemical systems. Great impetus was given to this development by the application of digital simulation (*1*) (explicit finite difference methods) to the differential equations describing diffusion, and subsequently these methods have found wide use, particularly in studies of electrochemical systems coupled with homogeneous reactions.

Even before the development of cyclic voltammetry, the importance of accurately describing current–potential curves at spherical electrodes in linear scan experiments was recognized and appropriate solutions were obtained by Frankenthal and Shain (*2*) and by Reinmuth (*3*). Other workers have treated the spherical diffusion problem including its extension to the consideration of amalgam formation ("inner" as well as "outer" diffusion) (*4*). The related problem of finite electrode volume has been addressed by workers studying anodic stripping (*5, 6*). Guminski and Galus (*7*) have published an empirical equation which relates the ratio of anodic to cathodic peak current in cyclic voltammetry to diffusion coefficient (d), switching potential (E_λ), scan rate (ν), and electrode radius (r_0):

$$-i_{\text{anod}} = i_{\text{cathod}} \left\{ 1 + 3.2 \left[\frac{D_{\text{red}}(E_{\text{Pc}} - E_\lambda)}{\nu r_o^{\,2}} \right]^{1/2} \right\}$$

The purpose of this study was to adapt the digital simulation technique to the calculation of cyclic voltammograms at spherical electrodes with amalgam formation and to generate sufficient data to allow one to establish the extent to which the useful diagnostic criteria (peak position, peak separation and peak current ratio) are affected by spherical diffusion and/or finite electrode volume. Calculations were made for a simple reversible system and all diffusion coefficients were assumed to be equal.

The usual calculation of linear sweep voltammograms at planar electrodes by either the solution of integral equations or by simulation results in a single current function $\pi^{1/2}\chi(at)$ which is independent of scan rate. For spherical electrodes the interaction of scan rate, diffusion coefficient, and electrode radium is most conveniently expressed in terms of the dimensionless parameter $\phi = D^{1/2}/a^{1/2}r_0$ where $a = nF\nu/RT$. As ν and r_0 are increased for a given chemical system, the conditions of linear diffusion are approached.

In developing the simulation, the volume element equations suggested by Feldberg (*1*) were employed. Fixed model values of $n = 1$, $D = 0.45$, $\nu = 0.25$ mV/time increment, and $\Delta t = 1$ were employed. The value of ϕ was varied by varying the model radius. The model can be related to a real system through ϕ and the switching potential. For a typical experiment ($r_0 = 0.05$ cm, $D = 6 \times 10^{-6}$ cm^2/s, $\nu = 0.1$ V/s), the number of volume increments in the drop will be about 300. The effect of finite electrode volume falls naturally out of the use of this model. Single scan currents calculated by the simulation show excellent agreement with those calculated using the empirical correction parameters of Beyerlein and Nicholson (*4*). Anodic peak currents were measured from extensions of the cathodic scans.

Current functions generated by varying ϕ over a wide range at constant switching potential are shown in Figure 1. The transition from the usual cyclic voltammogram to that more resembling a stripping experiment is evident.

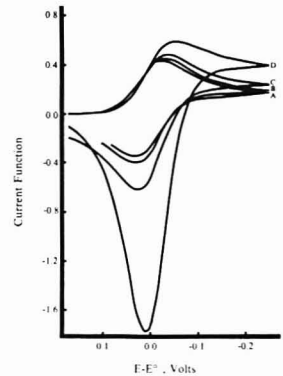

Figure 1. Current functions for different values of ϕ: (A) 0.00726, (B) 0.0229, (C) 0.0725, (D) 0.227

Table I. Cathodic and Anodic Peak Potentials and Peak Current Ratio as Functions of Switching Potential and ϕ

	$E_\lambda - E^\circ$, mV			
ϕ	-75	-164	-253	-342
0.227	−57[a]	−57	−57	−57
	16[b]	10	7	6
	1.84[c]	2.70	3.54	4.35
0.0725	−37	−37	−37	−37
	28	24	23	22
	1.27	1.47	1.66	1.84
0.0229	−31	−31	−31	−31
	32	28	28	27
	1.09	1.14	1.18	1.22
0.00726	−29	−29	−29	−29
	33	30	29	28
	1.03	1.04	1.06	1.07
0.00229	−29	−29	−29	−29
	33	30	29	29
	1.01	1.01	1.02	1.02

[a,b] Cathodic and anodic peak potentials, $E - E^\circ$, mV. [c] i_a/i_c.

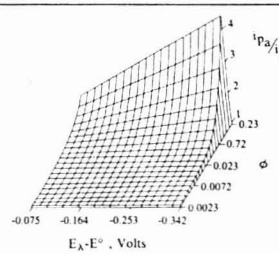

Figure 2. Peak current ratio as a function of ϕ (logarithmic scale) and switching potential

Unlike the planar system where the ratio of anodic to cathodic peak current is independent of switching potential (assuming the potential scan is reversed no closer than $35/n$ mV to the cathodic peak (*8*)), the switching potential affects —voltammograms in the system under consideration. Results

0003-2700/79/0351-2287$01.00/0

Table II. Comparison of Peak Current Ratios from Digital Simulation and from the Equation of Guminski and Galus

ϕ	$E_\lambda - E^\circ$, mV	i_a/i_c, sim.	i_a/i_c, calcd
0.027	−342	4.35	3.42
0.119	−298	2.43	2.20
0.0725	−253	1.66	1.67
0.0229	−164	1.14	1.17
0.00726	−75	1.03	1.03

of changes in both ϕ and switching potential on peak potentials and peak current ratios are given in Table I. Though peak potentials are seen to vary, the separation is little affected. The peak current ratio, the most common diagnostic criterion, undergoes large changes as expected.

These results are most easily seen by the use of the pseudo-three-dimensional map shown in Figure 2. Use of this diagram allows one to easily estimate the peak current ratio for a given set of experimental conditions.

Finally, measured peak current ratios taken from the simulations were compared to those calculated by the equation of Guminski and Galus. This comparison, shown in Table II, indicates that the equation is a good predictor under typical experimental conditions.

LITERATURE CITED

(1) Feldberg, S. W. *Electroanal. Chem.* **1969**, *3*, 199–296.
(2) Frankenthal, R. P.; Shain, E. *J. Am. Chem. Soc.*, **1956**, *78*, 2969.
(3) Reinmuth, W. H. *J. Am. Chem. Soc.* **1957**, *79*, 6358.
(4) Beyerlein, F. H.; Nicholson, R. S. *Anal. Chem.* **1972**, *44*, 1647.
(5) Shain, I.; Lewinson, J. *Anal. Chem.* **1961**, *33*, 187.
(6) DeVries, W. T.; Van Dalen, E. *J. Electroanal. Chem.* **1967**, *8*, 366.
(7) Guminski, C.; Galus, Z. *Rocz. Chem.* **1969**, *43*, 2147; *Chem. Abstr.* **1970**, *72*, 106569.
(8) Nicholson, R. S.; Shain, I. *Anal. Chem.* **1964**, *36*, 706.

J. Everett Spell
Robert H. Philp, Jr.*

Department of Chemistry
University of South Carolina
Columbia, South Carolina 29208

RECEIVED for review March 16, 1979. Accepted July 26, 1979.

Enhancement of Luminol Chemiluminescence with Halide Ions

Sir: Chemiluminescence (CL) analysis of trace Cr(III) has been reported previously (*1*). The technique is based upon the Cr(III)-catalyzed oxidation of luminol by hydrogen peroxide in basic aqueous solution. The intensity of light emission is proportional to the "free" Cr(III) concentration, if luminol and hydrogen peroxide are present in excess. The detection limit has been reported to be 5×10^{-10} M (0.025 ppb) (*1*, *2*).

We have been concerned with the speciation of chromium in marine and freshwater environments. Previous studies have used only Cl analysis for the determination of Cr(III) in freshwater systems (*1–3*). While attempting to extend this technique to seawater analysis, we have determined that concentrated inorganic salt solutions can cause an enhancement of the Cl intensity. Table I indicates the ions which were tested for interferences. The concentration of 0.56 M is based upon the chloride concentration in natural seawater (*4*). The anions Cl^-, F^-, SO_4^{2-} have the same effect upon the light emission. The bromide ion is unique with its eightfold increase in luminescence intensity. Some ions, which are not listed in Table I (I^-, SCN^-, $S_2O_3^{2-}$), reacted with the hydrogen peroxide. For iodide and thiocyanate, a chemiluminescent reaction occurred in the absence of Cr(III).

Upon further investigation of the bromide enhancement, it was discovered that the CL signal remained proportional to the Cr(III) concentration. Furthermore, as indicated in Table II, light emission is not a linear function of the bromide concentration. Below 10^{-3} M Br^-, no signal enhancement is observed. A bromide concentration of 0.5 M was chosen for future CL analysis and in all cases background solutions, of 0.56 M NaBr and 10^{-2} M EDTA, were measured for a chemiluminescence signal. This is important because commercial KBr and KCl have impurities of heavy metals.

These anionic enhancements were not observed in earlier reports. One paper (*1*) used anionic concentrations of 1×10^{-4} M, which are below the minimum concentration needed to observe the enhancement. Another group reported no effect on the CL signal when high concentrations of NaCl were added (*5*). Their work used chemiluminescence as a detection system for the chromatographic separation of metals. They chose a cell pH of 12.5 as optimum for their purpose, while the usual cell pH for Cr(III) is approximately 10.5. The chloride experiments (*5*) we have repeated at pH 12.5, and indeed no change in the CL peak intensity was observed.

Table I. Effect of Anions on the Chemiluminescence of Cr(III)

anion (0.56 M)	% light emission (Cr only = 100%)	anion (0.56 M)	% light emission (Cr only = 100%)
Cl^-	145	Br^-	800
SO_4^{2-}	146	PO_4^{3-}	0
SO_4^{2-} (0.028 M)[a]	100	NO_3^-	100
F^-	140		

[a] Concentration found in seawater.

Preliminary results indicate these anionic enhancements are not unique to Cr(III). Tests with Co(II), Fe(II), and Ni(II) as catalysts yielded responses with 2–4 times the intensity observed with no Cl^- or Br^- present. The chemiluminescence system of MnO_4^-–luminol (no H_2O_2 present) also gave increased signals in the presence of chloride or bromide ion. Bromide ion appears to be unique for the Cr(III) system, but peak enhancement was the same for chloride and bromide addition in the metal catalysts used above. It should be stressed that experimental conditions were not optimized for the metals other than chromium, and the final CL enhancements may be greater than those indicated.

The mechanism of this bromide effect is thought to be an ion-pairing phenomenon. The formation of a chromium–bromide–peroxide complex is postulated. The bromide, associated with the complex, facilitates the transfer of electrons in the reaction with luminol. A similar mechanism was proposed by Seitz for Co(II) catalysis (*6*). Work is now in progress in our laboratory to elucidate the mechanism of bromide interaction.

Analyses for this work were obtained using a flow system, which incorporates two 20-mL plastic syringes driven by a Sage Model 351 syringe pump. One syringe contains the chromium(III) sample to be analyzed, while the second syringe has a solution of luminol and hydrogen peroxide at pH 11.2. The solutions are mixed immediately before entering a quartz flow cell contained in a Perkin-Elmer MPF-44A Fluorescence

0003-2700/79/0351-2288$01.00/0

Table II. Chemiluminescence as a Function of Bromide Concentration

[Br^-], M	% light emission (Cr only = 100%)	[Br^-], M	% light emission (Cr only = 100%)
0.003	100	0.1	470
0.005	106	0.3	620
0.007	120	0.5	780
0.01	150	1.0	850
		2.0	940

Spectrophotometer. Light emission is monitored at 430 nm. Samples have been analyzed as outlined previously (*1*, *2*) using standard addition methods and heating the samples in the presence of EDTA to determine the background signal. The signal responses have been corrected for the blank response in the absence of Cr(III).

In summary, the addition of chloride or bromide ions has been found to increase the sensitivity of the chemiluminescence analysis of trace metals. The detection limit for Cr(III) has been lowered to 1.3×10^{-10} M (ca. 7 parts-per-trillion) for freshwater systems, when 0.5 M Br^- is present. These results may be compared to the 50 parts-per-trillion detection limit we found for the reference (*1*) method using our MPF-44A spectrafluorimeter. Further, we have extended the chemiluminescence technique to the determination of chromium in seawater. Chemiluminescence intensity enhancements, with chloride or bromide ions, have also been observed for Co(II), Fe(II), and Ni(II) ions.

LITERATURE CITED

(1) W. R. Seitz, W. W. Suydam, and D. M. Hercules, *Anal. Chem.*, **44**, 957 (1972).
(2) S. D. Hoyt and J. D. Ingle, Jr., *Anal. Chim. Acta*, **87**, 163 (1976).
(3) J. L. Bowling, J. A. Dean, G. Goldstein, and J. M. Dale, *Anal. Chim. Acta*, **76**, 47 (1975).
(4) D. R. Kester et al., *Limnol. Oceanogr.*, **12**, 176 (1967).
(5) R. Delumyea and A. V. Hartkopf, *Anal. Chem.*, **48**, 1402 (1976).
(6) T. G. Burdo and W. R. Seitz, *Anal. Chem.*, **47**, 1639 (1975).

Daniel E. Bause
Howard H. Patterson*

Department of Chemistry
University of Maine
Orono, Maine 04469

RECEIVED for review May 4, 1979. Accepted July 16, 1979. The work upon which this publication is based was supported in part by funds provided by the Office of Water Research and Technology (No. B-016-ME), U.S. Department of the Interior, Washington, D.C., as authorized by the Water Research and Devlopment Act of 1978.

Brominating Solution for the Preconcentration of Mercury from Natural Waters

Sir: In recent papers, workers have reported the application of a brominating solution (*1*, *2*) and bromine vapor (*3*) for the pretreatment of water samples prior to mercury determination by the cold vapor technique. The reagent makes available the Hg^{2+} ion from organomercury associations in the sample. The use of a brominating solution as a preservative for water samples prior to analysis for mercury has also been suggested (*2*). As a consequence, it might be inferred that the brominating reagent has a high affinity for the inorganic mercury ion. This has prompted us to use it in a preconcentration technique for mercury determination.

A well documented general procedure (*3–5*) for preconcentrating mercury from natural waters prior to measurement by the cold vapor technique involves purging the sample after treatment with a powerful reducing agent and collection of the volatilized mercury vapor on a suitable absorbing medium. We have experimented with an acid–bromate–bromide solution (0.7% w/v HCl, 0.011% w/v $KBrO_3$, 0.04% w/v KBr) as an absorbing medium in the apparatus shown in Figure 1.

The solution is prepared by adding 40 mL of 1% w/v potassium bromide–0.28% w/v potassium bromate reagent and 20 mL of hydrochloric acid (36% w/v) to distilled water and diluting to 1 L. Purging 850 mL of the sample and added stannous chloride for 10 min with argon gas at a flow of 2 L/min, we found that 10 mL of the solution acted as an effective trap for mercury vapor. This is in spite of the fact that part of the bromine volatilizes from the solution during the passage of gas. With 2 such traps connected in series to a 25 ng/L mercury standard, <4% of the mercury collected in the first trap was detected in the second. Immediately following preconcentration, 1-mL aliquots of the reagent are injected into an Atomic Fluorescence detection unit according to the method of Thompson and Godden (*6*). The system is calibrated between every 5 sample analyses by adding mercury standards to previously reduced and stripped samples. The detection limit of the system depends on the blank value and is about 0.5 ng/L. The relative standard deviation on a series of 10 standards of 10 ng/L is 8% and on 7 river water samples of 9 ng/L from a bulk sample, 16%, after correction for the reagent blank. We use this method for the determination of mercury in natural waters with mercury levels below 100 ng/L and the technique is linear in this range.

Seawater sampled from the outer Thames Estuary on three occasions was analyzed for mercury using the above technique.

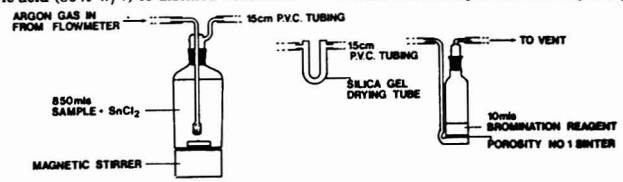

Figure 1. Mercury preconcentration apparatus

0003-2700/79/0351-2289$01.00/0

Table I. Hg in Outer Thames Estuary Water

date	position	samples collected	Hg, ng/L	ref.
Aug. 1978	North Oaze Buoy	2	13	this work
	NE Mouse Buoy	2	12	
	Mid Barrow Buoy	2	2.5	
	Barrow No. 7 Buoy	2	5	
Dec. 1978	North Oaze Buoy	1	31	
	NE Mouse Buoy	1	27	
	Mid Barrow Buoy	1	25	
	Barrow No. 7 Buoy	1	12	
Apr. 1979	North Oaze Buoy	1	24	
	NE Mouse Buoy	1	13	
	Mid Barrow Buoy	1	11	
	Barrow No. 7 Buoy	1	11	
1976		2	18 and 12	(7)

Unfiltered samples, 1 L, were collected in glass bottles, 10 mL of concentrated nitric acid were added, and the samples were analyzed up to 24 h after collection. The results are displayed in Table I. It may be seen that these show good agreement with the values obtained by Baker (7) in water collected from the same area.

LITERATURE CITED

(1) B. J. Farey, L. A. Nelson, and M. G. Rolph, *Analyst (London)*, **103**, 656 (1978).
(2) B. J. Farey and L. A. Nelson, *Anal. Chem.*, **50**, 14, 2147 (1978).
(3) J. Olafsson, *Mar. Chem.*, **6**, 87 (1978).
(4) W. F. Fitzgerald, W. B. Lyons, and C. D. Hunt, *Anal. Chem.*, **46**, 13, 1882 (1974).
(5) R. A. Vitkun, T. B. Kravchenko, Yu. V. Zelyukova, and N. S. Poluektov, *Ind. Lab.*, **41**(6), 815 (1975).
(6) K. C. Thompson and R. G. Godden, *Analyst (London)*, 100, 544 (1975).
(7) C. W. Baker, *Nature (London)*, **270**, 230 (1977).

L. Andrew Nelson

Directorate of Scientific Services
Thames Water Authority
177 Rosebery Avenue
London, EC1R 4TP, U.K.

RECEIVED for review March 26, 1979. Accepted June 14, 1979.

AIDS FOR ANALYTICAL CHEMISTS

Phase Solubility Analysis as the Basis of a Separation Method

George B. Smith* and George V. Downing

Merck Sharp & Dohme Research Laboratories, P.O. Box 2000, Rahway, New Jersey 07065

Phase solubility analysis (*1*) is known as a tedious and exacting purity method and is used routinely in only a few laboratories. Different amounts of a crystalline sample are equilibrated with a fixed amount of a solvent of choice. Then the solution compositions are measured, usually by mass, in order to determine the purity of the sample. An extensive discussion of the technique is given by Mader (*2*).

A successful solubility analysis is a separation process. Both a pure solid phase and an impure solution phase, whose solute is richer in the impurities than the original sample, result from the clean separation that ideally occurs during the equilibration. The purpose of this paper is to call attention to the usefulness of the general technique of phase solubility analysis for separations. We emphasize that the experience and careful laboratory manipulation needed to obtain meaningful phase purity results are usually not required for the separations.

Effecting a phase equilibration based on solubility analysis (to separate impurities and/or to prepare a pure solid) is called "swishing" in our laboratories. The resulting solution or solid phases are characterized by whatever analytical methods are appropriate and convenient, often thin-layer chromatography (TLC), liquid chromatography (LC), or nuclear magnetic resonance (NMR). TLC has been used most frequently, and the method is called "swish TLC."

The applications of swishing, either to purify the sample or to concentrate impurities, are diverse. Swish purification of several grams or several hundred grams of material is accomplished by overnight equilibration in a suitable solvent, with magnetic stirring on a small scale or with mechanical agitation in a Morton flask for larger quantities. Swish concentration enhances observation or identification of impurities and improves the detection limit. Swish TLC is a forensic method by which impurity patterns can be "fingerprinted" in order to indicate the particular process used to manufacture the sample. Solid solutions are detected by comparison of the impurity concentrate and the original sample.

THEORETICAL

Phase solubility analysis for purity involves measurement of the solution concentration at several system compositions after equilibration at constant temperature. (System composition is the amount of solid sample per unit weight of solvent.) In general, the measured solution concentrations, plotted vs. the corresponding system compositions, define two straight lines as shown in Figure 1. The solution is unsaturated at system compositions less than X_1, and such points fall on the 45° line OA through the origin. The system be-

0003-2700/79/0351-2290$01.00/0

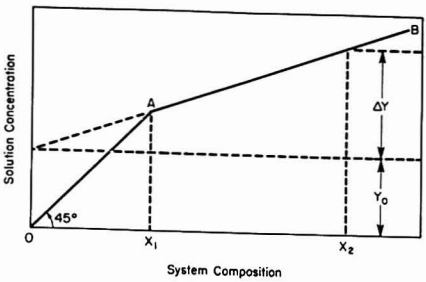

Figure 1. Solubility analysis diagram

comes saturated with respect to the main component at system composition X_1, and points at system compositions greater than X_1 fall on the line AB. The positive slope of the line AB is due to soluble impurities. The solution concentration Y_0, found by extrapolation of the line AB to the y axis, is the solubility of the main component. A solubility measured in this way is termed an extrapolated solubility and is unaffected by the presence of impurities in the sample.

Swishing in order to bring about a phase separation usually involves equilibration at just one system composition, X_2 in Figure 1. Temperature control is optional and serves mainly to control the solution concentration of the main component. The enrichment of impurities in the solution phase can be calculated as follows with the assumption that the solid phase at equilibrium contains only the main component.

$$m_1 = \Delta Y/X_2 \quad (1)$$

$$m_2 = \Delta Y/(Y_0 + \Delta Y) \quad (2)$$

where m_1 represents the fraction of impurity present in the original sample, and m_2 represents the fraction of impurity in the solute of the equilibrated solution. The ratio m_2/m_1 is the impurity enrichment factor, i.e., the impurity content of the solute is m_2/m_1 times that of the original sample.

$$m_2/m_1 = X_2/(Y_0 + \Delta Y) \quad (3)$$

The enrichment factor for minor impurities is approximately equal to the ratio of system composition to extrapolated solubility, X_2/Y_0. The same factor applies to each minor impurity in the sample.

APPLICATIONS

In phase solubility analysis for purity, thorough agitation is usually required in order to approach equilibrium satisfactorily. Equilibration of the solid phase, i.e., the main component, is often rate-determining. On the contrary, reaching equilibrium in phase separation applications is desirable but is not necessary. Most of the impurities may dissolve and hence separate before the main component is equilibrated.

Observation of phase separation by a chromatographic method such as TLC is a powerful and necessary complement. Phase separation involves removal of the impurities as a group from the main component. Chromatography provides detailed qualitative information about the impurity composition.

Examples are given below to illustrate the varied applications of phase separations.

Purification. The results of a swish purification, as observed by TLC detected by scanning densitometry, are shown in Figure 2. This phase separation was confirmed by solubility analyses of the separated phases.

Solubility analysis of the original sample showed 0.4% impurity with an extrapolated solubility of the main component of 14 mg/g of solvent. One-gram and 100-g samples

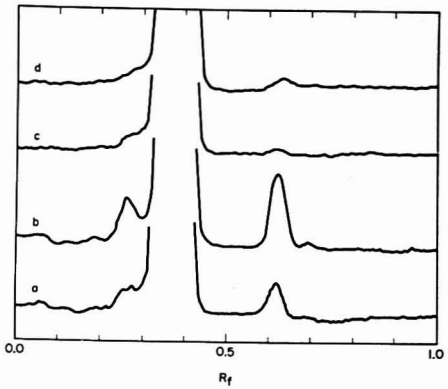

Figure 2. Swishing monitored by TLC: (a) original sample, (b) swish solution residue, (c) purified solid from 1-g swish, (d) purified solid from 100-g swish

Figure 3. Enrichment of TLC impurities: left, original sample; right, swish solution residue

were swished at 50 mg/g system composition; the expected enrichment factor was 50/14 or about 3.6.

TLC comparison of the original sample and the swish solution residue at equal loads showed the expected enrichment of the impurities at R_f 0.27 and 0.62. The solution residue was 1.5% impure by solubility analysis, or about 3.6 times 0.4%. Traces of the TLC impurities remained in the purified solids, which were measurably pure by solubility analysis.

Enhancing Detection of Impurities. Impurities in a crystalline solid can be enriched by an order of magnitude or more by swishing. The purpose of swishing may be to concentrate a particular impurity for better determination by a particular method or to gain a more detailed view of the impurity composition, e.g., by TLC.

TLC results are shown in Figure 3 for a study in which swish TLC helped to establish both TLC and phase solubility

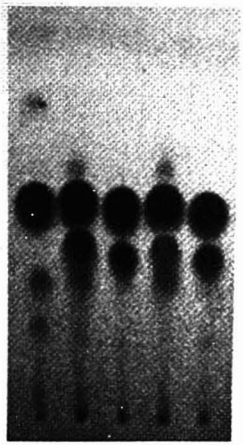

Figure 4. "Fingerprint" TLC impurity patterns

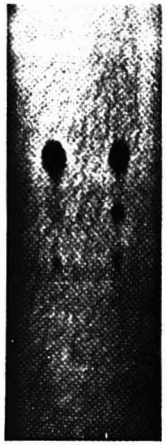

Figure 5. Detection of solid solution: left, original sample; right, swish solution residue

analysis as reliable methods. The first analyzed sample of a new compound showed 1.5% impurity by solubility analysis, but the sample was essentially single spot by TLC. An explanation for the absence of TLC impurities was required.

TLC comparison, at equal loads, of the sample and its swish solution residue (system composition 30 mg/g; extrapolated solubility 4 mg/g; enrichment factor 7.5) revealed several impurities at levels in the sample just below the detection limits. (A streaked main spot resulted at higher loading.)

Isolation and Identification of Impurities. Concentration of the impurities of a crystalline solid by swishing is a good initial step toward isolation and identification. High enrichment factors can be achieved by successive swishes.

For example, 10 g of sample with solubility of 5 mg/g of solvent, equilibrated in 100 g of solvent, would yield about 500 mg of solution residue (system composition 100 mg/g; enrichment factor 20). Subsequent swishing of the residue at the same system composition, 500 mg in 5 g of solvent, would yield about 25 mg of twice-enriched impurity concentrate. This would be ample material for TLC or LC separation followed by spectroscopic studies, e.g., MS or NMR, to identify impurities.

Trace impurities would be enriched as the square of the enrichment factor, or 400-fold, unless they became saturated. This means that impurities present in the original sample at 0.001 to 0.01% would appear in the impurity concentrate at quite tractable levels. Saturation would be a deterrent only if impurities were essentially insoluble.

"Fingerprinting". A manufacturer has legal protection, which varies in different parts of the world, concerning the production and sale of his product. The impurity composition of a given product may uniquely identify the process by which it was made, and this information can be important in patent infringements.

TLC is a convenient, rapid tool for separating and viewing impurities in the industrial laboratory. But today the quality of many products, e.g., pharmaceuticals, is such that TLC impurities are invisible. The trend in recent years toward higher and higher purity is well known. Impurities of quality products can be enriched by swishing in order to make them visible by TLC.

The swish TLC "fingerprints" of five samples of the same product are shown in Figure 4. Before swishing, these samples were essentially single spot by TLC. Reading from left to right the swish TLC results reveal one process used to make the sample in channel 1, another process in channels 2 and 4, and a third process in channels 3 and 5.

Detection of Solid Solution. Phase separation may be incomplete in swishing or in solubility analysis purity determinations. Slow equilibration may be overcome by increasing the equilibration time, by increasing the equilibration temperature, by improving the agitation, or by grinding the sample. If complete phase separation cannot be achieved by varying the equilibration conditions, solid solution is indicated. An impurity or impurities is distributed in both the solid and solution phases at equilibrium. (This assumes that the possibility of insoluble impurities has been ruled out.)

TLC results illustrating detection of solid solution are shown in Figure 5. TLC comparison, at equal loads, of a sample and its swish solution residue (system composition 50 mg/g; extrapolated solubility 5 mg/g; enrichment factor 10) revealed two impurities behind the main spot. The more mobile impurity, distributed entirely in the solution phase, was enriched about 10-fold in the solution residue. The less mobile impurity formed a solid solution with the main component and was enriched by a much smaller factor.

Solid solution may be avoided if the crystal form can be changed. The key is to find a solvent that forms a stable solvate with the main component or one that forms a compound such as a salt (*3*, *4*).

CONCLUSION

Thus the process of equilibrating a crystalline solid with a solvent, where the solid is present in considerable excess over its solubility in the solvent, is seen to be a powerful method of separation of the pure main component and of simultaneously providing a solution enriched in the impurities. This simple, rapid method effects the separation under mild conditions and is capable of handling appreciable amounts of material.

With the increasing emphasis on the amount and nature of impurities, the method is excellent for obtaining impurities in amounts sufficient for characterization or for demonstrating their absence or presence at a negligible level. In addition to the examples given here, the method can be useful for examination of process-change samples, stability samples, or

whenever the great excess of the main component interferes with other separation methods.

LITERATURE CITED

(1) Webb, T. J. *Anal. Chem.* **1948**, *20*, 100.
(2) Mader, W. J. "Organic Analysis", Vol. 2; Interscience: New York and London, 1954; p 253.
(3) Downing, G. V., Jr.; Smith, G. B.; White, A. B. *Anal. Chem.* **1971**, *43*, 260.
(4) Repta, A. J.; Bansal, P. *J. Pharm. Sci.* **1972**, *61*, 1069.

RECEIVED for review February 2, 1979. Accepted August 8, 1979.

Critical Parameters in the Barium Perchlorate/Thorin Titration of Sulfate

J. C. Haartz,* Peter M. Eller, and Richard W. Hornung

National Institute for Occupational Safety and Health, 4676 Columbia Parkway, Cincinnati, Ohio 45226

The analysis for sulfur-containing species such as sulfur dioxide, sulfur trioxide, and sulfates in the atmosphere — both ambient and workplace — is an area of continuing and intense interest. The titrimetric determination of sulfate using barium perchlorate and the indicator Thorin (*1*, *2*) has been recommended for the determination of sulfur dioxide (*3–6*), sulfur trioxide (*6*), and sulfuric acid (*7*). The original description of the method (*2*) recommends an apparent pH in the range of 2.5 to 4.0 and a nonaqueous solvent (alcohol) concentration of between 70 and 90% (v/v) for the titration, but little attention has been directed to the critical nature of these parameters in the analytical methods subsequently derived from this procedure (*3–7*). Indeed, one of the methods (*6*) does not even specify solution pH, although the titration has been reported to be sensitive to this factor (*1*, *2*, *8*). We report herein the results of an investigation of these parameters and the fact that careful control of both pH and solvent concentration is necessary for the accurate determination of the above mentioned sulfur species in the small samples encountered in industrial hygiene analyses. There is, however, a range of values for these parameters over which acceptable recoveries are obtained.

EXPERIMENTAL

For these experiments, a pH meter (Ionalyzer Model 801, Orion Research), with a standard glass pH electrode (Fisher Scientific Co., #13-629-1) and calomel reference electrode (Fisher Scientific Co., #13-639-52), were used to determine the apparent pH of the solutions titrated. "Apparent pH" is used (*2*) to denote the fact that the pH values for the alcohol solution are read directly from the meter, although the meter is standardized using aqueous pH standard solutions. The alcohol used in this study was that recommended in the industrial hygiene methods (*3–7*), 2-propanol (PrOH) (Fisher Scientific Company, ACS reagent grade). The pH was adjusted using 0.2 N $HClO_4$ (J. T. Baker Chemical Company, Analyzed Reagent); the volume used was ≤1 mL for these studies and did not alter the total volume significantly.

Titrations were performed according to standard procedures (*4*, *7*) using a 2-mL microburet for the 0.005 M $Ba(ClO_4)_2$. The titrant was standardized by titrating to a visual end point 5.0 mL of 0.00403 N H_2SO_4 to which had been added 40.0 mL of PrOH and 3 drops of the indicator Thorin. Aliquots of standard sulfate solution (60 μg/mL, prepared from analytical reagent grade Na_2SO_4, J. T. Baker Chemical Company) were titrated after adjustment of solution pH and % PrOH to the desired values with a final volume of 50 mL. Two preliminary sets of titrations were run, using parameters based on the ranges suggested in the NIOSH Criteria Document (*4*). In the first set, the pH was held at 3.5 and the PrOH concentrations were varied from 60% to 100%. In the second set, the PrOH concentration was held constant at 85% v/v and the solution pH was varied over the range 2.0 to 8.0. For the data to be used for determination of the response surface, titrations were performed using 21 combinations of experimental factors covering the ranges of pH 2.0 to 4.6 and PrOH 60% to 95%. For each pH–% PrOH combination, the volumes of titrant used for sample and blank were recorded and a subjective evaluation was made of the visual end-point sharpness (1 = very diffuse, 2 = diffuse, etc., to 5 = very sharp). Duplicate titrations were run at eight combinations of the experimental factors which covered all of the end-point sharpness ratings. The magnitude of the RSD was inversely proportional to the sharpness ratings, and ranged from 0 to 5% with a mean value of 2.3%.

RESULTS AND DISCUSSION

In the preliminary titrations at pH 3.5, end points tended to be obscure and delayed at low (<80%) PrOH concentrations. At concentrations above 90% PrOH, the observed end points were grossly premature (Figure 1). The net effect is that low recoveries are obtained for solvent compositions below 70% PrOH and above 90% PrOH at pH 3.5. The problems with end-point determination were also evident in the substantially higher "blank" values obtained when titrations were run at pH ≤3.0 (Figure 2) or at PrOH concentrations ≤80% (Figure 1). These increases in "blank" values contribute to a decreased precision for analyses and effectively raise the lower concentration limit for the procedure. At low pH (e.g., pH ~3.0 at 85% PrOH or pH ~2.5 at 80% PrOH), titrant volumes tend to increase for both samples and blanks. Below pH 2.0 (at 85% PrOH), no end points were reached even with very large volumes of titrant (Figure 2). It has been shown previously that the titration is subject to interferences from "foreign" ions, including various cations (*1*, *2*, *8*) as well as anions (*1*, *2*). This interference leads to a positive or negative bias which is related both to the species and relative concentration thereof. However, at low concentrations (*8*), a 20-fold excess of $NaNO_3$ produces only a small (<1%) error in the end point. The 2-fold excess of Na^+ at a concentration of 10^{-4} M used in this study should therefore have at most a very small effect. Accordingly, ion exchange was not used to remove the Na^+ prior to the titrations. Obviously, ion-exchange pretreatment should be considered in applications of the technique to field samples which might contain significant quantities of concomitant ions.

The data obtained in the last set of titrations were used for a response surface analysis, the object of which was to determine the range of combinations of pH and % PrOH which yielded acceptable (~100%) recoveries of sulfate ion. This analysis was carried out by using a weighted regression technique to determine the best mathematical model which fits an appropriate function of the independent variables, pH and % PrOH, to the dependent variable, fraction of sulfate recovered. The subjective evaluation of end-point sharpness was used as a statistical weight for the experimental observations because the observed recovery values were not equally reliable. Therefore, the more reliable values (values subject

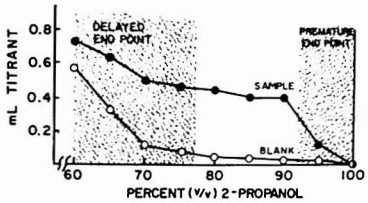

Figure 1. Volume of titrant (0.0053 M $Ba(ClO_4)_2$) required for sulfate (200 μg) sample and blank solutions as a function of PrOH concentration, at pH 3.5

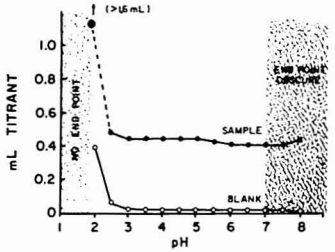

Figure 2. Volume of titrant (0.0053 M $Ba(ClO_4)_2$) required for sulfate (200 μg) sample and blank solutions as a function of pH at 85% PrOH

to less variance) which were associated with high values of end-point sharpness were given more weight in the analysis than those subject to greater variability. The end result is that the surface is forced to fit more closely to the more reliable values than to those more subject to error.

A fourth degree polynomial model was fitted to the data. Terms were removed in a stepwise manner, until every remaining term had an associated p-value of 0.15 or less. The final model selected was:

$$Y = -126.355 + 683.065\ X_2 + 30.324\ X_1X_2 - 1.3603\ X_1^2 - 1496.49\ X_2^2 + 1.500\ X_1^2X_2 - 53.726\ X_1X_2^2 + 1469.85\ X_2^3 - 528.635\ X_2^4 + 22.325\ X_1X_2^3$$

where Y = fraction of sulfate recovered, X_1 = pH, and X_2 = fraction PrOH. From this model, a contour plot was drawn to provide a "map" of the sulfate recovered as a function of the various combinations of pH and % PrOH (Figure 3). The contours shown correspond to predicted fractional recoveries of 0.6, 0.7, 0.8, 0.9, and 1.0. Anticipated recoveries would be optimal in the areas included within the 1.0 contours.

Shown superimposed on Figure 3 is a crosshatched area in which the end points were visually sharpest (end-point sharpness = 5). This information, used in conjunction with the results of the surface response analysis, indicates that optimum percent recovery and low variance would be obtained only in the region where the optima overlap. Thus, the experimental conditions recommended for titrations would include an apparent pH between 3.5 and 4.5 and a corresponding nonaqueous solvent concentration of 82–87% PrOH. These intervals constitute the largest rectangle fitting entirely within both the crosshatched area and the contour of predicted fractional recovery of 1.0. Other combinations of pH and PrOH concentration will also lead to acceptable recovery values but cannot be included if fixed, continuous intervals for these parameters are to be recommended. A broader pH range can be tolerated if the PrOH concentration range is limited; conversely, careful adjustment of pH allows more latitude in the PrOH concentration range. In the implementation of these titrations, the effects of dilution by the addition of the titrant and the aqueous acid solution used to adjust the pH must be taken into account to maintain the PrOH concentration in the optimum range. Also, the apparent

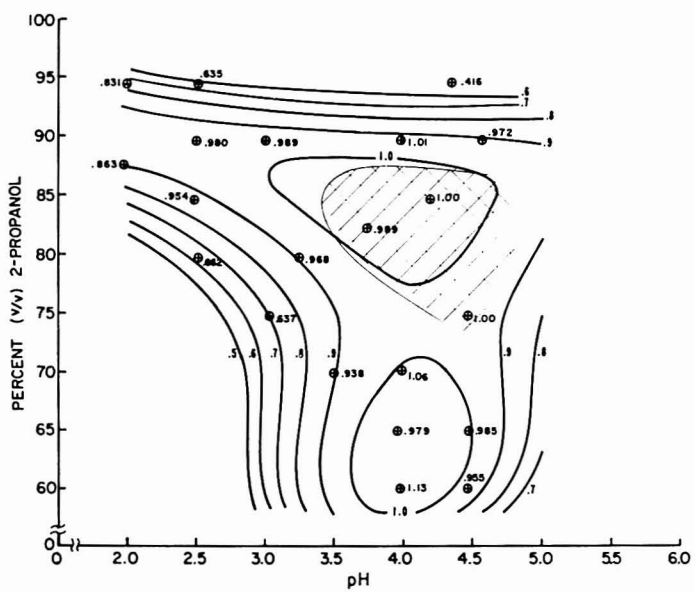

Figure 3. Fraction of sulfate recovered as a function of pH and % PrOH. Experimentally determined points are indicated by ⊕, with the corresponding fractional recovery. Cross-hatching indicates region of sharpest end points.

pH of the solution to be titrated must be carefully adjusted to be within the recommended range using a pH meter (not pH paper) for measurement.

ACKNOWLEDGMENT

The assistance of Michael A. Kraus in performing the sulfate titrations is appreciated. We also thank R. J. Smith for writing the program which produced the contour plots from the best-fit equation.

LITERATURE CITED

(1) Fritz, J. S.; Freeland, M. Q. *Anal. Chem.* **1954**, *26*, 1593–95.
(2) Fritz, J. S.; Yamamura, S. S. *Anal. Chem.* **1955**, *27*, 1461–64.
(3) U.S. Dept. of Labor, OSHA: Sulfur Dioxide Occupational Exposure. *Fed. Reg.* **1975**, *40*, 54520–54534.
(4) "Criteria for a Recommended Standard . . . Occupational Exposure to Sulfur Dioxide"; DHEW Pub. (NIOSH) 74-111, 1974.
(5) "NIOSH Manual of Analytical Methods", 2nd ed., Taylor, D. G., Ed.; DHEW Pub. (NIOSH) 77-157-A,B,C 1977; Methods 163 and S-174.
(6) "Methods of Air Sampling and Analysis," 2nd ed., Katz, M., Ed.; American Public Health Association: Washington, D.C. 20036, 1977; Method 711, p 737.
(7) "Criteria for a Recommended Standard . . . Occupational Exposure to Sulfuric acid"; DHEW Pub. (NIOSH) 74-128, 1974.
(8) Butler, J. W., Locke, D. N. *J. Environ. Sci. Health-Environ. Sci. Eng.* **1976**, *A11*, 79–92.

RECEIVED for review May 18, 1979. Accepted August 20, 1979.

High-Speed Algorithm for Simplex Optimization Calculations

Gregory F. Brissey, Robert B. Spencer,[1] and Charles L. Wilkins*

Department of Chemistry, University of Nebraska—Lincoln, Lincoln, Nebraska 68588

In recent years the importance of optimization of experimental procedures and parameters affecting any given chemical analysis has been recognized. As a result, a number of workers have investigated the application of the sequential simplex method of Spendley and co-workers (*1*), as well as the later modifications by Nelder and Mead (*2*) to problems of chemical interest (*3–7*). Denton and co-workers derived the most recent modification of the simplex procedure for chemical applications and demonstrated its efficacy in optimization of the operation of a computer-controlled flame spectrophotometer (*8*). A number of studies of the application of simplex optimization methods to the development of weight vectors for chemical pattern recognition studies, primarily spectral data interpretation, have also been reported (*9–13*). In these latter studies, one of the major disadvantages of the technique has been the large amount of computer time required when high-dimensional problems are involved. For experiment optimization applications, computation time is often a secondary consideration, since problems frequently involve adjustment of only two or three operating parameters and their actual adjustment times may significantly exceed the computer time required to determine what the new settings should be. However, with the increasing advent of instruments capable of making rapid computer-controlled adjustment of a larger number of electronically controlled parameters, the need for more rapid simplex computation procedures may soon be felt even in experiment optimization applications. In the context of the previously-mentioned pattern recognition studies, the need for optimizing as many as 60 or more parameters, which are subsequently used in an automatic discriminant function for spectral analysis, makes the speed of the simplex algorithm employed a dominant factor in that application. Accordingly, a search for an even faster algorithm than those previously reported was initiated. We report here the successful outcome of that search.

DESCRIPTION OF THE HIGH-SPEED SIMPLEX ALGORITHM

Both the Modified Simplex method (*2*, *4*) and the Super Modified Simplex procedure (*8*, *9*) have been described in detail elsewhere as has their application to the problem of weight vector development for pattern recognition purposes (*9–13*). Therefore, only a brief summary of the fundamentals of the techniques will be given here to facilitate discussion of the improved algorithm. As originally defined (*1*), a simplex consists of a figure with $d + 1$ vertices located in a d dimensional space. Thus, in a two-dimensional space a simplex is a triangle, and in three-dimensional space, a tetrahedron. The coordinates of each vertex represent values of the d control variables, and the simplex algorithm provides a systematic procedure for exploring the experimental response obtained as a result of modifications in the control variables. By this means, if the simplex search is successful, an optimized response is ultimately obtained.

For pattern recognition, the simplex method was applied to the determination of the appropriate set of weights in a linear discriminant function which would produce an optimum response (defined as the maximum recognition of members of a training set of patterns which are classified with respect to some property of interest) (*9*). In order that the space searched be continuous, an additional response criterion (minimization of the perceptron (*14*) value) was combined with the recognition criterion. Subsequently, other response functions have been examined for that particular type of application (*13*).

Whatever protocol is used, the simplex optimization procedure involves searching for an optimum in response space by successively replacing the worst vertex of the simplex with better vertices. This is accomplished by reflecting the worst vertex through the centroid of the remaining vertices (CR). Therefore, the new vertex (W_{ki}^{new}) is simply a linear combination of the worst vertex and CR. As originally implemented for pattern recognition applications (*9*), the reflection procedure required complete recalculation of the value of CR on each iteration, using Equation 1.

$$CR_i = (1/(n-1)) \sum_{j \neq k}^{n} W_{ji} \qquad (1)$$

For the d dimensional space, n is equal to $d + 1$, the number of vertices of the simplex and the remaining vertices, j, are summed, excluding k, the vertex (weight vector) being replaced. Thus, each of the i coordinates of the centroid are calculated. This is unnecessary, since a running *overall centroid* (C) may be computed on each iteration by considering only the *changed* vertex (for pattern recognition, this is a weight vector). Equation 2 summarizes these relationships.

$$C_i^{new} = C_i^{old} + (1/n)(W_{ki}^{new} - W_{ki}^{old}) \qquad (2)$$

However, because the new summation, W_{ji}^{new}, changes from the old one only as a result of the changes in the vertex

[1] Present address: Nicolet Instrument Corp., Madison, Wis. 53711.

0003-2700/79/0351-2295$01.00/0

Table I. Chemical Categories of the Compounds Whose Mass Spectra Comprise the Training Set Pool

category	number
phenyls	7245
aldehydes and ketones	887
ether	362
aliphatic alcohols	463
phenols	1618
carboxylic acids	294
thiol/thioethers	138
esters	1657
amines	370
amides	459
nitrites	121

replaced, the full summation need only be done for the initial vertex, with the subsequent centroids being computed by modifying the sum. If a weight vector (vertex) k is excluded, the values of CR_i follow directly from the discussion above as expressed in Equation 3 which uses the excluded vertex to compute CR_i

$$CR_i = (1/(n-1))(nC_i - W_{ki}^{old}) \quad (3)$$

In any of the simplex methods mentioned above, new vertices in hyperspace are chosen by placing them on a line defined by the worst vertex and the centroid of the remaining vertices. The methods differ only in the algorithm used to determine where on that line to place the new vertex. For pattern recognition, a new trial weight vector results at each iteration. Therefore, the algorithms used may be viewed as corresponding to linear combinations of the centroid and the worst vertex with a proportionality constant, α, dictated by the method used. Equation 4 summarizes this relationship.

$$W_{ki}^{new} = CR_i + \alpha(CR_i - W_{ki}^{old}) \quad (4)$$

The equation represents the linear combination of the centroid, CR_i, with the vector difference of the centroid and the old weight vector. Using the relation expressed by Equation 3, it follows that W_{ki}^{new} can be computed directly from the overall centroid, C, the old vertex, W_{ki}^{old}, and the proportionality constant, α.

$$W_{ki}^{new} = (1+\alpha)(n/n-1)C_i - (1+(n\alpha)/n-1)W_{ki}^{old} \quad (5)$$

Thus, wherever the centroid of the remaining vertices was previously used, the overall centroid, C, can be used instead. The centroid of the unreflected vertices need never be calculated. For pattern recognition applications, the response of a vertex is obtained by forming the dot products of that vertex with each member of the training set, in turn, and tabulating the recognition performance. A major increase in speed can be realized by recognizing the fact that the dot product of the new vertex with any particular member of the training set, X_{li}, is also a linear combination with the dot product of the member with both the overall centroid, C_i, and the worst vertex, W_{ki}^{old}, having the same coefficients as those in Equation 5. The expression for directly computing the dot products of the new vertex with the members of the training set is given by Equation 6.

$$W_{ki}^{new} \cdot X_{li} = (1+\alpha)(n/n-1)X_{li}C_i - (1+(n\alpha)/N-1)W_{ki}^{old}X_{li} \quad (6)$$

Because the dot products on the right-hand side of Equation 6 are calculated directly only once (taking 60 multiplications per training set member in our example) and subsequently these and updated values are used (requiring 4 multiplications per training set member), the speed improvement is ca. $N/4$, where N is the dimension of training set members. Thus, for the present 60-dimension example, a speed improvement of a factor of 15 is expected.

Note that the various modifications of the simplex technique basically differ in how the coefficient α, which defines the weighting of the linear combination, is determined. For example, in the Super-Modified Simplex method described by Denton and co-workers (8), the responses of the worst vertex, the centroid of the remaining vertices, and the reflected point of the worst vertex through the centroid are calculated and fitted to a second-order polynomial curve. The position of the maximum of this curve defines α, and a new vertex is calculated. If this vertex has a better response than the reflected point it is kept, otherwise the reflected point is kept.

As the dot product of a particular pattern with the overall centroid is changed, it too can be updated in an analogous fashion (Equation 7).

$$(C_iX_{li})^{new} = (C_iX_{li})^{old} + (1/n)(W_{ki}^{new}X_{li} - W_{ki}^{old}X_{li}) \quad (7)$$

Furthermore, the weight vector that bisects the means of the two classes of spectra in the training set ($W_{d+1,i}$) is used as the initial vertex in the construction of the simplex. The remaining initial d vertices (weight vectors) are obtained by adding a constant called the "Spanning Constant" (SC) to only one of the d elements in the initial weight vector for each new weight vector created, with no two having the constant added to the same d element. This initial step can be avoided by recognizing that the dot products of the d starting weight vectors may be obtained directly from the dot products of the initial weight vector and the spanning constant (Equation 8).

$$W_{ji} \cdot X_{li} = W_{d+1,i} \cdot X_{li} + SC \cdot X_{lj} \quad (8)$$

As a result, for the initial, expanded, or contracted simplex, only the dot products for an initial weight vector and centroid of the simplex need to be calculated from the training set spectra.

Another speed improvement which can be realized is achieved by the simple expedient of ranking the responses of vertices initially and as they are generated, using a binary search method to locate the ranking of new responses. In this way, a running pointer to the worst current vertex is easily maintained.

Table II. Comparison of Optimum Weight Vector Development Time and Performance for the SMS and ISMS Methods[a,b]

	total CPU time (s)		iteration/second		total iterations		% correct recognition	
category	SMS	ISMS	SMS	ISMS	SMS	ISMS	SMS	ISMS
phenyl	392.8	44.0	0.87	12.09	342	532	92	90
carboxylic acid	1309.2	68.7	1.01	13.48	1321	926	90	94
thiol/thioether	2014.6	144.4	1.06	15.88	2131	2294	99	100
ester	1798.2	80.8	1.05	13.52	1883	1092	88	91
amide	737.6	51.4	0.93	13.30	686	653	83	84
average	1250.5	77.9	0.98	13.65	1273	1099	90	92

[a] Calculations done using an IBM 360/65 computer. [b] Prediction performances of the weight vectors produced were comparable. In the absence of round-off error, identical weight vectors would be expected.

EXPERIMENTAL

Data. In order to test the efficacy of the new algorithms, a training set pool of 13614 low resolution mass spectra of monofunctional compounds were drawn from the NIH/EPA/MSDC mass spectral data base of 25560 spectra, leased from the Office of Standard Reference Data, National Bureau of Standards. For each of 5 categories of compounds (selected from those listed in Table I), training sets of 200 spectra were chosen. The training sets were constructed so as to contain equal numbers of class and nonclass spectra. For example, the training set for recognition of the ether function was comprised of the spectra of 100 ethers and 100 additional spectra were chosen from among the other 10 categories listed in Table I. For training with each category, the 60 most frequent m/e peak positions were chosen as the features to be used.

Computations. Super-modified Simplex (SMS) and Improved Super-modified Simplex (ISMS) programs were written in Fortran IV and all computations were done using an IBM 360/65 computer. Spanning constants used were the same for both SMS and ISMS calculations. The extrapolation factor used was 50% of the distance between the worst vertex and its reflection about the centroid of remaining vertices and the safety factor was 5% of the same distance.

RESULTS AND DISCUSSION

Table II summarizes the data relevant for comparison of the SMS and ISMS simplex pattern recognition speed and performance in development of weight vectors for recognition of each of the 5 categories chosen for testing. When total computation times are compared, it is seen that the improved algorithm described here was, on the average, 14 times faster in locating an optimal weight vector. Recognition performance of the vector thus produced was generally as good as, or better than, those obtained using the SMS method. Closer examination of the tabulated data shows that this speed improvement derives primarily (as expected) from the ability of the ISMS technique to complete many more iterations in a given amount of time. The total number of iterations carried out with each of the methods was approximately the same. Because the dot products of the vertices must be stored when the ISMS method is used, memory requirements are somewhat greater than with the SMS technique. In the present instance, the program size increased from 150 Kbytes to 200 Kbytes when the ISMS technique was implemented. However, this modest memory increase is more than compensated by the additional computational speed obtained.

LITERATURE CITED

(1) Spendley, W; Hext, G. R; Himsworth, F. R. *Technometrics* **1962**, *4*, 441.
(2) Nelder, J. A; Mead, R. *Comput. J.* **1965**, *7*, 308.
(3) Ernst, R. R. *Rev. Sci. Instrum.*, **1968**, *39*, 998.
(4) Deming, S. N; Morgan, S. L. *Anal. Chem.* **1973**, *45*, 278A.
(5) Long, D. E. *Anal. Chim. Acta* **1969**, *46*, 193.
(6) Deming, S. N; Morgan, S. L. *Anal. Chem.* **1974**, *46*, 1170.
(7) Johnson, E. R.; Mann, C. K; Vickers, T. J. *Appl. Spectrosc.* **1976**, *30*, 415.
(8) Routh, M. W. Swartz, P. A; Denton, M. B. *Anal. Chem.* **1977**, *49*, 1422.
(9) Ritter, G. L; Lowry, S. R; Wilkins, C. L; Isenhour, T. L. *Anal. Chem.* **1975**, *47*, 1951.
(10) Brunner, T. R; Wilkins, C. L; Lam, T. F; Soltzberg, L. J; Kaberline, S. L. *Anal. Chem.* **1976**, *48*, 1146.
(11) Lam, T. F; Wilkins, C. L; Brunner, T. R; Soltzberg, L. J; Kaberline, S. L. *Anal. Chem.* **1976**, *48*, 1768.
(12) Kaberline, S. L; Wilkins, C. L. *Anal. Chim. Acta* **1978**, 103, 417.
(13) Ritter, G. L; Lowry, S. R; Isenhour, T. L; Wilkins, C. L., submitted for publication in *J. Chem. Inf. Comput. Sci.*
(14) Duda, R. O; Hart, P. E. "Pattern Classification and Scene Analysis", Wiley-Interscience: New York, 1973; p 141.

RECEIVED for review June 25, 1979. Accepted August 10, 1979. The support of the National Science Foundation under grant CHE-76-21295 is gratefully acknowledged.

Quantitative Analysis of Silicates by Instrumental Epithermal Neutron Activation Using (n,p) Reactions

Ernest S. Gladney* and Daniel R. Perrin

University of California, Los Alamos Scientific Laboratory, P.O. Box 1663, Los Alamos, New Mexico 87545

Instrumental epithermal neutron activation (IENA) involves the use of a neutron filter to screen out the thermal portion of the reactor neutron energy spectrum. Both Cd and B are efficient neutron filters. The former is essentially opaque to neutrons with kinetic energies of less than 0.4 eV, while the absorption cross section of the latter follows a $1/v$ relationship and reaches a small value at approximately 280 eV (*1*). The advantages of epithermal over conventional thermal neutron activation for elemental analysis of geological materials have been well summarized by Steinnes (*2*). The principal advantage is that the most common rock forming elements, which activate strongly with thermal neutrons (e.g., Na, Al, P, K, Fe, and Sc), have their activities suppressed, relative to elements which have cross-sectional resonances in the epithermal energy region.

The reduction in activity from common (n,γ) products permits the observation of activation products from the lower cross section (n,p) reactions. Elements with potentially useful (n,p) reaction products are shown in Table I. Cross-sectional data are taken from Steinnes (*2*) and Erdtmann (*3*) and are presumably for Cd filtered epithermal fluxes. The energy threshold values are from Howerton et al. (*4*). Only ^{54}Mn and ^{58}Co are commonly observed in spectra of thermal neutron activated geological samples. The remainder are usually obscured by the background caused by those species that are produced in greater abundance by thermal neutron capture. The threshold energies for (n,p) events are also shown in the table. For most of the reactions, neutrons with 0.5 MeV kinetic energy or more are required. When the thermal component of the flux is absorbed, neutrons of this energy become a much more prominent part of the remaining spectrum.

Steinnes has carefully explored the (n,p) reaction for Ni determination in silicate rocks (*5*), and Ni measurements in geological materials using this reaction have been reported by other investigators (*6–9*). The determination of Si through the ^{28}Al reaction has been reported in bulk iron ore samples (*10*) and in lymph node samples (*11*). The quantitative study of the application of (n,p) reactions to the analysis of geological materials is the subject of this paper.

EXPERIMENTAL

One-gram samples of various silicate standard reference materials were encapsulated in polyethylene vials and irradiated in the Los Alamos Omega West Reactor epithermal facility. The epithermal neutron flux is boron filtered and is described in detail elsewhere (*12*). The flux is approximately 5×10^{10} n/cm^2/s. Samples may be pneumatically transferred in a few seconds from the reactor to the counting room. Each irradiation is monitored by use of a known amount of an Au solution pipetted onto filter paper disks lodged in the rabbit caps. These monitors may be

0003-2700/79/0351-2297$01.00/0

Table I. Epithermal Neutron (n,p) Reactions

target nuclide	isotopic abundance, %	activation product	(n,p) cross section, mb	energy threshold, MeV(3)	half-life	prominent γ-rays, keV	interfering reactions and γ rays, keV	epithermal cross sections of interfering reactions, mb
^{19}F	100	^{19}O	1.35	E[a]	27 s	193	^{18}O(n,γ)^{19}O	0.070
							^{22}Ne(n,α)^{19}O	0.056
^{23}Na	100	^{23}Ne	1.5	3.76	38 s	439	^{26}Mg(n,α)^{23}Ne	0.027
^{24}Mg	79	^{24}Na	1.53	4.93	15 h	1368, 2754	^{23}Na(n,γ)^{24}Na	290
^{27}Al	100	^{27}Mg	4.0	1.90	9.4 m	844, 1013	^{26}Mg(n,γ)^{27}Mg	13
							^{30}Si(n,α)^{27}Mg	0.155
							847-keV ^{56}Mn	-
^{28}Si	92.2	^{28}Al	6.4	3.99	2.2 m	1779	^{27}Al(n,γ)^{28}Al	180
							^{31}P(n,α)^{28}Al	0.118
							1268-keV ^{28}Al single escape	-
^{29}Si	4.7	^{29}Al	560	3.00	6.5 m	1273	^{30}Si(n,γ)^{31}Si	47
							^{34}S(n,α)^{31}Si	22
							1268-keV ^{28}Al single escape	-
^{46}Ti	8.0	^{46}Sc	10.5	1.62	84 d	889, 1021	^{45}Sc(n,γ)^{46}Sc	10,700
^{47}Ti	7.5	^{47}Sc	16.3	E	3.4 d	160	^{50}V(n,α)^{47}Sc	1.5
							^{46}Ca(n,γ)^{47}Ca(β$^-$)^{47}Sc	320
^{48}Ti	73.7	^{48}Sc	0.27	3.27	43.7 h	983, 1037, 1312	^{51}V(n,α)^{48}Sc	0.022
^{54}Fe	5.8	^{54}Mn	82.5	E	312 d	835	834 keV ^{72}Ga	-
							^{55}Mn(n,2n)^{54}Mn	0.258
^{58}Ni	68.3	^{58}Co	113	E	71 d	811	^{59}Co(n,2n)^{58}Co	0.72

[a] Exothermic.

Table II. Concentrations in Various Standard Reference Materials

material	Ti, ppm IENA (n,p)	Ti, ppm AV (ref.)[a]	Ti, ppm R^b	Fe, % IENA (n,p)	Fe, % AV (ref.)	Fe, % R	Si, % IENA (n,p)	Si, % AV (ref.)	Si, % R
USGS AGV-1	5500	6190 (*14*)	0.89	4.21	4.73 (*14*)	0.89	31.2	28.0 (*14*)	1.11
BCR-1	12600	12750	0.99	8.77	9.37	0.94	23.2	25.5	0.91
G-2	2900	2780	1.04	1.93	1.85	1.04	33.6	32.3	1.04
GSP-1	3900	3990	0.98	3.41	3.03	1.13	30.4	31.5	0.97
PCC-1	90	90	1.00	5.71	5.84	0.98	19.6	19.6	1.00
GXR-1	650	<200 (*17*)	-	24.4	23.7 (*16*)	1.03	23.0	23.0 (*16*)	1.00
GXR-2	2800	3000	0.93	1.86	1.88	0.99	23.0	21.6	1.06
GXR-3	1000	1200	0.83	18.2	18.1	1.01	6.2	6.4	0.97
GXR-4	2600	2600	1.00	2.86	3.03	0.94	31.2	31.0	1.01
GXR-5	2100	2600	0.81	3.02	3.42	0.88	19.1	19.1	1.00
GXR-6	5000	5100	0.98	5.45	5.59	0.97	22.3	22.4	1.00
NBS SRM 91	<350	114 (*15*)	-	0.06	0.057 (*15*)	1.05	32.2	31.5 (*15*)	1.02
120	780	900	0.87	0.77	0.77	1.00	2.12	2.18	0.97
633	1700	1400	1.21	2.78	2.94	0.95	11.2	10.3	1.09
635	2600	1900	1.37	2.04	1.86	1.10	9.8	8.7	1.13
			$\overline{X} \pm \sigma$ 0.99 ± 0.15		$\overline{X} \pm \sigma$ 0.99 ± 0.07				$\overline{X} \pm \sigma$ 1.02 ± 0.06

[a] AV = Accepted or Certified Value. [b] R = Ratio IENA/AV.

counted simultaneously with the sample or removed and counted later if the 411-keV transition from the ^{198}Au interferes. Flux variations of about 10% are encountered during the normal work day.

National Bureau of Standards (NBS) Standard Reference Material (SRM) #79a (fluorspar) was used to standardize the F and Ca determinations. NBS SRM #194 (ammonium dihydrogen phosphate) was employed as the P standard. Oxides or carbonates of Na, Mg, Al, Si, and Ti were used as standards for these elements. Elemental Fe and Ni were dissolved and known amounts of the concentrated stock solutions were pipetted onto filter paper. The filter paper was air dried and folded to the same geometry as the samples.

The wide range of half-lives of the (n,p) activation products in Table I precludes the use of a single irradiation. Fluorine and Na were determined using a 20-s epithermal irradiation and three 10-s counts. A 1-min irradiation and three 1-min counts were used for ^{28}Si. At the conclusion of these counts, one 5-min count was taken for the measurement of Al and ^{29}Si. A third irradiation of 1 h was employed for the remainder of the elements examined. Magnesium and P were counted for 30 min after 1-h decay. After 24-h decay, Ti was measured through both ^{47}Sc and ^{48}Sc reaction products with 15–30 min counts. Titanium (via ^{46}Sc), Ni, and Fe were eventually attempted after an additional 2–3 weeks' decay by 500-min counts.

Special decay corrections for rapidly decaying sources (*13*) were not employed in the determination of the elements with short-lived (n,p) products. Rather, the initial analyzer dead-times were kept to under 10% and multiple short counts taken. These data were later plotted and force fit to the appropriate half-life for a graphical determination of the initial activity. Initial activities of longer-lived species were determined by single counts and mathematical extrapolation.

Samples and monitors were counted on large (60–80 cm^3) Ge(Li) detectors connected to 4096 channel pulse-height analyzers. The resolution of the detectors was typically 2.0 keV (full-width at half maximum) at the 1332-keV ^{60}Co line. Spectra were stored on magnetic tape for off-line processing by computer. The γ-rays used for each isotope are shown in Table I, along with potential interferences.

Table III. Concentrations in Various Standard Reference Materials

material	Na, % IENA (n,p)	Na, % AV (ref.)[a]	Na, % R^b	F, % IENA (n,p)	F, % AV (ref.)	F, % R	Ni, ppm IENA (n,p)	Ni, ppm AV (ref.)	Ni, ppm R
USGS AGV-1	3.20	3.16 (*14*)	1.01	<0.5	0.043 (*14*)	-	14	13 (*5*)	1.08
BCR-1	2.14	2.08	1.03	<0.5	0.047	-	10	10	1.00
G-2	3.11	3.01	1.03	<0.5	0.13	-	2.9	2.3	1.26
GSP-1	2.18	2.17	1.00	<0.5	0.32	-	7.8	7.0	1.11
PCC-1	<0.6	0.53	-	<0.5	0.0015	-	2400	2430	0.99
NBS SRM-91	6.23	6.29 (*15*)	0.99	5.16	5.72 (*15*)	0.90	0.79	none (*15*)	-
120	<0.5	0.35	-	3.82	3.84	1.00	12	none (*15*)	-
633	<0.6	0.50	-	<0.5	0.08	-	14	none (*15*)	-
635	<0.6	0.52	-	<0.5	0.03	-	34	none (*15*)	-
		$\bar{X} \pm \sigma$ 1.01 ± 0.02			$X = \bar{0.95}$			$\bar{X} \pm \sigma$ 1.09 ± 0.10	

[a] AV = Accepted or Certified Value. [b] R = Ratio IENA/AV.

Table IV. Evaluation of Severity of Interferences from Competing Nuclear Reactions

radioactive product	production ratio reactions	production ratio ratio	average crustal abundance ratio (Mason)	activity ratio in average crustal material
^{19}F	(n,p)/(n,γ)	9600	(0.01 at DL)	96
^{19}F	(n,p)/(n,α)	260	[Ne not in rocks]	-
^{23}Na	(n,p)/(n,α)	500	1.35	680
^{24}Mg	(n,p)/(n,γ)	0.004	0.74	0.003
	(n,p)/(n,α)	1.68	0.26	0.44
^{27}Al	(n,p)/(n,γ)	2.8	3.9	11
	(n,p)/(n,α)	810	0.29	230
^{28}Si	(n,p)/(n,γ)	0.03	3.4	0.10
	(n,p)/(n,α)	49	264	13000
^{29}Si	no interfering reactions		-	-
^{31}P	(n,p)/(n,γ)	25	0.004	0.10
	(n,p)/(n,α)	390	4.0	1600
^{46}Ti	(n,p)/(n,γ)	0.000079	200	0.016
^{47}Ti	(n,p)/(n,γ)	130	0.12	16
	(n,p)/(n,α)	330	32	11000
^{48}Ti	(n,p)/(n,α)	10	32	320
^{54}Fe	(n,p)/(n,2n)	18	53	950
^{58}Ni	(n,p)/(n,2n)	110	3	330

RESULTS AND DISCUSSION

Only six elements (F, Si, Na, Fe, Ni, and Ti) were successfully determined in geological matrices via (n,p) reactions. The data in Tables II and III represent means of three or more determinations on each material for each element. The single standard deviations among the measurements were less than 10% in all cases. Data from the certifying agencies and other investigators are shown for comparison. A ratio of elemental determinations by IENA to an accepted value for each element in each matrix is calculated. The ratios for a given element are then summarized as a mean ± one standard deviation. A ratio greater than one indicates a positive bias in our data, relative to the accepted value, while a ratio of less than one indicates a negative bias. With the exception of F and Ni, these summarized mean ratios are all within 2% of agreement with the accepted or certified values. This agreement demonstrates that (n,p) reactions are an excellent means for quantitative analysis in geological materials. The mean ratios of F and Ni are within 10% of the accepted or certified values. The following detection limits (3σ above background) have been achieved: F and Na = 0.5%, Si ≐ 2%, Ti and Fe = 100 ppm, and Ni = 1 ppm.

Several problems contributed to the failure to report quantitative data from the remaining (n,p) products in Table I. Insufficient sensitivity for crustal abundance levels of P prevented its measurement. Competing (n,γ) and (n,α) reactions degraded the accuracy of data from (n,p) products of ^{28}Si, ^{46}Ti, and ^{24}Mg. Competition from (n,γ) reactions, while reduced in epithermal flux, is not entirely eliminated. The contribution of interfering reactions to the product of interest may be calculated using the induced activity equation (*3*). Since the radioactive product from each pair of reactions compared is the same, the equation simplifies to the product of the cross section, isotopic abundance, and elemental abundance. The latter is estimated for average crustal material using Mason's data (*18*), the cross sections are given in Table I and the isotopic abundances extracted from Erdtmann (*3*). The exception is F, which is not sufficiently abundant to be observed in average crustal materials. For the purpose of the calculation the 0.5% detection limit value has been substituted for Mason's data. The change in neutron filter material from Cd to B will have little impact on the (n,p) and (n,α) cross sections in Table I. The (n,γ) cross sections will be somewhat reduced and the interference from this source will be somewhat overestimated.

The production ratio of (n,p) to (n,γ) and (n,p) to (n,α) interfering reactions from Table I are given in Table IV, for silicate materials having Mason's average crustal abundance of elements. A ratio of 1.0, 9.0, 19, and 99 indicates that 50%, 10%, 5%, and 1% of the product is derived from the interfering reaction, respectively. For the data reported in Tables II and III, the interferences with F, Na, Si, Fe, and Ni determination by (n,p) produce 1% or less of the observed activity and have been neglected. The same is true for Ti determinations utilizing $^{48}Ti(n,p)^{48}Sc$, but the situation is complicated if ^{47}Sc is employed. The degree of interference from $^{46}Ca(n,\gamma)^{47}Ca(\beta^+)^{47}Sc$ depends upon the decay time after irradiation. In the worst case, if all the ^{47}Ca has decayed to ^{47}Sc, the interference accounts for 6% of the total ^{47}Sc in the sample. Counting after only 24-h decay reduces this con-

tribution to less than 2%, at which point it is neglected.

The use of ^{24}Na, ^{28}Al, ^{31}Si, and ^{46}Sc for the determination of Mg, Si, P and Ti, respectively, is shown to be strongly influenced by one or more interfering reactions (production ratios <1). In order to use these four (n,p) reactions, one must have prior knowledge of the concentration of Al, Na, Si, and Sc to properly correct for the (n,γ) contribution. The $^{27}Al(n,p)^{27}Mg$ reaction could be used for Al determination with minimal (n,γ) correction; however, the precision achieved is not comparable to that using thermal neutrons and conventional (n,γ) activation for Al. Even though analytical data on these four elements can be resolved from among the competing reactions with a sacrifice of precision, Si, Al, and Ti can be more easily measured by other (n,p) or (n,γ) reactions. Neither (n,γ) nor (n,p) methods are particularly sensitive for Mg determination and nonnuclear techniques are preferred.

Epithermal activation via (n,p) reactions provides an alternative, although less sensitive, method for the determination of Fe, Al, Na, Ni, and F. The preferred techniques are probably thermal neutron activation for the first three elements, atomic absorption for Ni, and ion selective electrode for F. Titanium and Si can be measured much more sensitively using the (n,p) reaction than by thermal neutron activation.

ACKNOWLEDGMENT

We thank the staff of the OWR for assistance with the neutron irradiations.

LITERATURE CITED

(1) Rossitto, F.; Terrani, M.; Terrani, S. *Nucl. Instrum. Methods* **1972**, *103*, 77.
(2) Steinnes, E. "Epithermal Neutron Activation Analysis of Geological Material", in "Activation Analysis in Geochemistry and Cosmochemistry", Brunfelt, A. O., Steinnes, E., Eds.; Universitetsforlaget: Oslo, 1971; pp 113–128.
(3) Erdtman, G. "Neutron Activation Tables", Verlag Chemie: Weinheim, 1976.
(4) Howerton, R. J.; Braff, D.; Cahill, W. J.; Chazan, N. "Thresholds of Neutron Induced Reactions", Report UCRL-14000, Scientific Information Systems Group, Lawrence Radiation Laboratory, Livermore, Calif., May 1964.
(5) Steinnes, E. *Anal. Chim. Acta* **1974**, *68*, 25.
(6) Ondov, J. M.; Zoller, W. H.; Olmez, I.; Aras, N. K.; Gordon, G. E.; Rancitelli, L. A.; Abel, K. H.; Filby, R. H.; Shah, K. R.; Ragaini, R. C. *Anal. Chem.* **1975**, *47*, 1102.
(7) Baedecker, P. A.; Rowe, J. J.; Steinnes, E. *J. Radioanal. Chem.* **1977**, *40*, 115.
(8) Rowe, J. J.; Steinnes, E. *J. Radioanal. Chem.* **1977**, *37*, 849.
(9) Lavi, P. *Radiochem. Radioanal. Lett.* **1976**, *27*, 163.
(10) Borsarn, M.; Holmes, R. J. *Anal. Chem.* **1978**, *50*, 296.
(11) Ordogh, M.; Orban, E.; Miskovits, G.; Appel, J.; Sazbo, E. *Int. J. Appl. Radiat. Isot.* **1974**, *25*, 61.
(12) Wangen, L. E.; Gladney, E. S. *Anal. Chim. Acta* **1978**, *96*, 271.
(13) Fremien, J. H., "Applications of Nuclear Physics"; Hart Publishing Co.: New York, 1970; pp 340–341.
(14) Flanagan, F. J. *Geochim. Cosmochim. Acta* **1973**, *37*, 1189.
(15) National Bureau of Standards, Certificates of Analysis.
(16) Allcott, G. H.; Lakin, H. W. "Tabulation of Geochemical Data Furnished by 109 Laboratories for Six Geochemical Exploration Reference Samples", U.S. Geological Survey Open File Report 78-163, 1978.
(17) Hubert, A. E.; Chao, T. T. *Anal. Chim. Acta* **1977**, *92*, 197.
(18) Mason, B. "Principles of Geochemistry", 3rd ed.; John Wiley: New York, 1966; pp 45–46.

RECEIVED for review May 18, 1979. Accepted August 20, 1979. Work performed under the auspices of the U.S. Department of Energy.

High-Speed Device for Synchronization of Natural-Drop Experiments with a Dropping Mercury Electrode

Paul D. Tyma,* Michael J. Weaver,* and C. G. Enke

Department of Chemistry, Michigan State University, East Lansing, Michigan 48824

There are many types of experiments performed with dropping mercury electrodes (DME) in which measurements must be made at times that are well defined relative to the birth of the drop. The simplest method for measurement synchronization is to dislodge the drop forcibly and simultaneously trigger a timing circuit. However, mechanical drop dislodgment may cause significant disturbance of polarographic diffusion profiles in the growing drop, particularly at subsecond current sampling times (*1*). An alternative approach is to detect the birth of a new drop following natural gravitational drop fall. Such drop-fall detectors also enable natural drop times to be determined, providing a simple route to the interfacial tension (*2*).

We have been investigating dc polarographic current–time curves at short times (0.01–1 s) following drop birth to evaluate rapid dc polarography (*1*, *3*) as a method for monitoring the kinetics of electrode reactions (*4*, *5*). For this purpose, as well as other applications where accurate knowledge of the drop time and/or electrode area is required, it is desirable to detect the time of consecutive natural drop fall with millisecond accuracy and in a manner which is compatible with potentiostatic circuitry and automated data acquisition by a laboratory microcomputer.

Although a sizable number of detection techniques have been reported (for example, see citations in refs. 6 and 7), few fulfil the above criteria. Nearly all use either a superimposed ac voltage or light as probes, although an FM transmitter and receiver have been employed to exploit the behavior of a DME as an antenna (*8*). While the optical detectors (*7*) offer the advantage of requiring no electrical connection with the cell, they are subject to serious errors of up to 100 ms (*4*). A number of the ac devices described either are not compatible with conventional potentiostat-based instrumentation (e.g., ref. 9), have response times on the order of tens of milliseconds (*10*), or continuously impose an undesirable ac perturbation on the cell and require remote activation and disabling because of a limited noise immunity (*6*). A recently reported technique (*11*) for making drop time measurements averaged over successive drops is simple in concept but requires adjustment as the cell current is changed, and in the vicinity of the potential of zero charge (pzc) it relies on stray impurity currents. Since these limitations render the previously described detectors inadequate for our purposes, we have developed a faster, more sensitive and versatile device which is described here.

PRINCIPLES OF OPERATION

Operation of the detector can be understood with reference to the block diagram (Figure 1) and schematic (Figure 2). Late in the drop life, the monostable which produces the delay for measurement of the dc current (D) returns to its stable state and closes the analog switch. An ac perturbation of 10 mV peak-to-peak at 100 kHz is imposed on the cell, and the resulting ac component of the cell current is detected by a tuned amplifier (A). When the electrode area is large enough so that the magnitude of the ac current exceeds the threshold selected by the potentiometer, the logic-level output of the level detector (B) will change states at the frequency of the

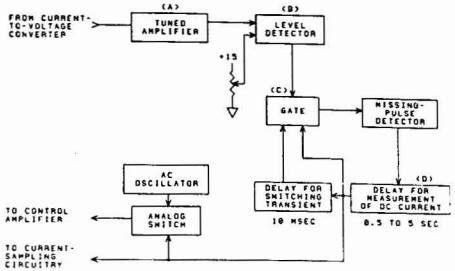

Figure 1. Block diagram of drop-fall detector

ac source and activate the missing-pulse detector after a delay to allow for switching transients. The precipitous decrease in electrode area concomitant with drop fall causes the tuned amplifier output to remain below the threshold throughout several ac cycles, long enough for detection of the missing transitions in the level-detector output. Within 100 to 200 μs of the fall of the drop, the ac source is disconnected from the potentiostat so that dc measurements can be made. The missing-pulse detector input is inhibited by the gate (C) to prevent noise transients from retriggering the detector, and a signal is sent to the current-sampling circuitry.

The time interval between the fall of the drop and its detection is due to three causes. First, at potentials away from the pzc, the potentiostat must supply charging current to the nascent drop. The resultant current spike (typically 50 μs)

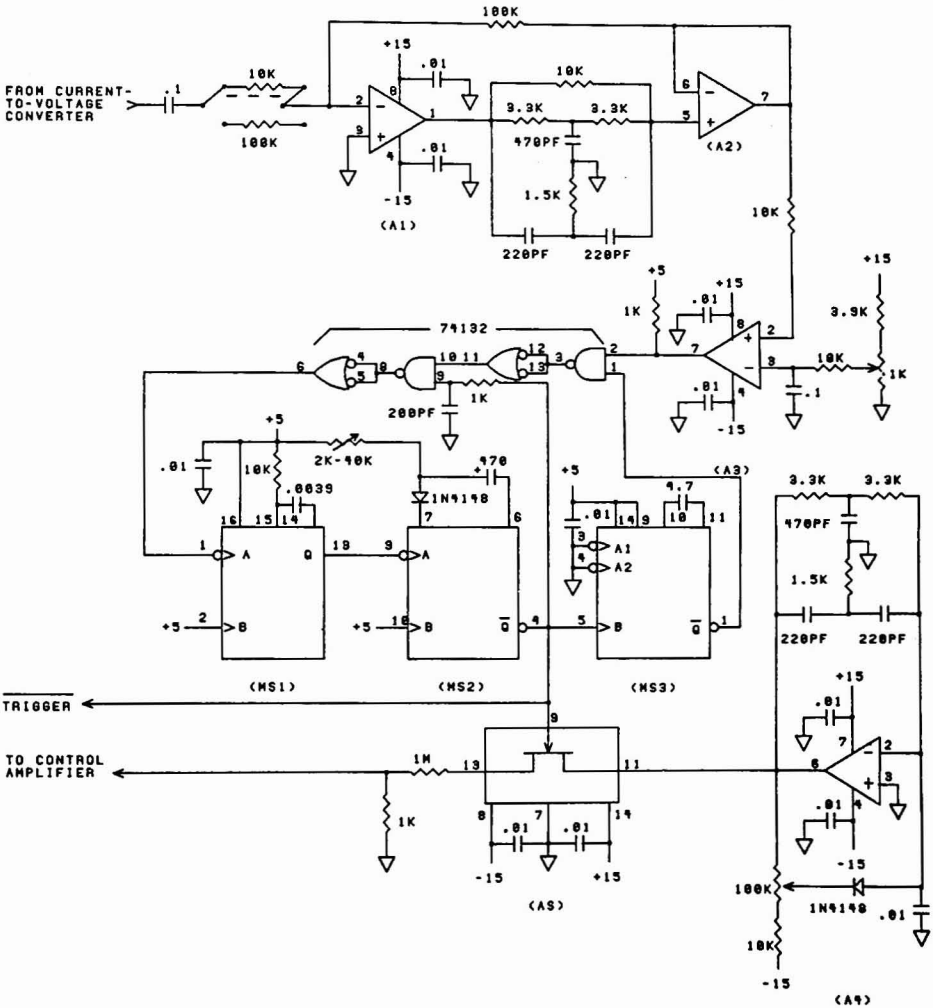

Figure 2. Schematic diagram. A1, A2, National LF353N; A3, National LM311N; A4, Signetics NE535V; MS1, MS2, SN74123; MS3, SN74121; AS, Siliconix DG300CJ

contains frequency components which can be detected by the tuned amplifier and which may keep the amplifier output above the level-detector threshold for a brief time after the drop has fallen. Second, the tuned amplifier must respond to the sudden change at its input with a deliberately constrained frequency response. Several periods of oscillation at the center frequency are required to accomplish this. Third, a full period (15 to 20 μs) of the missing-pulse detection monostable must elapse between the last output transition of the level detector and the production of the trigger signal for the current-sampling circuitry. Finally, noise in the current-to-voltage converter whose power spectrum overlaps the frequency range of the tuned amplifier can delay detection of drop-fall a few additional ac cycles.

The drop-fall detector operates reliably even in noisy environments provided the potentiostat employed has sufficient response at the frequency of the ac perturbation. Although we have chosen a frequency of 100 kHz, the detector is suitable for slower potentiostats providing that a lower frequency is selected, albeit with some lengthening in drop-detection time. This modification needs to be performed only once and is accomplished by varying the passive components in the twin-T networks around amplifiers A1 and A4 (*12*) and the timing capacitor on MS1. A single selection of the suitable gain (two are available) for the tuned amplifier and of a threshold level appropriate to the current-to-voltage converter setting, to the electrode capacitance, and to the cell resistance generally suffices over a wide potential range (2 V or more) for a given set of cell conditions. Since no further adjustments are required, this circuit is very useful as a trigger device for automated instruments, especially those under the control of a laboratory computer. The circuit's independent nature allows the computer to perform lower priority tasks between measurements, instead of requiring that the processor continually monitor portions of the detection circuitry in order to discern drop fall (*6*).

PERFORMANCE SUMMARY

The features of the detector include the temporary disconnection of the self-contained oscillator from the potentiostat by means of an analog switch as soon as drop fall has been detected which eliminates the need for filtering. A single adjustment generally suffices for a wide range of potentials, and the operation of the detector is unaffected by the presence of the pzc within that range. The response time, between 100 and 200 μs, is dictated by electrochemical cell characteristics, the frequency of the ac perturbation, and the time window of the missing-pulse detector. Unfavorable cell conditions are those in which large faradaic and nonfaradaic components are present so that the output of the tuned amplifier remains substantial even after the drop has fallen. Such circumstances are encountered, for example, with a solution of 1 mM Cr^{3+} in 1 M $NaClO_4$ (pH 3) at an electrode potential of −1100 mV. vs. SCE where the diffusion-controlled reduction of Cr^{3+} occurs, and the excess electrode charge density is large and negative (ca. −13 μC cm^{-2}) (*13*). The response time was assessed by observing the current-to-voltage converter output on a Biomation Model 820 transient recorder in the pretrigger mode. Detection was considered to have occurred when sinusoidal variations at 100 kHz could no longer be distinguished in the cell current. Thirty determinations yielded an average detection time of 185 μs with a standard deviation of 36 μs. Measurements at the growing mercury drop are essentially unaffected by the ac perturbation since it is automatically disconnected within this time scale. Either individual or successive natural drop times can be conveniently determined to this accuracy, so that current–time curves may be monitored even at subsecond sampling times with high accuracy. In addition to its use as a synchronization device for rapid dc polarography (see ref. 4 for details) and determinations of the excess electrode-charge density from charge–time curves (*14*), we have also found it to be highly suitable for obtaining precise surface-tension data from drop-time measurements (*11*).

LITERATURE CITED

(1) Canterford, D. R. *J. Electroanal. Chem.* **1977**, *77*, 113.
(2) Corbusier, P.; Gierst, L. *Anal. Chim. Acta* **1956**, *15*, 254.
(3) Bond, A. M.; O'Halloran, R. J. *J. Phys. Chem.* **1973**, *77*, 915.
(4) Tyma, P. D. *J. Electrochem. Soc.* **1978**, *125*, 284C.
(5) Tyma, P. D.; Weaver, M. J., to be published.
(6) De Blasi, M.; Giannelli, G.; Papoff, P.; Rotunno, T. *Ann. Chim.* **1975**, *65*, 315.
(7) Hahn, B. K.; Enke, C. G. *Anal. Chem.* **1974**, *46*, 802.
(8) Yarnitzky, C. *J. Electroanal. Chem.*, **1974**, *51*, 207. Yarnitsky, C.; Wijnhorst, C. A.; Van Der Laar, B.; Reyn, H.; Skuyters, J. H. *Ibid.*, **1977**, *77*, 391.
(9) Papeschi, G.; Costa, M.; Borda, S. *Electrochim. Acta* **1970**, *15*, 2015.
(10) Lawrence, J.; Mohilner, D. M. *J. Electrochem. Soc.* **1971**, *118*, 259.
(11) Peerce, P. J.; Anson, F. C. *Anal. Chem.* **1977**, *49*, 1270.
(12) Malmstadt, H. V.; Enke, C. G.; Crouch, S. R.; Horlick, G. "Optimization of Electronic Measurements"; W. A. Benjamin: Menlo Park, Calif., 1974; pp 47–53.
(13) Weaver, M. J.; Anson, F. C. *J. Electroanal. Chem.* **1975**, *65*, 711.
(14) Lauer, G.; Osteryoung, R. A. *Anal. Chem.* **1967**, *39*, 1866.

RECEIVED for review April 30, 1979. Accepted August 24, 1979. P.D.T. gratefully acknowledges support from an American Chemical Society Analytical Chemistry Division Fellowship which was sponsored by the Procter and Gamble Company. M.J.W. is indebted to the Air Force Office of Scientific Research for support of his research program.

Apparatus for the Dynamic Coating of Capillary Columns

Eduardo O. Murgia and Joaquin A. Lubkowitz*

Instituto Tecnológico Venezolano del Petróleo, Apartado 76343, Caracas 107, Venezuela

The use of glass capillary columns is expanding rapidly in the analysis of the complex substances by gas chromatography. The glass column is still costly and it is sometimes convenient for the user to control length, nature of liquid phase, and thickness of stationary phase of the columns to be used.

Recently several workers (*1–3*) have reviewed the numerous recipes available for the preparation of columns. Thus many of the myths have disappeared. The manufacture of a column requires the careful attention of the pretreatment of the glass surface, the deactivation of its Lewis acidity, and finally the coating of the stationary phase. One of the most reproducible methods of coating the column is a variation of the dynamic method developed by Schomburg and which has been called the mercury plug technique (*4*). The method consists of introducing a short mercury plug immediately after the liquid phase has entered the column. This technique aims at achieving a thin film from a highly viscous solution which can resist drainage and non-uniformity of the coating during the evaporation stage. This method is relatively fast and has the potential that the same equipment can be used for other steps such as coating with a deactivating agent or rinsing the column.

A simple apparatus has been developed which is designed to coat the columns and is capable of introducing a short plug

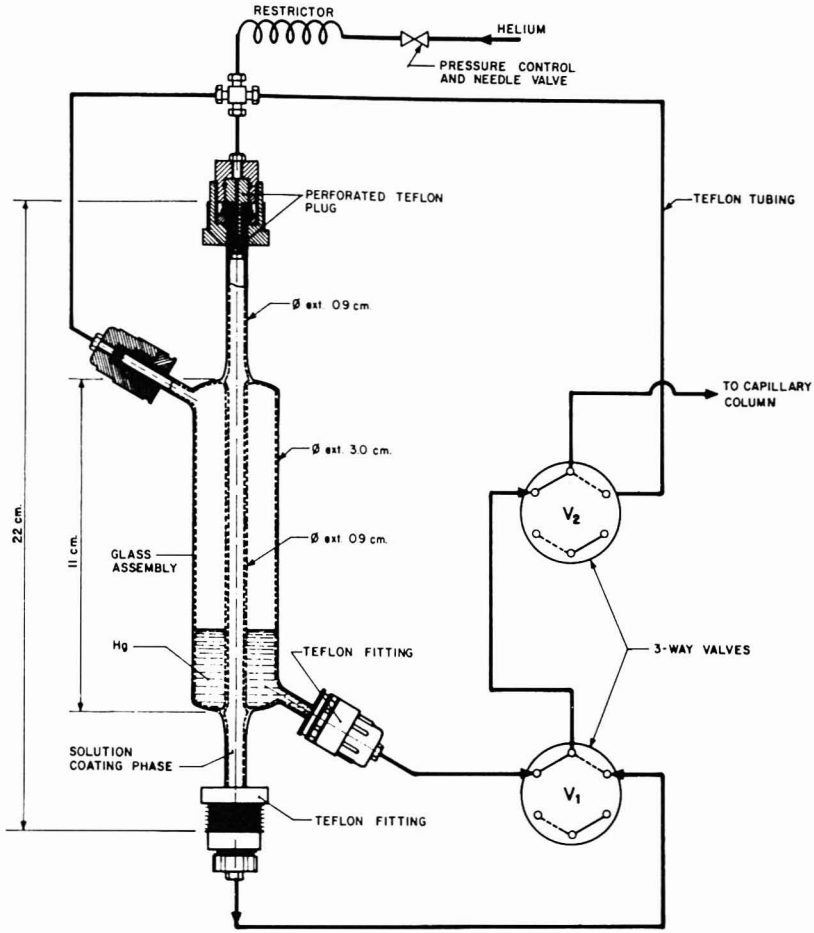

Figure 1. Schematic diagram of the coating apparatus

of mercury. Furthermore, the liquid phase and the mercury are contained in separated sections. The apparatus is simple to construct and operate.

EXPERIMENTAL

Apparatus Construction. The assembled apparatus is shown in Figure 1. It consists of a replacement column tube (Altex Scientific, Berkeley, Calif., catalogue no. 252-00-001) and a glass-jacketed column built around this tube. Two pieces of microbore column of 2-mm i.d. (Altex, catalogue no. 251-00) were joined to the main body. Thus, all four ports use the liquid chromatography Teflon fittings which can be hand-tightened. The two lower exit ports are connected to the three-way valves (Rheodyne, Berkeley, Calif., model no. 50-31). A flow controller (Brooks, 4480, Brooks Instrument, Hatfield, Pa.) and a 2-m long, 1.59-mm o.d. stainless-steel capillary tubing are used in order to carefully control the flow so that the liquid flow through the column is adjustable from 0.2–2 m/s.

The outer jacket contains about 3 mL of mercury which is introduced via the left port. The inner glass tube is capable of holding 4 mL of liquid. The connections between valves and the glass container are made with Teflon tubing (1.15-mm o.d.).

Operation. After introducing the liquid phase though the upper port, the needle valve is adjusted to give the desired flow rate through the column and its dummy. The valves V_1 and V_2 should be in the coating sequence as shown in Figure 1. Immediately after the liquid coating phase is in the column, usually 15% of total column volume, the valves are switched to the mercury plug position as shown in Figure 1. Valve V_2 is kept in this position for a short time, usually 2–3 s, since this time

determines the length of the mercury plug. The valves are then switched to the gas flushing sequence whereby the inert gas finishes the coating and dries the column.

RESULTS AND DISCUSSION

The system designed has been tested repeatedly and offers several advantages over other reported apparatus. It depends on valves rather than on using a moving capillary to introduce the mercury plug. The coating phase is physically separated from the mercury and, thus, the mercury supply remains essentially noncontaminated. The mercury is isolated from the liquid phase container. Only the delivery Teflon pathway toward the column presents a contact of liquid and mercury. The apparatus handles mercury safely making it difficult to spill mercury during such operations as loading, cleaning, and pressurizing the assembly.

The same apparatus can be used to rinse the column or for the passage of deactivating solutions. It is possible to expand the unit by attaching an additional glass cylinder to the unused ports of one valve. Thus the second glass container can be used exclusively for washing or deactivation treatments. This would reduce further the possibilities of contamination. The additional cylinder can be made of plastic and used for etching the columns with liquid solutions (*5*) or by attaching a gas generator. Finally, the assembled unit as shown in Figure 1 has components which are found in most separation laboratories and has a cost of less than $150.

We have repeatedly used this system in coating columns obtaining theoretical plates number of 2000–3000 for k = 14–20 (C-14) and internal column diameters of 0.25 mm.

LITERATURE CITED

(1) Jennings, W. "Gas Chromatography with Glass Capillary Columns"; Academic Press: New York, 1978; p 31.
(2) Sandra, P.; Verzele, M. *Chromatographia* **1977**, *10*, 419–425.
(3) Onuska, F. I.; Comba, M. E.; Bistrikl, T.; Wilkinson, R. J. *J. Chromatogr.* **1977**, *142*, 117–125.
(4) Schomburg, G.; Husmann, H. *Chromatographia* **1975**, *8*, 517–519.
(5) Heckman, R. A.; Green, R.; Best, F. *Anal. Chem.* **1978**, *50*, 2157–2158.

RECEIVED for review April 23, 1979. Accepted August 6, 1979.

Surge Control Unit for Mercury Manometers

Jesse S. Ard

Eastern Regional Research Center, Agricultural Research, Science and Education Administration, 600 E. Mermaid Lane, Philadelphia, Pennsylvania 19118

The reading of a mercury meniscus can be critical to obtaining correct pressure and volume measurements. Sometimes corrections have to be applied for local gravity, temperature, capillary depression, the height of a cylinder equivalent to the volume of a curved section, glass refraction, static electricity, and dryness of the gas exposed (*1*, *2*). These factors can produce errors, but these can be reduced or eliminated by the use of wide-diameter glass tubing where the meniscus is read. Such tubing is also desirable for obtaining large displacement volumes for McCleod gauges, hydrogenation apparatus, Toepler pumps, and other gas handling systems.

However, glass walls of large chambers cannot well survive the liquid hammering action of large masses of surging mercury, which often occurs through careless handling of valves or other accidents. The usual provision for surge control has been a constriction in the lower connections, but this, if small enough, may retard normal flow and may result in long delays in reading the meniscus.

A simple glass unit (Figure 1) that provides division and reunion of a liquid stream has been designed to overcome these difficulties. Diameters of the channels can be chosen to fit particular circumstances. Normally, the unit would be placed in the lower part of a glass structure. Connecting units in tandem may be used to enhance the dampening effect.

Glass tubing may be bent to form a unit. A somewhat less efficient unit may be made more easily by blowing a bulb, flattening it, and pushing in each side with carbon to form an island-like structure encircled by channels. The glass units should be annealed well to overcome local stresses that are likely to occur if one branch contracts more than the other.

The unit does not trap bubbles, avoids the need for narrow constrictions, and offers resistance to flow that is an increasing function of the mercury velocity. Thus, surging is prevented without appreciable effect on normal flow rates. Resistance to mercury motion approaches zero as the velocity approaches zero, and the meniscus settles to the correct level with negligible hysteresis. Surges upward and downward are dampened alike. For example, on upward flow, collision of the mercury streams produces a resistance to flow at the top

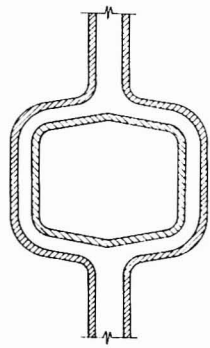

Figure 1. Glass unit for mercury surge control by divergent-convergent actions

juncture. At the same time, the velocity is attenuated at the bottom juncture because of the division of the mercury into two streams. This attenuation not only minimizes the forces from the moving mercury but also nearly balances the lateral forces through opposing symmetry. In actual operation, no tendency for the unit to jump could be observed, and the small glass structure withstood the internal forces well.

These units have served for manometers, hydrogenation apparatus, and large fixed McCleod gauges. For example, a surge control unit measuring 40 mm across the squared part and containing channels 2.7 mm in diameter for the divided stream proved satisfactory in controlling mercury hammer in a 200-mL volume bulb and overshoot in the comparison column of a McCleod gauge.

LITERATURE CITED

(1) "International Critical Tables," H. H. Kimball, Ed., No. 1, Maple Press Co., York, Pa., 1926, p 68.
(2) W. Cawood and H. S. Patterson, *Trans. Faraday Soc.*, **29**, 514 (1933).

RECEIVED for review July 19, 1979. Accepted August 23, 1979.

Author Index

Future Articles

Solvent System Optimization in the Separation of Indole Alkaloids by Silica Gel Liquid Chromatography
S. Hara, N. Yamauchi, C. Nakae, and S. Sakai

Reduction of Argon Consumption by a Water Cooled Torch in Inductively Coupled Plasma Emission Spectrometry
G. R. Kornblum, W. van der Waa, and L. de Galan

Major and Trace Elements Determination in Geological and Biological Samples by Energy-Dispensive X-Ray Fluorescence Spectrometry
K. Matsumoto and K. Fuwa

Modification of a Gas Chromatographic Inlet for Thermal Desorption of Adsorbent-Filled Sampling Tubes
W. K. Fowler, C. H. Duffey, and H. C. Miller

Vacuum-Ultraviolet Atomic Absorption Spectrometry of Mercury with Cold Vapor Generation
K. Tanabe, J. Takahashi, H. Haraguchi, and K. Fuwa

Determination of Binding Protein and Labeled Analyte Concentrations Which Optimize the Response in Immunoassays
C. J. Halfman

Elemental Analysis of Thick Obsidian Samples by Proton Induced X-Ray Emission Spectrometry
P. E. Deurden, E. Clayton, J. R. Bird, D. D. Cohen, W. R. Ambrose, and B. F. Leach

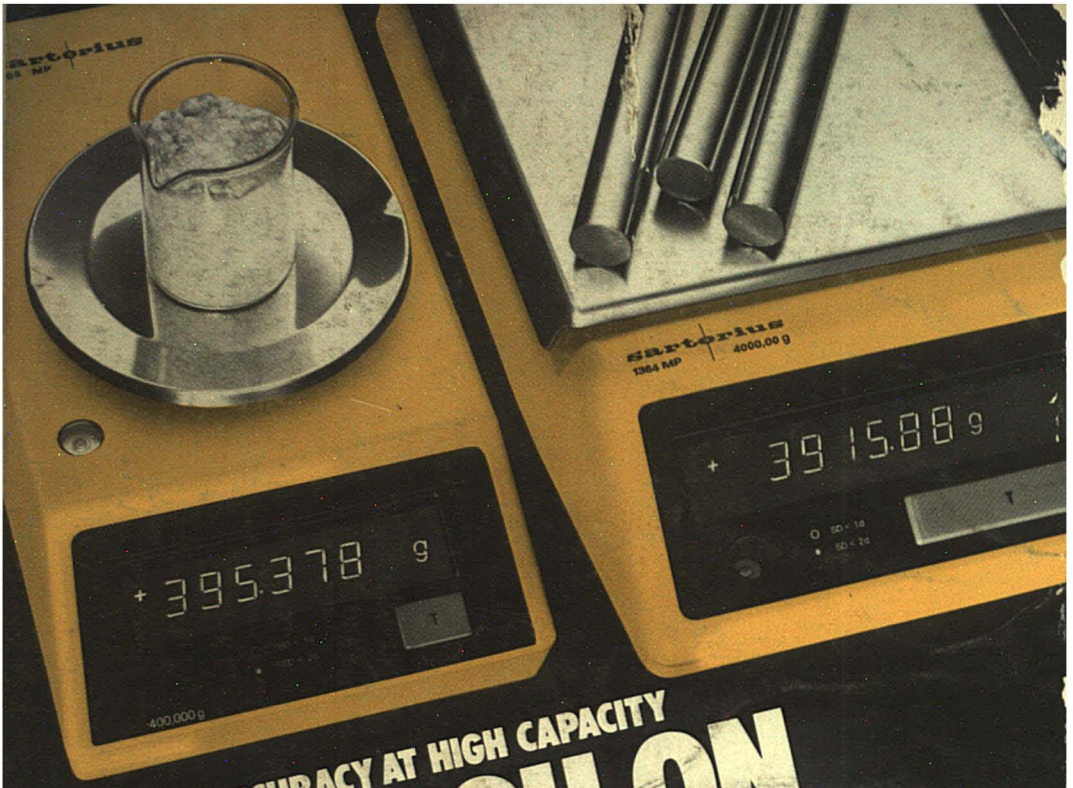

HIGHER ACCURACY AT HIGH CAPACITY

GET HIGH ON SUPER RANGE

ELECTRONIC BALANCES ONLY BY SARTORIUS

Only Super Range combines high capacity with higher accuracy.

Super Range is an expanded weighing range to the full capacity of the balance, resulting in higher readout accuracy. With Super Range, you can weigh 400 grams to 0.001g (Model 1265MP, above left), or 4,000 grams to 0.01g (Model 1364MP, above right). Balances with 'dual range' or 'movable fine range' cannot match this readability when weighing to full capacity.

With Super Range, the final decimal place never disappears.

Super Range avoids the confusion of the 'disappearing' final decimal place common to 'movable fine range' balances when weighing to full capacity. With Super Range, the number of decimal places in the readout is constant, regardless of sample weight.

Today's most advanced balances to meet the needs of tomorrow.

Super Range Balances are microprocessor-equipped and feature instant electronic taring, built-in BCD output to interface with printers and calculators, adjustable integration time, and large, bright 7-segment displays. Super Range is another weighing first from Sartorius.

For literature, write: Sartorius Balances Division, Brinkmann Instruments, Inc., Subsidiary of Sybron Corporation, Cantiague Road, Westbury, N.Y. 11590, or call 516/334-7500.

SYBRON | Brinkmann

CIRCLE 21 ON READER SERVICE CARD